U.S. DEPARTMENT OF LABOR MSHA
00032260

copy 2 open file - Std for Telecommunication Surveys (no supplement for this copy)

Electromagnetic Fields in Mine Environments

Final Report

USBM Contract J0199115

Continuation of H0155008

1 May 1980

U.S. Bureau of Mines
Twin Cities Research Center
LIBRARY

OFR
81-32 (1)

The views and conclusions contained in this document are those of the authors and should not be interpreted as necessarily representing the official policies or recommendations of the Interior Department's Bureau of Mines or of the U.S. Government.

OFR 32-81
C.2

(this page replaces old Title Page)

REPORT DOCUMENTATION PAGE

1. Report No.	2.	3. Recipient's Accession No.

4. Title and Subtitle	5. Report Date
ELECTROMAGNETIC FIELDS IN MINE ENVIRONMENTS	1 May 1980
	6.

7. Author(s)	8. Performing Organization Report No.
Wait, James R. and Hill, David A. Rm 242, RB1 U.S. Dept. of Commerce, Boulder, Colo. 80303	

9. Performing Organization Name and Address	10. Project/Task/Work Unit No.
Institute for Telecommunication Science U.S. Dept. of Commerce Boulder, Colo. 80309	J0199115 Cont. of H0155008
	11. Contract or Grant No.
12. Sponsoring Organization Name and Address	13. Type of Report
Office of the Assistant Mining Director U.S. Bureau of Mines Department of the Interior Washington, D.C.	Final
	14.

15. Supplementary Notes

16. Abstract

The present final report constitutes the total productivity of a series of contracts from the U.S. Bureau of Mines and the Institute for Telecommunication Sciences over the period 1971-1979. The emphasis on the research has been analytical. In this "executive summary" we give a succinct description of each phase of the investigation. In the first phase of the investigation that was stimulated by the National Academy of Engineering, we concentrated on the analytical studies of techniques relevant to mine rescue. Several specific procedures for locating a buried source were analyzed. In the next, but overlapping phase of the investigation, we dealt with the fundemental character of how electromagnetic waves propagate in mine tunnels. At the outset we allowed for the finite conductivity of the tunnel walls and the presence of axial conductors such as cables, pipes and tracks. The third phase of the investigation was devoted to the analyses of various specific geophysical engineering problems. The related fourth phase dealt with the general subject of non-destructive testing of wire ropes such as used for mine hoists.

17. Originator's Key Words	18. Availability Statement
Mine Communications Electromagnetics Mine Rescue Transients Transfer Impedance	The publishers indicated have kindly granted permission to include reprinted material in the copies of this report submitted to the U.S. Government sponsor.

19. U. S. Security Classif. of the Report	20. U. S. Security Classif. of This Page	21. No. of Pages	22. Price
Unclassified	Unclassified	448	

Electromagnetic Fields in Mine Environments

TABLE OF CONTENTS

Executive Summary..... 2
Acknowledgement (Foreword)..... 3
State of Knowledge of Analytical Techniques for Thru-the-Earth E.M. (Electromagnetic) Wave Problems Relevant to Mine Rescue..... 5
E.M. (Electromagnetic) Induction Technique for Locating a Buried Source..... 9
Criteria for Locating Oscillating Magnetic Dipole Buried in the Earth..... 13
Transient Signals from Buried Magnetic Dipole..... 16
Transient Magnetic Fields Produced by Step-Function-Excited Buried Loop..... 20
E.M. Surface Fields Produced by Buried Pulse-Excited Loop..... 22
Transient E.M. Fields of Circular Loop in Presence of a Conducting Half-Space..... 26
Locating an Oscillating Magnetic Dipole in the Earth..... 29
Low-Frequency Impedance of a Circular Loop Over Conducting Ground..... 31
E.M. Fields of a Small Loop Buried in Stratified Earth..... 34
E.M. Response of Buried Sphere for Buried-Dipole Excitation..... 36
Perturbation of Magnetic Dipole Fields by Perfectly Conducting Prolate Spheroid.... 42
E.M. Transient Response of Small Wire Buried Loop..... 45
Source Location Errors for Magnetic Dipole Buried in Inhomogeneous Earth..... 55
Subsurface E.M. Fields of a Line Source on Two-Layer Earth..... 67
Array Technique for E.M. Positional Determination of Buried Receiving Point..... 73
Subsurface E.M. Fields of Line Source on Conducting Half-Space..... 75
Effect of Buried Conductor on Subsurface Fields for Line Source Excitation..... 81
The Sub-Surface Magnetic Fields Produced by Line Current on Non-Flat Earth..... 86
Subsurface Electromagnetic Fields of Grounded Cable of Finite Length..... 93
Excitation of Conductive Cylinder by Prescribed Axial Current..... 100
Subsurface Electric Fields of Grounded Cable of Finite Length..... 108
Transient Excitation of the Earth by Line Source of Current..... 117
Analytical Studies of E.M. Waves on Mono-filar and Bi-Filar Structures..... 120
Theory of E.M. Wave Propagation Through Tunnels..... 125
H.F. Communication in Tunnels Using Open Transmission Lines and Leaky Cables..... 132
Theory of Transmission of E.M. Waves Along Multi-Conductor Lines..... 135
Theory of Wave Propagation Along a Thin Wire Inside Rectangular Waveguide..... 139
Guided E.M. Waves in Curved Rectangular Mine Tunnel..... 143
Geometrical Optical Approach for E.M. Propagation in Rectangular Tunnel..... 149
Guided E.M. Waves Along an Axial Conductor in a Circular Tunnel..... 161
Excitation of Monofilar and Bifilar Modes on Transmission Line in Tunnel..... 165
Gap Excitation of Axial Conductor in Circular Tunnel..... 170
E.M. Fields of a Coaxial Cable with Interrupted Shield Located in Tunnel..... 174
Coupling Between Radiating Coaxial Cable and Dipole Antenna..... 179
Channel Characteristics of Braided Coaxial Cable in Mine Tunnel..... 183
Transmission Loss for Leaky Feeder Communication System in Circular Tunnel..... 189
L.F. Radio Transmission in a Circular Tunnel Containing Wire Conductor Near Wall... 196
Eccentrically Located Wire in a Cylindrical Cavity in Conducting Medium..... 197
Attenuation on a Surface Wave G-Line Suspended Within Circular Tunnel..... 200
E.M. Fields of a Dipole Source in Circular Tunnel Containing Surface Wave Line..... 202
Propagation Along a Braided Coaxial Cable in Circular Tunnel..... 217
Spatial Dispersion of Shield Transfer Impedance of Braided Cable..... 222
Impedance of an Electric Dipole Located in Cylindrical Cavity..... 225

Page

Impedance of Dipoles in a Circular Tunnel with Axial Conductor..... 231
Analysis of R.F. Transmission Along a Trolley Wire in Mine Tunnel..... 240
R.F. Transmission via Trolley Wire in Tunnel with Rail Return..... 245
Quasi-Static Limit for Propagating Mode Along Thin Wire in Circular Tunnel..... 251
R.F. Transmission in Semicircular Mine Tunnel Containing Two Axial Conductors..... 254
Dedicated Communication Line in Mine Tunnel for Shunt-Loaded Trolley Wire..... 259
Transmission Modes in Braided Coaxial Cable and Coupling to Tunnel..... 266
Guided Electromagnetic Waves in Periodically Nonuniform Tunnel..... 272
Controlled Mode Conversion in Leaky Feeder Mine Communication Systems..... 276
Mode Conversion by Tunnel Nonuniformities in Leaky Feeder Systems..... 281
Bandwidth of Leaky Coaxial Cable in Circular Tunnel..... 285
Comparison of Loop and Dipole Antennas in Leaky Feeder Systems..... 292
Transmission in Elliptical Tunnel with Contained Axial Conductor..... 304
Low-Frequency Propagation Along thin Wire in Arbitrarily Shaped Mine Tunnel..... 308
Electromagnetic Guided Waves in Mine Environments..... 314
Theory of Transmission of E.M. Waves Down Mine Hoist..... 319
Theory of Transmission of E.M. Waves in a Coal Seam..... 327
Analysis for E.M. Fields of Dipole Located Within Metal-Cased Borehole..... 330
E.M. Shielding of Sources Within Metal-Cased Bore Hole..... 334
Calculated Admittance of Idealized Drill Rod Antenna in Lossy Medium..... 339
Electromagnetic Basis of Drill-Rod Telemetry..... 343
Theory of Transmission of E.M. Waves Along a Drill Rod in Conducting Rock..... 345
Theory of E.M. Methods for Nondestructive Testing of Wire Ropes..... 349
Review of E.M. Methods in Nondestructive Testing of Wire Ropes..... 362
E.M. Basis for Nondestructive Testing of Cylindrical Conductors..... 374
E.M. Nondestructive Testing of Cylindrically Layered Conductors..... 377
Analysis of A.C. Excitation of Wire Rope by Toroidal Coil..... 380
Scattering by Slender Void in Homogeneous Conducting Wire Rope..... 385
E.M. Field Perturbation by Void in Conducting Cylinder Excited by Wire Loop..... 393
E.M. Response of Anisotropic Conducting Cylinder to External Source..... 400
E.M. Interaction Between Conducting Cylinder and Solenoid in Relative Motion..... 404
Dynamic E.M. Response of Homogeneous Conducting Cylinder for Symmetric Excitation.. 409
Fields of a Horizontal Loop of Arbitrary Shape in Two Layer Earth..... 417

Acknowledgement

We should like to acknowledge the support and encouragement we received from the following individuals in the course of this intensive study: J.C. Powell, J.N. Murphy, H. Parkinson, H.K. Sacks and H. Dobroski, all of the U.S. Bureau of Mines; R.L. Lagace, R.H. Spencer and A. Emslie of A.D. Little, Inc.; A.J. Farstad and R.G. Olsen of Westinghouse - Boulder; G.V. Keller and C.H. Stoyer of Colorado School of Mines in Golden; K.P. Spies of ITS/NTIA in Boulder, P. Delogne of Louvain University in Belgium; L. Deryck of Liege University in Belgium; R. Gabillard and P. Degauque in Lille University, France; Q. Davis and R. Haining of University of Surrey in the United Kingdom; David Martin of the United Kingdom National Coal Board, S.F. Mahmoud of Cairo University, formerly CIRES; D. Seidel of Sandia Corp., formerly CIRES; D.C. Chang and E.F. Kuester of the Electromagnetics Lab at Colorado University in Boulder; D.D. Crombie, Director of I.T.S./NTIA in Boulder; W.N. Hess, Director of ERL/NOAA in Boulder and C. Kisslinger, Director of CIRES in Boulder; R.L. Gardner of CIRES, and finally but certainly not least, Loys Gappa, Lana Hope and Jeri Bacon in CIRES Boulder for manuscript preparation.

EXECUTIVE SUMMARY

The present final report constitutes the total productivity of a series of contracts from the U.S. Bureau of Mines and the Institute for Telecommunication Sciences over the period 1971-1979. The emphasis on the research has been analytical and the topics selected for investigation were suggested by the staff of the Pittsburgh Mining and Safety Research Center in Bruceton, Pa. Other Bureau of Mines contractors also provided valuable advice.

[redacted] (i.e., the U.S. Bureau of Mines). After revision, this material was [redacted] so there was [redacted] The present collection is essentially a compilation of this material arranged in a reasonably coherent order. In all cases the publications were prepared in the Cooperative Institute for Research in Environmental Sciences (see acknowledgements below) that is a joint venture between NOAA and the University of Colorado. The support of NOAA to CIRES to facillitate the publication of the journal articles was crucial.

In this "executive summary" we give a succinct description of each phase of the investigation. As appropriate, we refer to the page number in parenthesis where the particular article can be found in the collection. The table of contents that procedes this summary lists all the articles.

In the first phase of the investigation that was stimulated by the National Academy of Engineering, we concentrated on the analytical studies of techniques relevant to mine rescue (5). [redacted] using an idealized model of the conductive overburden (9, 13). In such cases the trapped miner was considered to have limited means but some type of emergency power source was assumed to be available. Various [redacted] and the [redacted] (20-124). Some attention was also given to [redacted] (45, 73), but these results did not appear too promising.

In the next, but overlapping, phase of the investigation, we dealt with the [redacted] (125, 132). This work was done in collaboration with workers in the United Kingdom, France and Belgium. At the outset we allowed for the finite conductivity of the tunnel walls and the presence of axial conductors such as cables, pipes and tracks. Numerous configurations were considered in a sequential fashion and an attempt was made to present the results in a form convenient for the use of experimentalists and systems engineers (135-308). In many cases we either derived simplified working formulas or provided the justifications for the use of empirical prediction procedures for transmission loss. Many of these results were the focus of discussion at an international workshop conference that we sponsored (314).

The third phase of the investigation was devoted to the analyses of various specific geophysical engineering problems that the sponsor suggested from time to time (330-361). The related fourth phase dealt with the general subject of [redacted] such as used for mine hoists (349). Here a general review was prepared (362) and various specific configurations (374-403) were considered, in detail, including the effect of the motional velocity of the ropes (404, 809).

16 July 1973

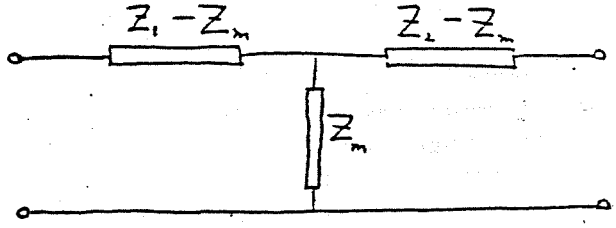
State of Knowledge of Analytical Techniques for Thru-the-Earth Electromagnetic Wave Problems Relevant to Mine Rescue

by James R. Wait

It is the purpose of this paper to review theoretical model concepts in through-the-earth transmission of electromagnetic waves. While the subject is very broad in its defined scope, we will be conscious of the specific applications to mine rescue and emergency telecommunications in coal mine environments.

The plan of the paper is to outline previous theoretical efforts without attempting to attach names or organizations to the specific developments. However, we include a guide to the literature as an appendix. Without pretending to be entirely impartial we include a critique of the limitations of the available analytical models.

As I see it the central problem is to calculate the steady state mutual impedance of a four-terminal network that is the black box characterizing the through-the-earth path. Problems of secondary importance include the determination of the input impedances of the two pairs of terminals and the associated transient responses.



The simple equivalent circuit given tells us a lot about the problem that we are seeking a solution for. The mutual impedance Z_m describes the propagation phenomena involved in transmission from input (source) to the output (receiver). Z_1 and Z_2, on the other hand, are the input impedances. Clearly the latter are needed in a total systems study since we have only a finite amount of power available at the source and the receiver must be matched in some sense to the output terminals of the receiving antenna.

Most of the past literature deals with the calculation or merely the derivation of the mutual impedance Z_m for some highly idealized geometrical configuration. For example, the source for an ungrounded loop is a magnetic dipole that is assigned a fixed magnetic moment. In the most extreme case this magnetic dipole is an infinitesimally small loop (of area dA) with a total circulating current I amps. The moment is IdA! Now we can still use this concept for a multi-turn loop if I is the total azimuthal current and provided the uniform current assumption is valid. Also, of course, we recognize that the finite size of the loop needs to be accounted for in some cases.

Reprinted from Proceedings of "Thru-the-Earth Electromagnetics Workshop", pp. 9-14, Final Report on U.S. Bureau of Mine Contract No. G 133023, 31 December 1973.

In some of the earliest work the fields of this dipole were calculated as if the conduction currents in the earth were negligible. Of course, this is a useful beginning. The next refinement was to correct these magneto-static fields by assuming that we need only multiply them by exp $(-s/\delta)$ where s was the transmission range and δ was the skin-depth in the earth for the operating frequency being adopted. With the benefit of hindsight we can criticize this correction as being grossly pessimistic for many cases of interest to mine rescue or to communication to a receiving station above or below the source loop.

By using the correct electrodynamic forms of the magnetic dipole fields in an homogeneous conductive medium of infinite extent, we can obtain a better estimate of the relevant value of Z_m. For example, if we are transmitting between two small coaxial loops, we can easily show that

$$Z_m = Z_o (1+\Gamma s)\, e^{-\Gamma s}$$

where $\Gamma = (1+i)\delta^{-1}$ and Z_o is the static or D.C. coupling limit.

Now usually the transmission takes place from the earth's surface to a buried receiving terminal. Or the converse situation may exist if we are dealing with up-link communication. In both cases the air-earth interface must be considered. Here we can immediately call attention to the classical formulation of Arnold Sommerfeld that dates back to 1909 in its earlies version. This was used as the basis of much analysis in later years but the interest was mainly for the case where the range exceeded a free-space wavelength. Here we are interested in the near zone where the significant distances are small compared with the wavelength in the air but such distances (i.e. depth or offset) may be comparable with the wavelength in the earth. This is quasi-statics in the vernacular of the current workers. To obtain field estimates we now have to "do" some integrations. Fortunately it was found that identities in Bessel function theory, recognized by mathematicians of the late 19th Century, were ripe for the picking. Thus some closed form field expressions were obtained and published in the 1950's for a fairly broad class of such problems. Numerical results required the manipulation of modified Bessel functions whose arguments were complex. Fortunately for cases of interest, the phase angles were near $\pi/4$ radians or 45 so that the tabulated Thomson's functions could be used. These are sometimes called the Kelvin functions and denoted ber, bei, kei, etc. [Note William Thomson became Lord Kelvin who was also noted for his work on laying the first Trans-Atlantic cable.]

With the ready availability of high speed computers, the use of intricate closed form field formulas is giving way to direct numerical integration of the Sommerfeld integrals. This is OK provided the programmer has some limiting checks or if he can refer back to some of the earlier work where the more elegant closed-form expressions in terms of special functions are used. Also, as has been shown quite recently, in the treatment of a finite-length source elements the special function representations for the dipole source is a convenient starting point. Otherwise double numerical integration is needed!

As we have indicated above, the air-earth interface problem is treated by regarding the overburden as a homogeneous half-space. A rather straightforward extension is the stratified half-space wherein the intermediate interfaces are plane and parallel to the air-earth interface. Further extensions involve electric dipoles rather than magnetic dipoles. These are appropriate when dealing with grounded electrodes connected by insulated cables. No new basic difficulties are encountered here.

In the class of problems discussed above, all three of the impedance elements Z_m, Z_1 and Z_2, are determinable. Thus, in principle, a complete determination or prediction of the system performance is possible. This includes down-link and up-link communication efficiency and estimates of source location accuracy for the models assumed.

Traditionally, the source current is assumed to vary harmonically in time. For dealing with transient excitation or in estimating signalling rate we need to understand the time-domain behavior of the system. Formally this is obtained by Fourier or Laplace transform inversion of the preceding transfer functions. In general, this is not a trivial task. However, some rather interesting closed-form results can be obtained if the original spatial wave number integration be deferred until after the Laplace transforms are inverted.

Now that the homogeneous and stratified half-space models have been exhausted it is appropriate to consider more realistic situations. For example, the earth's surface is not always flat. One approach to allow for this situation, was to adapt cylindrical and spherical boundaries. In such cases, the local radius of curvature was chosen to (more-or-less) match the local topography. Results of calculations from such models indicated that transmission ranges were not markedly affected but that source location errors could be significant. An even simpler method conceptually was to retain the uniform half-space model but to allow the plane interference to be tilted at such an angle that the local slope of the terrain was matched. Further analytical work on such models is justified since much insight can be gained without excessive numerical effort. Unfortunately, formally exact solutions for such models are strictly limited. One class of boundary that could be treated for line source excitation is a parabolic or hyperbolic interface. The three dimensional version involving dipoles in the presence of a paraboliodal interface is extremely intricate but it may be worth doing also.

One must clearly recognize that the overburden is not a homogeneous slab whether it be bounded by plane or uniformly curved interfaces. Thus, the influence of omni-present inhomogeneities needs to be understood. An extreme case is when metallic tracks and pipes are in the vicinity of the normal transmission path. To treat such configurations, two dimensional models have been used. An example is the line source excited buried cylinder of infinite length. This is not a trivial problem if one considers the interactions between the buried cylindrical inhomogeneity and the air-earth interface. Two specific analytical techniques have been used to get numerical results for this problem. One is essentially a perturbation procedure that

involves successive reflections between the cylinder and the plane interface while the other is a sophisticated integral equation procedure. The results between those methods agree in a common region of validity. The extension to three dimensional versions of these problems is nontrivial. Some progress has been made, however, in using perturbation procedures. An example is the buried sphere in the presence of a surface based dipole source. Some work has also been done on cylinders of finite length where certain assumptions were made about the nature of the axial induced current flow at the ends of the cylinder. Among other things this analysis showed that predictions based on infinite cylinders may be quite misleading.

Within the scope of these analytical techniques, we encompass both active and passive location concepts. In the active method, of course, the unknown source is energized by the to-be-rescued party. On the other hand, in the passive method, the target to be located is typically a loop of wire or a similar configuration. Various geometries, for such problems, have been considered in both the frequency and the time domain.

The foregoing account of theoretical analyses of electromagnetic induction problems is, by no means, claimed to be exhaustive. The selection has been based mainly on work that the author is familar with.

APPENDIX

A rather brief "guide" to the literature is as follows:

E.D. Sunde - Earth Conduction Effects in Transmission Systems - Dover Pulications, New York 1968 - (Comprehensive review of much of the early work in the 1930-1940 period carried out at Bell Telephone Labs. - includes many useful formulations for mutual impedances of grounded circuits relevant to coupling between power and communication circuits).

D.B. Large, L. Ball and A.J. Farstad - Radio Transmission from Underground Coal Mines - Theory and measurement trans. IEEE Comm 21, 194-10204, 1973 (good recent account of Westinghouse' s investigations).

R.E. Collin and F.J. Zucker (editors) - Antenna Theory Part II - McGraw Hill 1969 - (Chap. 24 by J.R. Wait gives a basic account of the theory for sources in conducting media - also an extensive bibliography is included).

L.L. Vanyan - Electromagnetic Depth Soundings (edited and translated by G.V. Keller) - Plenum Press 1967 - (An authorative review of Russian work on electromagnetic induction in the earth).

Also see recent volumes of the Journal Radio Science, IEEE Transactions on Antenna and Propagations, Journal of Applied Physics, and Geophysics.

Reprinted from Proceedings of "Thru-the-Earth Workshop" held at the Colorado School of Mines, Golden, Colo., August 1973, pp. 9-14, Available from NTIS under Accession No. PB 231 154.

IEEE Trans. Geosci. Electr., vol. GE-9, No. 2, 95-98 (April 1971)

Electromagnetic Induction Technique for Locating a Buried Source

JAMES R. WAIT, FELLOW, IEEE

Abstract—The field structure of a buried vertical oscillating magnetic dipole is examined. For an observer on the earth's surface, it is indicated that the finite conductivity of the earth will modify the geometrical character of the vertical and horizontal magnetic field components. However, this effect is quite small if the burial depth is less than an electrical skin depth.

Introduction

THERE IS A possibility that electromagnetic waves can be employed to locate coal miners following a disaster. A number of studies supporting this thesis are currently being sponsored by the U. S. Bureau of Mines. In this paper, without any claim to originality, I wish to present the basic theory of a technique that may hold some promise.

Manuscript received January 14, 1971.
The author is with the Institute for Telecommunication Sciences, Office of Telecommunications, Boulder, Colo. 80302.

The specific configuration considered is a small wire loop contained in a horizontal plane and buried at some depth h beneath the earth's surface. The objective here is to examine the structure of the electromagnetic field on the earth's surface produced by an alternating current injected into the loop. The situation is illustrated in Fig. 1 with respect to a cylindrical coordinate system (ρ, ϕ, z). The earth is represented as a homogeneous half-space of conductivity σ. All displacement currents can be neglected because we may assume that all linear

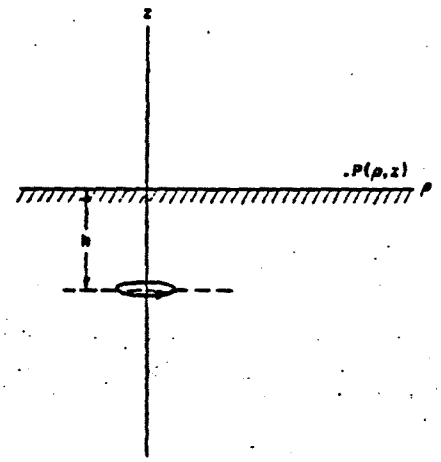


Fig. 1. Geometry of buried loop.

distances involved are small compared with the free-space wavelength.

Formulation and Solution

Considering the loop, whose area × turns product is IA, as a vertical magnetic dipole, we can derive the resultant magnetic fields in the air (i.e., $z>0$) from the following [1]:

$$i\mu_0\omega H_\rho = \partial^2 F/(\partial\rho\partial z) \tag{1}$$

and

$$i\mu_0\omega H_z = \partial^2 F/\partial z^2 \tag{2}$$

where μ_0 is the permeability of free space, ω is the angular frequency, and F is a scalar function. A straightforward boundary value analysis leads to the following integral form [1]:

$$F = \frac{i\mu_0\omega IA}{2\pi}\int_0^\infty \frac{\lambda}{u+\lambda} e^{-\lambda h} J_0(\lambda\rho)\,d\lambda \tag{3}$$

where $u=(\lambda^2+\gamma^2)^{1/2}$, $\gamma^2 = i\sigma\mu_0\omega$, and J_0 is a Bessel function of order zero.

Using (1) and (2) along with (3), we find that the fields at the location (ρ, z) for $z>0$ are

$$H_\rho = b_0 P \tag{4}$$

and

$$H_z = b_0 Q \tag{5}$$

where

$$P = h^3\int_0^\infty \frac{\lambda^2}{\lambda+u} e^{-\lambda z} e^{-uh} J_1(\lambda\rho)\,d\lambda \tag{6}$$

and

$$Q = h^3\int_0^\infty \frac{\lambda^2}{\lambda+u} e^{-\lambda z} e^{-uh} J_0(\lambda\rho)\,d\lambda \tag{7}$$

and the normalizing factor is

$$b_0 = IA/(2\pi h^3). \tag{8}$$

By changing the variable of integration to $x=\lambda h$, the integrals P and Q are expressible in the form

$$P = \int_0^\infty \frac{x^2 e^{-xZ}}{x+(x^2+iH^2)^{1/2}} e^{-(x^2+iH^2)^{1/2}} J_1(xD)\,dx \tag{9}$$

and

$$Q = \int_0^\infty \frac{x^2 e^{-xZ}}{x+(x^2+iH^2)^{1/2}} e^{-(x^2+iH^2)^{1/2}} J_0(xD)\,dx \tag{10}$$

where $H=(\sigma\mu_0\omega)^{1/2}h$, $D=\rho/h$, and $Z=z/h$ are dimensionless parameters. Equations (9) and (10) are in a form suitable for numerical integration, and a computer program has been prepared to accomplish this task. Before discussing the results, some special limiting cases will be mentioned.

Limiting Cases

When the conductivity σ and/or the frequency ω are sufficiently low, the parameter H is effectively zero. Then, without difficulty, the integrals P and Q are expressible in the closed forms

$$P = (3/2)D(Z+1)R^{-5} \tag{11}$$

and

$$Q = (1/2)[3(Z+1)^2R^{-5} - R^{-3}] \tag{12}$$

where $R=[D^2+(Z+1)^2]^{1/2}$. These simple results for the normalized magnetic fields P and Q correspond to static conditions.

The other limiting case of interest is when the conductivity σ and/or the frequency ω are sufficiently high that the integrals P and Q may be approximated in an asymptotic sense. Essentially, this amounts to arguing that when $|\gamma\rho|\gg 1$, the exponential factor $\exp(-uh)$ in (3), (6), and (7) may be adequately approximated by $\exp(-\gamma h)$. Then, treating both H and D as large parameters, we find that

$$P \sim -e^{i\pi/4}(3/H)D^{-4}\exp\left[-e^{i\pi/4}H\right] \tag{13}$$

and

$$Q \sim +e^{i\pi/2}(9/H^2)D^{-4}\exp\left[-e^{i\pi/4}H\right]. \tag{14}$$

A precise description of the validity of these asymptotic forms is subtle, but on comparison with numerical integration on the exact forms, it appears that they are useful when both H and HD are $\gg 1$.

Another interesting check is to let h be identically zero. Then for $z=0$, we have [1]

$$F = \frac{i\mu\omega IA}{2\pi}\int_0^\infty \frac{\lambda}{u+\lambda} J_0(\lambda\rho)\,d\lambda \tag{15}$$

$$= \frac{i\mu\omega IA}{2\pi}\frac{1}{\gamma^3\rho^3}\left[1-(1+\gamma\rho)e^{-\gamma\rho}\right] \tag{16}$$

where we have made use of a known identity. Then, again for $z=0$, we have

$$R_\phi = \partial F/\partial\rho = \frac{i\mu_0\omega IA}{2\pi}\cdot\frac{3}{\gamma^3\rho^4}\alpha \tag{17}$$

where

$$\alpha = 1 - [1 + \gamma\rho + (\gamma^2\rho^2/3)]e^{-\gamma\rho}. \tag{18}$$

If we now assume $|\gamma\rho| \gg 1$ and utilize the approximate (Leontovich) boundary condition [1], we have

$$H_\rho \simeq \eta E_\phi, \qquad \eta = i\mu_0\omega/\gamma \tag{19}$$

$$\simeq -\frac{IA}{2\pi}\cdot\frac{3}{\gamma\rho^4}. \tag{20}$$

This is consistent with (13) given above if we note that the right-hand side of (20) is $\lim_{h\to 0} b_0 P$. Also, we can obtain an exact expression for H_z at $z=0$ by using $i\mu_0\omega H_z = -(1/\rho)/(\partial/\partial\rho)\rho E_\phi$ and (17); thus $H_z = -IA\rho/(2\pi\gamma^2\rho^5)\beta$ where

$$\beta = 1 - [1 + \gamma\rho + (4/9)\gamma^2\rho^2 + (1/9)\gamma^3\rho^3]e^{-\gamma\rho}. \tag{21}$$

Again, if $|\gamma\rho| \gg 1$, $\beta \simeq 1$, and (21) is consistent with (14).

As a matter of theoretical interest, we have one final special case which deserves mention. Specifically, we take $\rho=0$, which means the observer is directly above the source loop. Then, of course, $P=0$, but Q is finite. If, in fact $z=0$, we have

$$Q = Q_z = h^3\int_0^\infty \lambda^3(u+\lambda)^{-1}e^{-uh}d\lambda. \tag{22}$$

Now,

$$(u+\lambda)^{-1} = (u-\lambda)(u^2-\lambda^2)^{-1} \doteq \gamma^{-2}(u-\lambda),$$

and therefore

$$Q_z = \frac{h^3}{\gamma^2}\left[\int_0^\infty u\lambda^3 e^{-uh}d\lambda - \int_0^\infty \lambda^4 e^{-uh}d\lambda\right]. \tag{23}$$

We can now verify that

$$Q_z = \frac{h^3}{\gamma^2}\left[\frac{\partial^4 p}{\partial h^4} - \gamma^2\frac{\partial^2 p}{\partial h^2} + \frac{\partial^5 q}{\partial h^5} - 2\gamma^2\frac{\partial^3 q}{\partial h^3} + \gamma^4\frac{\partial q}{\partial h}\right] \tag{24}$$

where

$$p = \int_0^\infty e^{-uh}\frac{\lambda}{u}d\lambda \tag{25}$$

and

$$q = \int_0^\infty \frac{e^{-uh}}{u}d\lambda. \tag{26}$$

These latter two integrals are known to be

$$p = e^{-\gamma h}/h \tag{27}$$

and

$$q = K_0(\gamma h) \tag{28}$$

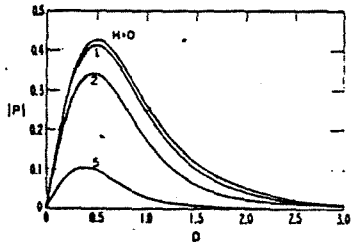


Fig. 2. Horizontal component of normalized magnetic field on surface as function of distance parameter D.

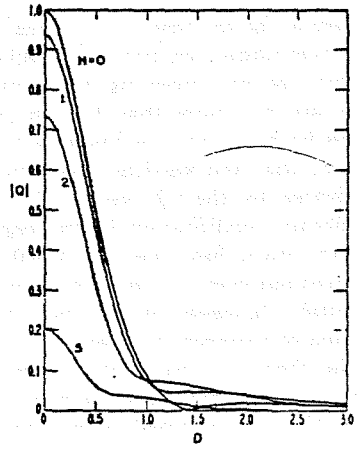


Fig. 3. Vertical component of normalized magnetic field on surface as function of distance parameter D.

where K_0 is a modified Bessel function of order zero. Using only the well-known identities $K_0'(Z) = -K_1(Z)$ and $K_1'(Z) = -[K_0(Z) + Z^{-1}K_1(Z)]$, it turns out that (24) can be reduced to the compact form

$$Q_z = 2e^{-x}x^{-2}[(12 + 12x + 5x^2 + x^3)] - 3[(x + (8/x))K_1(x) + 4K_0(x)]$$

where $x = \gamma h = \sqrt{i}H$. This provides an alternative method to compute the field directly above the source dipole.

Discussion of Results and Final Remarks

As indicated above, P and Q are the normalized components of the horizontal and the vertical magnetic field on the surface for the buried loop source. The magnitudes $|P|$ and $|Q|$ plotted as a function of the normalized distance D (or ρ/h) are illustrated in Figs. 2 and 3, respectively. The parameter on the curve is the normalized depth parameter H (or $(\sigma\mu_0\omega)^{1/2}h$). This can be calculated from the simple formula $H = 0.086(\sigma_{\text{mmho}}f)^{1/2}h_{\text{km}}$ where σ_{mmho} is the earth conductivity in millimhos per meter, f is the frequency in hertz, and h_{km} is the burial depth in kilometers. For example, if $\sigma_{\text{mmho}} = 1$, $f = 10^2$, and $h_{\text{km}} = 0.2$, we have $H = 0.17$. In this case, we can make the rather important observation that the character of the $|P|$ versus D curves in Fig. 2 are essentially

the same as for the case $H=0$. Thus, the conductivities of the overburden are probably negligible for this configuration of the receiving loop provided the burial depths are not more than 0.5 km and the operating frequencies are in the low audio range. It is significant, however, that the vertical magnetic field component as indicated by the $|Q|$ versus D curve in Fig. 3 has a significant modification in the region near $D=\sqrt{2}$. Here, the static field (i.e., for $H=0$) has a null which is smeared out even for small values of the parameter H. This effect, however, is still not detrimental to the operation of a detection scheme.

While there are many other aspects of a practical scheme for using the induction field for source location, we feel that this approach is worthy of critical examination. Furthermore, by applying some simple notions of reciprocity, we can adapt the present results to the situation when the source loop is located on the surface and the receiving loop is located at depth. Other factors receiving our attention are the influence of an inhomogeneous overburden and the effect of irregular terrain.

Acknowledgment

The author wishes to thank K. P. Spies for his assistance with the numerical calculations and Dr. D. B. Large for several stimulating discussions.

References

[1] J. R. Wait, "Electromagnetic fields of sources in lossy media," in *Antenna Theory*, pt. II, R. E. Collin and F. J. Zucker, Eds. New York: McGraw-Hill, 1969, ch. 24, pp. 468–471.

Proc. IEEE (Letters), Vol. 59, No. 6
1033-1035 (June 1971)

Criteria for Locating an Oscillating Magnetic Dipole Buried in the Earth

Abstract—The possibility is discussed of locating miners, after a disaster, by an electromagnetic technique. Specifically, it is suggested that the complex ratio of the horizontal and the vertical field components be measured. The limitation due to the finite conductivity of the overburden is also considered and shown to be a not insurmountable problem.

Following a disaster in a coal mine, there is a need to locate personnel who may be trapped or lost. The possibility that they can be found by an electromagnetic direction-finding scheme is intriguing. Unfortunately, the waves must propagate through a conductive overburden. Apart from the resulting attenuation, there is a distortion of the field vectors which can be be expected to produce errors. However, as indicated in a recent report[1] on this subject, the effect of the conductive environment can be minimized if a current-carrying loop source is used at a sufficiently low frequency. Such a method may be a useful complement to the highly promising seismic location technique being developed elsewhere.[2]

In this letter, we consider an analytical model of the direction-finding scheme and provide some quantitative criteria that may form the basis of working models. Also, hopefully, the results should provide useful information to other groups or individuals who are giving this matter their attention.

Conceptually, the simplest case is where we seek to determine the location of a small horizontal loop of area A carrying a total current I at an

Manuscript received January 22, 1971; revised February 10, 1971.

[1] *Mine Rescue and Survival Techniques*, National Academy of Engineering, Washington, D.C., 1969.

[2] D. B. Large, Westinghouse Georesearch Labs., Boulder, Colo., private communication.

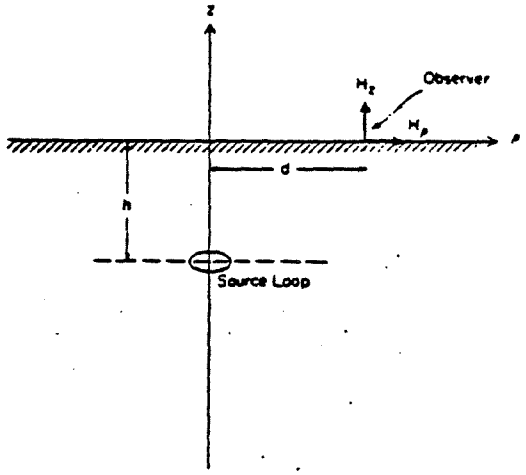


Fig. 1. Horizontal loop (i.e., vertical magnetic dipole) buried at depth h in a homogeneous half-space.

angular frequency ω. Thus we are interested in the detailed structure of the fields produced on the surface with a view to specifying meaningful measurements. To simplify the analysis, we represent the earth as a homogeneous half-space of conductivity σ and permeability μ. Here we assume $\mu = \mu_0$, where μ_0 is the permeability of free space. Also, because of the low frequencies involved, we can neglect all displacement currents in the problem. The situation is illustrated in Fig. 1 where the earth's surface is the plane $z=0$ and the loop is located at $z=-h$ on the axis of a cylindrical coordinate system (ρ, ϕ, z).

The magnetic field components H_ρ and H_z produced on the surface at $\rho=d$ can be calculated from integral expressions that have a well-known form.[3] The numerical task, however, is not trivial since the distances involved may be comparable with the effective wavelength or skin depth in the conductor. Thus the otherwise exhaustive asymptotic and near-field derivations scattered throughout the literature could not be used directly. Here we resort to a numerical evaluation of the integrals but utilize the static (i.e., $\omega \to 0$) results and other special cases as a check. Details of the analysis and computations are to be given elsewhere.

The desired field components at $\rho=d$ and $z=0$ are given explicitly as

$$H_\rho = \frac{IA}{2\pi h^3} P \tag{1}$$

$$H_z = \frac{IA}{2\pi h^3} Q \tag{2}$$

where P and Q are convenient normalized quantities. The latter are to be obtained from

$$\begin{Bmatrix} P \\ Q \end{Bmatrix} = \int_0^\infty \frac{x^3}{x + (x^2 + iH^2)^{\frac{1}{2}}} \exp\left[-(x^2 + iH^2)^{\frac{1}{2}}\right] \begin{Bmatrix} J_1(xD) \\ J_0(xD) \end{Bmatrix} dx \tag{3}$$

where J_0 and J_1 are Bessel functions, $H = (\sigma\mu\omega)^{\frac{1}{2}} h$, and $D = \rho/h$.

The ratio of the magnitudes of H_ρ and H_z at the observing station is simply $|P|/|Q|$ or $|P/Q|$. This ratio is plotted in Fig. 2 as a function of the distance parameter D. Not surprisingly, this function rises from a sharp null at $D=0$ to a maximum that is near $D=1.4$ for the small H values in accordance with the expected static behavior of the dipole (i.e., a static or dc theory predicts $Q=0$ at $D=\sqrt{2}$). This pronounced maximum is blurred as H increases and, to a first order, it shifts to smaller values of D. Nevertheless, the curves in Fig. 2 indicate that, for a single measurement of $|H_\rho/H_z|$ or $|P/Q|$, two admissible values of D can be ascertained.

The phase difference between H_ρ and H_z is a quantity of interest since it can be measured at the observer station without any phase reference

[3] J. R. Wait, "Electromagnetic sources in lossy media," in *Antenna Theory*, pt. 2, Collin and Zucker, Ed. New York: McGraw-Hill, 1969, ch. 24.

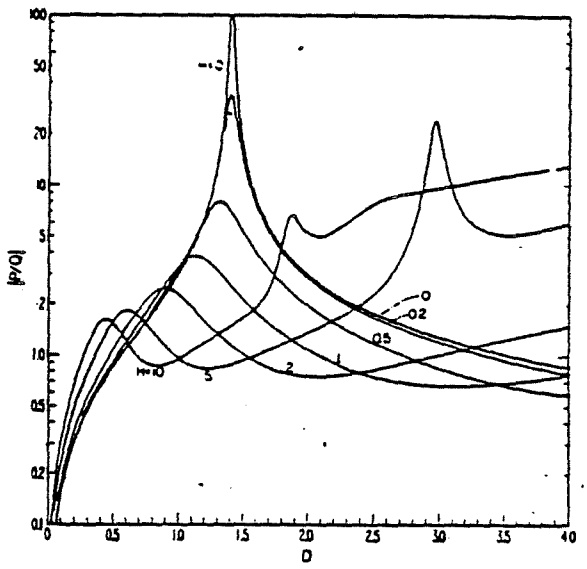


Fig. 2. The magnitude of the ratio of the horizontal and the vertical magnetic field.

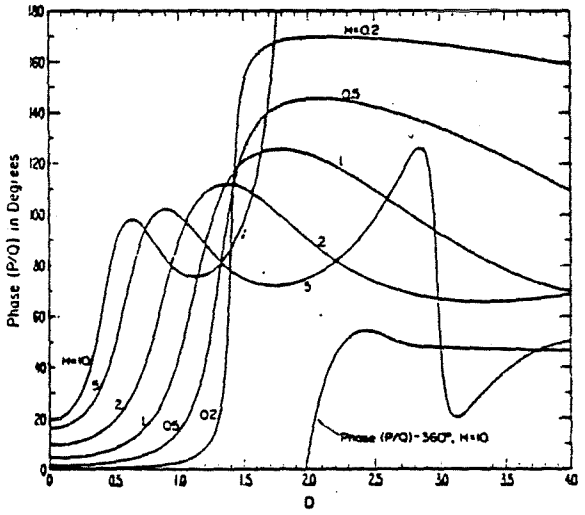


Fig. 3. The difference in phase between the horizontal and the vertical magnetic fields.

from the source. This quantity is of course equal to the argument of the ratio P/Q. It is plotted in Fig. 3 as a function of D for the same range of H. Clearly, we see that, for sufficiently small H, the phase is near either 0 or 180°, depending on whether $D<1.4$ or $D>1.4$, respectively. This fact permits us to eliminate the ambiguity from the single measurement of the amplitude ratio alluded to in the foregoing. Thus, in principle, we can deduce the appropriate value of D from the measurement of the complex P/Q. Of course, if h is known, we then can find the desired radial coordinate ρ.

In our discussion here, we have required that H be a small parameter if the conductive effects in the overburden are to be minimized. In terms of actual quantities, this can be written

$$H = 2\sqrt{2}\,\pi\sqrt{\sigma_m f}\, h_m \times 10^{-2} \simeq 0.086\sqrt{\sigma_m f}\, h_m$$

where σ_m is the earth conductivity in millimhos per meter, f is the frequency in hertz, and h_m is the burial depth h expressed in kilometers. For

example, if $\sigma_m = 1$, $f = 100$, and $h_{tm} = 0.2$, we see that $H \simeq 0.17$ which is sufficiently small that the fields should have a static-like behavior.

The results given here, while not at all exhaustive, indicate that direction-finding possibilities definitely exist for a buried magnetic dipole source, provided the field structure can be measured at a single observation station on the surface. Conversely, we can reverse the roles of the source and the observer and locate the receiving apparatus in the earth and transmit from a grounded loop on the surface. The latter may be a more practical scheme from the operational point of view, since the to-be-rescued miners would then need only to utilize a cross-loop receiver with suitable switching provisions to measure both the field ratios and the phase differences. Also, of course, the vertical loop (i.e., horizontal axis) can be oriented to give the radial direction toward the source. For feasibility tests, however, it is recommended that the loop transmitter be buried and the field quantities be measured on the surface. From an experimental point of view, this would seem to have major advantages in the scope of the measurements and the variety of situations to be examined.

Analytical studies on this subject are continuing.[4] Among some of the problems being discussed are the effect of a stratified and nonuniform overburden, other dipole and line-source configurations, and the transient solutions for pulsed dipole sources. The work bears a close similarity to earlier investigations in geophysical exploration using electromagnetic methods.[5] The configurations are sufficiently different, however, that the previous numerical data cannot be used directly.

ACKNOWLEDGMENT

The author wishes to thank K. P. Spies for his numerical analysis and general assistance in this task.

JAMES R. WAIT
Inst. Telecommun. Sci.
Boulder, Colo. 80302

[4] These studies are being carried out under Task 5 of a contract from the U.S. Bureau of Mines to the Office of Telecommunications.
[5] G. V. Keller and F. Frischknecht, *Electrical Methods in Geophysical Prospecting*, Oxford, England: Pergamon, 1967.

JOURNAL OF APPLIED PHYSICS VOLUME 42, NUMBER 10 SEPTEMBER 1971

Transient Signals from a Buried Magnetic Dipole

James R. Wait and David A. Hill
Cooperative Institute for Research in the Environmental Sciences, University of Colorado, Boulder, Colorado 80302
(Received 28 January 1971)

The solution for a pulse-excited magnetic dipole is carried through for a conducting half-space model of the earth. All displacement currents are neglected so the solution is not valid at very small times in the transient response. It is shown that the waveforms of the magnetic field components on the surface depend both on the conductivity of the earth and the geometrical parameters of the problem. The results have possible application to electromagnetic signaling and direction finding for a buried source.

I. INTRODUCTION

One method of signaling to the surface from a terminal buried in the earth is to shock excite an underground loop of wire. Because of the Ohmic conduction in the overburden, we can expect only that the low-frequency spectral components will reach the surface. Also, because of the dispersion, the radiated transient signal will undergo considerable distortion in waveform. It is of interest to examine this situation in a quantitative fashion. To facilitate the analysis, we shall adopt a homogeneous half-space model for the earth. The unground loop buried at depth h is represented by a magnetic dipole with a vertical axis. The situation is illustrated in Fig. 1.

The time-harmonic problem of a magnetic dipole in the presence of a half-space is very well known. A great deal of attention has been given to the numerical evaluation of the integrals for the range of parameters of interest in geophysical prospecting.[1] In such cases, the linear distances involved are very small compared with the wavelength in air, but not necessarily with the wavelength in the conductor. Except for certain second-order effects, this means that all displacement currents can be neglected at the outset. In spite of this simplification, the integrals in the time-harmonic problem are nonelementary and numerical integration is the order of the day.[1,2] However, we wish to point out that the pulse solution of the problem can be carried through in a relatively simple fashion. This fact was demonstrated earlier for a buried electric dipole,[3] but the method we adopt here for the magnetic dipole seems more straightforward.

II. TIME-HARMONIC FORMULATION

As indicated above, the formal integral solution of the time-harmonic problem is well known.[1] Thus, if the time factor is $e^{i\omega t}$, the magnetic field components H_ρ and H_z in the air (i.e., $z>0$) are given by

$$H_\rho = b_0(i\omega)\ P(i\omega) \tag{1}$$

and

$$H_z = b_0(i\omega)\ Q(i\omega), \tag{2}$$

where $b_0(i\omega)$ is a normalizing quantity which is proportional to the current in the small loop, while

$$P(i\omega) = h^3 \int_0^\infty F(i\omega, \lambda, h)\lambda^3 e^{-\lambda z} J_1(\lambda\rho)\ d\lambda,$$
$$Q(i\omega) = h^3 \int_0^\infty F(i\omega, \lambda, h)\lambda^3 e^{-\lambda z} J_0(\lambda\rho)\ d\lambda, \tag{3}$$

where J_0 and J_1 are Bessel functions of order zero and order one, respectively. The function of $i\omega$, λ, and h in the integrand of (3) is

$$F(i\omega, \lambda, h) = [(\lambda^2 + i\sigma\mu\omega)^{1/2} + \lambda]^{-1} \exp[-(\lambda^2 + i\sigma\mu\omega)^{1/2} h]. \tag{4}$$

For a loop of area A, turns N, and current $I(i\omega)$, we have

$$b_0(i\omega) = AN(2\pi h^3)^{-1} I(i\omega). \tag{5}$$

III. TRANSIENT FORMULATION

We now consider the fact that the loop current (assumed uniform) is $I_0\delta(t)$, where $\delta(t)$ is the unit impulse function. We then wish to calculate the time-dependent voltages $v_\rho(t)$ and $v_z(t)$ induced in a small receiving loop oriented in the ρ and z directions, respectively. If the receiving loop has area A_r and turns N_r, these voltages are obtained as follows:

$$v_\rho(t) = A_r N_r \mu \frac{\partial}{\partial t} h_\rho(t),$$

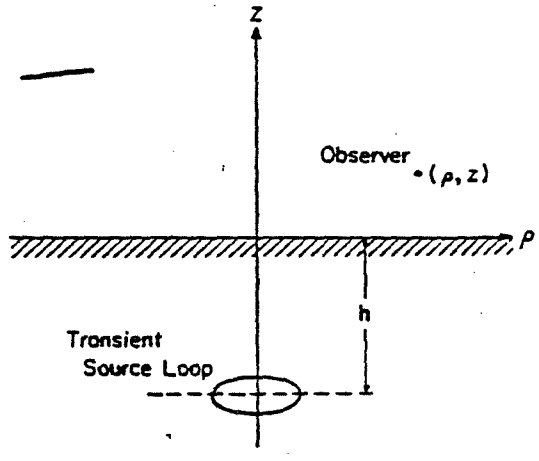


FIG. 1. Geometry for the situation.

$$v_z(t) = A_r N_r \mu \frac{\partial}{\partial t} h_z(t), \tag{6}$$

where

$$h_z(t) = \mathcal{L}^{-1} b_0(s) P(s),$$
$$h_r(t) = \mathcal{L}^{-1} b_0(s) Q(s), \tag{7}$$

and

$$b_0(s) = AN(2\pi h^3)^{-1} I_0. \tag{8}$$

Here μ is the magnetic permeability of the whole space. $\mathcal{L}^{-1}$ denotes the inverse Laplace transform operator and s is the transform variable which can be identified formally with $i\omega$ in the time-harmonic problem. Thus, consolidating the above developments, we have

$$v_z(t) = \frac{ANA_r N_r \mu I_0}{2\pi h^3} p(t),$$
$$v_r(t) = \frac{ANA_r N_r \mu I_0}{2\pi h^3} q(t), \tag{9}$$

where

$$p(t) = \mathcal{L}^{-1} s P(s), \tag{10}$$
$$q(t) = \mathcal{L}^{-1} s Q(s), \tag{11}$$

or, equivalently,

$$p(t) = h^3 \int_0^\infty [\mathcal{L}^{-1} sF(s, \lambda, h)] \lambda^3 e^{-\lambda z} J_1(\lambda\rho)\, d\lambda,$$
$$q(t) = h^3 \int_0^\infty [\mathcal{L}^{-1} sF(s, \lambda, h)] \lambda^3 e^{-\lambda z} J_0(\lambda\rho)\, d\lambda, \tag{12}$$

and

$$\mathcal{L}^{-1} sF(s, \lambda, h) = \mathcal{L}^{-1} s[(\lambda^2 + \sigma\mu s)^{1/2} + \lambda]^{-1} \times \exp[-(\lambda^2 + \sigma\mu s)^{1/2} h]. \tag{13}$$

The inverse transform can be evaluated by performing the following sequences of operations:

$$\begin{aligned}
\mathcal{L}^{-1} sF(s, \lambda, h) &= (\sigma\mu)^{-1} \mathcal{L}^{-1}[(\lambda^2 + \sigma\mu s)^{1/2} - \lambda] \\
&\quad \times \exp[-(\lambda^2 + \sigma\mu s)^{1/2} h] \\
&= -\frac{1}{\sigma\mu} \left(\lambda + \frac{\partial}{\partial h}\right) \mathcal{L}^{-1} \\
&\quad \times \exp[-(\lambda^2 + \sigma\mu s)^{1/2} h] \\
&= -\frac{1}{\sigma\mu} \left[\left(\lambda + \frac{\partial}{\partial h}\right) \frac{(\sigma\mu)^{1/2} h}{2\pi^{1/2} t^{3/2}}\right] \\
&\quad \times \exp\left(-\frac{\sigma\mu h^2}{4t} - \frac{\lambda^2 t}{\sigma\mu}\right) \\
&= \frac{1}{2(\pi\sigma\mu)^{1/2} t^{3/2}} \left(1 - \frac{\sigma\mu h^2}{2t} + \lambda h\right) \\
&\quad \times \exp\left(-\frac{\sigma\mu h^2}{4t} - \frac{\lambda^2 t}{\sigma\mu}\right).
\end{aligned} \tag{14}$$

Here, we have used a standard Laplace transform relation[4] to perform the inversion before applying the derivative operation.

Combining (12) and (14), we see that the desired time-dependent waveforms are

$$p(t) = -\frac{h^3 \exp(-\sigma\mu h^2/4t)}{2(\pi\sigma\mu)^{1/2} t^{3/2}} \int_0^\infty \lambda^3 \left(1 - \frac{\sigma\mu h^2}{2t} + \lambda h\right) e^{-\lambda z} \times \exp\left(-\frac{\lambda^2 t}{\sigma\mu}\right) J_1(\lambda\rho)\, d\lambda, \tag{15}$$

$$q(t) = -\frac{h^3 \exp(-\sigma\mu h^2/4t)}{2(\pi\sigma\mu)^{1/2} t^{3/2}} \int_0^\infty \lambda^3 \left(1 - \frac{\sigma\mu h^2}{2t} + \lambda h\right) e^{-\lambda z} \times \exp\left(-\frac{\lambda^2 t}{\sigma\mu}\right) J_0(\lambda\rho)\, d\lambda,$$

where it is understood that the right-hand side is zero if $t < 0$. For a general location (ρ, z) of the observer in the air, the integrals are of a form which can be evaluated numerically without undue difficulty. In particular, we note that for $t > 0$, the integrands are highly damped as λ approaches infinity along the real axis. Also, the convergence is improved if $z > 0$, corresponding to an observer in the air *above* the ground.

IV. REDUCTION TO WORKING FORM

For the important special case $z = 0$, the integrals in (15) can be treated analytically. The integrals to contend with are all of the form

$$A_{m,n} = \int_0^\infty \lambda^m e^{-\alpha\lambda^2} J_n(\lambda\rho)\, d\lambda, \tag{16}$$

where $\alpha = t/\sigma\mu$, $m = 3, 4$, and $n = 0, 1$. Using the ascending series definition of the Bessel function $J_n(\lambda\rho)$, we can deduce without difficulty that

$$A_{3,0} = \frac{1}{2\alpha^2} \left(1 - \frac{\rho^2}{4\alpha}\right) \exp\left(-\frac{\rho^2}{4\alpha}\right), \tag{17}$$

$$A_{4,1} = \frac{\rho}{2\alpha^3} \left(1 - \frac{\rho^2}{8\alpha}\right) \exp\left(-\frac{\rho^2}{4\alpha}\right), \tag{18}$$

$$A_{4,0} = \frac{1}{8\alpha^{5/2}} \sum_{n=0}^{\infty} \frac{\Gamma(n + \frac{5}{2})}{(n!)^2} \left(-\frac{\rho^2}{4\alpha}\right)^n, \tag{19}$$

$$A_{3,1} = \frac{\rho}{4\alpha^{5/2}} \sum_{n=0}^{\infty} \frac{\Gamma(n + \frac{5}{2})}{(n+1)(n!)^2} \left(-\frac{\rho^2}{4\alpha}\right)^n. \tag{20}$$

Actually, the latter two relations can be expressed in terms of derivatives of the modified Bessel function I_0. For example, if we start with the known form[5]

$$A_{0,0} = \tfrac{1}{2}(\pi/\alpha)^{1/2} \exp(-\rho^2/8\alpha) I_0(\rho^2/8\alpha), \tag{21}$$

we see that

$$A_{4,0} = \frac{\partial^2 A_{0,0}}{\partial \alpha^2} \tag{22}$$

and

$$A_{3,1} = \frac{\partial^2 A_{0,0}}{\partial \alpha \partial \rho}. \tag{23}$$

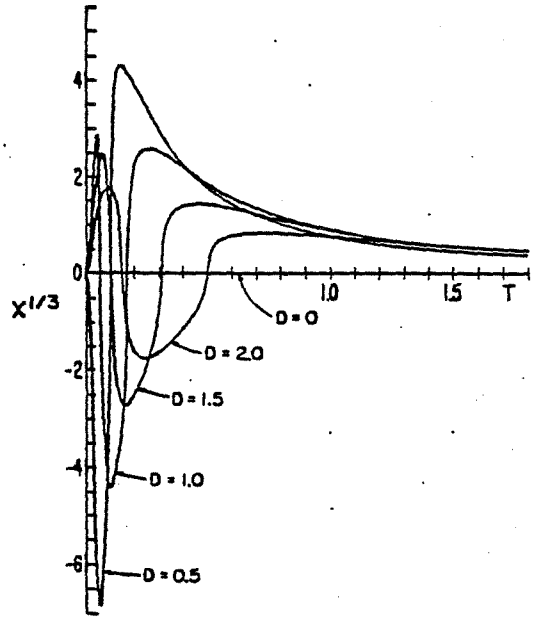


FIG. 2. Waveform of the time derivative of the horizontal magnetic field on the surface for an impulsive current in the buried source loop.

These can be further reduced to a complicated combination of exponential factors and modified Bessel functions I_0 and I_1. Thus, we have

$$A_{1,0}=\frac{\pi^{1/2}}{8\alpha^{3/2}}\exp\left(-\frac{\rho^2}{8\alpha}\right)\left[\left(3-\frac{3}{2}\frac{\rho^2}{\alpha}+\frac{\rho^4}{8\alpha^2}\right)I_0+\left(\frac{\rho^2}{\alpha^2}-\frac{5\rho^4}{16\alpha^2}\right)I_1\right] \tag{22'}$$

and

$$A_{2,1}=\frac{\pi^{1/2}\rho}{8\alpha^{3/2}}\exp\left(-\frac{\rho^2}{8\alpha}\right)\left[\left(\frac{3}{2}-\frac{\rho^2}{4\alpha}\right)I_0+\left(\frac{\rho^2}{4\alpha}-\frac{1}{2}\right)I_1\right], \tag{23'}$$

where the arguments of the modified Bessel functions are $\rho^2/8\alpha$.

Using the results (17)–(20), the waveform functions defined by (15) are given by

$$p(t)=-\left[4\pi^{1/2}(\sigma\mu h^2)^2\right]^{-1}X(D,T) \tag{24}$$

and

$$q(t)=-\left[4\pi^{1/2}(\sigma\mu h^2)^2\right]^{-1}Y(D,T), \tag{25}$$

where

$$X(D,T)=\exp\left(-\frac{1}{4T}\right)\frac{1}{T^{1/2}}\left[\left(1-\frac{1}{2T}\right)\frac{D}{T^{1/2}}\times\sum_{n=0}^{\infty}\frac{\Gamma(n+\frac{3}{2})}{(n+1)(n!)^2}\left(-\frac{D^2}{4T}\right)^n+\frac{D}{T}\left(1-\frac{D^2}{8T}\right)\exp\left(-\frac{D^2}{4T}\right)\right] \tag{26}$$

and

$$Y(D,T)=\exp\left(-\frac{1}{4T}\right)\frac{1}{T^{1/2}}\left[\left(1-\frac{1}{2T}\right)\left(1-\frac{D^2}{2T}\right)\exp\left(-\frac{D^2}{4T}\right)+\frac{1}{T^{1/2}}\sum_{n=0}^{\infty}\frac{\Gamma(n+\frac{5}{2})}{(n!)^2}\left(-\frac{D^2}{4T}\right)^n\right], \tag{27}$$

where $T=\alpha/h^2=t/\sigma\mu h^2$ and $D=\rho/h$. Here, we note that X and Y are dimensionless functions of the time parameter T and the distance parameter D. As a consequence, $p(t)$ and $q(t)$ have dimensions of $\sec^{-2}$ which is consistent with our formulation.

The series expansions indicated in (26) and (27) are rapidly convergent provided T is not zero and D is not too large compared with unity. In fact, if $D=0$ (corresponding to locating the observer right over the source loop), we see that $X(0,T)=0$ and

$$Y(0,t)=\exp\left(-\frac{1}{4T}\right)\frac{1}{T^{1/2}}\left[\left(1-\frac{1}{2T}\right)+\frac{3\pi^{1/2}}{4}\frac{1}{T^{1/2}}\right]. \tag{28}$$

Equivalent forms of (26) and (27) involving modified Bessel functions are found, from (22b) and (23b), to be

$$X(D,T)=\frac{1}{T^{1/2}}\exp\left(-\frac{1}{4T}\right)\left(\frac{D}{T}\left(1-\frac{D^2}{8T}\right)\exp\left(-\frac{D^2}{4T}\right)+\left(1-\frac{1}{2T}\right)\left\{\frac{D}{4}\left(\frac{\pi}{T}\right)^{1/2}\exp\left(-\frac{D^2}{8T}\right)\times\left[\left(\frac{3}{2}-\frac{D^2}{4T}\right)I_0+\left(\frac{D^2}{4T}-\frac{1}{2}\right)I_1\right]\right\}\right) \tag{29}$$

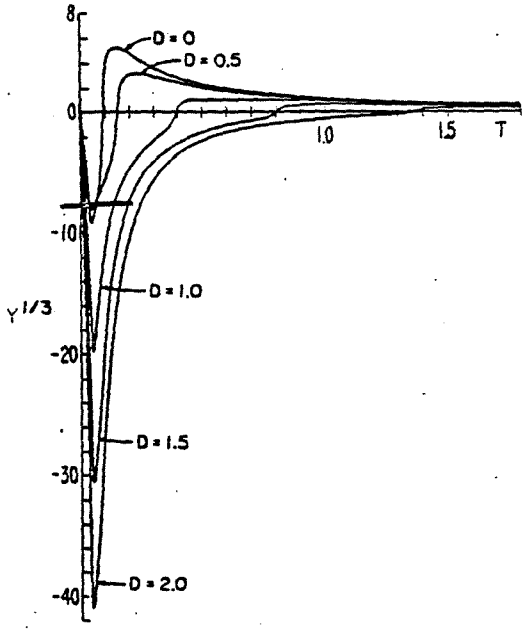


FIG. 3. Waveform of the time derivative of the vertical magnetic field on the surface.

and

$$Y(D,T)=\frac{1}{T^{7/2}}\exp\left(-\frac{1}{4T}\right)\left\{\left(1-\frac{1}{2T}\right)\left(1-\frac{D^2}{4T}\right)\right.$$
$$\times\exp\left(-\frac{D^2}{4T}\right)+\frac{1}{4}\left(\frac{\pi}{T}\right)^{1/2}\exp\left(-\frac{D^2}{8T}\right)\left[\left(3-\frac{3D^2}{2T}+\frac{D^4}{8T^2}\right)I_0\right.$$
$$\left.\left.+\left(\frac{D^2}{T}-\frac{5D^4}{16T^2}\right)I_1\right]\right\}, \qquad (30)$$

where the arguments of I_0 and I_1 are $D^2/8T$. The functions X and Y are plotted in Figs. 2 and 3 vs the time parameter. To facilitate the presentation, the cube roots of X and Y are shown as a function of T on a linear scale. Various values of the parameter $D(=\rho/h)$ are chosen, including the value $D=0$, which corresponds to the observer directly underneath the source loop.

We may observe that the waveforms shown in Figs. 2 and 3 have a characteristic shape which is significantly dependent upon D. Thus, it is not inconceivable that the shape can be used as a criterion to locate the source from an observer on the surface. We note that the normalized time axis T may be read directly in msec, if $4\pi\sigma h^2=10^4$; if, for example, $\sigma=10^{-2}$ mhos/m, we find that $h=283$ m.

We stress that in our formulation, all displacement currents have been neglected. This means that our results are only valid when t is somewhat greater than ϵ/σ sec.[3] If, for example, $\sigma=10^{-2}$ and $\epsilon/\epsilon_0=10$ for the half-space, we have $\epsilon/\sigma=8.85\times10^{-9}$ sec.

Further work on this subject should allow for the inhomogeneity and possible layering of the conducting half-space. Also, without additional difficulty, we can allow for the finite duration of the current pulse in the source loop and the transient response of the loop receiving antennas.

---

[1] J. R. Wait, J. Geophys. 20, 630 (1955).
[2] J. H. Coggon and H. F. Morrison, J. Geophys. 35, 476 (1970).
[3] J. R. Wait, Appl. Sci. Res. (Sec. B) 8, 213 (1960).
[4] Here, we use the classical result

$$\mathcal{L}^{-1}\exp(-s^{1/2})=\tfrac{1}{2}(\pi t^3)^{-1/2}\exp(-1/4t)$$

along with a simple change of variable.
[5] A. D. Wheelon, *Tables of Summable Series and Integrals Involving Bessel Functions* (Holden-Day, Los Angeles, 1968), p. 81, No. 1.704.

TRANSIENT MAGNETIC FIELDS PRODUCED BY A STEP-FUNCTION-EXCITED LOOP BURIED IN THE EARTH

Indexing terms: Magnetic fields, Transients

Using a previously developed formalism, we obtain explicit results for the field waveforms observed on the Earth's surface for a small horizontal loop buried in a conducting halfspace. It is shown that the shape of the waveform is diagnostic of the relative location of the buried source. The results have possible application in mine rescue operations.

In a previous paper,[1] we derived expressions for the transient electromagnetic fields of a small wire loop buried in the Earth and excited by an impulsive current. Here we use this formalism to calculate the fields on the surface of the Earth when the current in the loop varies with time as a step function.

The model used before is described briefly here. As indicated in Fig. 1, we adopt a homogeneous halfspace model for the Earth with conductivity σ. The loop buried at depth h is represented by a magnetic dipole with a vertical axis. In terms of a cylindrical co-ordinate system (ρ, ϕ, z), the Earth's surface is $z = 0$ and the homogeneous Earth of conductivity σ occupies the region $z < 0$. The loop is located at $z = -h$ on the z axis. The quantities of interest are the voltages $v_\rho(t)$ and $v_z(t)$ induced in small receiving loops oriented in the radial and vertical directions, respectively. In the previous paper, we derived closed-form expressions for these voltage waveforms when the current was $I_0\delta(t)$ Amperes, where $\delta(t)$ is the unit impulse and I_0 is a constant. Numerical results for the impulse-response waveforms $p(t)$ and $q(t)$ were given for the special case where the observer was located at the Earth's surface $z = 0$. The results have also been generalised for a source loop of finite size.[2] In this case, the inverse transforms required numerical integration. In what follows here, we will restrict attention to the magnetic-dipole

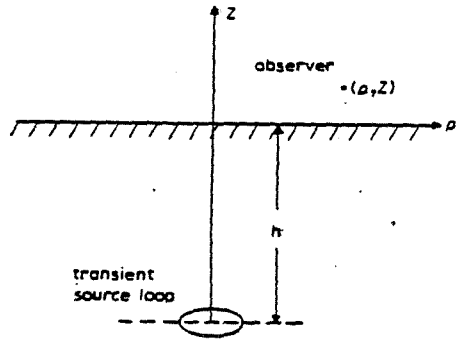


Fig. 1 *Geometry of the situation*

approximation, so that the dimensions h and ρ should be at least five times the radius a of the source loop. As before, we neglect all displacement currents.

We now consider that the current in the source loop is $I(t)\,u(t)$ amperes, where $u(t) = 1$ for $t > 0$ and 0 for $t < 0$. Then, by an application of the convolution theorem, the corresponding voltage responses are

$$\left.\begin{matrix} v_\rho(t) \\ v_z(t) \end{matrix}\right\} = \frac{ANA_r N_r \mu_0}{2\pi h^3} \int_0^t \left\{\begin{matrix} p(\tau) \\ q(\tau) \end{matrix}\right. I(t-\tau)\,d\tau \quad . \quad . \quad (1)$$

where $\mu_0 = 4\pi \times 10^{-7}$ H/m, $A = \pi a^2$ = area of source loop (i.e. magnetic dipole) of radius a, N = number of turns in source loop, A_r = area of receiving loop (of infinitesimal size) and N_r = number of turns of receiving loops. Explicit expressions were given before[1] for the functions $p(\tau)$ and $q(\tau)$. For what follows, it is convenient to rewrite eqn. 1 as follows:

$$\left.\begin{matrix} v_\rho(t) \\ v_z(t) \end{matrix}\right\} = \underbrace{\frac{ANA_r N_r \mu_0}{2\pi h^3}}_{\text{henrys}} \times \underbrace{\left\{\begin{matrix} -1 \\ 4\pi^3(\sigma\mu_0)^2 h^4 \end{matrix}\right\}}_{(\text{seconds})^{-2}} \int_0^t \underbrace{\left\{\begin{matrix} X(D,\hat{T}) \\ Y(D,\hat{T}) \end{matrix}\right. I(t-\tau)\,d\tau}_{\text{ampere-seconds}} \quad (2)$$

volts

where we have indicated the physical dimensions of the various factors. Here, X and Y are dimensionless functions defined by[1]

$$\left.\begin{matrix} X(D,\hat{T}) \\ Y(D,\hat{T}) \end{matrix}\right\} = \frac{2}{\hat{T}^4} \exp\left(-\frac{1}{4\hat{T}}\right) \int_0^\infty \left(1 + x - \frac{1}{2\hat{T}}\right) x^3 \times \exp(-x^2\hat{T}) \left\{\begin{matrix} J_1(xD) \\ J_0(xD) \end{matrix}\right. dx \quad (3)$$

where $\hat{T} = \tau(\sigma\mu_0 h^2)^{-1}$ and $D = \rho/h$. As mentioned above, the functions X and Y were evaluated by both analytical and numerical integration for this situation. Thus for a specified form for $I(t)$, we need to perform a further integration as indicated by eqn. 2.

When the source current is a step function, $I(t) = I_0 u(t)$, we see that

$$\left.\begin{matrix} v_\rho(t) \\ v_z(t) \end{matrix}\right\} = \frac{ANA_r N_r \mu_0}{2\pi h^3} \left(\frac{-1}{4\pi^2 \sigma\mu_0 h^2}\right) I_0 \left\{\begin{matrix} X_s(D,T) \\ Y_s(D,T) \end{matrix}\right. \quad . \quad . \quad (4)$$

where

. . . . 1972 Vol. 8 No. 11

$$\left.\begin{matrix} X_s(D,T) \\ Y_s(D,T) \end{matrix}\right\} = \int_0^T \left\{\begin{matrix} X(D,\hat{T}) \\ Y(D,\hat{T}) \end{matrix}\right. d\hat{T} \quad . \quad . \quad . \quad . \quad . \quad (5)$$

where $T = t/(\sigma\mu_0 h^2)$.

Using numerical integration, the dimensionless functions X_s and Y_s are plotted in Figs. 2A and 2B as functions of T for

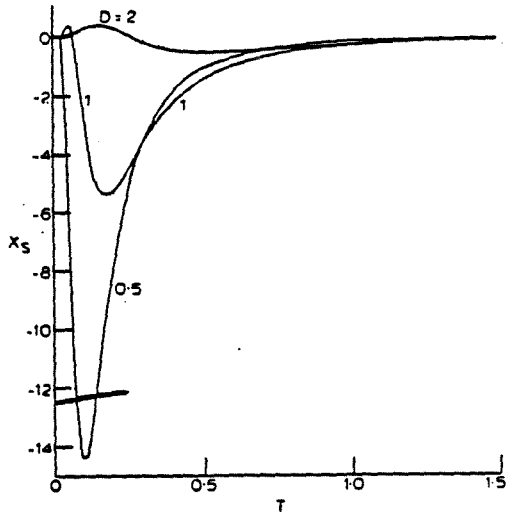


Fig. 2A *Waveform of the voltage in the receiving loop with radially oriented axis*

several values of D. As indicated, these step-function responses approach zero for large values of the time parameter T. This can easily be demonstrated analytically, and thus it is a check on the accuracy of the numerical integration.

We stress that, in our formulation, all displacement currents have been neglected. This means that our results are only valid when t is somewhat greater than ε/σ seconds. If, for example, $\sigma = 10^{-2}$ and $\varepsilon/\varepsilon_0 = 10$ for the half-space, we have $\varepsilon/\sigma = 8{\cdot}85 \times 10^{-9}$ s.

It is believed that these waveform functions X_s and Y_s can be useful to interpret signals received on the surface for a pulse-excited buried loop. The latter could be any unearthed wire lying more or less in a horizontal plane. The power source could be a battery connected to the loop by a simple on/off toggle switch.

It is evident that the waveform shape depends on D. Thus

Reprinted from ELECTRONICS LETTERS Vol. 8 No. 11

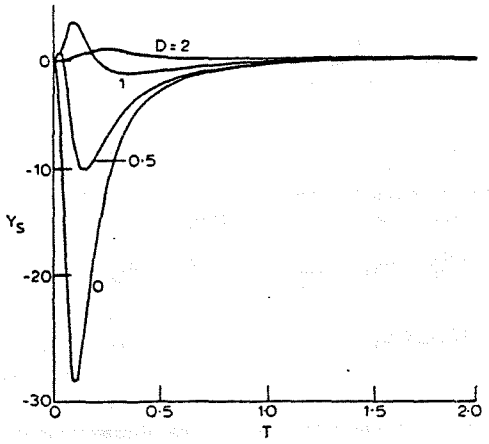


Fig. 2a *Waveform of the voltage in the receiving loop with vertically oriented axis*

it is possible that the waveform can be used as a readily detected criterion of source location for a single observation point on the surface. We note that the time parameter T can be read directly in milliseconds if $4\pi\sigma h^2 = 10^4$; if, for example, $\sigma = 10^{-2}$ S/m, we see that $h = 283$ m. The feasibility of such a scheme in mine rescue operations needs to be examined.

JAMES R. WAIT

5th May 1972

Environmental Research Laboratories
National Oceanic & Atmospheric Administration
US Department of Commerce
Boulder, Colo. 80302, USA

DAVID A. HILL

Institute for Telecommunication Sciences
Office of Telecommunications
US Department of Commerce
Boulder, Colo. 80302, USA

References

1 WAIT, J. R., and HILL, D. A.: 'Transient signals from a buried magnetic dipole', *J. Appl. Phys.*, 1971, 42, pp. 3866–3869
2 WAIT, J. R., and HILL, D. A.: 'Transient electromagnetic fields of a finite circular loop in the presence of a conducting half-space', *ibid.*, 1972, 43 (to be published)

Electromagnetic surface fields produced by a pulse-excited loop buried in the earth

James R. Wait
Environmental Research Laboratories, National Oceanic and Atmospheric Administration

David A. Hill
Institute for Telecommunication Sciences, Office of Telecommunications, U. S. Department of Commerce, Boulder, Colorado 80302

(Received 30 May 1972)

A transient excited magnetic dipole immersed in a conducting half-space is considered. Explicit results for the field waveforms observed on the surface are obtained for the case where the exciting current is an exponential time function. It is shown that the shape of the waveform is diagnostic of the relative location of the buried source. The results have possible application in mine rescue operations.

I. INTRODUCTION

We derived expressions earlier for the transient electromagnetic fields of a small wire loop buried in the earth and excited by an impulsive current.[1] Here, we extend this formalism to calculate the fields on the surface of the earth when the current in the loop varies with time as an exponential function of time. This is relevant to the situation where the source is a condenser discharge.

The model used before is described briefly here. As indicated in Fig. 1, we adopt a homogeneous half-space model for the earth with conductivity σ. The loop buried at depth h is represented by a magnetic dipole with a vertical axis. In terms of a cylindrical coordinate system (ρ, ϕ, z), the earth's surface is $z=0$ and the homogeneous earth of conductivity σ occupies the region $z<0$. The loop is located at $z=-h$ on the z axis. The quantities of interest are the voltages $v_\rho(t)$ and $v_z(t)$ induced in small receiving loops oriented in the radial and vertical directions, respectively. In the previous paper, we derived closed-form expressions for these voltage waveforms when the current was $I_0\delta(t)$ (A), where $\delta(t)$ is the unit impulse and I_0 is a constant. Numerical results for the impulse response waveforms $p(t)$ and $q(t)$ were given for the special case where the observer was located at the earth's surface $z=0$. The results have also been generalized for a source loop of finite size.[2] In this case, the inverse transforms required numerical integration. In what follows here, we will restrict attention to the magnetic dipole approximation so that the dimensions h and ρ should be at least five times the radius a of the source loop. As before, we neglect all displacement currents.

II. APPLICATION OF CONVOLUTION THEOREM

We now consider that the current in the source loop is $I(t)u(t)$(A), where $u(t)=1$ for $t>0$, $u(t)=0$ for $t<0$. Then, by an application of the convolution theorem, the corresponding voltage responses are

$$v_\rho(t)=\frac{ANA_rN_r\mu_0}{2\pi h^3}\int_0^t p(\tau)I(t-\tau)\,d\tau,$$
$$v_z(t)=\frac{ANA_rN_r\mu_0}{2\pi h^3}\int_0^t q(\tau)I(t-\tau)\,d\tau, \tag{1}$$

where $\mu_0=4\pi\times10^{-7}$ H/m, $A=\pi a^2$ is the area of source loop (i.e., magnetic dipole) of radius a, N is the number of turns in source loop, A_r is the area of receiving loop (of infinitesimal size), and N_r is the number of turns in receiving loop. Explicit expressions were given before[1] for the functions $p(\tau)$ and $q(\tau)$. For what follows, it is convenient to rewrite (1) as follows:

$$v_\rho(t)=\frac{ANA_rN_r\mu_0}{2\pi h^3}\left(\frac{-1}{4\pi^{1/2}(\sigma\mu_0)^2h^4}\right)\int_0^t X(D,\hat{T})I(t-\tau)\,d\tau, \quad \text{(HA/sec)}$$
$$v_z(t)=\frac{ANA_rN_r\mu_0}{2\pi h^3}\left(\frac{-1}{4\pi^{1/2}(\sigma\mu_0)^2h^4}\right)\int_0^t Y(D,\hat{T})I(t-\tau)\,d\tau, \quad \text{(HA/sec)} \tag{2}$$

where we have indicated the physical dimensions of the various factors. Here X and Y are dimensionless functions defined by,[1]

$$X(D,\hat{T})=\frac{2}{\hat{T}^{3/2}}\exp\left(-\frac{1}{4\hat{T}}\right)\times\int_0^t\left(1+x-\frac{1}{2\hat{T}}\right)x^3\exp(-x^2\hat{T})J_1(xD)\,dx,$$
$$Y(D,\hat{T})=\frac{2}{\hat{T}^{3/2}}\exp\left(-\frac{1}{4\hat{T}}\right)\times\int_0^t\left(1+x-\frac{1}{2\hat{T}}\right)x^3\exp(-x^2\hat{T})J_0(xD)\,dx, \tag{3}$$

where $\hat{T}=\tau(\sigma\mu_0h^2)^{-1}$ and $D=\rho/h$. As mentioned above, the functions X and Y were evaluated by both analytical and numerical integration for this situation. Thus, for a specified form for $I(t)$, we need to perform a further integration as indicated by (2).

In the case where the source current is a step function, $I(t)=I_0u(t)$, we see that

$$v_\rho(t)=\frac{ANA_rN_r\mu_0}{2\pi h^3}\left(\frac{-1}{4\pi^{1/2}\sigma\mu_0h^2}\right)I_0X_0(D,T),$$

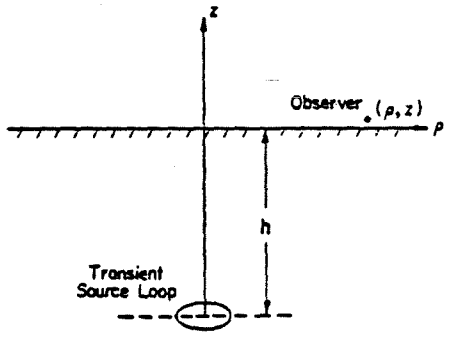


FIG. 1. Geometry of the situation.

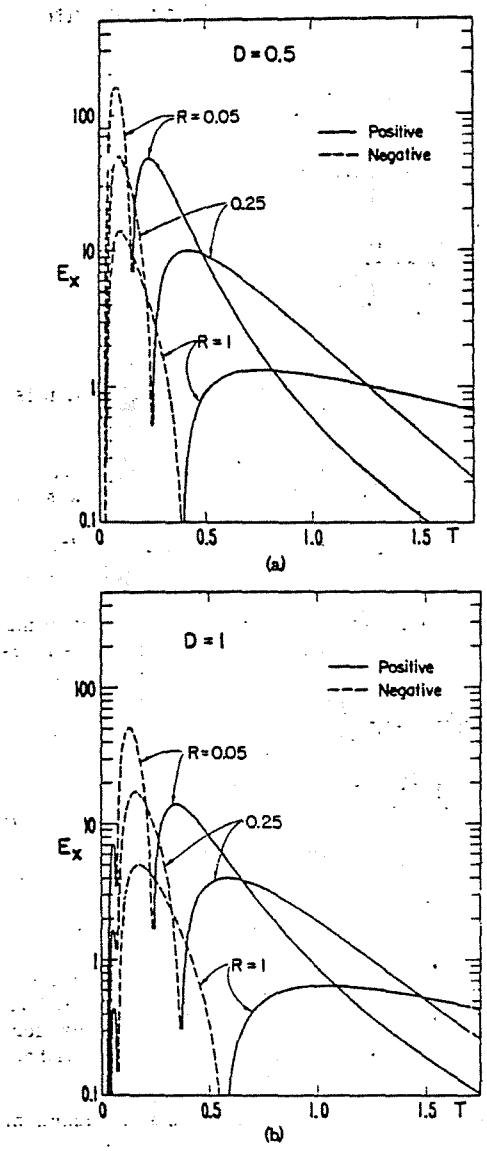


FIG. 2. Waveform of the voltage in the receiving loop with radially oriented axis.

$$v_s(t)=\frac{ANA_rN_r\mu_0}{2\pi h^3}\left(\frac{-1}{4\pi^{1/2}\sigma\mu_0h^2}\right)I_sY_s(D,T), \tag{4}$$

where

$$X_s(D,T)=\int_0^t X(D,\hat{T})\,d\hat{T},$$
$$Y_s(D,T)=\int_0^t Y(D,\hat{T})\,d\hat{T}, \tag{5}$$

where $T=t/(\sigma\mu_0h^2)$.

We specify that the total charge, discharged into the loop, is Q_0 (C). Thus, on the assumption that the loop inductance is negligible, the loop current is

$$I(t)=(Q_0/t_c)\exp(-t/t_c)u(t), \tag{6}$$

where t_c is the time constant of the circuit. This is equivalent to

$$I(t)=[Q_0/(\sigma\mu_0h^2R)]\exp(-T/R), \tag{7}$$

where $R=t_c/(\sigma\mu_0h^2)$ and $T=t/(\sigma\mu_0h^2)$. Therefore, we see that the loop voltage responses are

$$v_\rho(t)=Q_0\frac{ANAN_r\mu_0}{2\pi h^3}\left(\frac{-1}{4\pi^{1/2}(\sigma\mu_0)^2h^4}\right)E_X(D,R,T),$$
$$v_z(t)=Q_0\frac{ANAN_r\mu_0}{2\pi h^3}\left(\frac{-1}{4\pi^{1/2}(\sigma\mu_0)^2h^4}\right)E_Y(D,R,T), \tag{8}$$

where

$$E_X=\frac{1}{R}\exp\left(-\frac{T}{R}\right)\int_0^T\exp\left(\frac{T'}{R}\right)X(D,T')\,dT',$$
$$E_Y=\frac{1}{R}\exp\left(-\frac{T}{R}\right)\int_0^T\exp\left(\frac{T'}{R}\right)Y(D,T')\,dT'. \tag{9}$$

The functions E_X and E_Y are the normalized voltage responses functions for an exponential source current. As indicated, they are functions of the dimensionless parameters D, R, and T. A special case is the impulse response:

$$\lim_{R\to0}E_X=X(D,T),$$
$$\lim_{R\to0}E_Y=Y(D,T). \tag{10}$$

Another special case is the step-function response:

$$\lim_{R\to\infty}RE_X=X_s(D,T),$$
$$\lim_{R\to\infty}RE_Y=Y_s(D,T). \tag{11}$$

The function E_X is plotted in Figs. 2(a) and 2(b) for $D=0.5$ and 1, respectively. [Note that $E_X=0$ for $D=0$.] The function for E_Y is plotted in Figs. 3(a)–3(c) for $D=0$, 0.5, and 1, respectively. In each case, the value of the normalized time constant R is indicated on the curves.

III. MAGNETIC FIELD RESPONSES

It is also of interest to examine the waveforms of the actual magnetic field components $H_\rho(t)$ and $H_z(t)$ at the observer for the step-function source current. Obviously, these are given by

$$H_\rho(t)=\frac{1}{\mu_0A_rN_r}\int_0^t v_\rho(t)\,dt,$$
$$H_z(t)=\frac{1}{\mu_0A_rN_r}\int_0^t v_z(t)\,dt, \tag{12}$$

where $v_\rho(t)$ and $v_z(t)$ are given by (4). Using (5) and changing the integration variable, these are equivalent to

$$H_\rho(t)=\frac{ANI_s}{2\pi h^3}X_R(D,T),$$
$$H_z(t)=\frac{ANI_s}{2\pi h^3}Y_R(D,T), \tag{13}$$

where

$$X_R(D,T)=-\frac{1}{4\pi^{1/2}}\int_0^T\left(\int_0^{\hat{T}}X(D,T')\,dT'\right)d\hat{T},$$
$$Y_R(D,T)=-\frac{1}{4\pi^{1/2}}\int_0^T\left(\int_0^{\hat{T}}Y(D,T')\,dT'\right)d\hat{T}, \tag{14}$$

and $T=t/(\sigma\mu_0h^2)$.

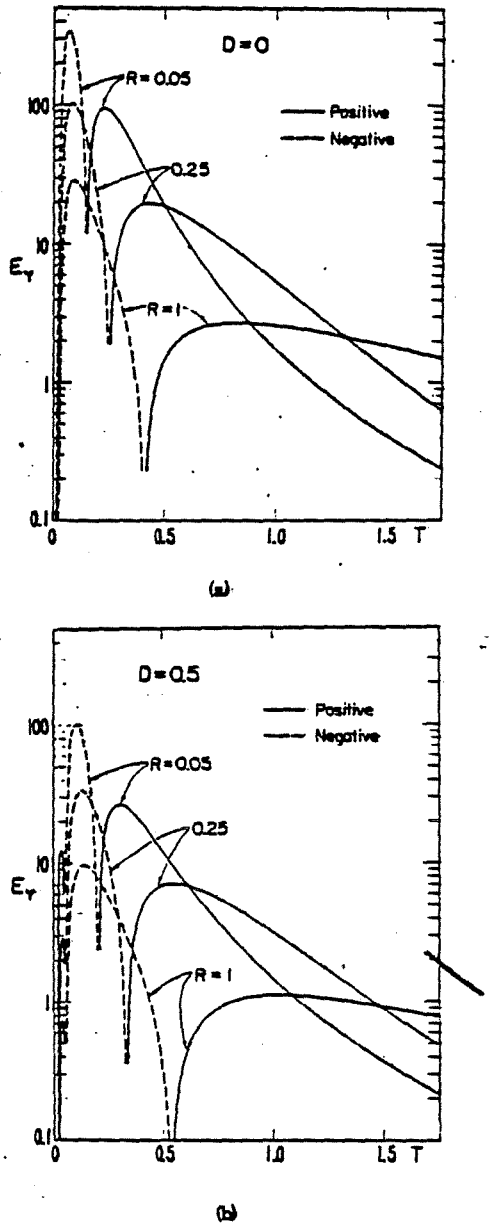


FIG. 3. Waveform of the voltage in the receiving loop with vertically oriented axis.

The dimensionless functions X_R and Y_R are plotted in Figs. 3(a) and 3(b). These are seen to approach the static values for large T. In accordance with potential theory, the latter are given by

$$X_R(D,\infty)=\frac{3D}{2(1+D^2)^{5/2}} \tag{15}$$

and

$$Y_R(D,\infty)=\frac{1-(\frac{1}{2}D^2)}{(1+D^2)^{5/2}}. \tag{16}$$

As mentioned above, X_R and Y_R as a function of T are the waveforms of the magnetic field components for a step-function current source. It is also apparent that X_R and Y_R are also the waveforms for the voltage responses in the receiving loops for a ramp-function current in the source loop.

IV. FINAL REMARKS

We stress that, in our formulation, all displacement currents have been neglected. This means that our results are only valid when t is somewhat greater than ϵ/σ sec. If, for example, $\sigma=10^{-2}$ and $\epsilon/\epsilon_0=10$ for the half-space, we have $\epsilon/\sigma=8.85\times10^{-9}$ sec.

It is believed that these waveform functions E_X, E_Y, X_R, and Y_R can be useful to interpret signals received on the surface for a pulse-excited buried loop. The latter could be any ungrounded wire lying more or less in a horizontal plane. The power source could be a condenser

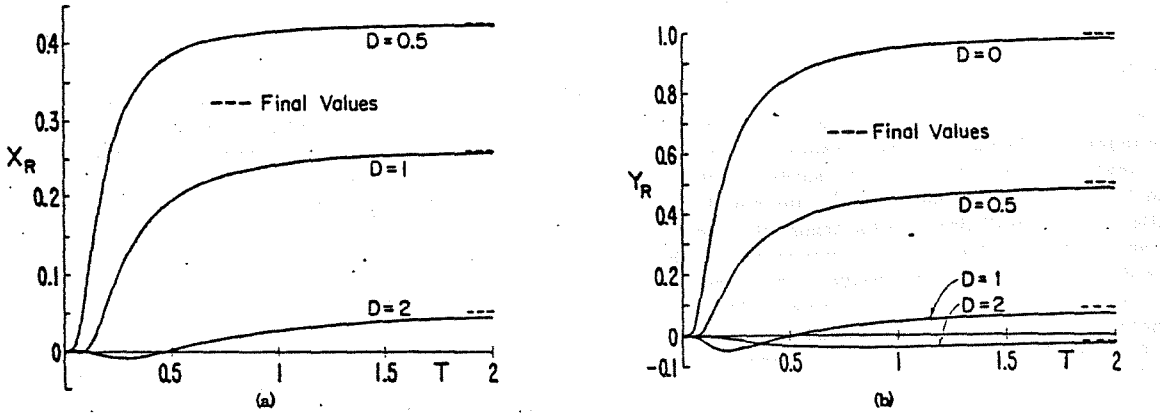


FIG. 4. (a) Waveform of the radial component of the magnetic field component. (b) Waveform of the vertical component of the magnetic field component.

charged up by a portable battery with provision for discharge through the loop.

It is evident that the waveform shape depends on D. Thus, it is possible that the waveform can be used as a readily detected criterion of source location for a single observation point on the surface. We note that the time parameter T can be read directly in msec if $4\pi\sigma h^2 = 10^4$; if, for example, $\sigma = 10^{-2}$ mho/m, we see that $h = 283$ m, or roughly 900 ft. The feasibility of such a scheme in mine rescue operations needs to be examined.

ACKNOWLEDGMENT

The authors are grateful for the useful suggestions from Dr. Hans Balke of the Westinghouse Corporation.

[1] J. R. Wait and D. A. Hill, J. Appl. Phys. 42, 3866 (1971).
[2] J. R. Wait and D. A. Hill, J. Appl. Phys. (to be published).

Transient electromagnetic fields of a finite circular loop in the presence of a conducting half-space

James R. Wait and David A. Hill
Cooperative Institute for Research in Environmental Sciences, University of Colorado, Boulder, Colorado 80302
(Received 27 December 1971)

A previous solution for a pulse-excited dipole is extended to allow for the finite size of the buried source loop. Numerical results for the above surface fields are presented. We also consider the situation when the finite source loop is located on the surface and the observer is buried. It is suggested that the waveform of the received pulse signals can be used for direction-finding and source location.

I. INTRODUCTION

In a previous paper[1] we presented a theoretical analysis for the transient magnetic fields produced by a pulse-excited magnetic dipole buried in the earth. All displacement currents were neglected, so the solution was not valid at very small times in the transient response. It was shown that the magnetic field waveforms on the surface depended on the conducitivity of the earth and the geometrical parameters of the problem. The results have possible application to mine-rescue operations. We consider here a number of new aspects of this problem.

II. FORMULATION

An important extension of the theory pertains to the use of a source loop of finite size.[2] The situation is indicated in Fig. 1(a) where we have located a horizontal single-turn loop of radius a at depth h. For an impulsive uniform current $I_0\delta(t)$, we then wish to calculate the waveform of the field at an observer point P, at a radial coordinate ρ on the surface. The theory given before is almost directly applicable to this situation. In particular, we again consider the time-dependent voltages $v_\rho(t)$ and $v_z(t)$ induced in small receiving loops, of area A_r and N_r turns, oriented in the ρ (radial) and the z (vertical) loops, respectively. Then it follows that

$$v_\rho(t)=[AA_rN_r\mu I_0/(2\pi h^3)]p(t), \tag{1}$$

$$v_z(t)=[AA_rN_r\mu I_0/(2\pi h^3)]q(t), \tag{2}$$

where $A=\pi a^2$,

$$p(t)=h^3\int_0^\infty [\mathcal{L}^{-1}sF(s,\lambda,h)]\lambda^3 e^{-\lambda\rho}J_1(\lambda\rho)f(\lambda)\,d\lambda, \tag{3}$$

$$q(t)=h^3\int_0^\infty [\mathcal{L}^{-1}sF(s,\lambda,h)]\lambda^3 e^{-\lambda\rho}J_0(\lambda\rho)f(\lambda)\,d\lambda, \tag{4}$$

with

$$f(\lambda a)=2J_1(\lambda a)/(\lambda a) \tag{5}$$

and

$$\mathcal{L}^{-1}sF(s,\lambda,h)=\mathcal{L}^{-1}s[(\lambda^2+\sigma\mu s)^{1/2}+\lambda]^{-1}\times\exp[-(\lambda^2+\sigma\mu s)^{1/2}h]. \tag{6}$$

The inverse Laplace transform indicated above was treated explicitly before.[1] But now the added complication[2] is the function $f(\lambda a)$ that can only be replaced by 1 if a becomes vanishingly small (i.e., the magnetic dipole limit).

Following the normalization used before, we write

$$p(t)=-[4\pi^{1/2}(\sigma\mu)^2h^4]^{-1}X(D,\ T,\ Z,\ A), \tag{7}$$

$$q(t)=-[4\pi^{1/2}(\sigma\mu)^2h^4]^{-1}Y(D,\ T,\ Z,\ A), \tag{8}$$

where X and Y are functions of the dimensionless parameters $D=\rho/h$, $T=t/(\sigma\mu h^2)$, $Z=z/h$, and $A=a/h$. From (7) and (8) in the earlier paper[1] it follows that

$$\frac{X}{Y}=\frac{2}{T^{3/2}}\exp\left(-\frac{1}{4T}\right)\int_0^\infty\left(1+x-\frac{1}{2T}\right)x^2\times\exp(-x^2T)\begin{Bmatrix}J_1(xD)\\J_0(xD)\end{Bmatrix}f(xA)\exp(-xZ)\,dx, \tag{9}$$

where $f(xA)=2J_1(xA)/(xA)$.

III. SOME RESULTS FOR BURIED SOURCE LOOPS

The case of immediate practical interest is when the observer is located at the earth's surface (i.e., $Z=0$). The waveform functions X and Y have been calculated using numerical integration for this case and for a range of values of T, D, and A. These results for X are shown in Figs. 2(a) and 2(b) where the abscissa is the time parameter T. The curves in Fig. 2(a) are for $A=0$, and the results are in agreement with those given before[1] for the magnetic dipole case. The influence of having a nonzero value of A is seen in Fig. 2(b). While the curves have a qualitative similarity, there is a sig-

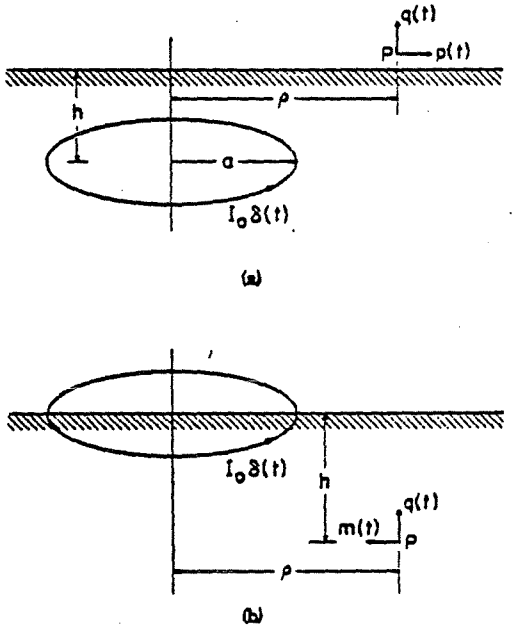


FIG. 1. (a) Buried circular loop excited by an impulsive current. (b) Circular source loop on surface.

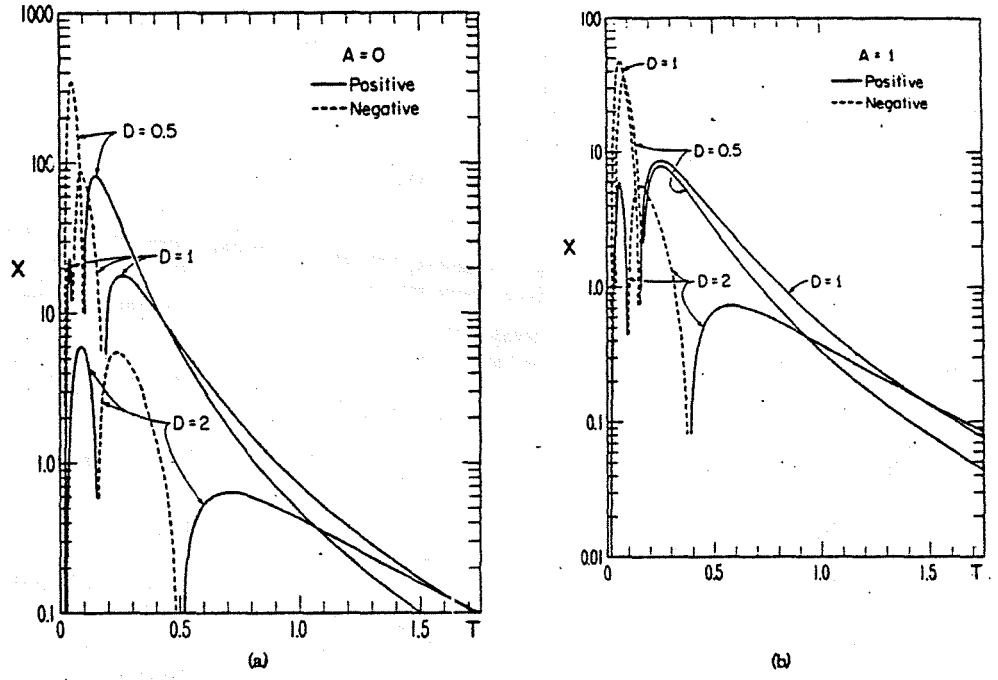


FIG. 2. Normalized impulse response of voltage in small vertical loop on surface (with axis oriented in radial direction) for buried source loop.

nificant difference between the two cases. The agreement between the results based on the analytical formula for X (for $A=0$) and the numerical integration results (for $A=0$) gives confidence to the curves.

The corresponding waveform functions Y for $Z=0$ are shown in Figs. 3(a)–3(c) for the same range of the parameters. The case for $A=0$ here disagreed with the numerical results given before,[1] but this was traced to an algebraic error in the derivation of the working formula. To correct the earlier development,[1] we note that the factor multiplying I_1 in (22′) should be

$$\rho^2/\alpha - \rho^4/8\alpha^2$$

and the factor multiplying I_1 in (30) should be

$$D^2/T - D^4/8T^2.$$

The earlier numerical results[1] for Y, when corrected for $D>0$, agreed to within five digit accuracy with the

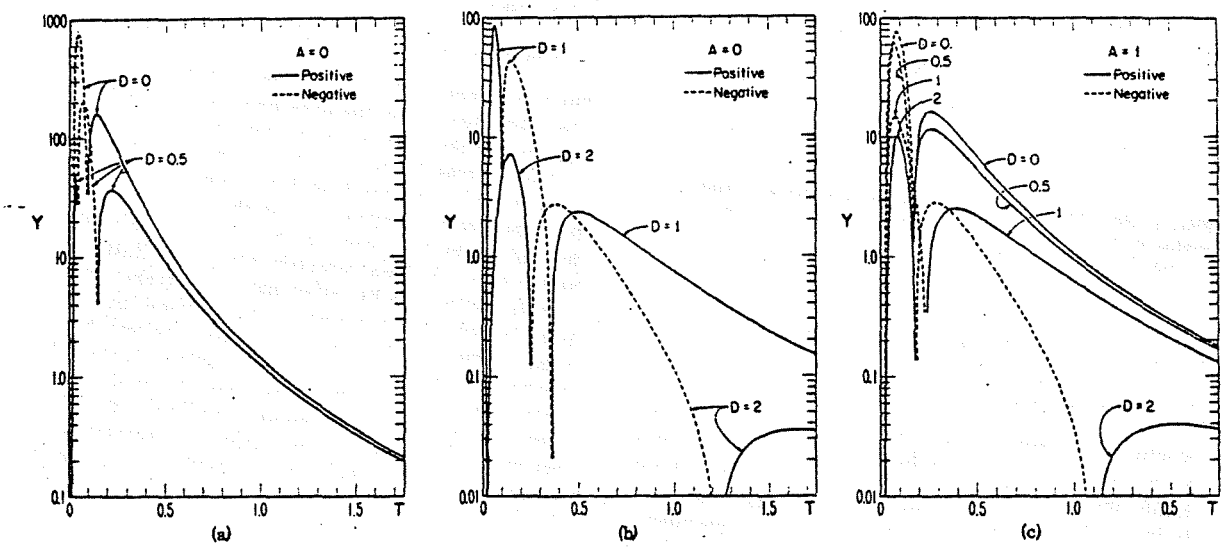


FIG. 3. Normalized impulse response of voltage in small horizontal loop on surface (with axis vertical) for buried source loop. Also applicable to small buried horizontal loop and source loop on surface (see text).

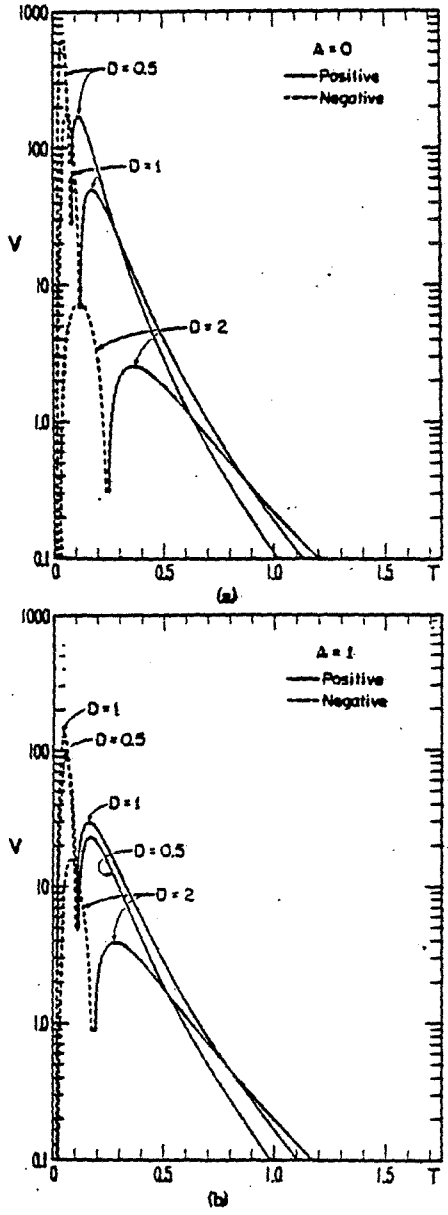


FIG. 4. Normalized impulse response of voltage in small buried vertical loop (with axis oriented in radial direction) for source loop on surface.

numerical integration data shown in Figs. 3(a) and 3(b).

IV. SOURCE LOOP ON SURFACE

A situation of even more practical interest is when the source loop of radius a is located on the surface and the fields are to be observed within the earth. The situation is indicated in Fig. 1(b). We again consider that the source current is $I_0\delta(t)$, and then the time-dependent voltages $v_p(t)$ and $v_z(t)$ induced in small receiving loops at P are given by

$$v_p(t) = -[AA_rN_r\mu I_0/(2\pi h^3)]m(t), \tag{10}$$

$$v_z(t) = [AA_rN_r\mu I_0/(2\pi h^3)]q(t). \tag{11}$$

The waveform $v_z(t)$ is the same here as in the reciprocal situation mentioned above: Thus, $q(t)$ is again defined by (4). On the other hand, $m(t)$ is to be obtained from

$$m(t) = -h^3\frac{\partial}{\partial h}\int_0^\infty \mathcal{L}^{-1}[sF(s,\lambda,h)]\lambda^2 J_1(\lambda\rho)e^{-\lambda z_0}f(a\lambda)\,d\lambda, \tag{12}$$

where now z_0 corresponds to the elevation of the source loop above ground and h is the depth of the observer.

Evaluating the inverse transform, as indicated before,[1] we get

$$m(t) = -h^3\frac{\partial}{\partial h}\frac{1}{2(\sigma\mu\pi)^{1/2}t^{3/2}}\int_0^\infty\left(\lambda h + 1 - \frac{\sigma\mu h^2}{2t}\right)$$
$$\times\exp\left(-\frac{\sigma\mu h^2}{4t}\right)\exp\left(-\frac{\lambda^2 t}{\sigma\mu}\right)\lambda^2 J_1(\lambda\rho)f(\lambda a)\,d\lambda$$
$$= \frac{h^3}{2(\sigma\mu\pi)^{1/2}t^{3/2}}\exp\left(-\frac{\sigma\mu h^2}{4t}\right)$$
$$\times\int_0^\infty\left[\lambda^2\left(\frac{(\sigma\mu)^2h^3}{4t^2} - \frac{3\sigma\mu h}{2t}\right) + \lambda^3\left(1 - \frac{\sigma\mu h^2}{2t}\right)\right]$$
$$\times\exp-(\lambda^2/\sigma\mu)tJ_1(\lambda\rho)f(\lambda a)\,d\lambda.$$

Putting this in dimensionless form, we find that

$$m(t) = -[4\pi^{1/2}(\sigma\mu)^2h^4]^{-1}V(D,\ T,\ Z,\ A),$$

where

$$V = \frac{2}{T^{5/2}}\exp\left(-\frac{1}{4T}\right)\int_0^\infty\left[x^2\left(\frac{3}{2T} - \frac{1}{4T^2}\right) - x^3\left(1 - \frac{1}{2T}\right)\right]$$
$$\times\exp(-x^2T)J_1(xD)f(xA)\,dx,$$

where $D = \rho/h$, $A = a/h$, $T = t/(\sigma\mu h^2)$, and $Z = z_0/h$.

Using numerical integration, the waveform function V for $Z = 0$ is shown plotted in Figs. 4(a) and 4(b) for the same range of the parameters.

V. CONCLUDING REMARKS

The waveforms $p(t)$, $q(t)$, and $m(t)$ shown here all depend significantly on the parameter D, which is the ratio of the observer's radial coordinate ρ to the depth h. This is true for both finite and infinitesimal loops. Also, we note that the transient coupling between a finite horizontal source loop on the surface and an infinitesimal buried receiving horizontal loop is the same as for the reciprocal situation where the finite source loop is buried. On the other hand, the transient coupling between the horizontal finite source loop and a small vertical receiving loop depends on whether the source loop is on the surface or buried. In the latter case, there is a difference between the up-link and the down-link situation. We stress, however, that this is not inconsistent with the principle of electromagnetic reciprocity, since the mutual impedance for a given configuration does not depend on which loop transmits.

[1] J. R. Wait and D. A. Hill, J. Appl. Phys. 42, 3866 (1971).
[2] J. R. Wait, Geophysics 19, 290 (1954).

LOCATING AN OSCILLATING MAGNETIC DIPOLE IN THE EARTH

Indexing terms: Magnetic fields, Mining

The merits of a horizontal magnetic dipole in a source-location scheme are considered. The results have possible applications in locating trapped miners following disasters.

In a previous communication,[1] we pointed out the possibility that, following a disaster, miners could be located by an electromagnetic technique. The basis of the method was to observe the structure of the vector magnetic field on the surface produced by a buried magnetic dipole whose location was to be determined. Specifically, we considered the source to be a vertically oriented magnetic dipole (i.e. a small horizontal loop) buried at a depth h in the conducting halfspace. It was indicated that the radial co-ordinate of the observer, relative to the source, could be ascertained from measurements of the horizontal and vertical magnetic fields at the surface. In such a scheme, it is necessary that the trapped miner(s) have available a means to excite a loop of wire with sufficient audio-frequency current to be detected on the surface.

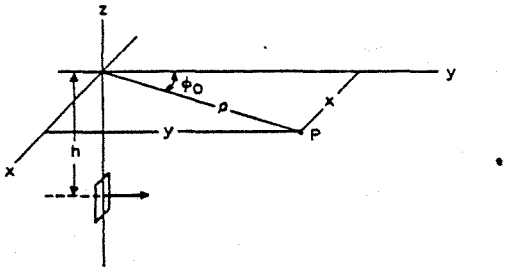


Fig. 1 *Horizontal magnetic dipole located at depth h in a conducting halfspace*

Current field investigations of the e.m. location scheme have shown that the null of the horizontal magnetic field directly over a buried vertical magnetic dipole is a relatively simple and useful criterion that may have promise in a practical scheme.*† Unfortunately, in this case, the received magnetic field must compete with atmospheric noise that always has significant horizontal components of magnetic field. This immediately suggests that a better scheme would be

* FARSTAD, A. J. (Personal communication, April 1972)
† GEYER, R. G. (Personal communication, April 1972)

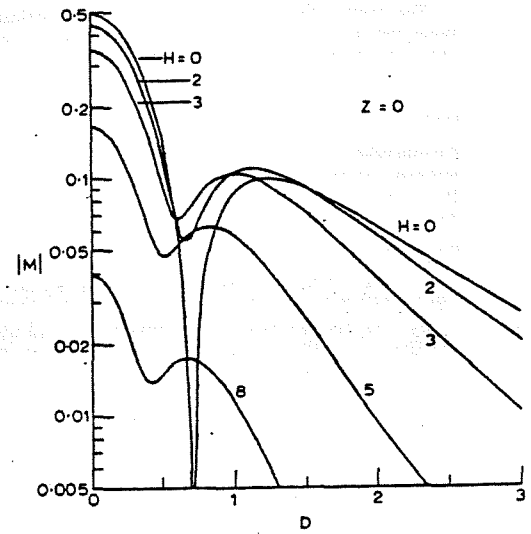


Fig. 2 *Function $|M|$, proportional to $|H_z|$, for observer at (0, y, 0) as a function of $D = y/h$ for various values of $H = (\sigma\mu_0\omega)^{\frac{1}{2}}h$*

netic-dipole source, in which case
urs in the vertical magnetic-field
tmospheric noise is then much
on, we consider here the structure
d by a buried horizontal magnetic
ained in a vertical plane). Also,
e other features of this configura-

cated in Fig. 1, where we choose
em (x, y, z), with the space $z < 0$
geneous nonmagnetic earth of
s a small loop or frame of area A
an angular frequency ω. The
ource is located at $z = -h$ on the
y direction. As before,[1] we can
currents because of the low

d components H_x, H_y and H_z at a
can be calculated from integral
own.[2] The latter are evaluated
ain special cases can be expressed

the fields in the region $z > 0$ can
ential Φ via

. . . . . (1)

where

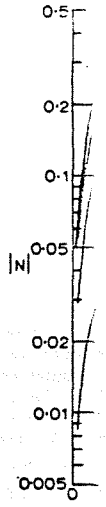
$$\Phi = \int_0^\infty J_0(\lambda\rho)\exp(-uh-\lambda z)\,d\lambda \qquad (2)$$

where ρ = $(\lambda^2 + i\sigma\mu_0\omega)^{\frac{1}{2}}$. If the conductivity σ and ω are sufficiently low, eqn. 1 is reduced to

$$\Phi \approx \exp\{-\lambda(h+z)\}\,d\lambda$$

$$= (\lambda^2)^{-\frac{1}{2}} \quad . \quad . \quad . \quad . \quad . \quad (3)$$

On carrying out the integrations in eqns. 1 and 2 and changing the variable to dimensionless form, we



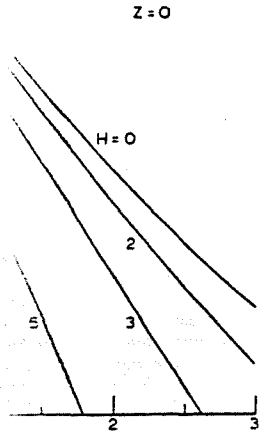


Fig. 3 *Fu... (0, y, 0) as ... to $|H_z|$, for observer at*

readily ob... forms for the fields for $z > 0$. Thu...

$$H_x = \ldots D)-M\} \quad . \quad . \quad . \quad . \quad (4)$$

$$H_y = \ldots I+C^2M\} \quad . \quad . \quad . \quad (5)$$

$$H_z = \ldots \quad . \quad . \quad . \quad . \quad . \quad . \quad (6)$$

where

$$C = (y/\rho) = \cos\phi_0$$

$$S = (x/\rho) = \sin\phi_0$$

and

$$D = (x^2+y^2)^{\frac{1}{2}}/h = \rho/h$$

The dimensionless integral functions M, N and T are defined by

$$M = \int_0^\infty gF(g,H,Z)(J_0(gD) - \frac{1}{gD} J_1(gD))dg \quad . \quad (7)$$

$$N = \int_0^\infty gF(g,H,Z) J_1(gD)\, dg \quad . \quad (8)$$

$$T = \int_0^\infty F(g,H,Z) J_1(gD)\, dg \quad . \quad (9)$$

where

$$F(g,H,Z) = \frac{g(g^2+iH^2)^{\frac{1}{2}}}{g+(g^2+iH^2)^{\frac{1}{2}}} \exp\{-(g^2+iH^2)^{\frac{1}{2}} - gZ\} \quad (10)$$

where $H = (\sigma\mu_0\omega)^{\frac{1}{2}} h$ and $Z = z/h$.

The corresponding static forms for the basic integrals M, N, and T are the elementary functions

$$M_s = \tfrac{1}{2}\left[\frac{1}{(D^2+(Z+1)^2)^{3/2}} - \frac{3D^2}{(D^2+(Z+1)^2)^{5/2}}\right] \quad (11)$$

$$N_s = \tfrac{1}{2}\frac{3D(Z+1)}{(D^2+(Z+1)^2)^{5/2}} \quad . \quad (12)$$

and

$$T_s = \tfrac{1}{2}\frac{D}{(D^2+(Z+1)^2)^{3/2}} \quad . \quad (13)$$

The following cases are of special interest. If $x = 0$ (i.e. $S = 0$ we find that

$$\left.\begin{aligned} H_x &= 0 \\ H_y &= -(IA/(2\pi h^3))\, M \\ H_z &= IA/(2\pi h^3)\, N \end{aligned}\right\} \quad . \quad (14)$$

On the other hand, if $y = 0$ (i.e. $C = 0$ we see that

$$\left.\begin{aligned} H_x &= 0 \\ H_y &= -(IA/(2\pi h^3))(T/D) \\ H_z &= 0 \end{aligned}\right\} \quad . \quad (15)$$

A general computer program has been written for the integrals M, N, and T/D that will yield numerical results for any value of the parameters D, H and Z. To illustrate the situation here, we plot $|M|$, $|N|$ and $|T/D|$ as functions of D in Figs. 2, 3 and 4, respectively, for the case $Z = 0$ and various values of H. The appropriate static behaviour is evident for the case $H = 0$. In general, we note that $H \simeq 0{\cdot}086(\sigma_m f)^{\frac{1}{2}} h_m$, where σ_m is the earth conductivity in millisiemens per metre, f is the frequency in hertz and h_m is the burial depth in kilometres. For example, if $\sigma_m = 1$, $f = 100$ and $h_m = 0{\cdot}2$, we see that $H = 0{\cdot}17$.

The functional behaviour of $|N|$ indicated in Fig. 3 shows that, in general, the vertical component H_z has a null directly over the source. This would appear to be a useful diagnostic property. On the other hand, the functional dependences of M and T provide secondary criteria that could also be exploited.

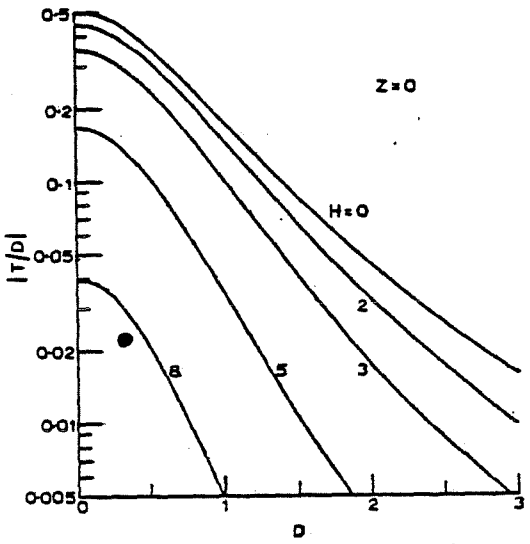


Fig. 4 *Function $|T/D|$, proportional to $|H_y|$ for observer at $(x, 0, 0)$ as a function of $D = x/h$*

The results described here are part of analytical study supported by the US Bureau of Mines under a contract monitored by H. E. Parkinson. I am grateful to K. P. Spies for performing the calculations.

JAMES R. WAIT

30th June 1972

Environmental Research Laboratories
National Oceanic & Atmospheric Administration
US Department of Commerce
Boulder, Colo. 80302, USA

References

1 WAIT, J. R.: 'Criteria for locating an oscillating magnetic dipole buried in the earth', *Proc. Inst. Elec. Electron. Eng.*, 1971, 59, pp. 1033–1035

2 WAIT, J. R., and CAMPBELL, L. L.: 'The fields of an oscillating magnetic dipole immersed in a semi-infinite conducting medium', *J. Geophys. Res.*, 1953, 58, pp. 167–178 (In eqn. 22, $2\gamma_0^2$ in the numerator should be $2\gamma_1^2$.)

LOW-FREQUENCY IMPEDANCE OF A CIRCULAR LOOP OVER A CONDUCTING GROUND

Indexing terms: Antenna theory, loop antennas, Electrical impedance

Using a quasistatic approach, the input impedance of a circular wire loop is calculated for the case where the Earth is represented as a homogeneous conducting halfspace. It is shown that the input resistance is only proportional to the ground conductivity when the loop radius is small compared with the electrical skin depth.

In various technical applications, one is interested in transmitting useful power from a ground-based loop antenna. For example, in proposed mine-rescue techniques,[1] it is desired to communicate with a subsurface observer via a transmission path through the overburden. In a previous analytical study,[2] we considered the subsurface fields for an insulated circular loop of wire on or just above the Earth's surface. We did not, however, consider the power required to maintain the specified uniform current I in the wire loop. In this letter, we consider this problem.

As before, the frequency is assumed to be sufficiently low for the current round the loop to be uniform. Alternatively, the feed points are sufficiently numerous for an adequately uniform current to be maintained, even for higher frequencies. The quantity of interest here is the self impedance Z, which is defined by $Z = V/I$, where V is the total voltage integrated round the loop.

The geometry is indicated in Fig. 1, where the Earth is taken to be a homogeneous halfspace of conductivity σ for $z < 0$ with respect to a cylindrical-co-ordinate system (ρ, ϕ, z). The loop of radius a is located at $z = h_0$ in the vacuum region for $z > 0$. The single-turn wire making up the loop has a radius c, where $c \ll a$. The wire itself is assumed to be perfectly conducting.

For the model adopted, the electric field E_ϕ in the space $z > 0$ can be derived from $E_\phi = \partial F/\partial \rho$, where F is a scalar function of ρ and z. Under quasistatic conditions, the latter is given by[2]

$$F = \frac{i\mu_0 \omega a^2 I}{2} \int_0^\infty \frac{2J_1(\lambda a)}{\lambda a} J_0(\lambda \rho) \times [\exp(-\lambda|z-h_0|) + (\lambda-u)(\lambda+u)^{-1} \exp\{-\lambda(z+h_0)\}]d\lambda \quad . \quad . \quad . \quad (1)$$

where $u = (\lambda^2 + i\sigma\mu_0\omega)^{\frac{1}{2}}$. The time factor adopted is $\exp(i\omega t)$, and the angular frequency ω is assumed to be sufficiently

low for all the displacement currents to be negligible. The magnetic permeability of the whole space is taken to be $\mu_0 (= 4\pi \times 10^{-7}$ H/m).

The self impedance Z is now calculated from

$$Z = \frac{-2\pi a E_\phi}{I}\Bigg]_{\substack{\rho=a \\ z=h_0+c}} \quad . \quad . \quad . \quad . \quad . \quad . \quad . \quad . \quad (2)$$

If we now write

$$Z = i\mu_0 \omega a (P + S) \quad . \quad . \quad . \quad . \quad . \quad . \quad . \quad . \quad . \quad (3)$$

it easily follows that

$$P = \pi \int_0^\infty \{J_1(x)\}^2 \exp(-B_0 x)\, dx \quad . \quad . \quad . \quad . \quad (4)$$

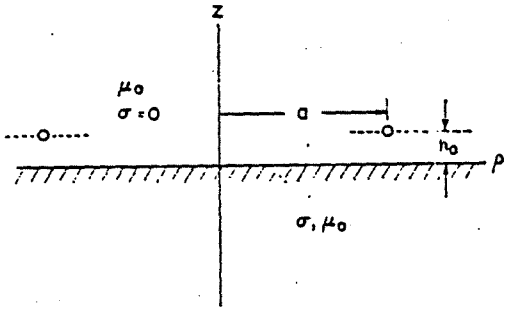


Fig. 1 *Side view of circular loop over the conducting halfspace model of the ground*

and

$$S = \pi \int_0^\infty \{J_1(x)\}^2 \frac{x - (x^2 + i2A^2)^{\frac{1}{2}}}{x + (x^2 + i2A^2)^{\frac{1}{2}}} \exp(-Bx)\, dx \quad (5)$$

where

$$A = \frac{a}{\delta} = \frac{\text{loop radius}}{\text{skin depth}} \qquad \delta = \left(\frac{2}{\sigma\mu_0\omega}\right)^{\frac{1}{2}}$$

$$B_0 = \frac{c}{a} = \frac{\text{wire radius}}{\text{loop radius}}$$

and

$$B = \frac{2h_0 + c}{a} \simeq \frac{2h_0}{a} = \frac{2 \times \text{loop height}}{\text{loop radius}}$$

Here, of course, P is the (normalised) primary inductance of the loop, and can be expressed in terms of the complete elliptic integrals as follows:

$$P = \frac{2}{k_0}\left\{\left(1 - \frac{k_0^2}{2}\right) K(k_0) - E(k_0)\right\} \quad . \quad . \quad . \quad . \quad (6)$$

where $k_0 = 2(B_0^2 + 4)^{-\frac{1}{2}}$. Here, following standard notation,

$$K(k) = \int_0^{\pi/2} \frac{d\theta}{(1 - k^2 \sin^2\theta)^{\frac{1}{2}}}$$

and

$$E(k) = \int_0^{\pi/2} (1 - k^2 \sin^2\theta)^{\frac{1}{2}}\, d\theta$$

In the general case, it appears that the secondary influence characterised by S must be evaluated by numerical methods. For small values of A, we can write

$$S \simeq -if(B) A^2 \quad . \quad . \quad . \quad . \quad . \quad . \quad . \quad . \quad . \quad . \quad (7)$$

where

$$f(B) = \frac{\pi}{2} \int_0^\infty \frac{\{J_1(x)\}^2}{x^2} \exp(-Bx)\, dx \quad . \quad . \quad . \quad (8)$$

If, in addition, $B \ll 1$, we can replace the exponential by $1 - Bx$ in eqn. 8, yielding standard integrals.[3] Then

$$f(B) \simeq \frac{2}{3} - \frac{\pi}{4} B \quad . \quad . \quad . \quad . \quad . \quad . \quad . \quad . \quad . \quad (9)$$

The other limiting case is when A is very large. To illustrate this case, we first note that

$$S = S_\infty + \Delta S \quad . \quad . \quad . \quad . \quad . \quad . \quad . \quad . \quad . \quad (10)$$

where

$$S_\infty = S|_{A=\infty} = -\frac{2}{k}\left\{\left(1 - \frac{k^2}{2}\right) K(k) - E(k)\right\} \quad (11)$$

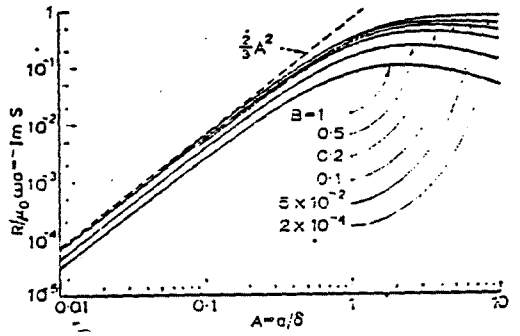


Fig. 2A *Normalised input resistance of the loop as a function of the loop radius for several elevations*

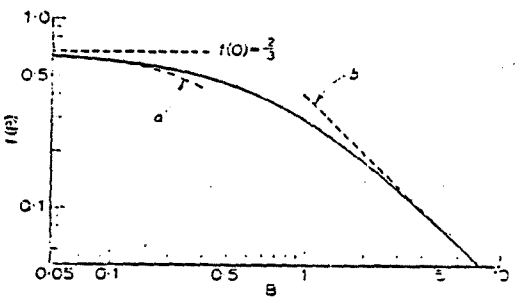


Fig. 2B *Function f(B) showing its limiting behaviour for small and large B values*

a Small-B approximation, $f(B) \simeq \frac{2}{3} - (\pi/4) B$
b Large-B approximation, $f(B) \simeq \pi/4B$

where $k = 2(B^2 + 4)^{-\frac{1}{2}}$, and

$$\Delta S = \pi \int_0^\infty \frac{2x}{x + (x^2 + i2A^2)^{\frac{1}{2}}} \{J_1(x)\}^2 \exp(-Bx)\, dx \quad (12)$$

If A is sufficiently large, we see that

$$\Delta S \simeq \left(\frac{2}{i}\right)^{\frac{1}{2}} \frac{\pi}{A} \int_0^\infty x \exp(-Bx) \{J_1(x)\}^2\, dx \quad . \quad . \quad (13)$$

is the leading term in an expansion in inverse powers of A. This integral has been given by Luke;[4] thus

$$\Delta S \simeq \left(\frac{2}{i}\right)^{\frac{1}{2}} \frac{Bk}{2A(1 - k^2)} \times \left\{\left(1 - \frac{k^2}{2}\right) E(k) - (1 - k^2) K(k)\right\}$$

It appears this is only a valid correction if the product AB is very large compared with 1.

Numerical values of P from eqn. 6 were obtained for several values of B_0 as follows:

$$B_0 = 10^{-6};\ P = 13{\cdot}89$$

$$B_0 = 10^{-5};\ P = 11{\cdot}59$$

$$B_0 = 10^{-4};\ P = 9{\cdot}29$$

The corresponding values of the inductance L of the loop in free space are then $L = \mu_0 aP$ henrys.

Using numerical integration, the complex quantity S was evaluated* from eqn. 5 for various values of B and A. Of particular interest is the resistive component $R = \mathrm{Re}\,Z = \mu_0 \omega a(-\mathrm{Im}\,S)$ ohms. The normalised quantity $R/\mu_0 \omega a$ is plotted in Fig. 2A as a function of A for various values of B. As indicated, R varies linearly with A^2 for A less than about 0·2. In this range, for the B values indicated, the approximation $S \simeq -iF(B)A^2$ is applicable. To aid the user, a plot of the function $F(B)$ is shown in Fig. 2B, along with the limiting asymptotes.

The limiting value of R for a/δ tending towards infinity is rather interesting. If B is sufficiently small, we see that the ordinate in Fig. 2A approaches $\pi/4$. This is entirely consistent with the concept that the resistance of the loop is equivalent to $2\pi a \times (\mu_0 \omega/8)$ ohms. The factor $\mu_0 \omega/8$ is identical to the resistance per unit length of an infinitely long current-carrying wire lying on or just above the surface of a conducting halfspace.[6]

* Numerical tables available on request from the authors

The present result can be used in estimating the total power requirements for a downlink communication system. For example, if we choose $a = 0{\cdot}5$ km, $f = 100$ Hz and $\sigma = 10^{-2}$ S/m, we see from Fig. 2A that $-\mathrm{Im}\,S \simeq 0{\cdot}25$ and that the corresponding value of the resistance R is $0{\cdot}10\,\Omega$. This is comparable to the ohmic resistance of the loop itself if, for example, we selected a single-turn copper wire with a radius of the order of 1·4 cm.

J. R. WAIT
K. P. SPIES

Institute for Telecommunication Sciences
Office of Telecommunications
US Department of Commerce
Boulder, Colo. 80302, USA

3rd July 1973

References

1 LARGE, D. B., BALL, L., and FARSTAD, A. J.: 'Radio transmission to and from underground coal mines—theory and measurement', *IEEE Trans.*, 1973, COM-21, pp. 194–202
2 WAIT, J. R., and SPIES, K. P.: 'Subsurface electromagnetic fields of a circular loop of current located above ground', *ibid.*, 1972, AP-20, pp. 520–522
3 WHEELON, A. D.: 'Tables of summable series and integrals involving Bessel functions' (Holden-Day, 1968) (e.g. see formulas 11.308 and 11.204)
4 LUKE, Y. L.: 'Integrals of Bessel functions', (McGraw-Hill, 1962), p. 316, no. 20
5 WAIT, J. R.: 'On the impedance of a long wire suspended over the ground', *Proc. Inst. Radio Engr.*, 1961, 49, p. 1429. (Note that the 3 in the denominator of the second term in the two equations for ΔR should be 3π)

ERRATA

BROOK, P., and SMITH, J. G.: 'Spreading resistance of multiple-layer cylindrical structures', *Electron. Lett.*, 1973, 9, pp. 253–254:

We regret that the following error occurred in the printing of the above letter: Eqn. 8 should read

$$\phi_i(r, Z_i) = f\frac{A^2}{B^2}\left(\frac{l_i - Z_i}{\sigma_i} + \sum_{k=i+1}^{n}\frac{l_k}{\sigma_k}\right) + \frac{2fA}{\sigma_1}\sum_{j=1}^{\infty}\frac{A_{1j}}{A_{ij}}\left\{\theta_{ij}\cosh\left(\frac{\alpha_j Z_i}{B}\right) - \sinh\left(\frac{\alpha_j Z_i}{B}\right)\right\} \times \left\{J_1\left(\frac{\alpha_j A}{B}\right)J_0\left(\frac{\alpha_j r}{B}\right)\Big/\alpha_j^2\, J_0^2(\alpha_j)\right\} \quad . \quad . \quad (8)$$

where

$$\frac{A_{ij}}{A_{1j}} = \frac{\sigma_1}{\sigma_i}\prod_{k=1}^{i-1}\left\{\cosh\left(\frac{\alpha_j l_k}{B}\right) - \theta_{kj}\sinh\left(\frac{\alpha_j l_k}{B}\right)\right\} \quad . \quad . \quad (8a)$$

NEELAKANTASWAMY, P. S., and BANERJEE, D. K.: 'Radiation characteristics of waveguide-excited dielectric spheres with matched sphere-air boundary', *Electron. Lett.*, 1973, 9, pp. 40–41:

The authors would like to make the following correction to their letter:

In Table 1, column 1, the heading should read 'serial number', and not 'sidelobe'

KINGSBURY, N. G.: 'Digital-filter 2nd-order element with low quantising noise for poles and zeros at low frequencies', *Electron. Lett.*, 1973, 9, pp. 271–273:

The author would like to make the following correction to his letter:

In Figs. 1A and 1B, there should be a minus sign next to the lower input of the first adder

DOWNING, B. J., and MYERS, F. A.: 'Q band (38 GHz) varactor-tuned Gunn oscillators', *Electron. Lett.*, 1973, 9, pp. 244–245:

We regret that the following error occurred in the printing of the above letter:

Figs. 1B and 2B, but not their captions, were transposed

BRAMER, B., and BANERJEE, A. R.: 'Fitting of measured data to a known relationship', *Electron. Lett.*, 1973, 9, pp. 184–186:

We regret that the following error occurred in the printing of the above letter:

There should be a footnote to the title reading as follows: The program listing and accompanying documentation are held in the IEE Computer-Program Library, Savoy Place, London WC2R 0BL, England. Copies are available on application and on payment of a charge. Please quote CP133

MUNRO, E. W., WHITAKER, A. J. T., and MCINNES, P. A.: 'Calculation of the secondary-radiation pattern for a paraboloid reflector with a given illumination function and feed position', *Electron. Lett.*, 1973, 9, pp. 234–235:

The authors would like to make the following correction to their letter:

The first equation should read

$$E(W, \phi) = \int_0^1\int_0^{2\pi} f(v)\exp j\left[2FLT\left\{1 - \frac{W_x v\cos\phi'}{FLT^2} + \frac{2W_z(2-T)}{LT^2} + \frac{(W_x^2 + W_z^2)}{L^2T^2}\right\}^{\frac{1}{2}} - Wv\cos\phi' + 2F(2-T)(L^2 - W^2)^{\frac{1}{2}}\right] v\, d\phi'\, dv$$

IEEE Trans. Antennas and Propagation, vol. AP-19, No. 5, (Communications) 717-718 (Sept. 1971)

Electromagnetic Fields of a Small Loop Buried in a Stratified Earth

Abstract—The field structure of a buried vertical oscillating magnetic dipole is examined. The earth is represented as a two-layer half-space, and the source is located in the bottom semi-infinite region. Using numerical integration, the magnitude of the ratio of the horizontal to the vertical magnetic field is examined for an observer on the earth's surface. It is shown that at sufficiently low frequencies, the field ratio is not appreciably modified by the finite conductivity and the geometry of the layers.

Communication to the earth's surface from a buried transmitter may be useful in emergency situations such as after a mine disaster [1]. Unfortunately, the conductive losses in the intervening rock will severely attenuate the signal unless extremely low frequencies are employed. Also, direction finding of the buried source, from the surface observer, is inhibited by the conductive overburden. In this communication, we wish to consider an analytical model which may shed some light on this problem.

As indicated in Fig. 1, we consider a vertical magnetic dipole or small loop (with vertical axis) located at a depth h beneath the surface of a flat earth. The current in the loop is taken to vary as $\exp(i\omega t)$. To simulate the effect of an inhomogeneous earth, we adopt a two-layer model. The upper layer has a conductivity σ_1 and a thickness b. The semi-infinite lower layer, which contains the source dipole, has a conductivity σ_2. A cylindrical coordinate system (ρ,ϕ,z) is chosen as illustrated in Fig. 1 with the observer located at $P(\rho,z)$ on or above the earth's surface at $z = 0$. It is our objective to evaluate the magnetic field components H_ρ and H_z at $P(\rho,z)$ for a specified total current I in the small loop of area A located at $z = -h$.

The formal solution for the problem as stated was given some time ago [2], although in the original derivation, it was assumed that the magnetic dipole was in the air above a two-layer stratified earth. Clearly, the solution has the same form as for the problem posed here. Also, as indicated before, all displacement currents can be neglected if the free-space wavelength is much greater than the significant dimensions of the problem. We assume this is the case here. Also, to simplify matters, we assume that both of the conductive layers have magnetic permeabilities which are the same as for free space. Thus, without difficulty, we find that

$$H_\rho = b_0 P \tag{1}$$

and

$$H_z = b_0 Q \tag{2}$$

where $b_0 = IA/(2\pi h^3)$ is a suitable normalizing factor, while P and Q are the dimensionless field quantities. Under the assumptions stated previously, we have the integral formulas

$$P = \frac{h^3}{2}\int_0^\infty \lambda^2 T(\lambda)\exp(-\lambda z) J_1(\lambda\rho)\, d\lambda \tag{3}$$

and

$$Q = \frac{h^3}{2}\int_0^\infty \lambda^3 T(\lambda)\exp(-\lambda z) J_0(\lambda\rho)\, d\lambda \tag{4}$$

where

$$T(\lambda) = \frac{\left(\frac{2\lambda}{u_1+\lambda}\right)\left(\frac{2u_1}{u_1+u_2}\right)\exp\left[-u_2(h-b)-u_1 b\right]}{\left[1-\left(\frac{u_1-\lambda}{u_1+\lambda}\right)\left(\frac{u_1-u_2}{u_1+u_2}\right)\exp(-2u_1 b)\right]} \tag{5}$$

$$u_1 = (\lambda^2 + i\sigma_1\mu_0\omega)^{1/2}, \text{ and } u_2 = (\lambda^2 + i\sigma_2\mu_0\omega)^{1/2}.$$

Manuscript received January 28, 1971.

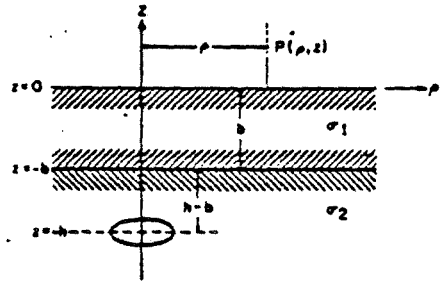


Fig. 1. Magnetic dipole located within two-layer stratified earth.

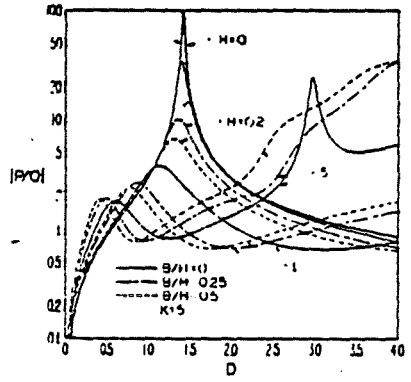


Fig. 2. Field ratio on surface for various values of $H = (\sigma_2\mu_0\omega)^{1/2}h$ and $B/H = b/h$ for fixed $K = (\sigma_1/\sigma_2)^{1/2} = 5$.

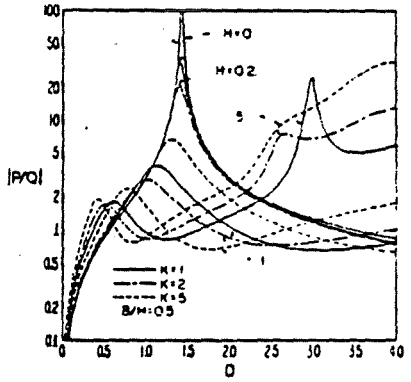


Fig. 3. Field ratio for various values of H and K for fixed $B/H = b/h = 0.5$.

While (3) and (4) can be evaluated analytically in certain limiting cases, the most direct approach is numerical integration. Convergence of the integrals is assured by the exponential factor in the numerator of the right-hand side of (5). Also, we note that P and Q are functions of the dimensionless parameters $B = (\sigma_2\mu_0\omega)^{1/2}b$, $H = (\sigma_2\mu_0\omega)^{1/2}h$, $D = \rho/h$, $Z = z/h$, and $K = (\sigma_1/\sigma_2)^{1/2}$. A digital computer program has been written for evaluating P and Q, and results have been obtained for a wide range of the parameters [3].

A quantity of special interest is the magnitude of the ratio H_ρ/H_z at $z = 0$ on the earth's surface. The magnitude of this ratio is $|P/Q|$ and typical plots are indicated in Figs. 2–4 for selected values of the parameters. The abscissa in each case is the distance parameter D or ρ/h. The limiting case designated $H = 0$ corresponds to purely static conditions (i.e., $\omega \to 0$). In this case, it is not difficult

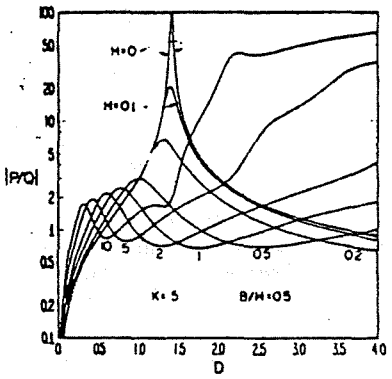


Fig. 4. Field ratio for various values of H for fixed $K = (\sigma_1/\sigma_2)^{1/2} = 5$ and $B/H = b/h = 0.5$.

cult to verify that, for $z = 0$, (3) and (4) reduce to

$$P = (3/2)DR^{-5}$$

and

$$Q = (1/2)[3R^{-5} - R^{-3}]$$

where $R = (D^2 + 1)^{1/2}$. The curves in Figs. 2–4 are consistent with these static field formulas for the small values of H. In particular, we see that the null for Q at $D = \sqrt{2}$ leads to an infinity for $|P/Q|$. This pronounced peak, however, is somewhat blurred when H is different from zero. In fact, the behavior of the ratio $|P/Q|$ becomes modified drastically for the larger values of H.

To consider a specific example, we choose $f = \omega/2\pi = 10^3$ Hz, $\sigma_2 = 10^{-3}$ mho/m, and $h = 200$ m; thus, $H = 0.17$. In this case, the upper layer of thickness $(B/H) \times 200$ m, has a conductivity $K^2 \times 10^{-3}$ mho/m. As indicated in Figs. 2 and 3, the presence of this masking layer deteriorates the ideal static-like behavior of the field ratio $|P/Q|$.

Using the analytical results from this study, it is possible to elucidate the effect of the stratification in the overburden and to provide improved criteria for direction finding techniques. The results given here are considered only as an example of the many possibilities that exist.

James R. Wait
Kenneth P. Spies
Inst. Telecommun. Sci.
Office of Telecommun.
U. S. Dep. Commerce
Boulder, Colorado 80302

References

[1] G. Meloy, G. V. Keller, *et al.*, "Mine rescue and survival," Nat. Acad. Eng., Washington, D. C., Tech. Rep. 1969.
[2] J. R. Wait, "The magnetic dipole over the horizontally stratified earth," *Can. J. Phys.*, vol. 29, 1951, pp. 577–592.
[3] J. R. Wait and K. P. Spies, "Evaluation of the surface EM fields," AFCRL Rep. 52, Feb. 1971, (available from Federal Clearinghouse, NTIS, Springfield, Va. 22151).

Radio Science, Volume 8, Numbers 8, 9, pages 813–818, August–September 1973

The electromagnetic response of a buried sphere for buried-dipole excitation

David A. Hill

Institute for Telecommunication Sciences, Office of Telecommunications, US Department of Commerce, Boulder, Colorado 80302

James R. Wait

Cooperative Institute for Research in Environmental Sciences, University of Colorado, Boulder, Colorado 80302 and National Oceanic and Atmospheric Administration, Environmental Research Laboratories, US Department of Commerce, Boulder, Colorado 80302

(Received April 4, 1973.)

The effect of a spherical inhomogeneity on the surface fields of a buried magnetic dipole source is determined from the reradiated fields of induced electric and magnetic dipole moments. For small spheres where the theory is valid, the errors introduced in source location are shown to be small. The results have possible application to rescue operations following coal mine disasters.

INTRODUCTION

The feasibility of locating a buried horizontal-loop source from surface measurements of the vertical and horizontal magnetic-field components has been investigated by *Wait* [1971]. For sufficiently low frequencies, the magnetic fields have a static-like behavior, and a single observation of the ratio and relative phases of the vertical and horizontal components is sufficient for location when the earth is homogeneous. However, when inhomogeneities are present, the surface fields will be modified, and source location may be more difficult.

In order to obtain a quantitative idea of the surface field modifications, we consider a spherical conducting ore zone as a perturbation to the homogeneous half-space. The corresponding rigorous problem of scattering by a buried sphere has been treated by *D'Yakanov* [1959]. Unfortunately, his solution is restricted to azimuthally symmetric excitation, and even then the solution is not in a convenient computational form. However, if the sphere is electrically small and is located at a sufficient distance from both the loop source and the interface, the scattered fields can be identified as the secondary fields of induced dipole moments. The latter are equal to the product of the incident fields and the polarizabilities of the sphere.

Wait [1968] has used this induced dipole approach for scattering by a small sphere above a conducting half-space. The method has the advantage that it is easily generalized to scatterers of other shapes for which both the electric and magnetic polarizabilities are known, such as spheroids [*van de Hulst*, 1957]. This concept has also been considered by *Ward* [1967] in the context of electromagnetic detection of massive sulphide-ore bodies from airborne platforms. In his applications, however, the induced electric dipole moments for his spheres and disk models were not used. This was justified for the low audio frequencies used in exploration systems such as AFMAG.

FORMULATION

The geometry is illustrated in Figure 1, which shows both the Cartesian coordinate system (x, y, z) and the cylindrical coordinate system (ρ, ϕ, z). The half-space $z < 0$ is free space, and, except for the sphere, the lower half-space $z > 0$ has conductivity σ, permittivity ϵ, and free-space permeability μ_0. The sphere of radius a is located at $(x_0, 0, z_0)$, and has conductivity σ_s, permittivity ϵ_s, and permeability μ_s.

The small source loop of area A is located at

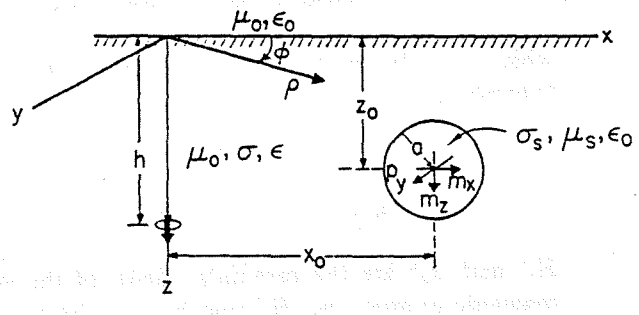


Fig. 1. Geometry for source loop and buried sphere with induced dipole moment.

$(0, 0, h)$ and carries a current I which varies as $\exp(i\omega t)$, where ω is the angular frequency. Since A is small, the source is equivalent to a vertical magnetic dipole. For an observer at the surface ($z = 0$), the vertical and horizontal components in the absence of the scattering sphere, H_ρ^i and H_z^i, have been given by *Wait* [1971]:

$$H_\rho^i = (-IA/2\pi h^3)P$$
$$H_z^i = (IA/2\pi h^3)Q \tag{1}$$

Here, P and Q are the dimensionless quantities:

$$\begin{matrix} P \\ Q \end{matrix} = \int_0^\infty \{[s^3 \exp(-u)]/(s+u)\} \begin{matrix} J_1(sD) \\ J_0(sD) \end{matrix} ds \tag{2}$$

where $u = (s^2 + iH^2)^{1/2}$, J_0 and J_1 are zero- and first-order Bessel functions, $H = (\sigma\mu_0\omega)^{1/2}h$, and $D = \rho/h$. The result in (2) assumes that displacement currents are negligible, and we retain this assumption throughout since we are interested in low frequencies. *Wait* [1971] has shown that for H sufficiently small, a single measurement of the complex ratio H_ρ^i/H_z^i is adequate to determine D and consequently ρ if h is known.

INDUCED DIPOLE MOMENTS

Although the distances involved here are much less than a free-space wavelength, they are not necessarily small compared to a wavelength in the lower half-space. Consequently, the induced electric dipole moment must be considered as well as the induced magnetic dipole moment. This is in contrast to the case in which the source and the scatterer are above ground [*Wait*, 1968].

Since both types of dipole moments are induced, both the unperturbed electric and magnetic fields at the sphere center $(x_0, 0, z_0)$ must be calculated. The unperturbed magnetic field has both z and x components, H_z^0 and H_x^0, and the unperturbed electric field has only a y component, E_y^0. These components can be obtained from *Wait* [1951; 1971], *Baños* [1966], or *Ward* [1967], and written in the following form which is similar to (1):

$$H_x^0 = (IA/2\pi h^3)Q^0$$
$$H_z^0 = (-IA/2\pi h^3)P^0 \tag{3}$$
$$E_y^0 = (-iH^2IA/4\pi\sigma h^4)Y^0$$

where

$$Q^0 = (1/2)\int_0^\infty \{\exp[-u|1-Z|] + [(u-s)/(u+s)]\exp[-u(1+Z)]\} \cdot \{[s^3 J_0(sX)]/u\}\, ds$$

$$P^0 = (1/2)\int_0^\infty \{\exp[-u|1-Z|] - [(u-s)/(u+s)]\exp[-u(1+Z)]\} \cdot s^2 J_1(sX)\, ds$$

$$Y^0 = \int_0^\infty \{\exp[-u|1-Z|] + [(u-s)/(u+s)]\exp[-u(1+Z)]\} \cdot \{[s^2 J_1(sX)]/u\}\, ds$$

$$Z = z_0/h$$

$$X = x_0/h$$

Note that Z must be positive, but X can be either positive or negative. The evaluation of the integrals will be discussed later.

The induced magnetic dipole moments, m_z and m_x, are given by the product of the magnetic polarizability and the incident magnetic field [*Wait*, 1960; 1968]

$$m_x = -2\pi a^3[3(M+iN)]H_x^0$$
$$m_z = -2\pi a^3[3(M+iN)]H_z^0 \tag{4}$$

where

$$3(M+iN) = -\frac{2\mu_s(\sinh\alpha - \alpha\cosh\alpha) + \mu_0(\sinh\alpha - \alpha\cosh\alpha + \alpha^2\sinh\alpha)}{\mu_s(\sinh\alpha - \alpha\cosh\alpha) - \mu_0(\sinh\alpha - \alpha\cosh\alpha + \alpha^2\sinh\alpha)}$$

where

$$\alpha = (i\omega\mu_s\sigma_s)^{1/2}a$$

We observe that the function $3(M + iN)$ has the following high-frequency limit

$$\lim_{|\alpha|\to\infty} [3(M + iN)] = 1 \tag{5}$$

If me assume that $\sigma_s \gg \sigma$, then the y-directed induced electric-current moment $(Ids)_y$ is given by [*van de Hulst*, 1957]

$$(Ids)_y = 4\pi\sigma a^3 E_y^0 \tag{6}$$

which is valid even if $|\alpha|$ is not large [*Wait*, 1960]. This electric-current moment has dimensions of current times length and differs by a factor of $i\omega$ from the electric-dipole moment which has dimensions of charge times length.

Several assumptions are implicit in the induced dipole-moment method used here to calculate the reradiated fields. First, the sphere radius a must be small in comparison to a wavelength in the lower half-space [*Stratton*, 1941]. Second, the sphere radius must be small compared to the geometric mean of the source and observer distances [*Wait*, 1960]. These conditions insure that higher-order multipoles are not important. Third, the sphere radius must be small compared to the distance between the sphere and the interface so that interactions between the sphere and the interface are not important. Actually, it is possible to compute correction terms which take into account interactions with the interface, and it has been done for a buried cylinder [*Wait*, 1972]. However, the correction terms are more complicated for a sphere because of coupling between the electric and magnetic modes [*Hill*, 1970]. At any rate, the interaction in the static limit has been shown to be unimportant for a sphere-interface separation of at least two sphere radii [*Hill and Wait*, 1972].

SCATTERED FIELDS

From the induced dipole moments in (4) and (6), it is possible to compute the scattered fields at any point on the surface by superposition. However, to simplify the discussion, we restrict our observation point to the x axis. This, of course, includes the point directly above the sphere ($x = x_0$) where the distortion of the surface fields is expected to be greatest. The scattered magnetic field on the x axis has only z and x components, H_z^s and H_x^s, which can be written as the sum of three contributions.

$$\begin{aligned} H_z^s &= H_z^v + H_z^h + H_z^e \\ H_x^s &= H_x^v + H_x^h + H_x^e \end{aligned} \tag{7}$$

H_z^v and H_x^v are the reradiated fields of the vertical magnetic moment m_z, H_z^h and H_x^h are the reradiated fields of the horizontal magnetic moment m_x, and H_z^e and H_x^e are the reradiated fields of the electric moment $(Ids)_y$.

The fields of the vertical magnetic moment can be written in the following form [*Wait*, 1971]

$$\begin{aligned} H_z^v &= (m_z/2\pi h^3)Q^r \\ H_x^v &= (-m_z/2\pi h^3)P^r \end{aligned} \tag{8}$$

where

$$\begin{matrix} P^r \\ Q^r \end{matrix} = \int_0^\infty \{[s^3 \exp(-uZ)]/(s + u)\} \begin{matrix} J_1[s(D - X)] \\ J_0[s(D - X)] \end{matrix} ds$$

Since we are observing the fields on the x axis, we redefine D to be x/h and let it be either positive or negative.

The fields of a horizontal magnetic moment have been given by *Wait* [1972], and for this geometry are given by

$$\begin{aligned} H_z^h &= (-m_x/2\pi h^3)N^r \\ H_x^h &= (-m_x/2\pi h^3)M^r \end{aligned} \tag{9}$$

where

$$N^r = \int_0^\infty \{[s^2 u \exp(-uZ)]/(s + u)\} \cdot J_1[s(D - X)]\, dx$$

$$M^r = \int_0^\infty \{[s^2 u \exp(-uZ)]/(s + u)\} \cdot ((J_0[s(D - X)] - \{J_1[s(D - X)]\}/[s(D - X)]))\, ds.$$

The fields of the electric moment are given by *Wait* [1961] and *Baños* [1966], and can be written in the following form

$$\begin{aligned} H_z^e &= \{[-(Ids)_y]/2\pi h^2\} S^r \\ H_x^e &= \{[-(Ids)_y]/2\pi h^2\} T^r \end{aligned} \tag{10}$$

where

$$S^r = \int_0^\infty \{[s^2 \exp(-uZ)]/(s+u)\} J_1[s(D-X)]\, ds$$

$$T^r = \int_0^\infty \{[\exp(-uZ)]/(s+u)\}((s^2 J_0[s(D-X)] - \{s J_1[s(D-X)]\}/(D-X)))\, ds$$

By substituting (3), (4), (6), (8), (9), and (10) into (7), the final expressions for the scattered field are obtained

$$\begin{aligned} H_z^s &= \{[-IA(a/h)^3]/2\pi h^3\} \\ &\cdot [3(M+iN)(Q^0Q^r + P^0N^r) - iH^2(Y^0S^r)] \\ H_x^s &= \{[IA(a/h)^3]/2\pi h^3\} \\ &\cdot [3(M+iN)(Q^0P^r - P^0M^r) + iH^2(Y^0T^r)] \end{aligned} \tag{11}$$

Note that the contribution from the electric moment goes to 0 as the frequency goes to 0 because H^2 vanishes. However, the contribution from the magnetic moment goes to 0 in the static limit only if the sphere is nonmagnetic ($\mu_s = \mu_0$). This can be seen by examining the behavior of $3(M + iN)$ in (4). This point has also been emphasized by *Ward* [1959].

The total fields observed on the surface are the sum of the incident and scattered fields

$$\begin{aligned} H_z^t &= H_z^i + H_z^s \\ H_x^t &= H_x^i + H_x^s \end{aligned} \tag{12}$$

where H_z^i and H_x^i are given by (1), and H_z^s and H_x^s are given by (11).

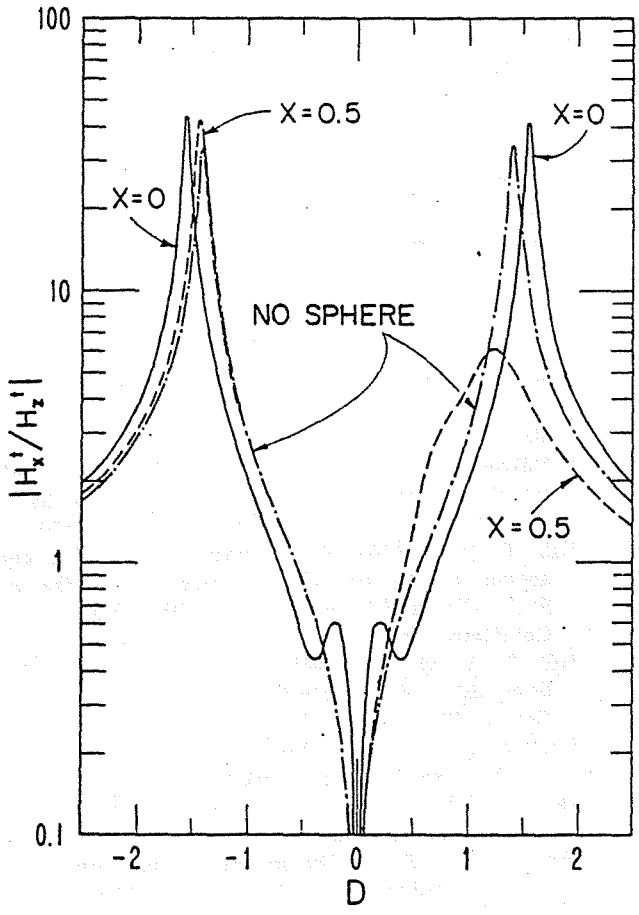


Fig. 2. Effect of sphere location on $|H_x^t/H_z^t|$. $H = 0.2$, $a/h = 0.3$, $Z = 0.5$, $|\alpha| = 5.0$, and $\mu_s = \mu_0$.

NUMERICAL RESULTS

Before performing a numerical evaluation of the integrals required for the magnetic components in (1) and (11), it is useful to obtain the static limits of the integrals by letting H approach 0. These limits are useful because they serve as a check on the general formulation and because H is sometimes quite small in realistic situations. By setting $H = 0$, the following static limits denoted by subscript s are obtained [*Wheelon*, 1968]:

$$\begin{aligned} P_s &= 3D/[2(1+D^2)^{5/2}] \\ Q_s &= (2-D^2)/[2(1+D^2)^{5/2}] \\ Q_s^0 &= [2(1-Z)^2 - X^2]/\{2[X^2+(1-Z)^2]^{5/2}\} \\ P_s^0 &= [3X(1-Z)]/\{2[X^2+(1-Z)^2]^{5/2}\} \\ Y_s^0 &= X/[X^2+(1-Z)^2]^{5/2} \\ P_s^r &= [3(D-X)Z]/\{2[(D-X)^2+Z^2)^{5/2}\} \\ Q_s^r &= [2Z^2 - (D-X)^2]/\{2[(D-X)^2+Z^2]^{5/2}\} \\ N_s^r &= [3(D-X)Z]/\{2[(D-X)^2+Z^2]^{5/2}\} \\ M_s^r &= [Z^2 - 2(D-X)^2]/\{2[(D-X)^2+Z^2]^{5/2}\} \\ S_s^r &= (D-X)/\{2[(D-X)^2+Z^2]^{3/2}\} \\ T_s^r &= -Z/\{2[Z^2+(D-X)^2]^{3/2}\} \end{aligned} \tag{13}$$

If these static results are subtracted from the general integral forms given earlier, then the convergence of the remaining numerical integral is improved if H is not too large. Of course, for $H = 0$, the integrands vanish and only the static terms remain. Computer programs were written for the numerical integrals, and the resultant quantities of

interest, $|H_z^t/H_x^t|$ and arg (H_z^t/H_x^t), were examined as a function of the various parameters.

Results for a nonmagnetic sphere ($\mu_s = \mu_0$) are shown in Figures 2 and 3. Parameter values are $H = 0.2$, $Z = 0.5$, $a/h = 0.3$, $|\alpha| = 5$, and $X = 0$ and 0.5. In a typical example where $f = 100$ Hz and $\sigma = 10^{-3}$ mhos m^{-1}, h would be 225 m. The amplitude curve in Figure 2 with no sphere present agrees with the previous result of *Wait* [1971]. With the sphere directly above the source ($X = 0$), the curve is still symmetrical about $D = 0$. The peak magnitudes are increased somewhat, but the peak locations are only slightly shifted. When the sphere is no longer above the source ($X = 0.5$), symmetry is lost and the peak for negative D increases while the peak for positive D decreases. The peak locations are again only slightly shifted. The phase curves in Figure 3 indicate that the greatest phase deviations occur close to the sphere location (D small for $X = 0$ and $D > 0$ for $X = 0.5$).

Results for smaller spheres and spheres farther from the source indicate smaller deviations. Another interesting result is that deviations were smaller for larger values of $|\alpha|$ due to the fact that the scattered field becomes more nearly real. Results were not obtained for larger spheres because the simplified treatment used here is not expected to be valid if a/h becomes too large.

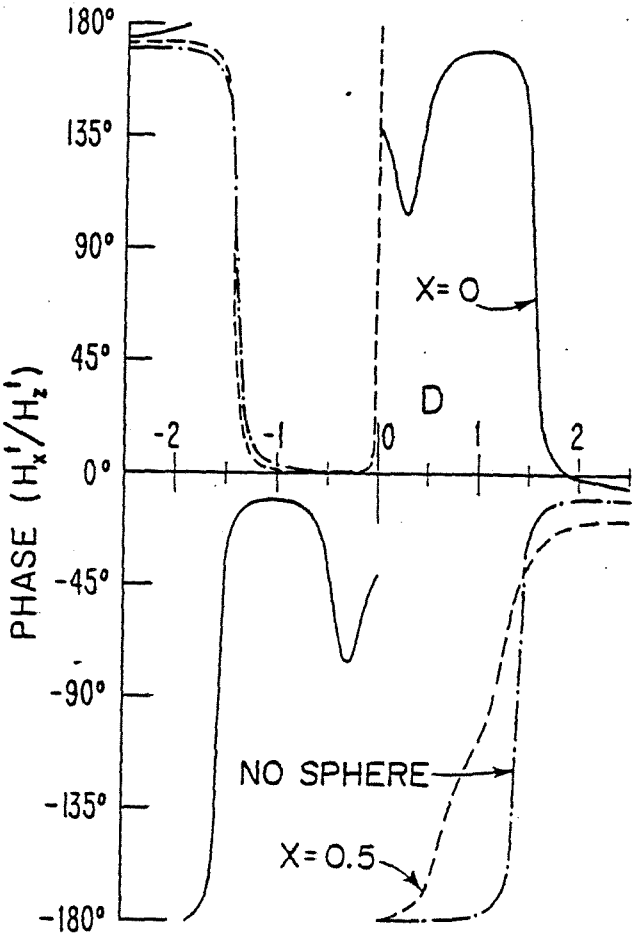


Fig. 3. Effect of sphere location on arg (H_z^t/H_x^t).

CONCLUDING REMARKS

A method for calculating the perturbation of the surface fields of a buried magnetic dipole has been developed. The method utilizes the reradiated fields of induced electric and magnetic dipole moments and is valid when the sphere radius is small compared with the source distance, the interface distance, and the wavelength in the earth.

A typical example shows that the magnitude and phase of the ratio of horizontal to vertical magnetic field can be noticeably altered by the presence of a sphere which is located at half the source depth and has a radius of 0.3 times the source depth. However, the variation of the surface fields as a function of position remains quite similar, and only small errors in source location should result.

Larger deviations can be expected when the sphere is larger or closer to the source or the interface, but the simplified theory presented here is not valid under such conditions. The study of this case is a worthwhile extension.

REFERENCES

Baños, A. (1966), *Dipole Radiation in the Presence of a Conducting Half-space*, pp. 195–230, Pergamon, New York.

D'Yakonov, B. P. (1959), The diffraction of electromagnetic waves by a sphere located in a half-space, *Bull. Acad. Sci. USSR, Geophys. Ser., 11*, 1120–1125.

Hill, D. A. (1970), Electromagnetic scattering concepts applied to the detection of targets near the ground, Ph.D. dissertation, pp. 90–100, Ohio State University, Columbus, Ohio.

Hill, D. A., and J. R. Wait (1972), Electromagnetic scattering of a small spherical obstacle near the ground, *Can. J. Phys., 50*(3), 237–243.

Stratton, J. A. (1941), *Electromagnetic Theory*, pp 563–573, McGraw-Hill, New York.

van de Hulst, H. C. (1957), *Light Scattering by Small Particles*, pp. xxx–xxx, John Wiley, New York.

Wait, J. R. (1951), The magnetic dipole over the horizontally stratified earth, *Can. J. Phys., 29*(6), 577–592.

Wait, J. R. (1960), On the electromagnetic response of a conducting sphere to a dipole field, *Geophysics, 25*(3), 649–658.

Wait, J. R. (1961), The electromagnetic fields of a horizontal dipole in the presence of a conducting half-space, *Can. J. Phys., 39*(7), 1017–1028.

Wait, J. R. (1968), Electromagnetic induction in a small conducting sphere above a resistive half-space, *Radio Sci., 3*(10), 1030–1034.

Wait, J. R. (1971), Criteria for locating an oscillating magnetic dipole buried in the earth, *Proc. IEEE, 59*(6), 1033–1035.

Wait, J. R. (1972), The effect of a buried conductor on the subsurface fields for line source excitation, *Radio Sci., 7*(5), 587–591.

Ward, S. H. (1959), Unique determination of conductivity, susceptibility, size, and depth in multifrequency electromagnetic exploration, *Geophysics, 24*, 531–546.

Ward, S. H. (1967), Electromagnetic theory for geophysical applications, in *Mining Geophysics*, vol. 2, edited by D. A. Hansen, W. R. Heinricks, Jr., R. C. Holmen, R. E. MacDougall, G. R. Rogers, J. S. S. Sumner, and S. H. Ward, pp. 10–196, Society of Exploration Geophysicists, Tulsa, Okla.

Wheelon, A. D. (1968), *Tables of Summable Series and Integrals Involving Bessel Function*, pp. 68–92, Holden-Day, San Francisco, Calif.

42

Radio Science, Volume 9, Number 1, pages 71–73, January 1974

Perturbation of magnetic dipole fields by a perfectly conducting prolate spheroid

David A. Hill and James R. Wait

Institute for Telecommunication Sciences, Office of Telecommunications, US Department of Commerce, Boulder, Colorado 80302

(Received September 6, 1973.)

The effect of a perfectly conducting prolate spheroid on the surface fields of a buried vertical magnetic dipole is examined in the quasi-static case. When the spheroid is in the vicinity of the source and near the surface, the errors introduced in source location can be significant. The results have possible application to rescue operations following coal mine disasters and in similar situations.

INTRODUCTION

The feasibility of locating a buried vertical magnetic dipole source (horizontal loop) from surface measurements of the vertical and horizontal magnetic field components has been investigated by *Wait* [1971]. For sufficiently low frequencies the air-earth interface has a negligible effect and a single observation of the complex ratio of the vertical and horizontal field components is sufficient for source location. Inhomogeneities in the earth distort the surface fields and may lead to errors in source location. To provide insight into this problem, the effect of a spherical inhomogeneity has been investigated [*Hill and Wait*, 1973].

Here we examine the effect of a perfectly conducting prolate spheroid for the case where the frequency is sufficiently low that currents in the surrounding medium can be neglected. Consequently, the situation reduces to a magnetostatic problem, and an exact solution is available [*Wait*, 1960]. The prolate spheroid is considered to be a reasonable model to study the influence of a finite or bounded conductor such as a metal pipe, railway conductor, or even an ore vein. At least it is not so idealized as a sphere.

FORMULATION

The geometry of the spheroid and source dipole is shown in Figure 1. The prolate spheroid is centered at the origin of a Cartesian coordinate system (x, y, z), and its major axis is coincident with the z axis. The semiminor axis a, semimajor axis b, and semifocal distance c are related by

$$c = (b^2 - a^2)^{1/2} \tag{1}$$

The prolate spheroidal coordinates are (η, δ, ϕ) and the surface of the spheroid is defined by $\eta = \eta_0$ where

$$\eta_0 = [1 - (a/b)^2]^{-1/2} \tag{2}$$

The boundary condition on the spheroid is that the normal component of the magnetic field must vanish. The resultant solution for the magnetic potential Ω of a magnetic point charge K located at (η', δ', ϕ') is [*Wait*, 1960]:

$$\Omega = (K/4\pi)\left[1/R - \sum_{n=0}^{\infty}\sum_{m=0}^{n} M_{mn} \cdot [P_n^m{}'(\eta_0)/Q_n^m{}'(\eta_0)]Q_n^m(\eta)P_n^m(\delta)\cos m(\phi - \phi')\right] \tag{3}$$

where

$$M_{mn} = [\epsilon_m(-1)^m/c](2n+1) \cdot [(n-m)!/(n+m)!]^2 Q_n^m(\eta')P_n^m(\delta')$$

$$\epsilon_m = \begin{cases} 1, & m = 0 \\ 2, & m \neq 0 \end{cases}$$

$$R = [(x-x')^2 + (y-y')^2 + (z-z')^2]^{1/2}$$

P_n^m and Q_n^m are associated Legendre functions of degree n and order m of the first and second kind, and prime denotes differentiation with respect to the argument. The definitions of P_n^m and Q_n^m follow those of *Smythe* [1968].

The magnetic field $\mathbf{H}$ of a y-directed magnetic dipole of strength Kdl is given by

$$\mathbf{H} = -dl\nabla(\partial/\partial y')\Omega \tag{4}$$

In order to simplify the results, we restrict both the source and the observer to the equatorial plane ($z = z' = 0$) as shown in Figure 1. Consequently, $H_z = 0$ and H_y is given by [*Wait*, 1960]

$$H_y = (Kdl/4\pi)\Big\{[3(y - y')^2/R^5 - 1/R^3] + (1/c)\sum_{n=0}^{\infty}\sum_{m=0}^{n}\epsilon_m(-1)^m \tag{5}$$
$$(2n + 1)[(n - m)!/(n + m)!]^2[P_n^{m\prime}(\eta_0)/Q_n^{m\prime}(\eta_0)] \cdot [P_n^m(0)]^2 V_n^m\Big\}$$

where

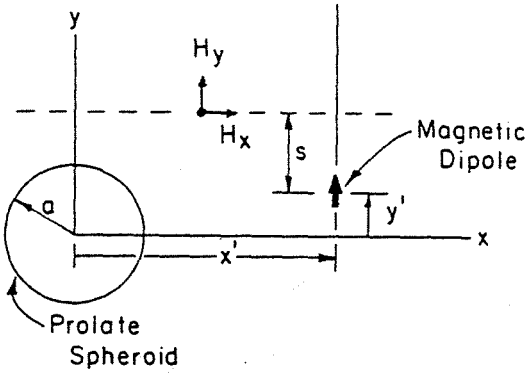


Fig. 1. Geometry for source and observer in the equatorial plane of a prolate spheroid ($z = 0$). The imagined earth-air interface is the plane $y = y' + s$.

$$V_n^m = Q_n^{m\prime}(\eta)Q_n^{m\prime}(\eta')\cos m(\phi - \phi')\{[(\sin\phi)/c](\eta^2 - 1)^{1/2}/\eta\}\{[(\sin\phi')/c][(\eta')^2 - 1]^{1/2}/\eta'\}$$
$$+ Q_n^m(\eta)Q_n^m(\eta')m^2\cos m(\phi - \phi)\{[(\cos\phi)/c](\eta^2 - 1)^{-1/2}\}\{[(\cos\phi')/c][(\eta')^2 - 1]^{-1/2}\}$$
$$- Q_n^m(\eta)Q_n^{m\prime}(\eta')m\sin m(\phi - \phi')\{[(\cos\phi)/c](\eta^2 - 1)^{-1/2}\}\{[(\sin\phi')/c][(\eta')^2 - 1]^{1/2}/\eta'\}$$
$$+ Q_n^{m\prime}(\eta)Q_n^m(\eta')m\sin m(\phi - \phi')\{[(\sin\phi)/c](\eta^2 - 1)^{-1/2}\}\{[(\cos\phi')/c][(\eta')^2 - 1]^{-1/2}\}$$

The following similar expression for H_x can be derived by applying (4) to (3):

$$H_x = (Kdl/4\pi)\Big\{-3(x - x')(y - y')R^{-5} + (1/c)\sum_{n=0}^{\infty}\sum_{m=0}^{n}\epsilon_m(-1)^m$$
$$(2n + 1)[(n - m)!/(n + m)!]^2[P_n^{m\prime}(\eta_0)/Q_n^{m\prime}(\eta_0)] \cdot [P_n^m(0)]^2 W_n^m\Big\} \tag{6}$$

where

$$W_n^m = Q_n^{m\prime}(\eta)Q_n^{m\prime}(\eta')\cos m(\phi - \phi')\{[(\cos\phi)/c](\eta^2 - 1)^{1/2}/\eta\}\{[(\sin\phi')/c][(\eta')^2 - 1]^{1/2}/\eta'\}$$
$$- Q_n^m(\eta)Q_n^m(\eta')m^2\cos m(\phi - \phi')\{[(\sin\phi)/c](\eta^2 - 1)^{-1/2}\}\{[(\cos\phi')/c][(\eta')^2 - 1]^{-1/2}\}$$
$$+ Q_n^m(\eta)Q_n^{m\prime}(\eta')m\sin m(\phi - \phi')\{[(\sin\phi)/c](\eta^2 - 1)^{-1/2}\}\{[(\sin\phi')/c][(\eta')^2 - 1]^{1/2}/\eta'\}$$
$$+ Q_n^{m\prime}(\eta)Q_n^m(\eta')m\sin m(\phi - \phi')\{[(\cos\phi)/c](\eta^2 - 1)^{1/2}/\eta\}\{[(\cos\phi')/c][(\eta')^2 - 1]^{-1/2}\}$$

The prolate spheroidal coordinates required in (5) and (6) are related to the Cartesian coordinates by:

$$\phi = \tan^{-1}(y/x),\ \eta = (1/c)(x^2 + y^2 + c^2)^{1/2} \tag{7}$$
$$\phi' = \tan^{-1}(y'/x'),\ \eta' = (1/c)[(x')^2 + (y')^2 + c^2]^{1/2}$$

NUMERICAL RESULTS

For the interesting case when both the source and observer are reasonably close to the observer, a large number of terms are required to achieve convergence of the summations in (5) and (6). Consequently, a computer subroutine was written for P_n^m which utilizes forward recurrence in n and m, and a subroutine was written for Q_n^m which utilizes backward recurrence in n and forward recurrence in m. The derivatives $P_n^{m\prime}$ and $Q_n^{m\prime}$ are easily obtained in terms of P_n^m and Q_n^m. Computed values for P_n^m, Q_n^m, $P_n^{m\prime}$, and $Q_n^{m\prime}$ checked exactly with tabulated six-figure values [*National Bureau of Standards*, 1945]. A computer program for H_x and H_y in (5) and (6) was then written and checked by requiring that the boundary condition was satisfied at the surface of the spheroid ($\eta = \eta_0$).

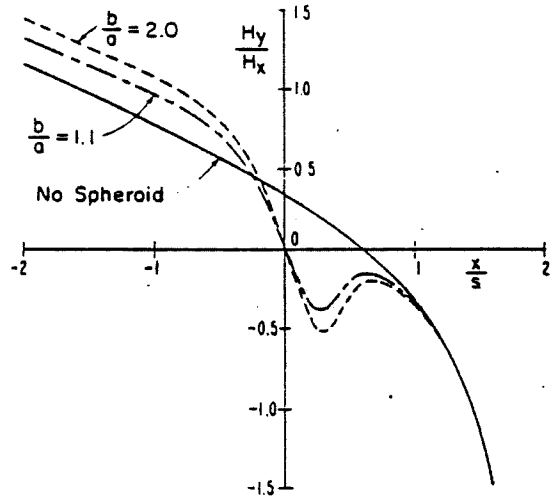


Fig. 2. Ratio of vertical to horizontal magnetic field component for a prolate spheroid which is tangent to the interface; $x'/s = 2$, $y'/s = -0.5$, and $a/s = 0.5$.

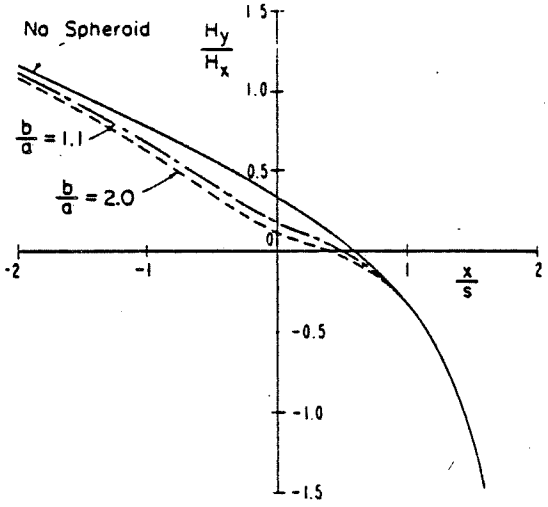


Fig. 3. Ratio of vertical to horizontal magnetic field component for a buried prolate spheroid; $x'/s = 2$, $y' = 0$, $a/s = 0.5$.

If we imagine that the earth-air interface is located at $y = s + y'$ as shown in Figure 1, then H_y and H_x are the vertical and horizontal magnetic field components that would be measured in a source location scheme. Since the ratio of vertical to horizontal components has been suggested as a useful quantity [*Wait*, 1971], the ratio H_y/H_x is shown as a function of x in Figure 2 for $a/s = 2$, $y'/s = -0.5$, and $x'/s = 2$. Since the spheroid is tangent to the interface at $x = 0$, the vertical component H_y is zero at $x = 0$. Note that a slightly larger anomaly occurs for the longer spheroid ($b/a = 2$). Results for the same case with the spheroid buried ($y' = 0$) are shown in Figure 3. The anomaly in H_y/H_x is somewhat weaker, but it occurs over a larger horizontal range.

CONCLUDING REMARKS

The exact quasi-static solution for a magnetic dipole in the presence of a perfectly conducting prolate spheroid has been used to calculate the perturbation of magnetic field components. Results in Figures 2 and 3 indicate that significant errors in source location could result when the spheroid is in the vicinity of the source and close to the interface.

REFERENCES

Hill, D. A., and J. R. Wait (1973), The electromagnetic response of a buried sphere for buried dipole excitation. *Radio Sci.*, *8*(8), in press.

National Bureau of Standards (1945), *Tables of Associated Legendre Functions*, 300 pp., Columbia University Press, New York.

Smythe, W. R. (1968), *Static and Dynamic Electricity*, 3rd ed., pp. 144–152, McGraw-Hill, New York.

Wait, J. R. (1960), Some solutions for electromagnetic problems involving spheroidal, spherical, and cylindrical bodies, *J. Res. Nat. Bur. Stand.*, *64B*(1), 15–32. (In this reference, in equation 12 and the following equations $-\partial/\partial y'$ should be $+\partial/\partial y'$ for a dipole in the positive y direction.)

Wait, J. R. (1971), Criteria for locating an oscillating magnetic dipole in the earth, *Proc. IEEE*, *59*(16), 1033–1035.

Pageoph
Vol. 105 (1973/IV)

Birkhäuser Verlag, Basel

Electromagnetic Transient Response of a Small Wire Loop Buried in a Homogeneous Conducting Earth

By DAVID A. HILL[1]) and JAMES R. WAIT[2])

Summary – The analysis extends previously obtained results for the transient magnetic fields of small loops in the presence of a homogeneous conducting half-space. Here, the secondary scattering of pulses by a buried target loop is examined for the case where both the source and receiver loops are located at the surface. While the response of the buried or target loop is orders of magnitude below the primary response, there is a significant difference in the respective transient waveforms. Thus, the results have possible application to mine rescue using a passive detection technique.

Introduction

A possible method of signaling to the earth's surface is to excite a buried loop with a transient current. The transmitted waveform undergoes considerable attenuation. It has been shown, however, that the waveform dispersion, as a function of source-receiver geometry, may provide a means of direction-finding and location of the active buried source (WAIT and HILL [1]).

Here, we consider scattering of a transient signal (generated at the surface) by a buried loop. This could be the basis of a passive location technique with possible application in mine rescue work following disasters. Naturally, the received scattered or secondary signal at the surface will be quite weak, but the characteristic wave shape may permit signal detection and location of the target loop. The latter could be any closed conductor, such as a one turn loop of No. 8 wire of radius of the order of 1 m. Of course, the advantage of such a system is that no power source is required at the buried terminal. Thus, it may have some possibility as the basis of a back-up scheme for the active methods which require a power source at the buried location.

We choose to work the problem entirely in the time domain since the necessary solutions for radiation by a small loop (magnetic dipole) in the presence of a conducting half-space can be represented in closed form in contrast to the Sommerfeld integral solutions that occur in the frequency domain solution in similar problems (TUAN and

[1]) Institute for Telecommunication Sciences, Office of Telecommunications, U.S. Department of Commerce.

[2]) Cooperative Institute for Research in Environmental Sciences, University of Colorado, Boulder, Colorado 80302, USA.

KING [2, 3]). Except in special cases, the latter require numerical integration (WAIT [4], COGGON and MORRISON [5]).

In the analysis that follows, displacement currents are considered negligible in comparison with conduction currents. This is not an intrinsic limitation of the method, and such neglect will not affect any of our conclusions.

Formulation of source field

In this section, we consider a source loop with an impulsive current located at the interface of a conducting half-space of conductivity σ, as shown in Fig. 1. The scattering or target loop is located at a depth h and at a horizontal distance ρ_s. Since we are interested in the voltage $v_s(t)$ induced in the scattering loop, we consider only the time derivative of the vertical magnetic field:

$$v_s(t) = A_s N_s \mu_0 \frac{\partial h_z^i(t)}{\partial t}, \tag{1}$$

where A_s is the area of the scattering loop, N_s is the number of turns in the scattering loop, μ_0 is the permeability of free space, and h_z^i is the vertical magnetic field incident on the loop.

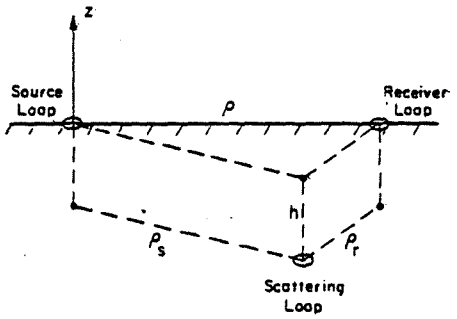


Figure 1
Geometry for source and receiver loops at the surface and scattering loop at depth h with the horizontal distances also shown

The current in the source loop $i(t)$ is assumed to be of the following form:

$$i(t) = Q_0 \delta(t), \tag{2}$$

where $\delta(t)$ is the unit impulse and Q_0 is a constant with dimensions of charge. MKS units are employed throughout. For this excitation, $v_s(t)$ is given by:

$$v_s(t) = -\frac{A_t N_t A_s N_s \mu_0 Q_0}{8\pi^{3/2} h^3 (\sigma \mu_0 h^2)^2} Y(D_s, T), \tag{3}$$

where A_t is the area of the transmitting loop (of infinitesimal size), N_t is the number of turns in the transmitting loop, $D_s = \rho_s/h$, and $T = t/(\sigma\mu_0 h^2)$. The function Y has been defined and tabulated earlier (WAIT and HILL [1]) and is given by:

$$Y(D,T) = \frac{\exp(-1/4T)}{T^{7/2}}\left\{\left(1-\frac{1}{2T}\right)\left(1-\frac{D^2}{4T}\right)\exp\left(-\frac{D^2}{4T^2}\right) + \left(\frac{\pi}{T}\right)^{1/2}\frac{\exp(-D^2/8T)}{4}\left[\left(3-\frac{3D^2}{2T}+\frac{D^4}{8T^2}\right)I_0\left(\frac{D^2}{8T}\right)+\left(\frac{D^2}{T}-\frac{D^4}{8T^2}\right)I_1\left(\frac{D^2}{8T}\right)\right]\right\}, \tag{4}$$

where I_0 and I_1 are the zero and first-order modified Bessel functions. All equations will hold only for positive t (or T) with all quantities equal to zero for negative t. Numerical results have also been given for loops of finite size (WAIT and HILL [6]).

The primary magnetic fields received at the surface in the absence of the scatterer are also of interest since the scattered field will be received in the presence of these fields. It is of course possible to construct a more sophisticated system of loops where these primary fields would be zero (under some assumptions of homogeneity), but the comparison for this simple system is still of some relevance. For a receiving loop oriented in the z and ρ directions, the primary received voltages v_z^p and v_ρ^p are given by:

$$\left.\begin{matrix} v_z^p(t) \\ v_\rho^p(t) \end{matrix}\right\} = A_r N_r \mu_0 \frac{\partial}{\partial t}\left\{\begin{matrix} h_z^p(t) \\ h_\rho^p(t) \end{matrix}\right., \tag{5}$$

where A_r is the area of the receiving loop, N_r is the number of turns in the receiving loop, and h_z^p and h_ρ^p are the z and ρ components of the primary magnetic field. By taking the limit, $h \to 0$, from previous results (WAIT and HILL [1]), the received voltages are found to be

$$\left.\begin{matrix} v_z^p(t) \\ v_\rho^p(t) \end{matrix}\right\} = K_p\left\{\begin{matrix} P_z(T_\rho) \\ P_\rho(T_\rho) \end{matrix}\right., \tag{6}$$

where

$$P_z(T_\rho) = \frac{\exp(-1/4T_\rho)}{T_\rho^{7/2}}\left(1-\frac{1}{4T_\rho}\right),$$

$$P_\rho(T_\rho) = \frac{\pi^{1/2}\exp(-1/8T_\rho)}{8T_\rho^4}\left[\left(3-\frac{1}{2T_\rho}\right)I_0\left(\frac{1}{8T_\rho}\right)+\left(\frac{1}{2T_\rho}-1\right)I_1\left(\frac{1}{8T_\rho}\right)\right],$$

$$T_\rho = t/(\sigma\mu_0\rho_r^2),$$

and

$$K_p = \frac{-A_t N_t A_r N_r \mu_0 Q_0}{8\pi^{3/2}\rho^2(\sigma\mu_0\rho^2)^2}.$$

The relatively simple form for v_z^p is expected since the corresponding frequency domain solution has a simple form involving exponential functions (WAIT [7], BANOS [8]). However, the same is not true for v_ρ^p, and it is only in the time domain that the closed form solution exists (WAIT [9]). Explicit curves for P_z and P_ρ are shown later in a comparison with the scattered waveforms.

Formulation of scattered field

In this section, we use a circuit theory approach to calculate the current in the scattering loop. This approach is equivalent to that used by GRANT and WEST [10] for a similar problem in the frequency domain. If the loop resistance and inductance are given by R_s and L_s, respectively, the impulse response $y_0(t)$ of the loop (i.e., the current produced by a unit voltage impulse) is given by

$$\begin{aligned} y_s(t) &= \frac{1}{L_s}\exp\left[\frac{-t}{(L_s/R_s)}\right] \\ &= \frac{1}{(\sigma\mu_0 h^2)R_s}\cdot\frac{\exp(-T/R)}{R}, \end{aligned} \tag{7}$$

where

$$R = \frac{L_s/R_s}{\sigma\mu_0 h^2}.$$

The quantity R is actually the ratio of the time constant of the loop (L_s/R_s) to the geometrical time constant ($\sigma\mu_0 h^2$).

The current $i_s(t)$ in the scattering or target loop is obtained from (3) and (7) by convolution. Thus

$$i_s(t) = \frac{-A_t N_t A_s N_s \mu_0 Q_0}{8\pi^{3/2} h^3 (\sigma\mu_0 h^2)^2 R_s}\, Y(D_s, T) * \frac{\exp(-T/R)}{R}, \tag{8}$$

where $D_s = \rho_s/h$ and where * denotes convolution in T.

$$\left\{\text{i.e., } Y(D,T)*\exp(-T/R) = \int_0^T Y(D,T')\exp[-(T-T')/R]\,dT'\right\}.$$

At this time, it is convenient to define two exponential response functions E_Y and E_X, which are given by the following convolution integral:

$$\begin{Bmatrix} E_Y(D,R,T) \\ E_X(D,R,T) \end{Bmatrix} = \frac{1}{R}\exp(-T/R) * \begin{Bmatrix} Y(D,T) \\ X(D,T) \end{Bmatrix}. \tag{9}$$

These functions are useful in cases where exponential currents occur, such as the inductor resistor model used here (or possibly a capacitor discharge source with inductance neglected) and they have the property of yielding the impulse or step responses under limiting conditions. The impulse responses are obtained by letting R approach zero:

$$\lim_{R\to 0}\begin{Bmatrix}E_Y(D,R,T)\\E_X(D,R,T)\end{Bmatrix}=\begin{matrix}Y(D,T)\\X(D,T)\end{matrix}. \tag{10}$$

The step responses $Y_s(D,T)$ and $X_s(D,T)$ (WAIT and HILL [11]) are obtained by letting R approach infinity:

$$\lim_{R\to\infty}\begin{Bmatrix}E_Y(D,R,T)\\E_X(D,R,T)\end{Bmatrix}=R\begin{Bmatrix}Y_s(D,T)\\X_s(D,T)\end{Bmatrix}. \tag{11}$$

We can use (9) to rewrite the current in (8) in a more compact form:

$$i_s(t)=\frac{-A_t N_t A_s N_s \mu_0 Q_0}{8\pi^{3/2}h^3(\sigma\mu_0 h^2)R_s}E_Y(D_s,T). \tag{12}$$

From the two limiting forms of E_Y, it is clear that the ratio of time constants R will have a strong effect on the current waveform.

Now that the current in the scattering loop is known, we can write the scattered field at the surface as the field of a magnetic dipole buried at a depth h and a horizontal distance ρ_r. If the vertical and horizontal components of the scattered magnetic field are detected by small loops with axes oriented vertically and horizontally, then the received voltages $v_z^s(t)$ and $v_\rho^s(t)$ are given by:

$$\begin{Bmatrix}v_z^s(t)\\v_\rho^s(t)\end{Bmatrix}=\frac{A_t N_t A_s^2 N_s^2 A_r N_r \mu_0^2 Q_0}{64\pi^3 h^6(\sigma\mu_0 h^2)^3 R_s}\cdot\begin{Bmatrix}E_Y(D_s,T)*Y(D_r,T)\\\cos\phi_r\, E_Y(D_s,T)*X(D_r,T)\end{Bmatrix}, \tag{13}$$

Here, A_r is the area of the receiving loop, N_r is the number of turns in the receiving loop, $D_r=\rho_r/h$, ϕ_r is the angle between the vertical plane containing the centers of the scattering and receiving loops and axis of the horizontal receiving loop. The function $X(D_r,T)$ in (13) was defined previously (WAIT and HILL [1]):

$$X(D,T)=\frac{\exp(-1/4T)}{T^{7/2}}\left\{\frac{D}{T}\left(1-\frac{D^2}{8T}\right)\exp\left(-\frac{D^2}{T}\right)\right.$$
$$\left.+\frac{D}{4}\left(\frac{\pi}{T}\right)^{1/2}\left(1-\frac{1}{2T}\right)\exp\left(-\frac{D^2}{8T}\right)\cdot\left[\left(\frac{3}{2}-\frac{D^2}{4T}\right)I_0\left(\frac{D^2}{8T}\right)+\left(\frac{D^2}{4T}-\frac{1}{2}\right)I_1\left(\frac{D^2}{8T}\right)\right]\right\}. \tag{14}$$

For simplicity, we choose to define two final dimensionless functions S_Y and S_X, which represent the received scattered waveforms:

$$\left.\begin{matrix} S_Y(D_s, D_r, T) \\ S_X(D_s, D_r, T) \end{matrix}\right\} = \left\{\begin{matrix} E_Y(D_s, T) * Y(D_r, T) \\ E_Y(D_s, T) * X(D_r, T) \end{matrix}\right. \tag{15}$$

Using (15), we can write (13) in the final form:

$$\left.\begin{matrix} v_z^s(t) \\ v_\rho^s(t) \end{matrix}\right\} = K_s \left\{\begin{matrix} S_Y(D_s, D_r, T) \\ S_X(D_s, D_r, T) \end{matrix}\right., \tag{16}$$

where

$$K_s = \frac{A_t N_r A_s^2 N_s^2 A_r N_r \mu_0^2 Q_0}{64\pi^3 h^6 (\sigma\mu_0 h^2)^3 R_s}.$$

Consequently, the wave shapes are described by the dimensionless functions S_Y and S_X, and the magnitudes are given by K_s which has dimensions of volts.

Numerical example

The number of parameters associated with this problem is so large that a complete numerical investigation of the various waveforms would be prohibitive. Consequently, we consider a representative case as shown in Fig. 2. The depth of the scattering loop is assumed to be known, and the received scattered waveforms are now calculated for

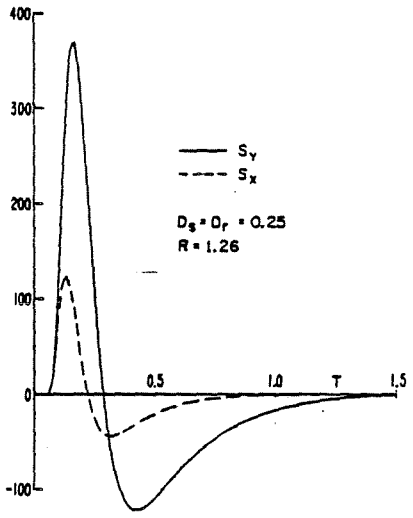


Figure 2
Waveforms for the vertical and horizontal scattering responses, S_Y and S_X, for $D_s = D_r = .25$

three different scatterer or target locations. Also, the source and receiver locations are fixed. The following numerical values are used in this example:

$$h = 200 \text{ m}; \quad \rho = 100 \text{ m}; \quad \rho_s = \rho_r = 50 \text{ m}, 100 \text{ m}, 200 \text{ m}; \quad \sigma = 10^{-2} \text{ mhos/m};$$
$$A_s = \pi \text{ m}^2; \quad N_s = 1; \quad R_s = .0259 \text{ ohms}; \quad L_s = 1.87 \times 10^{-5} \text{ Henries}. \tag{17}$$

The resistance of the loop R_s is calculated by using the resistance per unit length of No. 8 copper wire (MINER and SEASTONE [12]). The loop is assumed to be circular with radius 1 m. The inductance is calculated from the static formula (SMYTHE [13]):

$$L_s = \mu_0 a \left[\ln\left(\frac{8a}{b}\right) - 2 \right], \tag{18}$$

where a is the loop radius, and b is the wire radius (for No. 8 copper wire).

The use of circuit theory might be questioned in the present context. A possible verification is that the magnetic polarizability of a perfectly conducting loop calculated using the variational technique (KOUYOUMJIAN [14]) agrees with the circuit theory if the inductance as given by (18) is used. The inductance of multiturn loops has also been treated (KING [15]), but the expressions are quite complicated.

From (17), the following calculated quantities are:

$$\sigma\mu_0 h^2 = 500 \ \mu\text{sec}; \quad \sigma\mu_0 \rho^2 = 125 \ \mu\text{sec}; \quad L_s/R_s = 630 \ \mu\text{sec};$$
$$R = 1.26; \quad D_s = D_r = .25, .5, 1. \tag{18}$$

In Figs. 3–5, the scattered waveforms S_Y and S_X are shown for the three different scatterer locations. The significant dependence of waveform on the geometry indicates that the diagnosis of wave shapes may be useful in source location. The waveforms of the primary fields P_Y and P_X are shown in Fig. 6. A log scale is used so that the small, medium, and large time values can be seen. An interesting feature is that the primary waveforms have already passed into a smooth decay by the time the scattered waveforms are just beginning to rise ($T \simeq .1$ or $T_\rho \simeq .4$). This feature would be beneficial for the detection of the scattered waveforms. The fact that P_X has a $T_\rho^{-3/2}$ singularity at the origin is of no consequence, since none of the results are valid for very short times (i.e., for $t < \varepsilon/\sigma \simeq 10^{-3}$ μsec).

The relative magnitudes of the scattered and primary voltages are important considerations if waveforms are to be detected and diagnosed. The ratio of K_s to K_ρ is a good indication of signal strengths even though the peaks of previously plotted functions differ considerably. From (6) and (16), K_s/K_ρ is in general found to be:

$$K_s/K_p = \frac{-A_s^2 N_s^2 \mu_0}{8\pi^{3/2} h^3 (\sigma\mu h^2) R_s} \left(\frac{\rho}{h}\right)^7. \tag{19}$$

The ratio is seen to be highly dependent on depth and horizontal distance [i.e., it varies as ρ^7/h^{12}]. For the parameters given in (17), we find $K_s/K_\rho = -1.33 \times 10^{-11}$. However, this number can be increased many orders of magnitude by varying some of the parameters favorably. For instance, if we change h to 63.3 m and σ to 10^{-3} mhos/m, the

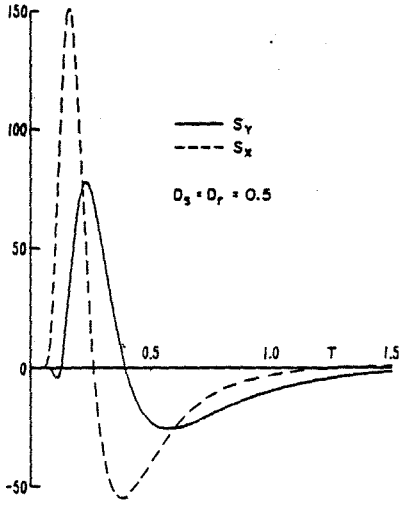


Figure 3
Waveforms for the vertical and horizontal scattering responses, S_Y and S_X, for $D_s = D_r = .5$

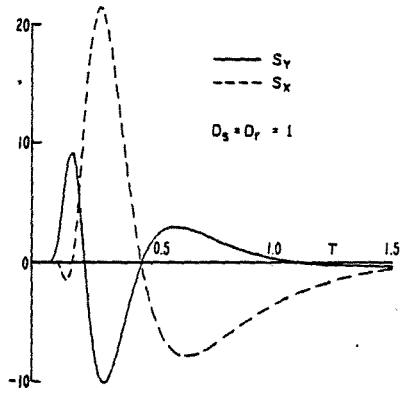


Figure 4
Waveforms for the vertical and horizontal scattering responses, S_Y and S_X, for $D_s = D_r = 1$

ratio becomes -1.33×10^{-4}. Also, major benefits could be realized by increasing loop area and wire radius. However, in any useful case, it appears that the significant difference in wave shape needs to be utilized to detect the scattered waveform.

If signal-to-noise level is to be considered, it is desirable to know the absolute magnitudes of v_z^s and v_ρ^s, which are proportional to K_s in (16). This can be readily computed if the values for A_r, N_r, A_t, N_t, and Q_0 are known.

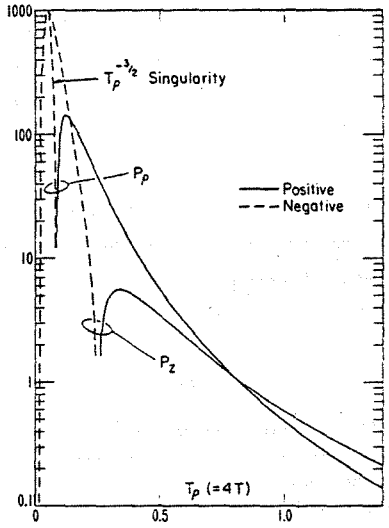


Figure 5
Vertical and horizontal primary responses, P_z and P_ρ, as a function of normalized time T_ρ

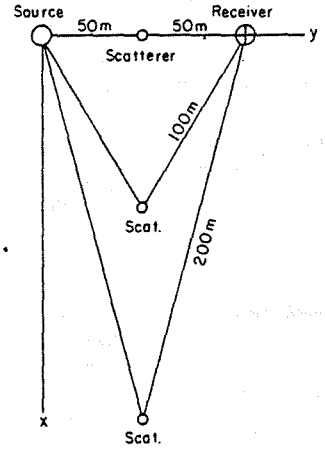


Figure 6
Top view of the source and receiver loops at the surface with three different locations of the scattering loop at a depth of 200 m

Concluding remarks

Previous results for the transient magnetic fields of small loops (magnetic dipoles) in the presence of a conducting half-space have been used to calculate, via circuit theory, the fields scattered by a buried loop. The application to direction-finding and target location has been considered. Even though the scattered response is many orders of magnitude below the primary response, we have shown that the time delay and difference in wave shape of the target response offers some hope for detection.

The results given here apply for an impulsive current in the source loop, but other excitations can be treated using convolution. In fact, a numerical convolution program is already used in the calculation of the scattered response. Another possible extension would be loading of the scattering loop which could again be treated by modifying the transient response of the loop in the convolution program. One further area of interest, both here and in the direct signaling problem, is the possibility of layering in the half-space. Frequency domain values have been computed (WAIT and SPIES [16]), and transient results could be obtained by numerical inverse transforms. It would be interesting to know whether layering would strongly influence the wave shape diagnosis which must be used in direction-finding.

REFERENCES

[1] J. R. WAIT and D. A. HILL, *Transient signals from a buried magnetic dipole*, J. Appl. Phys. *42* (10) (1971), 3866–3869. [Note that in (22′), the factor multiplying I_1 should be $[\rho^2/\alpha - \rho^4/(8\alpha^2)]$, and that multiplying I_1 in (30) should be $[D^2/T - D^4/(8T^2)]$. Also, in (27), the factor $[1 - D^2/(2T)]$ should be $[1 - D^2/(4T)]$.

[2] H. S. TUAN and R. W. P. KING, *Current in a scattering antenna embedded in a dissipative half space*, Radio Sci. *1* (11) (New Ser.) (1966), 1309–1319.

[3] H. S. TUAN and R. W. P. KING, *Radiation from a scattering antenna embedded in a dissipative half space*, Radio Sci. *3* (6) (New Ser.) (1968), 577–584.

[4] J. R. WAIT, *Mutual electromagnetic coupling of loops over a homogeneous ground*, Geophysics *20* (1955), 630–637.

[5] J. H. COGGON and H. F. MORRISON, *Electromagnetic investigation of the sea floor*, Geophysics *35* (1970), 476–489.

[6] J. R. WAIT and D. A. Hill, *Transient electromagnetic fields of a finite circular loop in the presence of a conducting half-space*, J. Appl. Phys. *43* (1972, in press).

[7] J. R. WAIT, *The magnetic dipole over the horizontally stratified earth*, Can. J. Phys. *29* (1951), 577–592.

[8] A. BANOS, *Dipole Radiation in the Presence of a Conducting Half Space* (Pergamon Press, Oxford, England 1965), p. 103.

[9] J. R. WAIT, *Electromagnetic fields of sources in lossy media*, Chapt. 24 in *Antenna Theory*, Pt. II (edited by R. E. COLLIN and F. J. ZUCKER) (McGraw-Hill Book Co., New York 1969).

[10] F. S. GRANT and G. F. WEST, *Interpretation Theory in Applied Geophysics* (McGraw-Hill Book Co., New York 1965), pp. 486–492.

[11] J. R. WAIT and D. A. HILL, *Transient magnetic fields produced by a step-function excited loop buried in the earth*, Elect. Letrs. (1972, in press).

[12] D. F. MINER and J. B. SEASTONE, *Handbook of Engineering Materials* (Wiley and Sons, New York 1965), pp. 1–90.

[13] W. R. SMYTHE, *Static and Dynamic Electricity* (McGraw-Hill Book Co., New York 1950), pp. 317–318.

[14] R. G. KOUYOUMJIAN, *The backscattering from a circular loop*, Appl. Sci. Res. (Sec. B) *6* (1956), 165–179.

[15] R. W. P. KING, *Fundamental Electromagnetic Theory* (Dover Publications, New York 1963), pp. 450–456.

[16] J. R. WAIT and K. P. SPIES, *Evaluation of the surface electromagnetic fields for a buried magnetic dipole source*, Air Force Cambridge Research Laboratories Scientific Rept. No. 52, 5 Feb. 1971, Contract No. PRO-Y-71-872.

(Received 19th August 1972)

Pageoph, Vol. 114 (1976), Birkhäuser Verlag, Basel

Analysis of Source Location Errors for a Magnetic Dipole Buried in a Laterally Inhomogeneous Conducting Earth

By C. H. STOYER[1]) and J. R. WAIT[2])

Summary – A numerical model is used to simulate a vertical magnetic dipole (VMD), with time harmonic excitation, buried under a segmented overburden. Results are presented in terms of readily measured field quantities. Of special interest are the ellipticities of the magnetic field in the vertical and horizontal planes. These turn out to be very sensitive to the lateral variation of the conductivity structure. Other parameters, such as the vertical magnetic field on the surface, are much less influenced. It is suggested that the combination of such measurements should lead to an optimum system for source location in application to mine rescue operations.

Introduction

Many experiments have been carried out in recent years to simulate the location of a buried vertical magnetic dipole (VMD) source, such as might be carried by, or made available to, trapped miners [LARGE, BALL and FARSTAD, 1973]. Even though the frequencies used are low (10^2–10^3 Hz), the conductive earth distorts the signal, and these distortions can give rise to appreciable errors in determining the location of the source. Major distortions are due to lateral variation of conductivity that can be natural or artificial (pipes, cables, etc.). In the case of artificial conductors, the location is usually well known, and can be accounted for. However, the natural conductivity structure of the earth in the vicinity of the buried dipole is not always so well known. Since the dipole location methods are primarily intended for the location of a miner trapped or lost in a mine accident, it is important that some knowledge of the conductivity structure be known, since mines are often located in the vicinity of anomalous conductors.

The purpose of this numerical modelling experiment is to look at the surface magnetic fields of a buried VMD in the presence of a laterally inhomogeneous overburden, to see if the field measurements normally made in an attempt to locate the buried source can show the structure of the earth as well. If this is so, then adjustments to the apparent location might be made in the field, to provide a more accurate

[1]) Now at Physics/Earth Science Depts., Box 3D, New Mexico State University, Las Cruces, New Mexico, 88001, USA.

[2]) Cooperative Institute for Research in Environmental Sciences, University of Colorado, Boulder, Colorado 80302, USA.

determination of the location of the buried VMD. For convenience, the observer is chosen to be at a height of 8 meters above the earth's surface. But for all practical purposes, the results for zero height would be the same.

The earth model chosen here is two-dimensional in that non-uniformity may exist in the vertical and in one of the horizontal directions. This is to be contrasted with the special three dimensional configurations treated by HILL and WAIT [1973].

Method

The three magnetic field components from a dipolar source are computed at a height of 8 m above the two-dimensional earth using the method developed by STOYER [1974] and STOYER and GREENFIELD [1975]. This is a finite difference method, whereby Maxwell's equations are solved on a rectangular grid in the wavenumber (k_x) domain, and inverse Fourier transformation of the computed fields for several k_x values yields space domain results. The strike of the structure is in the x-direction.

The model used for the segmented overburden is shown in Fig. 1. Tests were also made by replacing the conductive zone (10^{-1} mho/m) with conductivities of 10^{-3} mho/m and 10^{-2} mho/m (the half-space conductivity). The former did not yield significant distortions and are not presented. The latter was used as a check to detect distortions produced by the sides of the finite difference grid. The frequency is 400 Hz for all computations.

The three-component magnetic fields can be presented in the form of six different contour maps representing simulated measurements in a plane 8 m above the earth's surface. In each case the position (0, 0) marks the projection of the buried source on to this plane and is the true location. Apparent locations are derived from the simulated field measurements. These include the strike angle of the field (y direction = 0°) which goes from zero to 90 degrees, the horizontal ellipticity, which is the minor axis divided by the major axis of the polarization ellipse in the x-y plane, the tilt angle and vertical

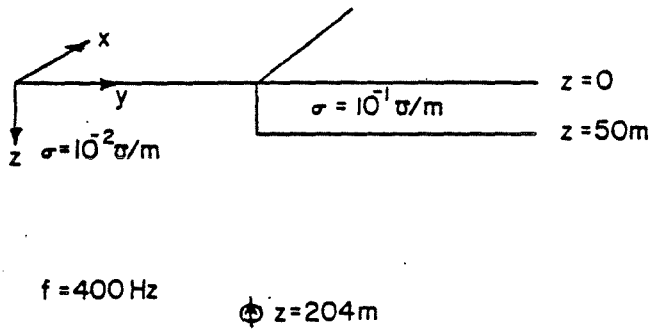


Figure 1
Two dimensional model used with a buried VMD source.

ellipticity, which lie in the vertical plane oriented in the direction of the strike angle, and the magnitude of the vertical and the horizontal magnetic fields, expressed as percent of maximum field. An explicit description of these parameters is given in Appendix A. The horizontal and vertical polarization ellipses are shown in Fig. 2. These measurements were chosen because they can all be made in the field with a wire coil attached to a filter and AC voltmeter without the use of more complicated electronic systems. A detailed discussion on the polarization ellipse is given by SMITH and WARD [1974].

Results

Apparent locations of a buried dipole are usually obtained from measurements made on the surface of the earth in the vicinity of the expected location. If these measurements are also required to indicate the conductivity structure of the earth, there must be a change in spatial pattern of the measured quantity with respect to structure and its position relative to the buried source. Indeed, the best indicator of subsurface structure might be a quantity which is zero in the absence of lateral inhomogeneities. In any case, parameters which are mainly a function of position with respect to the source will probably not be good indications of structure and quantities which are strongly structure dependent are probably poor indicators of source position. The contour maps presented here show measurable quantities which fall into both of these categories.

When the earth is flat and homogeneous, the projection of the source on to the surface is marked by maximum vertical magnetic field, minimum horizontal field, maximum (90°) tilt angle (the field vector points away from the source at all other points), and minimum vertical ellipticity. All of these quantities have concentric circular patterns when contour mapped over the surface. The horizontal ellipticity, however, is zero everywhere if conductivity is axially symmetric about the axis of the buried VMD. If this is not the case, non-radial components of horizontal fields are generated which are not in phase with the 'primary' field. The result is that the horizontal field does not have a true null, the apparent location is in error (it is moved away from the conductor), and the horizontal field is elliptical, in general. Hence, the

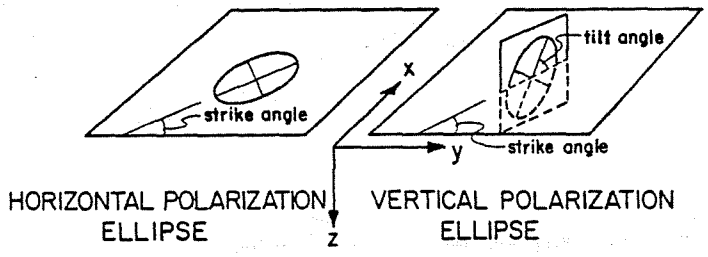


Figure 2
The polarization ellipses.

horizontal ellipticity should be a good indicator of near-surface lateral structure which gives rise to errors in apparent location.

The contour maps presented here give a good indication of which parameters are sensitive to source location and which are sensitive to structure. Maps of the vertical magnetic field are shown for two source positions, one with very small location error (~1 m) in Fig. 3 and one with large error (9 m) in Fig. 4. Note that the low contrast in this model will not give rise to large errors in apparent location, such as have been generated by a previous model [STOYER, 1974] or have been measured in the field [FARSTAD, 1973].

Note that these two patterns are essentially identical, although higher conductivity contrasts, which will yield larger apparent location errors, will probably produce some pattern difference. The broadness of the peak limits the usefulness of the vertical field in location of the buried source.

For the same source positions, the horizontal field $[|H_x|^2 + |H_y|^2]^{1/2}$ shows somewhat more change in pattern. These are shown in Figs. 5 and 6. Even though the horizontal field is often used in dipole location experiments, the minimum in the field can be significantly shifted by lateral variation in overburden conductivity [STOYER, 1974]. Figure 7 shows a contour map of horizontal field which yielded a location error of about 6 m. Note that the contours in the vicinity of the peak field (two 90% contours) show significant distortion.

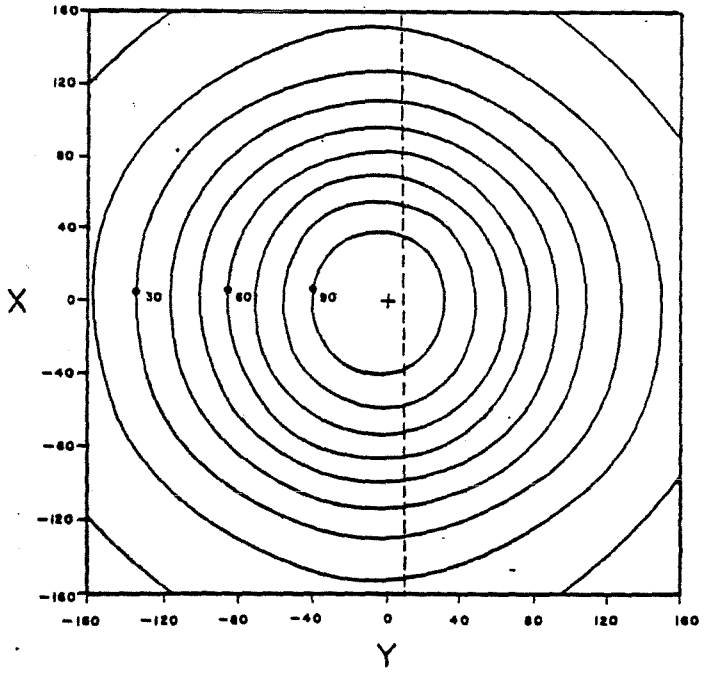


Figure 3
Contour map of vertical magnetic field (H_z) above a buried VMD source (d = 204 m). Overburden is segmented about dashed line with higher conductivity to the right. Location error is <1 m. Contours are percent of maximum field.

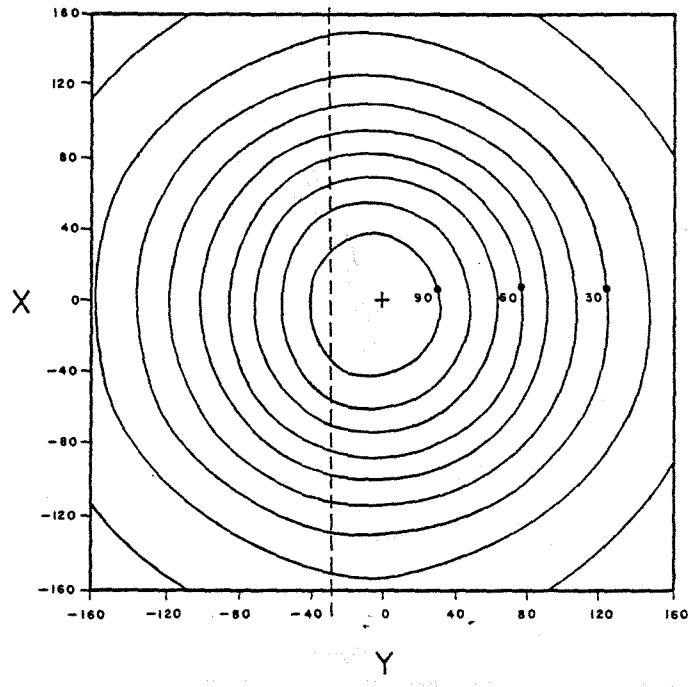


Figure 4
Contour map of vertical magnetic field (H_z) above a buried VMD source (d = 204 m). Overburden is segmented about dashed line with higher conductivity to the right. Location error is about 9 m. Contours are percent of maximum field.

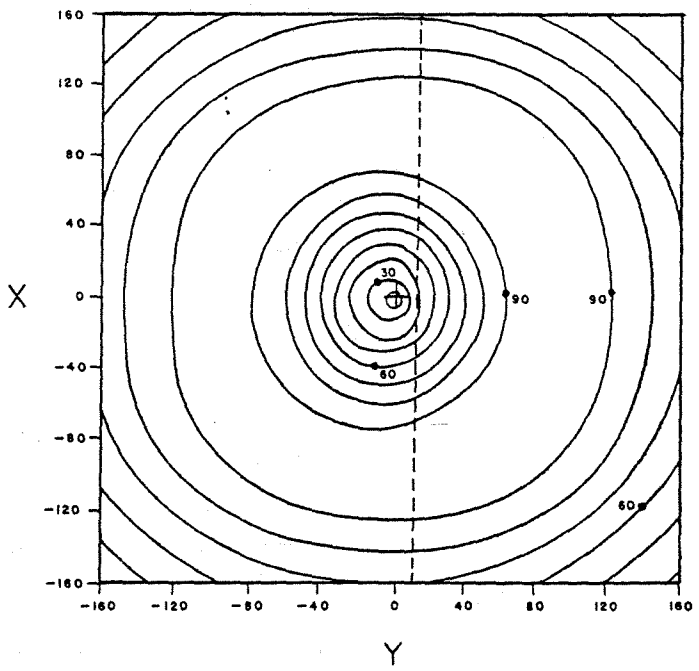


Figure 5
Contour map of the horizontal magnetic field in percent of maximum field. Contour interval is 10%. Overburden is segmented about dashed line with overburden on the right. Location error is < 1 m. (Note triangular form of contour is artifact of computer plotting.)

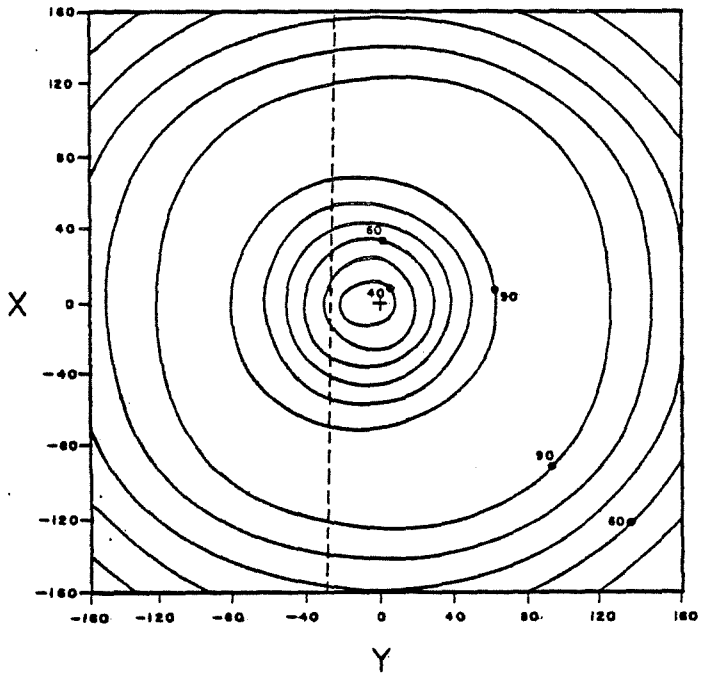


Figure 6
Contour map of horizontal magnetic field expressed as percent of maximum. Contour interval is 10%. Overburden is segmented about dashed line with higher conductivity to the right. Location error is 9 m.

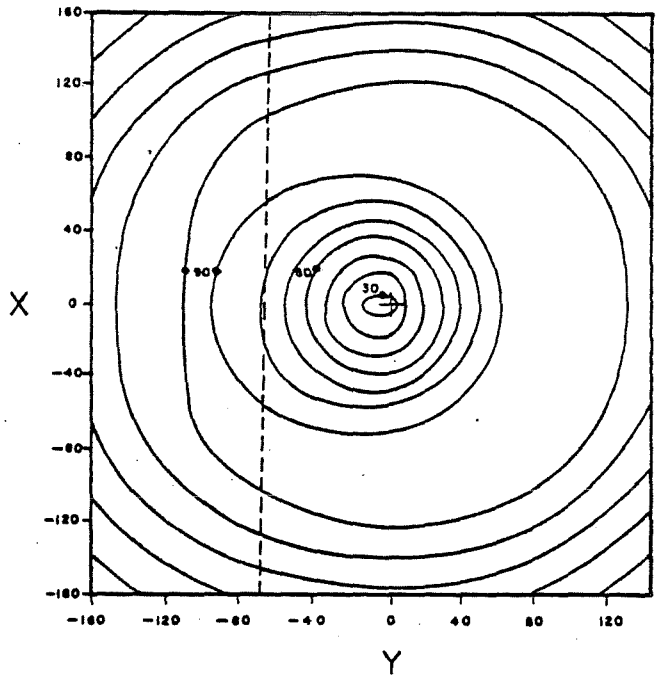


Figure 7
Contour map of horizontal field expressed as percent of maximum. Contour interval is 10%. Overburden is segmented about dashed line with higher conductivity to the right. Location error is 6 m.

Previous results [STOYER, 1974] indicate that the tilt angle measurement is the best indicator of source position in the x-y plane. Although it might seem that 90° tilt angle would coincide with minimum horizontal field, this is not so when lateral variation of conductivity is high, since secondary horizontal fields are not in phase with the strong primary vertical field. Hence, maximum (90°) tilt angle does not occur at the same location as minimum horizontal field. Contour maps of tilt angle show patterns of similar nature to the vertical field measurement but with sharper peaks. None of the tilt angle maps produced from this model show any significant pattern change with position and are not presented. However, for higher contrasts, and thus significant location errors, significant pattern differences should appear.

The most significant pattern differences in this experiment were observed in the contour maps of vertical and horizontal ellipticity. Different source locations had not only different patterns, but different magnitudes of ellipticities along with different location errors.

Vertical ellipticities always exist due to interfaces in the x-y plane (e.g., the surface of the earth). Figure 8 shows the vertical ellipticity pattern of a source which is under the lower conductivity overburden segment, 70 meters distant from the projected edge of the conductor. The ellipticities are of magnitude similar to the homogeneous case, except that the pattern is severely distorted (it is non-circular), especially in the vicinity of the conductor. Figure 9 shows the source projected 10 m from the conductor. The source is under the conductor in Fig. 10, 30 meters from the projected edge. Note that

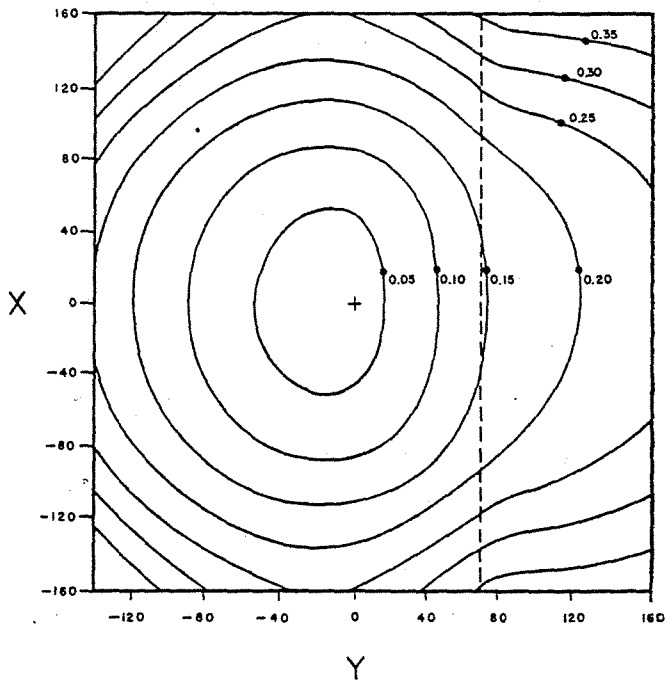


Figure 8
Vertical ellipticities contoured in intervals of 0.05. The overburden is segmented about the dashed line with the more conductive zone on the right.

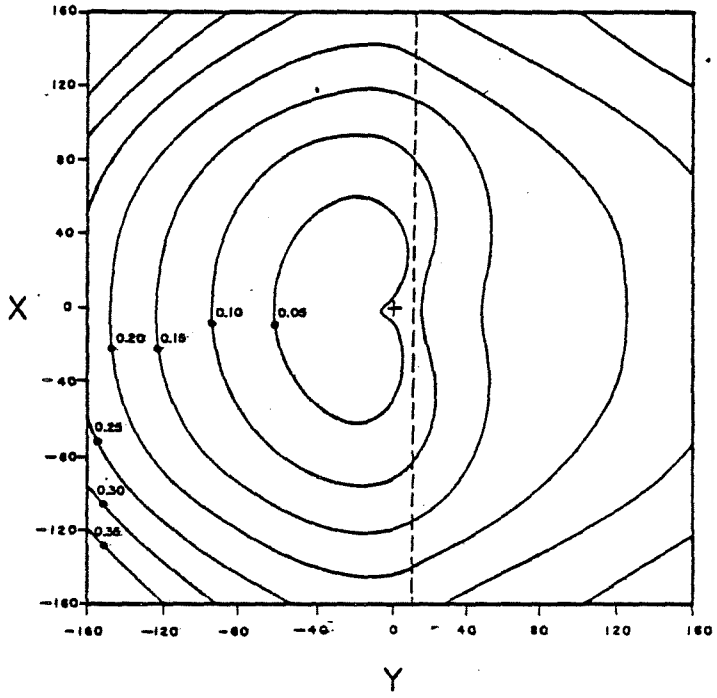


Figure 9
Vertical ellipticities contoured in intervals of 0.05. The overburden is segmented about the dashed line with the more conductive zone on the right.

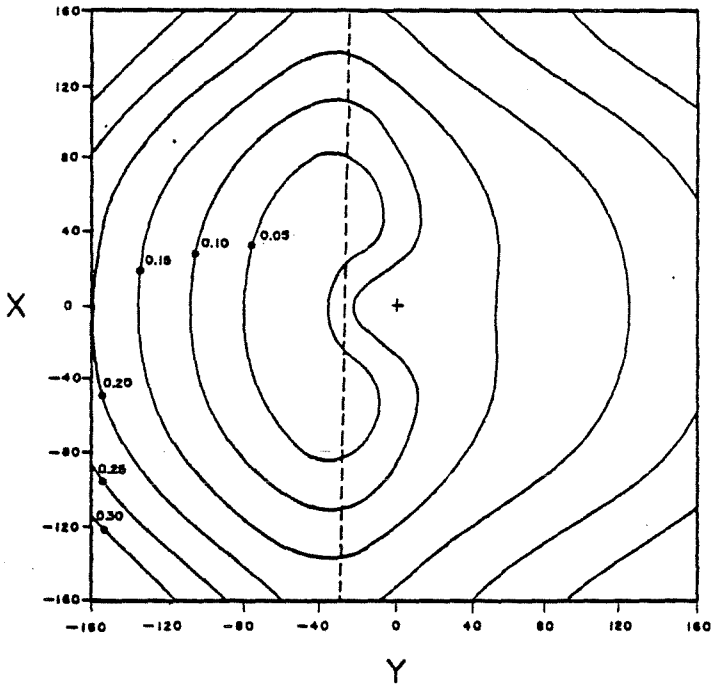


Figure 10
Vertical ellipticities contoured in intervals of 0.05. The overburden is segmented about the dashed line with the more conductive zone on the right.

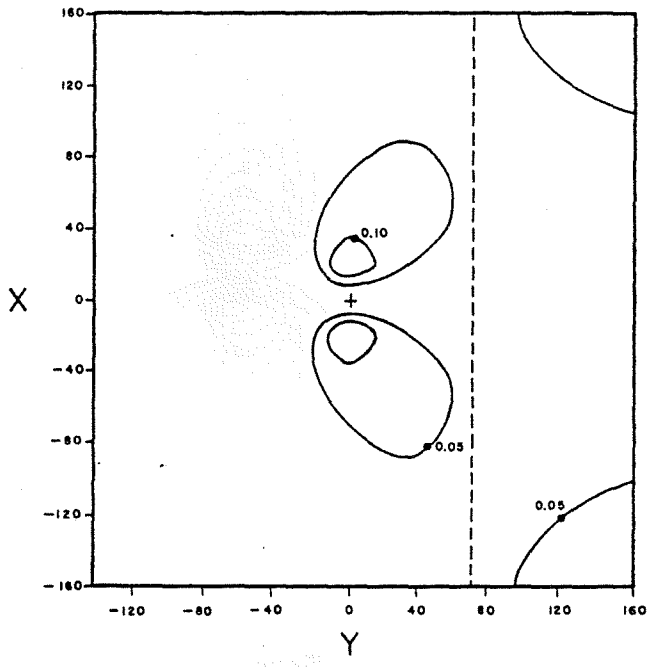


Figure 11
Horizontal ellipticity contoured in intervals of 0.05. The overburden is segmented with the more conductive side to the right of the dashed line.

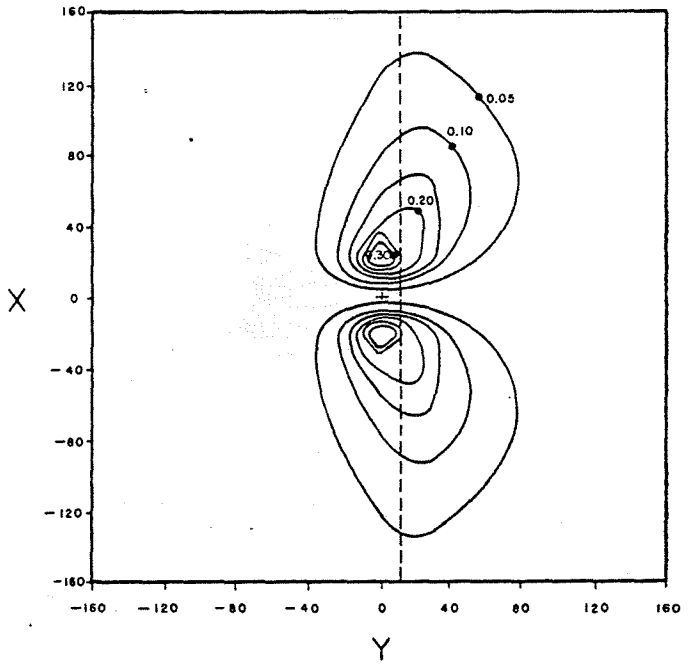


Figure 12
Horizontal ellipticity contoured in intervals of 0.05. The overburden is segmented with the more conductive side to the right of the dashed line.

64 64

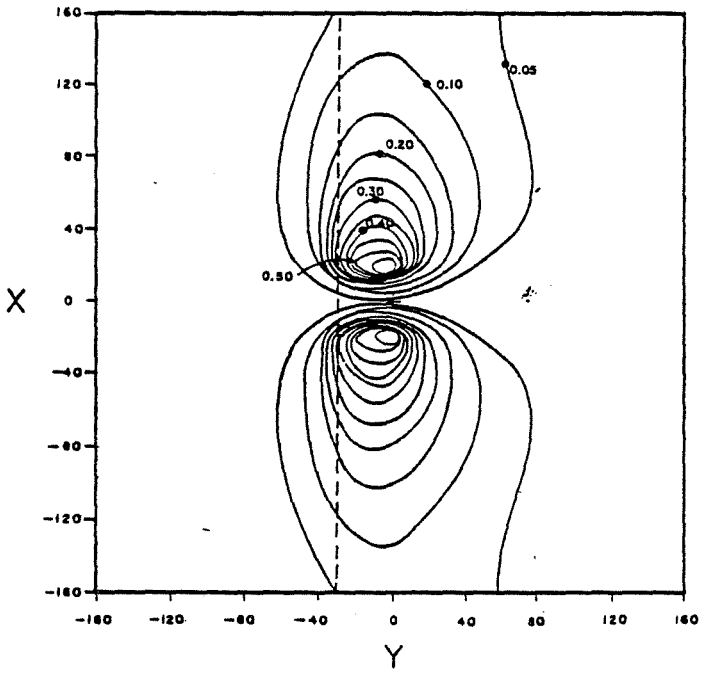


Figure 13
Horizontal ellipticity contoured in intervals of 0.05. The overburden is segmented with the more conductive side to the right of the dashed line.

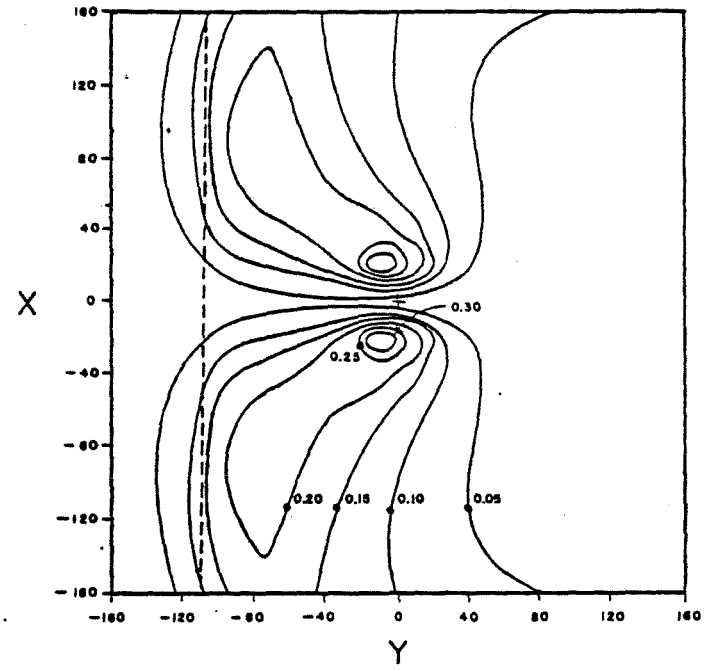


Figure 14
Horizontal ellipticity contoured in intervals of 0.05. The overburden is segmented with the more conductive side to the right of the dashed line.

the distortion in the ellipticities increases as the source moves under the conductor. Thus it seems that the vertical ellipticity measurements contain a significant amount of information about the relative positions of the source and conductor if not about the magnitude and direction of a location error.

The horizontal ellipticity, however, is a direct manifestation of lateral conductivity variation, since it is zero for a layered half-space. Like the vertical ellipticity, the horizontal ellipticity changes pattern as the source moves under the conductive overburden segment (Figs. 11, 12, 13, and 14), but the magnitude increases as well. The lobed pattern of the horizontal ellipticity seems to point in the direction of the conductor's edge. The maximum value increases from about 0.10 to about 0.55, but decreases again as the source moves under the conductor. This shows that horizontal ellipticity measurements might be quite useful in estimating the accuracy of an apparent location or in estimating a correction, and therefore in improving buried dipole location methods.

Discussion

The results presented in this paper show that low conductivity contrasts (~ 10) in the overburden do not significantly effect the apparent location of a buried VMD source. They also show that ellipticity patterns and magnitudes are quite responsive to the lateral conductivity variations which give rise to location errors. While the patterns of magnetic field amplitude and tilt angle are not nearly as sensitive to lateral conductivity changes as ellipticities, larger or more highly conducting bodies can produce changes in the patterns of these, as shown by a previous modelling experiment [STOYER, 1974].

Calculations at frequencies other than 400 Hz would also be worthwhile. In fact, there may be some advantage in a multi-frequency system but this, of course, would lead to undesirable complexity in the transmitter circuitry.

Several recommendations for future study are in order. To the authors' knowledge, none of the field experiments have measured ellipticities of magnetic fields. These should be measured and reported, especially in cases where significant location errors exist. Further modelling work needs to be done to see if conductors which do produce significant location errors can be detected from field measurements, and to see if these location errors can be corrected from raw field data. In addition, the effect of deeper conductors needs to be tested to see what sort of location errors and possible on site corrections might be made.

APPENDIX

The horizontal and vertical polarization ellipses

The three components of the magnetic field are not in phase, in general, and the total field vector sweeps out an ellipsoidal solid. By considering only the two

components which lie in a plane, we can discuss the behavior of the magnetic field in terms of two polarization ellipses. The derived parameters are readily measured by an amplitude sensitive field system.

SMITH and WARD [1974] give a detailed analysis of the polarization parameters in the y-z plane. We shall first consider the fields H_x and H_y, which lie in the plane $z = \text{const}$. The strike angle of the polarization ellipse (α) is the strike angle of the major axis, while the ellipticity (e_h) is the ratio of the major to the minor axis. (Note that this differs from the ellipticity used by pure mathematicians.) From Smith and Ward, we have

$$\alpha = \tfrac{1}{2} \arctan \left[\frac{\pm 2(H_x/H_y) \cos \Delta\phi}{1 - (H_x/H_y)^2} \right],$$

where the magnetic fields are $H_x \exp(i\phi_x)$ and $H_y \exp(i\phi_y)$ and $\Delta\phi = \phi_x - \phi_y$. The ellipticity, e_h, is given by

$$e_h = \frac{|H_x \exp(i\Delta\phi) \cos\alpha - H_y \sin\alpha|}{|H_x \exp(i\Delta\phi) \sin\alpha + H_y \cos\alpha|}.$$

Once these parameters are known, we can consider the vertical polarization ellipse which lies in the plane $x = y \sin\alpha$. The tilt angle (β) and the vertical ellipticity (e_v) are computed via the formulae

$$\beta = \tfrac{1}{2} \arctan \left[\frac{\pm 2(H_z/H_p) \cos \Delta\phi}{1 - (H_z/H_p)^2} \right]$$

$$e_v = \frac{|H_z \exp(i\Delta\phi) \cos\beta - H_p \sin\beta|}{|H_z \exp(i\Delta\phi) \sin\beta + H_p \cos\beta|}$$

where the magnetic fields are $H_z \exp(i\phi_z)$ and $H_p \exp(i\phi_p) = H_x \exp(i\phi_x) \sin\alpha + H_y \exp(i\phi_y) \cos\alpha$ and $\Delta\phi = \phi_z - \phi_p$.

These four measurements contain all of the information present in the three component magnetic fields, except for the absolute amplitude and phase of the fields. This is consistent with assumed ignorance of the amplitude and phase of the transmitted field.

REFERENCES

D. A. HILL and J. R. WAIT (1973), *The electromagnetic response of a buried sphere for buried-dipole excitation*, Radio Science *8* (8, 9), 813–818.

D. B. LARGE, L. BALL and A. J. FARSTAD (1973), *Radio transmission to and from underground coal mines – Theory and measurement*, IEEE Trans. on Comm. *COM-21* (3), 194–202.

B. D. SMITH and S. H. WARD (1974), *On the computation of polarization ellipse parameters*, Geophysics *39* (6), 867–869.

C. H. STOYER (1974), *Numerical solutions of the response of a two-dimensional earth to an oscillating magnetic dipole source with application to a groundwater field study*, Ph.D. thesis, The Pennsylvania State University.

C. H. STOYER and R. J. GREENFIELD (1975), *Numerical solutions of the response of a two-dimensional earth to an oscillating magnetic dipole source*, Paper accepted for publication in Geophysics.

(Received 19th February 1975)

Radio Science, Volume 8, Numbers 8, 9, pages 805–810, August-September 1973

Subsurface electromagnetic fields of a line source on a two-layer earth

James R. Wait and Kenneth P. Spies

Institute for Telecommunication Sciences, Office of Telecommunications, US Department of Commerce, Boulder, Colorado 80302

(Received January 22, 1973; revised January 29, 1973.)

A previous analysis for a line source on a homogeneous half-space model of the earth is extended to allow for the presence of stratification. The formal integral solution is reduced to a form suitable for numerical integration. Also, a number of special cases and limiting forms are considered. It is shown that the subsurface field has a structure that can be significantly modified when the half-space is no longer homogeneous. The results have application to the design of electromagnetic techniques in mine rescue operations.

INTRODUCTION

Communication from a surface-based transmitter and an observer buried in the earth must be established following mine disasters. Because telephone wires and other normal means of communication can be interrupted, it is desirable that the electromagnetic signals propagate directly through the earth medium. In such situations, a desirable transmitting facility consists of a long insulated cable excited by an audio-frequency electric current. The fields at a subsurface point can be detected either by a multiturn loop or by the voltage induced in wire connecting two electrodes. The latter may be metal roof bolts or other metal probes that have good contact with the host rock.

If the length of the transmitter cable is much greater than all other physical dimensions, we can assume, for purposes of analysis, that the subsurface fields are the same as those for an infinite line source of uniform current. In other words, the resultant fields are those produced by induction rather than by conduction. Unfortunately, the situation is complicated by the presence of the inhomogeneous overburden that both attenuates and distorts the subsurface fields. In a previous investigation, *Wait and Spies* [1971] considered a homogeneous conducting half-space model that permitted an explicit calculation of the fields for a time-harmonic source current. Also, *Wait* [1971] advocated the use of such cable fields in a direction-finding scheme. This would permit as subsurface observer to determine his location relative to the surface-based transmitter. In such cases, it may be necessary to employ an array of such cables with a capability to allow a subsurface point to be scanned in a regular sequence.

A fundamental limitation to any down-link communication or subsurface location scheme is imposed by the conductive inhomogeneous over-burden. With this motivation in mind, we extend our earlier analysis to a two-layer half-space. In particular, we are interested in how the structure of the subsurface field is modified when the conductivity of the upper layer differs from the conductivity of the lower layer. Such a condition is typical in most environments in the vicinity of coal mines, although we admit that the model is still highly idealized.

THE INTEGRAL FORMULATION

With reference to the rectangular coordinate system shown in Figure 1, a layered nonmagnetic half-space consists of a homogeneous slab of conductivity σ_1 occupying the region $0 < y < h_1$, and a semi-infinite homogeneous medium of conductivity σ_2 occupying the region $y > h_1$, while a uniform line-source current I coincides with the z axis. If the fields vary with time as $\exp(i\omega t)$, and the frequency is sufficiently low that displacement currents are negligible compared with conduction currents, the non-vanishing field components at a subsurface point (x, h) are given by

$$H_x = \begin{cases} -\frac{I}{\pi}\int_0^\infty \frac{u_1}{u_1+\lambda}\left[\frac{\exp(-u_1h) - R\exp[-u_1(2h_1-h)]}{1-RR_0\exp(-2u_1h_1)}\right]\cos\lambda x\,d\lambda & 0 < h \le h_1 \\ -\frac{I}{\pi}\int_0^\infty \frac{u_1}{u_1+\lambda}\left[\frac{(1-R)\exp(-u_1h_1)\exp[-u_2(h-h_1)]}{1-RR_0\exp(-2u_1h_1)}\right]\cos\lambda x\,d\lambda & h_1 \le h \end{cases} \tag{1}$$

$$H_y = \begin{cases} \frac{I}{\pi}\int_0^\infty \frac{\lambda}{u_1+\lambda}\left[\frac{\exp(-u_1h) + R\exp[-u_1(2h_1-h)]}{1-RR_0\exp(-2u_1h_1)}\right]\sin\lambda x\,d\lambda & 0 < h \le h_1 \\ \frac{I}{\pi}\int_0^\infty \frac{\lambda}{u_1+\lambda}\left[\frac{(1+R)\exp(-u_1h_1)\exp[-u_2(h-h_1)]}{1-RR_0\exp(-2u_1h_1)}\right]\sin\lambda x\,d\lambda & h_1 \le h \end{cases} \tag{2}$$

$$E_z = \begin{cases} -\frac{i\mu_0\omega I}{\pi}\int_0^\infty \frac{1}{u_1+\lambda}\left[\frac{\exp(-u_1h) + R\exp[-u_1(2h_1-h)]}{1-RR_0\exp(-2u_1h_1)}\right]\cos\lambda x\,d\lambda & 0 < h \le h_1 \\ -\frac{i\mu_0\omega I}{\pi}\int_0^\infty \frac{1}{u_1+\lambda}\left[\frac{(1+R)\exp(-u_1h_1)\exp[-u_2(h-h_1)]}{1-RR_0\exp(-2u_1h_1)}\right]\cos\lambda x\,d\lambda & h_1 \le h \end{cases} \tag{3}$$

where

$$R = (u_1 - u_2)/(u_1 + u_2)$$

$$R_0 = (u_1 - \lambda)/(u_1 + \lambda)$$

where

$$u_j = (\lambda^2 + \gamma_j^2)^{1/2}$$

$$\gamma_j^2 = i\sigma_j\mu_0\omega$$

$$j = 1, 2$$

The relevant formal theory for this layered geometry is available [*Wait*, 1970]. We remark here that (a) the field components satisfy the appropriate Helmholtz equation in the layers, (b) the field components are all continuous at the interface $y = h_1$, (c) the fields all decay exponentially as $y \to \infty$, and (d) the fields reduce to those for a uniform half-space if $h_1 \to \infty$ and/or if $\sigma_1 \to \sigma_2$.

For numerical work, it is convenient to express these components in terms of the following dimensionless parameters:

$$X = x/h$$

$$H = (\sigma_1\mu_0\omega)^{1/2}h$$

$$D = (\sigma_1\mu_0\omega)^{1/2}h_1$$

$$K = \sigma_2/\sigma_1$$

Also, as indicated below, we change the variable of integration to a dimensionless $s = \lambda h$. Then, the fields may be written as

$$H_x = -(I/2\pi h)A \tag{4}$$

$$H_y = (I/2\pi h)B \tag{5}$$

$$E_z = -(i\mu_0\omega I/2\pi)F \tag{6}$$

where A, B, and F are dimensionless field functions that conform to an earlier analysis for the homogeneous half-space model. For the configuration being considered here, we see that

$$A = \int_0^\infty a(s)\cos Xs\,ds \tag{7}$$

$$B = \int_0^\infty b(s)\sin Xs\,ds \tag{8}$$

and

$$F = \int_0^\infty f(s)\cos Xs\,ds \tag{9}$$

where

$$a(s) = \begin{cases} \frac{2(s^2+iH^2)^{1/2}}{(s^2+iH^2)^{1/2}+s}\,\frac{\exp[-(s^2+iH^2)^{1/2}] - R\exp[-(2D/H-1)(s^2+iH^2)^{1/2}]}{1-RR_0\exp[-2(D/H)(s^2+iH^2)^{1/2}]} & 0 \le H \le D \\ \frac{2(s^2+iH^2)^{1/2}}{(s^2+iH^2)^{1/2}+s}\,\frac{(1-R)\exp[-(D/H)(s^2+iH^2)^{1/2} - (1-D/H)(s^2+iKH^2)^{1/2}]}{1-RR_0\exp[-2(D/H)(s^2+iH^2)^{1/2}]} & D \le H \end{cases} \tag{10}$$

$$b(s) = \begin{cases} \dfrac{2s}{(s^2 + iH^2)^{1/2} + s} \dfrac{\exp\,[-(s^2 + iH^2)^{1/2}] + R \exp\,[-(2D/H - 1)(s^2 + iH^2)^{1/2}]}{1 - RR_0 \exp\,[-2(D/H)(s^2 + iH^2)^{1/2}]} \\ \qquad\qquad 0 \leq H \leq D \qquad (11) \\ \dfrac{2s}{(s^2 + iH^2)^{1/2} + s} \dfrac{(1 - R) \exp\,[-(D/H)(s^2 + iH^2)^{1/2} - (1 - D/H)(s^2 + iKH^2)^{1/2}]}{1 - RR_0 \exp\,[-2(D/H)(s^2 + iH^2)^{1/2}]} \\ \qquad\qquad D \leq H \end{cases}$$

$$f(s) = [b(s)]/s = \begin{cases} \dfrac{2}{(s^2 + iH^2)^{1/2} + s} \dfrac{\exp\,[-(s^2 + iH^2)^{1/2}] + R \exp\,[-(2D/H - 1)(s^2 + iH^2)^{1/2}]}{1 - RR_0 \exp\,[-2(D/H)(s^2 + iH^2)^{1/2}]} \\ \qquad\qquad 0 < H \leq D \qquad (12) \\ \dfrac{2}{(s^2 + iH^2)^{1/2} + s} \dfrac{(1 + R) \exp\,[-(D/H)(s^2 + iH^2)^{1/2} - (1 - D/H)(s^2 + iKH^2)^{1/2}]}{1 - RR_0 \exp\,[-2(D/H)(s^2 + iH^2)^{1/2}]} \\ \qquad\qquad D \leq H \end{cases}$$

$$R = \frac{(s^2 + iH^2)^{1/2} - (s^2 + iKH^2)^{1/2}}{(s^2 + iH^2)^{1/2} + (s^2 + iKH^2)^{1/2}} \qquad (13)$$

$$R_0 = \frac{(s^2 + iH^2)^{1/2} - s}{(s^2 + iH^2)^{1/2} + s} \qquad (14)$$

Our task is to calculate A, B, F, where X, H, D/H, and K are given.

SPECIAL CASES AND LIMITING FORMS

First of all, we note that if $K = 1$ (i.e., if $\sigma_1 = \sigma_2$), then $R = 0$ and

$$a(s) = \frac{2(s^2 + iH^2)^{1/2}}{(s^2 + iH^2)^{1/2} + s} \exp\,[-(s^2 + iH^2)^{1/2}] \qquad (15)$$

$$b(s) = sf(s)$$

$$= \frac{2s}{(s^2 + iH^2)^{1/2} + s} \exp\,[-(s^2 + iH^2)^{1/2}] \qquad (16)$$

thus, A, B, and F reduce, as they should, to the forms for a homogeneous half-space (1). On the other hand, if $H = 0$ corresponding to the frequency tending to 0, then $R = R_0$ and

$$a(s) = b(s) = \exp\,(-s) \qquad (17)$$

$$f(s) = [\exp\,(-s)]/s \qquad (18)$$

Therefore

$$A = \int_0^\infty [\exp\,(-s)] \cos\, Xs\, ds = 1/(1 + X^2) \qquad (19)$$

$$B = \int_0^\infty [\exp\,(-s)] \sin\, Xs\, ds = X/(1 + X^2) \qquad (20)$$

In this static limit, the integral for F does not converge, since the integrand behaves as $1/s$, near the origin. In this case, however, it is not difficult to show that

$$E_z \propto \lim_{\omega \to 0} (\omega \log \omega) \to 0$$

Another special case that is useful for checking the numerical data given below is to let $h_1 \to 0$. Thus, we should recover the results for a homogeneous half-space with conductivity σ_2. For example, if we use the functional notation $A = A(H, X, K, D)$ for the general two-layer case, we see that

$$A(H, X, K, 0) = A(K^{1/2}H, X) \qquad (21)$$

where

$$A(H, X) = 2 \int_0^\infty \frac{(s^2 + iH^2)^{1/2}}{(s^2 + iH^2)^{1/2} + s} \cdot \{\exp\,[-(s^2 + iH^2)^{1/2}]\} \cos\, sX\, ds \qquad (22)$$

This is one of the integrals considered before (1) for the homogeneous half-space. The same identity applies to the field functions B and F.

A limiting case of the two-layer formulation oc-

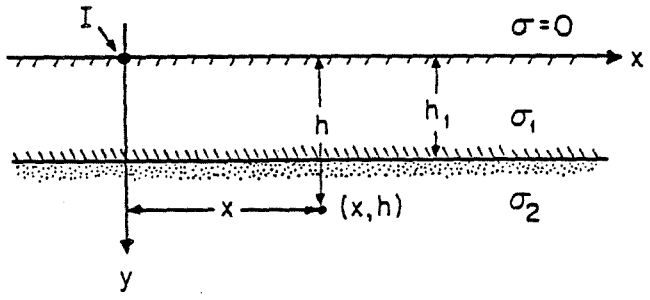


Fig. 1. Two-layer model of the earth for excitation by a uniform line current on the surface.

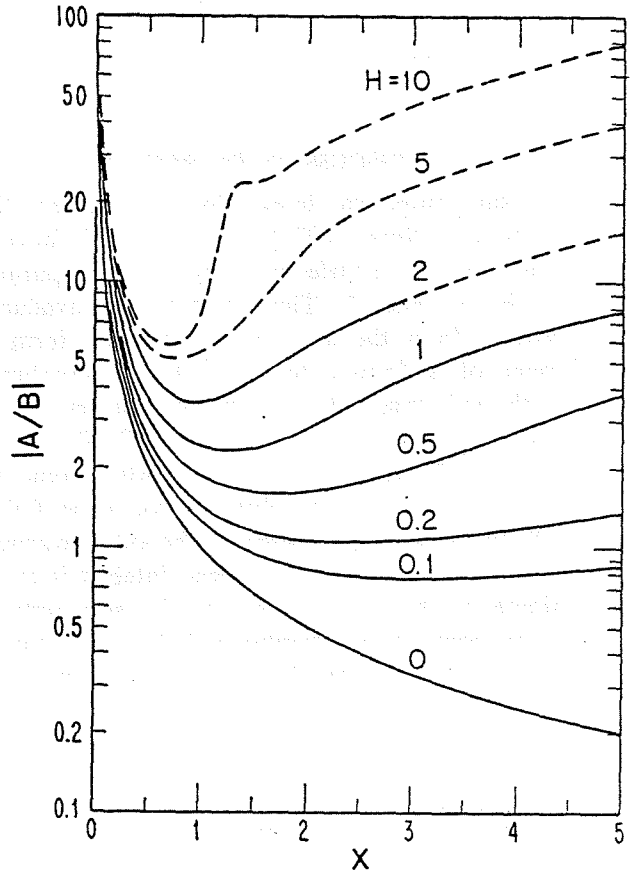


Fig. 2. Ratio between the horizontal and the vertical components of the magnetic field at a subsurface observing point located in the lower stratum of a two-layer earth. For this figure and for the succeeding ones, $X = x/h$, $H = (\sigma_2\mu_0\omega)^{1/2}\ h$, $D/H = h_1/h$, and $K = \sigma_2/\sigma_1$. For this figure $D/H = 0.5$, and $K = 10$.

curs when $x \to \infty$ [*Wait*, 1970]. In this high-frequency limit, the electric field E_z varies as $x^{-3/2}$ exp $(-i\ k_0\ x)$, where k_0 is the free-space wave number. This fact emerges from a general asymptotic development for the far-zone fields of a line source on a stratified half-space (3). Provided $|k_0\ x| \ll 1$, being consistent with the neglect of displacement currents, E_z varies simply as x^{-2} in this quasi-static asymptotic range. Some results for this case were given by *Bannister* [1968], who was specifically interested in the application to the measurement of the conductivity of the sea bed. In his case, the parameters equivalent to $|\gamma_1 x|$ and $|\gamma_2 x|$ were very large so that the fields could be described by their quasi-static asymptotic forms. In our contemplated application to mine rescue procedures, we would seldom be working in a frequency or distance range where these asymptotic results could be used. Nevertheless, they do serve as an excellent check on the numerical integration results discussed below.

In the notation used here, the quasi-static asymptotic results are valid if both HX and $K^{1/2}HX$ are sufficiently large (i.e., greater than about 5). Then we find that

$$A \simeq 2QP/(i^{1/2}HX^2) \tag{23}$$

$$B \simeq 2Q^2G/(iH^2X^3) \tag{24}$$

and

$$F \simeq 2Q^2G/(iH^2X^2) \tag{25}$$

where Q is the commonly encountered wave-tilt factor [*Wait*, 1970] given by

$$Q = [1 + r \exp(-2i^{1/2}D)]/[1 - r \exp(-2i^{1/2}D)] \tag{26}$$

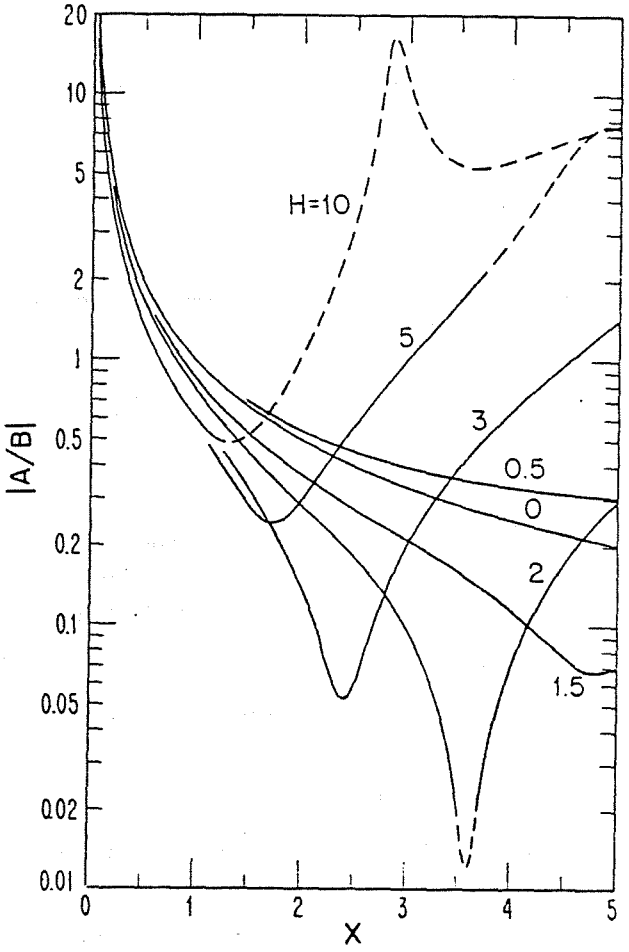


Fig. 3. Ratio between the horizontal and the vertical components of the magnetic field at a subsurface observing point located in the lower stratum of a two-layer earth. $D/H = 0.5$; $K = 0.1$.

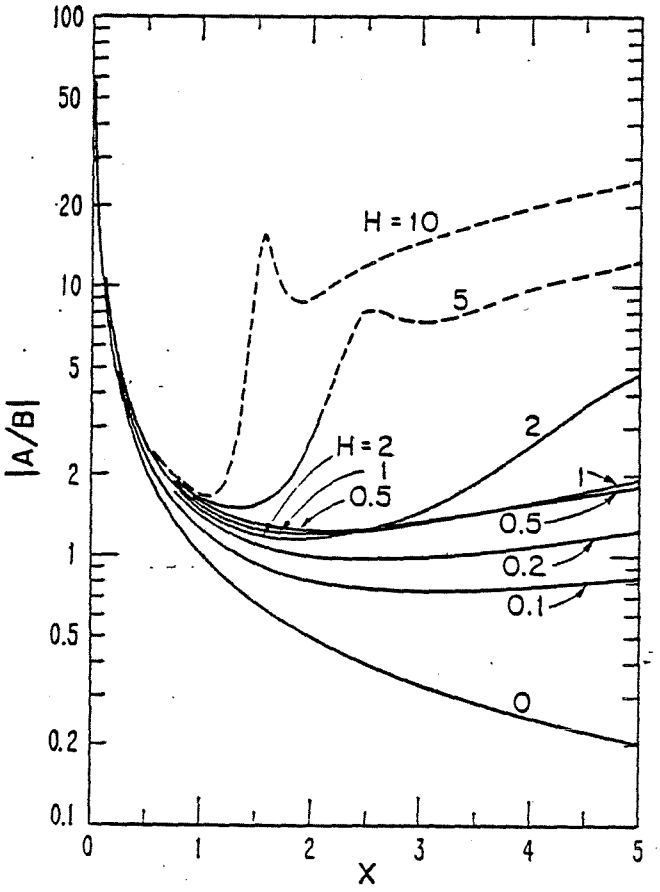


Fig. 4. Ratio of the field components when the observing point is within the upper stratum. $D/H = 2$; $K = 10$.

and r is a reflection coefficient defined by

$$r = \lim_{\epsilon \to 0} R = (1 - K^{1/2})/(1 + K^{1/2}) \qquad (27)$$

Here, G and P are depth-gain functions that correspond to the ratio of the field at depth H to that at the surface. These are found to have the form

$$G = [\exp(-i^{1/2}H) + r \cdot \exp(-2i^{1/2}D + i^{1/2}H)]/[1 + r\exp(-2i^{1/2}D)] \qquad (28)$$

$$P = [\exp(-i^{1/2}H) - r \cdot \exp(-2i^{1/2}D + i^{1/2}H)]/[1 - r\exp(-2i^{1/2}D)] \qquad (29)$$

for $0 < H \leq D$. The corresponding forms in the lower region are

$$G = \{(1 + r)/[1 + r\exp(-2i^{1/2}D)]\} \cdot \exp[-i^{1/2}D - i^{1/2}(H - D)K^{1/2}] \qquad (30)$$

$$P = \{(1 - r)/[1 - r\exp(-2i^{1/2}D)]\} \cdot \exp[-i^{1/2}D - i^{1/2}(H - D)K^{1/2}] \qquad (31)$$

for $H \geq D$.

DISCUSSION OF RESULTS

Using numerical integration as discussed before [*Wait and Spies*, 1971], A, B, and F have been evaluated for a selected range of the parameters X, H, K, and D. These results are available on request from the authors in tabulated form for a range of X from 0 to 5 and for all combinations of the following values of the parameters: $H = 0.1$, 0.2, 0.5, 1.0, 1.5, 0.2, 0.5, 1.0, 2.0; $D/H = h_1/h = 0.5$, 1.0, 2.0; $K = 0.1$, 10. Also, some values of A, B, and F were obtained for $K = 0.01$ and 100 for a restricted range of the other parameters.

A derived quantity of special interest is the magnitude of the ratio H_x/H_y at the sub-surface observer point. As we mentioned before (1), this ratio, equal to $|A/B|$, can be measured by two crossed

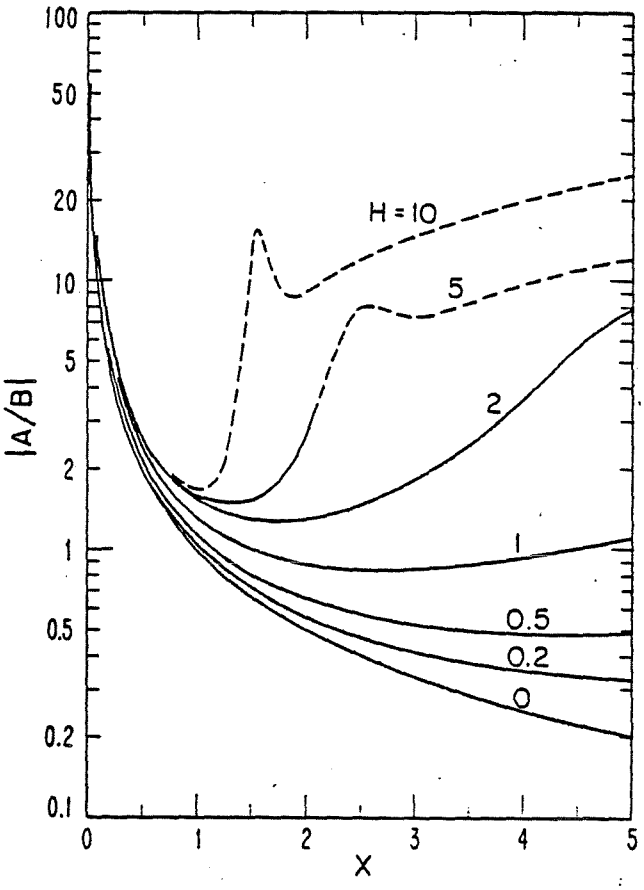


Fig. 5. Ratio of the field components when the observing point is within the upper stratum. $D/H = 2$; $K = 0.1$.

loops or by a single loop rotatable about an axis. Using the numerical data for A and B, this ratio is plotted in Figures 2 and 3 as a function of the displacement X for $K = 0.1$ and $K = 10$, respectively, for $D/H = 0.5$, and a range of H values. Here and in the figures that follow, the curves are broken whenever $|A|$ and/or $|B|$ is less than 10^{-3} (i.e., < -60 db). These results in Figures 2 and 3 correspond to locating the observer within the substratum. The corresponding results for the case in which the observer is within the upper layer are shown in Figures 4 and 5, where we choose $D/H = 2.0$.

The effect of varying the conductivity contrast $K(= \sigma_2/\sigma_1)$ is illustrated in Figures 6 and 7, where we choose $D/H = 0.5$ and 2, respectively, and fix $H = 1$ (i.e., $D = 0.5$ and 2).

In general, $|A/B|$ always has a pronounced peak at $X = 0$ corresponding to the observer directly beneath the source cable. On examining the curves in Figures 2, 3, 4, 5, 6, and 7 we see that the peak may be obscured to some extent by the presence of the stratification in the overburden. No doubt this behavior should be taken into account in any feasibility studies of source-location techniques that utilize subsurface magnetic-field measurements.

An important and nontrivial extension of the present analysis is to allow for the nonuniformity of the thickness of the upper layer. This subject is being currently investigated by using a wave-optical technique.

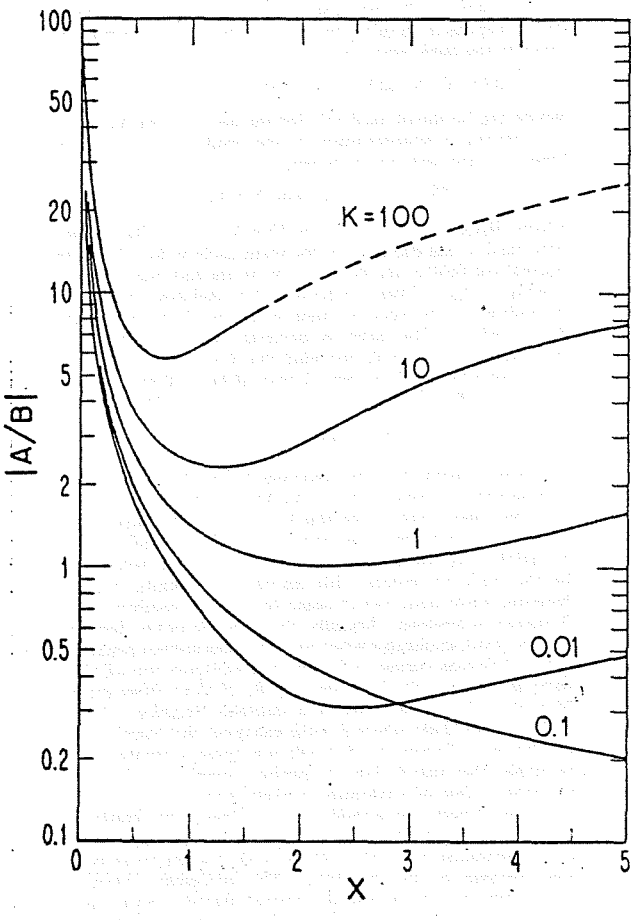


Fig. 6. Ratio of the field components illustrating the effect of conductivity contrast between the layers. $H = 1$; D/H = 0.5.

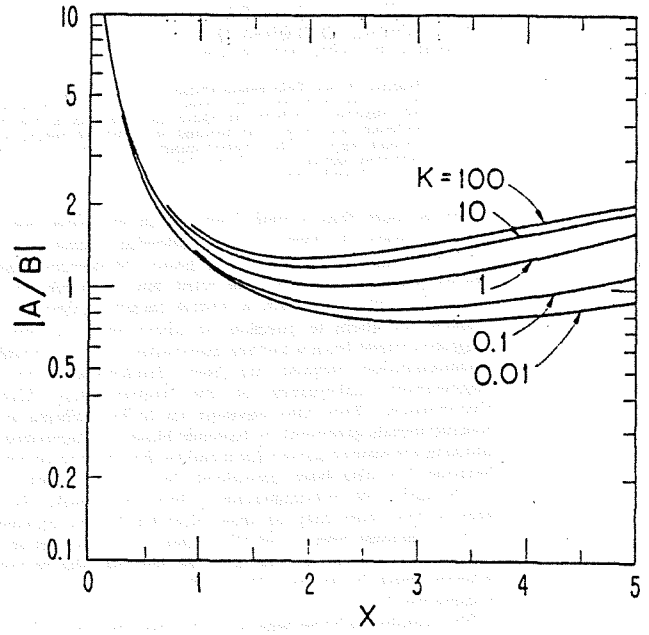


Fig. 7. Ratio of the field components illustrating the effect of conductivity contrast between the layers. $H = 1$; $D/H = 2.0$.

Acknowledgments. We would like to thank Dr. R. G. Geyer of the Colorado School of Mines for suggesting this problem, and Mrs. Loys Gappa for her help in preparing the manuscript. The research was supported by the US Bureau of Mines.

REFERENCES

Bannister, P. R. (1968) Electromagnetic fields within a a stratified earth produced by a long horizontal line source, *Radio Sci.*, *3*(4), 387–390.

Wait, J. R. (1970), *Electromagnetic Waves in Stratified Media*, 2nd ed., chap. 2, pp. 8–63, Pergamon, New York.

Wait, J. R. (1971), Array technique for electromagnetic positional determination of a buried receiving point, *Electron. Lett.*, *7*(8), 186–187.

Wait, J. R., and K. P. Spies (1971), Subsurface electromagnetic fields of a line source on a conducting half-space, *Radio Sci.*, *6*(8/9), 781–786.

ARRAY TECHNIQUE FOR ELECTROMAGNETIC POSITIONAL DETERMINATION OF A BURIED RECEIVING POINT

Indexing terms: Telecommunication links, Safety

We describe a scheme to locate personnel in a coal mine following a disaster. The method, while not yet tested, would require only that the trapped miner be equipped with a loop receiving device. Operating frequencies in the low audio range are called for.

There is more than a casual interest in exploiting electromagnetic waves to locate miners following a disaster. The possibility that all conventional means of communication are eliminated should not be ruled out. However, if the miners are equipped with a simple receiving device, it is feasible for them to perceive an audio-frequency electromagnetic signal from a surface transmitter. Such a downlink communication scheme has been demonstrated by the Georesearch Laboratory of the Westinghouse Electric Corporation. They also envisage an uplink scheme using seismic signals generated by hammer blows. A technique for utilising the seismic signals for direction finding and/or source location has also been considered (as described orally by D. B. Large of Westinghouse). Here, we would like to suggest that there may be some direction-finding capability using a scanning array of electromagnetic line sources on the surface. If such a method is to be feasible, the receiving terminal must be simple. We outline a possible scheme to achieve this goal.

The simplest scheme which we envisage is a parallel pair of long current-carrying cables on the earth's surface. If the earthed endpoints of these cables are sufficiently far away, the fields in the vicinity may be imagined to emanate from infinite line sources.

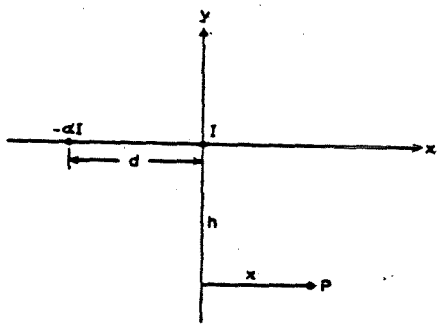


Fig. 1 *Cross-sectional view of situation*

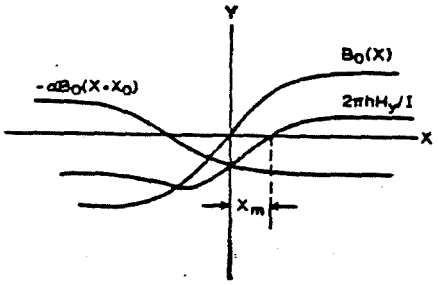


Fig. 2 *Illustrating superposition of 2-cable fields*

The configuration is illustrated in Fig. 1, which is a cross-sectional view of the situation. As indicated, a current I amperes flows in one cable, while a current $-\alpha I$ amperes flows in the other cable. Here α is a factor which can be varied by the operator on the surface. The two cables are separated by a distance d, which is kept constant for a given test.

We now choose a rectangular co-ordinate system (x, y, z) so that the Earth's surface is the plane $y = 0$ and the first cable is coincident with the z axis. Then, the second cable is located at $x = -d$ and $y = 0$. The receiving location is a depth $y = -h$, but its location relative to the cable pair is not known; i.e. we wish to determine the x co-ordinate of the subsurface point P indicated in Fig. 1.

A relatively simple quantity to detect at the subsurface point P is the vertical component of the resultant magnetic field. If the frequency of the alternating current in the cables is sufficiently low, the fields at P can be estimated from static theory. As discussed elsewhere, this calls for operating frequencies of the order of 100 Hz or less, and limits the depths to less than several hundred metres for moderately conducting overburdens. For purposes of this discussion, we will employ the static theory, even though there is a more refined analysis available[1, 2].

Under the conditions stated, the vertical magnetic-field component H_y at P is given by a simple adaptation of the Biot–Savart law. Thus,

$$H_y = \frac{I}{2\pi h}\left\{\frac{X}{1+X^2} - \alpha\frac{X+X_0}{1+(X+X_0)^2}\right\} \quad . \quad . \quad (1)$$

where $X = x/h$ and $X_0 = d/h$. If the observer is equipped with a rudimentary horizontal loop (i.e. vertical axis) and voltage detector, he is able to note by a seismic hammer blow when the signal has a maximum or a minimum. For example, if α is varied in some systematic pattern by the surface operator (e.g. a saw-tooth scan of one minute), there will be a point in time when H_y vanishes. For a fixed and known value of X_0, one can then determine X from eqn. 1 by setting the term in braces equal to zero. In general, this leads to the cubic equation

$$X\{1+(X+X_0)^2\} = \alpha(1+X^2)(X+X_0) \quad . \quad . \quad . \quad (2)$$

which can be solved explicitly for the desired root X_m.

A graphical interpretation of the results is useful at this stage. To this end, we write eqn. 1 in the form

$$H_y = \{I/(2\pi h)\}\{B_0(X) - \alpha B_0(X+X_0)\} \quad . \quad . \quad . \quad (3)$$

where $B_0(X) = X(1+X^2)^{-1} = (X+X^{-1})^{-1}$. The normalised field of the current I in the main cable is $B_0(X)$ and the normalised field of the current $-\alpha I$ in the secondary cable is $-\alpha B_0(X+X_0)$. These functions are sketched in Fig. 2. As indicated, the sum of these is the resultant normalised field $2\pi h H_y/I$. The latter is obviously zero at some point $X = X_m$ where $X_m > 0$, provided that $0 < \alpha < 1$.

It is easy to see from eqn. 2 that, if both X and $X_0 \ll 1$, the solution for the root is particularly simple. Then

$$X_m = \alpha X_0/(1-\alpha)$$

It is also evident that the resolving power of the scheme is only satisfactory when X_m and X_0 are not too large.

As mentioned above, the simple analysis given here is only valid when eddy currents induced in the overburden are negligible. At sufficiently low frequencies, this will always be the case. Of course, this imposes a difficulty with the receiving equipment, which needs to be more sensitive as the frequency is lowered. Actually, the principle of the detection scheme is still applicable when eddy currents are not negligible. It then becomes necessary to assume a halfspace model of the earth and replace the field function $B_0(x)$ by its more general form $B(X, H)$. The latter is a complex function of both X and $H = \sqrt{2}\,h/\delta$ where δ is the electrical skin depth of the overburden. Tables of $B(X, H)$ are given elsewhere.[1] In principle, they can be used to devise a detection scheme for the general case of a conductive overburden.

The discussion has considered a 2-dimensional configuration involving parallel-line sources. In a single application of the technique, it is only possible to deduce the value of the x co-ordinate of the observer. The procedure, however, can be repeated for current line sources parallel to the x axis, in which case the z co-ordinate of the observer could be determined.

Other possibilities include the use of arrays of line sources

operating either at the same frequency or at multiple frequencies. The feasibility of such schemes should be investigated at the earliest opportunity.

J. R. WAIT

9th March 1971

Institute for Telecommunication Sciences
Office of Telecommunications
Boulder, Colo. 80302, USA

References

1 WAIT, J. R., and SPIES, K. P.: 'Sub-surface electromagnetic fields of a line source on a conducting half-space', *Radio Sci.*, 1971, 6
2 WAIT, J. R.: 'Electromagnetic waves in stratified media' (Pergamon, 1962), chap. 2

Radio Science, Volume 6, Numbers 8, 9, pages 781–786, August-September 1971

Subsurface electromagnetic fields of a line source on a conducting half-space

James R. Wait and Kenneth P. Spies

Institute for Telecommunication Sciences
Office of Telecommunications, Boulder, Colorado 80302

(Received January 15, 1971.)

An infinite line source or current-carrying cable on the surface of a flat homogeneous earth is considered. The integral formula, for the case of negligible displacement currents, is reduced either to tabulated functions or to a form suitable for numerical integration. A table of numerical values of these basic integrals is presented. We also show that, in principle, the relative location of the line source can be deduced from measurements of the subsurface field The results have possible application to mine rescue operations.

INTRODUCTION

In certain aspects of applied geophysics [*Grant and West*, 1966], one is interested in the nature of the electromagnetic fields within the earth for a source on the surface. For example, if a communication link is to be established from a sender on the earth's surface to a receiving point in a mine or other subterranean terminal, it is necessary to choose a transmitting antenna and an operating frequency that are appropriate for the task. With this objective in mind, we shall consider a two-dimensional model which hopefully provides insight to this problem. The earth is regarded as a homogeneous conducting half-space in this formulation. We also consider the possibility that the structure of the measured subsurface field can be employed to deduce the relative location of the line source on the surface.

FORMULATION OF THE GREEN'S FUNCTION

We begin with the fields of a uniform line current I at (x', y') in a nonmagnetic homogeneous half-space ($y < 0$) of conductivity σ as indicated in Figure 1. Everything is considered to be invariant in the z direction, so the posed problem is entirely two-dimensional. The fields are taken to vary with time as $\exp(i\omega t)$, and the (angular) frequency ω is sufficiently low that all displacement currents are negligible compared with the conduction currents. The electric field at $P(x, y)$ has only a z component $E(x, y)$ and it can be conveniently written as follows [*Wait*, 1962]:

$$E = (-i\mu_0\omega I/2\pi)G(x, y; x', y') \qquad (1)$$

where $\mu_0 = 4\pi \times 10^{-7}$ is the permeability of free space. Then the 'Green's function,' for $y > 0$, is

$$G(x, y; x', y') = K_0[\gamma[(x - x')^2 + (y - y')^2]^{1/2}] - K_0[\gamma[(x - x')^2 + (y + y')^2]^{1/2}] + 2\int_0^\infty \frac{e^{-u(y+y')}}{u + \lambda} \cos[\lambda(x - x')]\, d\lambda \qquad (2)$$

where $u = (\lambda^2 + \gamma^2)^{1/2}$ and $\gamma^2 = i\sigma\mu_0\omega$. The first modified Bessel function on the right-hand side of (2) can be identified as the Green's function of the line source for an infinite medium, while the second term is associated with an 'image' of the line source at $x = x'$ and $y = -y'$. For the region $y < 0$, we have

$$G(x, y; x', y') = 2\int_0^\infty \frac{e^{-uy'}e^{\lambda y}}{u + \lambda} \cos[\lambda(x - x')]\, d\lambda \qquad (3)$$

It is not difficult to verify that G has the proper singularity at the source, and that G and $\partial G/\partial y$ are continuous at the interface $y = 0$. Also, we see that $(\nabla^2 - \gamma^2)\, G = 0$ for $y > 0$, while $\nabla^2 G = 0$ for $y < 0$. Furthermore, if Re $u > 0$, and noting that λ is also real, the solutions for G behave properly as $|y| \to \infty$. In establishing the correctness of (2) and (3), one makes use of the integral representation

$$K_0[\gamma(x^2 + y^2)^{1/2}] = \int_0^\infty \frac{e^{-u|y|}}{u} \cos \lambda x\, d\lambda \qquad (4)$$

This key formula is also used in the developments which follow.

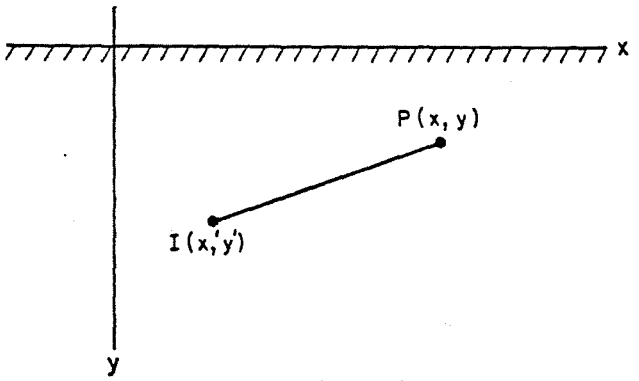


Fig. 1. Current line source in the presence of a homogeneous half-space.

SUBSURFACE MAGNETIC FIELDS FOR LINE CURRENT ON SURFACE

A situation of special interest is when the line source is on the earth's surface and we observe the resultant magnetic field H at a subsurface point $P(x, h)$, as indicated in Figure 2. Thus, in (1), we take $x' = y' = 0$ and use $i\mu_0\omega H_x = -\partial E/\partial y$ and $i\mu_0\omega H_y = \partial E/\partial x$ to obtain

$$H_x = -\frac{I}{\pi}\int_0^\infty \frac{u}{u+\lambda} e^{-uh} \cos \lambda x \, d\lambda \tag{5}$$

$$H_y = +\frac{I}{\pi}\int_0^\infty \frac{\lambda}{u+\lambda} e^{-uh} \sin \lambda x \, d\lambda \tag{6}$$

while, of course, $H_z \equiv 0$. While the evaluation of (5) and (6) for the general case requires numerical integration, the important special case for $x = 0$ is amenable to analytical treatment. Then the magnetic field is purely horizontal, (i.e., $H_y = 0$) and is reduced as follows:

$$\begin{aligned} H_x = H_x^0 &= -\frac{I}{\pi}\int_0^\infty \frac{u}{u+\lambda} e^{-uh} \, d\lambda \\ &= +\frac{I}{\pi}\frac{\partial}{\partial h}\int_0^\infty \frac{e^{-uh}}{u+\lambda} d\lambda \\ &= +\frac{I}{\pi\gamma^2}\frac{\partial}{\partial h}\int_0^\infty (u-\lambda)e^{-uh} \, d\lambda \end{aligned} \tag{7}$$

where we note that $(u - \lambda)(u + \lambda) = \gamma^2$. Now a special case of (4) is

$$\int_0^\infty \frac{e^{-uh}}{u} d\lambda = K_0(\gamma h) \tag{8}$$

thus

$$\int_0^\infty u e^{-uh} \, d\lambda = \frac{d^2}{dh^2} K_0(\gamma h) \tag{9}$$

Similarly, if we use the standard form

$$\int_0^\infty \lambda \frac{e^{-uh}}{u} d\lambda = \frac{e^{-\gamma h}}{h} \tag{10}$$

we have

$$\int_0^\infty \lambda e^{-uh} \, d\lambda = -\frac{\partial}{\partial h}\frac{e^{-\gamma h}}{h} \tag{11}$$

Thus, making use of (9) and (11), we see that (7) is equivalent to

$$H_x^0 = +\frac{I}{\pi\gamma^2}\left[\frac{\partial^3}{\partial h^3} K_0(\gamma h) + \frac{\partial^2}{\partial h^2}\frac{e^{-\gamma h}}{h}\right] \tag{12}$$

By utilizing the Bessel function relations

$$d K_0(\alpha)/d\alpha = -K_1(\alpha) \tag{13}$$

$$d K_1(\alpha)/d\alpha = -[K_0(\alpha) + \alpha^{-1} K_1(\alpha)] \tag{14}$$

we can express (12) in the form

$$H_x^0 = -[I/(2\pi h)] A_0(\alpha) \tag{15}$$

where

$$\begin{aligned} A_0(\alpha) = 2K_0(\alpha) + 2\left(\alpha + \frac{2}{\alpha}\right) K_1(\alpha) \\ - \alpha^{-2}(2 + 2\alpha + \alpha^2)e^{-\alpha} \end{aligned} \tag{16}$$

where $\alpha = \gamma h = (i\sigma\mu_0\omega)^{1/2} h$. At sufficiently low frequencies (i.e., $\alpha \to 0$), we see that $A_0(\alpha)$ approaches 1, and we recover the expected static form. On the other hand, the high-frequency limit (i.e., $\alpha \to \infty$) leads to

$$A_0(\alpha) \sim (2\pi\alpha)^{1/2} e^{-\alpha} \tag{17}$$

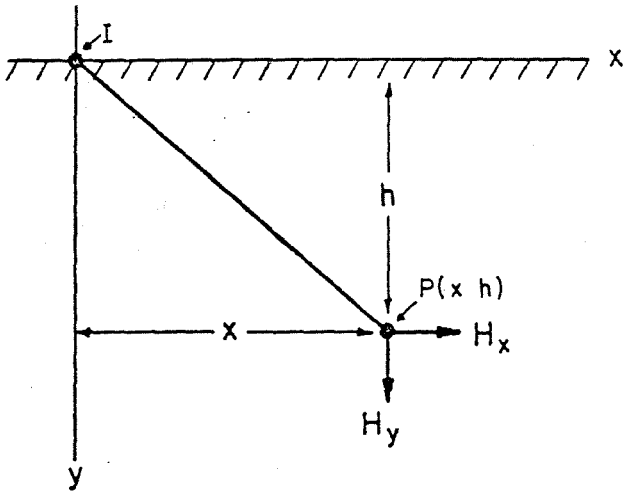


Fig. 2. Line source on surface and field components to be observed at subsurface point.

which is a factor of 2 greater than the corresponding result for an infinite medium. In this asymptotic limit, the air-ground interface has the effect of doubling the field of the line source.

In the general case, for numerical work, it is convenient to express (15) and (16) in terms of dimensionless parameters $H = (\sigma\mu_0\omega)^{1/2}h$ and $X = x/h$. Thus, on changing the integration variable to $s = \lambda h$, we have

$$H_z = -\frac{I}{2\pi h} A(H, X)$$

$$H_r = +\frac{I}{2\pi h} B(H, X)$$

where

$$A(H, X) = 2\int_0^\infty \frac{(s^2 + iH^2)^{1/2}}{(s^2 + iH^2)^{1/2} + s} \cdot \exp\left[-(s^2 + iH^2)^{1/2}\right] \cos(sX)\, ds \qquad (18)$$

$$B(H, X) = 2\int_0^\infty \frac{s}{(s^2 + iH^2)^{1/2} + s} \cdot \exp\left[-(s^2 + iH^2)^{1/2}\right] \sin(sX)\, ds \qquad (19)$$

The corresponding form for the electric field is

$$E = (-i\mu\omega I/2\pi)F(H, X)$$

where

$$F(H, X) = G(x, y; 0, 0) = 2\int_0^\infty \frac{1}{(s^2 + iH^2)^{1/2} + s} \cdot \exp\left[-(s^2 + iH^2)^{1/2}\right] \cos sX\, ds \qquad (20)$$

Because these integrals recur frequently in electromagnetic induction problems involving buried terminals, tables of the integrals A, B, and F have been prepared. Except for the case $X = 0$, numerical integration is necessary. First of all, however, we discuss some limiting situations which are useful for checking the numerical work.

LIMITING FORMS

A very simple limiting form is when the frequency tends to zero. Then $\gamma^2 \to 0$ and then (5) and (6) reduce to

$$H_z = H_{0z} = -\frac{I}{2\pi}\int_0^\infty e^{-\lambda h} \cos\lambda x\, d\lambda = \frac{-I}{2\pi h}\frac{h^2}{h^2 + x^2} \qquad (21)$$

$$H_r = H_{0r} = \frac{I}{2\pi}\int_0^\infty e^{-\lambda h} \sin\lambda x\, d\lambda = \frac{I}{2\pi h}\frac{xh}{h^2 + x^2} \qquad (22)$$

Then, the corresponding forms of (18) and (19) are simply

$$A(0, X) = A_0 = (1 + X^2)^{-1} \qquad (23)$$

$$B(0, X) = B_0 = X(1 + X^2)^{-1} \qquad (24)$$

Another useful limiting case is to allow the conductivity or frequency or both to be sufficiently high that $|\gamma x|$ can be regarded as a large parameter. Some consideration shows that this justifies the replacement of $\exp(-uh)$ by $\exp(-\gamma h)$ in the integrands of (5) and (6). Then also

$$F = 2\int_0^\infty \frac{\cos\lambda x}{u + \lambda} e^{-uh}\, d\lambda \sim 2e^{-\gamma h}\int_0^\infty \frac{\cos\lambda x}{u + \lambda}\, d\lambda \sim \frac{2}{\gamma^2 x^2} e^{-\gamma h} \qquad (25)$$

where we have used previously developed results

TABLE 1. Field calculations for a line source on a conducting half-space at zero frequency limit ($H = 0$)

X	A_0	B_0	A_0/B_0
0.0	1.000 + 0	0.000 + 0	∞
0.1	9.901 - 1	9.901 - 2	1.000 + 1
0.2	9.615 - 1	1.923 - 1	5.000 + 0
0.3	9.174 - 1	2.752 - 1	3.333 + 0
0.4	8.621 - 1	3.448 - 1	2.500 + 0
0.5	8.000 - 1	4.000 - 1	2.000 + 0
0.6	7.353 - 1	4.412 - 1	1.667 + 0
0.7	6.711 - 1	4.698 - 1	1.429 + 0
0.8	6.098 - 1	4.879 - 1	1.250 + 0
0.9	5.525 - 1	4.972 - 1	1.111 + 0
1.0	5.000 - 1	5.000 - 1	1.000 + 0
1.1	4.525 - 1	4.977 - 1	9.091 - 1
1.2	4.098 - 1	4.918 - 1	8.333 - 1
1.3	3.717 - 1	4.833 - 1	7.692 - 1
1.4	3.378 - 1	4.730 - 1	7.143 - 1
1.5	3.077 - 1	4.615 - 1	6.667 - 1
1.6	2.809 - 1	4.494 - 1	6.250 - 1
1.7	2.571 - 1	4.370 - 1	5.882 - 1
1.8	2.358 - 1	4.245 - 1	5.556 - 1
1.9	2.169 - 1	4.121 - 1	5.263 - 1
2.0	2.000 - 1	4.000 - 1	5.000 - 1
2.1	1.848 - 1	3.882 - 1	4.762 - 1
2.2	1.712 - 1	3.767 - 1	4.545 - 1
2.3	1.590 - 1	3.657 - 1	4.348 - 1
2.4	1.479 - 1	3.550 - 1	4.167 - 1
2.5	1.379 - 1	3.448 - 1	4.000 - 1
2.6	1.289 - 1	3.351 - 1	3.846 - 1
2.7	1.206 - 1	3.257 - 1	3.704 - 1
2.8	1.131 - 1	3.167 - 1	3.571 - 1
2.9	1.063 - 1	3.082 - 1	3.448 - 1
3.0	1.000 - 1	3.000 - 1	3.333 - 1
3.1	9.425 - 2	2.922 - 1	3.226 - 1
3.2	8.897 - 2	2.847 - 1	3.125 - 1
3.3	8.410 - 2	2.775 - 1	3.030 - 1
3.4	7.962 - 2	2.707 - 1	2.941 - 1
3.5	7.547 - 2	2.642 - 1	2.857 - 1
3.6	7.163 - 2	2.579 - 1	2.778 - 1
3.7	6.807 - 2	2.519 - 1	2.703 - 1
3.8	6.477 - 2	2.461 - 1	2.632 - 1
3.9	6.169 - 2	2.406 - 1	2.564 - 1
4.0	5.882 - 2	2.353 - 1	2.500 - 1
4.1	5.615 - 2	2.302 - 1	2.439 - 1
4.2	5.365 - 2	2.253 - 1	2.381 - 1
4.3	5.131 - 2	2.206 - 1	2.326 - 1
4.4	4.912 - 2	2.161 - 1	2.273 - 1
4.5	4.706 - 2	2.118 - 1	2.222 - 1
4.6	4.513 - 2	2.076 - 1	2.174 - 1
4.7	4.331 - 2	2.036 - 1	2.128 - 1
4.8	4.160 - 2	1.997 - 1	2.083 - 1
4.9	3.998 - 2	1.959 - 1	2.041 - 1
5.0	3.846 - 2	1.923 - 1	2.000 - 1

[*Wait*, 1962]. Thus, for the asymptotic limit $HX \to \infty$,

$$F \sim \left(\frac{2}{iH^2}\right) \frac{1}{X^2} \exp\left[-(i)^{1/2} H\right] \tag{26}$$

In a similar fashion, we readily find the corrsponding asymptotic forms

$$A \sim \left(\frac{2}{(i)^{1/2} H}\right) \frac{1}{X^2} \exp\left[-(i)^{1/2} H\right] \tag{27}$$

$$B \sim \left(\frac{4}{iH^2}\right) \frac{1}{X^3} \exp\left[-(i)^{1/2} H\right] \tag{28}$$

In particular, we see that

$$A/B \sim (i)^{1/2} H X/2 \tag{29}$$

TABLE 2. Field calculations for a line source on a conducting half-space

H = 0.10

X	A	PHASE(A) IN DEGREES	B	PHASE(B) IN DEGREES	A/B	PHASE(A/B) IN DEGREES	F	PHASE(F) IN DEGREES
0.00	1.843+000	1.14	0.000+000					
0.02	1.841+000	1.14	1.995-002	-0.59	5.215+001	1.73	2.986+000	-15.79
0.04	1.836+000	1.14	3.986-002	-0.59	2.608+001	1.73	2.985+000	-15.79
0.06	1.827+000	1.14	5.966-002	-0.59	1.739+001	1.73	2.984+000	-15.80
0.08	1.815+000	1.14	7.933-002	-0.59	1.304+001	1.74	2.983+000	-15.80
0.10	1.801+000	1.15	9.881-002	-0.59	1.843+001	1.74	2.981+000	-15.81
0.15	1.019+000	1.16	1.464-001	-0.60	6.960+000	1.76	2.975+000	-15.84
0.20	1.803+000	1.18	1.919-001	-0.61	5.224+000	1.79	2.967+000	-15.89
0.30	1.758+000	1.24	2.746-001	-0.63	3.490+000	1.87	2.944+000	-16.01
0.40	9.031+001	1.32	3.440-001	-0.66	2.625+000	1.98	2.914+000	-16.17
0.50	8.410-001	1.43	3.990-001	-0.70	2.108+000	2.13	2.879+000	-16.37
0.60	7.763-001	1.55	4.400-001	-0.75	1.764+000	2.30	2.838+000	-16.59
0.70	7.122-001	1.70	4.684-001	-0.81	1.520+000	2.51	2.794+000	-16.85
0.80	6.508-001	1.87	4.862-001	-0.87	1.339+000	2.74	2.744+000	-17.12
0.90	5.936-001	2.06	4.955-001	-0.94	1.198+000	3.00	2.701+000	-17.41
1.00	5.411-001	2.26	4.980-001	-1.02	1.087+000	3.28	2.654+000	-17.72
1.10	4.936-001	2.49	4.956-001	-1.10	9.961-001	3.59	2.606+000	-18.03
1.20	4.510-001	2.73	4.894-001	-1.19	9.215-001	3.92	2.559+000	-18.35
1.30	4.130-001	2.99	4.807-001	-1.28	8.590-001	4.27	2.513+000	-18.68
1.40	3.791-001	3.26	4.702-001	-1.38	8.061-001	4.64	2.467+000	-19.01
1.50	3.498-001	3.54	4.586-001	-1.49	7.606-001	5.03	2.423+000	-19.34
1.60	3.222-001	3.84	4.463-001	-1.59	7.215-001	5.43	2.380+000	-19.67
1.70	2.984-001	4.14	4.337-001	-1.72	6.880-001	5.85	2.338+000	-20.01
1.80	2.772-001	4.46	4.211-001	-1.82	6.584-001	6.28	2.298+000	-20.34
1.90	2.583-001	4.78	4.085-001	-1.94	6.324-001	6.72	2.258+000	-20.67
2.00	2.415-001	5.11	3.962-001	-2.07	6.094-001	7.17	2.220+000	-21.00
2.10	2.263-001	5.44	3.842-001	-2.19	5.891-001	7.63	2.183+000	-21.34
2.20	2.127-001	5.77	3.726-001	-2.32	5.710-001	8.09	2.148+000	-21.67
2.30	2.005-001	6.18	3.613-001	-2.46	5.550-001	8.56	2.113+000	-21.99
2.40	1.895-001	6.44	3.505-001	-2.59	5.406-001	9.03	2.079+000	-22.32
2.50	1.795-001	6.77	3.402-001	-2.73	5.278-001	9.50	2.047+000	-22.65
2.60	1.705-001	7.10	3.302-001	-2.87	5.163-001	9.98	2.015+000	-22.97
2.70	1.623-001	7.43	3.207-001	-3.02	5.060-001	10.45	1.985+000	-23.29
2.80	1.548-001	7.76	3.116-001	-3.17	4.967-001	10.92	1.955+000	-23.61
2.90	1.479-001	8.08	3.029-001	-3.32	4.885-001	11.39	1.927+000	-23.93
3.00	1.417-001	8.39	2.945-001	-3.47	4.810-001	11.86	1.899+000	-24.25
3.10	1.359-001	8.70	2.866-001	-3.62	4.744-001	12.33	1.871+000	-24.56
3.20	1.307-001	9.01	2.789-001	-3.78	4.685-001	12.81	1.846+000	-24.87
3.30	1.258-001	9.32	2.716-001	-3.94	4.632-001	13.31	1.821+000	-25.18
3.40	1.213-001	9.70	2.645-001	-4.11	4.587-001	13.80	1.797+000	-25.50
3.50	1.172-001	10.01	2.578-001	-4.27	4.546-001	14.28	1.773+000	-25.81
3.60	1.134-001	10.31	2.514-001	-4.44	4.511-001	14.75	1.750+000	-26.12
3.70	1.099-001	10.61	2.452-001	-4.60	4.481-001	15.21	1.728+000	-26.44
3.80	1.066-001	10.88	2.392-001	-4.77	4.455-001	15.66	1.709+000	-26.75
3.90	1.035-001	11.15	2.336-001	-4.94	4.432-001	16.09	1.689+000	-27.07
4.00	1.007-001	11.42	2.281-001	-5.11	4.414-001	16.51	1.669+000	-27.38
4.20	9.552-002	11.87	2.178-001	-5.46	4.385-001	17.32	1.622+000	-28.00
4.40	9.099-002	12.28	2.083-001	-5.80	4.368-001	18.09	1.583+000	-28.61
4.60	8.696-002	12.65	1.995-001	-6.16	4.359-001	18.81	1.545+000	-29.21
4.80	8.338-002	12.97	1.913-001	-6.51	4.356-001	19.49	1.539+000	-29.80
5.00	8.016-002	13.26	1.837-001	-6.88	4.364-001	20.13	1.474+000	-30.38

H = 0.50

X	A	PHASE(A) IN DEGREES	B	PHASE(B) IN DEGREES	A/B	PHASE(A/B) IN DEGREES	F	PHASE(F) IN DEGREES
0.00	1.092+000	-5.60	0.000+000				1.400+000	-34.91
0.02	1.092+000	-5.60	1.899-002	-6.46	5.751+001	2.86	1.400+000	-34.91
0.04	1.091+000	-5.61	3.793-002	-6.47	2.874+001	2.86	1.400+000	-34.92
0.06	1.089+000	-5.61	5.678-002	-6.48	1.918+001	2.87	1.399+000	-34.94
0.08	1.086+000	-5.62	7.549-002	-6.49	1.439+001	2.87	1.398+000	-34.97
0.10	1.082+000	-5.63	9.401-002	-6.51	1.152+001	2.88	1.396+000	-35.00
0.15	1.070+000	-5.67	1.392-001	-6.59	7.685+000	2.92	1.391+000	-35.10
0.20	1.054+000	-5.72	1.823-001	-6.69	5.780+000	2.97	1.384+000	-35.25
0.30	1.010+000	-5.87	2.604-001	-6.97	3.878+000	3.10	1.364+000	-35.67
0.40	9.544+001	-6.07	3.252-001	-9.36	2.934+000	3.29	1.338+000	-36.23
0.50	8.922-001	-6.31	3.756-001	-9.65	2.374+000	3.53	1.306+000	-36.92
0.60	8.273-001	-6.60	4.125-001	-10.42	2.006+000	3.82	1.271+000	-37.72
0.70	7.630-001	-6.91	4.369-001	-11.06	1.746+000	4.16	1.233+000	-38.62
0.80	7.014-001	-7.25	4.508-001	-11.81	1.556+000	4.55	1.194+000	-39.66
0.90	6.438-001	-7.63	4.564-001	-12.60	1.411+000	4.97	1.154+000	-40.63
1.00	5.910-001	-8.01	4.554-001	-13.45	1.298+000	5.44	1.114+000	-41.72
1.10	5.431-001	-8.41	4.497-001	-14.35	1.208+000	5.94	1.074+000	-42.89
1.20	5.000-001	-8.82	4.405-001	-15.30	1.135+000	6.47	1.035+000	-44.01
1.30	4.615-001	-9.24	4.288-001	-16.28	1.076+000	7.04	9.965-001	-45.15
1.40	4.270-001	-9.67	4.156-001	-17.30	1.028+000	7.62	9.598-001	-46.35
1.50	3.963-001	-10.11	4.014-001	-18.34	9.874-001	8.23	9.239-001	-47.60
1.60	3.689-001	-10.56	3.866-001	-19.42	9.541-001	8.86	8.896-001	-48.82
1.70	3.444-001	-11.01	3.718-001	-20.51	9.264-001	9.50	8.565-001	-50.05
1.80	3.225-001	-11.47	3.570-001	-21.63	9.034-001	10.16	8.241-001	-51.27
1.90	3.028-001	-11.94	3.424-001	-22.76	8.844-001	10.82	7.945-001	-52.58
2.00	2.851-001	-12.41	3.282-001	-23.90	8.687-001	11.49	7.655-001	-53.72
2.10	2.692-001	-12.89	3.145-001	-25.06	8.560-001	12.17	7.375-001	-54.94
2.20	2.547-001	-13.38	3.012-001	-26.23	8.457-001	12.85	7.109-001	-56.16
2.30	2.416-001	-13.87	2.885-001	-27.41	8.376-001	13.53	6.853-001	-57.37
2.40	2.297-001	-14.37	2.762-001	-28.59	8.314-001	14.22	6.609-001	-58.57
2.50	2.188-001	-14.89	2.644-001	-29.78	8.269-001	14.90	6.374-001	-59.76
2.60	2.088-001	-15.40	2.531-001	-30.98	8.236-001	15.57	6.150-001	-60.94
2.70	1.996-001	-15.93	2.422-001	-32.18	8.223-001	16.25	5.937-001	-62.12
2.80	1.911-001	-16.46	2.318-001	-33.38	8.218-001	16.92	5.729-001	-63.28
2.90	1.833-001	-17.01	2.219-001	-34.58	8.224-001	17.58	5.532-001	-64.44
3.00	1.761-001	-17.55	2.123-001	-35.79	8.240-001	18.24	5.342-001	-65.58
3.10	1.693-001	-18.10	2.032-001	-37.00	8.264-001	18.90	5.161-001	-66.71
3.20	1.630-001	-18.65	1.945-001	-38.20	8.297-001	19.54	4.988-001	-67.82
3.30	1.572-001	-19.23	1.862-001	-39.41	8.337-001	20.18	4.825-001	-68.94
3.40	1.517-001	-19.83	1.783-001	-40.62	8.384-001	20.82	4.668-001	-70.04
3.50	1.465-001	-20.39	1.707-001	-41.82	8.437-001	21.44	4.518-001	-71.13
3.60	1.416-001	-20.96	1.635-001	-43.02	8.496-001	22.06	4.375-001	-72.21
3.70	1.371-001	-21.53	1.566-001	-44.22	8.562-001	22.68	4.237-001	-73.27
3.80	1.327-001	-22.13	1.501-001	-45.42	8.629-001	23.28	4.075-001	-74.32
3.90	1.286-001	-22.73	1.438-001	-46.61	8.703-001	23.88	3.943-001	-75.36
4.00	1.247-001	-23.33	1.421-001	-47.80	8.782-001	24.47	3.816-001	-76.39
4.20	1.175-001	-24.53	1.313-001	-50.16	8.950-001	25.63	3.576-001	-78.40
4.40	1.110-001	-25.74	1.215-001	-52.51	9.134-001	26.77	3.353-001	-80.37
4.60	1.050-001	-26.98	1.125-001	-54.84	9.331-001	27.88	3.146-001	-82.29
4.80	9.949-002	-28.18	1.043-001	-57.14	9.540-001	28.96	2.952-001	-84.15
5.00	9.441-002	-29.40	9.672-002	-59.42	9.761-001	30.02	2.774-001	-85.96

H = 0.20

X	A	PHASE(A) IN DEGREES	B	PHASE(B) IN DEGREES	A/B	PHASE(A/B) IN DEGREES	F	PHASE(F) IN DEGREES
0.00	1.078+000	0.59	0.000+000				2.298+000	-21.19
0.02	1.078+000	0.59	1.982-002	-1.93	5.397+001	2.51	2.298+000	-21.19
0.04	1.078+000	0.59	3.960-002	-1.93	2.695+001	2.52	2.297+000	-21.20
0.06	1.067+000	0.59	5.928-002	-1.93	1.799+001	2.52	2.296+000	-21.20
0.08	1.064+000	0.59	7.882-002	-1.93	1.350+001	2.53	2.295+000	-21.22
0.10	1.060+000	0.60	9.817-002	-1.94	1.080+001	2.54	2.293+000	-21.23
0.15	1.048+000	0.61	1.454-001	-1.96	7.208+000	2.57	2.288+000	-21.28
0.20	1.032+000	0.62	1.906-001	-1.98	5.413+000	2.61	2.280+000	-21.35
0.30	9.877+001	0.67	2.727-001	-2.05	3.627+000	2.72	2.258+000	-21.55
0.40	9.323-001	0.73	3.415-001	-2.15	2.730+000	2.88	2.229+000	-21.81
0.50	8.702-001	0.88	3.959-001	-2.28	2.198+000	3.08	2.194+000	-22.13
0.60	8.055-001	0.90	4.362-001	-2.43	1.847+000	3.32	2.155+000	-22.51
0.70	7.413-001	1.01	4.641-001	-2.60	1.597+000	3.61	2.112+000	-22.93
0.80	6.799-001	1.13	4.813-001	-2.79	1.413+000	3.92	2.068+000	-23.38
0.90	6.226-001	1.27	4.899-001	-3.00	1.271+000	4.28	2.023+000	-23.86
1.00	5.708-001	1.43	4.919-001	-3.23	1.159+000	4.66	1.977+000	-24.37
1.10	5.245-001	1.59	4.889-001	-3.48	1.069+000	5.07	1.931+000	-24.89
1.20	4.797-001	1.77	4.823-001	-3.74	9.947-001	5.51	1.886+000	-25.43
1.30	4.416-001	1.96	4.730-001	-4.01	9.335-001	5.97	1.841+000	-25.97
1.40	4.076-001	2.15	4.620-001	-4.30	8.821-001	6.45	1.798+000	-26.53
1.50	3.773-001	2.35	4.499-001	-4.60	8.387-001	6.94	1.756+000	-27.09
1.60	3.505-001	2.54	4.372-001	-4.90	8.017-001	7.45	1.715+000	-27.65
1.70	3.265-001	2.75	4.241-001	-5.22	7.699-001	7.97	1.675+000	-28.21
1.80	3.052-001	2.95	4.110-001	-5.53	7.426-001	8.50	1.637+000	-28.78
1.90	2.861-001	3.14	3.980-001	-5.89	7.190-001	9.03	1.600+000	-29.35
2.00	2.691-001	3.34	3.852-001	-6.23	6.986-001	9.57	1.564+000	-29.92
2.10	2.538-001	3.53	3.728-001	-6.59	6.809-001	10.11	1.529+000	-30.48
2.20	2.400-001	3.71	3.607-001	-6.95	6.654-001	10.65	1.496+000	-31.05
2.30	2.276-001	3.88	3.491-001	-7.31	6.521-001	11.19	1.463+000	-31.61
2.40	2.164-001	4.05	3.379-001	-7.68	6.405-001	11.73	1.432+000	-32.17
2.50	2.062-001	4.20	3.272-001	-8.04	6.307-001	12.26	1.402+000	-32.73
2.60	1.970-001	4.35	3.168-001	-8.44	6.217-001	12.79	1.373+000	-33.29
2.70	1.886-001	4.48	3.070-001	-8.83	6.143-001	13.31	1.344+000	-33.84
2.80	1.808-001	4.61	2.975-001	-9.22	6.079-001	13.83	1.317+000	-34.40
2.90	1.738-001	4.72	2.884-001	-9.62	6.025-001	14.33	1.291+000	-34.94
3.00	1.673-001	4.81	2.798-001	-10.02	5.980-001	14.83	1.265+000	-35.49
3.10	1.613-001	4.90	2.715-001	-10.42	5.943-001	15.32	1.240+000	-36.04
3.20	1.558-001	4.97	2.635-001	-10.83	5.913-001	15.80	1.216+000	-36.57
3.30	1.507-001	5.02	2.559-001	-11.24	5.887-001	16.27	1.192+000	-37.11
3.40	1.459-001	5.07	2.486-001	-11.66	5.868-001	16.73	1.170+000	-37.64
3.50	1.415-001	5.10	2.417-001	+12.08	5.854-001	17.18	1.147+000	-38.17
3.60	1.374-001	5.12	2.350-001	-12.50	5.846-001	17.62	1.126+000	-38.69
3.70	1.335-001	5.13	2.286-001	-12.92	5.842-001	18.05	1.105+000	-39.21
3.80	1.299-001	5.13	2.224-001	-13.35	5.842-001	18.48	1.085+000	-39.73
3.90	1.265-001	5.12	2.165-001	-13.78	5.844-001	18.90	1.065+000	-40.25
4.00	1.234-001	5.10	2.108-001	-14.21	5.853-001	19.31	1.046+000	-40.77
4.20	1.176-001	5.01	2.001-001	-15.08	5.878-001	20.09	1.010+000	-41.79
4.40	1.124-001	4.89	1.901-001	-15.95	5.914-001	20.84	9.750-001	-42.81
4.60	1.078-001	4.73	1.809-001	-16.83	5.959-001	21.56	9.420-001	-43.81
4.80	1.036-001	4.52	1.723-001	-17.72	6.013-001	22.24	9.105-001	-44.80
5.00	9.982-002	4.28	1.644-001	-18.60	6.073-001	22.89	8.806-001	-45.76

H = 1.00

X	A	PHASE(A) IN DEGREES	B	PHASE(B) IN DEGREES	A/B	PHASE(A/B) IN DEGREES	F	PHASE(F) IN DEGREES
0.00	1.000+000	-21.52	0.000+000				7.775-001	-56.22
0.02	9.998-001	-21.52	1.663-002	-23.52	6.013+001	1.96	7.774-001	-56.24
0.04	9.986-001	-21.54	3.321-002	-23.53	3.007+001	2.00	7.770-001	-56.26
0.06	9.967-001	-21.56	4.969-002	-23.56	2.006+001	2.00	7.763-001	-56.29
0.08	9.940-001	-21.59	6.605-002	-23.60	1.505+001	2.01	7.753-001	-56.34
0.10	9.905-001	-21.64	8.222-002	-23.66	1.205+001	2.02	7.740-001	-56.39
0.15	9.787-001	-21.78	1.216-001	-23.86	8.044+000	2.05	7.698-001	-56.60
0.20	9.627-001	-22.01	1.598-001	-24.09	6.054+000	2.10	7.635-001	-56.85
0.30	9.198-001	-22.55	2.260-001	-24.88	4.071+000	2.25	7.476-001	-57.68
0.40	8.659-001	-23.32	2.803-001	-25.77	3.089+000	2.45	7.263-001	-58.78
0.50	8.056-001	-24.26	3.212-001	-26.97	2.508+000	2.72	7.010-001	-60.08
0.60	7.428-001	-25.35	3.490-001	-28.39	2.128+000	3.04	6.728-001	-61.61
0.70	6.807-001	-26.55	3.654-001	-29.99	1.863+000	3.44	6.429-001	-63.32
0.80	6.212-001	-27.86	3.726-001	-31.76	1.666+000	3.90	6.120-001	-65.18
0.90	5.658-001	-29.24	3.716-001	-33.66	1.523+000	4.43	5.810-001	-67.15
1.00	5.151-001	-30.67	3.652-001	-35.69	1.410+000	5.02	5.532-001	-69.22
1.10	4.692-001	-32.14	3.543-001	-37.81	1.324+000	5.67	5.282-001	-71.35
1.20	4.279-001	-33.63	3.417-001	-40.02	1.252+000	6.39	4.911-001	-73.53
1.30	3.911-001	-35.12	3.268-001	-42.29	1.197+000	7.17	4.633-001	-75.75
1.40	3.582-001	-36.62	3.109-001	-44.62	1.152+000	8.00	4.385-001	-77.98
1.50	3.289-001	-38.11	2.945-001	-47.00	1.117+000	8.88	4.113-001	-80.23
1.60	3.028-001	-39.61	2.782-001	-49.40	1.089+000	9.81	3.874-001	-82.48
1.70	2.796-001	-41.06	2.621-001	-51.84	1.067+000	10.78	3.647-001	-84.72
1.80	2.587-001	-42.51	2.465-001	-54.30	1.050+000	11.79	3.433-001	-86.94
1.90	2.400-001	-43.93	2.314-001	-56.77	1.037+000	12.84	3.232-001	-89.15
2.00	2.232-001	-45.33	2.171-001	-59.24	1.028+000	13.91	3.042-001	-91.34
2.10	2.081-001	-46.71	2.034-001	-61.72	1.023+000	15.01	2.863-001	-93.52
2.20	1.944-001	-48.07	1.903-001	-64.18	1.022+000	16.13	2.694-001	-95.62
2.30	1.820-001	-49.41	1.783-001	-66.64	1.020+000	17.27	2.539-001	-97.72
2.40	1.707-001	-50.72	1.669-001	-69.14	1.023+000	18.43	2.390-001	-99.77
2.50	1.604-001	-52.00	1.561-001	-71.60	1.027+000	19.60	2.251-001	-101.79
2.60	1.509-001	-53.27	1.460-001	-74.04	1.034+000	20.77	2.120-001	-103.77
2.70	1.422-001	-54.51	1.366-001	-76.47	1.042+000	21.96	1.997-001	-105.70
2.80	1.343-001	-55.73	1.277-001	-78.87	1.051+000	23.15	1.881-001	-107.59
2.90	1.269-001	-56.92	1.194-001	-81.26	1.063+000	24.34	1.773-001	-109.44
3.00	1.201-001	-58.09	1.116-001	-83.62	1.076+000	25.53	1.671-001	-111.24
3.10	1.138-001	-59.24	1.044-001	-85.96	1.090+000	26.72	1.575-001	-112.99
3.20	1.079-001	-60.37	9.761-002	-88.28	1.105+000	27.91	1.485-001	-114.69
3.30	1.024-001	-61.47	9.127-002	-90.57	1.122+000	29.10	1.400-001	-116.34
3.40	9.732-002	-62.55	8.533-002	-92.83	1.140+000	30.28	1.321-001	-117.93
3.50	9.255-002	-63.63	7.981-002	-95.06	1.160+000	31.45	1.246-001	-119.46
3.60	8.809-002	-64.64	7.463-002	-97.26	1.180+000	32.62	1.175-001	-120.93
3.70	8.390-002	-65.64	6.975-002	-99.43	1.202+000	33.78	1.108-001	-122.40
3.80	7.997-002	-66.63	6.527-002	-101.56	1.225+000	34.93	1.047-001	-123.78
3.90	7.627-002	-67.59	6.104-002	-103.66	1.249+000	36.07	9.881-002	-125.11
4.00	7.278-002	-68.52	5.705-002	-105.72	1.275+000	37.20	9.320-002	-126.37
4.20	6.640-002	-70.32	4.993-002	-109.74	1.329+000	39.42	8.325-002	-128.73
4.40	6.071-002	-72.02	4.368-002	-113.66	1.390+000	41.58	7.437-002	-130.84
4.60	5.561-002	-73.61	3.821-002	-117.29	1.456+000	43.69	6.652-002	-132.72
4.80	5.104-002	-75.09	3.342-002	-120.53	1.527+000	45.72	5.960-002	-134.34
5.00	4.692-002	-76.47	2.924-002	-124.15	1.605+000	47.68	5.345-002	-135.72

TABLE 2. (continued)

H = 2.00

X	A	PHASE(A) IN DEGREES	B	PHASE(B) IN DEGREES	A/B	PHASE(A/B) IN DEGREES	F	PHASE(F) IN DEGREES
0.00	6.843E-001	-58.87	0.000E+000				2.989E-001	-97.71
0.02	6.840E-001	-58.88	1.114E-002	-59.33	6.141E+001	0.45	2.984E-001	-97.73
0.04	6.830E-001	-58.92	2.224E-002	-59.37	3.071E+001	0.49	2.982E-001	-97.77
0.06	6.814E-001	-58.98	3.327E-002	-59.44	2.048E+001	0.46	2.977E-001	-97.83
0.08	6.792E-001	-59.06	4.418E-002	-59.53	1.537E+001	0.47	2.971E-001	-97.93
0.10	6.763E-001	-59.17	5.489E-002	-59.68	1.231E+001	0.48	2.964E-001	-98.04
0.15	6.664E-001	-59.54	8.181E-002	-60.17	8.227E+000	0.52	2.937E-001	-98.45
0.20	6.521E-001	-60.06	1.055E-001	-60.84	6.193E+000	0.58	2.900E-001	-99.02
0.30	6.174E-001	-61.49	1.448E-001	-62.29	4.173E+000	0.76	2.800E-001	-100.62
0.40	5.731E-001	-63.43	1.804E-001	-64.44	3.176E+000	1.02	2.671E-001	-102.76
0.50	5.239E-001	-65.78	2.023E-001	-67.16	2.589E+000	1.38	2.520E-001	-105.39
0.60	4.722E-001	-68.48	2.144E-001	-70.32	2.203E+000	1.84	2.356E-001	-108.43
0.70	4.207E-001	-71.46	2.181E-001	-73.88	1.963E+000	2.43	2.185E-001	-111.80
0.80	3.721E-001	-74.67	2.152E-001	-77.77	1.792E+000	3.14	2.012E-001	-115.44
0.90	3.282E-001	-77.93	2.075E-001	-81.94	1.611E+000	4.00	1.845E-001	-119.27
1.00	2.897E-001	-81.38	1.966E-001	-86.31	1.504E+000	5.02	1.684E-001	-123.23
1.10	2.564E-001	-84.89	1.838E-001	-90.87	1.423E+000	6.18	1.531E-001	-127.29
1.20	2.281E-001	-88.45	1.699E-001	-95.55	1.361E+000	7.58	1.388E-001	-131.38
1.30	2.044E-001	-91.95	1.557E-001	-100.32	1.314E+000	8.97	1.256E-001	-135.46
1.40	1.843E-001	-94.96	1.418E-001	-105.15	1.279E+000	10.59	1.134E-001	-139.50
1.50	1.616E-001	-97.66	1.286E-001	-110.02	1.254E+000	12.36	1.022E-001	-143.47
1.60	1.432E-001	-100.64	1.157E-001	-114.98	1.237E+000	14.27	9.197E-002	-147.58
1.70	1.276E-001	-103.67	1.042E-001	-119.77	1.228E+000	16.38	8.267E-002	-151.33
1.80	1.140E-001	-106.46	9.388E-002	-124.62	1.225E+000	18.45	7.423E-002	-155.84
1.90	1.021E-001	-108.78	8.314E-002	-129.41	1.228E+000	20.71	6.668E-002	-159.68
2.00	9.163E-002	-111.87	7.409E-002	-134.14	1.237E+000	23.07	5.976E-002	-162.01
2.10	8.241E-002	-113.29	6.590E-002	-138.81	1.251E+000	25.52	5.346E-002	-165.24
2.20	7.428E-002	-115.34	5.851E-002	-143.38	1.270E+000	28.04	4.788E-002	-168.29
2.30	6.718E-002	-117.24	5.186E-002	-147.85	1.294E+000	30.62	4.285E-002	-171.14
2.40	6.079E-002	-118.98	4.590E-002	-152.22	1.323E+000	33.24	3.835E-002	-173.77
2.50	5.512E-002	-120.56	4.057E-002	-156.47	1.358E+000	35.91	3.429E-002	-176.17
2.60	5.012E-002	-121.98	3.581E-002	-160.58	1.400E+000	38.59	3.068E-002	-178.34
2.70	4.562E-002	-123.26	3.157E-002	-164.55	1.447E+000	-41.29	2.746E-002	179.75
2.80	4.172E-002	-124.44	2.779E-002	-168.36	1.501E+000	43.97	2.459E-002	178.18
2.90	3.820E-002	-125.37	2.444E-002	-172.01	1.563E+000	46.62	2.204E-002	176.72
3.00	3.505E-002	-126.25	2.146E-002	-175.48	1.633E+000	49.23	1.979E-002	175.42
3.10	3.224E-002	-126.99	1.883E-002	-178.75	1.712E+000	51.77	1.780E-002	174.28
3.20	2.972E-002	-127.59	1.653E-002	178.14	1.801E+000	-309.78	1.604E-002	173.29
3.30	2.744E-002	-128.09	1.454E-002	175.35	1.902E+000	-307.44	1.450E-002	172.44
3.40	2.544E-002	-128.49	1.283E-002	172.75	2.014E+000	-305.24	1.314E-002	171.56
3.50	2.363E-002	-128.79	1.134E-002	170.42	2.141E+000	-299.21	1.196E-002	170.62
3.60	2.199E-002	-129.00	9.837E-003	168.37	2.282E+000	-297.37	1.094E-002	169.67
3.70	2.052E-002	-129.14	8.613E-003	166.63	2.439E+000	-295.77	1.004E-002	168.71
3.80	1.920E-002	-129.21	7.545E-003	165.21	2.614E+000	-294.42	9.267E-003	167.77
3.90	1.800E-002	-129.21	6.615E-003	164.15	2.808E+000	-293.36	8.595E-003	166.87
4.00	1.692E-002	-129.18	5.809E-003	163.46	3.016E+000	-292.53	8.012E-003	166.08
4.20	1.504E-002	-129.08	4.414E-003	163.24	3.467E+000	-292.22	7.043E-003	-179.98
4.40	1.349E-002	-128.89	3.367E-003	164.59	4.008E+000	-293.24	6.334E-003	178.02
4.60	1.219E-002	-128.59	2.589E-003	167.34	4.533E+000	-295.69	5.755E-003	-176.36
4.80	1.109E-002	-128.09	2.013E-003	171.08	5.011E+000	-299.54	5.286E-003	-175.03
5.00	1.015E-002	-127.56	1.602E-003	175.10	5.392E+000	-302.78	4.891E-002	-174.05

H = 10.00

X	A	PHASE(A) IN DEGREES	B	PHASE(B) IN DEGREES	A/B	PHASE(A/B) IN DEGREES	F	PHASE(F) IN DEGREES
0.00	5.781E-003	-20.49	0.000E+000				5.527E-004	-43.49
0.02	5.693E-003	-20.52	9.669E-005	-18.42	5.678E+001	-1.98	5.520E-004	-43.97
0.04	5.669E-003	-20.74	1.928E-004	-18.85	2.940E+001	-1.84	5.510E-004	-44.10
0.06	5.629E-003	-21.09	2.878E-004	-19.22	1.952E+001	-1.87	5.498E-004	-44.34
0.08	5.575E-003	-21.59	3.785E-004	-19.74	1.473E+001	-1.85	5.481E-004	-44.63
0.10	5.505E-003	-22.23	4.664E-004	-20.41	1.180E+001	-1.82	5.460E-004	-45.02
0.15	5.272E-003	-24.43	6.871E-004	-22.72	7.674E+000	-1.71	5.395E-004	-46.17
0.20	4.964E-003	-27.46	8.821E-004	-25.92	5.626E+000	-1.95	5.292E-004	-47.98
0.30	4.284E-003	-35.84	1.036E-003	-36.85	4.058E+000	-0.99	5.220E-004	-49.32
0.40	3.560E-003	-46.87	1.074E-003	-46.87	3.313E+000	-0.00	5.453E-004	-50.44
0.50	2.954E-003	-59.87	9.641E-004	-61.52	2.995E+000	1.65	2.693E-004	-133.67
0.60	2.497E-003	-74.06	8.225E-004	-78.31	2.256E+000	4.25	2.611E-004	-138.29
0.70	1.296E-003	-48.53	6.387E-004	-98.69	2.030E+000	8.16	1.439E-004	-133.51
0.75	1.864E-003	-99.89	5.496E-004	-108.29	1.942E+000	10.74	1.198E-004	-141.60
0.80	8.708E-004	-102.25	4.662E-004	-118.98	1.868E+000	13.87	9.872E-005	-148.46
0.85	7.036E-004	-108.46	3.899E-004	-129.98	1.804E+000	17.51	8.242E-005	-159.52
0.90	5.631E-004	-114.02	3.216E-004	-135.92	1.750E+000	21.90	6.473E-005	-162.11
0.95	4.464E-004	-114.69	2.620E-004	-145.43	1.706E+000	27.14	5.147E-005	-168.82
1.00	3.518E-004	-122.25	2.104E-004	-155.64	1.673E+000	33.39	4.061E-005	-173.83
1.05	2.758E-004	-124.48	1.669E-004	-165.28	1.650E+000	40.65	3.133E-005	-176.82
1.10	2.162E-004	-124.55	1.297E-004	-174.68	1.667E+000	49.75	2.403E-005	-178.98
1.15	1.711E-004	-123.38	9.933E-005	176.44	1.723E+000	-899.42	1.834E-005	-179.01
1.20	1.383E-004	-120.88	8.267E-005	168.38	1.859E+000	-218.68	1.498E-005	-178.37
1.25	1.157E-004	-115.15	9.468E-005	160.28	2.115E+000	-275.42	1.119E-005	-179.86
1.30	1.088E-004	-134.69	3.896E-005	153.59	2.587E+000	-263.28	1.216E-005	-163.18
1.32	9.647E-005	-107.56	3.378E-005	151.32	2.863E+000	-258.87	8.713E-006	-159.82
1.34	9.288E-005	-105.93	2.496E-005	149.34	3.707E+000	-254.47	8.323E-006	-156.52
1.36	8.982E-005	-103.65	2.471E-005	147.74	3.635E+000	-251.39	8.027E-006	-153.39
1.38	8.724E-005	-101.95	2.592E-005	146.68	4.170E+000	-244.84	7.826E-006	-150.51
1.40	8.501E-005	-100.43	1.756E-005	146.25	4.844E+000	-246.68	7.668E-006	-147.96
1.42	8.305E-005	-99.13	1.461E-005	146.28	5.683E+000	-248.38	7.515E-006	-145.78
1.44	8.128E-005	-97.99	1.205E-005	147.54	6.744E+000	-249.44	7.418E-006	-143.88
1.46	7.965E-005	-96.97	9.858E-006	150.17	8.080E+000	-247.24	7.337E-006	-142.23
1.48	7.812E-005	-96.06	8.048E-006	154.63	9.716E+000	-258.79	7.265E-006	-140.94
1.50	7.665E-005	-95.48	6.604E-006	161.41	1.161E+001	-256.49	7.196E-006	-139.93
1.52	7.522E-005	-94.83	5.564E-006	170.73	1.252E+001	-265.68	7.127E-006	-139.14
1.54	7.381E-005	-94.49	4.925E-006	-177.92	1.499E+001	83.42	7.053E-006	-138.54
1.56	7.241E-005	-94.15	4.653E-006	-168.07	1.556E+001	71.93	6.974E-006	-138.11
1.58	7.102E-005	-93.88	4.659E-006	-155.55	1.524E+001	61.47	6.888E-006	-137.82
1.60	6.962E-005	-93.66	4.837E-006	-147.32	1.440E+001	53.64	6.796E-006	-137.63
1.62	6.823E-005	-93.53	5.092E-006	-141.41	1.340E+001	47.88	6.698E-006	-137.54
1.64	6.684E-005	-93.43	5.363E-006	-137.40	1.246E+001	43.97	6.593E-006	-137.51
1.66	6.545E-005	-93.36	5.616E-006	-134.41	1.165E+001	41.45	6.483E-006	-137.53
1.68	6.407E-005	-93.32	5.832E-006	-133.23	1.099E+001	39.91	6.369E-006	-137.60
1.70	6.270E-005	-93.38	6.003E-006	-132.38	1.044E+001	39.08	6.251E-006	-137.69
1.72	6.132E-005	-93.29	6.231E-006	-132.19	9.928E+000	38.90	6.964E-006	-137.58
1.74	5.998E-005	-93.31	6.214E-006	-133.43	9.625E+000	38.12	5.635E-006	-138.27
1.76	5.859E-005	-93.31	6.018E-006	-135.18	9.607E+000	41.46	5.529E-006	-138.58
1.78	5.018E-005	-93.29	5.787E-006	-136.78	8.770E+000	43.69	5.538E-006	-138.44
1.79	4.748E-005	-93.22	5.335E-006	-138.59	8.895E+000	49.37	4.760E-006	-134.69
1.80	4.490E-005	-93.13	4.948E-006	-139.49	9.098E+000	46.76	4.583E-006	-138.69

H = 5.00

X	A	PHASE(A) IN DEGREES	B	PHASE(B) IN DEGREES	A/B	PHASE(A/B) IN DEGREES	F	PHASE(F) IN DEGREES
0.00	1.234E-001	-178.33	0.000E+000				2.516E-002	139.54
0.02	1.232E-001	-178.34	2.202E-003	-177.06	6.053E+001	-1.38	2.514E-002	139.51
0.04	1.226E-001	-178.44	4.393E-003	-177.17	3.028E+001	-1.29	2.506E-002	139.41
0.06	1.225E-001	-178.63	6.599E-003	-177.39	2.020E+001	-1.28	2.502E-002	139.33
0.08	1.217E-001	-178.87	8.689E-003	-177.60	1.514E+001	-1.27	2.492E-002	139.15
0.10	1.213E-001	-179.13	1.077E-002	-177.93	1.214E+001	-1.28	2.479E-002	138.88
0.15	1.201E-001	179.77	1.571E-002	-179.35	8.123E+000	358.62	2.424E-002	137.62
0.20	1.193E-001	178.32	2.013E-002	179.47	6.123E+000	-1.08	2.362E-002	136.15
0.30	1.221E-001	174.28	2.705E-002	175.05	4.142E+000	-0.77	2.199E-002	132.84
0.40	9.452E-002	168.91	3.118E-002	169.17	3.171E+000	-0.24	1.974E-002	128.95
0.50	8.444E-002	162.43	3.241E-002	161.94	2.605E+000	0.49	1.737E-002	119.98
0.60	7.682E-002	155.13	3.152E-002	153.56	2.263E+000	1.57	1.498E-002	112.32
0.70	6.807E-002	147.33	2.909E-002	144.25	1.997E+000	3.06	1.267E-002	104.09
0.80	6.206E-002	139.21	2.579E-002	134.21	1.829E+000	5.14	1.053E-002	95.44
0.90	5.763E-002	131.16	2.215E-002	123.64	1.701E+000	7.52	8.660E-003	85.62
1.00	2.590E-002	123.39	1.853E-002	112.71	1.614E+000	10.48	7.015E-003	77.87
1.10	2.356E-002	116.16	1.517E-002	101.61	1.553E+000	14.54	5.615E-003	69.40
1.20	1.844E-002	109.67	1.218E-002	90.44	1.515E+000	19.19	4.443E-003	61.47
1.30	1.641E-002	104.16	9.624E-003	79.44	1.497E+000	24.48	3.477E-003	54.23
1.40	1.124E-002	99.81	7.448E-003	68.74	1.502E+000	31.06	2.694E-003	48.88
1.50	8.792E-003	96.78	5.734E-003	58.41	1.533E+000	38.37	2.069E-003	43.05
1.55	7.795E-003	95.60	4.950E-003	53.45	1.575E+000	42.25	1.781E-003	41.16
1.60	6.925E-003	95.14	4.326E-003	48.64	1.602E+000	46.54	1.581E-003	39.70
1.65	6.183E-003	94.92	3.715E-003	44.03	1.665E+000	50.94	1.381E-003	38.73
1.70	5.535E-003	95.09	3.213E-003	39.62	1.723E+000	55.38	1.206E-003	38.28
1.75	4.982E-003	95.48	2.751E-003	35.45	1.811E+000	59.94	1.055E-003	38.38
1.80	4.510E-003	96.07	2.345E-003	31.57	1.923E+000	64.58	9.324E-004	39.04
1.85	4.106E-003	96.97	1.998E-003	28.01	2.054E+000	68.98	8.258E-004	40.25
1.90	3.766E-003	98.04	1.681E-003	24.82	2.241E+000	73.22	7.372E-004	41.95
1.95	3.467E-003	99.22	1.413E-003	22.07	2.460E+000	77.13	6.646E-004	44.08
2.00	3.229E-003	100.44	1.182E-003	19.84	2.732E+000	80.61	6.055E-004	46.47
2.05	3.018E-003	101.69	9.843E-004	18.24	3.066E+000	83.44	5.581E-004	49.03
2.10	2.836E-003	102.89	8.165E-004	17.37	3.473E+000	85.52	5.233E-004	51.60
2.15	2.679E-003	104.01	6.757E-004	17.39	3.964E+000	86.83	4.980E-004	54.05
2.20	2.540E-003	105.04	5.590E-004	18.44	4.549E+000	86.59	4.855E-004	56.25
2.25	2.418E-003	105.95	4.643E-004	20.68	5.208E+000	85.27	4.454E-004	58.26
2.30	2.308E-003	106.75	3.893E-004	24.19	5.929E+000	82.56	4.284E-004	59.93
2.35	2.208E-003	107.44	3.320E-004	28.91	6.651E+000	78.52	4.135E-004	61.15
2.40	2.117E-003	108.02	2.901E-004	34.57	7.295E+000	73.47	4.001E-004	61.98
2.45	2.032E-003	108.53	2.611E-004	40.66	7.781E+000	67.83	3.877E-004	62.29
2.50	1.953E-003	108.98	2.428E-004	46.62	8.068E+000	62.28	3.756E-004	62.09
2.55	1.878E-003	109.23	2.299E-004	51.92	8.169E+000	57.32	3.644E-004	64.36
2.60	1.808E-003	109.49	2.222E-004	56.28	8.136E+000	53.22	3.534E-004	64.66
2.65	1.742E-003	109.71	2.170E-004	59.68	8.027E+000	50.05	3.426E-004	64.89
2.70	1.679E-003	109.88	2.128E-004	62.14	7.888E+000	47.74	3.319E-004	65.02
2.75	1.619E-003	110.01	2.088E-004	63.96	7.751E+000	46.16	3.213E-004	65.09
2.80	1.561E-003	110.12	2.044E-004	64.97	7.637E+000	45.19	3.110E-004	65.11
2.85	1.507E-003	110.21	1.999E-004	65.63	7.538E+000	44.69	3.009E-004	65.10
2.90	1.454E-003	110.29	1.944E-004	65.94	7.473E+000	44.35	2.910E-004	65.07
2.95	1.405E-003	110.35	1.899E-004	66.00	7.428E+000	44.36	2.814E-004	65.04
3.00	1.357E-003	110.41	1.857E-004	65.88	7.427E+000	44.57	2.721E-004	65.01

NUMERICAL RESULTS

The numerical values of A, B, and A/B for the zero frequency limit (i.e., $H = 0$) are listed in Table 1 for X ranging from 0 to 5. Of course, in this static limit, both A and B are purely real.

The numerical results for the complex values of A, B, and A/B are given in Table 2 for H ranging from 0.1 to 10. Here, the amplitudes of the quantities and their phases are given. For the smaller H values, it is immediately evident that the results are consistent with the zero-frequency values in Table 1. Also, if HX is sufficiently large, the complex values of A, B, and A/B do appear to approach their respective asymptotic limits. On a point of theoretical interest, we note that the asymptotic results are really only valid at quite large values of the parameters X and H. Nevertheless, they do serve as a good check on the numerical integration, since this is just when the integrands have the greatest number of oscillations over the range of integration.

A key parameter in the above formulation is H. This can be expressed in a fairly simple form as follows:

$$H = (\sigma\mu\omega)^{1/2}h = 0.086(\sigma_m f)^{1/2}h_{km}$$

if σ_m is the conductivity expressed in mmho m^{-1}, f is the frequency in Hz, and h_{km} is the burial depth in km. Thus, for example, if $\sigma_m = 1$, $f = 100$, and $h_{km} = 0.2$, we have H = 0.17. As we can see from the tables, this value of H is sufficiently small that the behavior of the functions A and B is very similar to that for the static case (i.e., zero frequency) where $H \equiv 0$.

We stress that the present analysis and results are applicable only to a homogeneous half-space model

for the earth. Nevertheless, this should serve as a guide for further work on the subject.

FINAL REMARKS

A graphical presentation of the ratio $|A/B|$ is given in Figure 3. As is indicated, the ordinate is the magnitude of the ratio between the horizontal and the vertical magnetic field at the observer for a line source on the surface. The abscissa X or x/h is the normalized horizontal coordinate (i.e., $x = 0$ for the observer at a distance h directly beneath the source). The phase of the quantity A/B is shown in Figure 4. In each case, the H values range from 0 to 10.

Both the amplitude and phase of the quantity A/B are measurable quantities if the observer is equipped with a crossed loop receiving antenna and suitable switching facility. If the value of H is known (or if it can be assumed to be effectively zero), the value of X should, in principle, be estimated from the measured ratio $|A/B|$. Even if H is not known,

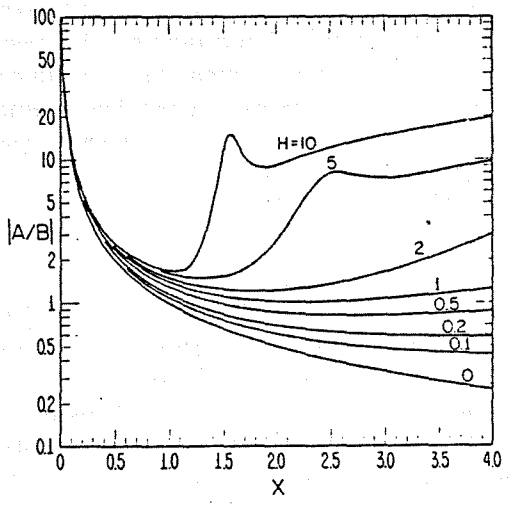


Fig. 3. Ratio of the magnitudes of the horizontal and vertical magnetic field components plotted as a function of the horizontal coordinate.

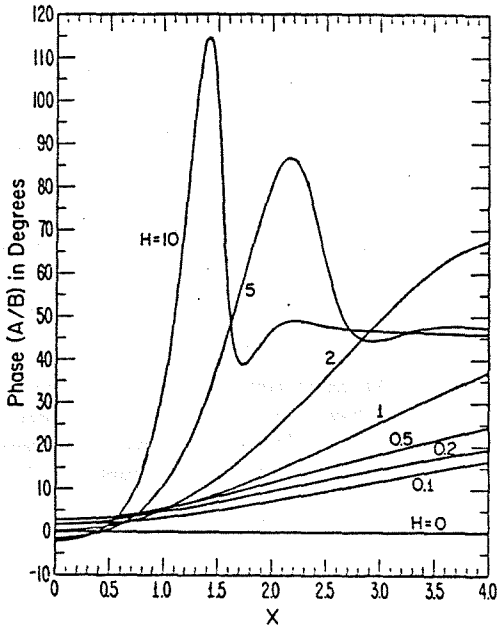


Fig. 4. Phase difference between the horizontal and the vertical magnetic field components plotted as a function of the horizontal coordinate.

the combined use of Figure 3 and Figure 4 should permit an unambiguous choice for X. Though operational procedures for carrying out this step have not been worked out, the approach seems promising.

The possibility of using an array of line sources on the surface is also being considered. At the expense of a more complicated source configuration with scanning capabilities, the observer would need only to signal the occurrence of a null. The up-link communication in this case could well be a seismically propagating impulse generated by a hammer blow.

REFERENCES

Grant, F. S., and G. F. West (1966), *Interpretation Theory in Applied Geophysics*, McGraw-Hill, New York.

Wait, J. R. (1962), *Electromagnetic Waves in Stratified Media*, chap. 2, Pergamon, New York.

Radio Science, Volume 7, Number 5, pages 587–591, May 1972

The effect of a buried conductor on the subsurface fields for line source excitation

James R. Wait[1]

Cooperative Institute for Research in the Environmental Sciences, University of Colorado, Boulder, Colorado 80302

(Received November 12, 1971.)

An approximate analytical method is presented for treating electromagnetic scattering from a slender cylindrical conductor buried in a homogeneous conducting half-space. The excitation is by a uniform line source of current located on the surface. The solution is achieved by an iterative method that accounts for the interaction of the induced current in the cylinder and the air-earth interface. It is shown that the cylindrical inhomogeneity will distort the profile of the subsurface magnetic field as the horizontal displacement is varied.

INTRODUCTION

In a previous paper [*Wait and Spies*, 1971] we considered an infinite line source or current-carrying cable on the surface of a flat homogeneous earth. The integral representation for the subsurface fields was reduced to tabulated functions. The results were of interest in mine communication problems, particularly during emergency conditions, for transmission paths through the overburden. The possibility that an array of such line sources could be used in direction-finding should not be overlooked [*Wait* 1971]. In the present paper, we wish to consider an inhomogeneous earth model that provides insight to the general problem. Specifically, we assume that the uniform half-space model adopted earlier [*Wait and Spies*, 1971] has a cylindrical conductor embedded within it. This is a possible means to account for the presence of conductive rails, pipes, or ore veins that would modify the total field at the subsurface observing point. In order to simplify the problem, we consider a two-dimensional model in which the buried cylindrical inhomogeneity is taken to be parallel to the surface line source.

Electromagnetic scattering from buried cylinders has been considered by *Parry and Ward* [1971] and *Hohmann* [1971] using integral equation formulations that require elaborate numerical techniques to achieve usable results. A modified integral equation technique for such problems has recently been developed (A. Q. Howard, Jr., personal communication, 1971). Also, we should point out that *D'Yakonov* [1959] has actually published a formally exact solution to the case for a buried cylinder of circular cross section. Unfortunately, his results are not in a form to obtain numerical data. Instead, we shall adopt an approximate analytical method that is particularly suitable when the buried conductor has a small cross section which is the case for a buried metallic pipe or rail.

[1] Consultant, Office of Telecommunications, Boulder, Colorado.

FORMULATION

We refer the reader to the previous paper [*Wait and Spies*, 1971] for the formulation of the necessary two-dimensional Green's function $G(x', y'; x, y)$ for the homogeneous nonmagnetic half-space of conductivity σ. As before, we neglect all displacement currents, and the time factor is exp $(i\omega t)$. Thus, the propagation constant in the half-space is $\gamma = (i\sigma\mu_0\omega)^{1/2}$.

We now consider the influence of an idealized inhomogeneity in the half-space for a current I on the surface. As indicated in Figure 1, the half-space is homogeneous for $y > 0$ except for a cylindrical region of conductivity $\hat{\sigma}$, radius a, centered at (x', y'). In order to simplify the analysis, we now consider the radius a to be sufficiently small that the currents induced in the cylinder are effectively symmetrical. As indicated in the Appendix, this is an adequate approximation provided $|\gamma a| \ll 1$ even though the exciting field is nonuniform. We note this does not place a restriction on the parameter $\hat{\gamma}a$ where $\hat{\gamma} = (i\hat{\sigma}\mu_0\omega)^{1/2}$. In fact, we wish to allow for the possibility

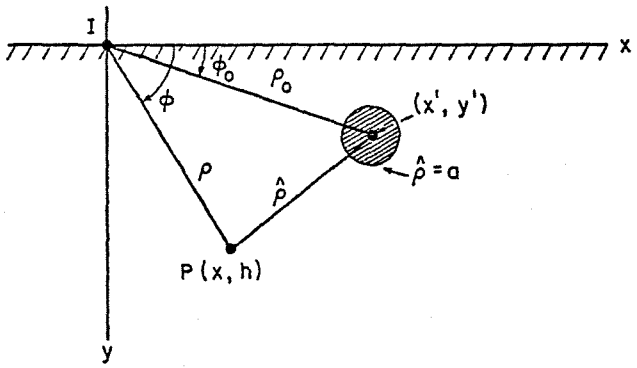


Fig. 1. Geometry for the buried cylinder in a conducting half-space.

that the cylindrical region has a high conductivity such as might exist for a metallic pipe or track buried in the earth.

In the first approximation, we argue that the field $E(x', y')$, which excites axial currents in the cylinder, is given by

$$E(x', y') = (-i\mu\omega I/2\pi)G(x', y'; 0, 0) \qquad (1)$$

Then the corresponding axial current $I_c^{(1)}$ is given by

$$I_c^{(1)} \simeq (Z)^{-1}E(x', y') \qquad (2)$$

where Z is the effective series impedance per unit length for excitation by a uniform axial field. In analogy to the development in the Appendix, we see that $Z = Z_i + Z_e$ which is the sum of the internal and external impedances, Z_i and Z_e, respectively. Without difficulty, we find that

$$Z_i = [\hat{\eta} I_0(\hat{\gamma}a)]/[2\pi a I_1(\hat{\gamma}a)] \qquad (3)$$

where I_0 and I_1 are modified Bessel functions of order zero and one, respectively, and $\hat{\eta} = i\mu_0\omega/\hat{\gamma}$ is the intrinsic impedance of the material inside the cylinder. Here, we note that in the low-frequency limit (i.e., $\omega \to 0$), Z_i approaches $(\pi a^2\sigma)^{-1}$, which is the direct-current resistance per unit length of the cylinder. On the other hand, at high frequencies where $|\hat{\gamma}a| \gg 1$, Z_i is well approximated by $Z_i \simeq \hat{\eta}/(2\pi a) = i\mu_0\omega/(2\pi\hat{\gamma}a)$ which, of course, vanishes in the perfect conductivity limit. Eddy current losses within the cylinder are accounted for by (3), and the numerical calculations can be facilitated by expressing I_0 and I_1 in terms of Thomson's ber and bei functions and their derivatives:

$$I_0[(i)^{1/2}Z] = \text{ber } Z + i \text{ bei } Z$$

and

$$i^{1/2}I_1[(i)^{1/2}Z] = \text{ber}' Z + i \text{ bei}' Z$$

An adequate form for the external impedance is

$$Z_e \simeq \frac{\eta K_0(\gamma a)}{2\pi a K_1(\gamma a)} \simeq \frac{i\mu_0\omega}{2\pi}\left(\log\frac{1}{\gamma a} + 0.116\right) \qquad (4)$$

since we have already adopted the premise that $|\gamma a| \ll 1$ (see Appendix).

The total field E_T at $P(x, h)$ is now regarded as the sum of the direct field due to the line source I at (0, 0) and the secondary or scattered field from the cylinder at (x', y'). Thus, to within the first-order approximation

$$E_T^{(1)}(x, h) = \frac{-i\mu\omega I}{2\pi} G(x, y; 0, 0) - \frac{i\mu\omega I_c^{(1)}}{2\pi} G(x, y; x', y') \qquad (5)$$

which automatically satisfies the boundary condition at the air-ground interface if we employ the form of the Green's function given in *Wait and Spies* [1971].

To obtain a second order approximation $I_c^{(2)}$, we correct $I_c^{(1)}$ in (5) to account for the interaction with the interface. Thus

$$I_c^{(2)} \simeq Z^{-1}E^{(1)} \qquad (6)$$

where

$$E^{(1)} \simeq -\frac{i\mu\omega I}{2\pi} G(x', y'; 0, 0)(1 - \Gamma^2 a^2 \hat{G})$$

where $\Gamma^2 a^2 = i\mu_0\omega/(2\pi Z)$ and $\hat{G}$ is the appropriate Green's function. Using $h \gg a$, we find that

$$\hat{G} \cong -K_0(2\gamma y') + 2\int_0^\infty \frac{\exp(-2uy')}{u + \lambda}\, d\lambda \qquad (7)$$

$$= -K_0(\beta) + 2\left[\frac{d^2}{d\beta^2} K_0(\beta) + \frac{d}{d\beta}\frac{\exp(-\beta)}{\beta}\right] \qquad (8)$$

where $\beta = 2\gamma y'$. Carrying out the derivative operations leads to

$$\hat{G} = +K_0(\beta) + (2/\beta)K_1(\beta) - (2/\beta^2)(1 + \beta)\exp(-\beta) \qquad (9)$$

The corresponding second-order approximated field at $P(x, h)$ is thus

$$E_T^{(2)}(x, h) = \frac{-i\mu\omega I}{2\pi} G(x, y; 0, 0) - \frac{i\mu\omega I_c^{(2)}}{2\pi} G(x, y; x', y') \qquad (10)$$

This in turn can be employed to calculate the third-order approximated current $I_c^{(3)}$. When the inter-

active process is continued indefinitely, we arrive at

$$I_e \simeq Z^{-1}E'(x', y') \tag{11}$$

where

$$E'(x', y') \simeq -\frac{i\mu_0\omega I}{2\pi} G(x', y'; 0, 0)$$
$$\cdot[1 - \Gamma^2a^2\hat{G} + (\Gamma^2a^2\hat{G})^2 - (\Gamma^2a^2\hat{G})^3 + \cdots] \tag{12}$$

which is formally summed to give

$$E'(x', y') \simeq -\frac{i\mu_0\omega I}{2\pi} G(x', y'; 0, 0)(1 + \Gamma^2a^2\hat{G})^{-1} \tag{13}$$

Using (11), we now obtain the final form of the perturbed total field at $P(x, h)$:

$$E_T(x, h) \simeq -\frac{i\mu_0\omega I}{2\pi}[G(x, h; 0, 0)$$
$$- \Omega G(x', y'; 0, 0)G(x, h; x', y')] \tag{14}$$

where

$$\Omega = \Gamma^2a^2/(1 + \Gamma^2a^2\hat{G}) \tag{15}$$

The corresponding magnetic field components are

$$H_{Tz}(x, h) \simeq \frac{I}{2\pi}\left[\frac{\partial G(x, y; 0, 0)}{\partial y}\right.$$
$$\left. - \Omega G(x', y'; 0, 0)\frac{\partial G(x, y; x', y')}{\partial y}\right]_{y=h} \tag{16}$$

$$H_{Ty}(x, h) \simeq -\frac{I}{2\pi}\left[\frac{\partial G(x, y; 0, 0)}{\partial x}\right.$$
$$\left. - \Omega G(x', y'; 0, 0)\frac{\partial G(x, y; x', y')}{\partial x}\right]_{y=h} \tag{17}$$

Using the integral forms $A(H, X)$, $B(H, X)$, and $F(H, X)$ defined in *Wait and Spies* [1971], we can express (14), (16), and (17) as follows:

$$E_T = \frac{-i\mu_0\omega I}{2\pi}[F(H, X)$$
$$- \Omega F(H', X')\{F(H + H', X - X')$$
$$+ K_0[\exp(i\pi/4)R_1] - K_0[\exp(i\pi/4)R_2]\}] \tag{18}$$

$$H_{Tz} = \frac{-I}{2\pi h}[A(H, X)$$
$$- \Omega F(H', X')\{K_1[\exp(i\pi/4)R_1]\exp(i\pi/4)HS_1$$
$$- K_1[\exp(i\pi/4)R_2]\exp(i\pi/4)HS_2$$
$$+ A(H + H', X - X')\}] \tag{19}$$

and

$$H_{Ty} = \frac{I}{2\pi h}[B(H, X)$$
$$- \Omega F(H', X')\{K_1[\exp(i\pi/4)R_1]\exp(i\pi/4)HC_1$$
$$- K_1[\exp(i\pi/4)R_2]\exp(i\pi/4)HC_2$$
$$+ B(H + H', X - X')\}] \tag{20}$$

where

$$H = (\sigma\mu_0\omega)^{1/2}h \qquad H' = (\sigma\mu_0\omega)^{1/2}y'$$
$$X = x/h \qquad X' = x'/h$$
$$R_1 = [H^2(X - X')^2 + (H - H')^2]^{1/2}$$
$$R_2 = [H^2(X - X')^2 + (H + H')^2]^{1/2}$$
$$C_1 = \frac{(x - x')}{[(x - x')^2 + (h - y')^2]^{1/2}}$$
$$C_2 = \frac{(x - x')}{[(x - x')^2 + (h + y')^2]^{1/2}}$$
$$S_1 = \frac{(h - y')}{[(x - x')^2 + (h - y')^2]^{1/2}}$$
$$S_2 = \frac{(h - y')}{[(x - x')^2 + (h + y')^2]^{1/2}}$$

AN ILLUSTRATIVE EXAMPLE

The explicit forms given by (18), (19), and (20) can be used to calculate the resultant fields at the subsurface observation point at depth x for any specified location of the cylindrical conductor. Of particular interest is the vertical component H_{Ty} of the magnetic field since this is readily detected by a rudimentary loop contained in the horizontal plane. In Figures 2 and 3, we illustrate the normalized field magnitude

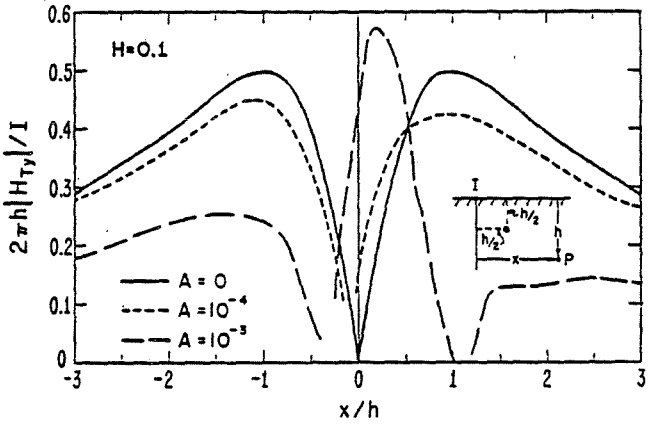


Fig. 2. Normalized vertical magnetic field at a depth h for $H = 0.1$.

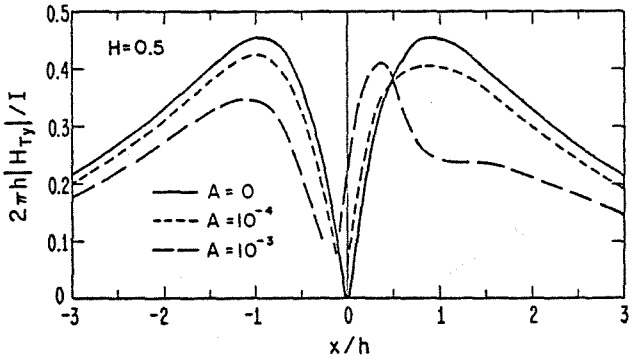


Fig. 3. Normalized vertical magnetic field at a depth h for $H = 0.5$.

$2\pi h\ |H_{Ty}|/I$ as a function of the relative horizontal displacement, x/h, of the observer. For this example, we located the buried metallic cylinder at $x = h/2$ and $y = h/2$. In Figures 2 and 3, we choose $H = (\sigma\mu_0\omega)^{1/2}h$ to be 0.1 and 0.5 respectively, while $A = |\gamma a| = (\sigma\mu_0\omega)^{1/2}a$ is 0.0, 10^{-4}, and 10^{-3} for each figure. Also, we assume that $\hat{\sigma}/\sigma = 10^7$.

First of all, we note the curves for $A = 0$ in Figures 2 and 3, corresponding to a homogeneous half-space, are perfectly symmetrical with the expected null of the vertical magnetic field directly beneath the line source. However, when $A > 0$, the asymmetry becomes evident, and the null is shifted. In this sense, the buried conductor distorts the subsurface field.

In order to attach a more physical meaning to the curves in Figures 2 and 3, we note first of all that the parameter $H = (\sigma_m f)^{1/2}h_{km} \times 8.6 \times 10^{-2}$, when σ_m is the overburden conductivity expressed in mmhos/m, f is the frequency in Hz and h_{km} is the depth of the observer expressed in km. Thus, if $\sigma_m = 1$ and $f = 100$, we see that $H = 0.1$ and 0.5 corresponds to $h_{km} = 0.116$ and 0.58, respectively. Then the parameter values $A = 10^{-4}$ and 10^{-3} correspond to a buried cylinder radius of 0.116 and 1.16 m, respectively, with a conductivity of 10^4 mhos/m. Of course, by a suitable scaling of the parameters, other possibilities exist. Also, with limited numerical effort, many other cases can be treated.

CONCLUDING REMARKS

The analytical method given in this paper permits quantitative estimates to be made of the effect of an idealized inhomogeneity in the conducting half-space. The method is admittedly not usable if the buried cylinder is very near the air-earth interface. Also, it is restricted to cylinder radii that are electrically small in terms of the wavelength in the external media. In other words, the parameter A should be small compared with 1. Recent numerical comparisons with integral equation formulations indicate, however, that the method works well for A as large as 0.1 (A. Q. Howard, Jr., personal communication, 1971).

APPENDIX

The method used to estimate the scattered field from a cylinder buried in the half-space employs certain concepts which can be clearly illustrated in the problem [*Wait*, 1959] of scattering from a cylinder of electrical constants $\hat{\sigma}$, $\hat{\epsilon}$, and μ_0, located in an infinite medium of electrical constants σ, ϵ, and μ_0.

The situation is illustrated in Figure 4, in which we take the line current I at (ρ_0, ϕ_0) to be parallel to the axis of the cylinder. Without repeating any details of the derivation, we can write down an exact expression for the electric field E_z external to the cylinder in the following form:

$$E_z = (-i\mu_0\omega I/2\pi)K_0(\gamma R) + E_z^s \tag{21}$$

where

$$R = [\rho^2 + \rho_0^2 - 2\rho\rho_0 \cos(\phi - \phi_0)]^{1/2}$$

$$\gamma = [i(\sigma + i\epsilon\omega)\mu_0\omega]^{1/2}$$

and E_z^s is the scattered or secondary field. We know that

$$E_z^s = -i\mu_0\omega I/2\pi \cdot \sum_{n=0}^{\infty} \epsilon_n A_n K_n(\gamma\rho_0) K_n(\gamma\rho) \cos n(\phi - \phi_0) \tag{22}$$

where

$$A_n = \frac{I_n'(\gamma a)}{K_n'(\gamma a)} \cdot \frac{\eta[I_n(\gamma a)]/[I_n'(\gamma a)] - \hat{\eta}[I_n(\hat{\gamma}a)]/[I_n'(\hat{\gamma}a)]}{Z_{s,n} + Z_{i,n}}. \tag{23}$$

where

$$Z_{s,n} = [-\eta K_n(\gamma a)]/[K_n'(\gamma a)]$$

$$Z_{i,n} = [\hat{\eta} I_n(\hat{\gamma}a)]/[I_n'(\hat{\gamma}a)]$$

and where $\eta = i\mu_0\omega/\gamma$, $\hat{\eta} = i\mu_0\omega/\hat{\gamma}$, and $\hat{\gamma} = [i(\hat{\sigma} + i\hat{\epsilon}\omega)\mu_0\omega]^{1/2}$.

If we now insist that $|\gamma a| \ll 1$ (without any restriction on $\hat{\gamma}a$), we can approximate the Bessel functions of argument γa by the leading term of their series expansions. Also, if additionally, we allow $\rho \gg a$, only

the $n = 0$ term in (22) need be retained. For this dominant term, we see that

$$A_0 \simeq \frac{-i\mu_0\omega}{2\pi(Z_e + Z_i)}\,[1 - (Z_i/2)(\sigma + i\epsilon\omega)a]$$

$$\simeq \frac{-i\mu_0\omega}{2\pi(Z_e + Z_i)} \tag{24}$$

where

$$Z_e = Z_{e,0}/2\pi a$$

$$Z_i = Z_{i,0}/2\pi a$$

are the external and the internal impedances of the cylinder as employed in the context of the previous derivation. Thus, (22) is expressible in the meaningful form

$$E_s^* \simeq \frac{-i\mu_0\omega I_e}{2\pi} K_0(\gamma\rho) \tag{25}$$

where

$$I_e = \frac{-i\mu_0\omega I}{2\pi} K_0(\gamma\rho_0)[Z_e + Z_i\Gamma^1 \tag{26}$$

is the total *induced* current in the cylinder. These results are consistent with the analysis for the half-space configuration provided we recognize that the appropriate Green's function here is simply the modified Bessel function $K_0(\gamma\rho)$.

Acknowledgments. I am indebted to Dr. David A. Hill for his cogent comments on an earlier version of this paper. Also, I wish to thank Allen Q. Howard, Jr., for carrying out the numerical calculations and for his collaboration on related integral equation approaches to the problem. The research was supported by the U. S. Bureau of Mines.

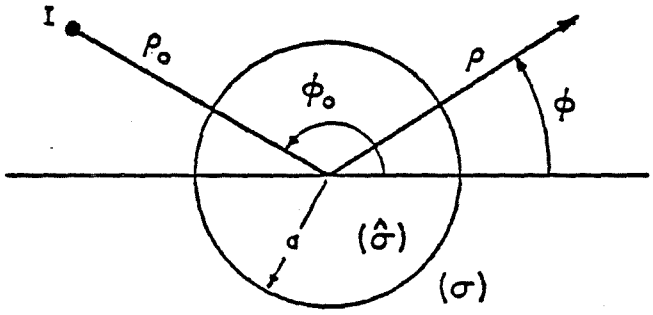


Fig. 4. Prototype problem of line source in presence of cylinder in an infinite medium.

REFERENCES

D'Yakonov, B. P. (1959), The diffraction of electromagnetic waves by a circular cylinder in a homogeneous half-space, *Bul. Acad. Sci. USSR, Geophys. Ser.*, no. 9, 950–955.

Hohmann, G. W. (1971), Electromagnetic scattering by conductors in the earth near a line source of current, *Geophysics, 36*, 101–131.

Parry, J. R., and S. H. Ward (1971), EM scattering from cylinders of arbitrary cross section in a conductive half-space, *Geophysics, 36*, 67–100.

Wait, J. R. (1959), *Electromagnetic Radiation from Cylindrical Structures*, Pergamon, Oxford, England.

Wait, J. R. (1971), Array technique for electromagnetic positional determination of a buried receiving point. *Elect. Lett. 7*(8), 186–187.

Wait, J. R., and K. P. Spies (1971), Subsurface electromagnetic fields of a line source on a conducting half-space, *Radio Sci. 6*(8/9), 781–786.

Reprint from the Review
PURE AND APPLIED GEOPHYSICS (PAGEOPH)
Formerly 'Geofisica pura e applicata'
Vol. 95, 1972/III BIRKHÄUSER VERLAG BASEL Pages 150–156

The Sub-Surface Magnetic Fields Produced by a Line Current Source on a Non-Flat Earth [1])

By JAMES R. WAIT [2]) and R. E. WILKERSON [2])

Summary – A simple cylindrical model is employed to estimate the effect of non-flatness of the ground on the sub-surface electromagnetic field from a current-carrying cable on the surface. It is shown that, if the surface curvature is sufficiently small, the fields in the cylinder model are very similar to those for the conducting half-space model of the earth employed earlier. The results can be used to provide estimates of expected errors in electromagnetic direction-finding of a buried receiving terminal.

1. Introduction

In a previous communication [1] [3]), we reported on the analysis and calculations of the sub-surface fields in a conducting half-space produced by a line current located on the surface. Similar calculations have since been brought to my attention [2], [3]. In our work, we were interested in the application of the basic Green's function to scattering from inhomogeneities such as longitudinal conductors. The latter can be expected to have a major effect on modifying the structure of the received field at the buried terminal. This could pose a serious limitation on the direction-finding capability of a simple crossed loop receiving device.

Here, we would like to consider an alternative and much simpler approach that should give needed insight to the effect of non-flatness on the ground surface. Thus, we adopt a cylindrical model chosen so that the curvature of the surface is matched to the local topography rather than the mean curvature of the earth (for present purposes, the latter is zero!).

2. A classical preliminary problem

The basic prototype problem is the classical one of a uniform line current source located outside an infinitely long homogeneous cylinder of radius R_0 [4]. The situation

---

[1]) The research reported here was supported in part by the Mine Safety Center, U.S. Bureau of Mines.

[2]) Institute for Telecommunication Sciences, Office of Telecommunications, Boulder, Colorado, 80302, U.S.A.

[3]) Numbers in brackets refer to References, page 156.

is illustrated in Figure 1 where we have chosen a cylindrical coordinate system (ϱ, ϕ, z). The external medium $\varrho > R_0$ is free space with permittivity ε_0 and the internal medium $\varrho < R_0$ has a conductivity σ and permittivity ε. The line source with current I amps, located at (ϱ_0, ϕ_0, z), varies harmonically as $\exp(i\,\omega\,t)$ where $\varrho_0 \geqq R_0$.

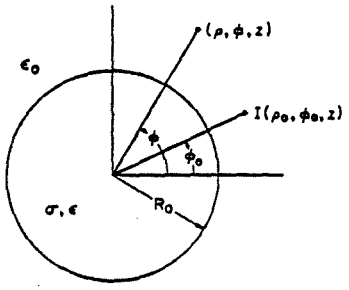


Figure 1
The prototype cylinder problem

For $\varrho > R_0$, we have only a z-component of the total electric field that can be written

$$E_z = E_z^p + E_z^s \tag{1}$$

as a sum of a primary and secondary parts. We know that [4]

$$E_z^p = -\frac{i\,\mu_0\,\omega\,I}{2\,\pi} K_0[\gamma_0[\varrho^2 + \varrho_0^2 - 2\,\varrho\,\varrho_0 \cos(\phi - \phi_0)]^{1/2}] \tag{2}$$

where $\gamma_0 = i(\varepsilon_0\,\mu_0)^{1/2}\,\omega$ and $\mu_0 = 4\,\pi \times 10^{-7}$. Using a standard addition theorem for modified Bessel functions, this, for $R_0 < \varrho < \varrho_0$, can be written

$$E_z^p = -\frac{i\,\mu_0\,\omega\,I}{2\,\pi} \sum_{m=0}^{\infty} \varepsilon_m\,K_m(\gamma_0\,\varrho_0)\,I_m(\gamma_0\,\varrho)\cos m(\phi - \phi_0) \tag{3}$$

where $\varepsilon_m = 1$ for $m = 0$, $= 2$ for $m = 1, 2, 3, \ldots$. Then, it follows that the secondary field for $\varrho > R_0$ will have the form

$$E_z^s = -\frac{i\,\mu_0\,\omega\,I}{2\,\pi} \sum_{m=0}^{\infty} \varepsilon_m\,A_m\,K_m(\gamma_0\,\varrho)\cos m(\phi - \phi_0) \tag{4}$$

where A_m is a coefficient yet to be determined.

The next step is to write down a suitable form for the total internal field. Thus, for the sourceless region $\varrho < R_0$, we have

$$E_z = -\frac{i\,\mu_0\,\omega\,I}{2\,\pi} \sum_{m=0}^{\infty} \varepsilon_m\,B_m\,I_m(\gamma\varrho)\cos m(\phi - \phi_0) \tag{5}$$

where $\gamma = (i\,\sigma\,\mu_0\,\omega - \varepsilon\,\mu_0\,\omega^2)^{1/2}$ and where B_m is also an unknown coefficient.

The boundary conditions for the present problem requires that E_z and $\partial E_z/\partial\varrho$ be continuous at $\varrho = R_0$. This leads to the system

$$K_m(\gamma_0\,\varrho_0)\,I_m(\gamma_0\,R_0) + A_m\,K_m(\gamma_0\,R_0) = B_m\,I_m(\gamma\,R_0) \tag{6}$$

$$K_m(\gamma_0\,\varrho_0)\,\gamma_0\,I_m'(\gamma_0\,R_0) + A_m\,\gamma_0\,K_m'(\gamma_0\,R_0) = B_m\,\gamma\,I_m'(\gamma\,R_0) \tag{7}$$

where the prime indicates differentiation with respect to the argument of the Bessel function. On eliminating A_m from (6) and (7), we get

$$B_m = -\frac{K_m(\gamma_0\,\varrho_0)}{\gamma_0\,R_0}\,\frac{1}{[I_m(\gamma\,R_0)\,K_m'(\gamma_0\,R_0) - (\gamma/\gamma_0)\,I_m'(\gamma\,R_0)\,K_m(\gamma_0\,R_0)]} \tag{8}$$

where we have used the Wronskian relation

$$K_m(x)\,I_m'(x) - K_m'(x)\,I_m(x) = 1/x.$$

Letting $\varrho_0 \to R_0$, we see that

$$B_m = -\left[I_m(\gamma\,R_0)\left(\frac{\gamma_0\,R_0\,K_m'(\gamma_0\,R_0)}{K_m(\gamma_0\,R_0)}\right) - \gamma\,R_0\,I_m'(\gamma\,R_0)\right]^{-1}. \tag{9}$$

This constitutes a statement of the exact solution of the problem.

For the present application, we can exploit the condition $|\gamma_0\,R_0| \ll 1$. Then, using the fact that for $x \ll 1$, $K_m'(x)/K_m(x) \sim -m/x$, (9) reduces to

$$B_m \simeq [m\,I_m(\gamma\,R_0) + \gamma\,R_0\,I_m'(\gamma\,R_0)]^{-1}. \tag{10}$$

Inserting this into (5), we have the following explicit expression for the internal fields for a line source on the surface of the cylinder

$$E_z = -\frac{i\,\mu_0\,\omega\,I}{2\,\pi}\sum_{m=0}^{\infty}\varepsilon_m\,\frac{I_m(\gamma\,\varrho)\cos m(\phi - \phi_0)}{m\,I_m(\gamma\,R_0) + \gamma\,R_0\,I_m'(\gamma\,R_0)}. \tag{11}$$

Corresponding expressions for the magnetic fields are

$$H_\varrho = -\frac{1}{i\,\mu_0\,\omega\,\varrho}\,\frac{\partial E_z}{\partial\phi} = \frac{I}{2\,\pi\,\varrho}\sum_{m=0}^{\infty}\varepsilon_m\,\frac{m\,I_m(\gamma\,\varrho)\sin m(\phi - \phi_0)}{m\,I_m(\gamma\,R_0) + (\gamma\,R_0)\,I_m'(\gamma\,R_0)} \tag{12}$$

and

$$H_\phi = \frac{1}{i\,\mu_0\,\omega}\,\frac{\partial E_z}{\partial\varrho} = \frac{I}{2\,\pi\,\varrho}\sum_{m=0}^{\infty}\varepsilon_m\,\frac{(\gamma\,\varrho)\,I_m'(\gamma\,\varrho)\cos m(\phi - \phi_0)}{m\,I_m(\gamma\,R_0) + (\gamma\,R_0)\,I_m'(\gamma\,R_0)}. \tag{13}$$

3. *Application to a topographic feature*

We now apply the prototype solution to the situation depicted in Figure 2. A Cartesian coordinate system (x, y, z) is chosen with the line source I located at the origin. The observer at P has coordinates (x, y, z) in the Cartesian system, and coordinates (ϱ, ϕ, z) in the cylindrical system where the latter has an origin at Q. The line Q is the center of curvature of the cylindrical surface, and it has Cartesian coordinates (x_0, y_0, z). [Note that the z-axes of the two coordinate systems are coincident but in opposite directions.]

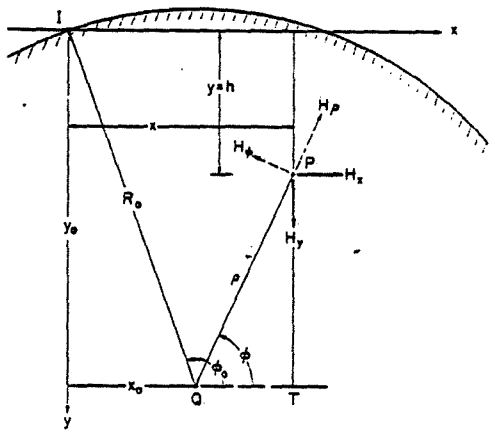


Figure 2
Geometry for a line current source on the cylindrical surface and the observer at buried location P

The quantities of interest are the orthogonal components of the magnetic field at the observer P expressed in the Cartesian system. Clearly, these are obtained as follows:

$$H_x = H_\varrho \cos\phi - H_\phi \sin\phi \tag{14}$$

$$H_y = -H_\varrho \sin\phi - H_\phi \cos\phi \tag{15}$$

where H_ϱ and H_ϕ are given by (12) and (13). For numerical work and comparisons with earlier studies (e.g. [1]), it is desirable to define two dimensionless field parameters A and B as follows:

$$A = -\frac{2\pi h}{I} H_x = A_\varrho \cos\phi - A_\phi \sin\phi \tag{16}$$

and

$$B = \frac{2\pi h}{I} H_y = A_\varrho \sin\phi + A_\phi \cos\phi \tag{17}$$

where

$$A_\varrho = -(2\pi h/I)\, H_\varrho \quad \text{and} \quad A_\phi = -(2\pi h/I)\, H_\phi$$

From (12) and (13), the latter are given explicitly as follows:

$$A_\varrho = -\left(\frac{h}{\varrho}\right) \sum_{m=0}^{\infty} \varepsilon_m \frac{m\, I_m(\gamma\, \varrho) \sin m(\phi - \phi_0)}{m\, I_m(\gamma\, R_0) + (\gamma\, R_0)\, I'_m(\gamma\, R_0)} \tag{18}$$

and

$$A_\phi = -\left(\frac{h}{\varrho}\right) \sum_{m=0}^{\infty} \varepsilon_m \frac{(\gamma\, \varrho)\, I'_m(\gamma\, \varrho) \cos m(\phi - \phi_0)}{m\, I_m(\gamma\, R_0) + (\gamma\, R_0)\, I'_m(\gamma\, R_0)} \tag{19}$$

where

$$I_m(\gamma\, R_0) = \sum_{n=0}^{\infty} \frac{(\gamma\, R_0)^{m+2n}}{n!(m+n)!\, 2^{m+2n}} \tag{20}$$

is the power series definition of the modified Bessel function. Of course, (18) and (19) are only valid if $\varrho \leqq R_0$.

In the case where displacement currents in the earth are negligible (i.e., where $\varepsilon\, \omega \ll \sigma$), we see that $\gamma \simeq (i\, \sigma\, \mu_0\, \omega)^{1/2}$. Then the modified Bessel functions of order m can be expressed in terms of Thompson's ber and bei function of order m. Specifically, $I_m(Z\, e^{i\pi/4}) = e^{-i(\pi/2)m}\, (\mathrm{ber}_m\, Z + i\, \mathrm{bei}_m\, Z)$ where $Z \cong |\gamma\, R_0| \simeq (\sigma\, \mu_0\, \omega)^{1/2}\, R_0$ is real.

Some needed geometrical relations follow immediately from Figure 2. First, we note that $y_0 = (R_0^2 - x_0^2)^{1/2}$, then $P\, T = y_0 - h$ and $Q\, T = x - x_0$. Consequently

$$\tan\phi = \frac{P\, T}{Q\, T} = \frac{(R_0^2 - x_0^2)^{1/2} - h}{x - x_0} \tag{21}$$

or

$$\phi = \arctan\left\{\frac{[(R_0/h)^2 - (x_0/h)^2]^{1/2} - 1}{(x/h) - (x_0/h)}\right\}. \tag{22}$$

Also, it is seen that

$$\varrho = [(P\, T)^2 + (Q\, T)^2]^{1/2}$$

and thus

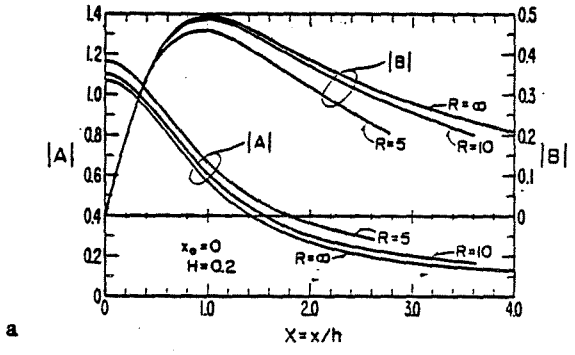
$$\gamma\, \varrho = (\gamma\, h)\left\{\left[\left[\left(\frac{R_0}{h}\right)^2 - \left(\frac{x_0}{h}\right)^2\right]^{1/2} - 1\right]^2 + \left(\frac{x}{h} - \frac{x_0}{h}\right)^2\right\}^{1/2} \tag{23}$$

where $\gamma\, h \simeq e^{i\pi/4}\, H$ and $H = (\sigma\, \mu_0\, \omega)^{1/2}\, h$. Furthermore, because P is an interior point, $\varrho < R_0$ and (23) tells us that $(x - x_0)^2 \leqq R_0^2 - (h - y_0)^2$.

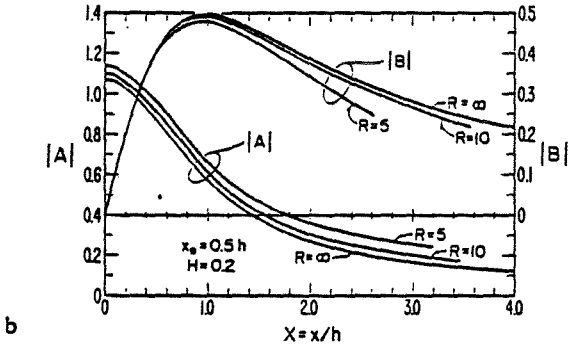
4. Discussion of some typical numerical results

Numerical calculations of the normalized field functions A and B have been carried for a range of the dimensionless parameters $H = |\gamma\, h|$, $R = |\gamma\, R_0|$, $X = x/h$ and $X_0 = x_0/h$. In order to illustrate the results here, we plot $|A|$ and $|B|$ as a function of the dimensionless distance parameter $X = x/h$ for $R = 5$, 10, and ∞. For the curves in Figure 3a,

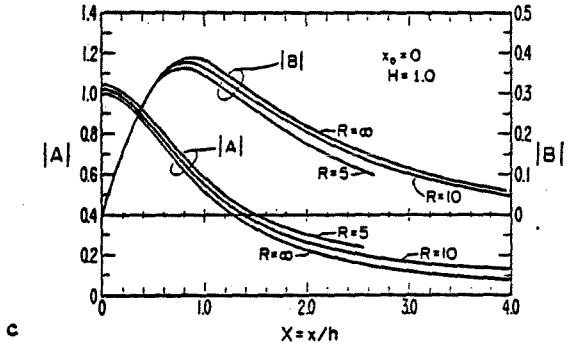
we have $x_0=0$ and $H=0.2$, in Figure 3b, we have $x_0=0.5h$ and $H=0.2$, and in Figure 3c, we have $x_0=0$ and $H=1.0$. The qualitative behavior of the curves is very similar in all three cases. The effect of finite curvature of the air-ground interface is to increase the level of the normalized horizontal field (i.e., $|A|$), while the maximum response of the vertical field (i.e., $|B|$) is lowered somewhat. Actually, the curves designated $R=\infty$ are based on the results for the conducting half-space or flat earth model as described before [1]. As we see, if the radius of curvature of the surface is sufficiently large, it



a



b



c

Figures 3, a, b and c
Normalized magnetic fields as a function of horizontal distance for geometry of Figure 2

appears that the conducting cylinder results approach those for the half-space. This is a reassuring check on the numerical data, since the method of calculation is vastly different in the two cases.

To deal with a specific example, we choose the ground conductivity σ to be 1 millimho/m and the operating frequency to be 100 Hz. Then the parameter $H=0.20$ if the observer depth $h=225$ m, while the parameter $H=1.0$ if $h=1.12$ km. Thus, if $R=10$, the radius of curvature R_0 of the surface is 11.2 km, while if $R=5$, we have $R_0=5.6$ km. These correspond to moderately rough terrain features.

The theory and the numerical data available for this problem should be useful for making various estimates of the expected errors introduced by the non-flatness of the ground on the direction of the magnetic field at a buried observer. In particular, the phase angle between the complex phasors A and B at the observer position will also depend on the radius of curvature R_0. This factor and other interesting questions are reserved for future work on this subject.

References

[1] J. R. Wait and K. P. Spies, *Sub-surface electromagnetic fields of a line source on conducting half-space*, Radio Sci. *6* (August–September 1971), 781-786.

[2] D. B. Large, Private communication (Westinghouse Georesearch Laboratory, Boulder, Colo. Jan. 1971).

[3] G. W. Hohmann, *Electromagnetic scattering by conductors in the earth near a line source of current*, Geophys. *36*, No. 1 (1971).

[4] J. R. Wait, *Electromagnetic radiation from cylindrical structures* (Pergamon Press, Oxford, England, 1959).

(Received 26th July 1971)

Canadian Journal of Physics, Vol. 51, No. 14, 1973, Published by the National Research Council of Canada

Subsurface Electromagnetic Fields of a Grounded Cable of Finite Length[1]

DAVID A. HILL AND JAMES R. WAIT

Institute for Telecommunication Sciences, Office of Telecommunications, U.S. Department of Commerce and Cooperative Institute for Research in Environmental Sciences, University of Colorado, Boulder, Colorado 80302

Received March 15, 1973

The subsurface fields of a finite line source or current-carrying cable are examined. Some special cases, such as the low-frequency limit, are treated analytically, and some simple working formulas are obtained. The general field expressions are reduced to single integrals with finite limits that are evaluated numerically. It is shown that if the source cable is sufficiently long, the fields are approximated by those for an infinite cable. The results have possible application to downlink communication and radio location of trapped miners.

On étudie les champs produits sous la surface du sol par une source constituée par une portion rectiligne finie d'un câble transportant du courant. Certains cas spéciaux, par exemple, la limite aux basses fréquences, sont traités analytiquement, et quelques formules directement applicables sont obtenues. Les expressions générales des composantes de champ sont réduites à des intégrales simples avec des limites finies, et ces intégrales sont évaluées numériquement. On montre que si le câble source est suffisamment long, les champs sont approximativement les mêmes que ceux d'un câble infini. Les résultats ont des applications pour les communications souterraines et la localisation par radio de mineurs emprisonnés.

[Traduit par le journal]

Can. J. Phys., 51, 1534 (1973)

Introduction

The subsurface fields of an infinite line source on a conducting half-space have been examined by Wait and Spies (1971). In any real communication link from the surface to an underground terminal, the line source or current-carrying cable is of finite length. Here, we examine the subsurface fields of a finite line source with the purpose of determining what cable length is sufficient, and when the infinite line source is a good approximation. The earth is taken to be a homogeneous conducting half-space, and the current in the cable is assumed to be constant. The latter assumption is well justified at audio frequencies when an insulated cable is terminated by grounded electrodes that are separated by distances small compared with a free-space wavelength (Wait 1952; Sunde 1968).

Formulation

The geometry of the line source of length $2l$ located on the half-space, and the observer in the half-space, are as shown in Fig. 1. The observer is located at (x, y, z), and the x-directed source current I runs from $-l$ to l on the x axis. The current varies as $\exp(i\omega t)$, and the angular frequency ω is sufficiently low that all displacement currents are negligible. The Hertz vector contains both x and z components (Π_x and Π_z) and the contribution from an incremental source of length dx' located at x' is given by Wait (1961) and Banos (1966):

$$d\Pi_x = \frac{I\,dx'}{2\pi\sigma}\int_0^\infty \frac{e^{uz}}{u+\lambda} J_0(\lambda\rho)\lambda\,d\lambda$$

$$d\Pi_z = \frac{I\,dx'}{2\pi\sigma}\frac{\partial}{\partial x}\int_0^\infty \frac{e^{uz}}{u+\lambda} J_0(\lambda\rho)\,d\lambda \qquad [1]$$

where

$$u = (\lambda^2 + \gamma^2)^{1/2}, \quad \gamma^2 = i\omega\mu_0\sigma,$$

$$\rho = [y^2 + (x - x')^2]^{1/2}$$

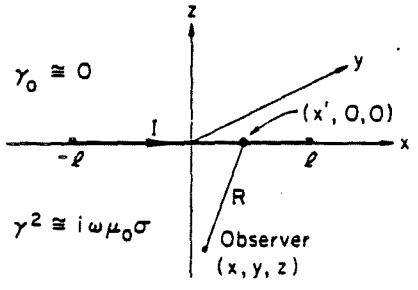


FIG. 1. Finite line source on a homogeneous half-space.

[1]The research reported here was supported by the U.S. Bureau of Mines, Pittsburgh Mining and Safety Research Center.

μ_0 is the permeability of free space, and σ is the conductivity of the half-space. Here, and in what follows, we restrict the observer to the subsurface region $z < 0$.

Since a numerical integration on x' will be required, it is desirable to eliminate the λ integration. For this quasi-static situation, Wait (1961) has shown that the λ integration can be performed to yield the result

$$d\Pi_x = \frac{I\,dx'}{2\pi\sigma\gamma^2}\left(\frac{\partial^2 P}{\partial z^2} - \frac{\partial^3 N}{\partial z^3} + \gamma^2\frac{\partial N}{\partial z}\right)$$

[2]

$$d\Pi_z = \frac{I\,dx'}{2\pi\sigma\gamma^2}\left(\frac{\partial^3 N}{\partial x\partial z^2} - \frac{\partial^2 P}{\partial x\partial z}\right)$$

where $N = I_0[(\gamma/2)(R + z)]K_0[(\gamma/2)(R - z)]$, $P = R^{-1}\exp(-\gamma R)$, $R = (\rho^2 + z^2)^{1/2}$, and I_0 and K_0 are modified Bessel functions of order zero. The magnetic field components are derived from the curl of the Hertz vector

[3] $$d\boldsymbol{H} = \sigma\,\text{curl}\,d\boldsymbol{\Pi}$$

By carrying out the curl operation in [3], and utilizing the fact that N satisfies the wave equation, $(\nabla^2 - \gamma^2)N = 0$, the magnetic field components are obtained:

$$dH_x = \frac{I\,dx'}{2\pi\gamma^2}\left(\frac{\partial^4 N}{\partial x\partial y\partial z^2} - \frac{\partial^3 P}{\partial x\partial y\partial z}\right)$$

[4]

$$dH_y = \frac{I\,dx'}{2\pi\gamma^2}\left(\frac{\partial^3 P}{\partial z^3} + \frac{\partial^3 P}{\partial x^2\partial z} + \frac{\partial^4 N}{\partial z^2\partial y^2}\right)$$

$$dH_z = \frac{I\,dx'}{2\pi\gamma^2}\left(\frac{\partial^4 N}{\partial y\partial z^3} - \gamma^2\frac{\partial^2 N}{\partial y\partial z} - \frac{\partial^3 P}{\partial y\partial z^2}\right)$$

The electric field components have been given by Wait (1961):

$$dE_x = \frac{-I\,dx'}{2\pi\sigma}\left(\frac{\partial^2 P}{\partial z^2} + \frac{\partial^3 N}{\partial y^2\partial z}\right)$$

[5]

$$dE_y = \frac{I\,dx'}{2\pi\sigma}\frac{\partial^3 N}{\partial y\partial x\partial z}$$

$$dE_z = \frac{I\,dx'}{2\pi\sigma}\frac{\partial^2 P}{\partial x\partial z}$$

To obtain the resultant fields for the finite-length cable, we integrate [4] and [5] over the range of x' from $-l$ to l.

The components of interest here are H_y, H_z, and E_x, since all other components vanish in the vertical plane $x = 0$. Also, these are the only nonzero components everywhere if the line source is of infinite length. For normalization purposes, it is useful to write the fields in the manner

$$H_y = \frac{I}{2\pi h}A(H, Y, X, L)$$

[6]

$$H_z = \frac{I}{2\pi h}B(H, Y, X, L)$$

$$E_x = \frac{-i\omega\mu_0 I}{2\pi}F(H, Y, X, L)$$

where $H = (\omega\mu_0\sigma)^{1/2}h$, $Y = y/h$, $X = x/h$, and $L = l/h$ and $h(= -z)$ is the observer depth. Note that A, B, and F are dimensionless. For the case of the infinite line source ($L = \infty$), these quantities have been tabulated (Wait and Spies 1971). By comparing [4] and [5] with [6], the following integral forms are found for A, B, and F:

$$A(H, Y, X, L) = \frac{h}{\gamma^2}\int_{-l}^{l}\left(\frac{\partial^3 P}{\partial z^3} + \frac{\partial^3 P}{\partial x^2\partial z} + \frac{\partial^4 N}{\partial z^2\partial y^2}\right)dx'$$

[7]

$$B(H, Y, X, L) = \frac{h}{\gamma^2}\int_{-l}^{l}\left(\frac{\partial^4 N}{\partial y\partial z^3} - \gamma^2\frac{\partial^2 N}{\partial y\partial z} - \frac{\partial^3 P}{\partial y\partial z^2}\right)dx$$

$$F(H, Y, X, L) = \frac{1}{\gamma^2}\int_{-l}^{l}\left(\frac{\partial^2 P}{\partial z^2} + \frac{\partial^3 N}{\partial y^2\partial z}\right)dx'$$

The specific expressions for the partial derivatives of P and N in [7] are given in the Appendix.

Low-Frequency Limit

The low-frequency limit is useful both as a check on the numerical work and as a simple means of determining trends at low frequencies. If the frequency approaches zero, then γ approaches zero and the Hertz components are given by

$$d\Pi_x = \frac{I\,dx'}{4\pi\sigma}\int_0^\infty e^{\lambda z}J_0(\lambda\rho)\,d\lambda = \frac{I\,dx'}{4\pi\sigma}\frac{1}{R}$$

[8]

$$d\Pi_z = \frac{-I\,dx'}{4\pi\sigma}\frac{(x - x')}{\rho}\int_0^\infty e^{\lambda z}J_1(\lambda\rho)\,d\lambda$$

$$= \frac{-I\,dx'}{4\pi\sigma}\frac{(x - x')}{\rho^2}(1 + z/R)$$

where we make use of the integrals listed by Wheelon (1968). It is important to note that $d\Pi_z$ does not vanish in this limit. This is consistent with the notion that the electric fields can be derived from a scalar potential Φ that is given by

$$\Phi = -\left(\frac{\partial \Pi_x}{\partial x} + \frac{\partial \Pi_z}{\partial z}\right) = \frac{-I\,dx'}{2\pi\sigma}\frac{\partial}{\partial x}\left(\frac{1}{R}\right)$$

for the static limit.

The magnetic field components are obtained from the curl operation in [3]. Thus

$$[9]\qquad dH_z = \frac{I\,dx'}{4\pi}\frac{y}{R^3}$$

$$dH_y = \frac{I\,dx'}{4\pi}\left\{\frac{-z}{R^3} + \frac{\partial}{\partial x}\left[\frac{x-x'}{\rho^2}\left(1+\frac{z}{R}\right)\right]\right\}$$

There is also an x component which is not of interest here. The quantities in [9] can be integrated from $x' = -l$ to $x' = +l$ to obtain the total fields

$$[10]\qquad H_y = \frac{I}{4\pi}\left\{\frac{-z}{y^2+z^2}\left[\frac{l-x}{[(l-x)^2+y^2+z^2]^{1/2}} + \frac{l+x}{[(l+x)^2+y^2+z^2]^{1/2}}\right] + \frac{l-x}{(l-x)^2+y^2}\left[1+\frac{z}{[(l-x)^2+y^2+z^2]^{1/2}}\right] + \frac{l+x}{(l+x)^2+y^2}\left[1+\frac{z}{[(l+x)^2+y^2+z^2]^{1/2}}\right]\right\}$$

$$H_z = \frac{I}{4\pi}\frac{y}{y^2+z^2}\left[\frac{l-x}{[(l-x)^2+y^2+z^2]^{1/2}} + \frac{l+x}{[(l+x)^2+y^2+z^2]^{1/2}}\right]$$

From [10], the normalized quantities A and B, as defined in [6], are found to be

$$[11]\qquad A(0, Y, X, L) = \frac{-1}{2(1+Y^2)}\left[\frac{L-X}{[(L-X)^2+1+Y^2]^{1/2}} + \frac{L+X}{[(L+X)^2+1+Y^2]^{1/2}}\right] + \frac{(L-X)/2}{(L-X)^2+Y^2}\left[1-\frac{1}{[(L-X)^2+1+Y^2]^{1/2}}\right] + \frac{(L+X)/2}{(L+X)^2+Y^2}\left[1-\frac{1}{[(L+X)^2+1+Y^2]^{1/2}}\right]$$

$$B(0, Y, X, L) = \frac{Y/2}{1+Y^2}\left[\frac{L-X}{[(L-X)^2+1+Y^2]^{1/2}} + \frac{L+X}{[(L+X)^2+1+Y^2]^{1/2}}\right]$$

As L approaches ∞, the following results are obtained:

$$[12]\qquad A(0, Y, X, \infty) = \frac{1}{1+Y^2}, \quad B(0, Y, X, \infty) = \frac{Y}{1+Y^2}$$

The results are of course independent of X and agree with infinite line source results (Wait and Spies 1971).

Results for finite L are shown in Figs. 2 and 3 for $X = 0$. Note that A in Fig. 2 overshoots its final value and that $L = 1$ is sufficient to obtain a horizontal magnetic field equal to that of the infinite line source. However, the B values in Fig. 3 approach their final values quite slowly, particularly for larger Y. Consequently, a fairly large value of L is required to obtain a vertical magnetic field nearly equal to that of the infinite line source.

High-Frequency Limit

The other useful limiting case is for high frequencies where $|\gamma y|$ is large. In this case, terms involving P are negligible, and N is asymptotically given by (Wait 1961)

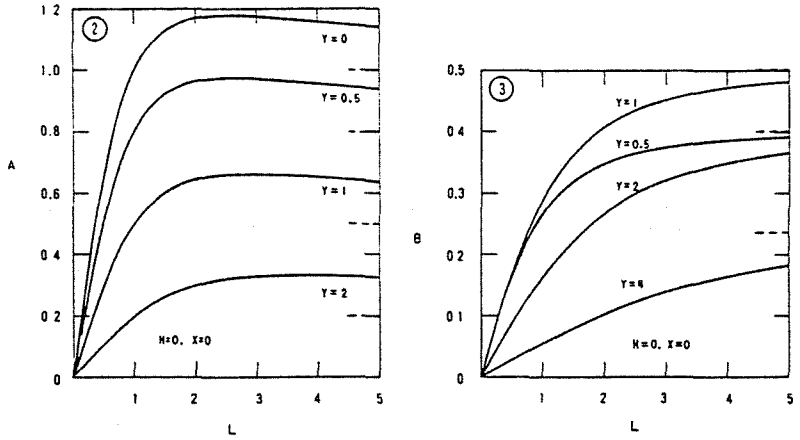


FIG. 2. Low-frequency limit of the horizontal magnetic field as a function of Y and L. Final values are dashed.
FIG. 3. Low-frequency limit of the vertical magnetic field as a function of Y and L. Final values are dashed.

[13] $$N \sim \frac{e^{\gamma z}}{\gamma \rho} \quad \text{for} \quad z \leqslant 0$$

Consequently, dE_x and dH_y are given by

[14] $$dE_x \sim -\frac{I\,dx'}{2\pi\sigma} e^{\gamma z} \frac{\partial^2}{\partial y^2}\left(\frac{1}{\rho}\right) \quad \text{and} \quad dH_y \sim -\frac{I\,dx'}{2\pi\gamma} e^{\gamma z} \frac{\partial^2}{\partial y^2}\left(\frac{1}{\rho}\right)$$

In order to determine dH_z, we must include higher-order terms in N. If this is done, the result is

[15] $$dH_z \sim -\frac{I\,dx'}{2\pi\gamma^2} e^{\gamma z} \frac{\partial}{\partial y}\left(\frac{1}{\rho^3}\right)$$

The x' integrations can be done in [14] and [15] to yield the total fields:

$$E_x \sim -\frac{I}{2\pi\sigma} e^{\gamma z} \frac{\partial^2}{\partial y^2} \{\ln [l - x + [(l - x)^2 + y^2]^{1/2}] - \ln [-(l + x) + [(l + x)^2 + y^2]^{1/2}]\}$$

[16] $$H_y \sim -\frac{I}{2\pi y} e^{\gamma z} \frac{\partial^2}{\partial y^2} \{\ln [l - x + [(l - x)^2 + y^2]^{1/2}] - \ln [-(l + x) + [(l + x)^2 + y^2]^{1/2}]\}$$

$$H_z \sim -\frac{I}{2\pi\gamma^2} e^{\gamma z} \frac{\partial}{\partial y}\left\{\frac{1}{y^2}\left[\frac{l - x}{[(l - x)^2 + y^2]^{1/2}} + \frac{l + x}{[(l + x)^2 + y^2]^{1/2}}\right]\right\}$$

If l approaches ∞, then [16] reduces to

[17] $$E_x|_{l=\infty} \sim \frac{-I}{\pi\sigma} \frac{e^{\gamma z}}{y^2}, \quad H_y|_{l=\infty} \sim \frac{I}{\pi\gamma} \frac{e^{\gamma z}}{y^2}, \quad H_z|_{l=\infty} \sim \frac{2I}{\pi\gamma^2} \frac{e^{\gamma z}}{y^3}$$

Thus, the normalized quantities A, B, and F are given by

$$A(H, Y, X, \infty) \sim \frac{2}{i^{1/2} H Y^2} \exp(-i^{1/2} H)$$

[18] $$B(H, Y, X, \infty) \sim \frac{4}{i H^2 Y^3} \exp(-i^{1/2} H)$$

$$F(H, Y, X, \infty) \sim \frac{2}{i H^2 Y^2} \exp(-i^{1/2} H)$$

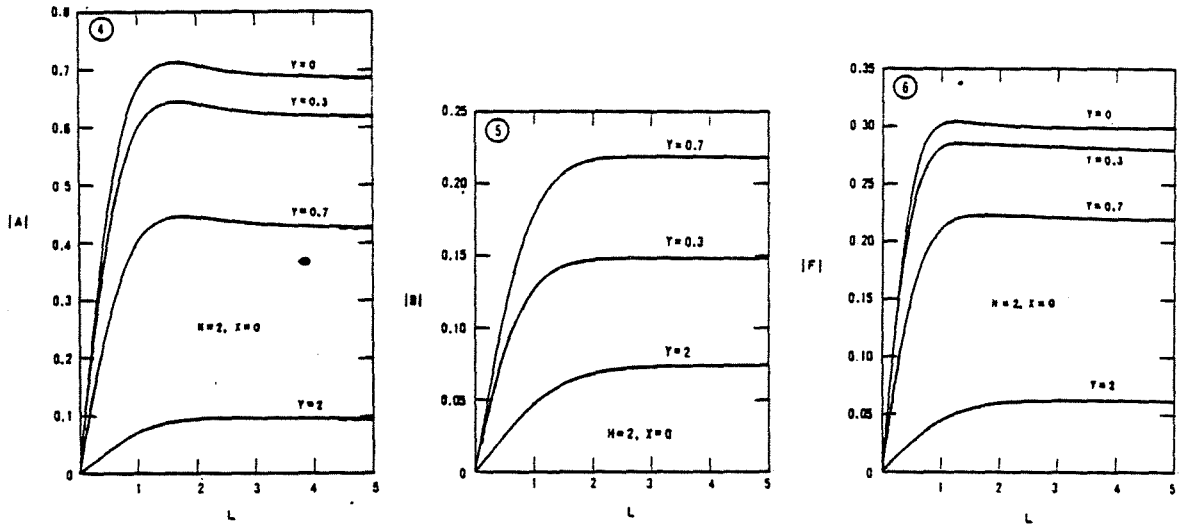


FIG. 4. Magnitude of the horizontal magnetic field as a function of Y and L.
FIG. 5. Magnitude of the vertical magnetic field as a function of Y and L.
FIG. 6. Magnitude of the horizontal electric field as a function of Y and L.

These results agree with those of the infinite line source (Wait and Spies 1971).

We stress that the "high-frequency" limit solutions discussed in this section are applicable when the horizontal distance, ρ, is much *greater* than a skin depth in the earth, and much *less* then the free-space wavelength. Thus, the formulas are of limited applicability, although they are useful for checking the results of the numerical integration.

General Numerical Results

For general values of H, a numerical integration over finite limits of the expressions in [7] is required. Even though the integrands are quite complicated, they are well behaved numerically. Consequently, the computer program for A, B, and F is quite fast, and the influence of the various parameters can be studied easily. Here, we illustrate some of the important features in graphical form.

Results for $H = 2$ and $X = 0$ are shown in Figs. 4, 5, and 6. For large L, all quantities approach those of the infinite line source (Wait and Spies 1971) which is reassuring. Although A, B, and F are now complex, only the magnitudes are plotted since the phases are relatively constant with L.

We note that $|A|$ in Fig. 4 still has a slight overshoot before settling down to its final value for large L. A similar trend for $|F|$ is shown in Fig. 6. In both cases, L greater than about 1 is sufficient to yield field strengths nearly equal to that of the infinite line source. However, a larger value of L would be required to reach a nearly maximum value of $|B|$ as shown in Fig. 5. Consequently, if the vertical magnetic field is important, a value for L in the neighborhood of 2 might be more appropriate, if we wish to simulate an infinitely long cable. This could be a crucial factor in designing a subsurface location scheme that makes use of the well-defined structure of the magnetic fields produced by an infinite line source.

Concluding Remarks

Analytical expressions for the subsurface fields of a finite line source have been derived for high-frequency and low-frequency limits. For the general case, a single numerical integration along the source is required. Although a constant current distribution has been assumed, an arbitrary distribution would present no problem since the source integration is done numerically. Also, multiple grounding of the source cable and arrays of such cables could be treated by simple extensions of the present formulation.

Results for low and medium frequencies indicate that the finite line source fields approach those of an infinite line source quite quickly. For instance, $L \simeq 1$ appears to be sufficient for the horizontal electric and magnetic fields, and $L \simeq 2$ is sufficient for the vertical magnetic field.

It is important to realize that the finite line source excites currents in the earth by induction and by conduction. The effect of the latter vanishes in the limit of an infinitely long cable when the magnetic field is measured at the subsurface point. The results shown in Figs. 2–6 for finite L implicitly account for the effect of the conduction currents injected at the electrodes.

In a sequel to this work, we plan to consider the fields produced by a finite source cable located within a coal mine.

Appendix

There are four terms in derivatives of P which are required in [7]. The differentiation is straightforward, and the resultant forms are

$$\frac{\partial^2 P}{\partial z^2} = \frac{e^{-\gamma R}}{R^2}\left[\frac{1}{R}\left(-1+\frac{3z^2}{R^2}\right)+\gamma\left(-1+\frac{3z^2}{R^2}\right)+\frac{\gamma^2 z^2}{R}\right]$$

$$\frac{\partial^3 P}{\partial z^3} = \frac{z\,e^{-\gamma R}}{R^3}\left[\frac{3}{R^2}\left(3-\frac{5z^2}{R^2}\right)+\frac{3\gamma}{R}\left(3-\frac{5z^2}{R^2}\right)+3\gamma^2\left(1-\frac{2z^2}{R^2}\right)-\frac{\gamma^3 z^2}{R}\right]$$

[19]
$$\frac{\partial^3 P}{\partial y \partial z^2} = \frac{y\,e^{-\gamma R}}{R^3}\left[\frac{3}{R^2}\left(1-\frac{5z^2}{R^2}\right)+\frac{3\gamma}{R}\left(1-\frac{5z^2}{R^2}\right)+\gamma^2\left(1-\frac{6z^2}{R^2}\right)-\frac{\gamma^3 z^2}{R}\right]$$

$$\frac{\partial^3 P}{\partial x^2 \partial z} = \frac{z\,e^{-\gamma R}}{R^3}\left\{\frac{3}{R^2}\left[1-\frac{5(x-x')^2}{R^2}\right]+\frac{3\gamma}{R}\left[1-\frac{5(x-x')^2}{R^2}\right]+\gamma^2\left[1-\frac{6(x-x')^2}{R^2}\right]-\frac{\gamma^3(x-x')^2}{R}\right\}$$

The four terms in derivatives of N can be simplified by replacing the derivatives of the modified Bessel functions by Bessel functions of zero and first order. This procedure, used previously by Wait and Campbell (1953*a*, *b*), yields the following expressions which are quite suitable for numerical evaluation.

[20]
$$\frac{\partial^2 N}{\partial y \partial z} = \frac{\gamma y}{2}[A_{00}I_0K_0 + A_{11}I_1K_1 + A_{01}I_0K_1 + A_{10}I_1K_0]$$

where

$$A_{00} = \frac{\gamma z}{R^2},\quad A_{11} = -\frac{\gamma z}{R^2},\quad A_{01} = \frac{1}{R^2}\left(-1+\frac{z}{R}\right),\quad A_{10} = -\frac{1}{R^2}\left(1+\frac{z}{R}\right)$$

$$\frac{\partial^3 N}{\partial y^2 \partial z} = \frac{\gamma}{2}[B_{00}I_0K_0 + B_{11}I_1K_1 + B_{01}I_0K_1 + B_{10}I_1K_0]$$

where

$$B_{00} = \frac{\gamma z}{R}\left(1-\frac{3y^2}{R^2}\right),\quad B_{11} = \frac{\gamma z}{R^2}\left(-1+\frac{3y^2}{R^2}+\frac{2y^2}{\rho^2}\right)$$

$$B_{01} = \frac{1}{R^2}\left[-1+\frac{z(1-\gamma^2y^2)}{R}+\frac{3y^2}{R^2}-\frac{3y^2z}{R^3}\right],\quad B_{10} = \frac{1}{R^2}\left[-1-\frac{z(1-\gamma^2y^2)}{R}+\frac{3y^2}{R^2}+\frac{3y^2z}{R^3}\right]$$

$$\frac{\partial^4 N}{\partial y^2 \partial z^2} = \frac{\gamma}{2}[C_{00}I_0K_0 + C_{11}I_1K_1 + C_{01}I_0K_1 + C_{10}I_1K_0]$$

where

$$C_{00} = \frac{\gamma z^2}{R^4}\left[-3+\gamma^2y^2+\frac{15y^2}{R^2}\right]$$

$$C_{11} = \frac{\gamma}{R^2}\left[-2+\frac{z^2(3-\gamma^2y^2)}{R^2}+\frac{6y^2}{R^2}-\frac{15y^2z^2}{R^4}+\frac{2y^2(R^2-2z^2)}{\rho^2R^2}\right]$$

$$C_{01} = \frac{1}{R^3}\left[\frac{z(3-\gamma^2y^2)}{R} - \gamma^2(y^2+z^2) - \frac{3z^2(1-2\gamma^2y^2)}{R^2} - \frac{15zy^2}{R^3} + \frac{15y^2z^2}{R^4} + \frac{\gamma^2y^2z(R+z)}{\rho^2}\right]$$

$$C_{10} = \frac{1}{R^3}\left[\frac{z(3-\gamma^2y^2)}{R} + \gamma^2(y^2+z^2) + \frac{3z^2(1-2\gamma^2y^2)}{R^2} - \frac{15zy^2}{R^3} - \frac{15y^2z^2}{R^4} + \frac{\gamma^2y^2z(R-z)}{\rho^2}\right]$$

$$\frac{\partial^4 N}{\partial y \partial z^3} = \frac{\gamma y}{2}\left[D_{00}I_0K_0 + D_{11}I_1K_1 + D_{01}I_0K_1 + D_{10}I_1K_0\right]$$

where

$$D_{00} = \frac{\gamma z}{R^4}\left(-3 + \frac{15z^2}{R^2} + \gamma^2z^2\right), \quad D_{11} = \frac{\gamma z}{R^4}\left(13 - \frac{15z^2}{R^2} - \gamma^2z^2\right)$$

$$D_{01} = \frac{1}{R^2}\left(\frac{3}{R^2} - \frac{3z}{R^3} - \frac{15z^2}{R^4} + \frac{15z^3}{R^5} - \gamma^2 - \frac{3\gamma^2z}{R} - \frac{\gamma^2z^2}{R^2} + \frac{6\gamma^2z^3}{R^3}\right)$$

$$D_{10} = \frac{1}{R^2}\left(\frac{3}{R^2} + \frac{3z}{R^3} - \frac{15z^2}{R^4} - \frac{15z^3}{R^5} - \gamma^2 + \frac{3\gamma^2z}{R} - \frac{\gamma^2z^2}{R^2} - \frac{6\gamma^2z^3}{R^3}\right)$$

The argument of I_0 and I_1 is $(\gamma/2)(R+z)$, and the argument of K_0 and K_1 is $(\gamma/2)(R-z)$.

Acknowledgments

We wish to thank Dr. R. G. Geyer, of the Colorado School of Mines, for his suggestions, and Mrs. Loys A. Gappa for her assistance in preparing the manuscript.

BANOS, A. 1966. Dipole radiation in the presence of a conducting half-space (Pergamon Press, New York).

SUNDE, E. D. 1968. Earth conduction effects in transmission systems (Dover Publications, New York), Chap. V, pp. 140–172.

WAIT, J. R. 1952. Can. J. Phys. 30, 512.

——— 1961. Can. J. Phys. 39, 1017.

WAIT, J. R. and CAMPBELL, L. L. 1953*a*. J. Geophys. Res. 58, 21.

——— 1953*b*. J. Geophys. Res. 58, 167.

WAIT, J. R. and SPIES, K. P. 1971. Radio Sci. 6, 781.

WHEELON, A. D. 1968. Tables of summable series and integrals involving Bessel functions (Holden-Day, San Francisco), p. 72.

160

Radio Science, Volume 8, Number 12, pages 1169–1176, December 1973

Excitation of a homogeneous conductive cylinder of finite length by a prescribed axial current distribution

James R. Wait

Cooperative Institute for Research in Environmental Sciences, University of Colorado, and Environmental Research Laboratories, National Oceanic and Atmospheric Administration, US Department of Commerce, Boulder, Colorado 80302

David A. Hill

Institute for Telecommunication Sciences, Office of Telecommunications, US Department of Commerce, Boulder, Colorado 80302

(Received June 14, 1973.)

The boundary value problem posed is a truncated cylindrical region excited by a specified distribution of electric current over a concentric cylindrical surface. The end conditions are that the total normal current density is zero. The solution is carried through for excitation by a symmetrically located axial current filament that is adjacent to the cylinder. Numerical results of the resultant magnetic field are given for the quasi-static situation for a perfectly conducting cylinder. It is indicated that the results depend significantly on the length of the cylindrical target. Even for very long cylinders, there is no quantitative similarity with the corresponding two-dimensional model of a cylinder of infinite length.

INTRODUCTION

The theory of the interaction of electromagnetic waves with finite or bounded structures is extremely involved except in a few special cases. For example, the vector wave solution for the sphere is about the only case that is tractable when the incident wave is arbitrary and the body dimensions are comparable with a wavelength. The class of obtainable solutions for scalar wave problems is somewhat broader, but even here we are restricted to separable geometries.

The need for useable results for finite body scattering has motivated many investigators to utilize numerical techniques [*Ward and Morrison,* 1971] such as the moment method [*Harrington,* 1968]. Even here the three-dimensional nature of the problem compounds the usual difficulty of excessive computation time. One well-known alternative to a direct numerical attack is to employ high frequency asymptotic techniques [*Fox,* 1964] such as J. B. Keller's geometrical theory of diffraction.

Here, we should like to point out the possibility of getting useful results from a special form of a truncated conducting cylinder that is excited by a finite axial current element. It is suggested that the results to this problem can provide insight to scattering by finite cylinders and, hopefully, they will be useful as a check on numerical procedures developed for more general three-dimensional structures. Also, we shall utilize the low frequency solutions to show graphically how the magnetic field varies in the vicinity of the cylinder for various positions of the adjacent current element.

FORMULATION

The specific situation of interest is illustrated in Figure 1. A conducting cylinder of conductivity σ and magnetic permeability μ occupies the space $\rho < a$ and $|z| < s$ in terms of a cylindrical coordinate system (ρ, ϕ, z). The region $\rho > a$ external to the cylinder has a conductivity σ_0 and magnetic permeability μ_0. To allow for the existence of displacement currents, we can allow both σ and σ_0 to be complex. Over the concentric cylindrical surface $\rho = \rho_0$, we specify that the axial current density is a known function $K(\phi, z)$ amp m^{-1}. Actually, in Figure 1 we only show the region for $z > 0$.

We now propose to find a solution of the problem under the stipulation that the normal current density is zero at the surface $z = |s|$. This, in turn,

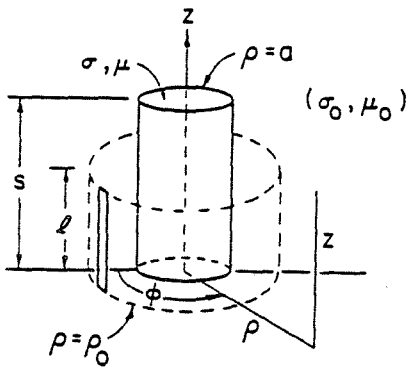


Fig. 1. General configuration showing only region for $z > 0$.

requires that the normal electric field E_z is also zero over this surface. On the other hand, since we are interested mainly in the situation of symmetry about the plane $z = 0$, we can utilize the fact that $E_\rho = 0$ on this plane. Thus, attention may be restricted just to the region $0 < z < s$, if we remember that the solutions for even symmetry are even about $z = 0$. In what follows, we shall adopt a time factor $\exp(i\omega t)$.

We fully appreciate that the posed problem is not directly applicable to an isolated finite cylinder, but we can assert that the solution of this idealized situation should tell us something about the effects of truncating the cylindrical structure. If the latter is relatively thin and highly conducting, it can be expected that the normal current density within the structure tends to vanish at the ends.

FORMAL SOLUTION

To facilitate the analysis of the posed problem, we express the total field in terms of electric and magnetic Hertz vectors that have only z components $\prod$ and $\prod^*$, respectively [*Wait*, 1959]. Thus, for the region $\rho < a$, the field components are obtained from

$$E_\rho = (\partial^2 \prod/\partial\rho\,\partial z) - (i\mu\omega/\rho)(\partial \prod^*/\partial\phi) \quad (1)$$

$$E_\phi = (1/\rho)(\partial^2 \prod/\partial\phi\,\partial z) + i\mu\omega(\partial \prod^*/\partial\rho) \quad (2)$$

$$H_\rho = (-i\gamma^2/\mu\omega\rho)(\partial \prod/\partial\phi) + (\partial^2 \prod^*/\partial\rho\,\partial z) \quad (3)$$

$$H_\phi = (i\gamma^2/\mu\omega)(\partial \prod/\partial\rho) + (1/\rho)(\partial^2 \prod^*/\partial\phi\,\partial z) \quad (4)$$

$$E_z = [-\gamma^2 + (\partial^2/\partial z^2)] \prod \quad (5)$$

$$H_z = [-\gamma^2 + (\partial^2/\partial z^2)] \prod^* \quad (6)$$

where $\gamma = (i\sigma\mu\omega)^{1/2}$ is the propagation constant for the cylinder. The solutions for the region $\rho > a$ have the same form as (1) through (6), but we add a subscript zero where appropriate.

The required forms of the solution for $\rho < a$ are

$$\prod = \sum_n \sum_m a_{m,n} I_m(v_n\rho) e^{-im\phi} \cos\lambda_n z \quad (7)$$

and

$$\prod^* = \sum_n \sum_m a_{m,n}^* I_m(v_n\rho) e^{-im\phi} \sin\lambda_n z \quad (8)$$

where $v_n = (\lambda_n^2 + \gamma^2)^{1/2}$. Here, I_m is a modified Bessel function of the first kind that remains finite at $\rho = 0$. For single-valuedness in ϕ, obviously m ranges from $-\infty$ to $+\infty$ through all integers. Also, since $E_z = 0$ at $z = s$, we note that $\lambda_n = (2n + 1)(\pi/2s)$ where $n = 0, 1, 2, 3, \cdots$. In addition, we readily confirm that $E_\rho = 0$ at $z = 0$, in accordance with our assumptions concerning symmetry.

In dealing with the region external to the cylinder, we choose the wave-functions to have the following form, for $a < \rho < \rho_0$,

$$\prod = \sum_n \sum_m [b_{m,n} I_m(u_n\rho) + c_{m,n} K_m(u_n\rho)] e^{-im\phi} \cos\lambda_n z \quad (9)$$

$$\prod^* = \sum_n \sum_m c_{m,n}^* K_m(u_n\rho) e^{-im\phi} \sin\lambda_n z \quad (10)$$

and, for $\rho > \rho_0$

$$\prod = \sum_n \sum_m d_{m,n} K_m(u_n\rho) e^{-im\phi} \cos\lambda_n z \quad (11)$$

$$\prod^* = \sum_n \sum_m d_{m,n}^* K_m(u_n\rho) e^{-im\phi} \sin\lambda_n z \quad (12)$$

where $u_n = (\lambda^2 + \gamma_0^2)^{1/2}$. Here, K_m is a modified Bessel function of the second kind that assures outgoing waves as $\rho \to \infty$. These forms of the solutions are chosen to allow for a possible discontinuity in H_ϕ at the surface $\rho = \rho_0$, while E_ϕ, E_z, and H_z are continuous. The latter immediately tells us that $c_{m,n}^* = d_{m,n}^*$.

We next express the prescribed current excitation as a double Fourier series in the manner

$$K(\phi, z) = \sum_n \sum_m F_{m,n} e^{-im\phi} \cos\lambda_n z. \quad (13)$$

where $F_{m,n}$ is easily determined. The boundary condition at $\rho = \rho_0$ written as

$$H_\phi|_{\rho=\rho_0+0} - H_\phi|_{\rho=\rho_0-0} = K(\phi, z) \quad (14)$$

is now easily applied. Using the Wronskian relation $I_m'(Z)K_m(Z) - I_m(Z)K_m'(Z) = 1/Z$, we determine that

$$b_{m,n} = (\eta_0\rho_0/\gamma_0) K_m(u_n\rho_0) F_{m,n} \quad (15)$$

where $\eta_0 = i\mu_0\omega/\gamma_0$. Thus, the coefficient $b_{m,n}$ is determined entirely by the excitation.

The boundary conditions at the surface of the cylinder are that E_z, H_z, E_ϕ, and H_ϕ are continuous at $\rho = a$. Application of these leads to four linear equations to solve for the four unknown coefficients. Omitting algebraic details, this process leads to

$$c_{m,n} = (-b_{m,n}/D)\{[(u^2/v^2) - 1]^2(im\lambda_n/a)^2 I_u K_u - [(\gamma u^2/v)(1/\eta)(I_u I_v'/I_v) - (\gamma_0 u/\eta_0) I_u'] \cdot [(\gamma u^2/v)(\eta I_v'/I_v) K_u - \gamma_0 u \eta_0 K_u']\} \quad (16)$$

and

$$c_{m,n}^* = (-b_{m,n}/D)(im\lambda_n/a^2)[(u^2/v^2) - 1]\gamma_0/\eta_0 \quad (17)$$

where

$$D = [(u^2/v^2) - 1]^2(im\lambda_n/a)^2 K_u^2 - [(\gamma u^2/v)(1/\eta)(K_u I_v'/I_v) - (\gamma_0 u/\eta_0) K_u'] \cdot [(\gamma u^2/v)(\eta I_v'/I_v) K_u - \gamma_0 u \eta_0 K_u'] \quad (18)$$

Here, we have used the following abbreviated notation $I_u = I_m(u_n a)$, $I_v = I_m(v_n a)$, $K_u = K_m(u_n a)$, $u = u_n$, $v = v_n$, and $\eta = i\mu\omega/\gamma$. The two coefficients for the internal fields can be obtained from

$$a_{m,n} = (u^2 b_{m,n} I_u + u^2 c_{m,n} K_u)/v^2 I_v \quad (19)$$

and

$$a_{m,n}^* = u^2 c_{m,n}^* K_u/v^2 I_v \quad (20)$$

To complete the statement of the formal solution of the posed problem, we observe that the Fourier inverse of (13) is

$$F_{m,n} = (1/\pi s) \int_0^s \int_0^{2\pi} K(\phi, z) e^{im\phi}\, d\phi \cos \lambda_n z\, dz \quad (21)$$

If we specialize this to an axial current I amp in a filamental strip of half-length l as indicated in Figure 2, we can replace (21) by

$$F_{m,n} = \int_0^l \cos \lambda_n z\, dz \int_{\phi_0 - \Delta/2}^{\phi_0 + \Delta/2} (I/\rho_0 \Delta) e^{im\phi}\, d\phi \quad (22)$$

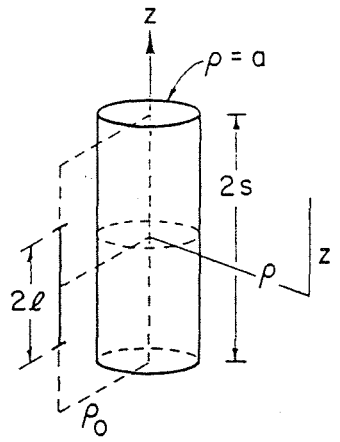


Fig. 2. Specialization to a linear current element adjacent to the conducting cylinder.

where Δ is the angular width of the strip. These elementary integrations yield

$$F_{m,n} = (I/\pi\rho_0)[\sin(m\Delta/2)/(m\Delta/2)] \cdot e^{im\phi_0}(\sin \lambda_n l)/\lambda_n s \quad (23)$$

The corresponding value for $b_{m,n}$ is given by (15). If $\Delta \to 0$ corresponding to a filamental line current, we have

$$b_{m,n} = (I/\pi)(\eta_0/\gamma_0) K_m(u_n \rho_0) e^{im\phi_0}(\sin \lambda_n l)/\lambda_n s \quad (24)$$

The corresponding electric dipole excitation is obtained by regarding $\lambda_n l$ as a small quantity whence

$$b_{m,n} \simeq (Il/\pi s)(\eta_0/\gamma_0) K_m(u_n \rho_0) e^{im\phi_0} \quad (25)$$

where Il is the current moment.

We shall now consider some aspects of the general solution before considering the static limit. Equation 16 can be written

$$c_{m,n} = -b_{m,n}[I_m(u_n a)/K_m(u_n a)]\Lambda_{m,n} \quad (26)$$

where

$$\Lambda_{m,n} = \frac{\left[\frac{\gamma}{v\eta}\frac{I_v'}{I_v} - \frac{\gamma_0}{u\eta_0}\frac{I_u'}{I_u}\right]\left[\frac{\gamma\eta}{v}\frac{I_v'}{I_v} - \frac{\gamma_0\eta_0}{u}\frac{K_u'}{K_u}\right] + \left(\frac{1}{v^2} - \frac{1}{u^2}\right)^2\left(\frac{m\lambda_n}{a}\right)^2}{\left[\frac{\gamma}{v\eta}\frac{I_v'}{I_v} - \frac{\gamma_0}{u\eta_0}\frac{K_u'}{K_u}\right]\left[\frac{\gamma\eta}{v}\frac{I_v'}{I_v} - \frac{\gamma_0\eta_0}{u}\frac{K_u'}{K_u}\right] + \left(\frac{1}{v^2} - \frac{1}{u^2}\right)^2\left(\frac{m\lambda_n}{a}\right)^2} \quad (27)$$

In the case of a perfectly conducting cylinder ($\gamma \to \infty$), we see that $\Lambda_m = 1$ and, in this case, $c_{m,n}^* = 0$ is a consequence of (17). An important special case of (27) is when $m = 0$. Then, in explicit notation,

$$\Lambda_{0,n} = \{(\gamma/v_n\eta)[I_0'(v_na)/I_0(v_na)] - (\gamma_0/u_n\eta_0)[I_0'(u_na)/I_0(u_na)]\} \div \{(\gamma/v_n\eta)[I_0'(v_na)/I_0(v_na)] - (\gamma_0/u_n\eta_0)[K_0'(u_na)/K_0(u_na)]\} \quad (28)$$

In this case, we also note that $c_{0,n}^* = 0$.

EXPLICIT FIELD EXPRESSIONS

We now consider the explicit forms for the electric Hertz potential Π, since this is of prime interest in calculating the fields in the principal plane $z = 0$. First of all, we note that this function for $\rho > a$ can be split into a primary and secondary portion as follows:

$$\Pi = \Pi_{pr} + \Pi_{sec}$$

The primary component, for $a < \rho < \rho_0$, is

$$\Pi_{pr} = (I/\pi)(\eta_0/\gamma_0) \sum_m \sum_n K_m(u_n\rho_0)I_m(u_n\rho) \cdot e^{im(\phi_0-\phi)}[(\sin \lambda_n l)/\lambda_n s] \cos \lambda_n z \quad (29)$$

For $\rho > \rho_0$, the corresponding expression is obtained by interchanging ρ_0 and ρ. Using a well-known addition theorem for modified Bessel functions, the summation over m is readily performed to yield

$$\Pi_{pr} = (I\eta_0/\pi\gamma_0) \sum_{n=0}^{\infty} K_0(u_n\rho_d) \cdot [(\sin \lambda_n l)/\lambda_n s] \cos \lambda_n z \quad (30)$$

where $\rho_d = [\rho^2 + \rho_0^2 - 2\rho\rho_0 \cos(\phi_0 - \phi)]^{1/2}$ is the radial distance from the observer to the source current element.

The secondary part of the electric Hertz potential in the region $\rho > a$ is conveniently written

$$\Pi_{sec} = -(I\eta_0/\pi\gamma_0) \sum_m \sum_n [K_m(u_n\rho_0)/K_m(u_na)] \cdot I_m(u_na)K_m(u_n\rho)\Lambda_{m,n}e^{im(\phi_0-\phi)} \cos \lambda_n z \quad (31)$$

where there is no apparent further simplicity.

To obtain the magnetic field components, we merely perform the differentiations indicated in (3) and (4). Restricting attention to the plane $z = 0$, it easily follows from (30) that the primary magnetic fields are

$$H_\rho^{pr} = [I\rho_0 \sin(\phi_0 - \phi)/\pi\rho_d] \cdot \sum_{n=0}^{\infty} K_1(u_n\rho_d)[(\sin \lambda_n l)/\lambda_n s]u_n \quad (32)$$

$$H_\phi^{pr} = \{I[\rho - \rho_0 \cos(\phi_0 - \phi)]/\pi\rho_d\} \cdot \sum_{n=0}^{\infty} K_1(u_n\rho_d)[(\sin \lambda_n l)/\lambda_n s]u_n \quad (33)$$

where $\lambda_n = (2n + 1)\pi/2s$. On the other hand, the secondary fields that follow from (31) are

$$H_\rho^{sec} = (I/\pi\rho) \sum_{m=-\infty}^{+\infty} \sum_{n=0}^{\infty} \Lambda_{m,n}[K_m(u_n\rho_0)/K_m(u_na)] \cdot I_m(u_na)K_m(u_n\rho)im e^{im(\phi_0-\phi)}[(\sin \lambda_n l)/\lambda_n s] \quad (34)$$

and

$$H_\phi^{sec} = (I/\pi) \sum_{m=-\infty}^{+\infty} \sum_{n=0}^{\infty} \Lambda_{m,n}[K_m(u_n\rho_0)/K_m(u_na)] \cdot I_m(u_na)u_n K_m'(u_n\rho)e^{im(\phi_0-\phi)}[(\sin \lambda_n l)/\lambda_n s] \quad (35)$$

Using (32) through (35), the total fields are obtained exactly from $H_\rho = H_\rho^{pr} + H_\rho^{sec}$ and $H_\phi = H_\phi^{pr} + H_\phi^{sec}$ in the plane $z = 0$ and for $\rho > a$. The double series expansions in (34) and (35) are rather cumbersome, but the convergence is rapid when $|\gamma a|$, $|\gamma_0 a|$, and $|\gamma_0 s|$ are not excessively large compared with unity.

SOME SPECIFIC RESULTS FOR THE QUASI-STATIC LIMIT

Some simplification is achieved in the low frequency or quasi-static case. For example, if $|\gamma_0 a|$, $|\gamma_0\rho|$, and $|\gamma_0\rho_0|$ are all $\ll 1$, we can effectively replace u_n by λ_n everywhere. However, unless $|\gamma a|$ is also small, we must retain the form for v_n. But, of course, if the cylinder is very highly conducting, such that $|\gamma a| \gg 1$, the complicated factor $\Lambda_{m,n}$ can be replaced by unity in (34) and (35). Thus, in the case of a perfectly conducting cylinder and in the quasi-static limit, we can use (32) through (35) with u_n replaced everywhere by λ_n and $\Lambda_{m,n}$ by unity. Some numerical data for this case are given below. To present these results, the reader is referred to Figure 3, where we have chosen a cartesian co-

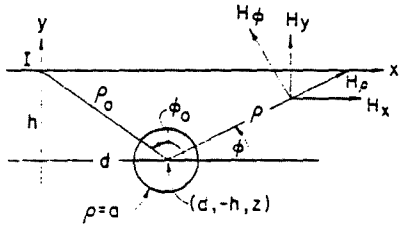


Fig. 3. Cross section (i.e., $z = 0$ plane) of the cylindrical target in the presence of the current cable.

ordinate system (x, y, z) with the current element at the origin. The field components H_x, H_y at the observer are thus obtained from

$$H_x = H_\rho \cos\phi - H_\phi \sin\phi$$

$$H_y = H_\rho \sin\phi + H_\phi \cos\phi$$

We can visualize this situation as the scanning of the resultant fields at the earth's surface ($y = 0$) for a buried cylindrical target centered at $x = d$ and $y = -h$. In view of our quasi-static assumptions, we have neglected the effects of the induced currents in the region external to the cylinder.

In Figure 4, we plot the normalized horizontal field $2\pi hH_x/I$ as a function of the normalized horizontal coordinate x/h in the transverse plane $z = 0$. Here, we choose $a/h = 0.5$, $d/h = 1$, $l/s = 0.5$, and $s/h = 2$, 10, and ∞. The case $s/h = \infty$ is based on the solution for the corresponding two-dimensional problem of a parallel line source carrying the same current I (see appendix A). The corresponding results for $2\pi hH_y/I$ are illustrated in Figure 5. A similar set of curves is shown in Figures 6 and 7, where the only difference is that $d/h = 0$. This case corresponds to having the cylindrical target located directly beneath the current element.

FINAL REMARKS

The general features of the response curves in Figures 4 through 7 are not surprising. In all cases they have the form expected for a secondary source of current induced in the target that tends to oppose the fields of the primary current. Of particular interest is the fact that the half-lengths of the truncated cylinder must be greater than a factor of 10 of the burial depth h before the magnitude of the response

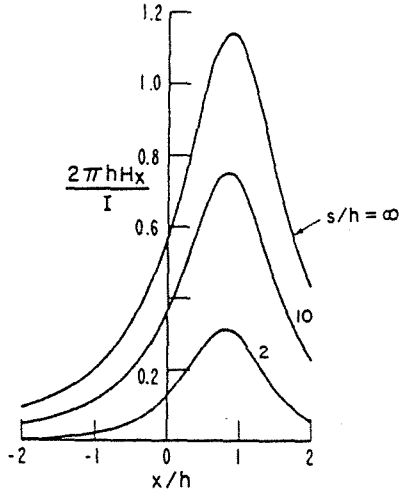


Fig. 4. Normalized horizontal magnetic field as a function of the horizontal displacement for a buried and displaced finite cylinder, $a/h = 0.5$, $d/h = 1.0$, $l/s = 0.5$, $y = 0$.

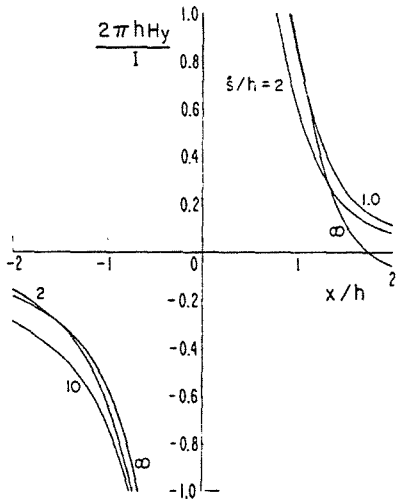


Fig. 5. Normalized vertical magnetic field as a function of the horizontal displacement for a buried and displaced finite cylinder, $a/h = 0.5$, $d/h = 1.0$, $l/s = 0.5$, $y = 0$.

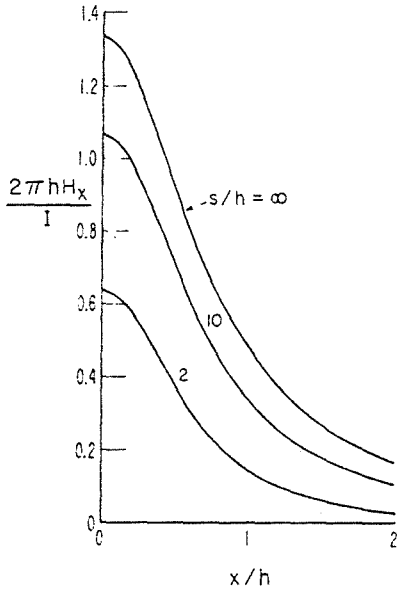


Fig. 6. Horizontal field for a finite cylinder buried directly beneath the source cable. $a/h = 0.5$, $d = 0$, $l/s = 0.5$, $y = 0$.

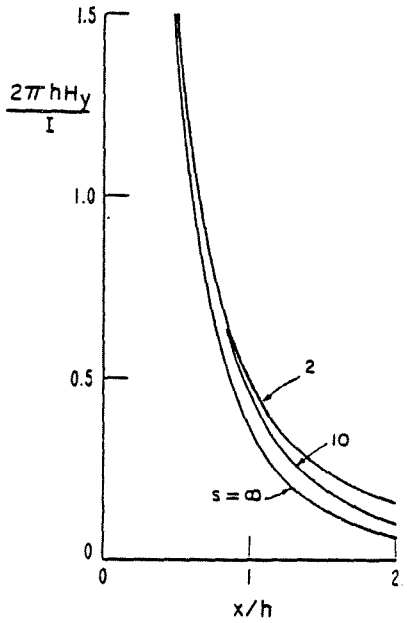


Fig. 7. Vertical field for a finite cylinder buried directly beneath the source cable, $a/h = 0.5$, $d = 0$, $l/s = 0.5$, $y = 0$.

approaches that for an infinite cylinder with the same transverse dimensions. This is an important factor to keep in mind when two-dimensional models are being employed to simulate the scattering from finite structures.

APPENDIX A: TWO-DIMENSIONAL MODEL

For comparison purposes, it is useful to consider the purely two-dimensional problem of a uniform line current parallel to a homogeneous circular cylinder of radius, a, with conductivity σ and permeability μ [*Wait*, 1952 (in equation 13 replace μ_2/μ_1 by $n\mu_2/\mu_1$, and in equation 14 replace $(k \pm n)$ by $n(k \pm 1)$), 1959]. This can be considered as the limit of the finite cylinder configuration as $s \to \infty$.

Using cylindrical coordinates (ρ, ϕ, z), the cylinder is defined by $\rho < a$ for $-\infty < z < \infty$. The line source is located at $\rho = \rho_0$ and $\phi = \phi_0$ where $\rho_0 > a$. The primary electric field of the line source has only a z component, given by

$$E_z^{pr} = (-i\mu_0\omega I/2\pi) K_0(\gamma_0\rho_d) \tag{A1}$$

where

$$\rho_d = [\rho_0^2 + \rho^2 - 2\rho_0\rho \cos(\phi_0 - \phi)]^{1/2} \tag{A2}$$

The corresponding magnetic field components are

$$H_\phi^{pr} = (1/i\mu_0\omega)(\partial E_z^{pr}/\partial\rho)$$

$$= \{I[\rho - \rho_0 \cos(\phi_0 - \phi)]/2\pi\rho_d\}\gamma_0 K_1(\gamma_0\rho_d) \tag{A3}$$

$$H_\rho^{pr} = (-1/\rho i\mu_0\omega)(\partial E_z^{pr}/\partial\phi)$$

$$= [+I\rho_0 \sin(\phi_0 - \phi)/2\pi\rho_d]\gamma_0 K_1(\gamma_0\rho_d) \tag{A4}$$

In the quasi-static case where $|\gamma_0\rho_d| \ll 1$, these are expressible in the simpler form

$$H_\phi^{pr} \simeq I[\rho - \rho_0 \cos(\phi_0 - \phi)]/2\pi\rho_d^2 \tag{A5}$$

and

$$H_\rho^{pr} \simeq I\rho_0 \sin(\phi_0 - \phi)/2\pi\rho_d^2 \tag{A6}$$

Using a previously known solution, we can write down the corresponding forms for the secondary fields external to the cylinder. The exact expressions for the two magnetic field components for the region $\rho > a$ are [*Wait*, 1952]

$$H_\phi^{sec} = -(I/2\pi\rho) \sum_{m=-\infty}^{+\infty} q_m[K_m(\gamma_0\rho_0)/K_m(\gamma_0 a)]$$

$$\cdot I_m(\gamma_0 a)e^{-im(\phi-\phi_0)}\gamma_0\rho_0 K_m'(\gamma_0\rho) \tag{A7}$$

and

$$H_\rho^{sec} = -(I/2\pi\rho) \sum_{m=-\infty}^{+\infty} q_m[K_m(\gamma_0\rho_0)/K_m(\gamma_0 a)]$$

$$\cdot I_m(\gamma_0 a)e^{-im(\phi-\phi_0)} im K_m(\gamma_0\rho) \tag{A8}$$

where

$$q_m = \{-(1/\eta)[I_m'(\gamma a)/I_m(\gamma a)]$$

$$+ (1/\eta_0)[I_m'(\gamma_0 a)/I_m(\gamma_0 a)]\}/\{(1/\eta)[I_m'(\gamma a)/I_m(\gamma a)]$$

$$- (1/\eta_0)[K_m'(\gamma_0 a)/K_m(\gamma_0 a)]\} \tag{A9}$$

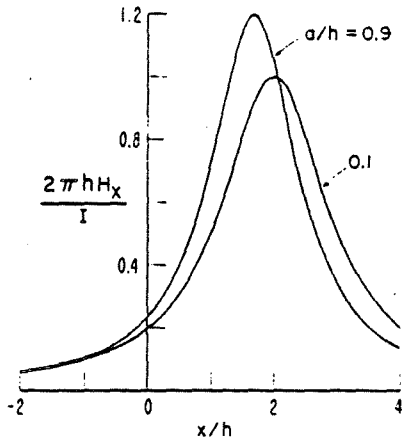


Fig. A1. Normalized field as a function of the horizontal displacement for a buried infinite cylinder, $d/h = 2$, $y = 0$.

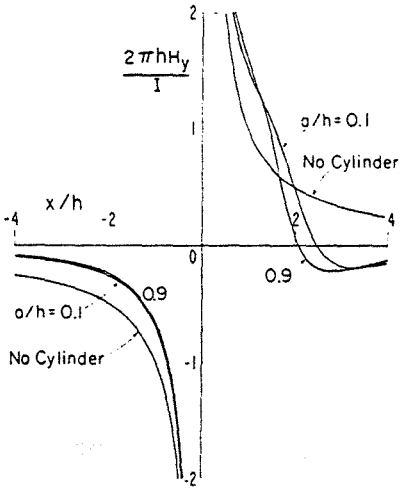


Fig. A2. Normalized field as a function of the horizontal displacement for a buried infinite cylinder, $d/h = 2$, $y = 0$.

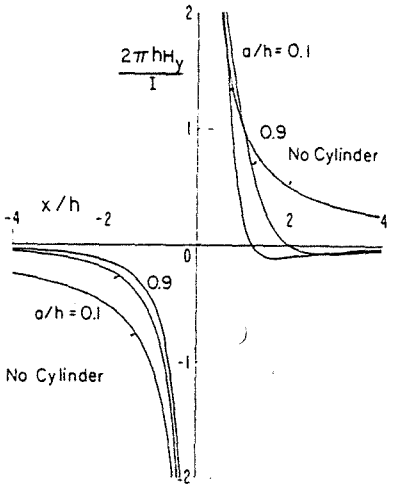


Fig. A4. Normalized field as a function of the horizontal displacement for a buried infinite cylinder, $d/h = 1$, $y = 0$.

The quasi-static forms for the secondary fields are then found to be

$$H_\phi^{sec} \simeq (I/2\pi\rho) \sum_{m=1}^{\infty} q_m (a^{2m}/\rho_0{}^m \rho^m) \cdot \cos m(\phi - \phi_0) + H_{0\phi}^{sec} \quad \text{(A10)}$$

and

$$H_\rho^{sec} \simeq (-I/2\pi\rho) \sum_{m=1}^{\infty} q_m (a^{2m}/\rho_0{}^m \rho^m) \cdot \sin m(\phi - \phi_0) \quad \text{(A11)}$$

where

$$H_{0\phi}^{sec} \simeq (I/2\pi\rho) q_0 \ln (0.89\gamma_0\rho_0)/\ln (0.89\gamma_0 a) \quad \text{(A12)}$$

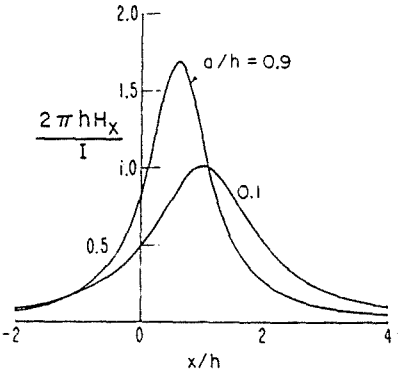


Fig. A3. Normalized field as a function of the horizontal displacement for a buried infinite cylinder, $d/h = 1$, $y = 0$.

In the limiting case where we let $\gamma_0 \to 0$, we see that $q_m = -1$ and $q_0 = -1$, and $H_{0\phi}^{sec} \simeq -I/(2\pi\rho)$. Then (A10) and (A11) can be summed as geometric series to give

$$H_\phi^{sec} = (-I/2\pi\rho) \cdot [1 - (a^2/\rho_0\rho) \cos (\phi - \phi_0)]/[1 - 2(a^2/\rho_0\rho) \cdot \cos (\phi - \phi_0) + (a^2/\rho_0\rho)^2] \quad \text{(A13)}$$

and

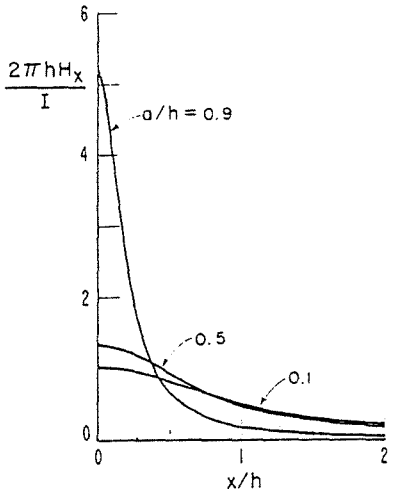


Fig. A5. Normalized field as a function of the horizontal displacement for a buried infinite cylinder, $d/h = 0$, $y = 0$.

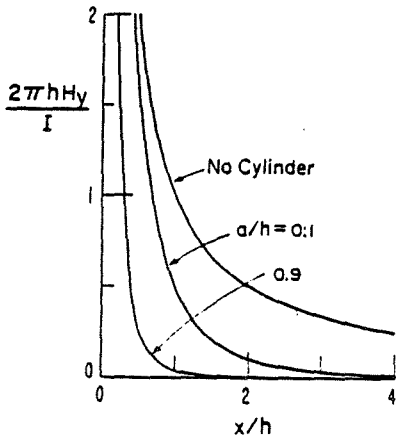


Fig. A6. Normalized field as a function of the horizontal displacement for a buried infinite cylinder, $d/h = 0$, $y = 0$.

$$H_\rho^{sec} = (I/2\pi\rho) \cdot [(a^2/\rho_0\rho)\sin(\phi - \phi_0)]/[1 - 2(a^2/\rho_0\rho) \cdot \cos(\phi - \phi_0) + (a^2/\rho_0\rho)^2] \quad \text{(A14)}$$

Again, referring to Figure 3, we consider the total H_x and H_y components in the plane $y = 0$, where now the buried cylinder (of perfect conductivity) is of infinite length. In Figure A1 we show a plot of $2\pi hH_x/I$ as a function of x/h for $d/h = 2$, for $a/h = 0.9$, and $a/h = 0.1$. The corresponding results for $2\pi hH_y/I$ are shown in Figure A2. Similar curves are shown in Figures A3 and A4, where $d/h = 1$, and finally in Figures A5 and A6 where $d/h = 0$.

REFERENCES

Fox, J. (Ed.) (1964), *Quasi-Optics*, pp. 1–25, Polytechnic, New York.

Harrington, R. F. (1968), *Field Computation by Moment Methods*, pp. 82–102, Macmillan, New York.

Wait, J. R. (1952), A cylindrical ore body in the presence of a cable carrying an oscillating current, *Geophys.*, *17*(2), 378–386.

Wait, J. R. (1959), *Electromagnetic Radiation from Cylindrical Structures*, pp. 182–183, Pergamon, New York.

Ward, S. H., and H. F. Morrison (Eds.) (1971), Special Issue on Electromagnetic Scattering, *Geophys.*, *36*(1), 1–183.

Pageoph
Vol. 111 (1973/X)

Birkhäuser Verlag, Basel

Subsurface Electric Fields of a Grounded Cable of Finite Length for both Frequency and Time Domain

By DAVID A. HILL[1]) and JAMES R. WAIT[2])

Summary – The subsurface electric fields of a current-carrying cable are examined for both steady-state and transient situations. Closed form expressions are obtained for two of the electric field components, and a numerical integration is used to obtain the third component. Waveforms for a step-function current excitation are displayed. The results have possible application to pulsed downlink communication in mine rescue operations.

1. Introduction

The time harmonic subsurface fields of a finite length line source or current-carrying cable on a conducting half-space have been examined by HILL and WAIT [1]. The emphasis was on examining the effects of finite cable length on the subsurface magnetic fields. Here we consider the electric field; also we extend the analysis to the time domain by treating a step-function current. The nature of the build-up of the subsurface electric field is of importance. This rise time dictates what pulse width and pulse repetition frequency can be used in a downlink communication system.

The half-space is taken to be homogeneous, and the current in the cable is assumed to be uniform. This is justified for an insulated cable with grounded ends for sufficiently low frequencies [4, 3, 8]. Actually, related problems of the transient subsurface fields of an infinitesimal horizontal dipole and transient coupling between surface cables have been treated by Wait [5]. The techniques employed here are similar.

2. Frequency domain solution

The line source extends from $-l$ to l on the x-axis, and the observer in the half-space ($z < 0$) is located at (x, y, z) as shown in Fig. 1. The x-directed current is $I\exp(i\omega t)$, and the angular frequency ω is sufficiently low that displacement currents are negligible

[1]) Institute for Telecommunication Sciences, Office of Telecommunications, U.S. Department of Commerce, Boulder, Colorado 80302.

[2]) Cooperative Institute for Research in Environmental Sciences, University of Colorado.

After carrying out the differentiation, E_z can be written in the following convenient form

$$E_z = -[I/(2\pi\sigma h^2)]\, E_{zn}(W, L, X, Y), \tag{3}$$

where

$$E_{zn} = R_1^{-3} \exp[-(iW)^{1/2} R_1][1 + (iW)^{1/2} R_1] - R_2^{-3} \exp[-(iW)^{1/2} R_2][1 + (iW)^{1/2} R_2],$$

$$W = \omega\mu_0 \sigma h^2, \qquad L = l/h, \qquad X = x/h, \qquad Y = y/h,$$

$$R_{\frac{1}{2}} = r_{\frac{1}{2}}/h = [(X \mp L)^2 + Y^2 + 1]^{1/2},$$

and h $(= -z)$ is the observer depth. Note that E_{zn}, W, L, X, and Y are all dimensionless and that W can be considered a normalized frequency since it is proportional to ω. The dependence of $|E_{zn}|$ on W is illustrated in Fig. 2 for $L = 1$ and various values of X and Y. In a typical example with $\sigma = 10^{-2}$ mhos/m and $h = 100$ m, the frequency f is given by

$$f = W/(2\pi\sigma\mu_0 h^2) = 1266\, W \text{ Hz}. \tag{4}$$

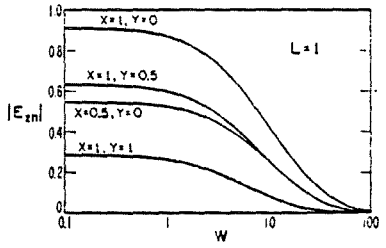


Figure 2
Frequency dependence of $|E_{zn}|$ for various observation points

Consequently, the frequency range in Fig. 2 is 126.6 Hz to 126.6 kHz for the above values of σ and h. The phase of E_{zn} is a generally decreasing function of W.

In order to express E_y in a convenient form, the differentiations in (2) are carried out and derivatives of the modified Bessel functions are replaced by zero- and first-order functions. The resultant E_y in normalized form is

$$E_y = -[I/(2\pi\sigma h^2)]\, E_{yn}(W, L, X, Y), \tag{5}$$

where

$$\begin{aligned} E_{yn} = \frac{(iW)^{1/2} Y}{2} \Bigg\{ & \left[\frac{(iW)^{1/2}}{R_1^2} (I_1 K_1 - I_0 K_0) \right|_{R=R_1} \\ & - \left(\frac{1}{R_1^3} + \frac{1}{R_1^2} \right) (I_0 K_1) \Big|_{R=R_1} + \left(\frac{1}{R_1^3} - \frac{1}{R_1^2} \right) (I_1 K_0) \Big|_{R=R_1} \Bigg] \\ & - \left[\frac{(iW)^{1/2}}{R_2^2} (I_1 K_1 - I_0 K_0) \right|_{R=R_2} - \left(\frac{1}{R_2^3} + \frac{1}{R_2^2} \right) (I_0 K_1) \Big|_{R=R_2} \\ & + \left(\frac{1}{R_2^3} - \frac{1}{R_2^2} \right) (I_1 K_0) \Big|_{R=R_2} \Bigg] \Bigg\}, \end{aligned}$$

After carrying out the differentiation, E_z can be written in the following convenient form

$$E_z = -[I/(2\pi\sigma h^2)]\, E_{zn}(W, L, X, Y), \tag{3}$$

where

$$E_{zn} = R_1^{-3} \exp[-(iW)^{1/2} R_1][1 + (iW)^{1/2} R_1] - R_2^{-3} \exp[-(iW)^{1/2} R_2][1 + (iW)^{1/2} R_2],$$

$$W = \omega\mu_0 \sigma h^2, \qquad L = l/h, \qquad X = x/h, \qquad Y = y/h,$$

$$R_{\frac{1}{2}} = r_{\frac{1}{2}}/h = [(X \mp L)^2 + Y^2 + 1]^{1/2},$$

and h $(= -z)$ is the observer depth. Note that E_{zn}, W, L, X, and Y are all dimensionless and that W can be considered a normalized frequency since it is proportional to ω. The dependence of $|E_{zn}|$ on W is illustrated in Fig. 2 for $L = 1$ and various values of X and Y. In a typical example with $\sigma = 10^{-2}$ mhos/m and $h = 100$ m, the frequency f is given by

$$f = W/(2\pi\sigma\mu_0 h^2) = 1266\, W \text{ Hz}. \tag{4}$$

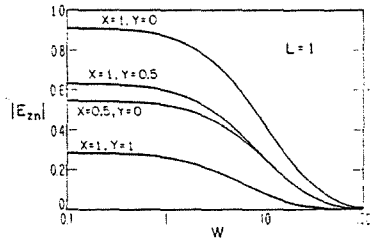


Figure 2
Frequency dependence of $|E_{zn}|$ for various observation points

Consequently, the frequency range in Fig. 2 is 126.6 Hz to 126.6 kHz for the above values of σ and h. The phase of E_{zn} is a generally decreasing function of W.

In order to express E_y in a convenient form, the differentiations in (2) are carried out and derivatives of the modified Bessel functions are replaced by zero- and first-order functions. The resultant E_y in normalized form is

$$E_y = -[I/(2\pi\sigma h^2)]\, E_{yn}(W, L, X, Y), \tag{5}$$

where

$$\begin{aligned} E_{yn} = \frac{(iW)^{1/2} Y}{2} \Bigg\{ & \left[\frac{(iW)^{1/2}}{R_1^2} (I_1 K_1 - I_0 K_0) \right|_{R=R_1} \\ & - \left(\frac{1}{R_1^3} + \frac{1}{R_1^2} \right) (I_0 K_1) \Big|_{R=R_1} + \left(\frac{1}{R_1^3} - \frac{1}{R_1^2} \right) (I_1 K_0) \Big|_{R=R_1} \Bigg] \\ & - \left[\frac{(iW)^{1/2}}{R_2^2} (I_1 K_1 - I_0 K_0) \Big|_{R=R_2} - \left(\frac{1}{R_2^3} + \frac{1}{R_2^2} \right) (I_0 K_1) \Big|_{R=R_2} \right. \\ & \left. + \left(\frac{1}{R_2^3} - \frac{1}{R_2^2} \right) (I_1 K_0) \Big|_{R=R_2} \right] \Bigg\}, \end{aligned}$$

the argument of I_0 and I_1 is $(iW)^{1/2}(R-1)/2$, and the argument of K_0 and K_1 is $(iW)^{1/2}(R+1)/2$. The dependence of $|E_{yn}|$ on W is illustrated in Fig. 3 for $L=1$ and various values of X and Y. The phase of E_{yn} is again a decreasing function of W.

The integration for E_x must be done numerically, and some results have been given [1]. However, here we wish to normalize in the following form

$$E_x = -[I/(2\pi\sigma h^2)]\, E_{xn}(W, L, X, Y), \tag{6}$$

where

$$E_{xn} = h^2 \int_{-l}^{l} \left(\frac{\partial^2 P}{\partial z^2} + \frac{\partial^3 N}{\partial y^2\, \partial z}\right) dx',$$

$$\frac{\partial^2 P}{\partial z^2} = \frac{\exp(-\gamma r)}{r^3}\left[\left(\frac{3z^2}{r^2} - 1\right) + \gamma r\left(\frac{3z^2}{r^2} - 1\right) + \gamma^2 z^2\right],$$

$$\frac{\partial^3 N}{\partial y^2\, \partial z} = \frac{\gamma}{2}\left[B_{00} I_0 K_0 + B_{11} I_1 K_1 + B_{01} I_0 K_1 + B_{10} I_1 K_0\right],$$

$$B_{00} = \frac{\gamma z}{r^2}\left(1 - \frac{3y^2}{r^2}\right),$$

$$B_{11} = \frac{\gamma z}{r^2}\left[-1 + \frac{3y^2}{r^2} + \frac{2y^2}{r^2 - z^2}\right],$$

$$B_{01} = \frac{1}{r^2}\left[-1 + \frac{3y^2}{r^2} + \frac{z(1 - \gamma^2 y^2)}{r} - \frac{3zy^2}{r^3}\right],$$

$$B_{10} = \frac{1}{r^2}\left[-1 + \frac{3y^2}{r^2} - \frac{z(1 - \gamma^2 y^2)}{r} + \frac{3zy^2}{r^3}\right],$$

the argument of I_0 and I_1 is $\gamma(r+z)/2$, and the argument of K_0 and K_1 is $\gamma(r-z)/2$. The x' integration was done numerically, and the resultant dependence of $|E_{xn}|$ on W for $L=1$ and various values of X and Y is illustrated in Fig. 4. It is interesting that the curves peak near $W=5$ before falling off for large W. As in the previous cases, the phase is a decreasing function of W.

A simple special case is the low frequency limit, where the electric field is given by the gradient of a scalar potential [6]. Thus

$$d\mathbf{E}^{dc} = \frac{I dx'}{2\pi\sigma}\, \nabla \frac{\partial}{\partial x}\left(\frac{1}{r}\right),$$

$$\mathbf{E}^{dc} = \frac{-I}{2\pi\sigma}\, \nabla\left(\frac{1}{r_1} - \frac{1}{r_2}\right). \tag{7}$$

Consequently, the normalized components are given by

$$E_{xn}^{dc} = (L - X)\,R_1^{-3} + (L + X)\,R_2^{-3},$$

$$E_{yn}^{dc} = -Y(R_1^{-3} - R_2^{-3}),$$

$$E_{zn}^{dc} = R_1^{-3} - R_2^{-3}. \tag{8}$$

All computed results in Figs. 2–4 agree with these limits as $W \to 0$. These limits are important because they are the final values of the step responses that are computed in the following section.

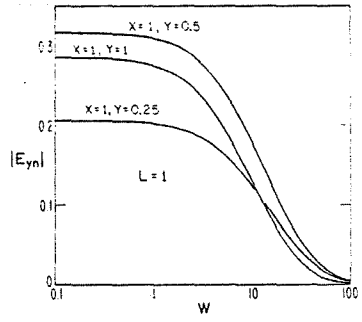


Figure 3
Frequency dependence of $|E_{yn}|$ for various observation points

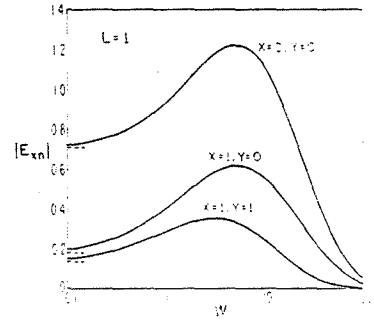


Figure 4
Frequency dependence of $|E_{xn}|$ for various observation points

3. *Step response*

In this case, the cable current is given by $IU(t)$ where $U(t)$ is the unit step function at $t = 0$. The step responses are given by the following inverse Fourier transform:

$$\begin{Bmatrix} \tilde{E}_x^s(t) \\ \tilde{E}_y^s(t) \\ \tilde{E}_z^s(t) \end{Bmatrix} = \frac{1}{2\pi} \int_{-\infty}^{\infty} \frac{\exp(i\omega t)}{i\omega} \begin{Bmatrix} E_x \\ E_y \\ E_z \end{Bmatrix} d\omega \tag{9}$$

where E_x, E_y, and E_z are given in the previous section.

The following standard inverse Fourier (or Laplace) transform is useful in obtaining $\tilde{E}_z^s$

$$\mathfrak{F}^{-1}[\exp(-a(i\omega)^{1/2})/(i\omega)] = \operatorname{erfc}[a/(2t^{1/2})]\, U(t), \tag{10}$$

where

$$\operatorname{erfc}(x) = \frac{2}{\pi^{1/2}} \int_x^\infty e^{-y^2}\, dy$$

is the complement of the error function for real argument x. By applying (10) to (2), we obtain

$$\tilde{E}_z^s(t) = \frac{-I}{2\pi\sigma} \frac{\partial}{\partial z} \{r_1^{-1} \operatorname{erfc}[(r_1/2)(\mu_0\sigma/t)^{1/2}] - r_2^{-1} \operatorname{erfc}[(r_2/2)(\mu_0\sigma/t)^{1/2}]\} \tag{11}$$

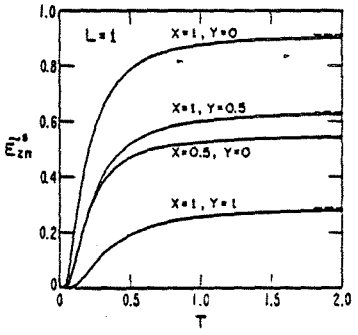


Figure 5
Step response $\tilde{E}_{zn}^s$ for various observation points

The unit step $U(t)$ has been omitted in (11), and it is understood from hereon that all time responses are zero for negative time. We now write (11) in the normalized form

$$\tilde{E}_z^s(t) = -[I/(2\pi\sigma h^2)]\, \tilde{E}_{zn}^s(T, L, X, Y), \tag{12}$$

where

$$\tilde{E}_{zn}^s = \frac{\operatorname{erfc}[(R_1/2)T^{-1/2}]}{R_1^3} - \frac{\exp[-R_1^2/(4T)]}{(\pi T)^{1/2} R_1^2} - \frac{\operatorname{erfc}[(R_2/2)T^{-1/2}]}{R_2^3} + \frac{\exp[-R_2^2/(4T)]}{(\pi T)^{1/2} R_2^2}$$

and $T = t/(\sigma\mu_0 h^2)$.

Curves of $\tilde{E}_{zn}^s$ vs. T are given in Fig. 5 for $L = 1$ and various values of X and Y. Note that, at $T = 2$, $\tilde{E}_{zn}^s$ has nearly reached its static limit as given by (8). For typical values of σ ($= 10^{-2}$ mhos/m) and h ($= 100$ m), the quantity $\sigma\mu_0 h^2$ is 0.1258 msec. Consequently, $T = 1$ corresponds to $t = 0.1258$ msec. The quantity $\sigma\mu_0 h^2$ has also appeared as the effective time constant for the transient fields of a pulsed loop [7].

In determining $\tilde{E}_y^s$, the following inverse Fourier (or Laplace) transform is useful [2]:

$$\mathfrak{F}^{-1}\{I_0[a(i\omega)^{1/2}]\,K_0[b(i\omega)^{1/2}]\} = \frac{\exp[-(a^2+b^2)/(4t)]}{2t}\cdot I_0\left(\frac{ab}{2t}\right). \tag{13}$$

Application of (13) to (2) allows the expression of the impulse response in closed form. Consequently, the step response can be written as an integral of the step response:

$$\tilde{E}_y^s(t) = -[I/(2\pi\sigma h^2)]\,\tilde{E}_{yn}^s(T, L, X, Y), \tag{14}$$

where

$$\tilde{E}_{yn}^s(T, L, X, Y) = \int_0^T \tilde{E}_{yn}^i(T', L, X, Y)\,dT'$$

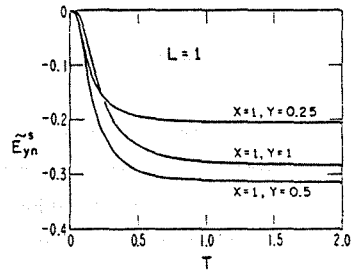


Figure 6
Step response $\tilde{E}_{yn}^s$ for various observation points

and

$$\tilde{E}_{yn}^i = \frac{Y}{16T^3}\left\{\exp\left(-\frac{R_1^2+1}{8T}\right)\left[I_1\left(\frac{R_1^2-1}{8T}\right) - I_0\left(\frac{R_1^2-1}{8T}\right)\right]\right.$$
$$\left. - \exp\left(\frac{R_2^2+1}{8T}\right)\left[I_1\left(\frac{R_2^2-1}{8T}\right) - I_0\left(\frac{R_2^2-1}{8T}\right)\right]\right\}.$$

The integration in (14) was done numerically, and the resultant step responses for $L = 1$ and various values of X and Y are shown in Fig. 6. Again, the final values as given by (8) have essentially been reached at $T = 2$.

In order to determine $\tilde{E}_x^s$, the inverse Fourier transform was done numerically as follows:

$$\tilde{E}_x^s(t) = -[I/(2\pi\sigma h^2)]\,\tilde{E}_{xn}^s(T, L, X, Y), \tag{15}$$

where

$$\tilde{E}_{xn}^s(T, L, X, Y) = \frac{1}{2\pi}\int_{-\infty}^{\infty} \frac{E_{xn}(W, L, X, Y)}{iW}\exp(iWT)\,dW,$$

and E_{xn} is given by (6). The resultant curves of $\tilde{E}^s_{xn}$ vs. T are shown in Fig. 7 for $L = 1$ and various values of X and Y. These waveforms, unlike those for $\tilde{E}^s_{zn}$ and $\tilde{E}^s_{yn}$, contain an overshoot and a slow recovery to the final value.

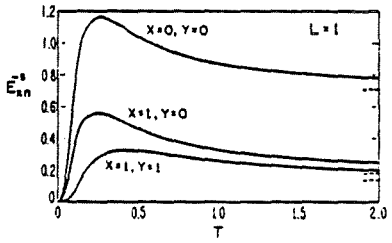


Figure 7
Step response $\tilde{E}^s_{xn}$ for various observation points

4. Concluding remarks

Both the time-harmonic and the transient subsurface electric field for a finite length cable carrying a step function current have been examined. Closed form expressions have been obtained for the y and z components, whereas numerical integration was required for the x component. The time-domain waveforms are fairly simple and the final values can be obtained from a scalar potential. However, the waveforms for the x component do contain an overshoot. The time constant of the waveforms is roughly $\sigma\mu_0 h^2$ which is consistent with previous results for loop sources.

Acknowledgements

We thank Dr. RICHARD G. GEYER for his useful suggestions, Drs. H. PARKINSON and J. POWELL for their encouragement, and their organization, the U.S. Bureau of Mines, for its support, and Mrs. LOYS GAPPA for her help in preparing the manuscript.

REFERENCES

[1] D. A. HILL and J. R. WAIT, *Subsurface Electromagnetic Fields of a Grounded Cable of Finite Length*, unpublished report, January 1973.

[2] G. E. ROBERTS and H. KAUFMAN, *Table of Laplace Transforms* (W. B. Saunders Co., Philadelphia 1966), 311 pp.

[3] E. D. SUNDE, *Earth Conduction Effects in Transmission Systems* (Dover Publications, New York 1968), pp. 140–172.

[4] J. R. WAIT, *Electromagnetic fields of current-carrying wires in a conducting medium*, Can. J. Phys. *30* (1952), 512–523.

[5] J. R. WAIT, *Propagation of electromagnetic pulses in a homogeneous conducting earth*, Appl. Sci. Res. *8B* (1960), 213–253.
[6] J. R. WAIT, *The electromagnetic fields of a horizontal dipole in the presence of a conducting half-space*, Can. J. Phys. *39* (1961), 1017–1028.
[7] J. R. WAIT and D. A. HILL, *Transient signals from a buried dipole*, J. Appl. Phys. *42* (10) (1971), 3866–3869.
[8] J. R. WAIT, *Electromagnetic wave propagation along a buried insulated wire*, Can. J. Phys. *50* (1972), 2402–2409.

(Received 29th March 1973)

Proc. IEEE (Letters), Vol. 59, No. 8
1287-1288 (August 1971)

Transient Excitation of the Earth by a Line Source of Current

Abstract—The electromagnetic fields in a conducting half-space are considered for a line source of current. Under the assumption that displacement currents are negligible, a closed form expression is obtained for the subsurface electric field when the source current is an impulse function. It is shown that the field has a relatively sharp spike which is followed by a slow-tail portion.

In a variety of situations, one is interested in the propagation of electromagnetic waves into the earth from a source on the surface. For example, in applied geophysics, this signal may excite currents in a buried ore deposit; they in turn produce a field on the surface which can be detected. Another possibility is that the subsurface signal may be detected in a mine or other underground working and thus provide a mechanism for downlink communication.

In most analytical studies of electromagnetic wave propagation in the earth, time harmonic fields are considered exclusively.[1] Except in special cases, quantitative estimates of field strength require numerical evaluation of integrals. Here we wish to point out that the transient solution for a relevant configuration is expressible in terms of tabulated functions. Specifically, we shall consider a long straight insulated wire lying on the earth's surface which is to be excited by an impulsive current.

First, we consider the time harmonic formulation of the problem. With respect to a Cartesian coordinate system (x, y, z), the assumed homogenous earth of conductivity σ and magnetic permeability μ_0 occupies the space $y<0$. The line source carrying a uniform current $I(i\omega)\exp(i\omega t)$ is coincident

Manuscript received December 23, 1970.

[1] J. R. Wait, Ed., *Electromagnetic Probing in Geophysics*. Boulder, Colo.: Golem Press, 1971.

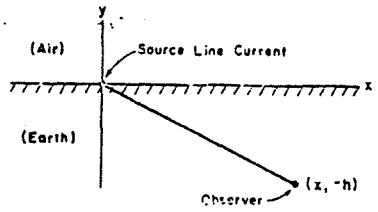


Fig. 1. Conducting half-space with a line source of current on the surface.

with the z axis. The situation is illustrated in Fig. 1. We now invoke the assumption that the significant angular frequencies ω are sufficiently low that all displacement currents can be neglected. As shown elsewhere[2] this is justified when all significant distances are small compared with the free space wavelength. For the problem as stated, the electric field has only a z component (i.e., parallel to the wire), and for $y=-h$ within the earth it is given by[2]

$$E_z(i\omega) = -\frac{i\mu_0\omega I(i\omega)}{\pi}\int_0^\infty \frac{\cos\lambda x}{u+\lambda}\exp(-uh)d\lambda \tag{1}$$

where $u=(\lambda^2+i\sigma\mu_0\omega)^{\frac{1}{2}}$ and the time factor $\exp(i\omega t)$ is understood.

We now allow the uniform current in the wire to be specified a function of time $J(t)$ which is zero for $t<0$. Thus in Laplace transform notation

$$I(s) = \mathcal{L}J(t) = \int_0^\infty J(t)\exp(-st)dt \tag{2}$$

and the corresponding electric field $e_z(t)$ within the earth at $y=-h$ is to be obtained from

$$e_z(t) = \mathcal{L}^{-1}E_z(s) = \frac{1}{2\pi i}\int_{c-i\infty}^{c+i\infty} E_z(s)\exp(st)ds, \tag{3}$$

where

$$E_z(s) = \frac{-\mu_0 sI(s)}{\pi}\int_0^\infty \cos\lambda x\,\frac{\exp[-(\lambda^2+\sigma\mu_0 s)^{\frac{1}{2}}h]}{[(\lambda^2+\sigma\mu_0 s)^{\frac{1}{2}}+\lambda]}d\lambda \tag{4a}$$

$$= \frac{I(s)}{\pi\sigma}\int_0^\infty \cos\lambda x\left(\frac{\partial}{\partial h}+\lambda\right)\exp[-(\lambda^2+\sigma\mu_0 s)^{\frac{1}{2}}h]d\lambda. \tag{4b}$$

We now consider specifically the impulse response so that $J(t)=I_0\delta(t)$ where $\delta(t)$ is the Dirac delta function and I_0 is a constant. Then $I(s)=I_0$ and the corresponding electric field, for $t>0$, is given by

$$e_z(t) = \frac{I_0}{\pi\sigma}\int_0^\infty \cos\lambda x\left(\frac{\partial}{\partial h}+\lambda\right)\left[\mathcal{L}^{-1}\exp\left[-(\sigma\mu_0)^{\frac{1}{2}}h\left(s+\frac{\lambda^2}{\sigma\mu_0}\right)^{\frac{1}{2}}\right]\right]d\lambda. \tag{5}$$

The Laplace inversion integral is a standard type, and we obtain

$$e_z(t) = \frac{I_0}{\pi\sigma}\int_0^\infty \cos\lambda x\left(\frac{\partial}{\partial h}+\lambda\right)\frac{(\sigma\mu_0)^{\frac{1}{2}}h}{2(\pi t^3)^{\frac{1}{2}}}\exp\left[-\frac{\lambda^2}{\sigma\mu_0}t-\frac{\sigma\mu_0 h^2}{4t}\right]d\lambda \tag{6}$$

Utilizing the easily proved relationships

$$\int_0^\infty \exp\left(-\frac{\lambda^2}{\sigma\mu_0}t\right)\cos\lambda x d\lambda = \frac{1}{2}\left(\frac{\pi\sigma\mu_0}{t}\right)^{\frac{1}{2}}\exp\left(-\frac{\sigma\mu_0 x^2}{4t}\right) \tag{7}$$

$$\int_0^\infty \exp\left(-\frac{\lambda^2}{\sigma\mu_0}t\right)\lambda\cos\lambda x d\lambda = \frac{\partial}{\partial x}\int_0^\infty \exp\left(-\frac{\lambda^2}{\sigma\mu_0}t\right)\sin\lambda x d\lambda$$

$$= \frac{\partial}{\partial x}\left[\left(\frac{\sigma\mu_0}{t}\right)^{\frac{1}{2}}\exp\left(-\frac{\sigma\mu_0 x^2}{4t}\right)\cdot\int_0^{(\sigma\mu_0/t)^{1/2}(x/2)}\exp(Z^2)dZ\right] \tag{8}$$

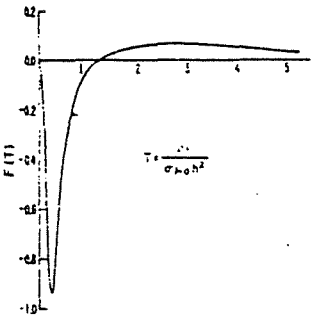


Fig. 2. Waveform of the electric field in the earth at depth h beneath the line source for an impulsive current.

we reduce (6) to the convenient form

$$e_z(t) = \frac{\mu_0 I_0}{2\pi t^2}\left\{\frac{1}{2}\left(1-\frac{\sigma\mu_0 h^2}{2t}\right)\exp\left(-\frac{\sigma\mu_0 x^2}{4t}\right)\right.$$

$$-\frac{\sigma\mu_0 xh}{2\pi^{\frac{1}{2}}t}\exp\left(-\frac{\sigma\mu_0 x^2}{4t}\right)\int_0^{(\sigma\mu_0/t)^{1/2}(x/2)}\exp(Z^2)dZ$$

$$\left.+\frac{1}{\pi^{\frac{1}{2}}}\left(\frac{\sigma\mu}{t}\right)^{\frac{1}{2}}\frac{h}{2}\right\}\exp\left(-\frac{\sigma\mu_0 h^2}{4t}\right). \tag{9}$$

Using tables of Dawson's integral,[3] the right-hand side can be readily computed for any value of the time parameter $4t/(\sigma\mu_0 h^2)$ or the ratio x/h.

A rather simple but, nevertheless, interesting case is when $x=0$ corresponding to having the observer, at depth h, directly beneath the source current. Then from (9), we see that

$$e_z(t) = \frac{8}{\pi\mu_0\sigma^2 h^4}F\left(\frac{4t}{\sigma\mu_0 h^2}\right) \tag{10}$$

where

$$F(T) = \frac{1}{T^2}\left[\left(\frac{1}{2}-\frac{1}{T}\right)+\left(\frac{1}{\pi T}\right)^{\frac{1}{2}}\right]\exp\left(-\frac{1}{T}\right). \tag{11}$$

The function $F(T)$ which is the waveform of the electric field is plotted as a function of the time parameter T in Fig. 2. As indicated, there is a rather strong negative spike followed by a "slow tail." Of particular interest is the fact that the field, for some particular feature of the waveform, decays algebraically as the inverse fourth power of the depth. This is to be contrasted with the exponential-like depth variation of the amplitude of time-harmonically varying fields.

For a typical case where $\sigma=10^{-2}$ (mho/m), it is easy to show that the abscissa T can be read directly in milliseconds if $h=563$ m, or approximately 1800 ft.

In the general case, where $x/h\neq 0$, we need to work with (9). Furthermore, if the corresponding magnetic fields $h_x(t)$ and $h_y(t)$ are desired, we can utilize Maxwell's equations

$$\mu_0\partial h_x(t)/\partial t = -\partial e_z(t)/\partial x \tag{12}$$

$$\mu_0\partial h_y(t)/\partial t = -\partial e_z(t)/\partial h. \tag{13}$$

In fact, the voltage responses of small loop receivers are proportional to the time derivatives of the appropriate magnetic field component so that the loop responses may be obtained without difficulty.

James R. Wait
Inst. Telecommun. Sci.
U. S. Dep. Commerce
Boulder, Colo. 80302

[2] J. R. Wait, Ed., *Electromagnetic Waves in Stratified Media*. Oxford, England: Pergamon, 1962.

[3] M. Abramowitz and I. A. Stegun, Eds., *Handbook of Mathematical Functions*. Washington, D. C.: NBS, 1964, p. 319.

Institut National des Industries Extractives

INTERNATIONAL CONFERENCE

" RADIO : Roads, Tunnels and Mines "

Liège (Belgium), 1 - 5 April 1974

II

MINES

Conference organized by INIEX with the financial assistance
of the Commission of the European Communities

ANALYTICAL STUDIES OF ELECTROMAGNETIC WAVES ON MONO-FILAR AND BI-FILAR STRUCTURES IN CIRCULAR AND RECTANGULAR MINE TUNNELS

James R. WAIT, David A. HILL, and Samir F. MAHMOUD
Cooperative Institute for Research in Environmental Sciences
University of Colorado
Boulder, Colorado 80302

ABSTRACT

This paper is a summary of recent analytical studies on guided waves on cylindrical conductors contained within hollow tubes that are bounded by imperfectly conducting walls. The boundary-value approach adopted (but not described here) is applicable for frequencies from the kilo-hertz to the giga-hertz range. The general purpose of the work is to provide understanding of important guided wave phenomena that are utilized in intra-mine radio communications. We present computed curves of attenuation rates, phase velocities, and transverse field patterns of the dominant modes. Finally, we consider the quantitative aspects of the mode conversion process, proposed by INIEX, that allows one to combine advantages of the mono-filar and the bi-filar modes.

SUMMARY

In many operational coal mines, it is desirable to communicate along tunnel-like structures that may extend up to 7 or 8 km. While conventional telephone lines may be used, it has been found very convenient and effective to transmit VLF signals directly through the haulageway[1]. Normally, the latter are more rectangular in cross section and contains a power cable that is suspended from the top wall. In order to understand observations and to improve communications procedures, it is worthwhile to analyze some idealized models.

Emslie, Lagace, and Strong[2] have developed an approximate theory for the empty rectangular guide with lossy dielectric walls. More recently, Mahmoud and Wait[3] and Mahmoud[4], have considered a rectangular guide with axial conductors, but with idealized perfect electric or magnetic side walls. The axial conductors are obviously important if the frequency is sufficiently low that the empty guide modes are "cut off".

Here we consider an idealized air-filled circular guide bounded by a lossy dielectric medium. We choose a cylindrical coordinate system (ρ,ϕ,z) to be coaxial with the guide, and an arbitrary number N of thin axial conductors are located within the guide. The objective is to calculate the complex propagation constant of the dominant modes of the structure. Thus, we assume that the fields and the wire currents of an individual mode vary with z as $\exp(-\Gamma z)$ for an $\exp(i\omega t)$ time dependence where the values of Γ are to be obtained. The fields due to each wire current can be derived

from z components of electric and magnetic Hertz vectors. An impedance condition is assumed on each wire, and a resultant homogeneous system of N equations for the N wire current results. The audience is referred to the written version of this analysis[6] for the single wire case. Numerical results based on this analysis show that the increase of attenuation as the wire conductor approaches the wall is in accordance with both observations of Delogne, Deryck, and Liegeois[7] in Belgian coal mines and numerical results of Mahmoud[4]. We show the amplitude and phase characteristics for the same mode at a frequency of 1000 MHz as a function of the distance of the wire from the tunnel center-line. Again, similar behavior has been obtained by Mahmoud[4].

For frequencies above the empty guide cutoff ($\sim$ 50 MHz), higher order modes appear. The attenuation of the TE_{01} and TE_{02} modes are also illustrated. These modes are not affected by the wire since their electric field has only an azimuthal component. Another class of modes can be described as perturbed TM and perturbed hybrid EH modes which do interact with the wire. The two-wire configuration is also of practical interest[7,8], and some results for both the mono-filar and bi-filar modes will be given.

REFERENCES

[1] A.E. Goddard, "Radio propagation measurements in coal mines at UHF and VLF", Proceedings of Thru-the-Earth Electromagnetics Workshop, Colo. School of Mines, Golden, Colo., 15-17, August 1973, available from National Technical Information Service, Alexandria, VA.

[2] A.G. Emslie, R.L. Lagace and P.F. Strong, "Theory of the propagation of UHF radio waves in coal mine tunnels", Proceedings of Thru-the-Earth Electromagnetics Workshop, Colo. School of Mines, Golden, Colo., 15-17 August 1973, available from National Technical Information Service, Alexandria, VA.

[3] S.F. Mahmoud and J.R. Wait, "Theory of wave propagation along a thin wire inside a rectangular waveguide", Radio Science, Vol. 9, No. 3, 417-420, 1974.

[4] S.F. Mahmoud, "Characteristics of EM guided waves for communication in coal mine tunnels", Submitted to IEEE Trans. on Communication, 1974.

[5] J.R. Wait, "Electromagnetic Radiation From Cylindrical Structures", Pergamon Press, Oxford, 1959.

[6] J.R. Wait and D.A. Hill, "Guided electromagnetic waves along an axial conductor in a circular tunnel", IEEE Trans. Ant. Prop., Vol. 22, No. 4, July issue (in press).

[7] P. Delogne, L. Deryck and R. Liégeois,"Guided propagation of radio waves", Proceedings of Thru-the-Earth Electromagnetics Workshop, Colo. School of Mines, Golden, Colo., 15-17 August 1973, available from National Technical Information Service, Alexandria, VA.

[8] D.A. Hill and J.R. Wait, Excitation of monofilar and bifilar modes on a transmission line in a circular tunnel", J. Appl. Phys., (in press) 1974.

The research reported was supported by the U.S. Bureau of Mines under a contract monitored by Dr. James A. Powell, Pittsburgh Mining and Safety Research Center, U.S. Bureau of Mines, 4800 Forbes Avenue, Pittsburgh, PA 15213. The opinions expressed here do not represent the official position of any agency of the U.S. Government.

DISCUSSION

K.F. TREEN

In considering the pure wave guide mode, is it not a fact that in the circular case, the attenuation of the TE_{01} mode would decrease fairly considerably as the frequency went up, but in practice, would it in fact be possible to sustain such a mode ?

J.R. WAIT

The TE or transverse electric modes in the circular wave guide are symmetric modes and it certainly is true that, with a very high frequency, particularly because of wall roughness, the attenuation rate would go up considerably. Here the calculations were shown for an imperfectly conducting smooth wall and I did not discuss roughness. I think, in any kind of practical wave guide consideration, some of these roughness factors could actually be treated by approximate methods such as that of A.G. Emslie (as quoted in the proceedings of the U.S. Bureau of Mines' sponsored conference on "Thru-the-Earth Electromagnetics", held in August 1973).

P. DELOGNE

This is not a question, but an addition to Mr. Wait's answer. The reduction in the specific attenuation of the monofilar mode at hyperfrequencies is linked with a surface-wave effect. If there are no walls, a wire of finite conductivity can serve as a guide for a surface wave, known as a Sommerfeld wave. The concentration of this wave around the wire increases with the frequency, so that when the effective radius of the wave reaches the order of magnitude of the wire-wall distance, this effect appears in Mr. Wait's theoretical model. If the frequency continues to increase, the fields in the vicinity of the wall decrease, as do also the losses in the wall. This finally results in a decreasing overall attenuation. To indicate the characteristic numerical

values, we can consider that at 1 GHz the effective radius of the Sommerfeld wave would be of the order of 30 cm. Nevertheless, such a theoretical wave could not be maintained in a tunnel unless the cable were so laid that no obstacle lies within the effective radius.

J.R. WAIT

I would like to point out that the modal solution of the boundary value problem that we obtained would include surface waves propagating along the centre conductor as a special case. In fact, we have looked into the Goubau type wave which has not been mentioned explicitly here. But this would be particularly applicable at a very high frequency. The energy would be localized to the region near the outer dielectric coating of the central conductor.

D.J. CREE

In the presence of structures within the wave guide like conveyors which run parallel with the wire, and also wagons which obstruct the wave guide and are parallel with the wire, is the mono- or the bi-filar configuration the best for the passage of electrical information down the wave guide ?

J.R. WAIT

The question relates to the effect of having large substructures in the wave guide and what these will do to the propagation. In fact, which type of mode, the bifilar or the monofilar would be better ? First of all, I should emphasize that I have been treating only uniform structures here; in other words, once the mode is launched, there is no conversion from one mode to the other, except at the source. But if there are non-uniformities along the cross-section, there would be a major conversion of energy and I think a greater conversion would probably take place in the monofilar case because the energy extends across the guide. Also, of course, we may get conversion into the wave guide modes and vice-versa from the waveguide mode to the monofilar and bifilar modes.

Radio Science, Volume 10, Number 7, pages 753–759, July 1975

Theory of EM wave propagation through tunnels

James R. Wait

Cooperative Institute for Research in Environmental Sciences, University of Colorado, Boulder, Colorado 80302

(Received March 13, 1975.)

A rather ingenious communication technique is being developed for use in Belgian coal mines. The idea is to use a two-wire transmission line or equivalent loosely braided coaxial cable that can be suspended from the upper wall. A transmitter placed in the vicinity of the line excites a strongly unbalanced mode that normally would propagate like a coaxial or TEM mode with relatively high attenuation. The key step in the Belgian system, and the closely related French system, is to convert this unbalanced mode to a balanced mode that is much less attenuated because the return current flows mostly in the second wire rather than through the surrounding rock. The physical basis of this system has many similarities with the leaky feeder device described by Martin and used in British coal mines. We summarize the analysis of the propagation characteristics for an idealized mine tunnel of circular cross section. The extension to a rectangular tunnel is also considered. Some comparison is made with relevant experimental data. Actually, we deal only with the twin open wire pair that is the basic ingredient of the so-called INIEX/Deryck system. However, as suggested above, the leaky braided cable system and the slotted cylindrical shielded cables have common features. The important point is that propagation modes which depend on current flow in the tunnel walls will suffer excessive attenuation while modes which utilize the second conductor as a return current path will have less attenuation.

INTRODUCTION

It is probable that Marconi was aware of the limitations of electromagnetic wave transmission through rock media. In all cases reported in the literature, Marconi chose signal paths that favored propagation of energy through the atmosphere. However, in some cases he observed the adverse influence of intervening hills and ridges.

For this centennial dedication to Marconi, we would like to select a subject that finds its motivation in a need to communicate from point to point in the Earth. While direct transmission is certainly possible over limited ranges, a much more attractive possibility is to utilize tunnels or other waveguiding channels in the Earth's crust.

Our immediate interest is to consider applications to coal mines where nature has provided us with extensive quasihomogeneous conductive regions. With a little help from man, such regions are often interspersed with tunnels whose cross sections vary from circular to rectangular form. Also, in such tunnels, we often find longitudinal conductors such as pipes and tracks that may or may not be grounded to the surrounding medium. In some cases, enterprising engineers have strung transmission lines of various forms that act as active or passive conveyors of electromagnetic energy [*Deryck*, 1970, 1972, 1973; *Delogne*, 1973; *Delogne et al.*, 1973; *Martin*, 1970; *Fontaine et al.*, 1973; *Goddard*, 1973].

We should mention that there is a closely related class of problems in antenna theory. For example, if we locate a radiating system in highly conductive media such as the Earth, it should come as no surprise that the structure needs to be insulated over at least part of its length. This topic, which is the subject of a special journal issue [*Wait*, 1974], is not discussed here.

The plan of this paper is to consider the guided mode theory of transmission in an air-filled cylindrical tunnel in a conductive medium. Also, we allow for the possibility that the tunnel contains an axial conductor or system of conductors of a specified form. We outline the analysis of the permissible modes that may propagate along this structure. Our derivations will be quite brief but the interested reader can find further details in the quoted references.

CIRCULAR TUNNEL MODEL

Specifically, we consider an air-filled tunnel of circular cross section with radius a bounded by

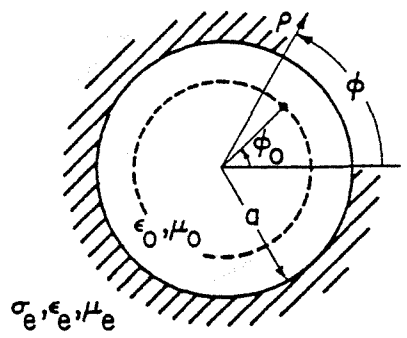


Fig. 1. Geometry for single wire conductor in a circular air-filled tunnel in homogeneous Earth.

a lossy dielectric medium. Within this uniform tunnel we locate a single relatively thin metal conductor of radius c_s whose conductivity is σ_s. The situation is illustrated in Figure 1 where we have chosen a cylindrical coordinate system (ρ,ϕ,z) to be coaxial with the guide. For the interior region $\rho < a$ the permittivity and permeability are ϵ_0 and μ_0 respectively. For the exterior region, the permittivity, conductivity and permeability are ϵ_e, σ_e, and μ_e respectively. The thin axial conductor is located at $\rho = \rho_0$ and $\phi = \phi_0$; its corresponding electric properties are ϵ_s, σ_s, and μ_s. Here we restrict attention to the case $0 < \rho_0 < a$. Later, we consider the effect of a second wire conductor that is parallel to the first.

We now consider the complex propagation constant of the dominant modes of the structure. Thus, we assume that the field of an individual mode varies with z according to $\exp(-\Gamma z)$ for an implied time factor $\exp(i\omega t)$ where the values of Γ are to be determined. As indicated elsewhere [*Wait and Hill*, 1974*a*], the fields can be determined by two scalar functions U and V that are, respectively, the z components of (axially directly) electric and magnetic Hertz vectors.

The current on the axial conductor can be designated $I\exp(-\Gamma z)$. The primary field within the tunnel from this travelling wave of current may be derived from the electric-type Hertz function U^p. It is well known that

$$U^p = (i\mu_0\omega/2\pi\gamma_0^2)\, I\exp(-\Gamma z)K_0\,[(\gamma_0^2 - \Gamma^2)^{1/2}\,\rho_d] \tag{1}$$

where $\gamma_0^2 = -\epsilon_0\mu_0\omega^2$, $\rho_d = [\rho^2 + \rho_0^2 - 2\rho\rho_0 \cdot \cos(\phi - \phi_0)]^{1/2}$, and K_0 is the modified Bessel function of the second kind. Now the total Hertz function within the guide can be written $U = U^p + U^s$, where U^s is the secondary part. The latter, for the region $\rho < a$, can be constructed by superimposing solutions of the type $I_m(v\rho) \cdot \exp(-im\phi)\exp(-\Gamma z)$ where I_m is a modified Bessel function of the first type, $v = (\gamma_0^2 - \Gamma^2)^{1/2}$ and m is any integer.

The above considerations, and the addition theorem for K_0 in (1), leads us to the representation [*Wait and Hill*, 1974*a*]

$$U = \sum_{m=-\infty}^{+\infty} U_m \exp[-im(\phi - \phi_0)] \tag{2}$$

where

$$U_m = (i\mu_0\omega/2\pi\gamma_0^2)\, Ie^{-\Gamma z}\, I_m(v\rho_0)\{K_m(v\rho) - R_m[K_m(va)/I_m(va)]\, I_m(v\rho)\} \tag{3}$$

for the region $\rho_0 < \rho < a$ where R_m is yet to be determined. Similar considerations lead us to the corresponding representation for the magnetic type Hertz function for the region $\rho < a$. Thus,

$$V = \sum_{m=-\infty}^{+\infty} V_m \exp[-im(\phi - \phi_0)] \tag{4}$$

where

$$V_m = (i\mu_0\omega/2\pi\gamma_0^2)\, Ie^{-\Gamma z}\,\Delta_m I_m(v\rho_0)\, I_m(v\rho) \tag{5}$$

For the external region $\rho > a$ the Hertz functions are both made up from solutions of the form

$$K_m(u\rho)\exp(-\Gamma z)\exp(-im\phi)$$

where

$$u = (\gamma_e^2 - \Gamma^2)^{1/2} \text{ and } \gamma_e^2 = i\mu_e\omega(\sigma_e + i\epsilon_e\omega)$$

The boundary conditions at the wall $\rho = a$ are that the tangential fields are continuous. Using these we may obtain expressions [*Wait and Hill*, 1974*b*] for the coefficients R_m and Δ_m in terms of modified Bessel functions of arguments va and ua. Then we can express the axial electric field E_z anywhere within the guide in terms of the still unknown current $I\exp(-\Gamma z)$ on the wire.

Now the boundary condition at the wire is

$$E_z = IZ_s\exp(-\Gamma z) \tag{6}$$

at $\rho_d = c_s$ for all values of z where Z_s is the series impedance of the wire. Because of the assumed

thinness of the wire, we can apply this condition at any point of the wire circumference. Thus, we choose the matching point at $\rho = \rho_0 + c_s$ and $\phi = \phi_0$. Thus (6) leads to the mode equation

$$(-i\mu_0\omega\nu^2/2\pi\gamma_0^2)\left\{K_0(\nu c) - \sum_{m=-\infty}^{+\infty} R_m[K_m(\nu a) \div I_m(\nu a)]\, I_m(\nu\rho_0)\, I_m[\nu(\rho_0 + c_s)]\right\} = Z_s \tag{7}$$

where the explicit result for the series impedance is

$$Z_s = (\eta_s/2\pi c_s)\, I_0(\gamma_s c_s)/I_1(\gamma_s c_s) \tag{8}$$

where $\gamma_s^2 = i\mu_s\omega(\sigma_s + i\epsilon_s\omega)$ and $\eta_s = i\mu_s\omega/\gamma_s$.

We now consider the extension [*Hill and Wait*, 1974*a*] of the solution to the case where two axial conductors of radii c_0 and c_1 are present. The situation is illustrated in Figure 2. Now I_0, the current on the conductor at (ρ_0,ϕ_0,z), is arbitrary, while I_1, the current on the conductor at (ρ_1,ϕ_1,z), is unknown. By superimposing solutions of the earlier single-wire source, we can construct an appropriate solution for E_z.

$$E_z = I_0 Z_{s0} e^{-\Gamma z} \quad \text{at} \quad \rho = \rho_0 + c_0, \phi = \phi_0 \tag{9}$$

$$E_z = I_1 Z_{s1} e^{-\Gamma z} \quad \text{at} \quad \rho = \rho_1 + c_1, \phi = \phi_1 \tag{10}$$

where Z_{s0} and Z_{s1} are the appropriate series impedances. The unknowns are I_1 (or I_1/I_0) and Γ. We can easily eliminate I_1 to yield a mode equation.

The method can be generalized to an arbitrary number of N thin axial conductors located within the guide. An impedance condition, as indicated above, can be assumed for each wire. This yields

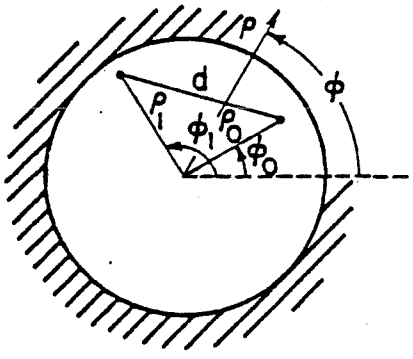


Fig. 2. Geometry for two arbitrarily located axial wires within tunnel.

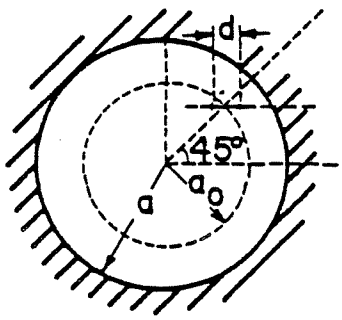


Fig. 3. Geometry for two axial wires located in a horizontal plane in the upper quadrant of the tunnel cross section. The mean distance to the tunnel wall is $a - a_0$.

a system of N linear equations for the N unknown wire currents. The system has a solution only if the following determinant is zero:

$$\begin{vmatrix} (A_{11} - Z_1) & A_{12} & \cdots & A_{1} \\ A_{21} & (A_{22} - Z_2) & \cdots & A_{2N} \\ \vdots & \vdots & & \vdots \\ A_{N1} & A_{N2} & \cdots & \end{vmatrix} = 0 \tag{11}$$

where A_{ij} is the z component of the electric field (primary plus secondary) produced at the match point on wire i by a unit current on wire j and Z_j is the series impedance of wire j. In what follows, we will just consider the case of two axial conductors, i.e., $N = 2$.

The modes that have transmission-line character as the frequency is lowered are of particular interest here. As we shall see, there are two classes of these: in one case the current ratio I_1/I_0 is approximately $+1$ and in the other case the ratio is approximately -1. For obvious reasons, these are designated the monofilar and bifilar modes, respectively. Actually, in the unlikely case that $\rho_0 = \rho_1$, we have exactly $I_1 = \pm I_0$. Using an adaptation of Newton's method, solutions of the desired type have been obtained for the specific configuration shown in Figure 3. This is considered a reasonable idealization of the situation encountered in practice where the transmission line is suspended from the tunnel wall but offset from the centerline. An example is shown in Figure 4 where the following parameters are assumed: $a = 2$ m, $\epsilon_e = 10\epsilon_0$, $\sigma_e = 10^{-2}$ mhos m^{-1}, $\sigma_s = 10^6$ mhos m^{-1}, $c_s = 10^{-3}$ m $= 1$ mm, and $d = 0.02$ m $= 2$ cm. Various values of the ratio a_0/a

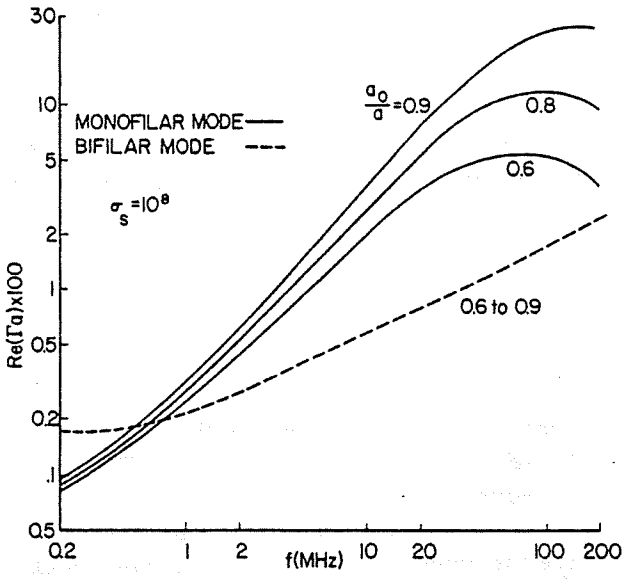


Fig. 4. The normalized attenuation rate as a function of frequency for the monofilar and bifilar modes for a wire conductivity $\sigma_s = 10^6$ mhos m^{-1}.

are shown for the monofilar mode but only the value 0.8 for the bifilar mode. In the latter case, the corresponding values for 0.9 and 0.6 are indistinguishable. Here the real part of (Γa), which is proportional to the attenuation rate, is plotted as

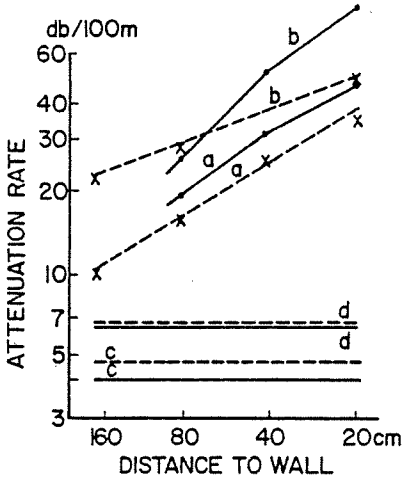


Fig. 5. Comparison of calculated (solid curves) and Deryck's observed (broken curves) data of attenuation rate as a function of the distance of the transmission line from the tunnel wall. Curves *a* and *b* are for the monofilar mode for 27 and 68 MHz, respectively, while curves *c* and *d* are for the bifilar mode for 27 and 68 MHz.

a function of frequency from 0.2 to 200 MHz. The increase of the monofilar mode attenuation as the wire conductor approaches the wall is apparent. Actually, the attenuation rates are quite dependent on the assumed wire conductivity but the dependence on the other parameters, such as c_s and d, is not so severe.

For the geometry of the tunnel guide considered in the preceding example, we can expect higher-order waveguide modes to appear when the frequency exceeds the cutoff value for the empty tube. This occurs at approximately 50 MHz in this case. For higher frequencies, we can expect the situation to be quite complicated. However, it appears we can always identify the monofilar and bifilar modes as the ones that are significantly influenced by the location and the series impedance of the wire conductor. Actually, we have calculated also these "waveguide modes" for various cylindrical geometries but the results are not given here. Suffice it to say that such modes have a very weak dependence on the conductivity of the axial wire conductors within the tunnel.

We can make a specific comparison of our calculated results of the attenuation rates with some experimental data published by *Deryck* [1973] for monofilar and bifilar mode propagation in a tunnel in Lanaye, Belgium. The actual tunnel has a total height of the order of 4 to 5 m and the width is of the order of 3 to 4 m. The comparison is indicated in Figure 5, where the abscissa is the distance of the transmission line from the tunnel wall and the ordinate is the attenuation rate in db per m. The calculated results use the same parameters as in Figure 4. As both the experimental and the theoretical curves show, there is a strong dependence on the proximity of the tunnel wall for the monofilar mode at both 27 and 68 MHz. On the other hand, there is virtually no dependence on the location of the transmission line for the case of the bifilar mode. This, of course, is an attractive feature for long distance communication. As *Deryck* [1972] indicates, conversion from the easily excited monofilar mode to the bifilar mode permits efficient point-to-point communication, even when the transmitting and/or receiving antennas are not closely coupled to the transmission line.

RECTANGULAR TUNNEL MODEL

A rigorous modal equation for the monofilar mode of a single wire in a rectangular tunnel has been

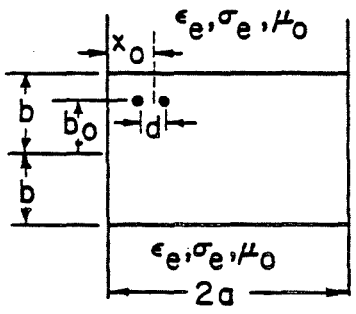


Fig. 6. The open wire T.L. (transmission line) inside a waveguide model of a rectangular tunnel.

recently obtained by *Mahmoud and Wait* [1974*a*] under some simplifying assumptions concerning the two side walls of the tunnel. Also, extensive numerical results on the properties of this mode have been reported [*Mahmoud and Wait*, 1974*a*; *Mahmoud*, 1974*a*]. We consider the configuration of the T.L. (transmission line) as shown in Figure 6. The two side walls of the tunnel are assumed to behave as either perfect electric or perfect magnetic conductors, while the other two walls are taken as generally lossy dielectric media. We adopt the nonrestrictive assumption that $d \gg c_s$ where c_s is the radius of any of the wires. As before, Γ is the complex propagation constant of the mode. So, apart from this common term, the currents in the two wires are given by I_1 and I_2. The boundary condition at the surface of each wire requires that the longitudinal electric field be equal to the current multiplied by the series impedance Z_w per unit length of the wire. Following *Mahmoud* [1974*b*], these conditions can be put in the convenient forms:

$$Z_{s1}(\Gamma)\, I_1 + Z_m(\Gamma)\, I_2 = Z_{w1}\, I_1 \tag{12}$$

$$Z_m(\Gamma)\, I_1 + Z_{s2}(\Gamma)\, I_2 = Z_{w2}\, I_2 \tag{13}$$

where $Z_{s1}(\Gamma)$ is defined as the longitudinal electric field at the surface of the first wire due to a unit current in that wire and a similar definition applied to $Z_{s2}(\Gamma)$. Here $Z_m(\Gamma)$ is the longitudinal electric field at the surface of one wire due to a unit current in the other wire.

By the elimination of I_1 and I_2 in (12) and (13), we obtain the modal equation for the unknown Γ as

$$[Z_{s1}(\Gamma) - Z_{w1}][Z_{s2}(\Gamma) - Z_{w2}] - Z_m^2 = 0 \tag{14}$$

This equation is greatly simplified when the two wires are identical since then $Z_{w1} = Z_{w2} = Z_w$. Furthermore, we can put $Z_{s1}(\Gamma) = Z_{s2}(\Gamma) = Z_s \cdot (\Gamma)$, which is a very good approximation since d is much less than the guide width. Under the above conditions, the modal equation, (14), reduces to two simple equations given by

$$Z_s(\Gamma) + Z_m(\Gamma) - Z_w = 0 \tag{15}$$

and

$$Z_s(\Gamma) - Z_m(\Gamma) - Z_w = 0 \tag{16}$$

where the first equation implies that $I_1 = I_2$ and the second implies that $I_1 = -I_2$. These are the two equations that correspond to the monofilar and the bifilar modes respectively and their solutions give the propagation constants of these modes.

Equations 15 and 16 were solved numerically by *Mahmoud* [1974*b*] for several configurations in the frequency range 200 kHz to 200 MHz. The resulting values of the attenuation $\alpha_{\text{monofilar}}$ and α_{bifilar} are plotted in Figures 7 and 8 for the case of interest here. The following physical constants are assumed in Figure 7: $2a = 4$ m, $2b = 3$ m, $x_0 = a/2$, $d = a/100$, $c_s = 1$ mm. Here σ_s (the conductivity of

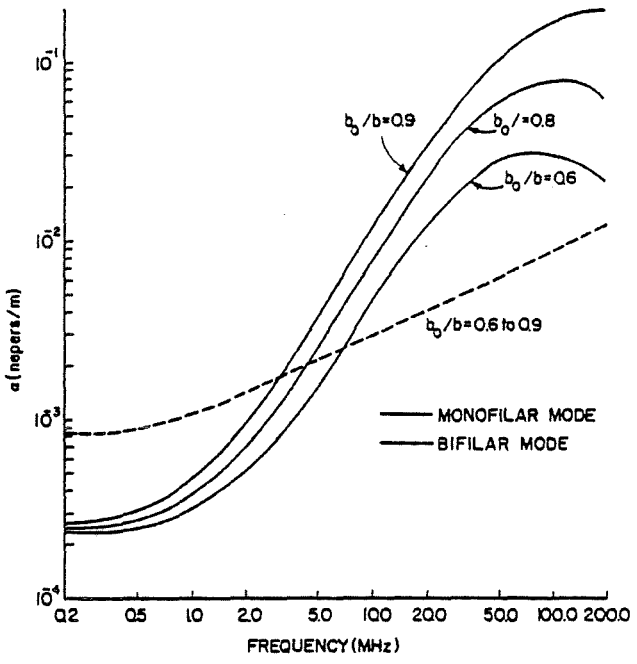


Fig. 7. Attenuation constant of the monofilar and the bifilar modes versus frequency for various values of b_0/b. Wire radii $c_s = 1$ mm.

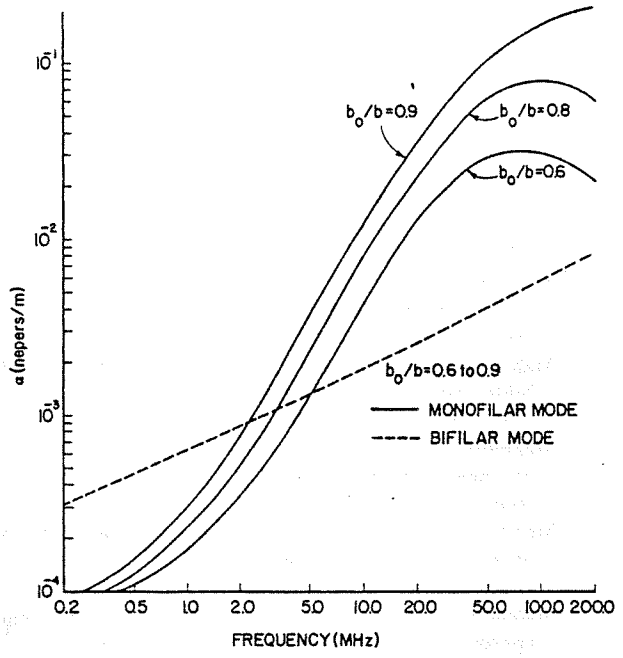


Fig. 8. Attenuation constant of the monofilar and the bifilar modes of configuration A versus frequency for various values of b_0/b. Wire radii $c_s = 2$ mm.

the wires) $= 10^6$ mho m^{-1}, $\epsilon_e = 10\,\epsilon_0$, and $\sigma_e = 10^{-2}$ mho m^{-1}.

In contrast with the monofilar mode, the attenuation of the bifilar mode is almost insensitive to variations of the parameter b_0/b in the frequency range considered and hence α_{bifilar} is shown for only one value of this parameter. To show the effect of varying the intrinsic parameters of the T.L., the wire radii are increased to 2 mm in Figure 8. By comparing with Figure 7 it is seen that α_{bifilar} is appreciably reduced at all frequencies, while $\alpha_{\text{monofilar}}$ is hardly affected for frequencies above about 12.5 MHz and considerably reduced at lower frequencies. Apparently, as the frequency is reduced below about 100 MHz, the guide walls behave more as good electrical conductors, hence reducing the attenuation of the monofilar mode. Thus, at low frequencies (of the order of few MHz and less), the attenuation of both modes becomes solely dependent on the intrinsic parameters σ_s and c_s. Furthermore, the ohmic losses of the T.L. are normally higher for the bifilar mode than those for the monofilar mode and hence the higher attenuation of the former mode at the low frequency end.

It is evident that the results presented here for the rectangular tunnel are very close to those for the circular tunnel. In fact, there is a complete consistency between the mode characteristics in the two guide geometries. This provides some confidence in the adequacy of the model used here for the rectangular tunnel.

Actually, the results shown in Figures 7 and 8 are obtained for a waveguide model with side walls that are perfect electric conductors. An alternative model is one in which these walls are perfect magnetic conductors. We computed values of attenuation rates for this model and it was found that the monofilar modes show much higher attenuation rates for frequencies below 25 MHz, while near 200 MHz the attenuation rates are only slightly different from those obtained for the first model. We believe, however, that the model with perfect electric side walls is a better approximation to the actual tunnel in the frequency range considered here, since the tunnel walls do tend to behave as good electrical conductors as the frequency is lowered.

FINAL REMARKS

In this paper, we have only considered the freely propagating modes of the axial structures. An important aspect in any communication design is how well these modes are excited. *Hill and Wait* [1974*a*,*b*] have considered the excitation mechanisms for both single and twin conductors in a circular tunnel model. Also, *Mahmoud* [1974*a*] had earlier treated the excitation by a dipole transmitter for the rectangular tunnel model. Other complicating factors that have been discussed are the effect of curvature of the tunnel axis [*Mahmoud and Wait*, 1974*b*] and the degrading influence of wall roughness [*Mahmoud and Wait*, 1974*c*]. An alternative method for allowing for finite wall conductivity using a geometrical optical approach is also given in the latter reference. In this method, all four walls of the rectangular waveguide may be lossy.

Acknowledgments. I am very grateful to D. A. Hill and S. F. Mahmoud for their contributions to this paper.

REFERENCES

Delogne, P. (1973), Les communications par radio en milieu souterrain, *Acta Tech. Belg. (Brussels)*, *9*(2), 18-26.

Delogne, P., L. Deryck, and R. Liegeois (1973), Guided propagation of radio waves, in *Proceedings of Thru-the-Earth Electromagnetics Workshop, Colorado School of Mines, Golden, Colorado, 15-17 August 1973*, pp. 49-53, National Technical Information Service, Springfield, VA 22151, acc. no. PB 231 154.

Deryck, L. (1970), Etude de modes de propagation d'ondes electromagnetiques, susceptibles d'exister sur une ligne bifilaire en milieu souterrain, *Ann. Mines Belg.*, *7*(8), 939-949.

Deryck, L. (1972), Radiocommunication in tunnels, *Electron. Lett.*, *8*(3), 71-72.

Deryck, L. (1973), Etude de la propagation des ondes electromagnetiques guidees dans les galerie souterraines, These de doctorat, Université de Liege, Belgium.

Fontaine, J., B. Demoulin, P. Degauque, and R. Gabillard (1973), Feasibility of radio communication in mine galleries by means of a coaxial cable having a high coupling impedance, in *Proceedings of Thru-the-Earth Electromagnetics Workshop, Colorado School of Mines, Golden, Colorado, 15-17 August 1973*, pp. 130-139, National Technical Information Service, Springfield VA 22151, acc. no. PB 231 154.

Goddard, A. E. (1973), Radio propagation measurements in coal mines at UHF and VLF, in *Proceedings of Thru-the-Earth Electromagnetics Workshop, Colorado School of Mines, Golden, Colorado, 15-17 August 1973*, pp. 54-61, National Technical Information Service, Springfield, VA 22151, acc. no. PB 231 154.

Hill, D. A., and J. R. Wait (1974*a*), Excitation of monofilar and bifilar modes on a transmission line in a circular tunnel, *J. Appl. Phys.*, *45*(8), 3402-3406.

Hill, D. A., and J. R. Wait (1974*b*), Gap excitation of an axial conductor in a circular tunnel, *J. Appl. Phys.*, *45*(11), 4774-4777.

Mahmoud, S. F. (1974*a*), Characteristics of EM guided waves for communication in coal mine tunnels, *IEEE Trans. Commun.*, *COM-22*(10), 1547-1554.

Mahmoud, S. F. (1974*b*), On the attenuation of monofilar and bifilar modes in mine tunnels, *IEEE Trans. Microwave Theory Tech.*, *MTT-22*(9), 845-847.

Mahmoud, S. F., and J. R. Wait (1974*a*), Theory of wave propagation along a thin wire inside a rectangular waveguide, *Radio Sci.*, *9*(3), 417-420.

Mahmoud, S. F., and J. R. Wait (1974*b*), Guided electromagnetic waves in a curved rectangular mine tunnel, *Radio Sci.*, *9*(5), 567-572.

Mahmoud, S. F., and J. R. Wait (1974*c*), Geometrical optical approach for electromagnetic wave propagation in rectangular mine tunnels, *Radio Sci.*, *9*(12), 1147-1158.

Martin, D. J. R. (1970), Radiocommunication in mines and tunnels, *Electron. Lett.*, *6*(18), 563-564.

Wait, J. R. (Ed.) (1974), Special Issue on ELF Communications, *IEEE Trans. Commun.*, *COM-22*(4), 353-588.

Wait, J. R., and D. A. Hill (1974*a*), Guided electromagnetic waves along an axial conductor in a circular tunnel, *IEEE Trans. Antennas Propagat.*, *AP-22*(4), 627-630.

Wait, J. R., and D. A. Hill (1974*b*), Coaxial and bifilar modes on a transmission line in a circular tunnel, *Appl. Phys.*, *4*(1), 1-6.

PRINCIPLES OF H.F. COMMUNICATION IN TUNNELS USING OPEN TRANSMISSION LINES AND LEAKY CABLES

James R. Wait, David A. Hill and David B. Seidel
Cooperative Institute for Research in Environmental Sciences
University of Colorado
Boulder, Colorado 80309

SUMMARY

A rather ingenious communication technique has been developed for use in coal mines. The idea is to use a two-wire transmission line or equivalent loosely braided coaxial cable that can be suspended from the upper wall (Wait, July, 1975). A transmitter placed in the vicinity of the line excites a strongly unbalanced mode that normally would propagate like a coaxial or TEM mode with relatively high attenuation. The key step in the Belgian system, and the closely related French system, is to convert this to a balanced mode that is much less attenuated because the return current flows mostly in the second wire rather than through the surrounding rock. The physical basis of this system has many similarities with the leaky feeder devices used in British coal mines when the mode conversion is inadvertent. We have examined a number of relevant problems of this type. Brief summaries are given in the following with appropriate references to where details can be found.

The braided coaxial cable was studied as a communication scheme in a mine tunnel. A simplified rectangular waveguide model was adopted for the tunnel, and the shield of the cable was assumed to behave as a single inductive transfer impedance. Specific results on the attenuation of the monofilar and bifilar (or coaxial) modes of propagation, taking into account the possible existence of a thin lossy film on the cable, were obtained (Mahmoud and Wait, Jan., 1976). In order to estimate the maximum possible range of communication, we considered the coupling factors of these modes to transmitting and receiving dipoles inside the tunnel, and we presented results on these factors for various cable parameters and over a wide range of frequencies (Mahmoud and Wait, Jan., 1976).

The transmission loss for a leaky coaxial cable communication system in a circular tunnel was calculated for an idealized model. The transmitting and receiving antennas were electric dipoles that could be located anywhere within the tunnel. For typical cable parameters, the optimum frequency was found to be in the range from 2 to 20 MHz. Calculations revealed that the use of a sparse braid and a high velocity cable will strongly improve the cable-dipole coupling with only a small penalty of a higher attenuation rate (Hill and Wait, April, 1976).

The previous development was extended to permit attenuation calculations when a braided cable is located close to a tunnel wall. This is an important case in mine communications utilizing leaky feeders. We found that the attenuation rate for the bifilar mode was hardly affected at all by the finite conductivity of the wall. On the other hand, the monofilar mode suffers a very high attenuation when the cable approaches the wall (Hill and Wait, July 1976). In a subsequent analysis, we examined the effect of the dependence of the braid transfer impedance on the propagation constant for a coaxial cable located in a circular tunnel (Wait and Hill, Jan., 1977).

The expression for the gap admittance of a coaxial cable within a circular tunnel was derived using a quasi-static method. Coupling between the TEM mode within the cable and the monofilar mode within the tunnel was computed, and 25% of the cable power was typically transferred to the tunnel from a single cable gap. The results have application to the use of leaky coaxial cables for communication in mine tunnels (Hill and Wait, Oct., 1975).

An idealized model of a trolley wire communication system was considered. To facilitate the analysis, the tunnel cross section was taken to be semicircular and the surrounding rock medium was homogeneous with a finite conductivity. The metallic rails or other conductors on the flat floor of the tunnel were represented by a plane metallic reflecting surface of infinite extent. The trolley wire and associated feeder line were assumed to be equivalent to a single cylindrical conductor that was parallel to the axis of the tunnel but located anywhere within the cross section. The appropriate modal equation was then solved for the propagation constant of the dominant mode. It was shown that the attenuation rate increases significantly as the trolley wire approaches the tunnel wall. However, even when the unloaded trolley wire was within 20 cm (8 in) of the wall, the attenuation rate at 200 kHz was still less than 2 dB per kilometer (Hill and Wait, Nov., 1976).

In a related study, the general theory for transmission in a circular tunnel containing a thin axial conductor was employed to calculate the attenuation rate of the propagating mode. The remarkable property was that the attenuation rate was approximately proportional to frequency and it did not depend critically on the wall conductivity for typical conditions (Wait and Hill, June, 1976).

A general analysis was given for the transmission of electromagnetic waves along a circular tunnel in the presence of axial conductors. One of these conductors was an idealization of a trolley wire with its bonded feeder line that may be located anywhere in the tunnel. The other was a metal rail that was located within the homogeneous rock medium at a finite distance from the tunnel wall. A mode equation for the propagation modes was obtained that was used to obtain numerical results for the attenuation rate in the frequency range 50 to 800 kHz. It was shown that the attenuation rate is only weakly dependent on the burial depth of the rail conductor, at least in the range up to 50 cm. Also, it was found that the rail conductor for the model adopted carries an appreciable fraction of the total return current when typical rock conductivities are assumed. A thin layer of insulation on the rail appears to have a negligible effect. In fact, there was little change even if the rail was within the tunnel and just above the tunnel floor (Wait and Hill, March, 1977).

The previous modal analysis for a circular tunnel containing a thin wire was shown to be greatly simplified at low frequencies provided the wall conductivity was high. The explicit formula for the propagation constant, so obtained when specialized to a perfectly conducting wire, was in agreement with a quasi-static analysis (Wait, May, 1977).

Propagation along a thin wire located in an air-filled tunnel was considered in the limiting case where the tunnel radius becomes indefinitely large but the distance of the wire to the tunnel wall remained finite. It was found that the results were consistent with the corresponding analysis for a thin wire located over a plane homogeneous earth (Wait, Nov., 1976).

We analyzed the fields excited by a dipole in a circular tunnel that contains a dielectric coated axial conductor. The integral form of the solution is generally valid provided the outer radius of the dielectric coated conductor is small compared with its distance to the tunnel wall. The propagation mode that behaves as an axial surface wave at high frequencies was examined for a frequency range from 1 MHz to 1 GHz. The attenuation reached a maximum value at frequencies of the order of 100 MHz where the absorption loss by the tunnel wall was most significant. In the range from 1 to about 10 MHz, the attenuation rate was approximately proportional to the frequency and was only weakly dependent on the conductivity of the region external to the tunnel walls. The results were consistent with earlier investigations for surface wave lines located over a homogeneous half space (Wait and Hill, Dec., 1976 and April, 1977).

The electromagnetic fields of dipole emitters located inside an empty tunnel or cylindrical cavity were first formulated. Both electric and magnetic types were considered. The results were used to deduce an expression for the change of self-impedance due to the presence of the tunnel walls. The input resistance R of the electric dipole was approximately a constant for frequencies less than about 25 MHz for a typical tunnel radius of 2m. In contrast, for the same conditions, R for the magnetic dipole or small loop varied approximately as the square of the frequency. The theory was extended to allow for the presence of an axial conductor or cable within the tunnel. The presence of the cable increases both R for a transversely oriented electric dipole and a circumferentially oriented magnetic dipole but R decreased for an axial electric dipole. Not surprisingly, the axial magnetic dipole is only weakly influenced by the presence of the cable (Hill and Wait, Dec., 1976, April, 1978).

Radio frequency transmission in a semi-circular tunnel containing a coaxial cable was again considered (Seidel and Wait, July, 1978). The general formulation accounted for both the ohmic losses in the tunnel wall and a thin lossy film layer on the outer surface of the dielectric jacket of the cable. Using the quasi-static approximation (Wait, May, 1977) it was found that the propagation constants of the low-frequency transmission line modes could be obtained from the solution of a cubic equation. However, for the special case when the conductivity thickness product of the lossy film layer vanishes, this cubic equation reduced to a quadratic. The spatially dispersive from of the braid transfer impedance (Wait and Hill, Jan., 1977) was also accounted for. It was shown that the quasi-static theory is well justified for frequencies as high as 100 MHz for typical tunnel geometries. Finally, special characteristic impedances were derived for the various modes of the equivalent multi-conductor transmission line.

Using a further application of the quasi-static theory (Wait, May, 1977), it is shown that the effect of ohmic losses in the wall, for two axial conductors (Hill and Wait, Sept., 1977), can be represented as series impedances per unit length in equivalent coupled transmission line circuits. This opens the way for a systematic calculation of the mode conversion phenomena that occur when one of the axial conductors has a discrete shunt load to the ground plane. Explicit formulas are obtained for the modal conversion coefficients. These are used to discuss the effect of a shunt load on the trolley wire on the performance of a radio frequency communication system (Wait and Hill, March, 1978). It is confirmed that the unloaded dedicated communication line provides for a low loss mode that is hardly affected by the shunt load on the adjacent trolley wire in the tunnel.

The role of controlled mode conversion in leaky feeder mine-communication systems was also considered (Seidel and Wait, Sept., 1978). The controlled interchange of energy between the propagation modes was used to optimize the communication range and allow for coupling to and from portable hand-held antennas. In particular, we showed that, for this model, the optimum lengths of the leaky cable sections or mode converters are not predicted adequately by the approximate coupled mode theory. However, it appears that simple modifications of this latter approach can be made that achieve compatibility (private communications from P. Delogne).

Using a somewhat different approach (Wait, July, 1978), we then considered guided electromagnetic waves in a periodically non-uniform tunnel. A boundary value analysis was outlined for the transmission in a circular tunnel that contained a thin axial conductor where the latter was allowed to vary in a periodic fashion throughout its length. Simplifications of the formal mode equation were achieved by invoking quasi-static conditions used as in previous studies (Wait, May, 1977). It is shown that the axial non-uniformity can be represented approximately as a modification of the series impedance of the equivalent transmission line of the composite tunnel structure.

Finally, we considered the operating bandwidth of a leaky coaxial cable in a circular tunnel (Hill and Wait, April 11, 1978). We examined both pulse transmission and the bandwidth limitations of the channel. The phase and group velocities of the bifilar mode were found to be nearly independent of frequency between 1 MHz and 100 MHz, and the channel bandwidth was found to be quite large. The effect of mode excitation was also examined by treating the mutual impedance between a pair of short electric dipoles.

REFERENCES

HILL, D.A. and WAIT, J.R., October 1975, "Electromagnetic fields of a coaxial cable with an interrupted shield located in a circular tunnel," Journal of Applied Physics, Vol. 46 No. 10, 4352-4356.

HILL, D.A. and WAIT, J.R., April 1976, "Calculated transmission loss for a leaky feeder communication system in a circular tunnel", Radio Science, Vol. 11, No. 4, 315-321.

HILL, D.A. and WAIT, J.R., July 1976, "Propagation along a braided coaxial cable located close to a tunnel wall," IEEE Transactions on Microwave Theory and Techniques, Vol. MTT-24, No. 7, 476-480.

HILL, D.A. and WAIT, J.R., November 1976, "Analysis of radio frequency transmission along a trolley wire in a mine tunnel," IEEE Transactions on Electromagnetic Compatibility, Vol. EMC-18, No. 4, 170-174.

HILL, D.A. and WAIT, J.R., Sept. 1977, "Analysis of radio frequency transmission in a semi-circular mine tunnel containing two axial conductors," IEEE Transactions on Communications, Vol. COM-25, No. 9.

HILL, D.A. and WAIT, J.R., April 1978, "The impedance of dipoles in a circular tunnel with an axial conductor," Accepted by the IEEE Transactions on Geoscience Electronics, Vol. GE-16, No. 2, 118-126.

HILL, D.A., and WAIT, J.R., Nov. 1978, "Bandwidth of a leaky coaxial cable in a circular tunnel," IEEE Transactions on Communications, Vol. COM-26, No. 11.

MAHMOUD, S.F. and WAIT, J.R., January 1976, "Calculated channel characteristics of a braided coaxial cable in a mine tunnel," IEEE Transactions on Communications, Vol. COM-24, No. 1, 82-87.

SEIDEL, D.B., and WAIT, J.R., July 1978, "Transmission modes in a braided coaxial cable and coupling to a tunnel environment," IEEE Transactions on Microwave Theory and Technique, Vol. MTT-26.

SEIDEL, D.B., and WAIT, J.R., Sept., 1978, "Role of controlled mode conversion in leaky feeder mine-communication systems," IEEE Transactions on Antennas and Propagation, Vol. AP-26, No. 5, 690-694.

WAIT, J.R., July 1975, "Theory of EM wave propagation through tunnels," Radio Science, Vol. 10, No. 7.

WAIT, J.R., Nov. 1976, "The eccentrically located wire in a cylindrical cavity in a conducting medium and the limit of a planar boundary," Radio Science, Vol. 11, No. 11, 897-899.

WAIT, J.R., May 1977, "Quasi-static limit for the propagating mode along a thin wire in a circular tunnel," IEEE Transactions on Antennas and Propagation, Vol. 25, No. 3, 441-443.

WAIT, J.R., July, 1978, "Guided electromagnetic waves in a periodically non-uniform tunnel," IEEE Transactions on Antennas and Propagation, Vol. AP-26, No. 4, 623-625.

WAIT, J.R. and HILL, D.A., June 1976, "Low-frequency radio transmission in a circular tunnel containing a wire conductor near the wall," Electronics Letters, Vol. 12, No. 13, 346-347.

WAIT, J.R. and HILL, D.A., Dec. 1976, "Attenuation on a surface wave G-line suspended within a circular tunnel," Journal of Applied Physics, Vol. 47, No. 12, 5472-5473.

WAIT, J.R. and HILL, D.A., December 1976, "Impedance of an electric dipole located in a cylindrical cavity in a dissipative medium," Applied Physics, Vol. 11, No. 4, 351-356.

WAIT, J.R. and HILL, D.A., January 1977, "Influence of spatial dispersion of the shield transfer impedance of a braided coaxial cable," IEEE Transactions on Microwave Theory and Techniques, Vol. 25, 72-74.

WAIT, J.R. and HILL, D.A., March 1977, "Radio frequency transmission via a trolley wire in a tunnel with a rail return," IEEE Transmission on Antennas and Propagation, Vol. AP-25, No. 2, 248-253.

WAIT, J.R. and HILL, D.A., April 1977, "Electromagnetic fields of a dipole source in a circular tunnel containing a surface wave line," International Journal of Electronics, Vol. 42, No. 4, 377-391.

WAIT, J.R. and HILL, D.A., March 1978, "Analysis of the dedicated communication line in a wire tunnel for a shunt-loaded trolley wire," IEEE Transactions on Communications, Vol. COM-26, No. 3, 355-361.

NOTE: The bibliographies in the above publications contain extensive references to the work of other investigators such as: B.A. Austin, J.C. Beal, D.C. Chang, J. Chiba, Q.V. Davis, P. Degauque, P. Delogne, L. Deryck, A.G. Emslie, R. Gabillard, R.W. Haining, E.F. Kuester, R.L. Lagace, R. Liegeois, N.A. Mackay, D.J.R. Martin, R.G. Olsen and R.L. Spencer. It was not our intention here to summarize all related work.

UDC 538.3:621.315.212.1:622.489

Theory of transmission of electromagnetic waves along multi-conductor lines in the proximity of walls of mine tunnels

JAMES R. WAIT, B.A.Sc., M.A.Sc., Ph.D.*

Based on a paper presented at the Symposium on Leaky Feeder Radio Communication Systems held at the University of Surrey on 9th and 10th April 1974.

SUMMARY

Using a boundary value analysis, the transmission of the propagation modes in the tunnel are considered. As expected, there is a conventional TEM-like mode that has relatively high loss due to the finite conductivity of the tunnel walls. In addition, however, we find that other modes exist when there are two or more axial conductors present in the tunnel. These have relatively low attenuation but such modes are difficult to excite. The optimum system requires the exploitation of both classes of modes. The object of this paper is to provide the analytical framework that can be used for the quantitative design of such systems.

* *Environmental Research Laboratories, National Oceanic and Atmospheric Administration, US Department of Commerce, Boulder, Colorado 80302.*

A rather ingenious communication technique is being developed for use in Belgian coal mines.[1-3] The idea is to use a two-wire transmission line or equivalent loosely braided coaxial cable that can be suspended from the upper wall. A transmitter placed in the vicinity of the line excites a strongly unbalanced mode that normally would propagate like a coaxial or TEM mode with relatively high attenuation. The key step in the Belgian system, and the closely related French system,[3] is to convert this unbalanced mode to a balanced mode that is much less attenuated because the return current flows mostly in the second wire rather than through the surrounding rock. The physical basis of this system has many similarities to the leaky feeder device described by Martin[4] and used in British coal mines.

Here we carry out an analysis of the propagation characteristics for an idealized mine tunnel of circular cross section. The extension to a rectangular tunnel is also mentioned. The theory is developed only for a uniform structure so that mode conversion is not accounted for, but in all other respects the problem is quite general. Some comparison is made with relevant experimental data. Actually, we deal only with a twin open wire pair that is the basic ingredient of the so-called INIEX/Deryck system. However, as suggested above, the leaky braided cable system and the slotted cylindrical shielded cables have common features. The important point is that propagation modes, that depend on current flow in the tunnel walls, will suffer excessive attenuation while modes that utilize the second conductor at a return current path will have less attenuation. While such features have been recognized by current workers, we have undertaken an analytical study that permits a quantitative understanding of the loss mechanisms.

Specifically, we consider an air-filled tunnel of circular cross-section with radius a bounded by a lossy dielectric medium. Within this uniform tunnel we locate a single relatively thin metal conductor of radius c, whose conductivity is σ_c. The situation is illustrated in Fig. 1(a) where we have chosen a cylindrical coordinate system (ρ, ϕ, z) to be coaxial with the guide. For the interior region $\rho < a$ the permittivity and permeability ε_0 and μ_0 respectively. For the exterior region, the permittivity, conductivity and permeability are ε_e, σ_e and μ_e respectively. The thin axial conductor is located at $\rho = \rho_0$ and $\phi = \phi_0$; its corresponding electric properties are ε_c, σ_c and μ_c. Here we restrict attention to the case $0 < \rho_0 < a$. Later, we consider the effect of a second wire conductor that is parallel to the first.

We now consider the complex propagation constant of the dominant modes of the structure. Thus, we assume that the fields of an individual mode varies with z according to $\exp(-\Gamma z)$ for an implied time factor $\exp(j\omega t)$ where the values of Γ are to be determined. As indicated elsewhere,[5] the fields can be determined by two scalar functions U and V that are, respectively, the z components of (axially directly) electric and magnetic Hertz vectors.

The current on the axial conductor can be designated $I\exp(-\Gamma z)$. The primary field within the tunnel from

this travelling wave of current may be derived from the electric-type Hertz function U^{e}. It is well known that

$$U^{\mathrm{e}} = \frac{\mathrm{j}\mu_0\omega}{2\pi\gamma_0^2} I \exp(-\Gamma z)\mathrm{K}_0[(\gamma_0^2-\Gamma^2)^{\frac{1}{2}}\rho_{\mathrm{d}}] \qquad (1)$$

where

$$\gamma_0^2 = -\varepsilon_0\mu_0\omega^2, \quad \rho_{\mathrm{d}} = [\rho^2+\rho_0^2-2\rho\rho_0\cos(\phi-\phi_0)]^{\frac{1}{2}},$$

and K_0 is the modified Bessel function of the second kind. Now the total Hertz function within the guide can be written, $U = U^{\mathrm{e}}+U^{\mathrm{s}}$, where U^{s} is the secondary part. The latter, for the region $\rho < a$, can be constructed by superimposing solutions of the type

$$\mathrm{I}_m(v\rho)\exp(-\mathrm{j}m\phi)\exp(-\Gamma z)$$

where I_m is a modified Bessel function of the first type, $v = (\gamma^2-\Gamma^2)^{\frac{1}{2}}$ and m is any integer.

The above considerations and the addition theorem for K_0 in (1) leads us to the representation

$$U = \sum_{m=-\infty}^{+\infty} U_m \mathrm{e}^{-\mathrm{j}m(\phi-\phi_0)} \qquad (2a)$$

where

$$U_m = \frac{\mathrm{j}\mu_0\omega}{2\pi\gamma_0^2} I \mathrm{e}^{-\Gamma z}\mathrm{I}_m(v\rho_0)\times$$

$$\times\left[\mathrm{K}_m(v\rho)-R_m\frac{\mathrm{K}_m(va)}{\mathrm{I}_m(va)}\mathrm{I}_m(v\rho)\right] \qquad (2b)$$

for the region $\rho_0 < \rho < a$ where R_m is yet to be determined. Similar considerations lead us to the corresponding representation for the magnetic type Hertz function for the region $\rho < a$. Thus,

$$V = \sum_{m=-\infty}^{+\infty} V_m \mathrm{e}^{-\mathrm{j}m(\phi-\phi_0)} \qquad (3a)$$

where

$$V_m = \frac{\mathrm{j}\mu_0\omega}{2\pi\gamma_0^2} I \mathrm{e}^{-\Gamma z}\Delta_m\mathrm{I}_m(v\rho_0)\mathrm{I}_m(v\rho). \qquad (3b)$$

For the external region $\rho > a$ the Hertz functions are both made up from solutions of the form

$$\mathrm{K}_m(u\rho)\exp(-\Gamma z)\exp(-\mathrm{j}m\phi)$$

where $u = (\gamma_{\mathrm{e}}^2-\Gamma^2)^{\frac{1}{2}}$ and $\gamma_{\mathrm{e}}^2 = \mathrm{j}\mu_{\mathrm{e}}\omega(\sigma_{\mathrm{e}}-\mathrm{j}\varepsilon_{\mathrm{e}}\omega)$.

The boundary conditions at the wall $\rho = a$ are that the tangential fields are continuous. Using these we obtain the following explicit results[5] for the coefficient R_m in (2b)

$$R_m = \frac{[(\gamma_0/v)\mathrm{K}'_m(va)/\mathrm{K}_m(va)]+Y_m\eta_0+\delta_m\eta_0}{[(\gamma_0/v)\mathrm{I}'_m(va)/\mathrm{I}_m(va)]+Y_m\eta_0+\delta_m\eta_0} \qquad (4)$$

where

$$\delta_m\eta_0 = \frac{(\mathrm{j}m\Gamma/a)^2[v^{-2}-u^{-2}]^2}{[(\gamma_0/v)\mathrm{I}'_m(va)/\mathrm{I}_m(va)]+(Z_m/\eta_0)} \qquad (5)$$

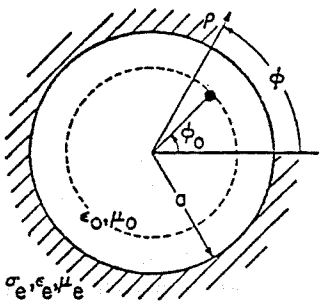
and $\eta_0 = \mathrm{j}\mu_0\omega/\gamma_0 \simeq 120\pi$ ohms, where

$$Z_m = -(\mathrm{j}\mu_{\mathrm{e}}\omega/u)\mathrm{K}'_m(ua)/\mathrm{K}_m(ua),$$

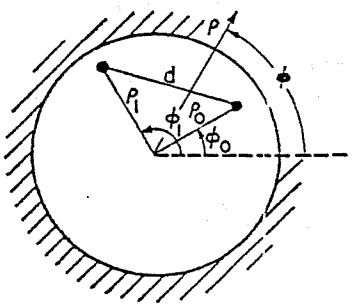
and

$$Y_m = (\mathrm{j}\gamma_{\mathrm{e}}^2/u\mu_{\mathrm{e}}\omega)\mathrm{K}'_m(ua)/\mathrm{K}_m(ua).$$

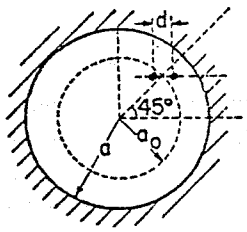
We can express the axial electric field E_z anywhere within the guide in terms of the still unknown current



(a) Geometry for single wire conductor in circular air-filled tunnel in homogenous earth.



(b) Geometry for two arbitrarily located axial wires within tunnel.



(c) Geometry for two axial wires located in a horizontal plane in the upper quadrant of the tunnel cross section. The mean distance to the tunnel wall is $a - a_0$.

Fig. 1.

$I\exp(-\Gamma z)$ on the wire. On combining (1), (2b) and the relation $E_z = -v^2U$, it follows that

$$E_z = -\frac{\mathrm{j}\mu_0\omega I v^2}{2\pi\gamma_0^2}\mathrm{e}^{-\Gamma z}\left[\mathrm{K}_0(v\rho_{\mathrm{d}})-\sum_{m=-\infty}^{+\infty}R_m\frac{\mathrm{K}_m(va)}{\mathrm{I}_m(va)}\times\right.$$

$$\left.\times\,\mathrm{I}_m(v\rho_0)(\mathrm{I}_m(v\rho)\,\mathrm{e}^{-\mathrm{j}m(\phi-\phi_0)}\right]. \qquad (6)$$

Now the boundary condition at the wire is

$$E_z = IZ_s\exp(-\Gamma z) \qquad (7)$$

at $\rho_{\mathrm{d}} = c_s$ for all values of z where Z_s is the series impedance of the wire. Because of the assumed thinness of the wire, we can apply this condition at any point of the wire circumference. Thus, we choose the matching point at $\rho = \rho_0+c_s$ and $\phi = \phi_0$. Thus (7) leads to the mode equation

$$\frac{-j\mu_0\omega v^2}{2\pi\gamma_0^2}\left[K_0(vc)-\sum_{m=-\infty}^{+\infty}R_m\frac{K_m(va)}{I_m(va)}\times\right.$$
$$\left.\times I_m(v\rho_0)I_m[v(\rho_0+c_s)]\right]=Z_s \qquad (8)$$

where the explicit result for the series impedance is

$$Z_s=\frac{\eta_s}{2\pi c_s}\frac{I_0(\gamma_s c_s)}{I_1(\gamma_s c_s)} \qquad (9)$$

where $\gamma^2=j\mu_s\omega(\sigma_s+j\varepsilon_s\omega)$ and $\eta_s=j\mu_s\omega/\gamma_s$.

We now consider the extension of the solution to the case where two axial conductors of radii c_0 and c_1 are present. The situation is illustrated in Fig. 1(b). Now I_0, the current on the conductor at (ρ_0, ϕ_0, z), is arbitrary, while I_1, the current on the conductor at (ρ_1, ϕ_1, z), is unknown. By superimposing solutions of the form (6) we can write

$$E_z=\frac{-j\mu\omega v^2}{2\pi\gamma^2}e^{-\Gamma z}\left\{I_0\left[K_0(v\rho_d)-\sum_{m=-\infty}^{\infty}R_m\frac{K_m(va)}{I_m(va)}\times\right.\right.$$
$$\times I_m(v\rho_0)I_m(v\rho)\,e^{-jm(\phi-\phi_0)}\Big]+I_1\left[K_0(v\rho_d')-\right.$$
$$-\sum_{m=-\infty}^{\infty}R_m\frac{K_m(va)}{I_m(va)}I_m(v\rho_1)I_m(v\rho)\times$$
$$\left.\left.\times e^{-jm(\phi-\phi_1)}\right]\right\} \qquad (10)$$

where

$$\rho_d=[\rho^2+\rho_0^2-2\rho\rho_0\cos(\phi-\phi_0)]^{\frac{1}{2}}$$

and

$$\rho_d'=[\rho^2+\rho_1^2-2\rho\rho_1\cos(\phi-\phi_1)]^{\frac{1}{2}}.$$

The two relevant boundary conditions are now:

$$E_z=I_0Z_{s0}e^{-\Gamma z}\quad\text{at}\quad\rho=\rho_0+c_0,\quad\phi=\phi_0. \qquad (11)$$

$$E_z=I_1Z_{s1}e^{-\Gamma z}\quad\text{at}\quad\rho=\rho_1+c_1,\quad\phi=\phi_1. \qquad (12)$$

where Z_{s0} and Z_{s1} are the appropriate series impedances. The unknowns are I_1 (or I_1/I_0) and Γ. We can easily eliminate I_1 to yield a mode equation.

The method can be generalized to an arbitrary number of N thin axial conductors located within the guide. An impedance condition as indicated above can be assumed for each wire. This yields a system of N linear equations for the N unknown wire currents. The system has a solution only if the following determinant is zero:

$$\begin{vmatrix}(A_{11}-Z_1) & A_{12} & \cdots\cdots & A_{1}\\ A_{21} & (A_{22}-Z_2) & \cdots\cdots & A_{2N}\\ \vdots & \vdots & & \vdots\\ A_{N1} & A_{N2} & \cdots\cdots & A_{NN}\end{vmatrix}=0 \qquad (13)$$

where A_{ij} is the z component of the electric field (primary plus secondary) produced at the match point on wire i by a unit current on wire j and Z_j is the series impedance of wire j. In what follows, we will just consider the case of two axial conductors, i.e. $N=2$.

For the high-frequency modes of interest in air-filled tunnels, we expect Γ to be of the order of $\gamma_0=jk$ where $k=\omega/c$ is the free space wave number. Also, the bounding medium will have a conductivity and/or permittivity sufficiently high that $|\gamma_e a|\gg 1$. Thus, we find that $Z_m\simeq(j\mu_e\omega)/(\gamma^2+k^2)^{\frac{1}{2}}$ and $Y_m\simeq\gamma^2/[j\mu_e\omega(\gamma^2+k^2)^{\frac{1}{2}}]$. Also, in most cases at high frequencies, the conductivity of the metal wire will be sufficiently high that both $|\gamma_s c_s|\gg 1$ and $\sigma_s\gg\varepsilon_s\omega$. Then we can write

$$Z_s\simeq(\mu_s\omega/2\sigma_s)^{\frac{1}{2}}(1+j)/(\pi c_s).$$

In the actual calculations, these approximations are only made when they are valid.

The modes that have a transmission-line character as the frequency is lowered are of particular interest here. As we shall see, there are two classes of these: in one case the current ratio I_1/I_0 is approximately $+1$ and in the other case the ratio is approximately -1. For obvious reasons, these are designated the coaxial and bifilar modes, respectively. Actually, in the unlikely case that $\rho_0=\rho_1$, we have exactly $I_1=\pm I_0$. Using an adaptation of Newton's method, solutions of the desired type have been obtained for the specific configuration shown in Fig. 1(c). This is considered a reasonable idealization of the situation encountered in practice where the transmission line is suspended from the tunnel wall but offset from the centreline. An example is shown in Fig. 2 where the following parameters are assumed: $a=2$m, $\varepsilon_e=10\varepsilon_0$, $\sigma_e=10^{-2}$ S/m, $\sigma_s=10^6$ S/m, $c_s=10^{-3}$ m $=1$ mm, and $d=0{\cdot}02$ m $=2$ cm. Various values of the ratio a_0/a are shown for the coaxial or monofilar mode but only the value 0·8 for the bifilar mode. In the latter case, the corresponding values for 0·9 and 0·6 are indistinguishable. Here the real part of (Γa), which is proportional to the attenuation rate, is plotted as a function of frequency from 0·2 to 200 MHz. The increase of the coaxial mode attenuation as the wire conductor approaches the wall is apparent. Actually, the attenuation rates are quite dependent on the assumed wire conductivity but the dependence on the other parameters, such as c_s and d, is not so severe.

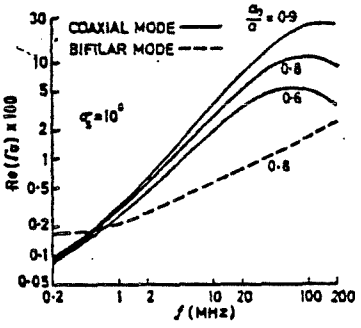


Fig. 2. The normalized attenuation rate as a function of frequency for the coaxial (or monofilar) and bifilar modes for a wire conductivity $\sigma_s=10^6$ S/m.

For the geometry of the tunnel guide considered in the preceding example, we can expect higher-order waveguide modes to appear when the frequency exceeds the cut-off value for the empty tube. This occurs approximately at 50 MHz in this case. For higher frequencies,

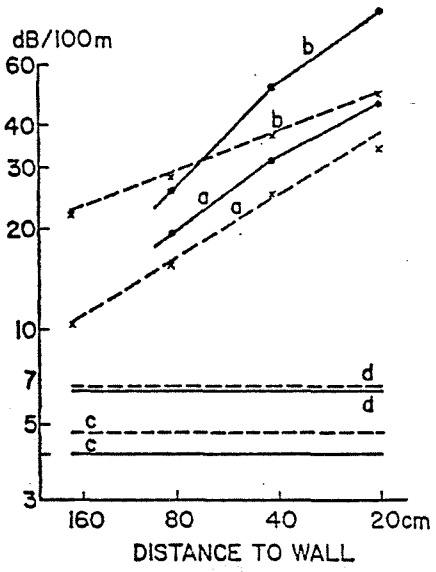


Fig. 3. Comparison of calculated (solid curves) and Deryck's observed (broken curves) data of attenuation rate as a function of the distance of the transmission line from the tunnel wall. Curves a and b are for the coaxial mode for 27 and 68 MHz, respectively, while curves c and d are for the bifilar mode for 27 and 68 MHz.

we can expect the situation to be quite complicated. However, it appears we can always identify the coaxial and bifilar modes as the ones that are significantly influenced by the location and the series impedance of the wire conductor. Actually, we have calculated also these 'waveguide modes' for various cylindrical geometries but the results are not given here. Suffice it to say that such modes have a very weak dependence on the conductivity of the axial wire conductors within the tunnel.

We can make a specific comparison of our calculated results of the attenuation rates with some experimental data published by Deryck[1] for coaxial and bifilar mode propagation in a tunnel in Lanaye, Belgium. The actual tunnel has a total height of the order of 4 to 5 m and the width is of the order of 3 to 4 m. The comparison is indicated in Fig. 3, where the abscissa is the distance of the transmission line from the tunnel wall and the ordinate is the attenuation rate in decibels per metre. The calculated results use the same parameters as in Fig. 2. As both the experimental and the theoretical curves show, there is a strong dependence on the proximity of the tunnel wall for the coaxial mode at both 27 and 68 MHz. On the other hand, there is virtually no dependence on the location of the transmission line for the case of the bifilar mode. This, of course, is an attractive feature for long distance communication. As Deryck[1] indicates, conversion from the easily excited coaxial mode to the bifilar mode permits efficient point-to-point communication, even when the transmitting and/or receiving antennas are not closely coupled to the transmission line.

In our analysis, we have adopted an idealized circular cross-section for the tunnel. Thus, strictly speaking, the calculated data are not valid for actual tunnels or haulageways in operational mines. However, it is interesting to note that the present results for the coaxial and bifilar modes are very similar to corresponding calculations carried out by Mahmoud[6] for rectangular tunnels. Unfortunately, an exact modal analysis[7] for the rectangular-shaped tunnel is only possible when the side walls are either perfectly electric or perfect magnetic conductors. Nevertheless, as we have illustrated in detail elsewhere,[8] the principal characteristics of the coaxial and bifilar modes are very similar in the two geometries. This suggests that the derived characteristics are qualitatively valid for non-circular tunnels provided the cross-sectional area is approximately the same.

Acknowledgments

I am very grateful to Dr. David A. Hill for his contributions to this paper. Also, I thank Dr. Samir F. Mahmoud for many useful discussions.

The views and conclusions contained in this document are those of the author and do not necessarily represent the official policy of the U.S. Bureau of Mines. The research was sponsored by USBM Contract HO122061, monitored by Dr. James A. Powell.

References

1. Deryck, L., 'Radio communication in tunnels', *Electronics Letters*, 8, No. 3, pp. 71–2, 10th February 1972; 'Echanges d'energie entre modes de propagation sur ligne bifilaire', *Bull. Tech. 'Mines et Carriers'*, No. 134, December 1971 (Institut National des Industries Extractives, Belgium).
2. Delogne, P., Deryck, L. and Liégeois, R., 'Guided propagation of radio waves', Proceedings of Thru-the-Earth Electromagnetics Workshop, pp. 49–53. Colorado School of Mines, Golden, Colo., 15th–17th August 1973, edited by R. G. Geyer. Final Report USBM Grant No. G133023. (Available from National Technical Information Service, Springfield, Va 22151, U.S.A.).
3. Fontaine, J., Demoulin, B., Degauque, P. and Gabillard, R., 'Feasibility of radio communication in mine galleries by means of a coaxial cable having a high coupling impedance', Proceedings of Thru-the-Earth Electromagnetics Workshop, pp. 130–9, 1973.
4. Martin, D. J. R., 'Radio communication in mines and tunnels', *Electronics Letters*, 6, pp. 563–4, 26th October 1970.
5. Wait, J. R. and Hill, D. A., 'Guided electromagnetic waves along an axial conductor in a circular tunnel', *IEEE Trans. on Antennas and Propagation*, AP-22, No. 4, pp. 627–30, July 1974.
6. Mahmoud, S. F., 'Characteristics of e.m. guided waves for communication in coal mine tunnels', *IEEE Trans. on Communications*, COM-22, No. 10, pp. 1547–54, October 1974.
7. Mahmoud, S. F. and Wait, J. R., 'Theory of wave propagation along a thin wire inside a rectangular waveguide', *Radio Science*, 9, No. 4, pp. 417–20, March 1974.
8. Wait, J. R., Hill, D. A. and Mahmoud, S. F., 'Studies of electromagnetic waves on monofilar and bifilar structures in circular and rectangular mine tunnels', International Conference 'Radio: Roads, Tunnels and Mines', Liège, Belgium, 1st–5th April 1974.

Manuscript received by the Institution on 5th August 1974. (Paper No. 1640/Com. 110).

Radio Science, Volume 9, Number 3, pages 417–420, March 1974

Theory of wave propagation along a thin wire inside a rectangular waveguide

Samir F. Mahmoud and James R. Wait

Cooperative Institute for Research in Environmental Sciences, University of Colorado, Boulder, Colorado 80302

(Received December 12, 1973.)

A modal equation for the propagation constants along a thin wire located inside a rectangular waveguide is derived. The regions external to the two horizontal broad walls are homogeneous lossy dielectrics. To facilitate the analysis, the two narrow vertical walls are assumed to be either perfect electric or perfect magnetic reflectors. Special cases that have been treated earlier [*Wait*, 1972] are recovered.

INTRODUCTION

The problem of wave propagation along an infinitely long straight wire located in a stratified medium has recently received attention [*Wait*, 1972] due to its importance in several applications. A related problem, which arises in dealing with radio propagation in coal mines (A. E. Goddard, personal communication, 1972; A. G. Emslie, R. L. Lagace, and P. F. Strong, personal communication, 1973) is that of wave propagation along an infinite wire located inside a rectangular waveguide with imperfectly reflecting boundaries. Here, we investigate a simplified version of this problem where one parallel pair of the guide boundaries is considered to be a perfect reflector. The other two boundaries are plane interfaces that separate the inside medium (air) from the outside media, which are lossy dielectrics in general.

We deduce a modal equation for the propagation constants along the wire which is in a suitable form to yield numerical results. These will be reported subsequently (by S. F. M.). The derivation is basically similar to that introduced by *Wait* [1972] and the obtained modal equation reduces to that in the above reference when the appropriate boundaries recede to ∞.

FORMULATION

The geometry of the problem is illustrated in Figure 1. The boundaries along the whole planes $x = 0$ and $x = 2a$ are assumed to be either perfect electric or perfect magnetic walls (i.e., infinite conductivity or infinite permeability, respectively). The semi-infinite media above the plane $y = 2b$ and below the plane $y = 0$ have electrical constants ϵ_1, μ_0 and ϵ_2, μ_0 respectively. Here the permittivities ϵ_1 and ϵ_2 may be generally complex to account for ohmic losses. The interior of the guide is filled with air with constants ϵ_0, μ_0 taken to be the same as free space. As before [*Wait*, 1972], we assume that the wire carries a current of the form $I \exp(i\omega t - \Gamma z)$ where ω is the angular frequency and Γ is the propagation constant that is to be determined. The factor $\exp(i\omega t - \Gamma z)$, common to all fields, is dropped for convenience in what follows.

SOLUTION

The total electromagnetic fields in each medium can be obtained from any two appropriate scalar potentials. In the present problem, it is most convenient to choose these potentials to be axial and transverse electric potentials Π_z and Π_y rather than two axial electric and magnetic potentials as used before [*Wait*, 1972]. This choice results in a considerable simplication of the algebra because the incident Π_y on any of the interfaces $y = 0$ and $y = 2b$ does not couple with a reflected Π_z (although the reverse is not true). However, now both potentials are coupled by the axial conductor.

Now assuming that the boundaries $x = 0$ and $x = 2a$ are perfect electric walls, appropriate forms for Π_z, and Π_y, in region 1, $2b \geq y \geq y_0$ are

$$\Pi_{z1} = \sum_m A_m \sin(m\pi x/2a)\{\exp[u_m(2b - y)] + R_{m1} \exp[-u_m(2b - y)]\} \quad (1)$$

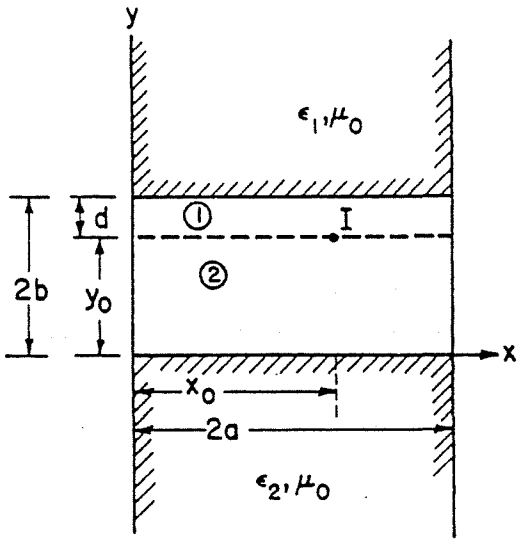


Fig. 1. Geometry for an infinite wire inside a rectangular waveguide.

$$\Pi_{y1} = \sum_m A_m R_{m1}^* \sin(m\pi x/2a) \cdot \exp[-u_m(2b - y)] + A_m^* \sin(m\pi x/2a) \cdot \{\exp[u_m(2b - y)] + S_{m1} \cdot \exp[-u_m(2b - y)]\} \quad (2)$$

Similarly for the region $y \geq 2b$, we write

$$\Pi_{z1} = \sum_m A_m T_{m1} \sin(m\pi x/2a) \cdot \exp[u_{m1}(2b - y)] \quad (3)$$

$$\Pi_{y1} = \sum_m (A_m T_{m1}^* + A_m^* \tau_{m1}) \cdot \sin(m\pi x/2a) \exp[u_{m1}(2b - y)] \quad (4)$$

where

$$u_m = [-k_0^2 - \Gamma^2 + (m\pi/2a)^2]^{1/2}$$

$$u_{m1} = [-k_1^2 - \Gamma^2 + (m\pi/2a)^2]^{1/2}$$

while $k_0^2 = \omega^2\mu_0\epsilon_0$, $k_1^2 = \omega^2\mu_0\epsilon_1$, and the integer m takes all values from 0 to ∞. The unknown reflection and transmission factors R_{m1}, R_{m1}^*, T_{m1}, T_{m1}^* and S_{m1}, and τ_{m1} are to be determined from the boundary conditions at the interface $y = 2b$. It is important to note that we can separately match those terms in equations 1 through 4 which involve the first four factors and those which involve the last two. The field components are related to the scalar potentials Π_z and Π_y by well-known formulas [*Wait*, 1959]. Thus we find that the resulting reflection coefficients are given by

$$R_{m1} = (u_m - u_{m1})/(u_m + u_{m1}) \quad (5)$$

$$R_{m1}^* = 2\Gamma[(u_m + u_{m1})^{-1} - k_0^2/(k_1^2 u_m + k_0^2 u_{m1})] \quad (6)$$

$$S_{m1} = (\epsilon_1 u_m - \epsilon_0 u_{m1})/(\epsilon_1 u_m + \epsilon_0 u_{m1}) \quad (7)$$

In a similar manner we obtain the potentials Π_z and Π_y in region 2, $y_0 \geq y \geq 0$, as:

$$\Pi_{z2} = \sum_m B_m \sin(m\pi x/2a) \cdot [\exp(u_m y) + R_{m2} \exp(-u_m y)] \quad (8)$$

$$\Pi_{y2} = \sum_m - B_m R_{m2}^* \sin(m\pi x/2a) \cdot \exp(-u_m y) + B_m^* \sin(m\pi x/2a) \cdot [\exp(u_m y) + S_{m2} \exp(-u_m y)] \quad (9)$$

where the reflection coefficients R_{m2}, R_{m2}^*, and S_{m2} are given by (5), (6), and (7) with a change of the subscript 1 to 2.

To proceed, we note that the coefficients A_m, A_m^*, B_m, and B_m^* are as yet unknowns to be determined from the boundary conditions at $y = y_0$. The source which has the form $I\,\delta(x - x_0)\,\delta(y - y_0)$ can be expanded in a Fourier series of the form

$$I\delta(x - x_0)\,\delta(y - y_0) = \delta(y - y_0) \sum l_m \sin(m\pi x/2a) \quad (10)$$

where

$$l_m = (I/a) \sin(m\pi x_0/2a) \quad (11)$$

The tangential fields at $y = y_0$ are continuous for each value of m, except for H_x which has a discontinuity equal to l_m. This reduces to the continuity of Π_z, Π_y, and $\partial\Pi_y/\partial y$, and the discontinuity of $\partial\Pi_z/\partial y$ such that

$$[\partial\Pi_{z2}/\partial y]_{y=y_0-} - [\partial\Pi_{z1}/\partial y]_{y=y_0+} = \sum_m l_m/i\omega\epsilon_0 \sin(m\pi x/2a)$$

Using (1) and (8) in the above equation and in the equation of the continuity of Π_z, and solving for the coefficients A_m and B_m we obtain:

$$A_m = (l_m/i\omega\epsilon_0 u_m) f_{m2}(y_0)/\Delta_m \quad (12)$$

$$B_m = (l_m/i\omega\epsilon_0 u_m) f_{m1}(d)/\Delta_m \quad (13)$$

where

$$f_{m1(2)}(y) = (1/2)[\exp(u_m y) + R_{m1(2)} \exp(-u_m y)] \quad (14)$$

$$\Delta_m = \exp(2u_m b)[1 - R_{m1}R_{m2} \exp(-4u_m b)] \quad (15)$$

The remaining two boundary conditions at $y = y_0$ give A_m^* and B_m^* as

$$A_m^* = [A_m R_{m1}^* S_{m2} \cdot \exp(-2u_m b) - B_m R_{m2}^*]/\Delta_m^* \quad (16)$$

$$B_m^* = [A_m R_{m1}^* - B_m R_{m2}^* S_{m1} \cdot \exp(-2u_m b)]/\Delta_m^* \quad (17)$$

where

$$\Delta_m^* = \exp(2u_m b)[1 - S_{m1}S_{m2} \exp(-4u_m b)] \quad (18)$$

In passing, we note that the natural modes of the empty guide are given by solutions of $\Delta_m = 0$ and $\Delta_m^* = 0$, corresponding to horizontally and vertically polarized modes respectively [*Wait*, 1970].

Now that all the terms in (1) and (2) are determined, we can obtain the axial electric field E_{z1} in region 1 as:

$$E_{z1} = -(i\omega\mu_0 I/\pi)B(\Gamma) \quad (19)$$

where

$$B(\Gamma) = (1 + \Gamma^2/k_0^2) \sum_m P_m(x; x_0) f_{m2}(y_0) \cdot f_{m1}(2b - y)/u_m \Delta_m - (\Gamma/k_0^2) \sum_m P_m(x; x_0) \cdot [R_{m1}^* f_{m2}(y_0) g_{m2}(y) + R_{m2}^* \cdot f_{m1}(d) g_{m1}(2b - y)]/\Delta_m \Delta_m^* \quad (20)$$

The only undefined terms in the above are

$$P_m(x; x_0) = (2\pi/a) \sin(m\pi x/2a) \sin(m\pi x_0/2a) \quad (21)$$

and

$$g_{m1(2)}(y) = (1/2)[\exp(u_m y) - S_{m1(2)} \exp(-u_m y)] \quad (22)$$

In the case when the planes $x = 0$ and $x = 2a$ correspond to perfect magnetic walls, equations 19 through 22 apply except that $P_m(x; x_0)$ is now redefined as

$$P_m(x; x_0) = (2\pi/a)\epsilon_m \cos(m\pi x/2a) \cos(m\pi x_0/2a)$$

where $\epsilon_m = 1$ for $m > 0$ and $1/2$ for $m = 0$.

Subject to the thin-wire assumption, we now obtain the desired modal equation for Γ by equating E_{z1} at $x = x_0$ and $y = y_0 + \rho$ by $Z_w I$ where ρ is the radius of the wire and Z_w is the series impedance of the wire. This is given in terms of the modified Bessel functions by *Wait* [1954],

$$Z_w = \eta_w I_0(\gamma_w \rho)/[2\pi\rho I_1(\gamma_w \rho)]$$

where

$$\eta_w = [i\mu_w\omega/(\sigma_w + i\epsilon_w\omega)]^{1/2}$$

$$\gamma_w = [i\mu_w\omega(\sigma_w + i\epsilon_w\omega)]^{1/2}$$

and ϵ_w, σ_w, and μ_w are the electrical parameters of the wire. Our modal equation is thus given by

$$D(\Gamma) + Z_w/(i\omega\mu_0/\pi) = 0 \quad (23)$$

where

$$D(\Gamma) = (1 + \Gamma^2/k_0^2) \sum P_m(x_0; x_0) f_{m2}(y_0) \cdot f_{m1}(d - \rho)/u_m \Delta_m - (\Gamma/k_0^2) \sum P_m(x_0; x_0) \cdot [R_{m1}^* f_{m2}(y_0) g_{m2}(y_0 + \rho) + R_{m2}^* \cdot f_{m1}(d) g_{m1}(d - \rho)]/\Delta_m \Delta_m^* \quad (24)$$

SPECIAL CASES

We now recover some of the important special cases of the modal equation, (23). First, when the wire lies on the upper boundary $y = 2b$, i.e., $y_0 = 2b - \rho$, and if $Z_w = 0$, a valid solution for Γ can be obtained from the behavior of the mth term in the summation of (23) as $m \to \infty$. Under this condition, the following approximations can be made:

$$u_m \to m\pi/2a$$

$$R_{m1}^* \to \Gamma[(\epsilon_1 - \epsilon_0)/(\epsilon_1 + \epsilon_0)]/u_m$$

$$f_{m1}(y), g_{m1}(y) \to \exp(u_m y)$$

$$\Delta_m, \Delta_m^* \to \exp(2u_m b)$$

Then the modal equation, (23), reduces to

$$(1 + \Gamma^2/k_0^2) - \Gamma^2/k_0^2(\epsilon_1 - \epsilon_0)/(\epsilon_1 + \epsilon_0) = 0$$

whose solution is $\Gamma^2 = -(k_0^2 + k_1^2)/2$.

This agrees with the result obtained earlier [*Coleman*, 1950; *Wait*, 1972] for the case of a thin wire on the interface between two semi-infinite homogeneous media.

Another important case is the case when the boundaries $x = 0$ and $x = 2a$ recede to $\mp \infty$ and the structure reduces to the parallel plate guide. In this case, the summation over m changes into an integration from $-\infty$ to $+\infty$ over the parameter λ which replaces $m\pi/2a$ everywhere. The trigonometric functions of x change into $\exp(-i\lambda x)$ and the

function $P_m(x; x_0)$ becomes simply $\exp(-i\lambda x)$ (for $x_0 = 0$).

Furthermore, if we allow the upper boundary $y = 2b$ to recede to $+\infty$ ($2b \to \infty$), we will have the case of a wire above a plane interface between two half spaces which has been treated earlier [*Wait*, 1972]. Upon using the following substitutions in (24):

$$2b \to \infty;\ R_1,\ R_1^*,\ S_1 \to 0;\ \text{and}\ \Delta,\ \Delta^* \to \exp(2ub)$$

we obtain $D(\Gamma)$ in the form

$$D(\Gamma) = (1/4)(1 + \Gamma^2/k_0^2)\int_{-\infty}^{\infty} \{\exp(-u\rho) + R_2 \exp[-u(2y_0 + \rho)]\}u^{-1}\, d\lambda - (1/2)(\Gamma^2/k_0^2)\int_{-\infty}^{\infty} [1/(u + u_2) - k_0^2/(k_2^2 u + k_0^2 u_2)] \cdot \exp[-u(2y_0 + \rho)]\, d\lambda \quad (25)$$

where the quantities u, u_2, R_2 are understood to be functions of λ. Equation 25 can be put in a slightly different form if we recognize that (see equation 5)

$$R_2 = -1 + 2u/(u + u_2)$$

Hence

$$D(\Gamma) = (1/2)(1 + \Gamma^2/k_0^2)\{K_0[i(k_0^2 + \Gamma^2)^{1/2}\rho] - K_0[i(k_0^2 + \Gamma^2)^{1/2}(2y_0 + \rho)]\} + \int_0^{\infty} [1/(u + u_2) + \Gamma^2/(k_2^2 u + k_0^2 u_2)] \cdot \exp[-u(2y_0 + \rho)]\, d\lambda \quad (26)$$

Equation 26 is the same as the corresponding one in [*Wait*, 1972] except for a different choice of the matching point on the wire perimeter.

CONCLUSIONS

The modal equation for the propagation constants along a thin wire located inside a rectangular waveguide is derived in a fashion similar to that used earlier [*Wait*, 1972]. The merits of the derived equation is that it is in a suitable form for a numerical treatment. Some of the important special cases are recovered and are seen to agree with previous work.

REFERENCES

Coleman, B. L. (1950), Propagation of electromagnetic disturbances along a thin wire in a horizontally stratified medium, *Phil. Mag., Ser. 7, 41*, 276–288.

Wait, J. R. (1954), Reflection at arbitrary incidence from a parallel wire grid, *Appl. Sci. Res., B4*(6), 393–400.

Wait, J. R. (1959), *Electromagnetic Radiation from Cylindrical Structures*, p. 10, Pergamon, New York.

Wait, J. R. (1970), *Electromagnetic Waves in Stratified Media*, chap. 6, pp. 132–195, Pergamon, New York.

Wait, J. R. (1972), Theory of wave propagation along a thin wire parallel to an interface, *Radio Sci., 7*(6), 675–679.

Radio Science, Volume 9, Number 5, pages 567–572, May 1974

Guided electromagnetic waves in a curved rectangular mine tunnel

Samir F. Mahmoud and James R. Wait

Cooperative Institute for Research in Environmental Sciences[1], *University of Colorado, Boulder, Colorado 80302*

(Received March 11, 1974.)

The transmission of VHF electromagnetic waves in a curved mine tunnel is analyzed using an idealized model in a cylindrical geometry. The tunnel cross section is assumed to be rectangular and the broad curved walls are imperfectly reflecting. The computations of the modal characteristics are facilitated by using a modified Airy function approximation of the rigorous cylindrical wave functions. The results indicated that the curvature of such tunnels will seriously increase the attenuation of the dominant low-order modes that are used for communications.

INTRODUCTION

The problem of guided wave propagation in waveguides with imperfectly reflecting boundaries arises in several applications, such as propagation in mine tunnels and in screened surface waveguides. It is observed that curvatures in these waveguides have a pronounced effect on the wave propagation losses [e.g., *Emslie et al.*, 1973]. In this paper we describe a quantitative investigation of this effect for the dominant modes of the guide.

We adopt a model of a rectangular waveguide with curved walls that are assumed to present a constant impedance or admittance to the tangential fields. The situation is illustrated in Figure 1. The other two straight walls are considered to behave as perfect electric or perfect magnetic conductors. In spite of the simplicity of such a model, it is believed to be capable of revealing the important characteristics of the dominant guided waves in a curved guide.

A great deal of work on curved rectangular waveguides has been carried out in the past. Attention, however, has been restricted to perfectly conducting walls. In this connection we mention the contributions of *Rice* [1948], *Waldron* [1957], *Cochran and Pecina* [1966], and *Wu* [1973].

FORMULATION

The geometry of the problem is illustrated in Figure 1. The fields are assumed to satisfy impedance boundary conditions on the walls $\rho = a - b$ and $\rho = a + b$ for $0 \leq z \leq 2h$, while the planes $z = 0$ and $z = h$ for $a - b \leq \rho \leq a + b$ are either electric or magnetic walls. Quite generally, the field components in the waveguide can be obtained from two z-directed electric and magnetic potentials Π and Π^* [*Wait*, 1959] for a time factor $\exp(i\omega t)$, as:

$$\begin{aligned} E_z &= (-\gamma^2 + \partial^2/\partial z^2)\Pi \\ E_\rho &= (\partial^2/\partial\rho\,\partial z)\Pi - (i\omega\mu/\rho)\,\partial\Pi^*/\partial\phi \\ E_\phi &= (\partial^2/\partial\phi\,\partial z)(\Pi/\rho) + i\omega\mu\,\partial\Pi^*/\partial\rho \end{aligned} \tag{1}$$

$$\begin{aligned} H_z &= (-\gamma^2 + \partial^2/\partial z^2)\Pi^* \\ H_\rho &= (-i\gamma^2/\omega\mu\rho)\,\partial\Pi/\partial\phi + \partial^2\Pi^*/\partial\rho\,\partial z \\ H_\phi &= (i\gamma^2/\omega\mu)\,\partial\Pi/\partial\rho + (1/\rho)\,\partial^2\Pi^*/\partial\phi\,\partial z \end{aligned} \tag{2}$$

General expressions of Π and Π^* are given as a double summation over all the possible modes, thus

$$\begin{pmatrix}\Pi\\ \Pi^*\end{pmatrix} = \sum_{m=0}^{\infty}\sum_{\nu=\nu_1,\nu_2} \left[\begin{pmatrix}a_{m,\nu}\\ c_{m,\nu}\end{pmatrix} J_\nu(u_m\rho) + \begin{pmatrix}b_{m,\nu}\\ d_{m,\nu}\end{pmatrix} H_\nu^{(2)}(u_m\rho)\right]\begin{pmatrix}\cos\lambda_m z\\ \sin\lambda_m z\end{pmatrix} \exp(-i\nu\phi) \tag{3}$$

where the Bessel and Hankel functions, J_ν and $H_\nu^{(2)}$ respectively, are the conveniently chosen independent solutions; $\lambda_m = m\pi/2h$, m being any integer including zero, and $u_m = -\gamma^2 - \lambda_m^2$; $\gamma^2 = -\omega^2\mu\epsilon = -k_0^2$ and $\nu = \nu_1, \nu_2, \cdots$ are the characteristic propagation constants to be determined from the boundary conditions.

In (3), it is assumed that the straight walls are perfect electric walls. In the case of perfect magnetic walls, we merely exchange the sine and cosine terms.

[1] CIRES is a cooperative venture between the University of Colorado and the National Oceanic and Atmospheric Administration.

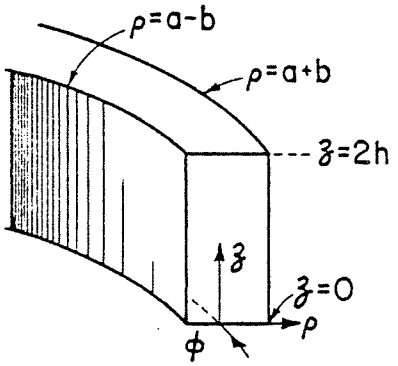


Fig. 1. Geometry of the problem. (Note that the medium within the tunnel is a homogeneous lossless medium with permittivity ϵ and permeability μ. Later we set these equal to their free-space values ϵ_0 and μ_0.)

THE CHARACTERISTIC MODES

The boundary conditions at the surfaces $\rho = a \pm b$ require that

$$E_z = \mp Z H_\phi \tag{4}$$

$$H_z = \pm Y E_\phi \tag{5}$$

with the higher sign applying to $\rho = a + b$ and the lower sign to $\rho = a - b$. The impedance Z and the admittance Y are assumed to represent the surface immittances presented by the outside media and should be chosen accordingly. Now we substitute in (4), from (1), (2), and (3), to obtain four homogeneous equations in the four coefficients, $a_{m,\nu}$, $b_{m,\nu}$, $c_{m,\nu}$, and $d_{m,\nu}$. For a nontrivial solution, it is required that the determinant of coefficients should vanish; thus we have:

$$\begin{vmatrix} (u^2 J_+ + Z_1 u J_+') & (u^2 H_+^{(2)} + Z_1 u H_+'^{(2)}) & J_+ Z i\nu\lambda/(a+b) & H_+^{(2)} Z i\nu\lambda/(a+b) \\ (u^2 J_- - Z_1 u J_-') & (u^2 H_-^{(2)} - Z_1 u H_-'^{(2)}) & -J_- Z i\nu\lambda/(a-b) & -H_-^{(2)} Z i\nu\lambda/(a-b) \\ -J_+ Y i\nu\lambda/(a+b) & -H_+^{(2)} Y i\nu\lambda/(a+b) & (u^2 J_+ - Y_1 u J_+') & (u^2 H_+^{(2)} - Y_1 u H_+'^{(2)}) \\ J_- Y i\nu\lambda/(a-b) & H_-^{(2)} Y i\nu\lambda/(a-b) & (u^2 J_- + Y_1 u J_-') & (u^2 H_-^{(2)} + Y_1 u H_-'^{(2)}) \end{vmatrix} = 0 \tag{6}$$

where the following abbreviations are used: $\lambda = \lambda_m$, $u = u_m$, $Z_1 = Zi\gamma^2/\omega\mu$, $Y_1 = Yi\omega\mu$, $J_\pm = J_\nu[u_m(a \pm b)]$,

$$J_\pm' = \left.\frac{\partial J_\nu(x)}{\partial x}\right|_{x = u_m(a \pm b)}$$

with similar definitions for $H_\pm^{(2)}$ and $H_\pm'^{(2)}$.

Now, for most cases of interest, the mean radius of curvature a is much greater than the free-space wavelength. Hence, both the order and the arguments of the Bessel functions in (6) are large, i.e., $|\nu|$, $|u_m(a \pm b)| \gg 1$ and for the important lower-order modes, the difference $|\nu - u_m(a \pm b)|$ is small. These conditions allow us to use the Airy function approximations for the Bessel functions [*Wait*, 1964, 1967], so

$$J_\nu(X) \simeq \pi^{-1/2}(2/X)^{1/3} v(t) \tag{7}$$

$$H_\nu^{(2)}(X) \simeq i\pi^{-1/2}(2/X)^{1/3} w_1(t) \tag{8}$$

where

$$v(t) = \pi^{1/2} Ai(t)$$

$$w_1(t) = \pi^{1/2}[Bi(t) - i\,Ai(t)]$$

and the functions $Ai(t)$ and $Bi(t)$ are those tabulated by *Miller* [1946]. The argument t is given by

$$(-t)^{1/2} = (X/2)^{1/3}(1 - \nu^2/X^2)^{1/2} \tag{9}$$

or

$$(t)^{1/2} = (X/2)^{1/3}(\nu^2/X^2 - 1)^{1/2} \tag{10}$$

The above form of t results in a better approximation of the Bessel functions as compared to the more familiar form used by *Wait* [1964]. For a complete discussion on the range of validity of the approximations in (7) and (8), the reader is referred to *Wait* [1967]. The logarithmic derivatives can also be approximated by:

$$J_\nu'(X)/J_\nu(X) \simeq -(2/X)^{1/3} v'(t)/v(t) \tag{11}$$

$$H_\nu'^{(2)}(X)/H_\nu(X) \simeq -(2/X)^{1/3} w_1'(t)/w_1(t) \tag{12}$$

Now using (7) through (12), the modal equation, (6), can be recast into the form:

$$\begin{vmatrix} [u^2 v(t_+) + q_1 u k_0 v'(t_+)] & [u^2 w(t_+) + q_1 u k_0 w'(t_+)] & (\omega\mu\nu\lambda q_1/x_+) v(t_+) & (\omega\mu\nu\lambda q_1/x_+) w(t_+) \\ [u^2 v(t_-) - q_1 u k_0 v'(t_-)] & [u^2 w(t_-) - q_1 u k_0 w'(t_-)] & -(\omega\mu\nu\lambda q_1/x_-) v(t_-) & -(\omega\mu\nu\lambda q_1/x_-) w(t_-) \\ -(k_0^2 q_2 \nu\lambda/x_+\omega\mu) v(t_+) & -(k_0^2 q_2 \nu\lambda/x_+\omega\mu) w(t_+) & [u^2 v(t_+) + q_2 u k_0 v'(t_+)] & [u^2 w(t_+) + q_2 u k_0 w'(t_+)] \\ (k_0^2 q_2 \nu\lambda/x_-\omega\mu) v(t_-) & (k_0^2 q_2 \nu\lambda/x_-\omega\mu) w(t_-) & [u^2 v(t_-) - q_2 u k_0 v'(t_-)] & [u^2 w(t_-) - q_2 u k_0 w'(t_-)] \end{vmatrix} \tag{13}$$

where $w(t) = w_1(t)$ and t_+ and t_- are given by (9) or (10) with X replaced by $u_m(a \pm b)$ respectively. The normalized quantities q_1, q_2, x_+, x_- are given by

$$q_1 = (iZ/\eta_0)(2/u_m a)^{1/3}$$

$$q_2 = (iY\eta_0)(2/u_m a)^{1/3}$$

$$x_\pm = k_0(a \pm b)(2/u_m a)^{1/3}$$

where $\eta_0 = (\mu/\epsilon)^{1/2}$ is the plane wave impedance. In what follows, $\mu = \mu_0$ and $\epsilon = \epsilon_0$, so $\eta_0 \simeq 120\pi$.

It is important to notice that when $m = 0(\lambda = 0)$, equation 13 reduces to two uncoupled modal equations for the $LSE_{0,n}$ modes (Longitudinal Section Electric: $E_z = 0$) and the $LSM_{0,n}$ modes (Longitudinal Section Magnetic: $H_z = 0$), corresponding to a waveguide with perfect magnetic or perfect electric narrow walls respectively. In this case $u^2 = u_0^2 = k_0^2$ and the modal equations of these modes are given by:

$$\{[w_1(t_+) + q_{1,2}w_1'(t_+)]/[v(t_+) + q_{1,2}v'(t_+)]\} \cdot \{[v(t_-) - q_{1,2}v'(t_-)]/[w_1(t_-) - q_{1,2}w_1'(t_-)]\} = 1 = e^{2in\pi} \qquad n = 0, 1, \cdots \tag{14}$$

where q_1 is used for the $LSM_{0,n}$ modes and q_2 for the $LSE_{0,n}$ modes. The above equation can also be written in terms of the functions $w_1(t)$ and $w_2(t)$ by use of the relation [*Wait*, 1970],

$$v(t) = i[w_1(t) - w_2(t)]$$

Equation 14 then takes the form

$$\{[w_1(t_+) + q_{1,2}w_1'(t_+)]/[w_2(t_+) + q_{1,2}w_2'(t_+)]\} \cdot \{[w_2(t_-) - q_{1,2}w_2'(t_-)]/[w_1(t_-) - q_{1,2}w_1'(t_-)]\} = 1 = e^{2in\pi} \tag{15}$$

which is similar to the modal equation obtained earlier [*Wait*, 1964] for TM modes in a cylindrical model of the earth-ionosphere waveguide.

Equation 14 is particularly suitable for numerical solution of the slow modes for which Re $(t) > 0$ since then $w_1(t)$ is exponentially growing and $v(t)$ is exponentially decaying. These slow modes are analogous to the whispering gallery modes treated earlier [*Wait*, 1967]. On the other hand, (15) is more suitable for fast modes (Re $(t) < 0$).

NUMERICAL RESULTS

For the purpose of numerical investigation of the modal equations, (13) through (15), values of Z and Y are chosen to represent an external lossy dielectric medium with a dielectric constant ϵ_e (assumed $\gg \epsilon_0$) and conductivity σ_e. This can correspond to a mine tunnel waveguide. From a consideration of the Fresnel reflection coefficients of TE and TM plane waves on the walls, we obtain Z and Y approximately as:

$$Z/\eta_0 = k_0/(k_e^2 - k_0^2)^{1/2} \tag{16}$$

$$Y\eta_0 = k_e^2/k_0(k_e^2 - k_0^2)^{1/2} \tag{17}$$

where $k_e^2 = \omega^2\mu_e(\epsilon_e - i\sigma_e/\omega)$.

The quantities $(1 - \beta/k_0)$ and α/k_0 are plotted versus the curvature parameter b/a in Figures 2 through 5 for two values of the guide half-electrical length $k_0 b$. Here α and β are given by

$$\alpha + i\beta = iv/a$$

The quantity $\tan \delta_e = \sigma_e/\omega\epsilon_e$ in Figures 2 and 3 is fixed at 0.018 and in Figures 4 and 5 at 0.045. ϵ_e/ϵ_0 is taken equal to 10. In fact, one set of physical parameters that correspond to the above figures is as follows: $b = 3.5$ ft ($\simeq 1.067$ m), $\epsilon_e = 10\epsilon_0$, $\sigma_e = 10^{-2}$ mho m^{-1}, and the frequency $f = 1000$ MHz (in Figures 2, 3) and 400 MHz (in Figures 4, 5), but

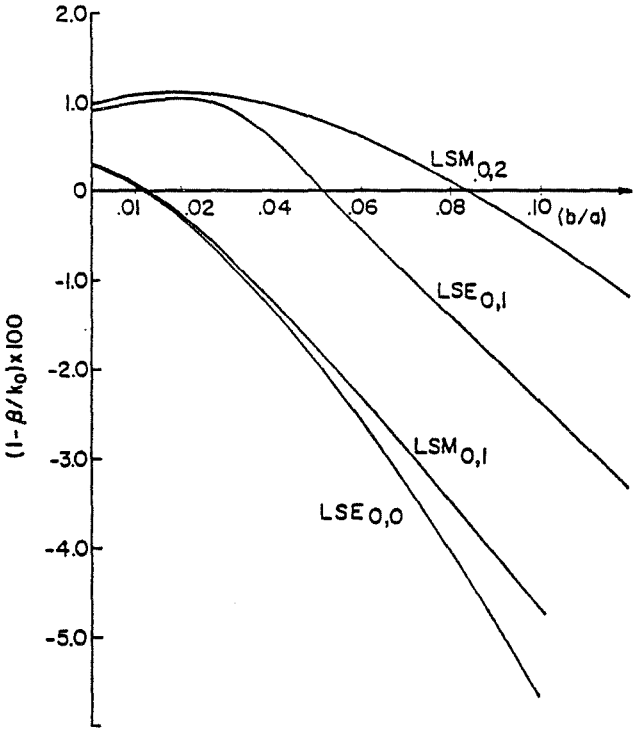


Fig. 2. Phase constants vs. b/a for $k_0 b = 22.4$, $\epsilon_e/\epsilon_0 = 10$, and $\tan \delta_e = 0.018$.

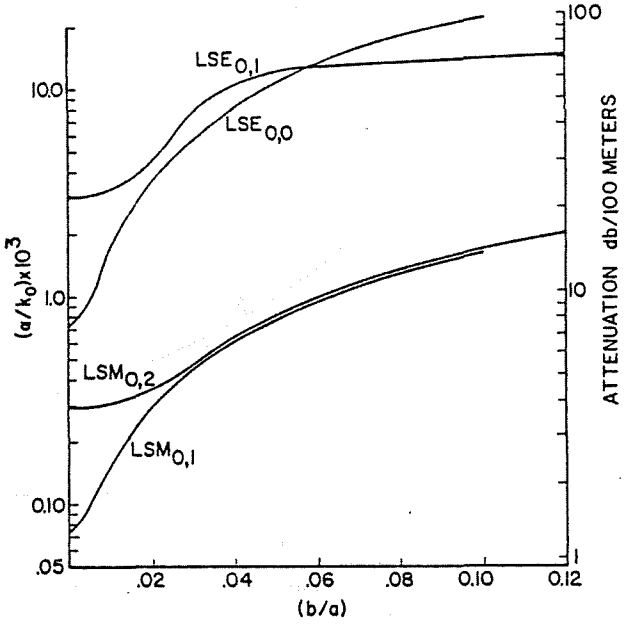


Fig. 3. Normalized attenuation rate vs. b/a for $k_0b = 22.40$, $\epsilon_e/\epsilon_0 = 10$ and $\tan \delta_e = 0.018$. The scale on the right-hand side gives the attenuation in db/100 m at 1000 MHz when $2b = 2.133$ m ($\simeq 7$ ft), and $\sigma_e = 10^{-2}$mho m^{-1}.

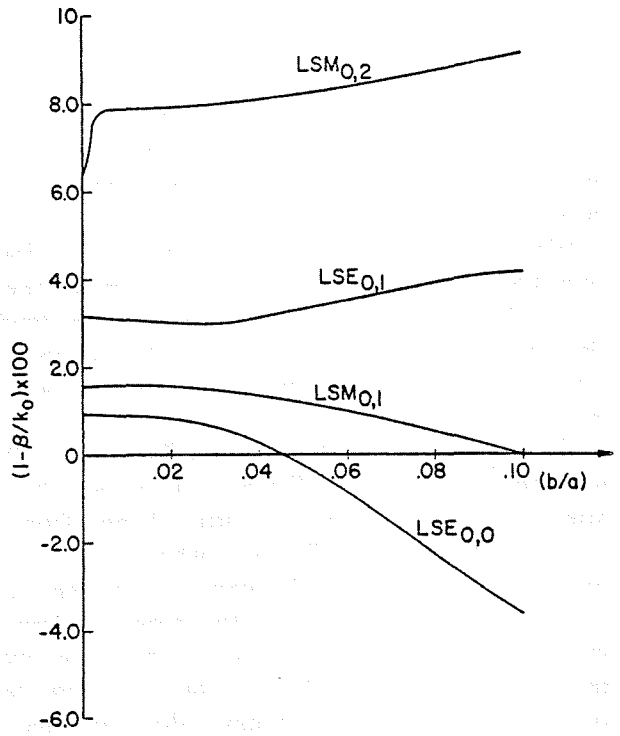


Fig. 4. Phase constants vs. b/a for $k_0b = 8.96$, $\epsilon_e/\epsilon_0 = 10$ and $\tan \delta_e = 0.045$.

with the dimensionless parameters used, the results are equally applicable to other sets of parameters. In the above figures, $m = 0$ and hence the modes are pure $LSE_{0,n}$ or $LSM_{0,n}$ according to type of walls at $z = 0, 2h$. In order to be consistent with the work of others [e.g., *Cochran and Pecina*, 1966], we choose the integer n to start from 0 for the LSE modes and from 1 for the LSM modes. The effect of curvature on the lowest-order mode ($LSE_{0,0}$ or $LSM_{0,1}$) is to lower its phase velocity and increase its attenuation. This mode tends to have its fields concentrated near the $\rho = a + b$ surface and hence behaves as the whispering gallery modes discussed by *Wait* [1967]. The curvature effects on the next higher order mode ($LSE_{0,1}$ or $LSM_{0,2}$) may be quite different; in particular, the attenuation of the $LSE_{0,1}$ mode may decrease with greater curvatures as a result of more grazing incidence of the rays on the guide wall at $\rho = a - b$, and hence this mode may become less attenuated than the lowest-order $LSE_{0,0}$ mode (Figures 3 and 5).

Normalized attenuation rates are plotted against the parameter k_0b for $LSE_{0,0}$ and $LSM_{0,1}$ modes in Figure 6. Here the product $\tan \delta_e \cdot k_0b$, rather than $\tan \delta_e$, is kept constant. This corresponds to a situation where the external medium of the guide has a constant conductivity σ_e while the frequency is varying. The ratio a/b takes the discrete values: ∞ (for a straight guide), 50, and 10. The typical decrease of attenuation with frequency observed in a straight waveguide is no longer a general characteristic in a curved waveguide. Similar effects are observed for the

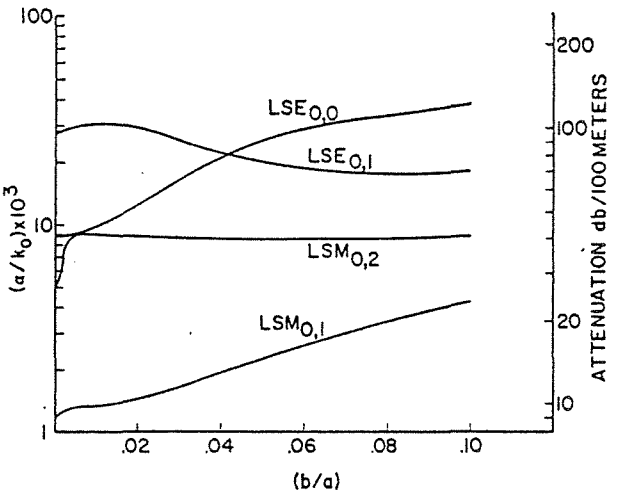


Fig. 5. Normalized attenuation rates vs. b/a for $k_0b = 8.96$, $\epsilon_e/\epsilon_0 = 10$ and $\tan \delta_e = 0.045$. The scale on the right-hand side gives the attenuation in db/100 m at 400 MHz when $2b = 2.133$ m ($\simeq 7$ ft) and $\sigma_e = 10^{-2}$mho m^{-1}.

next higher-order modes ($LSE_{0,1}$ and $LSM_{0,2}$) as illustrated in Figure 7. Of particular interest is the minimum of attenuation versus k_0b (or frequency) exhibited by the $LSE_{0,1}$ mode. The same phenomenon is observed with VLF modes in the earth-ionosphere guide [*Wait*, 1970, chap. 7] and is now considered to be a well-understood phenomenon.

When $m > 0$ (i.e., $\lambda > 0$), the modes are no longer pure LSE or LSM modes. However, we may continue to use the same nomenclature with the understanding that, e.g., $LSE_{m,n}$ is a hybrid mode that reduces to a longitudinal section electric mode when m becomes zero.

The attenuation of the modes $LSE_{1,0}$ and $LSM_{1,1}$ is plotted versus k_0b in Figure 8. It is seen that the attenuation rates show very little change from the corresponding case in Figure 6 where $m = 0$. This means that the coupling between the LSE and LSM modes is not appreciable in the range of electrical guide widths shown in these figures. It is worth mentioning that a reduction of tan δ_e to one tenth of its value in Figures 6 through 8 does not affect the attenuation rates by any significant amount. This is probably due to the fact that tan δ_e in these figures is already small (it has a maximum of 0.09) and hence the excess attenuation is due to more radiation rather than ohmic losses.

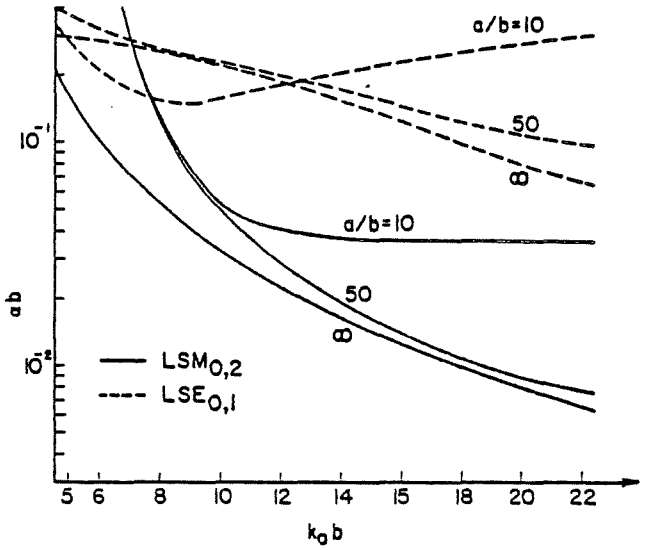


Fig. 7. Normalized attenuation rates vs. k_0b_1 for the same parameters as in Figure 6.

CONCLUDING REMARKS

In this paper, we have analyzed the propagating modes in a curved rectangular guide with imperfect but smooth walls. We found that the lowest-order mode has a whispering gallery character and as a result, the attenuation rate is increased significantly by the curvature. Actually, the attenuation of the $LSE_{0,1}$ mode may be decreased by the curvature and

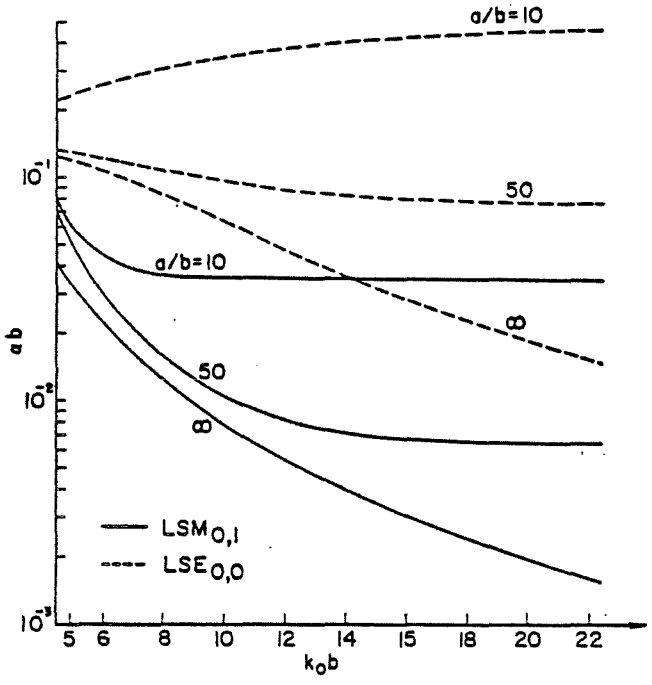


Fig. 6. Normalized attenuation rates vs. k_0b. $\epsilon_e/\epsilon_0 = 10$ and the product tan $\delta_e \cdot k_0b$ is kept constant and equal to 4.032.

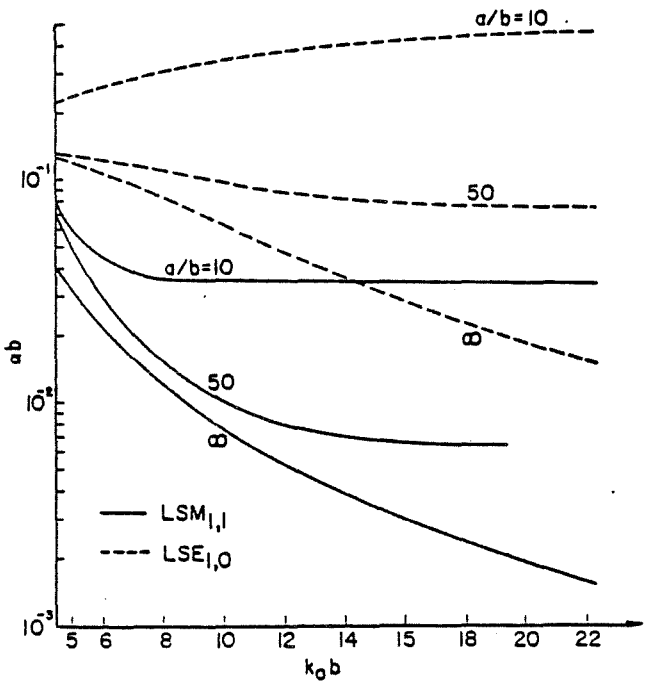


Fig. 8. Normalized attenuation rates vs. k_0b for the same parameters as in Figure 6.

hence this mode can become less attenuated than the lower $LSE_{0,0}$ mode.

REFERENCES

Cochran, J. A., and R. G. Pecina (1966), Mode propagation in continuously curved waveguides, *Radio Sci.*, *1*(6), 679–708.

Emslie, A. G., R. L. Lagace, and P. F. Strong (1973), Theory of propagation of UHF radio waves in coal mine tunnels, *Thru-the-Eaeth Electromagnetics Workshop*, eidted by R. G. Geyer, *Fin. Rep. USBM contract/grant G133023*, pp. 38–48, Department of the Interior, Bureau of Mines, Washington, DC.

Miller, J. C. P. (1946), *The Airy Integral*, Cambridge University Press, London.

Rice, S. O. (1948), Reflections from circular bends in rectangular wave guides—Matrix theory, *Bell Syst. Tech. J.*, *27*(2), 305–349.

Wait, J. R. (1959), *Electromagnetic Radiation from Cylindrical Structures*, p. 10, Pergamon, New York.

Wait, J. R. (1964), Two-dimensional treatment of mode theory of the propagation of VLF radio waves, *J. Res. Nat. Bur. Stand., Sect. D. 68D*(1), 81–93.

Wait, J. R. (1967), Electromagnetic whispering gallery modes in a dielectric rod, *Radio Sci.*, *2*(9), 1005–1017.

Wait, J. R. (1970), *Electromagnetic Waves in Stratified Media*, 2nd ed., pp. 76 and 112, Pergamon, New York.

Waldron, R. A. (1957), Theory of the helical waveguide of rectangular cross-section, *J. Brit. Inst. Radio Eng.*, *17*(10), 577–592.

Wu, C. P. (1973), Waveguide modes in curved waveguides, in *Computer Techniques for Electromagnetics*, edited by R. Mittra, pp. 279–281, Pergamon, New York.

Radio Science, Volume 9, Number 12, pages 1147–1158, December 1974.

Geometrical optical approach for electromagnetic wave propagation in rectangular mine tunnels

Samir F. Mahmoud[1] *and James R. Wait*[2]

Cooperative Institute for Research in Environmental Sciences, University of Colorado, Boulder, Colorado 80302

(Received August 30, 1974.)

Electromagnetic wave propagation inside an empty rectangular mine tunnel with imperfect walls is considered. The modal expansion of the fields is complicated by the coupling of the basic modes by the imperfect walls. To avoid this difficulty, and in view of the large guide dimensions relative to the free space wavelength, a geometrical ray approach is proposed. To provide a theoretical foundation for the method, we first consider an idealized waveguide model with two perfectly reflecting side walls. The modal field expansion for this prototype model is fully analyzed to provide a satisfactory comparison between the modal and the geometrical ray sums. The proposed general ray method is then applied to the rectangular waveguide when all four walls are imperfectly conducting. Finally, the influence of wall roughness is considered by a relatively simple method.

INTRODUCTION

Recently, much attention has been paid to the possibility of radio communication in a mine tunnel environment [e.g., *Goddard*, 1973; *Emslie et al.*, 1973]. An interesting and rather fundamental problem arises in relation to electromagnetic wave propagation in a rectangular waveguide (representing the tunnel) which is assumed perfect in shape but whose four walls are generally characterized by a lossy dielectric medium. A close investigation of this problem shows that, although the Helmholtz wave equation is separable in Cartesian coordinates, the boundary conditions on the walls of the guide necessitate the coupling of the basic modal functions. As indicated by *Wait* [1967], this raises a fundamental difficulty in obtaining the modal eigenvalues and eigenfunctions for such a waveguide or any other whose cross section is different from the circular shape.

In this paper, a geometrical ray approach is proposed to obtain the fields at any point in the waveguide as a summation of rays from the source and all possible images, avoiding the elaborate task of determining the modal propagation constants. This approach is applicable when the waveguide dimensions are somewhat greater than a free-space wavelength, a condition that is usually satisfied in mine tunnel applications.

PROTOTYPE MODEL AND MODAL FORMULATION

An important idealized model of the above rectangular waveguide is one with perfectly reflecting side walls while the top and bottom walls are still lossy dielectric media. For this waveguide, the free modal propagation constants and modal fields are straightforward to obtain [*Mahmoud and Wait*, 1974] and hence it provides a means of checking the modal versus the geometrical ray sums for the field. For this reason, we present a detailed field analysis for the above guide in the next section. This is followed by a formulation of the geometrical ray sum for the general waveguide with four imperfect walls. The effect of roughness of the guide walls is also considered by using an approximate technique. Finally, some numerical results are presented for specific situations of practical interest.

The geometry of the problem is shown in Figure 1. The source is assumed to be an infinitesimally short horizontal dipole of moment $P \exp(i\omega t)$ and located at the point $(x_0, y_0, 0)$ in the Cartesian frame. The resulting current density in the guide can be expressed, apart from the time factor $\exp(i\omega t)$, as

[1] Present address: Electrical Engineering Department, Cairo University, Egypt.

[2] Consultant to the Institute for Telecommunication Sciences, Office of Telecommunications.

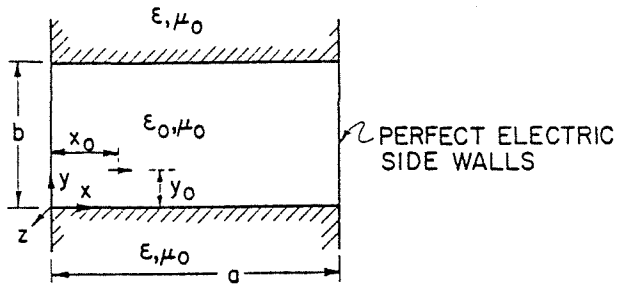


Fig. 1. A horizontal dipole inside a rectangular waveguide with perfect side walls.

$$J(x, y, z) = P\ \delta(x - x_0)\ \delta(y - y_0)\ \delta(z)\mathbf{x} \quad (1)$$

where x is a unit vector in the x direction. Applying the z Fourier transform operator, we transform $J(x, y, z)$ into $J(x, y; \beta)$ given by

$$J(x, y; \beta) = \int_{-\infty}^{\infty} \exp(i\beta z)\, J(x, y, z)\, dz = P\ \delta(x - x_0)\ \delta(y - y_0)\mathbf{x} \quad (2)$$

All the fields in the waveguide are transformed in a similar fashion and, as a result, the derivative $\partial/\partial z$ is now equivalent to the multiplication factor $(-i\beta)$. Generally, the fields can be obtained from two appropriate scalar potentials. The most convenient two potentials, for the present waveguide, are electric and magnetic potentials directed normally to the two imperfect walls (i.e., in the y direction). Let these be denoted by Π_y and Π_y^* respectively. This choice simplifies the analysis to follow since Π_y and Π_y^* are not coupled at the interfaces $y = 0$ and $y = b$ (although they are coupled by the source). It should be noted here, however, that for the general waveguide with four imperfect walls, any two chosen potentials will always be coupled at two or more of the walls.

The lossless waveguide region $0 < x < a$, $0 < y < b$ has electrical characteristics ϵ_0, μ_0 that can be assumed to be the same as free space. The lossy regions for $0 < x < a$ and, $y < 0$ and $y > b$ have corresponding parameters ϵ, μ_0 where $\epsilon = \epsilon_1 - i\sigma_1/\omega$ in terms of the real permittivity ϵ_1 and real conductivity σ_1.

Suitable expansions for Π_y and Π_y^* (assuming perfect electric side walls) are given below. For $b \geq y \geq y_0$,

$$\Pi_y = \sum_m A_m \sin(m\pi x/a)\{\exp[u_m(b - y)] + S_m \exp[-u_m(b - y)]\} \quad (3)$$

$$\Pi_y^* = \sum_m A_m^* \cos(m\pi x/a)\{\exp[u_m(b - y)] + R_m \exp[-u_m(b - y)]\} \quad (4)$$

while for $y \geq b$,

$$\Pi_{y1} = \sum_m T_m \sin(m\pi x/a) \exp[u_{m1}(b - y)] \quad (5)$$

$$\Pi_{y1}^* = \sum_m T_m^* \cos(m\pi x/a) \exp[u_{m1}(b - y)] \quad (6)$$

where the above potentials are functions of β which appears in u_m and u_{m1} as

$$u_m = [-k_0^2 + (m\pi/a)^2 + \beta^2]^{1/2}$$

$$u_{m1} = [-k_1^2 + (m\pi/a)^2 + \beta^2]^{1/2}$$

$$k_0^2 = \omega^2\mu_0\epsilon_0, \quad k_1^2 = \omega^2\mu_0\epsilon$$

and the summation over m is from 0 to $+\infty$. The tangential field components at the interface $y = b$ are given in terms of Π_y and Π_y^* as follows [*Wait*, 1959].

$$e_x = \partial^2\Pi_y/\partial x\,\partial y + \omega\mu_0\beta\Pi_y^*$$

$$e_z = -i\beta\,\partial\Pi_y/\partial y - i\omega\mu_0\,\partial\Pi_y^*/\partial x$$

$$h_x = -\omega\epsilon_0\beta\Pi_y + \partial^2\Pi_y^*/\partial x\,\partial y$$

$$h_z = i\omega\epsilon_0\,\partial\Pi_y/\partial x - i\beta\,\partial\Pi_y^*/\partial y$$

for $b \geq y \geq y_0$, while for $y \geq b$, ϵ_0 is replaced by ϵ. The continuity of these field components at $y = b$ reduces to the continuity of Π_y, Π_y^*, and their y derivatives. This results in S_m and R_m given by

$$S_m = (\epsilon u_m - \epsilon_0 u_{m1})/(\epsilon u_m + \epsilon_0 u_{m1}) \quad (7)$$

$$R_m = (u_m - u_{m1})/(u_m + u_{m1}) \quad (8)$$

While A_m and A_m^* are still arbitrary and unrelated. This means that the two potentials are uncoupled by the interface as stated above. We recognize S_m and R_m as the Fresnel reflection coefficients for vertically and horizontally polarized waves respectively [*Wait*, 1970]. The present choice of y-directed Hertz vectors is a simplification over the forms used previously by *Mahmoud and Wait* [1974].

In a similar fashion, the potentials Π_y and Π_y^* for $0 \leq y \leq y_0$ are obtained as

$$\Pi_y = \sum_m B_m \sin(m\pi x/a)[\exp(u_m y) + S_m \exp(-u_m y)] \quad (9)$$

$$\Pi_y^* = \sum_m B_m^* \cos(m\pi x/a)[\exp(u_m y) + R_m \exp(-u_m y)] \quad (10)$$

The four coefficients A_m, A_m^*, B_m, and B_m^* are to be determined from the continuity of e_x, e_z, and h_x at $y = y_0$ plane and the discontinuity of h_z by the source. This reduces to the continuity of Π_y^* and $\partial\Pi_y/\partial y$ at $y = y_0$ and the discontinuity of both Π_y and $\partial\Pi_y^*/\partial y$ such that

$$h_x|_{y_0+} - h_x|_{y_0-} = -\omega\epsilon_0\beta(\Pi_y|_{y_0+} - \Pi_y|_{y_0-}) + (\partial/\partial x)[(\partial\Pi_y^*/\partial y)_{y_0+} - (\partial\Pi_y^*/\partial y)_{y_0-}] = 0 \quad (11)$$

$$h_z|_{y_0+} - h_z|_{y_0-} = i\omega\epsilon_0(\partial/\partial x)(\Pi_y|_{y_0+} - \Pi_y|_{y_0-}) - i\beta[(\partial\Pi_y^*/\partial y)_{y_0+} - (\partial\Pi_y^*/\partial y)_{y_0-}] = P\,\delta(x - x_0) = (2P/a)\sum_m \delta_m \cos(m\pi x_0/a)\cos(m\pi x/a) \quad (12)$$

where $\delta_m = 1$ for $m \neq 0$ and $= \frac{1}{2}$ for $m = 0$. The last equality is obtained by expanding the delta function in a cosinusoidal series in the interval $(0, a)$.

Substituting from (3), (4), (9), and (10) in (11) and (12), we obtain

$$A_m g_m(b - y_0) - B_m g_m(y_0) = X_m \quad (13)$$

$$A_m^* f_m'(b - y_0) + B_m^* f_m'(y_0) = Y_m \quad (14)$$

where

$$X_m = (P/i\omega\epsilon_0 a)\,\delta_m \cos(m\pi x_0/a)(m\pi/a)/(k_0^2 + u_m^2)$$

$$Y_m = (P/ia)\beta/[u_m(k_0^2 + u_m^2)]$$

and the functions $f_m(y)$, $g_m(y)$, $f_m'(y)$, and $g_m'(y)$ are defined by

$$\left.\begin{matrix} f_m(y) \\ g_m(y) \end{matrix}\right\} = (1/2)\exp(u_m y) + (1/2)\left\{\begin{matrix} R_m \\ S_m \end{matrix}\right\}\exp(-u_m y) \quad (15)$$

$$\left.\begin{matrix} f_m'(y) \\ g_m'(y) \end{matrix}\right\} = (1/2)\exp(u_m y) - (1/2)\left\{\begin{matrix} R_m \\ S_m \end{matrix}\right\}\exp(-u_m y) \quad (16)$$

The equations for the continuity of Π_y^* and $\partial\Pi_y/\partial y$ at $y = y_0$ give

$$-A_m g_m'(b - y_0) = B_m g_m'(y_0) \quad (17)$$

$$A_m^* f_m(b - y_0) = B_m^* f_m(y_0) \quad (18)$$

Now, solving equations (13), (14), (17), and (18), we obtain

$$A_m = 2g_m'(y_0)X_m/\Delta_m$$

$$B_m = -2g_m'(b - y_0)X_m/\Delta_m$$

$$A_m^* = 2f_m(y_0)Y_m/\Delta_m^*$$

and

$$B_m^* = 2f_m(b - y_0)Y_m/\Delta_m^*$$

where

$$\left.\begin{matrix} \Delta_m \\ \Delta_m^* \end{matrix}\right\} = \exp(u_m b) - \left\{\begin{matrix} S_m^2 \\ R_m^2 \end{matrix}\right\}\exp(-u_m b) \quad (19)$$

Hence we obtain Π_y and Π_y^* in (3), (4), (9), and (10) in the form

$$\Pi_y = (4P/i\omega\epsilon_0 a)\sum_m \frac{(m\pi/a)}{k_0^2 + u_m^2}\,\delta_m \cos(m\pi x_0/a)\cdot\sin(m\pi x_0/a)\left\{\begin{matrix} g_m'(y_0)g_m(b - y) \\ -g_m'(b - y_0)g_m(y) \end{matrix}\right\}\Big/\Delta_m \quad (20)$$

$$\Pi_y^* = (4P/ia)\beta\sum_m \frac{1}{k_0^2 + u_m^2}\,\delta_m \cos(m\pi x_0/a)\cdot\cos(m\pi x/a)\left\{\begin{matrix} f_m(y_0)f_m(b - y) \\ f_m(b - y_0)f_m(y) \end{matrix}\right\}\Big/ u_m\Delta_m^* \quad \text{for} \quad \begin{cases} b \geq y \geq y_0 \\ y_0 \geq y \geq 0 \end{cases} \quad (21)$$

Finally, we take the inverse transform of (20) and (21) to obtain Π_y and Π_y^* as functions of x, y, z:

$$\Pi_y(x, y, z) = (1/2\pi)\cdot\int_{-\infty}^{\infty}\exp(-i\beta z)(\text{RHS of 20})\,d\beta \quad (22)$$

$$\Pi_y^*(x, y, z) = (1/2\pi)\cdot\int_{-\infty}^{\infty}\exp(-i\beta z)(\text{RHS of 21})\,d\beta \quad (23)$$

where RHS refers to the right-hand side.

The integration over β in (22) and (23) can be changed into a summation of residues in the complex β plane in a routine manner to obtain

$$\Pi_y(x, y, z) \simeq [-4\,\text{sgn}(z)P/\omega\epsilon_0 a]\cdot\sum_{n=1,2,\cdots}\sum_m [\exp(-i\beta_{mn}|z|)F_m'(x, x_0)(m\pi/a)/(k_0^2 + u_n^2)]g_n'(y_0)g_n(y)u_n/\beta_{mn}(\partial\Delta/\partial u)_{u_n} \quad (24)$$

$$\Pi_y^*(x, y, z) \simeq (-4P/a)\sum_{n=1,2,\cdots}\cdot\sum_m[\exp(-i\beta_{mn}^*|z|)F_m(x, x_0)/(k_0^2 + u_n^2)]\cdot f_n(y_0)f_n(y)/(\partial\Delta^*/\partial u)_{u_n} \quad (25)$$

where $f_n(y) = f_m(y)|_{\beta=\beta_n}$ etc. and where u_n and u_n^*, $n = 1, 2, \cdots$ are the roots of the equations $\Delta(u) = 0$ and $\Delta^*(u) = 0$ respectively. Also note that

$$\beta_{mn} = [k_0^2 - (m\pi/a)^2 + u_n^2]^{1/2}$$

and

$$\beta_{mn}^* = [k_0^2 - (m\pi/a)^2 + u_n^{*2}]^{1/2}$$

The functions $F_m(x, x_0)$ and $F_m'(x, x_0)$ are given by

$$\{F_m(x, x_0), F_m'(x, x_0)\} = \delta_m \cos(m\pi x_0/a) \cdot \{\cos(m\pi x/a), \sin(m\pi x/a)\}$$

Actually, the representations given by (24) and (25) are not exact since we have neglected the continuous spectrum associated with the branch line integrations around the branch point at $\beta = [k_1^2 - (m\pi/a)^2]^{1/2}$. The corresponding lateral waves are heavily damped when the external media are finitely conducting, e.g., $\epsilon_1\omega/\sigma_1 < 10$.

RAY SUM FOR PROTOTYPE MODEL

To cast equations (22) and (23) into a summation of rays, the terms $1/\Delta_m$ and $1/\Delta_m^*$ are first expanded in the manner

$$\left.\begin{matrix}1/\Delta_m \\ 1/\Delta_m^*\end{matrix}\right\} = \exp(-u_m b) \sum_n \left\{\begin{matrix}S_m^{2n} \\ R_m^{2n}\end{matrix}\right\} \exp(-2nu_m b)$$

Upon substituting back into (22) and (23), we encounter the following type of integral

$$I_{mi} = (1/2\pi) \int_{-\infty}^{\infty} \exp(-i\beta z) \cdot \exp[-u_m(y - y_i)]q(\beta)\, d\beta$$

This can be evaluated by the method of stationary phase to obtain:

$$I_{mi} \simeq \exp(i\pi/4)\lambda_m \cos\phi_i q(\lambda_m \sin\phi_i) \cdot \exp(-i\lambda_m r_i)/(2\pi\lambda_m r_i)^{1/2}$$

valid for $\lambda_m r_j \gg 1$. In the above q is a slowly varying function of β. In addition,

$$\lambda_m = (\beta^2 - u_m^2)^{1/2} = [k_0^2 - (m\pi/a)^2]^{1/2}$$
$$\phi_i = \tan^{-1} z/|y - y_i|$$
$$r_i = (z^2 + |y - y_i|^2)^{1/2}$$

The symbol j runs over all the images in the $y = 0$ and $y = b$ walls in any arbitrary order that we need not specify here. The location of these images are $y_j = 2lb \pm y_0$; $l = -\infty$ to ∞. We finally obtain Π_y and Π_y^* as the following summation of images

$$\Pi_y(x, y, z) = (P/i\omega\epsilon_0 a) \sum_m (m\pi/a) F_m'(x, x_0) \cdot \sum_j [(S)^{n_j}/(k_0^2 - \lambda_m^2 \cos^2\phi_j)] \cdot [\exp(-i\lambda_m r_j + i\pi/4)](2\pi\lambda_m r_j)^{-1/2} \quad (26)$$

$$\Pi_y^*(x, y, z) = (P/ia) \sum_m F_m(x, x_0) \cdot \sum_j [(R)^{n_j}/(k_0^2 - \lambda_m^2 \cos^2\phi_j)] \cdot [\exp(-i\lambda_m r_j + i\pi/4)](2\pi\lambda_m r_j)^{-1/2} \quad (27)$$

where n_j is the number of reflections on the $y = 0$ and $y = b$ walls involved in forming the jth images. It is easy to verify that for images at $y_j = 2lb + y_0$, $n_j = 2|l|$ and for images located at $y_j = 2lb - y_0$, $n_j = |l| + |l-1|$. We note that S and R are functions of u_m (see equations 7 and 8) for which we substitute $(i\lambda_m \cos\phi_j)$.

The fields excited by a vertical dipole can be obtained by following a similar analysis as above. In this case, however, the fields may be obtained from only one scalar potential Π_y (i.e., $\Pi_y^* = 0$). Alternatively, we can use the reciprocity theorem to derive these fields from those excited by the horizontal dipole. Here we shall only state the results. Thus, as a modal expansion, Π_y^v excited by an infinitesimally short vertical dipole of moment P located at $(x_0, y_0, 0)$, is given by

$$\Pi_y^v(x, y, z) = (-4P/\omega\epsilon_0 a) \sum_{n=1,2,\cdots} \cdot \sum_m \exp(-i\beta_{mn} z) F_m^v(x, x_0) \cdot g_n(y_0) g_n(y)/\beta_{mn}(\partial\Delta/\partial u)_{u_n} \quad (28)$$

where $F_m^v(x, x_0) = \sin(m\pi x_0/a) \sin(m\pi x/a)$. Then, the corresponding ray sum is

$$\Pi_y^v(x, y, z) = (P/i\omega\epsilon_0 a) \sum_m F_m^v(x, x_0) \sum_j (S)^{n_j} \cdot \exp(-i\lambda_m r_j + i\pi/4)/(2\pi\lambda_m r_j)^{1/2} \quad (29)$$

where the symbols occurring above have the same meaning as in (26). It should be noticed that the summation over m in (26), (27), and (29) can also be transformed into a ray sum from images in the side walls; however, this is not exploited here.

COMPARISON OF MODES AND RAYS FOR PROTOTYPE MODEL

A comparison between mode and ray summations of the electric field is shown in Figures 2 and 3. In Figure 2, the source is a $\lambda/2$ horizontal dipole and in Figure 3, it is a $\lambda/2$ vertical dipole. The following physical constants are assumed: $a = 2b = 4.26$ m ($\simeq 14$ ft), $x_0 = a/4$, $y_0 = 0.2b$, $y = 0.3b$. The frequency is 1 GHz and the effective wall impedances

Z_h, for horizontal polarization, and Z_v, for vertical polarization, are given by

$$Z_h = \eta_0/(\epsilon/\epsilon_0 - 1)^{1/2}$$

$$Z_v = \eta_0(\epsilon/\epsilon_0 - 1)^{1/2}/(\epsilon/\epsilon_0)$$

where ϵ is the complex dielectric constant of the walls, $\epsilon = \epsilon_1 - i\sigma_1/\omega\epsilon_0$, with $\epsilon_1 = 10\ \epsilon_0$ and $\sigma_1 = 10^{-2}$ mho m^{-1}. The electric fields E_x and E_y in the figures are obtained from the potentials Π_y, Π_y^*, and Π_y^v by

$$E_x|_{\text{horiz. dipole}} = \partial\Pi_y^2/\partial y\,\partial x + i\omega\mu_0\,\partial\Pi_y^*/\partial z$$

$$E_y|_{\text{vert. dipole}} = (k_0^2 + \partial^2/\partial y^2)\Pi_y^v$$

The comparison in Figures 2 and 3 shows a very close agreement between the mode and ray sums up to a distance of 2000 m for the horizontal dipole case and about 500 m for the vertical dipole case. The disagreement for distances greater than 500 m in the latter case is possibly due to the high total attenuation of the field and hence the severe cancellation of the terms of the ray series.

LIMIT TO THE PARALLEL PLATE GUIDE

The above results can be specialized to the parallel plate waveguide by allowing the two side walls to recede to $-\infty$ and $+\infty$ in the negative and positive x directions. In this case, the $\delta(x-x_0)$ term in (2) is expanded as

$$(1/2\pi)\int_{-\infty}^{+\infty} \exp\,[-i\kappa(x - x_0)]\,d\kappa$$

and hence all the preceding summations over m are replaced by a similar integral. Hence, as an example, equation 23 for Π_y^* now becomes

$$\Pi_y^*(x, y, z) = (1/2\pi)\int_{-\infty}^{\infty} \exp\,(-i\beta z)\beta\,d\beta(P/i\pi)$$

$$\cdot\int_{-\infty}^{\infty} \exp\,(-i\kappa x)\,d\kappa\begin{Bmatrix} f(y_0)f(b-y) \\ f(b-y_0)f(y)\end{Bmatrix} \Big/ [u\Delta^*(k_0^2 + u^2)]$$

$$\text{for } \begin{cases} b \geq y \geq y_0 \\ y_0 \geq y \geq 0 \end{cases} \qquad (30)$$

where $u^2 = -k_0^2 + \beta^2 + \kappa^2$, and x_0 is taken to be zero. To reduce the above expression into a modal sum, the second integral is transformed in the κ plane into a residue sum to give

$$\Pi_y^*(x, y, z) = (-P/\pi)\int_{-\infty}^{\infty} \exp\,(-i\beta z)\beta\,d\beta$$

$$\cdot\sum_{n=1,2,\cdots} \exp\,(-i\lambda_n\kappa)f_n(y_0)f_n(y)$$

$$\div [\lambda_n(k_0^2 + u_n^2)(\partial\Delta^*/\partial u)_{u_n}] \qquad (31)$$

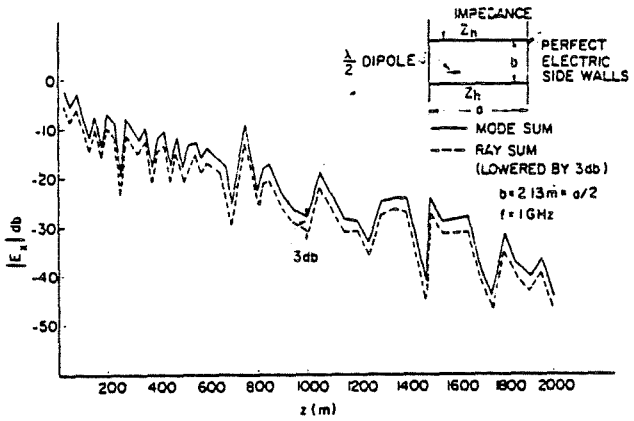


Fig. 2. Horizontal electric field versus distance z from the source. Modal and geometrical ray sums.

where u_n, $n = 1, 2, \ldots$, are the roots of the equation $\Delta^*(u) = 0$ and $\lambda_n^2 = k_0^2 + u_n^2 - \beta^2$. As before, we have neglected the continuous spectrum associated with the branch-line integration.

Now making use of the integral representation for the Hankel function

$$H_0^{(2)}[k(z^2 + x^2)^{1/2}] = (1/\pi)\int_{-\infty}^{\infty} \exp\,(-i\beta z)\,d\beta$$

$$\cdot \exp\,[-i(k^2 - \beta^2)^{1/2}x]/(k^2 - \beta^2)^{1/2}$$

equation 31 reduces finally to

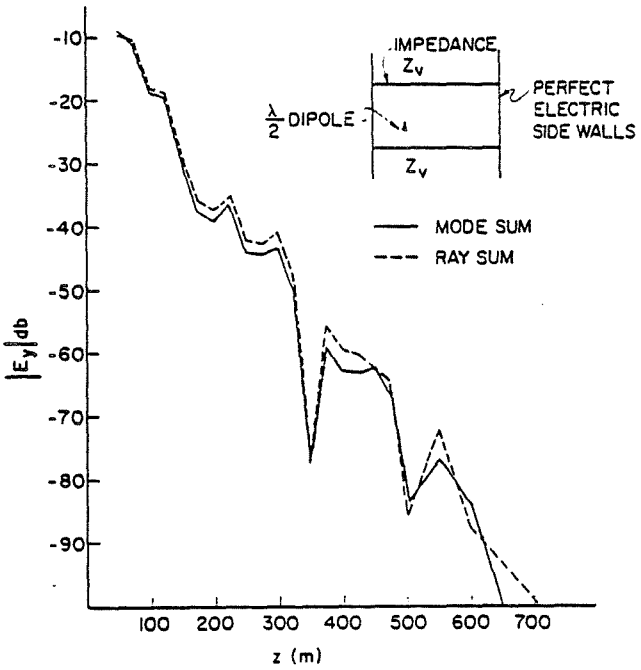


Fig. 3. Vertical electric field versus distance z from the source. Modal and geometrical ray sums.

$$\Pi_y^*(x, y, z) = -iP \sum_{n=1,2,\cdots} (\partial/\partial z) \cdot H_0^{(2)}[(k_0^2 + u_n^2)^{1/2}(z^2 + x^2)^{1/2}] \cdot f_n(y_0) f_n(y)/[(k_0^2 + u_n^2)(\partial\Delta^*/\partial u)_{u_n}] \quad (32)$$

To obtain a ray sum equivalent to (32), we expand the term $1/\Delta^*$ in (30) as before and perform the κ integration to get

$$(k_0^2 + \partial^2/\partial y^2)\Pi_y^*(x, y, z) = -(P/2) \cdot \int_{-\infty}^{\infty} \exp(-i\beta z)\beta\, d\beta \sum_i (R)^{n_i} H_0^{(2)}[(k_0^2 - \beta^2)^{1/2}\rho] = -(P/4\pi k_0) \sum_i (R)^{n_i}(\partial/\partial z)[\exp(-ik_0 r_i)/r_i] \quad (33)$$

where $\rho = [x^2 + (y-y_j)^2]^{1/2}$, $r_j = (\rho^2 + z^2)^{1/2}$, and j and n_j are defined as in equation 27. Similar expressions to (32) and (33) can also be derived for Π_y and Π_y^v.

SUMMATION OF RAYS FROM ONE-DIMENSIONAL ARRAY OF SOURCES

In what follows, an analytical expression for the geometrical ray sum from a source and its images in a parallel plate guide is obtained. The situation is illustrated in Figure 4 where the source at $y = y_0$, $z = 0$ produces images at $y_j = 2nb \pm y_0$, $z = 0$. The total field at an observation point (y, z) can be expressed as

$$S = S^+ + S^- \quad (34)$$

where S^+ is the contribution of the source and images as $y_j = 2nb + y_0$ while S^- is the contribution of images at $y_j = 2nb - y_0$, $n = -\infty$ to ∞. It is easy to verify that the number of reflections involved in producing an image at $y_j = 2nb + y_0$ is $2|n|$ and at $y_j = 2nb - y_0$ is $|n| + |n-1|$. Hence, apart from a possible directive pattern of the source, S^+ and S^- are given by

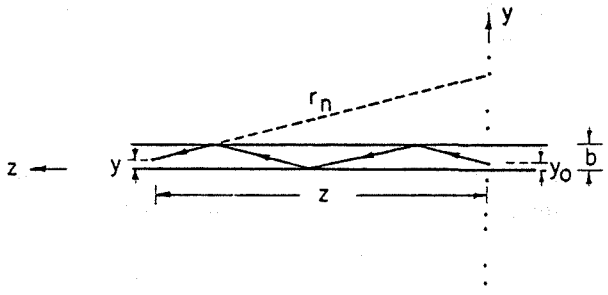


Fig. 4. The images in a parallel plate waveguide.

$$S^+ = \sum_{n=-\infty}^{\infty} (R)^{2|n|}[\exp(-ik_0 r_n^+)/r_n^+] \quad (35)$$

$$S^- = \sum_{n=-\infty}^{\infty} (R)^{|n|+|n-1|}[\exp(-ik_0 r_n^-)/r_n^-] \quad (36)$$

where $r_n^{\pm} = [z^2 + (2nb \pm y_0 - y)^2]^{1/2}$ and R is the reflection coefficient from the guide walls given by

$$R = -(C_v - \Delta)/(C_v + \Delta)$$

with $C_v = |2nb \pm y_0 - y|/r^{\pm}$, and Δ is a quantity related to the effective surface impedance. (This Δ should not be confused with that used in the previous section.) In particular, when $|\epsilon| \gg \epsilon_0$,

$$\Delta = (\epsilon/\epsilon_0 - 1 + C_v^2)^{1/2} \simeq (\epsilon/\epsilon_0 - 1)^{1/2}$$

for horizontally polarized waves or

$$\Delta = (\epsilon/\epsilon_0 - 1 + C_v^2)^{1/2}/(\epsilon/\epsilon_0) \simeq (\epsilon/\epsilon_0 - 1)^{1/2}/(\epsilon/\epsilon_0)$$

for vertically polarized waves, ϵ being the complex permittivity of the guide walls.

Since the images become weaker as they move away from the guide plates, we can assume that for the images of significant contribution to the field $z \gg |2nb \pm y_0 - y_r|$, which is valid as long as z is not in the very near field zone. Under this assumption we can use the following approximations:

$$r^{\pm} \simeq z + |2nb \pm y_0 - y|^2/2z \quad (37)$$

$$R \simeq -\exp(-2C_v/\Delta) \simeq -\exp(-2|2nb \pm y_0 - y|/z\Delta) \quad (38)$$

Substituting back in (35), S^+ becomes

$$S^+ = [\exp(-ik_0 z)/z]\left\{\sum_{n=1}^{\infty} \exp[-ik_0(2nb + y_0 - y)^2/2z - 4(2nb + y_0 - y)n/z\Delta] + \sum_{n=1}^{\infty} \exp[-ik_0(2nb - y_0 + y)^2/2z - 4(2nb - y_0 + y)n/z\Delta] + \exp[-ik_0(y_0 - y)^2/2z]\right\}$$

$$= [\exp(-ik_0 z)/z]\left[\sum_{n=1}^{\infty} \exp(-\alpha n^2 - \beta n - \gamma) + \sum_{n=1}^{\infty} \exp(-\alpha n^2 + \beta n - \gamma) + \exp(-\gamma)\right]$$

$$= [\exp(-ik_0 z)/z][\exp(-\gamma)] \cdot \left[1 + 2\sum_{n=1}^{\infty} \cosh \beta n \exp(-\alpha n^2)\right]$$

In the case of an incident Π_y plane wave on the $y = b$ interface, the Fresnel reflection coefficient is given by

$$S(k_y) = (\epsilon k_y - \epsilon_0 k_{y1})/(\epsilon k_y + \epsilon_0 k_{y1}) \qquad (44)$$

while no Π_x is needed.

Although the above reflection coefficients are strictly valid only for incident plane waves on infinite plane interfaces, they are practically as valid for incident spherical waves when these are several wavelengths from the source and when the interface is only of finite extent. In other words, the waves emanating from the source are assumed to be sharply defined rays far enough from the source, and hence their reflections are affected only by the local conditions of the interface. This is actually the basis of developing the ray series to follow for the fields in the waveguide whose cross-sectional dimensions are sufficiently greater than a free-space wavelength.

Now we define a 2 × 2 reflection coefficient matrix [Γ] for each interface as follows:

$$\begin{bmatrix} \Pi_x^{\text{refl}} \\ \Pi_y^{\text{refl}} \end{bmatrix} = [\Gamma] \begin{bmatrix} \Pi_x^{\text{inc}} \\ \Pi_y^{\text{inc}} \end{bmatrix}$$

This will be given by

$$[\Gamma] = \begin{bmatrix} R(k_y) & 0 \\ \pm R^*(k_x, k_y) & S(k_y) \end{bmatrix} \qquad (45)$$

for the interfaces at $y = b$ and $y = 0$ where the plus sign applies to the first interface and the minus sign to the second. Similarly

$$[\Gamma] = \begin{bmatrix} S(k_x) & \pm R^*(k_y, k_x) \\ 0 & R(k_x) \end{bmatrix} \qquad (46)$$

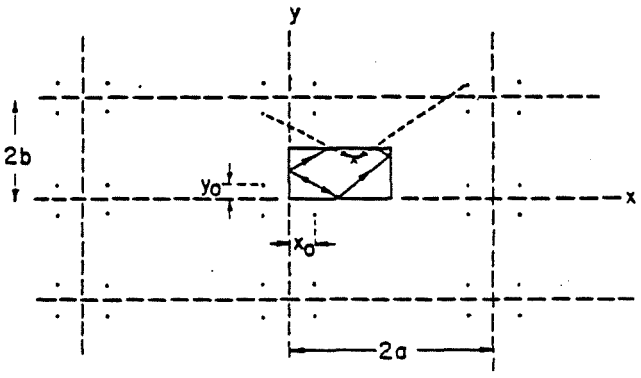


Fig. 6. The set of images in a rectangular waveguide.

for the interfaces at $x = a$ and $x = 0$ respectively. In the above, R, R^*, and S are defined by (42-44). The total field in the guide due to a given source is thus equal to the sum of ray contributions from all images added to that of the source. This situation is illustrated in Figure 6. Hence we have

$$\begin{bmatrix} \Pi_x^t(x, y, z) \\ \Pi_y^t(x, y, z) \end{bmatrix} = (1/4\pi i\omega\epsilon_0) \sum_l \cdot \sum_j [\exp(-ik_0 r_{lj})/r_{lj}][M_{lj}] \begin{bmatrix} P_x \\ P_y \end{bmatrix} \qquad (47)$$

where P_x and P_y are the x- and y-directed dipole moments of the source which is assumed to be an infinitesimally short dipole located at $(x_0, y_0, 0)$. The integers l and j run over all the images (and the source) in any arbitrary order that we need not specify here.

$$r_{lj} = [z^2 + (x - x_l)^2 + (y - y_j)^2]^{1/2}$$

(x_l, y_j) are the coordinates of the l-j image, where

$$x_l = 2ma \pm x_0, \qquad m = -\infty \text{ to } \infty$$

$$y_j = 2nb \pm y_0, \qquad n = -\infty \text{ to } \infty$$

and $[M_{lj}]$ is the product of all the reflection coefficient matrices involved in producting the l-j image with due care to the exact order of multiplication and the dependence of the reflection coefficients on the directional cosines of the ray. The horizontal and vertical electric field components are obtained from (47) and the following relations [*Wait*, 1959]:

$$E_x(x, y, z) = (k_0^2 + \partial^2/\partial x^2)\Pi_x^t + \partial^2\Pi_y^t/\partial y\,\partial x$$

$$E_y(x, y, z) = \partial^2\Pi_x^t/\partial x\,\partial y + (k_0^2 + \partial^2/\partial y^2)\Pi_y^t$$

Equation 47 is actually an exact equation, provided that the geometrical ray approximation is valid, since it takes account of the coupling between the Π_x and Π_y potentials through the term R^*. From equation 43 we see that for grazing rays ($k_x/k_0 \ll 1$, $k_y \ll k_{y1}$, and $\epsilon k_y \ll \epsilon_0 k_{y1}$), $R^* \simeq 2k_x k_y$, i.e., R^* becomes of a second-order magnitude relative to R and S (42 and 44), which then approaches unity. Since these grazing rays contribute most to the field, we may conclude that the coupling term R^* is of little importance. However, this statement is only true if we are interested in the fields of major polarization, e.g., Π_x (or E_x) due to a horizontal dipole moment P_x in which case, however, Π_y is appreciably affected

In the case of an incident Π_y plane wave on the $y = b$ interface, the Fresnel reflection coefficient is given by

$$S(k_y) = (\epsilon k_y - \epsilon_0 k_{y1})/(\epsilon k_y + \epsilon_0 k_{y1}) \qquad (44)$$

while no Π_x is needed.

Although the above reflection coefficients are strictly valid only for incident plane waves on infinite plane interfaces, they are practically as valid for incident spherical waves when these are several wavelengths from the source and when the interface is only of finite extent. In other words, the waves emanating from the source are assumed to be sharply defined rays far enough from the source, and hence their reflections are affected only by the local conditions of the interface. This is actually the basis of developing the ray series to follow for the fields in the waveguide whose cross-sectional dimensions are sufficiently greater than a free-space wavelength.

Now we define a 2×2 reflection coefficient matrix $[\Gamma]$ for each interface as follows:

$$\begin{bmatrix} \Pi_x^{refl} \\ \Pi_y^{refl} \end{bmatrix} = [\Gamma] \begin{bmatrix} \Pi_x^{inc} \\ \Pi_y^{inc} \end{bmatrix}$$

This will be given by

$$[\Gamma] = \begin{bmatrix} R(k_y) & 0 \\ \pm R^*(k_x, k_y) & S(k_y) \end{bmatrix} \qquad (45)$$

for the interfaces at $y = b$ and $y = 0$ where the plus sign applies to the first interface and the minus sign to the second. Similarly

$$[\Gamma] = \begin{bmatrix} S(k_x) & \pm R^*(k_y, k_x) \\ 0 & R(k_x) \end{bmatrix} \qquad (46)$$

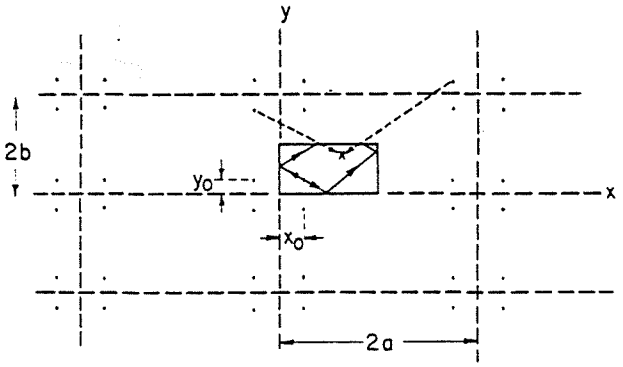


Fig. 6. The set of images in a rectangular waveguide.

for the interfaces at $x = a$ and $x = 0$ respectively. In the above, R, R^*, and S are defined by (42-44). The total field in the guide due to a given source is thus equal to the sum of ray contributions from all images added to that of the source. This situation is illustrated in Figure 6. Hence we have

$$\begin{bmatrix} \Pi_x'(x, y, z) \\ \Pi_y'(x, y, z) \end{bmatrix} = (1/4\pi i\omega\epsilon_0) \sum_l \cdot \sum_j [\exp(-ik_0 r_{lj})/r_{lj}][M_{lj}] \begin{bmatrix} P_x \\ P_y \end{bmatrix} \qquad (47)$$

where P_x and P_y are the x- and y-directed dipole moments of the source which is assumed to be an infinitesimally short dipole located at $(x_0, y_0, 0)$. The integers l and j run over all the images (and the source) in any arbitrary order that we need not specify here.

$$r_{lj} = [z^2 + (x - x_l)^2 + (y - y_j)^2]^{1/2}$$

(x_l, y_j) are the coordinates of the l-j image, where

$$x_l = 2ma \pm x_0, \qquad m = -\infty \text{ to } \infty$$

$$y_j = 2nb \pm y_s, \qquad n = -\infty \text{ to } \infty$$

and $[M_{lj}]$ is the product of all the reflection coefficient matrices involved in producting the l-j image with due care to the exact order of multiplication and the dependence of the reflection coefficients on the directional cosines of the ray. The horizontal and vertical electric field components are obtained from (47) and the following relations [*Wait*, 1959]:

$$E_x(x, y, z) = (k_0^2 + \partial^2/\partial x^2)\Pi_x' + \partial^2\Pi_y'/\partial y\,\partial x$$

$$E_y(x, y, z) = \partial^2\Pi_x'/\partial x\,\partial y + (k_0^2 + \partial^2/\partial y^2)\Pi_y'$$

Equation 47 is actually an exact equation, provided that the geometrical ray approximation is valid, since it takes account of the coupling between the Π_x and Π_y potentials through the term R^*. From equation 43 we see that for grazing rays ($k_x/k_0 \ll 1$, $k_y \ll k_{y1}$, and $\epsilon\, k_y \ll \epsilon_0 k_{y1}$), $R^* \simeq 2k_x k_y$, i.e., R^* becomes of a second-order magnitude relative to R and S (42 and 44), which then approaches unity. Since these grazing rays contribute most to the field, we may conclude that the coupling term R^* is of little importance. However, this statement is only true if we are interested in the fields of major polarization, e.g., Π_x (or E_x) due to a horizontal dipole moment P_x in which case, however, Π_y is appreciably affected

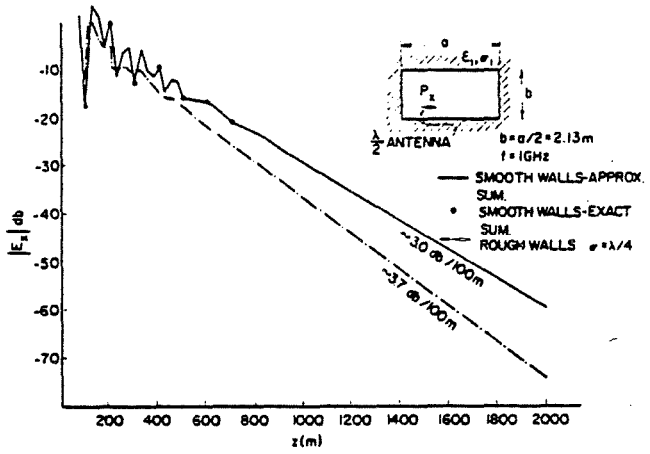


Fig. 7. Horizontal electric field versus distance z from the source inside a rectangular waveguide. Smooth and rough walls, 1 GHz.

by the coupling term. Hence, if we neglect R^* in (47) we can obtain the approximate formulas

$$\Pi_z^t(x, y, z) \simeq (1/4\pi i\omega\epsilon_0) \sum_l \cdot \sum_i \exp(-ik_0 r_{l,i}) S^{n_i} R^{n_j} P_z \qquad (48)$$

and

$$\Pi_y^t(x, y, z) \simeq (1/4\pi i\omega\epsilon_0) \sum_l \cdot \sum_i \exp(-ik_0 r_{l,i}) R^{n_i} S^{n_j} P_y \qquad (49)$$

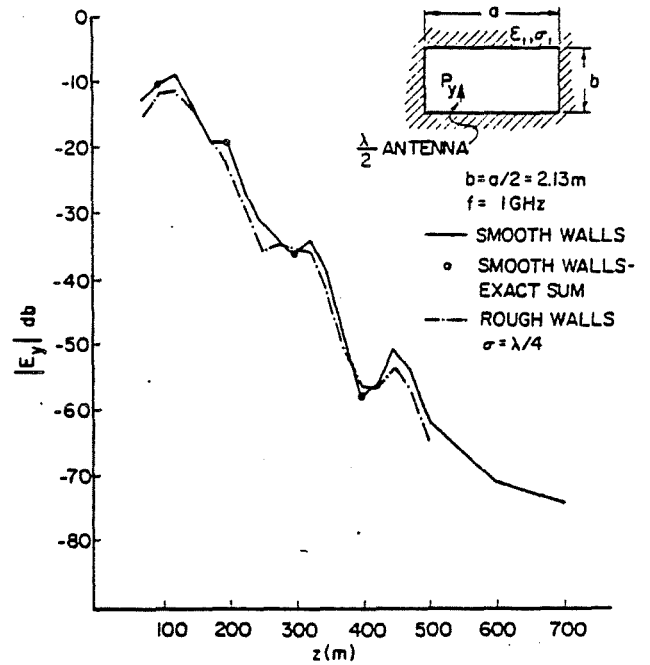


Fig. 8. Vertical electric field versus distance z from the source inside a rectangular waveguide. Smooth and rough walls, 1 GHz.

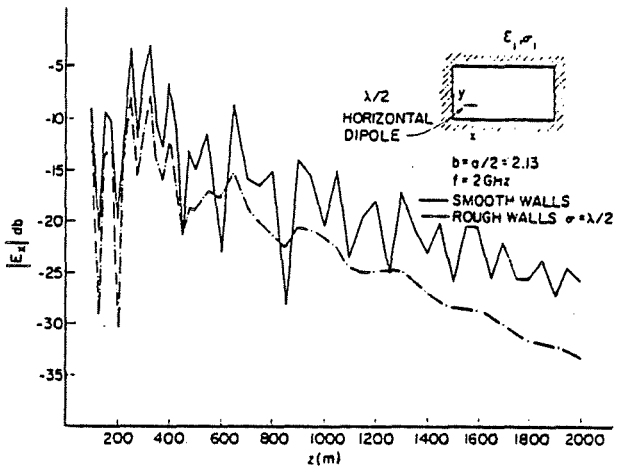


Fig. 9. Horizontal electric field versus distance z from the source inside a rectangular waveguide. Smooth and rough walls, 2 GHz.

where n_i and n_j are the numbers of reflection on the vertical and horizontal walls, respectively, involved in forming the l-j image.

Some specific numerical results for the horizontal and vertical excitations at 1 and 2 GHz are shown in Figures 7 through 10. The solid curves are computed from the approximate equations (48, 49) and the small circles in Figures 7 and 8 represent points computed on the basis of the more exact expression (47). It is seen that the agreement between the exact and approximate expressions is very good.

CONSIDERATION OF WALL ROUGHNESS

So far the wall roughness has been neglected. This, however, may be important at the range of

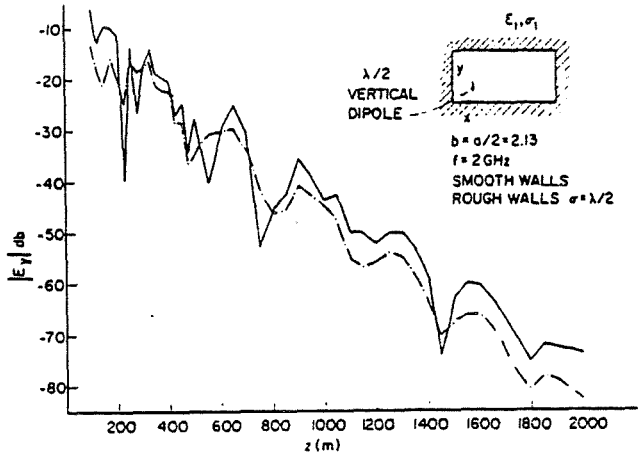


Fig. 10. Vertical electric field versus distance z from the source inside a rectangular waveguide. Smooth and rough walls, 2 GHz.

frequencies considered. For example, at 2 GHz the standard deviation of the mine tunnel walls may be of the order of $\lambda_0/2$. The simplest way to account for the roughness is to modify the Fresnel reflection coefficient in the specular direction while neglecting the nonspecular scattering. Using results obtained theoretically by *Beckmann and Spizzichino* [1963] and experimentally by *Beard* [1961], the specular Fresnel reflection coefficient R from a rough surface is given by

$$R = R_0 \exp(-\phi^2/2) \tag{50}$$

where R_0 is the Fresnel reflection coefficient from an average smooth surface, and $\phi = 4\pi\sigma \sin\psi/\lambda_0$. Here the rough surface is assumed to have a gaussian distribution with a standard deviation equal to σ, while ψ is the grazing angle of ray incidence. This expression is valid for values of $\sigma \sin\psi/\lambda_0 < 0.1$ [*Beard*, 1961], i.e., $\phi < 1.256$. Actually, for all cases of interest in the present investigation, this condition is well satisfied.

The simplicity of formula (50) makes it easy to incorporate the roughness effect in the geometrical ray series for the parallel plate waveguide (see Figures 5 and 11) as well as for the general rectangular waveguide (see Figures 7 through 10). We notice in these figures that the percentage increase of the attenuation due to roughness is greater when the horizontal polarization is dominant than when the vertical polarization is dominant. Also, this increase is greater for the higher frequencies (compare Figures 7 and 8 for 1 GHz with Figures 9 and 10 for 2 GHz).

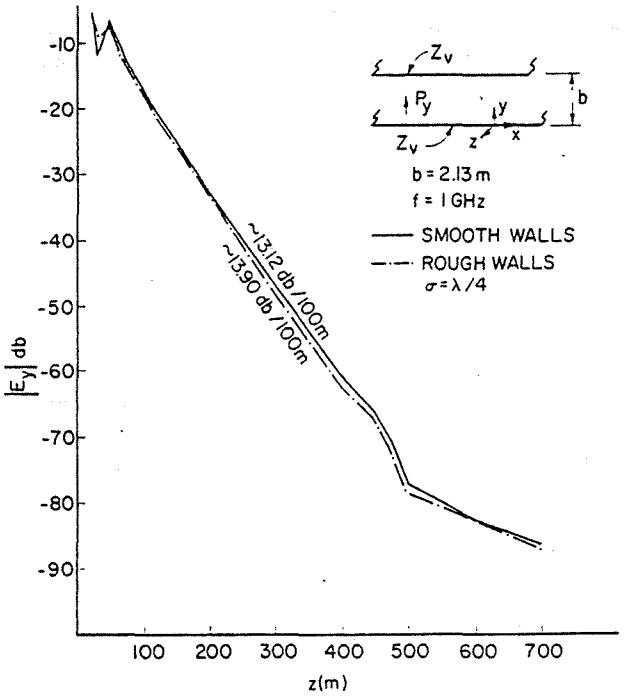


Fig. 11. Vertical electric field versus distance z from the source inside a parallel plate waveguide. Smooth and rough walls.

Equation 50 can also be incorporated in the modal equation for the parallel plate waveguide to study the effect of roughness on the first few dominant modes. This study should also help understand the same effect in the general rectangular waveguide. The modal equation for the parallel plate waveguide of width b is given by *Wait* [1970] as

$$R^2(k_y) \exp(-i2k_y b) = \exp(-i2n\pi) \tag{51}$$

For a rough surface guide, we substitute for $R(k_y)$ from (50), hence

$$R(k_y) = -[(k_y - k_0\Delta)/(k_y + k_0\Delta)] \exp(-2k_y^2\sigma^2)$$

where ϕ is replaced by $2k_y\sigma$, k_y is the wave number in the y direction (see Figure 4) and Δ is given by $\Delta = \Delta_h \simeq (\epsilon/\epsilon_0 - 1)^{1/2}$ for horizontally polarized waves and $\Delta = \Delta_v \simeq (\epsilon/\epsilon_0 - 1)^{1/2}/(\epsilon/\epsilon_0)$ for vertically polarized waves. Under the condition $n\pi/k_0 b\Delta \ll 1$, which is usually valid for lower-order modes, we can rewrite $R(k_y)$ in the approximate form

$$R(k_y) \simeq -\exp(-2k_y/k_0\Delta - 2k_y^2\sigma^2)$$

Hence (51) reduces to the quadratic equation

$$k_y^2\sigma^2 + k_y(1/k_0\Delta + ib) - in\pi = 0$$

whose solution can be put in the form

$$k_y \simeq k_{y0} + \delta k_{y0}$$

where

$$k_{y0} = n\pi/(b - i2/k_0\Delta)$$

and

$$\delta k_{y0} = i2(n\pi/b)^2\sigma^2(1 + i\sigma/k_0 b\Delta)/b$$

The corresponding longitudinal attenuation constant α is obtained from the relation

$$\alpha = R_e[(k_0^2 - k_y^2)^{1/2}] \simeq \alpha_0 + \delta\alpha$$

where

$$\alpha_0 \simeq 2(n\pi/b)^2/k_0^2\Delta b \tag{52}$$

$$\delta\alpha \simeq 2(n\pi/b)^3\sigma^2/k_0 b \tag{53}$$

and hence

$$\delta\alpha/\alpha_0 \simeq (n\pi/b)k_0\sigma^2\Delta \qquad (54)$$

In the above, k_{y0} and α_0 apply to the case of smooth walls ($\sigma = 0$) and δk_y and $\delta\alpha$ are the changes in these quantities due to roughness.

According to (54) we can see that $(\delta\alpha/\alpha_0)$ is a monotonically increasing function of frequency. However, the overall attenuation $\alpha + \delta\alpha$ decreases with frequency due to more grazing incidence of rays on the guide walls. Since Δ_v is smaller than Δ_h by a factor approximately equal to ϵ/ϵ_0, we also find from (54) that $\delta\alpha/\alpha_0$, for horizontal polarization, is greater than that for vertical polarization.

Numerical solutions of the modal equation (51) are presented in Figures 12 and 13 for horizontal and vertical polarizations. The parameter ϕ' on these figures is defined as $2n\pi\sigma/b$ and it is approximately equal to ϕ in (50) since $\sin\psi \simeq n\pi/k_0b$. These results are seen to agree with the remarks stated above. We should admit, however, that this rough surface modification of the mode equation is certainly not rigorous. For one thing, it ignores the possible reconversion of the incoherent energy back into the coherent portion following the multiple bounces in the guiding structure. We feel confident, however, that the present approach should give a reasonable estimate on the expected modification of the attenuation rate to roughness. If anything, it will lead to a more pessimistic picture than if we fully accounted for the reconverted energy from the incoherent waves.

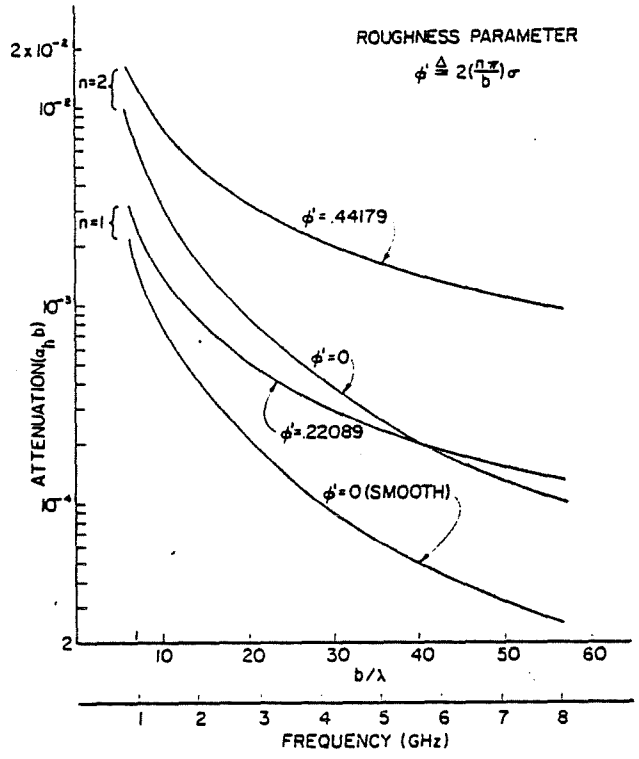


Fig. 12. Effect of roughness on the attenuation of horizontally polarized modes in a parallel plate waveguide. The lower horizontal scale corresponds to $b = 2.13$ m.

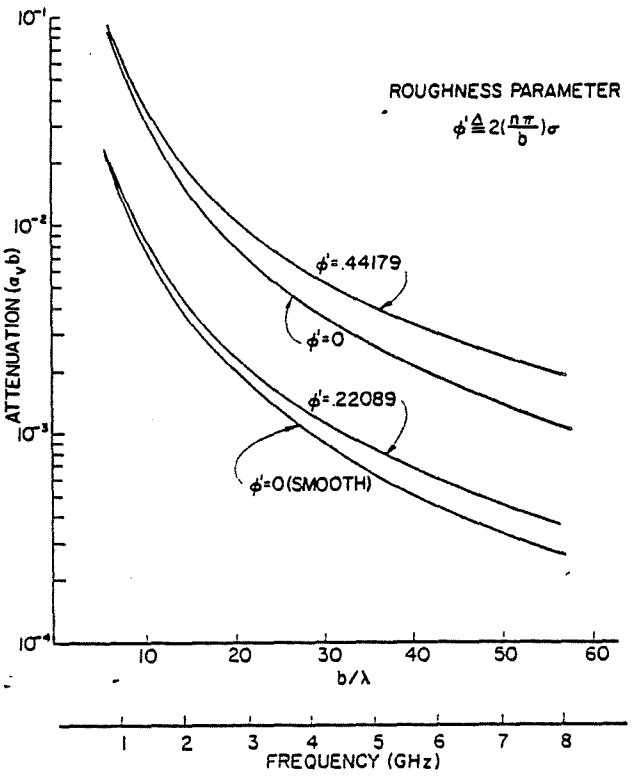


Fig. 13. Effect of roughness on the attenuation of vertically polarized modes in a parallel plate waveguide. The lower horizontal scale corresponds to $b = 2.13$ m.

CONCLUSIONS

Electromagnetic field excitation in a rectangular waveguide with imperfect walls, which may represent a mine tunnel, has been considered. Modal and geometrical ray sums have been obtained for the prototype model (i.e., when the two narrow side walls are assumed to be perfect reflectors). When all walls are imperfect, the modal propagation constants are not easy to obtain since the simple modes are intrinsically coupled. For this case, a geometrical ray summation has been derived, taking into account the coupling between the horizontally and vertically polarized rays. It is found, however, that this coupling can be neglected if only the field components of major polarization are of interest. Finally, the

effect of small roughness in the guide walls has been incorporated in the geometrical ray summation as well as in the modal equation for the case of a parallel plate waveguide. It has been demonstrated that the percentage increase in modal attenuation due to a typical wall roughness for mine tunnels increases with frequency although the overall attenuation is always a decreasing function of frequency due to a more grazing incidence of rays on the guide walls.

REFERENCES

Beard, C. I. (1961), Coherent and incoherent scattering of microwaves from the ocean, *IRE Trans. Antennas Propagat.*, *9*(9), 470–483.

Beckmann, P., and A. Spizzichino (1963), *The Scattering of Electromagnetic Waves from Rough Surfaces*, p. 124, Pergamon, New York.

Emslie, A. G., R. L. Lagace, and P. F. Strong (1973), Theory of propagation of UHF radio waves in coal mine tunnels, *Proceedings of Golden Workshop, School of Mines, Golden, Colorado, August 21–24*, pp. 38–48, Acc. No. PB 231 154, National Technical Information Service, Alexandria, Va.

Goddard, A. E. (1973), Radio propagation measurements in coal mines at UHF and VHF, *Proceedings of Thru-the-Earth Electromagnetic Workshop, Colorado School of Mines, Golden, Colorado, August 21–24*, pp. 54–61, Acc. No. PB 231 154, National Technical Information Service, Alexandria, Va.

Gradshteyn, L. S., and L. I. Ryzhik (1965), *Tables of Integrals, Series, and Products*, 4th ed., p. 923, Academic, New York.

Mahmoud, S. F., and J. R. Wait (1974), Theory of wave propagation along a thin wire inside a rectangular waveguide, *Radio Sci.*, *9*(3), 417–420.

Wait, J. R. (1959), *Electromagnetic Radiation from Cylindrical Structures*, p. 10, Pergamon, New York.

Wait, J. R. (1967), A fundamental difficulty in the analysis of cylindrical waveguides with impedance walls, *Electron. Lett.*, *3*(2), 87–88.

Wait, J. R. (1970), *Electromagnetic Waves in Stratified Media*, 2nd ed., chap. 6, p. 130, Pergamon, New York.

Reprinted by permission from IEEE TRANSACTIONS ON ANTENNAS AND PROPAGATION
Vol. AP-22, No. 4, July 1974, pp. 627-630

PRINTED IN THE U.S.A.

Guided Electromagnetic Waves Along an Axial Conductor in a Circular Tunnel

JAMES R. WAIT AND DAVID A. HILL

Abstract—A method to calculate the propagation characteristics of the guided modes in a circular tunnel bounded by lossy dielectric media is presented. The effect of an axial thin wire within the tunnel is also accounted for in the boundary value treatment of the problem. It is found that the attenuation of the transverse electromagnetic (TEM) or coax type mode is greatly increased when the conductor is moved toward the tunnel wall.

INTRODUCTION

In many operational coal mines, it is desired to communicate along tunnel-like structures that may extend up to 7 or 8 km. While conventional telephone lines may be used, it has been found very convenient and effective to transmit VHF radio signals directly through the haulageway [1]. Normally, these tend to be rectangular in cross section and are located within coal seams. In United States mines, these tunnels are crisscrossed by approximately an equal number at right angles. Also, within most tunnels, there is a high voltage power cable that is suspended from the top wall. In addition, numerous metal roof bolts are located throughout the mine. It is evident that the transmission of electromagnetic waves in such a structure is very complicated. Nevertheless, in order to understand observations and to improve communication procedures, it seems worthwhile to analyze some idealized models of the situation.

Emslie *et al.* [2] have developed an approximate theory for the empty rectangular guide with lossy dielectric walls. Their ingenious development is an extension of an earlier analysis by Marcatili and Schmeltzer [3] for rectangular dielectric rods surrounded by free space. More recently, Mahmoud and Wait [4] and Mahmoud [5] have considered a rectangular waveguide bounded on the horizontal walls by a finite conductivity and permittivity, but the (narrower) side wall was idealized as having perfect magnetic or electric boundaries. This model permitted the rigorous satisfaction of the boundary conditions. Also, it was feasible to include the effect of axial conductors within the tunnel. The latter are obviously important if the frequency is sufficiently low that the modes for the empty guides are "cut off." Here we consider another idealized model that should provide new insight into the problem.

Specifically, we consider an air-filled tunnel of circular cross section with radius a bounded by a lossy dielectric medium. Within this uniform tunnel we located a relatively thin metal conductor of radius c, whose conductivity is σ. The situation is illustrated in Fig. 1 where we have chosen a cylindrical coordinate system (ρ,ϕ,z) to be coaxial with the guide. For the interior region $\rho < a$, the permittivity and permeability are ϵ_0 and μ_0, respectively. For the exterior region, the

Manuscript received December 12, 1973; revised February 19, 1974.
The authors are with the Institute for Telecommunication Sciences, Office of Telecommunications, United States Department of Commerce, Boulder, Colo. 80302.

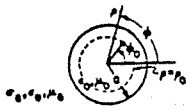


Fig. 1. Geometry of circular tunnel waveguide with axial conductor at distance ρ_0 from tunnel axis.

permittivity, conductivity, and permeability are ϵ_0, σ_0, and μ_0 respectively. The thin axial conductor is located at $\rho = \rho_0$ and $\phi = \phi_0$; its corresponding electric properties are ϵ_c, σ_c, and μ_c. Here we restrict attention to the case $0 < \rho_0 < a$.

FORMULATION

Our objective now is to calculate the complex propagation constant of the dominant modes of the structure. Thus we assume that the field of an individual mode varies with z according to $\exp(-\Gamma z)$ for an implied time factor $\exp(i\omega t)$ where the values of Γ are to be determined. To obtain the solution, we exploit the fact that the fields can be completely determined by two scalar functions U and V that are, respectively, the z components of the (axially directly) electric and magnetic Hertz vectors.

The current on the axial conductor can be designated $I \exp(-\Gamma z)$. The primary field within the tunnel from this traveling wave of current may be derived from the electric-type Hertz function U^p. It is well known that [6]

$$U^p = \frac{i\mu_0\omega}{2\pi\gamma_0^2} I \exp(-\Gamma z) K_0[(\gamma_0^2 - \Gamma^2)^{1/2}\rho_d] \tag{1}$$

where $\gamma_0^2 = -\epsilon_0\mu_0\omega^2$, $\rho_d = [\rho^2 + \rho_0^2 - 2\rho\rho_0\cos(\phi - \phi_0)]^{1/2}$, and K_0 is the modified Bessel function of the second kind. Now the total Hertz function within the guide can be written $U = U^p + U^s$ where U^s is the secondary part. The latter, for the region $\rho < a$, can be constructed by superimposing solutions of the type $I_m(v\rho)\exp(-im\phi)\exp(-\Gamma z)$ when I_m is a modified Bessel function of the first type, $v = (\gamma_0^2 - \Gamma^2)^{1/2}$, and m is any integer.

The above considerations and the addition theorem for K_0 in (1) lead us to the representation

$$U = \sum_{m=-\infty}^{+\infty} U_m \exp[-im(\phi - \phi_0)] \tag{2a}$$

or

$$U = \frac{i\mu_0\omega}{2\pi\gamma_0^2} I \exp(-\Gamma z) \sum_{m=-\infty}^{+\infty} I_m(v\rho_0)\left[K_m(v\rho) - R_m\frac{K_m(va)}{I_m(va)}I_m(v\rho)\right] \cdot \exp[-im(\phi - \phi_0)] \tag{2b}$$

for the region $\rho_0 < \rho < a$, where R_m is yet to be determined. Similar considerations lead us to the corresponding representation for the magnetic type Hertz function for the region $\rho < a$. Thus

$$V = \sum_{m=-\infty}^{+\infty} V_m \exp[-im(\phi - \phi_0)] \tag{3a}$$

or

$$V = \frac{i\mu_0\omega}{2\pi\gamma_0^2} I \exp(-\Gamma z) \sum_{m=-\infty}^{+\infty} \Delta_m I_m(v\rho_0) I_m(v\rho) \exp[-im(\phi - \phi_0)]. \tag{3b}$$

For the external region $\rho > a$ the Hertz functions are both made up from solutions of the form $K_m(u\rho)\exp(-\Gamma z)\exp(-im\phi)$ where $u = (\gamma_e^2 - \Gamma^2)^{1/2}$ and $\gamma_e^2 = i\mu_e\omega(\sigma_e + i\epsilon_e\omega)$.

For the region $\rho < a$, the tangential field components for the mth harmonic can be obtained from the mth harmonic of the Hertz functions as follows:

$$E_{\phi m} = \left(\frac{im\Gamma}{\rho}\right) U_m + i\mu_0\omega\frac{\partial V_m}{\partial\rho}$$

$$H_{\phi m} = \left(\frac{i\gamma_0^2}{\mu_0\omega}\right)\frac{\partial U_m}{\partial\rho} + \left(\frac{im\Gamma}{\rho}\right) V_m \tag{4}$$

$$E_{zm} = -v^2 U_m \text{ and } H_{zm} = -v^2 V_m$$

then, for example, the total axial field is

$$E_z = \sum_{m=-\infty}^{+\infty} E_{zm} \exp[-im(\phi - \phi_0)] \tag{5}$$

For the region $\rho > a$, the corresponding field quantities are obtained by replacing μ_0, γ_0^2, and v by μ_e, γ_e^2, and u, respectively.

WALL BOUNDARY CONDITIONS

The boundary conditions at the wall $\rho = a$ are that the tangential fields are continuous. For the present problem this is equivalent to applying the following conditions on the internal fields at $\rho = a$:

$$E_{\phi m} = \alpha_m E_{zm} + Z_m H_{zm} \tag{6}$$

$$H_{\phi m} = -Y_m E_{zm} + \alpha_m H_{zm} \tag{7}$$

where

$$\alpha_m = -\frac{im\Gamma}{(u^2 a)} \tag{8}$$

$$Z_m = -\left(\frac{i\mu_e\omega}{u}\right)\frac{K_m'(ua)}{K_m(ua)} \tag{9}$$

and

$$Y_m = \left(\frac{i\gamma_e^2}{u\mu_e\omega}\right)\frac{K_m'(ua)}{K_m(ua)}. \tag{10}$$

The wall impedance conditions in this form can be readily generalized to a concentrically layered external media and to certain anisotropic media. Here we will restrict attention to the homogeneous isotropic external region.

Using (2b), (3b), and (4), we readily obtain the following algebraic pair

$$\Delta_m[i\mu_0\omega v I_m' + Z_m v^2 I_m] + R_m\left[-\frac{im\Gamma}{a}K_m - \alpha_m\gamma^2 K_m\right] = -\frac{im\Gamma}{a}K_m - \alpha_m v^2 K_m \tag{11}$$

and

$$\Delta_m\left[\frac{im\Gamma}{a}I_m + \alpha_m v^2 I_m\right] + R_m\left[-\frac{i\gamma_0^2 v}{\mu_0\omega}\frac{K_m I_m'}{I_m} + Y_m v^2 K_m\right] = -\frac{i\gamma_0^2 v}{\mu_0\omega}K_m' + Y_m v^2 K_m \tag{12}$$

where the arguments of the Bessel functions and their derivatives are va. Eliminating Δ_m from (11) and (12), we obtain the explicit result

$$R_m = \frac{[(\gamma_0/v)K_m'(va)/K_m(va)] + Y_m\eta_0 + \delta_m\eta_0}{[(\gamma_0/v)I_m'(va)/I_m(va)] + Y_m\eta_0 + \delta_m\eta_0} \tag{13}$$

where

$$\delta_m\eta_0 = \frac{(im\Gamma/a)^2[v^{-2} - u^{-2}]^2}{[(\gamma_0/v)I_m'(va)/I_m(va)] + (Z_m/\eta_0)} \tag{14}$$

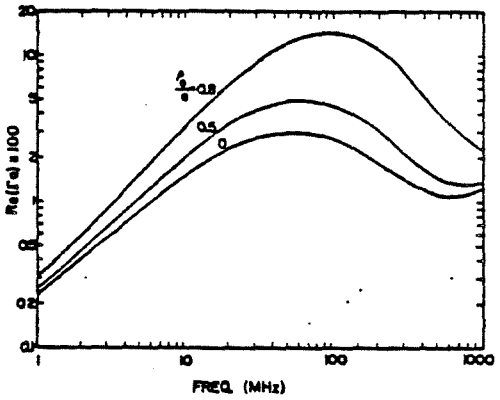


Fig. 2. Attenuation rate of COAX or TEM type mode as function of frequency for various locations of wire conductor. Multiply ordinate by 132.4 to convert to dB/100 ft.

and

$$\eta_0 = i\mu_0\omega/\gamma_0 \simeq 120\pi\ \Omega.$$

We now can express the axial electric field E_z anywhere within the guide in terms of the still unknown current $I \exp(-\Gamma z)$ on the wire. Using (1), (2b), and (4), this is given by

$$E_z = -\frac{i\mu_0\omega I\nu^2}{2\pi\gamma_0^2}\exp(-\Gamma z)\left[K_0(\nu\rho_0) - \sum_{m=-\infty}^{\infty} R_m \frac{K_m(\nu a)}{I_m(\nu a)} I_m(\nu\rho_0) \cdot I_m(\nu\rho)\exp(-im(\phi-\phi_0))\right]. \quad (15)$$

WIRE BOUNDARY CONDITION

The boundary condition at the wire is

$$E_z = IZ_s \exp(-\Gamma z) \quad (16)$$

at $\rho_0 = c_s$, for all values of z, where Z_s is the series impedance of the wire. Because of the assumed thinness of the wire, we can apply this condition at any point of the wire circumference. Thus we choose the matching point at $\rho = \rho_0 + c_s$ and $\phi = \phi_0$. Thus (16) leads to the mode equation

$$\frac{-i\mu_0\omega\nu^2}{2\pi\gamma_0^2}\left[K_0(\nu c) - \sum_{m=-\infty}^{\infty} R_m \frac{K_m(\nu a)}{I_m(\nu a)} I_m(\nu\rho_0) I_m[\nu(\rho_0 + c_s)]\right] = Z_s. \quad (17)$$

The explicit result for the series impedance [6] is

$$Z_s = \frac{\eta_0}{2\pi c_s}\frac{I_0(\gamma_s c_s)}{I_1(\gamma_s c_s)} \quad (18)$$

where $\gamma_s^2 = i\mu_s\omega(\sigma_s + i\epsilon_s\omega)$ and $\eta_s = i\mu_s\omega/\gamma_s$.

In principle, the problem as posed is solved when Γ is determined from (17). This mode equation is exact, subject only to the assumed thinness of the metal wire centered at (ρ_0, ϕ_0) inside the guide. In order to render the problem tractable, we will make a number of simplifying assumptions that are well justified on physical grounds.

SOME NUMERICAL RESULTS

For the high-frequency modes of interest we expect Γ to be on the order of $\gamma_0 = ik$, where $k = \omega/c$ is the free space wave number. Also, the bounding medium will have a conductivity and/or permittivity sufficiently high that $|\gamma_s a| \gg 1$. Invoking these assumptions, we can approximate (9) and (10) as follows:

$$Z_m \simeq \frac{(i\mu_s\omega)}{(\gamma_s^2 + k^2)^{1/2}}$$

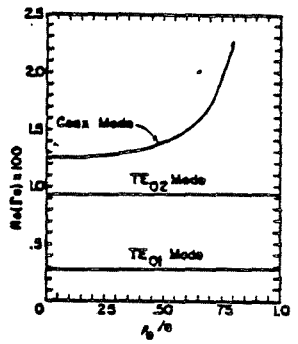


Fig. 3. Attenuation rate of COAX and TE modes for frequency of 1 MHz as function of wire conductor offset.

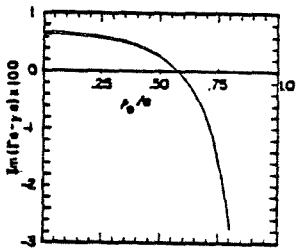


Fig. 4. Phase characteristic for COAX mode at 1 GHz.

and

$$Y_m \simeq \frac{\gamma_s^2}{[i\mu_s\omega(\gamma_s^2 + k^2)^{1/2}]}.$$

Also, in most cases at high frequencies, the conductivity of the metal wire will be sufficiently high that both $|\gamma_s c_s| \gg 1$ and $\sigma_s \gg \epsilon_s\omega$. Then from (18) we can obviously write

$$Z_s \simeq \left(\frac{\mu_s\omega}{2\sigma_s}\right)^{1/2}\frac{(1+i)}{(2\pi c_s)}.$$

With the simplifications indicated, some numerical solutions of (17) have been obtained. Of particular interest is the mode that has a transverse electromagnetic (TEM) character as the frequency is lowered. Using an adaptation of Newton's method, solutions of this type have been obtained. An example is shown in Fig. 2 where the following parameters are assumed: $a = 2m$, $\epsilon_s = 10\epsilon_0$, $\sigma_s = 10^{-2}$ mho/m, $\sigma_s = 10^5$ mho/m, $c_s = 10^{-2}$ m = 1 cm. Here the real part of (Γa) which is proportional to the attenuation rate, is plotted as a function of frequency from 1 to 1000 MHz. Three values of ρ_0/a, namely 0, 0.5, and 0.8 are indicated. *The ordinate in Fig. 2 is converted to dB per 100 ft in (obsolete) English units by multiplying by 132.4. Then the vertical scale extends from roughly 0.13 to 26 dB/100 ft.* The increase of the attenuation as the wire conductor approaches the wall is in accordance with the observations of Delogne *et al.* [7] in Belgian coal mines. Also Mahmoud [5] in his numerical studies of the rectangular guide has confirmed this effect.

For the geometry of the tunnel guide considered in the preceding example, we can expect higher order waveguide modes to appear when the frequency exceeds the cutoff value for the empty tube. This occurs approximately at 50 MHz in this case. For higher frequencies, we can expect the situation to be quite complicated. However, it appears we can always identify the TEM or COAX type mode as the one that is significantly influenced by the location and the series impedance of the wire conductor. In Figs. 3 and 4, we show the attenuation and phase characteristics for this COAX mode at a frequency of 1 GHz where the abscissa is the ratio ρ_0/a. The other parameters are the same as those shown in Fig. 2. We also show the attenuation rates for the TE_{01} and TE_{02} modes in Fig. 3 for the same

structures which are determined from the simplified mode equation $R_\phi^{-1} = 0$. In this case the wire conductor has no effect whatsoever on the modes of this type since the electric field has only a ϕ component. There is another class of modes here that can be described as perturbed TM and perturbed hybrid EH modes[1] that do interact with the wire conductor. A numerical study of these modes is presently underway. However, at least for the present geometry, they would appear to have attenuations greater than those shown in Fig. 3.

Another interesting point illustrated in Fig. 4 is that the phase velocity of the COAX mode is less than c when the wire conductor is at the center of the guide, but it becomes greater than c as the wire moves toward the wall. An analogous effect has been observed by Mahmoud [7] in his study of the rectangular guide.

[1] EH is standard nomenclature for modes that are neither E nor H type.

REFERENCES

[1] A. E. Goddard, "Radio propagation measurements in coal mines at UHF and VLF," in *Proc. Through-the-Earth Electromagnetics Workshop*, Colorado School of Mines, Golden, Colo., Aug. 15–17, 1973, available from Nat. Tech. Inform. Service, Alexandria, Va.

[2] A. G. Emslie, R. L. Lagace, and P. F. Strong, "Theory of the propagation of UHF radio waves in coal mine tunnels," in *Proc. Through-the-Earth Electromagnetics Workshop*, Colorado School of Mines, Golden, Colo., Aug. 15–17, 1973, available from Nat. Tech. Inform. Service, Alexandria, Va.

[3] E. A. J. Marcatili and R. A. Schmeltzer, "Hollow metallic and dielectric wave guides for long distance optical transmission and lasers," *Bell Syst. Tech. J.*, vol. 43, pp. 1783–1809, July 1964.

[4] S. F. Mahmoud and J. R. Wait, "Wave propagation along a thin wire inside a rectangular waveguide, Part I," *Radio Sci.*, vol. 9, Mar. 1974.

[5] S. F. Mahmoud, "Characteristics of EM guided waves for communication in coal mine tunnels," *IEEE Trans. Comm.*

[6] J. R. Wait, *Electromagnetic Radiation from Cylindrical Structures*. London: Pergamon, 1959.

[7] P. Delogne, L. Deryck, and R. Liegois, "*Guided propagation of radio waves*," in *Proc. Through-the-Earth Electromagnetics Workshop*, Colorado School of Mines, Golden, Colo., Aug. 15–17, 1973, available from Nat. Tech. Inform. Service, Alexandria, Va.

Excitation of monofilar and bifilar modes on a transmission line in a circular tunnel

David A. Hill

Institute for Telecommunications Sciences, Office of Telecommunications, U. S. Department of Commerce, Boulder, Colorado 80302

James R. Wait

Cooperative Institute for Research in Environmental Sciences, University of Colorado, Boulder, Colorado 80302
(Received 27 March 1974; in final form 9 May 1974)

We consider the excitation of monofilar and bifilar modes on a transmission line in a circular tunnel by a short dipole antenna. As expected, the monofilar mode is excited more strongly by an antenna placed in the tunnel, but the bifilar mode has lower attenuation. The excessive losses in the monofilar or coaxial mode are attributed to the return current flow along the tunnel walls. In the bifilar or transmission-line mode the fields are more confined to the region of the wire conductors.

I. INTRODUCTION

In coal mines it is desirable to communicate for long distances along tunnels and haulageways. An ingenious communication technique which is being developed for use in Belgian coal mines[1,2] utilizes a two-wire transmission line that can be suspended from the upper wall. A transmitter placed in the tunnel excites mainly the monofilar mode which propagates like a coaxial or TEM mode. The key step in the Belgian system is to convert this mode to a bifilar mode which is less attenuated because the return current flows in the second wire rather than through the surrounding rock. This mode converter, in its simplest form,[1,2] is often just an inductance inserted in one line and a capacitor inserted in the other so that the monofilar mode is transformed into the bifilar mode. The monofilar mode could also be called the balanced or symmetrical mode, and the bifilar mode could be called the unbalanced or asymmetrical mode. In other cases, this conversion is achieved by random imperfections in the system such as nonuniformities in the tunnel cross section and/or changes in the wire spacing. Here we consider only the excitation of the modes on an idealized uniform structure.

The propagation constants of these modes have been examined by Mahmoud[3] for a rectangular tunnel and by Wait and Hill[4] for a circular tunnel. Here, we examine the excitation of these modes by an electric dipole in a circular tunnel containing a two-wire line. The same principles would apply to the excitation of the corresponding type modes on a single braided coaxial cable that is often used in mine communications.[5] However, we do not consider this situation explicitly here.

II. FORMULATION

The geometry, of the tunnel and the source dipole of moment P in the plane $z=0$, is shown in Fig. 1. Consequently, the source current density J_s can be written

$$J_s(\rho, \phi, z) = P\delta(\rho-\rho_s)\delta(\phi-\phi_s)\delta(z)/\rho, \tag{1}$$

where δ is the Dirac delta function. As indicated cylindrical coordinates (ρ, ϕ, z) are adopted so that the source is located at $(\rho_s, \phi_s, 0)$. This current source produces an axial electric field $E_z(\rho, \phi, z)$ that can be determined by an application of the method of reciprocity. The method was used by Mahmoud[6] for a rectangular tunnel containing a single axial conductor. The technique of exploiting the reciprocity theorem has been used extensively in the calculation of excitation efficiencies for VLF modes in the earth–ionosphere waveguide.[7,8]

We will also determine the wire currents $I_0(z)$ and $I_1(z)$ excited by the current source at $(\rho_s, \phi_s, 0)$. These wire currents are indicative of the strength of the excited monofilar and bifilar modes.

To facilitate our analysis, we write the axial current density for $z>0$ carried by the wires J_z in the form

$$J_z(\rho, \phi, z) = \exp(-i\beta z)\rho^{-1}[I_0\delta(\rho-\rho_0)\delta(\phi-\phi_0) + I_1\delta(\rho-\rho_1)\delta(\phi-\phi_1)], \tag{2}$$

for a time factor $\exp(i\omega t)$. Here $i\beta$ is the propagation constant of a given mode on the structure. The total field e of this current can be separated into transverse and axial components in the following manner:

$$e(\rho, \phi, z) = \exp(-i\beta z)\{I_0[e_{t0}(\rho, \phi, \beta) + \hat{z}e_{z0}(\rho, \phi, \beta)] + I_1[e_{t1}(\rho, \phi, \beta) + \hat{z}e_{z1}(\rho, \phi, \beta)]\}. \tag{3}$$

Explicit field expressions can be derived from z components of electric and magnetic Hertz vectors[4] and will be given later.

We now apply the reciprocity theorem[9] to the current

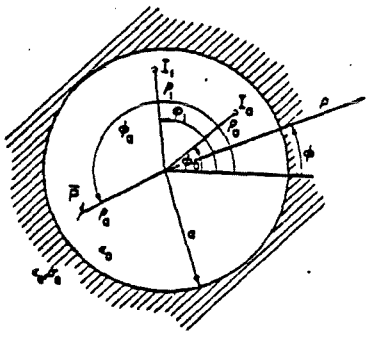


FIG. 1. Geometry for two wires and a source dipole in a circular air-filled tunnel in a homogeneous earth.

densities given by Eqs. (1) and (2) and their fields to yield the following:

$$\int_{-\infty}^{\infty}\int_0^{2\pi}\int_0^{\infty} J_a(\rho,\phi,z)\cdot[I_0\,e_{t0}(\rho,\phi,\beta) + I_1 e_{t1}(\rho,\phi,\beta)]\exp(-i\beta z)\rho\,d\rho\,d\phi\,dz = \int_{-\infty}^{\infty}\int_0^{2\pi}\int_0^{\infty} J_a(\rho,\phi,z)E_{za}(\rho,\phi,z)\rho\,d\rho\,d\phi\,dz. \quad (4)$$

The integrations in Eq. (4) can be carried out to obtain

$$I_0\mathbf{P}\cdot\mathbf{e}_{t0}(\rho_a,\phi_a,\beta)+I_1\mathbf{P}\cdot\mathbf{e}_{t1}(\rho_a,\phi_a,\beta) = I_0\int_{-\infty}^{\infty}E_{za}(\rho_0,\phi_0,z)\exp(-i\beta z)\,dz + I_1\int_{-\infty}^{\infty}E_{za}(\rho_1,\phi_1,z)\times\exp(-i\beta z)\,dz \triangleq I_0E'_{za}(\rho_0,\phi_0,\beta)+I_1E'_{za}(\rho_1,\phi_1,\beta), \quad (5)$$

where E'_{za} is the Fourier transform of E_{za}. Since I_0 and I_1 are arbitrary at this point, we can derive the following from Eq. (5):

$$E'_{za}(\rho_0,\phi_0,\beta)=\mathbf{P}\cdot\mathbf{e}_{t0}(\rho_a,\phi_a,\beta),\qquad E'_{za}(\rho_1,\phi_1,\beta)=\mathbf{P}\cdot\mathbf{e}_{t1}(\rho_a,\phi_a,\beta). \quad (6)$$

In order to obtain the induced wire currents, $I_0(z)$ and $I_1(z)$, we write them as Fourier transforms

$$I_0(z)=\frac{1}{2\pi}\int_{-\infty}^{\infty}I'_0(\beta)\exp(i\beta z)\,dz,\qquad I_1(z)=\frac{1}{2\pi}\int_{-\infty}^{\infty}I'_1(\beta)\exp(i\beta z)\,dz. \quad (7)$$

The boundary conditions at the wire match points require that

$$E'_{za}(\rho_0+c,\phi_0,\beta)+I'_0(\beta)e_{z0}(\rho_0+c,\phi_0,\beta)+I'_1(\beta)e_{z1}(\rho_0+c,\phi_0,\beta)=I'_0(\beta)Z_s,$$
$$E'_{za}(\rho_1+c,\phi_1,\beta)+I'_0(\beta)e_{z0}(\rho_1+c,\phi_1,\beta)+I'_1(\beta)e_{z1}(\rho_1+c,\phi_1,\beta)=I'_1(\beta)Z_s, \quad (8)$$

where

$$Z_s=\frac{\eta_s}{2\pi c}\frac{I_0(\gamma_s c)}{I_1(\gamma_s c)},\qquad \gamma_s^2\approx i\omega\mu\sigma_s,\qquad \eta_s=\frac{i\omega\mu}{\gamma_s},$$

σ_s is the wire conductivity, and c is the wire radius. The above expression for the wire series impedance per unit length[10,11] Z_s is actually an approximation which is valid for $|\gamma_s|^2 \gg |\beta|^2$. For sufficiently small values of c, Eq. (6) can be substituted into Eq. (8) to obtain

$$\begin{bmatrix}A_0(\beta) & A_1(\beta)\\ B_0(\beta) & B_1(\beta)\end{bmatrix}\begin{bmatrix}I'_0(\beta)\\ I'_1(\beta)\end{bmatrix}=\begin{bmatrix}-\mathbf{P}\cdot\mathbf{e}_{t0}(\rho_a,\phi_a,\beta)\\ -\mathbf{P}\cdot\mathbf{e}_{t1}(\rho_a,\phi_a,\beta)\end{bmatrix}, \quad (9)$$

where

$$A_0(\beta)=e_{z0}(\rho_0+c,\phi_0,\beta)-Z_s,\qquad A_1(\beta)=e_{z1}(\rho_0+c,\phi_0,\beta),$$
$$B_0(\beta)=e_{z0}(\rho_1+c,\phi_1,\beta),\qquad B_1(\beta)=e_{z1}(\rho_1+c,\phi_1,\beta)-Z_s.$$

Using Cramer's rule, $I'_0(\beta)$ can be written

$$I'_0(\beta)=[-B_1(\beta)\,\mathbf{P}\cdot\mathbf{e}_{t0}(\rho_a,\phi_a,\beta)+A_1(\beta)\,\mathbf{P}\cdot\mathbf{e}_{t1}(\rho_a,\phi_a,\beta)]\,[\Delta(\beta)]^{-1}, \quad (10)$$

where $\Delta(\beta)=A_0(\beta)B_1(\beta)-A_1(\beta)B_0(\beta)$.

A similar expression can be written for $I'_1(\beta)$. The zeros of $\Delta(\beta)$ are the characteristic values β_p of the waveguide modes that were examined previously.[4]

The wire current $I_0(z)$ is obtained by substituting Eq. (10) into Eq. (7) and converting the integral into the following residue series:

$$I_0(z)\approx i\sum_p[-B_1(\beta_p)\mathbf{P}\cdot\mathbf{e}_{t0}(\rho_a,\phi_a,\beta_p)+A_1(\beta_p)\mathbf{P}\cdot\mathbf{e}_{t1}(\rho_a,\phi_a,\beta_p)]\,[(d\Delta/d\beta)|_{\beta=\beta_p}]^{-1}\times\exp(-i\beta_p z), \quad (11)$$

where $I_m(\beta_p)<0$ and $|z|$ is sufficiently large that the heavily damped branch cut contribution can be ignored. At resonance, it is easy to see that

$$I'_1(\beta_p)/I'_0(\beta_p)=-B_0(\beta_p)/B_1(\beta_p). \quad (12)$$

Also, for sufficiently small c, $B_0(\beta)\approx A_1(\beta)$. Consequently, Eq. (11) can be rewritten in the following convenient form:

$$I_0(z)\approx-\operatorname{sgn}(z)i\sum_p\frac{B_1(\beta_p)}{(d\Delta/d\beta)|_{\beta=\beta_p}}\times\mathbf{P}\cdot\mathbf{e}_t(\rho_a,\phi_a,\beta_p)\exp(-i\beta_p|z|), \quad (13)$$

where

$$\mathbf{e}_t(\rho_a,\phi_a,\beta_p)=\mathbf{e}_{t0}(\rho_a,\phi_a,\beta_p)+\frac{I'_1(\beta_p)}{I'_0(\beta_p)}\mathbf{e}_{t1}(\rho_a,\phi_a,\beta_p).$$

Since $\mathbf{e}_t(\rho_a,\phi_a,\beta_p)$ can be considered the transverse modal field normalized to unity current in wire zero. Eq. (13) now contains the expected form of P dotted into the modal field. The denominator of Eq. (13) and the factor $B_1(\beta_p)$ have actually been computed in solutions of the mode equation $\Delta(\beta)=0$ by means of Newton's method for specific cases.[4] The behavior of $\mathbf{e}_t$ is considered in Sec. III.

III. TRANSVERSE FIELD VARIATIONS

The transverse electric field variation of a given mode is of interest in both the excitation problem as shown in Eq. (13) and the reception problem. For normalization purposes, let the current in wire zero be unity and the other current be $I'_1(\beta)$. For the monofilar mode, $I'_1(\beta_p)\approx 1$, and for the bifilar mode, $I'_1(\beta_p)\approx -1$. The exact values emerge from the solution of the mode equation.[4] All electric and magnetic field components can be derived from z components of electric and magnetic Hertz vectors, Π_z and Π_z^*. The transverse electric field required in Eq. (13) is

$$\mathbf{e}_t(\rho,\phi,\beta)=\hat{\rho}e_\rho(\rho,\phi,\beta)+\hat{\phi}e_\phi(\rho,\phi,\beta), \quad (14)$$

where

$$e_\rho=-\Gamma\frac{\partial\Pi_z}{\partial\rho}-\frac{i\omega\mu}{\rho}\frac{\partial\Pi_z^*}{\partial\phi}$$

and

$$e_\phi=-\frac{\Gamma}{\rho}\frac{\partial\Pi_z}{\partial\phi}+i\omega\mu\frac{\partial\Pi_z}{\partial\rho}.$$

Here we have let $\Gamma=i\beta$, and the z variation is $\exp(-\Gamma z)$. By substituting the known expressions[4] for Π_z and Π_z^* into Eq. (14) and carrying out the differentiations, the following expressions for e_ρ and e_ϕ are obtained in a form suitable for computation:

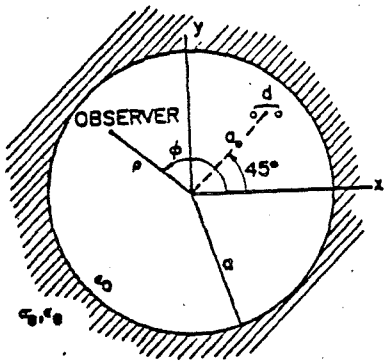


FIG. 2. Special geometry for a two-wire transmission line in a circular tunnel.

$$e_\rho = \frac{\eta_0}{2\pi}\left[\frac{\Gamma v}{\gamma}\left(\frac{\rho-\rho_0\cos(\phi-\phi_0)}{\rho_d}K_1(v\rho_d)\right.\right.$$
$$+I_1'(\beta)\frac{\rho-\rho_1\cos(\phi-\phi_1)}{\rho_d'}K_1(v\rho_d')\Big)$$
$$+\sum_{m=0}^{\infty}\left(\frac{\Gamma v}{\gamma}\epsilon_m R_m\frac{K_m(va)}{I_m(va)}I_m'(v\rho)+\frac{2i}{\rho}m\eta_0\Delta_m I_m(v\rho)\right)$$
$$\left.\times[I_m(v\rho_0)\cos m(\phi-\phi_0)+I_1'(\beta)I_m(v\rho_1)\cos m(\phi-\phi_1)]\right],$$
$$e_\phi = \frac{\eta_0}{2\pi}\left[\frac{\Gamma}{\gamma}\left(\frac{v\rho_0\sin(\phi-\phi_0)}{\rho_d}K_1(v\rho_d)\right.\right.$$
$$+I_1'(\beta)\frac{v\rho_1\sin(\phi-\phi_1)}{\rho_d'}K_1(v\rho_d')\Big)$$
$$-2\sum_{m=1}^{\infty}\left(\frac{\Gamma}{\gamma\rho}mR_m\frac{K_m(va)}{I_m(va)}I_m(v\rho)+vi\eta_0\Delta_m I_m'(v\rho)\right).$$
$$\left.\times[I_m(v\rho_0)\sin m(\phi-\phi_0)+I_1'(\beta)I_m(v\rho_1)\sin m(\phi-\phi_1)]\right] \quad (15)$$

where $\rho < a$,

$$\rho_d=[\rho^2+\rho_0^2-2\rho\rho_0\cos(\phi-\phi_0)]^{1/2},$$
$$\rho_d'=[\rho^2+\rho_1^2-2\rho\rho_1\cos(\phi-\phi_1)]^{1/2},$$
$$v=(\gamma^2-\Gamma^2)^{1/2},$$
$$\epsilon_m=1, \quad m=0$$
$$=2, \quad m\neq 0,$$

γ is the free-space propagation constant. a is the tunnel radius, η_0 is the characteristic impedance of free space, and I_m and K_m are modified Bessel functions of order m. The quantities R_m and Δ_m are determined from the tunnel boundary conditions and are given by[4]

$$R_m=\frac{\{(\gamma/v)K_m'(va)[K_m(va)]^{-1}\}+Y_m\eta_0+\delta_m\eta_0}{\{(\gamma/v)I_m'(va)[I_m(va)]^{-1}\}+Y_m\eta_0+\delta_m\eta_0},$$
$$\Delta_m=\left(\frac{K_m(va)}{I_m(va)}\frac{R_m-1}{\eta_0}\right)\frac{(im\Gamma/a)(v^{-2}-u^{-2})}{\{(\gamma/v)I_m'(va)[I_m(va)]^{-1}\}+Z_m/\eta_0}, \quad (16)$$

where

$$\delta_m\eta_0=\frac{(im\Gamma/a)^2(v^{-2}-u^{-2})^2}{\{(\gamma/v)I_m'(va)[I_m(va)]^{-1}\}+Z_m/\eta_0},$$

$$Z_m=-(i\omega\mu/u)K_m'(ua)[K_m(ua)]^{-1},$$
$$Y_m=(i\gamma_e^2/u\mu\omega)K_m'(ua)[K_m(u/a)]^{-1},$$
$$u=(\gamma_e^2-\Gamma^2)^{1/2},$$
$$\gamma_e^2=i\omega\mu(\sigma_e+i\omega\epsilon_e),$$

ω is the angular frequency, and σ_e and ϵ_e are the conductivity and permittivity of the surrounding rock. In the numerical evaluation of Eqs. (15) and (16), the required modified Bessel functions are quickly computed by recurrence (backward for I_m and forward for K_m).

In order to treat a specific numerical example, consider the special geometry of Fig. 2. Let x and y be the horizontal and vertical coordinates where a horizontal two-wire transmission line of wire spacing d is centered at $\rho=a_0$ and $\phi=45°$. The horizontal and vertical electric field components, e_x and e_y, at the observation point (ρ, ϕ) are given by

$$e_x=e_\rho\cos\phi-e_\phi\sin\phi,$$
$$e_y=e_\rho\sin\phi+e_\phi\cos\phi. \quad (17)$$

These rectangular components are the ones of interest when considering transmission or reception with horizontal or vertical dipoles. For convenience, we consider a case for which the propagation constants of the monofilar and bifilar modes have already been computed[4]: frequency = 20 MHz, $a=2$ m, $\epsilon_e/\epsilon_0=10$, $\sigma_e=10^{-2}$ mho/m, wire conductivity $\sigma_c=10^8$ mho/m, wire radius $c=10^{-3}$ m, $d=0.02$ m, and $a_0/a=0.8$. Solutions of this mode equation for this case yield for the monofilar mode:

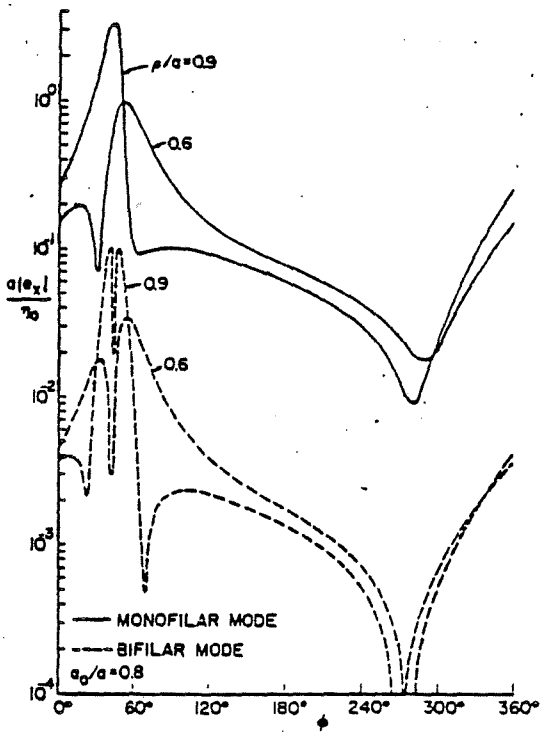


FIG. 3. Magnitude of the horizontal electrical field as a function of azimuth angle ϕ for both monofilar and bifilar modes.

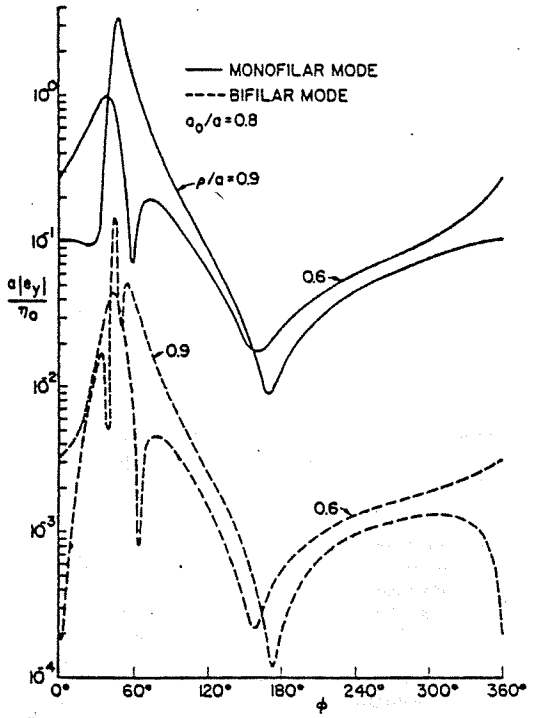


FIG. 4. Magnitude of the vertical electric field as a function of azimuth angle ϕ for both monofilar and bifilar modes.

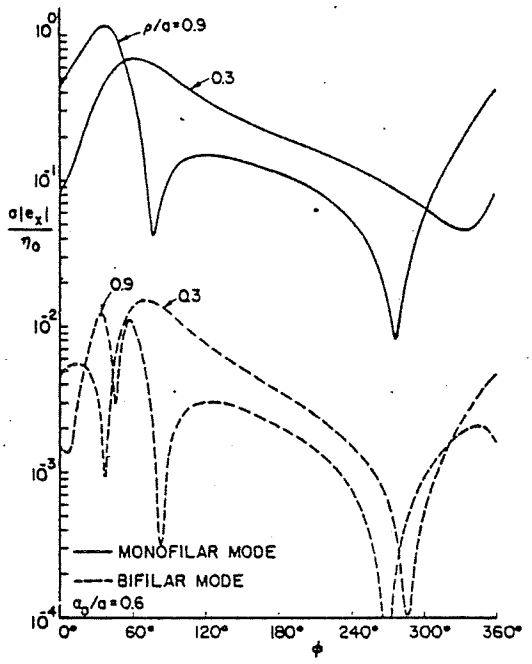


FIG. 5. Magnitude of the horizontal electric field as a function of azimuth angle ϕ for both monofilar and bifilar modes. The value of a_0/a has been decreased to 0.6.

$$\Gamma a = 5.478\times10^{-2} + i8.882\times10^{-1}, \qquad (18)$$

$$I_1/I_0 = 0.9189\angle -0.898°;$$

for the bifilar mode:

$$\Gamma a = 7.809\times10^{-3} + i8.547\times10^{-1},$$

$$I_1/I_0 = -1.0127\angle 0.264°.$$

Here we have designated the wire closest to the wall as wire zero. Note that the $R_e(\Gamma a)$, which proportional to the attenuation, is about seven times greater for the monofilar mode, and that the current ratios I_1/I_0 are close to ± 1 as expected. For the frequency and tunnel size considered here, only the monofilar and bifilar modes carry significant power since all other modes are "cut off".

Substitution of the numerical results of Eq. (18) into Eq. (15) yields the desired field quantities. In Fig. 3, the normalized horizontal field $a|e_x|/\eta_0$ is shown as a function of ϕ for $\rho/a=0.6$ and 0.9 for both modes, and in Fig. 4 the normalized vertical field $a|e_y|/\eta_0$ is shown for the same cases. The field variations are rather complicated in the vicinity of the transmission line ($\phi=45°$), but the important point is that field strength of the bifilar mode is generally down by a factor of about 100 from that of the monofilar mode throughout the tunnel.

In order to demonstrate that the above trends do not depend on the location of the transmission line, we consider a second example where the distance of the line from the wall is doubled, $a_0/a=0.6$. All other parameters are the same as above. Solution of the mode

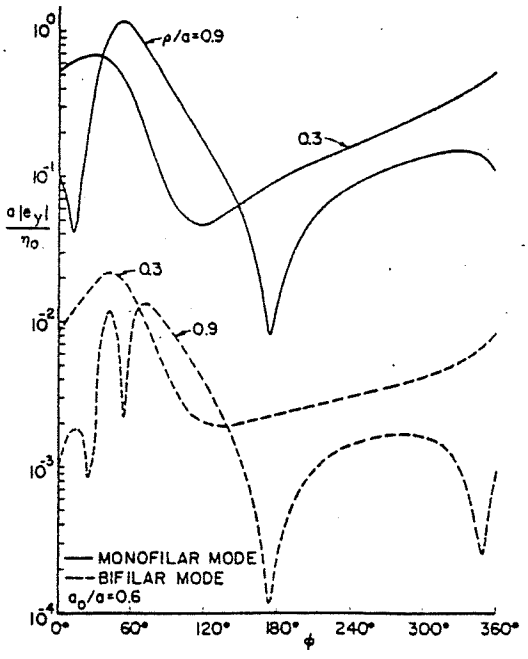


FIG. 6. Magnitude of the vertical electric field as a function of azimuth angle ϕ for both monofilar and bifilar modes. The value of a_0/a has been decreased to 0.6.

equation yields for the monofilar mode

$$\Gamma a = 3.505\times10^{-2} + i8.610\times10^{-1},$$
$$\text{and} \qquad I_1/I_0 = 0.9324\angle -0.810^\circ. \tag{19}$$

For the bifilar mode, Γa and I_1/I_0 are virtually unchanged from the previous values. In Figs. 5 and 6, the normalized horizontal and vertical electric fields are shown for $\rho/a = 0.3$ and 0.9. Again, the field strength of the bifilar mode is generally down by a factor of about 100 from that of the monofilar mode throughout the tunnel.

V. CONCLUDING REMARKS

We have examined the excitation of monofilar and bifilar modes on a two-wire transmission line in a circular tunnel. Although the circular tunnel model is highly idealized, previous attenuation calculations[4] have agreed quite closely with those of Mahmoud[3] for a rectangular tunnel with perfectly conducting side walls and with experimental data of Deryck[1] taken in actual mine tunnels.

The transverse field variations shown in Figs. 3 and 4 illustrate the expected result that the monofilar mode is much easier to excite or receive than the bifilar mode. Below about 50 MHz, these are the only modes which are not cut off. However, at higher frequencies (e.g., greater than about 50 MHz), there are perturbed empty tunnel modes which will propagate.

[1] L. Deryck, *Bulletin Technique "Mines et Carriers"*, *No.* 134 (Institut National des Industries Extractives, Belgium, 1971).
[2] P. Delogne, L. Deryck, and R. Liegeois, Proceedings of Thru-the-Earth Electromagnetics Workshop, edited by R. G. Geyer, pp. 49—53 (unpublished).
[3] S. F. Mahmoud (unpublished).
[4] J. R. Wait and D. A. Hill, Preliminary Report to U. S. Bureau of Mines, 1974 (unpublished).
[5] J. Fontaine, B. Demoulin, P. Degauque, and R. Gabillard, Proceedings of Thru-the-Earth Electromagnetics Workshop, edited by R. G. Geyer, pp. 130—139, (unpublished); Final Report on U. S. Bureau of Mines Contract No. G133023, 1973 (unpublished), available from N. T. I. S., Springfield, Va.
[6] S. F. Mahmoud (unpublished).
[7] J. R. Wait, *Electromagnetic Waves in Stratified Media*, 2nd. ed. (Pergamon, Oxford, England, 1970).
[8] J. Galejs, *Terrestrial Propagation of Long Electromagnetic Waves* (Pergamon, Oxford, England, 1972).
[9] G. D. Monteath, *Applications of the Electromagnetic Reciprocity Principle* (Pergamon, Oxford, England, 1973).
[10] S. A. Schelkunoff, *Electromagnetic Waves* (Van Nostrand, New York, 1943), 260—266.
[11] J. R. Wait, *Electromagnetic Radiation from Cylindrical Structure* (Pergamon, Oxford, England, 1959), pp. 142—148.

Gap excitation of an axial conductor in a circular tunnel

David A. Hill and James R. Wait

Institute for Telecommunication Sciences, Office of Telecommunications, U. S. Department of Commerce, Boulder, Colorado 80302

(Received 13 May 1974; in final form 25 July 1974)

We consider the excitation of modes on an axial conductor in a circular tunnel by a circumferential gap. Numerical results are presented for the power into the monofilar mode and the attenuation of the mode. The power delivered to the monofilar mode increases as the conductor approaches the tunnel wall, but the attenuation also increases. The results have application to systems which use coaxial cables for long-distance communication in mine tunnels.

I. INTRODUCTION

In order to communicate for long distances along mine tunnels and haulageways, it has been found advantageous to utilize a two-conductor transmission line which will support two types of dominant modes,[1] monofilar and bifilar. In the monofilar mode, the forward current is carried by the transmission line and the return current is carried by the tunnel walls. In the bifilar mode, the return current is carried by the second conductor. The monofilar mode has the advantage that it is readily excited (or received) by an antenna located in the tunnel, but also the disadvantage of higher attenuation due to loss in the surrounding rock. A key step in practical systems is the conversion from the monofilar or symmetrical mode to the bifilar or asymmetrical mode.

The actual transmission line can be either a two-wire line, as in the INIEX/Deryck[2] system, or a coaxial cable. The attenuation and excitation of the modes on a two-wire line have been studied both analytically[3,4] and experimentally.[2] When the transmission line is a coaxial cable, the bifilar mode propagates between the inner and outer conductors, and the monofilar mode propagates between the outer conductor and the tunnel walls. Mode conversion is accomplished either discretely by spaced slots as in the INIEX/Delogne system[1] or continuously through a loosely braided outer conductor.[5] Here we examine the excitation of a circular conductor by a circumferential voltage source. As far as the external fields are concerned the conductor itself appears to be solid metal.

In what follows, all field quantities vary harmonically with time according to the time factor $\exp(i\omega t)$, where ω is the angular frequency.

II. FORMULATION

A circular conductor of radius c_s is located within a circular tunnel as shown in Fig. 1. Since the conductor radius is assumed small compared to both a wavelength and the tunnel radius a, the primary fields[6] of the conductor current can be determined from the z component of a Hertz vector Π^p:

$$\Pi^p = \int_{-\infty}^{\infty} F(\lambda) K_0(v\rho_d) \exp(-i\lambda z)\, d\lambda \qquad (1)$$

$$= \int_{-\infty}^{\infty} F(\lambda) \sum_{m=-\infty}^{\infty} I_m(v\rho_0) K_m(v\rho) \exp[-im(\phi-\phi_0)] \times \exp(-i\lambda z)\, d\lambda \quad (\rho > \rho_0),$$

where $\rho_d = [\rho^2 + \rho_0^2 - 2\rho\rho_0\cos(\phi-\phi_0)]^{1/2}$, $v = (\lambda^2 - k^2)^{1/2}$, k is the free-space wave number, I_m and K_m are modified Bessel functions of order m, and $F(\lambda)$ is unknown at this point. For $\rho < \rho_0$, ρ and ρ_0 are interchanged. The boundary conditions at the tunnel wall ($\rho = a$) are that the tangential fields (E_z, E_ϕ, H_z, H_ϕ) are continuous. Consequently, the total fields in the tunnel can be derived from the following z components of the electric and magnetic Hertz vectors,[4,7] Π and Π^m:

$$\Pi = \int_{-\infty}^{\infty} F(\lambda) \sum_m I_m(v\rho_0)\left(K_m(v\rho) - R_m(\lambda)\frac{K_m(va)}{I_m(va)} I_m(v\rho)\right) \times \exp[-im(\phi-\phi_0)] \exp(-i\lambda z)\, d\lambda, \qquad (2)$$

$$\Pi^m = \int_{-\infty}^{\infty} F(\lambda) \sum_m \Delta_m(\lambda)\, I_m(v\rho_0)\, I_m(v\rho) \exp[-im(\phi-\phi_0)] \times \exp(-i\lambda z)\, d\lambda,$$

where

$$R_m(\lambda) = \frac{(ik/v)K_m'(va)[K_m(va)]^{-1} + Y_m\eta_0 + \delta_m\eta_0}{(ik/v)I_m'(va)[I_m(va)]^{-1} + Y_m\eta_0 + \delta_m\eta_0},$$

$$\Delta_m(\lambda) = [1 - R_m(\lambda)]\frac{K_m(va)}{I_m(va)} \frac{(m\lambda/a)(v^{-2} - u^{-2})\eta_0^{-1}}{(ik/v)I_m'(va)[I_m(va)]^{-1} + Z_m/\eta_0},$$

$$\delta_m\eta_0 = \frac{(m\lambda/a)^2(v^{-2} - u^{-2})^2}{(ik/v)I_m'(va)[I_m(va)]^{-1} + Z_m/\eta_0},$$

$$Z_m = -(i\omega\mu_0/u)K_m'(ua)[K_m(ua)]^{-1},$$

$$Y_m = (k_e^2/i\omega\mu_0 u)K_m'(ua)[K_m(ua)]^{-1},$$

$$u = (\lambda^2 - k_e^2)^{1/2}, \quad \text{and} \quad k_e^2 = -i\omega\mu_0(\sigma_e + i\omega\epsilon_e).$$

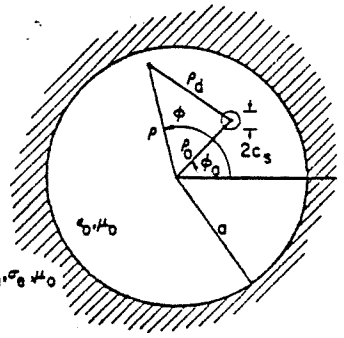


FIG. 1. Geometry for an axial conductor in a circular tunnel. The conductor is excited by a gap at $z = 0$.

The conductor is excited by a gap of width $2d$ centered at $z=0$. In the gap, the electric field E_z is approximately given by $V/2d$, where V is the gap voltage. In order to determine $F(\lambda)$ in Eq. (2), we assume that E_z and the conductor current $I(z)$ satisfy the following impedance relationship for all z:

$$E_z=(V/2d)\,p_d(z)+Z_s I(z) \quad \text{at } \rho_d=c_s, \tag{3}$$

where

$$p_d(z)=1, \quad |z|<d$$
$$=0, \quad |z|>d.$$

Z_s is the series impedance per unit length which is explicitly given by[6]

$$Z_s=\frac{\eta_s}{2\pi c_s}\frac{I_0(ik_s c_s)}{I_1(ik_s c_s)}, \tag{4}$$

where $k_s^2=-i\omega\mu_0(\sigma_s+i\omega\epsilon_s)$, $\eta_s=\omega\mu_0/k_s$, and σ_s and ϵ_s are the conductivity and permittivity of the axial conductor. The following expression for E_z at the match point $(\phi=\phi_0, \rho=\rho_0+c_s)$ can be derived from Eq. (2):

$$E_{z|_{\substack{\rho=\rho_0+c_s\\ \phi=\phi_0}}}=\left(k^2+\frac{\partial^2}{\partial z^2}\right)\Pi_{|_{\substack{\rho=\rho_0+c_s\\ \phi=\phi_0}}}$$
$$=-\int_{-\infty}^{\infty} v^2 F(\lambda)\exp(-i\lambda z)\left(K_0(vc_s)-\sum_m R_m(\lambda)\right. \tag{5}$$
$$\left.\times\frac{K_m(va)}{I_m(va)}I_m(v\rho_0)\,I_m[v(\rho_0+c_s)]\right)d\lambda.$$

The current $I(z)$ can be determined approximately by examining the azimuthal magnetic field H_ϕ around the conductor. Thus

$$I(z)\simeq 2\pi c_s H_\phi\simeq 2\pi c_s\frac{k^2}{i\omega\mu_0}\frac{\partial\Pi}{\partial\rho_d}\bigg|_{\rho_d=c_s}$$
$$=-2\pi c_s\frac{k^2}{i\omega\mu_0}\int_{-\infty}^{\infty} vF(\lambda)K_1(vc_s)\exp(-i\lambda z)\,d\lambda. \tag{6}$$

Since vc_s is small, Eq. (6) reduces to

$$I(z)=\frac{-2\pi k^2}{i\omega\mu_0}\int_{-\infty}^{\infty}F(\lambda)\exp(-i\lambda z)\,d\lambda. \tag{7}$$

The following expansion for the source function in Eq. (3) is also useful:

$$\frac{V}{2d}p_d(z)=\frac{V}{2\pi}\int_{-\infty}^{\infty}\frac{\sin(\lambda d)}{\lambda d}\exp(-i\lambda z)\,d\lambda. \tag{8}$$

By substituting Eqs. (5), (7), and (8) into Eq. (3), we can solve for $F(\lambda)$:

$$F(\lambda)=\frac{-V}{2\pi D(\lambda)}\frac{\sin(\lambda d)}{\lambda d}, \tag{9}$$

where

$$D(\lambda)=v^2\left(K_0(vc_s)-\sum_m R_m(\lambda)\frac{K_m(va)}{I_m(va)}I_m(v\rho_0)I_m[v(\rho_0+c_s)]\right)$$
$$+\frac{2\pi ik}{\eta_0}Z_s.$$

The zeros of $D(\lambda)$ are the characteristic values of the waveguide modes λ_s which have been examined previously.[7] There is also a branch point at $\lambda=k_e$, but the branch cut contribution corresponds to lateral waves in the lossy external medium and is heavily damped. Consequently, the branch cut contribution can be neglected for most applications (sufficiently large $|z|$). In evaluating the λ integrations in Eq. (2) by the residue theorem, it is necessary to close the contour in the lower half-plane for positive z and in the upper half-plane for negative z with the following results:

$$\Pi=iV\sum_s\frac{\sin(\lambda_s d)}{\lambda_s d}\frac{\exp(-i\lambda_s|z|)}{D'(\lambda_s)}$$
$$\times\sum_m\exp[-im(\phi-\phi_0)]I_m(v_s\rho_0)$$
$$\times\left(K_m(v_s\rho)-R_m(\lambda_s)\frac{K_m(v_s a)}{I_m(v_s a)}I_m(v_s\rho)\right), \tag{10}$$

$$\Pi^m=iV\,\mathrm{sgn}(z)\sum_s\frac{\sin(\lambda_s d)}{\lambda_s d}\frac{\exp(-i\lambda_s|z|)}{D'(\lambda_s)}$$
$$\times\sum_m\exp[-im(\phi-\phi_0)]\,\Delta_m(\lambda_s)I_m(v_s\rho_0)I_m(v_s\rho),$$

where $v_s^2=\lambda_s^2-k^2$,

$$\mathrm{sgn}(z)=+1, \quad z>0,$$
$$=-1, \quad z<0,$$

and the branch cut contribution has been neglected. The actual field components are given by

$$E_z=\left(k^2+\frac{\partial^2}{\partial z^2}\right)\Pi, \quad H_z=\left(k^2+\frac{\partial^2}{\partial z^2}\right)\Pi^m,$$
$$E_\rho=\frac{\partial^2\Pi}{\partial z\,\partial\rho}-\frac{i\omega\mu_0}{\rho}\frac{\partial\Pi^m}{\partial\phi},$$
$$H_\rho=\frac{i\omega\epsilon_0}{\rho}\frac{\partial\Pi}{\partial\phi}+\frac{\partial^2\Pi^m}{\partial z\,\partial\rho}, \tag{11}$$
$$E_\phi=\frac{1}{\rho}\frac{\partial^2\Pi}{\partial z\,\partial\phi}+i\omega\mu_0\frac{\partial\Pi^m}{\partial\rho},$$
$$H_\phi=-i\omega\epsilon_0\frac{\partial\Pi}{\partial\rho}+\frac{1}{\rho}\frac{\partial^2\Pi^m}{\partial z\,\partial\phi}.$$

III. CALCULATION OF POWER

In order to judge the effectiveness of the modal excitation, it is useful to calculate the power which is supplied to the waveguide modes by the source gap. The total power supplied to the tunnel is most easily determined by integrating the Poynting vector over the entire axial conductor and tunnel wall surfaces. The ρ component of the Poynting vector S_ρ at the tunnel wall $(\rho=a)$ is given by

$$S_\rho=(E_\phi H_z^*-E_z H_\phi^*)\big|_{\rho=a}, \tag{12}$$

where $*$ denotes complex conjugate and the usual factor of $\frac{1}{2}$ is omitted because rms values are assumed for the field quantities. The normal component of the Poynting vector S_ρ at the conductor surface is approximately given by

$$S_\rho\simeq-(E_z H_\phi^*)\big|_{\rho=c_s}=-(Z_s/2\pi c_s)\,I(z)\,I^*(z). \tag{13}$$

From Eqs. (7) and (9) and the residue theorem, $I(z)$ is

$$I(z)=\frac{2\pi kV}{\eta_0}\sum_s\frac{\sin(\lambda_s d)}{\lambda_s d}\frac{\exp(-i\lambda_s|z|)}{D'(\lambda_s)}. \tag{14}$$

The total power P is given by

$$P=P_t+P_w, \tag{15}$$

$$P_w = -4\pi c_s \int_d^{\infty} \mathrm{Re}(S_\rho)\, dz,$$

Re indicates the real part, and the evenness of S_ϕ and S_ρ in z has been utilized. The azimuthal symmetry of S_ρ in ϕ' has also been used in P_w. To simplify the following numerical results, it is useful to set d equal to zero. The singularity in the susceptance due to a delta-gap source is well known in linear antenna theory,[8] but the delta gap presents no problem in the calculation of real power here.

When the actual field expressions are substituted into Eq. (15), the ϕ and z integrations are easily performed because only exponentials are involved. The resultant forms for P_t and P_w are

$$P_t = \frac{-4\pi V^2}{\eta_0} \mathrm{Re} \sum_s \sum_p \frac{1}{D'(\lambda_s) D'(\lambda_p)^* i(\lambda_s - \lambda_p^*)} \tag{16}$$
$$\times \sum_m I_m(v_s\rho_0)\, I_m(v_p\rho_0)^* \Big\{ [v_p^2 \eta_0 \Delta_m(\lambda_p)\, I_m(v_p a)]^*$$
$$\times \{ m\lambda_s K_m(v_s a)[1 - R_m(\lambda_s)] + ikav_s \eta_0 \Delta_m(\lambda_s) I_m'(v_s a) \}$$
$$+ \Big[m\lambda_p \eta_0 \Delta_m(\lambda_p)\, I_m(v_p a) + ikav_p \Big(K_m'(v_p a) - R_m(\lambda_p) \cdot$$
$$\times \frac{K_m(v_p a)}{I_m(v_p a)} I_m'(v_p a) \Big) \Big]^* \{ v_s^2 K_m(v_s a)[1 - R_m(\lambda_s)] \} \Big\}$$

and

$$P_w = \frac{2V^2}{\eta_0} (2\pi k)^2 \mathrm{Re}\left(\frac{Z_s}{\eta_0} \sum_s \sum_p \frac{1}{D'(\lambda_s) D'(\lambda_p)^* i(\lambda_s - \lambda_p^*)} \right).$$

In a lossless waveguide, the modes are orthogonal and the cross terms in the summation ($s \neq p$) have no contribution. However, for the lossy waveguide case,[9] this is not necessarily true.

If only the total power P is desired, it can be derived in a simpler manner by integrating the Poynting vector over the source gap. For $d = 0$, this is equivalent to multiplying the real part of the current at $z = 0$ by V.

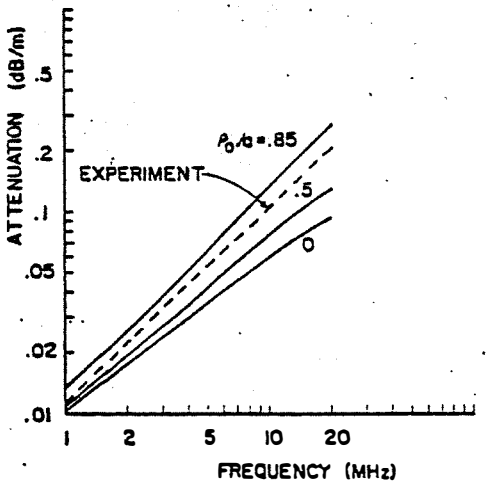


FIG. 2. Attenuation of the monofilar mode as a function of frequency for three conductor locations. The experimental curve corresponds to $\rho_0/a = 0.85$.

Strictly speaking, Eq. (14) is not valid in the gap ($|z| < d$), but the same result for P in Eq. (17) can be obtained by rigorously integrating the Poynting vector over the gap and letting d approach zero.[10]

We now consider a numerical example which is applicable to the use of a coaxial cable in a mine tunnel. The following tunnel parameters are assumed: $a = 2m$, $\epsilon_s/\epsilon_0 = 10$, and $\sigma_s = 10^{-2}$ mho/m. The conductor parameters are $\sigma_s = 10^5$ mho/m and $c_s = 0.35$ cm, where c_s is a fairly standard value.[5] The frequency range of interest[1,5] is roughly 1–20 MHz. In this frequency range, the perturbed empty tunnel modes are essentially "cut off" and can be neglected. However, at frequencies above about 50 MHz they can be important and their attenuation has been studied.[11] The first step is the numerical solution for the characteristic value of the monofilar mode, λ_1, from the equation $D(\lambda) = 0$. Newton's method has been used to solve this equation with the advantage that the solution automatically yields $D'(\lambda_1)$ which is needed in Eq. (16). The attenuation α_1 is given by

$$\alpha_1 = 8.686\, \mathrm{Im}(-\lambda_1) \quad (dB/\mathrm{m}), \tag{18}$$

where Im refers to the imaginary part. The attenuation as a function of frequency is plotted for three values of ρ_0/a in Fig. 2. Also plotted is an empirical curve for α_1 which is derived from coal mine measurements.[5] The tunnel shape was different, but the separation between the conductor and the wall was 0.3 m which corresponds to the $\rho_0/a = 0.85$ curve. Considering the uncertainties in the parameters, the agreement is quite good. The increase in attenuation with increasing frequency and decreasing wall conductor separation has been noted both experimentally[2] and theoretically.[7,12]

The preceding values of λ_1 and $D'(\lambda_1)$ can be used to calculate the power into the monofilar mode as given by Eq. (16) with only the $s = p = 1$ term included or by Eq. (17) with only the $s = 1$ term included. Higher-order modes should be negligible because they have large negative imaginary parts of λ_s. The normalized power is shown in Fig. 3 for the same parameters as used in Fig. 2. It is interesting that there is a slight local maximum at about 7 MHz which was determined by a different analysis to be the optimum frequency in the braided coaxial cable system.[5] The total power and the power into the conductor are shown as a function of ρ_0/a for 7 MHz in Fig. 4. As expected, the power lost in the conductor P_w is a small fraction of either the total power P or the power lost through the tunnel walls P_t. The attenuation is also shown and is seen to increase as ρ_0/a increases.

IV. CONCLUDING REMARKS

We have examined the gap excitation of modes on an axial conductor in a circular tunnel and given numerical results for the monofilar mode. For the range of frequencies and parameters of interest in mine communications, the power into the monofilar mode is increased as the conductor approaches the wall, but the attenuation also increases. Although the circular tunnel is

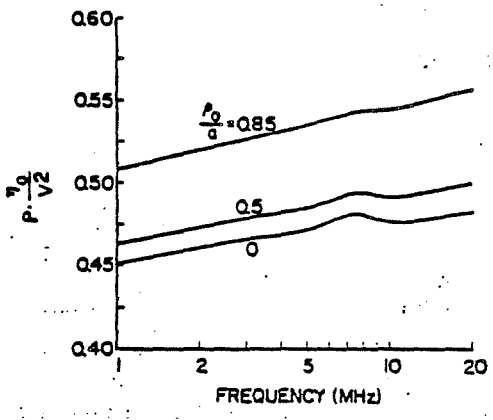


FIG. 3. Power supplied to the monofilar mode as a function of frequency for three conductor locations.

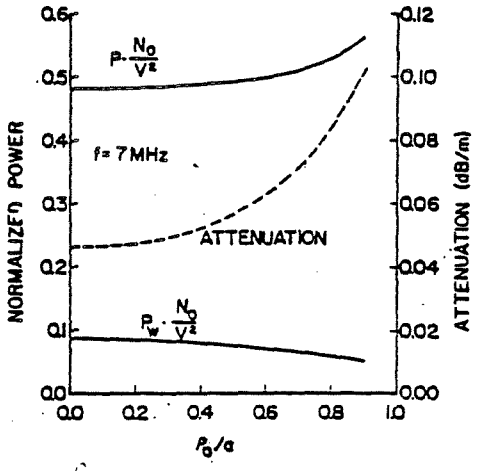


FIG. 4. Total power P supplied to the monofilar mode as a function of conductor position at 7 MHz. The power lost in the conductor P_w and the mode attenuation are also shown.

highly idealized, attenuation results[3,7] have shown good agreement with theory for a rectangular tunnel[12] and with experimental data taken in actual mine tunnels.[1]

The results here have application to coaxial cable systems for both discrete slot excitation and continuous excitation as through a leaky outer braid. However, a useful extension would be to solve a more complicated modal equation including directly the effects of the dielectric filler, the braid, and the jacket of the cable.

In this paper we have not considered the effect of the higher-order modes in the tunnel. A numerical evaluation of Eq. (17) for all integer values of s is needed to specify the *total* power supplied by the gap in the outer conductor of the coaxial cable. Also, for a complete systems design, we need to analyze the coupling of all the modes *inside* the coaxial conductor with all the modes in the tunnel region. These tasks are now occupying our serious attention.

ACKNOWLEDGMENT

The authors wish to thank Professor Paul Delogne for suggesting the simpler alternative method of calculating the power.

[1]P. Delogne, L. Deryck, and R. Liegeois, *Proceedings of Thru-the-Earth Electromagnetics Workshop*, edited by R.G. Geyer (N.T.I.S., Springfield, Va., 1973), pp. 49—53.
[2]L. Deryck, *Bulletin Technique "Mines et Carriers"*, *No.* 134 (Institut National des Industries Extractives, Belgium, 1971).
[3]J.R. Wait and D.A. Hill, J. Appl. Phys. (to be published).
[4]D.A. Hill and J.R. Wait, J. Appl. Phys. 45, 3402 (1974).
[5]J. Fontaine, B. Demoulin, P. Degnuque, and R. Gabillard, in Ref. 1, pp. 130—139.
[6]J.R. Wait, *Electromagnetic Radiation from Cylindrical Structures* (Pergamon, New York, 1959), pp. 142—148.
[7]J.R. Wait and D.A. Hill, IEEE Trans. Antennas Propag. 22, 627 (1974).
[8]T.T. Wu and R.W.P. King, J. Appl. Phys. 30, 74 (1959).
[9]J. Van Bladel, *Electromagnetic Fields* (McGraw-Hill, New York, 1964), pp. 304—306.
[10]Paul Delogne (private communication).
[11]D.A. Hill and J.R. Wait, IEEE AP-S International Symposium, Atlanta, 1974 (unpublished).
[12]S.F. Mahmoud (unpublished).

Electromagnetic fields of a coaxial cable with an interrupted shield located in a circular tunnel

David A. Hill

Institute for Telecommunication Sciences, Office of Telecommunications, U.S. Department of Commerce, Boulder, Colorado 80302

James R. Wait*

Cooperative Institute for Research in Enviromental Sciences, University of Colorado/NOAA, Boulder, Colorado 80302
(Received 5 May 1975)

An expression for the gap admittance of a coaxial cable within a circular tunnel is derived using a quasistatic method. Coupling between the TEM mode within the cable and the monofilar mode within the tunnel is computed, and 25% of the cable power is typically transferred to the tunnel from a single cable gap. The results have application to the use of leaky coaxial cables for communication in mine tunnels.

PACS numbers: 84.40.N

I. INTRODUCTION

One method of communication along mine tunnels utilizes a two-conductor transmission line which will support two dominant modes designated as monofilar and bifilar.[1] If the transmission line is an ideal coaxial cable, the bifilar mode is simply the TEM mode within the cable. In the monofilar mode, the forward current is carried by the cable shield and the return current is carried by the tunnel walls. The monofilar mode is readily excited or recieved by an antenna in the tunnel, but suffers from higher attenuation due to loss in the surrounding rock.[2] The INIEX/Delogne system[3] utilizes a circumferential gap in the cable shield to achieve conversion between the two modes.

In order to gain a quantitative understanding of this mode conversion, we examine such a coaxial cable in an idealized circular tunnel. The fields external to the cable for this geometry have been analyzed previously.[4] Here we consider the complete problem of coupling from a TEM mode inside the cable to the modes in the tunnel, particularly the monofilar mode. This situation is illustrated in Fig. 1 and is described in more detail below.

The gap voltage and field distribution are not assumed, but are determined from a quasistatic method similar to that employed by Chang[5] and Hurd[6] in a free-space analysis. The final result of our analysis is an efficiency factor for the coupling between the TEM cable mode and the monofilar mode. This is an essential parameter in the design of such systems for communications.

II. GAP ADMITTANCE

We first derive an expression for the gap voltage when a TEM wave within the coaxial cable is incident upon the gap. The cable geometry is shown in Fig. 1 with respect to a cylindrical coordinate system (ρ, ϕ, z). The solid inner conductor of radius a and the shield of radius b and of negligible thickness are assumed to be perfect conductors. The insulation $(a < \rho < b)$ has permittivity ϵ. A circumferential gap in the shield is centered at $z = 0$. The circular tunnel of radius a' is also shown in Fig. 1 with respect to a tunnel-centered cylindrical coordinate system (ρ', ϕ', z). The tunnel region for $\rho' < a'$ and $\rho > b$ is characterized by zero conductivity and free-space permittivity ϵ_0, and the external region $\rho' > a'$ is characterized by conductivity σ_e and permittivity ϵ_e. Free-space permeability μ_0 is assumed everywhere. Finally, we note that the axis of the coaxial cable is located at ρ_0, ϕ_0.

We first consider the fields in the tunnel $(\rho' < a')$, but external to the cable $(\rho > b)$. If the cable radius is small compared with a wavelength and the tunnel radius,

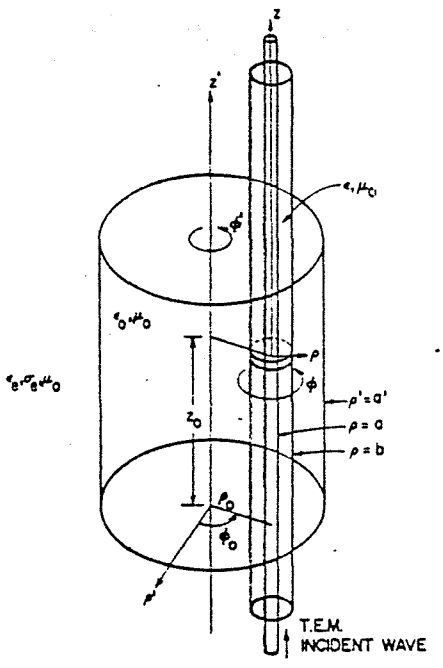


FIG. 1. Coaxial cable with an interrupted shield contained within a circular tunnel. A TEM incident wave is propagating in the positive z direction. (Note drawing is not to scale since b is much smaller than a'.) Gap is located at $z = 0$ or $z' = z_0$.

the primary fields can be derived from the following electric Hertz vector that has only a z component Π_p,

$$\Pi_p = \int_{-\infty} F(\lambda) K_0(v\rho) \exp(-i\lambda z)\, d\lambda, \tag{1}$$

where $v = (\lambda^2 - k_0^2)^{1/2}$, $k_0 = \omega(\mu_0\epsilon_0)^{1/2}$, K_0 is a modified Bessel function of zero order, and $F(\lambda)$ is unknown at this point. The time variation of all field quantities is $\exp(i\omega t)$, where ω is the angular frequency. The secondary fields are determined by applying the boundary conditions that the tangential electric and magnetic fields $(E_{z'}, E_{\phi'}, H_{z'}, H_{\phi'})$ are continuous at the tunnel wall ($\rho' = a'$). As indicated before,[4] the total fields in the tunnel region can be obtained from electric and magnetic Hertz vectors that have only z components Π_e and Π_m. These are given explicitly by

$$\Pi_e = \int_{-\infty} F(\lambda)\{K_0(v\rho) - \textstyle\sum_m R_m(\lambda)[K_m(va')/I_m(va')] \times I_m(v\rho_0) I_m(v\rho') \exp[-im(\phi' - \phi_0)]\} \exp(-i\lambda z)\, d\lambda, \tag{2}$$

$$\Pi_m = \int_{-\infty} F(\lambda) \textstyle\sum_m \Delta_m(\lambda) I_m(v\rho_0) I_m(v\rho') \times \exp[-im(\phi' - \phi_0)] \exp(-i\lambda z)\, d\lambda,$$

where

$$R_m = \frac{(ik_e/v)K_m'(va')/K_m(va') + Y_m\eta_0 + \delta_m\eta_0}{(ik_e/v)I_m'(va')/I_m(va') + Y_m\eta_0 + \delta_m\eta_0},$$

$$\delta_m\eta_0 = \frac{(m\lambda/a')^2(v^{-2} - u^{-2})^2}{[(ik_e/v)I_m'(va')/I_m(va')] + Z_m/\eta_0},$$

$$Z_m = \frac{-(i\omega\mu_0/u)K_m'(ua')}{K_m(ua')},$$

$$Y_m = \frac{(k_e^2/i\omega\mu_0 u)K_m'(ua')}{K_m(ua')},$$

$u = (\lambda^2 - k_e^2)^{1/2}$, $k_e^2 = -i\omega\mu_0(\sigma_e + i\omega\epsilon_e)$, $\eta_0 = (\mu_0/\epsilon_0)^{1/2}$, I_m and K_m are modified Bessel functions of order m, and the summations on m run over integers from $-\infty$ to ∞. The explicit expression for $\Delta_m(\lambda)$ has been given previously[4] but is not required here.

In order to derive the desired Green's function, we consider first a delta gap at $z = 0$. The axial electric field E_z at $\rho = b$ is thus given by

$$E_z\big|_{\rho=b} = V\delta(z) = (V/2\pi)\int_{-\infty} \exp(-i\lambda z)\, d\lambda, \tag{3}$$

where V is the delta gap voltage and the second expression is the integral representation of a delta function. We can also determine E_z by operating on Π_e and evaluating the expression at an equivalent point, $\phi' = \phi_0$ and $\rho' = \rho_0 + b$. Thus

$$E_z\Big|_{\substack{\rho'=\rho_0+b \\ \phi'=\phi_0}} = \left(k_0^2 + \frac{\partial^2}{\partial z^2}\right)\Pi_e\Big|_{\substack{\rho'=\rho_0+b \\ \phi'=\phi_0}} = -\int_{-\infty} F(\lambda) D(\lambda) \exp(-i\lambda z)\, d\lambda, \tag{4}$$

where

$$D(\lambda) = v^2\{K_0(vb) - \textstyle\sum_m R_m(\lambda)[K_m(va')/I_m(va')] \times I_m(v\rho_0) I_m[v(\rho_0 + b)]\}.$$

By equating (3) and (4), $F(\lambda)$ is found to be

$$F(\lambda) = -V/2\pi D(\lambda). \tag{5}$$

The azimuthal magnetic field in the unprimed space H_ϕ is given by

$$H_\phi = -i\omega\epsilon_0 \frac{\partial \Pi_e}{\partial \rho} + \frac{1}{\rho}\frac{\partial^2 \Pi_m}{\partial z\, \partial \phi}. \tag{6}$$

Now it is convenient to define an average magnetic field evaluated at $\rho = b$:

$$\bar{H}_\phi = (2\pi)^{-1}\int_0^{2\pi} H_\phi\big|_{\rho=b}\, d\phi. \tag{7}$$

Then $\bar{H}_\phi$ is approximately given by

$$\bar{H}_\phi = -i\omega\epsilon_0 \frac{\partial \Pi_e}{\partial \rho}\Big|_{\rho=b} = i\omega\epsilon_0 \int_{-\infty} vF(\lambda) K_1(vb) \exp(-i\lambda z)\, d\lambda, \tag{8}$$

bearing in mind that b is small compared with the wavelength. By introducing Hankel functions of the second kind $H_0^{(2)}$ and $H_1^{(2)}$ and using (4) and (5), $\bar{H}_\phi$ in (8) can be rewritten

$$\bar{H}_\phi = \frac{i\omega\epsilon_0 V}{2\pi}\int_{-\infty} \frac{H_1^{(2)}(\beta b)\exp(-i\lambda z)}{\beta[H_0^{(2)}(\beta b) + \Lambda(\lambda)]}\, d\lambda, \tag{9}$$

where

$$\Lambda(\lambda) = \frac{2}{\pi i}\sum_m R_m(\lambda)\frac{K_m(va')}{I_m(va')} I_m(v\rho_0) I_m[v(\rho_0 + b)],$$

$$\beta = -iv = (k_0^2 - \lambda^2)^{1/2}.$$

We now consider a finite gap of width δ centered at $z = 0$ with a voltage V and an electric field distribution $\hat{f}(z)$. The field distribution is normalized such that

$$\int_{-\delta/2}^{\delta/2} \hat{f}(z)\, dz = 1. \tag{10}$$

From (9), it is seen that the external field $\bar{H}_\phi$ can now be written as an integral of a Green's function over the gap

$$\bar{H}_\phi = (V/2\pi\delta)\int_{-\delta/2}^{\delta/2} \hat{f}(z') G_0(b, z, z')\, dz, \tag{11}$$

where

$$G_0(b, z, z') = i\omega\epsilon_0 \int_{-\infty} \frac{H_1^{(2)}(\beta b)\exp(-i\lambda|z - z'|)}{\beta[H_0^{(2)}(\beta b) + \Lambda(\lambda)]}\, d\lambda.$$

The internal magnetic field at the gap ($\rho = b^-$) can be written as the sum of an incident TEM mode and an integral over the gap:

$$\bar{H}_\phi = \frac{I_0}{2\pi b}\exp(-ikz) + \frac{V}{2\pi\delta}\int_{-\delta/2}^{\delta/2} \hat{f}(z') G(b, z, z')\, dz', \tag{12}$$

where $k = \omega(\mu_0\epsilon)^{1/2}$, $I_0 = 2\pi b h_0$, h_0 is the incident magnetic field at the center of the gap, and $G(b, z, z')$ has been given previously.[7] By equating (11) and (12), we obtain the following integral equation for $\hat{f}(z')$:

$$\frac{I_0}{2\pi b}\exp(-ikz) - \frac{V}{2\pi\delta}\int_{-\delta/2}^{\delta/2} \hat{f}(z')[G_0(b, z, z') - G(b, z, z')]\, dz' = 0. \tag{13}$$

This integral equation is of the same form as that obtained by Chang[5] and Hurd[6] and by Wait and Hill[7,8] for a coated cable. However, $G_0(b, z, z')$, as given by (11) is considerably more complicated because it includes the effect of the tunnel boundary.

In order to solve (13), we employ a quasistatic method which assumes that δ is small compared to a wavelength. Some of the details are omitted because the procedure is the same as that employed for the coated cable in free space.[8] As it turns out, $G_0(b, z, z')$ can be approximated

in the following manner:

$$G_0(b,z,z') = i\omega\epsilon_0\left[\int_{-\infty}^{\infty}\frac{1}{\beta}\left(\frac{H_1^{(2)}(\beta b)}{H_0^{(2)}(\beta b)+\Lambda(\lambda)}-i\right)\exp(-i\lambda|z-z'|)\,d\lambda + i\int_{-\infty}^{\infty}\frac{1}{\beta}\exp(-i\lambda|z-z'|)\,d\lambda\right] \quad (14)$$

$$\approx i\omega\epsilon_0\left[\int_0^{\infty}\frac{2}{\beta}\left(\frac{H_1^{(2)}(\beta b)}{H_0^{(2)}(\beta b)+\Lambda(\lambda)}\right)d\lambda - 2K_0(ik_0|z-z'|)\right]$$

$$\approx 2i\omega\epsilon_0[N_0+\ln|z-z'|+\ln(\tfrac{1}{2}k_0)+C]$$

$$= 2i\omega\epsilon_0\ln[\kappa_0|z-z'|],$$

where $\kappa_0=\frac{1}{2}k_0\exp(C+N_0)$,

$$N_0=\int_0^{\infty}\frac{1}{\beta}\left(\frac{H_1^{(2)}(\beta b)}{H_0^{(2)}(\beta b)+\Lambda(\lambda)}-i\right)d\lambda+\frac{i\pi}{2},$$

and $C=0.5772\cdots$ is Euler's constant. Since the interior problem has already been solved, we merely restate the desired approximation[8] for $G(b,z,z')$,

$$G(b,z,z')\approx -2i\epsilon\omega\left(\ln\kappa|z-z'|+\frac{i\pi}{2kb\ln(b/a)}\right), \quad (15)$$

where

$$\kappa=[\pi/(b-a)]\exp N,$$

$$N=\sum_{s=1}^{\infty}\left(\frac{1}{s}+\frac{i\pi}{bs}\frac{[J_0(u_s a)]^2}{[J_0(u_s a)]^2-[J_0(u_s b)]^2}\right),$$

$$u_s=(k^2-\lambda_s^2)^{1/2},$$

J_0 is the zero-order Bessel function, and λ_s is the propagation constant of the s-order evanescent TM mode. Since the dependence of G_0 and G on z and z' has been reduced to $\ln|z-z'|$, (13) can be solved for $\hat{f}(z')$:

$$\hat{f}(z')=\frac{\delta/2}{\pi[(\delta/2)^2-(z')^2]^{1/2}}, \quad (16)$$

where it has been noted that $\hat{f}(z')$ has the correct edge behavior as $|z'|\to\frac{1}{2}\delta$.

By substituting (14)–(16) into (13), it is possible to relate V to I_0 in terms of a total gap admittance Y_t which is the sum of an external admittance Y_e, an internal admittance Y_i, and a small capacitance term $i\omega C_0$. Thus

$$V=-I_0Y_t^{-1}=-I_0(Y_e+Y_i+i\omega C_0)^{-1}, \quad (17)$$

where

$$i\omega C_0=\frac{2ik_0b}{\eta_0}\left(1+\frac{\epsilon}{\epsilon_0}\right)\ln(2), \quad (18)$$

$$Y_e=-\frac{2ik_0b}{\eta_0}\left[\ln\left(\frac{k_0\delta}{4}\right)+N_0+C\right], \quad (19)$$

$$Y_i=\frac{Y_0}{2}-i\frac{2kb}{\eta}\left[\ln\left(\frac{\pi\delta}{2(b-a)}\right)+N\right], \quad (20)$$

and where $Y_0=2\pi[\eta\ln(b/a)]^{-1}$ and $\eta=(\mu_0/\epsilon)^{1/2}$. Y_0 is the characteristic admittance of the TEM mode in the cable. The expression for V in (17) is used in Sec. III to derive a coupling factor between the cable and the tunnel.

III. POWER COUPLING FACTOR

At frequencies of most interest to mine communications (< 50 MHz), most of the power supplied by the cable gap to the tunnel goes into the monofilar mode. Also, the small amount of power which goes into the waveguide modes and the continuous spectrum is rapidly attenuated away from the gap because the waveguide modes are evanescent and the continuous spectrum corresponds to heavily damped lateral waves in the lossy rock walls. Consequently, we consider the useful tunnel power to be the power in the monofilar mode P_m. Thus we define a power coupling factor C_m as the ratio

$$C_m=P_m/P_{\mathrm{TEM}}, \quad (21)$$

where $P_{\mathrm{TEM}}=\frac{1}{2}|I_0|^2/Y_0$ is the power in the coaxial cable incident on the gap.

The propagation constant of the monofilar mode λ_0 has been computed for a wide range of parameters from the mode equation[2]

$$D(\lambda_0)=0, \quad (22)$$

where $D(\lambda)$ has been defined in (4). For small gaps, the power in the monofilar mode is given by[4]

$$P_m=\frac{\pi k_0}{\eta_0}|V^2|\,\mathrm{Re}\left(\frac{1}{D'(\lambda_0)}\right) = \frac{\pi k_0}{\eta_0}\frac{I_0^2}{|Y_t|^2}\,\mathrm{Re}\left(\frac{1}{D'(\lambda_0)}\right), \quad (23)$$

where (17) has been used in obtaining the second expression for P_m. By substituting (23) into (21),

$$C_m=2\pi k_0Y_0\,\mathrm{Re}[1/D'(\lambda_0)]/|Y_t|^2\eta_0. \quad (24)$$

If we had considered all power external to the cable as useful power, as assumed by Delogne,[3] the external coupling factor C_e would have been

$$C_e=Y_0\,\mathrm{Re}(Y_e)/|Y_t|^2. \quad (25)$$

In general, $C_m<C_e$, although for frequencies well below 50 MHz the difference is small, in some cases.

IV. NUMERICAL RESULTS

Before considering a specific numerical example, we must consider some computational aspects involved in evaluating N_0 as given by the integral in (14). In order for the integral to converge, $\Lambda(\lambda)$ must approach zero more rapidly than $H_0^{(2)}(\beta b)$ as $\lambda\to\infty$. By employing asymptotic expansions, the ratio for large λ is found to be

$$\Lambda(\lambda)/H_0^{(2)}(\beta b)\sim f(\lambda)\exp[-2\lambda(a'-\rho_0-b)], \quad (26)$$

where $f(\lambda)$ is algebraic in λ. Note that $(a'-\rho_0-b)$ is the distance from the edge of the cable to the tunnel wall. If λ_t is the actual upper limit used in the numerical integration, then (26) implies that $\lambda_t(a'-\rho_0-b)\gg 1$. If this condition is satisfied then the asymptotic behavior of the integrand is the same as in the free-space case. However, even then it is required that $\lambda_t b\gg 1$ for a small truncation error and that $\lambda_t\delta\ll 1$ in order to neglect the factor $\exp(-i\lambda|z-z'|)$ in (14). In order to be able to choose λ_t to satisfy these three conditions,

TABLE I. N_0 and external admittance Y_e.

Frequency (MHz)	Free space ($a'=\infty$) N_0	Y_e (mmhos)
5	$-54.7+i230.6$	$1.281+i0.359$
10	$-32.5+i128.6$	$1.428+i0.464$
20	$-19.29+i72.56$	$1.612+i0.620$
50	$-9.58+i34.89$	$1.939+i0.958$

In tunnel ($a'=2$ m, $\epsilon_e/\epsilon_0=10$, $\sigma_e=10^{-2}$ mhos/m)

Frequency	ρ_0 (m)	N_0	Y_e (mmhos)
5	0.0	$-16.0+i270.2$	$1.501+i0.144$
5	1.0	$-16.2+i279.2$	$1.551+i0.145$
5	1.7	$-16.9+i314.5$	$1.747+i0.149$
10	0.0	$-11.9+i137.0$	$1.523+i0.235$
10	1.0	$-11.5+i142.0$	$1.577+i0.231$
10	1.7	$-11.0+i160.2$	$1.780+i0.226$
20	0.0	$-10.78+i69.90$	$1.553+i0.430$
20	1.0	$-9.86+i72.72$	$1.616+i0.410$
20	1.7	$-8.68+i82.65$	$1.837+i0.384$
50	0.0	$-12.70+i31.73$	$1.763+i1.132$
50	1.0	$-10.11+i32.65$	$1.814+i0.988$
50	1.7	$-6.04+i36.68$	$2.038+i0.726$

the following two conditions must be satisfied:

$$\delta/b \ll 1 \quad \text{and} \quad \delta/(a'-\rho_0-b) \ll 1. \tag{27}$$

These are not serious restrictions, so long as large gaps are not considered.

We now consider a numerical example which is applicable to mine communications. The following tunnel parameters are assumed: $a'=2$ m, $\epsilon_e/\epsilon_0=10$, and $\sigma_e=10^{-2}$ mhos/m. The following cable parameters are typical[8]: $a=2.68$ mm, $b=1$ cm, and $\epsilon/\epsilon_0=2.5$. A gap width δ of 1 mm is assumed, but the results are not very sensitive to changes in δ. We consider various cable locations in the tunnel and a frequency range from 5 to 50 MHz.

Table I contains numerical values of N_0 given by (14) and Y_e given by (19). Note that $\mathrm{Re}(Y_e)$ increases both with frequency and with ρ_0. The values for $\rho_0=1.7$ m are probably most representative of operational conditions since the cable will generally be located near the wall. For comparison, free-space results were also computed from (14) by setting $\Lambda(\lambda)=0$ and are shown in Table I. Again $\mathrm{Re}(Y_e)$ increases with frequency.

Table II contains numerical values of N given by (15), $i\omega C_0$ given by (18), and Y_i given by (20). Note that Re $\mathrm{Re}(Y_i)$ is independent of frequency and $\mathrm{Im}(Y_i)$ increases with frequency. Since these quantities are properties of the cable only, they are independent of ρ_0.

Table III contains results for C_m given by (24) and the attenuation rate. The attenuation rate in dB/100 m is given by $868.8\ \mathrm{Im}(-\lambda_0)$ where λ_0 is given by (22). The numerical solution of (22) is accomplished by a modification of Newton's method.[2] Note that attenuation rate increases considerably with both frequency and ρ_0. However, C_m has a rather weak frequency dependence and increases only slightly with ρ_0. Consequently, it appears

TABLE II. N, $i\omega C_0$, and internal admittance (Y_i).

Frequency (MHz)	N	$i\omega C_0$ (mmhos)	Y_i (mmhos)
5	-0.0514	$i0.013$	$10.006+i0.022$
10	-0.0514	$i0.027$	$10.006+i0.044$
20	-0.0514	$i0.054$	$10.006+i0.088$
50	-0.0514	$i0.135$	$10.006+i0.221$

that lower frequencies are more advantageous because of the lower attenuation rate which would permit a greater distance between slots for a given signal level.

V. CONCLUDING REMARKS

We have obtained results for coupling between a TEM mode within a coaxial cable and the monofilar mode within the surrounding tunnel resulting from a circumferential gap in the cable shield. The actual INIEX/Delogne cable has a dielectric coating which we have neglected here for simplicity. This simplification is not important in the frequency range which we consider here (5—50 MHz), but could be important at higher frequencies where the dielectric coating can support a tightly bound surface or Goubau wave.[7,9] The INIEX/Delogne cable also utilizes lumped circuit elements at the cable gap in order to control the radiated power [proportional to $\mathrm{Re}(Y_e)$] and to minimize the reflection of the TEM mode within the cable. Our calculations show that about 25% of the cable power is released to the tunnel, whereas the lumped circuit elements of the INIEX/Delogne cable are adjusted to release only about 10% of the power to the tunnel.[3] It would be a useful theoretical extension to modify the gap voltage expression in (17) to allow for lumped circuit elements.

The numerical results in Table III indicate that the decrease in attenuation of the monofilar mode with frequency favors lower frequencies for coupling from the cable to the tunnel at a significant distance from the gap. However, the efficiency of the receiving antenna decreases as the frequency is decreased. Consequently, we can expect a minimum in coupling loss at some frequency. It would be a useful extension to include the antenna efficiency and cable attenuation to enable a com-

TABLE III. Coupling factor (C_m) and attenuation rate.

Frequency (MHz)	ρ_0 (m)	Coupling factor, C_m (%)	Attenuation rate (dB/100 m)
5	0.0	23.3	3.42
5	1.0	23.7	4.23
5	1.7	25.6	7.04
10	0.0	22.8	6.04
10	1.0	23.4	8.13
10	1.7	25.6	15.50
20	0.0	22.9	9.51
20	1.0	23.6	14.1
20	1.7	26.0	31.8
50	0.0	21.7	12.0
50	1.0	23.3	20.0
50	1.7	27.0	65.0

plete calculation of path loss between two antennas in the presence of a cable with arbitrary gap locations. These extensions are now occupying our attention.

ACKNOWLEDGMENTS

The authors would like to thank Ms. Lana Slusher for her help in preparing the manuscript. They also acknowledge the support of the U.S. Bureau of Mines.

[1]P. Delogne, L. Deryck, and R. Liegeois, in *Proceedings of Thru-the-Earth Electromagnetics Workshop*, edited by R.G. Geyer (N.T.I.S., Springfield, Va., 1973), pp. 49—53.
[2]J.R. Wait and D.A. Hill, IEEE Trans. Antennas Propag. AP-22, 627 (1974).
[3]P. Delogne, International Conference on Radio: Roads, Tunnels and Mines, Liege, Belgium, 1974, pp. 129—136 (unpublished).
[4]D.A. Hill and J.R. Wait, J. Appl. Phys. 45, 4774 (1974).
[5]D C. Chang, IEEE Trans. Antennas Propag. AP-21, 792 (1973).
[6]R.A. Hurd, Can. J. Phys. 51, 946 (1973).
[7]J.R. Wait and D.A. Hill, IEEE Trans. Antennas Propag. AP-23, 470 (1975).
[8]J.R. Wait and D.A. Hill, IEEE Trans. Antennas Propag. (to be published).
[9]P. Delogne and R. Liegeois, Ann. Telecommun. 26, 85 (1971).

IEEE TRANSACTIONS ON COMMUNICATIONS, NOVEMBER 1975

Vol. 23

Coupling Between a Radiating Coaxial Cable and a Dipole Antenna

DAVID A. HILL, MEMBER, IEEE, AND
JAMES R. WAIT, FELLOW, IEEE

Abstract—The coupling loss between a coaxial cable with a circumferential gap and a dipole antenna is analyzed. The numerical results have application to continuous-access guided communication (CAGC) and to related leaky feeder systems now being used in intramine communications. It is shown that the coupling is very strong in the neighborhood of the cable axis even when the linear distance between the dipole and the cable gap is large. This, of course, is a desirable feature of such limited-access communication systems.

INTRODUCTION

Continuous-access guided communication (CAGC) is an interesting combination of a shielded channel and a radiating system. The CAGC technique usually utilizes some kind of a wave-guiding system that has provision for a controlled leakage to enable a neighboring point to have access to signal information. Current applications are to ground transportation systems [1] and mine communications [2] but there are many other possibilities in urban environments.

A key aspect of CAGC is how to control the leakage from the main guiding channel that usually is a coaxial cable of some type. One method [1] that has been proposed is to employ a number of circumferential slits or gaps in the solid shield of the coax. In this fashion, the structure becomes a form of radiating antenna by virtue of the currents excited on the external surface of the shield. A key parameter in such a system is the resulting coupling loss between an incident TEM mode within the coax and a portable linear dipole receiving antenna in the external neighborhood. In this concise paper, we present quantitative information for such a configuration consisting of an infinitely long coax with a single radiating gap and an arbitrarily located dipole antenna. The reciprocal problem, when the external dipole antenna transmits, is also considered.

Earlier we derived field expressions for a dielectric coated coaxial cable with an interrupted shield [3], [4]. This was used to evaluate the total power radiated from an idealized break in the outer cable shield of a CATV system. The boundary-value analysis mentioned above is extended here to determine the coupling loss between such a radiating cable and a receiving dipole antenna.

The geometry of the infinitely long cable is indicated in Fig. 1 with respect to a cylindrical coordinate system (ρ,ϕ,z). The inner conductor of radius a and the shield of radius b are both assumed to be perfectly conducting. The insulation in the space, $a < \rho < b$, has a dielectric constant ϵ_1 and the jacket in the space, $b < \rho < c$, has a dielectric constant ϵ_2. The region, $\rho > c$, external to the cable is assumed to be free space with dielectric constant ϵ_0. A gap of width δ in the shield is located at $z = 0$. Here we are concerned with how much power is coupled to an external dipole antenna when an internal TEM mode is incident on the gap.

MUTUAL IMPEDANCE FORMULATION

For an internal TEM mode of current I_0 incident on the gap, the power in the incident mode P_i is given by

$$P_i = \tfrac{1}{2} |I_0|^2 / Y_0. \tag{1}$$

Paper approved by the Associate Editor for Radio Communication of the IEEE Communications Society for publication without oral presentation. Manuscript received March 24, 1975; revised May 23, 1975.

The authors are with the Institute for Telecommunication Sciences, Office of Telecommunications, U. S. Department of Commerce, Boulder, Colo. 80302.

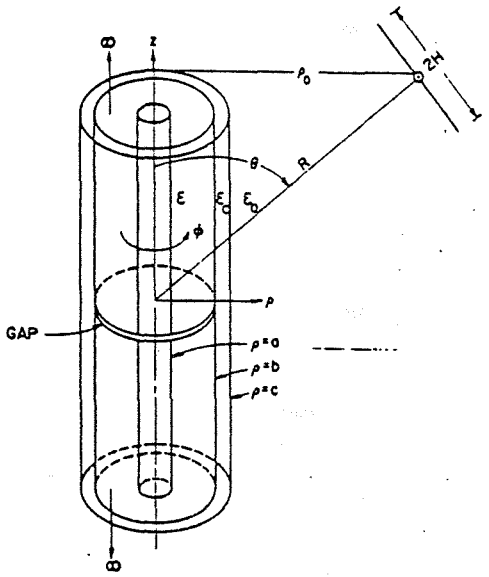


Fig. 1. Dielectric coated coaxial cable with a circumferential gap of width δ and the external dipole antenna (not to scale).

where $Y_c = 2\pi/\eta \ln (b/a)$ and $\eta = (\mu_0/\epsilon)^{1/2}$. Here Y_c is the characteristic admittance of the TEM mode in the coax. For a total gap admittance Y_t, the resultant gap voltage V is

$$V = I_c/Y_t. \tag{2}$$

Two different methods [3], [4] were used to calculate Y_t, and they gave very similar results over the parameter ranges of interest.

When the thickness of jacket $(c - b)$ is small, the external magnetic field $H_{c\phi}$ is given by [3]

$$H_{c\phi} = \frac{i\omega\epsilon_c bV}{2\pi} \int_{-\infty}^{\infty} \frac{H_1^{(2)}(u_c\rho) \exp(-i\lambda z) f(\lambda) d\lambda}{u_c b H_c^{(2)}(u_c b) + \Delta(\lambda) H_1^{(2)}(u_c b)}, \tag{3}$$

where $\Delta(\lambda) = (\epsilon_0/\epsilon_c) u_c^2 (c - b) b$,

$$f(\lambda) = \frac{\sin(\lambda\delta/2)}{(\lambda\delta/2)},$$

$$u_0 = (k_0^2 - \lambda^2)^{1/2}, \qquad u_c = (k_c^2 - \lambda)^{1/2},$$

$$k_c = \omega(\mu_0\epsilon_c)^{1/2}, \qquad k_0 = \omega(\mu_0\epsilon_0)^{1/2},$$

and $H_c^{(2)}$ and $H_1^{(2)}$ are zero- and first-order Hankel functions of the second kind. The time dependence is $\exp(i\omega t)$. The external electric field has ρ and z components, $E_{c\rho}$ and E_{cz}, that are given by

$$E_{c\rho} = \frac{ibV}{2\pi} \int_{-\infty}^{\infty} \frac{H_1^{(2)}(u_c\rho) \exp(-i\lambda z) f(\lambda) \lambda d\lambda}{u_c b H_c^{(2)}(u_c b) + \Delta(\lambda) H_1^{(2)}(u_c b)},$$

$$E_{cz} = \frac{bV}{2\pi} \int_{-\infty}^{\infty} \frac{H_0^{(2)}(u_c\rho) \exp(-i\lambda z) f(\lambda) u_c d\lambda}{u_c b H_c^{(2)}(u_c b) + \Delta(\lambda) H_1^{(2)}(u_c b)}. \tag{4}$$

For a general location of the receiving antenna, the electric field must be computed from (4) by numerical integration. Then, for a receiving antenna of finite length, another numerical integration of the electric field over the length of the antenna is required in order to compute the coupling loss. However, the calculations simplify considerably when the receiving antenna is located in the far field of the cable (i.e., $k_0\rho \gg 1$) [3]. The magnetic field, given by (3), then simplifies to

$$H_{c\phi} \simeq \frac{-iV}{\pi\eta_0} P(\theta) \frac{\exp(-ik_0 R)}{R}, \tag{5}$$

where $R = (\rho^2 + z^2)^{1/2}$, $\eta_0 = (\mu_0/\epsilon_0)^{1/2}$,

$$P(\theta) = \frac{f(k_0 \cos\theta) k_0 b}{k_0 b \sin\theta H_0^{(2)}(k_0 b \sin\theta) + \Delta(k_0 \cos\theta) H_1^{(2)}(k_0 b \sin\theta)},$$

and θ is the polar angle measured from the z axis. In the far field, the electric field has only a θ component $E_{c\theta}$:

$$E_{c\theta} \simeq \eta_0 H_{c\phi} \simeq \frac{-iV}{\pi} P(\theta) \frac{\exp(-ik_0 R)}{R}. \tag{6}$$

The receiving antenna is now taken to be a thin dipole of half-length H equal to or less than a quarter wavelength. Consequently, the antenna current $I(l)$ can be assumed to be sinusoidal [5]:

$$I(l) = \frac{I(0)}{\sin(k_0 H)} \sin[k_0(H - |l|)], \tag{7}$$

where l is the distance from the center of the antenna. In order to maximize the coupling (minimize the coupling loss), the dipole is oriented in the θ direction as shown in Fig. 1. The voltage V_d induced in the dipole is thus determined from the induced EMF method [5], [6] as follows:

$$V_d \simeq \frac{1}{I(0)} \int_{-H}^{H} E_{c\theta} I(l)\, dl$$

$$\simeq \frac{2E_{c\theta}(1 - \cos k_0 H)}{k_0 \sin(k_0 H)}, \tag{8}$$

where $E_{c\theta}$ is evaluated at the center of the dipole and is assumed constant over the length of the dipole. The mutual impedance between the cable and the dipole Z_m is now defined as the ratio of the voltage induced in the dipole to the current in the incident TEM mode of the cable. Thus

$$Z_m = V_d/I_c. \tag{9}$$

By reciprocity, Z_m is also equal to the ratio of the voltage in the excited TEM cable mode to the current at the terminals of the transmitting dipole.

NUMERICAL RESULTS FOR COUPLING LOSS

We define coupling loss L as the ratio of the incident power in the TEM mode [given by (1)] to the power absorbed in a matched load termination of the dipole. The current in the matched load is given by

$$I(0) = V_d/(2R_{in}) = I_c Z_m/(2R_{in}). \tag{10}$$

Here R_{in} is the input resistance of the dipole (assuming no losses) given by [5]

$$R_{in} = \frac{\eta_0}{4\pi} \{[1 - \cot^2(k_0 H)] \operatorname{Cin}(4k_0 H) + 4\cot^2(k_0 H) \operatorname{Cin}(2k_0 H) + 2\cot(k_0 H)[\operatorname{Si}(4k_0 H) - 2\operatorname{Si}(2k_0 H)]\}, \tag{11}$$

where

$$\operatorname{Si}(x) = \int_0^x \frac{\sin u}{u} du$$

and

$$\operatorname{Cin}(x) = \int_0^x \frac{1 - \cos u}{u} du.$$

Thus, the coupling loss is given by

$$L = \frac{|I_c|^2/(2Y_c)}{|I_c|^2 |Z_m|^2/(8R_{in})} = \frac{4R_{in}}{Y_c |Z_m|^2}. \tag{12}$$

To convert to decibels, we take $10 \log_{10}(L)$.

To deal with the reciprocal case of a transmitting dipole and a receiving cable, the expression for the coupling loss above remains the

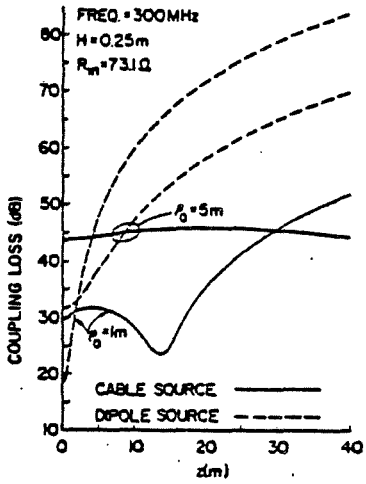


Fig. 2. Coupling loss between the cable and the dipole at 300 MHz. Dipole-to-dipole coupling loss is also shown at each location for comparison.

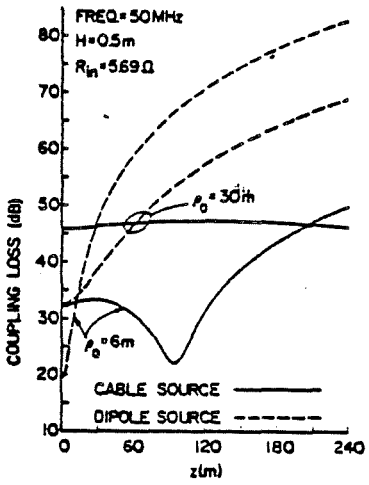


Fig. 3. Coupling loss at 50 MHz.

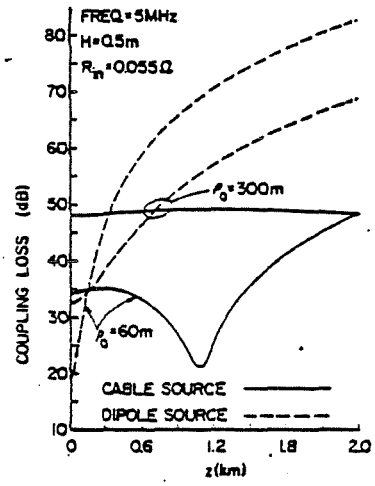


Fig. 4. Coupling loss at 5 MHz.

same if L is defined as the ratio of power transmitted by the dipole to the power transferred to either one of the TEM modes propagating away from the gap.

The equations required to compute L in (12) were programmed, and the results, shown in Figs. 2–4, were obtained for three frequencies (300 MHz, 50 MHz, and 5 MHz). The coupling loss, shown in Figs. 2–4, is for the geometry for the θ orientation of the dipole indicated in Fig. 1 that minimizes the coupling loss. In each case, the dipole remains at a radial distance ρ_0 of either one or five wavelengths from the cable while the z coordinate is increased from zero to 40 wavelengths. For these calculations, the cable parameters are: a = 1.25 mm, b = 1.0 cm, $c - b$ = 1.25 mm, δ = 1 mm, ϵ/ϵ_0 = 1.5, and ϵ_s/ϵ_0 = 2.5. For comparison, results are also shown for the case where the cable has been replaced by a transmitting dipole which is centered at the origin and z directed. The expressions used for the dipole–dipole coupling are given in the Appendix. Note that the coupling loss for the cable source is much lower than that for a dipole source for large z. This is in agreement with the results of Delogne and Liegeois [7] and our previous calculations [3] that show the cable radiation is concentrated mainly within 10 degrees of the z axis. The coupling losses shown for 5 MHz in Fig. 4 are probably too optimistic since a matched load is very difficult to obtain for such a low dipole resistance (0.055 Ω) and a large dipole reactance.

CONCLUDING REMARKS

Using an idealized model, we have computed coupling loss between a cable with a gap and a dipole for the special case where the dipole is in the far field. If the dipole is in the near field, coupling loss can still be calculated by the induced EMF method, but the complicated integral expressions for the electric field in (4) are required. Also, the optimum orientation of the dipole will, in general, be something other than the θ-orientation which is optimum in the far field.

Since CAGC and the related leaky feeder communication systems [8], [9] are sometimes employed in confined regions such as mine tunnels, an extension of the above treatment is needed. Using a model of an idealized circular tunnel, the relevant boundary value analysis has already been carried out [10] but further numerical work is needed to obtain the appropriate coupling losses. Also, we wish to combine the results to permit a systems evaluation of a point-to-point communication via two dipole antennas in the vicinity of the coax with a specified number of gaps in the shield. Another important extension is to consider the effect of locating the coax just above an imperfectly conducting ground. This is a configuration that is relevant to the study of the possible interference between a CATV system and aircraft navigation signals [11].

APPENDIX—COUPLING BETWEEN DIPOLES

The far field of a dipole of half-length H and feed current I_0 which is oriented in the z direction is given by [5]

$$E_\theta = \frac{i\eta_0}{2\pi} \frac{I_0}{\sin(k_0 H)} P(\theta) \frac{\exp(-ik_0 R)}{R}$$

where

$$P(\theta) = \frac{\cos(k_0 H \cos\theta) - \cos(k_0 H)}{\sin\theta}. \tag{13}$$

Consequently, the mutual impedance with the receiving dipole shown in Fig. 2 is

$$Z_m = \frac{2E_\theta(1 - \cos(k_0 H))}{I_0 k_0 \sin(k_0 H)}. \tag{14}$$

Utilizing the same approach used earlier, the coupling loss is found to be

$$L = 4R_{in}^2/|Z_m|^2. \tag{15}$$

REFERENCES

[1] J. C. Beal, J. Josiak, S. F. Mahmoud, and V. Rawat, "Continuous access guided communication (CAGE) for ground transportation systems," *Proc. IEEE*, vol. 61, pp. 502–508, May 1973.

[2] D. R. Martin and Q. Davis, Eds., *Proc. Int. Colloq. Leaky Feeder Radio Communication Systems*, University of Guildford, Surrey, England, 1974.

[3] J. R. Wait and D. A. Hill, "On the electromagnetic fields of a dielectric coated coaxial cable with an interrupted shield," *IEEE Trans. Antennas Propagat.*, vol. AP-23, pp. 470–479, July 1975.

[4] ——, "Electromagnetic fields of a dielectric coated coaxial cable with an interrupted shield—Quasi-static calculations," submitted to *IEEE Trans. Antennas Propagat.*

[5] J. D. Kraus, *Antennas*. New York: McGraw-Hill, 1950.

[6] P. S. Carter, "Circuit relations in radiating systems and applications to antenna problems," *Proc. IRE*, vol. 20, pp. 1004–1041, 1932.

[7] P. Delogne and R. Liegeois, "Le rayonment d'une interruption du conducteur exterieur d'un cable coaxial," *Annales des Telecommunicatons*, vol. 26, no. 3 and 4, pp. 85–100, 1971.

[8] P. Delogne, L. Deryck and R. Liegeois, "Guided propagation of radio waves," in *Proc. Thru-the-Earth Electromagnetics Workshop*, Colorado School of Mines, Golden, pp. 49–53; available from the Nat. Tech. Inform. Service (PB 231 154), 1973.

[9] D. J. R. Martin, "Very-high-frequency radio communication in mines and tunnels," Ph.D. dissertation, Dep. Electron. Elec. Eng., Univ. Surrey, Surrey, England, 1973.

[10] D. A. Hill and J. R. Wait, "Gap excitation of an axial conductor in a circular tunnel," *J. Appl. Phys.*, vol. 45, pp. 4774–4777, Nov. 1974.

[11] T. Harr, E. Haakinson, and S. Murahata, "Electromagnetic compatibility of simulated CATV signals and aircraft navigation receivers," Office Telecommunications, U. S. Dep. Commerce, Rep. OTR 74-27, 1974.

Calculated Channel Characteristics of a Braided Coaxial Cable in a Mine Tunnel

SAMIR F. MAHMOUD, MEMBER, IEEE, AND JAMES R. WAIT, FELLOW, IEEE

Abstract—The braided coaxial cable is studied as a communication scheme in a mine tunnel. A simplified rectangular waveguide model is adopted for the tunnel, and the shield of the cable is assumed to behave as a single inductive transfer impedance. Specific results on the attenuation of the monofilar and bifilar (or coaxial) modes of propagation, taking into account the possible existence of a thin lossy film on the cable, are presented. In order to estimate the maximum possible range of communication, we consider the coupling factors of these modes to transmitting and receiving dipoles inside the tunnel, and we present results on these factors for various cable parameters and over a wide range of frequencies.

INTRODUCTION

SEVERAL communication schemes in mine tunnels have recently been discussed. These include the two-wire open transmission line [1], the slotted coaxial cable [2], and the braided coaxial line [3], [4], all of which provide what is usually termed "continuous access guided communication." For any of these lines, one can identify two principal modes of propagation: the monofilar mode which provides a low coupling loss to the receiving or a transmitting antenna inside the tunnel, but which has a relatively high rate of attenuation; and the bifilar (or coaxial) mode which has the opposite properties. The design problem of a communication scheme in a given tunnel environment involves the best utilization of the properties of these two modes in order to achieve the longest range of communication.

In this paper, we consider the braided coaxial cable as a scheme of communication in mine tunnels. Thus, theoretical design data on the attenuation rates and coupling losses of the monofilar and bifilar modes are presented for various cable parameters and mine environments. Previous related work in the literature includes that due to Fontaine *et al.* [3], who considered the imperfect shield of the braided cable to provide a continuous coupling between two transmission lines, the first consisting of the outer shield of the cable and the earth, and the second being the cable itself with an assumed perfect shield. However, in their work, no detailed analysis of the tunnel walls and tunnel environment is attempted. Wait and Hill [4] have considered such effects on the attenuation of the modes in a circular tunnel.

Paper approved by the Associate Editor for Wire Communication of the IEEE Communications Society for publication after presentation at the U.S. National Meeting of URSI (International Union of Radio Science), Boulder, CO, October 1975. Manuscript received May 5, 1975; revised August 4, 1975.

S. F. Mahmoud was with the Cooperative Institute for Research in Environmental Sciences, University of Colorado, Boulder, CO 80302. He is now with the Department of Electrical Engineering, Cairo University, Giza, Egypt.

J. R. Wait is with the Cooperative Institute for Research in Environmental Sciences, University of Colorado, Boulder, CO 80302.

MODELING OF THE TUNNEL AND CABLE

The mine tunnel is modeled as a rectangular waveguide whose broad walls are a lossy dielectric medium with permittivity ϵ_e and conductivity σ_e. However, the narrow side walls are considered to behave as perfect electric conductors in order that a rigorous analytical treatment of the modes of propagation becomes possible. This tunnel model has been previously used, and has provided results for the case of a single wire inside the tunnel [5] that are in good agreement with measurements in an actual tunnel [1] and with theoretical results for a circular tunnel [6].

The outer shield of the braided coaxial cable is modeled as a transfer impedance $Z_T(\Omega/\text{m})$ which is taken equal to $j\omega L$, L being an inductance per unit length. A dielectric jacket of permittivity ϵ_c and an outer radius c surrounds the braid and is assumed to be covered by a thin outer lossy layer of mine dust or conducting fluid with a transfer impedance Z_L which is purely resistive. The filling dielectric of the cable has a permittivity ϵ, an outer radius b, and an inner radius a, and the inner conductor has a conductivity σ_w with a resulting series impedance $z_w(\Omega/\text{m})$. As indicated in Fig. 1, the cable is located with its axis at distances $(s - s_0)$ and $(l - l_0)$ from the top and the side walls, respectively. The outer radius c of the jacket is sufficiently small compared to distances from all the walls, so that an azimuthally symmetrical current distribution inside the cable can be assumed for the important modes of the tunnel. In the following, we derive an equation for the modal propagation constants inside the rectangular tunnel containing the braided cable by extending a previous derivation [7].

MODAL PROPAGATION CONSTANTS

The fields for a given mode are assumed to have the dependence $\exp(i\omega t - \Gamma z)$ where ω is the applied angular frequency, Γ is the modal propagation constant for which solutions are being sought, and z is a distance along the axis of the tunnel. Looking from outside the cable, this appears to the tunnel as a line source with a longitudinal current $I_c = 2\pi c H_\phi$ where H_ϕ is the azimuthal magnetic field on the outside surface of the jacket ($\rho = c$). This current produces fields everywhere inside the tunnel, and the average longitudinal electric field E_z at $\rho = c + 0$, i.e., just outside the jacket, has been derived in an earlier paper [7] and is given by

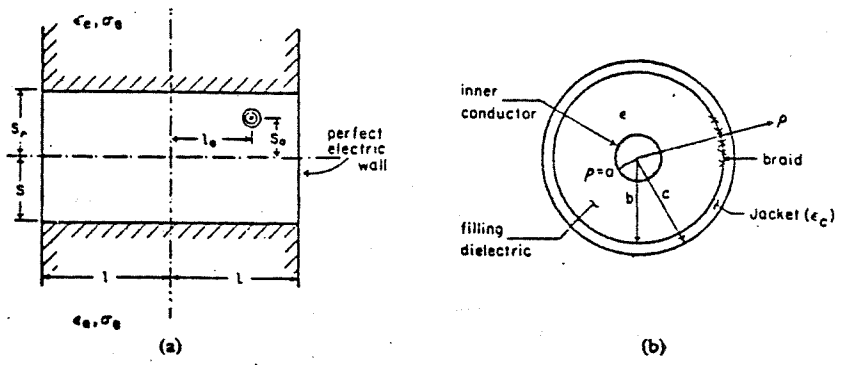


Fig. 1. (a) Rectangular waveguide model showing the location of the cable. (b) Internal structure of the braided coaxial cable.

$$E_z\,|_{\rho=c+0} = (i\omega\mu_0/\pi)D(\Gamma)\cdot I_c \tag{1}$$

where $D(\Gamma)$ is a function of the propagation constant Γ among other parameters pertaining to the tunnel dimensions, wall electrical constants, and the location and radius of the cable. $D(\Gamma)$ is given explicitly by a rather lengthy expression in the above reference, and hence will not be reproduced here.

In order to satisfy the boundary conditions requiring the continuity of E_z at the jacket outer surface, it is necessary to obtain this field at $\rho = c - 0$ from a consideration of the currents and fields inside the cable. Generally, this task involves expressing the fields in different regions in terms of appropriate Bessel functions and applying the boundary conditions at the respective interfaces. Considerable simplification results, however, if a quasi-static solution is used [4]. Such a solution requires that the condition βb, $\beta c \ll 1$ be satisfied where β is any transverse wavenumber in one of the dielectric regions inside the cable. This condition is usually met for the important modes of propagation except, perhaps, at UHF.

Wait and Hill [4] show that the effective series impedance per unit length $Z(\Gamma)$, defined as $E_z(\rho = c - 0)/I_c$, is given by

$$Z(\Gamma) = Z_L(Z_c + Z_b)/(Z_L + Z_c + Z_b) \tag{2}$$

where

$$Z_b = Z_T(Z' + Z_w)/(Z_T + Z' + Z_w) \tag{3}$$

where

$$Z'(\Gamma) = -(\omega^2\mu\epsilon + \Gamma^2)\ln(b/a)/2\pi i\omega\epsilon \tag{4}$$

and

$$Z_c(\Gamma) = -(\omega^2\mu\epsilon_c + \Gamma^2)\ln(c/b)/2\pi i\omega\epsilon_c. \tag{5}$$

This is just the input impedance looking to the right at point (c) of the circuit shown in Fig. 2. Here the series impedances $Z'(\Gamma)$ and $Z_c(\Gamma)$ account for the filling dielectric and the jacket. The currents I_a, I_b, and I_c are interpreted as $\oint H_\phi dl$ where H_ϕ is the azimuthal magnetic field integrated over the circumferences at $\rho = a$, b, and c, respectively.

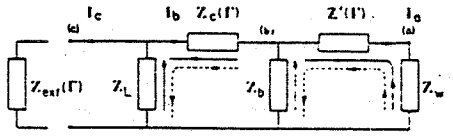


Fig. 2. Transverse equivalent circuit of the braided coaxial cable [4]. Solid and broken arrows represent the current flow lines for the monofilar and bifilar modes, respectively.

Now the modal equation is obtained by equating (1) by $I_cZ(\Gamma)$, and thus

$$(-i\omega\mu_0/\pi)\cdot D(\Gamma) = Z(\Gamma). \tag{6}$$

In relation to the equivalent circuit of Fig. 2, $(-i\omega\mu_0/\pi)\cdot D(\Gamma)$ is equal to minus the external impedance $Z_{ext}(\Gamma)$ looking into the tunnel from the jacket outer surface. Solutions of the modal equation (6) result in the monofilar mode, the bifilar mode, and the perturbed normal modes of the empty tunnel. The latter, however, have the property of being cut off at frequencies lower than about 50 MHz for typical tunnel dimensions, and hence will not be important for transmission in this range of frequency.

NUMERICAL SOLUTION OF THE MODAL EQUATION

The modal equation (6) has been solved for Γ of the monofilar and bifilar modes using the Newton-Raphson method. Previous results on Γ of the monofilar mode in a tunnel containing a single wire [5] have been used as initial roots in the above iterative method. For the bifilar mode, very good starting values of Γ are readily obtained from the equivalent circuit of Fig. 2 if we assume that both Z_L and Z_{ext} are much greater than Z_T, hence, by neglecting their effect, the modal equation takes the approximate form

$$Z_w + Z'(\Gamma) + Z_T \simeq 0. \tag{7}$$

Using (4) in (7), we obtain the approximate result

$$\Gamma_{bif}^2 = -\omega^2\mu\epsilon + [2\pi i\omega\epsilon(Z_w + Z_T)/\ln(b/a)]. \tag{8}$$

Now, it is convenient to define another excitation factor, say, $\Lambda_p'(x,y)$, according to

$$\Lambda_p'(x,y) = \bar{I} \cdot \bar{e}_p(x,y) \Big/ \left[\eta \int_S \bar{e}_p \times \bar{h}_p \cdot \bar{z}\, dS \right]^{1/2} \quad (12)$$

where $\eta = \sqrt{\mu_0/\epsilon_0}$ is the free-space wave impedance which has been added only to render $\Lambda_p'(x,y)$ a dimensionless quantity. Hence, expression (11) can be recast in the form

$$(V/\eta I) = \sum_p \Lambda_p'(x_0,y_0)\Lambda_p'(x_1,y_1) \exp(-\Gamma_p z_1). \quad (13)$$

We thus find that the received voltage is made up of a summation of individual voltages induced by each propagating mode in the tunnel. It is clear that as z_1 increases, there comes a distance beyond which only one mode is responsible for the total received voltage. This mode is the least attenuated mode which, in our case, is the bifilar mode. The maximum possible range of communication is clearly a function of the properties of this mode alone, specifically, its excitation factors and attenuation rate. To express these ideas more thoroughly, we define a total loss L_p (in decibels) for the pth mode as follows:

$$L_p = -20 \log_{10} |\Lambda_p'(x_0,y_0)\Lambda_p'(x_1,y_1)| + \alpha_p z_1 \quad (14)$$

where $\alpha_p = 8.7$ Re (Γ_p). For a given transmitted power and minimum S/N ratio at the receiver, the total loss L_p of the bifilar mode cannot exceed a certain maximum $\hat{L}_p$, which in turn determines the maximum possible communication range. In the following, we shall find an estimate to the quantity L_p for the monofilar and bifilar modes.

As is apparent from (14), L_p is dependent on the locations of the transmitting and receiving dipoles and their orientations. However, in order to obtain meaningful results without the specification of any particular dipole location or orientation, and which can still reflect the effects of the line and tunnel parameters, we use the following argument. The fields of the monofilar and the bifilar modes outside the cable are linearly proportional to their respective modal currents on the outside surface of the cable, that is, $I_c = 2\pi c H_\phi$ (at $\rho = c$). Furthermore, if we assume that the dipoles are always oriented to have maximum possible interaction with the modal fields, then a reasonable approximation to Λ_p' in (12) is

$$\Lambda_p' = \text{const}\, \eta^{1/2} \left| (I_c)_p f(\Gamma_p/k_0) \Big/ \left[\int_S \bar{e}_p \times \bar{h}_p \cdot \bar{z}\, dS \right]^{1/2} \right| \quad (15)$$

where k_0 is the free-space wavenumber and $f(\Gamma_p/k_0)$ is a function that represents the dependence of the modal fields on the modal propagation constant Γ_p and is, as yet, unknown. A look at the appropriate formulas [5, Appendix I] for the modal fields shows that the dependence on Γ_p is quite complicated. However, in the low-frequency limit, it is readily shown in Appendix I of this paper that the transverse fields are linearly proportional to Γ_p; hence, $f(\Gamma_p/k_0)$ in (15) is taken to be (Γ_p/k_0). This low-frequency approximation is believed to to be quite valid up to frequencies for which $2k_0 l \sim \pi$, and probably is still acceptable for higher frequencies. For typical tunnel dimensions, $2l = 4$ m; hence, the upper frequency limit is about 37.5 MHz.

Now the current I_c for the monofilar and bifilar modes is easily obtained from the circuit of Fig. 2 under the normalization $I_a = 1$. The flow of currents of the monofilar and bifilar modes are different, and are shown in Fig. 2 by solid and dashed arrows, respectively. It is straightforward to obtain $I_{c,\text{mono}}$ and $I_{c,bif}$ as

$$I_{c,\text{mono}} = [(Z_c(\Gamma_{\text{mono}}) + Z_L)(Z'(\Gamma_{\text{mono}}) + Z_T + Z_w) + Z_T(Z'(\Gamma_{\text{mono}}) + Z_w)]/Z_L Z_T \quad (16)$$

and

$$I_{c,bif} = Z_L Z_T / [(Z_c(Z_{bif}) + Z_T)(Z_{\text{ext}}(\Gamma_{bif}) + Z_L) + Z_{\text{ext}}(\Gamma_{bif}) Z_L]. \quad (17)$$

In the special case when the outer lossy film is absent, i.e., $Z_L = \infty$, (16) and (17) take the simple forms

$$I_{c,\text{mono}} = [Z'(\Gamma_{\text{mono}}) + Z_T + Z_w]/Z_T \quad (18)$$

$$I_{c,bif} = Z_T/[Z_{\text{ext}}(\Gamma_{bif}) + Z_c(\Gamma_{bif}) + Z_T], \quad (19)$$

and as a check, if $Z_T = 0$, corresponding to a perfect shielding of the cable, the above two equations will imply that the bifilar mode has zero fields outside the cable, while the monofilar mode has zero fields inside the cable, as we would expect. Finally, the integration in (15) is obtained by a seminumerical method using expressions for the modal fields that were given before [5].

By combining (15) and (14), we arrive at

$$L_p = \text{const} - 20 \log_{10} \left| \eta (\Gamma_p/k_0)^2 I_{cp}^2 \Big/ \left[\int_S \bar{e}_p \times \bar{h}_p \cdot \bar{z}\, dS \right] \right| + \alpha_p z_1. \quad (20)$$

The coupling loss may be obtained from the above by putting $z_1 = 0$. Computed results of α_{mono}, α_{bif}, and the coupling loss for the monofilar and bifilar modes are tabulated for a range of frequencies in Tables I–III for the following three cases.

Case a: $L = 40$ nH/m, $\epsilon = 2.5\epsilon_0$.
Case b: $L = 4$ nH/m, $\epsilon = 2.5\epsilon_0$.
Case c: $L = 40$ nH/m, $\epsilon = 1.5\epsilon_0$.

The other cable parameters are held constant in all three cases. These are $1/\sigma d = 10^3\ \Omega$, $\sigma_w = 5.7 \times 10^7$ S/m, $\epsilon_c = 3\epsilon_0$, and the cable and tunnel dimensions are the same as in Fig. 3.

In case *b*, the cable has the least braid leakage, and in case *c*, the permittivity of the dielectric filling is chosen low to allow for a higher coupling between the fields of the bifilar mode and a transmitting or a receiving dipole. As would be expected, the coupling loss for the bifilar mode is highest in case *b* and lowest in case *c*. The quantity $R_{\min}$ in the last columns of Tables I–III is defined as the communication range at which both the monofilar and bifilar modes contribute equally to the received signal. Hence, at this range ($z_1 =$

Some numerical computations on the attenuation rates of the monofilar and bifilar modes are shown in Figs. 3 and 4. Here $Z_L = 1/\sigma d$ with σd varying from 10^{-3} to 10^{-1} $\mho$ and $Z_T = i\omega L$ with $L = 40$ and 4 nH/m in Figs. 3 and 4, respectively. The following observations are evident from Figs. 3 and 4.

1) The attenuation of the bifilar mode is markedly affected by the conductivity of the inner conductor of the cable as it varies from $\sigma_w = 10^6$ to 5.7×10^7 $\mho$/m (Fig. 3). This is due to a concentration of the fields of this mode inside the cable.

2) The effect of the outer lossy film is to increase the attenuation of both modes, this increase being higher at higher frequencies and more pronounced for the bifilar mode.

3) The attenuation of the bifilar mode in Fig. 4 is seen to be much less sensitive to the conductivity of the outer lossy film. This is a result of reducing the braid transfer impedance Z_T relative to its value in Fig. 3. Such a reduction, however, causes a higher coupling loss to receiving or transmitting dipoles in the tunnel, as will be shown in the next section.

4) As has been observed in previous work [1], [5], [6], the attenuation of the monofilar mode increases as the cable approaches the tunnel wall (Fig. 3), while the bifilar mode remains almost unaffected.

It is quite interesting to notice a remarkable similarity between the above results and those obtained by Wait and Hill [4] for a circular tunnel model. The main difference occurs for the monofilar mode at the lower frequencies where the attenuation rate is very small in any case. Such differences can be attributed to the particular tunnel model being adopted. We may conclude, however, that the remarks 1)–4) stated above are, to a great extent, independent of the particular shape of the tunnel.

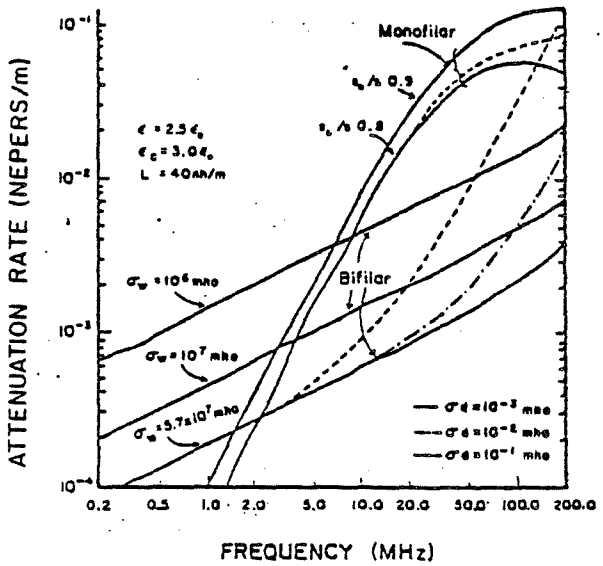


Fig. 3. Attenuation rates of the monofilar and bifilar modes versus frequency, $L = 40$ nH/m. In this figure and Fig. 4, $l = 2$ m, $s = 1.5$ m, $l/l_0 = 1/2$, $a = 1.5$ mm, $b = 10$ mm, and $c = 11.5$ mm, $\epsilon_c = 10\epsilon_0$ and $\sigma_c = 10^{-2}$ $\mho$/m.

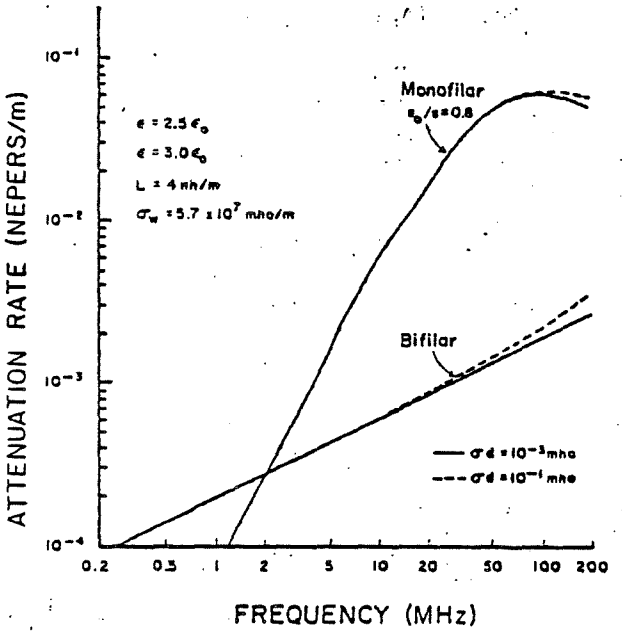


Fig. 4. Attenuation of the monofilar and bifilar modes versus frequency, $L = 4$ nH/m.

COUPLING LOSS AND COMMUNICATION RANGE

A transmitting dipole located inside the tunnel excites both the monofilar and bifilar modes among the normal modes of the empty tunnel. The latter, however, are of less importance due to their cutoff properties. Let $[\bar{e}_p, \bar{h}_p] \exp(-\Gamma_p z)$ for $p = 1, 2, \cdots$ represent the vector electric and magnetic field distributions of the pth mode, p being an integer that runs over all possible modes. Thus, a short dipole of moment $\bar{P} = \bar{I}\bar{l}$, located at the point $(x_0, y_0, 0)$, will excite a summation of these modes given by

$$[\bar{E}, \bar{H}] = \sum_p \Lambda_p(x_0, y_0)[\bar{e}_p, \bar{h}_p] \exp(-\Gamma_p |z|). \tag{9}$$

Here, $\Lambda_p(x_0, y_0)$ is the excitation factor of the pth mode, and is a function of the dipole orientation and location in the tunnel cross section [8]. Thus,

$$\Lambda_p(x_0, y_0) = \bar{I}\bar{l} \cdot \bar{e}_p(x_0, y_0) \Big/ \left[\int_S \bar{e}_p \times \bar{h}_p \cdot \bar{z}\, dS\right] \tag{10}$$

where the last integration is taken over the tunnel cross section.

Now, we assume that a similar dipole is used for reception and is located at (x_1, y_1, z_1); then, the received open-circuited voltage V is given by

$$V = \sum_p \bar{I}\bar{l} \cdot \bar{e}_p(x_1, y_1)\Lambda_p(x_0, y_0) \exp(-\Gamma_p z_1)$$

which, upon using (10), becomes

$$V = (1/\bar{I}\bar{l}) \sum_p \Lambda_p(x_1, y_1)\Lambda_p(x_0, y_0)\left[\int_S \bar{e}_p \times \bar{h}_p \cdot \bar{z}\, dS\right] \cdot \exp(-\Gamma_p z_1). \tag{11}$$

TABLE I
COUPLING LOSS (CASE *a*)

Freq. (MHz)	α_{mono} (dB/km)	α_{bif} (dB/km)	Coupling Loss		R_{min} (km)
			Monofilar	Bifilar	
100	521.2	19.2	7.22	88.7	0.162
50	419.5	12.5	7.75	91.1	0.205
25	203.6	8.60	8.33	92.4	0.431
12.5	72.1	5.91	9.10	93.1	1.26
6.25	20.3	4.10	9.84	93.8	5.26

TABLE II
COUPLING LOSS (CASE *b*)

Freq. (MHz)	α_{mono} (dB/km)	α_{bif} (dB/km)	Coupling Loss		R_{min} (km)
			Monofilar	Bifilar	
100	534.5	16.8	7.55	139.4	0.255
50	428.6	11.9	7.99	140.2	0.316
25	206.2	8.42	8.52	141.5	0.671
12.5	73.1	5.95	9.24	141.3	1.96
6.25	20.4	4.24	10.04	140.6	8.25

TABLE III
COUPLING LOSS (CASE *c*)

Freq. (MHz)	α_{mono} (dB/km)	α_{bif} (dB/km)	Coupling Loss		R_{min} (km)
			Monofilar	Bifilar	
100	516.8	19.8	7.33	75.4	0.137
50	415.0	13.6	7.79	76.7	0.172
25	201.0	9.42	8.40	76.2	0.354
12.5	71.1	5.84	9.11	75.5	1.02
6.25	20.0	3.55	9.91	73.4	3.85

R_{min}), $L_{mono} = L_{bif}$, and at distances greater than R_{min}, the bifilar mode becomes the dominant propagating mode. In any well-designed communication scheme, the received signal-to-noise ratio S/N at R_{min} is well above the minimum allowable ratio; hence the maximum possible communication range R should be greater than R_{min}. As an example, assuming that the transmitter power and the received noise are such that the total signal loss L_{bif} is limited to, say, 150 dB for acceptable reception, then from Tables I–III we find that the maximum possible communication ranges at 25 MHz in the three tabulated cases are, respectively, $R = 6.69$, 1.08, and 7.82 km.

To study the dependence of R on the operating frequency, a detailed consideration of the maximum transmitter power and received noise as functions of the frequency should be investigated. This is outside the scope of this paper. The above results, however, show clearly the effects of the main cable parameters on the communication range, and should help in the design of a communication link in an actual tunnel.

CONCLUSIONS

A study of the important characteristics of the braided coaxial cable for communication in a mine tunnel has been presented. The analysis used accounts fully for the continuous exchange of energy between the tunnel and the cable. This is in contrast to the method of Fontaine *et al.* [3], who employed a perturbation-type coupled mode formalism. The results on the attenuation rates and coupling losses of the two principal modes of propagation obtained are believed to reveal the role of the various cable parameters in system design. We should stress, however, that in the present analysis, the braided cable and the tunnel are assumed to be completely uniform in the axial direction. Lateral variations of the cable parameters will cause additional coupling between the propagating bifilar and monofilar modes and the higher order cutoff modes. These mode conversion effects, whether intentional or accidental, play a role in the overall performance of the leaky cable systems in a mine tunnel environment. This aspect of the subject is receiving our attention.

APPENDIX I

In this Appendix, we prove that the transverse modal fields are linearly proportional to the modal propagation constant Γ in the low-frequency limit. The reader is referred to an earlier paper [5, Appendix I] for the basic equations and the symbols that will be used here.

The transverse modal fields [5] e_x and e_y are given by

$$e_x = -\Gamma\partial\Pi_z/\partial x + \partial^2\Pi_y/\partial x\partial y \tag{I-1}$$

$$e_y = -\Gamma\partial\Pi_z/\partial y + (k_0^2 + \partial^2/\partial y^2)\Pi_y \tag{I-2}$$

where Π_z and Π_y are two electric potentials that are not reproduced here. In the low-frequency limit, k_0, k_e, and Γ are neglected relative to $(\partial/\partial x)$ or $(\partial/\partial y)$; hence, the following substitutions are valid: $u_m \to u_{m1} \to m\pi/2l$, $R_m \to 0$, $S_m \to (\epsilon_1 - \epsilon_0)/(\epsilon_1 + \epsilon_0)$, $R_m^* \to \Gamma(\epsilon_1 - \epsilon_0)/((\epsilon_1 + \epsilon_0)u_m)$, $\Delta_m \to \Delta_m^* \to \exp(2u_m s)$. Using the above substitutions in the expressions of Π_z and Π_y, we find

$$\begin{aligned}
\partial\Pi_z/\partial x &\to (-i\omega\mu_0 I_c/\pi k_0^2)\sum_{m=0}^{\infty}(2\pi/l)\sin(m\pi x_0/l) \\
&\quad \cdot \cos(m\pi x/l)\exp(-u_m|y-y_0|) \\
&= (-i\omega\mu_0 I_c/k_0^2 l)\,\mathrm{Im}\left\{\sum_{m=0}^{\infty}\exp[-(m\pi/2l) \right. \\
&\quad \cdot (|y-y_0| - i(x+x_0)] - \exp[-(m\pi/2l) \\
&\quad \left. \cdot (|y-y_0| - i(x-x_0)]\right\} \\
&= (-i\eta/k_0 l)\,\mathrm{Im}\{[1-\exp(-(\pi/2l) \\
&\quad \cdot (|y-y_0| - i(x+x_0))]^{-1} \\
&\quad - [1-\exp(-(\pi/2l)(|y-y_0| - i(x-x_0))]^{-1}\}
\end{aligned}$$

where $x_0 = l + l_0$, $y_0 = s + s_0$, and Im stands for the imaginary part. Similar expressions are obtained for $\partial^2\Pi_y/\partial x\partial y$, $\partial\Pi_z/\partial y$, and $\partial^2\Pi_y/\partial y^2$. Substituting in (I-1) and (I-2), we arrive after simple algebra at

$$\begin{aligned}
e_x \to (i\eta I_c\Gamma/k_0 l)\,\mathrm{Im}\,[&X(|y-y_0|) \\
&- \epsilon' X(3s - s_0 - y) - \epsilon' X(y + y_0) \\
&- \epsilon'^2 X(3s - s_0 + y) - \epsilon'^2 X(4s + y_0 - y)]
\end{aligned} \tag{I-3}$$

and

$$e_y \to (i\eta I_c \Gamma/k_0 l)\ \mathrm{Re}\ [\pm X(|y-y_0|) - \epsilon' X(3s-a_0-y) - \epsilon' X(y+y_0) - \epsilon'^2 X(3s-s_0+y) - \epsilon'^2 X(4s+y_0-y)], \quad y \le y_0 \quad \text{(I-4)}$$

where Re stands for the real part and the function $X(y)$ is defined as

$$X(y) = [1-\exp(-(\pi/2l)(y-i(x+x_0))]^{-1} - [1-\exp(-(\pi/2l)(y-i(x-x_0))]^{-1}$$

and $\epsilon' = (\epsilon_1 - \epsilon_0)/(\epsilon_1 + \epsilon_0)$. Equations (I-3) and (I-4) show that the transverse fields are linearly proportional to Γ in the low-frequency limit.

ACKNOWLEDGMENT

We would like to thank Dr. D. A. Hill for his useful comments and L. Hope for her help in preparing the manuscript.

REFERENCES

[1] L. Deryck, "Exchanges d'energie entre modes de propagation sur ligne bifilaire," *Bull. Tech. "Mines et Carriers"* (Institut National des Industries Extractives, Belgium), no. 134, Dec. 1971.

[2] R. DeKeyser, P. Delogne, J. Janssens, and R. Liegeois, "Radio communication and control in mines and tunnels," *Electron. Lett.*, vol. 6, Oct. 26, 1970.

[3] J. Fontaine, B. Demoulin, P. Degauque, and R. Gabillard, "Feasibility of a radio communication in mine galleries by means of a coaxial cable having a high coupling impedance," in *Proc. Thru-the-Earth Electromagn. Workshop*, Colorado School of Mines, Golden, Aug. 1973. Available from Nat. Tech. Inform. Service, Alexandria, VA, Publ. 231 154.

[4] J. R. Wait and D. A. Hill, "Propagation along a braided coaxial cable in a circular tunnel," *IEEE Trans. Microwave Theory Tech.*, vol. MTT-23, pp. 401–406, May 1975.

[5] S. F. Mahmoud, "Characteristics of EM guided waves for communication in coal mine tunnels," *IEEE Trans. Commun.*, vol. COM-22, pp. 1547–1554, Oct. 1974.

[6] J. R. Wait and D. A. Hill, "Guided electromagnetic waves along an axial conductor in a circular tunnel," *IEEE Trans. Antennas Propagat.* (Succinct Papers), vol. AP-22, pp. 627–630, July 1974.

[7] S. F. Mahmoud and J. R. Wait, "Theory of wave propagation along a thin wire inside a rectangular waveguide," *Radio Sci.*, vol. 9, pp. 417–420, Mar. 1974.

[8] R. E. Collin, *Field Theory of Guided Waves*. New York: McGraw-Hill, 1960, p. 484.

Radio Science, Volume 11, Number 4, pages 315–321, April 1976

Calculated transmission loss for a leaky feeder communication system in a circular tunnel

David A. Hill

Institute for Telecommunication Sciences, Office of Telecommunications, US Department of Commerce, Boulder, Colorado 80302

James R. Wait[1]

Cooperative Institute for Research in Environmental Sciences, National Oceanic and Atmospheric Administration, Environmental Research Laboratories, Boulder, Colorado 80302

(Received October 26, 1975; revised November 15, 1975.)

The transmission loss for a leaky coaxial cable communication system in a circular tunnel is calculated for an idealized model. The transmitting and receiving antennas are electric dipoles that may be located anywhere within the tunnel. For typical cable parameters, the optimum frequency is found to be in the range from 2 to 10 MHz. Calculations reveal that the use of a sparse braid and a high velocity cable will strongly improve the cable-dipole coupling with only a small penalty of a higher attenuation rate.

INTRODUCTION

The leaky feeder technique [*Beal et al.*, 1973; *Cree*, 1975] is now being developed and exploited for communication in mine tunnels [*Martin*, 1975]. In this method, first described by *Monk and Winbigler* [1956], the signals are guided by some type of transmission line such as a coaxial cable [*Fontaine et al.*, 1973] or a twin-wire line [*Deryck*, 1975; *Wait and Hill*, 1974]. The energy is coupled into or out of the channel by antennas in the vicinity of the transmission line. The advantage of this technique, of course, is that we do not have to make electrical contact with the axial conductor such as used in the "line radio" method developed many years ago by *Jakosky and Zellers* [1924, 1925] and now used extensively. An extremely interesting experimental study of transmission in tunnels has been published by *Gillette and Gilmour* [1975] that seems to confirm some of the theoretical concepts [*Wait and Hill*, 1974; *Delogne*, 1975; *Mahmoud and Wait*, 1976] relating to the respective roles of the monofilar and the bifilar modes in tunnel structures.

We have previously derived a mode equation for an idealized braided coaxial cable within a circular tunnel, and we presented some numerical results for the attenuation rates of the dominant modes [*Wait and Hill*, 1975]. Here we determine the mutual impedance and the related transmission loss between a pair of dipoles located in such a tunnel. Actually, this total transmission loss is the sum of the dipole-to-cable coupling losses and the attenuation of the dominant propagation mode. In our work we follow others [*Fontaine et al.*, 1973; *Delogne*, 1975; *Slaughter*, 1975] and assume that the braided sheath or shield of the coaxial cable can be described adequately by a surface transfer impedance [*Dummer and Blackband*, 1961]. Also, we do not consider mode conversion effects due to the inevitable lateral variations of the tunnel cross sections and other irregularities.

MODAL EXCITATION

The geometry of the circular tunnel is shown in the cylindrical coordinate system (ρ, ϕ, z) in Figure 1. The air-filled tunnel of radius a_0 has permittivity ϵ_0, and the surrounding rock has conductivity σ_e and permittivity ϵ_e. The free-space permeability μ_0 is assumed everywhere. The braided coaxial cable is located at (ρ_0, ϕ_0), and the source dipole is located at $(\rho_a, \phi_a, 0)$.

We now determine the total current $I(z)$ induced on the cable by a source current of moment $\vec{P}$. Here we follow a procedure, based on the reciprocity principle, that was used by *Mahmoud* [1974] for a single-wire transmission line in a rectangular

[1] Consultant to Institute for Telecommunication Sciences, Office of Telecommunications.

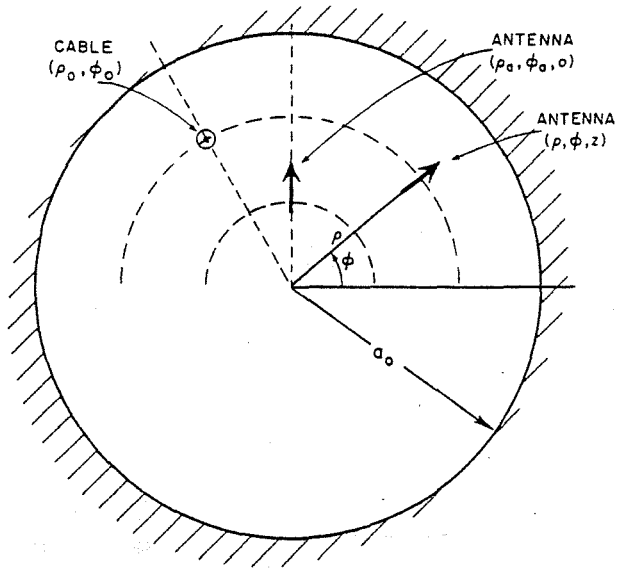


Fig. 1. Transmitting and receiving dipoles in a circular tunnel which contains a braided coaxial cable. (In the subsequent calculations we chose $\phi = \phi_a = \phi_0$.)

tunnel and by *Hill and Wait* [1974] for a two-wire line in a circular tunnel.

The source current density $\vec{J}_a$ is written

$$\vec{J}_a(\rho, \phi, z) = \vec{P}\delta(\rho - \rho_a)\,\delta(\phi - \phi_a)\,\delta(z)/\rho_a \tag{1}$$

where δ is the Dirac delta function and $\vec{P}$ is taken to be transverse to z. We now consider that for a given mode, the cable carries a total axial current I_0 that can, for an external observer, be localized at the center of the cable. Thus, the resulting current density is

$$J_z(\rho, \phi, z) = (I_0/\rho_0)\exp(-i\beta z)\,\delta(\rho - \rho_0)\,\delta(\phi - \phi_0) \tag{2}$$

where β is the propagation constant of the mode. Here and in what follows, we adopt an $\exp(i\omega t)$ time dependence. To be more specific, we can define I_0 as the line integral of the azimuthal magnetic field around the outer circumference of the coaxial cable.

The total electric field $\vec{e}(\rho, \phi, z)$ of the modal current can be written in terms of a z component e_z and a transverse component $\vec{e}_t$. Thus

$$\vec{e}(\rho, \phi, z) = \exp(-i\beta z)\, I_0[\vec{e}_t(\rho, \phi, \beta) + \hat{z}\, e_z(\rho, \phi, \beta)] \tag{3}$$

We now apply the reciprocity theorem [*Monteath*, 1973] to the two current densities $\vec{J}_a$ and J_z and their fields to yield:

$$\int_{-\infty}^{\infty}\int_0^{2\pi}\int_0^{\infty} \vec{J}_a(\rho, \phi, z) \cdot I_0\, \vec{e}_t(\rho, \phi, \beta) \cdot \exp(-i\beta z)\rho\, d\rho\, d\phi\, dz = \int_{-\infty}^{\infty}\int_0^{2\pi}\int_0^{\infty} J_z(\rho, \phi, z) \cdot E_{za}(\rho, \phi, z)\,\rho\, d\rho\, d\phi\, dz \tag{4}$$

where E_{za} is the z component of the field produced by the source dipole. When (1) and (2) are substituted into (4), the following is obtained:

$$\vec{P} \cdot \vec{e}_t(\rho_a, \phi_a, \beta) = \int_{-\infty}^{\infty} E_{za}(\rho_0, \phi_0, z)\exp(-i\beta z)\, dz = E'_{za}(\rho_0, \phi_0, \beta) \tag{5}$$

Each Fourier component $I'(\beta)$ of the cable current $I(z)$ must satisfy the following impedance boundary condition at the edge of the cable ($\rho = \rho_0 + c, \phi = \phi_0$):

$$E'_{za}(\rho_0 + c, \phi_0, \beta) + I'(\beta)\, e_z(\rho_0 + c, \phi_0, \beta) = I'(\beta)\, Z(\beta) \tag{6}$$

where $Z(\beta)$ is the effective impedance per unit length of the cable looking radially inwards. Since $E'_z(\rho_0, \phi_0, \beta) \simeq E'_z(\rho_0 + c, \phi_0, \beta)$, we can substitute (5) into (6) to obtain:

$$I'(\beta) = -\vec{P} \cdot \vec{e}_t(\rho_a, \phi_a, \beta)/A(\beta) \tag{7}$$

where $A(\beta) = e_z(\rho_0 + c, \phi_0, \beta) - Z(\beta)$.

The total cable current $I(z)$ is

$$I(z) = \frac{1}{2\pi}\int_{-\infty}^{\infty} I'(\beta)\exp(i\beta z)\, d\beta \tag{8}$$

By deforming the integration contour in the complex β plane, (8) can be converted to the following residue series:

$$I(z) \simeq -i\sum_p \frac{\vec{P} \cdot \vec{e}_t(\rho_a, \phi_a, \beta_p)\exp(-i\beta_p |z|)}{[dA(\beta)/d\beta]|_{\beta=\beta_p}} \tag{9}$$

where $\beta = \beta_p$ are the roots of the modal equation, $A(\beta) = 0$, and the heavily damped branch cut contribution can be neglected. $I(z)$, as given by (9), is actually valid for any axial conductor that can be characterized by a series impedance per unit length $Z(\beta)$.

The specific braided coaxial cable of interest here is modeled by: a center conductor of radius a and conductivity σ_w, insulation of outer radius b and permittivity ϵ, a metal braid of radius b that can be characterized by a transfer inductance per unit length L_T, a protective jacket of outer radius c and permittivity ϵ_c, and a thin lossy film of radius c that can be characterized by a conductivity-thickness product σd. The presence of such lossy films should be expected in realistic mine environments [*Rawat and Beal*, 1974]. The appropriate expression for $Z(\beta)$ for this structure has been derived previously for use in the solution of the mode equation [*Wait and Hill*, 1975]. For most cases of interest, the mode of lowest attenuation is the "bifilar" mode which carries most of its energy between the center conductor and the metal braid, but this mode also has "leakage" fields outside the cable. The propagation constant of this mode β_b is approximately that of the insulation, i.e., $\beta_b \sim \omega(\mu_0\epsilon)^{1/2}$.

The coaxial cable and the tunnel also support a monofilar mode which is characterized by a forward current in the cable and a return current in the rock wall. In addition, there are an infinite number of tunnel waveguide modes which are only weakly affected by the cable. However, for application to long-distance communication, we need retain only the bifilar mode in (9):

$$I(z) \simeq -i\frac{\vec{P}\cdot\vec{e}_t(\rho_a,\phi_a,\beta_b)\exp(-i\beta_b|z|)}{[dA(\beta)/d\beta]|_{\beta=\beta_b}} \tag{10}$$

MUTUAL IMPEDANCE

For large positive z, the transverse field external to the cable can be obtained from (3) and (10):

$$\vec{e}(\rho,\phi,z) = -i\{\vec{P}\cdot\vec{e}_t(\rho_a,\phi_a,\beta_b)/[dA(\beta)/d\beta]|_{\beta=\beta_b}\} \cdot \hat{e}_t(\rho,\phi,\beta_b)\exp(-i\beta_b z) \tag{11}$$

For a transverse receiving dipole of effective length $\vec{l}_{re}$ located at (ρ,ϕ,z), the received voltage is

$$v_r = \vec{e}(\rho,\phi,z)\cdot\vec{l}_{re} \tag{12}$$

The dipole moment $\vec{P}$ can be written as the input current i_a times an effective length $\vec{l}_{ae}$:

$$\vec{P} = i_a\vec{l}_{ae} \tag{13}$$

The mutual impedance Z_m is defined as the ratio of received voltage to transmitter current, and is found to be:

$$Z_m = \{-i[\vec{l}_{ae}\cdot\vec{e}_t(\rho_a,\phi_a,\beta_b)][\vec{l}_{re}\cdot\vec{e}_t(\rho,\phi,\beta_b)] \div [dA(\beta)/d\beta]|_{\beta=\beta_b}\}\exp(-i\beta_b z) \tag{14}$$

The specific expression for $\vec{e}_t$ has been given previously [*Wait and Hill*, 1974]. For a thin transmitting dipole of physical length l_a, the magnitude of the effective length, assuming a sinusoidal current distribution, is given by

$$|\vec{l}_{ae}| = 2[1-\cos(k_0 l_a/2)]/k_0\sin(k_0 l_a/2) \tag{15}$$

where $k_0 = \omega(\mu_0\epsilon_0)^{1/2}$. A similar expression can be used for the receiving dipole.

To illustrate some quantitative features of Z_m, we consider a special example. The receiving and transmitting dipoles are of the same length, location, and orientation. They are located on the same radial line as the cable (i.e., $\phi_a = \phi_0$), and they are oriented radially for maximum coupling. The assumed tunnel parameters are: $a_0 = 2$ m, ϵ_e/ϵ_0

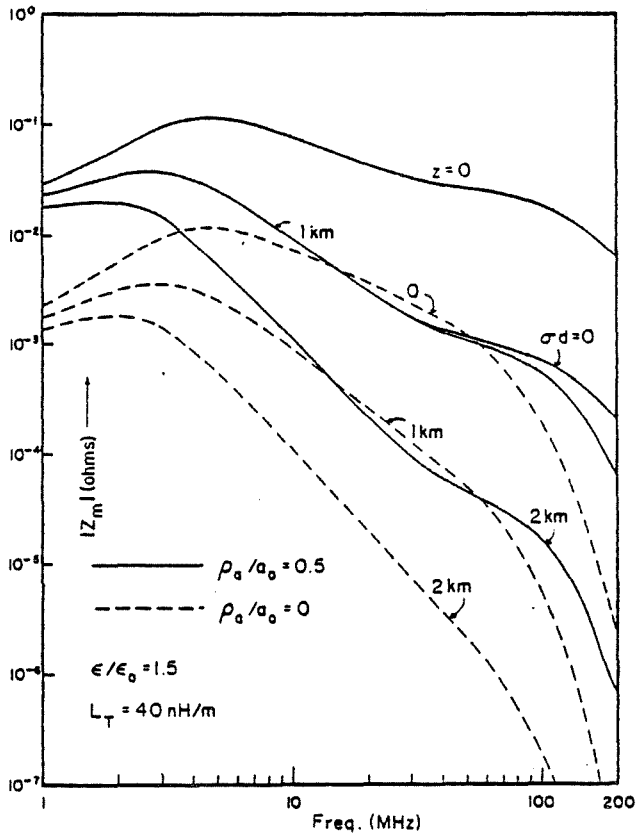


Fig. 2. Magnitude of mutual impedance for a large value of transfer inductance L_T. (Note that the cable location is fixed such that $\rho_0/a_0 = 0.9$ for this and subsequent figures.)

= 10, and $\sigma_e = 10^{-3}$ mhos/m. The cable is located at $\rho_0/a_0 = 0.9$, and the assumed cable parameters are: $a = 1.5$ mm, $b = 10$ mm, $c = 11.5$ mm, $\epsilon/\epsilon_0 = 1.5$, $\epsilon_c/\epsilon_0 = 3$, $\sigma_w = 5.7 \times 10^7$ mhos/m, and $\sigma d = 10^{-3}$ mhos. The antenna length l_a is taken to be 0.75 m, and the frequency range covered is 1 to 200 MHz. Figures 2-5 illustrate the magnitude of the mutual impedance as a function of various parameters. Note that $|Z_m|$ is at least an order of magnitude less when the dipoles are located at the tunnel center ($\rho_a = 0$) as compared to a location closer to the cable ($\rho_a = 0.5$). Antenna separations on the order of 1 km are of interest, and results for $z = 0$ are shown only to illustrate the portion of Z_m which is due to coupling in and out of the cable. Note from the spreading of the curves that attenuation becomes quite large at the higher frequencies. The results in Figure 2 are for $L_T = 40$ nH/m which represents a very sparse braid such as that employed in the FONT cable [*Fontaine et al.*, 1973]. Also shown is one curve

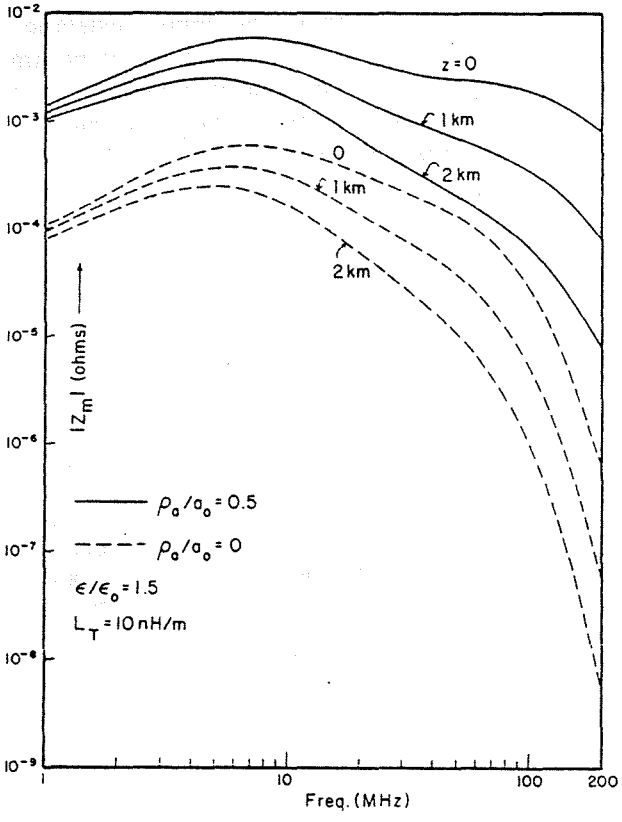


Fig. 3. Magnitude of mutual impedance for an intermediate value of transfer inductance L_T.

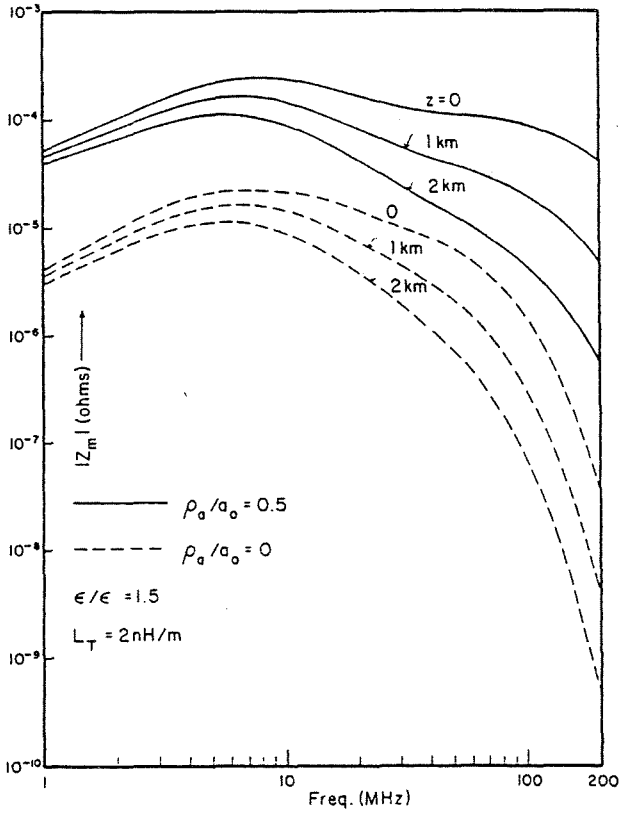


Fig. 4. Magnitude of mutual impedance for a small value of L_T.

where the lossy film is removed ($\sigma d = 0$). The lossy film increases the attenuation rate at the higher frequencies, but has no effect at the lower frequencies. Figure 3 shows results for a smaller value of L_T (10 nH/m) and, although the attenuation rate is lower, $|Z_m|$ is smaller due to reduced coupling. For Figure 4, $|Z_m|$ is reduced even further because of the very small value of L_T (2 nH/m). Figure 5 corresponds to Figure 2 except that the permittivity of the cable insulation has been increased ($\epsilon/\epsilon_0 = 2.5$). The attenuation rate is decreased slightly because of reduced leakage fields, but the dipole coupling is much weaker.

TRANSMISSION LOSS

If the input resistance of the transmitting antenna is R_a, then the input power is

$$P_a = |i_a|^2 R_a/2 \tag{16}$$

If the input resistance of the receiving antenna is R_r and the antenna is terminated in a matched load,

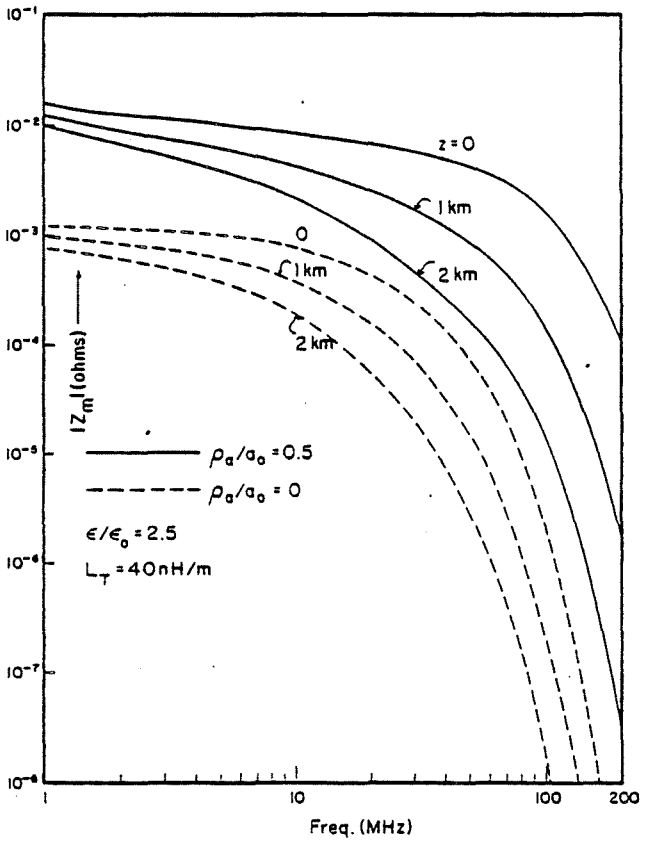


Fig. 5. Magnitude of mutual impedance for a larger value of insulation permittivity ϵ.

the received power is

$$P_r = |i_a|^2 |Z_m|^2 \gamma / (8R_r) \tag{17}$$

Thus the transmission loss L (in dB) is

$$L = 10 \log_{10}\left(\frac{P_a}{P_r}\right) = 10 \log_{10}\left(\frac{4R_a R_r}{|Z_m|^2}\right) \tag{18}$$

For the higher frequencies where the spacing between the dipole and the tunnel wall is on the order of a wavelength, the input resistance can be approximated by the free-space radiation resistance [*Kraus*, 1950]. However, for low frequencies, the loss resistance due to near field losses becomes much larger than the radiation resistance. This loss resistance has been computed for dipoles near a half space [*Wait*, 1969; *Chang and Wait*, 1970] but no such results are available for a dipole in a circular tunnel environment. Qualitatively, the loss resistance is expected to reach a constant value as the frequency decreases rather than continuing to decrease in the manner of the radiation resistance.

In Table 1 we show the input resistance and resultant transmission loss for the same parameters used in Figure 3. To qualitatively include the effect of loss resistance, a lower limit of either 2 or 0.5 ohms has been placed on R_{in}. The absolute level

TABLE 1. Transmission loss (parameters are those of Figure 3).

Frequency (MHz)	R_{in} (ohms)	ρ_a/a_0	Transmission loss (dB) $Z = 0$	$Z = 1$ km	$Z = 2$ km
200.0	73.1	0.0	167.0	187.0	207.0
200.0	73.1	0.5	104.9	125.0	145.0
114.5	18.1	0.0	126.6	142.1	157.6
114.5	18.1	0.5	86.3	101.8	117.3
65.6	5.50	0.0	102.1	114.3	126.5
65.6	5.50	0.5	73.4	85.7	97.9
37.5	2.0*,1.76	0.0	86.9,85.8	96.6,95.5	106.3,105.2
37.5	2.0*,1.76	0.5	63.6,62.5	73.3,72.2	83.0,81.9
21.5	2.0*,0.57	0.0	82.4,71.6	90.1,79.2	97.8,86.9
21.5	2.0*,0.57	0.5	61.1,50.2	68.7,57.8	76.4,65.5
12.3	2.0*,0.5*	0.0	78.4,66.4	84.4,72.3	90.3,78.2
12.3	2.0*,0.5*	0.5	57.9,45.8	63.8,51.8	69.7,57.7
7.04	2.0*,0.5*	0.0	76.6,64.5	80.9,68.9	85.3,73.3
7.04	2.0*,0.5*	0.5	56.5,44.4	60.8,48.8	65.2,53.2
4.03	2.0*,0.5*	0.0	78.3,66.2	81.4,69.3	84.4,72.4
4.03	2.0*,0.5*	0.5	58.2,46.1	61.3,49.2	64.4,52.3
2.30	2.0*,0.5*	0.0	82.8,70.8	85.0,73.0	87.2,75.1
2.30	2.0*,0.5*	0.5	62.3,50.3	64.5,52.5	66.7,54.6
1.0	2.0*,0.5*	0.0	91.4,79.4	92.8,80.7	94.1,82.1
1.0	2.0*,0.5*	0.5	69.3,57.2	70.6,58.6	71.9,59.9

*assumed values

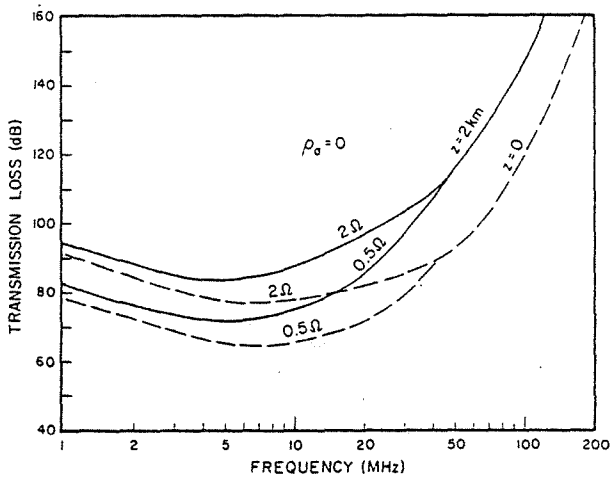


Fig. 6. Transmission loss as a function of frequency illustrating dependence on total range and antenna input resistances.

of path loss is strongly dependent on this value, but the frequency dependence is not.

Some of the results from Table 1 are illustrated graphically in Figures 6 and 7. A minimum transmission loss is noted at about 7 MHz. The results for $z = 0$ can be interpreted as the two-way coupling loss in and out of the cable, and the results are in reasonable agreement with the free-space calculations of *Rawat and Beal* [1974] using somewhat different assumptions. Also, there is a qualitative similarity with the recent approximate calculations of *Mahmoud and Wait* [1976] for a rectangular tunnel model.

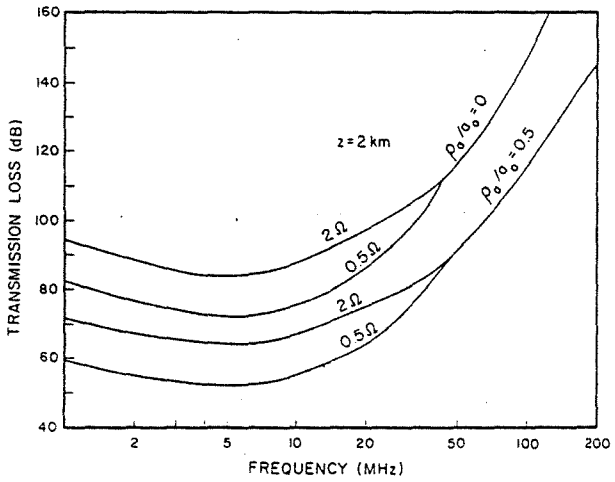


Fig. 7. Transmission loss as a function of frequency illustrating dependence of location of antennas relative to cable.

CONCLUDING REMARKS

The mutual impedance between a pair of dipole antennas in a circular tunnel has been computed for the case where the bifilar mode of the braided coaxial cable is the dominant mode. The coupling of the dipoles with the cable is improved by using a high transfer inductance [*Fontaine et al.*, 1973] and an insulation with a low dielectric constant. The large cable leakage fields produced by such a cable result in a slightly higher attenuation rate, but this is more than offset by the improvement in coupling loss. For typical parameters, an optimum frequency is observed in the range from 2 to 10 MHz.

In computing transmission loss, a better knowledge of the input resistance of dipoles in a tunnel environment would be desirable and could be obtained by theory or experiment. But conclusions regarding transmission loss are expected to follow those of mutual impedance as far as cable parameters and optimum frequency are concerned.

We should regard this analysis as the first step in a total systems study for communication using the leaky feeder system in mine tunnels and similar environments. The characterization of the braided cable is oversimplified and the neglected conversion between the propagation modes is not really justified in a fully realistic situation. Nevertheless, it is important to understand how a transmission may occur for the rather idealized model before attempting a study of all of the complicating influences such as longitudinal irregularities in the guiding structure.

REFERENCES

Beal, J. C., J. Josiak, S. F. Mahmoud, and V. Rawat (1973), Continuous-access guided communications (CAGC) for ground-transportation systems, *Proc. IEEE, 61*(5), 562-568.

Chang, D. C., and J. R. Wait (1970), Theory of a vertical tubular antenna located above a conducting half-space, *IEEE Trans. Antennas Propagat., AP-18*(2), 182-188.

Cree, D. J. (1975), Practical performance of radiating cables, *Radio Electron. Eng., 45*(5), 215-223.

Delogne, P. P. (1975), Electromagnetic theory of the leaky coaxial cable, *Radio Electron. Eng., 45*(5), 233-240.

Deryck, L. (1975), Control of mode conversions on bifilar lines in tunnels, *Radio Electron. Eng., 45*(5), 241-247.

Dummer, G. W. A., and W. T. Blackband (1961), *Wires and R. F. Cables*, pp. 112-115, Sir Isaac Pitman & Sons, London.

Fontaine, J., B. DeMoulin, P. DeGauque, and R. Gabillard (1973), Feasibility of radio communication in mine galleries by means of a coaxial cable having a high coupling impedance,

in *Proceedings of Thru-the-Earth Electromagnetics Workshop*, pp. 130–139, *Acc. No. PB 231 154*, National Technical Information Service, Springfield, VA 22151.

Gillette, M. R., and A. S. Gilmour (1975), Attenuation measurements in wet granite tunnels, *IEEE Trans. Electromagn. Compat.*, *EMC-7*(4), 201–206.

Hill, D. A., and J. R. Wait (1974), Excitation of monofilar and bifilar modes on a transmission line in a circular tunnel, *J. Appl. Phys.*, *45*(8), 3402–3406.

Jakosky, J. J., and D. H. Zellers (1924), Factors retarding transmission of radio signals underground and some further experiments and conclusions, Reports of investigations, *Serial No. 2651*, US Bureau of Mines, Washington, DC.

Jakosky, J. J., and D. H. Zellers (1925), Line radio and the effects of metallic conductors on underground communication, Reports of investigations, *Serial No. 2682*, US Bureau of Mines, Washington, DC.

Kraus, J. D. (1950), *Antennas*, pp. 254–262, McGraw-Hill, New York.

Mahmoud, S. F. (1974), Characteristics of EM guided waves for communication in coal mine tunnels, *IEEE Trans. Commun.*, *COM-22*(10), 1547–1554.

Mahmoud, S. F., and J. R. Wait (1976), Calculated channel characteristics of a braided coaxial cable in a mine tunnel, *IEEE Trans. Commun.*, *COM-24*(1), 82–87.

Martin, D. J. R. (1975), A general study of the leaky feeder principle, *Radio Electron. Eng.*, *45*(5), 205–214.

Monk, N., and H. S. Winbigler (1956), Communication with moving trains in tunnels, *IRE Trans. Vehicular Commun.*, *PGVC-7*, 21–28.

Monteath, G. D. (1973), *Applications of the Electromagnetic Reciprocity Principle*, Pergamon, New York.

Rawat, V., and J. C. Beal (1974), Leaky cables treated as open waveguides, in *Proc. Int. Colloquium Leaky-Feeder Communications*, Guildford, Surrey, England.

Slaughter, R. J. (1975), Field leakage and cross talk with special reference to radiating cables with tape screens, *Radio Electron. Eng.*, *45*(5), 248–252.

Wait, J. R. (1969), Impedance characteristics of electric dipoles over a conducting half-space, *Radio Sci.*, *4*(10), 971–975.

Wait, J. R., and D. A. Hill (1974), Coaxial and bifilar modes on a transmission line in a circular tunnel, *Appl. Phys.*, *4*(4), 307–312.

Wait, J. R., and D. A. Hill (1975), Propagation along a braided coaxial cable in a circular tunnel, *IEEE Trans. Microwave Theory Tech.*, *MTT-23*(5), 401–405.

Electronics Letters, Vol. 12, No. 13, pp. 346-347, 24th June 1976

LOW-FREQUENCY RADIO TRANSMISSION IN A CIRCULAR TUNNEL CONTAINING A WIRE CONDUCTOR NEAR THE WALL

Indexing term: Guided electromagnetic-wave propagation

The general theory for transmission in a circular tunnel containing a thin axial conductor is employed to calculate the attenuation rate of the propagating mode. The remarkable property is that the attenuation rate is approximately proportional to frequency and it does not depend critically on the wall conductivity for typical conditions.

In previous papers,[1,2] we have discussed the theory of electromagnetic-wave transmission in tunnels. Specific applications to high-frequency communication were described. Here we would like to report on some calculations that illustrate some of the remarkable features at low frequencies.

The model we choose is highly idealised. Specifically, the cross-section is circular with radius a, beyond which the rock is assumed to be homogeneous with conductivity σ_e and permittivity ε_e. To illustrate the effect of an axial wire within the tunnel, we locate a thin conductor of radius c and conductivity σ_w at a distance d from the tunnel wall. Of particular interest is the attenuation rate of the propagating mode in the tunnel, since this is an important factor in a communication system.

Some calculated results, based on our earlier paper,[1] are shown in Figs. 1 and 2 for the attenuation rate as a function of frequency for a tunnel radius $a = 2$ m. Three values of d are shown and two different sets of the electrical properties of the adjacent rock are chosen. For these calculations, the wire conductivity is taken to be infinite and the wire radius

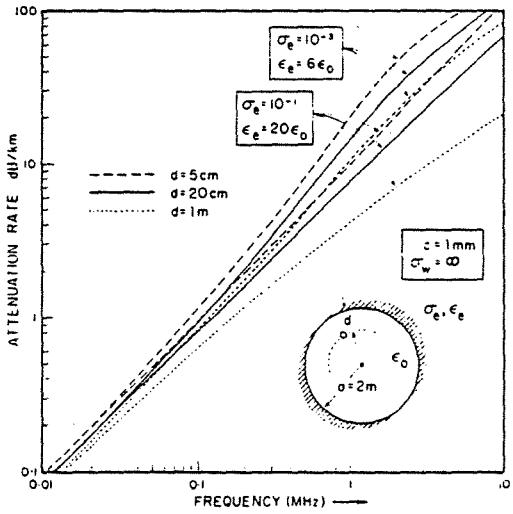


Fig. 1 *Attenuation rate function of frequency for model indicated by inset*

$c = 1$ mm. The results clearly show that the attenuation rate is almost a linear function of frequency. Also, the dependence on the rock conductivity is not great. In fact, the curves for $\sigma_e = 10^{-2}$ S/m would be between the curves for $\sigma_e = 10^{-1}$ and 10^{-3} S/m.

Some related calculations are shown in Fig. 2, where now the frequency is fixed at 50 kHz and the abscissa is the normalised distance of the wire conductor from the tunnel wall. Now the wire conductivity is $5{\cdot}7 \times 10^7$ S/m, corresponding to copper. Again the results show that the attenuation rate, while small, does increase significantly as the wire conductor approaches the tunnel wall. We also see that the dependence on conductivity σ_e is quite weak in the range from 10^{-2} to 10^{-3} S/m, while, for rather unrealistic higher conductivity, the attenuation rate has decreased in a significant fashion.

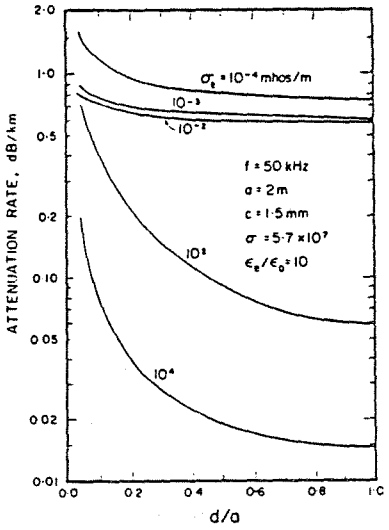


Fig. 2 *Attenuation rate as function of (normalised) distance of conductor to tunnel wall*

The behaviour of the attenuation rate for the parameters indicated in Figs. 1 and 2 is really not too surprising. For the very high wall conductivities, we have the classical skin effect that is familiar at microwave in metal-walled guides. Then the attenuation rate is varying with frequency f approximately as $(f/\sigma_e)^{\frac{1}{2}}$. For more realistic rock conductivities, however, the distance d is becoming small compared with the skin depth in the rock. Then we find the low-frequency attenuation rate is, to within first order, independent of rock conductivity, but proportional to frequency. This is consistent with the known behaviour of a linear wire at low height over the surface of the earth at very low frequencies.[3,4]

J. R. WAIT
D. A. HILL

Institute for Telecommunication Sciences
Office of Telecommunications
US Department of Commerce
Boulder, Colo. 80302, USA

1st June 1976

References

1 WAIT, J. R., and HILL, D. A.: 'Guided electromagnetic waves along an axial conductor in a circular tunnel', *IEEE Trans.*, 1974, AP-22, pp. 627–630
2 WAIT, J. R., and HILL, D. A.: 'Coaxial and bifilar modes on a transmission line in a circular tunnel', *Appl. Phys.*, 1974, 4, pp. 307–312
3 WAIT, J. R.: 'On the impedance of long wire suspended over the ground', *Proc. Inst. Radio Engr.*, 1961, 49, p. 1576
4 CHANG, D. C., and WAIT, J. R.: 'Extremely low frequency (ELF) propagation along a horizontal wire located above or buried in the earth', *IEEE Trans.*, (special issue, edited by WAIT J. R.), 1974, COM-22, pp. 421–426

Radio Science, Volume 11, Number 11, pages 897-899, November 1976

The eccentrically located wire in a cylindrical cavity in a conducting medium and the limit of a planar boundary

James R. Wait

Cooperative Institute for Research in Environmental Sciences, University of Colorado/Environmental Research Laboratories, National Oceanic and Atmospheric Administration, US Department of Commerce, Boulder, Colorado 80302

(Received July 23, 1976.)

Propagation along a thin wire located in an air-filled tunnel is considered in the limiting case where the tunnel radius becomes indefinitely large but the distance of the wire to the tunnel wall remains finite. It is found that the results are consistent with the corresponding analysis for a thin wire located over a plane homogeneous earth.

A modal analysis was performed earlier for the transmission of electromagnetic waves in a circular air-filled tunnel of radius a that contains an axial conductor [*Wait and Hill*, 1974]. The surrounding medium is homogeneous and unbounded with a conductivity σ_e, permittivity ϵ_e, and permeability μ_e. The modal equation, for the propagation constants Γ, was given in the form

$$K_0(vc) - \sum_{m=-\infty}^{+\infty} R_m \frac{K_m(va)}{I_m(va)} [I_m(v\rho_0)]^2 = 0 \qquad (1)$$

in the case when the axial wire of radius c was located at a distance ρ_0 from the tunnel axis. Also, we have assumed here that the wire conductivity is infinite and that the distance d of the wire from the tunnel wall is large compared with the wire radius (i.e., $d = a - \rho_0 \gg c$). Other factors in (1), in the notation used earlier, are defined as follows:

$$v = (\gamma_0^2 - \Gamma^2)^{1/2}, \quad u = (\gamma_e^2 - \Gamma^2)^{1/2},$$

$$\gamma_0^2 = -\epsilon_0 \mu_0 \omega^2, \quad \gamma_e^2 = i\mu_e \omega(\sigma_e + i\epsilon_e \omega)$$

and

$$R_m = \frac{(\gamma_0/v)K_m'(va)/K_m(va) + Y_m \eta_0 + \delta_m \eta_0}{(\gamma_0/v)I_m'(va)/I_m(va) + Y_m \eta_0 + \delta_m \eta_0} \qquad (2)$$

and

$$\delta_m \eta_0 = \frac{(im\Gamma/a)^2 [v^{-2} - u^{-2}]^2}{[(\gamma_0/v)I_m'(va)/I_m(va)] + (Z_m/\eta_0)} \qquad (3)$$

and

$$\eta_0 = \left(\frac{\mu_0}{\epsilon_0}\right)^{1/2} = 120\pi, \quad Z_m = -\frac{i\mu_0 \omega}{u} \frac{K_m'(ua)}{K_m(ua)},$$

$$\text{and } Y_m = (i\gamma_e^2/u\mu_0\omega)\, K_m'(ua)/K_m(ua)$$

Actually, (1) is an exact equation to determine the axial propagation constant Γ of the discrete modes for the structure. These include the modes that have a transmission line characteristic at low frequencies as well as the waveguide modes that propagate at high frequencies. This transmission line or monofilar mode has no low-frequency cutoff so it is of considerable practical interest in mine communication problems.

The attenuation rate (Re Γ in nepers/m) of the monofilar mode has a strong dependence on the distance $d = a - \rho_0$ from the tunnel wall. This is an important design consideration in communication schemes since it is convenient to locate the axial wire near the tunnel wall where d is somewhat less than a. Unfortunately, in this case, the summation over m in modal equation (1) is poorly convergent so computation is difficult. But physically, in this case, one would expect the configuration to be very similar to that of an infinite wire located at a height d over a flat earth of conductivity σ_e and permittivity ϵ_e. Mathematically this transition corresponds to letting $a \to \infty$ but keeping d finite.

We shall indicate here that the appropriate modal equation for the thin wire over the half-space is obtained as a limiting case of (1). The key step is to replace the infinite summation over integers m in (1) by an infinite integral with a variable λ

that is identified with m/a. Uniform asymptotic expansions [*Abramowitz and Stegun*, 1964] for the modified Bessel functions can be used here effectively. For example:

$$Z_m \to Z_{\lambda a} = -(i\mu_0\omega/u)\, K'_{\lambda a}(ua)/K_{\lambda a}(ua)$$
$$\simeq +(i\mu_0\omega/u)[1 + (u/\lambda)^2]^{1/2}/(u/\lambda) \tag{4}$$

Using such asymptotic forms, we find that

$$R_m \to R_{\lambda a} \cong \{\lambda^2\Gamma^2(1 - K^2) - [\epsilon_0\omega\hat{v} - (\epsilon_e - i\sigma_e \div \omega)\omega\hat{u}K](\mu_0\omega\hat{v} + \mu_e\omega\hat{u}K)\}/\{\lambda^2\Gamma^2(1 - K)^2 + [\epsilon_0\omega\hat{v} + (\epsilon_e - i\sigma_e/\omega)\omega\hat{u}K](\mu_0\omega\hat{v} + \mu_e\omega\hat{u}K)\} \tag{5}$$

where $K = (\Gamma^2 - \gamma_0^2)/(\Gamma^2 - \gamma_e^2)$. But, in the case $\mu_e = \mu_0$, we can reduce this to

$$R_{\lambda a} = \left[1 + \frac{2\gamma_0^2}{\gamma_0^2 - \Gamma^2}\frac{(\lambda^2 - \hat{u}\hat{v})\hat{v}}{\gamma_0^2\hat{u} + \gamma_e^2\hat{v}}\right] \tag{6}$$

where

$$\hat{u} = (\lambda^2 + u^2)^{1/2} = (\lambda^2 - \Gamma^2 + \gamma_e^2)^{1/2}$$

and

$$\hat{v} = (\lambda^2 + v^2)^{1/2} = (\lambda^2 - \Gamma^2 + \gamma_0^2)^{1/2}$$

Then, on making all the appropriate substitutions, the mode equation (1) is transformed to

$$\{K_0[(\gamma_0^2 - \Gamma^2)^{1/2}c] - K_0[(\gamma_0^2 - \Gamma^2)^{1/2}2d]\} \cdot (1 - \Gamma^2/\gamma_0^2) = 2\int_0^\infty [(\lambda^2 - \hat{v}\hat{u})/(\gamma_0^2\hat{u} + \gamma_e^2\hat{v})] \cdot \exp(-2\hat{v}d)\, d\lambda \tag{7}$$

This is entirely equivalent to the postulated form

$$Z - \Gamma^2 Y^{-1} = 0 \tag{8}$$

where

$$Z = [i\mu_0\omega/(2\pi)][\Lambda + 2(Q - iP)] \tag{9}$$

and

$$Y = (i2\pi\epsilon_0\omega)[\Lambda + 2(N - iM)]^{-1} \tag{10}$$

where

$$\Lambda = K_0[(\gamma_0^2 - \Gamma^2)c] - K_0[(\gamma_0^2 - \Gamma^2)2d] \tag{11}$$

and

$$Q - iP = \int_0^\infty \frac{\exp(-\hat{v}2d)}{\hat{u} + \hat{v}}\, d\lambda \tag{12}$$

and

$$N - iM = (\gamma_0/\gamma_e)^2 \int_0^\infty \frac{\exp(-\hat{v}2d)}{\hat{v} + (\gamma_0/\gamma_e)^2\hat{u}}\, d\lambda \tag{13}$$

There is no further approximation in writing the transformed mode equation in the form given by (8) rather than (7). But here one should note that Z and Y, while functions of Γ, can be interpreted as a series impedance and series admittance, respectively. Not surprisingly, (8) is the same as the result derived directly for the model of a thin wire over a uniform half space [*Wait*, 1972].

A similar transition analysis was carried out recently by *King et al.* [1974] who began with an approximate form for the fields of an eccentrically located wire in a cylindrical cavity. After making numerous approximations, they arrived at a form similar to (7) and (8) above but the $N - iM$ integral is not present. They suggest their result is valid if (in our notation), $|\gamma_e/\gamma_0|^2 \gg 1$ and $|\gamma_0 d| \ll 1$. Indeed this does seem to be true. But, at higher frequencies, it is necessary to include the modification to the generalized admittance Y from the $N - iM$ integral. The importance of this type of coupling has actually been considered by *Chang and Wait* [1974] and *Chang and Olsen* [1975] in a somewhat different context.

Thus we have shown that the mode equation, properly formulated for an axial wire in a cylindrical tunnel, does indeed transform into the appropriate form for a thin wire over a half space in the limit of the tunnel radius approaching infinity. But we should remain conscious of the different physical nature of the two problems even if the radius a becomes large compared with other physical dimensions.

REFERENCES

Abramowitz, M., and I. A. Stegun (1964), *Handbook of Mathematical Functions*, p. 378, US Government Printing Office, Washington, DC.

Chang, D. C., and R. G. Olsen (1975), Excitation of an infinite antenna above a dissipative earth, *Radio Sci.*, *10*(8,9), 823–832.

Chang, D. C., and J. R. Wait (1974), Extremely low frequency (ELF) propagation along a horizontal wire located above or buried in the earth, *IEEE Trans. Commun.*, *COM-22*(4), 421–426.

King, R. W. P., T. T. Wu, and L. C. Shen (1974), The horizontal wire antenna over a conducting or dielectric half space: Current

and admittance, *Radio Sci.*, 9(7), 701-709. [See also comments on this article, by J. R. Wait, *Radio Sci.*, 9(12), 1165.]

Wait, J. R. (1972), Theory of wave propagation along a thin wire parallel to an interface, *Radio Sci.*, 7(6), 675-679. [In (28) for $N - iM$, a factor $(k_1/k_2)^2$ should multiply the integral; in (17), delete the superscript $1/2$ in the factor $(\gamma^2 - u_1 u_2)$; in (36), the denominator of the integrand should be $k_1^2 u_2 + k_2^2 u_1$. This paper also contains numerous references to earlier work.]

Wait, J. R., and D. A. Hill (1974), Guided electromagnetic waves along an axial conductor in a circular tunnel, *IEEE Trans. Antennas Propagat.*, *AP-22*(4), 627-630.

Attenuation on a surface wave G-line suspended within a circular tunnel

James R. Wait and David A. Hill

Institute for Telecommunication Sciences, Office of Telecommunications, U.S. Department of Commerce, Boulder, Colorado 80302
(Received 14 June 1976)

Calculations indicate that a surface wave Goubau line may have useful transmission characteristics even if it is located within 20 cm from the rock wall of a tunnel. The results are consistent with previous theoretical and experimental data for a thin wire located at low heights over a finitely conducting plane earth.

PACS numbers: 84.40.Qp, 42.20.—y, 84.40.Cb, 84.40.Ts

In a number of instances, one needs to communicate through tunnels whether these be in coal mines or for roadways in mountainuous terrain. For air-filled empty tunnels with mean radii of the order of 2 m, the cutoff frequency for waveguide mode propagation is approximately 50 MHz. At lower frequencies the attenuation rate becomes very high unless axial metal conductors within the tunnel are utilized. There may be rails and pipes that would be present in any case in time tunnels. In order to control such transmissions, open wire and loosely braided coaxial cables have been used with considerable success.[1] Another possibility is to suspend a surface wave or G-line[2] from the roof of the tunnel. This scheme may have numerous practical difficulties, particularly in coal mines where the environment is hostile at best. Nevertheless, it is of interest to examine the transmission characteristics for an idealized analytical model. We wish to report some preliminary calculations for the attenuation rate of the mode that has the character of an axial surface wave at frequencies above about 100 MHz.

The analytic model we employ is an infinitely long and straight tunnel with a constant radius a_0 that contains an axial wire of radius c_0 located at a distance ρ_0 from the tunnel axis (see Fig. 1). The metal wire of conductivity σ_w is encased by a dielectric insulation of radius b with a permittivity ϵ. To facilitate the analysis, it is assumed that b is much less than $a_0 - \rho_0$. This restriction, which is not severe, means that the G-line should not be very close to the tunnel wall. The magnetic permeability of the whole space is also assumed to be μ_0, the same as for free space. A general mode equation that characterizes the discrete mode of propagation for this type of structure is already available.[3,4] There are no restrictions on the solutions other than the one mentioned above.

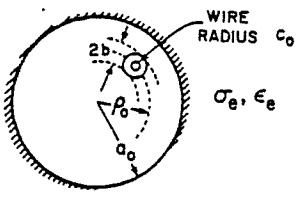


FIG. 1. Cross section of tunnel with G-line (not drawn to scale).

Using the theoretical formulation indicated, the attenuation rate of the "desired" mode was calculated for the values of the various parameters indicated in Fig. 2. In that figure, the attenuation rate, in dB/km, is plotted as a function of frequency from 1 MHz to 1 GHz for two values of the G-line—to—wall separation. The wire conductivity was chosen to be either infinite or 5.7×10^7 mho/m corresponding to copper.

The results shown in Fig. 2 are significant and they need to be discussed briefly. First of all, at the lower frequencies (i.e., less than 10 MHz), the results are almost indistinguishable from the case of a bare wire without insulation covering. In fact, on comparing the results with those in Ref. 3, the general shape of the curves is seen to be quite similar to that for a bare wire at all except the highest frequencies. The main effect of the dielectric covering is to lower the attenuation at the upper frequencies. There is also a close similarity in shape with the monofilar mode results in Ref. 4 where, in effect, the transmission mode "sees" the braided conductor as a single wire. For the calculations in Fig. 2, we see that the influence of finite conductivity of the center conductor is only felt at frequencies approaching 1 GHz.

It is evident that the low-frequency portions of the curves in Fig. 2 correspond to a transmission line type of mode wherein the return current is flowing entirely within the rock or earth media adjacent to the tunnel

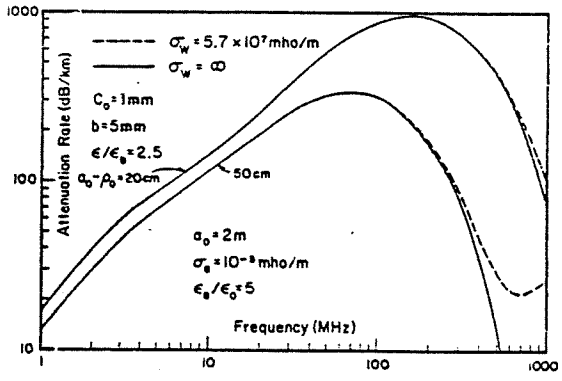


FIG. 2. Calculated attenuation rate of the transmission line mode that becomes a bound surface wave on the G-line at high frequencies.

 Copyright © 1976 American Institute of Physics

wall. For frequencies less than about 20 MHz, the attenuation rate is approximately proportional to frequency and reaches a maximum around 100 MHz where there is maximum absorption by the tunnel walls. For higher frequencies, the attenuation rate actually decreases because the energy flow is tightly bound to the G-line. In this case, the tunnel walls are having a minimal influence. At still higher frequencies, however, the almost pure Goubau mode is then influenced mainly by the finite conductivity of the conductor wire.

Actually, the calculations given here and those in Refs. 3 and 4 bear a striking resemblance to those obtained by Kikuchi[5] for a bare finitely conducting wire located in air over a homogeneous conducting half-space. The correspondence is particularly close when Kikuchi's results are scaled such that his frequencies are multiplied by 10 and his dimensions are multiplied by 0.1. In this way, the heights of his wire above ground are comparable to the distance of our G-line to the tunnel wall. The broad maxima for the attenuation rate shown in Fig. 2 and also those in Ref. 1 are then quite consistent with Kikuchi's results, although we do not attempt a detailed comparison because of the basic difference in the models employed. Similar results, both theoretical and experimental, were published recently by Chiba and Sato[6] where the scaling is not necessary to afford a direct qualitative comparison. They employ a wire conductor of radius 1.15 mm with a dielectric coating of radius 4.2 mm located at heights of 60 cm, 1.5 m, and 5 m over a conducting half-space model of the earth. Unfortunately, other parameters are not given; so a careful comparison is not possible. Nevertheless, a maximum attenuation of about 200 dB/km for the 60-cm height occurs at a frequency of about 70 MHz, while the high-frequency minimum of about 26 dB/km occurs at a frequency around 700 MHz. These are certainly consistent with the results shown in Fig. 2. Chiba and Sato also found good agreement with an experimental G-line of 100 m length that was excited by a horn transmitter.

While we do not expect quantitative agreement with calculations based on half-space models, it is reassuring that our results are entirely consistent with such independent investigations. In this connection, the portion of the curves in Fig. 2 for $a_0 - \rho_0 = 50$ cm are extremely close (within a few percent) to some results calculated by Lavrov and Knyazev.[7] Their bare wire is located at 50 cm height over a half-space of conductivity 10^{-3} and relative permittivity 6. This is a further check on our method of calculation.

We are currently making a comprehensive analytical evaluation of the G-line transmission characteristics located in a tunnel. By adapting the formulation given in Ref. 4, we are able to allow for the possible existence of a lossy film on the outer dielectric surfaces of the G-line. Such a coating can represent a thin layer of conductive mine dust or a mineralized water film. This will be a severe limiting factor in the use of the G-line at gigahertz frequencies in mine environments but should not be too upsetting at frequencies less than about 200 MHz.

[1]J.R. Wait, Radio Electron. Eng. 45, 229 (1975).
[2]G. Goubau, J. Appl. Phys. 21, 1119 (1950).
[3]J.R. Wait and D.A. Hill, IEEE Trans. Antennas Propagat. AP-22, 627 (1974).
[4]J.R. Wait and D.A. Hill, IEEE Trans. Microwave Theory Tech. MTT-23, 401 (1975).
[5]H. Kikuchi, Proc. IEE 120, 637 (1973).
[6]J. Chiba and R. Sato, Tech. Rep. Tokoku University 39, 133 (1974).
[7]G.A. Lavrov and A.S. Knyazev, *Near Earth and Buried Antennas* (Soviet Radio, Moscow, 1965), Chap. 3, Fig. 2.4.

INT. J. ELECTRONICS, 1977, VOL. 42, NO. 4, 377–391

Electromagnetic fields of a dipole source in a circular tunnel containing a surface wave line

JAMES R. WAIT† and DAVID A. HILL‡

We present a boundary value analysis for the fields excited by a dipole in a circular tunnel that contains a dielectric coated axial conductor. The integral form of the solution is generally valid provided the outer radius of the dielectric coated conductor is small compared with its distance to the tunnel wall. The propagation mode that behaves as an axial surface wave at high frequencies is examined for a frequency range from 1 MHz to 1 GHz. The attenuation reaches a maximum value at frequencies of the order of 100 MHz where the absorption loss by the tunnel wall is most significant. In the range from 1 to about 10 MHz, the attenuation rate is approximately proportional to frequency and is only weakly dependent on the conductivity of the region external to the tunnel walls. The results are consistent with earlier investigations for surface wave lines located over a homogeneous half-space.

1. Introduction

Communication through the tunnels is often needed for the control of trains. The use of coaxial cables in one form or another has been suggested (Mikoshiba and Nurita 1969, Okada *et al.* 1975, Beal *et al.* 1973, Gallawa *et al.* 1969, Davis 1975). Such techniques are found to be particularly applicable to communication in mines and such underground facilities where the environment is rather hostile. Such coaxial cable systems are operable even when a layer of conducting fluid or dust coats the outer surface of the cable jacket. Another possibility that is appropriate for relatively dry tunnels is the surface wave transmission line (SWTL). In its simplest form, this is a metallic wire with a concentric dielectric coating. As pointed out by Goubau (1950), such a line will guide electromagnetic waves with small loss. The use of the SWTL in high-speed ground transportation systems shows considerable promise (Gallawa *et al.* 1969). The basic advantage is that the desired signal is confined to the vicinity of the line yet physical contact is not needed for access.

By their very nature, continuous access communication systems (CAGC) should not be unduly influenced by the environment except in the neighbourhood of the SWTL. However, if the SWTL is located close to a conductor such as the ground or the wall of a tunnel, we should expect some degradation of the propagation (Davis 1975). This effect would be self-evident after examining the calculations by Gallawa *et al.* (1969) of the axial power flow for a SWTL located in free space. They show that, for a typical SWTL operating in the frequency range 500–1000 MHz, the radial extent of the power flow extends out to distances of the order of 50 cm. Thus a valid question is : how close to a tunnel wall could we locate an SWTL and still maintain the advantage of low attenuation ?

Received 27 September 1976.

† Cooperative Institute for Research in Environmental Sciences, University of Colorado/NOAA/ERL, Boulder, Colorado 80309, U.S.A.

‡ Institute for Telecommunication Sciences, Office of Telecommunications, U.S. Department of Commerce, Boulder, Colorado 80302, U.S.A.

2. Statement of problem

With the motivation indicated above, we propose to analyse the configuration indicated in Fig. 1 which we will describe with reference to a cylindrical coordinate system (ρ, ϕ, z). The tunnel of radius a_0 is cut through a homogeneous rock medium (i.e. for $\rho > a_0$) of conductivity σ_e and permittivity ϵ_e. Without complicating the analysis we can also allow the external region to have a magnetic permeability μ_e that is different from the free space value μ_0.

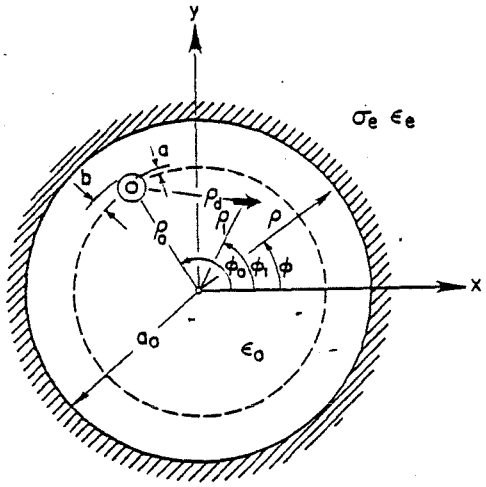


Figure 1. Cross-section geometry for the SWTL (Surface Wave Transmission Line) located in a circular tunnel and the dipole exciter.

Within the tunnel we locate a SWTL that consists of a solid cylindrical conductor of radius a with electrical properties σ_w, ϵ_w and μ_w. This conductor is coated with a lossless dielectric coating of outer radius b, with permittivity ϵ and assumed permeability μ_0. The axis of the SWTL is located at $\rho = \rho_0$ and $\phi = \phi_0$. To simplify the analysis, we require that $a_0 - \rho_0 \gg b$. This restriction will assume that the axial currents on the SWTL are essentially uniform in the circumferential direction and that the effect of non-axial current are neglible.

In previous analyses (Wait and Hill 1974, 1975) of this configuration, we have represented the field as a superposition of modes that individually satisfy the boundary conditions at the walls. For the applications intended, only a few such discrete modes were needed to represent the total field. However, it does seem that a preferred procedure is to deal explicitly with the fields of a source located anywhere within the tunnel. This representation leads very naturally to the excitation factors for the modal contributions. It also provides a convenient starting point to evaluate the continuous modes that are normally neglected.

The derivation given here will be quite brief since we can refer the reader to closely related papers for some aspects of the analysis (Wait and Hill 1974, 1975, Hill and Wait 1974, 1975). The general scheme will be to first construct

an integral representation of the fields of the dipole within the tunnel. Then we postulate a corresponding field representation for the fields of the SWTL (Surface Wave Transmission Line) that also satisfies the boundary conditions at the tunnel wall. We then insist that the total fields must satisfy an appropriate axial impedance condition at the surface of SWTL. In what follows, we deal with time harmonic fields in accordance with the factor exp ($i\omega t$).

3. Fields of dipole in empty tunnel

In general, we find it convenient to work with two scalar potential functions. These are really the z components of axially directed Hertz vectors of the electric and magnetic type. In the case of the dipole source in the empty tunnel, these Hertz potentials U and V have the following form

$$\begin{bmatrix} U \\ V \end{bmatrix} = \sum_{m=-\infty}^{+\infty} \int_{-\infty}^{+\infty} \left\{ \begin{bmatrix} A_m(\lambda) \\ B_m(\lambda) \end{bmatrix} K_m(v\rho) + \begin{bmatrix} P_m(\lambda) \\ Q_m(\lambda) \end{bmatrix} I_m(v\rho) \right\} \times \exp\left[-im(\phi-\phi_1)\right] \exp\left(-i\lambda z\right) d\lambda \qquad (1)$$

where $I_m(v\rho)$ and $K_m(v\rho)$ are modified Bessel functions, $v=(\lambda^2+\gamma_0^2)^{1/2}$ and $\gamma_0=i(\epsilon_0\mu_0)^{1/2}\omega$. The dipole of the electric or magnetic type is located at $(\rho, \phi_1, 0)$ where $\rho_1<a_0$. The functions $A_m(\lambda)$ and $B_m(\lambda)$ are determined by the strength and orientation of the dipole as indicated in the Appendix. The functions $P_m(\lambda)$ and $Q_m(\lambda)$ are related to $A_m(\lambda)$ and $B_m(\lambda)$ via the boundary conditions at the tunnel walls.

Here we digress slightly and express (1) in the form

$$\begin{pmatrix} U \\ V \end{pmatrix} = \Gamma \begin{pmatrix} U_m \\ V_m \end{pmatrix} \qquad (2)$$

where Γ is the indicated integral-summation operator. Then the corresponding field components tangential to the tunnel wall are obtained from

$$\begin{pmatrix} E_\phi \\ H_\phi \\ E_z \\ H_z \end{pmatrix} = \Gamma \begin{pmatrix} E_{\phi m} \\ H_{\phi m} \\ E_{zm} \\ H_{zm} \end{pmatrix} \qquad (3)$$

where

$$E_{\phi m} = -(m\lambda/\rho)U_m + i\mu_0\omega\partial V_m/\partial\rho \qquad (4)$$

$$H_{\phi m} = -i\epsilon_0\omega\partial U_m/\partial\rho - (m\lambda/\rho)V_m \qquad (5)$$

$$E_{zm} = -v^2 U_m \qquad (6)$$

and

$$H_{zm} = -v^2 V_m \qquad (7)$$

where $v^2=\lambda^2+\gamma_0^2$ and $\gamma_0^2=-\epsilon_0\mu_0\omega^2$. As we have shown before (Wait and Hill 1974), the boundary conditions at the cavity or tunnel wall are succinctly expressed by

$$\left.\begin{aligned} E_{\phi m} &= \alpha_m E_{zm} + Z_m H_{zm} \\ H_{\phi m} &= -Y_m E_{zm} + \alpha_m H_{zm} \end{aligned}\right]_{\text{at } \rho=a_0} \tag{8, 9}$$

where

$$\alpha_m = m\lambda/(u^2 a_0) \tag{10}$$

$$Z_m = -(i\mu_e\omega/u)K_m'(ua_0)/K_m(ua_0) \tag{11}$$

$$Y_m = [i\gamma_e^2/(u\mu_e\omega)]K_m'(ua_0)/K_m(ua_0) \tag{12}$$

$$\gamma_e^2 = i\mu_e\omega(\sigma_e + i\epsilon_e\omega)$$

$$u = (\lambda^2+\gamma_e^2)^{1/2}$$

The application of the boundary conditions expressed by (8) and (9) lead readily to the desired relationships of P_m and Q_m in terms of A_m and B_m. Thus

$$P_m(\lambda) = -[A_m(\lambda)r_m + B_m(\lambda)t_m]D_m^{-1} \tag{13}$$

$$Q_m(\lambda) = -[A_m(\lambda)s_m + B_m(\lambda)w_m]D_m^{-1} \tag{14}$$

where

$$r_m = \left[\left(\frac{m\lambda}{v^2a_0}-\alpha_m\right)^2 + \left(\frac{\gamma_0 K_m'}{vK_m}+\eta_0 Y_m\right)\left(\frac{\gamma_0 I_m'}{vI_m}+\frac{Z_m}{\eta_0}\right)\right] I_m K_m \tag{15}$$

$$t_m = \left(\frac{m\lambda}{v^2a_0}-\alpha_m\right)\frac{i\mu_0\omega}{v^2a_0} \tag{16}$$

$$s_m = -\left(\frac{m\lambda}{v^2a_0}-\alpha_m\right)\frac{i\epsilon_0\omega}{v^2a_0} \tag{17}$$

$$w_m = \left[\left(\frac{m\lambda}{v^2a_0}-\alpha_m\right)^2 + \left(\frac{\gamma_0 I_m'}{vI_m}+\eta_0 Y_m\right)\left(\frac{\gamma_0 K_m'}{vK_m}+\frac{Z_m}{\eta_0}\right)\right] I_m K_m \tag{18}$$

and

$$D_m = \left[\left(\frac{m\lambda}{v^2a_0}-\alpha_m\right)^2 + \left(\frac{\gamma_0 I_m'}{vI_m}+\eta_0 Y_m\right)\left(\frac{\gamma_0 I_m'}{vI_m}+\frac{Z_m}{\eta_0}\right)\right] I_m^2 \tag{19}$$

To achieve conciseness in notation, we have used above the following abbreviations: $I_m = I_m(va_0)$, $I_m' = I_m(va_0)$, $K_m = K_m(va_0)$, $K_m' = K_m'(va_0)$ while bearing in mind that α_m, Z_m and Y_m are defined by (10), (11) and (12). In the above $\eta_0 = (\mu_0/\epsilon_0)^{1/2} \simeq 120\pi$ is the characteristic impedance of the air inside the tunnel that we assume is the same as free space.

4. Fields due to SWTL

We now consider the fields in the tunnel region due to the axial current on the SWTL. In analogy to previous work (Wait and Hill 1974, 1975,

6. Application of axial impedance boundary condition

The (spatially dispersive) impedance boundary condition that characterizes the SWTL is simply expressed by

$$\hat{I}(\lambda) \cdot Z_b(\lambda) = \hat{E}_z(\lambda) \tag{28}$$

Here $\hat{E}_z(\lambda)$ is the spatial transform of the tangential electric field at the surface of the SWTL and $Z_b(\lambda)$ is the axial impedance that is defined in terms of the quantities λ, a, b, σ_w, ϵ_w, μ_w and ϵ. Strictly speaking, the actual tangential electric field given by $E_z(z) = (-\gamma_0^2 + \partial^2/\partial z^2)(U + U_s)$ at $\rho' = b$ will vary with ϕ' around the circumference of the SWTL. But, in view of our assumption on the smallness of b, we may select the matching point at $\phi = \phi_0$ and $\rho = \rho_0 + b$. This leads to the result that

$$2\pi i \epsilon_0 \omega Z_b(\lambda) \cdot F(\lambda) = -v^2 \sum_m [A_m(\lambda) K_m(v\rho_0) + P_m(\lambda) I_m(v\rho_0)] \times \exp[-im(\phi_0 - \phi_1)] - v^2 F(\lambda) \left[K_0(vb) - \sum_n R_n(\lambda) \frac{K_n(va_0)}{I_n(va_0)} \times I_n(v\rho_0) I_n[v(\rho_0 + b)] \right] \tag{29}$$

This can be immediately solved for $F(\lambda)$ in the form

$$F(\lambda) = -v^2 D^{-1}(\lambda) \sum_{m=-\infty}^{+\infty} [A_m(\lambda) K_m(v\rho_0) + P_m(\lambda) I_m(v\rho_0)] \times \exp[-im(\phi_0 - \phi_1)] \tag{30}$$

where

$$D(\lambda) = 2\pi i \epsilon_0 \omega Z_b(\lambda) + v^2 \left[K_0(vb) - \sum_{n=-\infty}^{+\infty} R_n(\lambda) \frac{K_n(va_0)}{I_n(va_0)} \times I_n(v\rho_0) I_n[v(\rho_0 + b)] \right] \tag{31}$$

To be consistent with our earlier assumption about the smallness of b, we should really replace $I_n[v(\rho_0 + b)]$ by $I_n(v\rho_0)$ in both (29) and (30).

This completes the formal development of the problem. The resultant fields are obtained from the resultant Hertz potentials $U + U_s$ and $V + V_s$ by using (1), (13), (14), (20), (21), (30) and (31). Also, of course, the coefficients $A_m(\lambda)$ and $B_m(\lambda)$ are specified by the nature of the source dipole as indicated in the Appendix.

A remaining consideration is the specification of the series impedance $Z_b(\lambda)$. This can be obtained by solving an auxiliary boundary value problem involving a dielectric coated wire in free space that is excited by a plane wave. The solution, considered as a special case of an earlier analysis (Wait and Hill 1975), can be written simply in quasi-static form as follows :

$$Z_b(\lambda) \simeq Z + Z_i \tag{32}$$

where

$$Z = \frac{(\lambda^2 - k^2)}{2\pi i \epsilon \omega} \ln \frac{b}{a} \quad \text{with } k^2 = \epsilon \mu_0 \omega^2 \tag{33}$$

6. Application of axial impedance boundary condition

The (spatially dispersive) impedance boundary condition that characterizes the SWTL is simply expressed by

$$\hat{I}(\lambda) \cdot Z_b(\lambda) = \hat{E}_z(\lambda) \tag{28}$$

Here $\hat{E}_z(\lambda)$ is the spatial transform of the tangential electric field at the surface of the SWTL and $Z_b(\lambda)$ is the axial impedance that is defined in terms of the quantities λ, a, b, σ_w, ϵ_w, μ_w and ϵ. Strictly speaking, the actual tangential electric field given by $E_z(z) = (-\gamma_0^2 + \partial^2/\partial z^2)(U + U_s)$ at $\rho' = b$ will vary with ϕ' around the circumference of the SWTL. But, in view of our assumption on the smallness of b, we may select the matching point at $\phi = \phi_0$ and $\rho = \rho_0 + b$. This leads to the result that

$$2\pi i \epsilon_0 \omega Z_b(\lambda) \cdot F(\lambda) = -v^2 \sum_m [A_m(\lambda) K_m(v\rho_0) + P_m(\lambda) I_m(v\rho_0)] \times \exp[-im(\phi_0 - \phi_1)] - v^2 F(\lambda) \left[K_0(vb) - \sum_n R_n(\lambda) \frac{K_n(va_0)}{I_n(va_0)} \times I_n(v\rho_0) I_n[v(\rho_0 + b)] \right] \tag{29}$$

This can be immediately solved for $F(\lambda)$ in the form

$$F(\lambda) = -v^2 D^{-1}(\lambda) \sum_{m=-\infty}^{+\infty} [A_m(\lambda) K_m(v\rho_0) + P_m(\lambda) I_m(v\rho_0)] \times \exp[-im(\phi_0 - \phi_1)] \tag{30}$$

where

$$D(\lambda) = 2\pi i \epsilon_0 \omega Z_b(\lambda) + v^2 \left[K_0(vb) - \sum_{n=-\infty}^{+\infty} R_n(\lambda) \frac{K_n(va_0)}{I_n(va_0)} \times I_n(v\rho_0) I_n[v(\rho_0 + b)] \right] \tag{31}$$

To be consistent with our earlier assumption about the smallness of b, we should really replace $I_n[v(\rho_0 + b)]$ by $I_n(v\rho_0)$ in both (29) and (30).

This completes the formal development of the problem. The resultant fields are obtained from the resultant Hertz potentials $U + U_s$ and $V + V_s$ by using (1), (13), (14), (20), (21), (30) and (31). Also, of course, the coefficients $A_m(\lambda)$ and $B_m(\lambda)$ are specified by the nature of the source dipole as indicated in the Appendix.

A remaining consideration is the specification of the series impedance $Z_b(\lambda)$. This can be obtained by solving an auxiliary boundary value problem involving a dielectric coated wire in free space that is excited by a plane wave. The solution, considered as a special case of an earlier analysis (Wait and Hill 1975), can be written simply in quasi-static form as follows :

$$Z_b(\lambda) \simeq Z + Z_i \tag{32}$$

where

$$Z = \frac{(\lambda^2 - k^2)}{2\pi i \epsilon \omega} \ln \frac{b}{a} \quad \text{with } k^2 = \epsilon \mu_0 \omega^2 \tag{33}$$

and

$$Z_i \simeq \frac{i\mu_w\omega}{2\pi(\sigma_w + i\epsilon_w\omega)^{1/2}a} \frac{I_0(\gamma_w a)}{I_1(\gamma_w a)} \tag{34}$$

with $\gamma_w = [(i\mu_w\omega)(\sigma_w + i\epsilon_w\omega)]^{1/2}$. Here Z is the λ dependent series impedance of the dielectric coating and Z_i is the axial impedance at the surface of the inner metal conductor. The latter is essentially independent of λ because $|\gamma^2| \gg \lambda^2$. By using the equations given in a previous paper (Wait and Hill 1975), a more accurate form of $Z_b(\lambda)$ is available for either this dielectric coated conductor or for a more complicated structure.

7. Modal spectrum

In general, a field component $\Phi(\rho, \phi, z)$ produced by the specific dipole source can be written in the following integral form

$$\Phi(\rho, \phi, z) = \sum_{n=-\infty}^{+\infty} \int_{-\infty}^{+\infty} \frac{G_n(\lambda)}{D(\lambda)} \exp(-in\phi) \exp(-i\lambda z)\, d\lambda \tag{35}$$

where $G_n(\lambda)$ is a generalized excitation coefficient that does not have any pole singularities in the complex λ plane. On the other hand, $D(\lambda)$ has zeroes for values of λ corresponding to the modes of the composite tunnel structure. Thus, for $z > 0$, we may close the λ integration contour in the lower half-plane by an infinite semi-circle to yield

$$\Phi(\rho, \phi, z) = -2\pi i \sum_{n=-\infty}^{+\infty} \sum_{s} \frac{G_n(\lambda_s)}{D'(\lambda_s)} \exp(-in\phi) \exp(-i\lambda_s z) + \text{C.S.} \tag{36}$$

Here λ_s are the solutions of the eigenvalue equation $D(\lambda) = 0$ and $D'(\lambda_s) = [dD(\lambda)/d\lambda]$ evaluated at $\lambda = \lambda_s$.

The continuous spectrum of modes denoted in (36) by C.S. corresponds to the contribution from the branch-line integrations that arise in the contour deformation mentioned above. In this paper we do not consider the C.S. but we can immediately make some remarks about the relative insignificance of such contributions in the present context. The branch point in question is located at $\lambda = -i\gamma_e$ where γ_e is the propagation constant of the conducting medium external to the tunnel wall. Contributions from the associated branch line for $z > 0$ behave as $\exp(-\gamma_e z)$ and thus the associated waves are highly attenuated for any value of n. Also, we should mention that the general mode equation $D(\lambda) = 0$ will yield an infinite number of solutions. A finite number of these will be ' propagating ' in the sense that the $|\text{Im} \cdot \lambda_s| \ll |\text{Re} \cdot \lambda_s|$. But of particular interest is the propagating mode that has the character of an axial surface wave. This can be clearly identified as the solution which has the desired character at high frequencies when the SWTL is not near the wall.

8. Numerical results for the modal attenuation

Using the theoretical formulation indicated, the attenuation rate of the ' desired ' mode was calculated for the values of the various parameters indicated in Fig. 2. In that figure, the attenuation rate, in dB per km, is

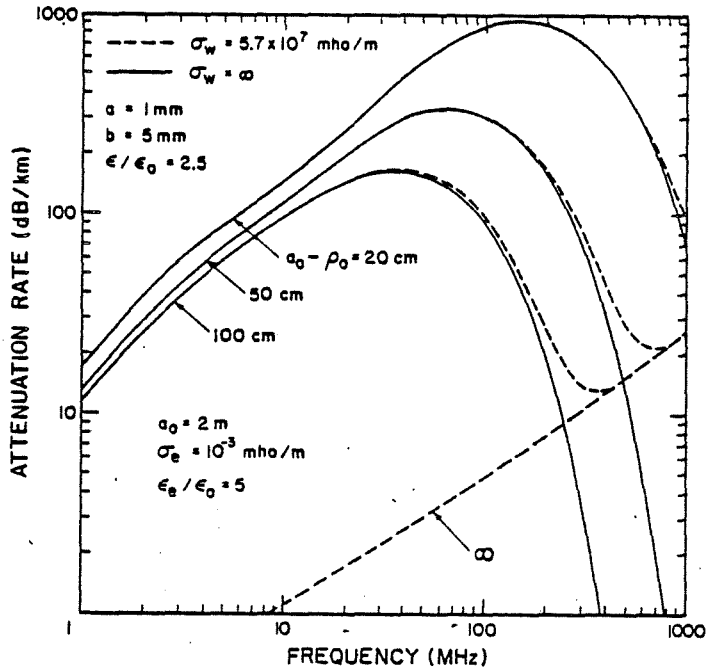


Figure 2. Attenuation rate of the mode that behaves as an axial surface wave at very high frequencies for several distances of the SWTL to the tunnel wall. The case indicated by ' ∞ ' corresponds to locating the SWTL in free space.

plotted as a function of frequency from 1 MHz to 1 GHz for three values of the SWTL to wall separation. The case where the SWTL is located in free space is indicated by the curve labelled ∞ (corresponding to an ' infinite ' distance from the tunnel wall). The wire conductivity was chosen to be either infinite or $5{\cdot}7 \times 10^7$ mho/m corresponding to copper.

The results shown in Fig. 2 are significant and they need to be discussed briefly. First of all, at the lower frequencies (i.e. less than 10 MHz), the results are almost indistinguishable from the case of a bare wire without insulation covering. In fact, on comparing the results with previous calculations (Wait and Hill 1974), the general shape of the curves are seen to be quite similar to those for a bare wire at all except the highest frequencies. The main effect of the dielectric covering is to lower the attenuation at the upper frequencies. There is also a close similarity in shape with the earlier obtained monofilar mode results (Wait and Hill 1975) where, in effect, the transmission mode ' sees ' the braided conductor as a single wire. For the calculations in Fig. 2, we note that the influence of finite conductivity of the centre conductor is only felt at frequencies approaching 1 GHz.

It is evident that the low frequency portions of the curves in Fig. 2 correspond to a transmission line type of mode wherein the return current is flowing entirely within the rock or earth media adjacent to the tunnel wall. For frequencies less than about 20 MHz, the attenuation rate is approximately proportional to frequency and reaches a maximum around 100 MHz where there is maximum absorption by the tunnel walls. For higher frequencies,

the attenuation rate actually decreases because the energy flow is tightly bound to the SWTL line. In this case, the tunnel walls are having a minimal influence. At still higher frequencies, however, the almost pure Goubau-type mode is then influenced mainly by the finite conductivity of the conductor wire.

Actually, the calculations given here and those described earlier (Wait and Hill 1974, 1975), bear a striking resemblance to those obtained by Kikuchi (1973) for a bare finitely-conducting wire located in air over a homogeneous conducting half-space. The correspondence is particularly close when Kikuchi's results are scaled such that his frequencies are multiplied by 10 and his dimensions are multiplied by 0·1. In this way, the heights of his wire above ground are comparable to the distance of our G-line to the tunnel wall. The broad maxima for the attenuation rate shown in Fig. 2 and also those in the special issue edited by Davis (1975), are then quite consistent with Kikuchi's results, although we do not attempt a detailed comparison because of the basic difference in the models employed. Similar results, both theoretical and experimental, were published recently by Chiba and Sato (1974) where the scaling is not necessary to afford a direct qualitative comparison. They employ a wire conductor of radius 1·15 mm with a dielectric coating of radius 4·2 mm located at heights of 60 cm, 1·5 and 5 m over a conducting half-space model of the earth. Unfortunately, other parameters are not given so a careful comparison is not possible. Nevertheless, a maximum attenuation of about 200 dB/km for the 60 cm height occurs at a frequency of about 70 MHz, while the high frequency minimum of about 26 dB/km occurs at a frequency around 700 MHz. These are certainly consistent with the results shown in Fig. 2. Chiba and Sato also found good agreement with an experimental SWTL line of 100 m length that was excited by a horn transmitter.

While we do not expect quantitative agreement with calculations based on half-space models, it is reassuring that our results are entirely consistent with such independent investigations. In this connection, the portion of the

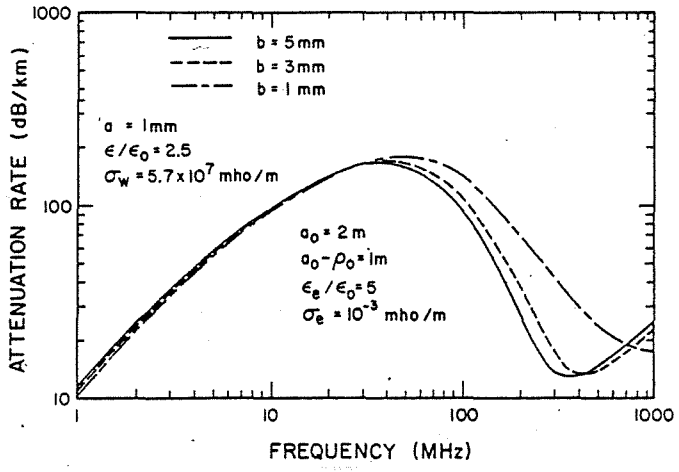


Figure 3. The influence of the thickness of the dielectric coating on the attenuation characters when the SWTL is located 1 m from the tunnel wall.

curves in Fig. 2 for $a_0 - \rho_0 = 50$ cm are extremely close (within a few per cent) to some results calculated by Lavrov and Knyazev (1965). Their bare wire is located at 50 cm height over a half space of conductivity 10^{-3} and relative permittivity of six. This is a further check on our method of calculation.

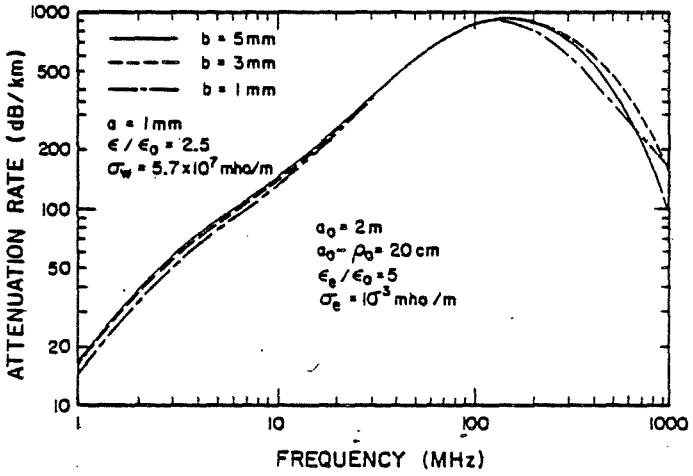


Figure 4. The influence of the thickness of the dielectric coating on the attenuation characters when the SWTL is located 20 cm from the tunnel wall.

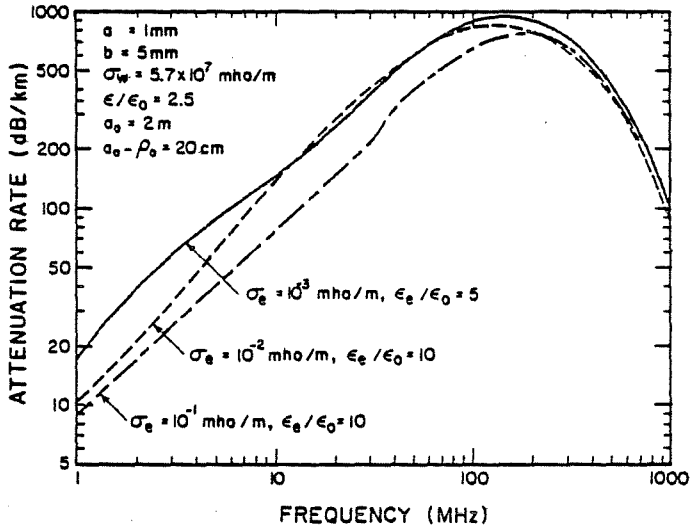


Figure 5. Influence of the electric properties of the external medium (e.g. rock) on the attenuation characteristics.

The influence of the thickness of the dielectric coating on the SWTL is illustrated in Fig. 3 where the distance to the tunnel wall is 1 m. At the lower frequencies, the dielectric coating has a negligible effect and, in this instance, the mode is monofilar in character. However, at the higher

frequencies, the thicker dielectric coating is associated with lower attenuation even though the effect is not pronounced. Similar results are shown in Fig. 4 where the distance of the SWTL to the wall is reduced to 20 cm. Now the mode has the mono-filar character even at high frequencies. For this same spacing, the influence of the conductivity of the external medium is illustrated in Fig. 5. The dependence is quite complicated but, in general, the lower conductivities are associated with higher attenuations.

9. Phase velocity of the ' desired ' mode

The phase velocity V_{ph} of the ' desired ' mode as a function of frequency is tabulated in the table for one of the examples considered in Fig. 2. As indicated, V_{ph} is always less than the velocity of light c for the whole frequency range from 1 to 1000 MHz. The ' slowness', however, is more apparent at the lower frequencies where the influence of the tunnel wall is

Phase velocity and radial field extent. $a_0=2$ m, $\sigma_e=10^{-3}$ mho/m, $\epsilon_e/\epsilon_0=5$, $a=1$ mm, $b=5$ mm, $\epsilon/\epsilon_0=2{\cdot}5$, $\sigma_w=5{\cdot}7\times10^7$, $a_0-\rho_0=50$ cm.

Frequency (MHz)	V_{ph}/c	Re (v) (m)
1·000	0·7874	60·98
1·279	0·7952	48·96
1·635	0·8040	39·47
2·091	0·8137	31·96
2·674	0·8240	25·97
3·420	0·8346	21·16
4·373	0·8449	17·24
5·593	0·8543	14·03
7·152	0·8630	11·40
9·146	0·8709	9·250
11·70	0·8782	7·496
14·96	0·8863	6·075
19·13	0·8955	4·932
24·46	0·8993	4·014
31·28	0·9062	3·271
40·00	0·9127	2·667
76·15	0·9242	1·517
117·0	0·9254	0·9971
179·7	0·9226	0·6358
276·0	0·9172	0·3982
423·9	0·9100	0·2472
651·0	0·9011	0·1525
1000·0	0·8901	0·0933

most significant. A related quantity listed in the table is the parameter $1/\mathrm{Re}\cdot v$ that can be identified as the radial extent of the field of the SWTL. Not surprisingly, at the lower frequencies this quantity is much greater than the cross-sectional dimension of the tunnel. This is compatible with the fact that the monofilar mode is influenced significantly by the tunnel walls.

At the higher frequencies, however, the parameter $1/\mathrm{Re}\cdot v$ is much less than the distance of the SWTL to the tunnel wall. Not surprisingly, this is associated with a tightly-bound surface wave mode of relatively low attenuation.

10. Concluding remarks

The present analysis is sufficiently general to allow for the prediction of the complete electromagnetic field produced by a dipole source of arbitrary orientation located in a circular tunnel that contains a 'thin' axial structure. In this context, 'thin' means that the wave guiding structure has an outer diameter that is small compared with its distance to the tunnel wall. For the numerical results described here, we specialized the axial cylindrical structure to be a SWTL (Surface Wave Transmission Line) that consists of a dielectric coated metallic conductor of circular cross section. Such an SWTL located in free space is known to support a weakly attenuating axial surface wave that is tightly bound in the radial direction. The calculations indicate that the proximity of the tunnel wall will have a very significant influence, at the lower frequencies, on the characteristics of this mode. Nevertheless, there may be some merit in utilizing the SWTL in tunnels if limited access communication is to be desired.

Further work on this subject should consider the question of the relative excitation efficiency of the surface-wave mode and the associated tunnel waveguide modes that are certainly implicit in our formulation. The effect of axial non-uniformities should also be considered since these will produce both undesirable and possibly desirable mode conversion phenomena.

Appendix

Primary field representations

The cross section of the tunnel or cylindrical cavity is indicated in Fig. 1 where both cylindrical coordinates (ρ, ϕ, z) and cartesian coordinates (x, y, z) have been chosen. We first consider an electric dipole of current moment $I\,ds$ is located at $(\rho_1, \phi_1, 0)$ that is oriented in the x direction. Our objective is to obtain an expression for the electric Hertz vector for the indicated dipole on the assumption that the tunnel walls are at an infinite distance. Such a vector, that has only an x component $\Pi_x{}^p$ in the cartesian system, is given by

$$\Pi_x{}^p = [I\,ds/(4\pi i\epsilon_0\omega)]R^{-1}\exp(-\gamma_0 R) \tag{37}$$

where the assumed time factor is $\exp(i\omega t)$, where $\gamma_0 = i(\epsilon_0\mu_0)^{1/2}\omega$ and where $R = [\rho^2 + \rho_1{}^2 - 2\rho\rho_1\cos(\phi - \phi_1) + z^2]^{1/2}$.

We now introduce two well known identities from Bessel function theory that are often exploited in problems of this type (Wait 1959):

$$\frac{\exp(-\gamma_0 R)}{R} = \frac{1}{\pi}\int_{-\infty}^{+\infty} K_0(v\hat{\rho})\exp(-i\lambda z)\,d\lambda \quad \text{where } v = (\lambda^2 + \gamma_0{}^2)^{1/2} \tag{38}$$

and

$$K_0(v\hat{\rho}) = \sum_{m=-\infty}^{+\infty} I_m(v\rho_1)K_m(v\rho)\exp[-im(\phi - \phi_1)] \quad (\text{for } \rho_1 < \rho) \tag{39}$$

where $\hat{\rho}=[\rho^2+\rho_1{}^2-2\rho\rho_1\cos(\phi-\phi_1)]^{1/2}$. Then, we see that

$$\Pi_x{}^p=\frac{I\,ds}{4\pi^2 i\epsilon_0\omega}\,\Gamma(I_m(v\rho_1)K_m(v\rho)) \tag{40}$$

where Γ denotes the operation

$$\sum_{-\infty}^{+\infty}\int_{-\infty}^{+\infty}(\ldots)\exp[-im(\phi-\phi_1)]\exp(-i\lambda z)\,d\lambda$$

on the quantity in parenthesis. The integration contour here is taken along the entire real axis in the complex λ plane. The summation is over all integer values of m from $-\infty$ to $+\infty$ including zero.

The corresponding axial electric field is obtained as follows :

$$E_z{}^p=\frac{\partial^2\Pi_x{}^p}{\partial x\partial z}=\left(\cos\phi\,\frac{\partial}{\partial\rho}-\sin\phi\,\frac{1}{\rho}\,\frac{\partial}{\partial\phi}\right)\frac{\partial\Pi_x{}^p}{\partial z}$$

$$=\frac{I\,ds}{4\pi^2 i\epsilon\omega_0}\int(-i\lambda)P(\lambda)\exp(-i\lambda z)\,d\lambda \tag{41}$$

where

$$P(\lambda)=\sum\left((\cos\phi)\,\frac{\partial K_m}{\partial\rho}+\frac{im}{\rho}\,(\sin\phi)K_m\right)I_m\exp[-im(\phi-\phi_1)] \tag{42}$$

The argument of K_m, in the above expression for $P(\lambda)$, is $v\rho$ and that of I_m is $v\rho_1$. Then, by using the Bessel function

$$K_m{}'=-(1/2)[K_{m-1}+K_{m+1}] \tag{43}$$

and

$$K_m=(v\rho/2m)[K_{m+1}-K_{m-1}] \tag{44}$$

it follows that

$$P(\lambda)=-\frac{v}{2}\sum K_{m-1}I_m\exp[-i(m-1)\phi+im\phi_1]$$

$$+K_{m+1}I_m\exp[-i(m+1)\phi+im\phi_1] \tag{45}$$

$$=-\frac{v}{2}\sum K_m\exp[-im(\phi-\phi_1)][\exp(i\phi_1)I_{m+1}$$

$$+\exp(-i\phi_1)I_{m-1}] \tag{46}$$

By we can also write

$$E_z{}^p=(-\gamma_0{}^2+\partial^2/\partial z^2)U^p \tag{47}$$

in terms of electric Hertz potential U^p which is the z component of an axially directed electric Hertz vector. Clearly,

$$U^p=\Gamma(A_m(\lambda)K_m(v\rho)) \tag{48}$$

where

$$A_m(\lambda)=\frac{-I\,ds}{4\pi^2\epsilon_0\omega}\left(\frac{\lambda}{2v}\right)[\exp(i\phi_1)I_{m+1}(v\rho_1)+\exp(-i\phi_1)I_{m-1}(v\rho_1)] \tag{49}$$

because (41) and (47) must be identical.

In a very similar fashion to the above, we can work with the axial magnetic field. Thus, in this case, we invoke the equivalence of

$$H_z^p = i\epsilon_0\omega\partial\Pi_x^p/\partial y \tag{50}$$

and

$$H_z^p = (-\gamma_0^2 + \partial^2/\partial z^2)\, V^p \tag{51}$$

where V^p is the magnetic Hertz potential. This has the representation

$$V^p = \Gamma(B_m(\lambda)K_m(v\rho)) \tag{52}$$

where

$$B_m(\lambda) = \frac{I\,ds}{4\pi^2}\left(\frac{i}{2v}\right)[\exp(-i\phi_1)I_{m-1}(v\rho_1) - \exp(i\phi_0)I_{m+1}(v\rho_1)] \tag{53}$$

The extension to magnetic dipole excitation is entirely analogous to the preceding derivation for the electric dipole. Thus we need only indicate the required changes in a very brief fashion.

The source is now a small loop of area dA carrying a current I. Again, with reference to Fig. 1, we can locate this dipole at $(\rho_1, \phi_1, 0)$ and orient it (i.e. the axis of the loop) in the x direction. The primary fields of this magnetic dipole can be derived from a magnetic Hertz vector that has only an x component Π_x^{*p} given by

$$\Pi_x^{*p} = [I\,dA/(4\pi)]R^{-1}\exp(-\gamma_0 R) \tag{54}$$

that is analogous to (1). The corresponding electric and magnetic Hertz potentials are given by (48) and (52), respectively, but now

$$A_m(\lambda) = \frac{i\mu_0\omega I\,da}{4\pi^2}\left(\frac{i}{2v}\right)[\exp(-i\phi_1)I_{m-1}(v\rho_1) - \exp(i\phi_1)I_{m+1}(v\rho_1)] \tag{55}$$

and

$$B_m(\lambda) = \frac{I\,dA}{4\pi^2}\left(\frac{-i\lambda}{2v}\right)[\exp(i\phi_1)I_{m+1}(v\rho_1) + \exp(-i\phi_1)I_{m-1}(v\rho_1)] \tag{56}$$

The other orientation of the dipoles that is of less practical interest would be when they are oriented in the axial or z direction. In this case we would have, for the electric dipole, that

$$A_m(\lambda) = [I\,ds/(4\pi^2 i\epsilon_0\omega)]I_m(v\rho_1) \tag{57}$$

and $B_m(\lambda) = 0$ while, for the magnetic dipole, $A_m(\lambda) = 0$ and

$$B_m(\lambda) = [I\,dA/(4\pi^2)]I_m(v\rho_1) \tag{58}$$

These expressions are valid for $\rho_1 < \rho$ and, as before, the dipole is located at $z = 0$.

The expressions for $A_m(\lambda)$ and $B_m(\lambda)$ given in this appendix enable any orientation of electric or magnetic dipoles to be obtained by appropriate superposition of the results for the transverse and axial dipoles.

References

Beal, J. C., Josiak, J., Mahmoud, S. F., and Rawat, V., 1973, *Proc. I.E.E.E.*, **61**, 562.

Chiba, J., and Sato, R., 1974, *Tech. Rep. Tokoku Univ.*, **39**, 183.

Davis, Q. V., 1975, *J. Br. Instn Rado Engr*, **45**, 201.

Gallawa, R. L., Beery, W. M., Chu, T. M., Cook, K. R., Fitzgerrell, R. G., Haidle, L. L., Partch, J. E., and Rosner, K., 1969, *I.E.E.E. Trans. Commun. Techn.*, **17**, 518.

Goubau, G., 1950, *J. appl. Phys.*, **21**, 1119.

Hill, D. A., and Wait, J. R., 1974, *J. appl. Phys.*, **45**, 4774 ; 1975, *Ibid.*, **46**, 4352.

Kikuchi, H., 1973, *Proc. Instn elect. Engrs*, **120**, 637.

Lavrov, G. A., and Knyazev, A. S., 1965, *Prizemnyye i Podzemnyye Antenny* (*Near Earth and Buried Antennas*), Sovetskoye (Soviet) Radio.

Mikoshiba, K., and Nurita, Y., 1969, *I.E.E.E. Trans. veh. Techn.*, **18**, 66.

Okada, S., Kishimoto, T., Akagawa, K., Nakahara, Y., Mikoshiba, K., Horiguchi, F., and Okamoto, K., 1975, *J. Br. Instn Radio Engrs*, **45**, 224.

Wait, J. R., 1959, *Electromagnetic Radiation from Cylindrical Structures* (Oxford : Pergamon).

Wait, J. R., and Hill, D. A., 1974, *I.E.E.E. Trans. Antennas Propag.*, **22**, 627 ; 1975, *I.E.E.E. Trans. microw. Theory Tech.*, **23**, 401.

IEEE TRANSACTIONS ON MICROWAVE THEORY AND TECHNIQUES, VOL. MTT-23, NO. 5, MAY 1975

Propagation Along a Braided Coaxial Cable in a Circular Tunnel

JAMES R. WAIT, FELLOW, IEEE, AND DAVID A. HILL, MEMBER, IEEE

Abstract—The modes of propagation along a coaxial structure contained within a circular tunnel are considered. The primary objective is to develop an approximate impedance boundary condition at the outer surface of the shielded cable that can be used in previously developed formalisms for axial conductors in tunnels. It is assumed that the metal braid can be characterized by a surface-transfer impedance. We also account for the possibility that a lossy film exists on the outer surface of the dielectric jacket of the cable.

INTRODUCTION

THERE IS A NEED to understand how electromagnetic waves propagate in tunnels if improved communication systems in mines are to be developed in a logical fashion. One approach now being developed is to exploit the leaky-feeder principle [1]. In this method, which can be described as continuous-access communications, the signals are guided by transmission lines or shielded conductors. The principal idea is that energy can be coupled into and out of the transmission channel by antennas that only need be in the general vicinity of the two-wire line or cable.

In developing the theory of mode propagation along axial conducting structures in cylindrical tunnels, we need to apply an impedance boundary condition at the outer surface of the guiding structure. In the case of a bare metallic wire, the appropriate expression to use is the series impedance Z_i defined as follows: $Z_i = E_z/I$ where $I = \oint H_t\, ds$. Here, E_z is the average axial field at the surface of the conductor, while H_t is the azimuthal magnetic field. For a thin circular wire of radius a with electromagnetic constants σ_w, ϵ_w, and μ_w, we can use the following argument.

FORMULATION FOR IMPEDANCE OF AN INNER CONDUCTOR

A cylindrical coordinate system (ρ, ϕ, z) is adopted such that the surface of the wire is $\rho = a$. If the external fields are now locally uniform, we can neglect the azimuthal variation around the wire and consider only the axial current flow. For fields that vary as $\exp(-\Gamma z + i\omega t)$ where Γ is a propagation constant, the Hertz vector has only a z component Π_w. Thus, within the wire $\rho \leq a$, we can write

$$E_z = (k_w^2 + \partial^2/\partial z^2)\Pi_w = (k_w^2 + \Gamma^2)\Pi_w$$
$$H_\phi = -(\sigma_w + i\epsilon_w\omega)\partial\Pi_w/\partial\rho \qquad (1)$$

where

$$ik_w = [(i\mu_w\omega)(\sigma_w + i\epsilon_w\omega)]^{1/2}.$$

The appropriate form of the solution for Π_w is the modified Bessel function $I_0[i(k_w^2 + \Gamma^2)^{1/2}\rho]$ times a constant factor. Thus according to our basic definition

$$Z_i = E_z/(2\pi\rho H_\phi)\,|_{\rho=a} \qquad (2)$$

or

$$Z_i = \frac{i(k_w^2 + \Gamma^2)^{1/2}}{2\pi(\sigma_w + i\epsilon_w\omega)a}\,\frac{I_0[i(k_w^2 + \Gamma^2)^{1/2}a]}{I_1[i(k_w^2 + \Gamma^2)^{1/2}a]}. \qquad (3)$$

In the usual case where $|\Gamma^2| \ll |k_w^2|$ this simplifies to

$$Z_i \simeq \frac{(i\mu_w\omega)^{1/2}}{2\pi(\sigma_w + i\epsilon_w\omega)^{1/2}a}\,\frac{I_0(ik_wa)}{I_1(ik_wa)}. \qquad (4)$$

In the dc limit (i.e., $\omega \to 0$) we see that Z_i reduces to the expected form $(\pi a^2\sigma_w)^{-1}$.

In previous papers on this subject, we have used the boundary condition $E_z = IZ_i$ to apply to the surface of the thin wire even when the external region is complex. Two examples were axial conductors in a circular tunnel [2] and an axial conductor in a rectangular tunnel [3]. The justification for this type of boundary condition is that the external fields are locally uniform. Thus, on physical grounds, we expect the results to be valid when the wire radius is small compared with the distance to neighborhood surfaces and when the quantity $|\beta a| \ll 1$. Here β is the effective transverse wavenumber in the external region. There is some experimental support for this analytical approach to such problems [4].

EXTENSION TO BRAIDED SHIELD, DIELECTRIC LAYERS, AND OUTER LOSSY FILM

We now wish to extend this series-impedance concept to the case where the axial wire conductor is covered by a layer of perfect insulation of radius b with dielectric constant ϵ and free-space permeability μ_0. To allow for the presence of a metal braided shield, we assume that there is a thin uniform sheath of radius b with a designated transfer impedance Z_T in ohms/meter. Surrounding this, we have a coating whose dielectric constant is ϵ_c; it is also assumed lossless and a has a free-space permeability. Finally, to allow for a layer of mine dust or conducting

Manuscript received July 31, 1974; revised November 22, 1974.
The authors are with the Institute for Telecommunication Sciences, Office of Telecommunications, U.S. Department of Commerce, Boulder, Colo. 80302.

fluid, we assume there is a thin outer layer of conductive material with a transfer impedance Z_L. This situation is illustrated in Fig. 1 where the cross section of this braided coaxial cable with lossy outer sheath is depicted.

The situation is admittedly simplified, particularly with regard to the thin uniform sheath representation of the braided shield. In fact, the nonuniformities of the braid and random perforations of the shield will play an important role in the performance of an actual system. However, for present purposes we will consider just a uniform or smoothed-out version of the braid. We can rely on other work [5] to give us an estimate on the expected value of the transfer impedance Z_T. In a similar fashion, we justify the use of the transfer impedance Z_L for the external lossy film. The appropriate value here can be estimated from the approximate formula $Z_L \simeq (2\pi c\sigma d)^{-1}\ \Omega/\text{m}$, where σd is the conductivity–thickness product of the lossy film. Such an easily recognizable expression is justified wher. d is small compared with the electric skin depth $(2/\sigma\mu\omega)^{1/2}$ of the film material, and also d should be small compared with the radius c.

The brief derivation given below for the effective series impedance follows the classical approach for cylindrical structures [6], [7].

The axial electric field and the azimuthal magnetic field for the three regions thus have the following form for fields that vary as $\exp(i\omega t - \Gamma z)$:

$$\left.\begin{aligned} E_z &= (k^2 + \Gamma^2)\Pi = \beta^2\Pi \\ H_\phi &= -i\epsilon\omega\partial\Pi/\partial\rho \end{aligned}\right\} \quad \text{for} \quad a < \rho < b \tag{5}$$

$$\left.\begin{aligned} E_z &= (k_c^2 + \Gamma^2)\Pi_c = \beta_c^2\Pi_c \\ H_\phi &= -i\epsilon_c\omega\partial\Pi_c/\partial\rho \end{aligned}\right\} \quad \text{for} \quad b < \rho < c \tag{6}$$

and

$$\left.\begin{aligned} E_z &= (k_0^2 + \Gamma^2)\Pi_0 = \beta_0^2\Pi_0 \\ H_\phi &= -i\epsilon_0\omega\partial\Pi_0/\partial\rho \end{aligned}\right\} \quad \text{for} \quad \rho > c \tag{7}$$

where Π, Π_c, and Π_0 are the Hertz potentials for the three respective regions. Also β, β_c, and β_0 are the corresponding transverse wavenumbers and they are defined as indicated above. Now in any of the three regions, the Hertz potentials can be written as linear combinations of the Bessel functions J_0 and Y_0 with arguments $\beta\rho$, $\beta_c\rho$, and $\beta_0\rho$, respectively. Then, for example, for the first region we deduce readily that

$$\left.\begin{aligned} E_z &= \beta^2[PJ_0(\beta\rho) + QY_0(\beta\rho)] \\ H_\phi &= i\epsilon\omega\beta[PJ_1(\beta\rho) + QY_1(\beta\rho)] \end{aligned}\right\} \quad \text{for} \quad a < \rho < b \tag{8}$$

and

$$\left.\begin{aligned} E_{cz} &= \beta_c^2[MJ_0(\beta_c\rho) + NY_0(\beta_c\rho)] \\ H_{c\phi} &= i\epsilon_c\omega\beta_c[MJ_1(\beta_c\rho) + NY_1(\beta_c\rho)] \end{aligned}\right\} \quad \text{for} \quad b < \rho < c. \tag{9}$$

Here P, Q, M, and N are constants yet to be determined. We have similar expressions in the external region, but here we utilize the fact that the "scattered" field is an outgoing wave and thus the solution for Π_0 is characterized by a linear combination of J_0 and $H_0^{(2)}$ where the latter is the Hankel function of the second kind. Thus we can write

$$\left.\begin{aligned} E_{0z} &= A[J_0(\beta_0\rho) + R_0H_0^{(2)}(\beta_0\rho)] \\ H_{0\phi} &= Ai\epsilon_0\omega\beta_0^{-1}[J_1(\beta_0\rho) + R_0H_1^{(2)}(\beta_0\rho)] \end{aligned}\right\} \quad \text{for} \quad \rho > c. \tag{10}$$

Here A can be regarded as the strength of the axial electric field of the "primary" wave at $\rho = 0$ that would exist if the structure were not present. The coefficient R_0 then determines the relative strength of the scattered field. Obviously, if the parameter $|\beta_0 c|$ is not sufficiently small, we would need to include Bessel functions of order m and the factor $\exp(im\phi)$ in the solutions for all the Hertz potentials.

The boundary conditions for the problem can now be stated succintly as follows:

$$E_z = 2\pi aZ_iH_\phi \quad \text{at} \quad \rho = a \tag{i}$$

$$E_z = E_{cz} \quad \text{at} \quad \rho = b \tag{ii}$$

$$H_\phi - H_{c\phi} = -(2\pi bZ_T)^{-1}E_z \quad \text{at} \quad \rho = b \tag{iii}$$

$$E_{cz} = E_{0z} \quad \text{at} \quad \rho = c \tag{iv}$$

$$H_{c\phi} - H_{0\phi} = -(2\pi cZ_L)^{-1}E_z \quad \text{at} \quad \rho = c. \tag{v}$$

Here (i) is the impedance boundary condition that we impose at the surface of the inner conductor. It is an "exact" condition if we use (3), but for practical purposes, Z_i can be taken to be independent of Γ so that (4) is adequate. Conditions (ii) and (iv) indicate that the axial electric field is effectively continuous through the braid and the lossy-film layer. This is a consequence of the assumed thinness of these layers (i.e., the thicknesses are small compared with the effective wavelength in the respective media).

From boundary condition (i) above, we easily deduce that

$$Q/P = R = -\frac{[J_0(\beta a) - i2\pi akZ_i(\beta\eta)^{-1}J_1(\beta a)]}{[Y_0(\beta a) - i2\pi akZ_i(\beta\eta)^{-1}Y_1(\beta a)]} \tag{11}$$

where $\eta = \mu\omega/k = (\mu/\epsilon)^{1/2}$. Similarly, from (ii) we find

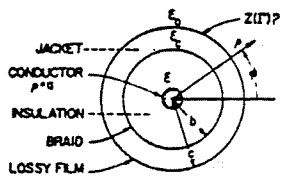


Fig. 1. The geometry of the coaxial structure showing the orientation of the cylindrical coordinate system.

that

$$P = M\frac{\beta_c^2 J_0(\beta_c b) + R_c Y_0(\beta_c b)}{\beta^2 J_0(\beta b) + R Y_0(\beta b)} \tag{12}$$

where $R_c = N/M$. Then an application of (iii) yields

$$R_c = \left\{\beta^2\left(\frac{i\beta_c k_c}{\eta_c} J_1(\beta_c b) - \frac{\beta_c^2 J_0(\beta_c b)}{2\pi b Z_T}\right) \times (J_0(\beta b) + R Y_0(\beta b)) - \frac{i\beta k}{\eta}\beta_c^2 J_0(\beta_c b)[J_1(\beta b) + R Y_1(\beta b)]\right\} \times \left\{-\beta^2\left(\frac{i\beta_c k_c}{\eta_c} Y_1(\beta_c b) - \frac{\beta_c^2 Y_0(\beta_c b)}{2\pi b Z_T}\right) \times (J_0(\beta b) + R Y_0(\beta b)) + \frac{i\beta k}{\eta}\beta_c^2 Y_0(\beta_c b)[J_1(\beta b) + R Y_1(\beta b)]\right\}^{-1}. \tag{13}$$

An application of (iv) tells us that $M\beta_c^2[J_0(\beta_c c) + R_c Y_0(\beta_c c)] = A[J_0(\beta_0 c) + R_0 H_0^{(2)}(\beta_0 c)]$. Combining this with (v) yields

$$R_c = -\frac{\left[\frac{ik_0}{\eta_0} J_1(\beta_0 c) - \frac{\beta_0 J_0(\beta_0 c)}{2\pi c Z_L} - \frac{ik_c}{\eta_c}\frac{\beta_0}{\beta_c}\frac{J_1(\beta_c c) + R_c Y_1(\beta_c c)}{J_0(\beta_c c) + R_c Y_0(\beta_c c)} J_0(\beta_0 c)\right]}{\left[\frac{ik_0}{\eta_0} H_1^{(2)}(\beta_0 c) - \frac{\beta_0 H_0^{(2)}(\beta_0 c)}{2\pi c Z_L} - \frac{ik_c}{\eta_c}\frac{\beta_0}{\beta_c}\frac{J_1(\beta_c c) + R_c Y_1(\beta_c c)}{J_0(\beta_c c) + R_c Y_0(\beta_c c)} H_0^{(2)}(\beta_0 c)\right]}. \tag{14}$$

Now the desired result is the effective series impedance defined by

$$Z(\Gamma) = \frac{E_{0z}}{2\pi c H_{0\phi}} \quad \text{at} \quad \rho = c$$

$$= \frac{\beta_0\eta_0[J_0(\beta_0 c) + R_0 H_0^{(2)}(\beta_0 c)]}{2\pi c i k_0[J_1(\beta_0 c) + R_0 H_1^{(2)}(\beta_0 c)]}. \tag{15}$$

QUASI-STATIC LIMITING FORM FOR $Z(\Gamma)$

The resulting expression for $Z(\Gamma)$ that is a function of the axial propagation constant Γ is rather involved. Fortunately, considerable simplification ensues if we consider the case where the arguments of the Bessel functions are sufficiently small that only the leading terms in their power-series expansions need be retained. In this connection it might be mentioned that in some important cases βc may not be "small" even when $\beta_0 c$ is small. For example, this could occur when $\Gamma \sim ik_0$, in which case $\beta_0 c$ is small even though $k_0 a$ may be comparable with one. However, in the quasi-static limit that we discuss below, it will be assumed that all the arguments are small.

To provide insight into the quasi-static limiting forms, we write out the field expressions that correspond to (8)–(10). Here we utilize the small-argument approximations $J_0(x) \to 1$, $J_1(x) \to x/2 \to 0$, $Y_0(x) \to (2/\pi)\ \ln 0.89x$, and $Y_1(x) \to -2/(\pi x)$. Thus

$$\left.\begin{aligned} E_\rho &\simeq \beta^2[P + (2/\pi)Q \ln 0.89\beta\rho] \\ H_\phi &\simeq -(2/\pi) i\epsilon\omega Q/\rho \end{aligned}\right\} a < \rho < b \tag{16}$$

$$\left.\begin{aligned} E_{c\rho} &\simeq \beta_c^2[M + (2/\pi)N \ln 0.89\beta_c\rho] \\ H_{c\phi} &\simeq -(2/\pi) i\epsilon_c\omega N/\rho \end{aligned}\right\} b < \rho < c \tag{17}$$

and

$$\left.\begin{aligned} E_{0z} &\simeq A[1 + R(1 - (i2/\pi) \ln 0.89\beta_0\rho] \\ H_{0\phi} &\simeq -A(2/\pi) i\epsilon_0\omega R/\rho \end{aligned}\right\} c < \rho < \hat{\rho}. \tag{18}$$

Here $\hat{\rho}$ is any value greater than c chosen such that $|\beta_0\hat{\rho}| \ll 1$. It is useful to note that in each region $H_\phi \times \rho$ is a constant in this limiting situation.

As an exercise, we can now apply boundary conditions (i)–(v) and get explicit quasi-static forms for the coefficients, or we can insert the small-argument approximations in the Bessel functions in (11)–(15). In either case, we obtain the following formula for the effective series impedance:

$$Z(\Gamma) \simeq \frac{Z_L(Z_c + Z_b)}{Z_L + Z_c + Z_b} \tag{19}$$

where

$$Z_b = \frac{Z_T(Z' + Z_i)}{Z_T + Z' + Z_i} \tag{20}$$

where

$$Z' = -\frac{k^2 + \Gamma^2}{2\pi i\epsilon\omega} \ln (b/a) \tag{21}$$

and

$$Z_c = -\frac{k_c^2 + \Gamma^2}{2\pi i\epsilon_c\omega} \ln (c/b). \tag{22}$$

The equivalent circuit for this situation is the ladder network shown in Fig. 2. The terminating element Z_i is the impedance of the inner conductor while the shunt elements Z_T and Z_L are the transfer impedances of the braid and

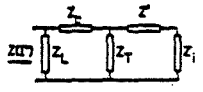


Fig. 2. The equivalent ladder network that yields the effective series impedance of the cable in the quasi-static approximation.

the external lossy film. The series elements Z_c and Z' can be identified as short sections of transmission lines whose properties depend on Γ. We stress that this quasi-static equivalent circuit is only valid when all the Bessel-function arguments are small compared with one. The expression for the series impedance given by (15) is not so restricted.

APPLICATION TO CIRCULAR-TUNNEL MODEL

We now consider the circular-waveguide model of a mine tunnel. The situation is depicted in Fig. 3 where the tunnel radius is a_0 while the cable is located at a distance ρ_0 from the tunnel axis. In an earlier paper [2], we determined the axial propagation constants of the permitted modes of the structure that satisfied both the impedance boundary conditions at the waveguide wall and at the surface of an axial conductor whose series impedance is specified. In the present case, the axial structure in the waveguide is the braided coaxial that we discussed previously. The impedance boundary condition is to be applied at the outer surface of the lossy-film coating whose radius is c. As indicated in Fig. 3, the distance of the cable from the tunnel wall is $a_0 - \rho_0$. In order for the solution to be valid, c should be small compared with $a_0 - \rho_0$.

As in the earlier paper, the homogeneous medium bounding the tunnel walls has a conductivity σ_s and a permittivity ϵ_s. In what follows, we choose $\sigma_s = 10^{-2}$ mho/m, $\epsilon_s = 10\epsilon_0$, and $a_0 = 2$ m. The interior region of the waveguide is free space, except at the braided coaxial. The dimensions of the latter, with reference to Fig. 1, are taken as follows: $a = 1.5$ mm, $b = 10$ mm, and $c = 11.5$ mm. Also, for purposes of illustration, we take the transfer impedance Z_T of the braid to be $i\omega L$ where $L = 40$ nH/m. This corresponds to the FONT cable developed by Fontaine *et al.* [5].

The relative dielectric constant ϵ/ϵ_0 of the insulator is taken to be 2.5 corresponding to polystyrene, for example. For an optimum system, we might have chosen a lower value but, for present purposes, this is not important. For the outer coating, the relative dielectric constant ϵ_c/ϵ_0 is taken to be 3.0 corresponding to typical jacket material. To allow for the presence of the outer lossy film, we choose the transfer impedance $Z_L = [2\pi c(\sigma d)]^{-1}$ where the conductivity–thickness product is to be specified. For example, a conducting fluid layer with $\sigma = 10$ mho/m whose thickness $d = 1$ mm leads to $(\sigma d) = 10^{-2}$ mho. As indicated by Rawat and Beal [8], the presence of such lossy films in realistic mine environments should be expected.

Using the above analytical machinery, we illustrate some results for the dominant modes of the braided cable located in the cylindrical structure. There are two important modes that we call the monofilar and bifilar modes. The first of these is similar to the situation treated before where we have a bare uncoated wire in the waveguide [2], [3]. In that case, the return current flows along the walls of the cylindrical waveguide. The second type is analogous to the currents flowing in a two-wire transmission line and the characteristic of this bifilar mode is almost independent of the waveguide walls. For the braided coaxial structure, this particular mode is the conventional one since the currents in the center conductor and braid are approximately equal but with opposite signs.

In Fig. 4, we show the attenuation rate (in nepers/meter) for the monofilar mode as a function of frequency from 0.2 to 200 MHz. Several values of ρ_0/a_0 are indicated as are two values of (σd). Also for this example, the conductivity σ_w of the center conductor is taken to be 10^7 mho/m, but for this mode, the attenuation is not critically dependent on σ_w. Also, except for higher frequencies, the attenuation rate is not influenced appreciably by (σd) for values even as high as 10^{-1} mho. As expected, of course, the attenuation rate for this monofilar mode increases as the coaxial is moved toward the wall. Note that $\rho_0/a_0 = 0.9$ corresponds to a distance $s - s_0 = 20$ cm ~ 8 in from the wall.

In Fig. 5 we show some corresponding results for the bifilar or coaxial-type mode. Since there is a strong dependence on the conductivity σ_w of the inner conductor, three different values are selected. The highest value $\sigma_w \sim 5.7 \times 10^7$ mho/m corresponds to copper. In this case, we also see that the results depend somewhat on the (σd) values, particularly at the upper frequencies. The

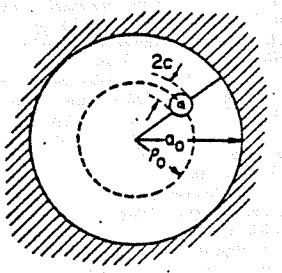


Fig. 3. The circular-waveguide model showing the location of the cable.

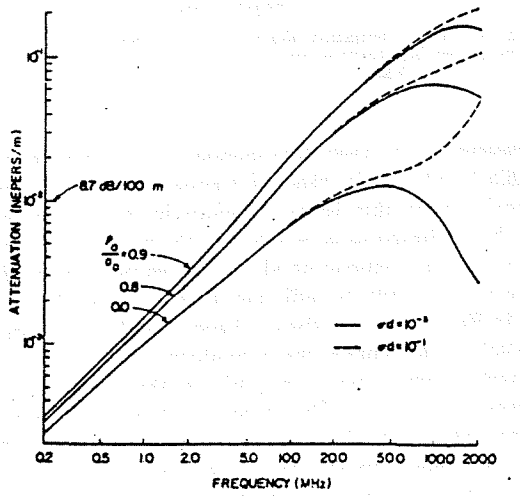


Fig. 4. The attenuation rate of the monofilar mode as a function of frequency. $a_0 = 2$ m.

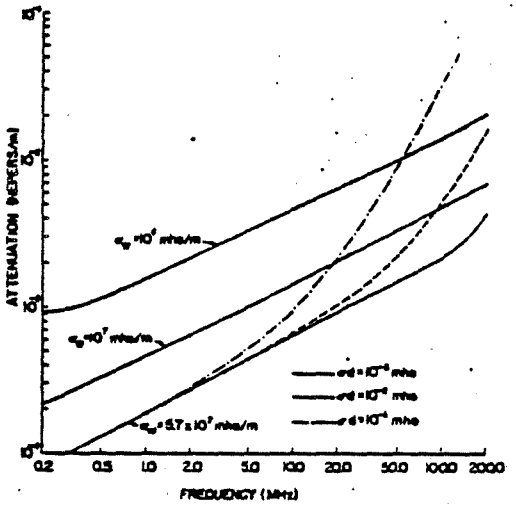


Fig. 5. The attenuation rate of the bifilar mode illustrating the dependence on the conductivity of the inner conductor and the effect of the external lossy film. $\epsilon = 2.5\epsilon_0$; $\epsilon_e = 3.0\epsilon_0$; $L = 40$ nH/m.

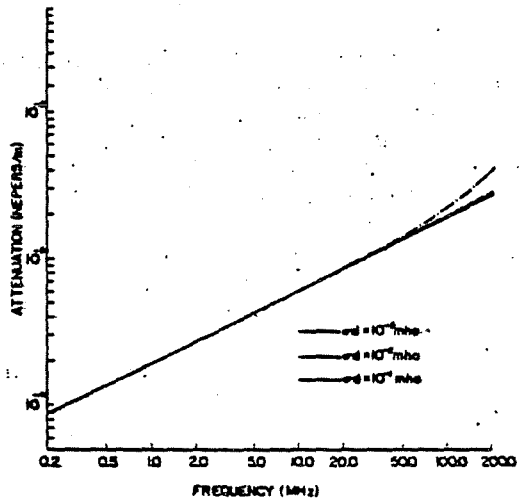


Fig. 6. The attenuation rate of the bifilar mode for a smaller value of the surface transfer impedance. $\sigma_w = 5.7 \times 10^7$ mho/m; $L = 4$ nH/m; $\epsilon = 2.5\epsilon_0$; $\epsilon_e = 3.0\epsilon_0$.

presence of the lossy film increases the attenuation of the bifilar mode for the range of frequencies and σd parameter considered in this figure. Actually, for the curves in Fig. 5 we have chosen $\rho_0/a_0 = 0.8$, but the results for this bifilar mode hardly depend at all on the value of ρ_0/a_0. In fact, the curves would be indistinguishable for $0 \leq \rho_0/a_0 \leq 0.9$.

In Fig. 6 we show the corresponding bifilar mode attenuation for the copper inner conductor. Here we choose the transfer inductance $L = 4$ nH/m that is a factor of 10 lower than before. The important point here is that the attenuation rate depends only slightly on the conductivity–thickness product (σd) of the outer lossy film. Thus, while high values of L are desirable from the standpoint of coupling to the desired bifilar mode, we can expect a greater susceptibility to the presence of lossy fluid or mine-dust layers on the outer jacket.

CONCLUDING REMARKS

The present results are believed to be a useful basis for the design of leaky-feeder communications systems that employ shielded cables in mine tunnels. The analytical method can be applied equally well to rectangular tunnels [9]. The effect of axial nonuniformities in the guiding structures needs to be considered if we are to utilize fully the capabilities of both the monofilar and the bifilar modes.

In principle, the method could be applied at much higher frequencies for single dielectric-coated conductors where the dominant mode would be a surface wave [10]–[12] whose energy is confined to the cable. Several difficulties emerge here. First of all, the assumption of local uniformity of the fields about the cable would need to be removed. Also, the hostile environment in most mine tunnels would produce very high attenuation due to moisture and coal dust. Also, the coupling to the surface-wave line would be not feasible for a roving miner. Nevertheless, we should keep an open mind on the possible relevance of Goubau-type surface-wave lines in mine environments.

ACKNOWLEDGMENT

The authors wish to thank their colleague Dr. S. F. Mahmoud for his useful comments and private communications.

REFERENCES

[1] J. C. Beal, J. Josiak, S. F. Mahmoud, and V. Rawat, "Continuous-access guided communication (CAGC) for ground-transportation systems," *Proc. IEEE (Special Issue on Ground Transportation for the Eighties)*, vol. 61, pp. 562–568, May 1973.

[2] J. R. Wait and D. A. Hill, "Guided electromagnetic waves along axial conductors in a circular tunnel," *IEEE Trans. Antennas Propagat.* (Succinct Papers), vol. AP-22, pp. 627–630, July 1974.

[3] S. F. Mahmoud and J. R. Wait, "Theory of wave propagation along a thin wire inside a rectangular waveguide," *Radio Sci.*, vol. 9, pp. 417–420, Mar. 1974.

[4] J. R. Wait and D. A. Hill, "Coaxial and bifilar modes on a transmission line in a circular tunnel," *Appl. Phys.*, vol. 4, pp. 307–312, Sept. 1974.

[5] J. Fontaine, B. DeMoulin, P. deGauque, and R. Gabillard, "Feasibility of radio communication in mine galleries by means of a coaxial cable having a high coupling impedance," in *1973 Proc. Thru-the-Earth Electromagnetics Workshop*, (Colorado School of Mines), U.S. Bureau of Mines Contract G-133023, Final Rep. Dec. 31, 1973, pp. 130–139 (Available from NTIS, Springfield, Va.).

[6] J. R. Wait, *Electromagnetic Radiation from Cylindrical Structures*. New York: Pergamon, 1959, pp. 142–148.

[7] R. E. Collin, *Field Theory of Guided Waves*. New York: McGraw-Hill, 1961, pp. 477–483.

[8] V. Rawat and J. C. Beal, "Leaky cables treated as open waveguides," in *Proc. Int. Colloquium Leaky-Feeder Communications* (Guilford, Surrey, England, Apr. 1974).

[9] J. R. Wait and S. F. Mahmoud, "Propagation along a braided coaxial cable in a rectangular tunnel," Informal Rep. U.S. Bureau of Mines, June 15, 1974.

[10] G. Goubau, "Single-conductor surface-wave transmission lines," *Proc. IRE*, vol. 39, pp. 619–624, June 1951.

[11] R. L. Gallawa *et al.*, "The surface-wave transmission line and its use in communicating with high-speed vehicles," *IEEE Trans. Commun. Technol.*, vol. COM-17, pp. 518–525, Oct. 1969.

[12] W. J. Dewar and J. C. Beal, "Coaxial-slot surface wave launchers," *IEEE Trans. Microwave Theory Tech.*, vol. MTT-18, pp. 449–455, Aug. 1970.

72 Vol. 25 IEEE TRANSACTIONS ON MICROWAVE THEORY AND TECHNIQUES, JANUARY 1977

Influence of Spatial Dispersion of the Shield Transfer Impedance of a Braided Coaxial Cable

J. R. WAIT AND D. A. HILL

Abstract—The effect of the dependence of the braid transfer impedance on the propagation constant is discussed for a coaxial cable located in a circular tunnel.

In recent papers [1], [2] in this TRANSACTIONS, we have presented attenuation calculations for a braided coaxial cable located within a circular tunnel bounded by a homogeneous

Manuscript received May 4, 1976.
J. R. Wait is with the Cooperative Institute for Environmental Sciences, University of Colorado, Boulder, CO 80309.
D. A. Hill is with the Office of Telecommunications, Institute for Telecommunication Sciences, U.S. Department of Commerce, Boulder, CO 80302.

lossy medium. Following previous engineering practice, the metal braid was represented by a transfer impedance Z_T that was assumed not to vary with the propagation constant of the desired mode. In fact, for the calculations, we assumed that $Z_T = i\omega L_T$ where L_T was the transfer inductance expressed in nanohenries per meter. But this is a limitation in the calculations, not in the theoretical formulation.

Recent theoretical work [3]–[5] on wire mesh screens suggests that the effective transfer impedance is better represented by the form

$$Z_T = A(\omega) + B(\omega)\Gamma^2 \tag{1}$$

where $A(\omega)$ and $B(\omega)$ are frequency-dependent parameters that do not depend on the propagation constant Γ. In the specific case of the uncoated braided coaxial cable model used earlier, we would have

$$Z_T = i\omega L_T[1 + \Gamma^2/(k_0^2 + k^2)] \tag{2}$$

where k_0 is the wave number for the region (i.e., air) adjacent to the cable and k is the wave number for the insulating dielectric on the inside of the shield. This particular form would apply if the weave or pitch angle ψ of the braid wires (angle subtended with the cable axis) is 45° and if the axial separation of the braid wires is small compared with a wavelength and with the radius of the shield. Of course, the formula, but not the form, for Z_T is modified if other factors are considered, such as the influence of the jacket material and any external lossy coatings. Also, if the weave angle is different from 45°, we should replace the bracketed term in (2) by $[1 + (2\Gamma^2 \cos^2 \psi)/(k_0^2 + k^2)]$ according to an analysis by Casey [5].

The general mode equations [1], [2] we have derived for the braided cable in the tunnel may still be used if Z_T is regarded to be Γ dependent. The iterative calculation is only slightly more complicated. However, it is useful to examine how much error is incurred by adopting an appropriate Γ-independent model for Z_T since this has been used frequently in the past. For the coaxial cable or bifilar mode, Γ is of the order of ik; thus we propose to use the approximation

$$Z_T(\Gamma) \simeq Z_T(ik) = i\omega L_T(1 - k^2/(k_0^2 + k^2)]$$
$$= i\omega L_T k_0^2/(k_0^2 + k^2). \tag{3}$$

The limiting case is obtained by setting $\Gamma = 0$ in (2). Then we recover the simple form $Z_T \simeq i\omega L_T$.

To illustrate the significance of the present results, we plot in Figs. 1–3 the attenuation rate of the bifilar mode in decibels per kilometer for the three cases mentioned previously. Specifically, the transfer impedance takes the respective forms $Z_T(\Gamma)$, $Z_T(ik)$, and $Z_T(0)$ as indicated on each figure.

The cable parameters, in terms of the earlier notation [1], [2], are a_0 (tunnel radius) = 2 m, σ_e (earth conductivity) = 10^{-3} mhos/m, $\varepsilon_e/\varepsilon_0 = 10$, a (inner conductor radius) = 1.5 mm, b (sheath radius) = 10 mm, $\varepsilon/\varepsilon_0$ (dielectric constant of insulator) = 1.5, and σ_w (conductivity of inner conductor) = 5.7×10^7 mhos/m. Also, as mentioned previously, the influence of the jacket and/or lossy external layer is ignored here. This corresponds to setting $c = b$ and $\sigma d = 0$ in the previous formulation [1], [2]. As indicated in the figures, ρ_0 (offset distance of cable from tunnel axis) is either zero or $0.9a_0 = 1.8$ m. In Fig. 1, where the reference value of L_T is 40 nH/m, it is seen that the attenuation rates for $Z_T(\Gamma)$ and $Z_T(ik)$ are considerably lower than that for $Z_T(0)$. In Fig. 2, where $L_T = 10$ nH/m, the difference is somewhat reduced, while in Fig. 3 where $L_T = 2$ nH/m, the difference is negligible. In all cases shown the difference between the curves for $Z_T(\Gamma)$ and $Z_T(ik)$ would seem to be insignificant.

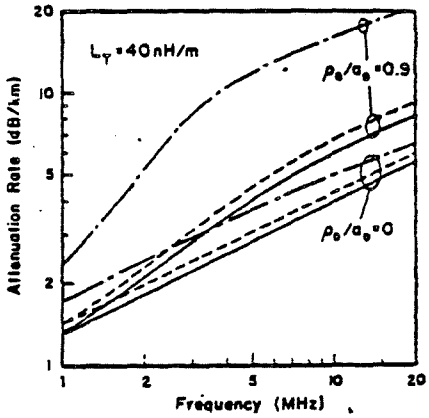


Fig. 1. Attenuation rate of a braided coaxial cable in a circular tunnel for three different representations of the sheath transfer impedance. The reference transfer inductance L_T is 40 nH/m. $Z_T(0)$: —·—·—. $Z_T(ik)$: - - - - -. $Z_T(\Gamma)$: ————.

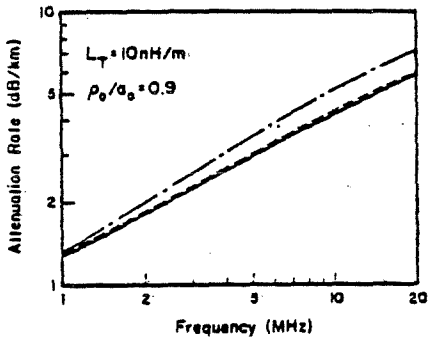


Fig. 2. Attenuation rate of a braided coaxial cable in a circular tunnel for three different representations of the sheath transfer impedance. The reference transfer inductance is $L_T = 10$ nH/m. $Z_T(0)$: —·—·—. $Z_T(ik)$: - - - - -. $Z_T(\Gamma)$: ————.

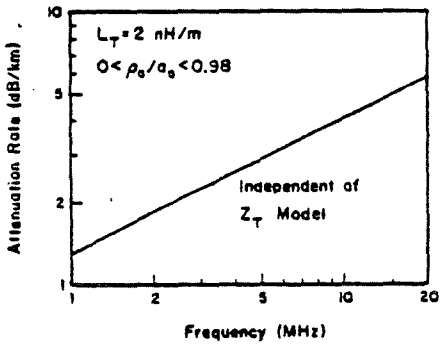


Fig. 3. Attenuation rate of a braided coaxial cable in a circular tunnel for three different representations of the sheath transfer impedance. The reference transfer inductance is $L_T = 2$ nH/m. Curves are indistinguishable.

Certainly from a practical standpoint, the use of an effective Γ-independent value of the transfer impedance such as $Z_T(ik)$ would lead to a negligible error. But, of course, the use of $Z_T(0)$ as may be obtained from a static test measurement is liable to produce significant discrepancies. Thus in interpreting the

calculated data from previous attenuation calculations [1], [2], one should identify the given sheath transfer impedance as an effective value for that mode (e.g., $Z_T(ik)$ for the bifilar mode and $Z_T(ik_0)$ for the monofilar mode).

Using the method discussed recently by the authors [6], the influence of the Γ dependence on Z_T on the excitation factor of the desired bifilar mode was investigated. The results showed that the ratio of the excitation factor for the $Z_T(0)$ assumption was typically 6 dB higher than for either the $Z_T(\Gamma)$ or $Z_T(ik)$ assumptions. This is not surprising since the cable is less leaky in the latter cases. To some extent, this compensates for the decreased attenuation rates insofar as the total system loss is concerned. The important point is that the excitation factors calculated for an effective $Z_T(ik)$ never differ more than 2 dB from the Γ-dependent form $Z_T(\Gamma)$ (even for the worst case where $L_T = 40$ nH/m).

Not surprisingly, the calculated transmission characteristics for such problems will depend on the many details of the assumed model. The large number of parameters, even in such an idealized configuration, makes it extremely difficult to form a comprehensive picture of the overall phenomena. Nevertheless, it appears highly worthwhile to develop engineering design criteria that can be used to estimate system performance. Work on this subject continues.

References

[1] J. R. Wait and D. A. Hill, "Propagation along a braided coaxial cable in a circular tunnel," *IEEE Trans. Microwave Theory Tech.*, vol. MTT-23, pp. 401–405, May 1975.
[2] D. A. Hill and J. R. Wait, "Propagation along a braided coaxial cable located close to a tunnel wall," *IEEE Trans. Microwave Theory Tech.*, to be published.
[3] M. I. Astrakhan, "Reflecting and screening properties of plane wire grids," *Radio Engr.* (USSR), vol. 23, pp. 76–83, Jan. 1968.
[4] D. A. Hill and J. R. Wait, "EM scattering of an arbitrary plane wave by a wire mesh with bonded junctions," *Can. J. Phys.*, vol. 54, pp. 353–361, Feb. 15, 1976.
[5] K. F. Casey, private communication, Kansas State University, 1975.
[6] D. A. Hill and J. R. Wait, "Calculated transmission loss for a leaky feeder communication system in a circular tunnel," *Radio Sci.*, vol. 11, pp. 315–322, Apr. 1976.

Appl. Phys. 11, 351—356 (1976)

Applied Physics

Impedance of an Electric Dipole Located in a Cylindrical Cavity in a Dissipative Medium

J. R. Wait
Cooperative Institute for Research in Environmental Sciences, University of Colorado, Boulder, CO 80309, USA

D. A. Hill
Institute for Telecommunication Sciences, Office of Telecommunications, U. S. Department of Commerce, Boulder, CO 80302, USA

Received 29 July 1976

Abstract. The electromagnetic fields of an electric dipole located inside a cylindrical cavity or empty tunnel are formulated. The results are used to deduce an expression for the change of self-impedance due to the presence of the cavity or tunnel walls. A numerical evaluation of the resultant convergent integral and a summation of the angular harmonic series were performed. An important finding is that the input resistance of the dipole is approximately a constant for frequencies less than about 25 MHz for a typical tunnel radius of 2 m. Such results are shown to be in qualitative agreement with an earlier analysis of an electric dipole over a dissipative half-space.

PACS Code: 84

When an antenna is located near a lossy region such as the earth's surface, a fraction of the power is lost. This is a well-known, if not a well understood problem in designing communication links for paths parallel to the ground [1]. Many theoretical studies have been carried out where the earth's surface is modelled as a dissipative half-space. An early paper by Sommerfeld and Renner [2] is particularly noteworthy in this connection. Some of the more recent work is discussed in the context of remotely determining the electrical properties of a planetary surface from a dipole impedance measurement [3]. In that work, it was shown that the functional dependence of the input resistance on the "loss tangent" of the half-space is consistent with electrostatic concepts provided the frequency is sufficiently low. On the other hand, at the higher frequencies, the results are compatible with the surface impedance formulations based on the compensation theorem. In this latter frequency range, the results were essentially equivalent to the Sommerfeld-Renner formulation mentioned above.

In recent years the transmission properties of electromagnetic waves in mine and railway tunnels have been exploited for communication purposes [4]. One of the parameters needed for an engineering design is the power efficiency of the antennas. This has motivated us to examine the near fields of an electric dipole located in an air-filled circular tunnel of radius a where the surrounding medium is homogeneous with conductivity σ_e and permittivity ε_e. Specifically, we are interested in how the self-impedance of the dipole is modified by the presence of the tunnel wall. Thus we are led to formulate the problem in such a manner that the calculable quantity is the *change* of the self impedance rather than its absolute value. In this way, we are permitted to adopt the Hertzian dipole idealiza-

tion provided only that the length of the antenna is small compared with both the free-space wavelength *and* with the distance of the antenna to the tunnel wall.

Formulation

The cross section of the tunnel or cylindrical cavity is indicated in Fig. 1 where both cylindrical coordinates (ϱ, ϕ, z) and cartesian coordinates (x, y, z) have been chosen. The electric dipole of current moment Ids is located at $(\varrho_0, \phi_0, 0)$ and is oriented in the x direction. The electrical properties of the surrounding medium are σ_e, ε_e and μ_e where the permeability μ_e is allowed to be different from the free space value μ_0 at least in the formulation. The tunnel or cavity region, for $\varrho < a$, has electrical properties ε_0 and μ_0 that are assumed to be the same as free space.

Our first step is to write down the electric Hertz vector for the indicated dipole on the assumption that the tunnel walls are at an infinite distance. Such a vector, that has only an x component Π^p_x in the cartesian system, is given by

$$\Pi^p_x = [Ids/(4\pi i\varepsilon_0\omega)]R^{-1}\exp(-\gamma_0 R) \tag{1}$$

where the assumed time factor is $\exp(i\omega t)$, where $\gamma_0 = i(\varepsilon_0\mu_0)^{1/2}\omega$ and where $R = [\varrho^2 + \varrho_0^2 - 2\varrho\varrho_0\cos(\phi - \phi_0) + z^2]^{1/2}$. However, in order to match the subsequent boundary conditions for the total fields. it is desirable to express the primary fields in terms of axially directed electric and magnetic Hertz vectors.

We now introduce two well known identities from Bessel function theory that are often exploited in problems of this type [5]

$$\frac{e^{-\gamma_0 R}}{R} = \frac{1}{\pi}\int_{-\infty}^{+\infty} K_0(v\hat{\varrho})\exp(-i\lambda z)d\lambda \qquad \text{where} \quad v = (\lambda^2 + \gamma_0^2)^{1/2} \tag{2}$$

and

$$K_0(v\hat{\varrho}) = \sum_{m=-\infty}^{+\infty} I_m(v\varrho_0)K_m(v\varrho)\exp(-im(\phi - \phi_0)] \qquad (\text{for } \varrho_0 < \varrho) \tag{3}$$

where $\hat{\varrho} = [\varrho^2 + \varrho_0^2 - 2\varrho\varrho_0\cos(\phi - \phi_0)]^{1/2}$.

Then, we see that

$$\Pi^p_x = \frac{Ids}{4\pi^2 i\varepsilon_0\omega}\sum\int I_m(v\varrho_0)K_m(v\varrho)\exp[-im(\phi - \phi_0)] \cdot \exp(-i\lambda z)d\lambda . \tag{4}$$

In the above and in what follows, we need not indicate that the summation is over all integer values of m from

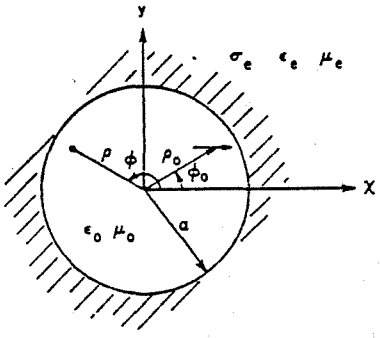


Fig. 1. Cross section of the cylindrical cavity or tunnel showing the location of the transversely oriented electric dipole

$-\infty$ to $+\infty$ and the integration contour is along the entire real axis in complex λ plane.

The corresponding axial electric field is obtained as follows

$$E^p_z = \frac{\partial^2\Pi^p_x}{\partial x\partial z} = \left(\cos\phi\frac{\partial}{\partial\varrho} - \sin\phi\frac{1}{\varrho}\frac{\partial}{\partial\phi}\right)\frac{\partial\Pi^p_x}{\partial z} = \frac{Ids}{4\pi^2 i\varepsilon_0\omega}\int(-i\lambda)F(\lambda)\exp(-i\lambda z)d\lambda \tag{5}$$

where

$$F(\lambda) = \sum\left((\cos\phi)\frac{\partial K_m}{\partial\varrho} + \frac{im}{\varrho}(\sin\phi)K_m\right) \cdot \exp[-im(\phi - \phi_0)]I_m . \tag{6}$$

The argument of K_m in the above expression for $F(\lambda)$, is $v\varrho$ and that of I_m is $u\varrho_0$. Then, by using the Bessel function identities

$$K'_m = -(1/2)[K_{m-1} + K_{m+1}] \tag{7}$$

and

$$K_m = [1/(2m)][K_{m+1} - K_{m-1}]vp \tag{8}$$

it follows that

$$F(\lambda) = -\frac{v}{2}\sum K_{m-1}I_m\exp[-i(m-1)\phi + im\phi_0] + K_{m+1}I_m\exp[-i(m+1)\phi + im\phi_0] \tag{9}$$

$$= -\frac{v}{2}\sum K_m\exp[-im(\phi - \phi_0)] \cdot [\exp(i\phi_0)I_{m+1} + \exp(-i\phi_0)I_{m-1}] . \tag{10}$$

But we can also write

$$E^p_z = (-\gamma_0^2 + \partial^2/\partial z^2)U^p \tag{11}$$

in terms of electronic Hertz potential U^p which is the z component of an axially directed electric Hertz vector. Clearly,

$$U^p = \sum \int A_m(\lambda) K_m(v\varrho) \exp[-im(\phi-\phi_0)] \exp[-i\lambda z] d\lambda \tag{12}$$

where

$$A_m(\lambda) = \frac{-Ids}{4\pi^2 \varepsilon_0 \omega} \left(\frac{\lambda}{2v}\right) \cdot [\exp(i\phi_0) I_{m+1}(v\varrho_0) + \exp(-i\phi_0) I_{m-1}(v\varrho_0)] \tag{13}$$

because (5) and (11) must be identical.

In a very similar fashion to the above, we can work with the axial magnetic field. Thus, in this case, we invoke the equivalence of

$$H_z^p = i\varepsilon_0 \omega \partial \Pi_z^p / \partial y \tag{14}$$

and

$$H_z^p = (-\gamma_0^2 + \partial^2/\partial z^2) V^p \tag{15}$$

where V^p is the magnetic Hertz potential. This has the representation

$$V^p = \sum \int B_m(\lambda) K_m(v\varrho) \exp[-im(\phi-\phi_0)] \exp(-i\lambda z) d\lambda \tag{16}$$

where

$$B_m(\lambda) = \frac{Ids}{4\pi^2} \left(\frac{i}{2v}\right) \cdot [\exp(-i\phi_0) I_{m-1}(v\varrho_0) - \exp(i\phi_0) I_{m+1}(v\varrho_0)] . \tag{17}$$

Secondary Fields

To account for the influence of the cavity or tunnel walls, we add the secondary fields. Thus, the total fields are to be obtained from electric and magnetic Hertz potentials represented by

$$U = \sum \int [A_m(\lambda) K_m(v\varrho) + P_m(\lambda) I_m(v\varrho)] \cdot \exp[-im(\phi-\phi_0)] \exp(-i\lambda z) d\lambda \tag{18}$$

and

$$V = \sum \int [B_m(\lambda) K_m(v\varrho) + Q_m(\lambda) I_m(v\varrho)] \cdot \exp[-im(\phi-\phi_0)] \exp(-i\lambda z) d\lambda \tag{19}$$

that are valid for $\varrho_0 < \varrho < a$. The factors $A_m(\lambda)$ and $B_m(\lambda)$ are specified by (13) and (17) while $P_m(\lambda)$ and $Q_m(\lambda)$ are yet to be determined.

In general, we note that (18) and (19) have the form

$$\begin{pmatrix} U \\ V \end{pmatrix} = \sum \int \begin{pmatrix} U_m \\ V_m \end{pmatrix} \exp[-im(\phi-\phi_0)] \exp(-i\lambda z) d\lambda . \tag{20}$$

Similarly, the field expressions can be written

$$\begin{pmatrix} E_\phi \\ H_\phi \\ E_z \\ H_z \end{pmatrix} = \sum \int \begin{pmatrix} E_{\phi m} \\ H_{\phi m} \\ E_{zm} \\ H_{zm} \end{pmatrix} \exp[-im(\phi-\phi_0)] \exp(-i\lambda z) d\lambda \tag{21}$$

where

$$E_{\phi m} = -(m\lambda/\varrho) U_m + i\mu_0 \omega \partial V_m / \partial \varrho$$
$$H_{\phi m} = -i\varepsilon_0 \omega \partial U_m / \partial \varrho - (m\lambda/\varrho) V_m$$
$$E_{zm} = -v^2 U_m \quad \text{and} \quad H_{zm} = -v^2 V_m .$$

As we have indicated before [6, 7], the boundary conditions at the cavity or tunnel wall are succinctly expressed by

$$\left.\begin{aligned} &E_{\phi m} = \alpha_m E_{zm} + Z_m H_{zm} \\ &\text{and} \\ &H_{\phi m} = -Y_m E_{zm} + \alpha_m H_{zm} \end{aligned}\right\}_{\text{at } \varrho = a} \tag{23}$$

where

$$\alpha_m = m\lambda/(u^2 a) ,$$
$$Z_m = -(i\mu_e \omega/u) K_m'(ua)/K_m(ua) \tag{24}$$
$$Y_m = [i\gamma_e^2/(u\mu_e \omega)] K_m'(ua)/K_m(ua) , \tag{25}$$
$$\gamma_e^2 = i\mu_e \omega(\sigma_e + i\varepsilon_e \omega) ,$$

and

$$u = (\lambda^2 + \gamma_e^2)^{1/2} .$$

The boundary conditions, given by (23), in conjunction with (18), (19), and (22), can be immediately applied to yield

$$P_m(\lambda) = -\left\{ A_m \left[\left(\frac{m\lambda}{v^2 a} - \alpha_m\right)^2 + \left(\frac{\gamma_0 K_m'}{v K_m} + \eta_0 Y_m\right)\left(\frac{\gamma_0 I_m'}{v I_m} + \frac{Z_m}{\eta_0}\right) \right] I_m K_m + B_m \left(\frac{m\lambda}{v^2 a} - \alpha_m\right) \frac{i\mu_0 \omega}{v^2 a} \right\} D_m^{-1} \tag{26}$$

and

$$Q_m(\lambda) = -\left\{ B_m \left[\left(\frac{m\lambda}{v^2 a} - \alpha_m\right)^2 + \left(\frac{\gamma_0 I_m'}{v I_m} + \eta_0 Y_m\right)\left(\frac{\gamma_0 K_m'}{v K_m} + \frac{Z_m}{\eta_0}\right) \right] I_m K_m - A_m \left(\frac{m\lambda}{v^2 a} - \alpha_m\right) \frac{i\varepsilon_0 \omega}{v^2 a} \right\} D_m^{-1} , \tag{27}$$

where

$$D_m = \left[\left(\frac{m\lambda}{v^2 a} - \alpha_m\right)^2 + \left(\frac{\gamma_0 I'_m}{v I_m} + \eta_0 Y_m\right)\left(\frac{\gamma_0 I'_m}{v I_m} + \frac{Z_m}{\eta_0}\right)\right] I_m^2$$

In (26) and (27) the following notational simplicity has been used: $A_m = A_m(\lambda)$, $B_m = B_m(\lambda)$, $I_m = I_m(va)$, $I'_m = I'_m(va)$, $K_m = K_m(va)$, $K'_m = K'_m(va)$ while bearing in mind that Z_m and Y_m are defined by (24) and (25) where the modified Bessel functions have argument ua. As usual, the prime over the modified Bessel function indicates differentiation with respect to the argument.

Impedance Formulation

It is now desirable to digrees slightly and talk about the primary fields of the source dipole. In particular, we easily deduce from (1) that

$$E_x^p = (-\gamma_0^2 + \partial^2/\partial x^2)\Pi_x^p. \tag{28}$$

At the broadside point $(x_0, y, 0)$ we see that

$$E_x^p = \frac{iIds}{4\pi\varepsilon_0\omega s^3}(1 + iks - k^2 s^2)\exp(-iks) \tag{29}$$

where $k = -i\gamma_0 = (\varepsilon_0\mu_0)^{1/2}\omega$ and $s = y - y_0 > 0$. In accordance with the E.M.F. method [3], we now can obtain the well known result for the "radiation resistance" of the dipole as follows

$$R_0 = \lim_{s\to 0}\left[-\frac{\mathrm{Re}\{E_x^p\}}{I}ds\right] = \frac{k^2(ds)^2}{6\pi}\eta_0 = 20k^2(ds)^2 \text{ ohms}. \tag{30}$$

As mentioned earlier, this simple approach cannot be used to calculate the self reactance of the dipole unless its finite length is explicitly accounted for. On the other hand, as we indicate below, the dipole dealization is satisfactory for deducing the change of both the input resistance and the input reactance from its free space value.

In accordance with the above discussion, we write the resultant Hertz potentials as the sum of two parts as follows

$$U = U^p + \Delta U \tag{31}$$

and

$$V = V^p + \Delta V \tag{32}$$

where ΔU and ΔV can be described as the secondary Hertz potentials. From (18) and (19), we see that

$$\Delta U = \sum\int P_m(\lambda) I_m(v\varrho)\exp[-im(\phi - \phi_0)]\exp(-i\lambda z)d\lambda \tag{33}$$

and

$$\Delta V = \sum\int Q_m(\lambda) I_m(v\varrho)\exp[-im(\phi - \phi_0)]\exp(-i\lambda z)d\lambda \tag{34}$$

which are valid for $0 < \varrho < a$. Now it is clear that the x component ΔE_x of the secondary field can be obtained from

$$\Delta E_x = \Delta E_\varrho \cos\phi_0 - \Delta E_\phi \sin\phi_0 \tag{35}$$

where

$$\Delta E_\varrho = (\partial^2/\partial\varrho\partial z)\Delta U - (i\mu_0\omega/\varrho)\partial\Delta V/\partial\phi \tag{36}$$

and

$$\Delta E_\phi = (1/\varrho)(\partial^2/\partial z\partial\phi)\Delta U + i\mu_0\omega\partial\Delta V/\partial\varrho. \tag{37}$$

If then the self impedance Z of the dipole is written

$$Z = Z_0 = \Delta Z \tag{38}$$

where Z_0 is the free space impedance, it follows that

$$\Delta Z = -\Delta E_x ds/I \tag{39}$$

in the limit $x \to x_0$, $y \to y_0$, and $z \to 0$. Explicitly

$$\Delta Z = \frac{ds}{I}\sum\int\{[i\lambda v\cos\phi_0 I'_m(v\varrho_0) - (m\lambda/\varrho_0)\sin\phi_0 I_m(v\varrho_0)]P_m(\lambda) + [(\mu_0\omega m/\varrho)\cos\phi_0 I_m(v\varrho_0) + i\mu_0\omega\sin\phi_0 v I'_m(v\varrho_0)]Q_m(\lambda)\}d\lambda \tag{40}$$

where $P_m(\lambda)$ and $Q_m(\lambda)$ are defined by (26) and (27), respectively.

Numerical Examples

The quantity of particular interst insofar as the power budget is concerned is the real part of ΔZ which is denoted ΔR. This quantity ΔR is the change of the input resistance due to the presence of the cavity or tunnel walls from the value R_0 of the dipole located in free space. To obtain values of the ratio R/R_0 where $R = R_0 = \Delta R$, the expression ΔZ given by (40) was evaluated numerically for frequencies from 1 to 200 MHz.

To facilicate the computation, the summation was moved inside the integral. Also, to avoid the difficulty at the singular points $\lambda = \pm k$, the integration contour was taken to be along the real axis in the complex λ plane with suitable small semi-circular indentations above $\lambda = +k$ and below $\lambda = -k$.

Some illustrative numerical results are indicated in Figs. 2 and 3 where R/R_0 is plotted as a function of frequency for three values of ϱ_0/a (0, 0.5, and 0.8). The conductivity σ_e of the surrounding medium is taken to be 10^{-2} mhos/m and the permittivity ε_e is taken to be $10\varepsilon_0$. We also set $\mu_e = \mu_0$ which is appropriate for 99% of all cases involving geological media. In Fig. 2, $\phi_0 = 0°$ so the electric dipole is along a radius while in Fig. 3, $\phi_0 = 90°$ so that the dipole is along a circumference. In both cases the input resistance increases significantly as the dipole approaches the tunnel wall. Also, not surprisingly, R oscillates about the value R_0 at sufficiently high frequencies due to constructive and destructive interference. However, at the lower frequencies, R increases very significantly and in fact, R/R_0 varies approximately as (frequency)$^{-2}$. Since R_0 itself varies as (frequency)^2 the upshot is that R is approximately a constant in this low frequency range. Such a conjecture was made in a previous study

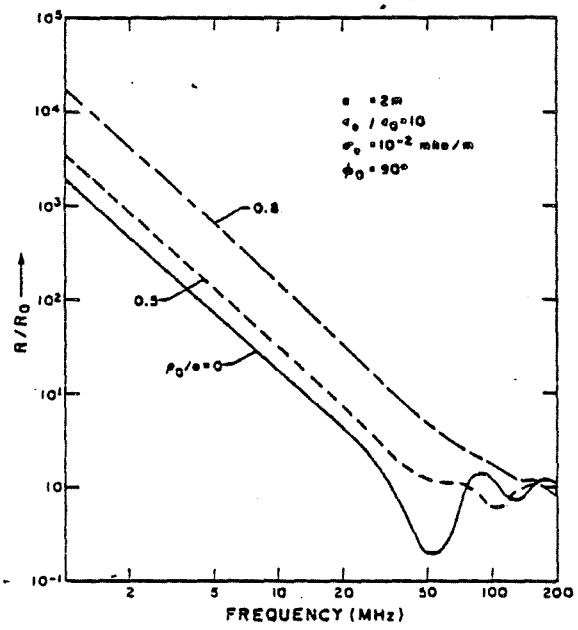


Fig. 3. The input resistance R of the circumferentially oriented dipole normalized by the free-space resistance R_0 as a function of frequency

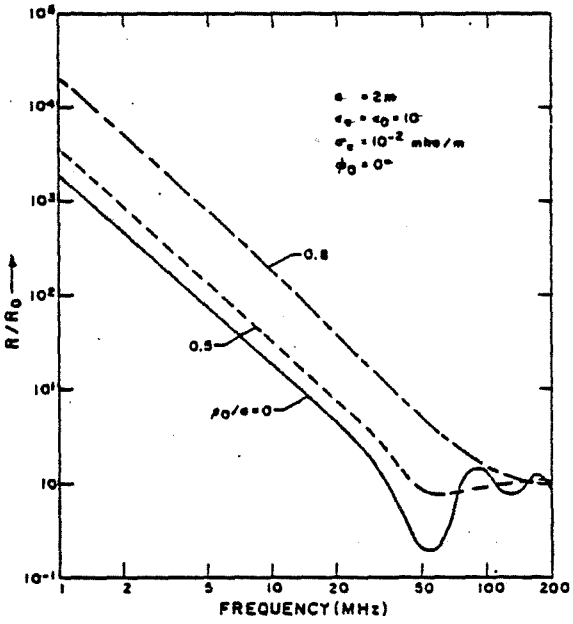


Fig. 2. The input resistance R of the radially oriented dipole normalized by the free-space resistance R_0 as a function of frequency

[8] for an electric dipole located in a tunnel. Also, the qualitative behavior of the results are entirely consistent with the earlier impedance analysis [3] of the vertical and horizontal electric dipole located over a dissipative halfspace.

Concluding Remarks

Further numerical results are obviously needed to clarify the dependence on the various physical parameters on the impedance characteristics. The qualitative relationship between the conductivity σ_e and permittivity ε_e and the distance $a - \varrho_0$ of the dipole from the tunnel wall should be quite similar to the earlier halfspace model [3]. In any case, we can certainly conclude that the influence of the tunnel walls plays a major role in determining the input impedance of both the transmitting and receiving antennas for any communication system that exploits the efficacious transmission properties of tunnels. Of course, the presence of an axial conductor within the tunnel should also be accounted for. This could also be a subject for further analysis using models considered earlier for analyzing the modes in such structures [6, 7]. Another significant

extension would be to consider magnetic dipoles or small loop antennas located within the cylindrical cavity. The formulation would be very similar but the numerical results, particularly at the lower frequencies, would be vastly different. In this case, the input resistance would not exhibit the approximate constancy with decreasing frequency; nor would the dimishing distance of the dipole to the tunnel wall result in such a rapid increase of the input resistance. However, the Q factor of such small loops are extremely high at such low frequencies and the matching of the transmitter to the loop would be difficult. Nevertheless, the extension of the analysis and the computations to the magnetic dipole would be worthwhile.

A final extension would be to treat explicitly the finite dimensions of the source dipole whether it be a linear wire or a loop. This, however, should not modify any of our conclusions here provided we remember that our deductions about the impedance increment ΔZ are restricted to electrically small antennas that are not too close to the tunnel wall.

References

1. A. D. Watt: *V.L.F. Radio Engineering* (Pergamon Press, Oxford 1967) p. 73
2. A. N. Sommerfeld, F. Renner: Ann. Physik (1) **41**, 1 (1942)
3. J. R. Wait: Radio Sci. **4**, 971 (1969)
4. Q. V. Davis: Radio and Electron. Engr. **45**, 201 (1975)
5. J. R. Wait: *Electromagnetic Radiation from Cylindrical Structures* (Pergamon Press, Oxford 1959)
6. J. R. Wait, D. A. Hill: IEEE Trans. AP-**22**, 627 (1974)
7. J. R. Wait, D. A. Hill: Appl. Phys. **4**, 307 (1974)
8. D. A. Hill, J. R. Watt: Radio Sci. **11**, 315 (1976)

118 IEEE TRANSACTIONS ON GEOSCIENCE ELECTRONICS, VOL. GE-16, NO. 2, APRIL 1978

The Impedance of Dipoles in a Circular Tunnel with an Axial Conductor

DAVID A. HILL, SENIOR MEMBER, IEEE, AND JAMES R. WAIT, FELLOW, IEEE

Abstract—The electromagnetic fields of dipole emitters located inside an empty tunnel or cylindrical cavity are first formulated. Both electric and magnetic types are considered. The results are used to deduce an expression for the change of self-impedance due to the presence of the tunnel walls. The input resistance R of the electric dipole is approximately a constant for frequencies less than about 25 MHz for a typical tunnel radius of 2 m. In contrast, for the same conditions, R for the magnetic dipole or small loop varies approximately as the square of the frequency. The theory is extended to allow for the presence of an axial conductor or cable within the tunnel. The presence of the cable increases R for both a transversely oriented electric dipole and a circumferentially oriented magnetic dipole but decreases R for an axial electric dipole. Not surprisingly, the axial magnetic dipole is only weakly influenced by the presence of the cable.

Introduction

IN RECENT YEARS the transmission properties of electromagnetic waves in mine and railway tunnels have been exploited for communication purposes [1]. One of the parameters needed for an engineering design is the power efficiency of the antennas. This motivated us [2] to examine the near fields of an electric dipole located in an air-filled circular tunnel of radius a where the surrounding medium is homogeneous with conductivity σ_e and permittivity ϵ_e. Specifically, we were interested in how the self-impedance of the dipole is modified by the presence of the tunnel wall. Thus we were led to formulate the problem in such a manner that the calculable quantity is the *change* of the self-impedance rather than its absolute value. In this way, we were permitted to adopt the Hertzian dipole idealization [3], [4] provided only that the length of the antenna is small compared with both the free-space wavelength *and* with the distance of the antenna to the tunnel wall.

In the present paper, we consider a more general situation. Both electric and magnetic dipoles are treated, and later we also allow for the presence of an axial conductor within the tunnel.

Manuscript received April 11, 1977; revised August 11, 1977.

D. A. Hill is with the Institute for Telecommunication Sciences, Office of Telecommunications, U.S. Department of Commerce, Boulder, CO 80302.

J. R. Wait is with the Cooperative Institute for Research in Environmental Sciences, University of Colorado/NOAA, Boulder, CO 80309.

Formulation

The cross section of the tunnel or cylindrical cavity is indicated in Fig. 1, where both cylindrical coordinates (ρ, ϕ, z) and Cartesian coordinates (x, y, z) have been chosen. The electric dipole of current moment Ids is located at $(\rho_0, \phi_0, 0)$, and is oriented in the x direction. The electrical properties of the surrounding medium are σ_e, ϵ_e, and μ_e where the permeability μ_e is allowed to be different from the free-space value μ_0, at least in the formulation. The tunnel or cavity region, for $\rho < a$, has electrical properties ϵ_0 and μ_0 that are assumed to be the same as free space.

Our first step is to write down the electric Hertz vector for the indicated dipole on the assumption that the tunnel walls are at an infinite distance. Such a vector, that has only an x component Π_x^p in the Cartesian system, is given by

$$\Pi_x^p = [Ids/(4\pi i\epsilon_0\omega)]R^{-1}\exp(-\gamma_0 R) \tag{1}$$

where the assumed time factor is $\exp(i\omega t)$, $\gamma_0 = i(\epsilon_0\mu_0)^{1/2}\omega$, and $R = [\rho^2 + \rho_0^2 - 2\rho\rho_0\cos(\phi - \phi_0) + z^2]^{1/2}$. However, in order to match the subsequent boundary conditions for the

U.S. Government work not protected by U.S. copyright.

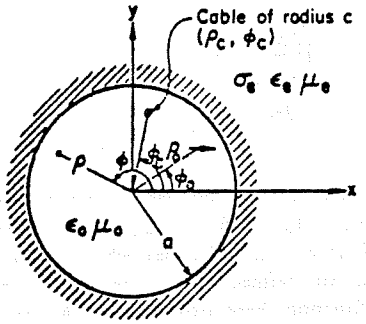


Fig. 1. Cross section of the cylindrical cavity or tunnel showing the location of the transversely oriented electric or magnetic dipole. The axial cable, that may be present, is also shown.

total fields, it is desirable to express the primary fields in terms of axially directed electric and magnetic Hertz vectors.

We now introduce two well-known identities from Bessel function theory that are often exploited in problems of this type [5]:

$$\frac{e^{-\gamma_0 R}}{R} = \frac{1}{\pi}\int_{-\infty}^{+\infty} K_0(v\hat{\rho}) \exp(-i\lambda z)\, d\lambda, \quad \text{where } v = (\lambda^2 + \gamma_0^2)^{1/2} \tag{2}$$

and

$$K_0(v\hat{\rho}) = \sum_{m=-\infty}^{+\infty} I_m(v\rho_0) K_m(v\rho) \exp[-im(\phi - \phi_0)], \quad \text{for } \rho_0 < \rho \tag{3}$$

where $\hat{\rho} = [\rho^2 + \rho_0^2 - 2\rho\rho_0 \cos(\phi - \phi_0)]^{1/2}$.

Then, we see that

$$\Pi_z^p = \frac{Ids}{4\pi^2 i\epsilon_0\omega}\,\Gamma(I_m(v\rho_0) K_m(v\rho)) \tag{4}$$

where Γ denotes the operation

$$\int_{-\infty}^{+\infty} \sum_{-\infty}^{+\infty} (\cdots) \exp[-im(\phi - \phi_0)] \exp(-i\lambda z)\, d\lambda$$

on the quantity in parenthesis. The integration contour here is taken along the entire real axis in the complex λ plane. The summation is overall integer values of m, from $-\infty$ to $+\infty$, including zero.

The corresponding axial electric field is obtained as follows:

$$E_z^p = \frac{\partial^2 \Pi_z^p}{\partial x \partial z} = \left(\cos\phi\,\frac{\partial}{\partial\rho} - \sin\phi\,\frac{1}{\rho}\,\frac{\partial}{\partial\phi}\right)\frac{\partial \Pi_z^p}{\partial z} = \frac{Ids}{4\pi^2 i\epsilon_0\omega}\int(-i\lambda) F(\lambda) \exp(-i\lambda z)\, d\lambda \tag{5}$$

where

$$F(\lambda) = \sum\left((\cos\phi)\,\frac{\partial K_m}{\partial\rho} + \frac{im}{\rho}(\sin\phi) K_m\right) I_m \cdot \exp[-im(\phi - \phi_0)]. \tag{6}$$

The argument of K_m in the above expression for $F(\lambda)$ is $v\rho$, and that of I_m is $v\rho_0$. Then, by using the Bessel function identities

$$K_m' = -(1/2)[K_{m-1} + K_{m+1}] \tag{7}$$

and

$$K_m = [1/(2m)]\,[K_{m+1} - K_{m-1}]\, v\rho \tag{8}$$

it follows that

$$F(\lambda) = -\frac{v}{2}\sum K_{m-1} I_m \exp[-i(m-1)\phi + im\phi_0] + K_{m+1} I_m \exp[-i(m+1)\phi + im\phi_0] \tag{9}$$

$$= -\frac{v}{2}\sum K_m \exp[-im(\phi - \phi_0)]\,[\exp(i\phi_0) I_{m+1} + \exp(-i\phi_0) I_{m-1}]. \tag{10}$$

But we can also write

$$E_z^p = (-\gamma_0^2 + \partial^2/\partial z^2)\, U^p \tag{11}$$

in terms of electric Hertz potential U^p which is the z component of an axially directed electric Hertz vector. Clearly,

$$U^p = \Gamma(A_m(\lambda) K_m(v\rho)) \tag{12}$$

where

$$A_m(\lambda) = \frac{-Ids}{4\pi^2\epsilon_0\omega}\left(\frac{\lambda}{2v}\right)[\exp(i\phi_0) I_{m+1}(v\rho_0) + \exp(-i\phi_0) I_{m-1}(v\rho_0)] \tag{13}$$

because (5) and (11) must be identical.

In a fashion very similar to the above, we can work with the axial magnetic field. Thus, in this case, we invoke the equivalence of

$$H_z^p = i\epsilon_0\omega\partial\Pi_z^p/\partial y \tag{14}$$

and

$$H_z^p = (-\gamma_0^2 + \partial^2/\partial z^2)\, V^p \tag{15}$$

where V^p is the magnetic Hertz potential. This has the representation

$$V^p = \Gamma(B_m(\lambda) K_m(v\rho)) \tag{16}$$

where

$$B_m(\lambda) = \frac{Ids}{4\pi^2}\left(\frac{i}{2v}\right)[\exp(-i\phi_0) I_{m-1}(v\rho_0) - \exp(i\phi_0) I_{m+1}(v\rho_0)]. \tag{17}$$

Secondary Fields

To account for the influence of the cavity or tunnel walls, we add the secondary fields. Thus the total fields are to be obtained from electric and magnetic Hertz potentials represented by

$$U = \Gamma(A_m(\lambda) K_m(v\rho) + P_m(\lambda) I_m(v\rho)) \tag{18}$$

and

$$V = \Gamma(B_m(\lambda) K_m(v\rho) + Q_m(\lambda) I_m(v\rho)) \tag{19}$$

that are valid for $\rho_0 < \rho < a$. The factors $A_m(\lambda)$ and $B_m(\lambda)$ are specified by (13) and (17) while $P_m(\lambda)$ and $Q_m(\lambda)$ are yet to be determined.

In general, we note that (18) and (19) have the form

$$\begin{pmatrix} U \\ V \end{pmatrix} = \Gamma \begin{pmatrix} U_m \\ V_m \end{pmatrix}. \tag{20}$$

Similarly, the field expressions can be written

$$\begin{pmatrix} E_\phi \\ H_\phi \\ E_z \\ H_z \end{pmatrix} = \Gamma \begin{pmatrix} E_{\phi m} \\ H_{\phi m} \\ E_{zm} \\ H_{zm} \end{pmatrix} \tag{21}$$

where

$$\begin{aligned} E_{\phi m} &= -(m\lambda/\rho)\, U_m + i\mu_0 \omega \partial V_m/\partial\rho \\ H_{\phi m} &= -ie_0 \omega \partial U_m/\partial\rho - (m\lambda/\rho)\, V_m \\ E_{zm} &= -v^2 U_m \quad \text{and} \quad H_{zm} = -v^2 V_m. \end{aligned} \tag{22}$$

As we have indicated before [6], [7], the boundary conditions at the cavity or tunnel wall are succinctly expressed by

$$\left.\begin{aligned} E_{\phi m} &= \alpha_m E_{zm} + Z_m H_{zm} \\ H_{\phi m} &= -Y_m E_{zm} + \alpha_m H_{zm} \end{aligned}\right\} \text{at } \rho = a \tag{23}$$

where

$$\alpha_m = m\lambda/(u^2 a)$$

$$Z_m = -(i\mu_e \omega/u)\, K'_m(ua)/K_m(ua) \tag{24}$$

$$Y_m = [i\gamma_e^2/(u\mu_e \omega)]\, K'_m(ua)/K_m(ua) \tag{25}$$

$$\gamma_e^2 = i\mu_e \omega(\sigma_e + ie_e \omega)$$

and

$$u = (\lambda^2 + \gamma_e^2)^{1/2}.$$

The boundary conditions, given by (23), in conjunction with (18), (19), and (22), can be immediately applied to yield

$$\begin{aligned} P_m(\lambda) = -\Bigg\{ & A_m \left[\left(\frac{m\lambda}{v^2 a} - \alpha_m \right)^2 \right. \\ & \left. + \left(\frac{\gamma_0 K'_m}{v K_m} + \eta_0 Y_m \right) \left(\frac{\gamma_0 I'_m}{v I_m} + \frac{Z_m}{\eta_0} \right) \right] I_m K_m \\ & + B_m \left(\frac{m\lambda}{v^2 a} - \alpha_m \right) \frac{i\mu_0 \omega}{v^2 a} \Bigg\} D_m^{-1} \end{aligned} \tag{26}$$

and

$$\begin{aligned} Q_m(\lambda) = -\Bigg\{ & B_m \left[\left(\frac{m\lambda}{v^2 a} - \alpha_m \right)^2 \right. \\ & \left. + \left(\frac{\gamma_0 I'_m}{v I_m} + \eta_0 Y_m \right) \left(\frac{\gamma_0 K'_m}{v K_m} + \frac{Z_m}{\eta_0} \right) \right] I_m K_m \\ & - A_m \left(\frac{m\lambda}{v^2 a} - \alpha_m \right) \frac{ie_0 \omega}{v^2 a} \Bigg\} D_m^{-1} \end{aligned} \tag{27}$$

where

$$\begin{aligned} D_m = \Bigg[& \left(\frac{m\lambda}{v^2 a} - \alpha_m \right)^2 \\ & + \left(\frac{\gamma_0 I'_m}{v I_m} + \eta_0 Y_m \right) \left(\frac{\gamma_0 I'_m}{v I_m} + \frac{Z_m}{\eta_0} \right) \Bigg] I_m^2. \end{aligned}$$

In (26) and (27) the following notational simplicity has been used: $A_m = A_m(\lambda)$, $B_m = B_m(\lambda)$, $I_m = I_m(ua)$, $I'_m = I'_m(ua)$, $K_m = K_m(ua)$, $K'_m = K'_m(ua)$, while bearing in mind that Z_m and Y_m are defined by (24) and (25), where the modified Bessel functions have argument ua. As usual, the prime over the modified Bessel function indicates differentiation with respect to the argument.

Impedance Formulation

It is now desirable to digress slightly and talk about the primary fields of the source dipole. In particular, we easily deduce from (1) that

$$E_x^p = (-\gamma_0^2 + \partial^2/\partial x^2)\, \Pi_x^p. \tag{28}$$

At the broadside point $(x_0, y, 0)$ we see that

$$E_x^p = \frac{Ids}{4\pi e_0 \omega s^3} (1 + iks - k^2 s^2) \exp(-iks) \tag{29}$$

where $k = -i\gamma_0 = (\epsilon_0 \mu_0)^{1/2} \omega$ and $s = y - y_0 > 0$. In accordance with the EMF method [3], we now can obtain the well-known result for the "radiation resistance" of the dipole as follows:

$$R_0 = \lim_{s \to 0} \left[-\frac{Re E_x^p}{I}\, ds \right] = \frac{k^2 (ds)^2}{6\pi} \eta_0 = 20 k^2 (ds)^2\ \Omega. \tag{30}$$

As mentioned earlier, this simple approach cannot be used to calculate the self-reactance of the dipole unless its finite length is explicitly accounted for. On the other hand, as we indicate below, the dipole idealization is satisfactory for deducing the change of both the input resistance and the input reactance from its free-space value.

In accordance with the above discussion, we write the resultant Hertz potentials as the sum of two parts as follows:

$$U = U^p + \Delta U \tag{31}$$

and

$$V = V^p + \Delta V \tag{32}$$

where ΔU and ΔV can be described as the secondary Hertz potentials. From (18) and (19), we see that

$$\Delta U = \Gamma(P_m(\lambda) I_m(v\rho)) \tag{33}$$

and

$$\Delta V = \Gamma(Q_m(\lambda) I_m(v\rho)) \tag{34}$$

which are valid for $0 < \rho < a$. Now it is clear that the x component ΔE_x of the secondary field can be obtained from

$$\Delta E_x = \Delta E_\rho \cos\phi_0 - \Delta E_\phi \sin\phi_0 \tag{35}$$

where

$$\Delta E_\rho = (\partial^2/\partial\rho\partial z)\,\Delta U - (i\mu_0\omega/\rho)\,\partial\Delta V/\partial\phi \tag{36}$$

and

$$\Delta E_\phi = (1/\rho)\,(\partial^2/\partial z\partial\phi)\,\Delta U + i\mu_0\omega\partial\Delta V/\partial\rho. \tag{37}$$

If then the self-impedance Z of the dipole is written as

$$Z = Z_0 + \Delta Z \tag{38}$$

where Z_0 is the free-space impedance, it follows that

$$\Delta Z = -\Delta E_x\,ds/I \tag{39}$$

in the limit $x \to x_0, y \to y_0$, and $z \to 0$. Explicitly

$$\Delta Z = \frac{ds}{I}\int_{-\infty}^{+\infty}\sum_{m=-\infty}^{+\infty}\{[i\lambda v\cos\phi_0 I_m'(v\rho_0) - (m\lambda/\rho_0)\cdot\sin\phi_0 I_m(v\rho_0)]P_m(\lambda) + [(\mu_0\omega m/\rho)\cos\phi_0 I_m(v\rho_0) + i\mu_0\omega\sin\phi_0 v I_m'(v\rho_0)]Q_m(\lambda)\}\,d\lambda \tag{40}$$

where $P_m(\lambda)$ and $Q_m(\lambda)$ are defined by (26) and (27), respectively.

The extension to magnetic dipole excitation is entirely analogous to the preceding derivation for the electric dipole. Thus we need only indicate the required changes in a very brief fashion.

The source is now a small loop of area dA carrying a current I. Again, with reference to Fig. 1, we can locate this dipole at $(\rho_0, \phi_0, 0)$ and orient it (i.e., the axis of the loop) in the x direction. The primary fields of this magnetic dipole can be derived from a magnetic Hertz vector that has only an x component Π_x^{*p} given by

$$\Pi_x^{*p} = [IdA/(4\pi)]R^{-1}\exp(-\gamma_0 R) \tag{41}$$

which is analogous to (1). The corresponding electric and magnetic Hertz potentials are given by (12) and (16), respectively, but now

$$A_m(\lambda) = \frac{i\mu_0\omega IdA}{4\pi^2}\left(\frac{i}{2v}\right)[\exp(-i\phi_0)\,I_{m-1}(v\rho_0) - \exp(i\phi_0)\,I_{m+1}(v\rho_0)] \tag{42}$$

and

$$B_m(\lambda) = \frac{IdA}{4\pi^2}\left(\frac{-i\lambda}{2v}\right)[\exp(i\phi_0)\,I_{m+1}(v\rho_0) + \exp(-i\phi_0)\,I_{m-1}(v\rho_0)]. \tag{43}$$

The total fields in the region $\rho_0 < \rho < a$ are again obtained from (18) and (19), where $P_m(\lambda)$ and $Q_m(\lambda)$ are as given by (26) and (27) in conjunction with (42) and (43).

We again can express the input impedance in the form given by (38), but now

$$\Delta Z = i\mu_0\omega\Delta H_x dA/I \tag{44}$$

in the limit $x \to x_0, y \to y_0$, and $z \to 0$. Here

$$\Delta H_x = \cos\phi_0\,\Delta H_\rho - \sin\phi_0\,\Delta H_\phi \tag{45}$$

$$\Delta H_\rho = \frac{i\epsilon_0\omega}{\rho}\frac{\partial\Delta U}{\partial\phi} + \frac{\partial^2\Delta V}{\partial\rho\partial z} \tag{46}$$

and

$$\Delta H_\phi = -i\epsilon_0\omega\frac{\partial\Delta U}{\partial\rho} + \frac{1}{\rho}\frac{\partial^2\Delta V}{\partial\phi\partial z}. \tag{47}$$

Then, the explicit form of (44) is

$$\Delta Z = \frac{i\mu_0\omega dA}{I}\int_{-\infty}^{+\infty}\sum_{-\infty}^{+\infty}\{[(\epsilon_0\omega m/\rho)\cos\phi_0 I_m(v\rho_0) + i\epsilon_0\omega v\sin\phi_0 I_m'(v\rho_0)]P_m(\lambda) + [-i\lambda v\cos\phi_0 I_m'(v\rho_0) + (m\lambda/\rho)\sin\phi_0 I_m(v\rho_0)]Q_m(\lambda)\}\,d\lambda. \tag{48}$$

As before, the input resistance R is the real part of Z. In free space (i.e., considering primary fields only), we readiiy deduce that the "radiation resistance" R_0 for the small loop is given by

$$R_0 = \eta_0 k^4 (dA)^2/(6\pi) \tag{49}$$

which is a well-known result. Thus, again writing $R = R_0 + \Delta R$, the change of the input resistance for the loop from its free-space value is obtained from $\Delta R = \mathrm{Re}\cdot\Delta Z$, where ΔZ is given by (48).

Numerical Results for Empty Tunnel

To obtain values of the ratio R/R_0, the expression ΔZ given by (40) for the electric dipole and (48) for the magnetic dipole were evaluated numerically for frequencies from 2 to 200 MHz. To avoid the difficulty at the singular points $\lambda = \pm k$, the integration contour was taken to be along the real axis in the complex λ plane with suitable small semicircular indentations above $\lambda = +k$ and below $\lambda = -k$.

Some illustrative numerical results for the electric dipole are indicated in Figs. 2 and 3, where R/R_0 is plotted as a function of frequency for three values of ρ_0/a (C, 0.5, and 0.8). The conductivity σ_e of the surrounding medium is taken to be 10^{-2} mho/m, and the permittivity ϵ_e is taken to be $10\epsilon_0$. We also set $\mu_e = \mu_0$, which is appropriate for virtually all cases involving geological media. In Fig. 2 $\phi_0 = 0°$ so the electric dipole is along a radius, while in Fig. 3 $\phi_0 = 90°$ so the dipole is along a circumference. In both cases the input resistance increases significantly as the dipole approaches the tunnel wall. Also, not surprisingly, R oscillates about the value R_0 at sufficiently high frequencies due to constructive and destructive interference. However, at the lower frequencies, R/R_0 increases very significantly, and, in fact, R/R_0 varies approximately as (frequency)$^{-2}$. Since R_0 itself varies as (frequency)^2 the upshot is that R, for an electric dipole, is approximately a constant in this low-frequency range. Such a conjecture was made in a previous study [8] for an electric dipole located in a tunnel. Also, the qualitative behavior of the results is entirely consistent with the earlier impedance analyses [4], [9] of vertical and horizontal electric dipoles located over a dissipative half-space.

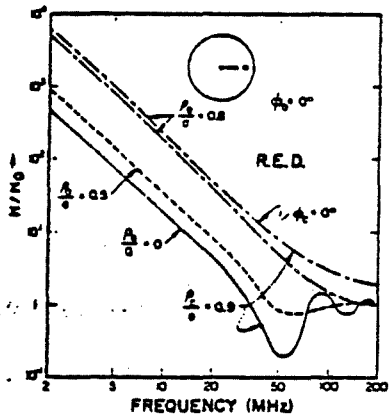


Fig. 2. The input resistance R of the RED normalized by the free-space resistance R_0 as a function of frequency. Results for both an empty and cable contained tunnel are shown for cases where $\rho_0/a = 0$ and 0.8.

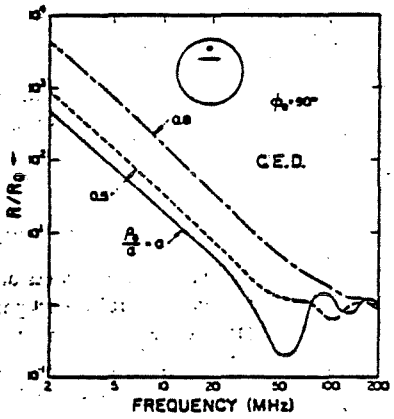


Fig. 3. The normalized input resistance of the CED. These results apply to the empty tunnel and to the case where the cable is located at $\phi_c = 90°$ for any $\rho_c \neq \rho_0$.

The illustrative numerical results for the magnetic dipole are indicated in Figs. 4 and 5 for the same parameters as used above for the electric dipole. In Fig. 4, $\phi_0 = 0°$ so the magnetic dipole (or small loop) is oriented with its axis along a radius. In Fig. 5, $\phi_0 = 90°$ so the dipole is along a circumference. The curves of R/R_0 as a function of frequency for the magnetic dipole have a very similar shape to those for the electric dipole. However, here we note that R_0 for the magnetic dipole varies as (frequency)^4, while R/R_0 still varies approximately as (frequency)$^{-2}$ at low frequencies. Thus the input resistance R for the magnetic dipole varies approximately as (frequency)^2 in contrast to the approximate constancy of R for the electric dipole. This behavior is consistent with earlier calculations for magnetic dipoles located over a conducting half-space [9], [10] and also for the case where the magnetic dipole is located within a spherical insulating cavity [11], [12].

As specified above, the conductivity σ_e of the ambient medium has been assigned the value, 10^{-2} mho/m, that may be typical of the rock through which the tunnel is cut. In the

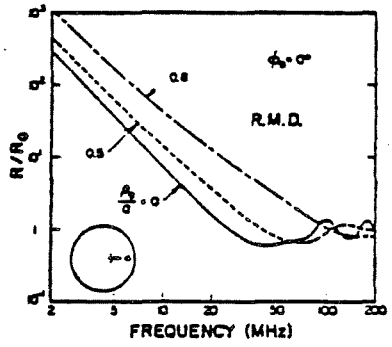


Fig. 4. The normalized input resistance of the RMD. Results for both an empty and cable contained tunnel are shown for cases where $\rho_0/a = 0$ and 0.8.

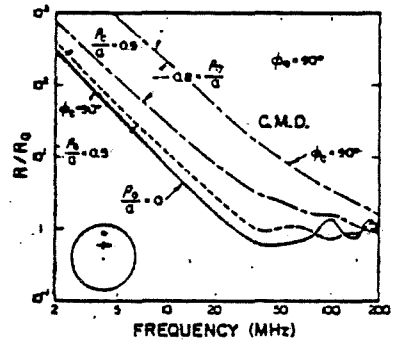


Fig. 5. The normalized input resistance of the CMD. These results apply to empty tunnel and to the case where the cable is located at $\phi_c = 0°$ for any $\rho_c \neq \rho_0$.

case of the electric dipole, the input resistance varies approximately as $1/\sigma_e$ at low frequencies (i.e., less than about 20 MHz); for the magnetic dipole it varies approximately as σ_e at low frequencies.

Extension of the Theory to Allow for an Axial Conductor and also for Axial Source Dipoles

In most practical situations, the tunnel will not be empty. More than not, the presence of rails, trolley wires, and cables will further modify the impedance of the dipoles from the free-space value. It is important to know if the neglect of these axial conductors will be of any serious consequence. The answer to this question has a bearing on two aspects of the general problem. In the first place, the input resistance of the dipoles will affect the overall transmission loss for a communication circuit, and secondly the measured dipole impedance may be used as a probe to determine the tunnel wall conductivity. Thus we modify the formulation for the dipole located in the empty tunnel to allow for the presence of an axial conductor. At the same time we also consider axially oriented dipole sources in addition to the transverse variety.

The situation is illustrated in Fig. 6 where the axial conductor or cable of radius c is located at (ρ_c, ϕ_c). To simplify the analysis, the radius c is assumed to be small compared with all other significant dimensions. Then the cable may be characterized by an axial impedance boundary condition as we indicate below.

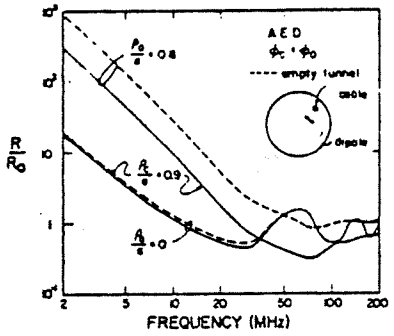


Fig. 6. The normalized input resistance of the AED. Results for both an empty and cable contained tunnel are shown.

The electric and magnetic Hertz potentials are now $U + U_c$ and $V + V_c$, respectively, where U and V have the same form as (18) and (19), while U_c and V_c are the Hertz potentials due to the cable currents. Using a certain amount of hindsight [13] we may write down the appropriate forms:

$$U_c = \int_{-\infty}^{+\infty} F_c(\lambda)\left[K_0(v\rho_d) - \sum_{n=-\infty}^{+\infty} R_n(\lambda)\frac{K_n(va)}{I_n(va)} I_n(v\rho) I_n(v\rho_c)\right] \cdot \exp\left[-in(\phi - \phi_c)\right] \exp(-i\lambda z)\, d\lambda \quad (50)$$

and

$$V_c = \int_{-\infty}^{+\infty} F_c(\lambda) \sum_{n=-\infty}^{+\infty} I_n(v\rho_c)\,\Delta_n(\lambda)\, I_n(v\rho) \cdot \exp\left[-in(\phi - \phi_c)\right] \exp(-i\lambda z)\, d\lambda \quad (51)$$

where $F_c(\lambda)$ is yet to be determined and where

$$\rho_d = [\rho^2 + \rho_0^2 - 2\rho\rho_c \cos(\phi - \phi_c)]^{1/2}.$$

To satisfy the boundary conditions at the tunnel wall, the expressions for $R_n(\lambda)$ and $\Delta_n(\lambda)$ are to be identical with those given in the earlier reference [13]. But actually, it is not difficult to see that

$$-R_n(\lambda)\frac{K_n(va)}{I_n(va)} = \frac{P_m(\lambda)}{A_m(\lambda)}, \quad \text{for } m = n \text{ and } B_m = 0 \quad (52)$$

and

$$\Delta_n(\lambda) = \frac{Q_m(\lambda)}{A_m(\lambda)}, \quad \text{for } m = n \text{ and } B_m = 0 \quad (53)$$

where $P_m(\lambda)$ and $Q_m(\lambda)$ are given by (26) and (27).

We now obtain $F_c(\lambda)$ by invoking the condition that the total fields should satisfy the impedance boundary condition at the cable. The latter relates the average values of the axial electric field and the current $I(z)$ in the cable. Here we find it convenient to introduce a coordinate system (ρ', ϕ', z) centered at the cable. Now, quite generally,

$$H_{\phi'} = -i\epsilon_0\omega\frac{\partial}{\partial\rho'}(U + U_c) + \frac{1}{\rho'}\frac{\partial^2}{\partial z\,\partial\phi'}(V + V_c). \quad (54)$$

Then clearly, if $|\gamma_0 c| = kc \ll 1$, and if the dipole is not too close to the cable, it follows that an excellent approximation is

$$\bar{H}_{\phi'} \simeq -i\epsilon_0\omega\frac{\partial}{\partial\rho'}U_c = i\epsilon_0\omega\int_{-\infty}^{+\infty} F(\lambda)\,K_1(vc)\,v \cdot \exp(-i\lambda z)\, d\lambda. \quad (55)$$

Furthermore, $|vc| \ll 1$ over the important range of the integration so that $K_1(vc) \simeq (vc)^{-1}$ and thus the cable current $I(z)$ is

$$I(z) = 2\pi c\bar{H}_{\phi'} \simeq 2\pi i\epsilon_0\omega\int_{-\infty}^{+\infty} F_c(\lambda)\exp(-i\lambda z)\, d\lambda. \quad (56)$$

The impedance boundary condition in its spatially dispersive form [14] is now written:

$$2\pi i\epsilon_0\omega\int_{-\infty}^{+\infty} Z_a(\lambda)\,F_c(\lambda)\exp(-i\lambda z)\, d\lambda = \left(-\gamma_0^2 + \frac{\partial^2}{\partial z^2}\right)(U + U_c)\Big|_{\substack{\rho=\rho_c+c\\ \phi=\phi_c}} \quad (57)$$

where the quantity on the right in the axial electric field evaluated at the point $(\rho_c + c, \phi_c)$ and $Z_a(\lambda)$ is the series impedance of the cable. In our examples, we will use the expression for Z_a that is appropriate to a solid conductor.

Using (57), it is straightforward to show that

$$2\pi i\epsilon_0\omega Z_a(\lambda)\,F_c(\lambda) = -v^2\sum_m\left[A_m(\lambda)\,K_m(v\rho_c) + P_m(\lambda)\,I_m(v\rho_c)\right] \cdot \exp\left[-im(\phi_c - \phi_0)\right] - v^2F_c(\lambda)\left[K_0(vc) - \sum_{n=-\infty}^{+\infty} R_n(\lambda) \cdot \frac{K_n(va)}{I_n(va)}\, I_n(v\rho_c)\, I_n[v(\rho_c + c)]\right]. \quad (58)$$

Solving this equation for $F(\lambda)$ we obtain

$$F_c(\lambda) = \left\{\hat{E}_z^p(\lambda) - v^2\sum_{m=-\infty}^{+\infty} P_m(\lambda)\,I_m(v\rho_c) \cdot \exp\left[-im(\phi_c - \phi_0)\right]\right\} D^{-1}(\lambda) \quad (59)$$

where

$$\hat{E}_z^p(\lambda) = -v^2\sum_{m=-\infty}^{+\infty} A_m(\lambda)\,K_m(v\rho_c)\exp\left[-im(\phi_c - \phi_0)\right] \quad (60)$$

and

$$D(\lambda) = 2\pi i\epsilon_0\omega Z_a(\lambda) + v^2\left[K_0(vc) - \sum_{n=-\infty}^{+\infty} R_n(\lambda)\frac{K_n(va)}{I_n(va)} I_n(v\rho_c)\, I_n[v(\rho_c + c)]\right]. \quad (61)$$

The modal equation to determine the discrete propagation modes in the tunnel is simply $D(\lambda) = 0$. This aspect of the problem has been adequately discussed elsewhere [6], [13]. For our impedance analysis, it is necessary to deal directly with the integral as we indicate below.

The quantity $\hat{E}_z^p(\lambda)$ defined by (60) is actually the Fourier transform of the axial electric field, due to the direct or primary influence of the dipole, evaluated at the cable. For convenience, we list the explicit forms as follows.

i) For an x-directed electric dipole

$$\hat{E}_z^p(\lambda) = \frac{Ids}{4\pi^2\epsilon_0\omega}(\lambda v)\frac{\rho_c\cos\phi_c - \rho_0\cos\phi_0}{\hat{\rho}_c} K_1(v\hat{\rho}_c) \quad (62)$$

where

$$\hat{\rho}_c = [\rho_c^2 + \rho_0^2 - 2\rho_c\rho_0\cos(\phi_c - \phi_0)]^{1/2}.$$

ii) For an x-directed magnetic dipole

$$\hat{E}_z^p(\lambda) = -\frac{i\mu_0\omega IdA}{4\pi^2} v\frac{(\rho_c\sin\phi_c - \rho_0\sin\phi_0)}{\hat{\rho}_c} K_1(v\hat{\rho}_c). \quad (63)$$

iii) For a z-directed electric dipole

$$\hat{E}_z^p(\lambda) = -\frac{Ids}{4\pi^2 i\epsilon_0\omega} v^2 K_0(v\hat{\rho}_c). \quad (64)$$

iv) For a z-directed magnetic dipole

$$\hat{E}_z^p(\lambda) = 0.$$

To facilitate the computation, we now express the self-impedance of the dipole as a superposition of the form

$$Z = Z_0 + \Delta Z + \Delta Z_c \quad (65)$$

where Z_0 is the free-space value, ΔZ is the correction computed as if the direct effect of the cable were ignored, and ΔZ_c is this direct contribution due to the cable.

i) For the x-directed electric dipole, ΔZ is given by (40) with $P_m(\lambda)$ replaced by $P_m^c(\lambda)$ where

$$P_m^c(\lambda) = P_m(\lambda) - F(\lambda) R_m(\lambda)\frac{K_m(va)}{I_m(va)} I_m(v\rho_c) \cdot \exp[-im(\phi_0 - \phi_c)]$$

$$\Delta Z_c = -\frac{ds}{I}\left[\frac{\rho_0\cos\phi_0 - \rho_c\cos\phi_c}{\hat{\rho}_c}\right] \cdot \int_{-\infty}^{+\infty} (i\lambda v) K_1(v\rho_c) F_c(\lambda)\, d\lambda. \quad (66)$$

ii) For the x-directed magnetic dipole, ΔZ is given by (44) with $Q_m(\lambda)$ replaced by $Q_{in}^c(\lambda)$ where

$$Q_m^c(\lambda) = Q_m(\lambda) + F(\lambda) I_m(v\rho_c)\Delta_m(\lambda)\exp[-im(\phi_0 - \phi_c)]$$

and

$$\Delta Z_c = k^2\frac{dA}{I}\left[\frac{\rho_0\sin\phi_0 - \rho_c\sin\phi_c}{\hat{\rho}_c}\right] \cdot \int_{-\infty}^{+\infty} vK_1(v\hat{\rho}_c) F_c(\lambda)\, d\lambda. \quad (67)$$

iii) For the z-directed electric dipole

$$\Delta Z = \frac{ds}{I}\int_{-\infty}^{+\infty} v^2 \sum_{m=-\infty}^{+\infty} P_m^c(\lambda) I_m(v\rho_0)\, d\lambda \quad (68)$$

and

$$\Delta Z_c = \frac{ds}{I}\int_{-\infty}^{+\infty} v^2 F_c(\lambda) K_0(v\hat{\rho}_c)\, d\lambda. \quad (69)$$

iv) For the z-directed magnetic dipole

$$\Delta Z = -\frac{i\mu_0\omega dA}{I}\int_{-\infty}^{+\infty} v^2 \sum_{m=-\infty}^{+\infty} Q_m^c(\lambda) I_m(v\rho_0)\, d\lambda \quad (70)$$

and, of course, $\Delta Z_c = 0$.

Numerical Results for Conductor Contained Tunnel

Using numerical integration and summation, results for the impedance increments ΔZ and ΔZ_c were obtained for a selected set of the parameters (e.g., $a = 2$ m, $\sigma_e = 10^{-2}$ mho/m, $\epsilon_e/\epsilon_0 = 10$ and for a solid cable of radius $c = 1.5$ cm with conductivity $\sigma = 5.7 \times 10^7$ mho/m). We discuss below the normalized input resistance as a function of frequency. The geometry is indicated in Fig. 1.

The results for the radially oriented electric dipole (RED) located at $\phi_0 = 0$, $\rho_0 = 0$, and $\rho_0 = 0.8a$, with the cable at $\phi_c = 0$ and $\rho_c = 0.9a$, are shown in Fig. 2 along with the earlier described results for the empty tunnel. As before, the tunnel radius $a = 2$ m. We see that the normalized input resistance R/R_0 for the case $\rho_0 = 0.8a$ is increased due to the presence of the cable at $\rho_c = 0.9a$, although the effect is not very pronounced. In the case where the RED is at the center of the tunnel, i.e., $\rho_0 = 0$, the presence of the axial conductor is not noticeable in so far as the input resistance of the dipole is concerned.

The next case is really trivial. That is, we locate the cable at $\phi_c = 90°$ with the circumferentially oriented dipole (CED) at $\phi_0 = 90°$. Then the input impedance is not affected by the presence of the cable. Thus the results in Fig. 3 computed for the empty tunnel apply to this special configuration.

The following case is the radially oriented magnetic dipole (RMD) located at $\phi_0 = 0°$ with the cable also located at $\phi_c = 0°$. Not surprisingly, the results are again unaffected by the presence of the cable so the earlier computed curves shown in Fig. 4 are also applicable to this special configuration.

Now, if we consider the circumferentially oriented magnetic dipole (CMD) located at $\phi_0 = 90°$, with the cable at $\phi_c = 90°$, the input resistance is again increased due to the presence of the cable. This effect is illustrated in Fig. 5 for the two cases where $\rho_0 = 0$ and $\rho_0 = 0.8a$. The effect is particularly noticeable in the latter case when the magnetic dipole is closely coupled to the cable (i.e., $\rho_c - \rho_0 = 0.1a = 20$ cm).

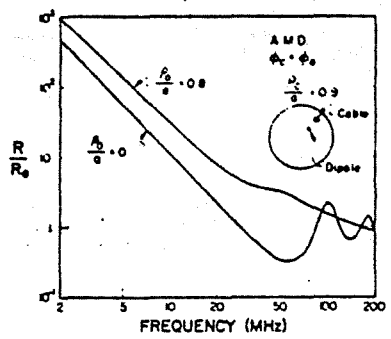


Fig. 7. The normalized input resistance of the AMD. The curves apply to both the empty and cable contained tunnel for the parameters indicated.

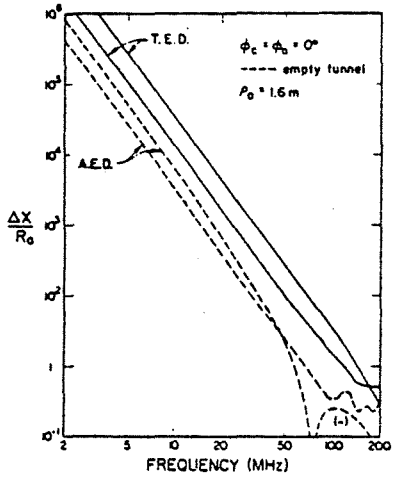


Fig. 8. The normalized change in input reactance for both an RED and AED. Results for both an empty and cable contained tunnel are shown for $\rho_0/a = 0.8$ and $\phi_0 = \phi_c = 0°$.

To complete the picture, we also show some results for the axially oriented electric and magnetic dipoles (AED and AMD, respectively) in Figs. 6 and 7. In the case of the AED, the input resistance is decreased due to the presence of the cable, while in the case of the AMD the change due to the cable is not perceptible.

The change in input reactance, $\Delta X = \mathrm{Im}(\Delta Z)$, is also available from the calculation of ΔZ. This quantity could provide additional information in attempting to remotely measure the electric properties of the tunnel wall and could also play a role in the total transmission loss of a tunnel communication system [8]. In Fig. 8 we show some results for the normalized change in input reactance $\Delta X/R_0$ for both radial and axial electric dipoles (RED and AED) for $\rho_0 = 0.8a$. The other parameters are the same as those in Fig. 2. For low frequencies, $\Delta X/R_0$ varies as (frequency)$^{-3}$ and ΔX varies as (frequency)$^{-1}$ which is in agreement with earlier half-space results [4]. For magnetic dipoles at low frequencies, $\Delta X/R_0$ tends to be much smaller. The high-frequency behavior in Fig. 8 is more complicated, but $\Delta X/R_0$ does approach zero in an oscillatory manner as expected.

Although we have given results for the specific case where the cable is a solid conductor, the formulation is valid for any thin conductor which can be characterized by a series impedance $Z_s(\lambda)$. Because leaky coaxial cables and dielectric coated wires are used in guided-access communication systems, the general computer programs included these situations. In fact, specific calculations for a leaky coaxial cable reveal that for typical cable parameters [14] the effect on the dipole impedance is very similar to that of a solid conductor as shown in Figs. 2-8. Nevertheless, there may be other situations where the spatial dispersive property of the axial surface impedance will affect the effective dipole impedance.

Concluding Remarks

The results indicated that the input resistance of both electric and magnetic dipoles within the tunnel are significantly influenced by the presence of the finitely conducting tunnel walls. However, the presence of axial conductors such as a trolley wire does not seem to produce a major perturbation, at least in the input impedance of the dipole. Also, there are certain configurations where the effect of such an axial conductor or cable is zero. This, of course, is due to the symmetry or asymmetry of the field configuration.

The model we have developed and the rather complicated computer program can be used to obtain specific results for the impedance increments ΔZ and ΔZ_c for any type of cable that can be characterized by a series impedance Z_a. In fact, the latter may also be spatially dispersive such as a leaky coaxial cable or a dielectric coated wire suspended in the tunnel.

The formulation can be extended without difficulty to tunnels that contain any number of axial conductors of various types. The increased complexity of the working formulas, however, becomes forbidding (i.e., the law of diminishing returns prevails).

As we have indicated elsewhere [8], [13], a knowledge of the input resistance of the dipoles is needed to make a satisfactory estimate of the total transmission loss of a tunnel communication system. But also, there is a good possibility that the measured input resistance and/or possibly the input reactance of the dipoles can be used to remotely measure the electric properties of the wall of the tunnel. The interpretation of the results at low frequencies may be very straightforward when the dependence of the input resistance R or wall conductivity is particularly simple [10]. This question certainly merits further attention.

References

[1] Q. V. Davis, Ed., "Leaky feeder communication systems," *Radio Electron. Engr.* (Special Issue), vol. 45, no. 5, Apr. 1975.

[2] J. R. Wait and D. A. Hill, "Impedance of an electric dipole located in a cylindrical cavity in a dissipative medium," *Applied Phys.*, vol. 11, no. 4, pp. 351-356, Dec. 1976.

[3] A. N. Sommerfeld and F. Renner, "Strahlungsenergie und Erdabsorption bei Dipolantennen," *Ann. Phys.*, vol. 41, no. 1, pp. 1-36, 1942.

[4] J. R. Wait, "Impedance characteristics of electric dipoles over a conducting half-space," *Radio Sci.*, vol. 4, no. 10, pp. 971-975, Oct. 1969.

[5] —, *Electromagnetic Radiation from Cylindrical Structures*. Oxford, England: Pergamon, 1959.

[6] J. R. Wait and D. A. Hill, "Guided electromagnetic waves along

an axial conductor in a circular tunnel." *IEEE Trans. Antennas Propagat.*, vol. AP-22, pp. 627–630, July 1974.

[7] —, "Coaxial and bifilar modes on a transmission line in a circular tunnel," *Appl. Phys.*, vol. 4, no. 4, pp. 307–312, Sept. 1974.

[8] D. A. Hill and J. R. Wait, "Calculated transmission loss for a leaky feeder communication system in a circular tunnel," *Radio Sci.*, vol. 11, no. 4, pp. 315–321, Apr. 1976.

[9] L. V. Kochmanova and V. P. Perov, "Power dissipated in dipole excitation of an electromagnetic field above a conducting half-space," *Radio Engrg. and Electron. Phys.*, vol. 19, no. 9, pp. 17–23, 1974.

[10] J. R. Wait, "Characteristics of antennas over lossy earth," in *Antenna Theory*, R. E. Collin and F. J. Zucker, Eds. New York: McGraw-Hill Book Co., 1969, part 2, ch. 23, pp. 386–437.

[11] —, "The magnetic dipole antenna immersed in a conducting medium," *Proc. IRE*, vol. 40, pp. 1244–1245, Oct. 1952.

[12] J. R. Wait and K. P. Spies, "A note on the insulated loop antenna immersed in a conducting medium," *Radio Sci. J. Res. NBS*, vol. 68D, no. 11, pp. 1249–1240, Nov. 1964.

[13] D. A. Hill and J. R. Wait, "Gap excitation of an axial conductor in a circular tunnel," *J. Appl. Phys.*, vol. 45, no. 11, pp. 4774–4777, Nov. 1974.

[14] J. R. Wait and D. A. Hill, "Influence of spatial dispersion of the shield transfer impedance of a braided coaxial cable," *IEEE Trans. Microwave Theory Tech.*, vol. MTT-25, pp. 72–74, Jan. 1977.

240

BAILEY R. HALL

Analysis of Radio Frequency Transmission Along a Trolley Wire in a Mine Tunnel

DAVID A. HILL AND JAMES R. WAIT, FELLOW, IEEE

Abstract—An idealized model of a trolley wire communication system in a tunnel is considered. To facilitate the analysis the tunnel cross section is taken to be semicircular and the surrounding rock medium is homogeneous with a finite conductivity. The metallic rails or other conductors on the flat floor of the tunnel are represented by a plane metallic reflecting surface of infinite extent. The trolley wire and associated feeder line are assumed to be equivalent to a single cylindrical conductor that is parallel to the axis of the tunnel but located anywhere within the cross section. The appropriate modal equation is then solved for the propagation constant of the dominant mode. It is shown that the attenuation rate increases significantly as the trolley wire approaches the tunnel wall. However, even when the trolley wire is within 20 cm (8 in) of the wall, the attenuation rate at 200 kHz is still less than 2 dB per kilometer.

INTRODUCTION

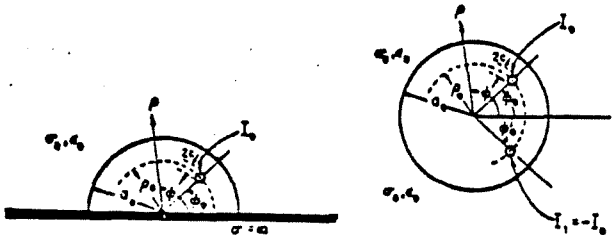
IT IS COMMON practice in communications in mines to utilize the trolley wire and its ground return as a radio frequency transmission line [1]. A potential problem in such a configuration is the influence of the finite conductivity of the rock adjacent to the tunnel or passageway in the mine. A similar situation can arise for communication lines in road and railway tunnels. For practical reasons, it is desirable to locate the trolley wire, that carries the dc or ac power, very close to the tunnel wall or rib. For power frequencies, this would not be of any consequence but for the radio frequencies used in the communication circuits, the eddy currents induced in the adjacent rock can lead to attenuation of the signal. To provide some insight to this problem, we hereby carry out an analysis of an idealized situation. Specifically, we consider a straight tunnel that has a semicircular cross section. In order to focus attention on the influence of the proximity of the trolley wire to the rock wall, we assume that the ground return circuit is ideal. Actually, this is not an inappropriate assumption when well bonded metal rails are located on the floor of the tunnel. In fact, to facilitate the analysis, we assume that the floor is a flat perfectly conducting surface. The trolley wire and any associated feeder line are assumed to be represented by a single axial cylindrical conductor with radius c. In the present model c is restricted to be much less than the tunnel radius a_0.

Manuscript received January 14, 1976.

The authors are with the Institute for Telecommunication Sciences, Office of Telecommunications, U.S. Department of Commerce, Boulder, CO 80302. (303) 499-1000.

FORMULATION

The situation to be considered is shown in Fig. 1(a). With respect to a cylindrical coordinate system, the wall of the tunnel for the semicylindrical model is defined by $\rho = a_0$ and $0 < \phi < \pi$. The perfectly conducting floor



(a) (b)

Fig. 1. (a) Axial conductor or trolley wire located in semicircular tunnel. (b) Equivalent twin-wire line in circular tunnel.

is the surface $\phi = 0$ and π for $0 < \rho < \infty$. The trolley wire of conductivity σ_w is centered at $\rho = \rho_0$ and $\phi = \phi_0$. The homogeneous rock with conductivity σ_e and permittivity ε_e occupies the region $\rho > a_0$ for $0 < \phi < \pi$.

By some means we now inject an oscillating current of angular frequency ω on to the trolley wire. This current flows axially along the wire down the tunnel to a suitable termination or matched load. Under the condition that there are infinite impedance chokes to prevent current drain to locomotives and other intervening loads, the return current will return along the ground plane and to some extent, in the tunnel walls. We can therefore assume that the current between the transmitter (at say $z = 0$) and the terminal load has the form $I_0 \exp(-\Gamma z)$ for the implied time factor $\exp(i\omega t)$. Of course, higher order modes will also be excited but they will be highly attenuated if the tunnel diameter $2a_0$ is small compared with the free-space wavelength. The problem thus boils down to the determination of the propagation constant Γ of the propagation mode in the semicircular tunnel that is effectively infinite in length. In particular, the real part of Γ so determined will indicate the attenuation of the propagating mode.

It now turns out that, because of the fortunate and nonaccidental choice of the geometry, the problem as posed in Fig. 1(a) is entirely equivalent to the fully circular tunnel shown in Fig. 1(b). The external region, now defined by $\rho > a_0$ for all ϕ, is homogeneous with conductivity σ_e and ε_e. In this case, however, we must locate an identical trolley wire at the proper image location. The current I_1 on this second wire located at $\rho = \rho_0$ and $\phi = -\phi_0$ must be equal to $-I_0$. Thus the problem originally posed is transformed to the task of finding the bifilar mode for the symmetrically disposed wires contained in what is otherwise an empty tunnel in a homogeneous rock medium.

As a slight digression, we should point out that the circular tunnel configuration shown in Fig. 1(b) also will support a monofilar mode that corresponds to choosing $I_1 = +I_0$. In this case the return currents are now flowing entirely in the rock adjacent to the tunnel walls. The corresponding semicircular tunnel mode would still look like Fig. 1(a) but the postulated perfect electric conductor on the floor would need to be a perfect magnetic conductor. Such a situation cannot be approximated in any sensible way so we will not pursue further the monofilar mode solution.

Modal Solution

A modal analysis to determine Γ for the bifilar mode on a transmission line in a circular tunnel has been obtained previously by the authors [2]. For the present symmetrical case shown in Fig. 1(b) that general mode equation may be factored and written in the form

$$A_0 - A_1 = 0 \tag{1}$$

where

$$A_0 = \frac{\gamma_0}{v^2}\frac{2\pi Z}{\eta_0} + K_0(va) - S_0 \tag{2}$$

and

$$A_1 = K_0(v\rho_d) - S_1 \tag{3}$$

where

$$\gamma_0^2 = -\varepsilon_0\mu_0\omega^2 = -(2\pi/\lambda_0)^2 = k_0^2 \qquad \rho_d = 2\rho_0 \sin\phi_0$$

$$v^2 = \gamma_0^2 - \Gamma^2 \qquad \eta_0 = (\mu_0/\varepsilon_0)^{1/2} = 120\pi$$

$$Z = \frac{\eta_w}{2\pi a}\frac{I_0(\gamma_w a)}{I_1(\gamma_w a)} \qquad \gamma_w^2 = i\sigma_w\mu_0\omega \qquad \eta_w = i\mu_0\omega/\gamma_w$$

and where S_0 and S_1 are factors that account for the presence of the tunnel walls. The latter two factors are given by

$$\begin{bmatrix} S_0 \\ S_1 \end{bmatrix} = \sum_{m=-\infty}^{+\infty} R_m \frac{K_m(va_0)}{I_m(va_0)} I_m(v\rho_0) I_m(v(\rho_0 + c)) \cdot \begin{bmatrix} 1 \\ \exp(-i2m\phi_0) \end{bmatrix} \tag{4}$$

where

$$R_m = \frac{(\gamma_0/v)K_m'(va_0)/K_m(va_0) + Y_m\eta_0 + \delta_m\eta_0}{(\gamma_0/v)I_m'(va_0)/I_m(va_0) + Y_m\eta_0 + \delta_m\eta_0} \tag{5}$$

and where

$$\delta_m\eta_0 = \frac{(im\Gamma/a_0)^2[v^{-2} - u^{-2}]^2}{(\gamma_0/v)I_m'(va_0)/I_m(va_0) + (Z_m/\eta_0)} \tag{6}$$

$$Y_m = \frac{i\gamma_e^2}{u\mu_0\omega}\frac{K_m'(ua_0)}{K_m(ua_0)} \qquad Z_m = -\frac{i\mu_0\omega}{u}\frac{K_m'(ua_0)}{K_m(ua_0)}$$

$$u = (\gamma_e^2 - \Gamma^2)^{1/2} \quad \text{and} \quad \gamma_e^2 = i\mu_0\omega(\sigma_e + i\varepsilon_e\omega).$$

In the present analysis we have tacitly assumed that the magnetic permeability takes its free space value μ_0 ($= 4\pi \times 10^{-7}$ H/m). However, it is a simple matter to account for the finite susceptibility of the axial conductor or trolley wire by using the appropriate value of the permeability μ_w in place of μ_0 in the expression for the series internal impedance Z given above.

The modal equation (1), while appearing to be rather complex, can be used to obtain numerical results without making any further approximations. For frequencies of the order of 100 kHz, the diameter of the tunnel is quite small compared with the free-space wavelength. In this case, $I_m(va_0)$ becomes very large and $K_m(va_0)$ becomes small. This causes numerical overflow problems so we find it

convenient to use small argument approximations so that the relevant factor in (4) is given by

$$\frac{K_m(va_0)}{I_m(va_0)} I_m(v\rho_0)I_m(v(\rho_0 + c)) \simeq \begin{cases} [(\rho_0 + c)\rho_0/a_0^2]^m(2m)^{-1}, & m \neq 0 \\ -\ln(va_0), & m = 0. \end{cases} \quad (7)$$

On the other hand, the modified Bessel functions of arguments $\gamma_w c$ and ua_0 are not approximated.

Limiting Cases

Before discussing some typical numerical results, we consider the limit of perfectly conducting walls of the tunnel. In this case it can be seen that $R_m \to 1$. Then, using the small argument approximation indicated by (7), it follows that

$$S_0 \simeq -\ln va_0 + \sum_{m=1}^{\infty} \left[\frac{(\rho_0 + c)\rho_0}{a_0^2}\right]^m \frac{1}{m} \quad (8)$$

and

$$S_1 \simeq -\ln va_0 + \sum_{m=1}^{\infty} \left[\frac{(\rho_0 + c)\rho_0}{a_0^2}\right]^m \frac{1}{m} \cos 2m\phi_0. \quad (9)$$

Using the well-known summation formula [3]

$$\sum_1^{\infty} b^m \frac{1}{m} \cos mx = -\tfrac{1}{2} \ln [1 - 2b \cos x + b^2] \quad (10)$$

we see that

$$S_1 - S_0 \simeq \ln (1 - r) - (1/2) \ln [1 - 2r \cos 2\phi_0 + r^2] \quad (11)$$

where

$$r = \frac{(\rho_0 + c)\rho_0}{a_0^2} \simeq \frac{\rho_0^2}{a_0^2}.$$

The relevant mode equation is now obtained from (11) by using the small argument approximations for the K_0 functions. Thus

$$\ln (\rho_d/c) + (\gamma_0/v^2)(2\pi Z/\eta_0) + S_1 - S_0 = 0. \quad (12)$$

Making use of (11), this can be solved explicitly for Γ^2 to yield

$$\Gamma = \gamma_0 \left[1 + \frac{2\pi Z}{i\mu_0\omega \ln R}\right]^{1/2} \quad (13)$$

where

$$R = (\rho_d/c)(1 - r)[1 - 2r \cos 2\phi_0 + r^2]^{-1/2}.$$

Equation (13) can be written in the form $\Gamma = (\hat{Y}\hat{Z})^{1/2}$ where $\hat{Y} = 2\pi i\varepsilon_0\omega/\ln R$ and $\hat{Z} = (i\mu_0\omega/2\pi) \ln R + Z$. Here $\hat{Y}$ and $\hat{Z}$ are the series admittance and series impedance, respectively, per unit length. The corresponding characteristic impedance is then $(\hat{Z}/\hat{Y})^{1/2}$ or $\Gamma/\hat{Y}$. As a check we can let the tunnel radius become infinite (i.e., $a_0 \to \infty$). Then R becomes ρ_d/c. The corresponding expressions for $\hat{Z}$ and $\hat{Y}$ are then the appropriate values for a single wire at a height $\rho_d/2$ over a perfect ground plane. Another check is let $\phi_0 \to 90°$ when we obtain $R = (\rho_d/c)(1 - r)/(1 + r)$. Using these limiting forms and setting $Z = 0$, we recover the handbook values of the characteristic impedance for perfectly conducting configurations [4].

TABLE I
Effect of Wire Position and Conductivity
($a_0 = 2$ m, $\varepsilon_e/\varepsilon_0 = 10$, $\sigma_e = 10^{-3}$ mhos/m, $\phi_0 = 45°$, $c = 1.5$ cm)

Frequency (kHz)	Normalized Phase $\mathrm{Im}(\Gamma)/k_0$ ($a_0 - \rho_0 = 80$cm)	($a_0 - \rho_0 = 40$cm)	($a_0 - \rho_0 = 20$cm)	($a_0 - \rho_0 = 10$cm)
50.0	1.060	1.149	1.271	1.274
66.0	1.060	1.149	1.271	1.273
87.1	1.060	1.149	1.271	1.273
114.9	1.060	1.149	1.270	1.272
151.6	1.060	1.149	1.270	1.271
200.0	1.060	1.148	1.269	1.270
264.0	1.059	1.148	1.268	1.269
348.2	1.059	1.147	1.267	1.268
459.5	1.059	1.146	1.264	1.265
606.3	1.058	1.144	1.261	1.262
800.0	1.057	1.142	1.255	1.256
	$\sigma_w = 5.7 \times 10^7$ mhos/m			$\sigma_w = 5 \times 10^7$ mhos/m

TABLE II
Effect of Wall Conductivity
($a_0 = 2$ m, $\varepsilon_e/\varepsilon_0 = 10$, $\phi_0 = 45°$, $a_0 - \rho_0 = 20$ cm, $\sigma_w = 5.7 \times 10^7$ mhos/m, $c = 1.5$ cm)

Frequency (kHz)	Normalized Phase $\mathrm{Im}(\Gamma)/k_0$ ($\sigma_e = 10^{-1}$)	($\sigma_e = 10^{-2}$)	($\sigma_e = 10^{-3}$)	($\sigma_e = 10^{-4}$)
50.0	1.266	1.271	1.271	1.266
66.0	1.264	1.270	1.271	1.260
87.1	1.262	1.270	1.271	1.254
114.9	1.259	1.269	1.270	1.247
151.6	1.257	1.269	1.270	1.238
200.0	1.253	1.268	1.269	1.228
264.0	1.248	1.267	1.268	1.221
348.2	1.244	1.266	1.267	1.216
459.5	1.238	1.265	1.266	1.212
606.3	1.232	1.264	1.261	1.209
800.0	1.224	1.262	1.255	1.208

TABLE III
Effect of Wire Size
($a_0 = 2$ m, $\varepsilon_e/\varepsilon_0 = 10$, $\sigma_e = 10^{-3}$ mhos/m, $\phi_0 = 45°$, $a_0 - \rho_0 = 40$ cm, $\sigma_w = 5.7 \times 10^7$ mhos/m)

Frequency (kHz)	Attenuation Rate (dB/km) ($c = 1.5$cm)	($c = 2.5$cm)	Phase $\mathrm{Im}(\Gamma)/k_0$ ($c = 1.5$cm)	($c = 2.5$cm)
50.0	2.14×10^{-2}	2.02×10^{-2}	1.149	1.173
66.0	3.11×10^{-2}	3.09×10^{-2}	1.149	1.172
87.1	4.68×10^{-2}	4.87×10^{-2}	1.149	1.172
114.9	7.30×10^{-2}	7.87×10^{-2}	1.149	1.172
151.6	1.168×10^{-1}	1.296×10^{-1}	1.149	1.172
200.0	1.907×10^{-1}	2.159×10^{-1}	1.148	1.171
264.0	3.149×10^{-1}	3.618×10^{-1}	1.148	1.171
348.2	5.224×10^{-1}	6.062×10^{-1}	1.147	1.170
459.5	8.631×10^{-1}	1.008	1.146	1.169
606.3	1.406	1.649	1.144	1.167
800.0	2.233	2.623	1.142	1.164

Numerical Results

We now present some numerical examples for the general configuration shown in Fig. 1(a) or its symmetrical equivalent in Fig. 1(b). In view of the large number of parameters involved, we selected certain typical values only. For example, we choose $\phi_0 = 45°$ for all cases and the wire radius c is taken to be 1.5 cm. The frequency range is taken to extend from 50 to 800 kHz since this encompasses frequencies used in trolley-wire communication systems. Also, we restrict attention to the attenuation rate (real part of Γ) of the propagating mode. This is expressed throughout in terms of decibels per kilometer.[1]

In the first example, in Fig. 2, the influence of the distance $a_0 - \rho_0$ of the trolley wire from the tunnel wall is exhibited.

[1] Some values of the normalized phase factor $\mathrm{Im}(\Gamma)/k_0$ are appended in Tables I–III. The relatively small influence of changing the wire radius c, on both attenuation and phase, is shown in Table III.

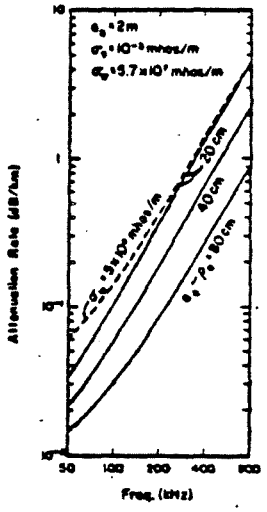


Fig. 2. Influence of distance of trolley wire to tunnel wall on attenuation rate.

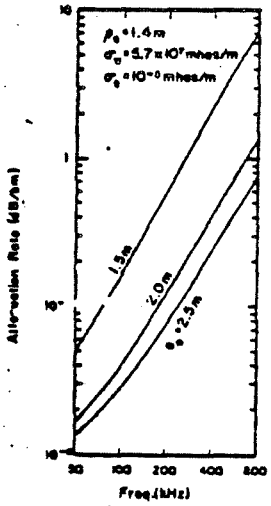


Fig. 4. Effect of varying tunnel radius for fixed height of trolley wire to ground plane or tunnel floor.

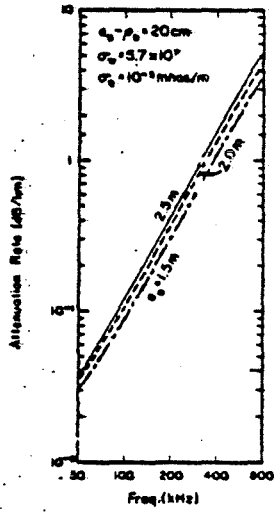


Fig. 3. Effect of varying tunnel radius for fixed separation between trolley wire and tunnel wall.

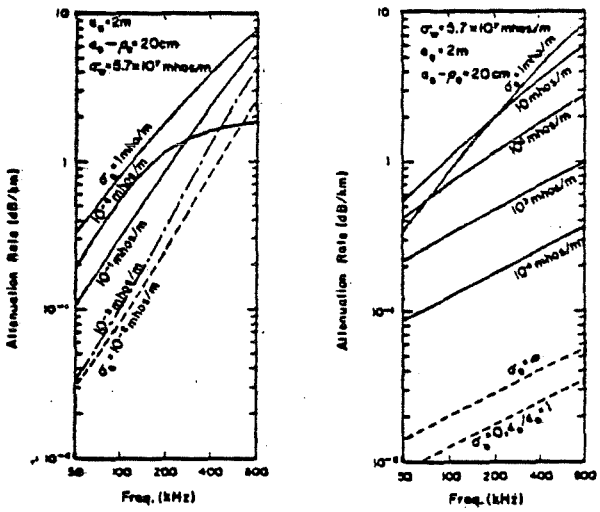


Fig. 5. (a) Dependence of attenuation rate on rock conductivity σ_e for range from 10^{-4} to 1 mhos/m. (b) Dependence of attenuation rate on rock conductivity σ_e for range from 1 mhos/m to ∞.

For this case the tunnel radius is 2 m and the rock conductivity $\sigma_e = 10^{-3}$ mhos/m. The relative permittivity ϵ_e/ϵ_0 of the rock is taken to be 10 and this value is adopted throughout the remaining examples. The wire conductivity σ_w is taken to be 5.7×10^7 mhos/m corresponding to copper but the effect of decreasing this to 5.7×10^6 is shown for the case $a_0 - \rho_0 = 20$ cm. As indicated in Fig. 2, the attenuation rate increases significantly as the trolley wire is moved toward the wall although the total attenuation for a 1-km path is still only 4.5 dB at 800 kHz even when $a_0 - \rho_0 = 20$ cm $\simeq 8$ in.

The influence of the tunnel radius for a fixed distance of the trolley wire to the wall is illustrated in Fig. 3. (The same parameters are used in Fig. 2). There appears to be only a very slight increase of attenuation when the tunnel radius is increased. This is probably due to the increasing fringing of the fields when the separation between the trolley wire and the image is increased.

If we keep the distance from the trolley wire to the ground plane fixed then, as indicated in Fig. 4, the attenuation rate increases as the tunnel radius is decreased. This again shows that the important parameter insofar as losses are concerned, is the distance of the trolley wire to the tunnel wall.

The dependence of the attenuation rate on the conductivity σ_e of the rock surrounding the tunnel is complicated. This is not surprising when one considers the various physical mechanisms that are responsible for the extraction of energy from the propagating mode. Some results to illustrate the dependence are shown in Fig. 5(a) and (b) for a wide range of values. For very small values of σ_e (e.g.,

10^{-4} mhos/m), the loss is determined primarily by the leakage radiation into the rock that has the character of a low loss dielectric at 800 kHz. As the rock conductivity is increased, this leakage radiation is lowered because of an increased impedance mismatch at the air/tunnel boundary. There is a local minimum of the attenuation at σ_e approximately equal to 10^{-2} mhos/m which occurs because, for further increases of σ_e, the induced eddy currents become a dominant factor and the skin depth in the surrounding rock is still quite large. However, with further increases of σ_e, the attenuation rate is again decreased because the skin depth is now becoming much less than the tunnel diameter.

Finally, as indicated before, in the limit when $\sigma_e = \infty$, the only loss mechanism is due to the finite conductivity σ_w of the trolley wire. This is indicated in Fig. 5(b). The corresponding limit when the rock conductivity is zero and the relative permittivity ϵ_e/ϵ_0 is unity, is also shown in Fig. 5(b). As discussed earlier, this is the case when the corresponding two-wire transmission line is located in free space, or the equivalent situation of a single wire over a perfect ground plane.

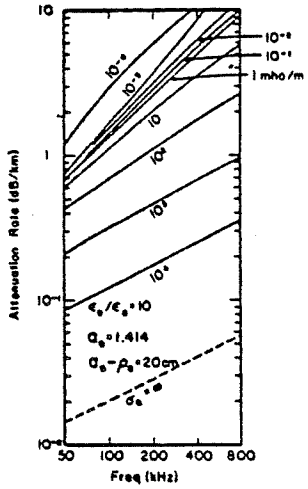


Fig. 6. Dependence of attenuation rate on rock conductivity σ_e for single conductor in fully circular tunnel. Other conditions are same as in Fig. 5(a) and (b) except that $a_0 = 1.414$ m.

Concluding Remarks

The tunnel model used above is admittedly very idealized. Nevertheless, the results do indicate that the influence of the finite conductivity of the adjacent rock is significant for frequencies from 50 to 800 kHz. Because we have represented the ground plane or floor of the tunnel as a perfect conductor, losses from the imperfect bonding of the rails are ignored. The influence of the leakage currents from the rails to the rock floor should be considered.

While this problem could be treated by a more sophisticated model, some insight is obtained by examining the results for a fully circular tunnel where the walls are uniformly conducting [5]. Essentially, this is the situation depicted in Fig. 1(b) where now we have only one conductor. Thus the return current must flow entirely in the adjacent rock. The mode equation is now $A_0 = 0$ where A_0 is defined by (2). We choose the same parameters as used in Fig. 5(a) and (b) except we set $a_0 = 1.414$ m so that the cross-sectional area of the tunnel is the same as before. Not surprisingly, the attenuation rates, as shown in Fig. 6, increase monitonically as the conductivity σ_e of the rock is decreased. Also, for σ_e in the range from 10^{-2} to 10^{-3} mhos/m, the attenuation rate is an order of magnitude greater than with the semicircular model.

If we again consider the special case $\sigma_e = \infty$, and use the small argument approximations for the Bessel functions, it is not difficult to show that $\Gamma \simeq (\hat{Y}_0\hat{Z}_0)^{1/2}$ where $\hat{Y}_0 = 2\pi i\epsilon_0\omega(\ln R_0)^{-1}$ and $\hat{Z}_0 = (i\mu_0\omega/2\pi)\ln R_0 + Z$ where

$$R_0 \cong \frac{a_0}{c}\left(1 - \frac{\rho_0^2}{a_0^2}\right).$$

This limiting case and one discussed earlier suggest that a meaningful definition for the characteristic impedance is $\Gamma/\hat{Y}$ for the semicircular model and $\Gamma/\hat{Y}_0$ for the fully circular model. This assertion, however, becomes invalid for the low rock conductivity (e.g., $\sigma_2 < 10^{-2}$) and for the higher frequencies (e.g., $f > 200$ kHz).

There is an obvious need for some controlled experimental tests for transmission in tunnels with various types of conductors such as rails and pipes. An important step in this direction has just been described by Gillette and Gilmour [6] for frequencies somewhat higher than considered here. Also, the theoretical models should be extended to account for the presence of insulated and un-insulated conductors buried in the adjacent rock.

Acknowledgment

We are grateful to Richard H. Spencer and Robert L. Lagace of the A. D. Little, Inc., for their useful comments that motivated this analysis.

References

[1] J. N. Murphy and H. E. Parkinson, "Mine communications: Research and development in the U.S.A.," *Proc. Int. Conf. Radio: Tunnels and Mines*, vol. II, Liege, Belgium, April 1–5, 1974, pp. 42–64.

[2] J. R. Wait and D. A. Hill, "Coaxial and bifilar modes on a transmission line in a circular tunnel," *Appl. Phys.*, vol. 4, pp. 307–312, 1974.

[3] A. D. Wheelon, *Tables of Summable Series and Integrals Involving Bessel Functions*. San Francisco, CA: Holden-Day, 1968, p. 44.

[4] L. A. DeRosa and A. G. Kandoian, Eds., *Reference Data For Radio Engineers*, 5th ed. New York: H. W. Sams & Co., 1968, ch. 22, pp. 21–22.

[5] J. R. Wait and D. A. Hill, "Guided electromagnetic waves along an axial conductor in a circular tunnel," *IEEE Trans. Antennas Propagat.*, vol. AP-22, pp. 627–630, July 1974.

[6] M. R. Gillette and A. S. Gilmour, "Attenuation measurements in the 1 to 1000 MHz frequency range in wet granite tunnels," *IEEE Trans. Electromagn. Compat.*, vol. EMC-17, pp. 201–206, Nov. 1975.

Radio Frequency Transmission via a Trolley Wire in a Tunnel with a Rail Return

JAMES R. WAIT, FELLOW, IEEE, AND DAVID A. HILL, SENIOR MEMBER, IEEE

Abstract—An analysis is given for the transmission of electromagnetic waves along a circular tunnel in the presence of axial conductors. One of these conductors is an idealization of a trolley wire with its bonded feeder line that may be located anywhere in the tunnel. The other is a metal rail that is located within the homogeneous rock medium at a finite distance from the tunnel wall. A mode equation for the propagation modes is obtained that is used to obtain numerical results for the attenuation rate in the frequency range 50 to 800 kHz. It is shown that the attenuation rate is only weakly dependent on the burial depth of the rail conductor, at least in the range up to 50 cm. Also, it is found that the rail conductor for the model adopted carries an appreciable fraction of the total return current when typical rock conductivities are assumed. A thin layer of insulation on the rail appears to have a negligible effect. In fact, there is little change even if the rail is within the tunnel and just above the tunnel floor.

INTRODUCTION

AN EXTREMELY interesting problem occurs when a radio frequency signal used in mine communications [1] is coupled to a trolley wire or its associated feeder line in a tunnel. If the tunnel wall is suffiently well conducting, the return current path through the rock is uninhibited. However, if the rock is of low conductivity, the resultant attenuation of the signal may be severe due to ohmic losses. Fortunately, in many such cases, the situation is improved by the presence of metal rails that would be in intimate contact with the floor of the tunnel. Ideally, such rails could act as a perfect ground plane. Then the trolley wire would be imaged, and the loss would result from the finite conductivity of the upper and side walls and the finite conductivity of the trolley wire and its bonded feeder. This configuration was analyzed earlier [2] and the results indicated that the attenuation was indeed very small (e.g., less than 2 dB/km at 200 kHz). A more realistic case, however, should explicitly consider the rail or other axial conductors that may be located in close proximity to the floor of the tunnel. This is the subject of the present investigation. Alas, we still employ a highly idealized model that, nevertheless, contains the essential ingredients. Specifically, we consider a tunnel of circular cross section with an eccentrically located trolley wire and a single rail that may be insulated from the rock. Whilst the formulation is fairly general and could be applicable to other tunnel configurations [6], numerical results are obtained only for the case where the diameter of the tunnel is small compared with the operating (free space) wavelength.

Manuscript received January 26, 1976; revised April 25, 1976. This work was supported by a contract from the U.S. Bureau of Mines monitored by Dr. H. K. Sacks.

J. R. Wait is with the Cooperative Institute for Research in Environmental Sciences, University of Colorado, Boulder, CO 80309.

D. A. Hill is with the Institute for Telecommunication Sciences, U.S. Department of Commerce, Boulder, CO 80302.

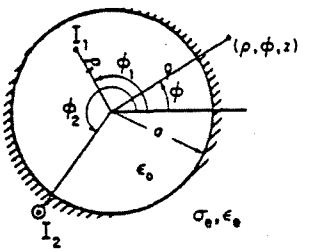


Fig. 1. Circular tunnel with trolley wire at (ρ_1,ϕ_1,z) carrying current I_1 and buried rail or earth conductor at (ρ_2,ϕ_2,z) carrying current I_2.

STATEMENT OF PROBLEM

The situation we wish to analyze is illustrated in Fig. 1. The tunnel of radius a, with free space permittivity ϵ_0, is cut through a homogeneous rock medium of conductivity σ_e and permittivity ϵ_e. The magnetic permeability μ_0 of the whole space is taken to be the same as that of free space. With respect to a cylindrical coordinate system (ρ,ϕ,z), the tunnel wall is defined by $\rho = a$. A trolley wire of radius c_0 and conductivity σ_s is located at $\rho = \rho_1$ and $\phi = \phi_1$, where $\rho_1 < a$. A rail or other heavy metal conductor is now represented by a cylindrical structure of outer radius c and centered at $\rho = \rho_2$ and $\phi = \phi_2$, where $\rho_2 > a + c$. Actually c is taken to be the radius of the insulation or coating that can be assigned a conductivity σ_c and permittivity ϵ_c. This coating is concentric with an assumed circular metal conductor of radius b that has a conductivity σ_w. Normally, we would expect the coating thickness $c - b$ to be small compared with all other dimensions of the problem. Also, all displacement currents in the metal conductors can be safely ignored, but, without additional complexity, their magnetic permeabilities may be taken to be different from the free space value μ_0 assumed elsewhere.

We are interested in seeking solutions for a propagation mode in the tunnel that has the form $\exp(-\Gamma z + i\omega t)$, where Γ is the complex propagation constant and ω is the angular frequency. Thus subject to the relative thinness of the wire and rail, we can assert that the currents will have the respective forms $I_1 \exp(-\Gamma z + i\omega t)$ and $I_2 \exp(-\Gamma z + i\omega t)$, where I_1 and I_2 are as yet undetermined. In what follows, we drop the harmonic time factor $\exp(i\omega t)$; its presence is understood. The solution is greatly simplified by invoking appropriate axial impedance conditions on the trolley wire and rail. The form of these are taken from previous work [3]-[5] but, in any case, they have a self contained plausibility.

WIRE BOUNDARY CONDITIONS

The impedance condition, on the axial electric field E_{0z}, at the trolley wire is taken to be [4]

$$E_{0z}\Big|_{\substack{\rho=\rho_1+c_0\\ \phi=\phi_1}} = Z_s I_1 \exp(-\Gamma z) \tag{1}$$

where

$$Z_s = \frac{\eta_s}{2\pi c_0}\frac{I_0(\gamma_s c_0)}{I_1(\gamma_s c_0)}. \tag{2}$$

$\gamma_s = (i\sigma_s\mu_s\omega)^{1/2}$ and $\eta_s = i\mu_s\omega/\gamma_s$. $I_0(\cdot)$ and $I_1(\cdot)$ are the modified Bessel functions not to be confused with the axial current I_1 on the trolley wire. In the case where $|\gamma_s c_0| \ll 1$, the axial impedance reduces to the usual series resistance $1/\pi c_0^2\sigma_s$ (in ohms per meter) that loses its dependence on the magnetic permeability μ_s. An analogous condition is to be applied at the coating surface of the rail conductor. For the axial electric field E_{ez} in the rock, it reads

$$E_{ez}\Big|_{\substack{\rho=\rho_2+c\\ \phi=\phi_2}} = Z_c(\Gamma) I_2 \exp(-\Gamma z) \tag{3}$$

where $Z_c(\Gamma)$ is the effective axial impedance of the rail or coated earth conductor. In general, it would be a function of the propagation constant Γ. For the present problem we can write

$$Z_c(\Gamma) \cong z_c + Z_b \tag{4}$$

being the sum of the impedance z_c of the coating and the impedance Z_b of the metal rail itself. For an earlier quasi-static analysis [3]

$$z_c \cong \frac{k_c^2 + \Gamma^2}{2\pi(\sigma_c + i\epsilon_c\omega)} \ln\frac{c}{b} \tag{5}$$

where $k_c^2 = -i\mu_0\omega(\sigma_c + i\epsilon_c\omega)$. Since $c - b \ll b$ this is equivalent to

$$z_c \cong \frac{i\mu_0\omega}{2\pi b}(c-b)\left(1 + \frac{\Gamma^2}{k_c^2}\right). \tag{6}$$

In addition, we note that

$$Z_b = \frac{\eta}{2\pi b}\frac{I_0(\gamma_w b)}{I_1(\gamma_w b)} \tag{7}$$

where $\gamma_w = (i\sigma_w\mu_w\omega)^{1/2}$ and $\eta_w = i\mu_w\omega/\gamma_w$. Also, if $|\gamma_w b| \ll 1$, Z_b reduces to $1/\pi b^2\sigma_w$, as it should.

THE REQUIRED FIELD EXPRESSIONS

We now return to the general configuration shown in Fig. 1 and for the moment ignore the presence of the rail conductor. The axial electric field $E_{0z}^{(1)}$ in the region $a > \rho > \rho_1$ due to the current $I_1 \exp(-\Gamma z)$ in the trolley wire is known from previous work [4], [5]. It is given explicitly by

$$E_{0z}^{(1)} = -\nu^2 \frac{i\mu_0\omega I_1}{2\pi\gamma_0^2} e^{-\Gamma z} \sum_{m=-\infty}^{+\infty} I_m(\nu\rho_1)\left[K_m(\nu\rho) - R_m\frac{K_m(\nu a)}{I_m(\nu a)} I_m(\nu\rho)\right] e^{-im(\phi-\phi_1)} \tag{8}$$

where $\nu = (\gamma_0^2 - \Gamma^2)^{1/2} = i(\Gamma^2 - \gamma_0^2)^{1/2}$ and $\gamma_0^2 = -k_0^2 = -\epsilon_0\mu_0\omega^2$. $I_m(\cdot)$ and $K_m(\cdot)$ are modified Bessel functions of

where

$$A_1 = -\frac{i\mu_0\omega\nu^2}{2\pi\gamma_0^2}\left\{ K_0(\nu c_0) - \sum R_m I_m(\nu\rho_1)\frac{K_m(\nu a)}{I_m(\nu a)} I_m(\nu(\rho_1 + c_0))\right\} - Z_s \quad (22)$$

$$A_2 = -\frac{i\mu_0\omega u^2}{2\pi\gamma_e^2}\sum K_m(u\rho_2)I_m(ua) \cdot (1 - S_m)\frac{I_m(\nu(\rho_1 + c_0))}{I_m(\nu a)} e^{-im(\phi_1-\phi_2)} \quad (23)$$

$$B_1 = -\frac{i\mu_0\omega\nu^2}{2\pi\gamma_0^2}\sum I_m(\nu\rho_1)K_m(\nu a) \cdot (1 - R_m)\frac{K_m(u(\rho_2+c))}{K_m(ua)} e^{-im(\phi_2-\phi_1)} \quad (24)$$

and

$$B_2 = -\frac{i\mu\omega u^2}{2\pi\gamma_e^2}\left\{ K_0(uc) - \sum S_m K_m(u\rho_2) \cdot \frac{I_m(ua)}{K_m(ua)} K_m(u(\rho_2 + c))\right\} - Z_c(\Gamma). \quad (25)$$

The summations in each case extend from $-\infty$ to $+\infty$ through integer values including zero. In dealing with radio frequencies, the tunnel diameter $2a$ is much smaller than a free-space wavelength. Then, for the modes of interest, the modal equation can be simplified somewhat by replacing Bessel functions of argument νa and $\nu\rho_1$ by their small argument approximations. Thus, for example,

$$\frac{K_m(\nu a)}{I_m(\nu a)} I_m(\nu\rho_1)I_m(\nu(\rho_1 + c)) \cong \begin{cases} \left[\frac{(\rho_1+c)\rho_1}{a^2}\right]^m \frac{1}{2m}, & m \neq 0 \\ -\ln(\nu a), & m = 0. \end{cases}$$

However, Bessel functions of argument ua and $u\rho_2$ are not so approximated.

While, in principle, there are an infinite number of solutions of the modal equation, we may anticipate that the mode of most practical interest is the one where Γ is of the order of ik_0, where $k_0 = 2\pi/(\text{free-space wavelength})$. Also, at least in the case of low rock conductivity, the currents I_1 and I_2 would be of the same order of magnitude but would tend to be antiphase. Thus, ideally, such a bifilar type mode is what would be expected for a two-wire line when the currents are antiphase. Of course, at higher frequencies, other propagation modes would be possible including those that would have their energy confined to tunnel or to the insulation in the coated rail.

NUMERICAL EXAMPLE

For the present illustration of the analytical model, we choose the following values for the parameters.

Trolley wire: radius $c_0 = 1.5$ cm,
conductivity $\sigma_s = 5.7 \times 10^7$ mhos/m,
permeability $\mu_s = \mu_0 = 4\pi \times 10^{-7}$.

Rail or buried earth conductor: radius $b = 4$ cm,
conductivity $\sigma_w = 10^7$ mhos/m,
permeability $\mu_w = \mu_0$
coating thickness $c - b = 0$.

Tunnel radius: $a = 1.414$ m (i.e., $2a \cong 9$ ft).

Trolley wire location: $\phi_1 = 120°$, $a - \rho_1 = 20$ cm.

Rail location: $\phi_2 = 240°$, $\rho_2 - a = 10$ cm.

Rock medium: conductivity σ_e (various values from 10^{-4} mhos/m to ∞)
permittivity $\epsilon_e = 10\epsilon_0$.

Frequency: from 50 to 800 kHz.

The attenuation rate which is the real part of Γ is plotted in Figs. 2(a) and 2(b) as a function of frequency. The vertical scale is decibels (dB) per kilometer (km) of path length along the tunnel. As illustrated, the attenuation increases monotonically as the rock conductivity σ_e is decreased from infinity to about 1 mho/m. In fact, in the case where $\sigma_e \geq 10$ mhos/m, the attenuation of the mode is almost identical to that computed for a tunnel with a trolley wire and no rail conductor present. This is the case considered earlier [2] and it corresponds to the dominant mode solution of the equation $A_1 = 0$, where A_1 is defined by (22). For lower and more typical rock conductivities, the results are influenced by the presence of the rail conductor. Such values are those shown in Fig. 2(b).

An important related parameter is the complex ratio I_2/I_1 since this is a measure of the relative amount of current being carried by the rail. For the same conditions described above, the amplitude and phase of this ratio is plotted in Fig. 3(a) and 3(b), respectively. Not surprisingly, as the rock conductivity is decreased, the relative current carried by the rail increases and, in fact, the ratio I_2/I_1 is actually tending to -1 at the lowermost frequencies. Of course, in the limit of high σ_e, the rail current is very small, which is not surprising since the return current flows very easily in the well conducting rock walls of the tunnel.

While the above results were obtained for a buried rail located at $\rho_2 - a = 10$ cm from the tunnel wall, other calculations showed that there was virtually no change in the results from $\rho_2 - a$ varying from 5 to 40 cm. Also, the presence of a thin lossless dielectric coating (e.g., $c - b = 0.1$ mm) on the rail conductor leads to a negligible change in the results. Of course, other values of these parameters may lead to significant changes but no major modifications should result for the present configuration in the frequency range considered.

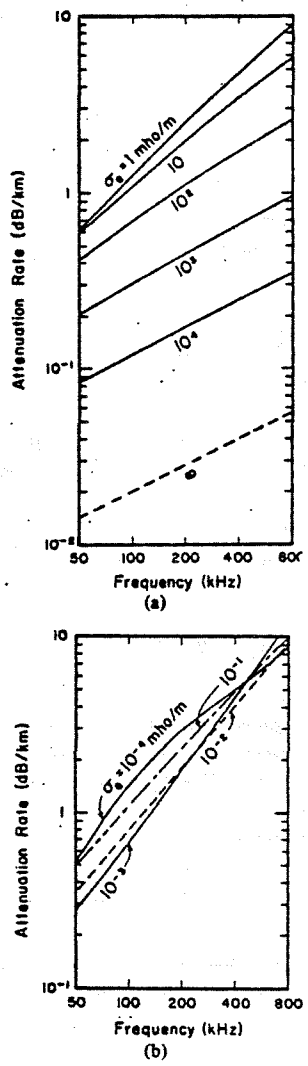


Fig. 2. Attenuation rate of dominant mode for model shown in Fig. 1.

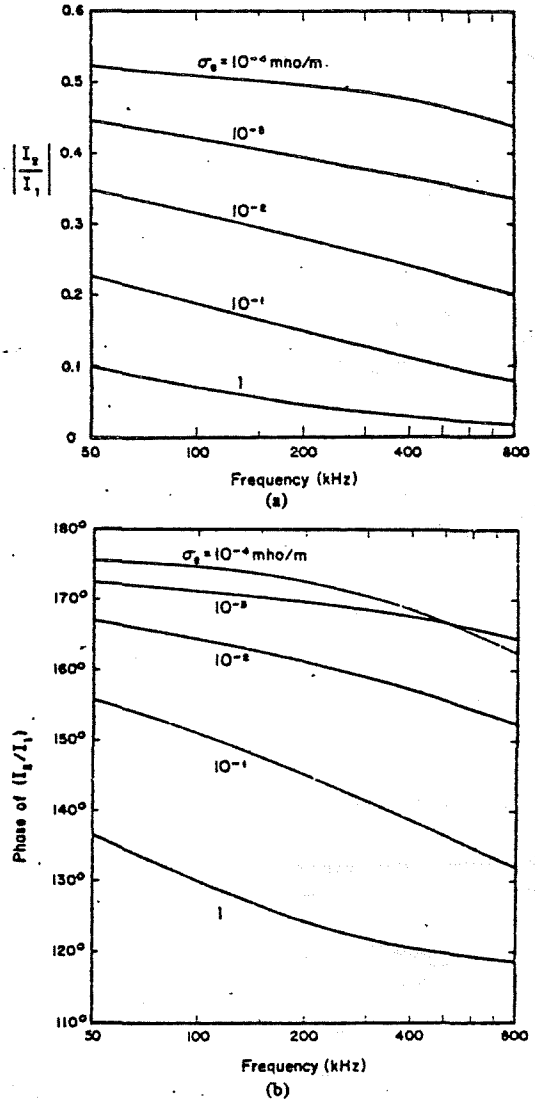


Fig. 3. Complex ratio of current I_2 in rail to current I_1 in trolley wire.

COMPARISON WITH RAIL IN TUNNEL

In the above model, we have assumed that the rail is a cylindrical dielectric-coated wire located in the conductive medium surrounding the tunnel. This could be criticized as unrealistic since the rail may be actually in the interface between the tunnel and the rock. However, as we pointed out, the dependence on the quantity $\rho_2 - a$ is very weak, and in fact, for all practical purposes, it makes little difference in the deduced propagation constant Γ whether the rail is just below or just above the floor of the tunnel. This assertion is confirmed by calculations, using another formulation [5] for the same model but with the parameter $a - \rho_2$ being positive. Such an example is illustrated in Fig. 4 for the same geometrical parameters used above with the exceptions indicated. As can be seen, as $a - \rho_2$ is decreasing, the attenuation rate is approaching the value for the rail conductor located within the rock medium (i.e., indicated by $\rho_2 - a = 10$ cm). Actually, in this latter situation, the results are essentically the same for $\rho_2 - a$ from 5 to 20 cm.

THE MONOFILAR MODE

Following the suggestion of the editor (W. F. Croswell), a search was made for other modes that may have low attenuation. A mode was found that had the character of the monofilar mode for a twin-wire transmission line in a circular tunnel [5]. The magnitude of the ratio I_2/I_1 for this mode varies considerably with the geometrical configuration but the phase of I_2/I_1 is close to zero. Thus, physically, both the trolley

integer order m. The coefficient R_m is given by

$$R_m = \frac{\frac{\gamma_0}{\nu}\frac{K_m'(\nu a)}{K_m(\nu a)} + Y_m\eta_0 + \delta_m\eta_0}{\frac{\gamma_0}{\nu}\frac{I_m'(\nu a)}{I_m(\nu a)} + Y_m\eta_0 + \delta_m\eta_0} \tag{9}$$

and

$$\delta_m\eta_0 = \frac{(im\Gamma/a)^2[\nu^{-2} - u^{-2}]^2}{\frac{\gamma_0}{\nu}\frac{I_m'(\nu a)}{I_m(\nu a)} + \frac{Z_m}{\eta_0}} \tag{10}$$

where

$$Y_m = \frac{i\gamma_e^2}{u\mu_0\omega}\frac{K_m'(ua)}{K_m(ua)} \tag{11}$$

$$Z_m = -\frac{i\mu_0\omega}{u}\frac{K_m'(ua)}{K_m(ua)} \tag{12}$$

$$u = (\gamma_e^2 - \Gamma^2)^{1/2} = i(\Gamma^2 - \gamma_e^2)^{1/2}$$

$$\gamma_e^2 = i\mu_0\omega(\sigma_e + i\epsilon_e\omega)$$

and

$$\eta_0 = (\mu_0/\epsilon_0)^{1/2} \cong 120\pi.$$

The corresponding expression for the field $E_{ez}^{(1)}$ in the region $\rho > a$ due to the current $I_1 \exp(-\Gamma z)$, is given by

$$E_{ez}^{(1)} = -\frac{i\mu_0\omega\nu^2}{2\pi\gamma_0^2} I_1 e^{-\Gamma z} \sum_{m=-\infty}^{+\infty} I_m(\nu\rho_1)K_m(\nu a) \cdot (1 - R_m)\frac{K_m(u\rho)}{K_m(ua)} e^{-im(\phi-\phi_1)}. \tag{13}$$

This can be checked by noting that $E_{ez}^{(1)}$ satisfies the appropriate wave equation for a medium of constants σ_e, ϵ_e, and μ_0, and that at $\rho = a$, $E_{ez}^{(1)} = E_{0z}^{(1)}$.

We now consider the complementary problem of deducing the axial field $E_{ez}^{(2)}$ in the region $\rho > a$ due to the current $I_2 \exp(-\Gamma z)$ in the rail conductor. The solution for this problem can be carried out in a straightforward manner if we first ignore the presence of the trolley wire. The result is

$$E_{ez}^{(2)} = -\frac{i\mu_0\omega u^2 I_2}{2\pi\gamma_e^2} e^{-\Gamma z}\left\{K_0(u\hat{\rho}_d) - \sum_{m=-\infty}^{+\infty} K_m(u\rho_2)S_m\frac{I_m(ua)}{K_m(ua)}K_m(u\rho)e^{-im(\phi-\phi)}\right\} \tag{14}$$

where $\hat{\rho}_d = [\rho^2 + \rho_2^2 - 2\rho\rho_2\cos(\phi - \phi_2)]^{1/2}$. The factor S_m has an analogous form to R_m, and in fact they are related as follows:

$$\frac{\nu^2}{\gamma_0^2}\frac{K_m(\nu a)}{K_m(ua)}(1 - R_m) = \frac{u^2}{\gamma^2}\frac{I_m(ua)}{I_m(\nu a)}(1 - S_m). \tag{15}$$

An equivalent form of (14) valid in the region $a < \rho < \rho_2$ is obtained by replacing $K_0(u\hat{\rho}_d)$ in its series form for this region referring to the origin $\rho = 0$. Thus

$$K_0(u\hat{\rho}_d) = \sum_{m=-\infty}^{+\infty} K_m(u\rho_2)I_m(u\rho)e^{-im(\phi-\phi_2)}. \tag{16}$$

The corresponding expression for the field $E_{0z}^{(2)}$, in the region $\rho < a$, due to the current $I_2 \exp(-\Gamma z)$, is found to be

$$E_{0z}^{(2)} = -\frac{i\mu_0\omega u^2}{2\pi\gamma_e^2} I_2 e^{-\Gamma z} \sum_{m=-\infty}^{+\infty} K_m(u\rho_2)I_m(ua) \cdot (1 - S_m)\frac{I_m(\nu\rho)}{I_m(\nu a)} e^{-im(\phi-\phi_2)}. \tag{17}$$

This again is an appropriate solution of the wave equation in a homogeneous region of electrical constants ϵ_0 and μ_0. It can be verified that $E_{0z}^{(2)} = E_{ez}^{(2)}$ at $\rho = a$.

Another useful check is to note that as a consequence of the reciprocity principle,

$$E_{ez}^{(1)}(\rho_2,\phi_2)/I_1 = E_{0z}^{(2)}(\rho_1,\phi_1)/I_2. \tag{18}$$

This, of course, could have been used at the outset to obtain the solution of one complementary problem from the other.

THE MODAL EQUATION

The principal remaining task is now to determine the propagation constant(s) Γ by requiring that the total fields satisfy the appropriate impedance conditions on the trolley wire and rail. Thus, on applying (1) and (3), we require that

$$E_{0z}^{(1)}(\rho_1 + c_0, \phi_1) + E_{0z}^{(2)}(\rho_1 + c_0, \phi_1) = Z_s I_1 \exp(-\Gamma z) \tag{19}$$

and

$$E_{ez}^{(1)}(\rho_2 + c, \phi_2) + E_{ez}^{(2)}(\rho_2 + c_0, \phi_1) = Z_c I_2 \exp(-\Gamma z). \tag{20}$$

These must be satisfied simultaneously for all values of z. This in turn requires that the determinant of the coefficients of I_1 and I_2 should vanish, i.e.,

$$\begin{vmatrix} A_1 & A_2 \\ B_1 & B_2 \end{vmatrix} = 0 \tag{21}$$

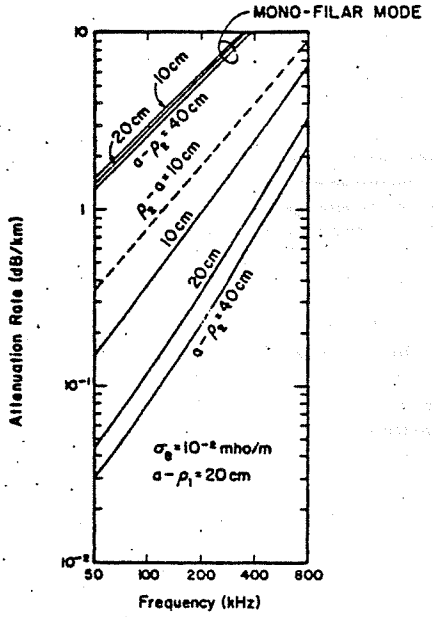


Fig. 4. Attenuation rate for corresponding situation where rail conductor is located within tunnel (i.e., $a - \rho_2 > 0$) and comparison curve for case of buried rail (i.e., $\rho_2 - a > 0$). Some results for corresponding monofilar mode are also shown.

wire and the rail carry the current in the same direction with all the return current being carried by the adjacent rock. Not surprisingly, this monofilar mode has an attenuation rate of the order of at least ten times that of the desired bifilar mode over the frequency range from 50 to 800 kHz. The results for the monofilar mode are shown in Fig. 4 for the parameters indicated. The case for $\rho_2 - a = 10$ cm is not shown since the attenuation rate is always greater than 10 dB/km.

There are also evanescent type solutions of the mode equation that are analogous to the cutoff modes in a waveguide. Their attenuation is enormous and would plot well over the upper limit of Figs. 2(a) and 4. As indicated elsewhere [4], modes of the waveguide type do not become propagating until the frequency is increased to 50 MHz or so for typical tunnels. This is true even if the surrounding medium was a perfect dielectric.

CONCLUDING REMARKS

The present analysis should provide some insight into the propagation mechanism that is exploited in radio frequency transmission on a trolley wire or other axial conductors in a tunnel. The presence of rails or other conductors on the floor of the tunnel assures that the return current path is effective particularly in the case where the conductivity of the surrounding rock is low. In our discussion, we have not considered the influence of various loads on the trolley wire such as locomotives. The latter are usually isolated to some extent by radio frequency chokes that nevertheless will influence the performance of an actual communication system.

Further work on this subject needs to consider all the relevant factors. Also, it appears that some carefully controlled experiments are badly needed if the relative importance of the various parameters are to be properly understood.

REFERENCES

[1] J. N. Murphy and H. E. Parkinson, "Mine communications: Research and development in the U.S.A.," in *Proceedings of International Conference on "Radio: Tunnels and Mines*, vol. II, pp. 42–64, April 1–5, 1974, Liege, Belgium.

[2] D. A. Hill and J. R. Wait, "Analysis of radio frequency transmission along a trolley wire in a mine tunnel," Report submitted to U.S. Bureau of Mines, December 19, 1975.

[3] J. R. Wait and D. A. Hill, "Propagation along a braided coaxial cable in a circular tunnel," *IEEE Trans. Microwave Theory Tech.*, vol. MTT-23, pp. 401–405, May 1975.

[4] —, "Guided electromagnetic waves along an axial conductor in a circular tunnel," *IEEE Trans. Antennas Propagat.*, vol. AP-22, pp. 627–630, July 1974.

[5] —, "Coaxial and bifilar modes on a transmission line in a circular tunnel," *Applied Physics* (Springer Verlag), vol. 4, pp. 307–312, 1974.

[6] M. R. Gillette and A. S. Gilmour, "Attenuation measurements in the 1 to 1000 MHz frequency range in wet granite tunnels," *IEEE Trans. Electromagn. Compat.*, vol. EMC-17, pp. 201–206, Nov. 1975.

COMMUNICATIONS Vol. 25, No. 3

Quasi-Static Limit for the Propagating Mode along a Thin Wire in a Circular Tunnel

JAMES R. WAIT

Abstract—A previous modal analysis for a circular tunnel containing a thin wire is shown to be greatly simplified at low frequencies provided the wall conductivity is high. The explicit formula for the propagation constant, so obtained when specialized to a perfectly conducting wire, is in agreement with a quasi-static analysis by Wu *et al.* [2] for a similar configuration.

A general modal analysis was given earlier [1] for the transmission in a straight circular tunnel bounded by a homogeneous medium and containing a thin axial wire running parallel to the tunnel wall. The medium external to the tunnel has a conductivity σ_e, permittivity ϵ_e, and permeability μ_e.

The modal equation for the propagation constants Γ was given in the form

$$-\frac{i\mu_0\omega v^2}{2\pi\gamma_0^2}\left[K_0(vc)-\sum_{m=-\infty}^{+\infty} R_m \frac{K_m(va)}{I_m(va)}[I_m(v\rho)]^2\right]=Z_s \tag{1}$$

in the case when the axial wire with series impedance Z_s of radius c was located at a distance ρ_0 from the tunnel axis and for an implied time factor $\exp(i\omega t)$. Also, we have assumed here that the distance d of the wire from the tunnel wall is large compared with the wire radius (i.e., $d = a - \rho_0 \gg c$). Other factors in (1), in the notation used earlier [1], are defined as follows:

$$R_m=\frac{(\gamma_0/v)K_m'(va)/K_m(va)+Y_m\eta_0+\delta_m\eta_0}{(\gamma_0/v)I_m'(va)/I_m(va)+Y_m\eta_0+\delta_m\eta_0} \tag{2}$$

$$\delta_m\eta_0=\frac{(im\Gamma/a)^2[v^{-2}-u^{-2}]^2}{[(\gamma_0/v)I_m'(va)/I_m(va)]+(Z_m/\eta_0)} \tag{3}$$

$$v=(\gamma_0^2-\Gamma^2)^{1/2},\quad u=(\gamma_e^2-\Gamma^2)^{1/2},$$

$$\gamma_0^2=-\epsilon_0\mu_0\omega^2,\quad \gamma_e^2=i\mu_e\omega(\sigma_e+i\epsilon_e\omega),$$

$$\eta_0=(\mu_0/\epsilon_0)^{1/2}\cong 120\pi,\quad Z_m=-\frac{i\mu_0\omega}{u}\frac{K_m'(ua)}{K_m(ua)},$$

Manuscript received June 8, 1976; revised September 8, 1976.

The author is with the Cooperative Institute for Research in Environmental Sciences, University of Colorado, Boulder, CO 80309.

and

$$Y_m = \frac{i\gamma_e^2}{u\mu_0\omega}\frac{K_m'(ua)}{K_m(ua)}.$$

The tunnel region is assumed to be free space with permittivity ϵ_0 and permeability μ_0 except for the thin wire that, as mentioned, is characterized by a series impedance Z_s. The latter is given explicitly by

$$Z_s = \frac{\eta_s}{2\pi c_s}\frac{I_0(\gamma_s c)}{I_1(\gamma c)}$$

where $\gamma_s^2 = i\mu_s\omega(\sigma_s + i\epsilon_s\omega)$ and $\eta_s = i\mu_s\omega/(\sigma_s + i\epsilon_s\omega)$ in terms of the conductivity σ_s, permittivity ϵ_s, and permeability μ_s of the wire.

Actually, (1) is an exact equation to determine the axial propagation constant Γ of the discrete modes for the structure. These include the modes that have a transmission line characteristic at low frequencies as well as the waveguide modes that propagate at high frequencies.

Here we would like to identify a low frequency approximation to (1) that can permit an explicit evaluation of the desired propagation constant for the desired mode. However, first of all, we will recast (1) into an equivalent form as follows:

$$\frac{-i\mu_0\omega v^2}{2\pi\gamma_0^2}[\Lambda + (\gamma_0^2\Omega/v^2)] = Z_s \tag{4}$$

where

$$\Lambda = K_0(vc) - \sum_{m=-\infty}^{+\infty}\frac{K_m(va)}{I_m(va)}[I_m(v\rho_0)]^2 \tag{5}$$

and

$$\Omega = -\frac{v^2}{\gamma_0^2}\sum_{m=-\infty}^{+\infty}(R_m - 1)\frac{K_m(va)}{I_m(va)}[I_m(v\rho_0)]^2. \tag{6}$$

Then we deduce from (4) that

$$\Gamma^2 = \gamma_0^2\left[1 + \frac{\Omega}{\Lambda} + \frac{2\pi Z_s}{i\mu_0\omega\Lambda}\right] \tag{7a}$$

or alternatively,

$$\Gamma^2 = ZY$$

where

$$Z = \frac{i\mu_0\omega}{2\pi}(\Lambda + \Omega) + Z_s \quad \text{and} \quad Y = 2\pi i\epsilon_0\omega/\Lambda. \tag{7b}$$

This is not an explicit equation for Γ^2 since Ω and Λ are functions of Γ^2. However, it becomes an explicit form if the frequency is sufficiently low and if the wall conductivity and/or wall permittivity are/is high. Specifically, we invoke the conditions $|va| \ll 1$, $|\gamma_e/\gamma_0|^2 \gg 1$, and $\mu_e = \mu_0$. Then, on using small argument approximations for the modified Bessel functions, we see that

$$\Lambda \cong \ln\frac{a}{c} - \sum_1^{\infty}\frac{1}{m}\left(\frac{\rho_0}{a}\right)^{2m} \tag{8}$$

$$\cong \ln\frac{a}{c} - \ln\frac{a^2}{a^2 - \rho_0^2}. \tag{8}$$

Clearly, $\Lambda \cong \ln(2d/c)$ when $d = a - \rho_0 \ll a$.

To reduce Ω, we note first that

$$\delta_m\eta_0 \cong -\Gamma^2 m/(\gamma_0 v^2 a) \tag{9}$$

where m is a positive integer, and

$$Y_m\eta_0 \cong -\frac{\gamma_e}{\gamma_0}\left[\frac{m}{\gamma_e a} - \frac{K_{m+1}(\gamma_e a)}{K_m(\gamma_e a)}\right]. \tag{10}$$

In writing the latter, we have also utilized the derivative relation $K_m'(x) = (m/x)K_m(x) - K_{m+1}(x)$. Then it follows that

$$(R_m - 1)\frac{K_m(va)}{I_m(va)}[I_m(v\rho_0)]^2 \cong -\frac{\gamma_0}{v^2 a}\left(\frac{\rho_0}{a}\right)^{2m}\left[\frac{m}{\gamma_0 a} + Y_m\eta_0\right]^{-1} \cong -\frac{\gamma_0^2}{v^2\gamma_e a}\left(\frac{\rho_0}{a}\right)^{2m}\frac{K_m(\gamma_e a)}{K_{m+1}(\gamma_e a)}. \tag{11}$$

Thus (6) is approximated by

$$\Omega = \frac{1}{\gamma_e a}\left[\frac{K_0(\gamma_e a)}{K_1(\gamma_e a)} + 2\sum_1^{\infty}\left(\frac{\rho_0}{a}\right)^{2m}\frac{K_m(\gamma_e a)}{K_{m+1}(\gamma_e a)}\right]. \tag{12}$$

Using expressions (8) and (12), we see that (7) is an explicit formula to calculate Γ. Here we choose the root corresponding to $\Gamma = \gamma_0$ in the case where Ω and Z_s are both zero. Clearly we have a transmission line type mode within this low frequency approximation. With appropriate change of notation and conventions, the results obtained here for the special case $Z_s = 0$ are in agreement with the quasi-static analysis by Wu *et al.* [2]. Following their suggestion, we could improve the convergence of the representation by rewriting it in the equivalent form

$$\Omega = \frac{1}{\gamma_e a}\left\{\frac{K_0(\gamma_e a)}{K_1(\gamma_e a)} + 2\sum_{m=1}^{\infty}\left[\frac{K_m(\gamma_e a)}{K_{m+1}(\gamma_e a)} - \frac{\gamma_e a}{2m}\right]\left(\frac{\rho_0}{a}\right)^{2m}\right\} + \ln\frac{a^2}{a^2 - \rho_0^2} \tag{13}$$

where we have merely added and subtracted a series of the form

$$\sum_{m=1}^{\infty}\frac{1}{my^m} = \ln\frac{y}{y-1}, \quad \text{where} \quad y > 1. \tag{14}$$

A very simple limiting case of (12) is obtained if we assume that $|\gamma_e a| \gg 1$ and then approximate the modified Bessel functions by the leading term of their asymptotic forms. Then

$$\Omega \cong \frac{1}{\gamma_e a}\left[1 + 2\sum_{m=1}^{\infty}\left(\frac{\rho_0}{a}\right)^{2m}\right] \cong \frac{1}{\gamma_e a}\frac{1 + (\rho_0/a)^2}{1 - (\rho_0/a)^2} \tag{15}$$

or if $d = (a - \rho_0) \ll a$, $\Omega \cong 1/(\gamma_e d)$ and then

$$\Gamma \cong \gamma_0 \left[1 + \frac{1}{\gamma_e d} \ln \frac{2d}{c} \right]^{1/2} \tag{16}$$

This simple result is consistent with an approximate quasi-static analysis by Sunde [3] who considered a thin wire at an equivalent height d over a homogeneous half-space with a propagation constant γ_e.

REFERENCES

[1] J. R. Wait and D. A. Hill, "Guided electromagnetic waves along an axial conductor in a circular tunnel," *IEEE Trans. Antennas Propagat.*, Vol. AP-22, pp. 627–630, July 1974.

[2] T. T. Wu, L. C. Shen, and R. W. P. King, "The dipole antenna with eccentric coating in a relatively dense medium," *IEEE Trans. Antennas Propagat.*, Vol. AP-23, pp. 57–62, January 1975.

[3] E. D. Sunde, *Earth Conduction Effects in Transmission Systems*. New York: Dover, 1968, p. 113.

Analysis of Radio Frequency Transmission in a Semicircular Mine Tunnel Containing Two Axial Conductors

DAVID A. HILL, MEMBER, IEEE, AND JAMES R. WAIT, FELLOW, IEEE

Abstract—We present an analysis of the propagation in a uniform tunnel of semicircular cross section that contains two axial conductors. In particular, we show that, even if one of these conductors has high ohmic loss, one of the two propagating modes has relatively low attenuation. This corresponds to the situation where an unloaded dedicated wire is used to improve radio frequency communication in a mine tunnel that contains a heavily loaded trolley wire.

INTRODUCTION

In mine communications it is common practice to use the trolley wire and its ground return for radio frequency transmission [1]. For an unloaded trolley wire, the attenuation rate of the dominant mode of propagation is of the order of 1 dB per kilometer at a frequency of 200 kHz. In this case, the losses are due mainly to the ohmic dissipation in the surrounding rock. Transmission in uniformly smooth tunnels of circular and semicircular shapes has been analyzed for axial conductors contained within the cross section [2–5]. These results are consistent with experimental data [6, 7] although detailed comparisons have not yet been made.

Since the trolley wire is intended primarily to provide power to locomotives, the characteristics of the carrier transmission will be modified. The upshot is that the effective signal attenuation is much higher than predicted by the unloaded trolley wire. An attempt can be made to use radio frequency chokes to present a high impedance to the carrier signal and a much lower impedance to the a.c. power. But this scheme is both expensive and not wholly effective. To circumvent this difficulty, it has been suggested that an additional unloaded axial conductor be located in the tunnel (private communication from R. H. Spencer). This "dedicated wire" will then permit an additional mode that has low attenuation even when the trolley wire is heavily loaded. We wish to present an analysis of this situation using an idealized configuration that is amenable to a full wave theory. We deal with the time harmonic situation where all field quantities vary as $\exp(i\omega t)$ where ω is the angular frequency.

FORMULATION

The assumed model is shown in Fig. 1a where we may use a cylindrical coordinate system (ρ, ϕ, z) to describe the configuration. As indicated, the tunnel cross section is semicircular with radius a. The floor of the tunnel, including the railway tracks, is represented by a plane perfect conductor while the external region defined by $\rho > a$ and $0 < \phi < \pi$ has a conductivity σ_e and permittivity ϵ_e. The trolley wire and its associated feeder line are represented by a single circular con-

Paper approved by the Editor for Transmission Systems of the IEEE Communications Society for publication without oral presentation. Manuscript received February 8, 1977; revised March 21, 1977.

D. A. Hill is with the Institute for Telecommunication Sciences, Office of Telecommunications, U.S. Department of Commerce, Boulder, CO 80302.

J. R. Wait is with the Cooperative Institute for Research in Environmental Sciences, University of Colorado, Boulder, CO 80309.

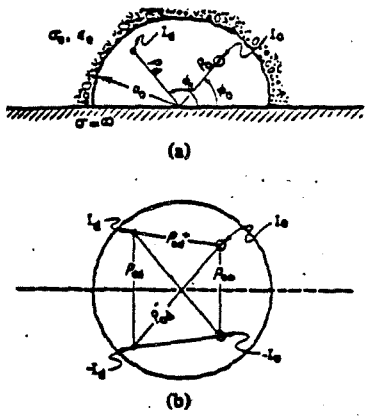


Fig. 1. (a) Semicircular tunnel showing trolley wire carrying current I_0 and "dedicated" wire carrying current I_d. (b) Equivalent circular tunnel showing anti-symmetric image currents.

ductor of radius c_0 that is located at $\rho = \rho_0$ and $\phi = \phi_0$. The dedicated wire is represented by a circular conductor of radius c_d and it is located at $\rho = \rho_d$ and $\phi = \phi_d$. The radii c_0 and c_d of these wires are both assumed to be much less than any other significant dimension such as their separation or the distances of the wires to the tunnel wall. Thus we need only be concerned with the total axial current carried by the wires. A convenient descriptor in this case is the axial surface impedance which is denoted Z_w for the trolley wire and Z_d for the dedicated wire. From previous work [2-5], we know these have the respective forms

$$Z_w \cong \frac{\eta_w}{2\pi c_0} \frac{I_0(\gamma_w c_0)}{I_1(\gamma_w c_0)} \tag{1}$$

and

$$Z_d \cong \frac{\eta_d}{2\pi c_d} \frac{I_0(\gamma_d c_d)}{I_1(\gamma_d c_d)} \tag{2}$$

where $\eta_w = i\mu_w\omega/\gamma_w$, $\gamma_w = (i\sigma_w\mu_w\omega)^{1/2}$ and $\eta_d = i\mu_d\omega/\gamma_d$, $\gamma_d = (i\sigma_d\mu_d\omega)^{1/2}$. Here σ_w and σ_d are the respective conductivities of the wires while μ_w and μ_d are the respective magnetic permeabilities. The above formulas for Z_w and Z_d are valid when $|\gamma_w{}^2|$ and $|\gamma_d{}^2|$ are much greater than $|\Gamma^2|$ where Γ is the axial propagation constant of the mode in question. Also, we have neglected the displacement currents in the wires which is certainly valid in the cases being considered. Of course, as $\omega \to 0$, we recover the appropriate d.c. results, i.e., $Z_w \to (\pi c_0{}^2\sigma_w)^{-1}$ and $Z_d \to (\pi c_d{}^2\sigma_d)^{-1}$. These are valid when $|\gamma_w c_0|$ and $|\gamma_d c_d| \ll 1$.

THE MODE EQUATION

We now consider the modal equation that determines the resultant propagation constants for the composite structure shown in Fig. 1 and described above. From previous work [3-5], we can easily obtain the following conditions that must be satisfied for a current I_0 on the trolley wire and a current I_d on the dedicated wire:

$$A_0 I_0 + A_d I_d = 0 \tag{3}$$

and

$$B_0 I_0 + B_d I_d = 0 . \tag{4}$$

The mode equation, of course, is

$$\begin{vmatrix} A_0 & A_d \\ B_0 & B_d \end{vmatrix} = 0 \tag{5}$$

where

$$A_0 = \frac{\gamma_0}{v^2} \frac{2\pi Z_w}{\eta_0} + K_0(vc_0) - S_{00}{}^+ - K_0(v\rho_{00}) + S_{00}{}^- \tag{6}$$

$$A_d = K_0(v\rho_{0d}{}^+) - S_{0d}{}^+ - K_0(v\rho_{0d}{}^-) + S_{0d}{}^- \tag{7}$$

$$B_0 = A_d \text{ (because of symmetry)} \tag{8}$$

$$B_d = \frac{\gamma_0}{v^2} \frac{2\pi Z_d}{\eta_0} + K_0(vc_d) - S_{dd}{}^+ - K_0(v\rho_{dd}) + S_{dd}{}^- \tag{9}$$

and where $v = (\gamma_0{}^2 - \Gamma^2)^{1/2}$, $\gamma_0{}^2 = -\epsilon_0\mu_0\omega^2 = -(2\pi/\lambda_0)^2$, $\eta_0 = (\mu_0/\epsilon_0)^{1/2} \cong 120\pi$. The geometrical parameters used here are:

$$\rho_{00} = 2\rho_0 \sin\phi_0, \qquad \rho_{dd} = 2\rho_d \sin\phi_d$$

$$\rho_{0d}{}^+ = [\rho_0{}^2 + \rho_d{}^2 - 2\rho_0\rho_d \cos(\phi_0 - \phi_d)]^{1/2}$$

$$\rho_{0d}{}^- = [\rho_0{}^2 + \rho_d{}^2 - 2\rho_0\rho_d \cos(\phi_0 + \phi_d)]^{1/2}.$$

As indicated in Fig. 1b, these can be identified with the linear distances between the wires and their images in the ground plane. The other quantities in (6) to (9) are expressed as column matrices as follows:

$$\begin{bmatrix} S_{00}{}^+ \\ S_{00}{}^- \end{bmatrix} = \sum_{m=-\infty}^{+\infty} R_m \frac{K_m(va_0)}{I_m(va_0)} I_m{}^2(v\rho_0) \begin{bmatrix} 1 \\ \exp(-i2m\phi_0) \end{bmatrix} \tag{10}$$

$$\begin{bmatrix} S_{dd}{}^+ \\ S_{dd}{}^- \end{bmatrix} = \sum_{m=-\infty}^{+\infty} R_m \frac{K_m(va_0)}{I_m(va_0)} I_m{}^2(v\rho_d) \begin{bmatrix} 1 \\ \exp(-i2m\phi_d) \end{bmatrix} \tag{11}$$

$$\begin{bmatrix} S_{0d}{}^+ \\ S_{0d}{}^- \end{bmatrix} = \sum_{m=-\infty}^{+\infty} R_m \frac{K_m(va_0)}{I_m(va_0)} I_m(v\rho_0) I_m(v\rho_d) \cdot \begin{bmatrix} \exp[-im(\phi_0 - \phi_d)] \\ \exp[-im(\phi_0 + \phi_d)] \end{bmatrix} \tag{12}$$

The coefficient R_m is a rather complicated coefficient that arises consistently in early circular tunnel models [2-5] and is given by

$$R_m = \frac{(\gamma_0/v)K_m'(va_0)/K_m(va_0) + Y_m\eta_0 + \delta_m\eta_0}{(\gamma_0/v)I_m'(va_0)/I_m(va_0) + Y_m\eta_0 + \delta_m\eta_0} \tag{13}$$

where

$$\delta_m \eta_0 = \frac{(im\Gamma/a_0)^2[v^{-2} - u^{-2}]^2}{(\gamma_0/v)I_m'(va_0)/I_m(va_0) + (Z_m/\eta_0)}$$

$$Y_m = \frac{i\gamma_e^2}{u\mu_0\omega}\frac{K_m'(ua_0)}{K_m(ua_0)} \qquad Z_m = -\frac{i\mu_0\omega}{u}\frac{K_m'(ua_0)}{K_m(ua_0)}$$

$$u = (\gamma_e^2 - \Gamma^2)^{1/2} \text{ and } \gamma_e^2 = i\mu_0\omega(\sigma_e + i\epsilon_e\omega). \tag{14}$$

As usual, we assume that the magnetic permeability of the surrounding rock and the air in the tunnel can be replaced by the free space value μ_0.

The mode equation (5) can be solved for Γ numerically by methods used earlier for similar configurations [2-5]. At sufficiently low frequencies, the tunnel wall and the axial conductors will behave as perfect conductors. In this low frequency limit there will be two TEM mode solutions. This is consistent with the succinct statement by Collin [8] that "*if we have a transmission line with N separate conductors, there will be N − 1 basic TEM modes of propagation.*" In our case, $N = 3$ since the tunnel wall and floor act as one conductor in this limiting situation. Now when the finite conductivity of the wires and the tunnel wall are considered, we still expect two dominant modes when the overall cross section of the tunnel is small compared with a free space wavelength. In addition, of course, we also have the highly attenuated evenescent modes; these do not concern us.

SPECIFIC RESULTS

A special case of the present formulation is to allow the radius c_d of the dedicated wire to vanish. We then recover the mode equation given in a previous analysis [4]. We now consider this case in the context of the present problem. Specifically, we first consider the following situation: $a_0 = 2m$, $a_o - \rho_0 = 20$ cm, $\phi_0 = 45°$, $c_0 = 1.5$ cm, $\sigma_e = 10^{-3}$mho/m, $\epsilon_e/\epsilon_0 = 10$, $c_0 = 0$, and $\sigma_\omega = 5.7 \times 10^7$mho/m and $\mu_\omega = \mu_0$. The corresponding attenuation rate for such a single unloaded copper trolley wire is indicated in Fig. 2. As indicated, the attenuation rate is quite low being less than 0.4 dB/km at 200 kHz. To simulate the effect of loading the trolley wire, we now decrease the wire conductivity σ_w continuously until the attenuation rate rises to 10 dB/km at a frequency of 200 kHz. The attenuation rate, for this hypothetical conductivity σ_w of 2.5×10^3mho/m, is shown plotted as a function of frequency in Fig. 2. The dependence with frequency is very weak because the series impedance of the line can be approximated by its d.c. value. Thus we have achieved, albeit somewhat artificially, the order of the attenuation rate that is experienced when transmitting a radio frequency signal on a loaded trolley wire.

Our objective is now to insert the dedicated wire into the tunnel and solve for the expected two propagating modes. At the same time, we can obtain the ratio for I_0/I_d of the currents for these two cases by merely using either (3) or (4). Since the dedicated wire is not intended to carry a heavy current, it may have a relatively smaller diameter than the trolley wire. We choose the same parameters as before but now we specify that $\sigma_w = 2.5 \times 10^3$mho/m, $c_d = 1.5$ mm, $a_0 - \rho_d = 20$ cm, $\phi_d = 135°$ and $\sigma_d = 5.7 \times 10^7$mho/m.

The attenuation rates, plotted as a function of frequency, are indicated in Fig. 3 for the two modes—one where $|I_0| \gg |I_d|$ and one for $|I_d| \gg |I_0|$. Not surprisingly, the mode of low attenuation corresponds to the situation where the current being carried by the lossy trolley wire is much less than the current on the dedicated wire. Conversely, the mode of high attenuation is associated with a small current on the dedicated wire. In fact, this mode has very similar characteristics to the mode on the lossy trolley line in the tunnel in the absence of the dedicated wire (e.g., compare upper curves in Fig. 2 and 3).

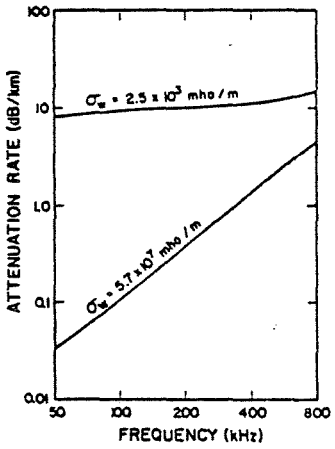


Fig. 2. Attenuation rate for a single (trolley) wire in the tunnel with the following parameters: $a_0 = 2m$, $\sigma_e = 10^{-3}$ mho/m, $\epsilon_e/\epsilon_0 = 10$, $a_0 - \rho_0 = 20$ cm, $\phi_0 = 45°$, and $c_0 = 1.5$ cm.

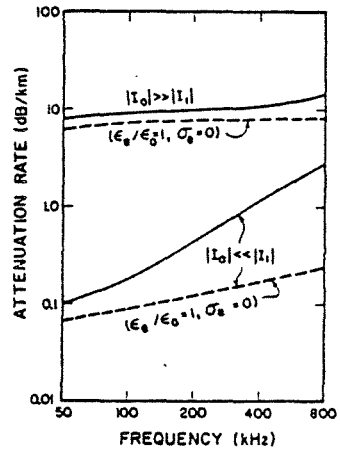


Fig. 3. Attenuation rate for the two modes in the tunnel when a dedicated wire is added. The parameters used are: $a_0 - \rho_0 = a_0 - \rho_d = 20$ cm, $\phi_0 = 45°$, $\phi_d = 135°$, $a_0 = 2m$, $\epsilon_e/\epsilon_0 = 10$, $\sigma_e = 10^{-3}$ mho/m, $c_o = 1.5$ cm, $\sigma_0 = 2.5 \times 10^3$ mho/m, $c_d = 1.5$ mm, and $\sigma_d = 5.7 \times 10^7$ mho/m. The corresponding results for the absence of the curved tunnel wall are also shown, i.e., $\sigma_e = 0$ and $\epsilon_e/\epsilon_0 = 1$.

The actual complex ratio I_0/I_d is shown in Fig. 4a and 4b for the same conditions as assumed in Fig. 3. As indicated in Fig. 4a, at the lower frequencies, the magnitude of the current on the trolley wire is very small for the desired "communication mode."

For comparison purposes, we also show corresponding results in Figs. 3, 4a and 4b for the case where the tunnel wall is ignored. As indicated in the Appendix, this is really a special case of the present formulation when $\sigma_e = 0$ and $\epsilon_e/\epsilon_0 = 1$.

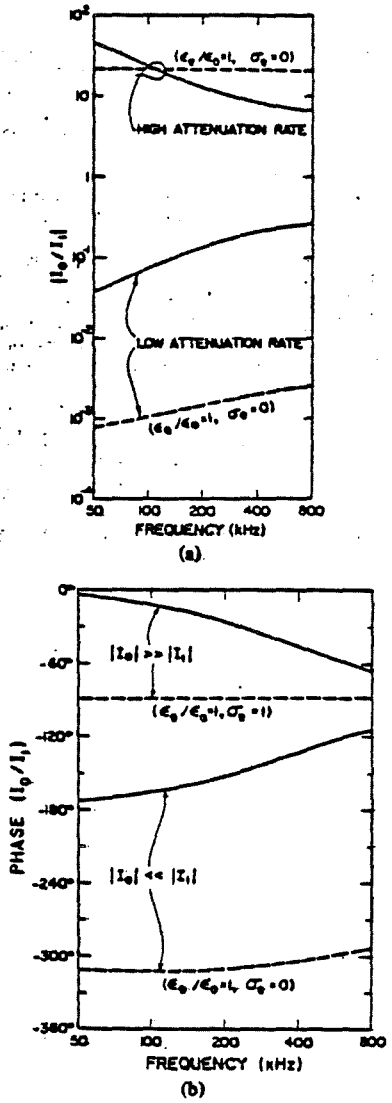


Fig. 4. (a) Amplitude of the ratio of trolley wire current to the dedicated wire current for the two propagating modes. The parameters are the same as in Fig. 3. (b) The corresponding phase difference between the trolley wire current and the dedicated wire current.

Not surprisingly, the attenuation rate for the mode of high attenuation is not affected in a major way by the presence of the lossy tunnel wall. However, the mode of low attenuation is changed rather drastically.

CONCLUDING REMARKS

The model we have chosen is admittedly very idealized. Actually, the trolley wire will be loaded at a fixed number of discrete points so the propagating mode will not be a simple traveling wave. Nevertheless, our model of the trolley wire with continuous series loading does indeed give the expected order of magnitude of the total attenuation. Also, with this model, we can demonstrate in a convincing fashion that an accompanying unloaded wire, referred to as the dedicated wire, does indeed introduce a new mode of much lower attenuation. It is this mode that can be utilized for telecommunication purposes. The wave theory, as given, accounts fully for the interchange of energy between the power and the communication modes.

Further work on this subject should probably attempt a more realistic model of the discretely loaded trolley wire and other axial nonuniformities of the configuration. However, it is doubtful if this will modify any of our conclusions arrived at here.

APPENDIX

APPROXIMATE ANALYTIC SOLUTION WHEN CURVED TUNNEL WALL IS IGNORED

Here we consider the case when the tunnel region effectively extends to infinity. This corresponds to the case where $\sigma_e = 0$ and $\epsilon_e/\epsilon_0 = 1$ so that the two axial conductors are now located in a semi-infinite free space region about the perfectly conducting ground plane. Now (6) and (7) become:

$$A_0 = \frac{\gamma_0}{v^2}\frac{2\pi Z_w}{\eta_0} + K_0(vc_0) - K_0(v\rho_{00}) \tag{15}$$

$$A_d = K_0(v\rho_{0d}^{+}) - K_0(v\rho_{0d}^{-}) \tag{16}$$

and

$$B_d = \frac{\gamma_0}{v^2}\frac{2\pi Z_d}{\eta_0} + K_0(vc_d) - K_0(v\rho_{dd}) . \tag{17}$$

When the arguments of the modified Bessel functions are all small, we can approximate (15), (16) and (17) as follows:

$$A_0 = \frac{\gamma_0}{v^2}\frac{2\pi Z_w}{\eta_0} + \ln(\rho_{00}/c_0) \tag{18}$$

$$A_d = \ln(\rho_{0d}^{-}/\rho_{0d}^{+}) \tag{19}$$

and

$$B_d = \frac{\gamma_0}{v^2}\frac{2\pi Z_d}{\eta_0} + \ln(\rho_{dd}/c_d). \tag{20}$$

The mode equation (5) now becomes

$$\left[\frac{\gamma_0}{v^2}\frac{2\pi Z_w}{\eta_0} + \ln(\rho_{00}/c_0)\right]\left[\frac{\gamma_0}{v^2}\frac{2\pi Z_d}{\eta_0} + \ln(\rho_{dd}/c_d)\right] - [\ln(\rho_{0d}^{-}/\rho_{0d}^{+})]^2 = 0. \tag{21}$$

This is equivalent to the quadratic form

$$v^4 a + v^2 b + c = 0 \tag{22}$$

where

$$a = \ln(\rho_{00}/c_0)\ln(\rho_{dd}/c_d) - [\ln(\rho_{0d}^{-}/\rho_{0d}^{+})]^2 \tag{23}$$

$$b = [Z_d \ln(\rho_{00}/c_0) + Z_w \ln(\rho_{dd}/c_d)](2\pi\gamma_0/\eta_0) \tag{24}$$

and

$$c = (2\pi\gamma_0/\eta_0)^2 Z_w Z_d. \quad (25)$$

We find from (22) that

$$v^2 = [-b \pm (b^2 - 4ac)^{1/2}]/2a = \gamma_0^2 - \Gamma^2 \quad (26)$$

and thus we have an explicit formula to calculate the propagation constants of the two modes for this configuration:

$$\Gamma^2 = \gamma_0^2 + [b \mp (b^2 - 4ac)^{1/2}](2a)^{-1}. \quad (27)$$

Of course, we select the two roots where Re. $\Gamma > 0$. Results for this case are illustrated in Figs. 3, 4a and 4b to compare with the corresponding curves when the tunnel walls are accounted for.

ACKNOWLEDGMENT

The authors would like to thank Dr. R. H. Spenser of A. D. Little, Inc. for his private communications on this subject. These have motivated the present study which is intended to complement their coupled transmission line analysis of such problems.

REFERENCES

[1] J. N. Murphy and H. E. Parkinson, "Mine communications: Research and development in the U.S.A.", *Proc. Int. Conf. Radio: Tunnels and Mines*, vol. II, Liege, Belgium, April 1-5, 1974, pp. 42-64.

[2] J. R. Wait and D. A. Hill, "Guided electromagnetic waves along an axial conductor in a circular tunnel", *IEEE Trans. Antennas Propagat.*, vol. AP-22, pp. 627-630, July 1974.

[3] J. R. Wait and D. A. Hill, "Coaxial and bifilar modes on a transmission line in a circular tunnel", *Appl. Phys.*, vol. 4, pp. 307-312, 1974.

[4] D. A. Hill and J. R. Wait, "Analysis of radio frequency transmission along a trolley wire in a mine tunnel", *IEEE Trans. Electromagn. Compat.*, vol. EMC-18, pp. 170-174, Nov. 1976.

[5] J. R. Wait, "Theory of transmission of electromagnetic waves along multi-conductor lines in the proximity of walls of mine tunnels", *The Radio and Electronic Eng.* (London), vol. 45, pp. 229-232, May 1975.

[6] M. R. Gillette and A. S. Gilmour, "Attenuation measurements in the 1 to 1000 MHz frequency range in wet granite tunnels", *IEEE Trans. Electromagn. Compat.*, vol. EMC-17, pp. 201-206, Nov. 1975.

[7] L. Deryck, "Radio communication in tunnels", *Electronics Letters*, vol. 8, pp. 71-72, Feb. 1972.

[8] R. E. Collin, *Field Theory of Guided Waves*. New York, McGraw-Hill Book Co., Inc., 1960, p. 124.

IEEE TRANSACTIONS ON COMMUNICATIONS, VOL. COM-26, NO. 3, MARCH 1978

Analysis of the Dedicated Communication Line in a Mine Tunnel for a Shunt-Loaded Trolley Wire

JAMES R. WAIT, FELLOW, IEEE, AND DAVID A. HILL, SENIOR MEMBER, IEEE

Abstract—The theory of transmission in a semicircular tunnel containing two axial conductors is simplified for the case of radio frequencies. It is shown that the effect of ohmic losses in the wall can be represented as series impedances per unit length in the equivalent coupled transmission line circuits. This opens the way for a systematic calculation of the mode conversion phenomena that occur when one of the axial conductors has a discrete shunt load to the ground plane. Explicit formulas are obtained for the modal conversion coefficients. These are used to discuss the effect of a shunt load on the trolley wire on the performance of a radio frequency communication system. It is confirmed that the unloaded dedicated communication line provides for a low loss mode that is hardly affected by the shunt load on the adjacent trolley wire in the tunnel.

INTRODUCTION

RADIO frequency transmission in mine tunnels is made possible by the presence of axial conductors. In fact, the trolley wire may be used effectively as a conveyor of communication signals at frequencies of the order of 100 kHz [1]. In such cases, the rails or other conductors in the tunnel carry the return current. Both theory and experiment [2-4] indicate that the attenuation rate for the unloaded trolley wire is as low as 2 dB per km of path length. However, the effects of shunt loads on the trolley wire will greatly increase the effective attenuation. To partially circumvent this difficulty, a separate unloaded line has been used for the purpose of carrying the radio frequency transmission [3]. The modal analysis of the performance of this dedicated line had been carried out where we assumed, for convenience, that the trolley wire loading could be simulated by an increase of continuous series resistance [4]. A more meaningful analysis is to consider explicitly the effect of a discrete shunt load on the trolley wire. This is the purpose of the present paper. At the same time, we reexamine some aspects of the theory that lead to simpler design concepts, particularly with regard to the effect of the ohmic loss in the tunnel walls.

Paper approved by the Editor for Transmission Systems of the IEEE Communications Society for publication after presentation at the National Radio Science Meeting, Boulder, CO, January 1977. Manuscript received August 29, 1977; revised September 27, 1977.

J. R. Wait is with the National Oceanic and Atmospheric Administration and the Cooperative Institute for Research in Environmental Sciences, University of Colorado, Boulder, CO 80309. He is also a Consultant to the Office of Telecommunications.

D. A. Hill is with the Institute for Telecommunication Sciences, Office of Telecommunications, U.S. Department of Commerce, Boulder, CO 80302.

FORMULATION

The assumed model is shown in Fig. 1 where we employ a cylindrical coordinate system (ρ, ϕ, z) to describe the configuration. The tunnel cross section is semicircular with radius a_0. The floor of the tunnel, including the effect of the rails, is represented by a plane perfect conductor. On the other hand, the external region defined by $\rho > a_0$ and $0 < \phi < \pi$ has a conductivity σ_e and magnetic permeability μ_e. The trolley wire and its associated feeder line are represented by a single circular conductor of radius c_0 that is located at $\rho = \rho_0$ and $\phi = \phi_0$. The communication or dedicated line is represented by a circular conductor of radius c_d and it is located at $\rho = \rho_d$ and $\phi = \phi_d$. We make the usual thin wire assumption which permits us to deal only with the axial currents I_0 and I_d on the trolley and dedicated wire, respectively. Furthermore, these are characterized by series impedance per unit length designated Z_w and Z_d. As we have indicated before [4], these do not depend significantly on the propagation constants Γ of the dominant modes.

Our previous analysis [4] showed that for a given mode of propagation

$$A_0 I_0 + A_d I_d = 0 \tag{1}$$

0090-6778/78/0300-0355$00.75

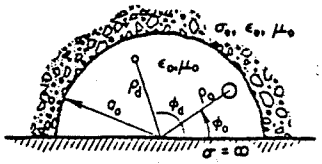


Fig. 1 Cross-section of the semicircular tunnel model showing the location of the trolley wire at (ρ_0, ϕ_0) and the dedicated communication line at (ρ_d, ϕ_d).

and

$$B_0 I_0 + B_d I_d = 0. \tag{2}$$

For our purposes here, the coefficients can be written conveniently in the following form

$$A_0 = K_0(\upsilon c_0) - K_0(\upsilon \rho_{00}) - \sum_{m=-\infty}^{+\infty} \frac{K_m(\upsilon a_0)}{I_m(\upsilon a_0)} \cdot I_m{}^2(\upsilon \rho_0)(1 - e^{-im2\phi_0}) + \frac{\gamma_0}{\upsilon^2}\frac{2\pi}{\eta_0}(Z_w + Z_{we}) \tag{3}$$

$$A_d = B_0 = K_0(\upsilon \rho_{0d}{}^+) - K_0(\upsilon \rho_{0d}{}^-) - \sum_{m=-\infty}^{+\infty} \frac{K_m(\upsilon a_0)}{I_m(\upsilon a_0)} \cdot I_m(\upsilon \rho_0) I_m(\upsilon \rho_d) e^{-im\phi_0}(e^{im\phi_d} - e^{-im\phi_d}) + \frac{\gamma_0}{\upsilon^2}\frac{2\pi}{\eta_0} Z_{wed} \tag{4}$$

and

$$B_d = K_0(\upsilon c_d) - K_0(\upsilon \rho_{dd}) - \sum_{m=-\infty}^{+\infty} \frac{K_m(\upsilon a_0)}{I_m(\upsilon a_0)} \cdot I_m{}^2(\upsilon \rho_d)(1 - e^{-im2\phi_d}) + \frac{\gamma_0}{\upsilon^2}\frac{2\pi}{\eta_0}(Z_d + Z_{de}) \tag{5}$$

Algebraically, (3), (4), and (5) are identical to the previous definitions [4] provided

$$\frac{2\pi Z_{we}}{\eta_0} = -\frac{\upsilon^2}{\gamma_0}\sum_{m=-\infty}^{+\infty}(R_m - 1)\frac{K_m(\upsilon a_0)}{I_m(\upsilon a_0)} \cdot I_m{}^2(\upsilon \rho_0)(1 - e^{-2im\phi_0}) \tag{6}$$

$$\frac{2\pi Z_{wed}}{\eta_0} = -\frac{\upsilon^2}{\gamma_0}\sum_{m=-\infty}^{+\infty}(R_m - 1)\frac{K_m(\upsilon a_0)}{I_m(\upsilon a_0)} \cdot I_m(\upsilon \rho_0) I_m(\upsilon \rho_d) e^{-im\phi_0}(e^{im\phi_d} - e^{-im\phi_d}) \tag{7}$$

and

$$\frac{2\pi Z_{de}}{\eta_0} = -\frac{\upsilon^2}{\gamma_0{}^2}\sum_{m=-\infty}^{+\infty}(R_m - 1)\frac{K_m(\upsilon a_0)}{I_m(\upsilon a_0)}$$

The notation and terminology remain the same as in the previous paper [4] but, for convenience, we note here that

$$\gamma_0 = i(\epsilon_0\mu_0)^{1/2}\omega = i2\pi/(\text{free space wavelength})$$

$$\eta_0 = (\mu_0/\epsilon_0)^{1/2} = 120\pi \text{ ohms}$$

$$\upsilon = (\gamma_0{}^2 - \Gamma^2)^{1/2} = i(\Gamma^2 - \gamma_0{}^2)^{1/2}$$

$$\rho_{00} = 2\rho_0 \sin\phi_0, \qquad \rho_{dd} = 2\rho_d \sin\phi_d$$

$$\rho_{0d}{}^+ = [\rho_0{}^2 + \rho_d{}^2 - 2\rho_0\rho_d \cos(\phi_0 - \phi_d)]^{1/2}$$

$$\rho_{0d}{}^- = [\rho_0{}^2 + \rho_d{}^2 - 2\rho_0\rho_d \cos(\phi_0 + \phi_d)]^{1/2}.$$

The coefficient R_m also defined earlier [2, 3] is a rather complicated function involving modified Bessel functions I_m and K_m of both arguments νa_0 and ua_0 where $u = (\gamma_e{}^2 - \Gamma^2)^{1/2}$ and $\gamma_e{}^2 = iu_0\omega(\sigma_e + i\epsilon_e\omega)$ in terms of the conductivity σ_e, permeability μ_e, and permittivity ϵ_e of the surrounding rock. For all cases encountered in practice we can neglect $\epsilon_e\omega$ compared with σ_e and furthermore μ_e may be replaced by the free-space permeability μ_0.

THE QUASI-STATIC APPROXIMATION

The mode equation that determines the permissible values Γ from (1) and (2) is clearly

$$A_0 B_d - B_0 A_d = 0. \tag{9}$$

In the previous paper [4], this equation was solved numerically using definitions of A_0, B_0, A_d, and B_d that were equivalent to (3), (4), and (5) above. There we allowed the series resistance (Real part of Z_w) of the trolley wire to be sufficiently large to account for the effect of possible shunt loads. Here we will treat the problem of discrete shunt loads in a more direct fashion. But this will be done at the expense of invoking some low frequency or quasi-static approximations [5] that we will closely identify.

The first step is to note that, provided $|\gamma_e/\gamma_0|^2 = |\sigma_e + i\epsilon_e\omega|/\epsilon_0\omega \gg 1$ and $|\gamma_0 a_0| = 2\pi a_0/(\text{free space wavelength}) \ll 1$, the general expressions given by (6), (7), and (8) can be simplified to

$$\frac{2\pi}{i\mu_0\omega}Z_{we} \cong \frac{2}{\gamma_e a_0}\sum_{m=1}^{\infty}\left(\frac{\rho_0}{a_0}\right)^{2m}\frac{K_m(\gamma_e a_0)}{K_{m+1}(\gamma_e a_0)} \cdot [1 - \cos(2m\phi_0)] \tag{10}$$

$$\frac{2\pi}{i\mu_0\omega}Z_{wed} \cong \frac{2}{\gamma_e a_0}\sum_{m=1}^{\infty}\left(\frac{\rho_0\rho_d}{a_0{}^2}\right)^{m}\frac{K_m(\gamma_e a_0)}{K_{m+1}(\gamma_e a_0)} \cdot [\cos m(\phi_0 - \phi_d) - \cos m(\phi_0 + \phi_d)] \tag{11}$$

and

$$\frac{2\pi}{i\mu_0\omega}Z_{de} \cong \frac{2}{\gamma_e a_0}\sum_{m=1}^{\infty}\left(\frac{\rho_d}{a_0}\right)^{2m}\frac{K_m(\gamma_e a_0)}{K_{m+1}(\gamma_e a_0)}$$

To within this approximation Z_{we}, Z_{wed}, and Z_{de} do not depend on the propagation constant Γ for the mode in question. In fact, Z_{we} can be interpreted as the effective series impedance of the trolley wire due to the influence of the tunnel wall. As indicated by (3), it is directly additive to Z_w the internal series impedance of the trolley wire itself. In a similar sense, Z_{de} is the contribution of the tunnel wall to the total series impedance of the dedicated line. On the other hand, Z_{wed} can be interpreted as the contribution of the tunnel wall to the mutual impedance between the lines.

Within the same quasi-static approximation

$$A_0 \cong \ln\frac{\rho_{00}}{c_0} - \sum_{m=1}^{\infty}\frac{1}{m}\left(\frac{\rho_0^2}{a_0^2}\right)^m (1-\cos 2m\phi_0) + \frac{\gamma_0}{v^2}\frac{2\pi}{\eta_0}(Z_w + Z_{we}) \tag{13}$$

$$A_d = \ln\frac{\rho_{0d}^-}{\rho_{0d}^+} - \sum_{m=1}^{\infty}\frac{1}{m}\left(\frac{\rho_0\rho_d}{a_0^2}\right)^m (\cos m(\phi_0^- - \phi_d) - \cos m(\phi_0 + \phi_d)) + \frac{\gamma_0}{v^2}\frac{2\pi}{\eta_0}Z_{wed} \tag{14}$$

and

$$B_d = \ln\frac{\rho_{dd}}{c_d} - \sum_{m=1}^{\infty}\frac{1}{m}\left(\frac{\rho_d^2}{a_0^2}\right)^m (1-\cos 2m\phi_d) + \frac{\gamma_0}{v^2}\frac{2\pi}{\eta_0}(Z_d + Z_{de}). \tag{15}$$

These are equivalent to

$$A_0 \cong \ln\frac{\rho_{00}}{c_0} + \frac{1}{2}\ln\frac{[1-\rho_0^2/a_0^2]^2}{\left[1-2\frac{\rho_0^2}{a_0^2}\cos 2\phi_0 + \left(\frac{\rho_0^2}{a_0^2}\right)^2\right]} + \frac{\gamma_0}{v^2}\frac{2\pi}{\eta_0}(Z_w + Z_{we}) \tag{16}$$

$$A_d \cong \ln\frac{\rho_{0d}^-}{\rho_{0d}^+} + \frac{1}{2}\ln\frac{\left[1-2\left(\frac{\rho_0\rho_d}{a_0^2}\right)\cos(\phi_0-\phi_d) + \left(\frac{\rho_0^2\rho_d}{a_0^2}\right)^2\right]}{\left[1-2\left(\frac{\rho_0\rho_d}{a_0^2}\right)\cos(\phi_0+\phi_d) + \left(\frac{\rho_0\rho_d}{a_0^2}\right)^2\right]} + \frac{\gamma_0}{v^2}\frac{2\pi}{\eta_0}Z_{wed} \tag{17}$$

and

$$B_d \cong \ln\frac{\rho_{dd}}{c_d} + \frac{1}{2}\ln\frac{[1-\rho_d^2/a_0^2]^2}{\left[1-2\frac{\rho_d^2}{a_0^2}\cos 2\phi_d + \left(\frac{\rho_d^2}{a_0^2}\right)^2\right]} + \frac{\gamma_0}{v^2}\frac{2\pi}{\eta_0}(Z_{de} + Z_d) \tag{18}$$

where we have utilized the known summation formulation

$$\sum_{n=1}^{\infty}\frac{a_n}{n}\cos nx = -\frac{1}{2}\ln[1-2a\cos x + a^2], \qquad \text{for } a^2 < 1$$

given by Wheelon [6] in his extraordinarily useful little book. More compact forms of (16), (17), and (18) are

$$A_0 = \ln\frac{R_0}{c_0} + \frac{\gamma_0}{v^2}\frac{2\pi}{\eta_0}(Z_w + Z_{wed}) \tag{19}$$

$$B_d = \ln\frac{R_d}{c_0} + \frac{\gamma_0}{v^2}\frac{2\pi}{\eta_0}(Z_{de} + Z_d) \tag{20}$$

and

$$A_d = B_0 = \ln\frac{R^-}{R^+} + \frac{\gamma_0}{v^2}\frac{2\pi}{\eta_0}Z_{wed}. \tag{21}$$

where R_0, R_d, R^- and R^+ are defined accordingly. Then, after some manipulation, the mode equation $A_0B_d - B_0A_d = 0$ can be put into a quadratic form

$$(v^2)^2 a + v^2 b + c = 0$$

where

$$a = \left(\ln\frac{R_0}{c_0}\right)\left(\ln\frac{R_d}{c_d}\right) - \left(\ln\frac{R^-}{R^+}\right)^2 \tag{22}$$

$$b = \gamma_0\frac{2\pi}{\eta_0}\left[\left(\ln\frac{R_0}{c_0}\right)(Z_d + Z_{de}) + \left(\ln\frac{R_d}{c_d}\right)(Z_w + Z_{we}) + 2\left(\ln\frac{R^-}{R^+}\right)(Z_{wed})\right] \tag{23}$$

and

$$c = \left(\frac{\gamma_0 2\pi}{\eta_0}\right)^2[(Z_w + Z_{we})(Z_d + Z_{de}) - (Z_{wed})^2]. \tag{24}$$

Consequently, the propagation constants are obtained from

$$\Gamma^2 = \gamma_0^2 + v^2 = \gamma_0^2 + [-b \pm (b^2 - 4ac)^{1/2}](2a)^{-1}. \tag{25}$$

We thus conclude immediately that there are two propagating modes in the system. This is consistent with the behavior of the shielded two-wire transmission line discussed by King [7].

It is also not too difficult to show that within the quasi-static approximation, the fields for a given mode E_ρ and E_ϕ can be deduced from

$$E_\rho = \partial^2 U/\partial\rho\partial z = -\Gamma\partial U/\partial\rho \tag{26}$$

and

$$E_\phi = \partial^2 U/\rho\partial\phi\partial z = -\Gamma\partial U/\rho\partial\phi \tag{27}$$

when the z dependence is of the form $\exp(-\Gamma z)$. Here U has the form [4]

$$U \triangleq \frac{i\mu_0\omega}{2\pi{\gamma_0}^2} e^{-\Gamma z}\left[I_0\left\{\ln\frac{{\rho_0}^-}{{\rho_0}^+} - \sum_{m=1}^{\infty}\left(\frac{\rho\rho_0}{{a_0}^2}\right)^m \frac{1}{m} \cdot [\cos m(\phi-\phi_0) - \cos m(\phi+\phi_0)]\right\} + I_d\left\{\ln\frac{{\rho_d}^-}{{\rho_d}^+} - \sum_{m=1}^{\infty}\frac{1}{m}\left(\frac{\rho\rho_d}{{a_0}^2}\right)^m \cdot [\cos m(\phi-\phi_d) - \cos m(\phi+\phi_d)]\right\}\right] \tag{28}$$

where

$${\rho_0}^+ = [{\rho_0}^2 + \rho^2 - 2\rho\rho_0\cos(\phi-\phi_0)]^{1/2}$$
$${\rho_0}^- = [{\rho_0}^2 + \rho^2 - 2\rho\rho_0\cos(\phi+\phi_0)]^{1/2}$$
$${\rho_d}^+ = [{\rho_d}^2 + \rho^2 - 2\rho\rho_d\cos(\phi-\phi_d)]^{1/2}$$
$${\rho_d}^- = [{\rho_d}^2 + \rho^2 - 2\rho\rho_d\cos(\phi+\phi_d)]^{1/2}.$$

Using the summation form used earlier, we find that

$$U = \frac{i\mu_0\omega}{2\pi{\gamma_0}^2} e^{-\Gamma z}\left[I_0\left\{\ln\frac{{\rho_0}^-}{{\rho_0}^+} + \frac{1}{2}\ln\left[1 - 2\frac{\rho\rho_0}{{a_0}^2}\cos(\phi-\phi_0) + \left(\frac{\rho\rho_0}{{a_0}^2}\right)^2\right] - \frac{1}{2}\ln\left[1 - 2\frac{\rho\rho_0}{{a_0}^2}\cos(\phi+\phi_0) + \left(\frac{\rho\rho_0}{{a_0}^2}\right)^2\right] + I_d\left\{\ln\frac{{\rho_d}^-}{{\rho_d}^+} + \frac{1}{2}\ln\left[1 - 2\frac{\rho\rho_d}{{a_0}^2}\cos(\phi-\phi_d) + \left(\frac{\rho\rho_d}{{a_0}^2}\right)^2\right] - \frac{1}{2}\ln\left[1 - 2\frac{\rho\rho_d}{{a_0}^2}\cos(\phi+\phi_d) + \left(\frac{\rho\rho_d}{{a_0}^2}\right)^2\right]\right\}\right]. \tag{29}$$

We now define the "voltage" V_0 of the trolley wire as follows:

$$V_0 = -\int_0^{\rho_0 - c_0} E_\rho(\phi=\phi_0)\,d\rho = \Gamma U\Big|_0^{\rho_0-c_0}, \quad \text{at } \phi=\phi_0. \tag{30}$$

The corresponding characteristic impedance is then given by

$$K_0 = \frac{V_0}{I_0\exp(-\Gamma z)} = \frac{\eta_0}{2\pi}\Gamma\left[\left\{\ln\frac{2\rho_0\sin\phi_0}{c_0} + \frac{1}{2}\ln\frac{[1-(\rho_0/a_0)^2]^2}{\left[1 - \frac{2{\rho_0}^2}{{a_0}^2}\cos 2\phi_0 + \left(\frac{\rho_0}{a_0}\right)^4\right]}\right\} + \frac{I_d}{I_0}\left\{\frac{1}{2}\ln\left[\frac{{\rho_d}^2 + {\rho_0}^2 - 2\rho_d\rho_0\cos(\phi_0+\phi_d)}{{\rho_d}^2 + {\rho_0}^2 - 2\rho_d\rho_0\cos(\phi_0-\phi_d)}\right] + \frac{1}{2}\ln\left[\frac{1 - \frac{2\rho_d\rho_0}{{a_0}^2}\cos(\phi_0-\phi_d) + \left(\frac{\rho_d\rho_0}{{a_0}^2}\right)^2}{1 - \frac{2\rho_d\rho_0}{{a_0}^2}\cos(\phi_0+\phi_d) + \left(\frac{\rho_d\rho_0}{{a_0}^2}\right)^2}\right]\right\}\right] \tag{31}$$

where, of course, $I_d/I_0 = -A_0/A_d$. It is important to recognize here that K_0 assumes a different value for each mode. Thus, if the two solutions of the mode equation for the propagation constant are Γ_1 and Γ_2, then the corresponding values of the characteristic impedance are designated ${K_0}^{(1)}$ and ${K_0}^{(2)}$, respectively.

The characteristic impedance K_d of the dedicated wire is given by the same expression as (31) if ρ_0, c_0, and ϕ_0 are interchanged everywhere with ρ_d, c_d, and ϕ_d, respectively. The corresponding characteristic impedances for the two modes are then designated ${K_d}^{(1)}$ and ${K_d}^{(2)}$.

This completes the specification of the quasi-static field solution for the uniform structure consisting of the trolley wire and the dedicated communication line in the semicircular tunnel. The eigen-modes propagate according to $\exp(\mp\Gamma_1 z)$ or $\exp(\mp\Gamma_2 z)$ in the $\binom{\text{positive}}{\text{negative}}$ z direction. Such eigen modes are uncoupled for a longitudinally uniform structure.

EXTENSION TO SHUNT LOADING OF THE TROLLEY WIRE

To demonstrate the effectiveness of the dedicated communication line, we need to introduce some form of nonuniformity in the structure. The most striking case is when the trolley wire has a discrete shunt load as indicated schematically in Fig. 2. Here we show an impedance Z_l connected from the trolley wire to the ground plane. This could represent a locomotive or a rectifier or similar power load. The question then is how will this modify the transmission characteristics of the two propagating modes? We deal with this situation in a straightforward fashion as follows.

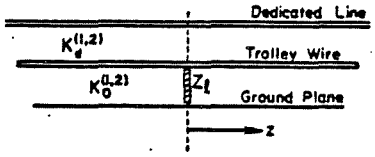


Fig. 2. Schematic representation of the shunt loaded trolley wire and the (unloaded) dedicated line.

With reference to Fig. 2, a mode of, say, type 1 is incident from the left (i.e., from the negative z direction). If the plane $z = 0$ that contains the shunt load is regarded as a junction, this incident mode of type 1 will be reflected and transmitted into both types 1 and 2. Thus we really have a 4 port network to deal with and its properties can be described formally by a scattering matrix [8, 9]. Without extra effort, we prefer to work explicitly with the current and voltage quantities. Thus we may write down the appropriate representations on either side of the junction plane.

The current and voltage on the trolley wire now assume the forms

$$I_0(z) = I_0^{(1)}[e^{-\Gamma_1 z} - R_{11}^0 e^{\Gamma_1 z} - R_{21}^0 e^{\Gamma_2 z}]; \quad z<0 \tag{32}$$

$$V_0(z) = I_0^{(1)}[K_0^{(1)} e^{-\Gamma_1 z} + K_0^{(1)} R_{11}^0 e^{\Gamma_1 z} + K_0^{(2)} R_{21}^0 e^{\Gamma_2 z}]; \quad z<0 \tag{33}$$

$$I_0(z) = I_0^{(1)}[T_{11}^0 e^{-\Gamma_1 z} + T_{21}^0 e^{-\Gamma_2 z}]; \quad z>0 \tag{34}$$

$$V_0(z) = I_0^{(1)}[K_0^{(1)} T_{11}^0 e^{-\Gamma_1 z} + K_0^{(2)} T_{21}^0 e^{-\Gamma_2 z}]; \quad z>0 \tag{35}$$

where $I_0^{(1)}$ denotes the amplitude of the incident current on the trolley wire. R_{11}^0 is the reflection coefficient of the current on the trolley wire from mode 1 to mode 1 while R_{21}^0 is the corresponding reflection coefficient from mode 1 to mode 2. Then T_{11}^0 is the transmission coefficient of the current on the trolley wire from mode 1 to mode 1 while T_{21}^0 is the corresponding transmission coefficient from 1 to mode 2.

The current and voltage for the dedicated line have precisely the same forms as given by (32) to (35); however, the indexes 0 are replaced everywhere by d. Now the incident current is $I_d^{(1)} \exp(-\Gamma_1 z)$ which must be the same as $P_1 I_0^{(1)} \exp(-\Gamma_1 z)$ where

$$P_1 = I_d/I_0, \quad \text{for mode 1}$$
$$= [-A_0/A_d], \quad \text{for } \Gamma = \Gamma_1. \tag{36}$$

Thus the current and voltage representations for the dedicated line are

$$I_d(z) = I_0^{(1)}[P_1 e^{-\Gamma_1 z} - P_1 R_{11}^0 e^{\Gamma_1 z} - P_2 R_{21}^0 e^{\Gamma_2 z}]; \quad z<0 \tag{37}$$

$$V_d(z) = I_0^{(1)}[K_d^{(1)} P_1 e^{-\Gamma_1 z} + K_d^{(1)} P_1 R_{11}^0 e^{\Gamma_1 z} + K_d^{(2)} P_2 R_{21}^0 e^{\Gamma_2 z}]; \quad z<0 \tag{38}$$

$$I_d(z) = I_0^{(1)}[P_1 T_{11}^0 e^{-\Gamma_1 z} + P_2 T_{21}^0 e^{-\Gamma_2 z}]; \quad z>0 \tag{39}$$

$$V_d(z) = I_0^{(1)}[K_d^{(1)} P_1 T_{11}^0 e^{-\Gamma_1 z} + K_d^{(2)} P_2 T_{21}^0 e^{-\Gamma_2 z}]; \quad z>0 \tag{40}$$

where

$$P_2 = I_d/I_0, \quad \text{for mode 2}$$
$$= [-A_0/A_d], \quad \text{for } \Gamma = \Gamma_2. \tag{41}$$

The following circuit conditions now apply at the junction plane $z = 0$:

$$I_0(0^-) = [V_0(0^\pm)/Z_l] + I_0(0^+) \tag{42}$$

$$V_0(0^-) = V_0(0^+) \tag{43}$$

$$I_d(0^-) = I_d(0^+) \tag{44}$$

$$V_d(0^-) = V_d(0^+). \tag{45}$$

Here, for example, $I_0(0^-)$ and $I_0(0^+)$ means $I_0(z)$ in the limit as z tends to zero from negative and positive values, respectively. In what follows, it is convenient to define $k_0^{(1)} = K_0^{(1)}/Z_l$ and $k_0^{(2)} = K_0^{(2)}/Z_l$.

The application of the above junction conditions to (32) to (35) and (37) to (41) lead to

$$1 - R_{11}^0 - R_{21}^0 = k_0^{(1)} + k_0^{(1)} R_{11}^0 + k_0^{(2)} R_{21}^0 + T_{11}^0 + T_{21}^0 \tag{46}$$

$$P_1 - P_1 R_{11}^0 - P_2 R_{21}^0 = P_1 T_{11}^0 + P_2 T_{21}^0 \tag{47}$$

$$K_0^{(1)} + K_0^{(1)} R_{11}^0 + K_0^{(2)} R_{21}^0 = K_0^{(1)} T_{11}^0 + K_0^{(2)} T_{21}^0 \tag{48}$$

$$K_d^{(1)} P_1 + K_d^{(1)} P_1 R_{11}^0 + K_d^{(2)} P_2 R_{21}^0 = K_d^{(1)} P_1 T_{11}^0 + K_d^{(2)} P_2 T_{21}^0. \tag{49}$$

These can be solved readily for the desired coefficients.

$$R_{11}{}^{0} = \frac{k_0{}^{(1)}}{(P_1/P_2)(k_0{}^{(2)} + 2) - (k_0{}^{(1)} + 2)} \tag{50}$$

$$T_{11}{}^{0} = \frac{(P_1/P_2)(k_0{}^{(2)} + 2) - 2}{(P_1/P_2)(k_0{}^{(2)} + 2) - (k_0{}^{(1)} + 2)} \tag{51}$$

$$R_{21}{}^{0} = T_{21}{}^{0} = \frac{-(P_1/P_2)k_0{}^{(1)}}{(P_1/P_2)(k_0{}^{(2)} + 2) - (k_0{}^{(1)} + 2)}. \tag{52}$$

On examining (37) to (40), it is a simple matter to show that corresponding coefficients for the dedicated line are related to the above by

$$R_{11}{}^{d} = R_{11}{}^{0}, \qquad T_{11}{}^{d} = T_{11}{}^{0}$$

$$R_{21}{}^{d} = (P_2/P_1)R_{21}{}^{0}, \qquad T_{21}{}^{d} = (P_2/P_1)T_{21}{}^{0}.$$

Thus we have completely solved the problem as stated.

An insertion loss in dB may be simply defined as $-20 \log_{10} | T_{11} |$ or $-20 \log_{10} | T_{22} |$ for modes of type 1 or 2, respectively. As indicated above, these apply both to the trolley wire or to the dedicated line even though only the trolley wire is shunt loaded.

Some numerical examples were examined for the following set of typical parameters: tunnel radius $a_0 = 2$ m, wall conductivity $\sigma_e = 10^{-3}$ mho/m, wall permittivity $\epsilon_e = 10\epsilon_0$, trolley wire radius $c_0 = 1.5$ cm, trolley wire conductivity $\sigma_w = 5.7 \times 10^7$, trolley wire location $\rho_0 = 1.8$ m and $\phi_0 = 45°$, dedicated wire radius 1.5 mm, dedicated wire conductivity $\sigma_d = 5.7 \times 10^7$ mho/m, dedicated wire location $\rho_d = 1.8$ m and $\phi_d = 135°$.

Using the above parameters for a frequency of 100 kHz, we find that, for mode 1: $[I_d/I_0] \cong 0.25 \angle -3°$ and $K_0{}^{(1)} \cong (250 - i1)\Omega$ while, for mode 2: $[I_d/I_0] \cong 2.5 \angle -177°$ and $K_0{}^{(2)} \cong (160 - i4)\Omega$. These deduced parameters varied only slightly over the frequency range from 50 to 800 kHz. As indicated, mode 1 is defined as the case where $| I_d |$ is somewhat less than $| I_0 |$. On the other hand, mode 2 is defined as the case where $| I_d |$ is somewhat greater than $| I_0 |$. For reasons that certainly are obvious later, mode 2 is aptly described as the "communication mode".

The insertion loss for mode 1 is shown in Fig. 3 as a function of frequency from 50 to 800 kHz. The selected values of the shunt impedance in real ohms are indicated. Not surprisingly, the insertion loss is fairly significant since for this mode most of the current is being carried by the trolly wire. On the other hand, the insertion loss for mode 2, as shown in Fig. 4, is for the same conditions. Clearly, it is very much reduced. This certainly serves as a dramatic confirmation of the concept of the dedicated communication line proposed by R. H. Spencer *et al.* [3].

Of course, the computed insertion loss will depend on the specified values for the numerous parameters of the problem. To illustrate one such dependence, the angular location ϕ_d of the dedicated line is allowed to vary from 50° to 170° but maintaining the radial position ρ_d constant at 1.8 m. These results for 100 kHz are shown in Figs. 5 and 6 for mode 1 and

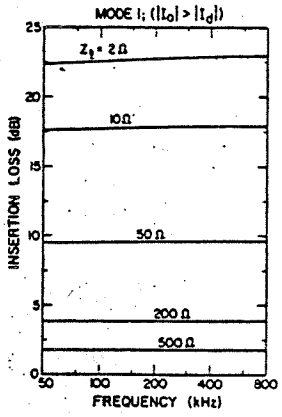


Fig. 3. The insertion loss ($-20 \log_{10} | T_{11} |$) of mode 1 for a shunt load on the trolley wire.

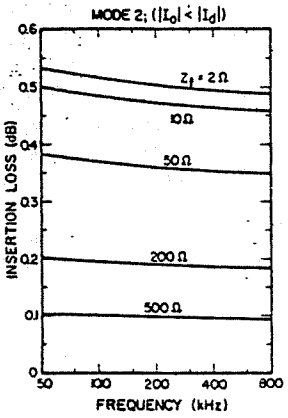


Fig. 4. The insertion loss ($-20 \log_{10} | T_{22} |$) of mode 2 for a shunt load on the trolley wire.

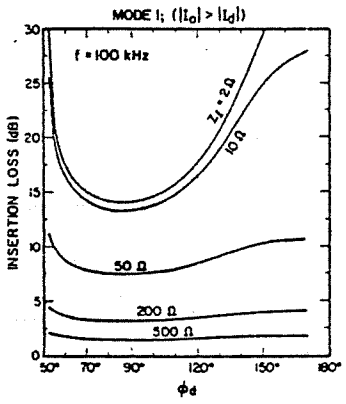


Fig. 5. The effect of the dedicated wire location on the insertion loss for mode 1. $\phi_0 = 45°$ (the 10 Ω curve should be labeled 5 Ω).

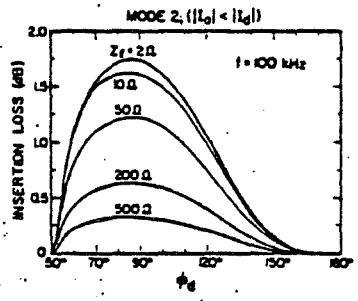


Fig. 6. The effect of the dedicated wire location on the insertion loss for mode 2. $\phi_0 = 45°$.

mode 2, respectively. The conditions are otherwise the same as adopted for Figs. 3 and 4.

As indicated in Fig. 5, the insertion loss becomes very large for mode 1 when ϕ_d tends toward 45°. In this case, mode 1 is monofilar (i.e., $I_d \cong I_0$) in character and most of the return current is via the tunnel walls and ground plane. Thus it is not surprising that the shunt load has a drastic effect on the transmission. In the other limiting directions where ϕ_d tends to 180°, the dedicated line is effectively being decoupled by the ground plane and we have, in effect, a tunnel with a single conductor (i.e., the trolley wire). Here the resulting monofilar type mode is again significantly influenced by the shunt load.

The corresponding behavior of mode 2 shown in Fig. 6 indicates that the insertion loss is very small as ϕ_d tends to 45°. In this case, mode 2 is bifilar (i.e., $I_d \cong -I_0$) in character and thus, not surprisingly, a connection to ground via Z_l has little effect. As ϕ_d tends to 180°, mode 2 has a small insertion loss because, as pointed out above, the coupling to the trolley wire is negligible.

CONCLUDING REMARKS

We have developed here a rudimentary theory for radio frequency transmission in a tunnel that contains a trolley wire and a dedicated communication line. As pointed out by Spencer and colleagues [3], the dedicated line provides for a low loss mode that is weakly coupled to the trolley wire circuit. Thus the performance of a carrier communication system in the tunnel is not seriously degraded by shunt loads on the trolley wire.

ACKNOWLEDGMENT

We are grateful for the many useful discussions with and private communications from the staff of A. D. Little, Inc., Cambridge, MA. In particular, we are indebted to Dr. R. H. Spencer for his suggestions and encouragement. We also wish to thank Mrs. L. R. Hope for help in preparing the manuscript and Dr. D. B. Seidel for his cogent comments on the formulation of the mode conversion problem.

REFERENCES

[1] J. N. Murphy and H. E. Parkinson, "Mine communications: Research and development in the U.S.A.", *Proc. Int'l. Conf. Radio, Tunnels and Mines*, Vol. II, pp. 42-64, Liege, Belgium, April 1-5, 1974.

[2] D. A. Hill and J. R. Wait, "Analysis of radio frequency transmission along a trolley wire in a mine tunnel", *IEEE Trans. Electromag. Compat.*, Vol. EMC-18, pp. 170-174, Nov. 1976.

[3] R. H. Spencer, A. G. Emslie, J. D. Foulkes, R. L. Lagace, P. G. Martin, P. F. O'Brien, and P. F. Strong, "Improvements for mine carrier phone systems", *Report to U.S. Bureau of Mines*, Contract No. HO346045, April 1977.

[4] D. A. Hill and J. R. Wait, "Analysis of radio frequency transmission in a semicircular tunnel containing two axial conductors", *IEEE Trans. Commun.*, Vol. COM-25, pp. 1046-1050, Sept. 1977.

[5] J. R. Wait, "Quasi-static limit for the propagating mode along a thin wire in a cylindrical tunnel", *IEEE Trans. Antennas Propagat.*, Vol. AP-25, No. 3, pp. 441-443, May 1977.

[6] A. D. Wheelon, *Tables of Summable Series and Integrals Involving Bessel Functions*, San Francisco: Holden-Day, 1968, p. 44.

[7] R. W. P. King, *Transmission Line Theory*, New York: McGraw-Hill Book Co., 1955, pp. 34-39.

[8] R. Levy, "Directional couplers", *Advances in Microwaves*, Vol. 1, New York: Academic Press, 1966, pp. 115-209.

[9] P. Delogne, Diaphone et orthogonalite des modes, *Revue HF Tijdschrift* (Societe Belge des Ingeneurs), Vol. 7, No. 10, 255-258, 1969.

494 IEEE TRANSACTIONS ON MICROWAVE THEORY AND TECHNIQUES, VOL. MTT-26, NO. 7, JULY 1978

Transmission Modes in a Braided Coaxial Cable and Coupling to a Tunnel Environment

DAVID B. SEIDEL, MEMBER, IEEE, AND JAMES R. WAIT, FELLOW, IEEE

Abstract—Radio frequency transmission in a semicircular tunnel containing a braided coaxial cable is considered. The general formulation accounts for both the ohmic losses in the tunnel wall and a thin lossy film layer on the outer surface of the dielectric jacket of the cable. Using a quasi-static approximation, it is found that the propagation constants of the low-frequency transmission line modes are obtained through the solution of a cubic equation. However, for the special case when the conductivity thickness product of the lossy film layer vanishes, this cubic equation reduces to a quadratic. The spatially dispersive form of the braid transfer impedance is also accounted for. It is shown that the quasistatic theory is well justified for frequencies as high as 100 MHz for typical tunnel geometries. Finally, special characteristic impedances are derived for the various modes of the equivalent multiconductor transmission line.

I. Introduction

A COAXIAL CABLE that allows continuous leakage through its outer sheath can be exploited for continuous-access guided communications [1]. The environment, of course, plays an important role whether it be an adjacent roadway, railway right-of-way, or tunnel. A key aspect of such systems is the coupling (intentional or nonintentional) between the transmission modes within the cable and the transmission mode(s) in the external region. Before an optimum communication system can be designed to utilize these coupled modes, a better understanding of the propagation mechanisms is needed.

In this paper, we consider specifically a semicircular tunnel model with a coaxial cable whose sheath is characterized by a transfer impedance. We also allow for the presence of a lossy film on the outer surface of the concentric dielectric jacket. For applications in mine environments such a lossy layer can represent the effect of a thin conducting fluid (i.e., saline water) or conductive dust. Of course, the ohmic losses in the curved tunnel walls are also included.

The main objective is to obtain specific results for the attenuation rates of the dominant transmission modes and to provide convenient definitions for the corresponding characteristic impedances. We also demonstrate the validity of the quasi-static formulation of the problem by making a comparison with calculations based on a more general (and more complicated) mode equation.

Manuscript received October 10, 1977; revised January 12, 1978.

D. B. Seidel is with Cooperative Institute for Research in Environmental Sciences University of Colorado/NOAA Boulder, CO 80309.

J. R. Wait is a Consultant to the Institute for Telecommunication Sciences, U.S. Department of Commerce, Boulder, CO.

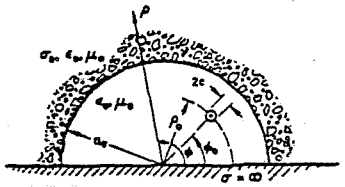


Fig. 1. Cross-section of semicircular tunnel containing coaxial cable (not to scale).

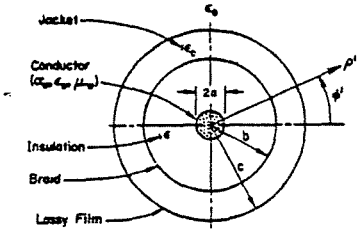


Fig. 2. The braided coaxial cable.

II. Formulation

The model assumed is described in terms of a cylindrical coordinate system (ρ,ϕ,z) and is shown in Fig. 1. The tunnel wall is located at $\rho=a_0$ for $0<\phi<\pi$, and the assumed perfectly conducting tunnel floor is located at $\phi=0$ and $\phi=\pi$ for $0<\rho<\infty$. The region defined by $\rho>a_0$ and $0<\phi<\pi$ is a homogeneous medium with conductivity σ_e and permittivity ϵ_e. The coaxial cable with outside radius c is centered at $\rho=\rho_0$ and $\phi=\phi_0$. The region defined by $\rho<a_0$, $0<\phi<\pi$, and $\rho'>c$, where ρ' is the radial component of a cylindrical coordinate system (ρ',ϕ',z) centered at (ρ_0,ϕ_0), is described by the free space permittivity and permeability ϵ_0 and μ_0, respectively. The geometry of the coaxial cable is shown in Fig. 2. The inner conductor has radius a and high but finite conductivity σ_w. The surrounding insulation of radius b is a lossless dielectric with permittivity ϵ. The braided sheath located at $\rho'=b$ is characterized by a surface transfer impedance Z_T. The outer dielectric coating has radius c and permittivity ϵ_c. We also allow for the possibility that a thin lossy film is located at $\rho'=c$ which is characterized by a transfer impedance Z_L. We assume that the fields of each mode of this structure vary as $\exp(-\Gamma z+i\omega t)$ where ω is the angular frequency, and Γ is the complex propagation constant for the particular mode.

U.S. Government work not protected by U.S. copyright

In a previous paper, Hill and Wait [2] obtained a modal solution for the similar problem of a single conductor trolley wire in a semicircular tunnel. This solution is general for any thin wire or cable that can be characterized by a series impedance. Their mode equation is given here in a more convenient form for our purpose:

$$K_0(\upsilon c) - K_0(\upsilon\rho_d) - S + \frac{2\pi\gamma_0}{\upsilon^2\eta_0}(Z(\Gamma)+Z_e) = 0 \qquad (1)$$

where

$$\gamma_0^2 = -\epsilon_0\mu_0\omega^2 = -(2\pi/\lambda_0)^2 = -k_0^2, \quad \rho_d = 2\rho_0\sin\phi_0$$
$$\upsilon^2 = \gamma_0^2 - \Gamma^2, \quad \eta_0 = (\mu_0/\epsilon_0)^{1/2} = 120\pi$$

where $Z(\Gamma)$ is an effective impedance of the cable that we define below. The factors S and Z_e account for the presence of the tunnel walls and are given by

$$S = 2\sum_{m=1}^{\infty}\frac{K_m(\upsilon a_0)}{I_m(\upsilon a_0)} I_m(\upsilon\rho_0) I_m(\upsilon(\rho_0+c))[1-\cos 2m\phi_0] \qquad (2)$$

and

$$Z_e = -\frac{\upsilon^2\eta_0}{\pi\gamma_0}\sum_{m=1}^{\infty}(R_m - 1)\frac{K_m(\upsilon a_0)}{I_m(\upsilon a_0)} \cdot I_m(\upsilon\rho_0) I_m(\upsilon(\rho_0+c))[1-\cos 2m\phi_0] \qquad (3)$$

where

$$R_m = \frac{[(\gamma_0/\upsilon)K_m'(\upsilon a_0)/K_m(\upsilon a_0)] + Y_m\eta_0 + \delta_m\eta_0}{[(\gamma_0/\upsilon)I_m'(\upsilon a_0)/I_m(\upsilon a_0)] + Y_m\eta_0 + \delta_m\eta_0}$$

$$Y_m = \left(\frac{i\gamma_c^2}{u\mu_0\omega}\right)\frac{K_m'(ua_0)}{K_m(ua_0)}$$

$$\delta_m\eta_0 = \frac{(im\Gamma/a_0)^2(\upsilon^{-2}-u^{-2})^2}{[(\gamma_0/\upsilon)I_m'(\upsilon a_0)/I_m(\upsilon a_0)] + Z_m/\eta_0}$$

$$Z_m = -\left(\frac{i\omega\mu_0}{u}\right)\frac{K_m'(ua_0)}{K_m(ua_0)}$$

$$\gamma_c^2 = i\omega\mu_0(\sigma_c + i\omega\epsilon_c) \quad u = (\gamma_c^2 - \Gamma^2)^{1/2}.$$

Note that S represents the reflected field from perfectly conducting cylindrical walls and thus Z_e accounts for the ohmic losses due to the finite conductivity of the tunnel walls.

Previously, Wait and Hill [3] derived an effective series impedance $Z(\Gamma)$ for a braided coaxial cable. In general, the resulting expression for $Z(\Gamma)$ is quite complicated. However, they show that, if some quasi-static approximations are invoked, $Z(\Gamma)$ can be expressed approximately by the simpler form where

$$Z(\Gamma) = \frac{Z_L(Z_c+Z_b)}{Z_L+Z_c+Z_b}$$
$$Z_b = \frac{Z_T(Z'+Z_i)}{Z_T+Z'+Z_i} \qquad (4)$$

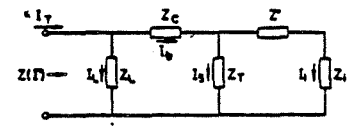


Fig. 3. The equivalent network which yields the effective series impedance of the cable in the quasi-static approximation.

$$Z_i = \frac{\eta_0\gamma_0}{2\pi a\gamma_w}\frac{I_0(\gamma_w a)}{I_1(\gamma_w a)} \qquad \gamma_w^2 = i\sigma_w\mu_0\omega$$
$$Z' = -(k^2+\Gamma^2)\alpha' \qquad k^2 = \omega^2\mu_0\epsilon$$
$$Z_c = -(k_c^2+\Gamma^2)\alpha_c \qquad k_c^2 = \omega^2\mu_0\epsilon_c$$
$$Z_L = [2\pi c(\sigma d)]^{-1}$$

$\alpha' = (2\pi i\omega\epsilon)^{-1}\ln(b/a)$ and $\alpha_c = (2\pi i\omega\epsilon_c)^{-1}\ln(c/b)$.

Here (σd) is the conductivity–thickness product of the thin lossy layer that may be present.

The equivalent circuit for $Z(\Gamma)$ is the network shown in Fig. 3. The general spatially dispersive form of the sheath transfer impedance Z_T can be employed here. An approximate Γ-dependent form [4],[5] appropriate for the present analysis is

$$Z_T = Z_0 + \alpha_t\Gamma^2$$

where

$$\alpha_t = 2Z_0(k^2+k_c^2)^{-1}\cos^2\psi$$

and $Z_0 = i\omega L_T$ where L_T is the static sheath transfer inductance, and ψ is the braid weave angle. Note that α_t accounts for the spatial dispersion of the sheath transfer impedance.

The proper mode equation for our problem is obtained by using (4) in (1). Normally, the numerical solution for the complex propagation constants Γ for the various modes of the structure are obtained by employing an iterative procedure for locating complex roots [3], [5]. However, here we take a different approach and we use an iterative solution of (1) only for purposes of comparison.

III. Quasi-Static Mode Equation

Solution of (1) for the modal propagation constants can be simplified if some quasi-static approximations are invoked. Specifically, we assume that $|\gamma_c/\gamma_0|^2 \gg 1$ and that $|\upsilon a_0| \ll 1$. In fact, using a previous result of Wait [6] and small argument approximations for the modified Bessel functions, we can represent (2) and (3) by

$$S \approx \sum_{m=1}^{\infty}\frac{r^m}{m}(1-\cos 2m\phi_0) \qquad (5)$$

and

$$Z_e \approx \frac{2\gamma_0\eta_0}{\pi\gamma_c a_0}\sum_{m=1}^{\infty} r^m\frac{K_m(\gamma_c a_0)}{K_{m+1}(\gamma_c a_0)}\sin^2 m\phi_0 \qquad (6)$$

where

$$r = \rho_0(\rho_0+c)/a_0^2.$$

Note that both S and Z_e are independent of Γ with this approximation. If we now use

$$\sum_{n=1}^{\infty} \frac{a^n}{n} \cos nx = -\frac{1}{2} \ln\left[1 - 2a\cos x + a^2\right], \qquad \text{for } a^2 < 1$$

given by Wheelon [7] in (5), we find that (1) becomes

$$v^2 \ln R + N(Z(\Gamma) + Z_e) = 0 \tag{7}$$

where

$$R = 2\rho_0 \sin\phi_0 c^{-1}(1-r)\left(1 - 2r\cos\phi_0 + r^2\right)^{-1/2}$$

and

$$N = 2\pi\gamma_0/\eta_0.$$

After considerable algebraic manipulation, (7) becomes a cubic equation of the form

$$a_3(\Gamma^2)^3 + a_2(\Gamma^2)^2 + a_1(\Gamma^2) + a_0 = 0 \tag{8}$$

where

$$a_3 = q_2(\ln R)/Z_L \tag{9}$$

$$a_2 = Nq_2 - s_1 \ln R + \left[(\gamma_0^2 q_2 - q_1)\ln R + NZ_e q_2\right]/Z_L \tag{10}$$

$$a_1 = N(Z_e s_1 + q_1) + (\gamma_0^2 s_1 - s_0)\ln R + \left[(\gamma_0^2 q_1 - q_0)\ln R + NZ_e q_1\right]/Z_L \tag{11}$$

$$a_0 = N(Z_e s_0 + q_0) + \gamma_0^2 s_0 \ln R + q_0(\gamma_0^2 \ln R + NZ_e)/Z_L \tag{12}$$

and

$$q_0 = (k^2\alpha' - Z_i)(k_c^2\alpha_c - Z_0) - k_c^2\alpha_c Z_0$$

$$q_1 = (\alpha_c - \alpha_t)(k^2\alpha' - Z_i) + \alpha'(k_c^2\alpha_c - Z_0) - \alpha_c(Z_0 + k_c^2\alpha_t)$$

$$q_2 = \alpha'(\alpha_c - \alpha_t) - \alpha_t\alpha_c$$

and

$$s_0 = Z_i + Z_0 - k^2\alpha' \qquad s_1 = \alpha_t - \alpha'.$$

Now (8) is a cubic equation and it has three roots which can be solved for algebraically. Two of these roots can be identified as the propagation constants of the well-known monofilar and bifilar modes. But, in addition, there is a third mode which we will refer to as the jacket mode since it is found that in this mode, the current and return current flows primarily in the braided sheath and the lossy film layer, respectively, and that the other currents are negligible. Examination of (9) reveals that in the absence of the outer lossy film ($Z_L \to \infty$), a_3 vanishes, and (8) reduces to a quadratic equation in Γ^2. Consequently, there are now only two solutions. As one would expect, the jacket mode has disappeared, leaving only the monofilar and bifilar modes.

These results are not unexpected. In the general case, we have four axial conductors (the tunnel wall and floor, the cable's inner conductor, the braided sheath, and the lossy film layer). Thus, at sufficiently low frequencies, there will be three TEM modes [8]. But, of course, in the absence of the lossy film, there remain only three conductors and thus only two TEM modes would exist in this low frequency limit. When ohmic losses in these conductors are considered, we still expect three (or two, if $\sigma d = 0$) dominant modes provided the tunnel cross section is small compared with the free space wavelength λ_0.

IV. Characteristic Impedances for Multiconductor Transmission Line

Because the dominant low-frequency modes of this system behave like TEM transmission-line modes, it is useful to treat the problem as a multiconductor transmission line using transmission-line concepts. Such an approach proves useful, for example, in considering the mode conversion problem resulting from the presence of axial nonuniformities in the cable or tunnel. Thus we need to derive the characteristic impedance of each line for each quasi-TEM mode. Specifically, we define

$$K_L = \frac{V_L}{I_L e^{-\Gamma z}}, \qquad K_s = \frac{V_s}{I_s e^{-\Gamma z}}, \qquad K_i = \frac{V_i}{I_i e^{-\Gamma z}} \tag{13}$$

as the impedance associated with the lossy film, the braided sheath, and inner conductor, respectively. The voltages V_L, V_s, and V_i are defined by

$$V_L = -\int_0^{\rho_0 - c} E_\rho(\phi = \phi_0)\, d\rho$$

$$V_s = V_L + \int_b^c E_{\rho'}\, d\rho'$$

$$V_i = V_s + \int_a^b E_{\rho'}\, d\rho' \tag{14}$$

and are the voltages of the lossy film, the braid, and the inner conductor, respectively, with reference to the tunnel floor. Similarly, I_L, I_s, and I_i are the currents in each conductor (see Fig. 3).

It is not difficult to show that within the quasi-static approximation, E_ρ can be determined from

$$E_\rho = \partial^2 U/\partial\rho\partial z = -\Gamma\partial U/\partial\rho \tag{15}$$

where U has the form

$$U \approx \frac{\eta_0}{2\pi\gamma_0} e^{-\Gamma z} I_t \left\{ \ln\frac{\rho_0^-}{\rho_0^+} - \sum_{m=1}^{\infty} \frac{1}{m}\left(\frac{\rho\rho_0}{a_0^2}\right)^m \cdot \left[\cos m(\phi - \phi_0) - \cos m(\phi + \phi_0)\right] \right\} \tag{16}$$

and

$$\rho_0^+ = \left[\rho_0^2 + \rho^2 - 2\rho\rho_0\cos(\phi - \phi_0)\right]^{1/2}$$

$$\rho_0^- = \left[\rho_0^2 + \rho^2 - 2\rho\rho_0\cos(\phi + \phi_0)\right]^{1/2}$$

$$I_t = I_L + I_s + I_i.$$

Similarly, we find that the radial electric field within the cable using these quasi-static approximations is given by

$$E_{\rho'} \approx \begin{cases} \dfrac{\Gamma I_t e^{-\Gamma z}}{2\pi i\omega\varepsilon\rho'}, & a < \rho' < b \\ \dfrac{\Gamma I_b e^{-\Gamma z}}{2\pi i\omega\varepsilon_c\rho'}, & b < \rho' < c \end{cases} \tag{17}$$

where $I_b = I_s + I_i$. Combining (13)–(17) and using the

summation form used earlier, we obtain

$$K_L = \left(\frac{1+p+q}{q}\right)\frac{\Gamma \ln R}{N}$$

$$K_2 = \Gamma\left[\left(\frac{1+p+q}{p}\right)\frac{\ln R}{N} + \left(\frac{1+p}{p}\right)\alpha_c\right] \qquad (18)$$

and

$$K_1 = \Gamma\left[(1+p+q)\frac{\ln R}{N} + (1+p)\alpha_c + \alpha'\right]$$

where the current ratios p and q are defined by

$$p \equiv \frac{I_2}{I_1} = \frac{Z'(\Gamma)+Z_1}{Z_T(\Gamma)} \qquad (19)$$

and

$$q \equiv \frac{I_L}{I_1} = (1+p)\frac{Z_b(\Gamma)+Z_c(\Gamma)}{Z_L}.$$

The characteristic impedances defined by (18) are dependent upon Γ and consequently they assume different values for each mode. Thus we have $K_L^{(j)}$, $K_2^{(j)}$, and $K_1^{(j)}$ corresponding to the propagation constant of each mode (Γ_j) for $j=1,2,3$. In the special case when there is no lossy film ($\sigma d=0$), I_L vanishes, and we consider only the two characteristic impedances $K_2^{(j)}$ and $K_1^{(j)}$ for $j=1,2$.

V. Some Numerical Results

We now present some examples of numerical results for typical configurations of the geometry shown in Figs. 1 and 2. In all examples that follow, we consider a tunnel with radius $a_0=2m$ and rock conductivity and permittivity of $\sigma_e=10^{-2}$ mhos/m and $\epsilon_e=10\epsilon_0$, respectively. The dimensions of the cable are as follows: $a=1.5$ mm, $b=10$ mm, and $c=11.5$ mm. The permittivities of the cable insulation and jacket are given by $\epsilon=2.5\epsilon_0$ and $\epsilon_c=3.0\epsilon_0$, which are typical values. Finally, in all cases, the cable is located at $\phi_0=45°$, and the cable's braid is woven at the angle $\psi=45°$.

In order to ascertain the accuracy of the quasi-static mode equation (7), we first consider a comparison of results computed using this approximation to results computed from (1) directly using iterative techniques. Fig. 4 compares the attenuation rates of the monofilar mode over the frequency range 0.2 to 100 MHz for various values of the cable's radial position ρ_0. (Attenuation rate in dB/km $=8686$ Re (Γ).) Here we take the braid transfer inductance L_T to be 40 nH/m which corresponds to the FONT cable [9], $\sigma_w=5.7\times10^7$ mhos/m, and $\sigma d=0$. A similar comparison for the bifilar mode shows the two solutions to be virtually indistinguishable over this range of frequencies. In addition, if a nonzero σd is introduced, a comparison of attenuation rate of the jacket mode also shows the two solutions to be virtually the same. These comparisons clearly demonstrate the utility of the quasi-static mode equation for typical tunnel parameters at radio frequencies. The remaining examples given here have been computed solely using the quasi-static approximation that is much more economic.

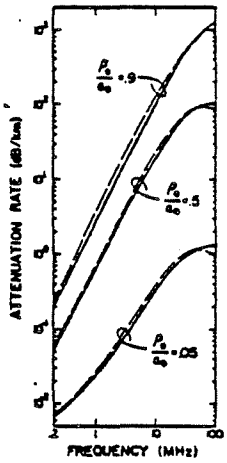


Fig. 4. Attenuation rate of the monofilar mode versus frequency for various valuses of (ρ_0/a_0). With quasi-static approximation:———. Without quasi-static approximation:- - - - - -.

In our next example, we again consider the case when $L_T=40$ nH/m but allow ρ_0, σ_w, and σd to assume various values. These results are shown in Fig. 5(a) and (b). It is found that the monofilar mode is essentially independent of the inner conductor's conductivity (σ_w) whereas the bifilar mode is essentially independent of the cable position within the tunnel. This is in agreement with similar results obtained for a coaxial cable in a circular tunnel [3]. It is interesting to note, however, that the attenuation rates for the monofilar mode (Fig. 5(a)) are significantly lower than those given [3] for similar parameters in a circular tunnel. This is not unexpected since, in the semicircular tunnel, a portion of the return current for the monofilar mode flows in the perfectly conducting tunnel floor and thus suffers less attenuation. On the other hand, there is virtually no difference between the bifilar modes, which are relatively insensitive to the environment outside the cable.

Now we turn our attention to the jacket mode. Fig. 6 shows the attenuation rate of this mode as a function of frequency for various values of L_T and σd. The most immediate observation to be made is that the attenuation rate for this mode is orders of magnitude higher than that of the other two modes. It is also observed that the attenuation is approximately proportional to $(\omega/\sigma d)^{1/2}$.

Another quantity of interest is the normalized phase defined by Im $(\Gamma)/k_0$ which is inversely proportional to the phase velocity with which the mode propagates along the tunnel. Some values of the normalized phase are given in Table I for the monofilar and bifilar modes. Here $L_T=2$ nH/m, $\sigma_w=5.7\times10^7$ mhos/m, and $\sigma d=0$. We note that for the monofilar mode, the normalized phase is slightly larger than unity when the cable–tunnel wall separation is large, but increases rapidly as the cable approaches the tunnel wall. On the other hand, the normalized phase of the bifilar mode is essentially independent of this separation and is slightly greater than $k/k_0=(\epsilon/\epsilon_0)^{1/2}=1.581$. This suggests the interesting possibility of adjusting the dielectric constant of the cable insulation

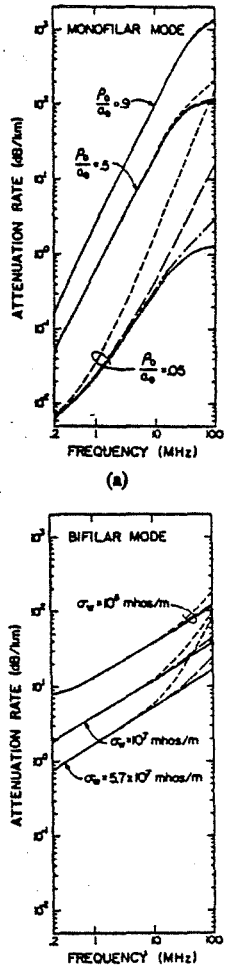


Fig. 5. Attenuation rate versus frequency for (a) monofilar mode, (b) bifilar mode. $\sigma d = 0$:———. $\sigma d = 10^{-3}$ mhos:— · —. $\sigma d = 10^{-2}$ mhos:———. $\sigma d = 10^{-1}$ mhos:------.

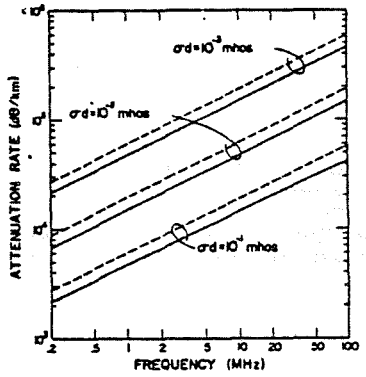


Fig. 6. Attenuation rate of jacket mode versus frequency for various values of σd. $L_T = 40$ nH/m:———. $L_T = 2$nH/m:------.

TABLE I
NORMALIZED PHASE Im $(\Gamma)/k_0$

f	Monofilar			Bifilar
	$\frac{\rho_0}{a_0} = .5$	$\frac{\rho_0}{a_0} = .9$	$\frac{\rho_0}{a_0} = .98$	$\frac{\rho_0}{a_0} = .5$
.2	1.058	1.251	1.685	1.604
.5	1.057	1.248	1.680	1.594
1.0	1.056	1.244	1.674	1.593
2.0	1.055	1.238	1.665	1.590
5.0	1.051	1.225	1.644	1.587
10.0	1.047	1.208	1.617	1.586
20.0	1.040	1.176	1.566	1.585
50.0	1.030	1.103	1.444	1.585
100.0	1.027	1.054	1.332	1.584

TABLE II
NORMALIZED PHASE Im $(\Gamma)/k_0$

f	Jacket Mode		
	$\sigma d = 10^{-3}$	$\sigma d = 10^{-2}$	$\sigma d = 10^{-1}$
.2	759.7	240.2	75.98
.5	480.5	151.9	48.06
1.0	339.8	107.4	34.00
2.0	240.2	75.98	24.06
5.0	151.9	48.06	15.25
10.0	107.4	34.00	10.82
20.0	75.98	24.06	7.699
50.0	48.06	15.25	4.967
100.0	34.00	10.82	3.630

and the cable–tunnel wall separation such that the two modes will propagate with the same phase velocity.

Finally, we consider the normalized phase for the jacket mode as given in Table II for three values of σd. Here $L_T = 2$ nH/m, and the values given are essentially independent of the other parameters. We see that, for typical values of the conductivity–thickness product of the lossy film, the normalized phase is much larger than one, and consequently, the mode propagates very slowly. It should be pointed out that, like this mode's attenuation rate, the phase is essentially proportional to $(\omega/\sigma d)^{1/2}$.

VI. Concluding Remarks

We have obtained a remarkably simple description of the dominant transmission modes for a leaky coaxial cable located in a uniform straight tunnel with a semicircular cross section. The formulation is facilitated by the assumption that the floor of the tunnel, including the effect of any metallic rails, is represented adequately by a perfectly conducting ground plane. This allows us to define characteristic impedances of the transmission modes in a meaningful fashion. In a subsequent study, we shall consider the application of these results to the case where the cable and/or the tunnel environment undergoes a lateral variation such as an abrupt modification of the effective series or shunt impedance.

References

[1] J. C. Beal, J. Josiak, S. F. Mahmoud, and V. Rawat, "Continuous access guided communication (CAGC) for ground transportation systems," *Proc. IEEE*, vol. 61, pp. 562–568, May 1973.

[2] D. A. Hill and J. R. Wait, "Analysis of radio frequency transmission along a trolley wire in a mine tunnel," *IEEE Trans. Electromagn. Compat.*, vol. EMC-18, pp. 170–174, Nov. 1976.

[3] J. R. Wait and D. A. Hill, "Propagation along a braided coaxial cable in a circular tunnel," *IEEE Trans. Microwave Theory Tech.*, vol. MTT-23, pp. 401–405, May 1975.

[4] K. F. Casey, "On the effective impedance of thin coaxial cable shields," *IEEE Trans. Electromagn. Compat.*, vol. EMC-18, pp. 110–117, Aug. 1976.
[5] J. R. Wait and D. A. Hill, "Influence of spatial dispersion of the shield transfer impedance of a braided coaxial cable," *IEEE Trans. Microwave Theory Tech.*, vol. MTT-25, pp. 72–74, Jan. 1977.
[6] J. R. Wait, "Quasi-static limit for the propagating mode along a thin wire in a circular tunnel," *IEEE Trans. Antennas Propagat.*, vol. AP-25, pp. 441–443, May 1977.
[7] A. D. Wheelon, *Tables of Summable Series and Integrals Involving Bessel Functions*. San Francisco: Holden-Day, 1968, p. 44.
[8] R. E. Collin, *Field Theory of Guided Waves*. New York: McGraw-Hill, 1960, p. 124.
[9] J. Fontaine, B. Demoulin, P. Degauque, and R. Gabillard, *Proc. of the Thru-the-Earth Electromagnetics Workshop*, U.S. Bureau of Mines, Aug. 1973 (available from the National Technical Information Service, 5285 Port Royal Road, Springfield, VA 22152, Document No. PB 231 154).

Guided Electromagnetic Waves in a Periodically Nonuniform Tunnel

JAMES R. WAIT, FELLOW, IEEE

Abstract—A boundary value analysis is outlined for the transmission in a circular tunnel that contains a thin axial conductor. The series impedance of the latter is allowed to vary in a periodic fashion throughout its length. Simplifications of the formal mode equation are achieved by invoking quasi-static conditions used in previous studies. It is shown that the axial nonuniformity can be represented approximately as a modification of the series impedance of the equivalent transmission line of the composite tunnel structure.

Manuscript received December 15, 1977.

The author is with the Cooperative Institute for Research in Environmental Sciences, University of Colorado and National Oceanographic and Atmospheric Administration, Boulder, CO 80309.

Electromagnetic wave transmission in tunnel-like structures has a number of important applications in mining technology and transportation. Analytical studies of such problems [1], [2] have usually assumed that the guiding structure is laterally uniform, although the influence and exploitation of mode converters have been considered [3]. It is our purpose to outline the analysis for an idealized periodic modulation of the lateral properties. Such results can provide insight to the physics of the wave propagation along laterally varying tunnel structures.

Insofar as possible, the notation will be the same as used previously [1], [2] and necessary derivations will be brief.

The model we chose is depicted in Fig. 1. The air-filled circular tunnel of radius a contains a thin axial conductor of radius c offset from the center of the tunnel by a distance ρ_0. The homogeneous medium external to the tunnel has conductivity σ_e, permittivity ϵ_e, and permeability μ_e. For convenience, a cylindrical coordinate system (ρ, ϕ, z) is chosen to be coaxial with the tunnel while an associated or displaced cylindrical coordinate system (ρ', ϕ', z) is chosen to be coaxial with the axial conductor. To be specific, $\rho' = 0$ corresponds to $\rho = \rho_0$ and $\phi = \phi_0$. Within the tunnel, the air (in spite of the presence of noxious fumes) is assumed to have zero conductivity, permittivity ϵ_0, and permeability μ_0. To allow for a lateral variation of the structure, we stipulate that the effective series impedance $Z_s(z)$ of the axial conductor varies periodically throughout its length. This condition can be succinctly stated as

$$\bar{E}_z(z) = Z_s(z)I(z), \qquad \text{at } \rho' = c \tag{1}$$

where $\bar{E}_z(z)$ is the average value of the axial electric field at the surface of the conductor and $I(z)$ is the total current carried by the conductor. Actually, because of the assumed thinness of the axial conductor, this impedance condition can be applied at any convenient value of ϕ' (i.e., $\bar{E}_z(z) \cong E_z\ (\rho' = c, \phi' = 0, z)$).

The periodic property is specified by

$$Z_s(z) = Z_s(z + nd) \tag{2}$$

for all values of z where n is an integer and d is the basic period. Floquet's theorem [4] now tells us that the axial propagation constants of the discrete modes have the form $\Gamma_n = \Gamma + i(2\pi n/d)$ where Γ is the propagation constant of a basic mode. For a time factor $\exp(i\omega t)$, the axial current on the conductor can thus be written

$$I(z) = \sum_{n=-\infty}^{+\infty} I_n \exp(-\Gamma_n z) \tag{3}$$

for a given basic mode, for example, in the limiting case of a uniform conductor $I(z) = I_0 \exp(-\Gamma z)$. This case was analyzed earlier [1]. Thus we use the same type of formulation to obtain the following expression for the z component U of the

U.S. Government work not protected by U.S. copyright.

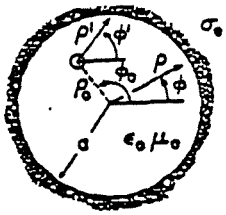


Fig. 1. Cross section of circular tunnel of radius a containing axial conductor of radius c that is offset by radial distance ρ_0 from tunnel axis.

electric Hertz vector within the tunnel:

$$U = \sum_{n=-\infty}^{+\infty} \frac{I_n}{2\pi i\epsilon_0\omega} \exp(-\Gamma_n z)\{K_0(v_n\rho') - \sum_{m=-\infty}^{+\infty} R_{m,n} \frac{K_m(v_n a)}{I_m(v_n a)} I_m(v_n\rho_0) I_m(v_n\rho) \times \exp[-im(\phi-\phi_0)]\}$$

where

$$R_{m,n} = \frac{(\gamma_0/v_n)K_m'(v_n a)/K_m(v_n a) + Y_{m,n}\eta_0 + \delta_{m,n}\eta_0}{(\gamma_0/v_n)I_m'(v_n a)/I_m(v_n a) + Y_{m,n}\eta_0 + \delta_{m,n}\eta_0} \quad (5)$$

$$\delta_{m,n} = \frac{(im\Gamma_n/a)^2[v_n^{-2} - u_n^{-2}]^2}{(\gamma_0/v_n)I_m'(v_n a)/I_m(v_n a) + (Z_{m,n}/\eta_0)} \quad (6)$$

$$Z_{m,n} = -\frac{i\mu_e\omega}{u_n}\frac{K_m'(u_n a)}{K_m(u_n a)} \quad (7)$$

$$Y_{m,n} = \frac{i\gamma_e^2}{u_n\mu_e\omega}\frac{K_m'(u_n a)}{K_m(u_n a)} \quad (8)$$

$$v_n = (\gamma_0^2 - \Gamma_n^2)^{1/2} = i(\Gamma_n^2 - \gamma_0^2)^{1/2} \quad (9)$$

$$u_n = (\gamma_e^2 - \Gamma_n^2)^{1/2} = i(\Gamma_n^2 - \gamma_e^2)^{1/2} \quad (10)$$

$$\eta_0 = (\mu_0/\epsilon_0)^{1/2} \qquad \gamma_0 = i(\epsilon_0\mu_0)^{1/2}\omega$$

$$\gamma_e = [(i\mu_e\omega)(\sigma_e + i\epsilon_e\omega)]^{1/2}.$$

It can be readily verified that

$$H_{\phi'}(c) = -i\epsilon_0\omega\left.\frac{\partial U}{\partial\rho'}\right|_{\rho'=c} \cong \frac{1}{2\pi c}\sum_{n=-\infty}^{+\infty} I_n \exp(-\Gamma_n z) \quad (11)$$

provided $c \ll a - \rho_0$.

To apply the impedance boundary condition specified by (1), we now assume that

$$Z_s(z) = \sum_{-N}^{N} Z_n \exp(-i2\pi nz/d) \quad (12)$$

where N is a finite but arbitrarily large integer and Z_n are coefficients that do not depend on z. Then, on noting that

$$E_z = (-\gamma_0^2 + \partial^2/\partial z^2)U, \quad (13)$$

and using (4), it readily follows that

$$-\frac{I_n v_n^2}{2\pi i\epsilon_0\omega}\left[K_0(v_n c) - \sum_{m=-\infty}^{+\infty} R_{m,n}\frac{K_m(v_n a)}{I_m(v_n a)}[I_m(v_n\rho_0)]^2\right] = \sum_{n'=-N}^{N} Z_{n'} I_{n-n'}. \quad (14)$$

This set of $2N + 1$ equations yields a nontrivial solution for the propagation constant Γ when the determinant of coefficients of I_n is set equal to zero. A rather extreme special case is when the axial conductor is uniform such that $Z_0 = Z_s$ and $Z_n = 0$ for $n \neq 0$. The resulting mode equation is then identical to the one obtained earlier [1].

In order to discuss the physical significance of the present general analysis, we consider the case of sinusoidal modulation of the impedance properties. Thus for example,

$$Z_s(z) = Z_s[1 + M\cos(2\pi z/d)] \quad (15)$$

where M is a spatial modulation index and d is the period. Then (14) can be written in the compact form

$$F_n I_n + I_{n+1} + I_{n-1} = 0 \quad (16)$$

where

$$F_n = \frac{2}{MZ_s}\left[\frac{v_n^2}{2\pi i\epsilon_0\omega}\Lambda_n + Z_{e,n} + Z_s\right] \quad (17)$$

$$v_n^2 = \gamma_0^2 - [\Gamma + i(2\pi n/d)]^2 \quad (18)$$

and

$$\Lambda_n = K_0(v_n c) - \sum_{m=-\infty}^{+\infty}\frac{K_m(v_n a)}{I_m(v_n a)}[I_m(v_n\rho_0)]^2 \quad (19)$$

$$\frac{2\pi Z_{e,n}}{\eta_0} = -\frac{v_n^2}{\gamma_0}\sum_{m=-\infty}^{+\infty}(R_{m,n} - 1)\frac{K_m(v_n a)}{I_m(v_n a)}[I_m(v_n\rho_0)]^2. \quad (20)$$

The quantities above have a clear physical meaning in the quasi-static limit [2] where we invoke the conditions $|v_n a| \ll 1$, $|\gamma_e/\gamma_0|^2 \gg 1$, and $\mu_e = \mu_0$. Then, we find that

$$\Lambda_n \cong \Lambda = \ln\frac{a}{c} - \sum_{m=1}^{\infty}\frac{1}{m}\left(\frac{\rho_0}{a}\right)^{2m} = \ln\frac{a}{c} - \ln\frac{a^2}{a^2 - \rho_0^2}. \quad (21)$$

If, in addition, $d = a - \rho_0 \ll a$, (21) simplifies to

$$\Lambda \cong \ln(2d/c) \quad (22)$$

provided we maintain our initial restriction that $d = a - \rho_0 \gg c$.

The quasi-static argument also yields the approximation

$$\frac{2\pi}{i\mu_0\omega} Z_{e,n} \cong \frac{2\pi}{i\mu_0\omega} Z_e = \frac{2}{\gamma_e a} \sum_{m=1}^{\infty} \left(\frac{\rho_0}{a}\right)^{2m} \frac{K_m(\gamma_e a)}{K_{m+1}(\gamma_e a)}. \tag{23}$$

These forms for Λ and Z_e were obtained earlier in the quasi-static analysis of the uniform axial conductor [2]. This suggests that, in general, $Z_{e,n}$ can be interpreted as an effective series impedance of the tunnel walls that is additive to the mean series impedance Z_s of the axial conductor.

Now, for the general case, we can deduce from (16) that

$$\frac{I_n}{I_{n\pm1}} = -\frac{1}{F_n - \dfrac{1}{F_{n\mp1} - \dfrac{1}{F_{n\mp2} - \cdots}}}. \tag{24}$$

Then, on equating the two resulting expressions for I_0/I_1, we obtain the mode equation

$$\left[F_0 - \frac{1}{F_{-1} - \dfrac{1}{F_{-2} - \dfrac{1}{F_{-3} - \cdots}}}\right] \times \left[F_1 - \frac{1}{F_2 - \dfrac{1}{F_3 - \dfrac{1}{F_4 - \cdots}}}\right] = 1. \tag{25}$$

Because F_n varies as n^2 for large n, these continued fractions converge very rapidly even for values of M as large as 1.

A particularly simple case corresponds to weak modulation wherein $M \ll 1$, and thus $I_{-1}/I_0 \cong -1/F_{-1}$ and $I_1/I_0 \cong -1/F_1$. The quasi-static form of the mode equation to determine Γ then has the relatively simple form

$$[v_0^2/(2\pi i\epsilon_0\omega)][\Lambda + Z_{eff}] = 0 \tag{26}$$

where

$$v_0^2 = \gamma_0^2 - \Gamma^2$$

$$Z_{eff} = Z_e + Z_s \left[1 - \frac{M}{2}\left(\frac{1}{F_1} + \frac{1}{F_{-1}}\right)\right] \tag{27}$$

and where

$$F_{\pm1} \cong \frac{(2\pi/d)^2}{\pi i\epsilon_0\omega}\left(1 \mp \frac{\gamma_0 d}{\pi}\right)\frac{\Lambda}{MZ_s}. \tag{28}$$

Here Z_{eff} can be interpreted as the effective total series impedance due to the ohmic wall losses in both the tunnel wall and in the periodically nonuniform center conductor. Of course (26) becomes an explicit formula to deduce Γ^2 if we write it in the equivalent form

$$\Gamma^2 = (ZY) \tag{29}$$

where

$$Z = \frac{i\mu_0\omega}{2\pi}\Lambda + Z_{eff}$$

and

$$Y = 2\pi i\epsilon_0\omega/\Lambda.$$

Here Z and Y are the effective line parameters that really only have a clear meaning within the quasi-static limit.

The general effect of the spatial modulation is to increase the attenuation of the basic propagation mode by virtue of energy converted into the Floquet harmonics. Also, at least for modulation periods less than the radio wavelength, the phase velocity of the basic mode is decreased.

The present approach can be adapted readily to study a random variation of the series impedance of the center conductor. Also, with some modification, lateral variations of the conductivity of the tunnel wall material can be encompassed. Finally, by using a similar formulation, the center conductor can be replaced by a coaxial cable that can have an outer braid with a spatially modulated transfer impedance. This particular configuration is useful in leaky feeder type communications [3] where the nonuniform braid can be designed to optimize the mode conversion between the modes in the tunnel that are internal and external to the braided sheath of the cable.

REFERENCES

[1] J. R. Wait and D. A. Hill, "Guided electromagnetic waves along an axial conductor in a circular tunnel," *IEEE Trans. Antennas Propagat.*, vol. AP-22, pp. 627-630, July 1974.

[2] J. R. Wait, "Quasi-static limit for the propagating mode along a thin wire in a circular tunnel," *IEEE Trans. Antennas Propagat.*, vol. AP-25, pp. 441-443, May 1977.

[3] L. Deryck, "Radio communications in tunnels," *Electron. Lett.*, vol. 8, pp. 71-72, Feb. 1972.

[4] R. E. Collin, *Field Theory of Guided Waves*. New York: McGraw-Hill, 1960.

Radiation Characteristics of a Dielectric Sphere Loaded Corrugated *E*-Plane Sectoral Horn

A. K. KAMAL, FELLOW, IEEE, S. C. GUPTA, AND R. A. NAIR

Abstract—The experimental results of the radiation characteristics of a dielectric sphere in front of a corrugated *E*-plane sectoral horn together with the design aspects of the horn are reported. The experiments were carried out with the test antenna system consisting of dielectric (paraffin wax) spheres kept offset at the minimum input VSWR position in front of the horn excited in the balanced HE_{11} mode. The test results have shown that such a feed system produces radiation patterns with reduced sidelobe levels and increased on-axis gain with reduced 3-dB beamwidths as compared to the same horn radiating in free space. The feed system may also produce a low input VSWR and can be used as a variable beamwidth feed for praraboloidal reflectors.

Manuscript received June 9, 1976; revised September 26, 1976.

The authors are with the Department of Electronics and Communication, University of Roorkee, Roorkee (U.P.), India.

0018-926X/78/0700-0625 $00.75 © 1978 IEEE

INTRODUCTION

The desirable features of dielectric loaded waveguides have been reported earlier [1]-[3]. Recently, it has been established that a dielectric sphere-mounted circular waveguide [4] and dielectric sphere-mounted corrugated pipe [5] have superior radiation characteristics with higher directivity and low sidelobe levels compared to those of an optimum horn of the same aperture. Here, the authors report the promising results of an experimental investigation into the radiation characteristics of an improved feed system having increased directivity and low sidelobe levels with variable beamwidth facility for paraboloidal reflector antennas for possible applications in satellite communication and radio astronomy.

THEORY

The geometry of the feed system is shown in Fig. 1. The paraffin wax ($\epsilon_r = 2.25$) sphere of radius a_1 is placed at an offset position for minimum input VSWR, in front of the corrugated E-plane sectoral horn. The dielectric sphere placed in front of the horn will act as a microwave lens illuminated by an aperture source. A corrugated sectoral horn was designed to have the corrugation specifications ($h = 1.3$ cm, $t = w = 0.15$ cm) and horn specifications ($\alpha_0 = 15^\circ$, $b = 5.2$ cm, $a = 2.28$ cm) so as to realize an impedance boundary from the corrugated surface required for the analysis of the fields in the axial region of the horn and to support a balanced HE_{11} mode. The corrugations were introduced only after a certain distance (≈ 1.5 cm) from the horn throat so as to obtain a low input VSWR.

EXPERIMENTAL RESULTS AND DISCUSSIONS

The corrugated horn was fabricated using the above specifications. Experiments were performed with parrafin wax ($\epsilon_r = 2.25$) spheres with diameters of 9 cm, 6 cm, and 4 cm placed offset in front of the sectoral horn excited in the balanced HE_{11} mode at an operating frequency of 8.64 GHz. The sphere offset positions were determined experimentally for the low input VSWR performance [7], and the optimum offset positions were found to lie between 1.1 cm and 1.4 cm from the horn aperture for the three sphere sizes tested. The E-plane and H-plane radiation patterns of the system for different sphere diameters were obtained, and are shown in Figs. 2 and 3 together with those for the corrugated sectoral horn alone. The gain of the antenna system was determined experimentally by the substitution method with a standard antenna of known gain (pyramidal horn of gain 52), and the measured values of gain are checked by the approximate formula $G = 41253/\theta_E\theta_H$, where θ_E and θ_H are the 3-dB beamwidths in degrees in the E-plane and H-plane, respectively. The results of the determined gain of the system are plotted in Fig. 4 as a function of the dielectric sphere diameter in wavelengths. The gain of the E-plane sectoral horn without dielectric sphere loading is also shown for comparison. The on-axis gain of the system increases in excess of 2 dB over that available from the corrugated E-plane sectoral horn of the same dimensions. From the experimental results it is obvious that the dielectric sphere loading reduces the sidelobe levels, particularly for dielectric spheres with diameters of two wavelengths or less. The system also has reduced 3-dB beamwidth and input VSWR.

It is concluded that the test feed system can be used as a variable beamwidth feed with increased directivity, low input VSWR, and low sidelobe levels for paraboloidal reflector antennas for special applications in radio astronomy and satellite communication.

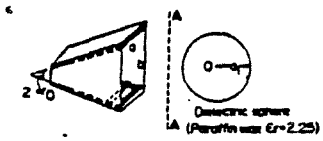


Fig. 1. Geometry of sphere loaded corrugated horn. $2\alpha_0$ = horn flare angle; A, A = arbitrary location of sphere; a, b = horn aperture dimensions.

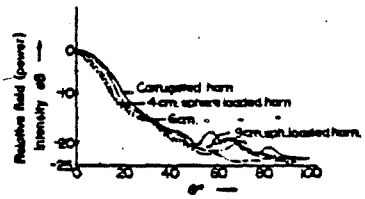


Fig. 2. E-plane radiation patterns (patterns measured at f_0 = 8.64 GHz).

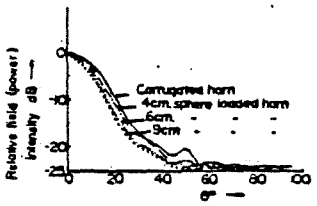


Fig. 3. H-plane radiation patterns (patterns measured at f_0 = 8.64 GHz).

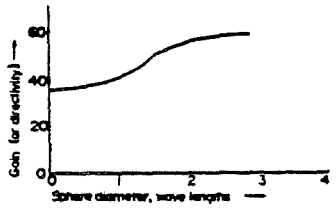


Fig. 4. Gain as function of sphere diameter.

REFERENCES

[1] J. S. Chatterjee and W. F. Crosswell "Waveguide excited dielectric sphere as feeds," *IEEE Trans. Antennas Propagat.*, pp. 206-208, Mar. 1972.

[2] M. A. K. Hamid and S. I. Towaij "A dielectric loaded circular waveguide antenna," *IEEE Trans. Antennas Propagat.*, pp. 96-97, 1972.

[3] P. S. Neelakanta Swamy and D. K. Banerjie "Radiation characteristics of a waveguide excited dielectric sphere backed by a metallic hemisphere," *IEEE Trans. Antennas Propagat.*, pp. 384-385, 1973.

[4] W. F. Crosswell, J. S. Chatterjee, V. B. Mason, and C. T. Tai "Radiation from a homogeneous sphere mounted on a waveguide aperture," *IEEE Trans. Antennas Propagat.*, pp. 647-654, Sept. 1975.

[5] P. S. Neelakanta Swamy and D. K. Banerjee, "Radiation characteristics of a dielectric sphere loaded corrugated pipe," *IEEE Trans. Antennas Propagat.*, pp. 728-730, Sept. 1975.

[6] M. S. Narasimhan and V. Venketaswara Rao, "Radiation characteristics of corrugated E-plane sectoral horn," *IEEE Trans. Antennas Propagat.*, pp. 321-327, May 1973.

[7] A. G. Martin, A. J. A. Oxtoby "Waveguide fed spherical dielectric antennas," *IEEE Trans. Antennas Propagat.*, pp. 338-340, Mar. 1974.

690 IEEE TRANSACTIONS ON ANTENNAS AND PROPAGATION, VOL. AP-26, NO. 5, SEPTEMBER 1978

Role of Controlled Mode Conversion in Leaky Feeder Mine Communication Systems

DAVID B. SEIDEL, MEMBER, IEEE, AND JAMES R. WAIT, FELLOW, IEEE

Abstract—Using an idealized model, we consider VHF wave transmission in a straight mine tunnel that contains a braided coaxial cable. The controlled interchange of energy between the propagation modes can be used to optimize the communication range and allow for coupling to and from portable hand-held antennas. In particular, we show that the optimum lengths for maximum transmission through the leaky cable sections or mode converters predicted here are compatible to those predicted by approximate coupled mode theory.

INTRODUCTION

RECENTLY, the leaky feeder concept has been utilized effectively in intramine communications [1], [2]. It had been previously found that such a system using a braided coaxial cable will propagate two low-frequency transmission line modes [3]. One of these eigen modes (defined here as the monofilar mode) is readily excited from an arbitrary point within the tunnel but suffers high attenuation because the return current flows mainly in the tunnel wall. Conversely, the other eigen mode (defined here as the bifilar mode) has low attenuation because the return current flows mostly in the sheath; but it is poorly excited for an external source in the tunnel. Thus, for an efficient limited access communication system, it is desirable to convert energy from one mode to the other. Such mode conversion can be obtained through insertion of axial nonuniformities in the coaxial line or within the tunnel environment. In this paper, transmission line techniques are used to develop a theory of controlled mode conversion for a braided coaxial cable in a semicircular tunnel. The formulation will also account for the ohmic losses of the tunnel wall as well as the spatially dispersive form of the braid transfer impedance.

The specific type of nonuniformity considered here is when the cable has a section of higher leakage. The case of a number of such uniformly spaced sections is also analyzed. This configuration can be used in practical mine-communication systems wherein the roving miners may use portable walkie-talkie type transceivers.

Manuscript received November 22, 1977; revised May 1, 1978.

The authors are with the Cooperative Institute for Research in Environmental Sciences, University of Colorado/NOAA, Boulder, CO 80309.

FORMULATION

The model assumed is described in terms of a cylindrical coordinate system (ρ, ϕ, z) and is shown in Fig. 1. The tunnel wall is located at $\rho = a_0$ for $0 < \phi < \pi$, and the assumed perfectly conducting tunnel floor is located at $\phi = 0$ and $\phi = \pi$ for $0 < \rho < \infty$. The region defined by $\rho > a_0$ and $0 < \phi < \pi$ is a homogeneous medium with conductivity σ_e and permittivity ϵ_e. The coaxial cable with outside radius c is centered at $\rho = \rho_0$ and $\phi = \phi_0$. The region defined by $\rho < a_0$, $0 < \phi < \pi$, and $\rho' > c$, where ρ' is the radial component of a cylindrical coordinate system (ρ', ϕ', z) centered at (ρ_0, ϕ_0), is described by the free space permittivity and permeability ϵ_0 and μ_0, respectively. The geometry of the coaxial cable is shown in Fig. 2. The inner conductor of radius a has a high but finite conductivity σ_w. The surrounding insulation of radius b is a lossless dielectric with permittivity ϵ. The braided sheath located at $\rho' = b$ is characterized by a surface transfer impedance Z_T. The outer dielectric coating has radius c and permittivity ϵ_c. We also allow for the possibility that a thin lossy film is located at $\rho' = c$ which is characterized by a transfer impedance Z_L. We assume that the fields of each mode of this structure vary as $\exp(-\Gamma z + i\omega t)$, where ω is the angular frequency

0018-926X/78/0900-0690$00.75

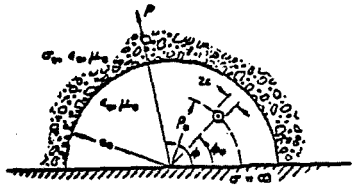


Fig. 1. Cross section of semicircular tunnel containing coaxial cable (not to scale).

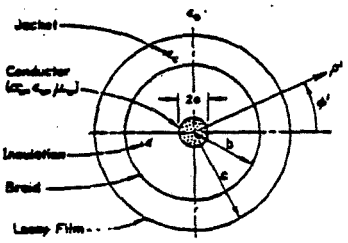


Fig. 2. Braided coaxial cable.

and Γ is the complex propagation constant for the particular mode.

In a previous paper [4], we obtained a quasistatic mode equation for the low-frequency quasi-TEM modes for this structure. There it was found that, in general, there are three distinct modes of this type. The corresponding propagation constants Γ_j were found to be the roots of a cubic equation with complex coefficients. In the special case where the lossy film layer is absent, there are only two modes, whose propagation constants are obtained from a quadratic equation. In each case, two modes can be identified as the well-known monofilar and bifilar modes. The third mode, when it exists, is referred to as the jacket mode [4].

Because the dominant low-frequency modes of this system behave like TEM transmission-line modes, it is useful to treat the problem as a multiconductor transmission line using transmission line concepts. For this purpose, characteristic impedances have been previously derived [4] for each line. Slightly modified expressions for those impedances are given as follows:

$$K_L = \left(\frac{1+P+Q}{Q}\right)\frac{\Gamma \ln R}{N},$$

$$K_s = \Gamma\left[(1+P+Q)\frac{\ln R}{N} + (1+P)\alpha_c\right],$$

and

$$K_l = \Gamma\left[\left(\frac{1+P+Q}{P}\right)\frac{\ln R}{N} + \left(\frac{1+P}{P}\right)\alpha_c + \alpha'\right] \tag{1}$$

are the impedances associated with the lossy film, the braided sheath, and the inner conductor, respectively. The current ratios P and Q are defined by

$$P \equiv \frac{I_l}{I_s} = \frac{Z_T(\Gamma)}{Z'(\Gamma) + Z_l}$$

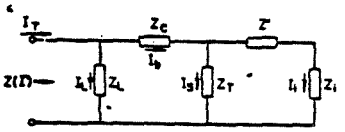


Fig. 3. Equivalent network which yields effective series impedance of cable in quasi-static approximation.

and

$$Q \equiv \frac{I_L}{I_s} = (1+P)\left[\frac{Z_b(\Gamma) + Z_c(\Gamma)}{Z_L}\right] \tag{2}$$

where I_L, I_s, I_l are the currents on each conductor (see Fig. 3). Other factors in (1) and (2) are defined in [4].

The characteristic impedances defined by (1) are dependent upon Γ, and consequently they assume different values for each mode. Thus we have $K_L^{(j)}$, $K_s^{(j)}$, and $K_l^{(j)}$ corresponding to the propagation constant of each mode Γ_j for $j = 1, 2, 3$. In the special case when there is no lossy film (i.e., $\alpha d = 0$), I_L vanishes, and we consider only the two characteristic impedances $K_s^{(j)}$ and $K_l^{(j)}$ for $j = 1, 2$.

These characteristic line impedances can be used in conjunction with transmission line concepts to consider axial nonuniformities or discontinuities in the tunnel/cable system. For example, the cable could be loaded by discrete shunt or series loads. Alternatively, there could be a short length of the tunnel in which tunnel and/or cable parameters change value, either intentionally or nonintentionally. Here we will specifically consider the case in which the value of the braid transfer impedance is changed over a short length (l) along the line. This corresponds in some sense to the mode converters suggested for use in tunnels by Deryck [5] and Delogne [1] who employed approximate coupled mode theory. Our multimode formulation is similar to that used by Wait and Hill [6] for analyzing the shunt loading on a two-wire system in a mine tunnel.

The geometry for this case is shown schematically in Fig. 4. In regions I and III, we have a sheath transfer inductance L_T, and the transmission characteristics in these regions are given by Γ_j, P_j, Q_j, $K_L^{(j)}$, $K_s^{(j)}$, and $K_l^{(j)}$. Similarly, region II is characterized by the sheath transfer inductance $\hat{L}_T$ as well as $\hat{\Gamma}_j$, $\hat{P}_j$, $\hat{Q}_j$, $\hat{K}_L^{(j)}$, $\hat{K}_s^{(j)}$, and $\hat{K}_l^{(j)}$. The line is excited by incident kth mode which impinges from the negative z direction. If we think of this as a junction problem, we will correspondingly expect a reflected wave in region I and a transmitted wave in region III, each containing all modes. Similarly, a forward and reverse traveling wave will be excited in region II. Thus we express the line currents and voltages in terms of reflection and transmission coefficients, as follows:

$$I_\alpha^{(k)}(z) = \begin{cases} I_k\left[W_\alpha^{(k)} \exp(-\Gamma_k z) - \sum W_\alpha^{(j)} R_{jk} \exp(\Gamma_j z)\right], \\ \qquad z < 0 \\ I_k \sum \hat{W}_\alpha^{(j)}\left[A_{jk} \exp(-\hat{\Gamma}_j z) - B_{jk} \exp(\hat{\Gamma}_j (z-l))\right], \\ \qquad 0 < z < l \\ I_k \sum W_\alpha^{(j)} T_{jk} \exp(-\Gamma_j (z-l)), \\ \qquad z > l \end{cases} \tag{3}$$

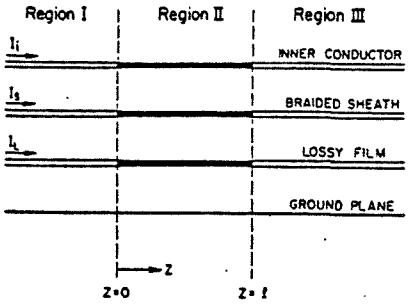


Fig. 4. Schematic diagram of multiconductor transmission line model of mode converter of length l.

$$V_\alpha^{(k)}(z) = \begin{cases} I_k[W_\alpha^{(k)}K_\alpha^{(k)}\exp(-\Gamma_k z) + \sum W_\alpha^{(j)}K_\alpha^{(j)}R_{jk}\exp(\Gamma_j z)], & z<0 \\ I_k\sum \hat{W}_\alpha^{(j)}\hat{K}_\alpha^{(j)}[A_{jk}\exp(-\hat{\Gamma}_j z) + B_{jk}\exp(\hat{\Gamma}_j(z-l))], & 0<z<l \\ I_k\sum W_\alpha^{(j)}K_\alpha^{(j)}T_{jk}\exp(-\Gamma_j(z-l)), & z>l \end{cases} \quad (4)$$

where α represents L, s, or i denoting the various conductors. The Σ denotes the sum over j of all modes and I_k is the incident sheath current in the kth mode at $z = 0$. R_{jk} and T_{jk} are the coefficients for the reflection and transmission into the jth mode due to an incident kth mode. Similarly, A_{jk} and B_{jk} are the coefficients for the forward and reverse traveling waves in region II. $W_\alpha^{(j)}$ represents 1, P_j, or Q_j for $\alpha = s$, i, or L, respectively.

In order to solve for these reflection and transmission coefficients, it is necessary to enforce the continuity of each current and voltage given by (3) and (4) at $z = 0$ and $z = l$. This results in a linear system of 12 equations and 12 unknowns (or 8 equations and 8 unknowns if $\sigma d = 0$) for each incident mode. The coefficients are then obtained by inverting the linear system using standard matrix techniques.

Actually, the structure we have described is a mode converter and its reflection and transmission coefficients are parameters which characterize its properties as a converter. For communications purposes, it is desirable for such converters to behave as forward directional couplers, and to couple energy from one forward-traveling mode to another at a rate determined by the particular application [7].

Before presenting some numerical examples, it is worthwhile to consider one important limiting case, that is, where $L_T = 0$. Now the cable braid is perfectly conducting, and the interior and exterior problems are decoupled. For the interior region, we have one coaxial cable mode (the bifilar mode). For this mode, $P = -1$ and $Q = 0$. Thus, from (1), we find that for the bifilar mode $QK_L = K_s = 0$. Similarly, for the exterior region, we have two modes (the monofilar and jacket modes). For each of these modes, $P = 0$, and thus $PK_l = K_s$.

NUMERICAL RESULTS

In what follows, we adopt the convention that modes 1, 2, and 3 denote the monofilar, bifilar, and jacket modes, respectively. It was previously found that for typical values of σd, the attenuation rate of mode 3 (jacket mode), was orders of magnitude larger than that of modes 1 or 2 [4]. Thus, for all practical purposes, the propagation effects of this mode are negligible. However, it is conceivable that significant amounts of energy could be converted to mode 3 from modes 1 and 2. Although the propagation effects of this energy can be ignored, the corresponding loss of energy in the other two modes may be significant. Consequently, in what follows, whilst the coefficients R_{ij} and T_{ij} for $i, j = 1, 2$ are of primary interest, the possible influence of the jacket mode is allowed for.

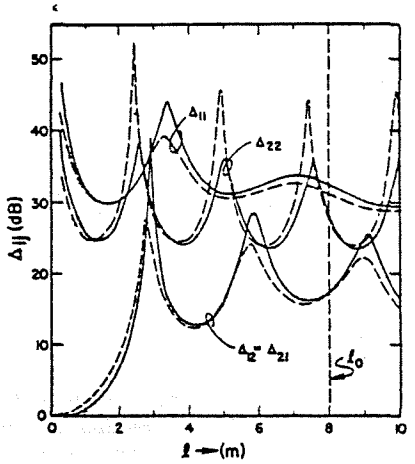


Fig. 5. Transmission-reflection ratio as function of converter length. $\sigma d = 0.1$ mho: ——; $\sigma d = 0$: - - -.

In the examples given here, we have chosen the following typical tunnel parameters: $f = \omega/2\pi = 36$ MHz, $a_0 = 2.0$ m, $\rho_0 = 1.8$ m, $\phi_0 = 45^\circ$, $\epsilon_e = 10\,\epsilon_0$, $\sigma_e = 10^{-2}$ mho/m, $a = 1.5$ mm, $b = 1.0$ cm, $c = 1.15$ cm, $\epsilon = 2.5\,\epsilon_0$, $\epsilon_c = 3.0\,\epsilon_0$, $\sigma_w = 5.7 \times 10^7$ mho/m, and $\psi = 45^\circ$.

We define the transmission-reflection ratio Δ_{ij} by

$$\Delta_{ij} = 20\log_{10}|T_{ij}/R_{ij}|.$$

Since we would like the mode converter to behave as a forward directional coupler, it is desirable to maximize Δ_{ij}. Fig. 5 shows the values of this parameter as a function of the segment length (l) of the converter. In this case, $L_T = 1.0$ nH/m and $\hat{L}_T = 100$ nH/m. Values are given for both $\sigma d = 0.1$ mhos and $\sigma d = 0$.

We find that there are converter lengths which maximize Δ_{ij} (and thus minimizing R_{ij}) for various i and j. It is also noted in Fig. 5 that the presence of lossy film does not have much effect on the value of these optimum lengths; however, it does appreciably affect the values at these peaks. We see that the lossy film reduces cross reflections (R_{12} and R_{21}) but increases self reflections (R_{11} and R_{22}). Also note that Δ_{12} is equal to Δ_{21}. This can be explained easily using reciprocity arguments, although, in general, for our mode normalizations $T_{12} \neq T_{21}$ and $R_{12} \neq R_{21}$.

Actually, in practical applications, it is particularly important to maximize Δ_{12}. Thus, for example, suppose that we have mode converters equally spaced along the length of the tunnel. Then, since the attenuation of mode 1 is higher than that of mode 2, a signal converted to mode 1 from mode 2 (via T_{12}) will attenuate faster than that transmitted to mode 2.

Thus, at some point down the tunnel, this signal in mode 1 will become smaller than the signal reflected by the next converter from mode 2 into mode 1 (via R_{12}). Since the reflected signal is out of phase with the transmitted signal, it is essentially interference. Thus Δ_{12} determines the distance between consecutive converters over which the reflected wave produces negligible interference.

Two other useful parameters are defined by

$$I_j = -20 \log_{10} |T_{jj}|$$

and

$$C = -20 \log_{10} |T_{21} T_{12}|$$

where I_j is the insertion loss in the jth mode in dB and C is the coupling loss in dB. C is important because, in a practical problem, the initial excitation will be predominately in mode 1 (monofilar). At a sufficiently large distance from this excitation, the predominant signal will be one which was converted to mode 2 (bifilar) by the first encountered converter, and then converted back to mode 1 at one of the following converters. Thus C represents the loss associated with this double conversion. Indeed this doubly converted signal will be dominant for distances (in meters) such that $C + \alpha_2 z < \alpha_1 z$ where $\alpha_j = 8.686$ Real (Γ_j) is the attenuation rate of the jth mode in dB/m.

Fig. 6 shows the insertion loss for the same parameters as in Fig. 5. Also, plotted is the curve $\alpha_j l$ which represents the attenuation of the same length of cable in the absence of the converter. Note that the insertion loss is to a large extent determined by this quantity, particularly for mode 1.

Fig. 7 shows the coupling loss for the same parameters. An additional curve is shown for different values of sheath transfer inductance (L_T = 2nH/m, $\hat{L}_T$ = 40 nH/m). As one would expect, the coupling loss increases as the length of the converter is decreased, and also as the contrast between the two cable types decreased. Note that there is in each case a length l which minimizes this loss. Delogne [6] has computed such a length using approximated coupled mode theory. His optimum length for maximum transmission coupling is given by $l_0 = \pi/(\beta_2 - \beta_1)$, where $\beta_j = \text{Im}\,(\Gamma_j)$ is the phase constant of the jth mode. This value is shown in Fig. 7 for L_T = 1 nH/m, $\hat{L}_T$ = 100 nH/m. It can be seen that this estimate by Delogne is relatively accurate for the model we have adopted. Note, however, that the simultaneous minimization of C and maximization of Δ_{12} is not, in general, possible (see Fig. 5).

Finally, we consider the case where identical converters are evenly spaced along the tunnel with period D. If the reflections from one of the converters are small, they can be neglected, and we can assume that the converters will not couple with one another. In a practical application, this system would be driven by a hand-held transmitter in the tunnel region. We choose a relatively analogous excitation to be a voltage source between the tunnel floor and the cable's braided sheath. This source is arbitrarily located between two converters at $z = -z_0$ (see Fig. 8). Similarly, signals will be received by a hand-held receiver in the tunnel region, and thus will be proportional to the field strength in this region. Since the fields outside the cable are proportional to the total axial current in the cable ($I_T = I_L + I_s + I_i$), we will compute $I_T(z)$ for each mode for this periodically loaded line.

Since the phase velocity of the two modes are different, signals traveling down the tunnel by different paths will, in general, have different phases. The strongest "signal" can be properly thought of as the desired signal, and the remaining weaker "signals" resulting from the different paths must be thought of as interference or noise. Similarly, reflected signals must also be thought of as interference.

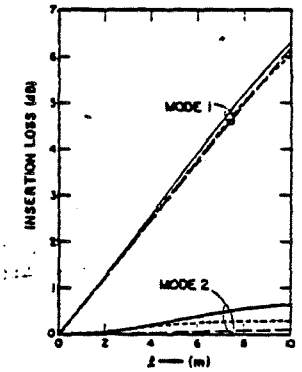


Fig. 6. Insertion loss as function of converter length. σd = 0.1 mho: ——; σd = 0: - - -; $\alpha_j l$: —— ——.

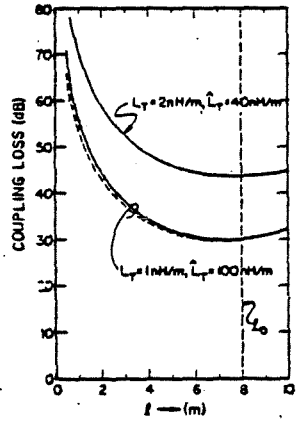


Fig. 7. Coupling loss as function of converter length. σd = 0.1 mho: ——; σd = 0: - - -.

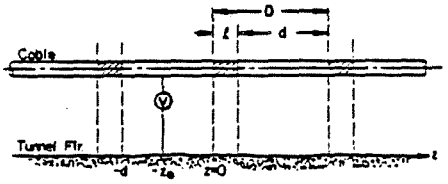


Fig. 8. Schematic diagram of uniformly spaced mode converters.

The voltage source at $z = -z_0$ will excite both the monofilar and bifilar modes. If we ignore the reflections from mode converters and neglect the coupling to the jacket mode, the following expression can be obtained for the relative strengths of the two incident modes at $z = 0$:

$$\frac{I_T^{(2)}(0)}{I_T^{(1)}(0)} = -\left(\frac{K_s^{(1)} - P_1 K_i^{(1)}}{K_s^{(2)} - P_2 K_i^{(2)}}\right)\left(\frac{1 + P_2 + Q_2}{1 + P_1 + Q_1}\right) \cdot \exp\left[(\Gamma_1 - \Gamma_2) z_0\right]. \quad (5)$$

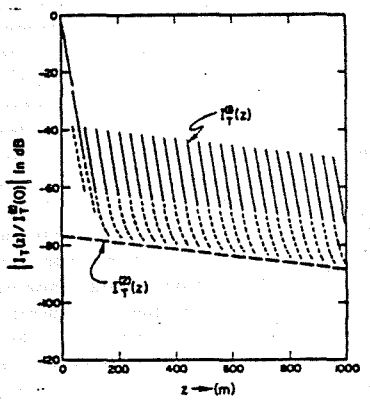


Fig. 9. Total axial current on uniformly loaded line. Dominant signal in modes 1 and 2: ——; interference in mode 1: - - -.

Note that, as expected, when $L_T = 0$, the bifilar mode is not excited and this ratio is zero.

Fig. 9 shows the total current in the monofilar and bifilar modes as a function of z for periodically spaced converters, each of which is described by the parameters in Fig. 5 with $\alpha d = 0.1$ mho. The converter length l was chosen to be 2.94 m, corresponding to a maximum of Δ_{12} (i.e., see Fig. 5). The separation between converters (D) was chosen to be 39.73 m. This choice was made in order that the ratio of signal to interference in the monofilar mode be the same immediately preceding and after the third converter (i.e., at $z = 2D$ and $z = 2D + l$).

Note that because of the difference in the attenuation rates of the two modes, (5) is dependent upon z_0 and assumes its largest value for $z_0 = d$. Even in this instance, for the data given in Fig. 9, its value is −92 dB, which is seen to be negligible compared to the current in the bifilar mode resulting from conversion from mode 1 to mode 2 at the first mode converter which is at −77 dB. Thus, although not shown in Fig. 9, the interference in mode 2 is at least 15 dB below the dominant signal.

We see from Fig. 9 that the dominant signal in the monofilar mode is the original incident signal preceding the first three converters, but after the third converter, the dominant signal is that converted from the bifilar mode by the previous converter. Also, note that the monofilar interference immediately preceding each converter is a reflected wave from the bifilar mode, illustrating the importance of maximizing Δ_{12}. Finally, we see that, because fields in the tunnel are proportional to the total current, the received signal will essentially be the dominant monofilar mode signal, and the bifilar mode currents must be thought of as additional interference.

We may generalize these results to similar systems in which the initial excitation is predominantly in the monofilar mode. We find that for large z, $I_T^{(1)}$ is bounded by (in dB)

$$|I_T^{(1)}|^{\max} = -C - \alpha_2 z$$

and

$$|I_T^{(2)}|^{\min} = -C - \alpha_1 l - \alpha_2 (z - l) \tag{6}$$

for $z > C/(\alpha_1 - \alpha_2)$. For small z, $I_T^{(1)}$ is given approximately (in dB) by

$$|I_T^{(1)}| \cong -\alpha_1 z \tag{7}$$

for $z < C/(\alpha_1 - \alpha_2)$.

CONCLUDING REMARKS

Using an idealized model, we have confirmed the general principle of leaky feeder systems as promulgated by Delogne [1] and his colleagues. The concept that such systems can be designed on the basis of controlled rather than inadvertent mode conversion would seem to be very important [7]. But, of course, there will always be a certain amount of spurious or nonintentional mode conversion due to irregularities in the tunnel wall such as ribs and other changes in the cross section. Actually, within the frame work of our theory, lateral changes in the effective surface impedance of the tunnel wall can be taken into account. This certainly remains as an important task for further work.

ACKNOWLEDGMENT

We are grateful for the useful and cogent comments from Prof. Paul Delogne.

REFERENCES

[1] P. Delogne, "Basic mechanisms of tunnel propagation," *Radio Sci.*, vol. 11, pp. 295–303, Apr. 1976.
[2] S. F. Mahmoud and J. R. Wait, "Calculated channel characteristics of a braided coaxial cable in a mine tunnel," *IEEE Trans. Commun.*, vol. COM-24, pp. 82–87, Jan. 1976.
[3] J. R. Wait and D. A. Hill, "Propagation along a braided coaxial cable in a circular tunnel," *IEEE Trans. Microwave Theory Tech.*, vol. MTT-23, pp. 401–405, May 1975.
[4] D. B. Seidel and J. R. Wait, "Transmission modes in a braided coaxial cable and coupling to a tunnel environment," submitted to *IEEE Trans. Microwave Theory Tech.*, vol. MTT-26, July 1978.
[5] L. De.yck, "Control of mode conversions on bifilar line in tunnels," *The Radio and Electronic Eng.*, vol. 45, pp. 241-247, May 1975.
[6] J. R. Wait and D. A. Hill, "Analysis of the dedicated communication line in a mine tunnel for a shunt-loaded trolley wire," *IEEE Trans. Commun.*, vol. COM-26, pp. 355–361, Mar. 1978.
[7] J. R. Wait, Ed., "Electromagnetic guided waves in mine environments" in Proceedings of a Workshop held in Boulder, Mar. 28–30 1978, sponsored by the U.S. Bureau of Mines, Contract No. HO155008. Document available from NTIS.

Mode Conversion by Tunnel Nonuniformities in Leaky Feeder Communication Systems

DAVID B. SEIDEL, MEMBER, IEEE, AND
JAMES R. WAIT, FELLOW, IEEE

Abstract—Using an idealized theoretical model, the inadvertent mode conversion between the bifilar and monofilar modes are dealt with in a tunnel that contains a braided coaxial cable. The tunnel is allowed to have various kinds of lateral nonuniformities such as changes of wall conductivity and permittivity. We conclude that such effects are very important in understanding leaky feeder systems.

Manuscript received September 20, 1978; revised January 24, 1979.

D. B. Seidel is with the Cooperative Institute for Research in Environmental Sciences, University of Colorado, Boulder, CO 80309.

J. R. Wait is with the Cooperative Institute for Research in Environmental Sciences, University of Colorado, Boulder, CO 80309, and is a consultant to the Institute for Telecommunications Sciences, National Telecommunications and Information Administration, U.S. Department of Commerce, Boulder, CO 80302.

INTRODUCTION

The leaky feeder concept has been utilized effectively in intra-mine communications [1], [2]. Previously, it was found that such a system using a braided coaxial cable will propagate two low frequency transmission line modes [3]. One of these eigen modes (i.e., the monofilar mode) is readily excited from an arbitrary point within the tunnel but suffers high attenuation because the return current flows mainly in the tunnel wall. The other eigen mode (i.e., the bifilar mode) has low attenuation because the return current flows mostly in the sheath; but it is poorly excited for an external source in the tunnel. Thus, for an efficient limited access communication system, it is desirable to convert energy from one mode to the other. Such mode conversion can be obtained through intentional insertion of axial nonuniformities in the coaxial line or within the tunnel environment. Alternately, such conversion may occur inadvertently due to existing nonuniformities along the tunnel's length. In an earlier paper [4], transmission line techniques were used to develop a theory of controlled mode conversion for a braided coaxial cable in a semicircular tunnel. Specifically, we had considered a cable that contains a short section of higher leakage corresponding to the "leaky stub" converter suggested by Delogne [1].

In the present sequel, we consider mode conversion of the inadvertent type, but we shall make use of the previous formulation [4]. Such results are relevant to mine communication systems, using the continuous leaky feeder concept [5], which rely mainly upon such inadvertent mode conversion for their operation. However, this point of view has not been universally adopted by the leaky feeder community.

FORMULATION

The model assumed is described in terms of a cylindrical coordinate system (ρ, ϕ, z) and is shown in Fig. 1. The tunnel wall is located at $\rho = a_0$ for $0 < \phi < \pi$, and the assumed perfectly conducting tunnel floor is located at $\phi = 0$ and $\phi = \pi$ for $0 < \rho < \infty$. The region defined by $\rho > a_0$ and $0 < \phi < \pi$ is a homogeneous medium with conductivity σ_e and permittivity ϵ_e. The coaxial cable with outside radius c is centered at $\rho = \rho_0$ and $\phi = \phi_0$. The region defined by $\rho < a_0$, $0 < \phi < \pi$, and $\rho' > c$, where ρ' is the radial component of a cylindrical coordinate system (ρ', ϕ', z) centered at (ρ_0, ϕ_0), is described by the free space permittivity and permeability ϵ_0 and μ_0, respectively. The geometry of the coaxial cable is shown in Fig. 2. The inner conductor, of radius a, has a high but finite conductivity σ_w. The surrounding insulation of radius b is a lossless dielectric with permittivity ϵ. The braided sheath located at $\rho' = b$ is characterized by a surface transfer impedance Z_T. The outer dielectric coating has radius c and permittivity ϵ_c. We also allow for the possibility that a thin lossy film is located at $\rho' = c$ which is characterized by a transfer impedance $Z_L = (2\pi c(\sigma d))^{-1}$ where σd is the conductivity-thickness product of the lossy layer. We assume that the fields of each mode of this structure vary as $\exp(-\Gamma z + i\omega t)$ where ω is the angular frequency and Γ is the complex propagation constant for the particular mode.

In a previous paper [6] we obtained a quasistatic mode equation for the low frequency quasi-TEM modes for this structure. There it was found that, in general, there are three distinct modes of this type. The corresponding propagation

0018-926X/79/0700-0560$00.75

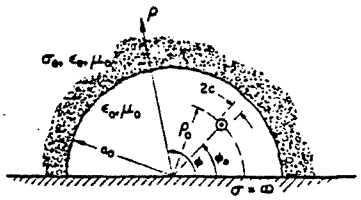


Fig. 1. Cross section of semicircular tunnel containing coaxial cable.

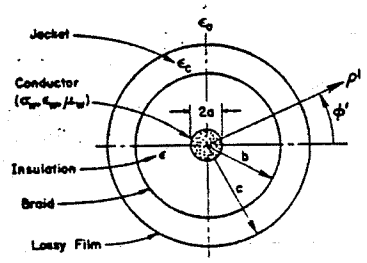


Fig. 2. Braided coaxial cable.

constants Γ_j were found to be the roots of a cubic equation with complex coefficients. In the special case where the lossy film layer is absent, there are only two modes, whose propagation constants are obtained from a quadratic equation. In each case, two modes can be identified as the well-known monofilar and bifilar modes. The third mode, when it exists, is referred to as the jacket mode [6].

Because the dominant low frequency modes of this system behave like TEM transmission-line modes, we can use transmission-line concepts to consider the effects of axial discontinuities along the extent of the tunnel [4]. This is accomplished by defining characteristic impedances which relate the currents and voltages on the various conductors present. These voltages and currents are then expressed in terms of incident, reflected, and transmitted waves on each side of any discontinuity, and associated coefficients of reflection and transmission between various modes are obtained by enforcing Kirchoff's voltage and current laws at the discontinuity. It goes without saying that this quasi-static approach is valid only in an approximate sense since higher order evenescent modes are neglected.

A solution for the reflection and transmission matrices $\bar{R}$ and $\bar{T}$ was obtained earlier [4] for the case of a tunnel containing a section of length l over which some physical characteristic of the tunnel was different from that in the remainder of the tunnel. Although the method was applied there only to one type of intentional converter, it is also suited to the consideration of many types of inadvertent mode conversions, such as uniform discontinuities of wall permittivity or conductivity. However, before pursuing these extensions, it is worthwhile to extend somewhat the previous quasi-static analysis [4].

It is well-known [7] by the reciprocity theorem, that for reciprocal, isotropic media, the reflection and transmission matricies $\bar{R}$ and $\bar{T}$ defined in [4] will be symmetric if the modes are normalized such that the power flow in the various modes are equal. However, in [4], the modes were normalized by the rather arbitrary convention that the current on the coaxial braid (I_s) be of unit amplitude for all modes and consequently the matrices are not symmetric. Henceforth, we will denote the nonsymmetric reflection and transmission matrices associated with this normalization by $\bar{R}'$ and $\bar{T}'$.

Now we define a new mode normalization by the convention that $I_s^{(j)} = a_j$ where $I_s^{(j)}$ is the coaxial braid current in the jth mode and $\{a_j\}$ are complex constants. We will constrain $\{a_j\}$ by demanding that the matrices $\bar{R}$ and $\bar{T}$ associated with this normalization be symmetric. Since [4] provides a solution for $\bar{R}'$ and $\bar{T}'$, we simply need to relate $\bar{R}$, $\bar{T}$, and $\{a_j\}$ to these quantities.

It is easy to show that $\bar{R}$ and $\bar{T}$ are related to $\bar{R}'$ and $\bar{T}'$ by

$$R_{ij} = (a_j/a_i)R_{ij}' \tag{1}$$

and

$$T_{ij} = (a_j/a_i)T_{ij}'.$$

Since we demand $R_{ij} = R_{ji}$ and $T_{ij} = T_{ji}$, (1) implies that

$$(a_j/a_i) = (R_{ji}'/R_{ij}')^{1/2} = (T_{ji}'/T_{ij}')^{1/2} \tag{2}$$

and thus

$$R_{ij} = (R_{ij}'R_{ji}')^{1/2}$$
$$T_{ij} = (T_{ij}'T_{ji}')^{1/2}. \tag{3}$$

From (2) we see that only the relative amplitudes of the eigencurrents need be restricted and hence we arbitrarily set $a_1 = 1$. Thus, for a structure propagating N modes, (2) gives us $N(N-1)$ equations for the $N-1$ unknowns $\{a_j\}, j = 2, \cdots, N$. Obviously, this system of equations is overdetermined for $N > 1$. If, in fact, the system has a solution, it is an indication that the modeling process has preserved reciprocity.

SOME NUMERICAL RESULTS

In what follows, we will adopt the convention that modes 1, 2, and 3 are the monofilar, bifilar, and jacket modes, respectively. For regions of the tunnel (see Fig. 3) where $z < 0$ (region 1) or $z > l$ (region 3), the parameters describing the physical properties of the tunnel are the same, and unless specifically indicated otherwise, will have the following typical values: $a_0 = 2$ m, $\rho_0 = 1.8$ m, $\phi_0 = 45°$, $\epsilon_e = 10\epsilon_0$, $\sigma_e = 10^{-2}$ mhos/m, $a = 1.5$ mm, $b = 1.0$ cm, $c = 1.15$ cm, $\epsilon = 2.5\ \epsilon_0$, $\epsilon_c = 3.0\ \epsilon_0$, $\sigma_w = 5.7 \times 10^7$ mhos/m, $\psi = 45°$, $\sigma d = 0$, and $f = \omega/2\pi = 36$ MHz. The coaxial braid is fairly leaky, with a surface transfer inductance $L_T = 40$ nH/m.

In the region described by $0 < z < l$ (region 2), we will let one of the parameters assume a different value than in the remainder of the tunnel; all other parameters are equal to those given above. Data will be given for the monofilar, bifilar, and conversion reflection coefficients (R_{11}, R_{22}, R_{12}) and similarly for the monofilar, bifilar, and conversion transmission coefficients (T_{11}, T_{22}, T_{12}). The situation is depicted in Fig. 4. Data are given in decibels, that is,

$$X_{ij}(\text{in dB}) = 20 \log_{10} |X_{ij}|$$

where X_{ij} denotes any one of the various reflection or transmission coefficients.

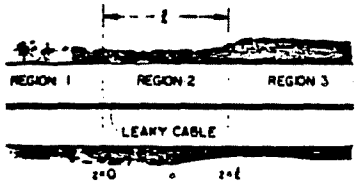


Fig. 3. Side view of tunnel showing three regions.

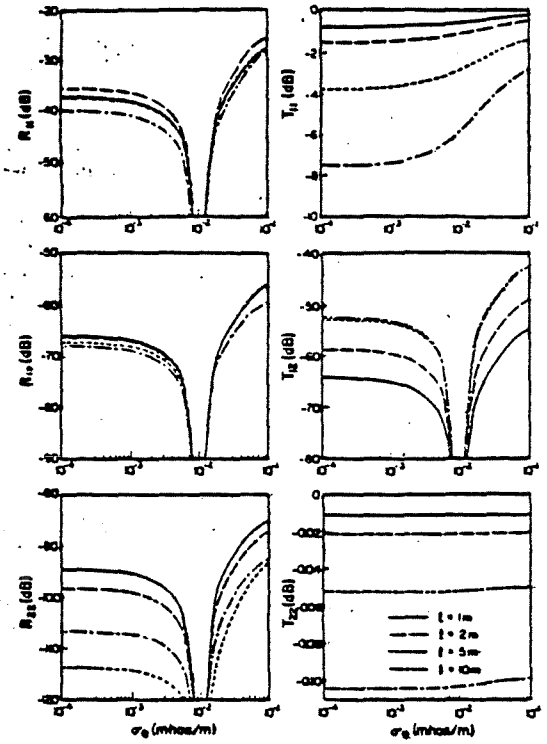


Fig. 4. Reflection and transmission coefficients as function of rock conductivity σ_e in region 2.

First we consider the effect of a change in the tunnel wall's conductivity σ_e in region 2. Fig. 4 plots X_{ij} as a function of σ_e for various values of l. It is seen that the reflection coefficients and the conversion transmission coefficient vary in the same manner, exhibiting maximum conversion and reflection when the conductivity is higher in region 2. When σ_e is lower in region 2, these coefficients level off, and are relatively insensitive to further downward changes in σ_e. Of course, at $\sigma_e = 10^{-2}$ mhos/m the regions are the same, and we expect R_{11}, R_{22}, R_{12}, and T_{12} to vanish. It is also interesting to note that T_{jj} (in dB) $\cong \alpha_j l$ where $\alpha_j = 8.686$ real $(\hat{\Gamma}_j)$ is the attenuation rate of the jth mode in region 2 (in dB/m). This means that, essentially, all energy in each mode is transmitted with only small reflection and conversion, and transmission loss is due, primarily, to the modal attenuation rate in region 2.

Fig. 5 shows a similar relation of these coefficients to a change in tunnel wall permittivity (ϵ_e). However, not unexpectedly, the maximum conversion and reflection occurs when ϵ_e is smaller in region 2 than in regions 1 and 3. Correspondingly, conversion and reflection are relatively insensitive to upward changes in region 2 permittivity.

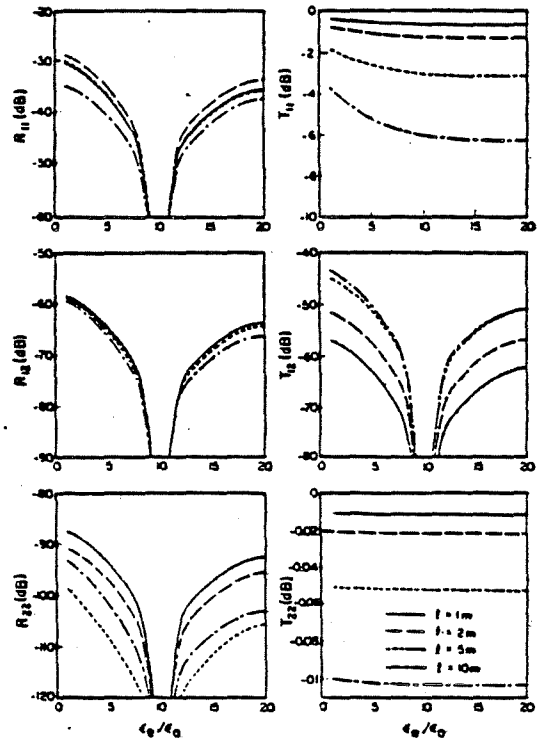


Fig. 5. Reflection and transmission coefficients as function of wall permittivity ϵ_e in region 2.

Another interesting source of inadvertent mode conversion is due to variations in the lossy film on the cable's outer surface. To consider this, we now let $\sigma d = 10^{-2}$ mhos in both regions 1 and 3. Fig. 6 shows the effect of varying σd in region 2 upon $\bar{R}$ and $\bar{T}$. We find that when σd is lower in region 2, there is little mode conversion or reflection, and the coefficients R_{11}, R_{22}, R_{12}, and T_{12} are relatively insensitive to downward changes in σd in region 2. Conversely, when σd in region 2 is increased above that in regions 1 and 3, we see an immediate increase in reflection and conversion. Again, as in previous examples, T_{11} and T_{22} are eseentially dependent upon the attenuation rates of the respective modes in region 2.

Although variations in σd along an actual mine tunnel are an unavoidable source of mode conversion, the behavior of T_{12} and R_{12} suggest the interesting idea of intentionally coating periodically spaced segments of cable with a conductive material to be used as mode converters. Indeed, we see that if $\sigma d = 10^{-2}$ mhos for the unperturbed system and 5 to 10 m lengths of cable are coated to increase this to 1 mho, we obtain a conversion transmission coefficient of about 30 dB. From [4], we found that for a typical leaky stub (i.e. leaky section) converter ($L_T = 40$ nH/m), T_{12} was about 20 to 25 dB. Intentional converters of this type woule be easy and inexpensive, and might be a quick and simple fix for areas of poor reception in existing continuous access leaky feeder systems.

In Fig. 7, we consider the effect that different cable insulation dielectrics have upon mode conversion for a given discontinuity. Specifically, consider $\sigma_e = 10^{-4}$ mhos/m in region 2 ($\sigma_e = 10^{-2}$ mhos/m in regions 1 and 3) and consider $\bar{R}$ and $\bar{T}$ for various permittivities of the cable insulation (ϵ). Note that ϵ is the same throughout all three regions. For this particular

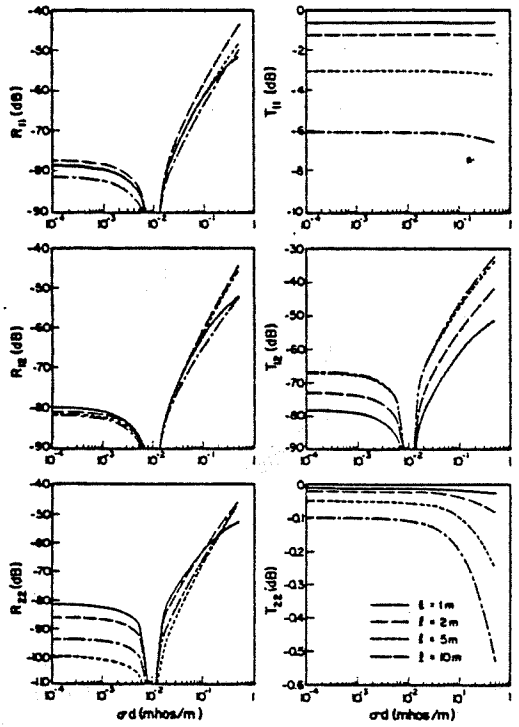


Fig. 6. Reflection and transmission coefficients as function of jacket conductance σd in region 2.

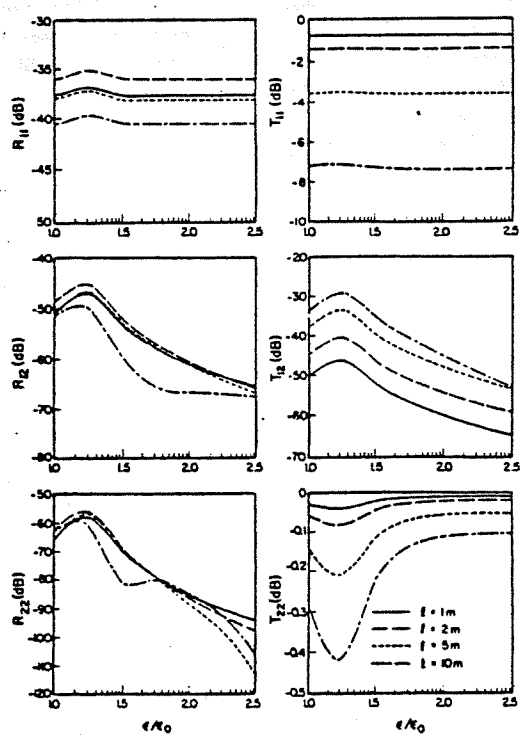


Fig. 7. Reflection and transmission coefficients as function of insulator permittivity ϵ of cable in region 2.

wall conductivity discontinuity, we see that mode conversion is maximized with $\epsilon \cong 1.25\ \epsilon_0$, indicating a fairly high velocity cable. This maximum seems to occur when the phase velocities of the two modes (monofilar and bifilar) are equal. This synchronous phase condition is well-known from coupled wave theory and is not peculiar to this problem.

Thus far, our technique has been applied only to changes in material parameters of the system. However, it can also be applied to changes in tunnel geometry. Obviously, because of the resulting abrupt geometrical discontinuities, our confidence in the method is somewhat less; such results are not given here (but they are available from the authors on request).

At this point, it is interesting to consider the consistency of the solutions for the normalization constants $\{a_j\}$ which symmetrized $\bar{R}$ and $\bar{T}$. Actually, in all cases, $\bar{R}$ and $\bar{T}$ were obtained by (3). However, in each case, all $N(N-1)$ solutions to (2) were also examined. For the results presented in Figs. 4-7 (that were characterized by changes in material parameters), all solutions for (2) were always in agreement in excess of four decimal places. It is worth mentioning here that this consistency was not found when the geometrical characteristics such as tunnel radius and cable location were modified over the section of length l. In the latter case the higher order evanescent modes should be taken into account.

CONCLUDING REMARKS

We have demonstrated by a rudimentary theory that inadvertent mode conversion can be a significant aspect of leaky feeder communication systems. In particular, if the phase velocities of the monofilar and bifilar mode are of the same order, relatively small lateral changes in the tunnel characteristics will produce significant energy conversion between the modes. This is probably the dominant mechanism in leaky feeder systems that employ a continuous loosely braided coaxial cable with a foam dielectric insulator. Unfortunately, it is difficult to predict the performance of such systems in a real world environment. On the other hand, controlled mode conversion by means of line converters can use cables with a higher permittivity of the dielectric. Then the inadvertent conversion is of much less consequence.

REFERENCES

[1] P. Delogne, "Basic mechanisms of tunnel propagation," *Radio Sci.*, vol. 11, pp. 295–303, April 1976.

[2] S. F. Mahmoud and J. R. Wait, "Calculated channel characteristics of a braided coaxial cable in a mine tunnel," *IEEE Trans. Communications*, vol. COM-24, pp. 82–87, January 1976.

[3] J. R. Wait and D. A. Hill, "Propagation along a braided coaxial cable in a circular tunnel," *IEEE Trans. Microwave Theory Tech.*, vol. MTT-23, pp. 401–405, May 1975.

[4] D. B. Seidel and J. R. Wait, "Role of controlled mode conversion in leaky feeder mine communication systems," *IEEE Trans. Antennas Propagat.*, vol. AP-26, pp. 690–694, Sept. 1978.

[5] D. J. R. Martin, "A general study of the leaky-feeder principle," *The Radio and Electronic Engineer*, vol. 45, no. 5, pp. 205–214, May 1975.

[6] D. B. Seidel and J. R. Wait, "Transmission modes in a braided coaxial cable and coupling to a tunnel environment," *IEEE Trans. Microwave Theory Tech.*, vol. MTT-26, pp. 494–499, July 1978.

[7] R. E. Collin, *Field Theory of Guided Waves*. New York: McGraw-Hill, 1960, p. 80.

IEEE TRANSACTIONS ON COMMUNICATIONS, VOL. COM-26, NO. 11, NOVEMBER 1978

Bandwidth of a Leaky Coaxial Cable in a Circular Tunnel

DAVID A. HILL, SENIOR MEMBER, IEEE, AND JAMES R. WAIT, FELLOW, IEEE

Abstract—Using the idealized model of a leaky coaxial cable in a circular tunnel to represent a leaky-feeder communication channel, we examine both pulse transmission and the bandwidth limitations of the channel. The phase and group velocities of the bifilar mode are found to be nearly independent of frequency between 1 MHz and 100 MHz, and the channel bandwidth is found to be quite large. The effect of mode excitation is also examined by treating the mutual impedance between a pair of short electric dipoles as the transfer function and the channel bandwidth is still large.

INTRODUCTION

THE leaky-feeder technique for communication in mine tunnels has recently been investigated in several theoretical [1–5] and experimental studies [6, 7]. Most theoretical studies have concentrated on the attenuation rates of the dominant modes and the coupling loss from the leaky cable to a nearby antenna. In addition to these signal amplitude effects, the bandwidth of leaky-feeder systems is of interest for cases where transmission of wide-band signals is desired. In this paper, we analyze an idealized leaky-feeder channel which consists of a uniform leaky coaxial cable located at an arbitrary position within a circular tunnel.

The frequency domain transfer function is expanded about the carrier frequency in constant, linear, and quadratic terms in both amplitude and phase. This transfer function is then used to study the dispersion of a Gaussian pulse propagating along the leaky-feeder channel. The same technique was previously applied for the case of a constant amplitude channel [8] and for amplitude and phase dispersion in optical waveguides [9, 10].

FREQUENCY DOMAIN TRANSFER FUNCTION

The specific geometry of the leaky coaxial cable located within a circular tunnel is shown in Fig. 1. The air-filled tunnel has radius a_0, and the surrounding rock has an effective conductivity σ_e and permittivity ϵ_e. Free space permeability μ_0 is assumed everywhere. The leaky coaxial cable is located at (ρ_0, ϕ_0) in cylindrical coordinates (ρ, ϕ, z). The center conductor has radius a and conductivity σ_w. The insulation has outer radius b and permittivity ϵ. The outer conductor of radius b is assumed to be a metal braid with a surface transfer impedance Z_T which is given by [11]

Paper approved by the Editor for Transmission Systems of the IEEE Communications Society for publication after presentation at the Workshop on Electromagnetic Guided Waves in Mine Environments, Boulder, CO, March 1978. Manuscript received April 17, 1978.

D. A. Hill is with the Institute for Telecommunication Sciences, U.S. Department of Commerce, Boulder, CO 80303.

J. R. Wait is with the Cooperative Institute for Research in Environmental Sciences, University of Colorado/NOAA, Boulder, CO 80309.

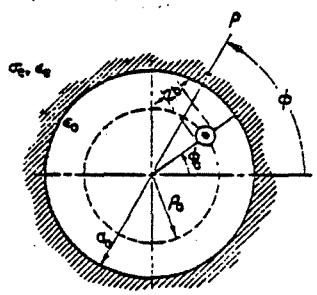


Fig. 1. Geometry for a leaky coaxial cable in a circular tunnel.

$$Z_T = i\omega L_T, \tag{1}$$

where L_T is the transfer inductance and $\exp(i\omega t)$ time dependence is assumed. The mode equation for the cable-tunnel configuration was derived and solved previously [4]. The convergence of this mode equation has been improved for the important special case when the cable is close to the tunnel wall [12]. The propagation constant Γ has been obtained for both the bifilar and monofilar modes for a wide variety of cases. For a uniform cable and tunnel, the bifilar mode is dominant in long distance transmission because it has a lower attenuation rate.

In our transfer function $P(\omega)$, we include only the propagation effect of a single mode over a distance z:

$$P(\omega) = \exp[-\Gamma(\omega)z], \tag{2}$$

where

$$\Gamma(\omega) = \alpha(\omega) + i\beta(\omega),$$

$\alpha(\omega)$ is the attenuation rate and $\beta(\omega)$ is the phase constant. Since we later consider a more general transfer function which includes excitation, we wish to write $P(\omega)$ in a more general form:

$$P(\omega) = \exp[-A(\omega) - i\Phi(\omega)], \tag{3}$$

where $A(\omega)$ and $\Phi(\omega)$ are real. For the propagation transfer function of (2), it is clear that

$$A(\omega) = \alpha(\omega)z \text{ and } \Phi(\omega) = \beta(\omega)z. \tag{4}$$

Since we expect to use $P(\omega)$ in a bandpass region centered about some carrier frequency ω_0, we expand $A(\omega)$ and $\Phi(\omega)$ in a Taylor series about ω_0:

U.S. Government work not protected by U.S. copyright

$$A(\omega) = A(\omega_0) + (\omega - \omega_0)A'(\omega_0) + (\omega - \omega_0)^2 A''(\omega_0)/2 \quad (5)$$

$$\Phi(\omega) = \Phi(\omega_0) + (\omega - \omega_0)\Phi'(\omega_0) + (\omega - \omega_0)^2\Phi''(\omega_0)/2.$$

At this stage, the following substitutions are useful:

$$A(\omega_0) = \alpha_0 z,\ A'(\omega_0) = 1/W_S,\ A''(\omega_0) = 1/(2W_A{}^2), \quad (6)$$

and

$$\Phi(\omega_0) = \omega_0\tau,\ \Phi'(\omega_0) = \tau_g,\ \Phi''(\omega_0) = 1/(2W)^2.$$

Following an earlier approach [8], we identify τ as the phase delay, τ_g as the group delay, and W as a phase bandwidth for the channel. Also, we can identify $\alpha_0 z$ as the total channel attenuation and W_S and W_A as amplitude bandwidths. The parameters W, W_S, and W_A are measures of the bandwidth over which the channel will depart significantly from a distortionless channel [13] of constant amplitude, linear phase.

From (4) and (6), the explicit expressions for the bandwidth quantities are found to be

$$W_S = 1/[\alpha'(\omega_0)z],\ W_A = [2\alpha''(\omega_0)z]^{-1/2} \quad (7)$$

and

$$W = [2\beta''(\omega_0)z]^{-1/2}.$$

At this point, we could calculate the bandwidth quantities from (7), but we first choose to examine the problem of pulse propagation in order to give more meaning to W_S, W_A, and W.

GAUSSIAN PULSE PROPAGATION

For simplicity, our source signal $f_0(t)$ as a function of time is taken to be a Gaussian-modulated carrier

$$f_0(t) = F_0 \exp(-\alpha^2 t^2) \exp(i\omega_0 t) \quad (8)$$

where F_0 is an amplitude factor. Strictly speaking, the time domain signals should be real functions of time. This can be accomplished by simply taking the real part of the time domain functions [13]. The frequency spectrum of (1) $F_0(\omega)$ is

$$F_0(\omega) = \int_{-\infty}^{\infty} f_0(t)e^{-i\omega t}\,dt = F_0(\pi^{1/2}/\alpha) \exp[-(\omega - \omega_0)^2/(4\alpha^2)]. \quad (9)$$

As indicated, the spectrum peaks at $\omega - \omega_0$ and diminishes rapidly for $\omega_0/\alpha \gg 1$. We define α here as the source bandwidth. Also, without additional complexity we can allow a receiver transfer function $R(\omega)$ of the following form:

$$R(\omega) = R(\omega_0) \exp[-(\omega - \omega_0)^2/(4\gamma^2)] \quad (10)$$

where γ is the receiver bandwidth.

The frequency spectrum of the detected signal is the product of the spectra of the source signal, the channel transfer function, and the receiver channel. Thus the detected transient signal $f(t)$ is given by the following inverse Fourier transform:

$$f(t) = \frac{1}{2\pi}\int_{-\infty}^{\infty} F_0(\omega)P(\omega)R(\omega)e^{i\omega t}\,dt. \quad (11)$$

By utilizing the integral property of the Gaussian [8, 9] we can evaluate the infinite integral in (11) and obtain the following for $f(t)$:

$$f(t) = \frac{F_0 R(\omega_0)}{2\alpha T} \exp(-\alpha_0 z) \exp[i\omega_0(t - \tau)]e(t), \quad (12)$$

where

$$e(t) = \exp[-[t - t_g + (i/W_S)]^2/(4T^2)]$$

and

$$T^2 = (1/4)(\alpha^{-2} + \gamma^{-2} + W_A{}^{-2} + iW^{-2}).$$

This result reduces to that of Kapron and Keck [9] if we set the receiver function equal to unity ($R(\omega_0) = 1$ and $1/\gamma^2 = 0$). The physical meaning of (12) is fairly clear. The factor $\exp(-\alpha_0 z)$ represents the total channel attenuation, the carrier phase is delayed by the time delay τ, and $e(t)$ is the signal envelope. However, $e(t)$ is complex and is a function of all three bandwidth quantities W_A, W, and W_S. In order to understand the effects of the three bandwidth quantities on $e(t)$, it is easiest to examine the individual effect of each one on an $e(t)$ in the absence of the other two. Thus we have the three following cases.

Case 1: quadratic amplitude term dominates ($1/W = 1/W_S = 0$). In this case, $e(t)$ is given by

$$e(t) = \exp[-(t - \tau_g)^2/(4T^2)] \quad (13)$$

where

$$4T^2 = \alpha^{-2} + \gamma^{-2} + W_A{}^{-2}.$$

It is clear that the envelope is delayed by the group delay τ_g and the pulse width, $2T$, is given by

$$2T = (\alpha^{-2} + \gamma^{-2} + W_A{}^{-2})^{1/2}. \quad (14)$$

In order to minimize the pulse width, the receiver bandwidth γ should be set equal to infinity ($1/\gamma^2 = 0$). Also, we note that for $W_A{}^{-2} \gg \alpha^{-2} + \gamma^{-2}$, the pulse width $2T$ is approximately equal to $W_A{}^{-1}$. For a digital system, this relationship fits the common definition of bandwidth (=reciprocal of the pulse width). Thus we call W_A the quadratic amplitude bandwidth.

Case 2: quadratic phase term dominates ($1/W_A = 1/W_S = 0$). This is the case treated previously [8] that is relevant to H.F. ionospheric wave transmission. Here $e(t)$ is given by

$$e(t) = \exp\left[-(t-\tau_g)^2/(4T^2)\right], \tag{15}$$

where

$$4T^2 = \alpha^{-2} + \gamma^{-2} + iW^{-2}.$$

Again the envelope is delayed by the group delay τ_g, but this time the envelope is complex. The magnitude of the envelope is given by

$$|e(t)| = \exp\left[-(t-\tau_g)^2/t_d^2\right], \tag{16}$$

where

$$t_d^2 = \left(\frac{1}{\alpha^2}+\frac{1}{\gamma^2}\right) + \left(\frac{1}{\alpha^2}+\frac{1}{\gamma^2}\right)^{-1}\frac{1}{W^4}.$$

To minimize t_d, γ is given by

$$\gamma = (W^{-2}-\alpha^{-2})^{-1/2}. \tag{17}$$

Under this condition, the pulse width t_d is $2^{1/2}/W$. Thus, except for a factor of $2^{1/2}$, we again have the reciprocal relationship between pulse width and bandwidth. Consequently, we call W the quadratic phase bandwidth.

Case 3: linear phase term dominates ($1/W = 1/W_A = 0$). In this case, $e(t)$ is given by

$$e(t) = \exp\left(\frac{1}{4T^2W_S^2}\right)\exp\left[\frac{-(t-\tau_g)^2}{4T^2}\right] \cdot \exp\left[\frac{-i(t-\tau_g)}{2T^2W_S}\right], \tag{18}$$

where

$$4T^2 = \alpha^{-2} + \beta^{-2}.$$

The first factor is a constant independent of t, and the second factor yields the delayed envelope with no stretching. The third factor has unity magnitude and represents an apparent shift $\omega_S = -(2T^2W_S)^{-1}$ in the frequency carrier. Since this frequency shift is inversely proportional to W_S, we call W_S the linear amplitude bandwidth. Apparently, Kapron and Keck [9] ignored this frequency shift because they were interested only in the magnitude of the pulse envelope. However, such an apparent frequency shift might cause a problem if coherent detection rather than envelope detection were used.

NUMERICAL RESULTS

The numerical solution of the mode equation for the cable-tunnel geometry configuration was described before [4, 12]. For our calculations here we choose the following tunnel parameters: $a_0 = 2$ m, $\sigma_e = 10^{-3}$ mho/m, and $\epsilon_e/\epsilon_0 = 10$. The cable parameters are: $a = 1.5$ mm, $\sigma_w = 5.7 \times 10^7$ mho/m, $\epsilon/\epsilon_0 = 1.5$, and $b = 1$ cm. Although the previous analyses [4, 12] included the possibility of a protective jacket and a lossy film, we do not include them here.

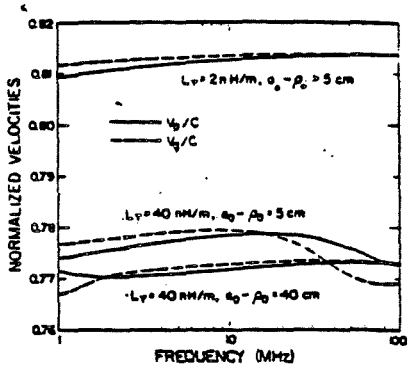


Fig. 2. Phase and group velocities of the bifilar mode.

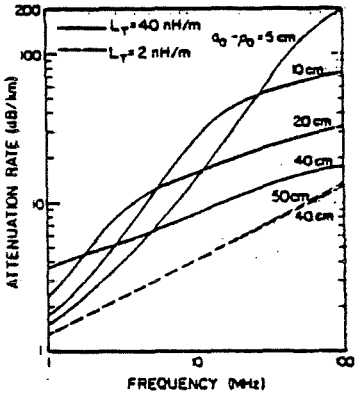


Fig. 3. Attenuation rate of the bifilar mode.

For the bifilar mode, the propagation constant is primarily determined by the dielectric constant of the insulation and is approximately given by

$$\Gamma \cong i\beta \cong (i\omega/c)(\epsilon/\epsilon_0)^{1/2} \cong i\omega/(0.816c), \tag{19}$$

where c is the free-space velocity of light. Since the phase velocity v_p is given by β/ω and the group velocity v_g is given by $d\omega/d\beta$, the approximate phase and group velocities are given by

$$v_p/c \cong v_g/c \cong c(\epsilon_0/\epsilon)^{1/2} \cong 0.816. \tag{20}$$

The actual values of v_p and v_g as computed from the mode equation is shown in Fig. 2 for frequencies from 1 MHz to 100 MHz. Note that the values for the low leakage cable ($L_T = 2$ nH/m) are nearly equal to the approximate value in (19). Also, the results are nearly independent of the distance of the cable from the wall, $a_0 - \rho_0$. For the high leakage cable ($L_T = 40$ nH/m), the velocities are lower and depend somewhat on the cable position.

In Fig. 3, we show the attenuation rate in dB/km ($=8.686 \times 10^3\alpha(\omega)$ where $\alpha(\omega)$ is given in nepers/m). For the low leakage cable, the attenuation rate is fairly low and nearly independent of the cable position. For the high leakage cable, the attenuation rate is higher and is quite sensitive to the cable position.

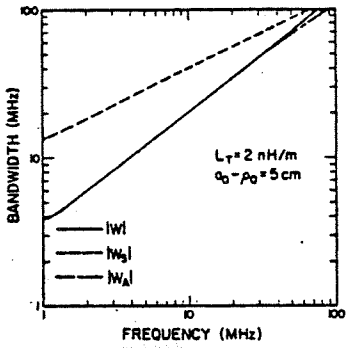


Fig. 4. Bandwidth quantities of the bifilar mode for a low-leakage cable.

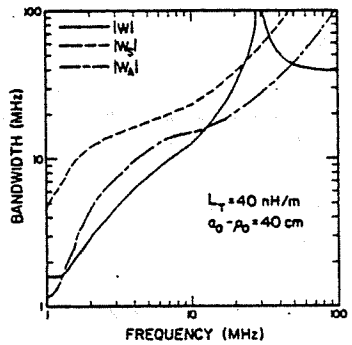


Fig. 5. Bandwidth quantities of the bifilar mode for a high-leakage cable.

From the numerically computed values of Γ, we can determine the bandwidth quantities from (7) by taking the required ω derivatives numerically. For all the results given in this paper, we set the propagation distance z at 1 km.

In Fig. 4, we show the bandwidths for the low-leakage cable (L_T = 2 nH/m), and they are all quite large. Actually, these results are for $a_0 - \rho_0 = 5$ cm, but the results are nearly independent of ρ_0. In Fig. 5, we show the bandwidths for the high leakage cable (L_T = 40 nH/m) located 40 cm from the wall. For the high-leakage cable close to the wall in Fig. 6, the bandwidths are smaller but never less than 10% of the carrier frequency.

Some recent work on wire mesh screens indicates that the surface transfer impedance actually depends on the propagation constant Γ [14]. If the weave angle of the braid wires (angle subtended with the cable axis) is 45°, then the appropriate form for the Z_T is

$$Z_T(\Gamma) \cong i\omega L_T[1 - \Gamma^2/(k_0^2 + k^2)], \tag{21}$$

where

$$k_0 = \omega/c \text{ and } k = (\omega/c)(\epsilon/\epsilon_0)^{1/2}.$$

The general effect of this change is to decrease Z_T and make the cable less leaky. In Figs. 7 and 8, we show the resultant velocities and attenuation rates for the Γ-dependent Z_T model. In comparing Figs. 3 and 8, we see that the attenuation rates

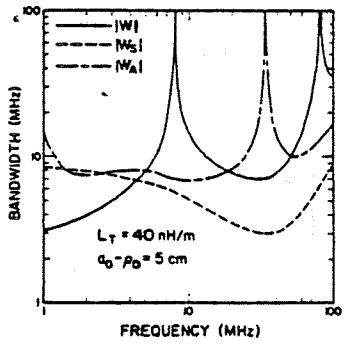


Fig. 6. Bandwidth quantities of the bifilar mode for a high-leakage cable located close to the tunnel wall.

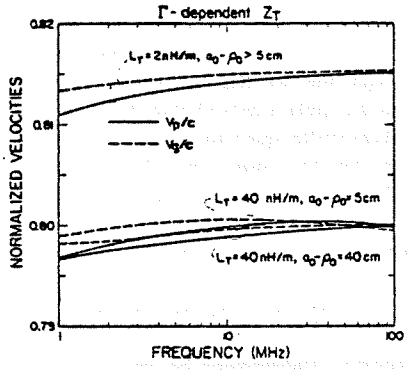


Fig. 7. Phase and group velocities of the bifilar mode for a Γ-dependent Z_T model.

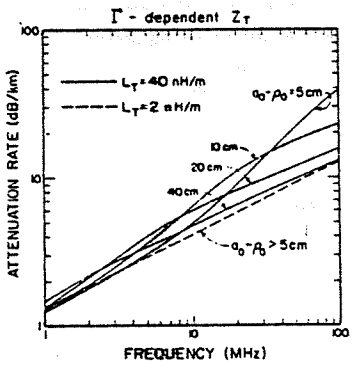


Fig. 8. Attenuation rate of the bifilar mode for a Γ-dependent Z_T model.

of the low leakage cable (L_T = 2 nH/m) are relatively independent of the Z_T model because they are mainly dependent on the center conductor losses. However, for the high leakage cable (L_T = 40 nH/m), the attenuation rates are much lower for the Γ-dependent Z_T model. In Fig. 9, we show the bandwidth quantities for the Γ-dependent model, and they are typically larger than those for the corresponding parameters in Fig. 6.

Although the monofilar mode typically has very high attenuation due to return current in the rock walls [4, 12], it could be of interest in some cases because it is easy to excite. The prop-

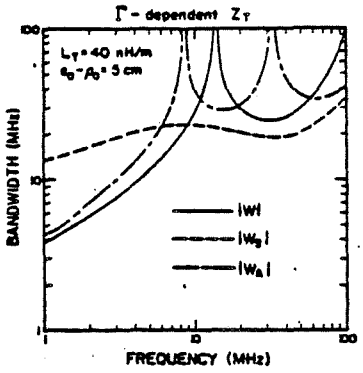


Fig. 9. Bandwidth quantities of the bifilar mode for a Γ-dependent Z_T model.

agation constant Γ of the monofilar mode is typical of a slow wave ($\beta > k_0$), and the attenuation rate increases and velocity decreases as the cable is moved close to the wall. In Fig. 10, we show the bandwidth quantities for the monofilar mode of a cable 20 cm from the tunnel wall. The L_T value is 2 nH/m, but the monofilar mode is weakly dependent on the cable walls. As Fig. 10 indicates, the bandwidths for the monofilar mode are considerably smaller than those of the bifilar mode.

EFFECT OF EXCITATION

If we consider transmission between a pair of short electric dipoles in the tunnel environment, then a more complete transfer function is the mutual impedance Z_m. Let the transmitting dipole have an arbitrary transverse orientation at $(\rho_t, \phi_t, 0)$, and let the receiving dipole have an arbitrary transverse orientation at (ρ_r, ϕ_r, z). For sufficiently large z, only the bifilar mode will contribute and Z_m is given by [5].

$$Z_m \cong -[l_{te} \cdot e_t(\rho_t, \phi_t, \Gamma_b)][l_{re} \cdot e_t(\rho_r, \phi_r, \Gamma_b)] \times \left[\frac{dM(\Gamma)}{d\Gamma}\right]^{-1}\Bigg|_{\Gamma=\Gamma_b} \cdot \exp(-\Gamma_b z), \tag{22}$$

where

$$M(\Gamma) = e_z(\rho_0 + b, \phi_0, \Gamma) - Z(\Gamma)$$

and

$$M(\Gamma_b) = 0.$$

In (22) l_{te} and l_{re} are the effective vector lengths of the transmitting and receiving electric dipoles, e_t is the transverse electric field of the bifilar mode, e_z is the axial electric field of the bifilar mode at the edge of the cable, $Z(\Gamma)$ is the effective series impedance of the coaxial cable, Γ_b is the propagation constant of the bifilar mode, and $M(\Gamma_b) = 0$ is the mode equation.

For frequencies below 100 MHz, l_{te}, l_{re}, and e_t are nearly independent of ω. Thus we can rewrite (22) in the following form:

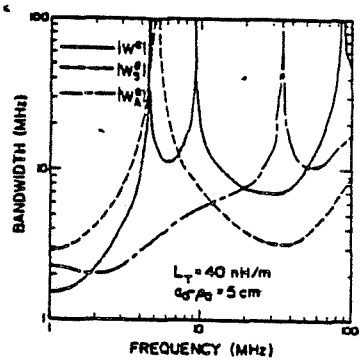


Fig. 10. Bandwidth quantities of the monofilar mode.

$$Z_m \cong K_e \left[\frac{dM(\Gamma)}{d\Gamma}\right]^{-1}\Bigg|_{\Gamma=\Gamma_b} \cdot \exp(-\Gamma_b z), \tag{23}$$

where K_e is independent of ω. We now define our new transfer function $P_e(\omega)$ as the frequency dependent part of Z_m:

$$P_e(\omega) = \frac{Z_m}{K_e} = \left[\frac{dM(\Gamma)}{d\Gamma}\right]^{-1}\Bigg|_{\Gamma=\Gamma_b} \exp(-\Gamma_b z)$$

$$= \exp\left\{-\Gamma_b z - \ln\left[\frac{dM(\Gamma)}{d\Gamma}\right]\Bigg|_{\Gamma=\Gamma_b}\right\}. \tag{24}$$

In a manner similar to (4), we can now define our new amplitude and phase functions, $A_e(\omega)$ and $\Phi_e(\omega)$:

$$A_e(\omega) = \mathrm{Re}\left\{\Gamma_b z + \ln\left[\frac{dM(\Gamma)}{d\Gamma}\right]\Bigg|_{\Gamma=\Gamma_b}\right\}$$

and (25)

$$\Phi_e(\omega) = \mathrm{Im}\left\{\Gamma_b z + \ln\left[\frac{dM(\Gamma)}{d\Gamma}\right]\Bigg|_{\Gamma=\Gamma_b}\right\}.$$

The quantity $dM(\Gamma)/d\Gamma$ is directly available from the solution of the mode equation which utilizes the Γ derivative in a Newton's method solution of the mode equation. As in (6) and (7), we can define the linear amplitude, quadratic amplitude, and quadratic phase bandwidths:

$$W_S{}^e = \frac{1}{A_e'(\omega_0)}, \quad W_A{}^e = \frac{1}{[2A_e''(\omega_0)]^{1/2}},$$

and (26)

$$W_e = \frac{1}{[2\Phi_e''(\omega_0)]^{1/2}}.$$

The ω derivatives in (26) again are computed numerically.

In Fig. 11, the bandwidth quantities of (26) are shown for a high leakage cable close to the tunnel wall. This case corresponds to the parameters used in Fig. 6. Note that the addition of the excitation factor changes the bandwidth curves some-

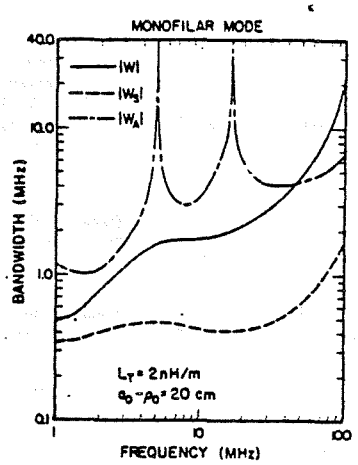


Fig. 11. Bandwidth quantities of the bifilar mode with excitation included.

what, but the minimum bandwidths are only slightly smaller. The same general trend has been found true for other cases.

CONCLUSIONS

The bandwidth limitations of an idealized leaky feeder channel have been evaluated by examining both the frequency response of the channel and the transmission of a Gaussian pulse along the channel. In either case the important quantities are the linear amplitude, quadratic amplitude, and quadratic phase bandwidths. However, for bifilar mode propagation for a distance of 1 km, these bandwidths are found to be quite large and never less than 10% of the carrier frequency for any of the cases investigated. The phase and group velocities of the bifilar mode are found to be quite frequency independent and determined primarily by the cable parameters.

For a cable braid model which utilizes a Γ-dependent surface transfer impedance, the cable is effectively less leaky. Consequently, the attenuation rate is lower and the bandwidths are even larger.

The monofilar mode was found to have bandwidths of only about 1% of the carrier for frequencies above 30 MHz. However, the attenuation rate for the monofilar mode above 30 MHz is so high (>600 dB/km) that this mode would be unusable anyway.

The effect of bifilar mode excitation was also included by using the mutual impedance between a pair of short dipoles as the transfer function. The effect of excitation on bandwidth was found to be fairly minor.

The primary conclusion of the bandwidth calculations is that bifilar propagation along a uniform cable in a uniform tunnel has a very wide bandwidth. However, for nonuniform cables or tunnels where mode conversion occurs, the channel could become quite frequency sensitive and have much smaller bandwidths. Such mode conversion could be either intentional [15, 16] or inadvertent [1].

Another possible extension is to allow for cubic terms in the expansion of the transfer function about the carrier frequency. This was done explicitly by Wait [17] for the phase term. The envelope is no longer Gaussian for the present model but is characterized by a more complicated yet tractable Airy function. Such cubic terms would be important in describing the envelope delay in cases where the effective bandwidths W and W_S of the quadratic terms are infinite (i.e. a point of inflection in the frequency dispersion curves).

REFERENCES

[1] D. J. R. Martin, "A general study of the leaky-feeder principle", *Radio and Electron. Engr.*, vol. 45, pp. 205-214, May 1975.

[2] P. P. Delogne and M. Safak, "Electromagnetic theory of the leaky coaxial cable", *Radio and Electron. Engr.*, vol. 45, pp. 233-240, May 1975.

[3] R. J. Slaughter, "Field leakage and crosstalk, with special reference to radiating cables with perforated tape screens", *Radio and Electron. Engr.*, vol. 45, pp. 248-252, May 1975.

[4] J. R. Wait and D. A. Hill, "Propagation along a braided coaxial cable in a circular tunnel", *IEEE Trans. Microwave Theory Tech.*, vol. MTT-23, pp. 401-405, May 1975.

[5] D. A. Hill and J. R. Wait, "Calculated transmission loss for a leaky feeder communication system in a circular tunnel", *Radio Sci.*, vol. 11, pp. 315-321, April 1976.

[6] D. J. Cree and L. J. Giles, "Practical performance of radiating cables", *Radio and Electron. Engr.*, vol. 45, pp. 215-223, May 1975.

[7] S. Okada, T. Kishomoto, K. Akagawa, Y. Nakahara, K. Mikoshiba, F. Horiguchi, and K. Okamoto, "Leaky coaxial cable for communication in high speed railway transportation", *Radio and Electron. Engr.*, vol. 45, pp. 224-228, May 1975.

[8] J. R. Wait, "On the optimum receiver bandwidth for propagated pulse signals", *Proc. IEEE*, vol. 57, pp. 1784-1785, October 1969.

[9] F. P. Kapron and D. B. Keck, "Pulse transmission through a dielectric optical waveguide", *Applied Optics*, vol. 10, pp. 1519-1523, July 1971.

[10] E. F. Kuester and D. C. Chang, "Single-mode pulse dispersion in optical waveguides", *IEEE Trans. Microwave Theory Tech.*, vol. MTT-23, pp. 882-887, November 1975.

[11] J. Fontaine, B. De Moulin, P. de Gauque and R. Gabillard, "Feasibility of radio communication in mine galleries by means of a coaxial cable having a high coupling impedance" in *1973 Proc. Thru-the-Earth Electromagn. Workshop*, Colorado School of Mines, U.S. Bureau of Mines, Contract G133023, Final Rept. Dec. 31, 1973, pp. 130-139, available from NTIS, Springfield, VA, Publ. 231 154.

[12] D. A. Hill and J. R. Wait, "Propagation along a braided coaxial cable located close to a tunnel wall", *IEEE Trans. Microwave Theory Tech.*, vol. MTT-24, pp. 476–480, July 1976.
[13] A. Fettweis, "On the significance of group delay in communication engineering", *AEÜ*, vol. 31, pp. 342-348, September 1977.
[14] J. R. Wait and D. A. Hill, "Influence of spatial dispersion of the shield transfer impedance of a braided coaxial cable", *IEEE Trans. Microwave Theory Tech.*, vol. MTT-25, pp. 72-74, January 1977.
[15] L. Deryck, "Control of mode conversions on bifilar line in tunnels", *Radio and Electron. Engr.*, vol. 45, pp. 241-247, May 1975.
[16] D. B. Seidel and J. R. Wait, "Role of controlled mode conversion in leaky feeder mine-communication systems", *IEEE Trans. Antennas and Propagation*, vol. AP-26, pp. 690-694, September 1978.
[17] J. R. Wait, "Distortion of pulsed signals when the group delay is a non-linear function of frequency", *Proc. IEEE*, vol. 58, no. 8, pp. 1292-1294, August 1970.

★

David A. Hill (M'72–SM'76), for a photograph and biography, see page 361 of the March 1978 issue of this TRANSACTIONS.

★

James R. Wait (SM'56–F'62), for a photograph and biography, see page 361 of the March 1978 issue of this TRANSACTIONS.

INT. J. ELECTRONICS, 1979, VOL. 47, NO. 2, 155–166

Comparison of loop and dipole antennas in leaky feeder communication systems

DAVID A. HILL and JAMES R. WAIT

Institute for Telecommunication Sciences,
NTIA/U.S. Department of Commerce, Boulder, Colorado 80303, U.S.A.

The mutual impedance between electric and/or magnetic dipoles in a circular tunnel containing a leaky coaxial cable is derived for arbitrary dipole positions. For the usual case of large dipole separation, the bifilar mode approximation is used to compute the mutual impedance and associated transmission loss. For typical cable parameters, a broad minimum in transmission loss is found in the range from 2 to 10 MHz. In this frequency range, the transmission loss is slightly less for magnetic dipoles (loops) than for electric dipoles. While the analytical model is a cable within a tunnel, the general approach and many of the conclusions would apply to similar above-ground systems. Thus the results are relevant to railway and roadway communications of the limited access type.

1. Introduction

The leaky feeder technique (Beal *et al.* 1973) has been developed for communication in mine tunnels (Martin 1975). The leaky transmission line is usually a coaxial cable (Fontaine *et al.* 1973), and the energy is coupled into or out of the channel by antennas in the vicinity of the transmission line. Both electric dipole (Haining 1974, Harms *et al.* 1974, Okada *et al.* 1975) and monopole (Delogne 1974, Cree 1975) antennas have been used. Small loops or coils (Breitenbach 1974, Cribbens 1974) have also been used to couple to the magnetic field.

In a previous paper (Hill and Wait 1976), we calculated the mutual impedance and transmission loss between a pair of electric dipole antennas located in a circular tunnel which contained a leaky coaxial cable. The previous formulation utilized a reciprocity derivation (Mahmoud 1974, Hill and Wait 1974) which was useful only when the transmitting and receiving dipoles were widely separated. Here we employ a more direct derivation which allows arbitrary dipole locations and includes both electric and magnetic (small loop) dipole antennas. In addition to calculating the transmission loss, we utilize the computed input resistance of the dipoles in the circular tunnel environment (Hill and Wait 1978). Thus the near field losses due to the lossy tunnel walls are accounted for.

When the dipoles are widely separated, the total transmission loss reduces to the sum of the dipole-to-cable coupling losses and the attenuation of the dominant mode. Numerical results are presented in order to compare the relative effectiveness of electric and magnetic dipole antennas.

2. Dipole excitation

The cross section of the circular tunnel is shown in the cylindrical coordinate system (ρ, ϕ, z) in Fig. 1. The air-filled tunnel of radius a_0 has free space permittivity ε_0 and permeability μ_0. The surrounding rock has conductivity σ_e. permittivity ε_e. and permeability μ_e.

Received 9 October 1978; accepted 5 February 1979.

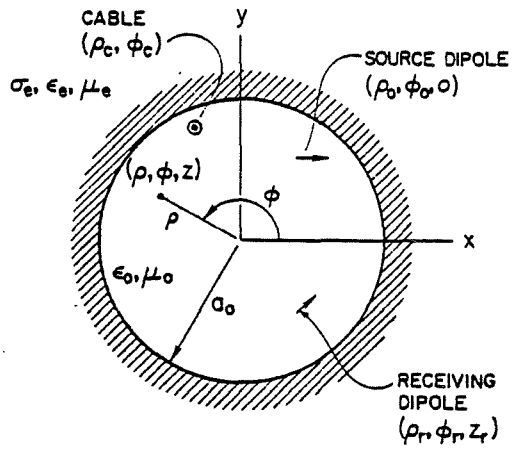


Figure 1. Transmitting and receiving dipoles (electric or magnetic) in a circular tunnel which contains a leaky coaxial cable.

The coaxial cable of radius c is centred at (ρ_c, ϕ_c), and it is assumed that c is small compared to both the free space wavelength and the distance of the cable from the tunnel wall. The specific leaky cable of interest here is modelled by: a centre conductor of radius a and conductivity σ_w, insulation of outer radius b and permittivity ε, a thin shield of radius b that can be characterized by a transfer inductance per unit length L_T, a protective jacket of outer radius c and permittivity ε_e, and a thin lossy film of radius c that can be characterized by a conductivity-thickness product σd. Actually, the results given in this paper apply for any thin axial conductor which can be represented by a series impedance per unit length $Z(\lambda)$ where λ is the axial wavenumber. The appropriate expression for $Z(\lambda)$ for this coaxial cable model has been derived previously for use in the solution of the mode equation (Wait and Hill 1975).

The x-directed dipole source at $(\rho_0, \phi_0, 0)$ can be either electric or magnetic. The electric dipole source has a dipole moment Il_{0e} where I is the current at the feed point and l_{0e} is the effective length. The usual $\exp(i\omega t)$ time dependence is suppressed. The magnetic dipole source has a magnetic dipole moment IA_{0e} where A_{0e} is the effective area.

The expressions for the fields of electric and magnetic dipoles of arbitrary orientation have been derived previously (Hill and Wait 1978). Here we consider only transverse orientations which generally are more effective in coupling to the leaky cable. In addition, x-directed orientation is sufficient to cover all transverse cases by proper selection of ϕ_0 and ϕ_c.

The total fields at any point in the tunnel can be derived from electric and magnetic Hertz potentials U_t and V_t which are the z-components of the electric and magnetic Hertz vectors, respectively (Wait 1959). Furthermore, we can write

$$U_t = U + U_c \tag{1}$$

and

$$V_t = V + V_c \tag{2}$$

U and V are the Hertz potentials that would exist in an empty tunnel, while U_c and V_c are the contributions (outside the cable) due to the axial cable current. The expressions for U_t and V_t have been derived previously (Hill and Wait 1978), and the derivation will not be repeated here. The specific expressions for electric and magnetic dipole excitation are given in Appendices A and B.

The component of the total field are obtained from U_t and V_t by the well known (Wait 1959) relations:

$$E_\rho = \frac{\partial^2 U_t}{\partial \rho \partial z} - \frac{i\omega\mu_0}{\rho}\frac{\partial V_t}{\partial \phi} \tag{3}$$

$$E_\phi = \frac{1}{\rho}\frac{\partial^2 U_t}{\partial \phi \partial z} + i\omega\mu_0 \frac{\partial V_t}{\partial \rho} \tag{4}$$

$$E_z = \left(\frac{\partial^2}{\partial z^2} - \gamma_0^2\right) U_t \tag{5}$$

$$H_\rho = \frac{i\omega\varepsilon_0}{\rho}\frac{\partial U_t}{\partial \phi} + \frac{\partial^2 V_t}{\partial \rho \partial z} \tag{6}$$

$$H_\phi = -i\omega\varepsilon_0 \frac{\partial U_t}{\partial \rho} + \frac{1}{\rho}\frac{\partial^2 V_t}{\partial \phi \partial z} \tag{7}$$

$$H_z = \left(\frac{\partial^2}{\partial z^2} - \gamma_0^2\right) V_t \tag{8}$$

where $\gamma_0^2 = -\omega^2\mu_0\varepsilon_0$.

3. Mutual impedance

We consider now a small receiving dipole of arbitrary transverse orientation located at (ρ_r, ϕ_r, z_r) as indicated in Fig. 1. For a receiving electric dipole of effective vector length $\mathbf{l}_{re}$, the received voltage v_r is

$$v_r = -\mathbf{l}_{re} \cdot \mathbf{E}_t \tag{9}$$

where

$$\mathbf{E}_t = \hat{\rho} E_\rho + \hat{\phi} E_\phi$$

Thus the mutual impedance Z_m is

$$Z_m = v_r/I = -\mathbf{l}_{re} \cdot \mathbf{E}_t/I \tag{10}$$

For a receiving magnetic dipole (loop of effective area A_{re}), the received voltage v_r is

$$v_r = i\omega\mu_0 A_{re} \hat{n} \cdot \mathbf{H}_t \tag{11}$$

where

$$\mathbf{H}_t = \hat{\rho} H_\rho + \hat{\phi} H_\phi$$

and $\hat{n}$ is a unit normal to the loop surface. Thus the mutual impedance Z_m for a small receiving loop is

$$Z_m = v_r/I = i\omega\mu_0 A_{re} \hat{n} \cdot \mathbf{H}_t/I \tag{12}$$

At this point, there is no restriction on the dipole locations (provided they are inside the tunnel and outside the cable). The formulation is also valid for mixed dipole types, such as electric source dipole and magnetic receiving dipole. When the dipoles are located close together (small $|z_r|$), the integral forms for the fields (as given in Appendices A and B) must be evaluated numerically in order to compute the mutual impedances. This is a rather tedious task, but it has been done in order to evaluate the change in the self impedance of electric and magnetic dipoles due to the tunnel walls and leaky cable (Hill and Wait 1978).

4. Bifilar mode approximation

For large values of $|z|$, the dominant contribution to the fields is from the mode of lowest attenutation. For most cases of interest, this is the 'bifilar' mode which carries most of its energy between the centre conductor and the braid but also has leakage fields outside the cable. The propagation constant λ_b of this mode satisfies the mode equation $D(\lambda_b)=0$ where $D(\lambda)$ is given by (B.7). This mode equation has been solved numerically (Wait and Hill 1975) and analytically for the quasi-static case (Seidel and Wait 1978 a). The propagation constant λ_b is approximately that of the cable insulation, i.e. $\lambda_b \simeq \omega(\mu_0\varepsilon)^{1/2}$.

The approximate expressions for the Hertz potentials for large $|z|$ are obtained by contour integration of (B.1) and (B.2). If only the pole contribution from the bifilar mode (at $\lambda=\lambda_b$) is included, the approximate expressions for U_t and V_t are found to be

$$U_t \simeq -2\pi i \frac{\hat{E}_z(\lambda_b)\exp(-i\lambda_b|z|)}{[dD(\lambda)/d\lambda]|_{\lambda=\lambda_b}} \cdot \left[K_0(v_b\rho_0) - \sum_{m=-\infty}^{\infty} R_m(\lambda_b) \times \frac{K_m(v_b a_0)}{I_m(v_b a_0)} I_m(v_b\rho) I_m(v_b\rho_c) \exp[-im(\phi-\phi_c)] \right] \tag{13}$$

and

$$V_t \simeq -2\pi i \frac{\hat{E}_z(\lambda_b)\exp(-i\lambda_b|z|)}{[dD(\lambda)/d\lambda]|_{\lambda=\lambda_b}} \sum_{m=-\infty}^{\infty} I_m(v_b\rho_c)\Delta_m(\lambda_b) \times I_m(v_b\rho)\exp[-im(\phi-\phi_c)] \tag{14}$$

where

$$v_b = (\lambda_b^2+\gamma_0^2)^{1/2}$$

Our previous solution of the mode equation, $D(\lambda)=0$, utilized a version of Newton's method (Hamming 1973) which yields the required derivative $dD(\lambda)/d\lambda$ with no additional effort. If other modes are needed, they can be handled in the same fashion. Then (13) and (14) would be a modal sum over λ_p where λ_p are the solutions of $D(\lambda_p)=0$.

For the mine communication application, the bifilar mode approximation is sufficient. The field components at large $|z|$ are approximately given by substituting (13) and (14) into (3)–(8). The approximate expressions for the mutual impedance of widely spaced dipoles are, in turn, given by substituting the resultant field expressions into (10) or (12). When this is done, the result in (10) agrees with the previous approximation for the mutual impedance of electric dipoles as obtained by reciprocity (Hill and Wait 1976).

5. Transmission loss

If the input resistance of the transmitting antenna is R_0, then the input power P_0 is

$$P_0 = |I|^2 R_0/2 \tag{15}$$

If the input resistance of the receiving antenna is R_r and the antenna is terminated in a matched load, then the received power P_r is

$$P_r = |I|^2 |Z_m|^2/(8R) \tag{16}$$

Thus the transmission loss L (in dB) is

$$L = 10\log_{10}\left(\frac{P_0}{P_r}\right) = 10\log_{10}\left(\frac{4R_0R_r}{|Z_m|^2}\right) \tag{17}$$

Since the transmitter power is limited in mine communications, it is the transmission loss which is of most interest to the systems engineer. The expression in (17) applies to both electric and magnetic dipoles as either transmitting or receiving antennas.

In order to compare the relative merits of dipole and loop antennas, a computer program was written for transmission loss between either a pair of electric dipoles or between a pair of magnetic dipoles. The required mutual impedances were computed from (10) and (12) using the bifilar mode approximation in (13) and (14). For the input resistances, the actual computed values in the tunnel environment (Hill and Wait 1978) were used. Thus the near field loss resistance due to the tunnel walls was accounted for.

In all numerical results, the following parameters were used. For the tunnel, $a_0 = 2$ m, $\sigma_e = 10^{-3}$ mho/m, $\varepsilon_e/\varepsilon_0 = 10$, and $\mu_e/\mu_0 = 1$. The cable was located at $\rho_c/a_0 = 0{\cdot}9$, and the parameters adopted were: $a = 1{\cdot}5$ mm, $b = 10$ mm, $c = 10$ mm, $\sigma_w = 5{\cdot}7 \times 10^7$ mho/m, $\varepsilon/\varepsilon_0 = 1{\cdot}5$, and $\sigma d = 0$. Thus the dielectric jacket and the lossy thin jacket have been excluded since they have been found to have a negligible effect.

Both electric dipoles were x-directed with $\phi_0 = \phi_r = \phi_c = 0°$ for maximum cable coupling. The effective dipole lengths, l_{0e} and $|l_{re}|$, were both taken to be 0·5 m. This could correspond to a physical length of 1 m with the usual triangular current distribution for electrically short dipoles.

Both magnetic dipoles were x-directed with $\phi_0 = \phi_r = \phi_c = 90°$ for maximum cable coupling. The loop areas, A_{0e} and A_{re}, were both taken to be 1 m^2.

In Fig. 2, the transmission loss L is shown for two dipole locations, $\rho_0/a_0 = \rho_r/a_0 = 0{\cdot}5$ and $\rho_0 = \rho_r = 0$. The transmission loss for the dipoles at the centre of the tunnel ($\rho_0 = \rho_r = 0$) is larger simply because the dipoles are farther from the cable. The curves for various separations z_r show the effect of the attenuation of the bifilar mode. The attenuation even for 2 km is seen to be quite small at 1 MHz but much larger at 50 MHz. The curves for $z_r = 0$ are shown merely to illustrate the two-way coupling loss to and from the cable. This coupling loss is fairly small because we have taken a rather large value of 40 nH/m for the surface transfer inductance L_T of the cable braid (Fontaine *et al.* 1973). Also, the low value of $\varepsilon/\varepsilon_0 = 1{\cdot}5$ yields a fairly high velocity for the bifilar mode which serves to decrease the coupling loss. In addition, the larger coupling loss quoted by many cable manufacturers applies to antennas located 20 feet ($\simeq 6$ m) from the cable. The antenna–cable separations in Fig. 2 are only 1·8 m and 0·8 m. Thus the parameters and the configuration represented in

Fig. 2 represent a very favourable situation. Still the results are in reasonable agreement with the free space coupling loss calculations of Rawat and Beal (1974) using somewhat different assumptions.

In Fig. 3, we show the corresponding transmission loss for a pair of identical magnetic dipoles (loops). The results are similar to those of the electric dipole, and the transmission loss is slightly lower for the low frequencies.

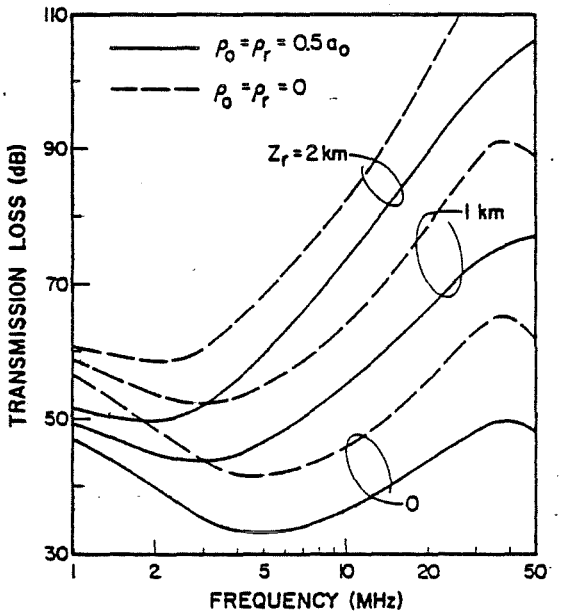


Figure 2. Transmission loss between a pair of identical electric dipoles for various dipole locations and axial separations. The curves for $z_r = 0$ represent the two-way coupling loss in and out of the cable. A high value of 40 nH/m is used for the surface transfer inductance of the cable braid.

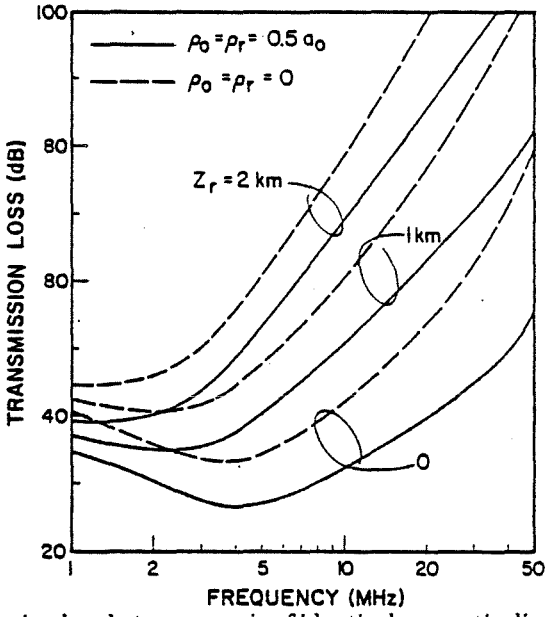


Figure 3. Transmission loss between a pair of identical magnetic dipoles (loops) for various dipole locations and axial separations. A high value of 40 nH/m is used for the surface transfer inductance of the cable braid.

As seen by (17), the transmission loss for matched loads depends only on the mutual impedance and the input resistances. Since matched loading is difficult for electrically small antennas, the mutual impedances and input resistances are of interest in their own right. In Fig. 4, the input resistances and the magnitude of the mutual impedances are shown for one dipole location. Below about 20 MHz the loss resistance dominates the radiation resistance for both electric and magnetic dipoles (Hill and Wait 1978). The result is that the electric dipole resistance is nearly independent of frequency and the magnetic dipole resistance is proportional to the square of the frequency. Another point is that both the input resistance and the mutual impedance of short electric dipoles are proportional to the length squared. For small loops (magnetic dipoles), both the input resistance and mutual impedance are proportional to the loop area squared. Thus, for the adopted model, the transmission loss is independent of dipole length or loop area as indicated by (17). Of course, this simple result neglects any difficulties in antenna matching or any wire resistance of the antennas.

In Figs. 5 and 6, the transmission losses for electric and magnetic dipoles are shown for smaller values of L_T. A value of $L_T = 10$ nH/m is probably more realistic for most cable shields, and a value of $L_T = 2$ nH/m represents a very low leakage cable braid. A decrease in L_T causes a large increase in coupling loss as seen in Figs. 5 and 6 and also a decrease in attenuation of the bifilar mode. Since the coupling loss dominates the attenuation loss for most cases of interest, a large value of L_T (very leaky cable) is most favourable. For very large dipole separations, z_r, this conclusion would no longer hold.

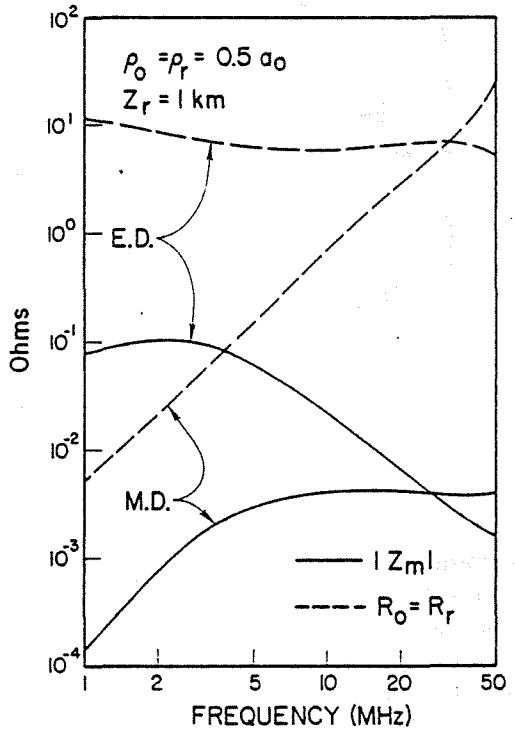


Figure 4. Mutual impedance, Z_m, and input resistance, $R_0 = R_r$, for electric dipoles (E.D.) and magnetic dipoles (M.D.). Again, $L_T = 40$ nH/m.

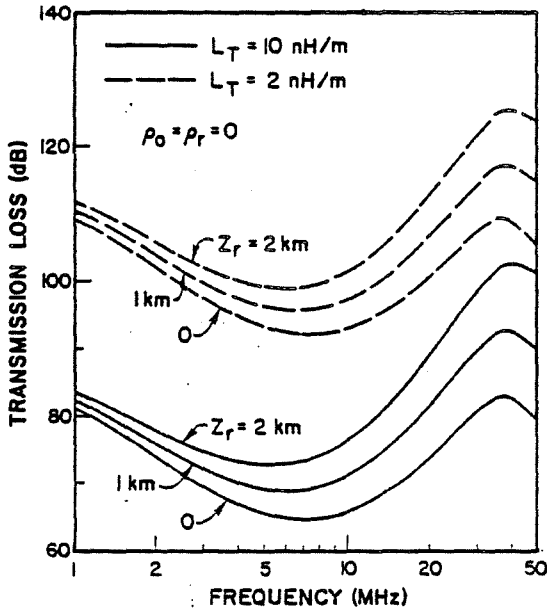


Figure 5. Transmission loss between a pair of identical electric dipoles for cables of lower leakage.

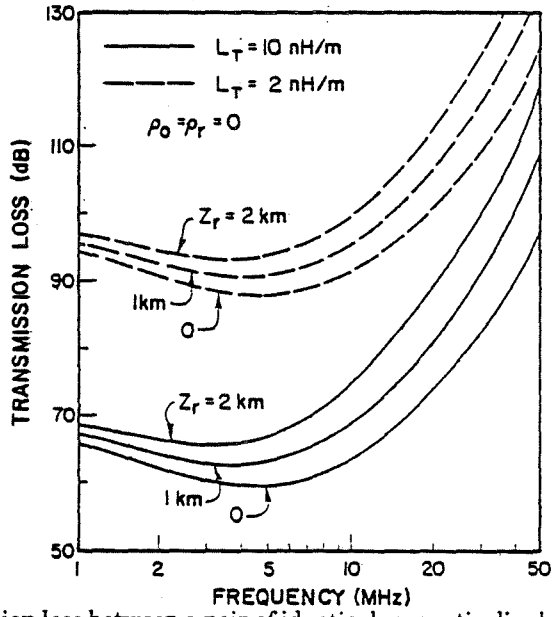


Figure 6. Transmission loss between a pair of identical magnetic dipoles for cables of lower leakage.

6. Concluding remarks

The mutual impedance between electric and/or magnetic dipoles has been derived for arbitrary dipole positions and orientations. For the usual case of large dipole separation, the single bifilar mode approximation is adequate. Numerical results for transmission loss indicate that a cable with a large transfer inductance and a low dielectric constant is most favourable. The large leakage fields of such a cable result in a slightly higher attenuation rate, but this is more than offset by a large reduction in coupling loss.

For typical parameters, a broad minimum in transmission loss is observed somewhere between 2 and 10 MHz. This is in agreement with Fontaine *et al.* (1973) who found 7 MHz to be an optimum frequency. In this frequency range, the transmission loss is somewhat lower for magnetic dipoles than for electric dipoles. This difference results primarily from the lower loss resistance (due to the tunnel walls) of the magnetic dipole. At higher frequencies where the loss resistance is less important, this advantage disappears.

The analysis given here assume a uniform tunnel and cable with no mode conversion. A remaining extension would be to include the effects of mode conversion between the monofilar and bifilar modes. Such mode conversion can be either intentional due to cable design (Deryck 1975, Seidel and Wait 1978 b) or inadvertent due to nonuniformities in the tunnel walls (Seidel and Wait 1978 c). However, it is doubtful if this more complicated analysis would modify our general conclusions on the relative merits of loop and dipole antennas in mine communications.

Appendix A. Empty tunnel fields

The empty tunnel fields are obtained from the Hertz potentials U and V which are given by Hill and Wait (1978)

$$U=\Gamma[A_m(\lambda)K_m(v\rho)+P_m(\lambda)I_m(v\rho)] \tag{A.1}$$

$$V=\Gamma[B_m(\lambda)K_m(v\rho)+Q_m(\lambda)I_m(v\rho)] \tag{A.2}$$

where

$$\Gamma[\ \ ]=\int_{-\infty}^{\infty}\sum_{-\infty}^{\infty}[\ \ ]\exp[-im(\phi-\phi_0)]\exp(-i\lambda z)\,d\lambda$$

$$v=(\lambda^2+\gamma_0^2)^{1/2},\quad \gamma_0=i\omega(\mu_0\varepsilon_0)^{1/2} \tag{A.3}$$

and I_m and K_m are modified Bessel functions. The integration contour is taken along the real axis in the complex λ plane, and the summation is taken over all integer values of m from $-\infty$ to $+\infty$.

The terms involving K_m represent the primary field (for $\rho_0<\rho<a_0$). For the electric dipole source, A_m and B_m are given by

$$A_m(\lambda)=\frac{-Il_{0e}}{4\pi^2\omega\varepsilon_0}\left(\frac{\lambda}{2v}\right)[\exp(i\phi_0)I_{m+1}(v\rho_0)+\exp(-i\phi_0)I_{m-1}(v\rho_0)] \tag{A.4}$$

$$B_m(\lambda)=\frac{Il_{0e}}{4\pi^2}\left(\frac{i}{2v}\right)[\exp(-i\phi_0)I_{m-1}(v\rho_0)-\exp(i\phi_0)I_{m+1}(v\rho_0)] \tag{A.5}$$

For the magnetic dipole source, A_m and B_m are given by

$$A_m(\lambda)=\frac{i\omega\mu_0 IA_{0e}}{4\pi^2}\left(\frac{i}{2v}\right)[\exp(-i\phi_0)I_{m-1}(v\rho_0)-\exp(i\phi_0)I_{m+1}(v\rho_0)] \tag{A.6}$$

$$B_m(\lambda)=\frac{IdA}{4\pi^2}\left(\frac{-i\lambda}{2v}\right)[\exp(i\phi_0)I_{m+1}(v\rho_0)+\exp(-i\phi_0)I_{m-1}(v\rho_0)] \tag{A.7}$$

The terms involving I_m in (A.1) and (A.2) represent the secondary fields due to the tunnel walls. P_m and Q_m are related to A_m and B_m by the following

$$P_m(\lambda) = -\left\{ A_m(\lambda)\left[\left(\frac{m\lambda}{v^2 a_0}-\alpha_m\right)^2 + \left(\frac{\gamma_0 K'_m}{vK_m}+\eta_0 Y_m\right)\left(\frac{\gamma_0 I'_m}{vI_m}+\frac{Z_m}{\eta_0}\right)\right] I_m K_m \right.$$
$$\left. + B_m(\lambda)\left(\frac{m\lambda}{v^2 a}-\alpha_m\right)\frac{i\omega\mu_0}{v^2 a} D_m^{-1}\right\} \tag{A.8}$$

$$Q_m(\lambda) = -\left\{ B_m(\lambda)\left[\left(\frac{m\lambda}{v^2 a_0}-\alpha_m\right)^2 + \left(\frac{\gamma_0 I'_m}{vI_m}+\eta_0 Y_m\right)\left(\frac{\gamma_0 K'_m}{vK_m}+\frac{Z_m}{\eta_0}\right)\right] I_m K_m \right.$$
$$\left. - A_m(\lambda)\left(\frac{m\lambda}{v^2 a_0}-\alpha_m\right)\frac{i\omega\varepsilon_0}{v^2 a}\right\} D_m^{-1} \tag{A.9}$$

where

$$D_m = \left[\left(\frac{m\lambda}{va_0}-\alpha_m\right)^2 + \left(\frac{\gamma_0 I'_m}{vI_m}+\eta_0 Y_m\right)\left(\frac{\gamma_0 I'_m}{vI_m}+\frac{Z_m}{\eta_0}\right)\right] I_m^2$$
$$\alpha_m = m\lambda/(u^2 a_0)$$
$$Z_m = -(i\omega\mu_e/u) K'_m(ua_0)/K_m(ua_0)$$
$$Y_m = [i\gamma_e^2/(u\omega\mu_e)] K'_m(ua_0)/K_m(ua_0)$$
$$\gamma_e^2 = i\omega\mu_e(\sigma_e + i\omega\varepsilon_e)$$

and

$$u = (\lambda^2+\gamma_e^2)^{1/2}$$

In (A.8) and (A.9), the following notational simplicity has been used: $I_m = I_m(va_0)$, $I'_m = I'_m(va_0)$, $K_m = K_m(va_0)$, and $K'_m = K'_m(va_0)$.

Appendix B. Cable fields

The fields due to the axial cable current are obtained from the Hertz potentials U_c and V_c which are given by Hill and Wait (1978)

$$U_c = \int_{-\infty}^{\infty} F_c(\lambda)\left[K_0(v\rho_d) - \sum_{m=-\infty}^{\infty} R_m(\lambda)\frac{K_m(va_0)}{I_m(va_0)} I_m(v\rho) I_m(v\rho_c)\right.$$
$$\left. \times \exp[-im(\phi-\phi_c)]\right] \exp(-i\lambda z)\, d\lambda \tag{B.1}$$

$$V_c = \int_{-\infty}^{\infty} F_c(\lambda) \sum_{m=-\infty}^{\infty} I_m(v\rho_c)\Delta_m(\lambda) I_m(v\rho) \exp[-im(\phi-\phi_c)] \exp(-i\lambda z)\, d\lambda \tag{B.2}$$

where

$$\rho_d = [\rho^2+\rho_c^2-2\rho\rho_c\cos(\phi-\phi_c)]^{1/2}$$

To satisfy the boundary conditions at the tunnel walls, $R_m(\lambda)$ and $\Delta_m(\lambda)$ are given by

$$-R_m(\lambda)\frac{K_m(va_0)}{I_m(va_0)} = \left.\frac{P_m(\lambda)}{A_m(\lambda)}\right|_{B_m=0} \tag{B.3}$$

and

$$\Delta_m(\lambda)=\left.\frac{Q_m(\lambda)}{A_m(\lambda)}\right|_{B_m=0} \tag{B.4}$$

where $P_m(\lambda)$ and $Q_m(\lambda)$ are given by (A.8) and (A.9).

The factor $F_c(\lambda)$ is given by

$$F_c(\lambda)=\hat{E}_z(\lambda)/D(\lambda) \tag{B.5}$$

where

$$\hat{E}_z(\lambda)=\hat{E}_z^p(\lambda)-v^2\sum_{m=-\infty}^{\infty}P_m(\lambda)I_m(v\rho_c)\exp\left[-im(\phi_c-\phi_0)\right] \tag{B.6}$$

and

$$D(\lambda)=2\pi i\omega\varepsilon_0 Z(\lambda)+v^2\left[K_0(vc)-\sum_{m=-\infty}^{\infty}R_m(\lambda)\frac{k_m(va_0)}{I_m(va_0)}I_m(v\rho_c)I_m[v(\rho_c+c)]\right] \tag{B.7}$$

The modal equation to determine the discrete propagation modes in the tunnel (Wait and Hill 1975) is simple $D(\lambda)=0$.

The quantity $\hat{E}_z^p(\lambda)$ is actually the Fourier transform of the axial electric field due to the direct or primary influence of the source dipole, evaluated at the cable. For an x-directed electric dipole, $\hat{E}_z^p(\lambda)$ is given by

$$\hat{E}_z^p(\lambda)=\frac{Il_{0e}}{4\pi^2\omega\varepsilon_0}(\lambda v)\frac{\rho_c\cos\phi_c-\rho_0\cos\phi_0}{\hat{\rho}_c}K_1(v\hat{\rho}_c) \tag{B.8}$$

Finally, for an x-directed magnetic dipole, $\hat{E}_z^p(\lambda)$ is given by

$$\hat{E}_z^p(\lambda)=-\frac{i\omega\mu_0 IA_{0e}}{4\pi^2}v\frac{\rho_c\sin\phi_c-\rho_0\sin\phi_0}{\hat{\rho}_c}K_1(v\hat{\rho}_c) \tag{B.9}$$

Acknowledgments

The problem was actually suggested by Dr. H. K. Sacks and we appreciate his sustained interest in this work. Also we would like to thank Mrs. Lana Hope for help in preparing the manuscript and Mr. Robert McDonald for drafting the figures.

References

Beal, J. C., Josiak, J., Mahmoud, S. F., and Rawat, V., 1973, *Proc. Inst. elect. electron. Engrs.* **61**, 562.

Breitenbach, O., 1974, *Proceedings of the International Colloquium on Leaky-Feeder Communications*, Surrey, England, pp. 197–225.

Cree, D. J., 1975, *J. Br. Instn Radio Engrs*, **45**, 215.

Cribbens, A. H., 1974, *Proceedings of the International Colloquium on Leaky-Feeder Communications*, Surrey, England, pp. 250–262.

Delogne, P., 1974, *Proceedings of the International Conference on Radio: Roads, Tunnels and Mines*, pp. 129–136.

Deryck, L., 1975, *J. Br. Instn Radio Engrs*, **45**, 241.

Fontaine, J., De Moulin, B., DeGauque, P., and Gabillard, R., 1973. *Proceedings of the Thru-the-Earth Electromagnetics Workshop*, Acc. No. PB 231 154, National Technical Information Service, Springfield, VA 22151, U.S.A., pp. 130–139.

Haining, R. W., 1974, *Proceedings of the International Colloquium on Leaky-Feeder Communications*, Surrey, England, pp. 236–249.

HAMMING, R. W., 1973, *Numerical Methods for Scientists and Engineers* (New York: McGraw-Hill).

HARMS, P. L., JOHANNESSEN, R., and FERNANDES, A. S. C., 1974, *Proceedings of the International Colloquium on Leaky-Feeder Communications*, Surrey, England, pp. 82–96.

HILL, D. A., and WAIT, J. R., 1974, *J. appl. Phys.*, **45**, 3402; 1976, *Radio Sci.*, **4**, 315; 1978, *I.E.E.E. Trans. Geosci. Electron.*, **16**, 118.

MAHMOUD, S. F., 1974, *I.E.E.E. Trans. Commun.*, **22**, 1547.

MARTIN, D. J. R., 1975, *J. Br. Instn Radio Engrs*, **45**, 205.

OKADA, O., KISHIMOTO, T., AKAGAWA, K., NAKAHARA, Y., MIKOSHIBA, K., HORIGUCHI, F., and OKAMOTO, K., 1975, *J. Br. Instn Radio Engrs*, **45**, 224.

RAWAT, V., and BEAL, J. C., 1974, *Proceedings of the Colloquium on Leaky-Feeder Radio Communications*, Surrey, England, pp. 108–124.

SEIDEL, D. B., and WAIT, J. R., 1978 a, *I.E.E.E. Trans. microw. Theory Tech.*, **26**, 494; 1978 b. *I.E.E.E. Trans. Antennas Propag.*, **26**, 690; 1978 c, Preliminary Report on Contract HO155008 to U.S. Bureau of Mines.

WAIT, J. R., 1959, *Electromagnetic Radiation from Cylindrical Structures* (New York: Pergamon).

WAIT, J. R., and HILL, D. A., 1975, *I.E.E.E. Trans. microw. Theory Tech.*, **23**, 401.

Radio transmission in an elliptical tunnel with a contained axial conductor

David B. Seidel and James R. Wait

Cooperative Institute for Research in Environmental Sciences, University of Colorado, Boulder, Colorado 80309

(Received 24 May 1978; accepted for publication 28 July 1978)

Electromagnetic transmission in a straight cylindrical tunnel with imperfectly conducting walls is considered when the cross section is in elliptical form. The presence of a thin axial conductor is also allowed for in the boundary-value formulation. The general matrix solution is simplified by invoking the quasistatic approximation which is shown, at least for circular tunnel geometry, to be valid for frequencies up to 20 MHz. The results of the quasistatic calculations indicated that the attenuation rate of the dominant mode is relatively insensitive to the ellipticity if the cross-section area and the cable-to-wall separation is kept constant.

PACS numbers: 41.10.Hv, 84.40.Cb

I. INTRODUCTION

The propagation of electromagnetic waves in a cylindrical tunnel with finitely conducting walls has been analyzed by Wait and Hill[1] where the effect of a contained axial conductor was also considered. To facilitate the boundary-value solution, the tunnel cross section was assumed to be circular and then the requisite radial wave solutions are Bessel functions. Also, in this case, the eigenmodes or characteristics modes were not coupled by the imperfectly conducting tunnel wall.

Of course, railway, road, and particularly mine tunnels are not circular in cross section. Thus, there is a need to know if the assumed cross-sectional shape is a critical parameter in the prediction of the attenuation rate of the dominant mode. This has motivated us to consider a cylindrical tunnel with an elliptical cross section.

II. FORMULATION

Specifically, we deal with an air-filled tunnel of elliptical cross section bounded by a lossy dielectric medium as shown in Fig. 1. The tunnel cross section's semimajor and minor axes are denoted by a and b, respectively. The tunnel interior is characterized by the permittivity and permeability of free space ϵ_0 and μ_0, respectively; for the exterior rock region, the conductivity, permittivity, and permeability are σ_e, ϵ_e, and μ_e, respectively.

We now define an elliptical cylindrical coordinate system whose z axis is aligned parallel to the tunnel and whose transverse coordinates are defined by

$$x = d\cosh\xi\cos\phi,$$
$$y = d\sinh\xi\sin\phi, \tag{1}$$

where x and y are the standard transverse Cartesian coordinates. Here d is the semifocal distance and is given by $d^2 = a^2 - b^2$. The tunnel wall surface is then characterized by $\xi = \xi_a$, where $\xi_a = \tanh^{-1}(b/a)$. A thin axial conductor or coaxial cable is suspended in the tunnel whose center point is located at $\xi = \xi_0$ and $\phi = \phi_0$. We assume that the fields vary as $\exp(i\omega t - \Gamma z)$, where Γ is the as yet unknown axial propagation constant. This dependence will be understood but suppressed in what follows.

The objective now is to find the complex propagation constants (Γ) of the dominant propagating modes. Toward this end, we formulate a mode equation by enforcing an impedance boundary condition at the surface of the thin wire or cable which is given by[1]

$$E_z(\xi_w, \phi_w) - I_0 Z_s = 0, \tag{2}$$

where (ξ_w, ϕ_w) is a point on the wire surface, I_0 is the total axial current on the wire or cable, and Z_s is the series impedance of the wire or cable. Expressions for the series impedance of a simple wire conductor and a leaky coaxial cable are available in Wait[2] and Wait and Hill,[3] respectively. It simply remains to find the axial electric field due to the current filament I_0.

III. GENERAL COUPLED MODE SOLUTION

To obtain a solution, we make use of the fact that the field can be determined by two scalar functions U and V which are, respectively, the z components of electric and

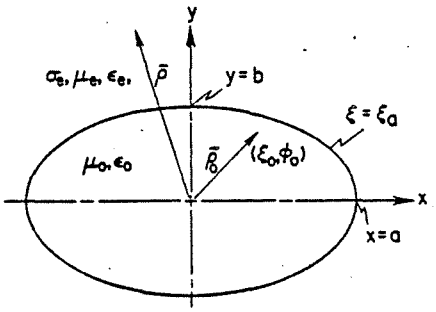


FIG. 1. Geometry of elliptical tunnel showing location of axial conductor or cable at (ξ_0, ϕ_0).

 0021-8979/79/020602-04$01.10

magnetic Hertz vectors. It is well known[2] that the primary fields due to I_e may be obtained from an electric Hertz potential

$$U^p = I_e(4\omega\epsilon_0)^{-1}H_0^{(2)}(vR), \tag{3}$$

where v is the transverse wave number inside the tunnel given by $v^2 = k_0^2 + \Gamma^2$, $k_0^2 = \omega^2\mu_0\epsilon_0$, and $R = |\bar{\rho} - \bar{\rho}_0|$. Here $H_0^{(2)}$ is the Hankel function of the second kind of order zero.

Using an appropriate addition theorem,[4] we express U^p as a sum of Mathieu functions:

$$U^p = I_e \sum_{\alpha,m,n} A\alpha_{mn} S\alpha_{2m+n}(vd,\cos\phi) \times H\alpha_{2m+n}^{(2)}(vd,\cosh\xi), \quad \xi > \xi_e, \tag{4}$$

where

$$A\alpha_{mn} = (1/\omega\epsilon_0) S\alpha_{2m+n}(vd,\cos\phi_0) J\alpha_{2m+n}(vd,\cosh\xi_0). \tag{5}$$

Here, and in what follows, we use the notation of Morse and Feshbach[4] with regard to Mathieu functions with the addition that here α represents either e or o denoting even or odd symmetry of the periodic Mathieu function. Hence, a sum over α denotes the sum of even and odd functions. Similarly, n assumes the values 0 or 1, representing π- and 2π-periodic Mathieu functions, respectively. Finally, m may be any nonnegative integer. Note that $A\alpha_{mn}$ is a known coefficient, dependent only upon the location of the axial conductor. It should also be noted that in Eq. (4), we have chosen the periodic Mathieu functions to be orthonormal, that is, for any complex s,

$$\int_0^{2\pi} [S\alpha_{2m+n}(s,\cos\phi)]^2 d\phi = 1.$$

The potential functions U and V are comprised of homogeneous solutions to the wave equation in addition to the particular solution U^p. Thus, we can respresent these functions in the tunnel interior (i.e., for $\xi_0 < \xi < \xi_e$) by

$$U = I_e \sum S\alpha_{2m+1}(vd,\cos\phi)[A\alpha_{mn} H\alpha_{2m+n}^{(2)}(vd,\cosh\xi) + R\alpha_{mn} J\alpha_{2m+n}(vd,\cosh\xi)] \tag{6}$$

and

$$V = I_e \sum P\alpha_{mn} S\alpha_{2m+n}(vd,\cos\phi) J\alpha_{2m+n}(vd,\cosh\xi), \tag{7}$$

where $R\alpha_{mn}$ and $P\alpha_{mn}$ are presently unknown coefficients of modal expansions of the homogeneous solutions for the potentials. By a similar argument, for $\xi > \xi_e$,

$$U = I_e \sum T\alpha_{mn} S\alpha_{2m+n}(ud,\cos\phi) H\alpha_{2m+n}^{(2)}(ud,\cosh\xi) \tag{8}$$

and

$$V = I_e \sum Q\alpha_{mn} S\alpha_{2m+n}(ud,\cos\phi) H\alpha_{2m+n}^{(2)}(ud,\cosh\xi) \tag{9}$$

where, analogously, $T\alpha_{mn}$ and $Q\alpha_{mn}$ are unknown coefficients. Here u is the transverse wave number in the medium exterior to the tunnel, given by $u^2 = k_e^2 + \Gamma^2$ where $k_e^2 = \omega\mu_e(\omega\epsilon_e - i\sigma_e)$.

From U and V, we can obtain the field components tangential to the tunnel wall. For the region $\xi < \xi_e$, these components are given by[2]

$$E_\phi = \frac{1}{D}\left(\Gamma\frac{\partial U}{\partial\phi} + i\omega\mu_0\frac{\partial V}{\partial\xi}\right),$$
$$H_\phi = \frac{1}{D}\left[\left(\frac{-ik_0^2}{\omega\mu_0}\right)\frac{\partial U}{\partial\xi} + \Gamma\frac{\partial V}{\partial\phi}\right], \tag{10}$$
$$E_z = v^2 U, \quad \text{and} \quad H_z = v^2 V,$$

where $D^2 = (\cosh^2\xi - \cos^2\phi)d^2$. For the region $\xi > \xi_e$, the corresponding field components are obtained by replacing k_0, v, and μ_0 by k_e, u, and μ_e, respectively.

We now solve for the four sets of unknown coefficients $R\alpha$, $P\alpha$, $Q\alpha$, and $T\alpha$ by forcing the four components of the tangential fields to be continuous at the tunnel wall. In a circular tunnel, because of the orthogonality between the trigonometric expansion functions and their derivatives, it is sufficient to enforce continuity for each mode of the field expansions independently.[1] However, for the case of elliptical cross section, this is no longer true because of the dependence of the periodic Mathieu functions upon the medium (through u and v). This results in a corresponding lack of orthogonality which complicates the solution.

We can, however, make use of the somewhat limited orthogonality between the two media, as indicated by

$$\int_0^{2\pi} S\alpha_{2m+n}(ud,\cos\phi) S\alpha_{2m'+n'}(vd,\cos\phi)\, d\phi = M\alpha_{mmn}\delta_{\alpha\alpha}\delta_{nn'} \tag{11}$$

and

$$\int_0^{2\pi} S\alpha_{2m+n}(ud,\cos\phi)\frac{d}{d\phi}[S\alpha_{2m'+n'}(vd,\cos\phi)]\, d\phi = K\alpha_{mmn}\delta_{\bar{\alpha}\alpha}\delta_{nn'}, \tag{12}$$

where $\bar{\alpha}$ denotes the opposite symmetry to α (i.e., if $\alpha = e$, then $\bar{\alpha} = o$ and vice versa). These relationships [Eqs. (11) and (12)] are also the definitions of the coupling coefficients $M\alpha$ and $K\alpha$. To solve for the unknown expansion coefficients in Eqs. (6)–(9), we enforce continuity of the four field components [Eq. (10)] at the tunnel wall, then multiply each of the resulting four equations by $S\alpha_{2m+n}(ud,\cos\phi)$ and integrate over ϕ. Now the two axial field continuity equations can be substituted into the remaining two equations. After considerable algebraic manipulation, we obtain the following equations for $R\alpha$ and $P\bar{\alpha}$:

$$\sum_j [R\alpha_{jn} f^{jm}_{an} + P\bar{\alpha}_{jn} g^{jm}_{an}] = \beta_{amn}, \tag{13}$$

$$\sum_j [R\alpha_{jn} h^{jm}_{an} + P\bar{\alpha}_{jn} s^{jm}_{an}] = \gamma_{amn}, \tag{14}$$

where

$$f^{jm}_{an} = M\alpha_{jmn}(\mu_0 k_e^2 v^2 t'_{amn} r_{ajn} - \mu_e k_0^2 u^2 t_{amn} r'_{ajn}),$$

$$g^{jm}_{an} = (i\omega\mu_0\mu_e\Gamma)(k_0^2 - k_e^2) K\alpha_{jmn} t_{amn} r_{\bar{a}jn},$$

$$h^{jm}_{an} = \Gamma(k_0^2 - k_e^2) K\bar{\alpha}_{jmn} t_{\bar{a}mn} r_{ajn},$$

$$s^{jm}_{an} = i\omega M\bar{\alpha}_{jmn}[\mu_e v^2 t'_{\bar{a}mn} a_{\bar{a}jn} - \mu_0 u^2 t_{\bar{a}mn} a'_{\bar{a}jn}], \tag{14}$$

$$\beta_{amn} = -\sum_j M\alpha_{jmn}(\mu_0 k_e^2 v^2 t'_{amn} a_{ajn} - \mu_e k_0^2 u^2 t_{amn} a'_{ajn}) A\alpha_{jn},$$

$$\gamma_{amn} = -\Gamma(k_0^2 - k_e^2) t_{\bar{a}mn} \sum_j K\bar{\alpha}_{jmn} a_{ajn} A\alpha_{jn}.$$

In Eq. (14) we have adopted the shorthand notation for the various radial Mathieu functions evaluated at the tunnel wall as follows:

$$a_{amn} = H\alpha^{(2)}_{2m+n}(vd, \cosh\xi_a),$$

$$r_{amn} = J\alpha_{2m+n}(vd, \cosh\xi_a), \tag{15}$$

$$t_{amn} = H\alpha^{(2)}_{2m+n}(ud, \cosh\xi_a).$$

Similarly, a prime on any of the left-hand sides in Eq. (15) denotes the derivative with respect to ξ of the radial Mathieu function in the corresponding right-hand side of Eq. (15) evaluated at $\xi = \xi_a$.

We note that Eq. (13) represents four independent pairs of coupled infinite matrix equations. Each of these four pairs corresponds to one of the four combinations of α and n (that is, one of the four combinations of even or odd symmetry and π or 2π periodicity). This partial decoupling is due to the limited orthogonality expressed in Eqs. (11) and (12). The solution obtained in Eq. (13) is similar in form to, and patterned after, that obtained by Yeh[3] when considering the propagating modes of an elliptical dielectric fiber. However, in that case, there is not an axial current-carrying conductor, and correspondingly, the infinite matrix equation analogous to Eq. (13) is homogeneous. Hence, zeros in the determinant of the matrix correspond to the characteristic eigenmodes of that system.

At this point, it is useful to consider some limiting cases of Eq. (13). First, we let the tunnel walls be perfectly conducting, that is, we let σ_e approach infinity. Because E_z must vanish at $\xi = \xi_a$, it is readily seen using Eqs. (6) and (10) that

$$R\alpha_{mn} = = -A\alpha_{mn} a_{amn}/r_{amn} \tag{16}$$

and, as in the case of a circular cross section, continuity is enforced in each mode of the field expansion independently.

Another useful limiting case is that when $\Gamma = 0$ (two-dimensional z-independent case). Here only a scalar function U is needed to determine the fields. Hence Eq. (13) reduces to the single infinite matrix equation

$$\sum_j R\alpha_{jn} f^{jm}_{an} = \beta_{amn}. \tag{17}$$

Also note that because now $v = k_0$ and $u = k_e$, the expressions for f and β in Eq. (14), and thus Eq. (17), can be somewhat simplified.

Now if Eq. (13) can be inverted, we can find $E_z(\xi_w, \phi_w)$ using Eqs. (6) and (10) for various values of Γ. Thus we can obtain characteristic values of Γ by employing some iterative root-finding procedure in the complex plane on Eq. (2).

IV. QUASISTATIC SOLUTION

Although a general numerical solution of Eq. (2) by iterative techniques is possible, such a solution would be very arduous. However, we can make some quasistatic approximations and obtain a much simpler solution that is adequate for many practical cases. In obtaining this solution, we will use some general results of previous quasistatic solutions for similar geometries.[6,7]

First we express Eq. (2) in the form

$$\Gamma^2 = ZY, \tag{18}$$

where $Z = Z_0 + Z_e + Z_s$ and $Y = -k_0^2/Z_0$. But this is not an explicit expression for Γ because Z and Y both depend upon Γ in a rather complicated fashion. However, it has been previously shown that under certain restrictions, Z_0 and Z_e are independent of Γ for a wire or cable suspended both within a circular tunnel[6] and above a lossy dielectric half-space.[7] In both cases, the restrictions are that $|va_0| \ll 1$ and $|k_e/k_0|^2 \gg 1$, where a_0 represents the tunnel radius or the height of the wire above the half-space, as the case may be. We will subsequently refer to this approximation as the three-dimensional quasistatic approximation.

In each case, if we further restrict $k_0 a_0 \ll 1$, then it is fairly simple to show that

$$Z_0 \simeq \lim_{\sigma_e \to \infty} (-E_z(\bar{\rho}_w)/I_0)\,|_{\Gamma=0}$$

and

$$Z_0 + Z_e \simeq -E_z(\bar{\rho}_w)/I_0\,|_{\Gamma=0}, \tag{19}$$

where $E_z(\bar{\rho}_w)$ is the axial field at a point $\bar{\rho}_w$ at the surface of the conductor due to a filamentary current I_0 at the center of the conductor. Thus we see that this more specialized quasistatic approximation (19) depends only upon the fields to the z-invariant problem and hence we will refer to it as the two-dimensional quasistatic approximation.

We now assume that this two-dimensional quasistatic approximation is also true for conductors in tunnels of elliptical cross section, as well as in circular tunnels and over lossy half-spaces. With this assumption, we can now obtain a much simpler solution for the propagation constants of the low-frequency dominant modes using solutions obtained using Eqs. (16) and (17) in Eqs. (18) and (19).

V. NUMERICAL ANALYSIS

Here we present some numerical results using the two-dimensional quasistatic approximation discussed above. The periodic and radial Mathieu functions were computed

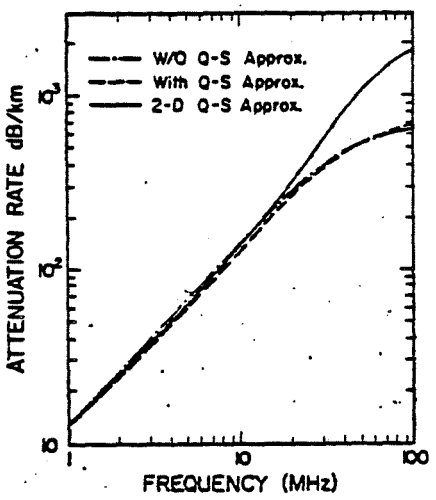


FIG. 2. Attenuation rate versus frequency for ciruclar tunnel showing validity of quasistatic approximations. Paramters: $a_0 = 2$ m, $a_0 - \rho_0 = 0.4$ m, $\epsilon_c = 10\epsilon_0$, $\sigma_c = 10^{-2}$ mhos/m, $c = 1$ cm, $\sigma_w = 10^5$ mhos/m.

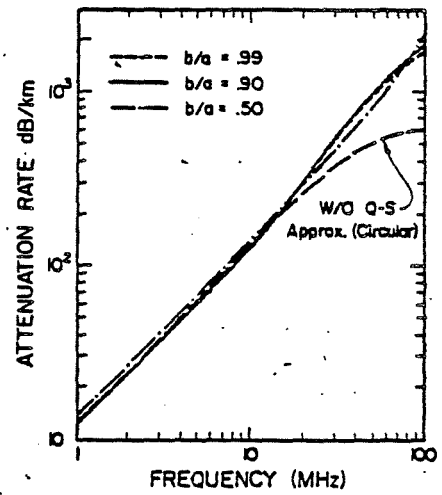


FIG. 3. Attenuation rate of elliptical tunnel model calculated for a quasistatic approximation and comparison with circular tunnel model. Parameters: $a_0 = (ab)^{1/2} = 2$ m, $\Delta = 0.4$ m, $\epsilon_c = 10\epsilon_0$, $\sigma_c = 10^{-2}$ mhos/m, $c = 1$ cm, $\sigma_w = 10^5$ mhos/m. Values of ellipticity b/a are indicated.

numerically using algorithms suggested by various expressions in Morse and Feshbach[4] and Blanch.[5] The infinite matrix equation in Eq. (17) was inverted by truncating the matrix to various sizes, inverting, and then observing the convergence of the solution to Eq. (17) as well as convergence of the truncated sum in Eq. (6).

Before proceeding with the numerical results for the elliptical tunnel, it is worthwhile to consider the accuracy and applicability of the two quasistatic approximations discussed earlier for a circular cylinder. Figure 2 shows a comparison of the two approximate solutions for the attenuation rate [proportional to Real(Γ)] versus frequency for a circular tunnel containing a simple wire conductor of radius 1 cm and conductivity of 10^5 mhos/m. Other parameters are $a_0 = 2$ m, $\epsilon_c = 10\epsilon_0$, and $\sigma_c = 10^{-2}$ mhos/m. The wire conductor is located at a distance $\rho_0 = 1.6$ m from the center of the tunnel. Here the exact solution is that obtained by iterative techniques without any quasistatic approximations. This solution is taken from Wait and Hill.[1] The three-dimensional quasistatic approximation is computed as described in Wait[6] and the two-dimensional approximation is computed using appropriate expressions for the fields in a z-invariant circular tunnel in Eq (19) and then Eq. (18). Note that the three-dimensional approximation is very accurate even as high as 100 MHz, whereas the two-dimensional approximation accuracy is good only to about 20 MHz. Indeed, it turns out that for all frequencies shown in Fig. 2, $|\nu a_0| < 0.05$, but at 20 MHz, $k_0 a_0 = 0.84$.

Figure 3 shows the attenuation rate versus frequecy for various elliptical cross-section eccentricities. All parameters are the same as in Fig. 2 if we define $a_0 = (ab)^{1/2}$ for the elliptical cross section. This definition of a_0 has the effect of keeping the cross-sectional area of the tunnel fixed for any eccentricity, so long as a_0 is held constant. Also, in all cases, the wire conductor is centered at a point along the major axis of the tunnel cross section and 0.4 m from the tunnel wall ($a - x_0 = 0.4$ m, $y_0 = 0$). In addition to the elliptical tunnel solutions, the corresponding exact circular solution from Wait and Hill[1] is also shown. As indicated, for frequencies less than about 20 MHz, the attenuation rate is essentially independent of tunnel eccentricity and corresponds to the circular tunnel solutions. Only above 20 MHz, where a two-dimensional quasistatic approximation is no longer valid, is any difference seen in the attenuation rate of the various tunnel cross sections. These results lead to the conclusion that the attenuation rate at relatively low frequencies is essentially independent of cross-sectional shape, but it is rather dependent upon the cross-sectional area of the tunnel. The influence of other parameters, including wire/tunnel wall proximity, remains essentially the same as in circular tunnels.

VI. FINAL REMARKS

While we certainly have not examined the full blown modal equation for the problem, we can assert with some certainty that the tunnel cross-sectional shape is not critical. Further support for this contention comes from earlier calculations for a rectangular tunnel model.[9] Of much importance in actual tunnels is how the tunnel cross section changes in the longitudinal direction. studies of nonuniform tunnel models are now underway.

[1] J.R. Wait and D.A. Hill, IEEE Trans. Antennas Propag. AP-22, 627 (1974).
[2] J.R. Wait, *Electromagnetic Radiation from Cylindrical Structures* (Pergamon, Oxford, 1959).
[3] J.R. Wait and D.A. Hill, IEEE Trans. Microwave Theory Tech. MTT-23, 401 (1975).
[4] P.M. Morse and H. Feshbach, *Methods of Theoretical Physics, Part II* (McGraw-Hill, New York, 1953).
[5] C. Yeh, J. Appl. Phys. 33, 3235 (1962).
[6] J.R. Wait, IEEE Trans. Antennas Propag. AP-25, 441 (1977).
[7] J.R. Wait, Radio Sci. 7, 675 (1972).
[8] G. Blanch, *Tables Relating to Mathieu Functions* (U.S. National Bureau of Standards, Washington, 1967).
[9] S.F. Mahmoud and J.R. Wait, IEEE Trans. Commun. COM-24, 82 (1976).

Low-Frequency Behavior of the Propagation Constant Along a Thin Wire in an Arbitrarily Shaped Mine Tunnel

EDWARD F. KUESTER, MEMBER, IEEE, AND DAVID B. SEIDEL, MEMBER, IEEE

Abstract—Seidel and Wait have investigated the complex propagation constant (phase and attenuation coefficients) of the fundamental mode of propagation for radio waves along a thin wire or cable, located in an elliptical mine tunnel, and found that the attenuation rate for low frequency is insensitive to the shape of the ellipse if the cable-wall distance and cross-sectional area are kept constant. We consider here tunnels of more general cross section, and obtain a characteristic equation for the propagation constant, valid for sufficiently low frequency, by means of a variational formulation of an integral equation. The characteristic equation involves only the electrical parameters of the tunnel walls, the radius of the wire, and the capacitance per unit length that the wire would have if the tunnel walls were perfectly conducting. Agreement with exact calculations for several geometries is found to be excellent below about 100 kHz, and acceptable even up to 1 MHz or more, for typical tunnel parameters. Since the wire capacitance can be shown to depend most importantly on its distance from the wall and on the area of the tunnel, the conclusion of Seidel and Wait can be made more precise and extended to tunnels of arbitrary cross section.

I. Introduction

MUCH INTEREST has been shown recently in the attenuation and propagation constants of waves propagating along wires, cables, rails, or other such structures in mine tunnels, because of the extensive use to which these have been put for communications purposes. When the adjacent rock which forms the tunnel wall has finite conductivity, it is necessary to idealize the problem by assuming some simple cross-sectional shape (usually circular) for the tunnel in order to formulate the problem exactly [1]–[3]. Recently, Seidel and Wait [4] investigated the case of an elliptical mine tunnel in order to determine the effect of a noncircular cross section on the attenuation constant. It was found that the attenuation rate at low frequency is insensitive to the eccentricity of the ellipse if the cable-wall distance and cross-sectional area are kept constant. It might reasonably be speculated that this result does not depend on the specific shape of the tunnel involved, but only on some more general property of the tunnel.

Manuscript received September 25, 1978; revised January 25, 1979. This work was supported by the U.S. Bureau of Mines under Contract with the Institute for Telecommunication Sciences/NTIA, U.S. Department of Commerce, Boulder, CO 80303, J. R. Wait, Principal Investigator, and H. K. Sacks, Project Officer for Bureau of Mines.

E. F. Kuester is with the Electromagnetics Laboratory, Department of Electrical Engineering, University of Colorado, Boulder, CO 80309.

D. B. Seidel was with the Cooperative Institute for Research in Environmental Sciences, University of Colorado/NOAA, Boulder, CO 80309. He is now with Sandia Laboratories, Albuquerque, NM 87115.

In this work, tunnels of arbitrary shape will be considered, and a characteristic equation for the propagation constant and attenuation rate at low frequencies will be obtained by means of a variational formulation of an integral equation for the electric field of the transmission-line mode. This equation involves only the electrical parameters of the tunnel walls, the radius of the wire, and the capacitance per unit length the wire would have if the tunnel walls were perfectly conducting. Comparisons of numerical results with those of more exact computations are presented.

II. Low-Frequency Characteristic Equation

A method for determining approximately the propagation constant at low frequency of a mode along a thin wire located within a mine tunnel of arbitrary cross section can be found by starting with Katsenelenbaum's [5] integral equation for the fields of a mode on an arbitrarily shaped dielectric rod. The tunnel geometry is indicated in Fig. 1. The medium external to the tunnel is assumed to be homogeneous and have permeability μ_0, permittivity ϵ, and conductivity σ, while the inside of the tunnel is air filled (μ_0, ϵ_0). The tunnel wall is denoted by the contour C, the circumference of the wire by the contour C_w, and the cross section of the tunnel (the region between C_w and C) by S. The interior cross section of the wire is denoted by S_w, and an outward normal unit vector to C or C_w will be denoted by $\bar{n}$ (or $\bar{n}'$, as appropriate).

By first assuming the wire to have a finite conductivity, we may express Katsenelenbaum's integral equation for this system as

$$\bar{E}(\bar{\rho}) = \frac{1}{2\pi}\left[\text{grad div} - \gamma_e^2\right] \cdot \int\int_{-\infty}^{\infty} \left(\frac{n^2(\bar{\rho}')}{N^2} - 1\right) \bar{E}(\bar{\rho}') K_0\left[u|\bar{\rho} - \bar{\rho}'|\right] dS' \quad (1)$$

where $\bar{\rho} = (x,y)$ and $\bar{\rho}' = (x',y')$ are points in the cross section, $\bar{E}$ is the vector electric field of the mode,

$$\gamma_e^2 = i\omega\mu_0(\sigma + i\omega\epsilon)$$

$$N^2 = (\epsilon - i\sigma/\omega)/\epsilon_0$$

$$n^2(\bar{\rho}) = \left[\epsilon(\bar{\rho}) - i\sigma(\bar{\rho})/\omega\right]/\epsilon_0$$

0018-9480/79/0800-0736$00.75

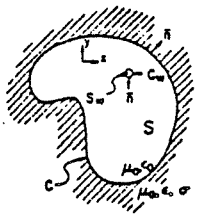


Fig. 1. Mine tunnel of arbitrary cross section.

$$u=(\gamma_e^2-\Gamma^2)^{1/2}, \qquad \mathrm{Re}(u)>0$$

and Γ is the yet unknown propagation constant, appropriate to an assumed propagation factor of exp $(i\omega t-\Gamma z)$ along the tunnel. The quantity $n^2(\bar{\rho})$ is the (complex) index of refraction at any point in the wire, in the tunnel or in the tunnel wall, so that the factor $(n^2(\bar{\rho})/N^2-1)$ vanishes outside of $S+S_w$, and the integral in (1) is only over a finite cross section. K_0 is the usual modified Bessel function of the second kind, and the operators "grad" and "div" are understood to have $\partial/\partial z$ replaced by $-\Gamma$ according to the implied propagation factor referred to above. A brief derivation of (1) is given in Appendix B.

A variational expression can be formed from (1) in the usual way [6] by taking the scalar product of both sides with $(n^2(\bar{\rho})/N^2-1)\bar{E}^T(\bar{\rho})$ and integrating over x and y (once again the integral is actually only over $S+S_w$). The superscript "T" denotes a transpose field which can be obtained from $\bar{E}(\bar{\rho})$ by changing the sign of $E_z(\bar{\rho})$. In what follows, we will assume for simplicity that the wire is perfectly conducting, though this is not essential to the technique. To handle this case, we let $\sigma(\bar{\rho})\to\infty$ and $\bar{E}(\bar{\rho})\to 0$ in S_w in such a way that $\sigma(\bar{\rho})\bar{E}(\bar{\rho})$ passes over into a surface current distribution $\bar{J}_s(\bar{\rho})$ concentrated on C_w. The resulting variational expression is

$$\begin{aligned}\Delta\int_S \bar{E}^T\cdot\bar{E}\,dS=&\frac{\Delta^2}{2\pi}\int_S \bar{E}^T(\bar{\rho})\\ &\cdot\left[\mathrm{grad\ div}-\gamma_e^2\right]\int_S \bar{E}(\bar{\rho}')K_0\,dS'\,dS\\ &-\frac{i\Delta}{2\pi\omega\epsilon_0N^2}\int_S \bar{E}^T(\bar{\rho})\cdot\left[\mathrm{grad\ div}-\gamma_e^2\right]\oint_{C_w}\bar{J}_s(\bar{\rho}')K_0\,dl'\,dS\\ &-\frac{i\Delta}{2\pi\omega\epsilon_0N^2}\oint_{C_w}\bar{J}_s^T(\bar{\rho})\cdot\left[\mathrm{grad\ div}-\gamma_e^2\right]\int_S \bar{E}(\bar{\rho}')K_0\,dS'\,dl\\ &-\frac{1}{2\pi}\frac{1}{(\omega\epsilon_0N^2)^2}\oint_{C_w}\bar{J}_s^T(\bar{\rho})\cdot\left[\mathrm{grad\ div}-\gamma_e^2\right]\oint_{C_w}\bar{J}_s(\bar{\rho}')K_0\,dl'\,dl\end{aligned} \tag{2}$$

where $\Delta=(1/N^2-1)$ and the argument of the Bessel function has been omitted for brevity.

Since the wire is assumed to be thin, proximity effects are neglected and $\bar{J}_s$ consists only of a longitudinal component J_{sz}. But conservation of charge and boundary conditions on $\bar{E}$ imply that

$$J_{sz}|_{C_w}=\frac{i\omega\epsilon_0}{\Gamma}n\cdot E\Big|_{C_w}=\frac{i\omega\epsilon_0}{\Gamma}\bar{n}\cdot\bar{E}^T\Big|_{C_w}=-J_{sz}^T|_{C_w} \tag{3}$$

and thus (2) reduces to

$$\begin{aligned}\Delta\int_S \bar{E}^T\cdot E\,dS=&\frac{\Delta^2}{2\pi}\int_S \bar{E}^T(\bar{\rho})\\ &\cdot\left[\mathrm{grad\ div}-\gamma_e^2\right]\int_S \bar{E}(\bar{\rho}')K_0\,dS'\,dS\\ &-\frac{\Delta}{2\pi N^2}\int_S \bar{E}^T(\bar{\rho})\cdot\mathrm{grad}\oint_{C_w}\left[\bar{n}'\cdot\bar{E}(\bar{\rho}')\right]K_0\,dl'\,dS\\ &+\frac{\Delta}{2\pi N^2}\oint_{C_w}\left[\bar{n}\cdot E(\bar{\rho})\right]\mathrm{div}\int_S \bar{E}(\bar{\rho}')K_0\,dS'\,dl\\ &+\frac{1}{2\pi}\frac{u^2}{N^4\Gamma^2}\oint_{C_w}\left[\bar{n}\cdot\bar{E}(\bar{\rho})\right]\oint_{C_w}\left[\bar{n}'\cdot\bar{E}(\bar{\rho}')\right]K_0\,dl'\,dl.\end{aligned} \tag{4}$$

As a trial function suitable for use when the frequency is sufficiently low, it seems appropriate to use the fields which would be present if the walls of the tunnel were perfectly conducting, i.e., the TEM fields $\bar{E}_0$, where

$$\bar{E}_0=-\nabla_t\Phi, \qquad \Phi|_{C_w}=V$$

$$\Phi|_C=0 \tag{5}$$

and "t" denotes the transverse part of an operator, obtained by setting $\partial/\partial z=0$. If $\bar{E}_0$ is inserted into (4) as the trial field, some simplification occurs because $\bar{E}_0$ has no z-component:

$$\begin{aligned}\Delta\int_S \bar{E}_0^2\,dS=&\frac{\Delta^2}{2\pi}\int_S \bar{E}_0(\bar{\rho})\cdot\left[\mathrm{grad}_t\,\mathrm{div}_t-\gamma_e^2\right]\int_S \bar{E}_0(\bar{\rho})K_0\,dS'\,dS\\ &-\frac{\Delta}{2\pi N^2}\int_S \bar{E}_0(\bar{\rho})\cdot\mathrm{grad}_t\oint_{C_w}\left[\bar{n}'\cdot\bar{E}_0(\bar{\rho}')\right]K_0\,dl'\,dS\\ &+\frac{\Delta}{2\pi N^2}\oint_{C_w}\left[\bar{n}\cdot\bar{E}_0(\bar{\rho})\right]\mathrm{div}_t\int_S \bar{E}_0(\bar{\rho}')K_0\,dS'\,dl\\ &+\frac{1}{2\pi}\frac{u^2}{N^4\Gamma^2}\oint_{C_w}\left[\bar{n}\cdot\bar{E}_0(\bar{\rho})\right]\oint_{C_w}\left[\bar{n}'\cdot E_0(\bar{\rho}')\right]K_0\,dl'\,dl.\end{aligned} \tag{6}$$

Moreover, by virtue of the special form (5) of $\bar{E}_0$, the individual terms of (5) can be reworked into more familiar quantities. These manipulations are carried out in Appendix A.

From (6), (A1), (A8)–(A11), we obtain an equation for determining Γ in the thin-wire approximation:

$$\begin{aligned}-\Delta=&\frac{-1}{2\pi}\left(\frac{C}{\epsilon_0}\right)\frac{u^2}{N^2\Gamma^2}\left[\ln\frac{ua}{2}+\gamma\right]-\Delta^2\Gamma^2N^2P\\ &+\frac{\Delta^2}{2\pi}u^2\Gamma^2N^2Q-\frac{\Delta}{\pi}u^2R\end{aligned} \tag{7}$$

where $\gamma=0.577\cdots$ is Euler's constant, C is the capacitance per unit length the wire would exhibit if the tunnel

walls were perfectly conducting, and

$$P=\frac{\epsilon_0}{CV^2}\int_S \Phi^2 dS \tag{8}$$

$$Q=\frac{\epsilon_0}{CV^2}\int_S \Phi(\bar{\rho})\int_S \Phi(\bar{\rho}')K_0 dS' dS \tag{9}$$

$$R=\frac{\epsilon_0}{CV^2}\oint_{C_w}\left[\bar{n}\cdot\bar{E}_0(\bar{\rho})\right]\int_S \Phi(\bar{\rho}')K_0 dS' dl. \tag{10}$$

Here V is the (arbitrary) potential difference associated with the trial field (5), and clearly drops out of (8)–(10).

As $\omega\to 0$, it can be seen that $N^2=0(1/\omega)$, $\gamma_e^2=0(\omega)$, $\Delta\to -1$, and with a certain amount of hindsight, $\Gamma=0(\omega)$[1], so that $u^2=0(\omega)$. Since (8)–(10) are $0(\omega^0)$ as $\omega\to 0$, it can be seen that, for sufficiently low frequencies, (7) will reduce to

$$\Delta=\frac{1}{2\pi}\left(\frac{C}{\epsilon_0}\right)\frac{u^2}{N^2\Gamma^2}\left[\ln\frac{ua}{2}+\gamma\right] \tag{11}$$

a result which involves the tunnel geometry only through the capacitance C, which is tabulated for many different cross-sectional shapes (see e.g., [7]). Since C is generally only weakly dependent on the dimensions of the tunnel, it can be seen that the low-frequency behavior of Γ will only weakly depend on these dimensions as well.

As a check on all of this, we can compare with a case for which a closed-form eigenvalue equation for Γ is available, namely a wire centered in a circular tunnel of radius b. Now, the exact equation is mathematically the same as that for the Goubau line [8], and the low-frequency limit is found by taking small argument forms for the Bessel functions involved (see [8]) and results in

$$\Delta\ln\left(\frac{b}{a}\right)=\frac{u^2}{N^2\Gamma^2}\left[\ln\frac{ua}{2}+\gamma\right] \tag{12}$$

which agrees with (11) since for this case, $C/\epsilon_0=2\pi/\ln(b/a)$.

A further comparison can be made with the quasi-static limit for the offset wire in a circular tunnel obtained by Wait [3]. Calling the radius of the tunnel b, once again, and denoting $v=(-\omega^2\mu_0\epsilon_0-\Gamma^2)^{1/2}$, Wait's approximations up to and including eq. (13) of [3] can be summarized in our notation as

$$|vb|\ll 1 \qquad |N^2|\gg 1$$

and hence, $u\simeq\gamma_e$. Since our assumptions correspond to $|\gamma_e b|\ll 1$, we must take the small argument forms of the modified Bessel functions in eq. (13) of [3], and insert this value into eq. (7) of the same reference. The result is

$$\Gamma^2=ZY \tag{13}$$

where

$$Z=-\frac{i\omega\mu_0}{2\pi}\left(\ln\frac{\gamma_e a}{2}+\gamma\right)+Z_s \tag{14}$$

[1]For present purposes, $0(\omega)$ will be understood to include behavior such as $\omega\ln\omega$, $\omega(\ln\omega)^2$, etc.

$$Y=2\pi i\omega\epsilon_0\left[\ln\frac{ab}{b^2-\rho_0^2}\right]^{-1} \tag{15}$$

where ρ_0 is the radial distance of the wire from the center of the tunnel, and Z_s is the axial impedance of the wire. Putting $Z_s=0$ in (14), making the previously indicated approximations in (11), and using the capacitance

$$\frac{C}{\epsilon_0}=2\pi\left[\ln\frac{b^2-\rho_0^2}{ab}\right]^{-1}$$

for the offset wire, we find that (13) and (11) give the same value for Γ.

Equation (11) can actually be cast in the suggestive form of (13) if we put

$$Z=\frac{i\omega\mu_0}{2\pi}\frac{u^2}{\Delta\gamma_e^2}\left(\ln\frac{ua}{2}+\gamma\right) \tag{16}$$

$$Y=i\omega C \tag{17}$$

in which case the real and imaginary parts of (16) can be related to the series resistance and inductance of the line, once the value of Γ is known. Equations (16) and (17) have the interesting interpretation that the low-frequency behavior of a wire in the tunnel is that of a transmission line whose shunt admittance is that which the wire would have if the tunnel walls were perfectly conducting (and thus is independent of the electric parameters of the rock) while the series impedance is that of the wire embedded in the rock with no tunnel surrounding it (and thus is independent of the shape of the tunnel)—see, e.g., [10].

III. Numerical Results

In order to compare results from this approximate analysis to exact results (which are only available for circular and elliptical cross sections), we need an expression for the distributed capacitance for these geometries. For the elliptical geometry shown in Fig. 2 (which includes the circular geometry as a special case) whose major and minor semi-axes are given by $A\equiv(d/2)\cosh\mu_1$ and $B\equiv(d/2)\sinh\mu_1$, respectively, and in which the wire is located at (μ_0,ϕ_0) in elliptic coordinates $(x+iy=(d/2)\cosh(\mu+i\phi))$, this capacitance is given by Morse and Feshbach [9] as

$$\frac{2\pi\epsilon_0}{C}=\ln\frac{d}{4a}+\mu_1-2\sum_{n=1}^{\infty}\frac{e^{-n\mu_1}}{n}\cdot\left[\frac{\cosh^2 n\mu_0\cos^2 n\phi_0}{\cosh n\mu_1}+\frac{\sinh^2 n\mu_0\sin^2 n\phi_0}{\sinh n\mu_1}\right]. \tag{18}$$

It is easily verified that (18) reduces to the expressions given in the previous section for the circular limit ($\mu_1\to\infty$, $d\to 0$, $d\exp(\mu_1)\to 4b$).

Results computed from (11) are compared with exact computations based upon the analysis of Wait and Hill [1] for a circular tunnel in Fig. 3. Here, the tunnel has radius $b=2$ m and contains a perfectly conducting thin wire with radius $a=1$ cm. The tunnel walls are characterized by

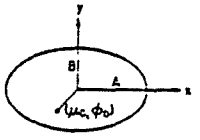


Fig. 2. Elliptical tunnel geometry.

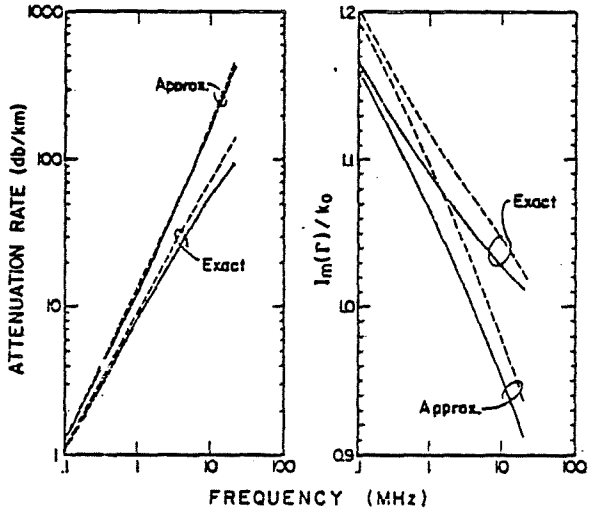


Fig. 3. Comparison of exact (Wait and Hill) and approximate (from (11)) solutions for attenuation rate and phase versus frequency, for a circular tunnel of radius $b=2$ m, with wire of radius $a=1$ cm, located at a radius ρ_0 from center of tunnel; $\epsilon=10\,\epsilon_0$, $\mu=\mu_0$, $\sigma=0.01$ mhos/m. $\rho_0=0$: ———. $\rho_0=1$ m: – – –.

$\epsilon=10\epsilon_0$, $\mu=\mu_0$, and $\sigma=0.01$ mhos/m. The wire is positioned at a distance ρ_0 from the center of the tunnel. The solid lines correspond to a concentrically located wire, while the dashed lines refer to a wire offset $\rho_0=1$ m from the center of the tunnel. It can be seen that good agreement is obtained for typical tunnel parameters at frequencies of 100 kHz or below, and that results are adequate (within a factor of 2 for the attenuation) up to about 1 MHz. The phase constant is predicted accurately up to much higher frequencies. Fig. 4 compares results for the elliptic cross section using the present variational approach ((11)—solid lines), and those obtained using the two-dimensional quasi-static approximation in [4] (broken lines). Here, $(AB)^{1/2}=2$ m, $B/A=0.5$, and the wire is located on the major axis 0.4 m from the tunnel wall. Other parameters are the same as in Fig. 3. The two give indistinguishable values for attenuation below about 1 MHz, and thus we find similar agreement with exact results as in the circular case, because the quasi-static limit was found to give good results in this low-frequency range.

Fig. 5 demonstrates the improvement in these computations for a concentric circular tunnel obtained by keeping one higher degree of approximation in (7); that is, still neglecting Q, but retaining P and evaluating R approximately using the small argument form of K_0. Relevant parameters are the same as those for Fig. 3 with $\rho_0=0$.

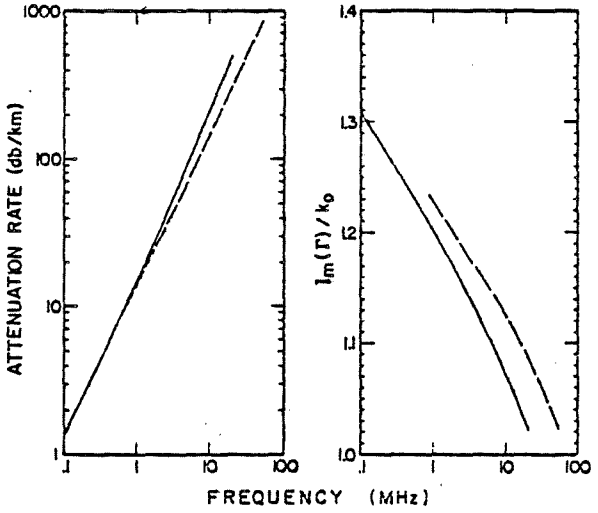


Fig. 4. Attenuation rate and phase versus frequency for an elliptical tunnel with $(AB)^{1/2}=2$ m, $B/A=0.5$, with wire of radius $a=1$ cm located on major axis 0.4 m from tunnel wall; $\epsilon=10\,\epsilon_0$, $\mu=\mu_0$, $\sigma=0.01$ mhos/m. Variational solution (from (11)): ———. Two-dimensional quasi-static solution (Seidel and Wait): ———.

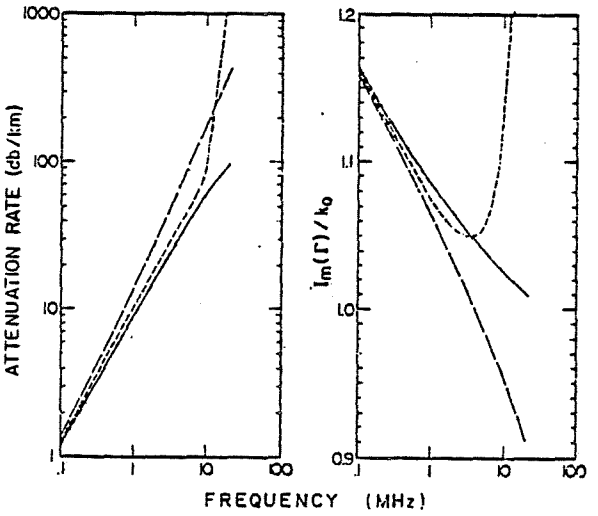


Fig. 5. Attenuation rate and phase versus frequency for a circular tunnel of radius $b=2$ m, with wire of radius $a=1$ cm located at center of tunnel ($\rho_0=0$); $\epsilon=10\,\epsilon_0$, $\mu=\mu_0$, $\sigma=0.01$ mhos/m. Zeroth-order variational (from (11)): ———. First-order variational (from (7), including P and R): ———. Exact (Wait and Hill): ———.

These calculations are elementary for the concentric circular case ($\rho_0=0$) and are omitted here. Here the exact solution is given by the solid lines, the zeroth-order variational solution from (11) by the broken lines, and the higher order solution by the dashed lines. The improvement is quite dramatic, especially in the attenuation, up to a few megahertz, but deteriorates rapidly thereafter. In view of the other idealizations involved in this problem (assumptions of an infinite homogeneous rock wall, no longitudinal irregularities, etc.) the effort necessary to compute P, Q, and R in more general situations does not

seem justified in terms of the increased accuracy they provide.

Appendix A

In this Appendix, the terms of (6) are manipulated into convenient forms for use in a low-frequency approximation.

First, consider the left-hand side:

$$\int_S \bar{E}_0^2 dS = \int_S \nabla_t\Phi\cdot\nabla_t\Phi\, dS$$
$$= \int_S \nabla_t\cdot\left[\Phi\nabla_t\Phi\right]dS \doteq \int_S \Phi\nabla_t^2\Phi\, dS$$
$$= -V\oint_{C_w} \bar{n}\cdot\nabla_t\Phi\, dl = \frac{C}{\epsilon_0}V^2 \tag{A1}$$

where C is the capacitance per unit length of the wire within a tunnel of identical cross section but with perfectly conducting walls. In deriving (A1), use is made of the divergence theorem and the fact that $\nabla_t^2\Phi=0$ in S.

Next, we have

$$\int_S \bar{E}_0(\bar{\rho})\cdot\left[\text{grad}_t\,\text{div}_t-\gamma_e^2\right]\int_S \bar{E}_0(\bar{\rho}')K_0 dS' dS$$
$$= \int_S \bar{E}_0(\bar{\rho})\cdot\left[\nabla_t^2-u^2-\Gamma^2+\text{curl}_t\,\text{curl}_t\right]\int_S \bar{E}_0(\bar{\rho}')K_0 dS' dS$$
$$= -2\pi\int_S \bar{E}_0^2 dS - \Gamma^2\int_S \bar{E}_0(\bar{\rho})\cdot\int_S \bar{E}_0(\bar{\rho}')K_0 dS' dS$$
$$+ \int_S \bar{E}_0(\bar{\rho})\cdot\text{curl}_t\,\text{curl}_t\int_S \bar{E}_0(\bar{\rho}')K_0 dS' dS \tag{A2}$$

since $(\nabla_t^2-u^2)K_0=-2\pi\delta(\bar{\rho}-\bar{\rho}')$. The first term is (A1); for the third term we have

$$\int_S \bar{E}_0(\bar{\rho})\cdot\text{curl}_t\,\text{curl}_t\int_S \bar{E}_0(\bar{\rho}')K_0 dS' dS$$
$$= -\int_S \nabla_t\Phi(\bar{\rho})\cdot\text{curl}_t\,\text{curl}_t\int_S \bar{E}_0(\bar{\rho}')K_0 dS' dS$$
$$= -\int_S \nabla_t\cdot\left\{\Phi(\bar{\rho})\text{curl}_t\,\text{curl}_t\int_S \bar{E}_0(\bar{\rho}')K_0 dS'\right\}dS$$
$$= V\oint_{C_w} \bar{n}\cdot\text{curl}_t\,\text{curl}_t\int_S \bar{E}_0(\bar{\rho}')K_0 dS' dl$$
$$= V\int_{S_w} \text{div}_t\,\text{curl}_t\,\text{curl}_t\int_S \bar{E}_0(\bar{\rho}')K_0 dS' dl = 0. \tag{A3}$$

The remaining integral in (A2) can be transformed by similar manipulations:

$$\int_S \bar{E}_0(\bar{\rho})\cdot\int_S \bar{E}_0(\bar{\rho}')K_0 dS' dS$$
$$= -\int_S \nabla_t\Phi(\bar{\rho})\cdot\int_S \bar{E}_0(\bar{\rho}')K_0 dS' dS$$
$$= -\int_S \nabla_t\cdot\left[\Phi(\bar{\rho})\int_S \bar{E}_0(\bar{\rho}')K_0 dS'\right]dS$$
$$+ \int_S \Phi(\bar{\rho})\nabla_t\cdot\int_S \bar{E}_0(\bar{\rho}')K_0 dS' dS. \tag{A4}$$

Consider the first integral:

$$-\int_S \nabla_t\cdot\left[\Phi(\bar{\rho})\int_S \bar{E}_0(\bar{\rho}')K_0 dS'\right]dS$$
$$= V\oint_{C_w} \bar{n}\cdot\int_S \bar{E}_0(\bar{\rho}')K_0 dS' dl$$
$$= V\int_{S_w} \nabla_t\cdot\int_S \bar{E}_0(\bar{\rho}')K_0 dS' dS$$
$$= \int_{S_w} \Phi(\bar{\rho})\nabla_t\cdot\int_S \bar{E}_0(\bar{\rho}')K_0 dS' dS \tag{A5}$$

defining $\Phi(\bar{\rho})=V$ in S_w, since $\bar{E}_0=0$ there. Thus (A4) becomes

$$\int_S \bar{E}_0(\bar{\rho})\cdot\int_S \bar{E}_0(\bar{\rho}')K_0 dS' dS = \int_{S+S_w}\Phi(\bar{\rho})\nabla_t\cdot\int_S \bar{E}_0(\bar{\rho}')\cdot K_0 dS' dS$$

and since

$$\nabla_t\cdot\int_S \bar{E}_0(\bar{\rho}')K_0 dS' = \int_S \nabla_t'\Phi(\bar{\rho}')\cdot\nabla_t' K_0 dS'$$
$$= \int_S \nabla_t'\cdot\left[\Phi(\bar{\rho}')\nabla_t' K_0\right]dS' - \int_S \Phi(\bar{\rho}')\nabla_t'^2 K_0 dS'$$
$$= -\int_{S+S_w}\Phi(\bar{\rho}')\nabla_t'^2 K_0 dS'$$
$$= 2\pi\Phi(\bar{\rho}) - u^2\int_{S+S_w}\Phi(\bar{\rho}')K_0 dS'. \tag{A6}$$

We obtain finally

$$\int_S \bar{E}_0(\bar{\rho})\cdot\int_S \bar{E}_0(\bar{\rho}')K_0 dS' dS$$
$$= 2\pi\int_{S+S_w}\Phi^2 dS - u^2\int_{S+S_w}\Phi(\bar{\rho})\int_{S+S_w}\Phi(\bar{\rho}')K_0 dS' dS$$
$$= 2\pi\int_S \Phi^2 dS - u^2\int_S \Phi(\bar{\rho})\int_S \Phi(\bar{\rho}')K_0 dS' dS \tag{A7}$$

upon neglecting the integrals over the wire cross section owing to our thin-wire assumption. Thus (A2) becomes

$$\int_S \bar{E}_0(\bar{\rho})\cdot\left[\text{grad}_t\,\text{div}_t-\gamma_e^2\right]\int_S \bar{E}_0(\bar{\rho}')K_0 dS' dS$$
$$= -2\pi\frac{C}{\epsilon_0}V^2 - 2\pi\Gamma^2\int_S \Phi^2 dS + u^2\Gamma^2$$
$$\cdot\int_S \Phi(\bar{\rho})\int_S \Phi(\bar{\rho}')K_0 dS' dS. \tag{A8}$$

Now, let us consider

$$\int_S \bar{E}_0(\bar{\rho})\cdot\text{grad}_t\oint_{C_w}\left[\bar{n}'\cdot\bar{E}_0(\bar{\rho}')\right]K_0 dl' dS$$
$$= \int_S \bar{E}_0(\bar{\rho})\cdot\oint_{C_w}\left[\bar{n}'\cdot\bar{E}_0(\bar{\rho}')\right]\nabla_t K_0 dl' dS$$
$$= \oint_{C_w}\left[\bar{n}'\cdot\bar{E}_0(\bar{\rho}')\right]\int_S \bar{E}_0(\bar{\rho})\cdot\nabla_t K_0 dS dl'$$
$$= -\oint_{C_w}\left[\bar{n}'\cdot\bar{E}_0(\bar{\rho}')\right]\text{div}_t'\int_S \bar{E}_0(\bar{\rho})K_0 dS dl' \tag{A9}$$

which is precisely in the form of the third term on the right side of (6). By virtue of (A6), we may evaluate this term as

$$\oint_{C_w}\left[\bar{n}\cdot\bar{E}_0(\bar{\rho})\right]\nabla_t\cdot\int_S\bar{E}_0(\bar{\rho}')K_0dS'dl$$

$$=2\pi V\oint_{C_w}\left[\bar{n}\cdot\bar{E}_0(\bar{\rho})\right]dl-u^2\oint_{C_w}\left[\bar{n}\cdot\bar{E}_0(\bar{\rho}')\right]$$

$$\cdot\int_S\Phi(\bar{\rho}')K_0dS'dl-u^2V\oint_{C_w}\left[\bar{n}\cdot\bar{E}_0(\bar{\rho})\right]\int_{S_w}K_0dS'$$

$$=2\pi\frac{C}{\epsilon_0}V^2-u^2\oint_{C_w}\left[\bar{n}\cdot\bar{E}_0(\bar{\rho})\right]\int_S\Phi(\bar{\rho}')K_0dS'dl \quad \text{(A10)}$$

the thin-wire assumption having been invoked once more.

The final term of (6) can be evaluated within the thin-wire constraint by using the fact that the surface charge (i.e., $\bar{n}\cdot\bar{E}_0$) is nearly uniform over the boundary C_w of the wire, and can be reckoned constant. We then find, for a wire of radius a, that

$$\oint_{C_w}\left[\bar{n}\cdot\bar{E}_0(\bar{\rho})\right]\oint_{C_w}\left[\bar{n}'\cdot\bar{E}_0(\bar{\rho}')\right]K_0dl'dl$$

$$\simeq-\left[\frac{CV}{\epsilon_0}\right]^2\left\{\ln\frac{ua}{2}+\gamma\right\} \quad \text{(A11)}$$

where $\gamma=0.577\cdots$ is Euler's constant.

Appendix B

In this Appendix, a derivation of (1) is presented essentially as given in [5]. Consider a volume V of electrical parameters $\mu(\bar{r})$, $\epsilon(\bar{r})$, and $\sigma(\bar{r})$ embedded in an infinite, homogeneous region with constant parameters μ_1, ϵ_1, and σ_1. Source-free field solutions (e.g., fields of guided modes) can be considered to arise from the polarization currents $\bar{J}_e$ and $\bar{J}_m$ radiating in the absence of the body V:

$$\bar{J}_e=i\omega(\hat{\epsilon}-\hat{\epsilon}_1)\bar{E} \qquad \bar{J}_m=i\omega(\mu-\mu_1)\bar{H} \quad \text{(B1)}$$

where $\hat{\epsilon}\equiv\epsilon-i\sigma/\omega$ and $\hat{\epsilon}_1=\epsilon_1-i\sigma_1/\omega$. Even though $\bar{E}$ and $\bar{H}$ are as yet unknown, the fields can be derived from Hertz vectors $\bar{\Pi}_e$ and $\bar{\Pi}_m$ according to

$$\bar{E}=(\text{grad div}+k_1^2)\bar{\Pi}_e-i\omega\mu_1\,\text{curl}\,\bar{\Pi}_m \quad \text{(B2)}$$

$$\bar{H}=(\text{grad div}+k_1^2)\bar{\Pi}_m+i\omega\hat{\epsilon}_1\,\text{curl}\,\bar{\Pi}_e \quad \text{(B3)}$$

where

$$\bar{\Pi}_e=\frac{1}{i\omega\hat{\epsilon}_1}\int_V\bar{J}_e(\bar{r}')\frac{e^{-ik_1|r-r'|}}{4\pi|r-r'|}d\bar{r}' \quad \text{(B4)}$$

$$\bar{\Pi}_m=\frac{1}{i\omega\mu_1}\int_V\bar{J}_m(\bar{r}')\frac{e^{-ik_1|r-r'|}}{4\pi|r-r'|}d\bar{r}'. \quad \text{(B5)}$$

We have defined $k_1^2=\omega^2\mu_1\hat{\epsilon}_1$ and $\text{Im}\,(k_1)<0$ for $\sigma_1>0$. If V, μ, ϵ, and σ are translationally invariant in the z-direction (i.e., V is some cylinder with constant cross-section S) and mode fields of the form $\bar{E}=\bar{E}(\bar{\rho})e^{-\Gamma z}$ and $\bar{H}=\bar{H}(\bar{\rho})e^{-\Gamma z}$ are assumed, with $\bar{\rho}=(x,y)$, then the z' integrations in (B4) and (B5) can be done in closed form provided $|\text{Re}\,\Gamma|<|\text{Im}\,k_1|$:

$$\bar{\Pi}_e=\frac{e^{-\Gamma z}}{2\pi}\int\left(\frac{\hat{\epsilon}(\rho')}{\hat{\epsilon}_1\bar{\rho}'}-1\right)\bar{E}(\rho')K_0\left[u|\bar{\rho}-\bar{\rho}'|\right]d\bar{\rho}' \quad \text{(B6)}$$

$$\bar{\Pi}_m=\frac{e^{-\Gamma z}}{2\pi}\int\left(\frac{\mu(\bar{\rho}')}{\mu_1}-1\right)\bar{H}(\bar{\rho}')K_0\left[u|\bar{\rho}-\bar{\rho}'|\right]d\bar{\rho}'. \quad \text{(B7)}$$

We have put $u=(-k_1^2-\Gamma^2)^{1/2}$ and $\text{Re}\,(u)>0$. Here K_0 is the modified Bessel function of the second kind. Upon putting $\mu(\bar{\rho})\equiv\mu_1$, $\bar{\Pi}_m$ vanishes and the integral (1) follows at once from (B2) by taking the observation point $\bar{\rho}$ inside S.

References

[1] J. R. Wait and D. A. Hill, "Guided electromagnetic waves along an axial conductor in a circular tunnel," *IEEE Trans. Antennas Propagat.*, vol. AP-22, pp. 627–630, 1974.

[2] D. A. Hill and J. R. Wait, "Analysis of radio frequency transmission along a trolley wire in a mine tunnel," *IEEE Trans. Electromagn. Compat.*, vol. EMC-18, pp. 170–174, 1976.

[3] J. R. Wait, "Quasi-static limit for the propagating mode along a thin wire in a circular tunnel," *IEEE Trans. Antennas Propagat.*, vol. AP-25, pp. 441–443, 1977.

[4] D. B. Seidel and J. R. Wait, "Radio transmission in an elliptical tunnel with a contained axial conductor," *J. Appl. Phys.*, vol. 50, pp. 602–605, 1979.

[5] B. Z. Katsenelenbaum, "Propagation of electromagnetic waves along an infinite dielectric cylinder at low frequencies," *Dokl. Akad. Nauk SSSR*, vol. 58, pp. 1317–1320, 1947, (in Russian).

[6] C. B. Shaw, B. T. French, and C. Warner, "Further research on optical transmission lines," Autonetics Div., North American Aviation, Anaheim CA., Sci. Rep. No. 2, AD-652501, 1967.

[7] M. A. R. Gunston, *Microwave Transmission-Line Impedance Data*. New York: Van Nostrand-Reinhold, 1972.

[8] R. E. Collin, *Field Theory of Guided Waves*. New York: McGraw-Hill, 1960, pp. 477–480.

[9] P. M. Morse and H. Feshbach, *Methods of Theoretical Physics*. New York: McGraw-Hill, 1953, p. 1203.

[10] E. D. Sunde, *Earth Conduction Effects in Transmission Systems*. New York: Dover, 1968.

NOAA Library Accession No. 78-0-1103
Also Bureau of Mines Open File Report -78

ELECTROMAGNETIC GUIDED WAVES IN MINE ENVIRONMENTS

Proceedings of a Workshop

Prepared for

United States Department of the Interior
Bureau of Mines

by

James R. Wait

Institute for Telecommunication Sciences
National Telecommunications and Information Administration
United States Department of Commerce
Boulder, Colorado 80303

Iterim Report for Period
2 February 1978 to 30 May 1978

Contract No. HO155008

31 May 1978

Available from NTIS (National Technical Information Service) as PB 289 742 in microfiche or photostat, Alexandria, Va.

I

REPORT DOCUMENTATION PAGE

1. Report No.	2.	3. Recipient's Accession No.

4. Title and Subtitle	5. Report Date
ELECTROMAGNETIC GUIDED WAVES IN MINE ENVIRONMENTS Proceedings of a Workshop	31 May 1978 6.

7. Author(s)	8. Performing Organization Report No.
James R. Wait (Editor) and others	N/A

9. Performing Organization Name and Address	10. Project/Task/Work Unit No.
Institute for Telecommunication Sciences National Telecommunications and Information Administration, U.S. Department of Commerce, Boulder, CO 80303	11. Contract or Grant No. H0155008

12. Sponsoring Organization Name and Address	13. Type of Report
Pittsburgh Mining and Safety Research Center U.S. Bureau of Mines 4800 Forbes Avenue Pittsburgh, PA 15213	Iterim 14.

15. Supplementary Notes
This document is the edited Proceedings of a workshop held from 28-30 March 1978 at the Institute of Telecommunication Sciences and published by the Cooperative Institute for Research in Environmental Sciences, University of Colorado.

16. Abstract
A unity of viewpoint emerged from the workshop. The concept that transmission is via characteristic modes was a common theme in many of the presentations. Also, the confusion on the meaning of *monofilar* and *bifilar* to describe these dominant modes was cleared up. But, there was still a healthy divergence of opinion on what constitutes an optimum system. It was generally agreed that further analytical and experimental work is definitely needed. In particular, it was stressed that independent measurements of the constitutive properties of the electromagnetic environment are needed. Also, there was considerable concern that laboratory measurements of rock samples could lead to misleading results for the effective conductivities. Also, there was a general recognition that over simplified propagation theory should not be used to interpret field data. From a theoretical and practical point of view, it was realized that mode coupling plays a vital role in the transmission channel. One must not only understand which and how many propagation modes are excited by the transmitting antenna, but the conversion of energy from one mode type to another must be accounted for. This conversion can either be done intentionally (by fixed mode convertors) or non intentionally (by random wall roughness). In fact, mode conversion can be quite complicated when various propagation paths exist such as when insulated cables, leaky feeders, grounded rails, coal seams, etc. all convey portions of the electromagnetic energy. However, this state of affairs should be regared as an opportunity for extended communication coverage in mines rather than a limitation of a design procedure based on preconceived notions of the dominant propagation mechanism.

17. Originator's Key Words	18. Availability Statement
mine communications, tunnel waveguides, radiowave propagation, carrier trolley wire transmission, geophysical probing, mine rescue	

19. U. S. Security Classif. of the Report	20. U. S. Security Classif. of this Page	21. No. of Pages	22. Price
UNCLASSIFIED	UNCLASSIFIED		

FOREWORD

This report was prepared by the Institute for Telecommunication Sciences, National Telecommunications and Information Administration, U.S. Department of Commerce, Boulder, Colorado under USBM Contract number H0155008. It was administered under the technical direction of the Pittsburgh Mining and Safety Research Center with H.K. Sacks acting as Technical Project Officer. This report is a summary of the work recently completed as a part of this contract during the period 2 February 1978 to 31 May 1978. This report was submitted by the authors on 31 May 1978.

The document is a compilation of the papers presented and discussed at a three day informal meeting on the general subject of mine communications. Active workers from the U.S., Canada, England, France, Belgium, South Africa, and Japan were invited to present their latest research results and exchange views. These papers are included here along with an edited record of the discussions that followed the presentations. Any views expressed or alluded to in the individual papers are not necessarily endorsed by the U.S. Bureau of Mines and, in no way, do they represent the official position of the U.S. Government on such matters.

All material contained herein is in the public domain and, as such, is not copyrighted. Each author has given a signed release of copyright so the material may be reproduced provided full acknowledgement to its source is given. After final approval by the U.S. Bureau of Mines, this document will be deposited in the National Technical Information Service (NTIS), Springfield, Virginia. Requests to purchase microfiche or photo-copies should be directed to the NTIS and not to the undersigned.

In organizing the workshop, the undersigned received a great deal of assistance from his colleague, David A. Hill, who was responsible for most of the physical arrangements. Secretarial support was provided by Lana Hope who also assisted in the preparation of these Proceedings. Our technical Project Officer, H.K. Sacks from the U.S. Bureau of Mines, was also a continuous source of encouragement. Also, much credit must go to my colleagues at Arthur D. Little, Inc.: R.L. Lagace, R.H. Spencer, and A.G. Emslie for their vital contributions and many useful suggestions. Robert Lagace, in particular, played a major role in making this workshop so successful. Their summary and suggestions for further research are included at the end of this document.

Speaking on behalf of my North American colleagues, I would like to warmly thank the following people who travelled a great distance to attend this workshop: Brian Austin from South Africa, Jiro Chiba from Japan, David Martin from England, Paul Delogne from Belgium, and Robert Gabillard from France. Their active participation was a key ingredient. Our only regret was that Quin Davis, the organizer of the 1974 Leaky Feeder Conference in Guildford, was not able to attend but his paper was ably presented by David Martin.

Finally, I would like to thank John N. Murphy of the U.S. Bureau of Mines, not only for his general support of the workshop, but for taking the time from his busy schedule to give an excellent and vigorously presented overview lecture on mine communi-ation research. This particular event was sponsored jointly by the local chapters of the IEEE Communications Society and the IEEE Antennas and Propagation Society.

31 May 1978

James R. Wait

TABLE OF CONTENTS

	Page
Foreword	2
"Experimental Results Obtained in a Mine on a Network of Leaky Cable" by P. Degauque, B. Demoulin, M. Cauterman and R. Gabillard	5
"Comparative Analysis of Leaky Cable Techniques for Mine Communications" by R. DeKeyser, P. Delogne, L. Derijck and L. Liégeois	15
"Modes in Braided Coaxial Cables in Circular and Elliptical Tunnels" by D.B. Seidel and J.R. Wait	26
"Use of Auxiliary Dedicated Wire as a Means of Aiding Carrier Current Propagation on a Trolley Wire/Rail Transmission Line" by A.G. Emslie, R.L. Lagace, R.H. Spencer, and P.F. Strong	28
"Analysis of the Dedicated Communication Line in a Mine Tunnel for a Shunt-Loaded Trolley Wire" by J.R. Wait and D.A. Hill	44
"Role of Controlled Mode Conversion in Leaky Feeder Mine-Communication Systems", by D.B. Seidel and J.R. Wait	45
"Pulse Transmission Along Cables in Circular Tunnels" by D.A. Hill and J.R. Wait	65
"Some Aspects of Leaky Feeder Radio Communication Being Studied by the UK National Coal Board" by D.J.R. Martin	66
"Field Measurements of Leaky-Feeder Signals" by Q.V. Davis, R.W. Haining, B.L. Critchley, and A.J. Motley	76
"Underground Radio Communication Techniques and Systems in South African Mines" by B.A. Austin	87
"Trapped Miner Communications and Location in Metal/Non Metal Mines" by A.J. Farstad	103
"Trapped Miner Through the Earth Communications in Coal Mines" by D. Kalvels	119
"A Radio Equipment for Mine Communication and Control" by P. Delogne	132
"Medium Frequency Radio Propagation and Coupling in Coal Mines" by A.G. Emslie, R.L. Lagace and M.A. Grossman	142
"Antenna Technology for Medium Frequency Portable Radio Communication in Coal Mines" by R.L. Lagace and A.G. Emslie	153
"Coupling of the Coal-Seam Mode to a Cable in a Tunnel at Medium Radio Frequencies" by R.L. Lagace and A.G. Emslie	170
"Wireless Radio Transmission at Medium Frequency in Underground Coal Mines - Summary of Measurements and Expected System Propagational Effects" by T.S. Cory	184
"Medium Frequency Communication Experiments" by H.R. Cooper	203
"Passive Reflectors as a Means for Extending UHF Signals Down Intersecting Cross Cuts in Mines" by R.L. Chufo and R.A. Isberg	204

Page

"Wireless Communication in the Tunnels and Underground Streets" by J. Chiba, T. Inaba, Y. Kuwamoto, O. Banno, and R. Sato 218
"The Testing of Leaky Coaxial Cables and Their Application to Guided Radar" by N.A.M. Mackay and J.C. Beal 227
"Guided Waves on Wires Near Ground" by D.C. Chang, E.F. Kuester, and S.W. Maley 242
"Electromagnetic Probing Through a Thin, Nonuniform Layer of Conductive Overburden" by R.G. Geyer and J.R. Wait 250
"Approximate Expressions for the Quasi-Static Fields Within and Outside a Conducting Slab" by P.R. Bannister and R.L. Dube 251
"Theory of Transmission of Electromagnetic Waves Along a Metal Rod in a Conducting Medium" by J.R. Wait and D.A. Hill 261
"Guide to the Use of Laboratory Electrical Measurements for Interpretation" by G.R. Olhoeft 276
"Electrical Properties of Eastern Bituminous Coal as a Function of Frequency, Polarization and Direction of the Electromagnetic Wave, and Temperature of the Sample" by C.A. Balanis, J.L. Jeffrey, and Y.K. Yoon 277
"Locating a Buried Magnetic Dipole" by T.W.H. Caffey 288
"Inversion of Geophysical Data" by C.H. Stoyer 297
"Finding High Contrast Anomalies Using Cross-Borehole High-Frequency CW Probing" by D.T. Davis, R.J. Lytle, E.F. Laine, and D.L. Lager 305
List of Attendees 307
Executive Summary (of Proceedings) by J.R. Wait 309
Bibliographic Note 311
"Summary of Current State of the Art and Suggestions for Further Research on Guided Wave Communication" by R.L. Lagace, A.G. Emslie and R.H. Spencer 312

Radio Science, Volume 10, Number 6, pages 625-632, June 1975

Theory of the transmission of electromagnetic waves down a mine hoist

James R. Wait

Cooperative Institute for Research in Environmental Sciences, University of Colorado, Boulder, Colorado 80302

David A. Hill

Institute for Telecommunication Sciences, Office of Telecommunications, US Department of Commerce, Boulder, Colorado 80302

(Received February 10, 1975.)

Using an idealized coaxial model, we consider the transmission, in the frequency range from 20 to 1000 kHz, down a mine hoist shaft from a symmetric source at the surface. The shaft is circular in cross section and the metal hoist cable is represented by a concentric conductor. To facilitate the analysis, the source is idealized as a, voltage-excited annular slot in a circular ground plane that is located in the air-earth interface. The earth itself is taken to be a homogeneous conducting half space. Using a modal type analysis, the total power supplied to the annular slot is calculated as the sum of the power delivered to the lower half space, the power dissipated at the air-earth interface and the power radiated into the atmosphere. Using these results, the relative power transmitted down the shaft to a specified depth is estimated. The resulting transmission efficiency is found to be almost completely dependent on the attenuation characteristics of the dominant TEM mode in the shaft.

INTRODUCTION

There is a need to transmit information from the earth's surface down a mine hoist shaft. In most cases, such shafts can be roughly represented as a cylindrical bore with a vertical axis. The metal hoist cable is then idealized as a circular metal conductor located on the axis of the shaft. A similar model of the shaft was considered by *Emslie and Lagace* [1974] who demonstrated the feasibility of this type of mine communication.

It is our purpose to analyze the electromagnetic wave transmission down such a shaft. The transmitter is to be located at the surface and the power transmitted downward is to be intercepted at some distance down the shaft. In this particular analysis, we do not consider any specific form of receiving antenna, nor do we allow for the effects of reflection from the bottom of the shaft. Thus, strictly speaking, our analysis applies only to a shaft of infinite depth.

The modal analysis we employ is straightforward and the methods are similar to those we used in analyzing transmission in circular mine tunnels [*Wait and Hill*, 1974*a*, *b*]. The additional complication arises here from the method of excitation and the influence of the air-earth interface. In fact, because of the latter, we resort to some approximations.

FORMULATION

We consider the model depicted in Figure 1. A cylindrical shaft, of radius a with center conductor of radius c, extends downward indefinitely into the earth. The latter is homogeneous with conductivity σ and permittivity ϵ and an assumed free-space permeability μ_0.

We imagine that power is to be provided to an annular slot in a simulated ground plane of effective radius ρ_0. Ideally, of course, $\rho_0 \to \infty$. We are interested to know how much of this power crosses the area $c < \rho < a$ at $z = l$ in the shaft.

While the annular slot is conceptually simple, it may be better to think of a toroidal coil as a more feasible source at VLF. But the electromagnetic problem is essentially the same and thus we consider here the problem only in the context of an annular slot that is excited uniformly by a

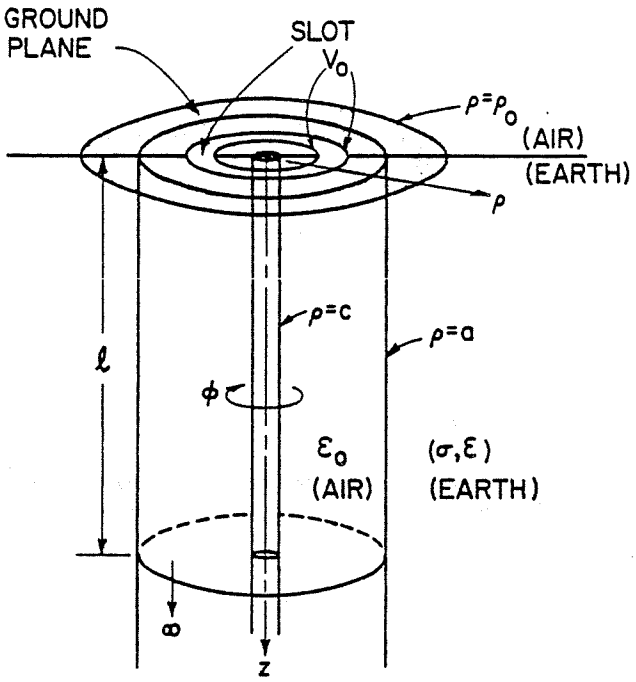


Fig. 1. Schematic view of the general configuration (in the analysis the annular slot of radius $\bar{\rho}$ is taken to have negligible width).

"voltage" V_0.

For the half space ($z > 0$), i.e., the earth, we can say that $E_\rho(z = 0) = f(\rho)$ is a prescribed function. For example, if the slot at $\rho = \bar{\rho}$ is of negligible width, then

$$f(\rho) = V_0\,\delta(\rho - \bar{\rho}) + e(\rho)u(\rho - \rho_0) \tag{1}$$

where $\delta(\rho - \bar{\rho})$ is a unit impulse function at $\rho = \bar{\rho}$ and $u(\rho - \rho_0)$ is a step function at $\rho = \rho_0$. Then, $e(\rho)$ is the tangential nonzero electric field on the earth's surface beyond the assumed perfectly conducting screen.

A fully rigorous solution of the posed problem is probably out of the question. However, if the distribution $f(\rho)$ over the significant range of ρ can be estimated, then the field at any other point in the earth or within the coaxial region can be predicted.

As indicated above, we have presupposed azimuthal symmetry. In terms of cylindrical coordinates (ρ,ϕ,z), derivatives involving $\partial/\partial\phi$ are zero. Thus, the nonvanishing field components are E_{0z}, $E_{0\rho}$, $H_{0\phi}$ for $c < \rho < a$ and E_z, E_ρ, H_ϕ for $\rho > a$.

The center conductor of radius c is to represent the metal hoist cable or "rope" as it is sometimes called. We can characterize this cable, insofar as external fields are concerned, by a series impedance Z_c in ohms per meter. Thus, the boundary condition at the cable is

$$E_{0z}\big|_{\rho=c} = I(z)Z_c \tag{2}$$

where $I(z) = 2\pi c H_{0\phi}\big|_{\rho=c}$ is the total axial current in the cable. Explicit expressions for Z_c are conveniently given by *Wait and Hill* [1974*b*].

MODAL SOLUTION

The fields for the present problem can be expressed in terms of a Hertz vector with a z component only. This is denoted Π_0 for $c < \rho < a$ and Π for $\rho > a$. Because of the impedance boundary condition imposed at $\rho = c$, it turns out that the fields everywhere in the region $\rho > c$ and $z > 0$ can be expressed in terms of a discrete set of modes. No continuous spectrum is needed. This leads us to write

$$\Pi = \sum_s A_s K_0(u_s\rho)\exp(-i\lambda_s z), \quad \text{for} \quad \rho > a \tag{3}$$

and

$$\Pi = \sum_s [B_s I_0(v_s\rho) + C_s K_0(v_s\rho)]\exp(-i\lambda_s z),$$

$$\text{for} \quad c < \rho < a \tag{4}$$

when I_0 and K_0 are modified Bessel functions, $u_s = (\lambda_s^2 + \gamma^2)^{1/2}$, $v_s = (\lambda^2 - k^2)^{1/2}$, $\gamma = [i\mu_0\omega \cdot (\sigma + i\epsilon\omega)]^{1/2}$, $k = (\epsilon_0\mu_0)^{1/2}\omega$, and λ_s are the eigenvalues of the problem. Physically, $i\lambda_s$ are the axial propagation constants for the coaxial structure that are yet to be determined. A_s, B_s, and C_s are coefficients, also yet to be determined.

On matching tangential fields at $\rho = a$, we obtain the pair

$$v_s^2[B_s I_0(v_s a) + C_s K_0(v_s a)] = u_s^2 A_s K_0(u_s a) \tag{5}$$

and

$$-i\epsilon_0\omega v_s[B_s I_1(v_s a) - C_s K_1(v_s a)] = (\sigma + i\epsilon\omega)u_s A_s K_1 \cdot (u_s a) \tag{6}$$

Solution of these leads to

$$B_s/C_s = -[K_0(\nu_s a)/I_0(\nu_s a)]\,R(\lambda_s) \tag{7}$$

where

$$R(\lambda_s) = [\eta_0 Y_s - (ik/\nu_s)\,K_1(\nu_s a)/K_0(\nu_s a)] \Big/ [\eta_0 Y_s + (ik/\nu_s)\,I_1(\nu_s a)/I_0(\nu_s a)] \tag{8}$$

and where

$$Y_s = [(\sigma + i\epsilon\omega)/u_s]\,K_1(u_s a)/K_0(u_s a)$$

$$\text{and} \quad \eta_0 = (\mu_0/\epsilon_0)^{1/2} \tag{9}$$

Furthermore,

$$A_s/C_s = (\nu_s^2/u_s^2)[K_0(\nu_s a)/K_0(u_s a)][1 - R(\lambda_s)] = \beta_s \tag{10}$$

Now the impedance boundary condition, given by (2), requires that

$$B_s/C_s = -[\nu_s K_0(\nu_s c) + 2\pi i\epsilon_0\omega c Z_c K_1(\nu_s c)] \Big/ [\nu_s I_0(\nu_s c) - 2\pi i\epsilon_0\omega c Z_c K_1(\nu_s c)] = \alpha_s \tag{11}$$

The equation to determine λ_s is then obtained by equating the right-hand sides of (7) and (11). Thus

$$\alpha_s + [K_0(\nu_s a)/I_0(\nu_s a)]\,R(\lambda_s) = 0 \tag{12}$$

is our mode equation.

ORTHOGONALITY CONSIDERATIONS AND THE NORMALIZING INTEGRAL

We now can write the following explicit forms for the radial electric field in the region $\rho > c$ and $z > 0$:

$$E_\rho = \sum_s C_s\beta_s i\lambda_s u_s K_1(u_s\rho)\exp(-i\lambda_s z) \tag{13}$$

and

$$E_{0\rho} = -\sum_s C_s i\lambda_s \nu_s [\alpha_s I_1(\nu_s\rho) - K_1(\nu_s\rho)] \cdot \exp(-i\lambda_s z) \tag{14}$$

In particular,

$$\left.\begin{matrix} E_\rho \\ E_{0\rho} \end{matrix}\right|_{z=0} = \sum_s C_s Z_s(\rho) \tag{15}$$

where

$$Z_s(\rho) = \begin{cases} i\beta_s\lambda_s u_s K_1(u_s\rho), & \text{for} \quad \rho > a \\ i\lambda_s\nu_s[K_1(\nu_s\rho) - \alpha_s I_1(\nu_s\rho)], & \text{for} \quad c < \rho < a \end{cases} \tag{16}$$

The function $Z_s(\rho)$ satisfies a form of the modified Bessel function of order one. Thus,

$$\rho^2 d^2 Z_s(\rho)/d\rho^2 + \rho\, dZ_s(\rho)/d\rho - [(w_s\rho)^2 + 1] \cdot Z_s(\rho) = 0 \tag{17}$$

where

$$w_s = \begin{cases} u_s, & \text{for} \quad \rho > a \\ \nu_s, & \text{for} \quad c < \rho < a \end{cases}$$

A similar equation applies to $Z_q(\rho)$ where q denotes another eigenvalue. From these it is easy to verify that

$$(\partial/\partial\rho)\{\rho[Z_q\, dZ_s/d\rho - Z_s\, dZ_q/d\rho]\} - \rho(w_s^2 - w_q^2) \cdot Z_s Z_q = 0 \tag{18}$$

Thus

$$\int_c^\infty \rho Z_s(\rho)Z_q(\rho)d\rho = -c[Z_q(\rho)\,\partial Z_s(\rho)/\partial\rho - Z_s(\rho) \cdot \partial Z_q(\rho)/\partial\rho]_{\rho=c}/(\nu_s^2 - \nu_q^2)$$

where we utilize the fact that $Z_s(\rho)$ vanishes exponentially as $\rho \to \infty$. We now confirm the orthogonality of the modes since

$$\int_c^\infty \rho Z_s(\rho)Z_q(\rho)d\rho = 0 \quad \text{if} \quad s \neq q \tag{20}$$

in view of the impedance boundary condition at the cable that is equivalent to

$$(\partial Z_s/\partial\rho)\big|_{\rho=c} = \Gamma\, Z_s(c) \tag{21}$$

where Γ is a constant. In fact,

$$\Gamma = 2\pi c i\epsilon_0\omega Z_c - c^{-1} \tag{22}$$

which is independent of the eigenvalue for our assumed constant value of Z_c. The latter assumption is certainly well justified for a metallic conductor at these frequencies. Of some importance is the case when $s = q$. Then we are interested in the normalizing integral

$$N_s = \int_c^\infty \rho[Z_s(\rho)]^2 d\rho \tag{23}$$

This can be treated as the limiting form of (19) as $q \to s$. Thus

$$N_s = cZ_s(c)\{(\Gamma - \partial/\partial\rho)[\partial/\partial\nu_q\, Z_q(\rho)]_s\}_{\rho=c}(2\nu_s)^{-1} \tag{24}$$

As indicated, the differentiation with respect to ν_q is carried out before setting $\nu_q = \nu_s$. Then the operation $\Gamma - \partial/\partial\rho$ is performed before setting $\rho = c$.

A direct approach to evaluate N_s is probably more feasible. Thus, using (16) we begin with

$$N_s = -\lambda_s^2[\,\nu_s^2 F_s + (\beta_s u_s)^2 G_s] \tag{25}$$

where

$$F_s = \int_c^a [K_1(\nu_s\rho) - \alpha_s I_1(\nu_s\rho)]^2 \rho\, d\rho$$

and

$$G_s = \int_a^\infty [K_1(u_s\rho)]^2 \rho\, d\rho$$

Now $K_1(x)$, or $I_1(x)$, satisfies the equation

$$x[K_1(bx)]^2 = -(\partial/\partial x)(((x^2/2)\{[K_1'(bx)]^2 - (1 + 1/b^2x^2)[K_1(bx)]^2\}))$$

which is readily verified. Thus,

$$F_s = -(a^2/2)[(Z_a')^2 - (1 + 1/\nu_s^2 a^2)Z_a^2] + (c^2/2) \cdot [(Z_c')^2 - (1 + 1/\nu_s^2 c^2)Z_c^2] \tag{26}$$

where

$$Z_a = K_1(\nu_s a) - \alpha_s I_1(\nu_s a)$$

$$Z_c = K_1(\nu_s c) - \alpha_s I_1(\nu_s c)$$

and

$$G_s = (a^2/2)\{[K_1'(u_s a)]^2 - (1 + 1/u_s^2 a^2) \cdot K_1^2(u_s a)\} \tag{27}$$

If $|\nu_s a| << 1$, we can write

$$N_s \simeq -\lambda_s^2[\ln(a/c) - (\nu_s^2/2)(a^2 - c^2)\alpha_s + (\beta_s u_s)^2 G_s]$$

FIELDS IN THE UPPER HALF SPACE

We now need to say something about the field in the air half space ($z < 0$). In general, here the fields can be derived from a Hertz potential $\hat{\Pi}$ given by

$$\hat{\Pi} = \int_0^\infty f(\lambda) e^{u_0 z} J_0(\lambda\rho)\, d\lambda \tag{28}$$

where $u_0 = (\lambda^2 - k^2)^{1/2}$. Then, for $z < 0$,

$$\hat{E}_\rho = \partial^2\hat{\Pi}/\partial\rho\partial z = -\int_0^\infty u_0 \lambda\, f(\lambda)\, J_1(\lambda\rho)\, d\lambda \tag{29}$$

Now if, for example, $\hat{E}_\rho = V_0\,\delta(\rho - \bar{\rho})$ at $z = 0$ for all values of ρ, we determine $f(\lambda)$ from

$$V_0\delta(\rho - \bar{\rho}) = -\int_0^\infty u_0 \lambda\, f(\lambda)\, e^{u_0 z} J_1(\lambda\rho)\, d\lambda \tag{30}$$

Using the Fourier Bessel transform pair [*Stratton*, 1941, p. 371]

$$G(\rho) = \int_0^\infty g(\lambda)\, J_1(\lambda\rho)\lambda\, d\lambda \tag{31}$$

$$g(\lambda) = \int_0^\infty G(\rho)\, J_1(\lambda\rho)\rho\, d\rho \tag{32}$$

it easily follows that

$$f(\lambda) = -(u_0\lambda)^{-1} V_0 J_1(\lambda\bar{\rho})\bar{\rho} \tag{33}$$

Thus

$$\hat{H}_\phi = i\epsilon_0\omega\, V_0\bar{\rho}\int_0^\infty (\lambda/u_0)\, J_1(\lambda\rho)\, J_1(\lambda\bar{\rho}) e^{u_0 z}\, d\lambda \tag{34}$$

for the region $z < 0$. If we now utilize the series

$$J_1(\lambda\bar{\rho}) = (1/2)[\lambda\bar{\rho} - (\lambda\bar{\rho})^3/8 + \ldots] \tag{35}$$

and the integral formula [*Stratton*, 1941, p. 576]

$$\int_0^\infty J_0(\lambda\rho)(\lambda/u_0)\, e^{u_0 z}\, d\lambda = (\rho^2 + z^2)^{-1/2}\exp[-ik \cdot (\rho^2 + z^2)^{1/2}] \tag{36}$$

it easily follows that

$$\hat{H}_\phi = [i\epsilon_0\omega V_0(\bar{\rho})^2/2]\{-\partial/\partial\rho + [(\bar{\rho})^2/8](\partial/\partial\rho) \cdot (k^2 + \partial^2/\partial z^2) + \ldots\}\, e^{-ikR}/R \tag{37}$$

where $R = (\rho^2 + z^2)^{1/2}$. In fact, the leading term will be adequate for most purposes; thus

$$\hat{H}_\phi \sim -[\epsilon_0\omega V_0(\bar{\rho})^2 k/2\rho](1 + 1/ik\rho)e^{-ik\rho} \tag{38}$$

for $z = 0$.

Now actually we are dealing with an imperfectly ground plane beyond $\rho > \rho_0$. But, to a good approximation, we can assume that the actual tangential magnetic field is not appreciably different. Also, we can employ the surface impedance boundary condition to make a good estimate for the tangential electric field $e(\rho)$ beyond the ground screen [*Wait*, 1969]. In fact, we say that

$$e(\rho) \simeq \eta \hat{H}_\phi \tag{39}$$

where $\hat{H}_\phi$ is given by (37) or (38) and $\eta = [i\mu_0\omega/(\sigma + i\epsilon\omega)]^{1/2}$. Then the power P^+ supplied to the ground by means of the upper half space is obtained from

$$P^+ \cong (1/2)\,\mathrm{Re}\,\eta \int_{\rho_0}^{\infty} (\hat{H}_\phi)^2\, 2\pi\rho d\rho \cong (\bar{\rho})(4\pi/8) \cdot [(\epsilon_0\omega)^2 V_0^2/\rho_0^2]\,\mathrm{Re}\,\eta \quad \text{if} \quad k\rho_0 << 1 \tag{40}$$

EVALUATION OF MODAL COEFFICIENTS C_s

We now determine the coefficients C_s by equating the right-hand sides of (1) and (15). That is

$$\sum_s C_s Z_s(\rho) = V_0 \delta(\rho - \bar{\rho}) + e(\rho) u(\rho - \rho_0) \tag{41}$$

Using the orthogonality relation (20), it readily follows that

$$\begin{aligned} C_s &= (V_0/N_s)\,\bar{\rho}\, Z_s(\bar{\rho}) + (1/N_s)\int_{\rho_0}^{\infty} e(\rho) Z_s(\rho)\rho\, d\rho \\ &= (V_0/N_s)\, i\lambda_s \nu_s \bar{\rho}[K_1(\nu_s\bar{\rho}) - \alpha_s I_1(\nu_s\bar{\rho})] \\ &\quad - (V_0\eta/N_s)(i\beta_s\lambda u_s)[\epsilon_0\omega(\bar{\rho})^2 k/2]\int_{\rho_0}^{\infty} (1 + 1/ik\rho) \cdot e^{-ik\rho} K_1(u_s\rho) d\rho \end{aligned} \tag{42}$$

While the integral above can be simplified, direct numerical evaluation is preferable, at least for the TEM mode. The integrand converges rapidly because $K_1(u_s\rho)$ behaves as $\rho^{-1/2}\exp(-u_s\rho)$ for large ρ.

Actually, for the higher-order modes, the integral in (42) can be approximated by

$$\int_{\rho_0}^{\infty} (1 + 1/ik\rho) e^{-ik\rho} K_1(u_s\rho) d\rho \simeq (\pi/2)^{1/2} \exp(-u_s\rho_0) / ik(u_s\rho_0)^{3/2} \tag{43}$$

This is valid, in an asymptotic sense, when $k\rho_0$ is small and $|u_s\rho|$ is large.

POWER RELATIONS

We now need to deduce the total power P^- supplied to the lower half space by the annular slot. Clearly, this is given by

$$\begin{aligned} P^- &= \left[(1/2)\,\mathrm{Re}\int_c^a E_{0\rho} H_{0\phi}^*\, 2\pi\rho d\rho\right]_{z=0} \\ &= \pi\bar{\rho} V_0 [\mathrm{Re}\, H_{0\phi}]_{\substack{\rho=\bar{\rho} \\ z=0}} \\ &= \pi\bar{\rho} V_0 \mathrm{Re}\{i\epsilon_0\omega \sum_s \nu_s C_s [K_1(\nu_s\bar{\rho}) - \alpha_s I_1(\nu_s\bar{\rho})]\} \end{aligned} \tag{44}$$

The total power supplied by the annular slot is thus $P = P^+ + P^- + P_r$ where P^+ is given adequately by (40) and P_r is the "radiated power" of the annular slot. A simple calculation indicates that the latter is

$$P_r = \lim_{R\to\infty} \eta_0 \pi \int_0^{\pi/2} |\hat{H}_\phi|^2 R^2 \sin\theta\, d\theta = (\pi/6)\, V_0^2\, (\epsilon_0\omega)^2 \cdot (\bar{\rho})^4 \eta_0 k^2 \tag{45}$$

In most cases, P_r will be negligible compared with either P^+ or P^-.

The "desired power" P_l is what can be intercepted at some depth l in the shaft. This quantity is to be obtained from

$$P_l = (1/2)\int_c^a E_{0\rho} H_{0\phi}^*\, 2\pi\rho d\rho \tag{46}$$

Since l is sufficiently large that $I_m\lambda_s l >> 1$ for $s > 0$, we need only use the zero-order mode (i.e., $s = 0$) in computing P_l. In other words, the other modes are "cut off". Thus, the relevant field quantities are

$$E_{0\rho} \simeq i\lambda_0 \nu_0 C_0 [K_1(\nu_0\rho) - \alpha_0 I_1(\nu_0\rho)] e^{-i\lambda_0 z} \tag{47}$$

and

$$H_{0\phi} \simeq i\epsilon_0\omega\nu_0 C_0 [K_1(\nu_0\rho) - \alpha_0 I_1(\nu_0\rho)] e^{-i\lambda_0 z} \tag{48}$$

The corresponding power is

$$\begin{aligned} P_l &\simeq (1/2)\,\mathrm{Re}\int_c^a [E_{0\rho} H_{0\phi}^*]_{z=l}\, 2\pi\rho\, d\rho \\ &= \pi\epsilon_0\omega |\nu_0 C_0|^2\, \mathrm{Re}\,\lambda_0 \int_c^a |K_1(\nu_0\rho) - \alpha_0 I_1 \\ &\quad \cdot (\nu_0\rho)|^2 \rho\, d\rho \exp[-il(\lambda_0 - \lambda_0^*)] \end{aligned} \tag{49}$$

Since $|\nu_0 a| << 1$ in cases of practical interest it

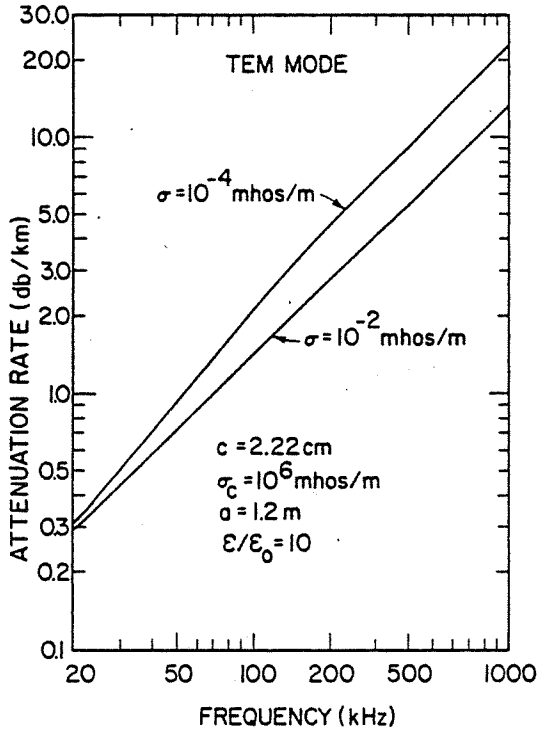


Fig. 2. Attenuation rate of the TEM mode.

follows that

$$P_l = \pi\epsilon_0\omega|C_0|^2\,[\ln(a/c) - (a^2 - c^2)\mathrm{Re}(\alpha_0 v_0/2)] \cdot \mathrm{Re}\{\lambda_0 \exp[-i(\lambda_0 - \lambda_0^*)l]\} \qquad (50)$$

SOME NUMERICAL RESULTS

Using the preceding formulation, some numerical results have been obtained for a number of specific cases using typical values of the relevant parameters. In Figure 2 we show the attenuation rate in db/km of the zero-order or TEM mode as a function of frequency in the cylindrical hoist shaft. The conductivity σ_c of the center conductor is taken to be 10^6 mhos/m and its radius c is 2.22 cm. The radius a of the shaft is 1.2 m. The surrounding homogeneous earth has a dielectric constant $\epsilon = 10\epsilon_0$, a conductivity σ that is either 10^{-2} or 10^{-4} mhos/m. The atmosphere and the air-filled shaft are assumed to have free-space permittivity ϵ_0 and magnetic permeability μ_0. The attenuation rates of the higher-order symmetric TM modes are shown in Figure 3 over the same frequency range and for the same conditions as in Figure 2. The attenuation rates of these evanescent type modes are virtually independent of the earth conductivity so, within graphical accuracy, the curves for $\sigma = 10^{-2}$ and 10^{-4} mhos/m are indistinguishable. In view of these results, it is not surprising that overall transmission efficiency (defined below) is dominated by the TEM mode attenuation characteristics.

An important design quantity is the transmission conductance G_0 of the annular slot. It is defined, in terms of the power delivered to the shaft, as follows:

$$P_l|_{l=0} = (1/2)\,V_0^2 G_0 \qquad (51)$$

where V_0 is the applied voltage (i.e., the rms voltage is $V_0/2^{1/2}$. In Figure 4, G_0 is plotted as a function of frequency for the same parameters as above but now we must specify the radius ρ_0 of the ground screen and the mean radius $\bar{P}$ of the annular slot. We choose $\rho_0 = 2.0$ m and $\bar{\rho} = 0.6$ m but the results are only weakly dependent on these parameters. In Figure 4 we also show the curve when there

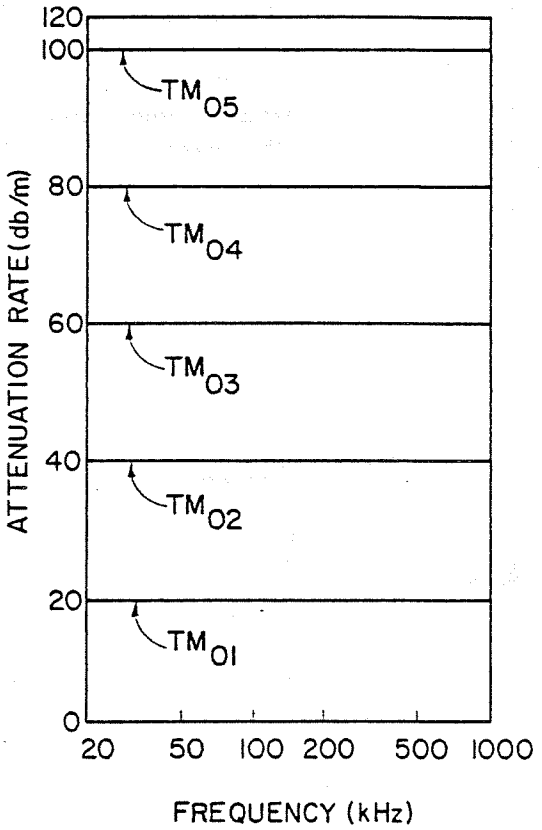


Fig. 3. Attenuation rate of the higher-order symmetric TM modes.

are no ohmic losses (i.e., $\sigma = \sigma_c = \infty$). In the latter case, it is easy to show that

$$G_0\big|_{\sigma=\sigma_c=\infty} = 2\pi/\eta_0 \ln(a/c) \tag{52}$$

As indicated in Figure 4, the transmission conductance increases somewhat with frequency as a result of ohmic losses.

We now define an overall transmission efficiency as the ratio $P_l/(P^- + P^+ + P_r)$. This quantity, expressed as a percentage, is plotted in Figure 5 as a function of frequency for the same parameter range. As indicated, two values of the depth l (= 0.5 and 2.0 km) are selected. Not surprisingly, the transmission efficiency becomes poorer as the depth l increases. In fact, the efficiency is proportional roughly to the factor $\exp(-2\alpha l)$ where α is the attenuation rate of the TEM mode.

CONCLUDING REMARKS

The present analysis and sample calculations show that, for such a configuration, most of the transmitter power can be delivered to the shaft. The key factor seems to be the manner of impressing the source voltage between the center conductor (i.e., hoist rope) and the wall of the shaft. Most of the power is dissipated in ohmic losses in the surrounding earth. For this reason, the transmission efficiency decreases roughly in an exponential fashion with depth to the observer in the shaft.

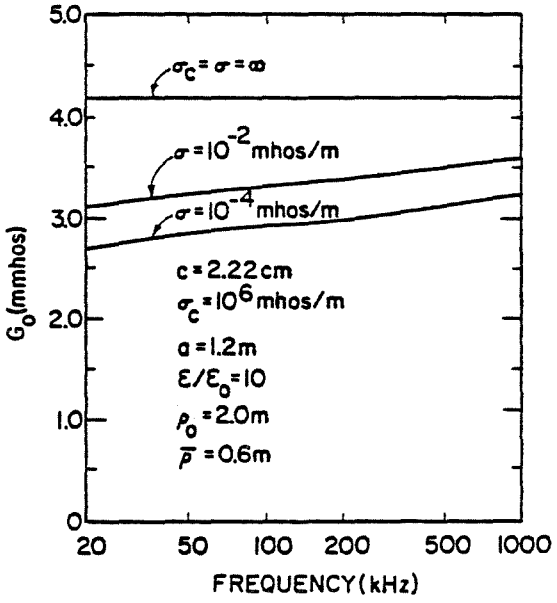


Fig. 4. Transmission conductance of the annular slot.

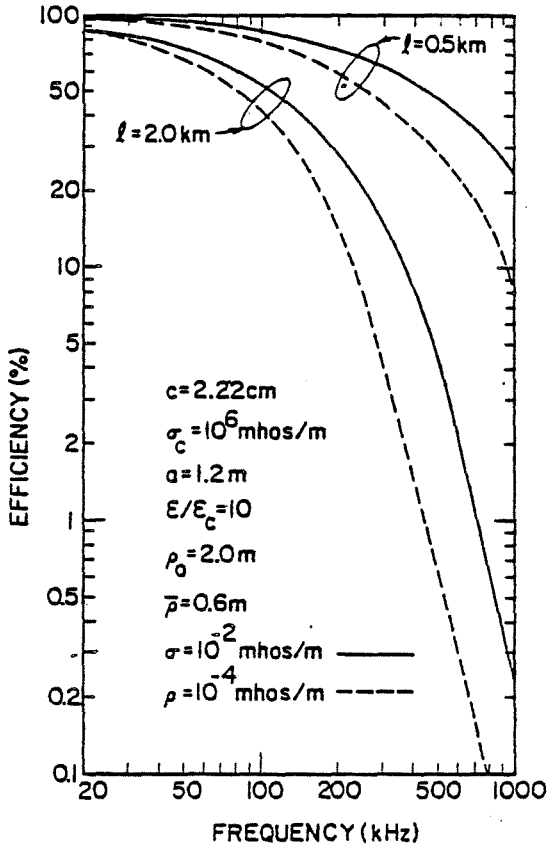


Fig. 5. Transmission efficiency of the system (this is a measure of the relative power that is transmitted down to a depth l in the shaft).

In our calculations we have neglected the continuous spectrum so this conclusion may be modified somewhat at the lowest frequencies and for low rock conductivity. However, in a practical scheme the upper few meters of the wall shaft would be lined with wire mesh so the neglected lateral wave, in the external conductor, would have a negligible effect. A recent calculation has shown this to be the case.

In an actual system we would use a toroidal-coil coupler rather than an annular slot. This should not change the overall features. On the other hand, the practical method of receiving the downward-propagated signal would be a major aspect of the overall capability to communicate. This subject is now occupying our attention.

REFERENCES

Emslie, A. G., and R. Lagace (1974), Hoist shaft mine communications, *Rep. to US Bureau of Mines*, sec. 5, A. D. Little,

Inc., Cambridge, Mass.

Stratton, J. A. (1941), *Electromagnetic Theory*, pp. 371, 576, McGraw-Hill, New York.

Wait, J. R. (1969), Characteristics of antennas over lossy earth, in *Antenna Theory, Part 2*, edited by R. E. Collin and F. J. Zucker, chap. 23, pp. 386-437, McGraw-Hill, New York.

Wait, J. R., and D. A. Hill (1974*a*), Coaxial and bifilar modes on a transmission line in a circular tunnel, *Appl. Phys.*, *4*(4), 307-312.

Wait, J. R., and D. A. Hill (1974*b*), Guided electromagnetic waves along an axial conductor in a circular tunnel, *IEEE Trans. Antennas Propagat.*, *AP-22*(4), 627-630.

Radio Science, Volume 11, Number 4, pages 263-265, April 1976

Note on the theory of transmission of electromagnetic waves in a coal seam

James R. Wait

Environmental Research Laboratories, National Oceanic and Atmospheric Administration, US Department of Commerce, Boulder, Colorado 80302

(Received October 27, 1975; revised November 13, 1975.)

A coal seam is idealized as a resistive slab bounded by more conductive rock. The source is taken to be a vertical electric dipole. It is shown that the dominant mode has relatively low attenuation.

Electromagnetic waves can propagate laterally via highly resistive layers in the earth [*Wait*, 1971]. In such cases, it is necessary to locate the source and observer within or near the waveguide. Such a waveguide could be formed by a coal seam bounded by well conducting rock. Our wave model is very simple and probably overly idealized but, in spite of this fact, the calculations are nontrivial.

The waveguide configurations and the cylindrical coordinate system (ρ,ϕ,z) we adopt are illustrated in Figure 1. We show a homogeneous slab of width $2h$, of conductivity σ, and of permittivity ϵ. This is bounded above and below by homogeneous and semi-infinite regions of conductivity σ_1 and permittivity ϵ_1. The source is a vertical electric dipole of moment $2Ids$ located at $z = 0$, which is the center of the slab. We first consider the vertical electric field E_z within the region $-h < z < h$. Formally, it is represented as a contour integral over a spectrum of plane waves. This, in turn, can be expressed as a sum of residues plus branch line integrals. For the present problem, the dominant contribution is the residue corresponding to the zero-order mode at the eigenvalue $C = C_0$ defined below. Thus, for our purposes, we write [*Wait*, 1970]:

$$E_z \simeq E_0 W \tag{1}$$

where

$$E_0 = -[i\mu_0 \omega Ids/(2\pi\rho)] \tag{2}$$

is a reference field and W is an attenuation function. The latter is given by

$$W = (2\pi k\rho)^{1/2}(kh)^{-1}\exp(-i\pi/4)\Lambda \cdot \cos(kC_0 z)S_0^{3/2}\exp(-ik\rho S_0) \tag{3}$$

where

$$ik = [i\mu_0\omega(\sigma + i\epsilon\omega)]^{1/2}, \quad S_0 = (1 - C_0^2)^{1/2},$$

$$\Lambda = \left[1 + \frac{i\partial R/\partial C}{2khR}\right]^{-1}_{C=C_0}, \quad R = \frac{C - \Delta}{C + \Delta},$$

$$\left(\frac{i\mu_0\omega}{\sigma + i\epsilon\omega}\right)^{1/2}\Delta = \frac{(k^2S^2 - k_1^2)^{1/2}}{\sigma_1 + i\epsilon_1\omega}$$

$$= i(k_1^2 - k^2S^2)^{1/2}/(\sigma_1 + i\epsilon_1\omega)$$

$$ik_1 = [i\mu_0\omega(\sigma_1 + i\epsilon_1\omega)]^{1/2}$$

Here C_0 is a solution of the equation $R\exp(-i2khC) = 1$. In writing (1), (2), and (3) we assume that $|k\rho| \gg 1$.

The mode equation can be written in equivalent form as

$$u\tanh uh + pv = 0 \tag{4}$$

where $p = (\sigma + i\epsilon\omega)/(\sigma_1 + i\epsilon_1\omega)$, $u = ikC$, and $v = (k^2S^2 - k_1^2)^{1/2} = ik_1(1 - p^2S^2)^{1/2}$. The attenuation rate is then $-Imk S_0$ nepers per unit length in the ρ direction. In this notation we see that the excitation factor Λ can be calculated from

$$\Lambda = \left[1 - \frac{1}{2hR}\frac{\partial R}{\partial u}\right]^{-1}, \quad R = \frac{u - pv}{u + pv}$$

Using the mode equation in the form

$$R - R^{-1} = 2\sinh 2uh$$

we see that

$$\Lambda = \left[1 - \frac{k_1^2 - k^2}{v^2}\frac{\sinh 2uh}{2uh}\right]^{-1} \tag{5}$$

Before presenting typical numerical results for the attenuation rates, we will discuss some limiting

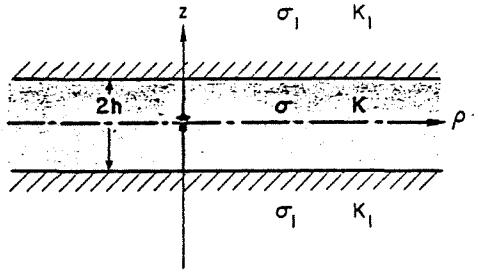


Fig. 1. Idealized coal seam of conductivity σ bounded by rock of conductivity σ_1. The relative permittivity values are taken to be $K_1 = \epsilon_1/\epsilon_0 = 15$ and $K = \epsilon/\epsilon_0 = 9$ throughout.

forms. If $|p| \to 0$, corresponding to perfectly conducting boundaries, it is evident from (4) that the zero-order mode corresponds to $u = 0$ or $S_0 = 1$. Thus the attenuation rate is the same as that for plane waves in a region of conductivity σ and permittivity ϵ. For this case, $\Lambda = 1/2$. The other limit results when the waveguide thickness h tends to 0, while all other parameters remain fixed. From (4) we see that this limit corresponds to $v = 0$, which means that $kS = k_1$. Thus, as is expected, the attenuation rate approaches that for an infinite medium of conductivity σ_1 and permittivity ϵ_1. Now, as is easily seen from (5), the excitation factor approaches 0. This result is not surprising, since we no longer have a waveguide but merely a conducting full-space. Some of these limiting cases were exhibited in some calculations reported earlier

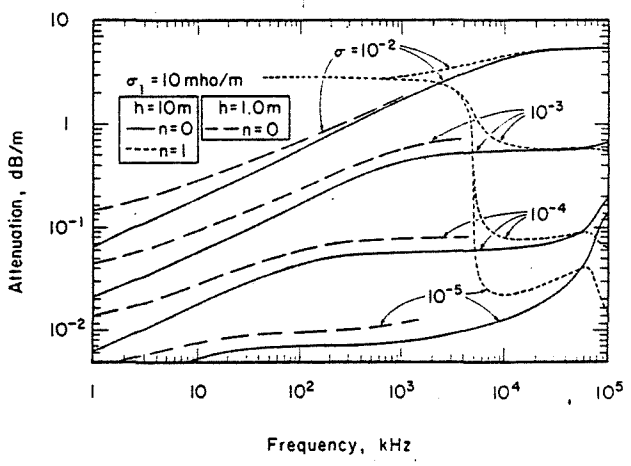


Fig. 2. Attenuation rates for dominant waveguide modes in a coal seam of thickness $2h$ for an optimistically high wall conductivity of $\sigma_1 = 10$ mhos/m.

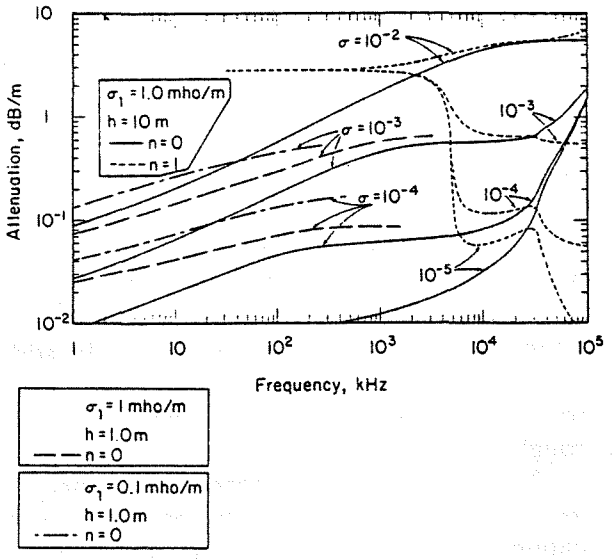


Fig. 3. Attenuation rates for dominant waveguide modes in a coal seam of thickness $2h$ for various wall conductivities.

[*Wait and Spies*, 1972] in the context of ultra-low frequency in a postulated waveguide in the crystalline basement of the earth's crust.

Using a numerical solution of (4), values of the attenuation rate $-Imk_0 S_0$ in decibels per meter have been obtained that are relevant to the coal seam situation. The frequency range extends from 1 to 10^5 kHz (i.e., 1000 Hz to 100 MHz). Some typical values of the parameters are chosen and they are indicated in a self-contained fashion in Figures 2 and 3. The curves apply to the important zero-order mode which is analogous to a TEM (Transverse Electromagnetic Mode) in a parallel plate waveguide. Such a mode, of course, has no cutoff as such and, for this reason, it has been proposed that it be the principal mechanism for low-loss transmission in stratified layers of the earth's crust. In Figure 2, however, we also show some results for the first order ($n = 1$) mode which for $h = 10$ m is "cut off" at frequencies below about 40 MHz, when the half-width h of the waveguide is equal to one-half of the effective wavelength. When $h = 1.0$ m this cutoff frequency would be approximately 400 MHz for the same condition.

Some important conclusions can be drawn fron Figures 2 and 3. As expected, on the basis of previous work on the earth-crust waveguide, the

attenuation rate is critically dependent on the bulk conductivity σ of the waveguide (i.e., the coal seam itself). In fact, at the higher frequencies, there is almost a direct proportionality as one would predict on the basis of propagation in an unbounded medium when the loss tangent is small (i.e., when $\epsilon\omega/\sigma \ll 1$). Also, we can see that, as the waveguide half-width h is changed from 10 m to 1.0 m, the attenuation is increased consistently. In addition, if we decrease the conductivity σ_1 of the bounding rock, the attenuation also increases in a manner roughly proportional to $(\sigma_1)^{-1/2}$.

These results confirm recent unpublished experimental and calculated results (personal communications, R. L. Lagace of A. D. Little, Inc.) that attenuation rates in such configurations can be expected to be as low as 0.1 dB/m for frequencies around 100 kHz if the bulk conductivity of the seam is less than about 1.0 millimho/meter.

In this analysis we have assumed that the coal seam is excited by a vertical electric dipole at its center. The same $n = 0$ mode is excited for a vertical electric dipole anywhere within the seam. However, if the electric dipole were located outside the seam it should be located in a horizontal orientation so that the desired mode is launched in the end-fire directions. Similarly, a horizontal-axis loop will also excite the desired mode but a vertical-axis loop will not. The excitation problem for the analogous earth-crust waveguide has been discussed recently [*Wait*, 1975] and the results would seem to apply directly to the coal-seam problem.

Acknowledgments. I am very grateful to R. G. Geyer and R. J. Lytle for their useful comments and critical remarks on this subject.

REFERENCES

Wait, J. R. (1970), *Electromagnetic Waves in Stratified Media*, 2nd Ed., p. 551, Pergamon, New York.

Wait, J. R. (1971), Analytical investigations of electromagnetic wave propagation in the earth's crust, in *The Structure and Physical Properties of the Earth's Crust, Geophys. Monogr. Ser.*, Vol. 14, edited by J. G. Heacock, p. 315, American Geophysical Union, Washington, DC.

Wait, J. R. (1975), Note on excitation of the electromagnetic earth-crust waveguide, *IEEE Trans. Antennas Propagat.*, *AP-23*, 425–428.

Wait, J. R., and K. P. Spies (1972), Dipole excitation of ultralow-frequency electromagnetic waves in the earth crust waveguide, *J. Geophys. Res.*, *77*, 7118–7120.

Analysis for the electromagnetic fields of a dipole located within a metal-cased borehole

James R. Wait

Cooperative Institute for Research in Environmental Sciences, University of Colorado/NOAA, Boulder, Colorado 80302
(Received 7 October 1976)

A solution is obtained for the electromagnetic fields of a dipole of arbitrary orientation located within a cylindrical metal tube of infinite length. The external medium is homogeneous with finite conductivity. The expressions for the resultant fields are given explicitly for the case where the wall of the tube has a thickness small compared with the skin depth of the metal. A numerical example for magnetic dipole excitation is given for the case where the observer is in the external medium at the same level as the source. Not surprisingly, the results show that the metal casing in a borehole will have a severe shielding effect on the external fields.

PACS numbers: 41.10.Hv, 84.40.Mk, 91.25.—r

I. INTRODUCTION

There are many practical situations where one is interested in transmitting electromagnetic waves directly through the earth. A particular case of some importance is when the source is located within an air-filled borehole that is surrounded by more or less uniform rock. Also, the hole may have a metal casing that can be envisaged as a thin-walled metal tube. We wish to present an analysis of this configuration under the assumption that end effects can be ignored or treated separately.

II. FORMULATION

Specifically we deal with a cylindrical hole of radius a cut through a homogeneous rock medium of conductivity σ_e and permittivity ϵ_e of infinite extent. To allow for the effect of a metal casing, the hole is lined with a thin metal tube of conductivity σ and thickness d. Since we ignore end effects, the hole can be considered infinite in length and described as the region $\rho < a$ and $-\infty < z < \infty$ in reference to a cylindrical coordinate system (ρ, ϕ, z). At some interior point (ρ_0, ϕ_0, z_0), we locate a point dipole exciter. This can be either an electric dipole (current element) or a magnetic dipole (small loop) with any specified orientation. The situation is illustrated in Fig. 1.

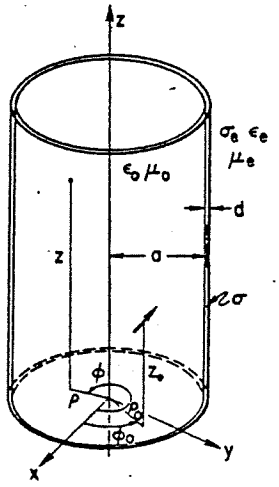


FIG. 1. Cylindrical borehole showing location of source dipole.

The derivation given below can be treated as an extension of earlier work so the many preliminary details of the formulation can be omitted.[1–4] Thus we can immediately write down suitable integral representations for the fields within the hole. These fields, for a time factor $\exp(i\omega t)$, can be obtained from electric and magnetic Hertz vectors that have only z components U and V, respectively. Thus, for the region $\rho_0 < \rho < a$, we may postulate that

$$U = \Gamma(A_m(\lambda)K_m(v\rho) + P_m(\lambda)I_m(v\rho)), \tag{1}$$

and

$$V = \Gamma(B_m(\lambda)K_m(v\rho) + Q_m(\lambda)I_m(v\rho)), \tag{2}$$

where Γ is an integral-summation operator defined by

$$\int_{-\infty}^{\infty} \sum_{m=-\infty}^{\infty} (\cdots) \exp[-im(\phi - \phi_0)] \exp[-i\lambda(z - z_0)]\, d\lambda.$$

$I_m(v\rho)$ and $K_m(v\rho)$ are modified Bessel functions of integer order m and argument $v\rho$ where $v = (\lambda^2 + \gamma_0^2)^{1/2}$ and $\gamma_0^2 = -\epsilon_0\mu_0\omega^2$. The functions $A_m(\lambda)$ and $B_m(\lambda)$ are specified by the source, while $P_m(\lambda)$ and $Q_m(\lambda)$ are yet to be determined.

In general, we see that Eqs. (1) and (2) have the form

$$\begin{pmatrix} U \\ V \end{pmatrix} = \Gamma \begin{pmatrix} U_m \\ V_m \end{pmatrix}. \tag{3}$$

Similarly, the field expressions can be written

$$\begin{pmatrix} E_\rho \\ H_\rho \\ E_z \\ H_z \end{pmatrix} = \Gamma \begin{pmatrix} E_{\rho m} \\ H_{\rho m} \\ E_{zm} \\ H_{zm} \end{pmatrix}, \tag{4}$$

where

$$E_{\rho m} = -\frac{m\lambda}{\rho} U_m + i\mu_0\omega \frac{\partial V_m}{\partial \rho}, \tag{5}$$

$$H_{\rho m} = -i\epsilon_0\omega \frac{\partial U_m}{\partial \rho} - \frac{m\lambda}{\rho} V_m, \tag{6}$$

$$E_{zm} = -v^2 U_m, \quad H_z = -v^2 V_m. \tag{7}$$

III. DEVELOPMENT OF GENERAL BOUNDARY CONDITIONS

An efficient way to proceed is to impose the following boundary conditions on the internal field at the surface $\rho = a - \frac{1}{2}d$:

$$E_{\phi m} = \alpha_m E_{zm} + Z_m H_{zm}\big|_{\text{at } \rho = a-(d/2)} \tag{8}$$

$$H_{\phi m} = -Y_m E_{zm} + \alpha_m H_{zm}\big|_{\text{at } \rho = a-(d/2)}$$

where α_m, Y_m, and Z_m are coefficients to be designated.

In the external region $\rho > a + \frac{1}{2}d$, similar field representations apply in place in Eqs. (1) and (2). We could write

$$U_e = \Gamma(\hat{P}_m(\lambda) K_m(u\rho)) \tag{9}$$

and

$$V_e = \Gamma(\hat{Q}_m(\lambda) K_m(u\rho)), \tag{10}$$

where $u = (\lambda^2 + \gamma_e^2)^{1/2}$ and $\gamma_e^2 = i\mu_0\omega(\sigma_e + i\epsilon_e\omega)$. Here $\hat{P}(\lambda)$ and $\hat{Q}_m(\lambda)$ are unknown coefficients but, for the present formulation, their explicit form is not needed. The corresponding field components $E_{\phi e}$, $H_{\rho e}$, etc., can be obtained from U_e and V_e by equations identical to Eqs. (5)—(7) with $i\epsilon_0\omega$ replaced by $\sigma_e + i\epsilon_e\omega$ and v replaced by u. Then, it is not difficult to show that for the external surface of the tube

$$E_{\phi om} = \alpha_{em} E_{zm} + Z_{em} H_{zm}\big|_{\text{at } \rho = a+(d/2)} \tag{11}$$

$$H_{\phi om} = -Y_{em} E_{zm} + \alpha_{em} H_{zm}\big|_{\text{at } \rho = a+(d/2)}$$

where

$$\alpha_{em} = \frac{m\lambda}{u^2(a + \frac{1}{2}d)}, \tag{12}$$

$$Z_m = -\frac{i\mu_0\omega}{u} \frac{K_m'[u(a+\frac{1}{2}d)]}{K_m[u(a+\frac{1}{2}d)]}, \tag{13}$$

$$Y_m = \frac{i\gamma_e^2}{u\mu_0\omega} \frac{K_m'[u(a+\frac{1}{2}d)]}{K_m[u(a+\frac{1}{2}d)]}. \tag{14}$$

By introducing appropriate wave functions in the tube region, $a - \frac{1}{2}d < \rho < a + \frac{1}{2}d$, we can complete the process. For example, in this region, we would have the following forms for the Hertz potentials:

$$U_i = \Gamma(M_m(\lambda) I_m(w\rho) + N_m(\lambda) K_m(w\rho)), \tag{15}$$

$$V_i = \Gamma(S_m(\lambda) I_m(w\rho) + T_m(\lambda) K_m(w\rho)), \tag{16}$$

where $w = (\lambda^2 + \gamma^2)^{1/2}$ and $\gamma^2 = i\mu\omega(\sigma + i\epsilon\omega)$. Here, the electrical properties of the tube are σ, ϵ, and μ. (The permeability μ of the tube may be quite different from the free space value.)

The coefficients M_m, N_m, S_m, and T_m can be determined in a very straightforward manner, although the algebra becomes complex. First of all, we note that the field equations are identical to Eqs. (5)—(7) with $i\mu_0\omega$ replaced by $i\mu\omega$, $\sigma_e + i\epsilon_e\omega$ replaced by $\sigma + i\epsilon\omega$, and u replaced by w. We then match the four tangential field components at the two boundaries $\rho = a \pm \frac{1}{2}d$ and obtain eight linear equations to determine the unknown coefficients P, Q, $\hat{P}$, $\hat{Q}$, M, N, S, and T in terms of A and B (the subscript m on these quantities is understood). Fortunately, this tedious operation can be avoided in the case of thin tubes with relatively high conductivity. Mathematically, we are saying that $\sigma \to \infty$, $d \to 0$ in such a way that σd, the transverse conductance, is finite. We are then permitted to use the following thin-sheet boundary conditions:

$$H_{\phi e}' = H_\phi + \sigma d E_z \qquad \text{at } \rho = a. \tag{17}$$
$$H_{\phi i} = H_\phi - \sigma d E_z$$

These merely state that the surface current density in the tube is equal to the discontinuity in the orthogonal tangential magnetic field—in accordance with Ampere's law. Under the same condition, the tangential electric field is continuous through the tube. That is,

$$E_{\phi e} = E_\phi \qquad \text{at } \rho = a. \tag{18}$$
$$E_{\phi i} = E_\phi$$

Now, in the limit $d \to 0$, Eq. (11) becomes

$$E_{\phi om} = \alpha_{em} E_{zm} + Z_{em} H_{zm} \tag{19}$$

and

$$H_{\phi om} = -Y_{em} E_{zm} + \alpha_{em} H_{zm}, \tag{20}$$

where

$$\alpha_{em} = m\lambda/(u^2 a), \tag{21}$$

$$Z_m = -\frac{i\mu_0\omega}{u} \frac{K_m'(ua)}{K_m(ua)}, \tag{22}$$

$$Y_m = \frac{i\gamma_e^2}{u\mu_0\omega} \frac{K_m'(ua)}{K_m(ua)}. \tag{23}$$

If we now use Eqs. (17) and (18), the pair (19) and (20) can be written

$$E_{\phi m} = \alpha_{em} E_{zm} + Z_{em}(H_{zm} - \sigma d E_{\phi m}) \tag{24}$$

and

$$H_{\phi m} + \sigma d E_{zm} = -Y_{em} E_{zm} + \alpha_{em}(H_{zm} - \sigma d E_{\phi m}). \tag{25}$$

These can be shown easily to be equivalent to Eq. (8) if

$$\alpha_m = \frac{\alpha_e}{1 + Z_{em}\sigma d}, \tag{26}$$

$$Y_m = Y_{em} + \sigma d + \frac{\alpha_{em}^2 \sigma d}{1 + Z_{em}\sigma d}, \tag{27}$$

$$Z_m = \frac{Z_{em}}{1 + Z_{em}\sigma d}. \tag{28}$$

Thus we can construct the desired solution by imposing the conditions

$$E_{\phi m} = \alpha_m E_{zm} + Z_m H_{zm} \tag{29}$$

and

$$H_{\phi m} = -Y_m E_{zm} + \alpha_m H_{zm} \tag{30}$$

at the interior surface of the tube. In this connection it is worth noting that $1/Z_m = 1/Z_{em} + \sigma d$ in all cases. However, $Y_m \simeq Y_{em} + \sigma d$ only in the case where the coupling term α_{em} can be ignored.

IV. INTEGRAL REPRESENTATIONS

The boundary conditions (29) and (30) can now be

applied to Eqs. (1), (2), and (5)—(7) to yield

$$P_m(\lambda) = -\left\{A_m\left[\left(\frac{m\lambda}{\nu^2 a} - \alpha_m\right)^2 + \left(\frac{\gamma_0 K_m'}{\nu K_m} + \eta_0 Y_m\right)\left(\frac{\gamma_0 I_m'}{\nu I_m} + \frac{Z_m}{\eta_0}\right)\right]\right.$$
$$\left. \times\, I_m K_m + B_m\left(\frac{m\lambda}{\nu^2 a} - \alpha_m\right)\frac{i\mu_0\omega}{\nu^2 a}\right\} D_m^{-1} \qquad (31)$$

and

$$Q_m(\lambda) = -\left\{B_m\left(\frac{m\lambda}{\nu^2 a} - \alpha_m\right)^2 + \left(\frac{\gamma_0 I_m'}{\nu I_m} + \eta_0 Y_m\right)\left(\frac{\gamma_0 K_m'}{\nu K_m} + \frac{Z_m}{\eta_0}\right)\right]$$
$$\times I_m K_m - A_m\left(\frac{m\lambda}{\nu^2 a} - \alpha_m\right)\frac{i\epsilon_0\omega}{\nu^2 a}\right\} D_m^{-1}, \qquad (32)$$

where

$$D_m = \left[\left(\frac{m\lambda}{\nu^2 a} - \alpha_m\right)^2 + \left(\frac{\gamma_0 I_m'}{\nu I_m} + \eta_0 Y_m\right)\left(\frac{\gamma_0 I_m'}{\nu I_m} + \frac{Z_m}{\eta_0}\right)\right] I_m^2. \qquad (33)$$

In Eqs. (31) and (32) the notation has been simplified such that $A_m = A_m(\lambda)$, $B_m = B_m(\lambda)$, $I_m = I_m(va)$, $I_m' = I_m'(va)$, $K_m = K_m(va)$, and $K_m' = K_m'(va)$ while bearing in mind that α_m, Y_m, and Z_m are defined by Eqs. (26)—(28). As usual, the prime over the Bessel function indicates differentiation with respect to the argument.

We have now actually completed the formal solution since the resulting field expressions are completely specified in terms of the "source coefficients" $A_m(\lambda)$ and $B_m(\lambda)$. The latter are quite simple for the two special cases of axial dipoles. For example, if we located an axial electric dipole of current moment at (ρ_0, ϕ_0, z_0), then[1]

$$A_m(\lambda) = \frac{Ids}{4\pi^2 i\epsilon_0\omega} I_m(\nu\rho_0), \quad B_m(\lambda) = 0. \qquad (34)$$

In the case of an axial magnetic dipole or small current loop of moment IdA we would have

$$B_m(\lambda) = \frac{IdA}{4\pi^2} I_m(\nu\rho_0), \quad A_m(\lambda) = 0. \qquad (35)$$

The other dipole orientation of interest is when it lies in the plane $z = z_0$ with its axis parallel to the x axis. We might describe this as the transverse dipole. The cross section for this situation is illustrated in Fig. 2. We note here that if $\phi_0 = 0°$, the transverse dipole is oriented in the radial direction, and if $\phi_0 = 90°$ it is oriented in the circumferential direction. Clearly any arbitrary orientation of the dipole can be regraded as the superposition of the three special cases mentioned above.

For the transverse electric dipole, it is not difficult

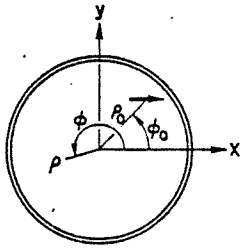


FIG. 2. Cross section for the case where the source dipole is perpendicular to the borehole axis.

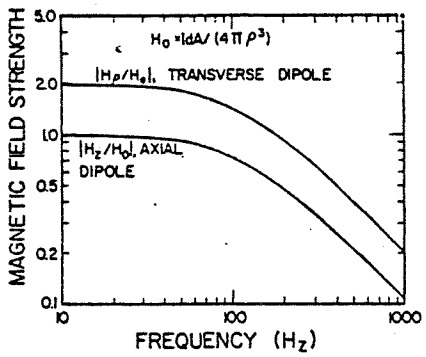


FIG. 3. Normalized fields in external region of axial and transverse dipoles located on the axis of the borehole. The following parameters are selected: $\phi_0 = \phi = 0°$, $z_0 = z = 0$, $\rho_0 = 0$, $\rho = 15.25$ m (= 50 ft), $a = 7.62$ cm (= 3 in.), $d = 0.635$ cm (= 0.25 in.), $\sigma = 5\times10^6$ mho/m, $\sigma_e = 10^{-2}$ mho/m, $\epsilon_e = 10\epsilon_0$.

to show that[3]

$$A_m(\lambda) = \frac{-Ids}{4\pi^2\epsilon_0\omega}\left(\frac{\lambda}{2\nu}\right)[\exp(i\phi_0)I_{m+1}(\nu\rho_0)$$
$$+\exp(-i\phi_0)I_{m-1}(\nu\rho_0)], \qquad (36)$$

$$B_m(\lambda) = \frac{Ids}{4\pi^2}\left(\frac{i}{2\nu}\right)[\exp(-i\phi_0)I_{m-1}(\nu\rho_0)$$
$$-\exp(i\phi_0)I_{m+1}(\nu\rho_0)]. \qquad (37)$$

On the other hand, for the transverse magnetic dipole[3]

$$A_m(\lambda) = \frac{i\mu_0\omega IdA}{4\pi^2}\left(\frac{i}{2\nu}\right)[\exp(-i\phi_0)I_{m-1}(\nu\rho_0)$$
$$-\exp(i\phi_0)I_{m+1}(\nu\rho_0)], \qquad (38)$$

$$B_m(\lambda) = \frac{IdA}{4\pi^2}\left(\frac{-i\lambda}{2\nu}\right)[\exp(i\phi_0)I_{m+1}(\nu\rho_0)$$
$$+\exp(-i\phi_0)I_{m-1}(\nu\rho_0)]. \qquad (39)$$

V. DISCUSSION OF A NUMERICAL EXAMPLE

In general, the computation for the fields require both an infinite summation over m and an infinite integration over λ. However, if the dipole is located on the axis, only the $m = 0$ terms are needed for the axial dipole and $m = \pm 1$ for the transverse dipole. We also should indicate that the transverse wave numbers u, v, and w are defined such that along the λ contour, $\mathrm{Re}\,u \geq 0$ and $\mathrm{Im}\,u \leq 0$.

To illustrate the situation, we consider two examples. In the first case we choose an axially oriented magnetic dipole located on the axis of the borehole (at $\rho_0 = 0$ and $z_0 = 0$). The magnetic field at a radial distance ρ in the external medium at $z = 0$ will then have only an H_z component. In presenting the numerical data for such a case, it is convenient to normalize this by dividing by $H_0 = IdA/(4\pi\rho^3)$, which is the corresponding static field. Thus, as $\omega \to 0$, $H_z/H_0 \to 1$. In the second case we locate a horizontal magnetic dipole at the same point and orient it in the $\phi_0 = 0$ direction. In this case, the observed field at $z = 0$ has only an H_ρ component. It is also convenient to normalize this by dividing by the same factor H_0. But now, as $\omega \to 0$, $H_\rho/H_0 \to 2$.

The magnitude of the ratios H_z/H_0 and H_ρ/H_0 are plotted in Fig. 3 as a function of frequency $\omega/2\pi$ from 10 to 1000 Hz for the parameters indicated in the figure caption. For this range of conditions, the thin-tube assumption is valid [i.e., $d \ll \delta$ where $\delta = (2/\sigma\mu\omega)^{1/2}$]. Also, in the present example, the distance ρ is very much less than the skin depth $\delta_e = (2/\sigma_e\mu_0\omega)^{1/2}$ in the external medium so that the results do not depend significantly on the conductivity σ_e. In fact, the curves plotted in Fig. 3 would not differ within plotting accuracy from the simple relationship

$$\frac{H_z}{H_0} \simeq \frac{H_\rho}{2H_0} \simeq \frac{1}{1 + i(\tfrac{1}{2}\mu_0\omega\sigma da)}. \tag{40}$$

This same shielding factor can be derived directly from a two-dimensional analysis of a magnetic line source at the axis of the tube. This is analogous to the case of the axial magnetic dipole. We also obtain the same factor by solving the two-dimensional analysis of a source that consists of two closely spaced wires carrying equal and opposite electric currents. When such a source is located at the axis of the tube, the fields are analogous to a small wire loop or magnetic dipole oriented in the transverse direction (i.e., loop axis is perpendicular to borehole axis).

It should be stressed that the close similarity of the numerical results for the dipole and the line source configuration is not true in general. Particularly, at higher frequencies and for other observer locations, major differences can be expected. Thus, generally dependable shielding calculations can only be guaranteed if the axial integrations are carried out explicitly.

VI. CONCLUDING REMARKS

The important physical conclusion is that shielding by thin metal tubes is governed primarily by the ratio $R = (ad)^{1/2}/\delta$. Where this ratio is small compared with unity, the shielding of an internal source is negligible, while if this ratio is large compared with unity, the external fields are reduced by a factor of the order of R^2. This relatively simple prediction is valid when $d \ll \delta$ (i.e., thin tubes) and when the observer distance $\rho \ll \delta_e$ in terms of the skin depth in the external medium. Actually, the condition that d be small is not overly stringent. For example, if $d/\delta < 0.2$, the fields will be within 10% of the more exact "thick tube" solution.[5] Shielding performance by thick-walled tubes, of course, is much more complicated but the present formulation can be adapted to consider any conceivable situation.

ACKNOWLEDGMENT

The author would like to thank David A. Hill for performing the numerical calculations and for his useful suggestions.

[1] J.R. Wait, *Electromagnetic Radiation from Cylindrical Structures* (Pergamon, Oxford, 1959).
[2] J.R. Wait and D.A. Hill, IEEE Trans. Antennas Propag. AP-22, 627 (1974).
[3] J.R. Wait and D.A. Hill, Preliminary Report to the U.S. Bureau of Mines, 1976 (unpublished).
[4] A.A. Kaufmann, *Theory of Induction Logging* (Nauka Press, Novosibersk, 1965), Chap. 13.
[5] J.R. Wait and D.A. Hill, Preliminary Report to the U.S. Bureau of Mines, 1976 (unpublished).

Electromagnetic Shielding of Sources Within a Metal-Cased Bore Hole

JAMES R. WAIT, FELLOW, IEEE, AND DAVID A. HILL

Abstract—An abbreviated derivation is given for the electromagnetic fields produced by a two-dimensional source located within a metal-cased bore hole surrounded by a homogeneous rock formation. Numerical results are presented for the fields in the external region. It is shown that the combined influence of the conductivity and permeability of the steel casing will severely attenuate the fields even at frequencies as low as 100 Hz.

Introduction

IN VARIOUS applications [1]–[4] in communications and geophysics, an estimate of how the metal casing of a drill hole will attenuate signals is needed. Whether we are dealing with a subsurface communication scheme or geophysically probing the adjacent formation, the presence of the casing cannot be ignored. It is the purpose of this paper to consider this question in a quantitative fashion.

Manuscript received December 16, 1976.

J. R. Wait is with the Cooperative Institute for Research in Environmental Sciences, University of Colorado/NOAA, Boulder, CO 80309.

D. A. Hill is with the Institute for Telecommunication Sciences, Office of Telecommunications, U.S. Department of Commerce, Boulder, CO 80302.

Formulation

The model we choose is rudimentary as indicated in Fig. 1. With respect to a cylindrical coordinate system (ρ, ϕ, z), the metal casing or tube is bounded by the surfaces $\rho = a$ and $\rho = b = a + d$. Here d is the thickness of the tubing, a is its inner radius, and b is its outer radius, which is flush with the external rock formation. The tube is composed of homogeneous metal with conductivity σ, permittivity ϵ, and permeability μ. The internal region, $\rho < a$, is assumed to be the same as free space with permittivity ϵ_0 and permeability μ_0. The external region, $\rho > b$, is assumed to be homogeneous with conductivity σ_e, permittivity ϵ_e, and permeability μ_0.

While it is possible to construct a general theory [5], [6] for any bounded source configuration within the tube, we will

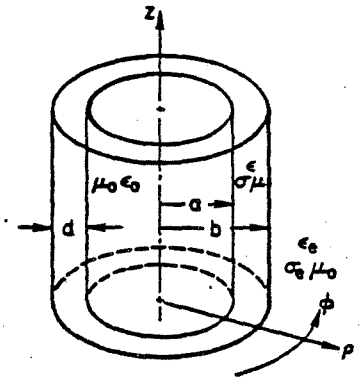


Fig. 1. Geometry of the metal-cased bore hole of assumed infinite length in a homogeneous rock formation.

employ here a much simpler two-dimensional formulation that predicts essentially the same shielding factors. Thus we allow the source to be an axially independent distribution of electric or magnetic currents, within the tube, that may vary individually as $\exp(-in\phi)$ where $n = 0, \pm 1, \pm 2, \pm 3, \cdots$. We also deal with time harmonic fields so that the common time factor is $\exp(i\omega t)$.

We deal first with the transverse electric (TE) fields excited by the equivalent magnetic currents. The z-directed magnetic field can be taken as having the following forms in the three regions [5], [7]:

$$H_{0z} = [A_n K_n(\gamma_0\rho) + B_n I_n(\gamma_0\rho)]e^{-in\phi}, \quad 0 < \rho < a \tag{1}$$

$$H_z = [M_n K_n(\gamma\rho) + N_n I_n(\gamma\rho)]e^{-in\phi}, \quad a < \rho < b \tag{2}$$

$$H_{ez} = C_n K_n(\gamma_e\rho)e^{-in\phi}, \quad \rho > b \tag{3}$$

where

$$\gamma_0 = i(\epsilon_0\mu_0)^{1/2}\omega = i2\pi/(\text{wavelength})$$

$$\gamma = [i\mu\omega(\sigma + i\epsilon\omega)]^{1/2}$$

$$\gamma_e = [i\mu_0\omega(\sigma_e + i\epsilon_e\omega)]^{1/2}.$$

I_n and K_n are modified Bessel functions of order n (in standard notation) with the indicated arguments. Summation over all the significant values of n is understood. The coefficients A_n determine the source configuration while B_n, M_n, N_n, and C_n are, as yet, unspecified.

The corresponding electric fields have only ρ and ϕ components but, for applying the boundary conditions, only the latter are needed. From Maxwell's equations, it follows that

$$E_{0\phi} = -\eta_0[A_n K_n'(\gamma_0\rho) + B_n I_n'(\gamma_0\rho)]e^{-in\phi}, \quad \rho < a \tag{4}$$

$$E_\phi = -\eta[M_n K_n'(\gamma\rho) + N_n I_n'(\gamma\rho)]e^{-in\phi}, \quad a < \rho < b \tag{5}$$

$$E_{e\phi} = -\eta_e C_n K_n'(\gamma_e\rho)e^{-in\phi}, \quad \rho > b \tag{6}$$

where

$$\eta_0 = (\mu_0/\epsilon_0)^{1/2} \simeq 120\pi$$

$$\eta = [(i\mu\omega)/(\sigma + i\epsilon\omega)]^{1/2}$$

$$\eta_e = [(i\mu_0\omega)/(\sigma_e + i\epsilon_e\omega)]^{1/2}.$$

The primes over the modified Bessel function indicate differentiation with respect to the argument.

The boundary conditions require that the tangential fields, as given by (1)–(6), are continuous at the interfaces $\rho = a$ and $\rho = b$. Thus

$$AK(\gamma_0 a) + BI(\gamma_0 a) = MK(\gamma a) + NI(\gamma a) \tag{7}$$

$$CK(\gamma_e b) = MK(\gamma b) + NI(\gamma b) \tag{8}$$

$$A\eta_0 K'(\gamma_0 a) + B\eta_0 I'(\gamma_0 a) = M\eta K'(\gamma a) + N\eta I'(\gamma a) \tag{9}$$

$$C\eta_e K'(\gamma_e b) = M\eta K'(\gamma b) + N\eta I'(\gamma b) \tag{10}$$

where, for the sake of brevity, the subscripts n have been dropped. The four unknown coefficients B, M, N, and C, can now be easily expressed in terms of A. Specifically, we find that

$$\begin{aligned}\frac{C}{A} = {} & \{[K(\gamma_0 a)I(\gamma b) + P(\eta_0/\eta)K'(\gamma_0 a)I'(\gamma b)] \\ & \times [I(\gamma_0 a)K(\gamma b) + P(\eta_0/\eta)I'(\gamma_0 a)K'(\gamma b)] \\ & - [K(\gamma_0 a)K(\gamma b) + P(\eta_0/\eta)K'(\gamma_0 a)K'(\gamma b)] \\ & \times [I(\gamma_0 a)I(\gamma b) + P(\eta_0/\eta)I'(\gamma_0 a)I'(\gamma b)]\} \\ & \times \{[K(\gamma_e b)I(\gamma a) + P(\eta_e/\eta)K'(\gamma_e b)I'(\gamma a)] \\ & \times [I(\gamma_0 a)K(\gamma b) + P(\eta_0/\eta)I'(\gamma_0 a)K'(\gamma b)] \\ & - [K(\gamma_e b)K(\gamma a) + P(\eta_e/\eta)K'(\gamma_e b)K'(\gamma a)] \\ & \times [I(\gamma_0 a)I(\gamma b) + P(\eta_0/\eta)I'(\gamma_0 a)I'(\gamma b)]\}^{-1}\end{aligned} \tag{11}$$

where

$$P = -\frac{K(\gamma a)I(\gamma b) - K(\gamma b)I(\gamma a)}{K'(\gamma a)I'(\gamma b) - K'(\gamma b)I'(\gamma a)}. \tag{12}$$

A limiting case is when $d = b - a \to 0$ so that we merely have an air-filled bore with no casing. This corresponds to setting $b = a$ in the above example and thus $P = 1$. It is convenient to normalize the numerical results to this case since we are primarily interested in evaluating the influence of the casing on the external fields.

Thin-Sheet Idealization

A more subtle limiting case is when the tube thickness d is small but the conductivity σ is large in such a way that their product σd (the transverse conductance) is a significant parameter. Mathematically this corresponds to evaluating the general expressions, given by C_n/A_n, for example, in the limit $d \to 0$ and $\sigma \to \infty$ but allowing σd to be finite. For obvious reasons, we call this the thin-sheet approximation. We can also obtain this solution directly by applying the following boundary conditions, in the limit $d \to 0$, to the field expressions (1), (3), (4), and (6)

$$H_{ez}\big|_{\rho=a+d} = H_{0z}\big|_{\rho=a} - \sigma d E_{e\phi}\big|_{\rho=a+d}$$

$$E_{e\phi}\big|_{\rho=a+d} = E_{0\phi}\big|_{\rho=a}. \tag{13}$$

Using either method, we obtain the "thin-sheet approximation" for the desired coefficient for TE waves in the external

region

$$\frac{C_n}{A_n}=\left\{\gamma_0 a I_n'(\gamma_0 a)\left[K_n(\gamma_e a)-\frac{\eta_e}{\eta_0}\frac{K_n'(\gamma_e a)I_n(\gamma_0 a)}{I_n'(\gamma_0 a)}\right.\right.$$
$$\left.\left.-\sigma d\eta_e K_n'(\gamma_e a)\right]\right\}^{-1}. \quad (14)$$

The transverse magnetic (TM) solution for excitation by axial electric currents is completely analogous to the TE solution. Thus we replace H_z with E_z, E_ϕ with $-H_\phi$, and η with η^{-1}. The corresponding coefficients are designated A_n^*, B_n^*, M_n^*, N_n^*, and C_n^*. Thus the ratio C_n^*/A_n^* is given by the right-hand side of (11) if ratios (η_e/η) and (η_0/η) are merely replaced by their reciprocals. The corresponding thin-sheet approximation is again obtained by letting $d\to 0$ and $\sigma\to\infty$ and keeping σd finite. The thin-sheet boundary conditions in the limit $d\to 0$ are now

$$H_{e\phi}|_{\rho=a+d}=H_\phi|_{\rho=a}+\sigma d E_{ez}|_{\rho=a+d}$$
$$E_{ez}|_{\rho=a+d}=E_z|_{\rho=a}. \quad (15)$$

For this case we find that

$$\frac{C_n^*}{A_n^*}=\frac{-(\eta_e/\eta_0)}{\gamma_0 a I(\gamma_0 a)}\left[K_n'(\gamma_e a)-\frac{\eta_e}{\eta_0}\frac{I'(\gamma_0 a)K(\gamma_e a)}{I_n(\gamma_0 a)}\right.$$
$$\left.-\sigma d\eta_e K_n(\gamma_e a)\right]^{-1}. \quad (16)$$

We see that if the external region is free space (i.e., $\gamma_e=\gamma_0$ and $\eta_e=\eta_0$) the corresponding thin-sheet approximations are

$$C_n/A_n=[1-\sigma d\eta_0\gamma_0 I_n'(\gamma_0 a)K_n'(\gamma_0 a)]^{-1} \quad (17)$$

$$C_n^*/A_n^*=[1+\sigma d\eta_0\gamma_0 I_n(\gamma_0 a)K_n(\gamma_0 a)]^{-1}. \quad (18)$$

For $|\gamma_0 a|\ll 1$, these are further simplified to

$$C_0/A_0\simeq[1+(\sigma d i\mu_0\omega a)/2]^{-1} \quad (19)$$

$$C_n/A_n\simeq[1+(\sigma d\eta_0|n|)/(2\gamma_0 a)]^{-1}, \quad \text{for } |n|=1,2,3,\cdots \quad (20)$$

$$C_0^*/A_0^*\simeq[1+\sigma d i\mu_0\omega a K_0(\gamma_0 a)]^{-1} \quad (21)$$

$$C_n^*/A_n^*\simeq[1+(\sigma d i\mu_0\omega a)/|2n|]^{-1}, \quad \text{for } |n|=1,2,3,\cdots. \quad (22)$$

The thin-sheet approximation is only valid if the tube thickness d is sufficiently small so that the tangential electric field is continuous across its width. In general, this would be true if $|\gamma d|\ll 1$, which is equivalent to the statement that $d\ll\delta$ where $\delta\cong[2/(\sigma\hat{\mu}\omega)]^{1/2}$ is the skin depth in the metal

Axial Coil Excitation

To illustrate the shielding effect of the metal casing, we will choose two important special cases. The first corresponds to a source consisting of a solenoidal coil that is located on the axis of the bore hole. The axial magnetic field in the external region is thus proportional to $C_0K_0(\gamma_e\rho)$. Then, clearly, the ratio of the magnetic field strength at a radial distance ρ for the cased hole to that for the uncased hole is $|C_0/C_0(d=0)|$ where C_0 is defined by (11) for $n=0$. This field strength ratio is plotted in Fig. 2(a) as a function of frequency from 1 to 10^4 Hz for casing permeabilities from $\mu=\mu_0$ to $1000\mu_0$, for

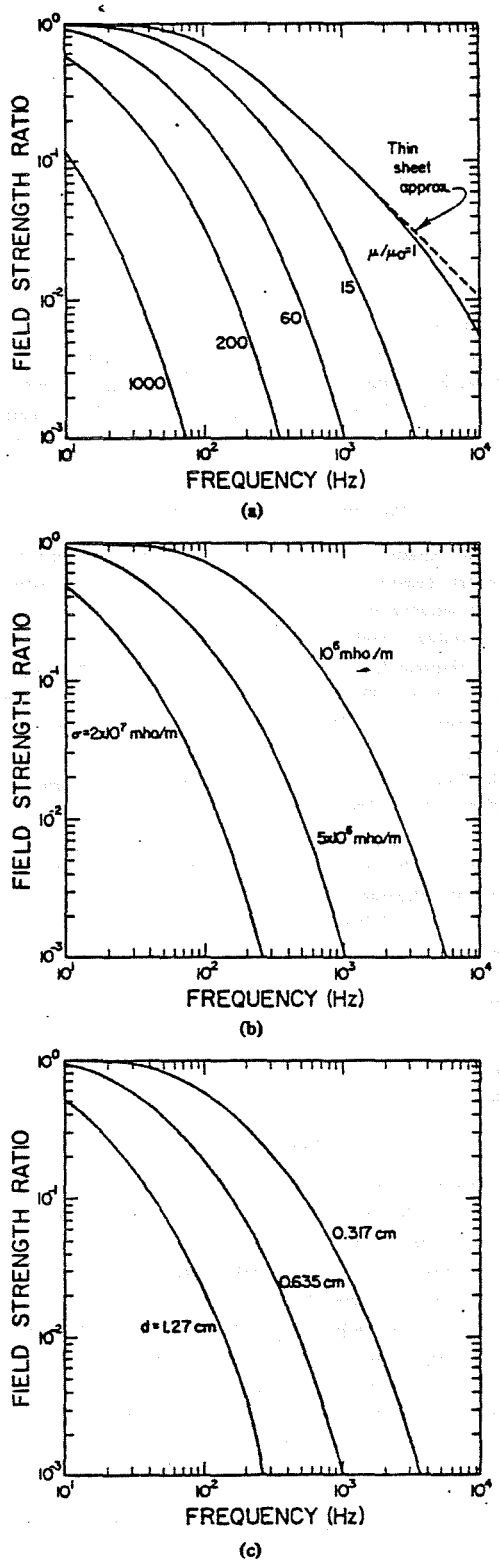


Fig. 2. Ratio of the field strength, in the external medium, of a cased hole to that of an uncased hole for an axial coil source. (a) For various permeabilities of the casing. (b) For various conductivities of the casing. (c) For various thicknesses of the casing.

casing thickness $d = 0.635$ cm, mean tube diameter $a + (d/2) = 7.62$ cm, tube conductivity $\sigma = 5 \times 10^6$ mho/m, rock conductivity $\sigma_e = 10^{-2}$ mho/m, and rock permittivity $\epsilon_e = 10\epsilon_0$. The thin-sheet approximation based on (14) with $n = 0$ is also shown. Not surprisingly, the shielding is most pronounced at higher frequencies. Also, the shielding is greater for the higher permeabilities. We also see that for this range of parameters, the thin-sheet approximation is only valid for the nonmagnetic case.

Similar results for $|C_0/C_0(d = 0)|$ are shown in Fig. 2(b) for the same parameters as those above but with $\mu = 60\mu_0$ fixed and various casing conductivities. As expected, the higher conductivities correspond to more severe shielding. For this same case, but with $\sigma = 5 \times 10^6$ mho/m fixed, the effect of varying the tube thickness is illustrated in Fig. 2(c). Again, as we would expect, the thicker tube or casing has the higher attenuation.

Two-Wire Line Excitation

The other special case of interest is when the source is an axial electric current. In particular, we consider the situation where the excitation is a centrally located two-wire transmission line whose spacing is small compared with the radius a. The axial electric field in the external medium is then equal to $C_1^e K_1(\gamma_e \rho) \cos \phi$. The corresponding H_ρ and H_ϕ components are then equal to $\eta_e^{-1} C_1^e K_1(\gamma_e \rho) \sin \phi$ and $\eta_e^{-1} C_1^e K_1'(\gamma_e \rho) \cos \phi$, respectively. Thus, for this configuration, the ratio of the magnetic field for the cased hole to that for the uncased hole is $|C_1^e/C_1^e(d = 0)|$. This field strength ratio is plotted in Fig. 3(a)–(c) in the same manner as the results shown above in Fig. 2(a)–(c). The results exhibit a similar behavior although there are quantitative differences. However, we note that the curves for $\mu = \mu_0$ follow quite closely the simple form of the thin-sheet approximation given by

$$\left|\frac{C_0}{C_0(d=0)}\right| = \left|\frac{C_1^e}{C_1^e(d=0)}\right| = \left[\frac{1}{1 + (\mu_0 \omega \sigma a d/2)^2}\right]^{1/2} \tag{23}$$

This relation is consistent with (19) and (22), which are valid for $|\gamma_e b| \ll 1$ and $|\gamma d| \ll 1$.

Discussion

The numerical results described above are strictly valid for excitation by magnetic and electric line sources that are located on the axis of the bore hole. The field strength ratios, as defined, then apply to all radial distances, in the external medium, from the bore hole axis. If, in general, the line sources are not centrally located in the hole, we need to sum over all the harmonics of order n that are excited. The formulation given above still applies but the field strength ratio now would depend on the radial distance ρ and the angular coordinate ϕ. Fortunately, however, if ρ is much greater than the outer diameter b of the casing, and if $|\gamma_e b| \ll 1$, the higher order harmonics (i.e., $|n| = 1, 2, 3, \cdots$) are insignificant. Thus the results shown in Figs. 2 and 3 do not require that the sources be on the axis of the bore hole.

As we have indicated, the two-dimensional formulation is based on the assumption that all field quantities do not vary in the axial direction. This, of course, is a severe idealization that is justified mainly on the basis that it leads to a great simplifi-

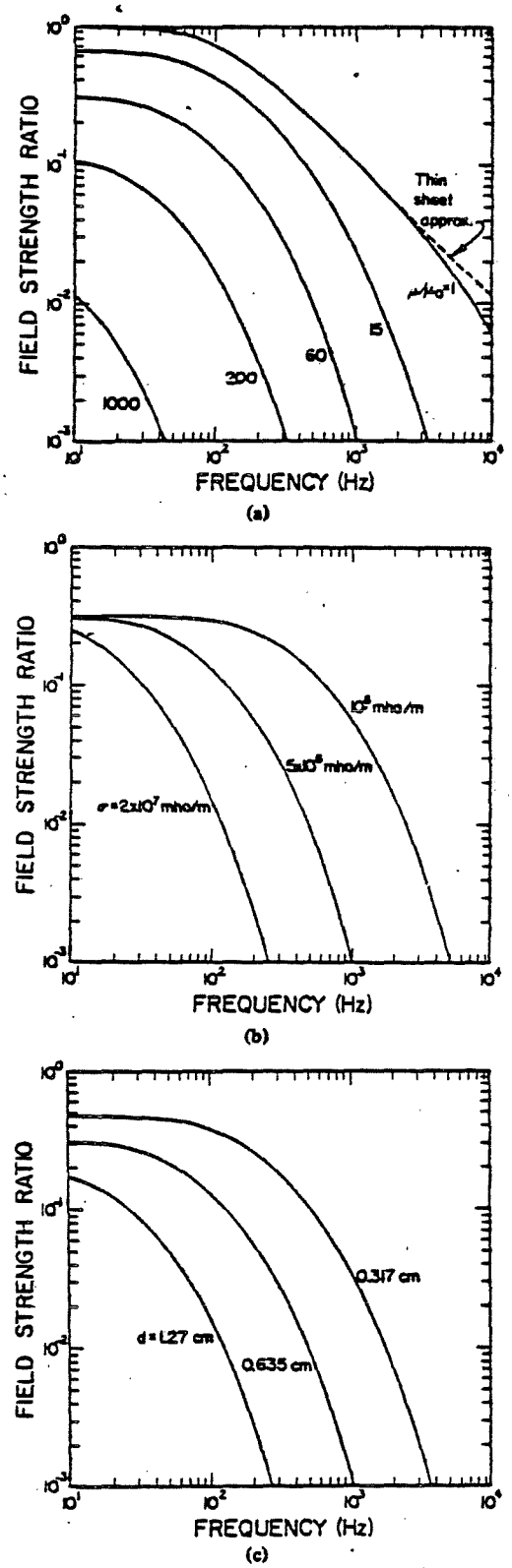


Fig. 3. Ratio of the field strength, in the external medium, of a cased hole to that of an uncased hole for a two-wire transmission line source. (a) For various permeabilities of the casing. (b) For various conductivities of the casing. (c) For various thicknesses of the casing.

cation in the numerical work. If indeed we had chosen finite sources such as axial or transverse magnetic dipoles, the formulation [5], [7], [8] would involve integrations over a spectrum of axial wavenumbers in addition to discrete summation of the angular harmonics. But if we focus our attention on the ratio of the fields of a cased hole in the external medium to that of an uncased hole, we can show that the results are quantitatively very similar to that for dipole excitation. Such a comparison test was actually carried out for magnetic dipoles oriented in both axial and transverse directions that were located on the axis of the bore hole [6]. In this calculation, the thin-sheet boundary conditions were invoked and the observer was located at $\rho = 15.25$ m (50 ft) with the same z coordinate as the source dipole. Within graphical accuracy the field strength ratios were indistinguishable from the "thin-sheet" results shown in Fig. 2(a) and (b). Thus we can assert with some confidence that all the numerical results are applicable, at least in an approximate sense, to dipole excitation if the observer is located in the adjacent medium at the same level as the source. Thus the curves in Fig. 2(a)–(c) would apply to the axial magnetic dipole source and those in Fig. 3(a)–(c) would apply to the transverse magnetic dipole source.

Conclusions

The main conclusion from the present analytical study is that a metal casing will certainly attenuate the fields in the external medium produced by a source within the bore hole. In particular, the combined effect of the conductivity and permeability of the casing steel will greatly reduce the field strengths at frequencies even as low as 100 Hz. In many shielding analyses in the past, the influence of the permeability has been overlooked. This is an important consideration when dealing with a bore hole casing since the steel may have permeability, relative to free space, of the order of 100, or even higher in some cases [9].

References

[1] S. J. Pirson, *Handbook of Well Log Analysis*. New York: Prentice Hall, 1963.

[2] A. A. Kaufman, *Theory of Induction Logging*. Novosibirsk: Nauka Press, 1965.

[3] G. V. Keller and F. C. Frischknecht, *Electrical Methods in Geophysical Prospecting*. New York: Pergamon Press, 1966.

[4] J. R. Wait, Ed., *Radio Science (Special Issue on Subsurface Telecommunications and Geophysical Probing)*, vol. 11, Apr. 1976.

[5] —, *Electromagnetic Radiation from Cylindrical Structures*. Oxford: Pergamon Press, 1959.

[6] —, "Analysis for the electromagnetic fields of electric and magnetic dipoles located within a metal-cased borehole," Preliminary Rep. to U.S. Bureau of Mines, Aug. 10, 1976.

[7] S. A. Schelkunoff, *Electromagnetic Waves*. New York: Prentice-Hall, 1943.

[8] J. A. Fuller and J. R. Wait, "Mutual electromagnetic coupling of coaxial loops in a borehole," *Radio Science*, vol. 8, pp. 453–457, May 1973.

[9] A. G. Kandoian (Chm. Edit. Bd.), *Reference Data for Radio Engineers*. New York: ITT Corporation, 1968, pp. 4–32.

IEEE TRANSACTIONS ON ANTENNAS AND PROPAGATION, VOL. AP-27, NO. 5, SEPTEMBER 1979

Calculated Admittance of an Idealized Drill Rod Antenna in a Lossy Medium

DAVID A. HILL, SENIOR MEMBER, IEEE, AND JAMES R. WAIT, FELLOW, IEEE

Abstract—Some calculated results for the input admittance of both insulated and uninsulated drill rods immersed in a lossy medium are given. The source can be either a voltage gap or a thin toroidal coil. For this input admittance calculation the drill rod is assumed to be of infinite length. Even a very thin insulating layer is found to greatly decrease the real part of the input admittance or the input power.

Manuscript received November 17, 1978; revised March 20, 1979.

The authors are with the Institute of Telecommunication Sciences, National Telecommunications and Information Administration, U.S. Department of Commerce, Boulder, CO 80303.

U.S. Government work not protected by U.S. copyright.

INTRODUCTION

There is a need to transmit signals from depth in a bore hole to the drill operator at the surface. A toroidal coil which completely encircles the drill rod will excite axial currents on the drill rod which will propagate to the surface where they can be detected. The toroidal coil is modeled by a ring of magnetic current K, and the excited drill rod current has been calculated for both infinitely long and truncated drill rods [1], [2].

The available power at depth will be limited; thus it is important to know the power required by the toroidal coil source. A specification of the input power is also needed to determine the total transmission loss between the toroid and the receiver. When the inner radius of the toroid coincides with the outer surface of the drill rod, the rod is essentially being excited by a voltage generator of magnitude K. Thus the input admittance and power can be computed from the model of voltage gap excitation of an infinitely long thin cylinder. Here we utilize a previous formulation for the input admittance of a coated cylinder [3] but allow the external medium to have a conductivity corresponding to that of the host rock.

FORMULATION

The basic cylindrical model is depicted in Fig. 1. The metal cylinder of radius b is infinitely long and has infinite conductivity. A voltage gap (or thin toroid) of width δ is centered at $z = 0$. The region $b < \rho < c$, which has conductivity σ_c and permittivity ϵ_c, can represent either an insulating layer or a region of conducting fluid in the drill hole. The region $\rho > c$ has conductivity σ and permittivity ϵ which are representative of the host rock. Free-space permeability μ_0 is assumed everywhere.

Under quasi-static conditions the external admittance of the gap Y_e is given by [3], [4]

$$Y_e = -2(\sigma_c + i\omega\epsilon_c)b[\ln(k_c\delta/4) + C + N_c], \tag{1}$$

where

$$k_c = \omega[\mu_0(\epsilon_c - i\sigma_c/\omega)]^{1/2}, \tag{2}$$

$$C = 0.5772, \tag{3}$$

$$N_c = \int_0^\infty \frac{1}{u_c}\left[\frac{Z_1(\lambda)}{Z_0(\lambda)} - i\right] d\lambda + i\pi/2. \tag{4}$$

$$Z_0(\lambda) = H_0^{(2)}(u_c b) + R(\lambda)H_0^{(1)}(u_c b), \tag{5}$$

$$Z_1(\lambda) = H_1^{(2)}(u_c b) + R(\lambda)H_1^{(1)}(u_c b), \tag{6}$$

$$R(\lambda) = -\frac{(\epsilon - i\sigma/\omega)u_c H_0^{(2)}(u_c c)H_1^{(2)}(uc) - (\epsilon_c - i\sigma_c/\omega)uH_1^{(2)}(u_c c)H_0^{(2)}(uc)}{(\epsilon - i\sigma/\omega)u_c H_0^{(1)}(u_c c)H_1^{(2)}(uc) - (\epsilon_c - i\sigma_c/\omega)uH_1^{(1)}(u_c c)H_0^{(2)}(uc)} \tag{7}$$

$$u_c = (k_c^2 - \lambda^2)^{1/2}, \tag{8}$$

$$u = (k^2 - \lambda^2)^{1/2}, \tag{9}$$

$$k = \omega[\mu_0(\epsilon - i\sigma/\omega)]^{1/2}, \tag{10}$$

$H_0^{(1)}$ and $H_1^{(1)}$ are Hankel functions of the first kind, and $H_0^{(2)}$ and $H_1^{(2)}$ are Hankel functions of the second kind.

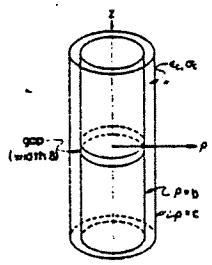


Fig. 1. Infinitely long drill rod with arbitrary coating.

The λ integration in (4) is taken along the real axis and must be performed numerically. The validity of (1) requires only that $|k_c|\delta$ and δ/b are small. The input power P is simply proportional to the real part of Y_e:

$$P = \tfrac{1}{2}|K|^2 \operatorname{Re}(Y_e) \tag{11}$$

where K is either the gap voltage or the magnetic current of the equivalent toroidal coil source.

NUMERICAL RESULTS

Previous results for Y_e [3], [4] were restricted to lossless media ($\sigma_c = \sigma = 0$). A new computer program was written to evaluate (1) for arbitrary values of σ_c and σ. The numerical integration in (4) required some care because the integrand decreases rather slowly for large λ and because a pole in the integrand near $\lambda = k_c$ causes rapid variation in the integrand near $\lambda = \operatorname{Re}(k_c)$. Both problems were overcome by using a variable sampling technique which utilizes closely spaced samples for small λ and widely spaced samples for large λ.

Figs. 2 and 3 illustrate $\operatorname{Re}(Y_e)$ for various insulation thicknesses over the frequency range from 1 Hz to 3 kHz. The insulating layer ($\epsilon_c = 2.5\epsilon_0$ and $\sigma_c = 0$) would normally be present for practical sources, at least in the source region. As expected, $\operatorname{Re}(Y_e)$ increases rapidly as the insulation thickness decreases. In Fig. 3 the rock conductivity σ is decreased from 10^{-2} mho/m to 10^{-3} mho/m, and a small decrease in $\operatorname{Re}(Y_e)$ results. The imaginary part of Y_e is not shown in Figs. 2 and 3 because it is much smaller than the real part. The gap width δ is 1 mm in both Figs. 2 and 3, but the results were found to be indistinguishable for $\delta = 2$ mm and 5 mm.

In Fig. 4 we illustrate Y_e for an uninsulated drill rod $\sigma_c = \sigma$ and $\epsilon_c = \epsilon$. Both the real and imaginary parts of Y_e are much larger than in the insulated cases of Figs. 2 and 3. The other difference is that the imaginary part of Y_e is negative. A negative value for the imaginary part of Y_e in the uninsulated case was also found by Shen [5] both by experiment and by an approximate theory. His results are actually for finite length antennas, but some of the results are for sufficiently long antennas so that the end reflections do not affect the input admittance. Many theoretical [6] and experimental [7] results are available for insulated finite length antennas, but in those studies the antennas need to be very long before the end effects can be neglected.

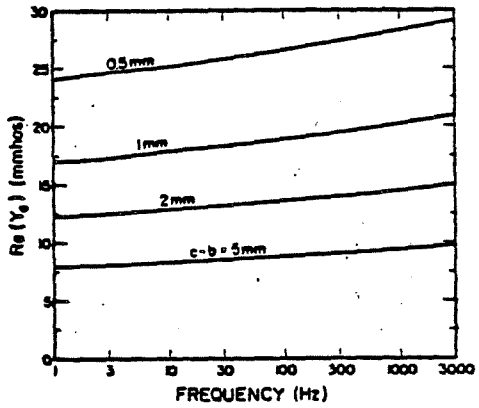


Fig. 2. Real part of admittance for various insulation thickness. Parameters: b = 2 cm, ϵ_c/ϵ_0 = 2.5, σ_c = 0, ϵ/ϵ_0 = 10, $\sigma = 10^{-2}$ mho/m, and δ = 1 mm.

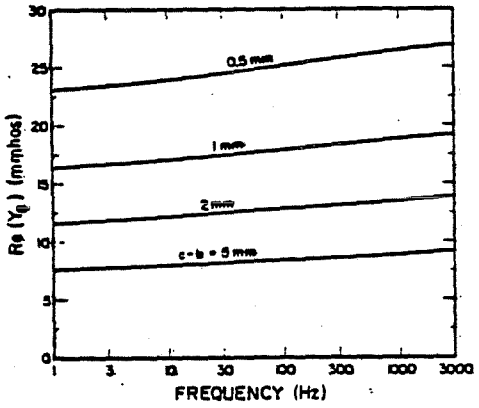


Fig. 3. Real part of admittance for lower rock conductivity, $\sigma = 10^{-3}$ mho/m. Other parameters are the same as those in Fig. 2.

In Fig. 5 we show the effect of a lossy coating on the drill rod admittance. This lossy coating could represent the highly conducting fluid which is often present in the drill hole. As expected, the results are similar to the uninsulated case in Fig. 4, but the real part of Y_e is larger due to higher near-field loss.

CONCLUDING REMARKS

The input admittance of both insulated and uninsulated drill rods immersed in a conducting medium has been calculated by a quasi-static method. The source can be either a voltage gap or a thin toroidal coil, and the results are useful for calculating total transmission loss in drill rod telemetry. Figs. 2 and 3 show that an insulating layer decreases the real part of the input admittance. This result can be interpreted as a decrease in the near-field loss due to the insulation. The input admittance is highly dependent on the thickness of the layer but is weakly dependent on frequency for the low frequencies of interest.

The calculations presented here for the input admittance tacitly assume that reflected waves from the bottom and the top of the drill rod are negligible. This will not always be the case, but their effects could be accounted for in an approximate fashion using the earlier formulation [1], [2] that dealt

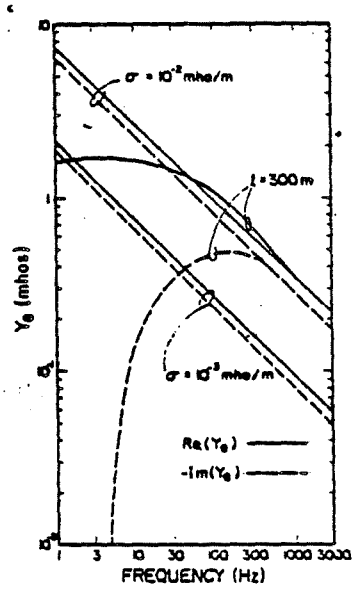


Fig. 4. Real and imaginary parts of input admittance for uninsulated drill rod of infinite length. Parameters: b = 2 cm, $\epsilon_c = \epsilon = 10\epsilon_0$, $\sigma_c = \sigma$, and δ = 1 mm. (Effect of having drill rod terminated at distance l below feed gap is also shown).

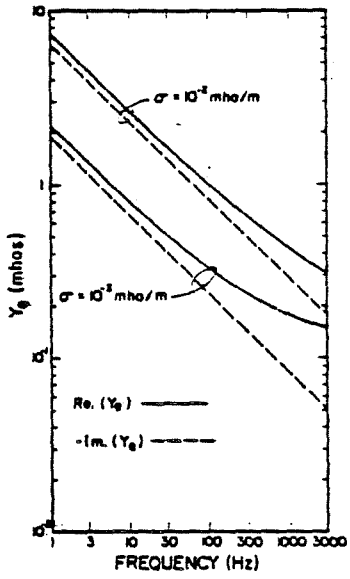


Fig. 5. Real and imaginary parts of input admittance for drill rod of infinite length surrounded by lossy layer. Parameters: b = 2 cm, c = 2.5 cm, $\epsilon_c = \epsilon_0 = 10_0$, and σ_c = 1 mho/m.

with how the signals actually propagate along the drill rod. Such a calculation is illustrated in Fig. 4, where the lower end of the drill rod is a distance l from the voltage gap. Assuming that the current is zero at the bottom end, we find that the admittance $Y_e(l)$ is given approximately by

$$Y_e(l) = Y_e + K^{-1}I(2l) \tag{12}$$

where Y_e is given by (1) and $I(2l)$ is given by [2, eq. (2)]. In

the example shown, $l = 300$ m and $\sigma = 10^{-2}$ mho/m. The corresponding curves for $\sigma = 10^{-3}$ mho/m are not shown, but they are very similar. As indicated in Fig. 4 the end effects are not significant for frequencies greater than about 300 Hz.

Another unsolved problem is to deal with the transient excitation of the drill rod since a condenser discharge device located behind the drill bit could be relatively economic in terms of power requirements.

REFERENCES

[1] J. R. Wait and D. A. Hill, "Theory of transmission of electromagnetic waves along a drill rod in conducting rock," *IEEE Trans. Geosci. Electron.*, vol. GE-17, pp. 21-24, Apr. 1979.

[2] D. A. Hill and J. R. Wait, "Electromagnetic basis of drill-rod telemetry," *Electron. Lett.*, vol. 14, pp. 532-533, Aug. 1978.

[3] J. R. Wait and D. A. Hill, "Electromagnetic fields of a dielectric coated coaxial cable with an interrupted shield—Quasi-static approach," *IEEE Trans. Antennas Propagat.*, vol. AP-23, pp. 679-682, Sept. 1975.

[4] J. R. Wait and D. A. Hill, "On the electromagnetic field of a dielectric coated coaxial cable with an interrupted shield," *IEEE Trans. Antennas Propagat.*, vol. AP-23, pp. 470-479, July 1975.

[5] L. C. Shen, "Theory of dipole antennas in dissipative media," *Proc. IEE*, vol. 117, pp. 27-29, Jan. 1970.

[6] K. M. Lee, T. T. Wu, and R. W. P. King, "Theory of an insulated linear antenna in a dissipative medium," *Radio Sci.*, vol. 12, pp. 195-203, Mar.-Apr. 1977.

[7] K. M. Lee and G. S. Smith, "Measured properties of bare and insulated antennas in sand," *IEEE Trans. Antennas and Propagat.*, vol. AP-23, pp. 664-670, Sept. 1975.

ELECTROMAGNETIC BASIS OF DRILL-ROD TELEMETRY

Indexing terms: Geophysical prospecting, Telemetering

Some calculated results are presented for the signal that can be propagated to the surface from a toroidal coil source near the bottom of a drill rod. Optimum frequencies are predicted to occur in the range 10–100 Hz for depths of the order of several kilometres.

There has been a long established need to communicate useful signals from depth in a bore hole to the drill operator at the surface. We have undertaken the task of deducing the expected attenuation for an idealised model. Specifically, we assume the adjacent rock is electrically homogeneous with conductivity σ, permittivity ϵ and permeability μ. The drill rod or stem is taken to be a metal cylinder of radius a that is assumed here to be in perfect contact with the host rock. The drill rod is excited by a toroidal coil wound tightly around the drill rod. This acts as a ring of magnetic current K of radius a; it is located at a depth d from the surface and at a distance l from the bottom of the drill rod.

For time-harmonic excitation, an expression was derived for the total induced current I_t in the drill rod at the surface for a specified value of the source magnetic current. This is based on the boundary-value solution for the rod of infinite length[1] with appropriate modifications made for the reflections at the top and bottom of the drill rod. In fact, to facilitate the solution, it is assumed that the top of the drill rod is effectively terminated in a perfect ground plane, whereas at the bottom the current is assumed to vanish. The perfect-ground-plane assumption at the top would be particularly appropriate in the offshore drilling situation where the sea water provides an excellent image plane.

On neglecting multiple reflections of the current waves, we obtain the desired expression for the induced current I_t at the drill-hole collar in the form

$$I_t = 2[I(d) - I(d + 2l)] \tag{1}$$

where $I(z)$ is the current that would be excited on a drill rod of infinite length at a distance z from the source toroid. The desired expression for $I(z)$ is found to be

$$I(z) = ia(\sigma + i\epsilon\omega)K \exp(ikz)S \tag{2}$$

where

$$S = \int_0^{-\exp(-i\arg k)} \frac{1}{\delta}\left[\frac{H_1^{(2)}(\delta ka)}{H_0^{(2)}(\delta ka)} - \frac{H_1^{(1)}(\delta ka)}{H_0^{(1)}(\delta ka)}\right] e^{-iyz}\,dy \tag{3}$$

where $\delta = -[y(y + 2i)]^{1/2}$. To achieve this highly convergent form, the original integration contour has been wrapped around the two sides of the branch line. Because the integrand of S is singular at $y = 0$, it is convenient to break the integration range into two parts; in the first, the range is from

(U.S. Gov't. work not protected by U.S. Copyright)

0 to d_0, and in the second, it is from d_0 to $\infty(-i \arg k)$. Here, as d_0 is sufficiently small, the small-argument approximations are valid for the indicated Hankel functions. Then we find that

$$S \approx S_d + \int_{d_0}^{\infty \exp(-i\arg k)} \frac{1}{\delta}[\ldots] e^{-iyz}\, dy \qquad (4)$$

where

$$S_d = \frac{2\pi}{kb}\int_0^{d_0} \frac{1}{y[\ln(\gamma k^2 a)]^2}\, dy = -\frac{2\pi}{kb \ln(d_0 k^2 a)} \qquad (5)$$

The numerical integration program for dealing with eqn. 4 uses a variable increment size to sample the variation over y.

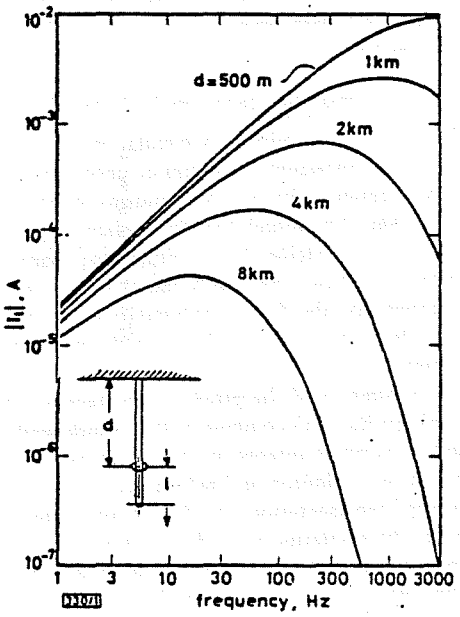


Fig. 1 *The total current on the drill rod at the surface (i.e. at the collar) for a source toroid at depth d*

$\sigma = 10^{-3}$ mS/m, $K = (f/5\,\text{kHz})$ V

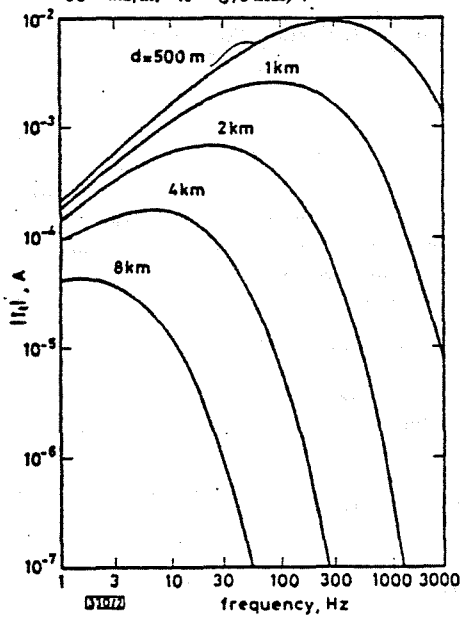


Fig. 2 *Total current on the drill rod at the surface (i.e. at the collar) for a source toroid at depth d*

$\sigma = 10^{-2}$ mS/m, $K = (f/5\,\text{kHz})$ V

The results can be checked, for large values of $|kz|$, against an asymptotic approximation based on an analysis by Kunz[2] for a similar problem. This form being strictly valid for $z \to \infty$ is given by

$$I(z) \approx -K(2\pi/\eta)e^{-ikz}/\ln\left[-\frac{2iz}{\Gamma^2 ka^2}\right]$$

where $\eta = [i\mu\omega/(\sigma + i\epsilon\omega)]^{1/2}$ and $\Gamma = 1{\cdot}781\ldots$. The extension of the above theory to allow for the finite conductivity of the drill rod has also been worked out.[3]

To plot meaningful curves of the current I_t at the collar as a function of frequency, it is desirable to normalise the excitation such that the effective magnetic current K in the source toroid is proportional to frequency. This is a consequence of the fact that K is proportional to the product of the electric current in the winding and the frequency. Such results are shown in Figs. 1 and 2, where the rock conductivity σ is taken to be 10^{-3} and 10^{-2} mS/m, respectively. Here the normalisation is such that $K = 1$ V if the frequency f is 5 kHz. The frequency range extends from 1 Hz to 3 kHz, and so the results are essentially independent of the permittivity of the rock. Also, we have assumed that the permeability μ takes its free-space value $4\pi \times 10^{-7}$, which also is a realistic supposition. The value of l, the distance from the toroid to the bottom of the drill rod, is taken to be 100 m. d, the distance from the collar to the toroid, takes the values indicated on the curves. In all cases, the radius a of the drill rod or stem is taken to be 2 cm.

A number of interesting features emerge in these calculations, which may have important practical implications. For large depths d the surface current signal is greatly attenuated, particularly at the higher frequencies for the higher rock conductivity. However, at lower frequencies, the relative attenuation is quite small. A further feature is that the current signal I_t is actually enhanced for the lowest frequency for the higher rock conductivity. This is related to the improved coupling of the toroid to the drill rod.

As a consequence of the various trade-offs, it is not surprising that there is an optimum frequency for a fixed depth d. For the great depths of drilling now being used, this frequency is in the range 10–100 Hz. Of course, many other factors may modify or invalidate any firm conclusions in this regard. In particular, the imperfect electrical contact between the drill-rod sections could inhibit the current flow, with a consequent increase of signal loss. Other generalisations of the model, such as allowing for the finite radial and lateral extent of the source toroid, would not lead to any significant change in the predicted performance However, the effect of insulation on the rod could conceivably lead to a lowering of the attenuation with a possible raising of the optimum operating frequency. Evidently, the problem requires much further study.

We are grateful to H. K. Sacks who suggested the need for these calculations.

D. A. HILL
J. R. WAIT

ITS/NTIA and ERL/NOAA
US Department of Commerce
Boulder, Co. 80303, USA

18th July 1978

References

1 WAIT, J. R.: 'Electromagnetic surface waves', *Adv. Radio Res.*, 1964, 1, pp. 157–217
2 KUNZ, K. S.: 'Asymptotic behavior of the current on an infinite cylindrical antenna', *J. Res. Natl. Bur. Stand. Sect. D*, 1963, 67D, pp. 417–431
3 WAIT, J. R., and HILL, D. A.: 'Theory of transmission of electromagnetic waves along a metal rod in a conducting medium'. Preliminary report to the US Bureau of Mines, 29 December 1976

IEEE TRANSACTIONS ON GEOSCIENCE ELECTRONICS, VOL. GE-17, NO. 2, APRIL 1979

Theory of Transmission of Electromagnetic Waves Along a Drill Rod in Conducting Rock

JAMES R. WAIT, FELLOW, IEEE, AND DAVID A. HILL, SENIOR MEMBER, IEEE

Abstract—We present an analysis of the electromagnetic fields excited by a toroidal coil that is coaxial with a circular metal rod located in a conducting medium. The integral representation for the induced axial current on the rod is cast in a form that is suitable for numerical evaluation. Some results for the electric current distribution on the infinitely long configuration are given for a fixed magnetic current source. Good agreement is obtained with an asymptotic estimate for this quantity. The effects of truncating the bottom end of the rod and terminating the top in an ideal ground plane are treated by an approximate method. Numerical results for this configuration are also given.

I. Introduction

THE POSSIBILITY exists that electromagnetic signals can be transmitted along a drill stem or metal rod in a conducting host rock. The idea is that the lower portion of the vertical rod is to be excited inductively in such a fashion that axial currents will propagate to the surface where they can be detected. Because the rod is in contact with the surrounding conducting medium, we expect that the attenuation rate will be fairly high even in the best of circumstances. Nevertheless, it is important to establish the theoretical limits of this type of transmission as a mechanism for transmitting information such as an indication of the orientation of the bore hole.

An initial examination of the problem suggested that the metal rod be excited by a coaxial solenoid that could be fed with alternating current. This configuration is sometimes employed in nondestructive testing of cables. However, some consideration indicated that this scheme would not excite axial currents on the rod of any substantial magnitude. A more promising configuration that suggests itself is a toroidal coil that encircles the rod. Electromagnetically, such a coil, when energized by an ac source, is equivalent to a circumferential magnetic current. If the inner radius of this toroid were allowed to coincide with the outer surface of the rod, we would, in effect, be exciting the rod by a voltage generator. Of course, this would be most effective in driving currents along the rod. It is not necessary, however, to require that the toroid be tightly wound about the rod. Thus in our analysis, we will consider the toroid to have a mean radius somewhat greater than the radius of the rod.

Another important practical consideration is that the rod will be of finite length. At the bottom end, the axially induced current will vanish, so this will be a boundary condition that must be imposed. At the surface, the rod could be terminated in various ways. However, we feel that the most desirable situation would be a simulated metal ground plane. Thus for this study, such is assumed.

Manuscript received April 28, 1978; revised November 18, 1978.

J. R. Wait is with the Cooperative Institute for Research in Environmental Sciences, University of Colorado/NOAA, Boulder, CO 80303.

D. A. Hill is with the Institute of Telecommunication Sciences, U.S. Department of Commerce, Boulder, CO 80303.

II. Formulation for the Infinitely Long Rod

We begin first with the model of a circular metal rod of radius a located in an unbounded medium of conductivity σ, permittivity ϵ, and permeability μ. A cylindrical coordinate system (ρ, ϕ, z) is then chosen such that the surface of the rod is $\rho = a$. The rod is to be excited by a uniform ring magnetic current K located at $z = z_0$, that has a radius b. To allow for subsequent generality, the finite conductivity of the metal in the rod can be characterized by an effective series impedance Z_s in ohms per meter.

In view of the symmetry of the problem, the excited magnetic field has only an $H_\phi(\rho, z)$ component that is independent of ϕ. The quantity of prime interest is the total axial current $I(z)$ on the rod that, by definition, is $2\pi a H_\phi(a, z)$.

A formal integral representation for $I(z)$ follows from an earlier analysis for the excitation of surface waves on a cylindrical structure in free space [1]. For a time factor $\exp(i\omega t)$, the corresponding result for the present configuration is

$$I(z) = -(\sigma + i\epsilon\omega) bK \cdot \int_{-\infty}^{+\infty} \frac{H_1^{(2)}(vb) \exp[-i\lambda(z - z_0)]\, d\lambda}{vH_0^{(2)}(va) - (\sigma + i\epsilon\omega)\, 2\pi a Z_s H_1^{(2)}(va)} \tag{1}$$

where $v = (k^2 - \lambda^2)^{1/2} = -i(\lambda^2 - k^2)^{1/2}$ and $ik = [i\mu\omega(\sigma + i\epsilon\omega)]^{1/2}$. Here $H_0^{(2)}$ and $H_1^{(2)}$ are Hankel functions of the second kind, of order zero and one, respectively. The integration here is along the entire real axis of the complex λ plane. Branch points occur in the second and fourth quadrants at $\lambda = \pm k$. We should also note that the integral has poles at $\lambda = \pm\lambda_s$, where λ_s is the solution of

$$vH_0^{(2)}(va) - (\sigma + i\epsilon\omega)\, 2\pi a Z_s H_1^{(2)}(va) = 0 \tag{2}$$

in the fourth quadrant of the λ plane.

It is worth pointing out here that the magnetic current ring could be a band with finite vertical extent as actually depicted in Fig. 1. The resultant electric current $I(z)$ for this case is then a superposition of elementary rings of thickness dz_0 over the range from say $z_0 = -s$ to $z_0 = +s$. The upshot is that to account for the finite vertical extent of the source, we would insert a factor $(\sin \lambda s)/(\lambda s)$ in the integrand of (1) when K is still regarded as the total ring magnetic current. In what follows, we will set $s = 0$, but we let $z = z_0$ denote the vertical

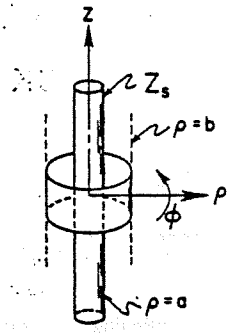


Fig. 1. The basic geometry of an infinitely long metal rod that is excited by a ring or band of magnetic current.

location of the teroid or ring source. As a matter of interest, the finite radial extent of the toroidal source coil could be handled in the same fashion.

In order to evaluate the integral for $z - z_0 > 0$, it is convenient to deform the contour about the singularities in the lower half of the λ plane. This immediately suggests that we write (1) in the form

$$I(z) = -(\sigma + i\epsilon\omega)bK \cdot \int_k^{k-i\infty} \left\{ \frac{H_1^{(2)}(vb)}{vH_0^{(2)}(va) - (\sigma + i\epsilon\omega)\, 2\pi a Z_s H_1^{(2)}(va)} - \frac{H_1^{(2)}(vbe^{-i\pi})}{ve^{-i\pi}H_0^{(2)}(vae^{-i\pi}) - (\sigma + i\epsilon\omega)\, 2\pi a Z_s H_1^{(2)}(vae^{-i\pi})} \right\} \cdot e^{-i\lambda(z-z_0)}\, d\lambda + I_s(z) \tag{3}$$

where the integral from k to $k - i\infty$ is the contribution from the two sides of the branch line, $I_s(z)$ in the residue at the pole $\lambda = \lambda_s$ that could be computed from

$$I_s(z) = 2\pi i(\sigma + i\epsilon\omega)\, bK \cdot \frac{H_1^{(2)}(v_s b) \exp(-i\lambda_s |z - z_0|)}{\left\{ \frac{\partial}{\partial\lambda} [vH_0^{(2)}(va) - (\sigma + i\epsilon\omega)\, 2\pi a Z_s H_1^{(2)}(va)] \right\}_{\lambda = \lambda_s}} \tag{4}$$

where $v_s = (k^2 - \lambda_s^2)^{1/2} = -ik(\lambda_s^2 - k^2)^{1/2}$.

The rotation formulas $H_0^{(2)}(xe^{-i\pi}) = -H_0^{(1)}(x)$ and $H_1^{(2)}(xe^{-i\pi}) = H_1^{(1)}(x)$ are useful to simplify the branch line integral in (3). Also, it is useful to change the variable to the dimensionless y via $\lambda = k(1 - iy)$. Then, without difficulty, (3) becomes

$$I(z) = i(\sigma + i\epsilon\omega)\, bK \exp(-ik|z - z_0|) \cdot \int_0^{\infty e^{-i \arg k}} \left\{ \frac{H_1^{(2)}(\delta kb)}{H_0^{(2)}(\delta ka) - gH_1^{(2)}(\delta ka)} - \frac{H_1^{(1)}(\delta kb)}{H_0^{(1)}(\delta ka) - gH_1^{(1)}(\delta ka)} \right\} \frac{1}{\delta} \cdot \exp(-ky|z - z_0|)\, dy + I_s(z) \tag{5}$$

where $\delta = -[y(y + 2i)]^{1/2}$ and $g = (\sigma + i\epsilon\omega)\, 2\pi a Z_s$.

While (5) appears rather complicated, it is in a suitable form for numerical computation due to the rapidly convergent exponential factor in the integrand. For the present application, the drill stem or rod is effectively a perfect conductor so g can be set equal to zero. Also, in this case, the surface wave is not excited. Thus for this case, we write

$$I(z) = ib(\sigma + i\epsilon\omega)\, Ke^{-ikz}\, S \tag{6}$$

where

$$S = \int_0^{\infty e^{-i \arg k}} \frac{1}{\delta} \left[\frac{H_1^{(2)}(\delta kb)}{H_0^{(2)}(k\delta a)} - \frac{H_1^{(1)}(\delta kb)}{H_0^{(1)}(k\delta a)} \right] e^{-iyz}\, dy \tag{7}$$

where we have set $z_0 = 0$. Since the integrand of S is singular at $y = 0$, it is convenient to break the integration range into two parts; in the first, the range is from 0 to d_0, and, in the second, it is from d_0 to $\infty \exp(-i \arg k)$. Here d is chosen to be sufficiently small that the small argument approximations are valid for the Hankel functions. Then we find that

$$S \simeq S_d + \int_{d_0}^{\infty e^{-i \arg k}} \frac{1}{\delta} [\cdots]\, e^{-iyz}\, dy \tag{8}$$

where

$$S_{d_0} = \frac{2\pi}{kb} \int_0^{d_0} \frac{dy}{y \ln^2(yk^2a^2)} = -\frac{2\pi}{kb \ln(dk^2a^2)}. \tag{9}$$

It is found that for small d_0, S evaluated in this manner is independent of d_0.

Integrals of the type given by (7) were evaluated asymptotically by Kunz [2]. Using his method, applied to the present configuration, we obtain, for $z \to +\infty$,

$$I(z) \simeq -\frac{K2\pi}{\eta} \frac{e^{-ikz}}{\ln\left[-\frac{2iz}{\Gamma^2 ka^2} \right]} \tag{10}$$

where $\eta = [i\mu\omega/(\sigma + i\epsilon\omega)]^{1/2}$ and $\Gamma = 1.781\cdots$. For lossless media, this reduces to Kunz's result.

III. Results for the Infinitely Long Rod

We now present some numerical results for the infinitely long rod shown in Fig. 1. Since $I(z) = I(-z)$, we only need consider the case $z > 0$. The integration program developed for dealing with (8) uses a variable increment size to sample the variation of the integrand over y. Some results for the magnitude of $I(z)$ are shown in Fig. 2 for a frequency of 5 kHz where the distance z varies from 10 to 1000 m. The radius a of the rod is 2 cm and the magnetic current K is fixed at a/b V. As indicated, the ratio b/a is either 1 or 2. For this example, the rock conductivity σ is 10^{-2} mho/m and the permittivity, relative to free space, ϵ/ϵ_0 is 10. But for comparison purposes, the corresponding results for a free-space environment are also shown. Both the numerical integration data and the corresponding asymptotic solution for these two cases are indicated in Fig. 2.

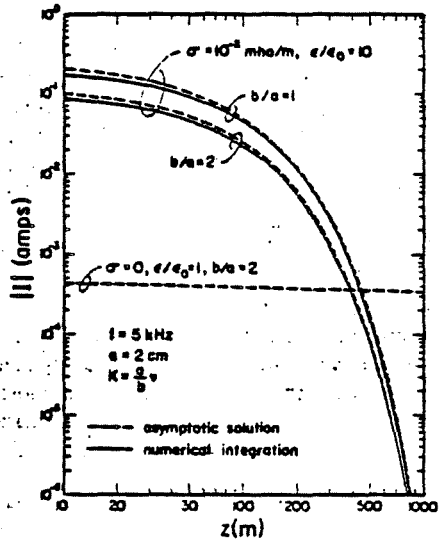


Fig. 2. The excited current on the infinitely long rod excited by the magnetic ring source for a frequency of 5 kHz.

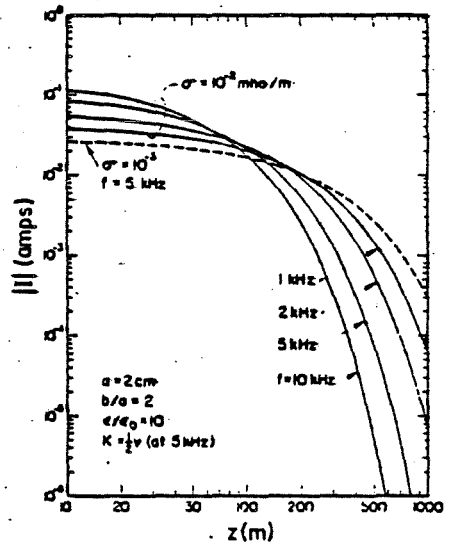


Fig. 3. The excited current on the infinitely long rod excited by the magnetic ring source for various frequencies normalized for a fixed electric current in the winding wires of the source toroid.

It is apparent that the excited current or the rod near the ring source of fixed K is much greater for the conductive environment than that for free space. However, beyond about $z = 500$ m, the rate of decay of the current on the rod is much greater in the case of the conductive environment. We also note that, in Fig. 2, the magnitude of the excited current for $b/a = 2$ is approximately half that for $b/a = 1$. In fact, we can say, in general, that the excited current is inversely proportional to b provided that $z >> b$. This dependence is explicitly shown in (10).[1]

[1]The method of normalizing the source calls for some explanation. We adjust K to be a/b V so that the electric current in the solenoid, the winding radius, and the number of turns remain constant.

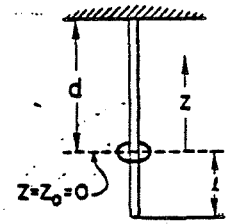


Fig. 4. The model employed to consider the finite depth extent of the rod and the termination of the rod at the surface.

In order to show a meaningful frequency dependence, the current magnitude of the magnetic current K itself is allowed to be proportional to frequency. This result follows from the fact that K of a solenoid is proportional to the product of the electric current in the winding and the frequency. Thus in Fig. 3, we plot the magnitude of $I(z)$ as a function of z for $\sigma = 10^{-2}$ mho/m for frequencies of 1, 2, 5, and 10 kHz and for $K = a/b$ V at 5 kHz, but otherwise proportional to frequency (i.e., $K = (a/b) \times f(\text{kHz})/5$). For comparison, the single curve for $\sigma = 10^{-3}$ mho/m and $f = 5$ kHz is also shown in Fig. 3. The frequency dependence for this case would be very similar.

Not surprisingly, the results in Fig. 3 show that the currents excited near the source toroid are greater for the higher frequencies, but the corresponding attenuation is much greater. This produces a "cross-over" effect wherein, at a distance z beyond about 100 m, the current magnitude is always much reduced with increases of frequency.

IV. Extension to the Truncated and Terminated Rod

We now consider an approximate extension of the foregoing analysis to allow for end effects. Specifically, we consider the configuration shown in Fig. 4. Here we represent the termination of the metal rod at the surface as a perfectly conducting ground plane. On the other hand, the rod is truncated at a distance l below the source toroid. An approximate solution for the total current $I_t(z)$, due to end effects, is then obtained by imposing the conditions of perfect reflection at the ground plane at $z = d$ and the vanishing of the current at $z = -l$. This leads to a superposition of "current waves" as follows:

$$I_t(z) = I(z) - I(z + 2l) + I(2d - z) - I(2(d + l) - z) + \cdots$$

where $d < z < -l$. In particular, the current at the top of the rod can be approximated by

$$I_t(d) \simeq 2[I(d) - I(d + 2l)]$$

where $I(d)$ and $I(d + 2l)$ can be obtained from (8) using appropriate numerical integration.

Some results for the magnitude of the total current I_t at $z = d$ are shown in Figs. 5 and 6 for $\sigma = 10^{-2}$ and 10^{-3} mho/m, respectively. In both cases the frequency is fixed at 5 kHz, $a = 2$ cm, $b/a = 2$, $\epsilon/\epsilon_0 = 10$, and $K = \frac{1}{2}$ V. As indicated in Figs. 5 and 6, the magnitude of the resultant current at the top of the rod generally decreases as l is reduced, except that there is slight enhancement for $l = 100$ m. This corresponds approximately to the condition that l is of the order of a quarter of an effective wavelength within the medium. The effect

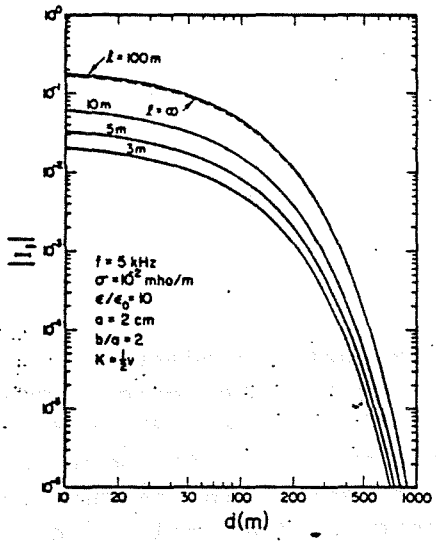


Fig. 5. The current at the top end of the rod as a function of the depth d of the source toroid for various values of the extension l of the rod below the toroid.

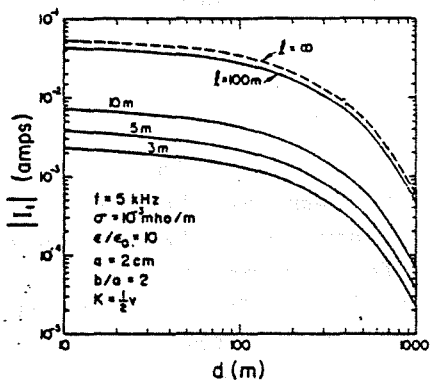


Fig. 6. The same as Fig. 5 but for a lower rock conductivity.

could be more noticeable for higher frequencies and when the rock conductivity is lower.

V. Concluding Remarks

Admittedly, the model we have employed is highly idealized. However, the assumption in the calculations that the rod is perfectly conducting can be easily relaxed by using an appropriate value for the series impedance Z_s. However, it appears that, to within graphical accuracy, the results would not be changed. A more important limitation would be the imperfect contact between sections of the rod if it were not continuous throughout its length. In such cases, the axial current flow could be inhibited with an effective increase of the total signal loss.

For the present model, the resultant attenuation will be at least as great as plane waves in the conducting medium that surrounds the rod. The only way this intrinsic loss could be circumvented would be to provide a layer of insulation on the rod. The formulation we have given could actually apply to this situation if, again, the effective (spatially dispersive) value [3] of Z_s was used. In such cases, the pole contribution to the integral representation would play an important role.

As indicated in the formulation, we can easily allow for the finite vertical and radial extent of the source toroid. However, for the numerical examples here, this would not have any noticeable effect on the current distributions. Also, the toroid itself could be ferrite loaded in order to improve the flux linkage for a given electrical current in the winding wires.

The concept that real-time sensor data can be transmitted from the drill bit to the surface operator is promising. The proposed mechanism of using a toroid or equivalent coupler appears to be fairly efficient in that the drill rod itself conveys the axial current.

References

[1] J. R. Wait, "Electromagnetic surface waves," in *Advances in Radio Research*, J. A. Saxton, Ed. London, England: Academic Press, 1964, vol. 1, pp. 157-217.

[2] K. S. Kunz, "Asymptotic behavior of the current on an infinite cylindrical antenna," *J. Res. NBS Sec. D (Radio Propagat.)*, vol. 67D, no. 4, pp. 417-431, July/Aug. 1963.

[3] J. R. Wait, "Electromagnetic wave propagation along a buried insulated wire," *Can. J. Phys.*, vol. 50, no. 20, pp. 2402-2409, Oct. 15, 1972.

From Proceedings of the Fourth West Virginia University Conference on Coal Mine Electrotechnology, August 2-4, 1978.

THEORY OF ELECTROMAGNETIC METHODS FOR NONDESTRUCTIVE TESTING OF WIRE ROPES*

David A. Hill
James R. Wait
ITS/NTIA and ERL/NOAA
U.S. Department of Commerce
Boulder, Colorado 80303

ABSTRACT

Past and current techniques for electromagnetic nondestructive testing of wire ropes are briefly reviewed. Recent theoretical work is also discussed. In particular, we mention prolate spheroidal void model for a broken strand or individual wire. Here we assume the wire rope is excited by an electric current loop. This primary field, in turn, induces both electric and magnetic dipole moments in the small void. The resulting external scattered field is then derived and numerical results are presented which suggest an effective configuration of sensing coils. The dual source of a magnetic current loop which is a model for a toroidal coil is also considered.

INTRODUCTION

Wire ropes are used extensively in many life sustaining situations. Elevator and mine hoist cables are two notable examples, but we might also mention the support cable for aerial tramways, ski chairlifts and gondolas, helicopter and suspension cables. In this paper, we will restrict attention to wire ropes used in mine hoists. There is an obvious need to perform tests of the integrity of such ropes without in any way impairing their function. Apart from careful visual examination and measurements of the external diameter, the nondestructive test methods available utilize electromagnetic fields, x-rays or mechanical waves. Here we consider only electromagnetic methods.

We begin with a brief review of the past and present techniques and principles of electromagnetic methods. Then we turn to some of the recent theoretical investigations starting with some idealized two-dimensional models. The three-dimensional theory of excitation of a homogeneous rope by either an encircling solenoid or toroid is then considered in more detail. The additional effect of idealized rope imperfections is treated by computing the induced electric and magnetic dipole moments. Finally, we present some numerical results for the anomalous external fields due to a rope imperfection or internal flaw. The properties of these anomalous fields are important in designing an effective configuration of sensing coils.

*This research was supported by U.S. Bureau of Mines Contract H0155008.

U.S. Gov't work not subject to U.S. Copyright.

REVIEW OF PAST AND CURRENT TECHNIQUES

Since a thorough review of electromagnetic methods containing numerous references has recently been prepared [1], we present here only a relatively brief summary. In all past and current systems, the rope is excited with an axial magnetic field which can be either A.C. or D.C. The operating frequency for A.C. systems is generally somewhere between 10 Hz and 100 Hz. The search coil is typically a loop which completely encircles the rope.

Wall [2] gives an early account of the design and operation of electromagnetic rope testers. He is an early proponent of the A.C. method as opposed to D.C. magnetic testing favored in more recent times. He lists some of the advantages as follows: a) the rope need not continuously move through the magnetic system, b) the A.C. signal is easy to detect and c) any remnant magnetism due, say, to a previous test is wiped out. Wall was interested in testing colliery ropes of the locked coil type up to 2¼ inch (5.6 cm) diameter. He was able to ascertain that the flux penetration was almost complete at 20 Hz but only partially so at 50 Hz.

Semmelink [3] gives an extremely interesting and comprehensive account of the early history of electromagnetic testing of wire ropes in South Africa. He also tested about fifty hoist ropes with an A.C. device at 50 Hz. In his measurements on steel, Semmelink found, what is now generally known, that an increase of tensile stress causes a significant increase in magnetic permeability but not in D.C. resistance. Lang [4] gives an extensive description of a very similar A.C. device, and most of his data are shown for a frequency of 30 Hz.

Hiltbrunner [5] gives a good description of what is known now as the D.C. magnetic testing method. The method is based on imposing a strong axial magnetic field to the sample by either a solenoid coil or a permanent magnetic. The search coil is oriented in the radial direction and produces a voltage response only when there is some type of lateral non-uniformity. Stachurski [6] gives a very useful summary of the physical concepts employed in D.C. magnetic testing for flaws in wire ropes. A number of interpretative schemes are outlined in a qualitative manner, and he uses prescribed forms of flaws, breaks, and cracks to calibrate the device. Using three D.C. devices, Egen and Benson [7] performed some very useful tests on a special prepared rope with seven types of faults.

Hochschild [8] has reviewed the theoretical papers by Förster [9-12]. Wait [1] points out that electromagnetic methods of non-destructive testing of solid conductors are closely akin to techniques now used in geophysical prospecting [13]. Most of the theoretical papers on wire rope testing are carried out for the special case of azimuthal symmetry [14-16]. Burrows [17] treats asymmetrical "flaws", but assumes azimuthal symmetry of the sensing coils.

TWO-DIMENSIONAL ANALYSIS

Wait [18] has recently derived the internal and external fields of an infinite circular cylinder which is excited by either an encircling solenoid or toroid of infinite length. The solenoid excites the rope with an axial magnetic field and an azimuthal electric field as do the current rope testers. The toroid, which is the dual source, excites the rope with an axial electric field and an azimuthal magnetic field. Such a source would be useful in probing the axial conductivity of the rope. The impedance of the encircling solenoid or toroid is also derived and is shown to be independent of the rope position under the usual quasi-static conditions.

Wait and Gardner [19] have extended the two-dimensional model to allow for the presence of a small cylindrical flaw of arbitrary conductivity and permeability. They derive an expression for the scattered magnetic and electric fields and the resultant change in the impedance of the encircling solenoid. They also present numerical results for various anomaly parameters at frequencies from 1 Hz to 1000 Hz.

Past theoretical work has assumed that the conductivity and permeability are isotropic, but Wait [20] has recently presented the theory for excitation of a wire rope where the conductivity and permeability are uni-axial tensors. This anisotropic model should be more representative of stranded wire ropes.

SOLENOID AND TOROID EXCITATION

In order to model excitation of a wire rope by a finite source, we have analyzed the configuration in Fig. 1. The source is either an electric or magnetic current loop which encircles an infinite wire rope. The first step is to determine the internal and external fields for the homogeneous rope in the absence of the void.

An electric current loop is an idealized model of a thin solenoid [21]. Due to the azimuthal symmetry of the rope and the source, the primary fields are TE (Transverse Electric) and independent of ϕ. The electric field has only an azimuthal component E_ϕ^{pr}, and the magnetic field has both an axial component H_z^{pr} and a radial component H_ρ^{pr}. The explicit integral forms of the fields have been derived and evaluated previously [21]. Actually, E_ϕ^{pr} and H_ρ^{pr} are zero at the center of the rope ($\rho=0$). Also, H_z^{pr} is nearly independent of ρ inside the rope for sufficiently low frequencies.

A magnetic current loop is an idealized model for a thin toroidal coil [22]. This source is the dual of the electric current loop, and the primary fields are TM (Transverse Magnetic) and independent of ϕ. The magnetic field has only an azimuthal component H_ϕ^{pr}, and the electric field has both an axial component E_z^{pr} and a radial component E_ρ^{pr}. The explicit integral forms have been derived and evaluated previously [22]. Both H_ϕ^{pr} and E_ρ^{pr} are zero at the center of the rope ($\rho=0$), but E_z^{pr} is nearly independent of ρ inside the rope for sufficiently low frequencies. The additional source complication of finite width in the axial direction and arbitrary azimuthal extent has also been considered [23]. This

more general source results in more complicated fields without azimuthal symmetry.

ANOMALOUS FIELDS OF ROPE IMPERFECTIONS

In order to model an individual wire or broken strand within the rope, we select a thin prolate spheroid of conductivity σ_v and permeability μ_v. The prolate spheroidal shape is a convenient one because its electric and magnetic polarizabilities are known. However, we would not expect a significant difference for a thin cylinder of the same length and volume. To account for the winding geometry of the rope, we allow a rotation of the major axis of the spheroid about the ρ' axis by an angle α. Thus the major axis is oriented at an angle α to the unit vector $\hat{z}'$ and an angle $\pi/2 + \alpha$ to the unit vector $\hat{\phi}'$ as indicated in Fig. 1c.

Since the void has a contrast in both the electric and magnetic properties, both electric and magnetic dipole moments will be induced [24]. The electric polarizabilities for the incident electric field applied along the major axis, α^e_{maj}, or along the minor axis, α^e_{min}, are given by

$$\alpha^e_{maj} = - V(\sigma_w - \sigma_v) \tag{1}$$

and

$$\alpha^e_{min} = - 2V(\sigma_w - \sigma_v)/(1 + \sigma_v/\sigma_w) , \tag{2}$$

where V is the volume of the thin prolate spheroid and σ_w is the rope conductivity. Because of the low operating frequency, we have neglected displacement currents. To include them, σ_w would be replaced by $\sigma_w + i\omega\varepsilon_w$ and σ_v would be replaced by $\sigma_v + i\omega\varepsilon_v$ in (1) and (2) for $\exp(i\omega t)$ time dependence. The magnetic polarizabilities for the incident magnetic field applied along the major axis, α^m_{maj}, or along the minor axis, α^m_{min}, are similarly given by

$$\alpha^m_{maj} = - Vi\omega(\mu_w - \mu_v) \tag{3}$$

and

$$\alpha^m_{min} = -2Vi\omega(\mu_w - \mu_v)/1 + \mu_v/\mu_w) , \tag{4}$$

where μ_w is the rope permittivity.

In order to compute the induced dipole moments, it is first necessary to resolve the incident electric and magnetic field into components along the major and minor axes. The resultant induced dipole moments can then be resolved into the more convenient ρ, ϕ, and z components. When this is done, the induced electric and magnetic dipole moments for an electric loop source are [21]

$$(Ids)_z = E^{pr}_\phi(\alpha^e_{min} - \alpha^e_{maj})\sin\alpha\cos\alpha, \tag{5}$$

$$(Ids)_\phi = E^{pr}_\phi(\alpha^e_{min}\cos^2\alpha - \alpha^e_{maj}\sin^2\alpha) , \tag{6}$$

$$(Ids)_\rho = 0 . \tag{7}$$

Similarly the induced magnetic dipole moments are found to be

$$(Kd\ell)_z = H_z^{pr}(\alpha_{maj}^m \cos^2\alpha + \alpha_{min}^m \sin^2\alpha) , \tag{8}$$

$$(Kd\ell)_\phi = H_z^{pr}(\alpha_{min}^m - \alpha_{maj}^m)\sin\alpha\cos\alpha , \tag{9}$$

$$(Kd\ell)_\rho = H_\rho^{pr}\alpha_{min}^m \tag{10}$$

In (5)-(10), the primary field components E_ϕ^{pr}, H_z^{pr}, H_ρ^{pr} are evaluated at ρ', ϕ', z'. For the magnetic current loop source, the induced electric and magnetic dipole moments are given by similar expressions [22]

$$(Ids)_z = E_z^{pr}(\alpha_{maj}^e \cos^2\alpha + \alpha_{min}^e \sin^2\alpha) , \tag{11}$$

$$(Ids)_\phi = E_z^{pr}(\alpha_{min}^e - \alpha_{maj}^e)\sin\alpha\cos\alpha , \tag{12}$$

$$(Ids)_\rho = E_\rho^{pr}\alpha_{min}^e , \tag{13}$$

$$(Kd\ell)_z = H_\phi^{pr}(\alpha_{min}^m - \alpha_{maj}^m)\sin\alpha\cos\alpha , \tag{14}$$

$$(Kd\ell)_\phi = H_\phi^{pr}(\alpha_{min}^m \cos^2\alpha - \alpha_{maj}^m \sin^2\alpha) , \tag{15}$$

$$(Kd\ell)_\rho = 0. \tag{16}$$

The scattered field external to the rope is the observable quantity in any nondestructive testing system. Bearing in mind the use of small coils for sensors, we will consider primarily the scattered magnetic field components $H_\rho^{sc}(\rho,\phi,z)$, $H_\phi^{sc}(\rho,\phi,z)$, and $H_z^{sc}(\rho,\phi,z)$. Each of these components can be written as a superposition of the contributions from each of the six dipole sources in the following compact matrix notation

$$\begin{bmatrix} H_\rho^{sc} \\ H_\phi^{sc} \\ H_z^{sc} \end{bmatrix} = \begin{bmatrix} G_{\rho\rho}^e & G_{\rho\phi}^e & G_{\rho z}^e \\ G_{\phi\rho}^e & G_{\phi\phi}^e & G_{\phi z}^e \\ G_{z\rho}^e & G_{z\phi}^e & G_{zz}^e \end{bmatrix} \begin{bmatrix} (Ids)_\rho \\ (Ids)_\phi \\ (Ids)_z \end{bmatrix} + \begin{bmatrix} G_{\rho\rho}^m & G_{\rho\phi}^m & G_{\rho z}^m \\ G_{\phi\rho}^m & G_{\phi\phi}^m & G_{\phi z}^m \\ G_{z\rho}^m & G_{z\phi}^m & G_{zz}^m \end{bmatrix} \begin{bmatrix} (Kd\ell)_\rho \\ (Kd\ell)_\phi \\ (Kd\ell)_z \end{bmatrix} \tag{17}$$

In the first 3 by 3 matrix, $G_{\rho\rho}^e$ is the ρ component of H at (ρ,ϕ,z) produced by a unit ρ-directed electric dipole at (ρ',ϕ',z'), $G_{\rho\phi}^e$ is the ρ component of H produced by a unit ϕ-directed electric dipole, etc. The second 3 by 3 matrix is similar except that the G^m elements correspond to unit magnetic dipoles. The specific expressions for the matrix elements have been derived previously [22]. A similar matrix expression is available for the scattered electric field [21].

The matrix expression in (17) is actually a general statement of the scattered fields produced by any small flaw in the rope. For the specific case of the thin prolate spheroidal flaw considered here, the induced dipole moments are given by (5)-(10) for electric current loop excitation or by (11)-(16) for magnetic current loop excitation. For other flaws or excitations, only the induced dipole moments will be different.

Computer programs have been written to obtain the scattered and primary fields for both electric [21] and magnetic [22] current loop excitation. Extensive numerical results in the form of computer plots have been generated for the electric current loop source [21] because this case is most representative of current rope testers. In Figs. 2-4, we present three representative plots of the azimuthal variation of the three scattered magnetic field components (H_ρ^{sc}, H_ϕ^{sc}, H_z^{sc}) normalized to the primary axial magnetic field H_z^{pr}. The parameters are: a = 1 cm, $\sigma_w = 1.1 \times 10^6$ mho/m, $\mu_w/\mu_o = 200$, $\sigma_v = 0$, $\mu_v/\mu_o = 1$, $\alpha = 0°$, $\phi' = 0$, $z'/a = 5$, $z/a = 5$, $\rho/a = 2$, and f = 10 Hz. The volume V of the void is taken to be $10^{-8}m^3$(= 1 cm × 1 mm × 1 mm), but the results are easily normalized to any other volume since the scattered fields are directly proportional to V.

Fig. 2 demonstrates that, for the void located near the center of the rope ($\rho'/a = 0.1$), the azimuthal variation of the scattered field is small. However, in Fig. 4, a large azimuthal variation is evident for the void located near the rope boundary ($\rho'/a = 0.9$). Most AC rope testers sense only the average azimuthal scattered electric field with a solenoid sensor which completely encircles the rope. In Fig. 5, the normalized scattered electric field $|E_\phi^{sc}/E_\phi^{pr}|$ is shown for the same parameters. It is again evident that a significant amount of information (and signal strength) is lost by sensing only the ϕ-averaged electric field.

CONCLUDING REMARKS

We have begun with a brief review of electromagnetic methods of wire rope testing. As indicated, the very practical and perhaps most useful work to date has been empirical in nature. There has been no attempt to deduce the magnitude of the secondary fields due to internal flaws; instead a large number of ropes have been tested and the results have been presented.

On the other hand, the analytical approaches have considered only highly idealized situations. Here we have analyzed a more realistic three-dimensional configuration without azimuthal symmetry. We have computed the three-dimensional scattered fields for a thin prolate spheroidal void which represents a broken strand. The results indicate that an effective configuration of sensing coils should make use of large asymmetrical portions of the scattered fields. Possible extensions of this work would include other types of small flaws which could be treated in a similar manner.

REFERENCES

[1] J.R. Wait, "Review of electromagnetic methods in nondestructive testing of wire ropes", Preliminary Report to U.S. Bureau of Mines on Contract No. H0155008, 28 March 1978.

[2] T.F. Wall, "Electromagnetic testing for mechanical flaws in steel wire ropes", *J. Inst. Elect. Engrs.*, Vol. 67, pp. 899-911, 1929.

[3] A. Semmelink, "Electromagnetic testing of winding ropes", *Trans. of the South African Institute of Electrical Engrs.*, Vol. 43, No. 5, pp. 113-129, May 1953.

[4] J.G. Lang, "The principle and practice of electromagnetic wire rope testing", *Canadian Mining and Metallurgical Bulletin*, pp. 415-424, April 1969.

[5] R.H. Hiltbrunner, "Le Controle Magnétique des câbles avec le defectoscope integra", *Économie et Technique des Transports*, No. 119, June 1957.

[6] J. Stachurski, "Magnetic testing of steel wire ropes", Report from Laboratory for Testing Wire Ropes, University of Mining and Metallurgy, Cracow, Poland, 1976.

[7] R.A. Egen and D.K. Benson, "Wire rope retirement criteria and procedures", Progress Report No. 16 (from Midwest Research Inst., 425 Volker Blvd., Kansas City, MO 64110) on U.S. Bureau of Mines Contract No. J0155187, 10 Nov. 1976.

[8] H. Hochschild, "Electromagnetic methods of testing metals", *Progress in Non-Destructive Testing*. New York: The Macmillan Co., 1959, Vol. 1, pp. 59-109.

[9] F. Förster, "Theoretical and experimental foundation of non-destructive testing using eddy current I. Test coil methods", *Zeitschrift Metallkunde*, Vol. 43, No. 5, pp. 163-171, 1952 (in German).

[10] F. Förster and H. Breitfeld, "Non-destructive testing using eddy current methods II. Practical results and industrial applications of methods using test coils", *Zeitschrift Metallkunde*, Vol. 43, No. 5, pp. 172-180, 1952 (in German).

[11] F. Förster and K. Stambke, "Theoretical and experimental foundation of non-destructive testing using eddy currents III. Quantitative methods of non-destructive testing using test object encircling coils", *Zeitschrift Metallkunde*, Vol. 45, No. 4, pp. 166-179, 1954 (in German).

[12] F. Förster, "Theoretical and experimental foundation of non-destructive testing using eddy currents IV. Practical apparatus for non-destructive testing using encircling coils for eddy currents", *Zeitschrift Metallkunde*, Vol. 45, No. 4, pp. 180-187, 1954 (in German).

[13] G.V. Keller and F.C. Frischknecht, *Electrical Methods in Geophysical Prospecting*. New York: Pergamon Press, 1966.

[14] P.R. Vein, "Inductance between two loops in the presence of solid conducting bodies", *J. Electronic Control*, Vol. 13, No. 5, pp. 471-494, 1962.

[15] C.V. Dodd, W.E. Deeds, and J.W. Luquire, "Integral solutions to some eddy current problems", *Int'l J. of NDT*, Vol. 1, pp. 29-90, 1969/1970.

[16] C.V. Dodd, C.C. Cheng, and W.E. Deeds, "Induction coils coaxial with an arbitrary number of cylindrical conductors", *J. Appl. Phys.*, Vol. 45, No. 2, pp. 638-647, Feb. 1974.

[17] M.L. Burrows, "A theory of eddy-current flaw detection", *Ph.D. Thesis, University of Michigan*, 1964 (available from University Microfilms, Ann Arbor, MI, Order No. 64-12,568).

[18] J.R. Wait, "The electromagnetic basis for non-destructive testing of cylindrical conductors", Preliminary Report to U.S. Bureau of Mines on Contract No. H0155008, 2 March 1978.

[19] J.R. Wait and R.L. Gardner, "Non-destructive testing of a cylindrical conductor with an internal anomaly - A two-dimensional model", Preliminary Report to U.S. Bureau of Mines on Contract No. H0155008, 24 May 1978.

[20] J.R. Wait, "Electromagnetic induction in an anisotropic cylinder", Preliminary Report to U.S. Bureau of Mines on Contract No. H0155008, as amended 14 Feb. 1978.

[21] D.A. Hill and J.R. Wait, "Electromagnetic field perturbation by an internal void in a conducting cylinder excited by a wire loop", Preliminary Report to U.S. Bureau of Mines on Contract No. H0155008, 14 July 1978.

[22] D.A. Hill and J.R. Wait, "Scattering by a slender void in a homogeneous conducting wire rope", *Appl. Phys.*, to be published, 1978.

[23] D.A. Hill and J.R. Wait, "Analysis of alternating current excitation of a wire rope by a toroidal coil", *J. Appl. Phys.*, Vol. 48, No. 12, pp. 4893-4897, Dec. 1977.

[24] W.R. Smythe, *Static and Dynamic Electricity*. New York: McGraw-Hill Book Co., 1950, 2nd Ed. (Third revised edition now available).

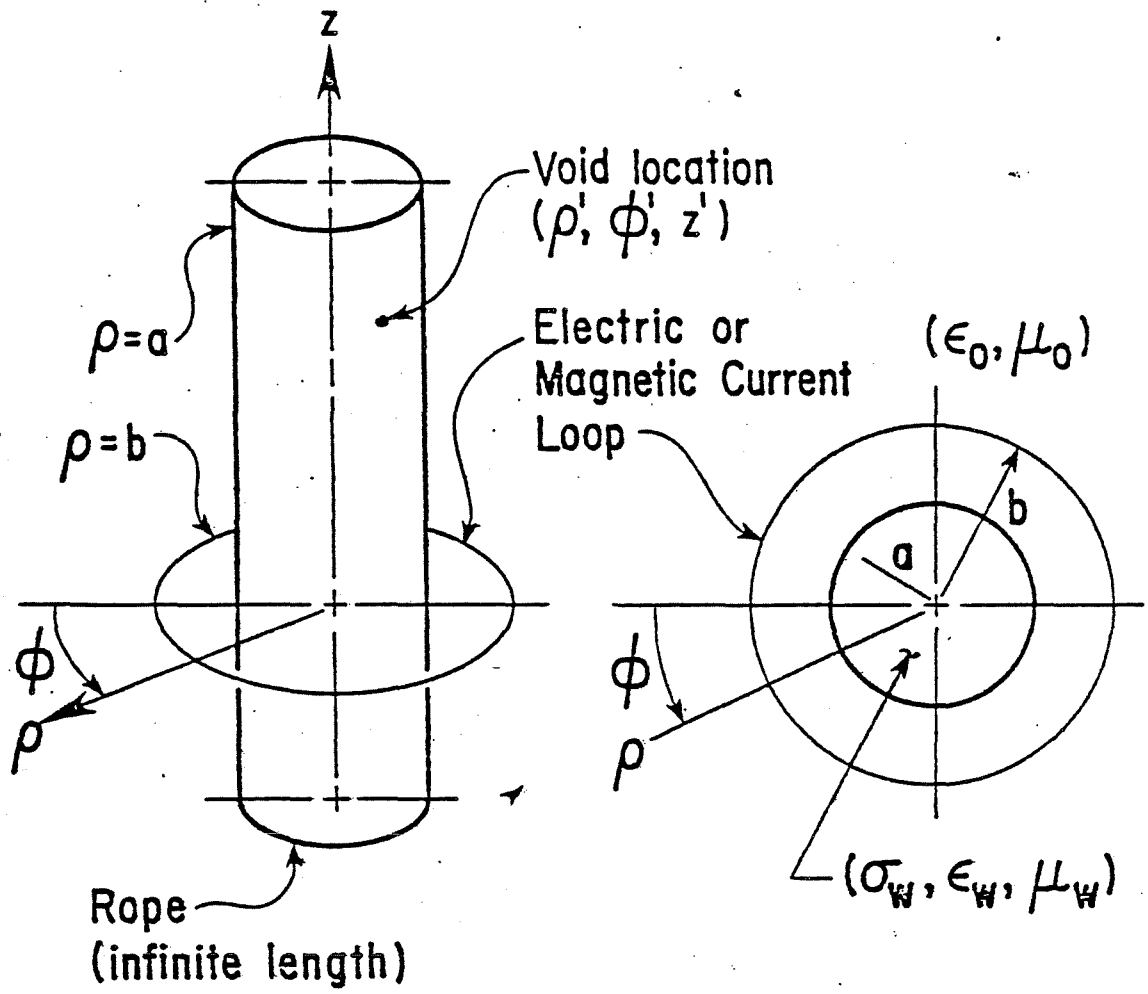


Fig. 1a

Fig. 1b

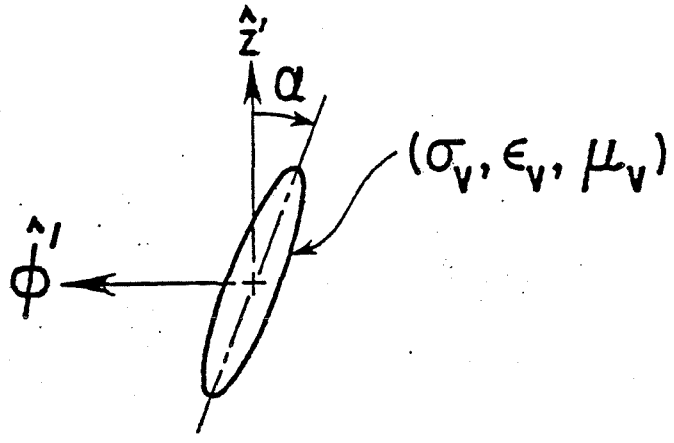


Fig. 1c

Fig. 1. Electric or magnetic current loop surrounding a metal rope of infinite length. a) Perspective view, b) Top view, c) Prolate spheroidal void.

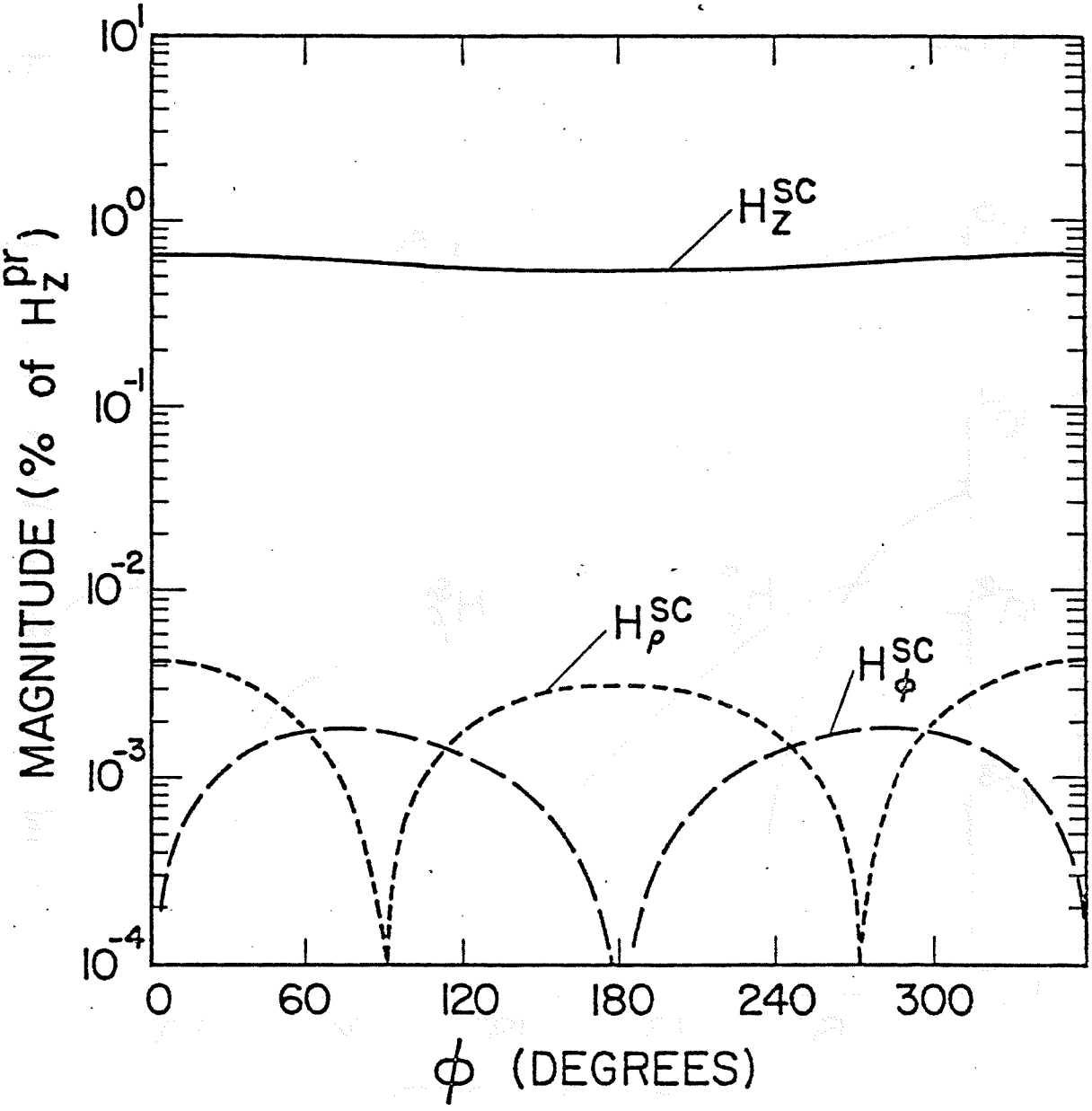


Fig. 2. Normalized magnitude of the scattered magnetic field components for $\rho'/a = 0.1$.

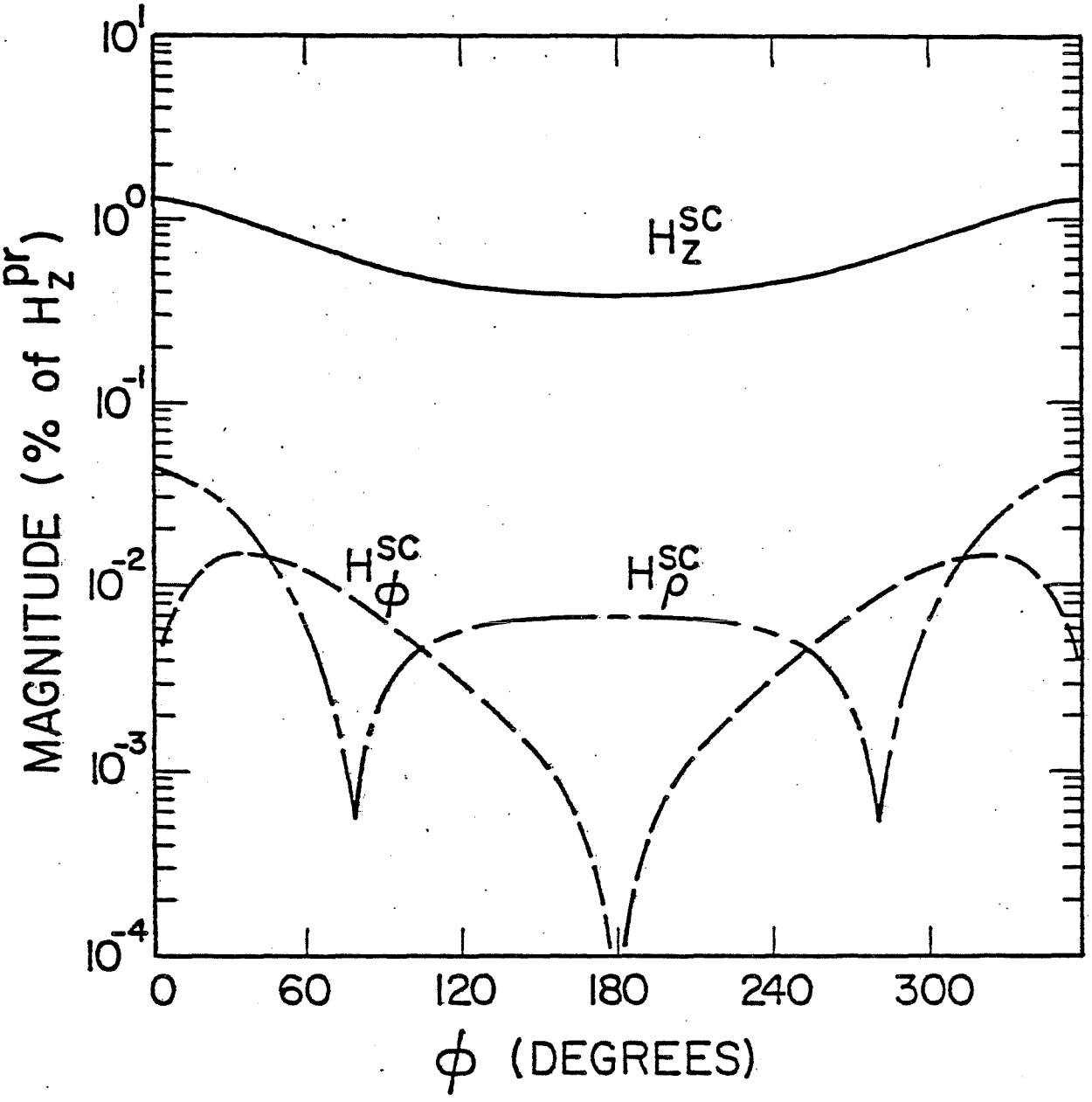


Fig. 3. Normalized magnitude of the scattered magnetic field components for $\rho'/a = 0.5$.

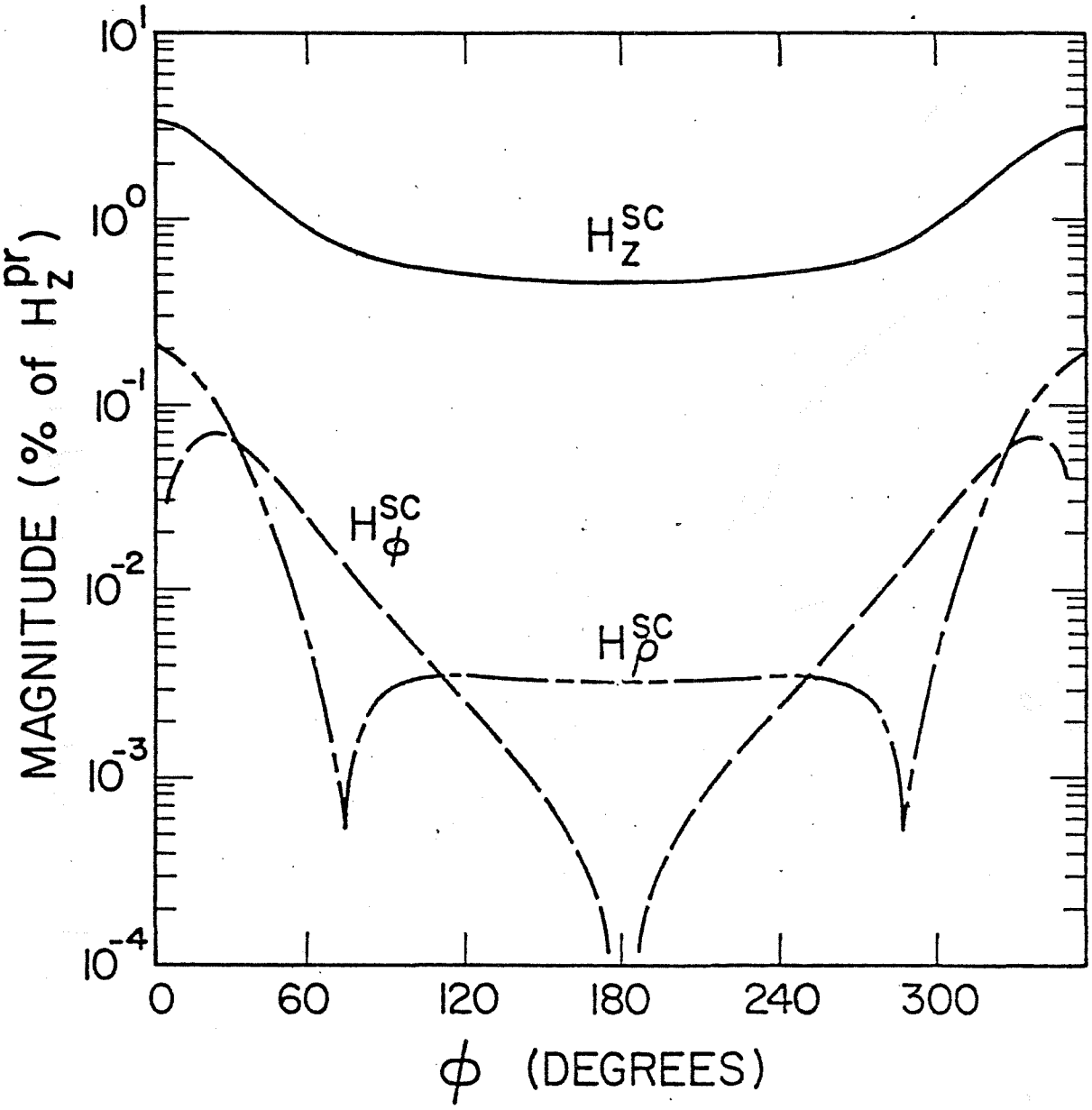


Fig. 4. Normalized magnitude of the scattered magnetic field components for $\rho'/a = 0.9$.

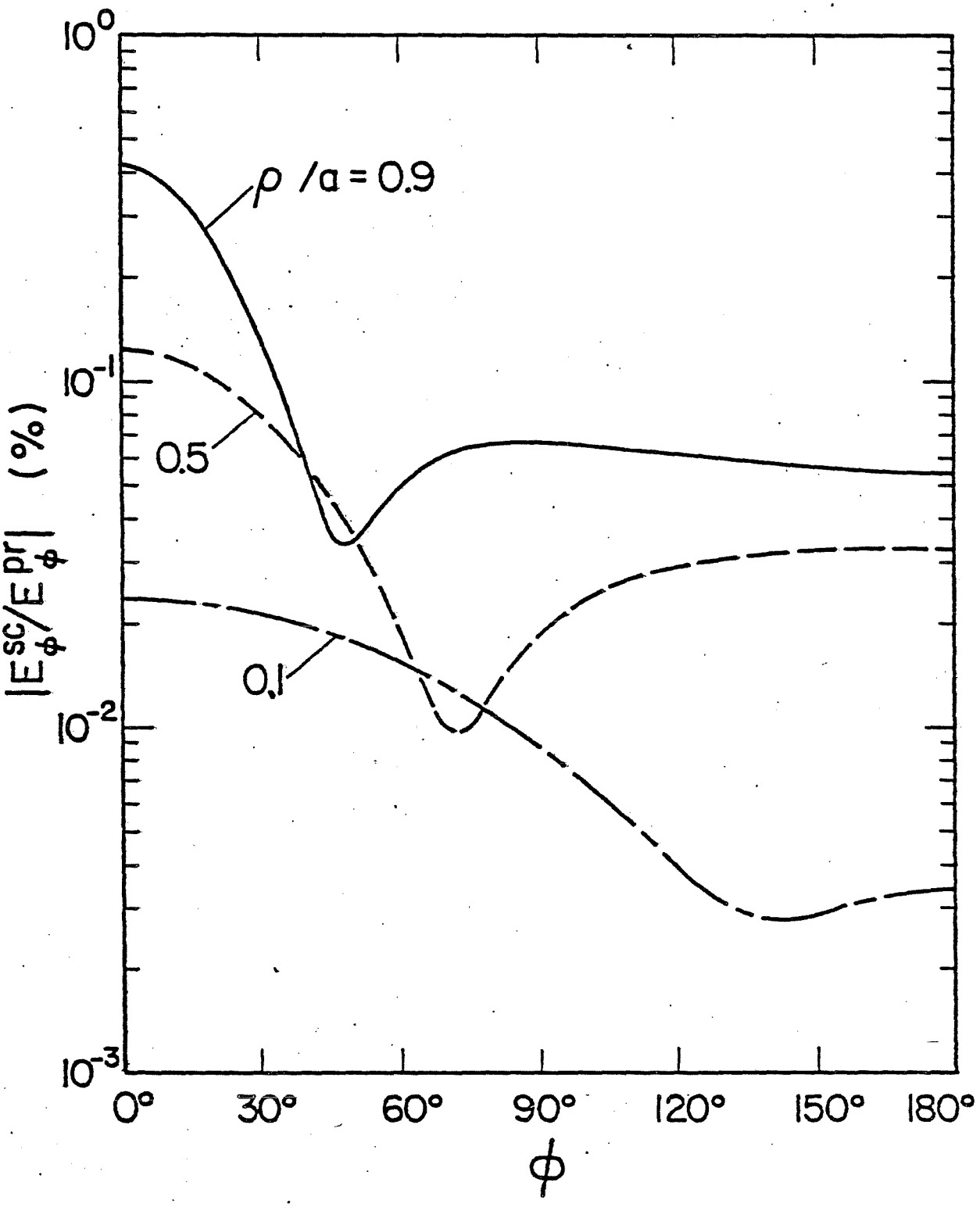


Fig. 5. Normalized magnitude of the scattered azimuthal electric field.

Review of Electromagnetic Methods in Nondestructive Testing of Wire Ropes

JAMES R. WAIT, FELLOW, IEEE

Abstract—Wire ropes are used extensively in many life sustaining situations. Elevator and mine-hoist cables are two notable examples, but the support cable for aerial tramways, ski chairlifts and gondolas, helicopter and suspension cables we might also mention. In this review, we will deal mainly with wire ropes used in mine hoists, but the results are also relevant for testing support cables for ski lifts. There is an obvious need to perform tests of the integrity of such ropes without in any way impairing their function. Apart from careful visual examination and measurements of the external diameter, the nondestructive test methods available utilize electromagnetic fields, X-rays, or mechanical waves. Here, we will review progress in the electromagnetic methods.

The early history of the subject will be described briefly, since this provides a remarkably good introduction to the working principles. We will then progress quickly to the current techniques and operating procedures. Next, we will summarize some of the basic papers that deal with the basic concepts and techniques for testing of cylindrical conductors by both electric and magnetic methods. At this juncture, we call our attention to the extensive related work on electromagnetic probing of geophysical targets such as ore bodies and other subsurface conductors. Finally, we turn to the various recent investigations, primarily of theoretical nature, that have been carried out; we include here only the most recent works.

INTRODUCTION

WIRE ROPES are used extensively in many life-sustaining situations. Both elevator and mine-hoist cables are two notable examples, but we might also mention the support cable for aerial tramways, ski chairlifts and gondolas, helicopter, and suspension cables. In this review, we will restrict attention to wire ropes used in mine hoists. There is an obvious need to perform tests of the integrity of such ropes without in any way impairing their function. Apart from careful visual examination and measurements of the external diameter, the nondestructive-test (NDT) methods available utilize electromagnetic fields, X-rays, or mechanical waves. Here we will review progress in the electromagnetic methods.

The early history of the subject will be described briefly since this provides a remarkably good introduction to the working principles. We will then progress quickly to the current techniques and operating procedures. Next we will summarize some of the basic papers that deal with the basic concepts and techniques for testing cylindrical conductors by both electric and magnetic methods. At this juncture, we call attention to the extensive related work on electromagnetic probing of geophysical targets such as ore bodies, and other subsurface conductors. Finally, we turn to the various investigations, primarily of a theoretical nature, that have been carried out; we include here only the most recent works.

Manuscript received May 17, 1978; revised November 16, 1978.

The author is with the Cooperative Institute for Research in Environmental Sciences, University of Colorado/NOAA, Boulder, CO 80309.

SOME EARLY NDT WORK IN ENGLAND

Wall [1] gives an early account of the design and operation of electromagnetic rope testers. The test results were given for specially constructed ropes. Using basically an ac technique, his method makes it possible to detect broken wires within a rope that represent less than 5-percent reduction in the total cross sectional area. As the author indicates, the investigation was motivated by the testing of wire ropes used in collieries in England. The author also indicates that other important applications are to tram cables, airship mooring ropes, and to suspension-bridge ropes.

Wall is an early proponent of the ac method as opposed to the dc magnetic testing favored in more recent times. He lists some of the advantages as follows: a) The rope need not continuously move through the magnetic system, b) The ac signal is easy to detect, and c) Any remnant magnetism due, say to a previous test, is wiped out.

He is interested in testing colliery ropes of the locked-coil type up to 2.25-in diameter. In such locked ropes, the outer and one or more of the inner layers are locked together to form flexible sheaths. This constrains the rope to maintain its circular form as it passes over the winding drum. He then quotes a classical skin-depth formula that gives a guide to the penetration of the ac currents into the core of the rope. He points out cogently, that once the ac energy penetrates through the outer locked-coil sheaths, it will be "practically" uniformly distributed through the remainder of the cross section since the wires are so effectively stranded.

The tests were made by means of a laminated iron yoke that has projecting limbs with machine-tunnelled holes as indicated in Fig. 1(a). The sample length of the rope was fixed concentrically in the holes. A search coil of 20 turns was wound around the center portion of the rope that is midway between the projecting limbs. The relationship between the flux density in the rope and the peak value of the magnetizing excitation at 20 and 50 Hz was measured. Wall was able to ascertain that the flux penetration was almost complete at 20 Hz, but only partially so at 50 Hz.

In the same pioneering paper, Wall studies the effect of mechanical strain on the magnetic permeability with special reference to ac excitation. He also examines the change in the reluctance of the air space due to the eccentricity of the rope in the magnet system.

Wall concludes that "whilst a flaw of about 3 percent of the total cross section is detectable, a flaw of about 5 percent produces a pronounced effect, whilst a flaw of about 18 percent gives a very striking disturbance of the record." Some of his results are summarized in Fig. 1(b).

U.S. Government work not protected by U.S. copyright

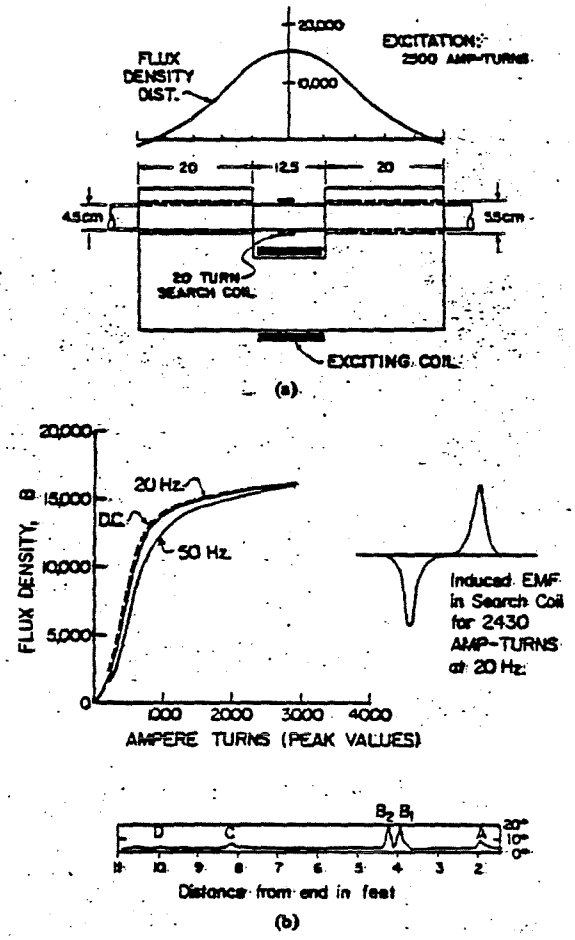


Fig. 1. (a) Sketch of Wall's device [1]. (b) Some data from Wall's test of a locked-coil rope. The B-H curve and the resulting induced EMF in the search coil. (EMF waveform amplitude not given.)

In a follow-up study, Wait and Hainsworth [2] investigate the way in which the flux is distributed within the rope. As they point out, this information is relevant to the estimation of the depth of a flaw in a locked coil or similar rope as used in collieries. They feel a mathematical approach to the problem is intractable. Instead, they build up a special sample or physical model with embedded search coils.

The experimental configuration was chosen to be a replica of a locked-coil rope except that the layers of wires were not so close as in actual ropes. Straight mild-steel wire rods of $\frac{1}{8}$ in diameter were employed, each rod was coated with insulating enamel before assembly. A first layer or central group of seven wires was formed and a search coil (A) of two-hundred turns was arranged to embrace this group. A second layer of twenty wires was then added and a search coil (B) embraced this layer. Next came the third layer with a further embracing search coil (C). Finally, a fourth layer of forty-four wires was formed and a search coil (D) embraced it. Each of the four search coils had two-hundred turns. Then by connecting pairs of consecutive search coils in opposition, it was possible to measure the flux magnitude associated with each layer.

The differences between the waveform of the induced EMF's in the various layers are very striking as indicated in Fig. 2.

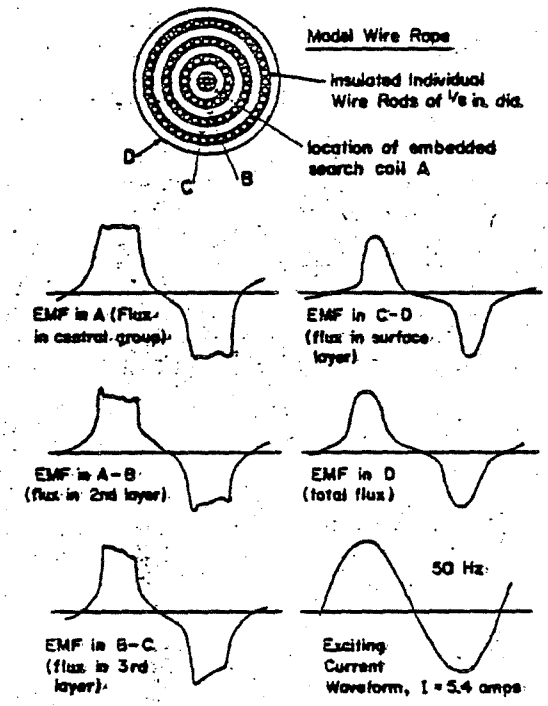


Fig. 2. Special model of a wire rope used by Wait and Hainsworth [2] to study internal fields.

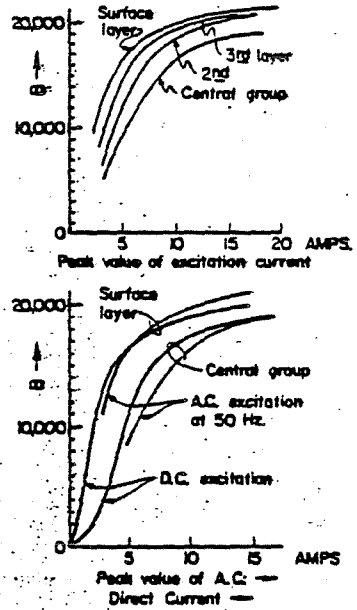


Fig. 3. Some measured data for the special wire rope model. (After Wait and Hainsworth [2].)

Also, as indicated in Fig. 3, the B-H response curves are shown for central group and the surface layer. Here the screening effect for the central group is very apparent. For the surface layer, the situation is somewhat different since apparently the ac excitation has the effect of increasing the apparent permeability. To some extent this tends to counteract the eddy current screening.

The Important Efforts by Semmelink in South Africa

Semmelink [3] gives an extremely interesting account of the early history of electromagnetic testing of wire ropes in South Africa. He indicated that in a paper read to the Transvaal Institute of Mechanical Engineering, in 1906, Mr. C. McCann proposed an "electrical apparatus" for ascertaining the cross sectional area of wire ropes. In this scheme, a detachable coil around the rope was supplied through a step-down transformer from the mains supply. A laminated yoke completed the magnetic circuit and an ammeter was connected in series with the coil. It was claimed that "the current falls exactly in proportion to the size of the rope." Semmelink was also well aware of T. F. Wall's [1] work in England that we described above. He points out that the disadvantage of Wall's method is that the rope speed must be very slow due to the very low frequencies being adopted. Furthermore, the locked-type ropes and the use of high-ac flux densities causes severe heating of the rope.

The first experiments described by Semmelink were conducted in 1946. A magnetizing coil of twenty turns of welding cable was used carrying a current of 100 A at 50 Hz together with a coaxial search coil of several thousand turns. The rope was passed through the centers of both coils. It was found that all visible corrosion and broken wires caused voltage variations in the search coil that were measured by a peak reading voltmeter and an oscilloscope. Semmelink [3] then tested about fifty main winding (hoist) ropes. The tensile strength of the wire was either 123/134 tons (2000 lb)/in^2, or 128/140 tons/in^2. The ropes had six strands of approximately thirty wires laid on a sisal core which was impregnated with lubricant. The diameter varied from 1.25 to 2 in. The ropes were similar to the type shown in Fig. 4. The steel was ascertained to have the following magnetic properties: relative permeability = 44 for a magnetizing force less than 1 Oe, maximum permeability = 320 for a magnetizing force of 25 Oe, maximum flux density = 14000 G for a magnetizing force of 200 Oe, retentivity = 9500 G, coercive force = 20 Oe, hysteresis loss = 0.35 W/cm^3 at 50 Hz. He found, what is now generally known, that an increase of tensile stress in the wire causes an increase of permeability. For example, a stress of 65 tons/in^2 causes an associated increase of permeability of 14 percent even for a magnetizing force of less than 1 Oe. He also noted that twisting of the wire caused a decrease of 8 percent of permeability for 180° of twist per foot of wire. Semmelink [3] also measured the change of dc resistance of the wire rope for stresses varying from 0 to 70 tons/in.^{2} Only 1.1 percent increase was noted over this range that was in accord with the percentage increase of length due to elasticity.

In deciding on an ac method, Semmelink chose to employ a low magnetizing current. This has two advantages: a) internal heating is minimized, and b) better penetration of the rope due to the relatively small initial permeability (i.e., he is working on the virgin part of the B-H curve). A schematic of his measuring scheme is indicated in Fig. 5.

In a later paper, Semmelink [4] describes a more sophisticated approach to the eddy-current testing of wire ropes. The schematic diagram of his measurement setup is illustrated in Fig. 6. As indicated, the rope is excited by spaced coaxial coils and the pickup coil is located centrally. The output of the pickup coil is amplified and detected by a phase-sensitive detector.

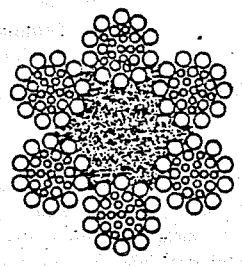


Fig. 4. Stranded wire rope.

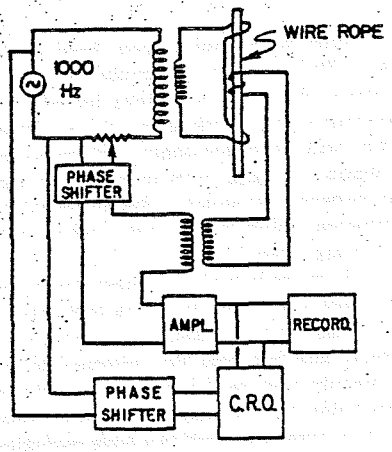


Fig. 5. Semmelink's [3] prototype ac scheme.

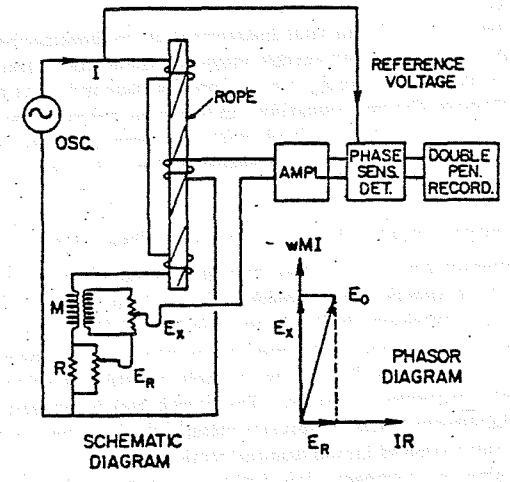


Fig. 6. Improved model use by Semmelink [4].

In the absence of eddy currents, the pickup or search-coil voltage leads the magnetizing current by 90°. However because of the eddy current losses, the phase shift is modified as indicated in Fig. 6. Both the reactive component E_x, and the resistive component E_R, can be balanced out in an appropriate adjustment of the potentiometers. Thus the "output" for a given rope can be indicated on a double pen recorder.

The rope speed during a test depends on the response of the recorder and the detector circuit. Furthermore, due to the

choice of a low-operating frequency (e.g., 80 Hz), the response of the detectors cannot be fast and Semmelink chooses a time-constant of 0.1 s. Thus if the shortest variation to be detected along the rope is 10 cm, the rope speed should not exceed 10 cm in 0.1 s (i.e., the rope speed should be less than 200 ft/min).

The coils, wound on a Bakelite former are 6 in long, with 5 in outer diameter, and 3-in inner diameter. The two magnetizing coils have 10 turns each. For a magnetizing current of 1 A, this gives an exciting field at the center of 0.43 Oe. The pickup or search coil also has ten turns. The whole assembly is hinged with spring-loaded contacts to maintain the electrical integrity needed when the two halves are clamped around the rope.

A number of interesting results have been obtained by Semmelink [4]. For example, a decrease of eddy currents causes an increase of flux with a resulting increase on the E_x trace and a corresponding decrease on the E_R trace. This often is associated with decreased contact between the strands. The reverse situation has also been found when there is increased contact between the strands. Such stressful situations occur at the crossover points where ropes pass from one layer to another on winding drums.

Slight corrosion in the rope leads to a deposit of nonconducting material between the wires, and to a reduction of eddy currents. This usually means a decrease of both E_x and E_R traces. Semmelink also indicates that internal corrosion appears to occur usually over relatively short lengths, often at intervals corresponding to the circumference of the drum.

External corrosion manifests itself in a large reduction of the E_x trace but only a small reduction in the E_R trace. Such corrosion can occur over long lengths of the rope (e.g., 1000 ft).

Semmelink [4] found that inadvertent dc magnetization of the rope (e.g., from the earth's magnetic field) could lead to violent transients in the E_x trace when the rope moves at high speed through the coil assembly. In one case, the rope had remained at rest for long periods with one section of the rope extending from the drum to the headgear sheave in a northerly direction.

More Recent Applications and Practices

Hiltbrunner gives a good description of what is known now as the dc magnetic-testing method [5]. This approach has been highly developed in Switzerland for the NDT of tramway wire ropes. Essentially, the method is based on imposing a strong axial magnetic field to the sample by either a solenoid coil and/or permanent magnet. The search coil is oriented in the radial direction and produces a voltage response only when there is some type of lateral nonuniformity.

Lang gives an extensive description of an ac testing device for wire ropes [6]. Although he does not acknowledge the fact, the concept, method, and operational procedure seem to be based on the earlier work of Semmelink [3], [4]. However, Lang uses only one single-turn transmitting coil with a coaxial search coil. Most of his data are shown for a frequency of 30 Hz. Lang found that in all cases of broken wires detected, the "X" trace shows a sharp reduction presumably due to a decrease in the axial magnetic flux. In a number of cases, sections of rope with apparent missing wires were found. This was believed to indicate a wire separation at a faulty spot weld. It is unfortunate that the numerous test results published by Lang are not accompanied by "ground truth" information on the actual state of the rope. He does show a few interesting comparisons between the measured breaking tensile strength and the "R" and "X" readings at 10 Hz, for locked-coil ropes. Such data however, were not provided for the 30 and 80 Hz tests on the stranded ropes.

Larsen *et al.* describes various devices for both dc and ac rope testing that are currently available [7]. They mention that the Rotesco device, as described by Lang [6], has been successful in 1970 in predicting tensile reductions of about 5 percent, although the extensive comparisons were not "quantitative."

Morgan [8] presents a general review of electromagnetic NDT methods applied to wire ropes. The discussion is entirely qualitative. He makes a number of recommendations for further development in Australia. Morgan and Symes [9] then describe the activities that led to the creation of a government-sponsored project at the University of New South Wales. They give a largely qualitative description of their current research on both methods of testing wire ropes. They also describe some tentative ideas about an ac device that is to operate at a frequency of 1 kHz. Surprisingly, they make no mention of many ac devices that hitherto have been used elsewhere. It is possible that they will find that 1 kHz is rather too high a frequency for effective penetration to the core of most mine-hoist ropes.

Stachurski [10] gives a very useful summary of the physical concepts employed in dc magnetic testing for flaws in wire ropes. A number of interpretative schemes are outlined in a qualitative manner. Also he uses prescribed forms of flaws, breaks, and cracks to calibrate the device. Much useful data on the design and implementation of the defectograph device are also given. It is evident that this Polish group has developed the dc magnetic technique to a high degree.

Egen and Benson [11] describe some interesting tests on a specially prepared rope with prescribed types of imperfections. There were seven types of faults: 1) splice; 2) two to three wires filed halfway through, over a length of about 0.5 in; 3) an added no. 18 AWG wire laid into groove of core; 4) spikes inserted into core and wires were spread apart; 5) three wires of 2 in length were removed from the core; 6) one wire in core was cut; and 7) a 2-in length of core was removed; all of these were done using three dc devices (the Polish MD-8 Defectoscope, the Swiss PMK-75 Kundig device, and the Canadian Rotesco device). None of these devices detected fault no. 6, and the Kundig device did not detect fault no. 2. Otherwise, all other faults were detected by all three instruments. The results indicated, that for the rope tested (i.e., $\frac{7}{8}$ in diameter, 6 X 25, FW, RLL, FC, XIPS), each instrument observed about the same magnetic-field variations. The very similar performance of these three instruments is probably a consequence of the basic similarity of the operating principle of each of these dc devices. It is a pity that the ac Rotesco device was not tested on the same rope.

Bergander [12] describes the Polish dc magnetic device for the NDT of wire ropes known as the Defectograph MD-8 that he developed with Stachurski [12]. The rope being tested moves through the permanent magnet which is magnetized to its saturation point. He claims that a 0.2-percent change of the rope cross section can be detected via a measurement of the external magnetic-leakage field. The EMF induced in the search coil can also be compensated for changes in the rope

speed. Using an empirical approach the probe-coil response is related to such parameters as the loss of cross section of the rope, the length over which the loss occurs, and the radial location of the internal flaw.

Early Theoretical Investigations

Hochschild [13] gives a review of papers by Förster [14]–[18] and presents some useful plots of the current density in conducting cylinders for ac excitation by a solenoidal coil. He points out that no matter how carefully the test-coil system is designed, small defects will go undetected unless, the response time of the instrument is less than the time taken from the defect to pass through the effective region of the coils. For example, a localized defect passing though a 0.03-in-wide differential test coil at 100 ft/min will not be detected unless the response extends upwards to at least 200 Hz. A common limitation on bandwidth is the ink-pen recording devices, whose frequency response seldom exceeds 200 Hz.

McClurg [19] also exhibits some of the results of Förster and colleagues in graphical form. In particular, he shows that the impedance variations of solenoids (i.e., feed-through coils) encircling cylindrical conductors that have surface and subsurface cracks. The empirical data used are from papers by Förster. McClurg discusses the application of these eddy-current techniques to metal-cutting operations where such things as uniformness of the hardness is desirable.

Graneau introduces the interesting concept that induced currents in a conductor, flowing along closed curves, can be represented by a number of filamentary circuits [20]. These currents and the energizing current can then be deduced in principle from a system of circuit equations with both self- and mutual inductances that are postulated from the physics of the problem. Using somewhat heuristic reasoning, Graneau obtains an expression for the current anywhere in the metallic object by infinite series of increasing powers of the energizing frequency. The coefficients are undetermined functions of the filament circuit resistance, and mutual inductances between the filaments. He concludes that there is a clear division between quantities depending on geometry and properties. As a consequence, the induced currents can be expressed as an explicit function of frequency. This is really quite strange since exact solutions of idealized forms such as layered cylinders with external dipole excitation do not exhibit this behavior [21]–[25].

Related Investigations in Geophysical Prospecting

Electromagnetic methods of NDT of solid conductors are closely akin to techniques that are now used in geophysical prospecting for metallic-ore bodies [21]–[34]. It is unfortunate that these two groups have had little interaction. This writer was involved in the theoretical developments in multifrequency and transient-electromagnetic methods in geophysical exploration. In fact, as long ago as 1950, it was proposed that conductivity and permeability of a spherical-ore body could be ascertained from its electromagnetic response in either the frequency or its time domain. A similar analysis was carried out for a cylindrical-ore body with a specified conductivity and permeability. The basic concept was that geometrical configuration of both the source and receiver coils with respect to the target could be arranged to have a negligible effect on the determination of ore body size, conductivity and permeability. The subject has advanced considerably since

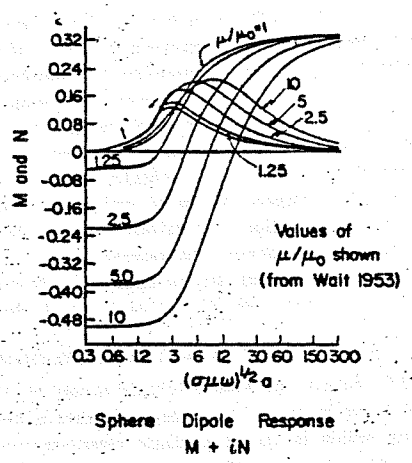


Fig. 7. Induced magnetic dipole for a conducting permeable sphere as a function of its conductivity σ, permeability μ, angular frequency ω, and radius a.

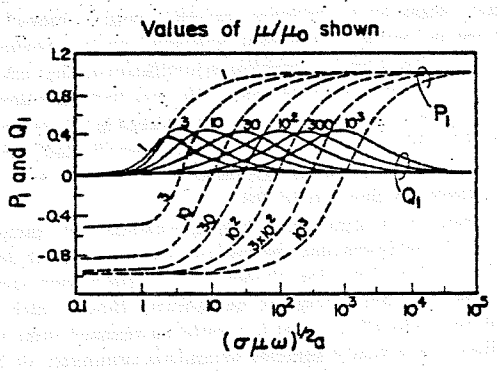


Fig. 8. Induced (line) magnetic dipole for a conducting permeable cylinder.

those "early days" and modern accounts are published regularly in *Geophysics*, the journal of the (U.S.) Society of Exploration Geophysicists, and *Geophysical Prospecting*, the journal of the European Society of Geophysical Exploration.

The work that is relevant to the electromagnetic probing of wire ropes is the analysis of a homogeneous conductive and permeable cylinder of infinite length. In an "early" paper [22], a general solution was given for the total fields produced when a line source or current-carrying cable was located parallel to the cylinder. An exact two-dimensional solution was obtained using a wave impedance approach. The low-frequency version of the general solution was expressed in a quasi-static form and numerical results for the induced dipole term were given. Some examples are shown in Figs. 7 and 8 for the induced magnetic-dipole responses of spheres and cylinders. In each case the ordinates are proportional to the induced-dipole moment. Strictly speaking, the monopole term should also be considered when dealing with cylinders

that are effectively infinite in length. This type of analysis was later extended to dipolar excitation of the infinite cylinder when again the monopole or azimuthally independent induced current was not considered in the numerical examples [22].

Further work on this subject was carried out by Hill and Wait [30], where more realistic situations were treated such as the excitation of a conductive cylinder of finite length by an external magnetic dipole where all significant induced monopole, dipole, and multipole contributions were retained in the calculations. The analytical and numerical techniques used in these papers would seem to be applicable in a quantitative analyses of electromagnetic NDT of solid conductors.

More Recent Analytical Studies

Vein [35] points out what is usually accepted—that the mutual impedance between two closed circuits is dependent on conducting solids in the immediate environments. He promotes the concept of transfer impedance but feels ill at ease in relating this to the reciprocity theorem for generally continuous media. With this motivation, he works through the analytical details of a number of classical problems such as the mutual impedance between coaxial-circular loops in the presence of planar, cylindrical, and spherical conductors. He assumes without really providing a justification, that azimuthal symmetry prevails in each case. No real harm is done, however, since no numerical results of any kind are provided. The derivations seem to be unnecessarily complicated, and even then, reliance is made on formulas quoted from exercises in W. R. Smythe's classic text [36].

Burrows, in a significant thesis, exploits the reciprocity theorem in eddy-current testing and the subsequent development of a flaw-detection theory [37]. He is very quick to recognize the limitations of quasi-static theory such as assumed by Vein [35]. But it should be stressed immediately that Burrows actually assumes azimuthal symmetry of his detection coils even though the "flaws" may be asymmetrical. This is a valid procedure but it appears that some fundamental information is lost when both the source and the probe coil fully encircle the cylindrical sample. Burrows represents internal flaws in terms of induced electric and magnetic dipoles, that in turn produce the secondary influence. He also provides some very useful tabulations of the infinite integrals that describe the internal fields within both solid cylindrical and tubular samples of circular cross sections for azimuthally symmetric excitation. These same integrals can be used to predict the response in a corresponding azimuthally symmetric detector coil due to an internal (small) flaw. Actually, this same approach has been followed up very recently by Hill and Wait who did not restrict the results to azimuthal symmetry of the probe coil [38].

Dodd *et al.* [39] have obtained integral solutions for the vector potential produced by a circular coil for a number of different geometrical configurations. The solutions are limited to axial symmetry. In calculating the exciting fields of a rectangular cross section circular coil, they assume that a straightforward superposition of current over the cross section is valid. This is a quasi-static assumption that probably needs to be investigated, particularly when the coil of finite width and length encircles a highly conducting cylinder.

Dodd *et al.* quote Burrows' formulation [37] for deducing the secondary-induced voltages due to a defect or flaw in an adjacent conductor. Here they write down a formula for the defect-produced voltage, induced in coil no. 2, by a current in coil no. 1 in terms of the electric and magnetic scattering matrices for an electrically small defect.

In the same paper, Dodd *et al.* give explicit solutions in integral form for the rectangular cross sectional coil located over a two-layer planar conductor. Actually, the form of these solutions are very similar to earlier investigations of electromagnetic induction in layered models of the earth's crust. The NDT community is apparently not aware of this extensive literature. An example is the book by Keller and Frischknecht [40] that reviews the current status of such problems at least up to 1965. Of course, Dodd *et al.* give the explicit form of the fields of a circular coil with rectangular cross section, while the geophysicists restrict their attention to small loops. Dodd *et al.* also give solutions for various combinations of pickup coils and the corresponding secondary effects due to embedded defects that can be characterized by the polarizability matrices mentioned above.

Cheng *et al.* [41] have presented a general formulation for the time-harmonic eddy currents, produced by a circular coil of rectangular cross section, for a underlying planar conductor of any number of layers. The integral solutions obtained in a straightforward fashion yield algebraically complicated results. A number of these results could have been obtained by use impedance methods based on analogies with transmission-line theory (see for example [42] and [43]).

Dodd *et al.* [44] give a formal vector potential solution to a coil coaxial with any number of cylindrical conductors. While they state the derivation is quite general, the solution is only carried through for complete symmetry about the common axis.

Dodd and Deeds [45] give the same solutions for a uniform coil with uniform ac current excitation over a two-layer planar conductor. They then repeat the solution for the coil encircling a two-layer cylindrical conductor of infinite length. A single numerical example is given for the normalized impedance of the coil as over the two-layer planar structure that exhibits the effect of the thickness of the upper layer.

Kahn *et al.* [46] present an interesting analysis of how eddy currents in a solid conductor are diverted around a surface crack. One of the basic assumptions is that the magnetic field tangent to the surface is a constant even in the presence of the crack. They also present solutions for diffraction by a semi-infinite crack (i.e., a *half*-plane) in an otherwise infinite medium. Neither of these solutions are "rigorous" as claimed by the authors, but the results do provide considerable insight into how defects, of other than infinitesimal size, will modify to external fields. Kahn and Spal [47] have also presented some results for the calculations of eddy currents in a long cylinder with a radial crack at the surface. Details of the analytical methods are not yet available but presumably the approach is similar to that used in treating the surface crack in the planar conductor. It is appropriate to call attention to the close similarity of such problems to earlier theoretical studies in geophysics, where one is interested in the perturbation of time-varying geomagnetic fields near coastlines [48] and other laterally varying features in the earth's crust [49].

An Alternative Formulation for Solenoid Excitation

As has been indicated, a common method of NDT of metal rods and tubes is to induce eddy currents by means of an encircling solenoid carrying an alternating current. The impedance of the solenoid is related to the cross sectional area

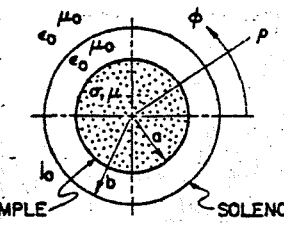


Fig. 9. Cross sectional view of cylindrical sample located centrally.

and the electrical properties of the sample. A formula for this impedance was obtained by Förster and Stambke [16] on the assumption that end effects could be ignored. Also they assumed that the cylindrical sample was centrally located within the solenoid. The same derivation was essentially repeated by Hochschild [13] and Libby [51].

A feature of the Förster-Stambke derivation is that the effect of the air gap is introduced in a somewhat heuristic fashion wherein the field in this concentric region is assumed to be the same as the one for the empty solenoid. We feel it is worthwhile to provide a more general derivation of the impedance formula. We also show it applies to the case of a nonconcentric air gap. Finally, we mention the relevance of the current analysis to the dual problem where the cylindrical sample is excited by a toroidal coil.

To simplify the discussion, we consider first the concentric air gap model with a homogeneous cylindrical sample of radius a, with conductivity σ, and magnetic permeability μ. The situation is indicated in Fig. 9 where the solenoid of radius b encloses the sample, both of which are assumed to be infinite in length. Our objective is to find an expression for the impedance of the solenoid per unit length since this is the basis of the NDT eddy-current methods that are commonly used.

In terms of cylindrical coordinates (ρ, ϕ, z), the only component of the magnetic field is H_z, since the exciting current in the solenoid is uniform in both the axial and azimuthal direction. Within the sample, H_z satisfies the Helmholtz equation

$$(\nabla^2 - \gamma^2) H_z = 0 \tag{1}$$

where $\gamma^2 = i\sigma\mu\omega$, and where we have adopted a time factor $\exp(i\omega t)$. Here, ω is the angular frequency that is sufficiently low so displacement currents in the sample can be neglected. If not, we merely replace σ by $\sigma + i\epsilon\omega$, where ϵ is the permittivity. Also, it goes without saying that the field amplitude is sufficiently small that nonlinear effects can be ignored.

For the highly idealized situation described, we can immediately write [52]

$$H_z = AI_0(\gamma\rho) \tag{2}$$

for $\rho < a$, where I_0 is a modified Bessel function of argument $\gamma\rho$, and where A is a constant. From Maxwell's equations the azimuthal component of the electric field is

$$E_\phi = -(1/\sigma)\,\partial H_z/\partial\rho = -A(\gamma/\sigma)\,I_1(\gamma\rho) \tag{3}$$

also for $\rho < a$. Now we can immediately form an expression for the "impedance" Z_c of the cylinder

$$Z_c = [-E_\phi/H_z]_{\rho=a} = \eta I_1(\gamma a)/I_0(\gamma a) \tag{4}$$

where, $\eta = \gamma/\sigma = (i\mu\omega/\sigma)^{1/2}$ is the intrinsic or wave impedance of the sample material.

Now, for the air gap region $a < \rho < b$, we write corresponding field expressions

$$H_{0z} = BI_0(\gamma_0\rho) + CK_0(\gamma_0\rho) \tag{5}$$

$$E_{0\phi} = -B\eta_0 I_1(\gamma_0\rho) + C\eta_0 K_1(\gamma_0\rho) \tag{6}$$

where B and C are constants $\eta_0 = \gamma_0/(i\epsilon_0\omega) = (\mu_0/\epsilon_0)^{1/2} \cong 120\pi$ in terms of the permittivity ϵ_0, and permeability μ_0, of the air region. Here and above, the Bessel function identities $\partial I_0(x)/\partial x = I_1(x)$ and $\partial K_0(x)/\partial x = -K_1(x)$ have been employed.

Compatible with the requirement that tangential fields must be continuous at $\rho = a$ we can write

$$[E_{0\phi} + Z_c H_{0z}]_{\rho=a} = 0. \tag{7}$$

This immediately tells us that

$$\frac{C}{B} = \frac{\eta_0 I_1(\gamma_0 a) - Z_c I_0(\gamma_0 a)}{\eta_0 K_1(\gamma_0 a) + Z_c K_0(\gamma_0 a)}. \tag{8}$$

In the external region $\rho > b$, the field expressions must clearly have the form:

$$H_{0z} = DK_0(\gamma_0\rho) \tag{9}$$

$$E_{0\phi} = D\eta_0 K_1(\gamma_0\rho) \tag{10}$$

where D is another constant.

Now the solenoid current is idealized as a continuous-current distribution j_0 amperes per meter in the azimuthal direction defined such that

$$\lim_{\Delta\to 0} \begin{cases} H_{0z}(\rho = b + \Delta) - H_{0z}(\rho = b - \Delta) = -j_0 & (11) \\ E_{0\phi}(\rho = b + \Delta) - E_{0\phi}(\rho = b - \Delta) = 0. & (12) \end{cases}$$

Application of these conditions immediately leads to

$$D = C - I_1(\gamma_0 b)\,B/K_1(\gamma_0 b) \tag{13}$$

and

$$B = j_0\gamma_0 b K_1(\gamma_0 b). \tag{14}$$

Among other things, this tells us that the magnetic field external to the solenoid (i.e., $\rho > b$) has the form

$$H_{0z} = \{-B[I_1(\gamma_0 b)/K_1(\gamma_0 b)] + C\}\,K_0(\gamma_0\rho). \tag{15}$$

The quantity of immediate interest is the impedance Z of the solenoid itself. Clearly, within the limits of our basic assumptions,

$$Z = \text{const.} \times E_{0\phi}(\rho = b)/j_0. \tag{16}$$

The corresponding impedance of the empty solenoid is denoted Z_0. Thus it follows that

$$\frac{Z}{Z_0} = 1 - \frac{C}{B}\frac{K_1(\gamma_0 b)}{I_1(\gamma_0 b)} \tag{17}$$

which is explicit since C/B is given by (8).

We now can simplify the impedance ratio formula if we invoke the small argument approximations for Bessel functions of order $\gamma_0 a$ and $\gamma_0 b$. That is, we use $I_0(x) \simeq 1$, $I_1(x) \simeq x/2$, $K_0(x) \simeq -\log x$, and $K_1(x) \simeq 1/x$. This exercise leads to

$$\frac{Z}{Z_0} \cong \left[1 - \frac{a^2}{b^2} + \frac{\mu}{\mu_0}\frac{a^2}{b^2}\frac{2}{\gamma a}\frac{I_1(\gamma a)}{I_0(\gamma a)}\right] = \frac{R + iX}{Z_0} \tag{18}$$

where no restriction has been placed on the magnitude of γa. Here R and X denote the resistance and reactance, respectively.

The formula for Z/Z_0 given by (18) is in agreement with Förster and Stambke [16] (if one remembers they used the old German designations J_0 and J_1 for modified Bessel functions). Förster and Stambke [16], Hochschild [13], and Libby [51] present extensive numerical data for this quasi-static approximation to Z/Z_0 in Argand diagrams in the complex plane for various values of $|\gamma a|$ and μ/μ_0. Two examples, using dimensionless parameters, are shown in Figs. 10 and 11 when the ordinates and abscissas are normalized by X_0 which is the reactance of the empty solenoid. That is, we assume $Z_0 \simeq iX_0$ corresponding to negligible ohmic losses in the solenoid itself. The real parameter α is defined by $\alpha = |\gamma a| \exp(-i\pi/4) = (\sigma\mu\omega)^{1/2}a$. In Fig. 10, the sample radius b is assumed to be the same as the sample radius a (i.e., no air gap). Different values of the magnetic permeability are shown. Not surprisingly, when α is small, R vanishes and X/X_0 tends to μ/μ_0. However, in general, the eddy currents have the effect of reducing X/X_0, which is the effective flux, and of introducing a resistive portion R/X_0. In Fig. 11, the relative permeability of the sample $\mu/\mu_0 = 1$ but the filling factor a^2/b^2 assumes different values. The results indicate that the presence of the air gap reduces the sensitivity of the device for probing the conductivity but the effect is predictable.

Actually, if α is sufficiently small (i.e., $|\gamma a| \ll 1$), equation (18) reduces to

$$Z/Z_0 \simeq X/X_0 \simeq 1 + (a^2/b^2)[\mu/\mu_0 - 1] \qquad (19)$$

which is consistent with the curves in Figs. 10 and 11. In this dc limit the results only depend on the magnetic permeability of the sample.

The formal extension of the theory to the case where the exciting solenoid is no longer concentric with the cylindrical sample can also be dealt with. The situation is indicated in Fig. 12. As before, cylindrical coordinates (ρ, ϕ, z) are chosen coaxial with the sample. But now, the shifted coordinates (ρ', ϕ', z) are chosen to be coaxial with the exciting solenoid. The shift is ρ_0 as indicated in Fig. 12 where we do impose the rather obvious physical restriction that $b > \rho_0 + a$. We may show that the field in the nonconcentric air gap has the form [50]

$$H_{0z} = BI_0(\gamma_0\rho') + \sum_{m=-\infty}^{+\infty} C_m \sum_{n=-\infty}^{+\infty} K_{m+n}(\gamma_0\rho') I_n \cdot (\gamma_0\rho_0)(-1)^n \exp(-i(n+m)\phi'). \qquad (20)$$

This is valid in the nonconcentric air gap region (i.e., $\rho > a$ and $\rho' < b$). The needed azimuthal component is obtained from

$$E_{0\phi'} = -\eta_0 \partial H_{0z}/\partial(\gamma_0\rho'). \qquad (21)$$

The relevant quantity for the impedance calculation is the "average" field $E_{0\phi'}$ at the solenoid. Then it follows that the impedance Z per unit length of the solenoid with the sample divided by the impedance Z_0 of the empty solenoid is given by

$$\frac{Z}{Z_0} = 1 - \frac{K_1(\gamma_0 b)}{I_1(\gamma_0 b)} \sum_{m=0}^{\infty} e_m \frac{C_m}{B}(-1)^m I_m(\gamma_0\rho_0) \qquad (22)$$

where $e_0 = 1$ and $e_m = 2$ for $m \neq 0$, and where C_m/B is known [50]. Not surprisingly, (22) reduces to (17) for the centrally located sample, i.e., $I_m(\gamma_0\rho_0) = 0$ for $\rho_0 \to 0$ when $m \neq 0$.

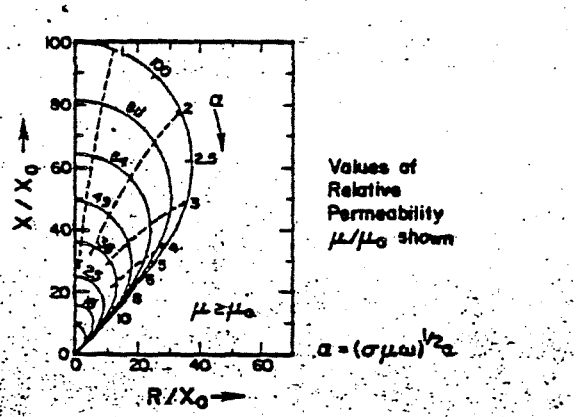


Fig. 10. Argand plot of the impedance $Z = R + iX$ normalized to the reactance X_0 of the empty solenoid, for $a = b$.

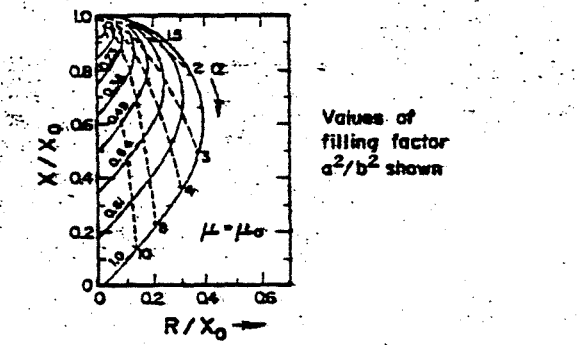


Fig. 11. Argand plot of the impedance $Z = R + iX$ normalized to the reactance X_0 of the empty solenoid, for $\mu = \mu_0$.

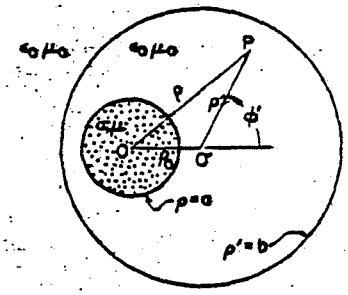


Fig. 12. Cross section view of the nonconcentrically located sample.

We again may invoke the small argument approximations for Bessel functions of order $\gamma_0 a$, $\gamma_0 b$, and $\gamma_0\rho_0$. Lo and behold, these show that Z/Z_0 reduces again to the formula given by (18)! This confirms the conjecture of Förster and Stambke [16] who seemed to be gifted with keen physical insight into such problems. Of course, we do not expect the result to hold in any sense when the dimensions of the solenoid become comparable with the free-space wavelength. In that case, many other complications arise such as the assumed uniformity of the solenoid current.

The Dual Problem

There is an extremely interesting dual to the problem we have discussed. That is, rather than exciting the cylindrical sample with an *azimuthal electric current*, we employ an

azimuthal magnetic current. This is an idealized representation for a thin toroidal coil, but again, it effectively is of infinite length in the z or axial direction. The assumed source discontinuity is now in the electric field at $\rho = b$ which has only a z component. The much more complicated case of the toroidal coil of finite axial extent was analyzed recently [53].

Under the present assumption of axial uniformity, the admittance Y per unit length of the toroid is the dual of the impedance Z of the solenoid discussed above. Thus all the earlier equations apply if we make the following transformations: $i\mu\omega \to \sigma$, $\mu_0 \to \epsilon_0$, $\eta \to \eta^{-1}$, $\eta_0 \to \eta_0^{-1}$, $H_z \to E_z$, $E_\phi \to -H_\phi$, $H_{0z} \to E_{0z}$, and $E_{0\phi} \to -H_{0\phi}$. Then, the dual of (18) is the ratio of the admittance Y of the toroidal coil with the sample to the admittance Y_0 without the sample. It is written explicitly

$$\frac{Y}{Y_0} = \left[1 - \frac{a^2}{b^2} + \frac{\sigma}{i\epsilon_0\omega}\frac{a^2}{b^2}\frac{2}{\gamma a}\frac{I_1(\gamma a)}{I_0(\gamma a)}\right] \tag{23}$$

for the case where $|\gamma_0 b| \ll 1$. That is, the radius of the toroidal coil should be much smaller than the free-space wavelength. Also, in full analogy to the earlier discussion, the quasi-state result holds for any location of the cylindrical sample within the toroid. Furthermore, in the low-frequency limit where $|\gamma a| = \alpha \ll 1$, we see that

$$Y \simeq Y_0\,[1 + (a^2/b^2)\,[(\sigma/i\epsilon_0\omega) - 1]] \tag{24}$$

which depends only on the conductivity of the sample. Thus this type of excitation should be preferred with probing the effective conductivity in the axial direction in the sample.

The Prolate Spheroidal Void Model of Hill and Wait

As we have indicated, an appropriate source for excitation of axial-electric currents is a toroidal coil which encircles the rope, and a magnetic-current model for the toroidal source coil has been analyzed [53]. Expressions for both the interior and exterior fields were derived for a homogeneous wire rope. As we shall outline here, the presence of a small slender void within the rope can be treated. Such a void can be considered a model for a broken strand. The void is also allowed to be oriented at any arbitrary angle to the rope axis to account for the winding geometry of the wire rope. The induced electric and magnetic dipole moments are computed from the primary fields and the electric and magnetic polarizabilities of the void. We then obtain expressions for the external fields of electric and magnetic dipoles of arbitrary orientation. Of course, it is these external fields which are the observable quantities in any electromagnetic NDT method. The particular expressions, derived for the external fields of internal electric and magnetic dipoles, should be useful in future analyses of other types of small imperfections in wire ropes. Of course in such cases, the electric and magnetic polarizabilities would be different.

In a previous analysis [53], we analyzed an azimuthal current sheet source which encircled the rope. The current sheet was allowed to have arbitrary width in the z or axial direction and arbitrary azimuthal extent. This source results in fairly complicated expressions for the electric and magnetic fields. Since in this paper we are primarily concerned with the fields scattered by the void, we take the simpler special case for the source shown in Fig. 13. Specifically, a magnetic-current ring of strength K is located at a radius b in the plane $z = 0$. This is

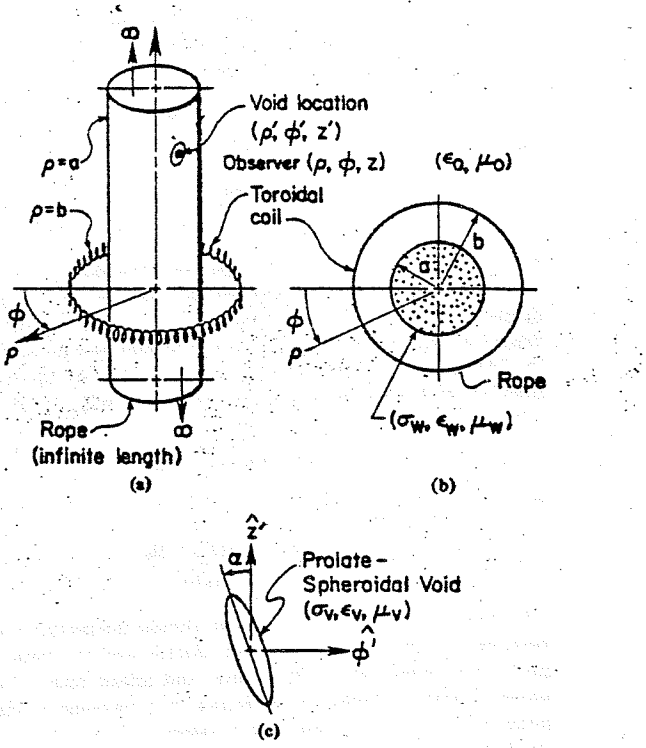


Fig. 13. Thin toroidal coil surrounding a metal rope of infinite length, (a) perspective view, (b) top view, (c) prolate spheroidal void.

a model for a thin toroidal coil which completely encircles the rope. The rope is assumed to be infinitely long and has radius a. It has conductivity σ_w, permittivity ϵ_w, and permeability μ_w. The surrounding free-space has permittivity ϵ_0, and permeability μ_0. For now, we defer discussion of the void properties and consider only the homogeneous rope.

Because of the symmetry of the source and the rope, the fields are transverse magnetic (TM) and independent of ϕ. The magnetic field has only a nonzero azimuthal component H_ϕ^{pr}, and the electric field has only nonzero axial and radial components E_z^{pr} and E_ρ^{pr}. The superscript pr denotes the fields in the absence of the void. These primary fields are derived elsewhere [53], and the explicit forms both inside and outside the rope are given in a recent report [38, Appendix A]. We note that E_ρ^{pr} and H_ϕ^{pr} are zero for $\rho = 0$. On the other hand, E_z^{pr} is nearly independent of ρ inside the rope for sufficiently low frequencies.

We now select a thin prolate spheroid of conductivity σ_v, permittivity ϵ_v, and permeability μ_v, in order to model a broken strand. The prolate-spheroidal shape is a convenient one because its electric and magnetic polarizabilities are known. However, we would not expect a significant difference for a thin circular cylinder of the same length and volume. To account for the winding geometry of the rope, we allow a rotation of the major axis of the spheroid about the ρ' axis by an angle α. Thus the major axis is oriented at an angle α to the unit vector $\hat{z}'$ and an angle $\pi/2 + \alpha$ to the unit vector $\hat{\phi}'$ as indicated in Fig. 1(c).

Since the void has a contrast in both the electric and magnetic properties, both electric and magnetic dipole moments

will be induced [36]. The electric polarizabilities for the incident electric field applied along the major axis α^e_{maj}, or along the minor axis α^e_{min}, are given by

$$\alpha^e_{maj} = -V(\sigma_w - \sigma_v) \tag{25}$$

and

$$\alpha^e_{min} = \frac{-2V(\sigma_w - \sigma_v)}{1 + \sigma_v/\sigma_w}. \tag{26}$$

where V is the volume of the thin prolate spheroid. Since we anticipate the use of very-low frequencies, we have neglected displacement currents. To include them, σ_w would be replaced by $\sigma_w + i\omega\epsilon_w$, and σ_v would be replaced by $\sigma_v + i\omega\epsilon_v$ in (25) and (26). The magnetic polarizabilities for the incident magnetic field applied along the major axis α^m_{maj}, or along the minor axis α^m_{min}, are similarly given by

$$\alpha^m_{maj} = -Vi\omega(\mu_w - \mu_v) \tag{27}$$

and

$$\alpha^m_{min} = \frac{-2Vi\omega(\mu_w - \mu_v)}{1 + \mu_v/\mu_w}. \tag{28}$$

In order to compute the induced dipole moments, it is first necessary to resolve the incident electric and magnetic fields into components along the major and minor axes. The resultant induced dipole moments can then be resolved into the more convenient ρ, ϕ, and z components. When this is done, the induced electric dipole moments are found to be

$$(Idz)_z = E^{pr}_z(\alpha^e_{maj}\cos^2\alpha + \alpha^e_{min}\sin^2\alpha) \tag{29}$$

$$(Idz)_\phi = E^{pr}_z(\alpha^e_{min} - \alpha^e_{maj})\sin\alpha\cos\alpha \tag{30}$$

$$(Idz)_\rho = E^{pr}_\rho\alpha^e_{min}. \tag{31}$$

In (29)–(31), the primary electric-field components E^{pr}_z and E^{pr}_ρ are evaluated at ρ', ϕ', z'. Similarly, the induced magnetic dipole moments are found to be

$$(Kdl)_z = H^{pr}_\phi(\alpha^m_{min} - \alpha^m_{maj})\sin\alpha\cos\alpha \tag{32}$$

$$(Kdl)_\phi = H^{pr}_\phi(\alpha^m_{min}\cos^2\alpha + \alpha^m_{maj}\sin^2\alpha) \tag{33}$$

$$(Kdl)_\rho = 0. \tag{34}$$

Note that the units of the induced electric dipole moments in (29)–(31) are ampere-meters, and the units of the induced magnetic dipole moments in (32) through (34) are volt-meters. These induced dipole moments are the sources of the scattered field.

The scattered field external to the rope is the observable quantity in any NDT system. Since we anticipate the use of coils for sensors, we have considered the scattered magnetic field components $H^{sc}_\rho(\rho, \phi, z)$, $H^{sc}_\phi(\rho, \phi, z)$, and $H^{sc}_z(\rho, \phi, z)$ [38]. Each of these components can be written as a superposition of the contributions from each of the six induced dipole sources. (Actually there are only five nonzero sources, since $(Kdl)_\rho$ is zero for the specific configuration considered here). Explicit expressions for the three scattered-field components are given elsewhere [38].

The quantities of most interest in NDT are the external ($\rho > a$) magnetic-field components which are observed with the sensing coils. The primary magnetic field has only a ϕ component H^{pr}_ϕ but the scattered magnetic field has all three components. For the numerical results, the following parametric values remain fixed: $a = 1$ cm, $\sigma_w = 1.1 \times 10^6$ mho/m, $\mu_w = 200\,\mu_0$, $b = 2$ cm, frequency = 10 Hz, $\rho = 2$ cm, $\sigma_v = 0$, and $\mu_v = \mu_0$. For this low frequency, the conduction currents dominate, and the permittivities ϵ_w and ϵ_v are unimportant. The above values of σ_w and μ_w are roughly representative of stainless steel, but the permeability of steel is quite variable [54]. For the above parameters, the radius a is approximately one-skin depth. For convenience here, we also choose $z = z' = 0$ and $\alpha' = 0$.

In Figs. 14, 15, and 16, we show the magnitude of the scattered magnetic-field components normalized by VH^{pr}_ϕ as a function of ϕ. The reason for showing the ϕ dependence is that, although the primary field is independent of ϕ, the scattered field varies considerably in ϕ. This variation might dictate the use of multiple-sensing coils spaced in azimuth around

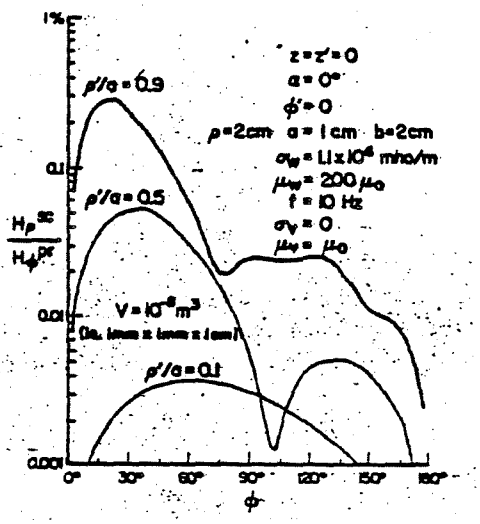


Fig. 14. The normalized magnitude of the scattered radial magnetic field for various void locations ρ'.

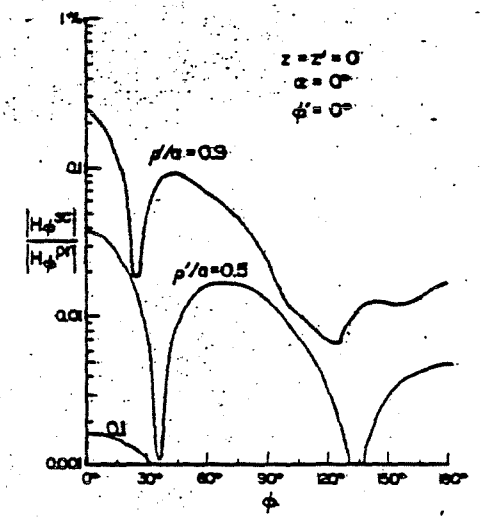


Fig. 15. The normalized magnitude of the scattered azimuthal magnetic field for various void locations ρ'.

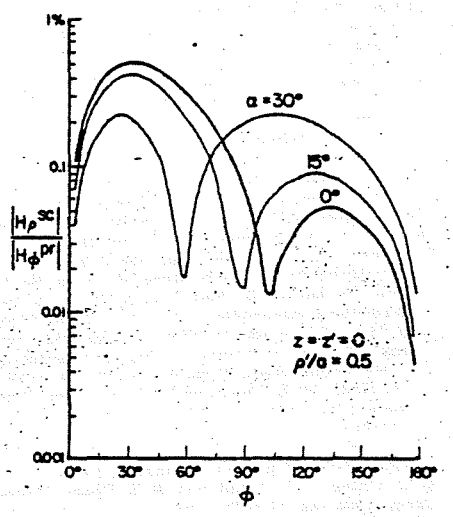


Fig. 16. The normalized magnitude of the scattered radial magnetic field for various void orientations α.

the rope. The curves are normalized by the primary field because the anomalous scattered field is measured in the presence of the primary field and their ratio is thus of interest. We also normalize the results to the volume V of the void in order to make the curves more general. However, a typical value for V might be on the order of 10^{-8} m^3 (=1 cm × 1 mm × 1 mm). As indicated in Figs. 14 and 15, H_ρ^{sc} and H_ϕ^{sc} are of approximately the same level, but H_ρ^{sc} is odd in ϕ while H_ϕ^{sc} is even. We also may note the decrease in scattered field as the void is moved from the outer region ($\rho'/a = 0.9$) toward the center ($\rho'/a = 0.1$) of the rope. Because $\alpha = 0°$ in Figs. 14 and 15, only the axial and radial electric dipole moments and the azimuthal magnetic dipole are excited. Also, the radial electric dipole is very small because its exciting field E_ρ^{pr} is small. The calculations reveal that $(Ids)_z$ and $(Kdl)_\phi$ contribute approximately equally to the scattered field. In Fig. 16, we have $z = z' = 0$ and $\rho'/a = 0.5$, but we allow α to vary from 0° to 30°. Nonzero values of α allow two additional dipole moments (the azimuthal-electric and the axial-magnetic dipoles) to be induced. The result is a decrease in the level of H_ϕ^{sc} and H_ρ^{sc} and an increase in the level of H_z^{sc}. These new results are elsewhere [38].

The phase of the scattered field was also computed, but was found to be of less interest. Also, the individual dipole contributions were computed, and they are of individual interest since they will be excited differently for other sources or other void configurations.

Although we have generated numerical results for the specific case of a thin prolate spheroidal void, the formulation given here actually yields the external fields for arbitrary induced electric and magnetic dipole moments. Thus the formulation is useful for any type of rope imperfection that can be characterized by induced electric and magnetic dipole moments. This requires only that the rope imperfection be small in terms of the rope radius and the rope skin depth. Larger imperfections should have a similar qualitative behavior, but could probably be rigorously analyzed only by solving an integral equation for the fields in the imperfection. Also, it would be a simple matter to perform similar calculations for a solenoidal coil of the type used in present NDT systems. The scattered field calculation remains unchanged, but the primary field would be $TE(E_z^{pr} = 0)$ rather than $TM(H_z^{pr} = 0)$. Some calculations for this case have been carried out by Burrows [37] for the special case, where both exciting and sensing coils are coaxial with the tubular specimen.

Concluding Remarks

We have attempted to give an overall view of NDT electromagnetic methods. As indicated, the investigations have proceeded along different lines. The very practical and perhaps most useful work to date has been empirical in nature. There has been no attempt made to deduce the magnitude of the secondary fields due to the internal flaw; instead a large number of actual ropes are tested and the results presented. On the other hand, the analytical approaches have considered only highly idealized situations. Nevertheless, some important principles are disclosed that may have an important bearing on operating procedures. For example, the toroidal coil exciter could be utilized in practical schemes in conjunction with localized sensor coils that can characterize the three-dimensional field configuration in an adequate fashion.

A basic theoretical aspect of the NDT problem that we have not really addressed is to account for the anisotropic nature of the effective conductivity and permeability of the wire rope. The spiral construction of stranded wire ropes sometimes described as a "twisted bunch of spaghetti" defies any simple microscopic description. However, from a macroscopic point, we might describe the effective anisotropy by conductivity and permeability tensors. Some preliminary efforts in this direction have begun [55]. It is obvious that much remains to be done.

Acknowledgment

The assistance of Ms. Lana Hope in preparing this report is much appreciated. He also thanks Dr. David A. Hill who provided the results shown in Figs. 14, 15, and 16.

References

[1] T. F. Wall, "Electromagnetic testing for mechanical flaws in steel wire ropes," *J. Inst. Elec. Eng.*, vol. 67, pp. 899–911, 1929.
[2] T. F. Wall and C. H. Hainsworth, "The penetration of alternating magnetic flux in wire ropes," *J. Inst. Elec. Eng.*, vol. 71, pp. 374–379, 1932.
[3] A. Semmelink, "Electromagnetic testing of winding ropes," *Trans. South African Inst. Elec. Eng.*, vol. 43, no. 5, pp. 113–129, May 1953.
[4] ——, "Electromagnetic testing of winding ropes," *Trans. South African Inst. Elec. Eng.*, vol. 47, no. 8, pp. 206–244, Aug. 1956.
[5] R. H. Hiltbrunner, "Le Contrôle Magnétique des câbles avec le défectoscope integra," *Economie Tech. Transports*, no. 119, June 1957.
[6] J. G. Lang, "The principle and practice of electromagnetic wire rope testing," *Can. Mining and Metallurgical Bull.*, pp. 415–424, Apr. 1969.
[7] C. H. Larsen, P. A. Egen, R. D. Jones, and H. A. Cross, "Wire rope applications and practices associated with underground coal mining in the U.S.," Final Rep. (from Battelle Laboratories) on U.S. Bureau of Mines Contract No. H0101741, June 22, 1971.
[8] J. P. Morgan, "Investigations on wire ropes in mine hoisting system," *Proc. Australian Inst. Min. Metal*, no. 215, pp. 59–85, 1965.
[9] J. P. Morgan and H. E. J. Symes, "Non-destructive testing of wire ropes," Australian Mineral Industries Research Assoc. Ltd., Bulletin No. 6, (National Library of Australia Card No. ISSN 0313-6973), 1976.
[10] J. Stachurski, "Magnetic testing of steel wire ropes," Rep. from Lab. for Testing Wire Ropes, Univ. of Mining and Metallurgy, Cracow, Poland, 1976.
[11] R. A. Egen and D. K. Benson, "Wire rope retirement criteria and procedures," Progr. Rep. 16 (from Midwest Research Inst., 425 Volker Blvd., Kansas City, MO 64110) on U.S. Bureau of Mines Contract No. J0155187, Nov. 10, 1976.

[12] M. J. Bergander, "Principles of magnetic defectoscopy of steel ropes," presented at the 47th Annu. Convention of the Wire Association, Boston, MA, Nov. 1977.
[13] H. Hochschild, "Electromagnetic methods of testing metals," in *Progress in Non-Destructive Testing*, vol. 1. New York: Macmillan, 1959, pp. 59–109.
[14] F. Förster, "Theoretical and experimental foundation of non-destructive testing using eddy currents I. Test coil methods," *Z. Metallkunde*, vol. 43, no. 5, pp. 163–171, 1952 (in German).
[15] F. Förster and H. Breitfeld, "Non-destructive testing using eddy current methods II. Practical results and industrial applications of methods using test coils," *Z. Metallkunde*, vol. 43, no. 5, pp. 172–180, 1952 (in German).
[16] F. Förster and K. Stambke, "Theoretical and experimental foundation of non-destructive testing using eddy currents III. Quantitative methods of non-destructive testing using test object encircling coils," *Z. Metallkunde*, vol. 45, no. 4, pp. 166–179, 1954 (in German).
[17] F. Förster, "Theoretical and experimental foundation of non-destructive testing using eddy currents IV. Practical apparatus for non-destructive testing using encircling coils for eddy currents," *Z. Metallkunde*, vol. 45, no. 4, pp. 180–187, 1954 (in German).
[18] F. Förster and H. Breitfeld, "Theoretical and experimental foundation of non-destructive testing using eddy currents V. Quantitative testing for cracks in metallic objects using test object encircling coils," *Z. Metallkunde*, vol. 45, no. 4, pp. 188–199, 1954 (in German).
[19] G. O. McClure, "Non destructive eddy current testing," *IRE Trans.*, vol. IE-11, no. 1, pp. 20–26, 1959.
[20] P. Grasseau, "Coupled circuit theory for electromagnetic testing," *Progress in Non-Destructive Testing*, E. G. Stanford and J. H. Fearson, Eds., vol. 2, pp. 163–188, 1961.
[21] J. R. Wait, "A conducting sphere in a time varying magnetic field," *Geophysics*, vol. XVI, pp. 666–672, Oct. 1951.
[22] ——, "The cylindrical ore body in the presence of a cable carrying an oscillating current," *Geophysics*, vol. XVII, pp. 378–386, Apr. 1952. (In eqs. (13), replace μ_2/μ_1 by $n\mu_2/\mu_1$ both in the numerator and denominator, similarly, in (14), replace $(k \pm n)$ by $n(k \pm 1)$. Also, the summations in (66), (67), etc. should include the $n = 0$ terms.)
[23] ——, "A conducting permeable sphere in the presence of a coil carrying an oscillating current," *Can. J. Phys.*, vol. 31, pp. 670–678, May 1953.
[24] ——, "Some solutions for electromagnetic problems involving spheroidal, spherical and cylindrical bodies," *J. Res. Nat. Bur. Stand.*, vol. 64B, pp. 15–32, Jan./Mar. 1960.
[25] S. H. Ward and D. C. Fraser, "A conducting permeable sphere and cylinder in an elliptically polarized alternating magnetic field," *J. Geomagn. Geoelec.*, vol. 18, no. 1, pp. 23–41, 1966.
[26] S. H. Ward, "The electromagnetic method," *Mining Geophysics*, vol. II, pp. 224–372, Oct. 1967. [Ward's quasi-static solution, Sec. 7a, does not include the effect of the induced monopole or azimuthally invariant currents, i.e., the $n = 0$ terms are missed.]
[27] S. K. Singh, "Transient electromagnetic response of a conducting infinite cylinder embedded in a conducting medium," *Geofis. Internacional (Mexico)*, vol. 12, no. 1, pp. 7–21, 1972.
[28] ——, "Transient electromagnetic response of a conducting cylinder in a conducting medium: numerical results," *Geofis. Internacional (Mexico)*, vol. 12, no. 4, pp. 267–280, 1972.
[29] Von J. Meyer, "Über die Richtungsveränderlichkeit des geomagnetischen Induktionspfeiles bei endlicher Leitfähigkeit," *Z. für Geophysik*, vol. 38, pp. 195–221, 1968.
[30] D. A. Hill and J. R. Wait, "Electromagnetic response of a conducting cylinder of finite length," *Geofis. Internacional (Mexico)*, vol. 12, no. 4, pp. 245–266, 1972.
[31] J. R. Wait, "On the electromagnetic induction in elongated ore bodies," *Geophysics*, vol. 38, no. 5, pp. 984–985, 1973. Correction: vol. 39, no. 2, p. 235, 1974.
[32] W. Kertz, "Leitungsfähiger Zylinder im transversalen magnetischen Wechselfeld," *Gerl. Beitr. Geophys.*, vol. 69, pp. 4–28, 1960.
[33] S. H. Ward, "Unique determination of conductivity susceptibility, size and depth in multi-frequency electromagnetic exploration," *Geophysics*, vol. 24, no. 3, pp. 531–546, July 1959.
[34] J. R. Wait, "Electromagnetic coupling between a circular loop and a conducting sphere," *Geophysics*, vol. 18, pp. 970–971, Oct. 1953.
[35] P. R. Vein, "Inductance between two loops in the presence of solid conducting bodies," *J. Electron. Contr.*, vol. 13, no. 5, pp. 471–494, 1962.
[36] W. R. Smythe, *Static and Dynamic Electricity*, 2nd ed. New York: McGraw-Hill, 1950. (3rd revised edition now available.)
[37] M. L. Burrows, "A theory of eddy-current flaw detection," Ph.D. dissertation, Univ. of Michigan, Ann Arbor, 1964 (available from University Microfilms, Ann Arbor, MI, Order No. 64–12,568).
[38] D. A. Hill and J. R. Wait, "Scattering by a slender void in a homogeneous conducting wire rope," *Appl. Phys.*, vol. 16, pp. 391–398, 1978 (and, by same authors, "Electromagnetic field perturbation by an internal void in a conducting cylinder excited by a wire loop," *Appl. Phys.*, vol. 18, pp. 141–147, 1973).
[39] C.-V. Dodd, W. E. Deeds, and J. W. Luquire, "Integral solutions to some eddy current problems," *Int. J. of NDT* vol. 1, pp. 29–90, 1969/1970.
[40] G. V. Keller and F. C. Frischknecht, *Electrical Methods in Geophysical Prospecting*. NY: Pergamon, 1966.
[41] C. C. Cheng, C. V. Dodd, and W. E. Deeds, "General analysis of probe coils near stratified conductors," *Int. J. of NDT*, vol. 3, 109–130, 1971/1972.
[42] J. R. Wait, *Electromagnetic Waves in Stratified Media*. New York: Pergamon Press, Chap. 2, 1st ed. 1962 and 2nd ed. 1970.
[43] J. R. Wait, "Fields of a horizontal dipole over a stratified half-space," *IEEE Trans. Antennas Propagat.*, vol. AP-14, no. 6, pp. 790–792, Nov. 1966.
[44] C. V. Dodd, C. C. Cheng, and W. E. Deeds, "Induction coils coaxial with an arbitrary number of cylindrical conductors," *J. Appl. Phys.*, vol. 45, no. 2, pp. 638–647, Feb. 1974.
[45] C. V. Dodd and W. E. Deeds, "Analytical solution to eddy current probe coil problems," *J. Appl. Phys.*, vol. 39, no. 6, pp. 2829–2838, May 1968.
[46] A. H. Kahn, R. Spal, and A. Feldman, "Eddy current losses due to a surface crack in conducting material," *J. Appl. Phys.*, vol. 48, no. 11, pp. 4454–4459, Nov. 1977.
[47] A. H. Kahn and R. D. Spal, "Electromagnetic theory and its relationship to standards," in *Proc. Workshop on Eddy Current Non-Destructive Testing* (National Bureau of Standards, Gaithersburg, MD, Nov. 3–4, 1977) (to be issued as an NBS Special Publication).
[48] J. T. Weaver, "The electromagnetic field within a discontinuous conductor with reference to geomagnetic micropulsations near a coast-line," *Can. J. Phys.*, vol. 41, pp. 484–495, 1963.
[49] J. R. Wait and K. P. Spies, "Magneto-telluric fields for a segmented overburden," *J. Geomagn. and Geoelec.*, vol. 26, pp. 449–458, 1974.
[50] J. R. Wait, "The electromagnetic basis for non-destructive testing of cylindrical conductors," *IEEE Trans. Instrum. Meas.*, vol. IM-27, No. 3, pp. 235–238, Sept. 1978.
[51] H. L. Libby, *Introduction to Electromagnetic Nondestructive Test Methods*. New York: Wiley, 1971, Sec. 5.2, pp. 135–150.
[52] J. R. Wait, *Electromagn. Radiation from Cylindrical Structures*. New York: Pergamon, 1959.
[53] D. A. Hill and J. R. Wait, "Analysis of alternating current excitation of a wire rope by a toroidal coil," *J. Appl. Phys.*, vol. 48, no. 12, pp. 4893–4897, 1977.
[54] A. G. Kandoian, *Reference Data for Radio Engineers*. ITT Corp., New York, 1968, pp. 4–32.
[55] J. R. Wait, "Electromagnetic response of an anisotropic conducting cylinder to an external source," *Radio Sci.*, vol. 13, no. 5, pp. 789–792, Sept./Oct. 1978.

The Electromagnetic Basis for Nondestructive Testing of Cylindrical Conductors

JAMES R. WAIT, FELLOW, IEEE

Abstract—Using an idealized model, we deduce the impedance per unit length of long solenoid of many turns that contains a cylindrical sample. The sample with a specified conductivity and magnetic permeability need not be centrally located within the solenoid provided all transverse dimensions are small compared with the free-space wavelength. The derivation is relatively straightforward and it provides a justification for earlier use of the impedance formula. The dual problem ,where the solenoid is replaced by a toroidal coil is also considered. It is shown that both excitation methods have merit in nondestructive testing procedures.

Introduction

A COMMON METHOD [1] of nondestructive testing (NDT) of metal rods and tubes is to induce eddy currents by means of an encircling solenoid carrying an alternating current. The impedance of the solenoid is related to the cross-sectional area and the electrical properties of the sample. A formula for this impedance was obtained by Förster and Stambke [2] on the assumption that end effects could be ignored. Also, they assumed that the cylindrical sample was centrally located within the solenoid. The same derivation was essentially repeated by Hochschild [3] and Libby [1].

A feature of the Förster–Stambke derivation is that the effect of the air gap is introduced in a somewhat heuristic fashion wherein the field in this concentric region is assumed to be the same as the one for the empty solenoid. We feel it is worthwhile to provide a more general derivation of the impedance formula. We also show it applies to the case of a nonconcentric air gap. Finally, we mention the relevance of the current analysis to the dual problem where the cylindrical sample is excited by a toroidal coil.

Formulation

To simplify the discussion, we consider first the concentric air gap model with a homogeneous cylindrical sample of radius a with conductivity σ and magnetic permeability μ. The situation is indicated in Fig. 1 where the solenoid of radius b encloses the sample, both of which are assumed to be infinite in length. Our objective is to find an expression for the impedance of the solenoid per unit length since this is the basis of the NDT eddy current methods that are commonly used.

In terms of cylindrical coordinates (ρ, ϕ, z), the only component of the magnetic field is H_z since the exciting current in the solenoid is uniform in both the axial and in the azimuthal direction. Within the sample, H_z satisfies the Helmholtz equation

$$(\nabla^2 - \gamma^2)H_z = 0 \tag{1}$$

where $\gamma^2 = i\sigma\mu\omega$ and where we have adopted a time factor $\exp(i\omega t)$. Here ω is the angular frequency that is sufficiently low that displacement currents in the sample can be neglected. If not, we merely replace σ by $\sigma + i\varepsilon\omega$ where ε is the permittivity. Also, it goes without saying that the field amplitude is sufficiently small that nonlinear effects can be ignored.

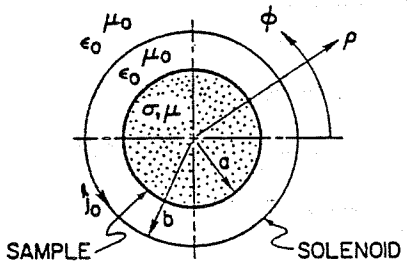


Fig. 1. Cross-sectional view of cylindrical sample located centrally within a solenoid of many turns.

Solution for Concentric Sample

For the highly idealized situation described, we can immediately write [4]

$$H_z = AI_0(\gamma\rho) \tag{2}$$

for $\rho < a$ where I_0 is a modified Bessel function of argument $\gamma\rho$ and where A is a constant. From Maxwell's equations the azimuthal component of the electric field is

$$E_\phi = -(1/\sigma)\,\partial H_z/\partial\rho = -A(\gamma/\sigma)I_1(\gamma\rho) \tag{3}$$

also for $\rho < a$. Now we can immediately form an expression for the "impedance" Z_c of the cylinder:

$$Z_c = [-E_\phi/H_z]_{\rho=a} = \eta I_1(\gamma a)/I_0(\gamma a) \tag{4}$$

where $\eta = \gamma/\sigma = (i\mu\omega/\sigma)^{1/2}$ is the intrinsic or wave impedance of the sample material.

Now, for the air gap region $a < \rho < b$, we write corresponding field expressions

$$H_{0z} = BI_0(\gamma_0\rho) + CK_0(\gamma_0\rho) \tag{5}$$

Manuscript received March 6, 1978.

The author is with the Cooperative Institute for Research in Environmental Sciences, University of Colorado/NOAA, Boulder, CO 80309.

U.S. Government work not protected by U.S. copyright

and

$$E_{0\phi} = -B\eta_0 I_1(\gamma_0\rho) + C\eta_0 K_1(\gamma_0\rho) \tag{6}$$

where B and C are constants and where $\eta_0 = \gamma_0/(i\varepsilon_0\omega) = (\mu_0/\varepsilon_0)^{1/2} \cong 120\pi$ in terms of the permittivity ε_0 and permeability μ_0 of the air region. Here and in the above, the Bessel function identities $\partial I_0(x)/\partial x = I_1(x)$ and $\partial K_0(x)/\partial x = -K_1(x)$ have been employed.

Compatible with the requirement that tangential fields must be continuous at $\rho = a$ we can write

$$[E_{0\phi} + Z_c H_{0z}]_{\rho=a} = 0. \tag{7}$$

This immediately tells us that

$$\frac{C}{B} = \frac{\eta_0 I_1(\gamma_0 a) - Z_c I_0(\gamma_0 a)}{\eta_0 K_1(\gamma_0 a) + Z_c K_0(\gamma_0 a)}. \tag{8}$$

In the external region $\rho > b$, the field expressions must clearly have the form

$$H_{0z} = DK_0(\gamma_0\rho) \tag{9}$$

$$E_{0\phi} = D\eta_0 K_1(\gamma_0\rho) \tag{10}$$

where D is another constant.

Now the solenoid current is idealized as a continuous current distribution j_0 A/m in the azimuthal direction defined such that

$$\lim_{\Delta\to 0} \begin{cases} H_{0z}(\rho = b + \Delta) - H_{0z}(\rho = b - \Delta) = -j_0 & (11) \\ E_{0\phi}(\rho = b + \Delta) - E_{0\phi}(\rho = b - \Delta) = 0 & (12) \end{cases}$$

Application of these conditions immediately leads to

$$D = C - I_1(\gamma_0 b)B/K_1(\gamma_0 b) \tag{13}$$

and

$$B = j_0\gamma_0 b K_1(\gamma_0 b). \tag{14}$$

Among other things, this tells us that the magnetic field external to the solenoid (i.e., $\rho > b$) has the form

$$H_{0z} = \{-B[I_1(\gamma_0 b)/K_1(\gamma_0 b)] + C\}K_0(\gamma_0\rho). \tag{15}$$

The quantity of immediate interest is the impedance Z of the solenoid itself. Clearly, within the limits of our basic assumptions,

$$Z = \text{constant} \times E_{0\phi}(\rho = b)/j_0. \tag{16}$$

The corresponding impedance of the empty solenoid is denoted Z_0. Thus it follows that

$$\frac{Z}{Z_0} = 1 - \frac{C}{B}\frac{K_1(\gamma_0 b)}{I_1(\gamma_0 b)} \tag{17}$$

which is explicit since C/B is given by (8).

Quasi-Static Form

We now can simplify the impedance ratio formula if we invoke the small argument approximations for Bessel functions of order $\gamma_0 a$ and $\gamma_0 b$. That is, we use $I_0(x) \simeq 1$, $I_1(x) \simeq x/2$, $K_0(x) \simeq -\log x$ and $K_1(x) \simeq 1/x$. This exercise leads to

$$\frac{Z}{Z_0} \cong \left[1 - \frac{a^2}{b^2} + \frac{\mu}{\mu_0}\frac{a^2}{b^2}\frac{2}{\gamma a}\frac{I_1(\gamma a)}{I_0(\gamma a)}\right] = \frac{R + iX}{Z_0} \tag{18}$$

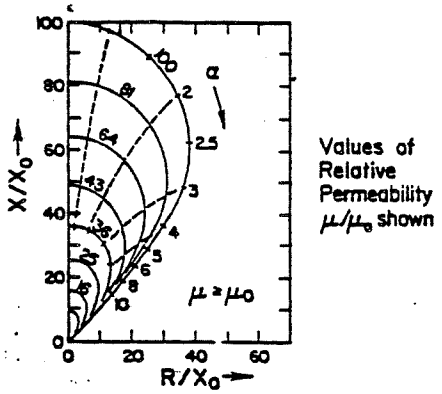


Fig. 2. Argand plot of the impedance $Z = R + iX$ normalized to the reactance X_0 of the empty solenoid, for $a = b$.

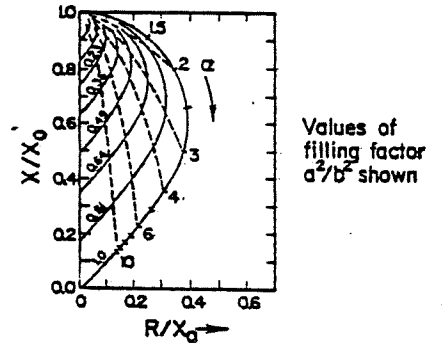


Fig. 3. Argand plot of the impedance $Z = R + iX$ normalized to the reactance X_0 of the empty solenoid, for $\mu = \mu_0$.

where no restriction has been placed on the magnitude of γa. Here R and X denote the resistance and reactance, respectively.

The formula for Z/Z_0 given by (18) is in agreement with Förster and Stambke [2] (if one remembers they used the old German designations J_0 and J_1 for modified Bessel functions). Förster and Stambke [2], Hochschild [3] and Libby [1] present extensive numerical data for this quasi-static approximation to Z/Z_0 in Argand diagrams in the complex plane for various values of $|\gamma a|$ and μ/μ_0. Two examples, using dimensionless parameters, are shown in Figs. 2 and 3 when the ordinates and abscissas are normalized by X_0 which is the reactance of the empty solenoid. That is, we assume $Z_0 \simeq iX_0$ corresponding to negligible ohmic losses in the solenoid itself. The real parameter α is defined by $\alpha = \gamma a \exp(-i\pi/4) = (\sigma\mu\omega)^{1/2}a$. In Fig. 2 the sample radius b is assumed to be the same as the sample radius a (i.e., no air gap). Different values of the magnetic permeability are shown. Not surprisingly, when α is small, R vanishes, and X/X_0 tends to μ/μ_0. However, in general, the eddy currents have the effect of reducing X/X_0, which is the effective flux, and to introduce a resistive portion R/X_0. In Fig. 3, the relative permeability of the sample $\mu/\mu_0 = 1$ but the filling factor a^2/b^2 assumes different values. The results indicate that the presence of the air gap reduces the sensitivity of the

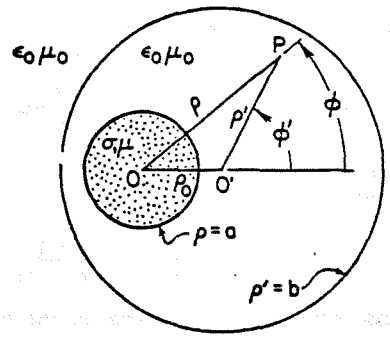


Fig. 4. Cross-section view of the noncentrally located sample.

device for probing the conductivity but the effect is predictable.

Actually, if α is sufficiently small (i.e., $|\gamma a| \ll 1$), (18) reduces to

$$Z/Z_0 \simeq X/X_0 \simeq 1 + (a^2/b^2)[\mu/\mu_0 - 1] \qquad (18')$$

which is consistent with the curves in Figs. 2 and 3. In this dc limit the results only depend on the magnetic permeability of the sample.

Analysis for Nonconcentric Sample

We now consider the formal extension of the theory to the case where the exciting solenoid is no longer concentric with the cylindrical sample. The situation is indicated in Fig. 4. As before, cylindrical coordinates (ρ, ϕ, z) are chosen coaxial with the sample. But now, the shifted coordinates (ρ', ϕ', z) are chosen to be coaxial with the exciting solenoid. The shift is ρ_0 as indicated in Fig. 4 where we do impose the rather obvious physical restriction that $b > \rho_0 + a$.

The field scattered from the solenoid now is no longer azimuthally symmetric. But, in analogy to (15), we can write

$$H_{0z} = BI_0(\gamma_0\rho') + \sum_{m=-\infty}^{+\infty} C_m K_m(\gamma_0\rho)e^{-im\phi} \qquad (19)$$

for the region $\rho > a$ and $\rho' < b$, while

$$H_{0z} = -B[I_1(\gamma_0 b)/K_1(\gamma_0 b)]K_0(\gamma_0\rho') + \sum_{m=-\infty}^{+\infty} C_m K_m(\gamma_0\rho)e^{-im\phi} \qquad (20)$$

for the region $\rho' > b$. As before, B is given by (14) in terms of the source current j_0 in the solenoid. Here C_m is to be determined.

To proceed further, we now note that the field inside the sample (i.e., $\rho < a$) must have the form

$$H_z = \sum_{m=-\infty}^{+\infty} H_{mz} \qquad (21)$$

where

$$H_{mz} = A_m I_m(\gamma\rho)e^{-im\phi}. \qquad (22)$$

Similarly, for the same region,

$$E_\phi = \sum_{m=-\infty}^{+\infty} E_{m\phi} \qquad (23)$$

where

$$E_{m\phi} = -(\gamma/\sigma)A_m I'_m(\gamma\rho)e^{-im\phi} \qquad (24)$$

where the prime indicates differentiation with respect to $\gamma\rho$. Now we define the cylinder impedance parameter Z_{mc} for harmonic waves of order m by

$$Z_{mc} = [-E_{m\phi}/H_{mz}]_{\rho=a} = \eta I'_m(\gamma a)/I_m(\gamma a) \qquad (25)$$

in analogy to (4). In fact, $Z_{0c} \equiv Z_c$.

A known addition theorem [5] for modified Bessel functions $I_0(\gamma_0\rho')$ allows us to write (19) in the form

$$H_{0z} = \sum_{m=-\infty}^{+\infty} H_{0mz} \qquad (26)$$

where

$$H_{0mz} = \{B(-1)^m I_m(\gamma_0\rho_0)I_m(\gamma_0\rho) + C_m K_m(\gamma_0\rho)\}e^{-im\phi}. \qquad (27)$$

Similarly, for the same region,

$$E_{0\phi} = \sum_{m=-\infty}^{+\infty} E_{0mz} \qquad (28)$$

where

$$E_{0mz} = -\eta_0\,\partial H_{0mz}/\partial(\gamma_0\rho). \qquad (29)$$

Application of the condition

$$[E_{0m\phi} + Z_{mc}H_{0mz}]_{\rho=a} = 0 \qquad (30)$$

now leads to the relation

$$\frac{C_m}{B} = \frac{(-1)^m I_m(\gamma_0\rho_0)[\eta_0 I'_m(\gamma_0 a) - Z_{mc}I_m(\gamma_0 a)]}{-\eta_0 K'_m(\gamma_0 a) + Z_{mc}K_m(\gamma_0 a)}. \qquad (31)$$

Inserting this result into (19) or (20) yields explicit expressions for the fields external to the sample. However, in order to deduce the resultant impedance of the solenoid, it is desirable to reexpress H_{0z} in terms of the (ρ', ϕ', z) coordinates. Here we use a known addition theorem [6] for $K_m(\gamma_0\rho)\exp(-im\phi)$. The rather horrendous result is

$$H_{0z} = BI_0(\gamma_0\rho') + \sum_{m=-\infty}^{+\infty} C_m \sum_{n=-\infty}^{+\infty} K_{m+n}(\gamma_0\rho')I_n(\gamma_0\rho_0)(-1)^n e^{-i(n+m)\phi'}. \qquad (32)$$

This is valid in the nonconcentric air gap region (i.e., $\rho > a$ and $\rho_0 < \rho' < b$). The needed azimuthal component is obtained from

$$E_{0\phi'} = -\eta_0\,\partial H_{0z}/\partial(\gamma_0\rho'). \qquad (33)$$

The relevant quantity for the impedance calculation is the "average" field $\bar{E}_{0\phi'}$ at the solenoid. Clearly, this is given by

$$\bar{E}_{0\phi'} = \frac{1}{2\pi}\int_0^{2\pi} [E_{0\phi'}]_{\rho'=b}\,d\phi' = -\eta_0 BI_1(\gamma_0 b) - \eta_0 \sum_{m=-\infty}^{+\infty} C_m K'_0(\gamma_0 b)I_m(\gamma_0\rho_0)(-1)^m. \qquad (34)$$

Thus it follows that the impedance Z per unit length of the solenoid with the sample divided by the impedance Z_0 of the empty solenoid is given by

$$\frac{Z}{Z_0} = 1 - \frac{K_1(\gamma_0 b)}{I_1(\gamma_0 b)} \sum_{m=0}^{\infty} \varepsilon_m \frac{C_m}{B} I_m(\gamma_0 \rho_0)(-1)^m \quad (35)$$

where $\varepsilon_0 = 1$ and $\varepsilon_m = 2$ for $m \neq 0$ and where C_m/B is given explicitly by (31). Not surprisingly, (35) reduces to (17) for the centrally located sample, i.e., $I_m(\gamma_0 \rho_0) = 0$ for $\rho_0 \to 0$ when $m \neq 0$.

We again may invoke the small argument approximations for Bessel functions of order $\gamma_0 a$, $\gamma_0 b$, and $\gamma_0 \rho_0$. That is, for $m = 1, 2, 3, \cdots$, we use

$$I_m(x) \simeq x^m/(m!\, 2^m),\ I'_m(x) \simeq x^{m-1}/[(m-1)!\, 2^m]$$

$$K_m(x) \simeq (m-1)!\, 2^{m-1}/x^m \text{ and } K'_m(x) \simeq -m!\, 2^{m-1}/x^{m+1}.$$

Lo and behold, these show that Z/Z_0 reduces again to the formula given by (18). This confirms the conjecture of Förster and Stambke who seemed to be gifted with keen physical insight into such problems. Of course, we do not expect the result to hold in any sense when the dimensions of the solenoid become comparable with the free-space wavelength. In that case, many other complications arise such as the assumed uniformity of the solenoid current.

The Dual Problem and Concluding Remarks

There is an extremely interesting duality to the problem we have discussed. That is, rather than exciting the cylindrical sample with an *azimuthal electric current*, we employ an *azimuthal magnetic current*. This is an idealized representation for a thin toroidal coil but, again, it effectively is of infinite length in the z or axial direction. The assumed source discontinuity is now in the electric field at $\rho = b$ which has only a z component. The much more complicated case of the toroidal coil of finite axial extent was analyzed recently [7].

Under the present assumption of axial uniformity, the admittance Y per unit length of the toroid is the dual of the impedance Z of the solenoid discussed above. Thus all the earlier equations apply if we make the following transformations: $i\mu\omega \to \sigma$, $\mu_0 \to \varepsilon_0$, $\eta \to \eta^{-1}$, $\eta_0 \to \eta_0^{-1}$, $H_z \to E_z$, $E_\phi \to -H_\phi$, $H_{0z} \to E_{0z}$, and $E_{0\phi} \to -H_{0\phi}$. Then the dual of (18) is the ratio of the admittance Y of the toroidal coil with the sample to the admittance Y_0 without the sample. It is written explicitly

$$\frac{Y}{Y_0} = \left[1 - \frac{a^2}{b^2} + \frac{\sigma}{i\varepsilon_0\omega}\frac{a^2}{b^2}\frac{2}{\gamma a}\frac{I_1(\gamma a)}{I_0(\gamma a)}\right]$$

for the case where $|\gamma_0 b| \ll 1$. That is, the radius of the toroidal coil should be much smaller than the free-space wavelength. Also, in full analogy to the earlier discussion, the quasi-static result holds for any location of the cylindrical sample within the toroid. Furthermore, in the low frequency limit where $|\gamma a| = \alpha \ll 1$, we see that

$$Y \simeq Y_0[1 + (a^2/b^2)[(\sigma/i\varepsilon_0\omega) - 1]]$$

which depends only on the conductivity of the sample. Thus this type of excitation should be preferred with probing the effective conductivity in the axial direction in the sample.

References

[1] H. L. Libby, *Introduction to Electromagnetic Nondestructive Test Methods*. New York: Wiley, 1971, Sect. 5.2, pp. 135–150.

[2] F. Förster and K. Stambke, "Theoretische und experimentelle Grundlagen der zerstörungfreien Werkstoffprüfung mit Wirbelstromverfahren. Pt. III," *Zeits. Metallkde.*, Bd. 45, Heft 4, pp. 166–179, 1954.

[3] H. Hochschild, "Electromagnetic methods of testing metals," in *Progress in Non-Destructive Testing*, E. G. Stanford and J. H. Fearon, Eds. New York: Macmillan, 1959, pp. 58–109.

[4] J. R. Wait, *Electromagnetic Radiation from Cylindrical Structures*. Oxford and New York: Pergamon Press, 1959.

[5] A. Erdélyi, Ed., *Higher Transcendental Functions*. New York: McGraw-Hill, 1953, vol. 2, p. 102 (no. 36 for $\nu = 0$).

[6] —— (*loc cit.*, p. 102, no. 35 with the substitutions $Z \to \gamma_0 \rho'$, $z \to -\gamma_0 \rho_0$, $\psi + \phi \to -\phi$, $\phi \to -\phi'$).

[7] D. A. Hill and J. R. Wait, "Analysis of alternating current excitation of a wire rope by a toroidal coil," *J. Appl. Phys.*, vol. 48, no. 12, pp. 4893–4897, 1977.

IEEE TRANSACTIONS ON INSTRUMENTATION AND MEASUREMENT, VOL. IM-28, NO. 2, JUNE 1979

Electromagnetic Nondestructive Testing of Cylindrically Layered Conductors

JAMES R. WAIT, FELLOW, IEEE, AND ROBERT L. GARDNER

Abstract—**We extend a previous analysis for the series impedance of a long solenoid to allow for the cylindrical layering of the encircled conductor. The results are discussed in the context of nondestructive testing of steel ropes that may have external or internal corrosion. It is shown that even an internal layer of reduced conductivity and permeability will be detectable if the frequency is sufficiently low to permit penetration of the primary field.**

I. Introduction and Formulation

IN AN EARLIER PAPER [1], we had described the electromagnetic basis for the nondestructive testing of cylindrical conductors. The model was highly idealized; it consisted of a long solenoid that encircled the homogeneous cylindrical sample. Here we wish to generalize the theory to account for concentric layering within the sample. This is a possible model to account for the effect of internal and external corrosion that can occur in cables or wire ropes.

The derivation is given in outline only since the method is well documented elsewhere [2], [3]. We deal specifically with a cylindrical sample that has an outer radius a_1 and a core of radius a_3. There is an intermediate annular region bounded by cylindrical surfaces of radii a_2 and a_3. The three regions have electrical properties σ_j, ε_j, and μ_j where $j = 1, 2, 3$.

The sample is located within a solenoid of radius b but it need not be centrally located provided the free-space wavelength is much greater than b. Then, proceeding in the same manner as in the previous paper [1], we can derive an expression for the series impedance Z of the solenoid per unit length in the form

$$\frac{Z}{Z_0} = 1 - \frac{a_1^2}{b^2} + Z_c \frac{2a_1}{i\mu_0 \omega b^2} \tag{1}$$

where Z_0 is the series impedance when the solenoid is free of the sample. Here Z_c is the inwards looking wave impedance at the sample. For example, if the latter were homogeneous with electrical properties σ_1, ε_1, and μ_1, we would have

$$Z_c = \frac{i\mu_1 \omega}{\gamma_1} \frac{I_1(\gamma_1 a_1)}{I_0(\gamma_1 a_1)} \tag{2}$$

where $\gamma_1 = [i\mu_1 \omega(\sigma_1 + i\varepsilon_1 \omega)]^{1/2}$ is the intrinsic propagation constant of the sample. Here I_0 and I_1 are modified Bessel functions of the first kind. This special case was derived in detail in the earlier paper [1].

Manuscript received September 26, 1978.

The authors are with the Cooperative Institute in Environmental Sciences, University of Colorado/NOAA, Boulder, CO 80309.

II. The General Wave Impedance

To account for the concentric layering of the sample, we need to employ the appropriate expression for the radial wave impedance Z_c. This can be obtained in a rather prosaic manner by setting up wave functions in each of the homogeneous regions and determining the unknown coefficients by matching tangential fields at the concentric interfaces. A more physically meaningful approach is to employ nonuniform transmission line theory as so elegantly promulgated by Schellkunoff [2]. The method has been applied to cylindrically layered plasma regions [3] so we can in effect, write down the answer here in terms of wave impedances, transmission factors, and reflection coefficients. Thus we find that

$$Z_c = \eta_1 \frac{I_1(\gamma_1 a_1)}{I_0(\gamma_1 a_1)} \frac{\left[1 + r \dfrac{I_1(\gamma_1 a_2) K_1(\gamma_1 a_1)}{I_1(\gamma_1 a_1) K_1(\gamma_1 a_2)}\right]}{\left[1 + R \dfrac{I_0(\gamma_1 a_2) K_0(\gamma_1 a_1)}{I_0(\gamma_1 a_1) K_0(\gamma_1 a_2)}\right]} \tag{3}$$

where

$$R = \left[\frac{\eta_1 I_1(\gamma_1 a_2)}{I_0(\gamma_1 a_2)} - \hat{Z}_c\right]\left[\frac{\eta_1 K_1(\gamma_1 a_2)}{K_0(\gamma_1 a_2)} + \hat{Z}_c\right]^{-1} \tag{4}$$

and

$$r = \left[\frac{I_0(\gamma_1 a_2)}{\eta_1 I_1(\gamma_1 a_2)} - \frac{1}{\hat{Z}_c}\right]\left[\frac{K_0(\gamma_1 a_2)}{\eta_1 K_1(\gamma_1 a_2)} + \frac{1}{\hat{Z}_c}\right]^{-1}. \tag{5}$$

Here K_0 and K_1 are modified Bessel functions of the second type and $\eta_1 = i\mu_1 \omega/\gamma_1$. The inward looking wave impedance $\hat{Z}_c$ at the cylindrical interface of radius a_2 is given by an analogous form:

$$\hat{Z}_c = \eta_2 \frac{I_1(\gamma_2 a_2)}{I_0(\gamma_2 a_2)} \frac{\left[1 + \hat{r} \dfrac{I_1(\gamma_2 a_3) K_1(\gamma_2 a_2)}{I_1(\gamma_2 a_2) K_1(\gamma_2 a_3)}\right]}{\left[1 + \hat{R} \dfrac{I_0(\gamma_2 a_3) K_0(\gamma_2 a_2)}{I_0(\gamma_2 a_2) K_0(\gamma_2 a_3)}\right]} \tag{6}$$

where

$$\hat{R} = \left[\frac{\eta_2 I_1(\gamma_2 a_3)}{I_0(\gamma_2 a_3)} - \frac{\eta_3 I_1(\gamma_3 a_3)}{I_0(\gamma_3 a_3)}\right] \cdot \left[\frac{\eta_2 K_1(\gamma_2 a_3)}{K_0(\gamma_2 a_3)} + \frac{\eta_3 I_1(\gamma_3 a_3)}{I_0(\gamma_3 a_3)}\right]^{-1} \tag{7}$$

and

$$\hat{r} = \left[\frac{I_0(\gamma_2 a_3)}{\eta_2 I_1(\gamma_2 a_3)} - \frac{I_0(\gamma_3 a_3)}{\eta_3 I_1(\gamma_3 a_3)}\right] \cdot \left[\frac{K_0(\gamma_2 a_3)}{\eta_2 K_1(\gamma_2 a_3)} + \frac{I_0(\gamma_3 a_3)}{\eta_3 I_1(\gamma_3 a_3)}\right]^{-1} \tag{8}$$

0018-9456/79/0600-0159$00.75

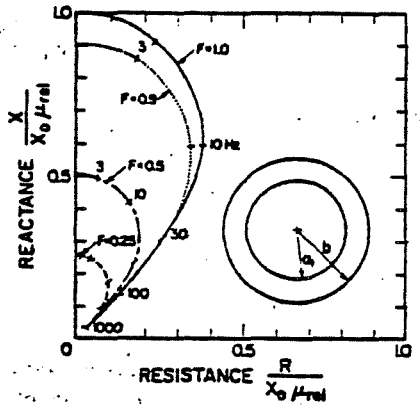


Fig. 1. Normalized series impedance of solenoid of radius b for a concentric homogeneous cylindrical sample of radius a_1 for various fill factors $F = a_1^2/b^2$.

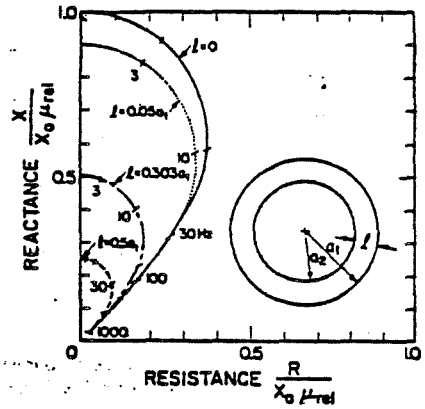


Fig. 2. Normalized series impedance of solenoid of radius $b = a_1$ for a sample with an external rust layer of thickness l.

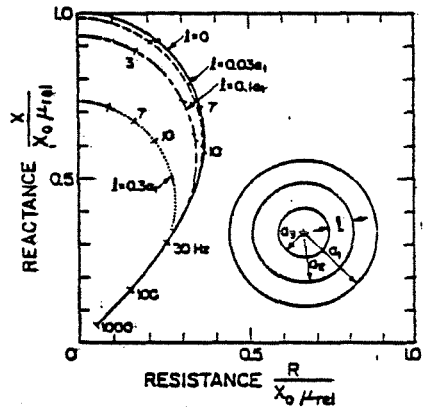


Fig. 3. Normalized series impedance of solenoid of radius $b = a_1$ for a sample of an interior rust layer of thickness l.

where $\gamma_j = [i\mu_j\omega(\sigma_j + i\varepsilon_j\omega)]^{1/2}$ and $\eta_j = i\mu_j\omega/\gamma_j$ for $j = 1, 2, 3$.

Actually, subject to such assumptions as axial and azimuthal uniformity, the expressions for Z_c and $\hat{Z}_c$ are exact. For computation, however, we can neglect displacement currents in the various layers. Thus, if $\varepsilon_j\omega \ll \sigma_j$, we see that $\gamma_j \simeq (i\sigma_j\mu_j\omega)^{1/2} = |\gamma_j| \exp(i\pi/4)$ whence all the modified Bessel functions have arguments with phase angles of 45°. The final results can then be written in terms of the tabulated Kelvin functions [4] via

$$I_0(\alpha i^{1/2}) = \text{ber}(\alpha) + i\,\text{bei}(\alpha)$$
$$iI_1(\alpha i^{1/2}) = \text{ber}_1(\alpha) + i\,\text{bei}_1(\alpha)$$
$$K_0(\alpha i^{1/2}) = \text{ker}(\alpha) + i\,\text{kei}(\alpha)$$
$$-iK_1(\alpha i^{1/2}) = \text{ker}_1(\alpha) + i\,\text{kei}_1(\alpha)$$

where α is a real parameter.

III. Numerical Examples

Computations have been carried out for the complex quantity Z/Z_0 for several specific conditions of practical interest. First of all, to provide a reference case, we let the sample be homogeneous with properties σ_1 and μ_1 and radius a_1. This, of course, corresponds to the general case under the condition $a_2 = a_3 = 0$. As indicated in the inset in Fig. 1, the sample is also located centrally within the solenoid of radius b. To be definite, we also choose the sample radius a_1 to be 2 cm which is kept fixed in all that follows. Also, the conductivity of the (uncorroded) sample is taken to be 1.1×10^6 mhos/m and its relative permeability $\mu_{rel} = \mu_1/\mu_0 = 200$. These are typical values for steel. The corresponding series impedance $Z = R + iX$ of the solenoid is shown plotted in Fig. 1 in an Argand diagram. The abscissa and ordinate are actually $R/X_0\mu_{rel}$ and $X/X_0\mu_{rel}$, respectively, where we have assumed that the impedance of the same empty solenoid is $Z = iX_0$ being purely inductive. Various fill factors $F = a_1^2/b^2$ are shown and the operating frequencies are indicated. As expected, at sufficiently low frequencies, R tends to zero and X approaches $X_0 \times \mu_{rel} \times F$. Not surprisingly, the series impedance of the solenoid is sensitive to the diameter of the sample.

We now consider an external rust or corrosion layer of thickness l at the outside of the sample as indicated in the inset in Fig. 2. This is a special case of the general analysis when $a_3 = 0$. The uncorroded region of radius a_2 has the same properties as before (i.e., $\sigma_2 = 1.1 \times 10^6$ mhos/m and $\mu_{rel} = \mu_2/\mu_0 = 200$) but the external layer now assumes the values $\sigma_1 = 1$ mho/m and $\mu_1 = \mu_0$. The results are shown in Fig. 2 where we have taken the fill factor F to be 1 (i.e., $a_1 = b$). Different values of l, the thickness of the rust layer, are shown. Not surprisingly, the effect of an external rust layer is to reduce the effective radius of the cylindrical steel sample.

Finally, we consider an internal corrosion layer. As indicated in Fig. 3, this corresponds to the case where the full formula for Z_c, as given by (3), is needed but we set $\sigma_1 = \sigma_3 = 1.1$ mhos/m and $\mu_1/\mu_0 = \mu_3/\mu_0 = \mu_{rel} = 200$ which are the "uncorroded" regions. In the central annular "corroded" region, we choose $\mu_2 = \mu_0$ and $\sigma_2 = 1.0$ mho/m. For the results shown in Fig. 3, we have also chosen the radius a_3 of the core to be $0.3a_1$ but the value of l ranges from

being zero (i.e., no rust layer) to a value of $0.3a_1$. As seen in Fig. 3, the series impedance of the solenoid is still markedly affected by the presence of the corrosion layer, even though it would not be visible to an outside observer. Of course, the frequency must be sufficiently low so that the primary fields of the solenoid can penetrate to the interior of the sample without significant dissipation.

IV. Concluding Remarks

The present calculations, while based on a highly idealized model, indicate the potential of nondestructive schemes using electromagnetic waves [5]. More sophisticated models based on the layered cylinder formulations can easily be implemented. Actually, three-dimensional models that allow for the finite extent of the primary field and the internal anomaly have been examined elsewhere [6], [7].

Certainly, the sensitivity of such devices to the electrical, magnetic, and geometrical properties needs further study. Here we have only indicated a few examples that might promote further developments in this area.

References

[1] J. R. Wait, "Electromagnetic basis for non-destructive testing of cylindrical conductors," *IEEE Trans. Instrum. Meas.*, vol. IM-27, pp. 235–238, Sept. 1978.

[2] S. A. Schelkunoff, *Electromagnetic Waves*. New York: Van Nostrand, 1943, p. 205.

[3] J. R. Wait, *Electromagnetic Waves in Stratified Media*. New York: Pergamon, 1970, 2nd ed., p. 534.

[4] N. W. McLachlan, *Bessel Functions for Engineers*. London, England: Oxford Univ. Press (corrected 2nd ed.), 1961, p. 211.

[5] H. Hochschild, "Electromagnetic methods of testing metals," *Progr. Non-Destructive Testing*, vol. I, pp. 58–109, E. G. Stanford and J. H. Fearon, Eds. New York: Macmillan, 1959.

[6] D. A. Hill and J. R. Wait, "Analysis of alternating current excitation of a wire rope by a toroidal coil," *J. Appl. Phys.*, vol. 48, no. 12, pp. 4893–4897, 1977.

[7] ——, "Scattering by a slender void in a homogeneous conducting wire rope," *Appl. Phys.* (Springer-Verlag), vol. 16, pp. 391–398, 1978.

Reprinted from Journal of APPLIED PHYSICS Vol. 48, No. 12, December 1977

Analysis of alternating current excitation of a wire rope by a toroidal coil

David A. Hill and James R. Wait

Institute for Telecommunication Sciences, Office of Telecommunications, U.S. Department of Commerce, Boulder, Colorado 80302

(Received 22 June 1977; accepted for publication 13 July 1977)

An idealized magnetic sheet current model for a toroidal coil which encircles a conducting ferromagnetic rope is analyzed. This configuration is suitable for the nondestructive testing of wire ropes and cables. Numerical results for the axial electric current density induced in the rope reveal that low frequencies on the order of 10 Hz are required to produced a uniform current in a typical rope. For a toroidal coil which does not completely encircle the rope, the azimuthal symmetry is lost and harmonics in ϕ are produced. These harmonics are large but decay rapidly away from the source.

PACS numbers: 41.10.Hv, 84.40.Mk

I. INTRODUCTION

A wide variety of electromagnetic nondestructive test methods are used in the metals industry to inspect and evaluate materials.[1] For inspection of wire ropes[2] which are made of electrically conducting ferromagnetic material, two electromagnetic methods, dc and ac, are currently available.[3] The dc (direct current) method excites the rope with a steady magnetic field, and the ac (alternating current) method[4] uses an alternating field. In both methods the magnetic field is applied along the axis of the rope, and rope irregularities produce magnetic field changes which induce voltages in the sensing coils. It is generally agreed that the dc method responds better to wire breaks and the ac method responds better to corrosion and wire flattening.[3]

In this paper we wish to examine an alternative ac method which excites the rope with an axial electric field rather than an axial magnetic field. Since axial electric currents would be induced, this method ought to be more sensitive to broken strands than the present ac method which induces only azimuthal currents which flow perpendicular to the strands. Also, such a method could be used on conductors which are not ferromagnetic. An appropriate source for excitation of axial electric currents is a toroidal coil which could either completely or partially encircle the rope. In this paper we consider an idealized flattened toroidal coil which can be represented by a magnetic current sheet. Expressions are derived for the fields both interior and exterior to the rope. The interior fields and currents are of particular interest and numerical results are given for the variation of the axial current density induced in a uniform rope. Later work will consider the associated problem of anomalous fields produced by rope imperfections such as broken strands or corrosion.

II. FORMULATION

The geometry of the rope and the concentric yoke coil are shown in Fig. 1 where cylindrical coordinates (ρ, ϕ, z) have been chosen. The rope of radius a has conductivity σ_w, permittivity ϵ_w, and magnetic permeability μ_w. The surrounding free space has permittivity ϵ_0 and permeability μ_0.

The idealized thin yoke coil has radius b and height l and extends in azimuth from $\phi=-\frac{1}{2}\psi$ to $\phi=\frac{1}{2}\psi$. For mathematical convenience, we represent the thin yoke coil by an azimuthal current sheet of strength M_ϕ located at $\rho=b$. M_ϕ could, in principle, be an arbitrary function of ϕ and z, but here is taken to be constant over the extend indicated in Fig. 1 and zero elsewhere:

$$M_\phi = G(\phi)F(z), \tag{1}$$

where

$$\begin{aligned} G(\phi) &= G_0, \quad -\tfrac{1}{2}\psi < \phi < \tfrac{1}{2}\psi \\ &= 0, \quad \text{elsewhere,} \end{aligned} \tag{2}$$

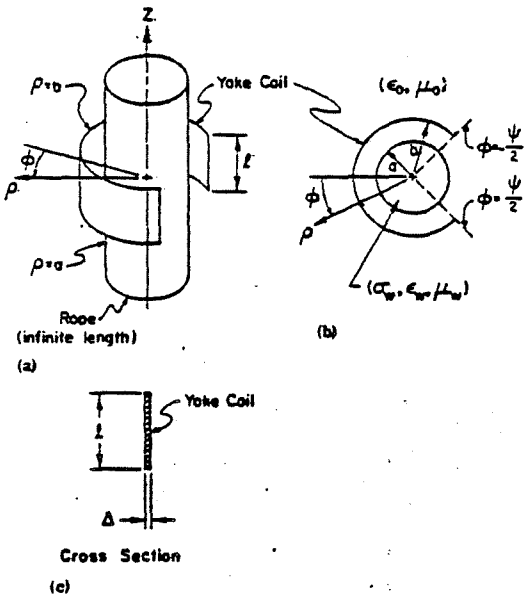


FIG. 1. Thin yoke coil surrounding a metal rope of infinite length. (a) Perspective view. (b) Top view. (c) Coil cross section. In the limit as Δ approaches zero, the coil becomes a magnetic current sheet.

 0021-8979/77/4812-4893$01.10

and

$$F(z)=F_\phi, \quad |z|<\tfrac{1}{2}l$$
$$=0, \quad |z|>\tfrac{1}{2}l. \tag{3}$$

The strength of the current sheet could be approximately related to a thin yoke coil of thickness Δ by

$$M_\phi=i\omega\mu\bar{H}_\phi\Delta, \tag{4}$$

where $\bar{H}_\phi$ is the azimuthal magnetic field inside the coil, μ is the permeability of the coil core, and $\exp(i\omega t)$ time dependence is assumed for all source and field quantities. It would also be possible to relate $\bar{H}_\phi$ to the yoke and winding parameters, but the details of the yoke design are not of primary interest here.

For the cylindrical geometry considered here, the fields can be derived from electric and magnetic Hertz vectors with only z components, Π and Π^*, respectively.[5] It is useful to express Π and Π^* in the following shorthand notation:

$$\Pi=\Gamma(\Pi_m) \quad \text{and} \quad \Pi^*=\Gamma(\Pi_m^*), \tag{5}$$

where

$$\Gamma(\,)=\int_{-\infty}^{\infty}\sum_{m=-\infty}^{\infty}(\,)\exp(-im\phi)\exp(-i\lambda z)\,d\lambda.$$

The integration contour is taken along the entire real axis in the complex λ plane, and the summation is over all integer values of m from $-\infty$ to ∞ including zero.

Outside the rope, Π_m and Π_m^* take the following form:

$$\Pi_m=A_m(\lambda)K_m(u\rho), \quad \rho>b$$
$$=B_m(\lambda)I_m(u\rho)+C_m(\lambda)K_m(u\rho), \quad a<\rho<b, \tag{6}$$

and

$$\Pi_m^*=A_m^*(\lambda)K_m(u\rho), \quad \rho>b$$
$$=B_m^*(\lambda)I_m(u\rho)+C_m^*(\lambda)K_m(u\rho), \quad a<\rho<b, \tag{7}$$

where $u=(\lambda^2+\gamma_0^2)^{1/2}$, $\gamma_0=i\omega(\mu_0\epsilon_0)^{1/2}$, I_m and K_m are modified Bessel functions, and A_m, B_m, C_m, A_m^*, B_m^* and C_m^* are coefficients to be determined from the boundary conditions. Inside the rope, Π_m and Π_m^* take the following form:

$$\Pi_m=a_m(\lambda)I_m(w\rho), \quad \rho<a \tag{8}$$

and

$$\Pi_m^*=a_m^*(\lambda)I_m(w\rho), \quad \rho<a, \tag{9}$$

where $w=(\lambda^2+\gamma_w^2)^{1/2}$, $\gamma_w^2=i\omega\mu_w(\sigma_w+i\omega\epsilon_w)$, and a_m and a_m^* are coefficients to be determined.

III. SOURCE CONDITIONS

The source conditions at $\rho=b$ involve the tangential electric (E_ϕ and E_z) and magnetic (H_ϕ and H_z) fields. E_z has a discontinuity of strength M_ϕ, and the other components are continuous:

$$E_z|_{\rho=b^+}-E_z|_{\rho=b^-}=-M_\phi, \tag{10}$$

$$E_\phi|_{\rho=b^+}-E_\phi|_{\rho=b^-}=0, \tag{11}$$

$$H_z|_{\rho=b^+}-H_z|_{\rho=b^-}=0, \tag{12}$$

and

$$H_\phi|_{\rho=b^+}-H_\phi|_{\rho=b^-}=0. \tag{13}$$

It is useful to employ shorthand notations for the electric and magnetic field components in all three regions:

$$\underset{z}{E_\phi}=\Gamma(\underset{z}{E_{\phi m}}) \quad \text{and} \quad \underset{z}{H_\phi}=\Gamma(\underset{z}{H_{\phi m}}). \tag{14}$$

The specific electric and magnetic field expressions required for $\rho>a$ are

$$E_{\phi m}=-\left(\frac{m\lambda}{\rho}\right)\Pi_m+i\omega\mu_0\frac{\partial\Pi_m^*}{\partial\rho},$$
$$H_{\phi m}=-\left(\frac{m\lambda}{\rho}\right)\Pi_m^*-i\omega\epsilon_0\frac{\partial\Pi_m}{\partial\rho}, \tag{15}$$

$$E_{zm}=-u^2\Pi_m \quad \text{and} \quad H_{zm}=-u^2\Pi_m^*.$$

It is also useful to obtain the Fourier representations of the source expressions defined in Eqs. (2) and (3):

$$F(z)=(1/2\pi)\int_{-\infty}^{\infty}\exp(-i\lambda z)f(\lambda)\,d\lambda, \tag{16}$$

where

$$f(\lambda)=F_\phi l\frac{\sin(\frac{1}{2}\lambda l)}{\frac{1}{2}\lambda l},$$

and

$$G(\phi)=(1/2\pi)\sum_{m=-\infty}^{\infty}g_m\exp(-im\phi), \tag{17}$$

where

$$g_m=G_\phi\psi\frac{\sin(\frac{1}{2}m\psi)}{\frac{1}{2}m\psi}.$$

Thus, M_ϕ can be written

$$M_\phi=\Gamma[f(\lambda)g_m/(4\pi^2)]. \tag{18}$$

The source conditions, Eqs. (10)—(13), can now be written

$$\begin{pmatrix}E_{zm}\\E_{\phi m}\\H_{zm}\\H_{\phi m}\end{pmatrix}\Bigg|_{\rho=b^+}-\begin{pmatrix}E_{zm}\\E_{\phi m}\\H_{zm}\\H_{\phi m}\end{pmatrix}\Bigg|_{\rho=b^-}=\begin{pmatrix}-f(\lambda)g_m/(4\pi^2)\\0\\0\\0\end{pmatrix}, \tag{19}$$

By substituting Eq. (15) into Eq. (19), we obtain the following four equations in six unknowns:

$$-u^2K_m(ub)A_m+u^2I_m(ub)B_m+u^2K_m(ub)C_m=-f(\lambda)g_m/(4\pi^2), \tag{20}$$

$$-u^2K_m(ub)A_m^*+u^2I_m(ub)B_m^*+u^2K_m(ub)C_m^*=0, \tag{21}$$

$$-(m\lambda/b)K_m(ub)A_m+i\omega\mu_\rho uK_m'(ub)A_m^*+(m\lambda/b)I_m(ub)B_m$$
$$-i\omega\mu_\rho uI_m'(ub)B_m^*+(m\lambda/b)K_m(ub)C_m$$
$$-i\omega\mu_\rho uK_m'(ub)C_m^*=0, \tag{22}$$

and

$$-(m\lambda/b)K_m(ub)A_m^*-i\omega\epsilon_\rho uK_m'(ub)A_m+(m\lambda/b)I_m(ub)B_m^*$$
$$+i\omega\epsilon_\rho uI_m'(ub)B_m+(m\lambda/b)K_m(ub)C_m^*$$
$$+i\omega\epsilon_\rho uK_m'(ub)C_m=0, \tag{23}$$

where the prime represents differentiation with respect to the argument. By substituting Eqs. (20) and (21) into Eqs. (22) and (23), we obtain

$$B_m = ub K_m'(ub) f(\lambda) g_m / (4\pi^2 u^2), \tag{24}$$

and

$$B_m^e = -[m\lambda/(i\omega\mu_0)] K_m(ub) f(\lambda) g_m (4\pi^2 u^2)^{-1}. \tag{25}$$

B_m and B_m^e, which are now known, specify the source fields in the region, $a < \rho < b$.

IV. BOUNDARY CONDITIONS

The electric and magnetic field expressions required inside the rope, $\rho < a$, are

$$\begin{aligned} E_{\phi m} &= -\left(\frac{m\lambda}{\rho}\right)\Pi_m + i\omega\mu_w \frac{\partial \Pi_m^e}{\partial \rho}, \\ H_{\phi m} &= -\left(\frac{m\lambda}{\rho}\right)\Pi_m^e - i\omega\hat{\epsilon}_w \frac{\partial \Pi_m}{\partial \rho}, \\ E_{zm} &= -w^2 \Pi_m \quad \text{and} \quad H_{zm} = -w^2 \Pi_m^e, \end{aligned} \tag{26}$$

where $i\omega\hat{\epsilon} = \sigma_w + i\omega\epsilon_w$. The boundary conditions at the rope boundary are that the tangential electric and magnetic fields are continuous:

$$\begin{pmatrix} E_{\phi m} \\ E_{zm} \\ H_{\phi m} \\ H_{zm} \end{pmatrix}\Bigg|_{\rho=a^-} - \begin{pmatrix} E_{\phi m} \\ E_{zm} \\ H_{\phi m} \\ H_{zm} \end{pmatrix}\Bigg|_{\rho=a^+} = \begin{pmatrix} 0 \\ 0 \\ 0 \\ 0 \end{pmatrix}. \tag{27}$$

By substituting Eqs. (15) and (26) into Eq. (27), we obtain the following four equations in four unknowns (a_m, a_m^e, C_m, and C_m^e):

$$-w^2 I_m(wa) a_m + u^2 I_m(ua) B_m + u^2 K_m(ua) C_m = 0, \tag{28}$$

$$-w^2 I_m(wa) a_m^e + u^2 I_m(ua) B_m^e + u^2 K_m(ua) C_m^e = 0, \tag{29}$$

$$\begin{aligned} &-(m\lambda/a) I_m(wa) a_m + i\omega\mu I_m'(wa) a_m^e + (m\lambda/a) I_m(ua) B_m \\ &\quad - i\omega\mu_\phi u I_m'(ua) B_m^e + (m\lambda/a) K_m(ua) C_m \\ &\quad - i\omega\mu_\phi u K_m'(ua) C_m^e = 0, \end{aligned} \tag{30}$$

and

$$\begin{aligned} &-(m\lambda/a) I_m(wa) a_m^e - i\omega\hat{\epsilon}_w u I_m'(wa) a_m + (m\lambda/a) I_m(ua) B_m^e \\ &\quad - i\omega\epsilon_\phi u I_m'(ua) B_m + (m\lambda/a) K_m(ua) C_m^e - i\omega\epsilon_\phi u K_m'(ua) C_m = 0. \end{aligned} \tag{31}$$

The simultaneous solution of Eqs. (28)—(31) yields

$$\begin{aligned} C_m = \Bigg\{ I_m K_m \Bigg[&-\left(\frac{m\lambda}{u^2 a} - \beta_m\right)^2 - \left(\frac{\gamma_0}{u}\frac{I_m'}{I_m} - \eta_0 y_m\right)\left(\frac{\gamma_0}{u}\frac{K_m'}{K_m} \right. \\ &\left. - \frac{z_m}{\eta_0}\right)\Bigg] B_m + \frac{\gamma_0\eta_0}{au^2}\left(\frac{m\lambda}{u^2 a} - \beta_m\right) B_m^e \Bigg\} D_m^{-1}, \end{aligned} \tag{32}$$

$$\begin{aligned} C_m^e = \Bigg\{ I_m K_m \Bigg[&-\left(\frac{m\lambda}{u^2 a} - \beta_m\right)^2 - \left(\frac{\gamma_0}{u}\frac{K_m'}{K_m} - \eta_0 y_m\right) \\ &\times \left(\frac{\gamma_0}{u}\frac{I_m'}{I_m} - \frac{z_m}{\eta_0}\right)\Bigg] B_m^e - \frac{\gamma_0}{\eta_0 u^2 a}\left(\frac{m\lambda}{au^2} - \beta_m\right) B_m \Bigg\} D_m^{-1}, \end{aligned} \tag{33}$$

$$\begin{aligned} a_m = \frac{u^2 K_m}{w^2 I_m(wa) D_m} \Bigg[&-\frac{\gamma_0}{u^2 a}\left(\frac{\gamma_0}{u}\frac{K_m'}{K_m} - \frac{z_m}{\eta_0}\right) B_m + \frac{\gamma_0\eta_0}{au^2} \\ &\times \left(\frac{m\lambda}{au^2} - \beta_m\right) B_m^e \Bigg], \end{aligned} \tag{34}$$

and

$$\begin{aligned} a_m^e = \frac{-u^2 K_m}{w^2 I_m(wa) D_m} \Bigg[&\frac{\gamma_0}{u^2 a}\left(\frac{\gamma_0}{u}\frac{K_m'}{K_m} - \eta_0 y_m\right) B_m^e \\ &+ \frac{\gamma_0}{\eta_0 u^2 a}\left(\frac{m\lambda}{au^2} - \beta_m\right) B_m \Bigg], \end{aligned} \tag{35}$$

where

$$\begin{aligned} D_m &= \Bigg[\left(\frac{m\lambda}{u^2 a} - \beta_m\right)^2 + \left(\frac{\gamma_0}{u}\frac{K_m'}{K_m} - \eta_0 y_m\right) \\ &\quad \times \left(\frac{\gamma_0}{u}\frac{K_m'}{K_m} - \frac{z_m}{\eta_0}\right)\Bigg] K_m^2, \\ z_m &= \frac{(i\omega\mu_w/w) I_m'(wa)}{I_m(wa)}, \\ y_m &= \frac{(i\omega\hat{\epsilon}_w/w) I_m'(wa)}{I_m(wa)}, \\ \beta_m &= \frac{m\lambda}{(w^2 a)}, \quad \text{and} \quad \eta_0 = \left(\frac{\mu_0}{\epsilon_0}\right)^{1/2}. \end{aligned}$$

The argument of I_m, K_m, I_m', and K_m' in Eqs. (32)—(35) is ua unless indicated otherwise. It is now possible to compute the internal fields from a_m and a_m^e, or the scattered external fields from C_m and C_m^e for any type of excitation. B_m and B_m^e depend only on the external source, and for the specific case of a magnetic sheet current considered here they are given by Eqs. (24) and (25).

V. NUMERICAL RESULTS

The quantity of most interest in probing the rope is the axial electric current density J_z ($=\sigma_w E_z$) which is given by

$$J_z = \Gamma(J_{zm}), \tag{36}$$

where

$$J_{zm} = -\sigma_w w^2 a_m I_m(w\rho).$$

Although the operator Γ as defined in Eq. (5) involves integration on λ from $-\infty$ to ∞ and summation on m from $-\infty$ to ∞, the evenness of J_{zm} in λ and m can be utilized to rewrite Eq. (36) and reduce the computation time by a factor of 4. Therefore,

$$J_z = \Gamma_e(J_{zm}), \tag{37}$$

where

$$\Gamma_e(\,) = 2\int_0^\infty \sum_0^\infty \epsilon_m(\,) \cos m\phi \cos\lambda z \, d\lambda,$$

and

$$\begin{aligned} \epsilon_m &= 1, \quad m = 0 \\ &= 2, \quad \text{otherwise.} \end{aligned}$$

Also, by substituting the asymptotic forms for the large argument for the modified Bessel functions,[6] it can be shown that J_{zm} decays as $\exp[-\lambda(b-\rho)]$ for large λ. Thus, the λ integration in Eq. (37) can be truncated for

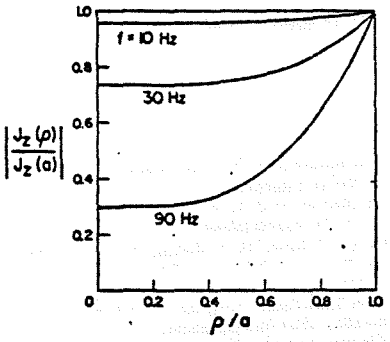


FIG. 2. The normalized magnitude of the axial current density as a function of ρ for symmetric excitation ($\psi = 360°$).

$\lambda(b-\rho)$ sufficiently large. A variable step size integration routine has been developed to effectively deal with the rapid variation in J_{z_m} for small λ and slower variation for larger λ. The convergence of the summation on m is more complicated and will be discussed later.

Calculations have been carried out for the following rope parameters: $a = 1$ cm, $\sigma_w = 1.1 \times 10^6$ mho/m, and $\mu_w = 200\,\mu_0$. This conductivity and permeability are roughly representative of stainless steel,[7] but the permeability of steel is quite variable.[8] The source parameters were chosen to be $b = 2a$ and $l = 2a$ with operating frequencies ($f = \omega/2\pi$) of 10, 30, and 90 Hz. Frequencies of 30 and 80 Hz are presently in use for rope testing and 10 Hz has been tried experimentally.[4] The plane wave skin depth δ for $\sigma_w \gg \omega\epsilon_w$ is given by

$$\delta = 1/(\pi f \mu_w \sigma_w)^{1/2}. \tag{38}$$

Thus, the frequencies chosen correspond to $a/\delta = 0.93$, 1.62, and 2.80.

The simplest toroidal coil to consider is one which completely encircles the rope ($\psi = 360°$) and produces fields and currents which are independent of ϕ. This type of yoke coil could be achieved in practice by using a hinge to allow the yoke to slip over the rope and close. For this case $a_m = 0$ for $m \neq 0$, and the m summation in Eq. (37) reduces to a single term. Results for the normalized magnitude and phase of J_z as a function of ρ are shown in Figs. 2 and 3. A nearly uniform current in magnitude and phase would be desirable for effectively probing the entire cross section of the rope, and this is nearly achieved at 10 but not at 30 and 90 Hz. However, there is at least some penetration to the center of the rope even at 90 Hz [$J_z(0)/J_z(a) \approx 0.3$]. The calculations in Figs. 2 and 3 were carried out for $z = 5a$, but examination of the rapid decay of J_{z_0} as a function of λ reveals that J_z is roughly constant in z for z small compared to a free-space wavelength. Thus, the result in Figs. 2 and 3 are nearly identical to those given previously for uniform current flow in the z direction.[3] It should also be noted that these results are quite different from those of the other polarization where the axial field is magnetic and the electric currents are azimuthal.[10]

Calculations have also been carried out for $\psi = 270°$ and 359°. The case of $\psi = 270°$ could represent a yoke coil which does not require a hinge to fit over the rope, and $\psi = 359°$ could represent a yoke coil which leaves a small gap when it closes down. Since a uniform current density is desirable in probing the rope, the relative strength of the higher harmonics in ϕ ($\cos m\phi$) compared to the constant term ($m = 0$) is of interest. Calculations reveal that for small values of z, the higher harmonics are quite large compared to the $m = 0$ term. However, for $|z|$ somewhat greater than a and $\frac{1}{2}l$, these higher harmonics begin to decay due to cancellation in the λ integration caused by the $\cos\lambda z$ factor. The rate of decay of the higher harmonics increases as m is increased. Consequently, it is sufficient to compare the first harmonic ($\cos\phi$) with the $m = 0$ term to determine how large $|z|$ must be in order to have a fairly uniform current in ϕ. Calculations reveal that for $|z| \gg a$, the first harmonic decays approximately as $|z|^{-3}$ which is consistent with the inverse distance cubed variation of quasistatic fields. Mathematically, this quasistatic incident magnetic field is produced by the formation of magnetic charge at ends of the magnetic current sheet ($\phi = \pm\frac{1}{2}\psi$) resulting in a large value of B_ϕ^i in Eq. (25). Due to TE to TM conversion (H_ϕ to E_z conversion) as indicated by Eq. (34), this quasistatic field couples to the higher harmonics of the axial electric field and current density. Whether this problem exists to any serious extent for any physical yoke coil or is simply a weakness of the discontinuous magnetic current model is an aspect of this problem which requires some further study. In any case it is possible to avoid higher ϕ harmonics by either (1) using a yoke coil which completely encircles the rope ($\psi = 360°$) or (2) observing the rope currents at a sufficient distance from the source. The second method must succeed for sufficiently large $|z|$ because the $m = 0$ current is essentially constant in z and the first harmonic decays as $|z|^{-3}$. Strictly speaking, these variations apply only for $|z|$ much less than a free-

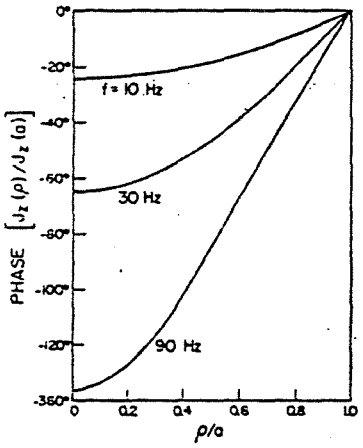


FIG. 3. The normalized phase of the axial current density as a function of ρ.

space wavelength, but this restriction will always be satisfied for the low frequencies considered here.

VI. CONCLUDING REMARKS

An idealized model of a flattened toroidal coil which encircles an infinitely long conducting rope has been analyzed. Calculations in Figs. 2 and 3 reveal that low frequencies on the order of 10 Hz are required to produce a uniform axial electric current in a typical wire rope. The field penetration is, however, somewhat better than would be predicted by simple plane wave skin depth theory.

For an exciting coil which does not completely encircle the wire rope, the symmetry in ϕ is lost, and harmonics in ϕ are produced in the axial rope current. These harmonics are large but decay fairly rapidly away from the source. The actual importance of these harmonics for a realistic exciting coil is a matter worthy of some further study.

A worthwhile extension of this work is to deduce the anomalous fields produced by internal rope imperfections such as broken strands or corrosion. These anomalies could be modeled by induced dipole moments whose strength is proportional to the exciting field multiplied by some effective polarizability.

[1] H. L. Libby, *Introduction to Electromagnetic Nondestructive Test Methods* (Wiley Interscience, New York, 1971).
[2] E. R. Hoskins, Report to U.S. Bureau of Mines on Contract No. H0346193, 1975 (unpublished).
[3] C. H. Larson, R. A. Egen, R. D. Jones, and H. A. Cross, Report to U.S. Bureau of Mines on Contract No. H0101741, 1971 (unpublished).
[4] J. G. Lang, The Canadian Mining and Metallurgical (CIM) Bulletin, 415—425, 1969 (unpublished).
[5] J. R. Wait, *Electromagnetic Radiation from Cylindrical Structures* (Pergamon, Oxford, 1959).
[6] M. Abramowitz and I. A. Stegun, *Handbook of Mathematical Function* (National Bureau of Standards, Washington, D.C., 1964), pp. 377—378.
[7] D. R. J. White, *Electromagnetic Shielding Materials and Performance* (Don White Consultants, Germantown, Md., 1975), Sec. 2.1.
[8] *Reference Data for Radio Engineers*, edited by I. G. Kandoian (ITT, New York, 1963), p. 4—32.
[9] N. W. McLachlan, *Bessel Functions for Engineers* (Clarendon Press, Oxford, 1955), Sec. 8.10.
[10] F. R. Bareham, Br. J. Appl. Phys. 11, 218—222 (1960).

Appl. Phys. 16, 391—398 (1978)

Applied Physics

Scattering by a Slender Void in a Homogeneous Conducting Wire Rope

D. A. Hill and *J. R. Wait*

Institute for Telecommunication Sciences, Office of Telecommunications, US Department of Commerce, Boulder, CO 80303, USA

Received 3 March 1978/Accepted 21 March 1978

Abstract. A thin prolate spheroidal void in an infinite conducting circular cylinder is used to model a broken strand in a wire rope. The rope is excited by an azimuthal magnetic line current which is a model for a thin toroidal coil. The anomalous external fields are computed from the induced electric and magnetic dipole moments of the void. The results have applications to nondestructive testing of wire ropes.

PACS: 41.10.Hv, 84.40Mk

Electromagnetic nondestructive testing is widely used in the metals industry to inspect and evaluate materials [1]. Both dc (direct current) and ac (alternating current) methods [2, 3] are currently used for inspection of wire ropes [4] which are made of electrically conducting ferromagnetic material. In both methods, the magnetic field is applied along the axis of the rope, and rope irregularities produce magnetic field changes which induce voltages in the sensing coils.

An alternative ac method would excite the rope with an axial electric field rather than an axial magnetic field. Since axial electric currents would be induced, this method might be more sensitive to broken strands than the present ac method which induces only azimuthal currents which tend to flow normally to the strands. Such a method could also be used on electrical conductors which are not ferromagnetic.

An appropriate source for excitation of axial electric currents is a toridal coil which encircles the rope, and a magnetic current model for the toroidal source coil has been analyzed [5]. Expressions for both the interior and exterior fields were derived for a homogeneous wire rope.

In this paper we wish to allow for the presence of a small slender void within the rope. Such a void can be considered a model for a broken strand. The void is also allowed to be oriented at any arbitrary angle to the rope axis to account for the winding geometry of the wire rope. The induced electric and magnetic dipole moments are computed from the primary fields and the electric and magnetic polarizabilities of the void. We then obtain expressions for the external fields of electric and magnetic dipoles of arbitrarily orientation. It is these external fields which are the observable quantities in any EM nondestructive testing method. The particular expressions, derived for the external fields of internal electric and magnetic dipoles, should be useful in future analyses of other types of small imperfections in wire ropes. Of course, in such cases, the electric and magnetic polarizabilities would be different.

Primary Field Excitation

In a previous analysis [5], we analyzed an azimuthal current sheet source which encircled the rope. The current sheet was allowed to have arbitrary width in the z or axial direction and arbitrary azimuthal extent. This source results in fairly complicated expressions for the electric and magnetic fields. Since, in this paper, we are primarily concerned with the fields scattered by the void, we take the simpler special case for the source shown in Fig. 1. Specifically, a magnetic current ring of strength K is located at a radius b in the plane $z=0$. This is a model for a thin toroidal coil which completely encircles the rope. The adopted time dependence is $\exp(i\omega t)$ for all source and field quantities.

The rope is assumed to be infinitely long and has radius a. It has conductivity σ_w, permittivity ε_w, and

0340-3793/78/0016/0391/$01.60

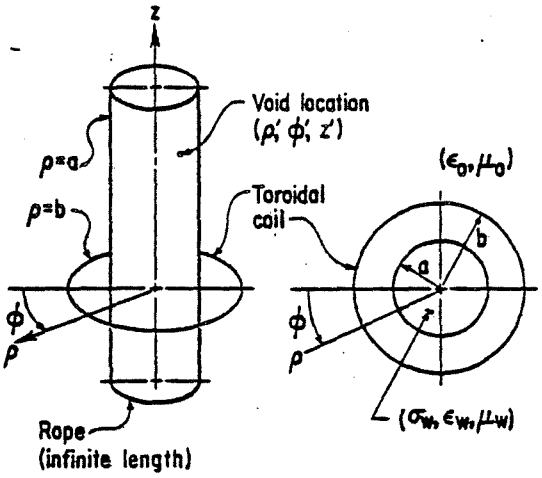


Fig. 1a

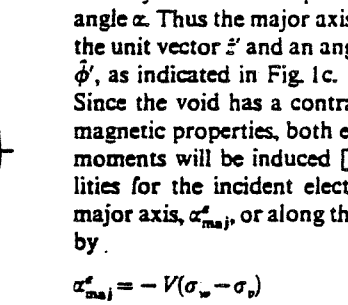


Fig. 1b

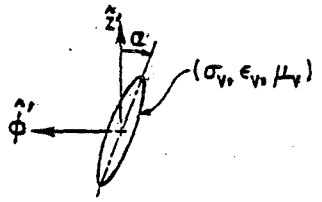


Fig. 1c

Fig. 1a–c. Thin toroidal coil surrounding a metal rope of infinite length (a) Perspective view, (b) Top view, (c) Prolate spheroidal void

permeability μ_w. The surrounding free space has permittivity ε_0 and permeability μ_0. For now, we defer discussion of the void properties and consider only the homogeneous rope.

Because of the symmetry of the source and the rope, the fields are TM (transverse magnetic) and independent of ϕ. The magnetic field has only a nonzero azimuthal component H_ϕ^{pr}, and the electric field has only nonzero axial and radial components E_z^{pr} and E_ϱ^{pr}. The superscript pr denotes the fields in the absence of the void. These primary fields have been derived previously [5], and the explicit forms both inside and outside the rope are given here in Appendix A. We note that E_ϱ^{pr} and H_ϕ^{pr} are zero for $\varrho=0$. On the other hand, E_z^{pr} is nearly independent of ϱ inside the rope for sufficiently low frequencies.

Induced Dipole Moments

We select a thin prolate spheroid of conductivity σ_v, permittivity ε_v, and permeability μ_v in order to model a broken strand. The prolate spheroidal shape is a convenient one because its electric and magnetic polarizabilities are known. However, we would not expect a significant difference for a thin circular cylinder of the same length and volume. To account for the winding geometry of the rope, we allow a rotation of the major axis of the spheroid about the ϱ' axis by an angle α. Thus the major axis is oriented at an angle α to the unit vector $\hat{z}'$ and an angle $\pi/2+\alpha$ to the unit vector $\hat{\phi}'$, as indicated in Fig. 1c.

Since the void has a contrast in both the electric and magnetic properties, both electric and magnetic dipole moments will be induced [6]. The electric polarizabilities for the incident electric field applied along the major axis, α^e_{maj}, or along the minor axis, α^e_{min}, are given by

$$\alpha^e_{maj} = -V(\sigma_w-\sigma_v) \tag{1}$$

and

$$\alpha^e_{min} = \frac{-2V(\sigma_w-\sigma_v)}{1+\sigma_v/\sigma_w}, \tag{2}$$

where V is the volume of the thin prolate spheroid. Since we anticipate the use of very low frequencies, we have neglected displacement currents. To include them, σ_w would be replaced by $\sigma_w+i\omega\varepsilon_w$ and σ_v would be replaced by $\sigma_v+i\omega\varepsilon_v$ in (1) and (2). The magnetic polarizabilities for the incident magnetic field applied along the major axis, α^m_{maj}, or along the minor axis, α^m_{min}, are similarly given by

$$\alpha^m_{maj} = -Vi\omega(\mu_w-\mu_v), \tag{3}$$

and

$$\alpha^m_{min} = \frac{-2Vi\omega(\mu_w-\mu_v)}{1+\mu_v/\mu_w}. \tag{4}$$

In order to compute the induced dipole moments, it is first necessary to resolve the incident electric and magnetic fields into components along the major and minor axes. The resultant induced dipole moments can then be resolved into the more convenient ϱ, ϕ, and z components. When this is done, the induced electric dipole moments are found to be

$$(Ids)_z = E_z^{pr}(\alpha^e_{maj}\cos^2\alpha+\alpha^e_{min}\sin^2\alpha), \tag{5}$$

$$(Ids)_\phi = E_z^{pr}(\alpha^e_{min}-\alpha^e_{maj})\sin\alpha\cos\alpha, \tag{6}$$

$$(Ids)_\varrho = E_\varrho^{pr}\alpha^e_{min}. \tag{7}$$

In (5)–(7), the primary electric field components E_z^{pr} and E_ϱ^{pr} are evaluated at ϱ', ϕ', z'. Similarly, the induced magnetic dipole moments are found to be

$$(Kdl)_z = H_\phi^{pr}(\alpha^m_{min}-\alpha^m_{maj})\sin\alpha\cos\alpha, \tag{8}$$

$$(Kdl)_\phi = H_\phi^{pr}(\alpha^m_{min}\cos^2\alpha+\alpha^m_{maj}\sin^2\alpha), \tag{9}$$

$$(Kdl)_\varrho = 0. \tag{10}$$

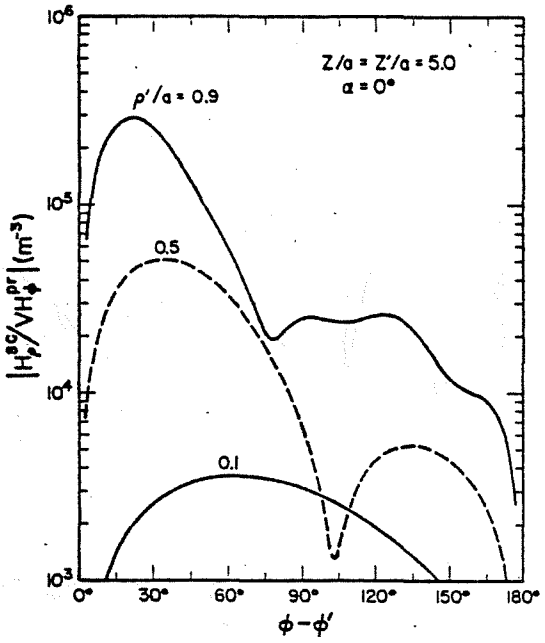


Fig. 2. The normalized magnitude of the scattered radial magnetic field for various void locations ϱ'

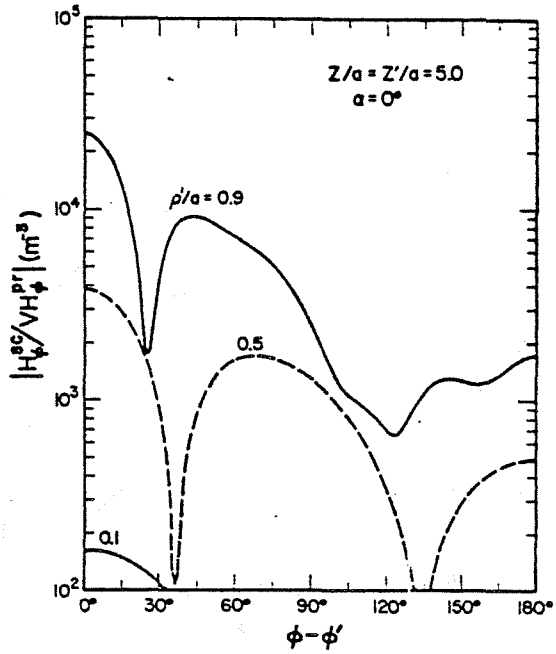


Fig. 3. The normalized magnitude of the scattered azimuthal magnetic field for various void locations ϱ'

Note that the units of the induced electric dipole moments in (5)–(7) are ampere meters, and the units of the induced magnetic dipole moments in (8)–(10) are volt-meters.

These induced dipole moments are the sources of the scattered field. In the following section, the specific expressions for the scattered field are discussed.

External Scattered Fields

The scattered field external to the rope is the observable quantity in any NDT system. Since we anticipate the use of coils for sensors, we will consider primarily the scattered magnetic field components $H_\varrho^{sc}(\varrho, \phi, z)$, $H_\phi^{sc}(\varrho, \phi, z)$, and $H_z^{sc}(\varrho, \phi, z)$. Each of these components can be written as a superposition of the contributions from each of the six induced dipole sources. [Actually, there are only five nonzero sources since $(Kdl)_\varrho$ is zero for the specific configuration considered here.]

The three scattered field components can be compactly written in the following matrix form

$$\begin{bmatrix} H_\varrho^{sc} \\ H_\phi^{sc} \\ H_z^{sc} \end{bmatrix} = \begin{bmatrix} G_{\varrho\varrho}^e & G_{\varrho\phi}^e & G_{\varrho z}^e \\ G_{\phi\varrho}^e & G_{\phi\phi}^e & G_{\phi z}^e \\ G_{z\varrho}^e & G_{z\phi}^e & G_{zz}^e \end{bmatrix} \cdot \begin{bmatrix} (Ids)_\varrho \\ (Ids)_\phi \\ (Ids)_z \end{bmatrix} + \begin{bmatrix} G_{\varrho\varrho}^m & G_{\varrho\phi}^m & G_{\varrho z}^m \\ G_{\phi\varrho}^m & G_{\phi\phi}^m & G_{\phi z}^m \\ G_{z\varrho}^m & G_{z\phi}^m & G_{zz}^m \end{bmatrix} \cdot \begin{bmatrix} (Kdl)_\varrho \\ (Kdl)_\phi \\ (Kdl)_z \end{bmatrix}. \quad (11)$$

In the first 3 by 3 matrix, $G_{\varrho\varrho}^e$ is the ϱ component of H at (ϱ, ϕ, z) produced by a unit ϱ-directed electric dipole at (ϱ', ϕ', z'). $G_{\varrho\phi}^e$ is the ϱ component of H produced by a unit ϕ-directed electric dipole at (ϱ', ϕ', z'), etc. The second 3 by 3 matrix is similar except that the G^m elements correspond to unit magnetic dipoles. We choose the above matrix notation rather than the elegant dyadic Green's function notation [7] because we are interested in the relative importance of each source and G term. Also, for the cylindrical geometry encountered here, all of the matrix elements can be derived in a systematic manner from z components of electric and magnetic Hertz vectors [8]. The specific expressions for the matrix elements are derived in Appendix B.

Numerical Results

The quantities of most interest in NDT are the external ($\varrho > a$) magnetic field components which are observed with the sensing coils. The primary magnetic field has only a ϕ component H_ϕ^{pr} which is given by (A.7) for $a < \varrho < b$ or by (A.11) for $\varrho > b$. The scattered magnetic field has all three components as given by (11). A computer program has been written to compute the external primary and scattered magnetic field components.

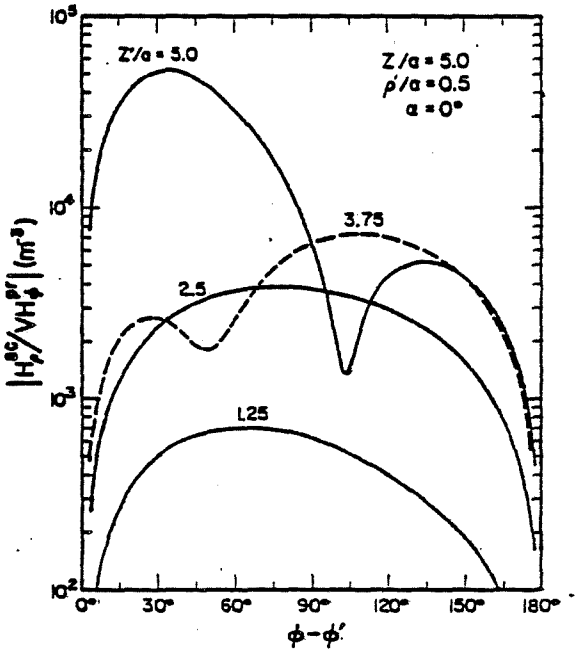


Fig. 4. The normalized magnitude of the scattered radial magnetic field for various void locations z'

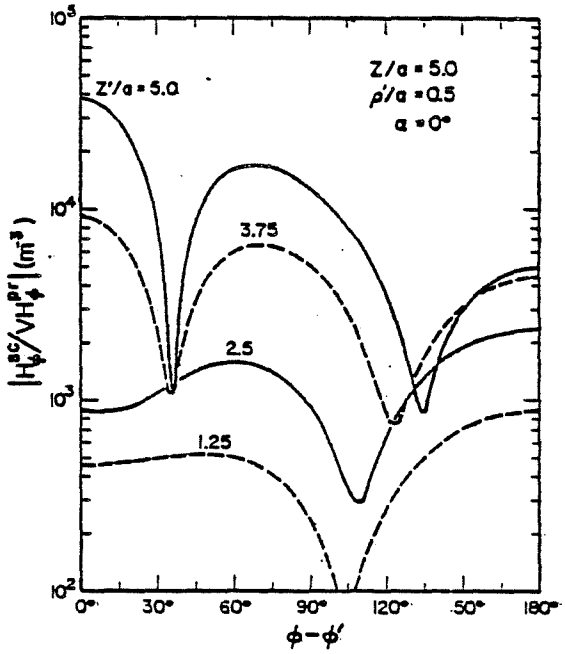


Fig. 5. The normalized magnitude of the scattered azimuthal magnetic field for various void locations z'

There are too many parameters to present a thorough parametric study here. For all numerical results shown the following parametric values remain fixed: $a=1$ cm, $\sigma_w=1.1\times10^6$ mho/m, $\mu_w=200\mu_0$, $b=2$ cm, frequency $=10$ Hz, $\varrho=2$ cm, $\sigma_v=0$, and $\mu_v=\mu_0$. For this low frequency, the conduction currents dominate, and the permittivities ε_w and ε_v are unimportant. The above values of σ_w and μ_w are roughly representative of stainless steel [9], but the permeability of steel is quite variable [10]. For the above parameters, the radius a is approximately one skin depth.

In Figs. 2–9, we show the magnitude of the scattered magnetic field components normalized by VH_ϕ^{pr} as a function of $\phi-\phi'$. The reason for showing the $\phi-\phi'$ dependence is that, although the primary field is independent of ϕ, the scattered field varies considerably in ϕ. This variation might dictate the use of multiple sensing coils spaced in azimuth around the rope. The curves are normalized by the primary field because the anomalous scattered field is measured in the presence of the primary field and their ratio is thus of interest. We also normalize the results to the volume V of the void in order to make the curves more general. However, a typical value for V might be on the order of 10^{-8} m^3 ($=1$ cm $\times$ 1 mm $\times$ 1 mm).

In Figs. 2 and 3, we set $z=z'=5a$ and $\alpha=0°$. By symmetry, $H_z^{sc}\simeq0$ for this case. H_ϱ^{sc} and H_ϕ^{sc} are of approximately the same level, but H_ϱ^{sc} is odd in $\phi-\phi'$ while H_ϕ^{sc} is even. Note the decrease in scattered field as the void is moved from the outer region ($\varrho'/a=0.9$) toward the center ($\varrho'/a=0.1$) of the rope.

In Figs. 4–6, we retain $z=5a$ and $\alpha=0°$ but allow z' to vary. Also, we set $\varrho'/a=0.5$. Note that the level of H_ϱ^{sc} and H_ϕ^{sc} increases as z' approaches z. However, H_z^{sc} is very small for $z'=z$, and its peak level is at about $z'/a=3.75$. Since $\alpha=0°$ in Figs. 2–6, only the axial and radial electric dipole moments, $(Ids)_z$ and $(Ids)_\varrho$, and the azimuthal magnetic dipole, $(Kdl)_\phi$, are induced. Also, $(Ids)_\varrho$ is very small because its exciting field E_ϱ^{pr} is small. The calculations reveal that $(Ids)_z$ and $(Kdl)_\phi$ contribute approximately equally to the scattered field.

In Figs. 7–9, we have $z=z'=5a$ and $\varrho'/a=0.5$, but we allow α to vary from 0° to 30°. Nonzero values of α allow two additional dipole moments, $(Ids)_\phi$ and $(Kdl)_z$ to be induced. The result is a decrease in the level of H_ϕ^{sc} and H_ϱ^{sc} and an increase in the level of H_z^{sc}.

The phase of the scattered field was also computed, but was found to be of less interest. Also, the individual dipole contributions were computed, and they are of individual interest since they will be excited differently for other sources on other void configurations.

Concluding Remarks

An idealized model for a wire break in an infinite conducting rope has been analyzed. The thin prolate

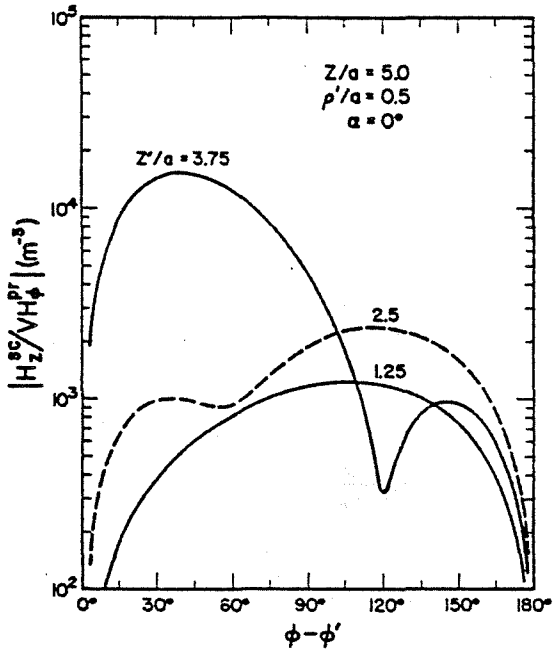


Fig. 6. The normalized magnitude of the scattered axial magnetic field for vaious void locations z'

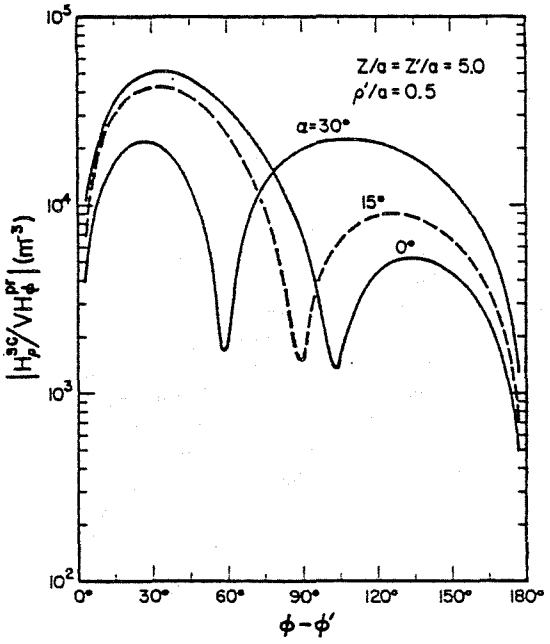


Fig. 7. The normalized magnitude of the scattered radial magnetic field for various void orientations α

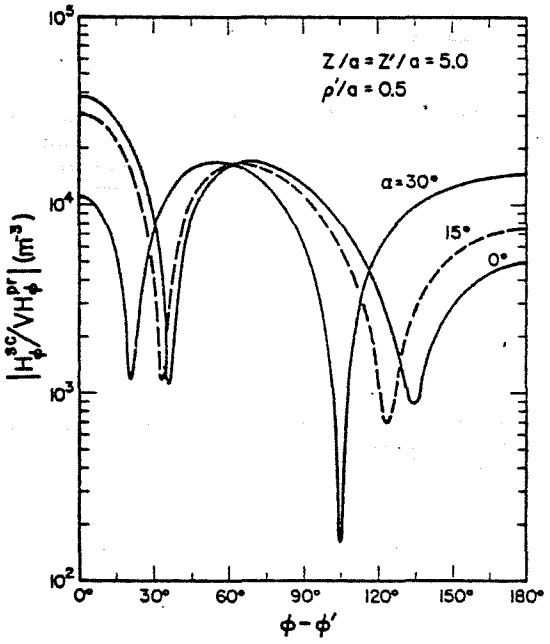


Fig. 8. The normalized magnitude of the scattered azimuthal magnetic field for various void orientations α

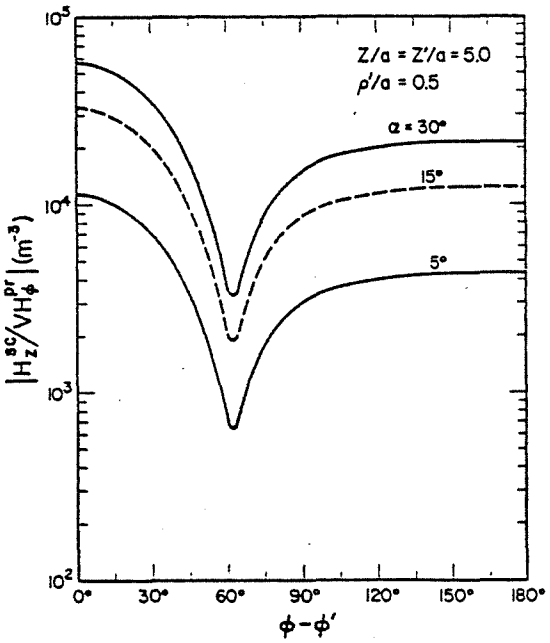


Fig. 9. The normalized magnitude of the scattered axial magnetic field for various void orientations α

spheroidal void has been shown to produce a significant anomaly in the external magnetic field when the rope is excited by a thin toroidal coil. In general, all three components of the scattered magnetic field are nonzero, but the azimuthal dependence is fairly complicated and contains some deep nulls. This suggests that multiple sensing coils of various locations and orientations might be worthwhile.

Although we have generated numerical results for the specific case of a thin prolate spheroidal void, the formulation given here actually yields the external fields for arbitrary induced electric and magnetic dipole moments. Thus the formulation is useful for any type of rope imperfection that can be characterized by induced electric and magnetic dipole moments. This requires only that the rope imperfection be small in terms of the rope radius and the rope skin depth. Larger imperfections should have a similar qualitative behavior, but could probably be rigorously analyzed only by solving an integral equation for the fields in the imperfection.

Also, it is a simple matter to perform similar calculations for a solenoidal coil of the type used in present NDT systems [3]. The scattered field calculation remains unchanged, but the primary field would be $TE(E_z^{pr}=0)$ rather than $TM(H_z^{pr}=0)$. Some calculations for this case have been carried out by Burrows [11] for the special case where both exciting and sensing coils are coaxial with the tubular specimen.

Appendix A

Primary Fields

The previous analysis for the homogeneous rope excitation [5] can be reduced to the present thin current ring source by letting the thickness l of the magnetic current source approach zero and by setting the azimuthal extent of the source equal to 2π. The resultant field expressions take different forms in the three regions, $\varrho<a$, $a<\varrho<b$, and $\varrho>b$.

Inside the rope ($\varrho<a$), we find

$$E_z^{pr}=-\int_{-\infty}^{\infty} w^2 a_0 I_0(w\varrho)\exp(-i\lambda z)d\lambda, \tag{A.1}$$

$$E_\varphi^{pr}=-\int_{-\infty}^{\infty} i\lambda w a_0 I_1(w\varrho)\exp(-i\lambda z)d\lambda, \tag{A.2}$$

$$H_\varphi^{pr}=-\int_{-\infty}^{\infty} i\omega\varepsilon_w a_0 I_1(w\varrho)\exp(-i\lambda z)d\lambda, \tag{A.3}$$

where $w=(\lambda^2+\gamma_w^2)^{1/2}$, $\gamma_w^2=i\omega\mu_w(\sigma_w+i\omega\varepsilon_w)$, $i\omega\hat{\varepsilon}_w=\sigma_w+i\omega\varepsilon_w$, and I_0 and I_1 are zero and first order modified Bessel functions. The factor a_0 is given by

$$a_0=\frac{-\gamma_0 B_0}{w^2 a I_0(wa)K_0(ua)}\cdot\left[\frac{\gamma_0 K_0'(ua)}{uK_0(ua)}-\eta_0 y_0\right]^{-1}, \tag{A.4}$$

where

$$B_0=\frac{Kb K_0'(ub)}{4\pi^2 u}, \qquad u=(\lambda^2+\gamma_0^2)^{1/2}$$

$$\gamma_0=i\omega(\mu_0\varepsilon_0)^{1/2}, \qquad \eta_0=(\mu_0/\varepsilon_0)^{1/2},$$

$$y_0=\frac{i\omega\hat{\varepsilon}_w}{w}\frac{I_1(wa)}{I_0(wa)}.$$

K is the strength of the magnetic current ring, K_0 is a zero-order modified Bessel function, and prime $'$ denotes differentiation with respect to the argument.

In the region between the rope and the source ($a<\varrho<b$), we find

$$E_z^{pr}=-\int_{-\infty}^{\infty} u^2[B_0 I_0(u\varrho)+C_0 K_0(u\varrho)]\exp(-i\lambda z)d\lambda, \tag{A.5}$$

$$E_\varphi^{pr}=-\int_{-\infty}^{\infty} i\lambda u[B_0 I_1(u\varrho)-C_0 K_1(u\varrho)]\exp(-i\lambda z)d\lambda, \tag{A.6}$$

$$H_\varphi^{pr}=-\int_{-\infty}^{\infty} i\omega\varepsilon_0 u[B_0 I_1(u\varrho)-C_0 K_1(u\varrho)]\exp(-i\lambda z)d\lambda, \tag{A.7}$$

where

$$C_0=-\frac{I_0(ua)\left[\frac{\gamma_0}{u}\frac{I_0'(ua)}{I_0(ua)}-\eta_0 y_0\right]}{K_0(ua)\left[\frac{\gamma_0}{u}\frac{K_0'(ua)}{K_0(ua)}-\eta_0 y_0\right]}B_0. \tag{A.8}$$

Outside the source ($\varrho>b$), we find

$$E_z^{pr}=-\int_{-\infty}^{\infty} u^2 A_0 K_0(u\varrho)\exp(-i\lambda z)d\lambda, \tag{A.9}$$

$$E_\varphi^{pr}=\int_{-\infty}^{\infty} i\lambda u A_0 K_1(u\varrho)\exp(-i\lambda z)d\lambda, \tag{A.10}$$

$$H_\varphi^{pr}=\int_{-\infty}^{\infty} i\omega\varepsilon_0 u A_0 K_1(u\varrho)\exp(-i\lambda z)d\lambda, \tag{A.11}$$

where

$$A_0=C_0-B_0 I_1(ub)/K_1(ub). \tag{A.12}$$

Appendix B

Dipole Fields

The derivation of the fields produced by a dipole source within a circular wire rope is analogous to that for a dipole source in a circular tunnel [8, 9], and some of the details are excluded here. The fields within the wire rope for $\varrho'<\varrho<a$ can be obtained from U_w and V_w which are the z components of electric and magnetic Hertz vectors

$$U_w=\Gamma[A_m(\lambda)K_m(w\varrho)+P_m(\lambda)I_m(w\varrho)], \tag{B.1}$$

$$V_w=\Gamma[B_m(\lambda)K_m(w\varrho)+Q_m(\lambda)I_m(w\varrho)], \tag{B.2}$$

where

$$\Gamma[\ ]=\int_{-\infty}^{\infty}\sum_{-\infty}^{\infty}[\ ]e^{-im(\phi-\phi')}e^{-i\lambda(z-z')}d\lambda. \tag{B.3}$$

$A_m(\lambda)$ and $B_m(\lambda)$ are functions of the source dipole and will later be given for the six dipole types. P_m and Q_m are determined from the boundary conditions at $\varrho=a$ and are given by

$$P_m=-\left\{A_m\left[\left(\frac{m\lambda}{w^2 a}-\alpha_m\right)^2+\left(\frac{\gamma_w K_m'}{wK_m}+\eta_w Y_m\right)\left(\frac{\gamma_w I_m'}{wI_m}+\frac{Z_m}{\eta_w}\right)\right]I_m K_m + B_m\left(\frac{m\lambda}{w^2 a}-\alpha_m\right)\frac{i\omega\mu_w}{w^2 a}\right\}D_m^{-1}, \tag{B.4}$$

$$Q_m=-\left\{B_m\left[\left(\frac{m\lambda}{w^2 a}-\alpha_m\right)^2+\left(\frac{\gamma_w I_m'}{wI_m}+\eta_w Y_m\right)\left(\frac{\gamma_w K_m'}{wK_m}+\frac{Z_m}{\eta_w}\right)\right]I_m K_m - A_m\left(\frac{m\lambda}{w^2 a}-\alpha_m\right)\frac{i\omega\hat{\varepsilon}_w}{w^2 a}\right\}D_m^{-1}. \tag{B.5}$$

where

$$D_m=\left[\left(\frac{m\lambda}{w^2a}-\alpha_m\right)^2+\left(\frac{\gamma_w I'_m}{wI_m}+\eta_w Y_m\right)\left(\frac{\gamma_w I'_m}{wI_m}+\frac{Z_m}{\eta_w}\right)\right]I_m^2,$$

$$\alpha_m=\frac{m\lambda}{u^2a},\quad Z_m=\frac{-i\omega\mu_0}{u}\frac{K'_m(ua)}{K_m(ua)},$$

and

$$Y_m=\frac{-i\omega\varepsilon_0}{u}\frac{K'_m(ua)}{K_m(ua)}.$$

The argument of the modified Bessel functions I_m and K_m is wa unless indicated otherwise.

The external fields ($\varrho>a$) can be obtained from

$$U=\Gamma[U_m]\quad\text{and}\quad V=\Gamma[V_m],\tag{B.6}$$

where

$$U_m=S_m(\lambda)K_m(u\varrho)$$

and

$$V_m=T_m(\lambda)K_m(u\varrho).$$

Continuity of E_z and H_z at $\varrho=a$ yields

$$S_m=\frac{w^2}{u^2}\left[\frac{A_mK_m(wa)+P_mI_m(wa)}{K_m(ua)}\right],\tag{B.7}$$

and

$$T_m=\frac{w^2}{u^2}\left[\frac{B_mK_m(wa)+Q_mI_m(wa)}{K_m(ua)}\right].\tag{B.8}$$

The external magnetic field components can be written

$$H_\varrho=\Gamma[H_{\varrho m}],\quad H_\phi=\Gamma[H_{\phi m}],\quad\text{and}\quad H_z=\Gamma[H_{zm}],\tag{B.9}$$

where

$$H_{\varrho m}=-i\lambda\frac{\partial V_m}{\partial\varrho}+\frac{\omega\varepsilon_0 m}{\varrho}U_m$$

$$=i\lambda uT_mK'_m(u\varrho)+\frac{\omega\varepsilon_0 m}{\varrho}S_mK_m(u\varrho),\tag{B.10}$$

$$H_{\phi m}=\frac{-m\lambda}{\varrho}V_m-i\omega\varepsilon_0\frac{\partial U_m}{\partial\varrho}$$

$$=\frac{-m\lambda}{\varrho}T_mK_m(u\varrho)-i\omega\varepsilon_0uS_mK'_m(u\varrho),\tag{B.11}$$

and

$$H_{zm}=-u^2V_m=-u^2T_mK_m(u\varrho).\tag{B.12}$$

Similar expressions are available for the electric field components. Equations (B.1)–(B.12) yield the external magnetic field components in terms of A_m and B_m which are functions of the source dipole. We now tabulate A_m and B_m for the six dipole types [8].

For a radial electric dipole $(Ids)_\varrho$, we have

$$A_m=(Ids)_\varrho\cdot\frac{-i\lambda}{4\pi^2i\omega\varepsilon_w w}I'_m(w\varrho')\tag{B.13}$$

and

$$B_m=(Ids)_\varrho\cdot\frac{im}{4\pi^2w^2\varrho'}I_m(w\varrho').\tag{B.14}$$

For an azimuthal electric dipole $(Ids)_\phi$, we have

$$A_m=(Ids)_\phi\cdot\frac{m\lambda}{4\pi^2i\omega\varepsilon_w w^2\varrho'}I_m(w\varrho')\tag{B.15}$$

and

$$B_m=(Ids)_\phi\cdot\frac{-1}{4\pi^2w}I'_m(w\varrho').\tag{B.16}$$

For an axial electric dipole $(Ids)_z$, we have

$$A_m=(Ids)_z\cdot\frac{I_m(w\varrho')}{4\pi^2i\omega\varepsilon_w}\tag{B.17}$$

and

$$B_m=0.\tag{B.18}$$

For a radial magnetic dipole $(Kdl)_\varrho$, we have

$$A_m=(Kdl)_\varrho\cdot\frac{im}{4\pi^2w^2\varrho'}I_m(w\varrho')\tag{B.19}$$

and

$$B_m=(Kdl)_\varrho\cdot\frac{-i\lambda}{4\pi^2wi\omega\mu_w}I'_m(w\varrho').\tag{B.20}$$

For an azimuthal magnetic dipole $(Kdl)_\phi$, we have

$$A_m=(Kdl)_\phi\cdot\frac{-1}{4\pi^2w^2}I'_m(w\varrho')\tag{B.21}$$

and

$$B_m=(Kdl)_\phi\cdot\frac{m\lambda}{4\pi^2w^2i\omega\mu_w\varrho'}I_m(w\varrho').\tag{B.22}$$

For an axial magnetic dipole $(Kdl)_z$, we have

$$A_m=0\tag{B.23}$$

and

$$B_m=(Kdl)_z\cdot\frac{I_m(w\varrho')}{4\pi^2i\omega\mu_w}.\tag{B.24}$$

We are now able to define the matrix elements required in (11) in terms of H_ϱ, H_ϕ, and H_z given in (B.9). For each of the six dipole types, we can define the required three elements in a column matrix as follows.

For a radial electric dipole $(Ids)_\varrho$, we have

$$\begin{bmatrix}G^e_{\varrho\varrho}\\G^e_{\phi\varrho}\\G^e_{z\varrho}\end{bmatrix}=\frac{1}{(Ids)_\varrho}\begin{bmatrix}H_\varrho\\H_\phi\\H_z\end{bmatrix}.\tag{B.25}$$

For an azimuthal electric dipole $(Ids)_\phi$, we have

$$\begin{bmatrix}G^e_{\varrho\phi}\\G^e_{\phi\phi}\\G^e_{z\phi}\end{bmatrix}=\frac{1}{(Ids)_\phi}\begin{bmatrix}H_\varrho\\H_\phi\\H_z\end{bmatrix},\tag{B.26}$$

For an axial electric dipole $(Ids)_z$, we have

$$\begin{bmatrix}G^e_{\varrho z}\\G^e_{\phi z}\\G^e_{zz}\end{bmatrix}=\frac{1}{(Ids)_z}\begin{bmatrix}H_\varrho\\H_\phi\\H_z\end{bmatrix}.\tag{B.27}$$

For a radial magnetic dipole $(Kdl)_\varrho$, we have

$$\begin{bmatrix}G^m_{\varrho\varrho}\\G^m_{\phi\varrho}\\G^m_{z\varrho}\end{bmatrix}=\frac{1}{(Kdl)_\varrho}\begin{bmatrix}H_\varrho\\H_\phi\\H_z\end{bmatrix}.\tag{B.28}$$

For an azimuthal magnetic dipole $(Kdl)_\phi$, we have

$$\begin{bmatrix}G^m_{\varrho\phi}\\G^m_{\phi\phi}\\G^m_{z\phi}\end{bmatrix}=\frac{1}{(Kdl)_\phi}\begin{bmatrix}H_\varrho\\H_\phi\\H_z\end{bmatrix}.\tag{5.29}$$

For an axial magentic dipole $(Kdl)_z$, we have

$$\begin{bmatrix}G^m_{\varrho z}\\G^m_{\phi z}\\G^m_{zz}\end{bmatrix}=\frac{1}{(Kdl)_z}\begin{bmatrix}H_\varrho\\H_\phi\\H_z\end{bmatrix}.\tag{B.30}$$

In order to numerically evaluate the G elements, we encounter the infinite summation and integration of the Γ operator, as indicated by (B.9). However, all of the G elements are either even or odd in m and

λ, and the summation and integration can be taken over positive values of m and λ to reduce the computation time by a factor of 4. Also, all G elements are calculated in parallel which means that the required modified Bessel are calculated only once resulting in a large time savings. In evaluating the λ integration, a variable step size integration is used to deal effectively with the rapid variation for small λ and the slower variation for large λ. Thus the subroutine which computes all 18 elements makes use of all these time saving features and is quite fast.

References

1. H.L. Libby: *Introduction to Electromagnetic Nondestructive Test Methods* (Wiley Interscience, New York 1971). [Gives numerous references]
2. C.H. Larsen, R.A. Egen, R.D. Jones, H.A. Cross: Report to the U.S. Bureau of Mines on Contract No. H0101741, June (1971)
3. J.G. Lang: The Canadian Mining and Metallurgical (CIM) Bulletin. 415 (1969)
4. E.R. Hoskins: Report to the U.S. Bureau of Mines of Contract No. H0346193 (South Dakota School of Mines & Technology) July (1975)
5. D.A. Hill, J.R. Wait: J. Appl. Phys. 48, 4893 (1977)
6. W.R. Smythe: *Static and Dynamic Electricity*, 3rd ed. (McGraw-Hill Book Co., New York 1968). Sec. 5.28, p. 171
7. C.T. Tai: *Dyadic Green's Functions in Electromagnetic Theory* (Scranton, Intext 1971)
8. J.R. Wait, D.A. Hill: Appl. Phys. 11, 351 (1976)
9. D.R.J. White: *Electromagnetic Shielding Material and Performance* (Don White Consultants, Inc., Germantown, MD 1975), Sec. 2.1
10. A.G. Kandoian: *Reference Data for Radio Engineers* (ITT Corp., New York 1968) pp. 4–32
11. M.L. Burrows: Ph.D. Thesis (Dept. of Electrical Engrg., University of Michigan, Ann Arbor 1964)

Appl. Phys. 18, 141—147 (1979)

Applied Physics

Electromagnetic Field Perturbation by an Internal Void in a Conducting Cylinder Excited by a Wire Loop

D. A. Hill and *J. R. Wait*

ITS/NTIA and ERL/NOAA, U.S. Department of Commerce, Boulder, CO 80303, USA

Received 14 August 1978/Accepted 26 September 1978

Abstract. A thin prolate spheroidal void in an infinite conducting circular cylinder is used to model an internal flaw in a wire rope. The rope is excited by an electric ring current which is a model for a thin solenoid or multi-turn wire loop. The anomalous external fields are computed from the induced electric and magnetic dipole moments of the void. For this type of excitation, the induced axial magnetic dipole moment is the dominant contributor to the scattered field. The results have application to nondestructive testing of wire ropes.

PACS: 41.10 Hv, 84.40 Mk.

Electromagnetic NDT (Nondestructive Testing) is widely used for inspection and evaluation of metals [1], and electromagnetic methods in NDT of wire ropes [2] have recently been reviewed [3]. Both DC and AC methods [4, 5] are currently in use. In both methods, the magnetic field is applied along the axis of the rope, and rope irregularities produce magnetic field changes which induce voltages in the sensing coils. A two-dimensional model of solenoidal (electric current ring) excitation of a homogeneous wire rope has now been analyzed fully [6]. The toroidal coil (magnetic current ring) excitation was also treated by invoking the principle of duality. A further analysis deals with a two-dimensional model for a wire rope with an internal anomaly [7], and the resulting change in the input impedance of the surrounding solenoid.

Here we consider a three-dimensional model in which an electric current ring is used to model a thin solenoid or multi-turn wire loop. The analogous problem of a magnetic current ring has already been solved [8]; thus the needed primary field expressions can be obtained from the magnetic ring current solution by duality. We allow for the presence of a small slender void within the otherwise homogeneous rope. Such a void can be considered a model for a broken wire within the rope or similar internal flaw. The void is allowed to be oriented at any arbitrary angle to the rope axis to account for the winding geometry. Following a previous analysis [9], we compute the induced electric and magnetic dipole moments from the primary fields and the electric and magnetic polarizabilities of the void. The external fields of the induced dipole moments are then calculated using the previous formulation for dipoles of arbitrary orientation [9]. These external fields are the observable quantities in any non-destructive testing method.

The most common methods of wire rope testing detect the average or integrated value of the circumferential electric field with a receiving solenoid which completely encircles the rope. Usually this is done by making and measuring the change in the mutual impedance of two coaxial loops or similar arrangement. But, in addition, one should be able to probe the detailed structure of the external magnetic field components with small sensing coils. Because this possibility has not been well explored, we present here, in graphical form, the azimuthal dependence of the three components of the external magnetic field for a significant range of the relevant parameters. These plots are intended to be an aid to the design of an effective con-

0340-3793/79/0018/0141/S01.40

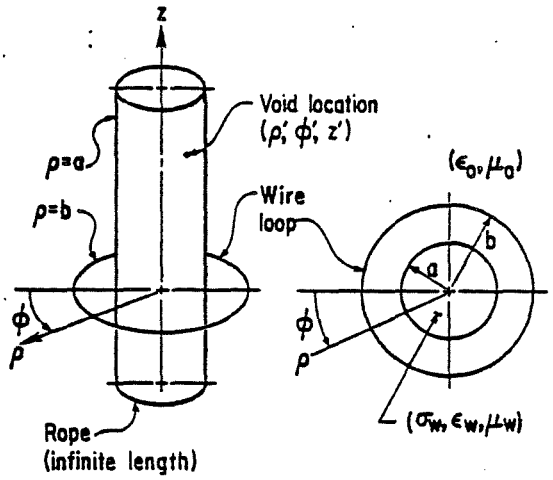


Fig. 1a Fig. 1b

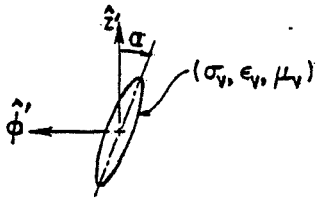


Fig. 1c

Fig. 1a–c. Thin solenoid surrounding a metal rope of infinite length. a) Perspective view, b) Top view, c) Prolate spheroidal void

figuration of sensing coils. Although the analysis is carried out for the AC case, DC excitation is included as a special case.

Primary Field Excitation

The geometry of the rope and the source are shown in Fig. 1. The rope is infinitely long and has radius a, conductivity σ_w, permittivity ε_w, and (magnetic) permeability μ_w. The surrounding free space has permittivity ε_0 and permeability μ_0. For now, we defer discussion of the void properties and consider only the homogeneous rope.

The source is an electric current ring of strength I located at $\varrho=b$ in the plane $z=0$. This is a model for a thin and narrow solenoid which completely encircles the rope. This source is the dual of the magnetic current ring or thin toroidal coil which was considered previously [9]. The time dependence is $\exp(i\omega t)$ for all source and field quantities.

Due to the symmetry of the source and the rope, the fields are TE to z (Transverse Electric) and independent of ϕ. The electric field has only a nonzero azimuthal component E_ϕ^{pr}, and the magnetic field has only nonzero axial and radial components H_z^{pr} and H_ϱ^{pr}. The superscript pr denotes the fields in the absence of the void. Since the dual problem of the magnetic ring source has already been solved [9], the fields of the electric ring source can be obtained by duality [10]. The resultant expressions for the primary fields both inside and outside the rope are given in Appendix A. The axial magnetic field H_z^{pr} is nearly independent of ϱ inside the rope for sufficiently low frequencies. On the other hand, H_ϱ^{pr} and E_ϕ^{pr} are zero at the rope center $\varrho=0$. For the DC limit ($\omega=0$), E_ϕ^{pr} is zero everywhere.

Induced Dipole Moments

To allow comparison between the toroid [9] and solenoid excitation, we again select a thin prolate spheroid in order to model a broken strand. As indicated in Fig. 1c, the spheroid has conductivity σ_v, permittivity ε_v, and permeability μ_v. We also allow a rotation of the major axis of the spheroid about the ϱ' axis by an angle α in order to account for the winding geometry of the rope. Consequently, the major axis is oriented at an angle α to the unit vector $\hat{z}'$ and an angle $\pi/2+\alpha$ to the unit vector $\hat{\phi}'$.

The prolate spheroidal void model is a convenient one because the electric and magnetic polarizabilities are known [11]. The electric polarizabilities for the incident electric field applied along the major axis, α_{maj}^e, or along the minor axis, α_{min}^e, are given by

$$\alpha_{maj}^e = -V(\sigma_w - \sigma_v) \tag{1}$$

and

$$\alpha_{min}^e = \frac{-2V(\sigma_w - \sigma_v)}{1+\sigma_v/\sigma_w}, \tag{2}$$

where V is the volume of the thin prolate spheroid. Displacement currents have been neglected in (1) and (2), but they can be included merely by replacing σ_w by $\sigma_w + i\omega\varepsilon_w$ and σ_v by $\sigma_v + i\omega\varepsilon_v$. The magnetic polarizabilities for the incident magnetic field applied along the major axis, α_{maj}^m, or along the minor axis, α_{min}^m, are given by

$$\alpha_{maj}^m = -V i\omega(\mu_w - \mu_v) \tag{3}$$

and

$$\alpha_{min}^m = \frac{-2V i\omega(\mu_w - \mu_v)}{1+\mu_v/\mu_w}. \tag{4}$$

Although the polarizabilities in (1)–(4) are derived for a thin prolate spheroid, we would not expect a significant difference for a thin circular cylinder of the same length and volume.

In order to compute the induced dipole moments, it is necessary to first resolve the incident electric and mag-

netic fields into components along the major and minor axes. The resultant dipole moments can then be resolved into the more convenient ϱ, ϕ, and z components. When this is done, the induced electric dipole moments are found to be

$$(Ids)_z = E^{pr}_{\phi}(\alpha^e_{min} - \alpha^e_{maj}) \sin\alpha \cos\alpha, \tag{5}$$

$$(Ids)_{\phi} = E^{pr}_{\phi}(\alpha^e_{min} \cos^2\alpha + \alpha^e_{maj} \sin^2\alpha), \tag{6}$$

$$(Ids)_{\varrho} = 0. \tag{7}$$

The induced magnetic dipole moments are found to be

$$(Kdl)_z = H^{pr}_z(\alpha^m_{maj} \cos^2\alpha + \alpha^m_{min} \sin^2\alpha), \tag{8}$$

$$(Kdl)_{\phi} = H^{pr}_z(\alpha^m_{min} - \alpha^m_{maj}) \sin\alpha \cos\alpha, \tag{9}$$

$$(Kdl)_{\varrho} = H^{pr}_{\varrho}\alpha^m_{min}. \tag{10}$$

In (5)–(7), the primary field components E^{pr}_{ϕ}, H^{pr}_z, and H^{pr}_{ϱ} are evaluated at ϱ', ϕ', z'.

External Scattered Field

The total scattered field can be written as a superposition of the contributions from each of the six induced dipole sources given in (5)–(10). (Actually, there are only five nonzero sources since $(Ids)_{\varrho}$ is zero for the specific configuration considered here.) The scattered magnetic field components $H^{sc}_{\varrho}(\varrho, \phi, z)$, $H^{sc}_{\phi}(\varrho, \phi, z)$, and $H^{sc}_z(\varrho, \phi, z)$ are of particular interest when small coils are used as sensors. However, the scattered electric field components $E^{sc}_{\varrho}(\varrho, \phi, z)$, $E^{sc}_{\phi}(\varrho, \phi, z)$, and $E^{sc}_z(\varrho, \phi, z)$ can also be computed with little additional effort. The ϕ-averaged value of E^{sc}_{ϕ} is of interest when a solenoid which completely encircles the rope is used as a sensor.

Both the magnetic and electric scattered fields can be compactly written in the following matrix form:

$$\begin{bmatrix} H^{sc}_{\varrho} \\ H^{sc}_{\phi} \\ H^{sc}_z \end{bmatrix} = \begin{bmatrix} G^e_{\varrho\varrho} & G^e_{\varrho\phi} & G^e_{\varrho z} \\ G^e_{\phi\varrho} & G^e_{\phi\phi} & G^e_{\phi z} \\ G^e_{z\varrho} & G^e_{z\phi} & G^e_{zz} \end{bmatrix} \begin{bmatrix} (Ids)_{\varrho} \\ (Ids)_{\phi} \\ (Ids)_z \end{bmatrix} + \begin{bmatrix} G^m_{\varrho\varrho} & G^m_{\varrho\phi} & G^m_{\varrho z} \\ G^m_{\phi\varrho} & G^m_{\phi\phi} & G^m_{\phi z} \\ G^m_{z\varrho} & G^m_{z\phi} & G^m_{zz} \end{bmatrix} \begin{bmatrix} (Kdl)_{\varrho} \\ (Kdl)_{\phi} \\ (Kdl)_z \end{bmatrix} \tag{11}$$

and

$$\begin{bmatrix} E^{sc}_{\varrho} \\ E^{sc}_{\phi} \\ E^{sc}_z \end{bmatrix} = \begin{bmatrix} F^e_{\varrho\varrho} & F^e_{\varrho\phi} & F^e_{\varrho z} \\ F^e_{\phi\varrho} & F^e_{\phi\phi} & F^e_{\phi z} \\ F^e_{z\varrho} & F^e_{z\phi} & F^e_{zz} \end{bmatrix} \begin{bmatrix} (Ids)_{\varrho} \\ (Ids)_{\phi} \\ (Ids)_z \end{bmatrix} + \begin{bmatrix} F^m_{\varrho\varrho} & F^m_{\varrho\phi} & F^m_{\varrho z} \\ F^m_{\phi\varrho} & F^m_{\phi\phi} & F^m_{\phi z} \\ F^m_{z\varrho} & F^m_{z\phi} & F^m_{zz} \end{bmatrix} \begin{bmatrix} (Kdl)_{\varrho} \\ (Kdl)_{\phi} \\ (Kdl)_z \end{bmatrix}. \tag{12}$$

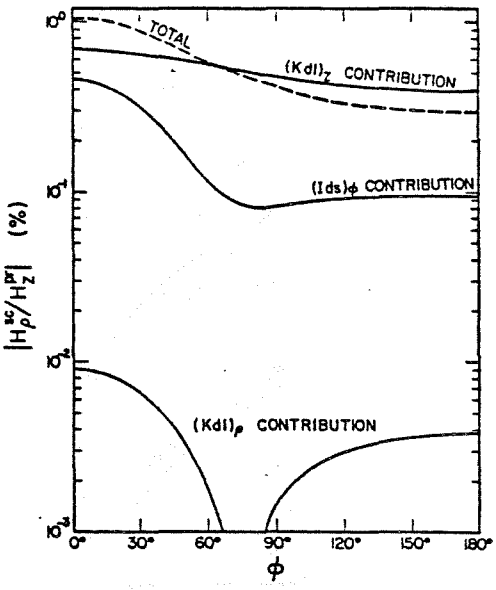


Fig. 2. Contribution of the individual dipole moments to H^{sc}_{ϱ} for an axially oriented void

In the first 3 by 3 matrix, $G^e_{\varrho\varrho}$ is the ϱ component of H at (ϱ, ϕ, z) produced by a unit ϱ-directed electric dipole at (ϱ', ϕ', z'), $G^e_{\varrho\phi}$ is the ϱ component of H produced by a unit ϕ-directed electric dipole at (ϱ', ϕ', z'), etc. The second 3 by 3 matrix is similar except that the G^m elements correspond to unit magnetic dipole sources. For the cylindrical geometry encountered here, all the matrix elements can be derived from z components of electric and magnetic Hertz vectors [12], and the specific expressions for the G elements have been given previously [9]. The expressions for the matrix elements in (12) are derived in Appendix B. The ϕ-averaged value of E^{sc}_{ϕ} which is of interest for solenoid reception is defined as

$$\overline{E^{sc}_{\phi}} = \frac{1}{2\pi} \int_0^{2\pi} E^{sc}_{\phi}(\varrho, \phi, z) d\phi. \tag{13}$$

The specific form of $\overline{E^{sc}_{\phi}}$ is also given in Appendix B. Of course, instead of (13), one could also obtain $\overline{E^{sc}_{\phi}}$ by integrating the flux over the area of the wire loop, but the present approach is simpler and more convenient.

Numerical Results

Numerically efficient computer programs have been written to evaluate the scattered fields as given by (11) and (12) and the primary fields as given by (A.5)–(A.7) for $a < \varrho < b$ and by (A.9)–(A.11) for $\varrho > b$.

In Figs. 2, 3, and 4 the magnitudes of the three scattered magnetic field components H^{sc}_{ϱ}, H^{sc}_{ϕ}, and H^{sc}_z are

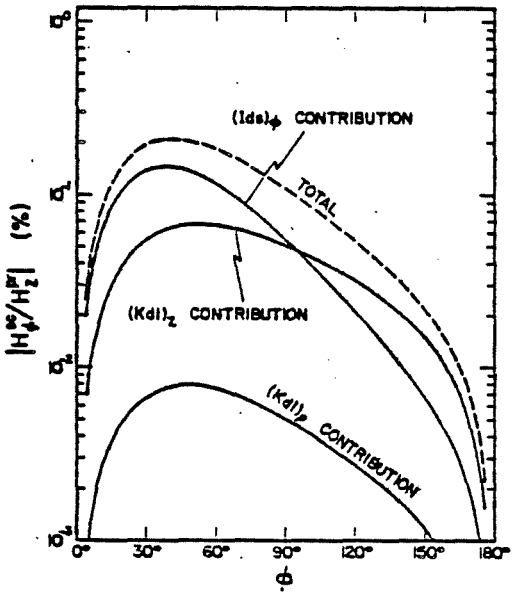


Fig. 3. Contribution of the individual dipole moments to H_ϕ^{sc}

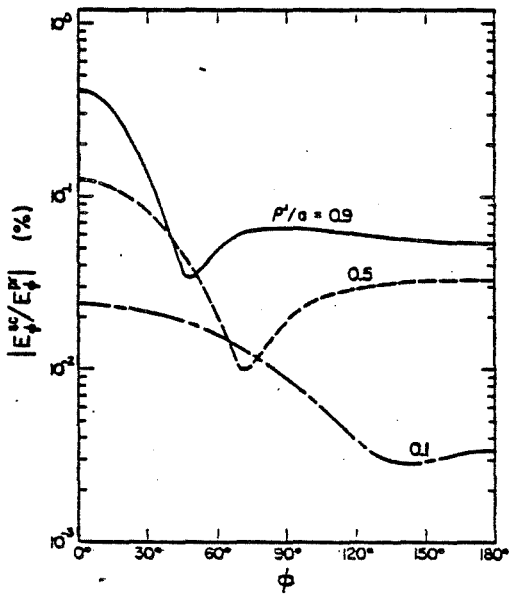


Fig. 5. Normalized magnitude of the scattered azimuthal electric field for various values of the void location ϱ'/a for $z'/a=5$

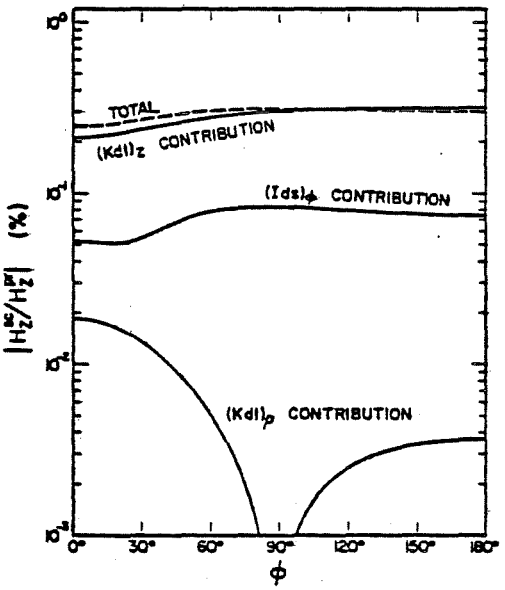


Fig. 4. Contribution of the individual dipole moments to H_z^{sc}

shown plotted as a function of ϕ for a selected set of the parameters. The vertical scale is in per cent of the primary axial magnetic field H_z^{pr} running from 10^{-3}% to 1%. The volume of the small slender void V is taken to be 10^{-6} m^3 ($=1$ mm $\times$ 1 mm $\times$ 1 cm) and the void itself is oriented in the axial direction (i.e. $\alpha=0°$). Since the scattered fields are proportional to V, the curves are easily scaled to other values of V. Also, the constitutive parameters of the void are taken to be those of free space: $\varepsilon_v=\varepsilon_0$, $\sigma_v=0$, and $\mu_v=\mu_0$. In these cases, ϕ' is taken to be zero, but for ϕ' not equal to zero, the horizontal axis can simply be replaced by $\phi-\phi'$. Other selected values of the parameters are: $a=1$ cm, $\sigma_w=1.1\times10^6$ mho/m, $\mu_w/\mu_0=200$, $b/a=2$, $\varrho'/a=0.5$, $z'/a=3.75$, $\varrho/a=2$, $z/a=5$, $f=10$ Hz.

The magnitudes of the individual dipole contributions to the total scattered field are also shown for each component of H in Figs. 2, 3, and 4. Since α is zero, there are only three induced dipole moments $(Kdl)_z$, $(Kdl)_\varrho$, and $(Ids)_\phi$. As expected, $(Kdl)_z$ is the major contributor. $(Kdl)_\varrho$ is small because H_ϱ^{pr} is very small inside the rope.

Actually, for solenoid reception, the value of $\overline{E_\phi^{sc}}$ is of primary importance. In Fig. 5, we also show the ϕ dependence of E_ϕ^{sc} for three values of ϱ'/a for $z'/a=5$. Of course, the greatest ϕ variation occurs for the void near the surface ($\varrho'/a=0.9$). In Table 1 the normalized averaged scattered azimuthal electric field $|\overline{E_\phi^{sc}}/E_\phi^{pr}|$ is shown for the same parameters which were used in Figs. 2–4. This is the quantity which indicates the sensitivity of the solenoid sensor used in present systems. The values of $|\overline{E_\phi^{sc}}/E_\phi^{pr}|$ are typically rather small ($\simeq0.01$%). Note in Fig. 5 that $|E_\phi^{sc}/E_\phi^{pr}|$ has a comparable level for $\varrho'/a=0.1$, but a much larger level for $\varrho'/a=0.5$ or 0.9. This is due to the higher ϕ harmonics in E_ϕ^{sc} which do not contribute to $\overline{E_\phi^{sc}}$. It is

also the case that the normalized scattered magnetic field components have a higher level because of the higher order harmonics in ϕ for $\varrho'/a \neq 0$.

Concluding Remarks

Excitation of a wire rope containing a slender void has been analyzed for a thin solenoid source. The prolate spheroidal void has been shown to produce an anomaly in the external fields which is typically larger than that produced for the case of toroidal excitation [9]. Again, the external scattered magnetic field components (not shown here) have a rather complicated azimuthal dependence containing some peaks and nulls. This suggests that multiple sensing coils of various locations and orientations might be worthwhile.

The ϕ-averaged value of the scattered azimuthal electric field $\overline{E_\phi^{sc}}$ has also been examined. This is the quantity which is sensed by a solenoidal sensor which encircles the rope, and Burrows [15] has also examined this quantity. This scattered field is typically quite small compared to the primary field as indicated in Table 1. Of course, the solenoid sensor does not make any use of the higher harmonics in ϕ which can be considerably larger than the ϕ-averaged value. However, a possible advantage of the solenoid sensor is that $\overline{E_\phi^{sc}}$ is not highly dependent on the void location. Thus the anomaly is related more to the void's volume than location. A system which senses the scattered field directly without any ϕ averaging will detect a greater anomaly when the void is located near the surface of the rope.

On the basis of calculations at other frequencies, one general conclusion is that 10 Hz is a good choice. Higher frequencies suffer from poor penetration of the rope. Also, the exciting solenoid and the sensors should be located as close to the rope as possible to maximize the relative scattered field.

The individual contributions of the various induced dipole moments to the scattered field are illustrated in Figs. 2–4. As expected for solenoidal excitation, the induced axial magnetic dipole moment is the dominant contributor to the scattered field. Actually, this dipole moment requires that the magnetic permeability of the rope be different from that of the void. In fact, calculations show that if the rope is nonmagnetic, the effect of the anomaly is quite small because only an electric dipole moment is induced.

A further worthwhile study would be to examine the response as a function of void location for a fixed geometry of the sensor. Some additional calculations, in a computer print-out format, that can give such information, may be obtained from the authors on request.

Table 1 - Normalized E_ϕ^{sc}

Parameters*	$\lvert E_\phi^{sc}/E_\phi^{pr}\rvert$ [%]
Same as Fig. 5	0.01044
$\varrho'/a = 0.1$	0.00986
$\varrho'/a = 0.9$	0.01472
$z'/a = 1.25$	0.01068
$z'/a = 2.5$	0.01058
$z'/a = 3.75$	0.01068
$\alpha = 15°$	0.01107
$\alpha = 30°$	0.01279
$f = 1$ Hz	0.01025
$f = 100$ Hz	0.00943
$f = 1000$ Hz	0.00009
$\varrho/a = 1.1$	0.01229
$\varrho/a = 1.5$	0.01124
$\sigma_w = 10^5$ mho/m	0.01025
$\sigma_w = 10^7$ mho/m	0.00993
$\mu_w/\mu_0 = 50$	0.02046
$\mu_w/\mu_0 = 10$	0.03367
$\mu_w/\mu_0 = 1$	0.00003
$b/a = 3$	0.01041
$b/a = 4$	0.01039
$z/a = z'/a = 2.5$	0.01049
$z/a = z'/a = 10$	0.01039
$\varrho/a = b/a = 1.1$	0.01229
$\varrho/a = b/a = 1.5$	0.01125
$\varrho/a = b/a = 3$	0.00937
$\varrho/a = b/a = 4$	0.00851
$a = 2$ cm	0.00143
$a = 2.5$ cm	0.00073

*Parameters for each entry are the same as Fig. 5 except where noted.

Although we have only examined the thin prolate spheroidal void, we have derived expressions which are useful for other shapes. The only requirement is that the imperfection be sufficiently small that its scattered fields can be represented by induced electric and magnetic dipole moments. Another convenient imperfection to treat would be an oblate spheroidal imperfection which could model a region of corrosion. Also, it might be possible to treat a rope model where the conductivity and permeability are tensors. This anisotropic feature of ropes is expected because of the winding geometry; the subject has been examined by Wait [16].

Appendix A

Primary Fields

The primary fields for excitation by a magnetic current ring of strength K have been derived previously [9]. By duality [10], the previous results hold for electric current ring excitation if we make the following transformations: $K \to I$, $H_\phi^{pr} \to E_\phi^{pr}$, $E_z^{pr} \to -H_z^{pr}$, $E_\varrho^{pr} \to -H_\varrho^{pr}$, $\mu_0 \to \varepsilon_0$, $\varepsilon_0 \to \mu_0$, $i\omega\mu_w \to \sigma_w + i\omega\varepsilon_w$, and $\sigma_w + i\omega\varepsilon_w \to i\omega\mu_w$. The resultant primary field expressions take different forms in the three regions, $\varrho < a$, $a < \varrho < b$, and $\varrho > b$.

Inside the rope ($\rho < a$), we find

$$H_z^w = -\int_{-\infty}^{\infty} w^2 a_0 I_0(w\rho)\exp(-i\lambda z)d\lambda, \quad (A.1)$$

$$H_\rho^w = -\int_{-\infty}^{\infty} i\lambda w a_0 I_1(w\rho)\exp(-i\lambda z)d\lambda, \quad (A.2)$$

$$E_\phi^w = i\omega\mu_w \int_{-\infty}^{\infty} w a_0 I_1(w\rho)\exp(-i\lambda z)d\lambda, \quad (A.3)$$

where $w=(\lambda^2+\gamma_w^2)^{1/2}$, $\gamma_w^2 = i\omega\mu_w(\sigma_w + i\omega\epsilon_w)$, and I_0 and I_1 are zero and first order modified Besesl functions. The factor a_0 is given by

$$a_0 = \frac{-\gamma_0 B_0}{w^2 a I_0(wa) K_0(ua)}\left[\frac{\gamma_0 K_0'(ua)}{u K_0(ua)} - \frac{z_0}{\eta_0}\right]^{-1}, \quad (A.4)$$

where

$$B_0 = \frac{IbK_0'(ub)}{2\pi u}, \quad u=(\lambda^2+\gamma_0^2)^{1/2},$$

$$\gamma_0 = i\omega(\mu_0\epsilon_0)^{1/2}, \quad \eta_0 = (\mu_0/\epsilon_0)^{1/2},$$

$$z_0 = \frac{i\omega\mu_w}{w}\frac{I_1(wa)}{I_0(wa)},$$

K_0 is a zero order modified Bessel function, and prime ' denotes differentiation with respect to the argument. (In the previous paper [9], the expression for B_0 should actually read $B_0 = -KbK_0'(ub)/(2\pi u\lambda)$)

In the region between the rope and the source ($a<\rho<b$), we find

$$H_z^w = -\int_{-\infty}^{\infty} u^2[B_0 I_0(u\rho) + C_0 K_0(u\rho)]\exp(-i\lambda z)d\lambda, \quad (A.5)$$

$$H_\rho^w = -\int_{-\infty}^{\infty} i\lambda u[B_0 I_1(u\rho) - C_0 K_1(u\rho)]\exp(-i\lambda z)d\lambda, \quad (A.6)$$

$$E_\phi^w = i\omega\mu_0 \int_{-\infty}^{\infty} u[B_0 I_1(u\rho) - C_0 K_1(u\rho)]\exp(-i\lambda z)d\lambda, \quad (A.7)$$

where

$$C_0 = -\frac{I_0(ua)\left[\frac{\gamma_0}{u}\frac{I_0'(ua)}{I_0(ua)} - \frac{z_0}{\eta_0}\right]}{K_0(ua)\left[\frac{\gamma_0}{u}\frac{K_0'(ua)}{K_0(ua)} - \frac{z_0}{\eta_0}\right]} B_0. \quad (A.8)$$

Outside the source ($\rho > b$), we find

$$H_z^w = -\int_{-\infty}^{\infty} u^2 A_0 K_0(u\rho)\exp(-i\lambda z)d\lambda, \quad (A.9)$$

$$H_\rho^w = \int_{-\infty}^{\infty} i\lambda u A_0 K_1(u\rho)\exp(-i\lambda z)d\lambda, \quad (A.10)$$

$$E_\phi^w = i\omega\mu_0 \int_{-\infty}^{\infty} u A_0 K_1(u\rho)\exp(-i\lambda z)d\lambda, \quad (A.11)$$

where

$$A_0 = C_0 - B_0 I_1(ub)/K_1(ub). \quad (A.12)$$

Appendix B

Scattered Electric Fields

The derivation for the electric fields produced by a dipole source within a wire rope is a direct extension of the derivation of the magnetic field derivation given previously [9], and some of the details are excluded here. The external fields can be obtained from U and V which are the z components of electric and magnetic Hertz vectors

$$U = \Gamma[U_m] \quad \text{and} \quad V = \Gamma[V_m], \quad (B.1)$$

where

$$U_m = S_m(\lambda)K_m(u\rho), \; V_m = T_m(\lambda)K_m(u\rho), \quad (B.2)$$

and

$$\Gamma[\;] = \int_{-\infty}^{\infty}\sum_{m=0}^{\infty}[\;]e^{-im(\phi-\phi')}e^{-i\lambda(z-z')}d\lambda. \quad (B.3)$$

The expressions for S_m and T_m have been given for each of the six dipole types [9].

The electric field components can be written

$$E_\rho = \Gamma[E_{\rho m}], E_\phi = \Gamma[E_{\phi m}] \quad \text{and} \quad E_z = \Gamma[E_{zm}], \quad (B.4)$$

where

$$E_{\rho m} = -i\lambda\frac{\partial U_m}{\partial\rho} - \frac{\omega\mu_0 m}{\rho}V_m$$

$$= -i\lambda u S_m K_m'(u\rho) - \frac{\omega\mu_0 m}{\rho}T_m K_m(u\rho), \quad (B.5)$$

$$E_{\phi m} = \frac{-m\lambda}{\rho}U_m + i\omega\mu_0\frac{\partial V_m}{\partial\rho}$$

$$= \frac{-m\lambda}{\rho}S_m K_m(u\rho) + i\omega\mu_0 u T_m K_m'(u\rho), \quad (B.6)$$

and

$$E_{zm} = -u^2 U_m = -u^2 S_m K_m(u\rho). \quad (B.7)$$

We are now able to define the matrix elements required in (12) in terms of E_ρ, E_ϕ, and E_z given in (B.4). For each of the six dipole types, we can define the required three matrix elements in a column matrix as follows.

For a radial electric dipole $(Ids)_\rho$ we have

$$\begin{bmatrix} F_{\rho\rho}^w \\ F_{\phi\rho}^w \\ F_{z\rho}^w \end{bmatrix} = \frac{1}{(Ids)_\rho}\begin{bmatrix} E_\rho \\ E_\phi \\ E_z \end{bmatrix}. \quad (B.8)$$

For an azimuthal electric dipole $(Ids)_\phi$ we have

$$\begin{bmatrix} F_{\rho\phi}^w \\ F_{\phi\phi}^w \\ F_{z\phi}^w \end{bmatrix} = \frac{1}{(Ids)_\phi}\begin{bmatrix} E_\rho \\ E_\phi \\ E_z \end{bmatrix}. \quad (B.9)$$

For an axial electric dipole $(Ids)_z$ we have

$$\begin{bmatrix} F_{\rho z}^w \\ F_{\phi z}^w \\ F_{zz}^w \end{bmatrix} = \frac{1}{(Ids)_z}\begin{bmatrix} E_\rho \\ E_\phi \\ E_z \end{bmatrix}. \quad (B.10)$$

For a radial magnetic dipole $(Kdl)_\rho$ we have

$$\begin{bmatrix} F_{\rho\rho}^m \\ F_{\phi\rho}^m \\ F_{z\rho}^m \end{bmatrix} = \frac{1}{(Kdl)_\rho}\begin{bmatrix} E_\rho \\ E_\phi \\ E_z \end{bmatrix}. \quad (B.11)$$

For an azimuthal magnetic dipole $(Kdl)_\phi$, we have

$$\begin{bmatrix} F^m_{\rho\phi} \\ F^m_{\phi\phi} \\ F^m_{z\phi} \end{bmatrix} = \frac{1}{(Kdl)_\phi} \begin{bmatrix} E_\rho \\ E_\phi \\ E_z \end{bmatrix}. \tag{B.12}$$

For an axial magnetic dipole $(Kdl)_z$, we have

$$\begin{bmatrix} F^m_{\rho} \\ F^m_{\phi} \\ F^m_{z} \end{bmatrix} = \frac{1}{(Kdl)_z} \begin{bmatrix} E_\rho \\ E_\phi \\ E_z \end{bmatrix}. \tag{B.13}$$

The ϕ-averaged value of E_ϕ as given by (B.4) can be written

$$\bar{E}_\phi = \frac{1}{2\pi} \int_0^{2\pi} E_\phi d\phi = \Gamma_0[E_{\phi 0}] \tag{B.14}$$

where

$$\Gamma_0[\ ] = \int_{-\infty}^{\infty} [\ ] e^{-i\lambda u(s-z')} d\lambda$$

and

$$E_{\phi 0} = i\omega\mu_0 T_0 K_0'(u\rho).$$

As expected, only the $m=0$ term of the electric Hertz vector contributes to $\bar{E}_\phi$.

References

1. H.L.Libby: *Introduction to Nondestructive Test Methods* (Wiley Interscience, New York 1971)
2. E.R.Hoskins: Report to the U.S. Bureau of Mines on Contract No. H0346193, South Dakota School of Mines and Technology (July 1975)
3. J.R.Wait: Review of electromagnetic methods in nondestructive testing of wire ropes, Preliminary Report to the U.S. Bureau of Mines on Contract No. H0155008 (March 1978)
4. C.H.Larsen, R.A.Egen, R.D.Jones, H.A.Cross: Report to the U.S. Bureau of Mines on Contract No. H0101741 (June 1971)
5. J.G.Lang: The Canadian Mining and Metalurgical (CIM) Bulletin, 415 (1969)
6. J.R.Wait: The electromagnetic basis for nondestructive testing of cylindrical conductors, IEEE Trans. IM-27, 235 (1978)
7. J.R.Wait, R.L.Gardner: Non-destructive testing of a cylindrical conductor with an internal anomaly – A two-dimensional model, Preliminary Report to the U.S. Bureau of Mines on Contract No. H0155008 (May 1978)
8. D.A.Hill, J.R.Wait: J. Appl. Phys. 48, 4893 (1977)
9. D.A.Hill, J.R.Wait: Appl. Phys. 16, 391 (1978)
   On pg. 396, In equation (A.3) replace $i\omega\varepsilon_w$ by $i\omega\hat{\varepsilon}_w$;
   On pg. 397, In equation (B.10) replace $i\lambda u T_m$ by $-i\lambda u T_m$
10. R.F.Harrington: *Time-Harmonic Electromagnetic Fields* (McGraw-Hill, New York 1961) Sect. 3.2
11. W.R.Smythe: *Static and Dynamic Electricity* (McGraw-Hill, New York 1968) Sect. 5.28
12. J.R.Wait, D.A.Hill: Appl. Phys. 11, 351 (1976)
13. A.G.Kandoian: *Reference Data for Radio Engineers* (ITT Corp., New York 1968) pp. 4–32
14. D.R.J.White: *Electromagnetic Shielding Material and Performance* (Don White Consultants, Inc., Germantown, MD 1975) Sect. 2.1
15. M.L.Burrows: Ph. D. Thesis, Department of Electrical Engineering, University of Michigan, Ann Arbor (1964)
16. J.R.Wait: Electromagnetic induction in an anisotropic cylinder, Radio Sci. 13 (September/October 1978)

Radio Science, Volume 13, Number 5, pages 789–792, September–October 1978

Electromagnetic response of an anisotropic conducting cylinder to an external source

James R. Wait

Cooperative Institute for Research in Environmental Sciences, University of Colorado/National Oceanic and Atmospheric Administration, Boulder, Colorado 80309

(Received February 23, 1978.)

A novel analytical solution is obtained for the boundary value problem of a circular cylinder of infinite length that is excited by a prescribed external field. The cylinder is anisotropic in the sense that the complex conductivity and magnetic permeability are diagonal uniaxial tensors with generally unequal elements. The solution involves Bessel functions of nonintegral order. Known special cases are recovered.

INTRODUCTION

Many years ago, *Lord Rayleigh* [1918] presented an exact solution for the electromagnetic plane-wave scattering from a homogeneous dielectric cylinder of circular cross section. His analysis was restricted to perpendicular incidence in that the incident wave vector was perpendicular to the axis of the cylinder. It was not until many years later that the complete solution was published for arbitrary plane-wave incidence [*Wait*, 1955, 1965*a*]. The extension to compressible plasma cylinders was also formulated [*Wait*, 1965*b*]. Since then, many related theoretical and numerical studies of scattering from penetrable cylinders have been carried out including excitation by dipole sources. Excellent reviews are given in two textbooks [*Kerker*, 1969; *Bowman et al.*, 1969]. Each of these contains numerous references even though they are not comprehensive.

Some interesting complexities arise when the cylinder becomes anisotropic. The best-known example is a plasma column in the presence of an axial dc magnetic field [*Wilhelmsson*, 1958; *Large and Wait*, 1965, 1967; *Wait*, 1966, 1967, 1968; *Kong*, 1975].

The problem we wish to deal with here is that of a homogeneous cylinder of circular cross section, but with the conductivity (σ) and permeability (μ) as axial tensors where the off-diagonal terms are zero. Specifically, we may write

$$(\sigma) = \begin{pmatrix} \sigma_\rho & 0 & 0 \\ 0 & \sigma_\phi & 0 \\ 0 & 0 & \sigma_z \end{pmatrix} \tag{1}$$

$$(\mu) = \begin{pmatrix} \mu_\rho & 0 & 0 \\ 0 & \mu_\phi & 0 \\ 0 & 0 & \mu_z \end{pmatrix} \tag{2}$$

Physically, the cylinder may be thought of as a homogeneous structure that could be finely layered in the radial, azimuthal, and axial directions. We will not dwell here on the material composition that leads to the above-postulated tensor properties.

FORMULATION

To be specific, we choose a cylindrical coordinate system (ρ,ϕ,z) such that the surface of the cylinder is $\rho = a$ where a is the radius. The external region $\rho > a$ will contain the sources but for the time being we will restrict our attention to the internal region $\rho < a$.

Maxwell's equations for the internal region, for a time factor $\exp(i\omega t)$, are

$$(\sigma)\vec{E} = \text{curl}\,\vec{H} \tag{3}$$

$$-i\omega(\mu)\vec{H} = \text{curl}\,\vec{E} \tag{4}$$

where $\vec{E}$ and $\vec{H}$ are the vector electric and magnetic fields, respectively.

Here it should be noted that σ_ρ, σ_ϕ, and σ_z are scalar complex conductivies; thus, for example, $\sigma_\rho = g_\rho + i\omega\varepsilon_\rho$ where g_ρ and ε_ρ are the real conductivity and the real permittivity in the ρ direction. Similarly we could write $\mu_\rho = \mu_\rho' - i\mu_\rho''$ where μ_ρ' and μ_ρ''

0048-6604/78/0910-0789$01.00

are both positive real. An important limitation is that we restrict attention to time-harmonic fields of sufficiently small magnitude that the elements of (σ) and (μ) do not vary with the field magnitude (i.e., we are within the linear regime).

Equations (1) and (2), expressed in cylindrical coordinates, are

$$(1/\rho)\,\partial E_z/\partial\phi - \partial E_\phi/\partial z = -i\omega\mu_\rho H_\rho \tag{5}$$

$$\partial E_\rho/\partial z - \partial E_z/\partial\rho = -i\omega\mu_\phi H_\phi \tag{6}$$

$$(1/\rho)(\partial/\partial\rho)(\rho E_\phi) - (1/\rho)\,\partial E_\rho/\partial\phi = -i\omega\mu_z H_z \tag{7}$$

$$(1/\rho)\,\partial H_z/\partial\phi - \partial H_\phi/\partial z = \sigma_\rho E_\rho \tag{8}$$

$$\partial H_\rho/\partial z - \partial H_z/\partial\rho = \sigma_\phi E_\phi \tag{9}$$

$$(1/\rho)(\partial/\partial\rho)(\rho H_\phi) - (1/\rho)\,\partial H_\rho/\partial\phi = \sigma_z E_z \tag{10}$$

Leading up to later developments, we now assume that the field components vary according to $\exp(-im\phi)\exp(-i\lambda z)$. For single-valuedness, m is restricted to positive or negative integers including zero. The parameter λ, as yet, is unrestricted. Maxwell's equations are now simplified to

$$-(im/\rho)\,E_z + i\lambda E_\phi = -i\omega\mu_\rho H_\rho \tag{11}$$

$$-i\lambda E_\rho - \partial E_z/\partial\rho = -i\omega\mu_\phi H_\phi \tag{12}$$

$$(1/\rho)(\partial/\partial\rho)(\rho E_\phi) + (im/\rho)\,E_\rho = -i\omega\mu_z H_z \tag{13}$$

$$-(im/\rho)\,H_z + i\lambda H_\phi = \sigma_\rho E_\rho \tag{14}$$

$$-i\lambda H_\rho - \partial H_z/\partial\rho = \sigma_\phi E_\phi \tag{15}$$

$$(1/\rho)(\partial/\partial\rho)(\rho H_\phi) + (im/\rho)\,H_\rho = \sigma_z E_z \tag{16}$$

To proceed further, we can now decompose or decouple the above set of equations into two cases. In the first case we set $H_z = 0$, whence it is a simple matter to deduce that E_z satisfies

$$\frac{1}{\rho}\frac{\partial}{\partial\rho}\rho\frac{\partial}{\partial\rho}E_z - \frac{\sigma_\phi}{\sigma_\rho}\frac{m^2}{\rho^2}\frac{\lambda^2 + i\sigma_\rho\mu_\phi\omega}{\lambda^2 + i\sigma_\phi\mu_\rho\omega}E_z - (\lambda^2 + i\sigma_\rho\mu_\phi\omega)(\sigma_z/\sigma_\rho)\,E_z = 0 \tag{17}$$

The other case is when we set $E_z = 0$, whence H_z is found to satisfy

$$\frac{1}{\rho}\frac{\partial}{\partial\rho}\rho\frac{\partial}{\partial\rho}H_z - \frac{\mu_\phi}{\mu_\rho}\frac{m^2}{\rho^2}\frac{\lambda^2 + i\sigma_\phi\mu_\rho\omega}{\lambda^2 + i\sigma_\rho\mu_\phi\omega}H_z - (\lambda^2 + i\sigma_\phi\mu_\rho\omega)(\mu_z/\mu_\rho)\,H_z = 0 \tag{18}$$

Now, clearly, the total field is the superposition of these two cases. In fact, it is not difficult to show that

$$E_\rho = \frac{1}{(\lambda^2 + i\sigma_\rho\mu_\phi\omega)}\left[i\lambda\frac{\partial E_z}{\partial\rho} + \frac{m\omega\mu_\phi}{\rho}H_z\right] \tag{19}$$

$$E_\phi = \frac{1}{(\lambda^2 + i\sigma_\phi\mu_\rho\omega)}\left[\frac{\lambda m}{\rho}E_z - i\omega\mu_\rho\frac{\partial H_z}{\partial\rho}\right] \tag{20}$$

$$H_\rho = \frac{1}{(\lambda^2 + i\sigma_\phi\mu_\rho\omega)}\left[\frac{im\sigma_\phi}{\rho}E_z + i\lambda\frac{\partial H_z}{\partial\rho}\right] \tag{21}$$

$$H_\phi = \frac{1}{(\lambda^2 + i\sigma_\rho\mu_\phi\omega)}\left[\sigma_\rho\frac{\partial E_z}{\partial\rho} + \frac{\lambda m}{\rho}H_z\right] \tag{22}$$

GENERAL SOLUTION

Solutions of (17) and (18) are modified Bessel functions. In fact, for fields that are finite at $\rho = 0$, we can verify that

$$E_z = f_{e,m}(\lambda)I_{\alpha_m}(u\rho)e^{-im\phi}e^{-i\lambda z} \tag{23}$$

$$H_z = f_{h,m}(\lambda)I_{\beta_m}(v\rho)e^{-im\phi}e^{-i\lambda z} \tag{24}$$

where

$$u^2 = (\lambda^2 + i\sigma_\rho\mu_\phi\omega)\,\sigma_z/\sigma_\rho \tag{25}$$

$$v^2 = (\lambda^2 + i\mu_\rho\sigma_\phi\omega)\,\mu_z/\mu_\rho \tag{26}$$

$$\alpha_m^2 = m^2(\sigma_\phi/\sigma_\rho)(\lambda^2 + i\sigma_\rho\mu_\phi\omega)/(\lambda^2 + i\sigma_\phi\mu_\rho\omega) \tag{27}$$

$$\beta_m^2 = m^2(\mu_\phi/\mu_\rho)(\lambda^2 + i\sigma_\phi\mu_\rho\omega)/(\lambda^2 + i\sigma_\rho\mu_\phi\omega) \tag{28}$$

and where $f_{e,m}(\lambda)$ and $f_{h,m}(\lambda)$ are unspecified functions of λ and m.

We are now in the position to write exact boundary conditions at the surface $\rho = a$ in the form

$$E_{\phi m}(a) = p_m E_{zm}(a) - z_m H_{zm}(a) \tag{29}$$

$$H_{\phi m}(a) = y_m E_{zm}(a) + q_m H_{zm}(a) \tag{30}$$

where

$$p_m = (\mu_z/\mu_\rho)(\lambda m/v^2 a) \tag{31}$$

$$q_m = (\sigma_z/\sigma_\rho)(\lambda m/u^2 a) \tag{32}$$

$$y_m = (\sigma_z/u)I'_{\alpha_m}(ua)/I_{\alpha_m}(ua) \tag{33}$$

$$z_m = (i\omega\mu_z/v)I'_{\beta_m}(va)/I_{\beta_m}(va) \tag{34}$$

The primes over the modified Bessel functions denote differentiation with respect to the indicated argument. The subscript m is indicated explicitly in (29) and (30) to remind the reader that these linear relations only hold for elemental wave func-

tions that behave as $\exp(-im\phi)$. The implicit functional dependence on $\exp(-i\lambda z)$ should also be understood.

In the free-space region external to the cylinder, we have, in general, a superposition of the incident or primary field and the scattered or secondary field. For the purpose of illustration, we imagine the source to be a prescribed electric or magnetic current distribution contained in the cylindrical surface $\rho = b$ where $b > a$. Clearly, in the outer region $\rho > b$, the solutions must contain the modified Bessel function $K_m(u_0\rho)$ of integer order m, where $u_0 = (\lambda^2 + \gamma_0^2)^{1/2}$ and $\gamma_0 = i(\varepsilon_0\mu_0)^{1/2}\omega$, since this decays to zero as $\rho \to \infty$. However, in the concentric region $a < \rho < b$, both $I_m(u_0\rho)$ and $K_m(u_0\rho)$ are involved.

The above suggests that we write

$$E_{zm} = -u_0^2 A_m K_m(u_0\rho) \tag{35}$$

$$H_{zm} = -u_0^2 A_m^* K_m(u_0\rho) \tag{36}$$

$$E_{\phi m} = -(m\lambda/\rho)A_m K_m(u_0\rho) + i\mu_0\omega u_0 A_m^* K_m'(u_0\rho) \tag{37}$$

$$H_{\phi m} = -(m\lambda/\rho)A_m^* K_m(u_0\rho) - i\varepsilon_0\omega u_0 B_m K_m'(u_0\rho) \tag{38}$$

for $\rho > b$, whereas

$$E_{zm} = -u_0^2 [B_m I_m(u_0\rho) + C_m K_m(u_0\rho)] \tag{39}$$

$$H_{zm} = -u_0^2 [B_m^* I_m(u_0\rho) + C_m^* K_m(u_0\rho)] \tag{40}$$

$$E_{\phi m} = -(m\lambda/\rho)[B_m I_m(u_0\rho) + C_m K_m(u_0\rho)] + i\mu_0\omega u_0 [B_m^* I_m'(u_0\rho) + C_m^* K_m'(u_0\rho)] \tag{41}$$

$$H_{\phi m} = -(m\lambda/\rho)[B_m^* I_m(u_0\rho) + C_m^* K_m(u_0\rho)] - i\varepsilon_0\omega u_0 [B_m I_m'(u_0\rho) + C_m K_m'(u_0\rho)] \tag{42}$$

for $a < \rho < b$.

APPLICATION OF SOURCE CONDITIONS

The exact boundary conditions given by (29) and (30) can be applied to (39) and (42). This is a straightforward way to invoke the required continuity of the tangential electric and magnetic fields across the cylindrical surface $\rho = a$. The result of this algebraic process is found to be

$$C_m = \left\{ B_m^* \left[\left(\frac{m\lambda}{au_0^2} - q_m \right) \frac{\gamma_0\eta_0}{u_0 a^2} \right] - B_m \left[\left(\frac{m\lambda}{u_0^2 a} - p_m \right) \cdot \left(\frac{m\lambda}{u_0^2 a} - q_m \right) + \left(\frac{\gamma_0 I_m'}{u_0 I_m} - y_m\eta_0 \right) \left(\frac{\gamma_0 K_m'}{u_0 K_m} - \frac{z_m}{\eta_0} \right) \right] I_m K_m \right\} D_m^{-1} \tag{43}$$

$$C_m^* = -\left\{ B_m \left[\left(\frac{m\lambda}{au_0^2} - p_m \right) \frac{\gamma_0}{\eta_0 u_0 a^2} \right] + B_m^* \left[\left(\frac{m\lambda}{u_0^2 a} - q_m \right) \left(\frac{m\lambda}{u_0^2 a} - p_m \right) + \left(\frac{\gamma_0 I_m'}{u_0 I_m} - \frac{z_m}{\eta_0} \right) \left(\frac{\gamma_0 K'}{u_0 K} - y_m\eta_0 \right) \right] I_m K_m \right\} D_m^{-1} \tag{44}$$

where

$$D_m = \left[\left(\frac{m\lambda}{au_0^2} - p_m \right) \left(\frac{m\lambda}{au_0^2} - q_m \right) + \left(\frac{\gamma_0 K_m'}{u_0 K_m} - y_m\eta_0 \right) \left(\frac{\gamma_0 K_m'}{u_0 K_m} - \frac{z_m}{\eta_0} \right) \right] K_m^2 \tag{45}$$

and where the arguments on the indicated I_m, I_m', K_m, and K_m' functions are $u_0 a$.

Now we need to say something about the source currents. These can be defined such that

$$E_z(b^+) - E_z(b^-) = -M_\phi \tag{46}$$

$$E_\phi(b^+) - E_\phi(b^-) = M_z \tag{47}$$

$$H_z(b^+) - H_z(b^-) = -j_\phi \tag{48}$$

$$H_\phi(b^+) - H_\phi(b^-) = j_z \tag{49}$$

where $b^\pm$ means $b \pm \Delta$ in the limit $\Delta \to 0$. Thus, for example, j_ϕ is the electric surface current density in the surface $\rho = b$ in the ϕ direction. Similarly, M_ϕ is the magnetic surface current density in the ϕ direction.

The discontinuity relations hold for the total fields so we can also apply them to the basic wave types that vary as $\exp(-im\phi)\exp(-i\lambda z)$. To this end, it is convenient to write the Fourier integral representation for the total z component of the electric field in the form

$$E_z = \Gamma(E_{zm}) \tag{50}$$

where

$$\Gamma(\ ) = \int_{-\infty}^{+\infty} \Sigma(\ ) e^{-im\phi} e^{-i\lambda z} d\lambda \tag{51}$$

and similarly for the other field components. Fur-

thermore, the source current density has a similar representation via

$$j_\phi = \Gamma(j_{\phi m}), \quad \text{etc.} \tag{52}$$

We now apply (46), (47), (48), and (49) to (39), (40), (41), and (42) to yield the following explicit results for the source coefficients:

$$B_m = u_0^{-2} \{u_0 b K'_m(u_0 b) M_{\phi m} + [m\lambda/(i\varepsilon_0\omega)] \cdot K_m(u_0 b) j_{\phi m}\} + [b/(i\varepsilon_0\omega)] K_m(u_0 b) j_{zm} \tag{53}$$

$$B^*_m = u_0^{-2} \{u_0 b K'_m(u_0 b) j_{\phi m} - [m\lambda/(i\mu_0\omega)] \cdot K_m(u_0 b) M_{\phi m}\} - [b/(i\mu_s\omega)] K_m(u_0 b) M_{zm} \tag{54}$$

The remaining coefficients are given by

$$A_m K_m(u_0 b) = u_0^{-2} \{B_m I_m(u_0 b) + C_m K_m(u_0 b) + M_{\phi m}\} \tag{55}$$

$$A^*_m K_m(u_0 b) = u_0^{-2} \{B^*_m I_m(u_0 b) + C^*_m K_m(u_0 b) + j_{\phi m}\} \tag{56}$$

This completes the formal solution of the problem since the coefficients are now all expressed in terms of the specified current source distribution.

CONCLUDING REMARKS

A number of interesting special cases emerge from the general solution presented here. If the electric and magnetic properties are isotropic (i.e., $\sigma_\rho = \sigma_\phi = \sigma_z$ and $\mu_\rho = \mu_\phi = \mu_z$), we recover the solution presented elsewhere [*Hill and Wait*, 1977]. Also, if the external excitation is a plane wave, the present general solution can be directly used to deduce the scattered field if λ is replaced by $k_0 \cos\theta$ where θ is the angle subtended by the incident wave normal and the z axis of the cylinder.

REFERENCES

Bowman, J. J., T. B. A. Senior, and P. L. E. Uslenghi (1969), *Electromagnetic and Acoustic Scattering from Simple Shapes*, North-Holland, Amsterdam.

Hill, D. A., and J. R. Wait (1977), Excitation of a wire rope by an azimuthal magnetic current sheet, *J. Appl. Phys.*, *48*, 4893–4897.

Kerker, M. (1969), *The Scattering of Light and Other Electromagnetic Radiation*, Academic, New York.

Kong, J. A. (1975), *Theory of Electromagnetic Waves*, John Wiley, New York.

Large, D. B., and J. R. Wait (1965), Cavity resonator modes in a cylindrically stratified magnetoplasma, *Radio Sci.*, *1*, 655–658.

Large, D. B., and J. R. Wait (1967), Resonances of a cylindrical earth-ionosphere cavity model with a dipolar magnetic field, *J. Geophy. Res.*, *72*, 5395–5400.

Rayleigh, Lord (J. W. Strutt) (1918), On the dispersal of light by a dielectric cylinder, *Phil. Mag.*, *36*, 365–376.

Wait, J. R. (1955), Scattering of a plane wave from a circular dielectric cylinder at oblique incidence, *Can. J. Phys.*, *33*, 189–195.

Wait, J. R. (1965*a*), The long wavelength limit in scattering from a dielectric cylinder at oblique incidence, *Can. J. Phys.*, *43*, 2212–2215.

Wait, J. R. (1965*b*), Scattering of electromagnetic and electroacoustic waves by a cylindrical object in a compressible plasma, *J. Res. Nat. Bur. Stand. Sect. D*, *69D*, 247–256.

Wait, J. R. (1966), Quasi-static theory of a cylindrical impedance probe for magnetoplasma, *Radio Sci.*, *1*, 1297–1301.

Wait, J. R. (1967), Further note on the quasi-static theory of cylindrical impedance probe for magnetoplasma, *Radio Sci.*, *2*, 253–256.

Wait, J. R. (1968), *Electromagnetics and Plasmas*, Holt, Rinehart, and Winston, New York.

Wilhelmsson, H. (1958), *The Scattering of Electromagnetic Waves by an Electron Beam and a Dielectric Cylinder*, Ph.D thesis, Chalmers Institute of Technology, Göteborg, Sweden.

Electromagnetic interaction between a conducting cylinder and a solenoid in relative motion

James R. Wait
Environmental Research Laboratories, National Oceanic and Atmospheric Administration, U.S. Department of Commerce, Boulder, Colorado 80303

David A. Hill
Institute for Telecommunication Sciences, U.S. Department of Commerce, Boulder, Colorado 80303

(Received 18 January 1979; accepted for publication 21 March 1979)

An analysis is presented for the mutual impedance between two solenoids that are coaxial with a conducting cylinder in relative motion. The formulation is based on the first-order Lorentz transformation and the results obtained are sufficiently general to encompass any such situation that could arise in nondestructive-testing schemes. A numerical example, relevant to steel-wire ropes of 2-cm radius used in mine hoists, indicates that even with relative velocities as high as 10 m/s, the mutual impedance at 10 Hz differs little from that calculated for zero velocity. However, the nonreciprocal effects could be significant for higher velocities and/or for more highly conducting and larger ropes.

PACS numbers: 41.10.Hv, 84.40.Mk, 91.25. – r

INTRODUCTION

An effective method for the nondestructive testing (NDT) of metal rods and tubes is to induce eddy currents by means of an encircling solenoid carrying an oscillating current.[1] The secondary field contains useful information about the geometry and the internal structure of the sample. The electromagnetic basis for such measurements has been recently reviewed.[2] Also, a method for predicting the influence of internal voids of idealized shape has been presented.[3,4]

There are some important applications when the sample is moving relative to the sensor. A good example is a mine-hoist rope that needs to be tested under dynamic conditions. Of course, if the motion of the rope is sufficiently slow, it might be justified to assume that the relative motion with the sensor is effectively zero. Obviously, a quantitative estimate of this effect is needed. This is the principal objective of the present study. It is also worth mentioning that in some sensing devices the rope motion induces eddy currents even though the exciting solenoid has direct current.[5] Thus a general formulation is worthwhile in order to provide insight into the relative merits of the various approaches that have been promoted particularly by articles in the trade literature.

FORMULATION

According to Einstein's general theory of relativity only the relative motion of the wire rope and the external sensor is important. Thus it will facilitate our discussion if the rope is taken to be stationary and the exciting solenoid is in uniform motion along its axis.

The situation is illustrated in Fig. 1. The wire rope is idealized as a stationary homogeneous circular cylinder of radius a of infinite length with conductivity σ, permittivity ϵ, and permeability μ. In terms of stationary cylindrical coordinates (ρ,ϕ,z), the rope is defined by $\rho < a$ and $-\infty < z < \infty$.

Now, as mentioned, the rope is to be excited by a concentrically located tightly wound solenoid of radius b that carries only an azimuthal current. The solenoid, which is of length l, is moving with a constant velocity v in the positive z direction. To specify the primary fields of the solenoid we choose a cylindrical coordinate system (ρ,ϕ,z') that is fixed in the moving frame. Thus we specify that the azimuthal current density $j'_\phi(z',t')$ is given by

$$j'_\phi(z',t') = j_0 \exp(i\omega t') \quad \text{for } \tfrac{1}{2}l > z' > -\tfrac{1}{2}l,$$
$$= 0 \quad \text{for } z' < -\tfrac{1}{2}l \quad \text{and} \quad z' > \tfrac{1}{2}l, \tag{1}$$

where t' is time in the moving (coil) frame and ω is the angular frequency. The needed spectral representation for the primary excitation is obtained from the Fourier transform pair

$$j'_\phi(z',t') = \frac{1}{2\pi}\int_{-\infty}^{+\infty} f(\lambda,t')\exp(-i\lambda z')\,d\lambda \tag{2}$$

and

$$f(\lambda,t') = \int_{-\infty}^{+\infty} j_\phi(z',t')\exp(i\lambda z')\,dz. \tag{3}$$

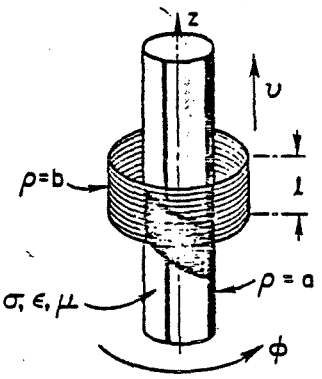


FIG. 1. Cylindrical conductor excited by an idealized azimuthal current sheet or solenoid in uniform relative motion.

Thus we find that

$$j'_\phi(z',t') = \frac{j_0 l}{2\pi}\int_{-\infty}^{+\infty} \frac{\sin\frac{1}{2}\lambda l}{\frac{1}{2}\lambda l}\exp(-i\lambda z')\exp(i\omega t')\,d\lambda. \quad (4)$$

Of course we understand that the physical quantity is the real part of the right-hand side of Eq. (4).

We now apply the first-order Lorentz transformation (FOLT) as discussed, for example, by Tai,[6] or Kong.[7] In this case quantities in the moving frame transform to the fixed (rope) frame as follows:

$$z' = z - vt,$$
$$t' = t - (v/c^2)z,$$
$$j'_\phi = j_\phi.$$

Thus the primary excitation in the rope frame is given by

$$j_\phi(z,t) = \frac{j_0 l}{2\pi}\int_{-\infty}^{+\infty} \frac{\sin\frac{1}{2}\lambda l}{\frac{1}{2}\lambda l}\exp\left\{-i\left[\lambda + \left(\frac{\omega v}{c^2}\right)\right]z\right\} \times \exp[i(\omega + \lambda v)t]\,d\lambda. \quad (5)$$

WAVE SOLUTIONS

The total fields inside the wire rope now must satisfy Maxwell's equations in the stationary frame. Also, since azimuthal symmetry prevails the fields can be obtained from a magnetic Hertz vector that has only a z component $\Pi(\rho,z,t)$ that must satisfy the scalar Helmholtz equation within the rope:

$$\left(\frac{1}{\rho}\frac{\partial}{\partial\rho}\rho\frac{\partial}{\partial\rho} + \frac{\partial^2}{\partial z^2} - \sigma\mu\frac{\partial}{\partial t} - \mu\epsilon\frac{\partial^2}{\partial t^2}\right)\Pi(\rho,z,t) = 0. \quad (6)$$

This and the form of Eq. (5) suggest that we utilize the Fourier-integral representation

$$\Pi(\rho,z,t) = \int_{-\infty}^{+\infty} \hat{\Pi}(\lambda,\rho)\exp\left\{-i\left[\lambda + \left(\frac{\omega v}{c^2}\right)\right]z\right\} \times \exp[i(\omega + \lambda v)t]\,d\lambda \quad (7)$$

for $\rho < a$. Clearly, $\hat{\Pi}$ must satisfy

$$\left[\frac{1}{\rho}\frac{\partial}{\partial\rho}\rho\frac{\partial}{\partial\rho} - \left(\lambda + \frac{\omega v}{c^2}\right)^2 - i\sigma\mu(\omega + \lambda v) + \mu\epsilon(\omega + \lambda v)^2\right]\hat{\Pi} = 0. \quad (8)$$

Now to be consistent in applying FOLT, all terms in v^2/c^2 can be dropped. Thus, for example,

$$\left[\lambda + \left(\frac{\omega v}{c^2}\right)\right]^2 \simeq \lambda^2 + \frac{2\lambda\omega v}{c^2}.$$

Then we see that, to within this order,

$$\left(\frac{1}{\rho}\frac{\partial}{\partial\rho}\rho\frac{\partial}{\partial\rho} - w^2\right)\hat{\Pi} = 0, \quad (9)$$

where

$$w \simeq \left(\lambda^2 + \frac{2\lambda\omega v}{c^2} + i\sigma\mu(\omega + \lambda v) - \mu\epsilon(\omega + \lambda v)^2\right)^{1/2}.$$

The appropriate internal solutions (i.e., for $\rho < a$) are thus

$$\hat{\Pi} = A(\lambda) I_0(w\rho), \quad (10)$$

where $A(\lambda)$ is a function of λ yet to be specified and $I_0(w\rho)$ is a modified Bessel function of order zero and argument $w\rho$.

The field components inside the cylidner can be written in the same integral form. Thus

$$\begin{matrix} H_\rho \\ E_\phi \\ H_z \end{matrix} = \int_{-\infty}^{+\infty} \begin{matrix} \hat{H}_\rho(\lambda) \\ \hat{E}_\phi(\lambda) \\ \hat{H}_z(\lambda) \end{matrix} \exp\left\{-i\left[\lambda + \left(\frac{\omega v}{c^2}\right)\right]z\right\} \times \exp[i(\omega + \lambda v)t]\,d\lambda, \quad (11)$$

where

$$\hat{H}_\rho(\lambda) = -i[\lambda + \omega v/c^2]\frac{\partial\hat{\Pi}}{\partial\rho}, \quad (12)$$

$$\hat{E}_\phi(\lambda) = i\mu(\omega + \lambda v)\frac{\partial\hat{\Pi}}{\partial\rho}, \quad (13)$$

$$\hat{H}_z(\lambda) = -w^2\hat{\Pi} \quad (14)$$

when $\hat{\Pi}$ is given by Eq. (10), and thus

$$\frac{\partial\hat{\Pi}}{\partial\rho} = wA(\lambda) I_1(w\rho). \quad (15)$$

In particular, we note that

$$-\left.\frac{\hat{E}_\phi(\lambda)}{\hat{H}_z(\lambda)}\right]_{\rho=a} = \frac{i\mu(\omega + \lambda v) I_1(wa)}{wI_0(wa)} = Z(\lambda), \quad (16)$$

where $Z(\lambda)$ is a boundary impedance. As indicated in the Appendix, Eq. (16) can be readily generalized to a concentrically layered cylinder.

The field components in the external region ($\rho > a$) have the same integral form as Eq. (11) but now

$$\hat{H}_{0\rho}(\lambda) = -i\left(\lambda + \frac{\omega v}{c^2}\right)\frac{\partial\hat{\Pi}_0}{\partial\rho}, \quad (17)$$

$$\hat{E}_{0\phi}(\lambda) = i\mu_0(\omega + \lambda v)\frac{\partial\hat{\Pi}_0}{\partial\rho}, \quad (18)$$

$$\hat{H}_{0z}(\lambda) = -u^2\hat{\Pi}_0, \quad (19)$$

where $u = [\lambda^2 - (\omega/c)^2]^{1/2}$ and $c = (\mu_0\epsilon_0)^{-1/2}$. Suitable solutions are of the form

$$\hat{\Pi}_0 = B(\lambda) I_0(u\rho) + C(\lambda) K_0(u\rho) \quad \text{for } a < \rho < b$$
$$= D(\lambda) K_0(u\rho) \quad \text{for } \rho > b, \quad (20)$$

where B, C, and D are yet to be determined. We now apply the source conditions

$$H_{0z}(b - 0) - H_{0z}(b + 0) = j_\phi(z,t), \quad (21)$$

$$E_{0\phi}(b - 0) - E_{0\phi}(b + 0) = 0, \quad (22)$$

and the impedance condition

$$[\hat{E}_{0\phi}(\lambda) = -Z(\lambda)\hat{H}_{0z}(\lambda)]_{\rho=a} \quad (23)$$

to yield

$$B = -\frac{j_0 l b}{2\pi u}\frac{\sin\frac{1}{2}\lambda l}{\frac{1}{2}\lambda l}K_1(ub), \quad (24)$$

$$\frac{B}{C} = \frac{i\mu_0(\omega + \lambda v)K_1(ua) + uZ(\lambda)K_0(ua)}{i\mu_0(\omega + \lambda v)I_1(ua) - uZ(\lambda)I_0(ua)}, \quad (25)$$

and

$$D = C - \frac{BI_1(ub)}{K_1(ub)}. \quad (26)$$

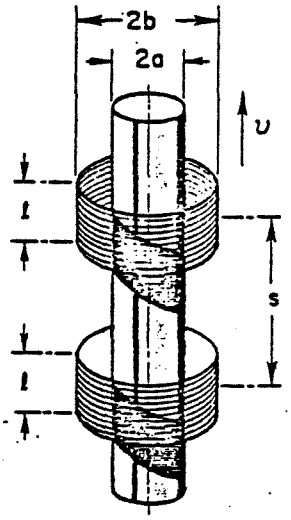


FIG. 2. Configuration of the concentric solenoids for the mutual-impedance formulation.

To complete the story we can use the continuity of H_z and H_{0z} at $\rho = a$ to give

$$A(\lambda) = \left(\frac{u^2}{w^2}\right)\frac{BI_0(ua) + CK_0(ua)}{I_0(wa)}. \tag{27}$$

Expressions for the fields everywhere in the stationary (rope) frame are now available in terms of the known parameters. But, in any practical sensing device, the fields E' and H' will be measured in the same frame as the source loop (i.e., the moving or primed frame in our convention). According to the first-order Lorentz transformation,

$$\mathbf{E}'(\rho,z',t') = \mathbf{E}(\rho,z,t) + \mu_0 v \mathbf{i}_z \times \mathbf{H}(\rho,z,t), \tag{28}$$

and

$$\mathbf{H}'(\rho,z',t') = \mathbf{H}(\rho,z,t) - \epsilon_0 v \mathbf{i}_z \times \mathbf{E}(\rho,z,t), \tag{29}$$

where $\mathbf{i}_z$ is a unit vector in the positive z direction. Here we are particularly interested in the $E'_{0\phi}$ field component which, after cancellation of various terms is written for $\rho > a$ explicitly in the form

$$E'_{0\phi} = i\mu_0\omega \int_{-\infty}^{+\infty} uB\,[I_1(u\rho) - (C/B)K_1(u\rho)] \times \exp(-i\lambda z')\exp(i\omega t')\,d\lambda. \tag{30}$$

To be consistent with FOLT we have also dropped various terms of order v^2/c^2.

MUTUAL IMPEDANCE REPRESENTATION

In practical sensing scheme we could measure the mutual impedance between the source loop of finite length l and a second coaxial loop of N turns of the same dimension that is separated from the first by a distance s. This situation is illustrated in Fig. 2. The mutual impedance Z'_m is obtained from

$$Z'_m = \frac{V'}{I'\exp(i\omega t')}, \tag{31}$$

where

$$V' = -\frac{2\pi bN}{l}\int_{s-l/2}^{s+l/2} E'_{0\phi}(b,z',t')\,dz'. \tag{32}$$

[In writing Eq. (32), the relation $NI' = j_0 l$ is implied.] Again after some fortuitous cancellation we obtain the explicit expression

$$Z'_m = i\mu_0\omega b^2 N^2 \int_{-\infty}^{+\infty} \left(\frac{\sin\frac{1}{2}\lambda l}{\frac{1}{2}\lambda l}\right)^2 K_1(ub)\exp(-i\lambda s) \times \left[I_1(ub) - \left(\frac{C}{B}\right)K_1(ub)\right] d\lambda, \tag{33}$$

where C/B is given by Eq. (25). This expression for the mutual impedance at the operating frequency $\omega/2\pi$ applies to any situation where the relative axial velocity of the sensor is v in the positive z direction with respect to the rope. Also, we should note that Z'_m is not an even function of s except in the trivial case where $v = 0$.

A useful check on the mutual-impedance result is to allow the radius of the rope to vanish whence $C/B = 0$. Now we have the coaxial-loop system in free space and there is no dependence on v; this is consistent with relativity theorey.

Actually, in any nondestructive testing for such configurations the external dimensions such as s and b will be extremely small compared with the free-space wavelength. Thus in Eq. (33) it is permissible to replace u by $|\lambda|$ over the whole range of integration. Physically, this just means that the external fields are Laplacian in character, and we might have assumed this quasistatic assumption at the outset. But, in general, it is not permissible to make a similar substitution for w as it appears in Eq. (9) and in subsequent expressions. However, the displacement currents in the cylinder will be small, i.e., $\epsilon(\omega + \lambda v) \ll \sigma$ for all significant values of the integration variable λ. Thus

$$w \simeq [\lambda^2 + i\sigma\mu(\omega + \lambda v)]^{1/2} \tag{34}$$

which is what we will use in the subsequent calculations. It is also worth pointing out that a special case of Eq. (33) for $u = |\lambda|$, $\omega = 0$ (i.e., dc excitation), and $l = 0$ was considered by Klyuev and Faingoiz[4] and our general formula reduces to their quasistatic result.

Within the quasistatic approximation the free-space mutual impedance between the loops takes the form

$$Z'_m = Z_0 = 2i\mu_0\omega b^2 N^2 \int_0^{\infty} K_1(\lambda b)I_1(\lambda b)\left(\frac{\sin\frac{1}{2}\lambda l}{\frac{1}{2}\lambda l}\right)^2 \cos\lambda s\,d\lambda. \tag{35}$$

This integral is not expressible in closed form except for the limiting case where the lengths l of the solenoids are vanishingly small (i.e., $l \ll s$). Then, using a known formula, we find

$$Z_0 = i\mu_0\omega b N^2 Q_{1/2}[(2b^2 + s^2)/2b^2], \tag{36}$$

where $Q_{1/2}$ is a Legendre function of the second kind. In the case where also $b \ll s$, the free-space mutual-impedance formula reduces to the expected form

$$Z_0 \simeq i\mu_0\omega(\pi b^2)^2 N^2/2\pi s^3, \tag{37}$$

which we might call the magnetic dipole approximation. In what follows we do not need to invoke any approximations about the relative magnitude of the ratios l/s and b/s; this

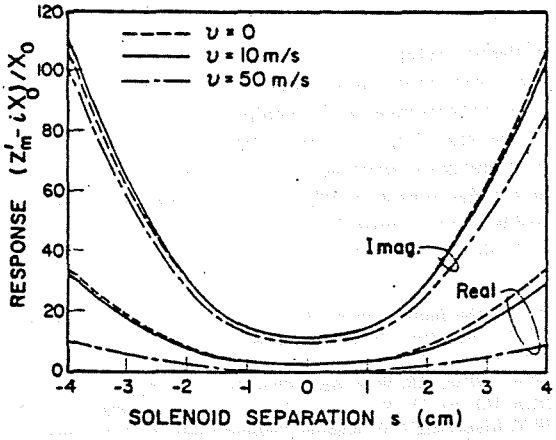


FIG. 3. The normalized secondary field as detected in the upper solenoid in Fig. 2 as a function of the separation between the solenoids.

entails, of course, numerical evaluations of the requisite integrals. These are of the same type that have been considered previously by the authors.[9]

AN ILLUSTRATIVE EXAMPLE

For a specific numerical example we select a conducting and permeable cylinder with the following parameters: $a = b = l = 2$ cm, $\sigma = 1.1 \times 10^6$ mhos/m, $\mu/\mu_0 = 200$. These are somewhat representative of a steel hoist rope, although the actual properties could vary widely, not to mention hystersis effects that we ignore. The operating frequency $\omega/2\pi = 10$ Hz, which is sufficiently low to permit reasonable penetration to the center of the cylinder.[10]

The quantity in Fig. 3 is the normalized response defined by $(Z'_m - iX_0)/X_0$, where X_0 is the mutual reactance between the coaxial solenoids in free space (note that $Z_0 = iX_0$ where X_0 is real). The response function so defined is plotted as a function of the loop separation s over the range from $s = -4$ to $+4$ cm, where the sign of s is in accord with our stated convention. Of course, for the case of zero relative motion (i.e., $v = 0$), the curves are symmetrical, but in the case of nonzero relative velocity (i.e., $v = 10$ and 50 m/s) there is a noticeable asymmetry. Calculations for other frequencies showed similar results.[11] Also, the results for lower velocities indicated that the departure from the $v = 0$ curves is negligible i.e., the curves for $v = 1$ m/s were indistinguishable from the curves for $v = 0$. Also, the results did not seem to be critically dependent on the geometry and dimension of the solenoid.

CONCLUDING REMARKS

The results of the present analysis indicate that the relative motion of the conducting cylinder or wire rope with the sensor can be ignored if the velocity is somewhat less than 10 m/s. However, it should be realized that in any design of the sensor, the bandwidth must be sufficiently large to respond to the effect of any internal flaw within the rope. This is a separate question that we have not considered here.

APPENDIX: EXTENSION TO LAYERED CYLINDERS

Without difficulty we can extend the theory to a concentrically layered conducting cylinder. This extension is outlined here, where we make use of nonuniform-transmission-line theory. The method has been applied previously to cylindrical plasma regions, so we may, in effect, write down the desired results.[12]

The model of the wire rope is three homogeneous regions with electrical properties defined as follows:

$$a_1 > \rho > a_2 \quad \text{with } \sigma_1, \epsilon_1, \text{ and } \mu_1,$$

$$a_2 > \rho > a_3 \quad \text{with } \sigma_2, \epsilon_2, \text{ and } \mu_2,$$

and

$$a_3 > \rho > 0 \quad \text{with } \sigma_3, \epsilon_3, \text{ and } \mu_3.$$

As before, the concentric exciting solenoid moves with a velocity v relative to this layered conductor. In terms of equivalent transmission-line parameters the radially directed propagation constants are given by

$$w_j \simeq [\lambda^2 + 2\lambda\omega v/c^2 + i\sigma\mu_j(\omega + \lambda v) - \mu\epsilon_j(\omega + \lambda v)^2]^{1/2}, \tag{38}$$

where λ is the common axial wave number. Here $j = 1,2,$ or 3 to designate the appropriate region. Now in the jth region we can decompose the Hertz potential $\hat{\Pi}_j(\lambda)$ into "ingoing" and "outgoing" wave functions; these are proportional to $I_0(w_j\rho)$ and $K_0(w_j\rho)$, respectively. The radial impedance associated with the "ingoing" waves is defined by

$$M_j^i = -E_{\phi,j}^i(\lambda)/H_{z,j}^i(\lambda), \tag{39}$$

while the radial impedance for the outgoing waves is defined by

$$M_j^0 = E_{\phi,j}^0(\lambda)/H_{z,j}^0(\lambda). \tag{40}$$

In accordance with Eqs. (13) and (14), we see that

$$M_j^i = \eta_j \frac{I_1(w_j\rho)}{I_0(w_j\rho)} \tag{41}$$

and

$$M_j^0 = \eta_j \frac{K_1(w_j\rho)}{K_0(w_j\rho)}, \tag{42}$$

where $\eta_j = i\mu_j(\omega + \lambda v)/w_j$.

We are now in the position to solve any concentrically layered model in terms of these wave impedances and appropriate field-transmission ratios. The quantity of particular interest is the resultant inward-looking wave impedance $Z(\lambda)$ at the outer surface $\rho = a$. Using the outlined procedure, this is found to be given by

$$Z(\lambda) = Z_1 = \eta_1 \frac{I_1(w_1a_1)}{I_0(w_1a_1)} \times \frac{1 + r_2 I_1(w_1a_2)K_1(w_1a_1)/I_1(w_1a_1)K_1(w_1a_2)}{1 + R_2 I_0(w_1a_2)K_0(w_1a_1)/I_0(w_1a_1)K_0(w_1a_2)}, \tag{43}$$

$$R_2 = \left(\frac{\eta_1 I_1(w_1a_2)}{I_1(w_1a_2)} - Z_2\right)\left(\frac{\eta_1 K_1(w_1a_2)}{K_0(w_1a_2)} + Z_2\right)^{-1} \tag{44}$$

and

$$r_2 = \left(\frac{I_0(w_1a_2)}{\eta_1 I_1(w_1a_2)} - \frac{1}{Z_2}\right)\left(\frac{K_0(w_1a_2)}{\eta_1 K_1(w_1a_2)} + \frac{1}{Z_2}\right)^{-1}. \quad (45)$$

Here R_2 and r_2 are reflection coefficients, defined such that

$$R_2 = H^0_{z,1}(\lambda)/H^i_{z,1}(\lambda) \quad \text{for } \rho = a_2 \quad (46)$$

$$r_2 = E^0_{\phi,1}(\lambda)/E^i_{\phi,1}(\lambda) \quad \text{for } \rho = a_2. \quad (47)$$

Clearly, Z_2 is the resultant wave impedance looking inward at $\rho = a_2$. It has precisely the same form as Eq. (43) if the indexes on $\eta_1, w_1, a_1, r_2, R_2$, and η_2 are stepped up by 1. Then, of course,

$$Z_3 = \eta_3 I_1(w_3a_3)/I_0(w_3a_3), \quad (48)$$

so our formula for $Z(\lambda)$ is explicit. This can be utilized directly in the expression for B/C in Eq. (25).

The further extension of the theory to any number of concentric homogeneous layers is straightforward, if not an obvious generalization of the formula for $Z(\lambda)$ given by Eq. (43).

Some final remarks of a general nature might be made at this stage. When $v^2/c^2 \ll 1$ and displacement currents are negligible, i.e., $\epsilon_j(\omega + \lambda v) \ll \sigma$, the effective formula for the transverse propagation constant is

$$w_j \simeq [\lambda^2 + i\sigma_j\mu_j(\omega + \lambda v)]^{1/2}$$

in the jth region. Evidently, the effect of the relative velocity v can be ignored if $|\sigma_j\mu_j v| \ll |\lambda|$ for all significant values of the axial wave number λ. Typically, λ^{-1} is of the order of a typical scale length l of the configuration (e.g., such as the diameter of the solenoid). Thus the condition $\sigma_j\mu_j vl \ll 1$ must be satisfied if motion effects are to be ignored. Clearly, this will be violated most easily for highly conducting cylinders with high permeabilities.

[1] H.L. Libby, *Introduction to Electromagnetic Nondestructive Test Methods* (Wiley, New York, 1971), Sec. 5.2, pp. 135–150.
[2] J.R. Wait, IEEE Trans. Instrum. Meas. 27, 235–238 (1978).
[3] D.A. Hill and J.R. Wait, Appl. Phys. 18, 141–147 (1979).
[4] D.A. Hill and J.R. Wait, Appl. Phys. 16, 391–398 (1978).
[5] V.V. Klyuev and G.G. Kapelin, Defektoskopiya 5, 69–76 (1968).
[6] C.T. Tai, Proc. IEEE 52, 685–689 (1964).
[7] J.A. Kong, *Theory of Electromagnetic Waves* (Wiley, New York, 1975).
[8] V.V. Klyuev and G.G. Kapelin, Defektoskopiya 8, 100–106 (1972).
[9] D.A. Hill and J.R. Wait, J. Appl. Phys. 48, 4893–4897 (1977).
[10] I.S. Gradshteyn and I.M. Ryzhik, *Tables of Integrals, Series and Products*, 2nd ed. (Academic, New York, 1965), pp. 732, No. 6.672–4, with $v = 1$ and $a = b$.
[11] J.R. Wait and D.A. Hill, Appl. Phys. (to be published).
[12] J.R. Wait, *Electromagnetic Waves in Stratified Media* (Pergamon, New York, 1970), p. 534.

Appl. Phys. 20, 89–96 (1979)

Applied Physics

Dynamic Electromagnetic Response of a Homogeneous Conducting Cylinder for Symmetric Excitation

James R. Wait

Environmental Research Laboratories, NOAA
US Dept. of Commerce, Boulder, CO 80303, USA

David A. Hill

Institute for Telecommunication Sciences/NTIA
US Dept. of Commerce, Boulder, CO 80303, USA

Received 8 March 1979/Accepted 12 April 1979

Abstract. A stranded wire rope is idealized as a hornogeneous conducting and permeable cylinder of circular cross section and of infinite length. The rope is excited by a coaxial solenoid or finite-length multi-turn coil that carries an azimuthally directed alternating current. The rope and the enclosing solenoid may have a uniform velocity relative to each other. Using a nonrelativistic analysis, the nature of this dynamic interaction is examined and numerical results are presented for parameter values that are relevant to both static and dynamic conditions in nondestructive testing of such cylindrical conductors. It is shown that for motional velocities v larger than about 50 m/s the dynamic interaction with the rope specimen is appreciably modified from that for the static condition (i.e., for $v=0$).

PACS: 41.10 Hv, 84.40 Mk

The nondestructive testing of metallic structures often utilizes the interaction of electromagnetic fields with the specimen [1, 2]. A particularly good example is a steel stranded wire rope such as is used in mine hoists. In this case it may be desirable to test the rope under dynamic conditions such that the sensor and the rope have a uniform velocity relative to each other. It is the purpose of the present paper to examine the effect of the motional velocity on the nature of the electromagnetic fields excited by a coaxial solenoid or finite length coil that carries an alternating current. We also consider the mutual impedance between two solenoids that are both coaxial with the rope. Such a configuration is quite common in testing both solid and tubular conductors.

Formulation

We consider a simple model; the rope is treated as a uniform cylindrical structure of radius a. It is excited by a current-carrying concentric solenoid of radius b as indicated in Fig. 1. Cylindrical coordinates (ϱ, ϕ, z) fixed within the rope are chosen such that the surface of the cylindrical conductor is $\varrho=a$ while the solenoid is idealized as an azimuthal current sheet of axial length l located at $\varrho=b$. The solenoid is taken to be moving with a uniform velocity v in the positive z direction relative to the rope frame. (ϱ, ϕ, z). Azimuthal variations of the fields are assumed to be negligible which is the case when the azimuthal current is constant and the rope is located concentrically within the solenoid.

The solenoid current surface density in amperes/meter at $\varrho=b$ is specified to be

$$j_\phi(z,t) = \text{Real part of } (NI/l)\exp(i\omega t) \qquad (1)$$

for $(l/2)+vt>z>(-l/2)+vt$ and zero outside this interval. Here N is the total number of turns that are wound uniformly throughout the axial length l of the solenoid. I is the magnitude of the current. The angular

0340-3793/79/0020/0089/$01.60

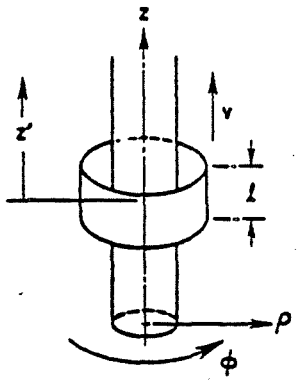


Fig. 1. Cylindrical conductor of radius a excited by a concentric solenoid of radius b that has a velocity v relative to conductor. In examples that follow $a=2$ cm, $b=2.5$ cm, and $l=2$ cm

frequency is ω and t is the time. Now it is not difficult to show that

$$j_\phi(z,t)=\frac{NI}{2\pi}\int_{-\infty}^{+\infty}\frac{\sin(\lambda l/2)}{(\lambda l/2)}e^{-i\lambda z}e^{i\lambda vt}d\lambda e^{i\omega t}, \tag{2}$$

where it is understood here and in what follows that we take the real part of the indicated complex quantity.

We are now interested in the interaction of the fields from this primary current with the conducting cylinder. While the analysis can be carried through quite rigorously by using the full-blown Lorentz transformation [3, 5], here we will use a nonrelativistic approach [6] that is justified when terms containing v^2/c^2 are negligibly small. This will certainly be the case in any practically realizable remote sensing scheme [e.g., even for a motional velocity $v=100$ m/s, $v^2/c^2\simeq 10^{-13}$ where $c=3\times10^8$ m/s]. Also we will assume that the fields in the region external to the rope are quasi-static in nature. This is justified when the significant dimensions of the sensor and the rope diameter are small compared with the operating free-space wavelength λ_0 [e.g., at a typical operating frequency of 10 Hz the $\lambda_0\simeq 3\times10^7$ m]. In this context it is worth pointing out that $|\lambda|^{-1}$, where λ is the axial wave number, should also be small compared with λ_0 over the significant range of the integration variable λ.

External Fields

In view of our assumption the fields in the region $\varrho>a$ can be obtained from a magnetic type Hertz vector that has only a z component $\Pi_0(\varrho,z,t)$ which satisfies Laplace's equation

$$\left(\frac{1}{\varrho}\frac{\partial}{\partial\varrho}\varrho\frac{\partial}{\partial\varrho}+\frac{\partial^2}{\partial z^2}\right)\Pi_0=0. \tag{3}$$

Taking a cue from (2) we construct the following appropriate integral form for Π as

$$\Pi_0(\varrho,z,t)=\int_{-\infty}^{+\infty}\hat{\Pi}_0(\lambda,\varrho)e^{-i\lambda z}e^{i(\omega+\lambda v)t}d\lambda, \tag{4}$$

where, in view of (3), $\hat{\Pi}_0$ must satisfy

$$\left(\frac{1}{\varrho}\frac{\partial}{\partial\varrho}\varrho\frac{\partial}{\partial\varrho}-\lambda^2\right)\hat{\Pi}_0=0. \tag{5}$$

Suitable solutions are

$$\hat{\Pi}_0=B(\lambda)I_0(|\lambda|\varrho)+C(\lambda)K_0(|\lambda|\varrho)\quad\text{for}\quad a<\varrho<b \tag{6}$$

and

$$\hat{\Pi}_0=D(\lambda)K_0(|\lambda|\varrho)\quad\text{for}\quad \varrho>b, \tag{7}$$

where I_0 and K_0 are modified Bessel functions. The particular form $K_0(|\lambda|\varrho)$ is indicated in the region $\varrho>b$ since it vanishes exponentially for all positive and negative real values of λ when $\varrho\to\infty$. Then, to assure field matching for all λ, the other Bessel functions in the air region must have the same argument. The functions B, C, and D are *yet* to be determined.

The field components in the region $\varrho>b$ can be obtained from

$$H_{0\phi}=\hat{c}^2\Pi_0/\partial\varrho\partial z \tag{8}$$

$$E_{0\phi}=\mu_0\partial^2\Pi_0/\partial t\partial\varrho \tag{9}$$

and

$$H_{0z}=\partial^2\Pi_0/\partial z^2. \tag{10}$$

The corresponding integral representations are

$$\begin{bmatrix}H_{0\varrho}\\E_{0\phi}\\H_{0z}\end{bmatrix}=\int_{-\infty}^{+\infty}\begin{bmatrix}\hat{H}_{0\varrho}(\lambda)\\\hat{E}_{0\phi}(\lambda)\\\hat{H}_{0z}(\lambda)\end{bmatrix}e^{-i\lambda z}e^{i(\omega+\lambda v)t}d\lambda, \tag{11}$$

where

$$\hat{H}_{0\varrho}(\lambda)=-i\lambda\partial\Pi_0/\partial\varrho \tag{12}$$

$$\hat{E}_{0\phi}(\lambda)=i\mu_0(\omega+\lambda v)\partial\hat{\Pi}_0/\partial\varrho \tag{13}$$

and

$$\hat{H}_{0z}(\lambda)=-\lambda^2\hat{\Pi}_0. \tag{14}$$

We are now in the position to apply the source conditions

$$H_{0z}(b-0)-H_{0z}(b+0)=j_\phi(z,t) \tag{15}$$

$$E_{0\phi}(b-0)-E_{0\phi}(b+0)=0 \tag{16}$$

and the impedance condition

$$[\hat{E}_{0\phi}(\lambda)=-Z(\lambda)\hat{H}_{0z}(\lambda)]_{\varrho=a}, \tag{17}$$

where $Z(\lambda)$ is discussed below. Thus we deduce that

$$B(\lambda)=-\frac{NIb}{2\pi|\lambda|}\frac{\sin(\lambda l/2)}{(\lambda l/2)}K_1(|\lambda|b) \tag{18}$$

$$\frac{B(\lambda)}{C(\lambda)}=\frac{i\mu_0(\omega+\lambda v)K_1(|\lambda|a)+|\lambda|Z(\lambda)K_0(|\lambda|a)}{i\mu_0(\omega+\lambda v)I_1(|\lambda|a)-|\lambda|Z(\lambda)I_0(|\lambda|a)} \tag{19}$$

and

$$D(\lambda)=C(\lambda)-B(\lambda)I_1(|\lambda|b)/K_1(|\lambda|b). \tag{20}$$

Here we have made use of the Wronskian relation

$$I_0(\chi)K_1(\chi)+I_1(\chi)K_0(\chi)=1/\chi. \tag{21}$$

Solution for Internal Field

Now we must specify the internal structure of the cylinder in order to obtain an explicit expression for $Z(\lambda)$. For present purposes we will assume homogeneity with a conductivity σ and magnetic permeability μ. Displacement currents in the cylinder are also neglected.

The fields within the cylinder (i.e., $\varrho<a$) can also be obtained from an azimuthally independent magnetic Hertz vector that has only an axial component Π. In the rope frame (ϱ,ϕ,z), it satisfies the time dependent wave equation

$$\left(\frac{1}{\varrho}\frac{\partial}{\partial\varrho}\varrho\frac{\partial}{\partial\varrho}+\frac{\partial^2}{\partial z^2}-\sigma\mu\frac{\partial}{\partial t}\right)\Pi=0. \tag{22}$$

The corresponding integral form is

$$\Pi(\varrho,z,t)=\int_{-\infty}^{+\infty}\hat{\Pi}(\lambda,\varrho)e^{-i\lambda z}e^{i(\omega+\lambda v)t}d\lambda, \tag{23}$$

where $\hat{\Pi}$ satisfies

$$\left(\frac{1}{\varrho}\frac{\partial}{\partial\varrho}\varrho\frac{\partial}{\partial\varrho}-w^2\right)\hat{\Pi}=0, \tag{24}$$

where

$$w=[\lambda^2+i\sigma\mu(\omega+\lambda v)]^{1/2}.$$

The field components is the region $\varrho<a$ are obtained from

$$H_\varrho=\partial^2\Pi/\partial\varrho\,\partial z \tag{25}$$

$$E_\phi=\mu\partial^2\Pi/\partial t\,\partial\varrho \tag{26}$$

and

$$H_z=\left(-\sigma\mu\frac{\partial}{\partial t}+\frac{\partial^2}{\partial z^2}\right)\Pi. \tag{27}$$

The corresponding expressions for the field components are then

$$\begin{bmatrix}H_\varrho\\E_\phi\\H_z\end{bmatrix}=\int_{-\infty}^{+\infty}\begin{bmatrix}\hat{H}_\varrho(\lambda)\\\hat{E}_\phi(\lambda)\\\hat{H}_z(\lambda)\end{bmatrix}e^{-i\lambda z}e^{i(\omega+\lambda v)t}d\lambda, \tag{28}$$

where

$$\hat{H}_\varrho(\lambda)=-i\lambda\,\partial\hat{\Pi}/\partial\varrho \tag{29}$$

$$\hat{E}_\phi(\lambda)=i\mu(\omega+\lambda v)\partial\hat{\Pi}/\partial\varrho \tag{30}$$

$$\hat{H}_z(\lambda)=-w^2\hat{\Pi}. \tag{31}$$

The appropriate solution of (24) that is finite at $\varrho=0$ is clearly

$$\hat{\Pi}=A(\lambda)I_0(w\varrho), \tag{32}$$

where $A(\lambda)$ is determined below.

Thus, we readily deduce that, at $\varrho=a$,

$$-\hat{E}_\phi(\lambda)/\hat{H}_z(\lambda)=Z(\lambda)=i\mu(\omega+\lambda v)I_1(wa)/I_0(wa). \tag{33}$$

This completes the specification of the ratio $B(\lambda)/C(\lambda)$ as given by (19). Also since $\hat{H}_{0z}$ and $\hat{H}_z$ are continuous at $\varrho=a$ we ascertain from (4) and (31) that

$$A(\lambda)=(\lambda^2/w^2)[B(\lambda)I_0(|\lambda|a)+C(\lambda)K_0(|\lambda|a)]/I_0(wa). \tag{34}$$

The fields everywhere in the (ϱ,ϕ,z) frame are now given in terms of the known parameters of the problem.

To express the fields $\mathbf{E}_0'$ and $\mathbf{H}_0'$ in the (ϱ,ϕ,z') coordinates in the frame of the solenoid we need to apply the transformation law

$$\mathbf{E}_0'=\mathbf{E}_0+\mu_0 v\mathbf{i}_z\times\mathbf{H}_0 \tag{35}$$

and

$$\mathbf{H}_0'=\mathbf{H}_0-\varepsilon_0 v\mathbf{i}_z\times\mathbf{E}_0, \tag{36}$$

where $\mathbf{i}_z$ is a unit vector in the positive z direction. These forms are valid for the external region $\varrho>a$; the corresponding forms for $\varrho<a$ are similar. The important point is that the axial magnetic field is not changed as a result of the uniformly axial motion.

Results for Internal Field

In any non-destructive testing scheme the internal field of the sample interacts with the material properties and, in turn, produces a secondary field that is detected in the external region [7]. Thus, it is of interest to examine the internal axial magnetic H_z at some fixed distance z' from the solenoid as indicated in Fig. 1.

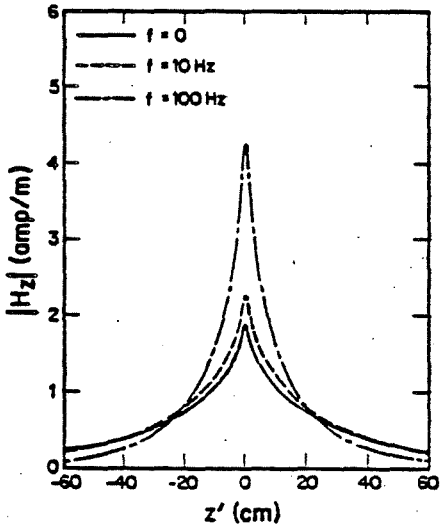


Fig. 2. Axial magnetic field at surface $\varrho = a$ of cylindrical conductor for $v = 0$, $\sigma = 10^6$ mho/m and $\mu/\mu_0 = 200$ for frequencies $f = 0$, 10 and 100 Hz

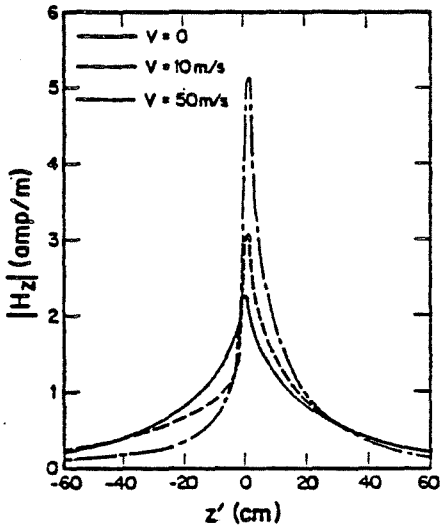


Fig. 4. Field at surface $\varrho = a$, for velocities $v = 0$, 10, and 50 m/s, for $f = 10$ Hz and other conditions as above

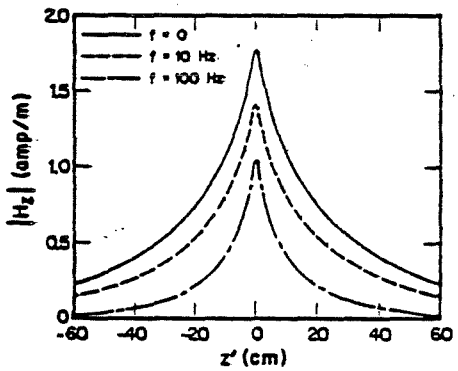


Fig. 3. Axial magnetic field at axis ($\varrho = 0$) for same conditions as in Fig. 2

The field in question is given by

$$H_z = -\int_{-\infty}^{+\infty} w^2 A(\lambda) e^{-i\lambda z} e^{j(\omega + \lambda v)t} I_0(w\varrho) d\lambda . \qquad (37)$$

Now $z = z' + vt$ if the solenoid is located at $z = 0$ at $t = 0$. Thus we have simply that

$$H_z = -\int_{-\infty}^{+\infty} w^2 A(\lambda) e^{-i\lambda z'} I_0(w\varrho) d\lambda \cdot e^{j\omega t} . \qquad (38)$$

The v dependence is contained entirely in $A(\lambda)$ that is defined by (34) where $B(\lambda)$ and $C(\lambda)$ are given explicitly by (18) and (19).

The integration over λ indicated by (38) is performed numerically using a variable step size in order to deal effectively with the relatively rapid variation for small values of $|\lambda|$. In general, at least for the case $v \sim 0$, the integrand is not an even function of λ so the integration must be carried out over the full range of λ from $-\infty$ to $+\infty$. Here we maintain the requirement that $\mathrm{Re}\{w\} > 0$ or that w tends to $|\lambda|$ tends to $\pm\infty$. Some results for $|H_z|$ plotted as a function of z' are shown in Figs. 2 through 9 where the curves are normalized by choosing $NI = 1$ ampere as the total current in the solenoid. Positive values of z' correspond to points that are ahead of the solenoid in the sense that the solenoid is moving with a uniform velocity v in the positive z direction *relative* to the rope. Of course, the results apply to the special case when the solenoid is fixed and the rope moves with a relative velocity v in the negative z direction.

In each of the curves for $|H_z|$ shown in Figs. 2 through 9, the rope radius $a = 2$ cm, the solenoid radius $b = 2.5$ cm, and the solenoid length $l = 2$ cm. We then choose various values and combinations of the following parameters: operating frequency $\omega/2\pi$, rope conductivity σ, rope magnetic permeability (relative to free space) μ/μ_0 and the velocity v.

In Fig. 2 we consider the case of a solenoid that is stationary with respect to the rope (i.e., $v = 0$) and illustrate the effect of frequency on the field $|H_z|$ at the surface of the rope, $\varrho = a$. Here $\mu/\mu_0 = 200$ and $\sigma = 10^6$ mho/m. As expected the curves are symmetrical about $z' = 0$. In each there is a pronounced peak within the region of the solenoid which again is not surprising. However, there is an enhancement of the peak for the ac cases (i.e., $f = 10$ and 100 Hz) over that

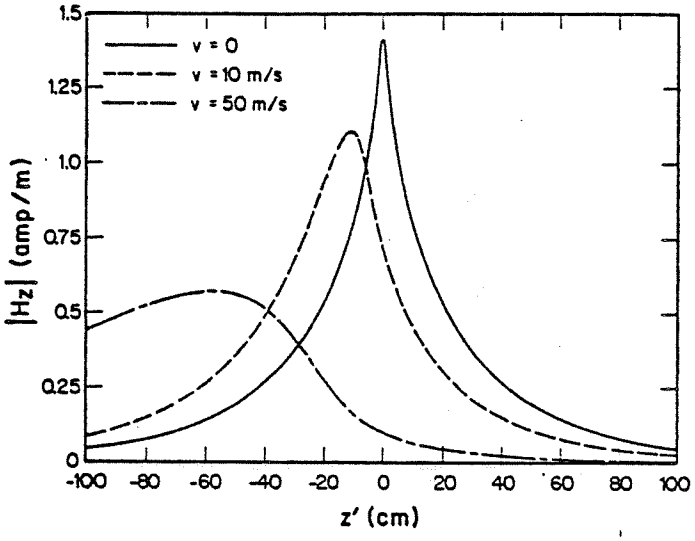


Fig. 5. Field at axis $\varrho=0$, for conditions as in Fig. 4

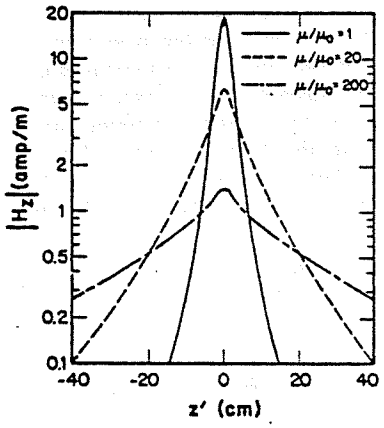


Fig. 6. Field at axis $\varrho=0$ for $f=10$ Hz, $v=0$, $\sigma=10^6$ mho/m and $\mu/\mu_0=1$, 20, and 200

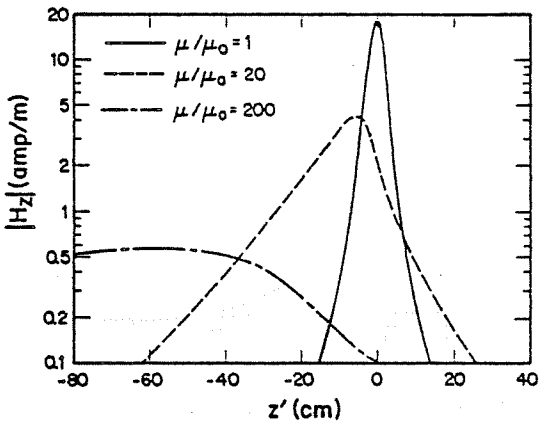


Fig. 7. Field at axis $\varrho=0$ for $v=50$ m/s and other conditions as in Fig. 6

for the DC case (i.e., $f=0$). At 100 Hz this is particularly noticeable since the magnetic flux is being excluded from the interior of the rope. In Fig. 3 the corresponding curves are shown for $|H_z|$ at the center of the rope, $\varrho=0$. Here we can see that, particularly at 100 Hz, the field magnitude is much reduced which is consistent with our statement above.

In Fig. 4. we now illustrate the influence of the motional velocity on the field H_z at the surface $\varrho=a$ for frequency $f=\omega/2\pi=10$ Hz, rope conductivity $\sigma=10^6$ mho/m and a relative permeability $\mu/\mu_0=200$. The three cases shown are for rope velocities $v=0$, 10 and 50 m/s. The corresponding results are shown in Fig. 5 for the internal field at the rope center $\varrho=0$ where there is a decided "delay" of the buildup of the field magnitude; this effect becomes quite appreciable at $v=50$ m/s.

In Fig. 6 we show the influence of the relative permeability μ/μ_0 for the case $\varrho=0$, $f=10$ Hz, $v=0$, and for $\sigma=10^6$ mho/m. The curves are particularly peaked when $\mu/\mu_0=1$ corresponding to a nonmagnetic metal but the maxima become smoothed out as μ/μ_0 increases. Corresponding results are shown in Fig. 7 for $v=50$ m/s. Again these show the pronounced "delay" of the maximum which we might describe as a *hydromagnetic drag.*

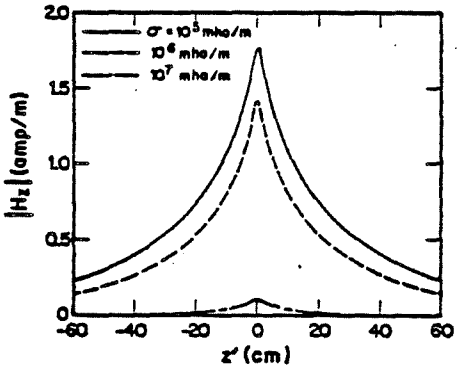


Fig. 8. Field at axis $\varrho=0$ for $v=0$, $f=10$ Hz, $\mu/\mu_0=200$, and $\sigma=10^5$, 10^6, and 10^7 mho/m

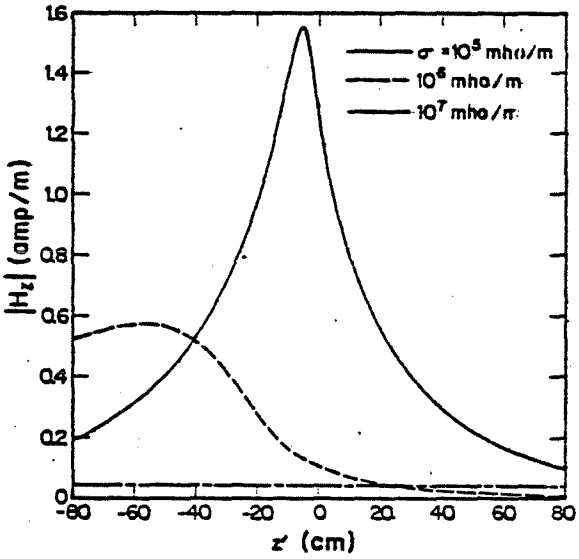


Fig. 9. Field at axis $\varrho=0$ for $v=50$ m/s and other conditions as in Fig. 8

In Fig. 8 we illustrate the influence of the rope conductivity σ on the internal field for the case where $v=0$, $f=10$ Hz, and $\mu/\mu_0=200$. Not surprisingly there is a progressive decrease of the field magnitude as σ increases from 10^5, to 10^6, to 10^7 mho/m. In the latter case the attenuation is quite severe. The corresponding curves are shown in Fig. 9. for a motional velocity $v=50$ m/s. Again we have a good illustration of the hydromagnetic drag effect that is particularly evident for $\sigma=10^6$ mho/m.

Mutual Impedance for Coaxial Solenoids

In various nondestructive testing schemes for wire ropes and similar tubular metal specimens the mutual

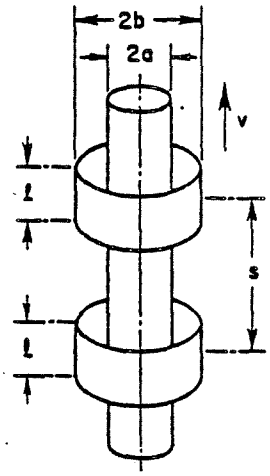


Fig. 10. Coaxial solenoid arrangement that moves with a velocity v (upwards in figure) relative to cylindrical conductor or rope

impedance between two coaxial solenoids is measured. Such a configuration is depicted in Fig. 10 where we can specify that the bottom solenoid is excited by a current I and the induced voltage V' is measured in the upper solenoid. Both solenoids have a fixed separation s and they move in the upward direction with a velocity v relative to the cylindrical rope. For convenience we select both solenoids to have N turns uniformly spaced over a length l. Clearly the voltage V' is to be obtained from

$$V'=-\frac{2\pi bN}{l}\int_{s-l/2}^{s+l/2}E'_{0\phi}(b,z',t)\,dz' \tag{39}$$

where

$$E'_{0\phi}(b,z',t)=E_{0\phi}(b,z',t)+v\mu_0 H_{0\varrho}(b,z',t). \tag{40}$$

Then if we define the mutual impedance Z'_m according to

$$Z'_m=V'/(Ie^{i\omega t}) \tag{41}$$

it follows readily, after cancellation of terms, that

$$Z'_m=i\mu_0\omega b^2N^2\int_{-\infty}^{+\infty}\left[\frac{\sin(\lambda l/2)}{(\lambda l/2)}\right]^2 K_1(|\lambda|b)e^{-i\lambda s}\cdot[I_1(|\lambda|b)-(C/B)K_1(|\lambda|b)]\,d\lambda \tag{42}$$

where C/B is given explicitly by (19). In the limiting case where the rope is absent we have the simpler formula

$$Z'_m=iX_0=2i\mu_0\omega b^2N^2\int_0^{\infty}\left[\frac{\sin(\lambda l/2)}{(\lambda l/2)}\right]^2\cdot K_1(\lambda b)I_1(\lambda b)\cos\lambda s\,d\lambda. \tag{43}$$

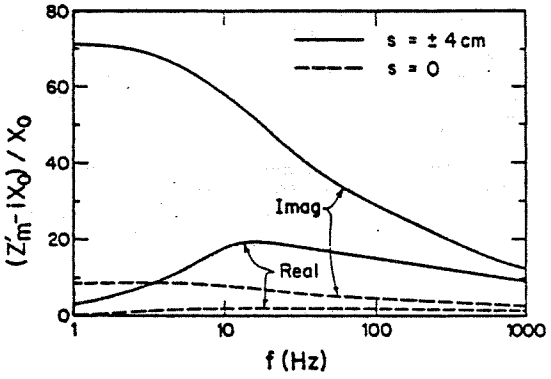


Fig. 11. Normalized response for sensor shown in Fig. 10 due to cylindrical conductor as a function of frequency for $v=0$, $\sigma=10^6$ mho/m, $\mu/\mu_0=200$, $s=\pm 4$ cm, and $s=0$

Here X_0 is the free-space mutual reactance between the two solenoids.

The quantity we consider for the final numerical examples is the *normalized response* defined by the complex ratio $(Z'_m - iX)/X_0$. In Fig. 11 the real and imaginary parts are plotted as a function of frequency from 1 to 1000 Hz for the following parameters: $v=0$, a rope radius $a=2$ cm, radius of both solenoids $b=2.5$ cm, rope conductivity $\sigma=10^6$ mho/m, rope permeability $\mu/\mu_0=200$. The two sets of curves in Fig. 11 correspond to $s=0$ and $s=4$ cm. In the first case of zero separation we are dealing with the self impedance of one solenoid whereas in the second case the solenoids are distinctly separated. In both situations it is evident that the imaginary part considerably exceeds the real part at the lowermost frequencies. The corresponding results for a motional velocity of $v=50$ m/s are shown in Fig. 12. Now we must distinguish between positive and negative values of s according to whether the "receiving" solenoid is above or below the "transmitting" solenoid, respectively. The marked changes between the curves in Figs. 11 and 12 are entirely due to the difference between motional velocity of zero and 50 m/s. It is particularly significant that in the latter case the reciprocity theorem is violated but such an effect is really not unexpected because of the lack of symmetry in the problem.

Finally, in Fig. 13, the normalized response at 10 Hz is plotted as a function of the motional velocity v from 1 to 1000 m/s for the three conditions $s=0$, $+4$, and -4 cm. Otherwise the parameters are the same as before. These curves show very clearly that, for v somewhat less than 10 m/s, the influence of the relative motion is negligible. In fact if $v=1$ m/s the curves have reached the $v=0$ asymptotes.

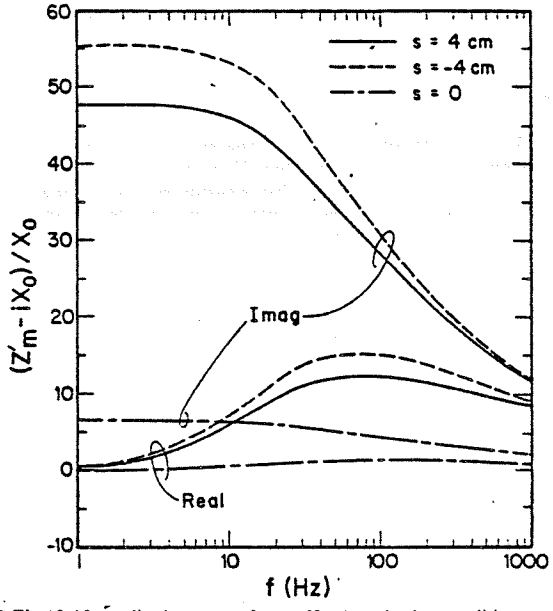


Fig. 12. Normalized response for $v=50$ m/s and other conditions as in Fig. 11

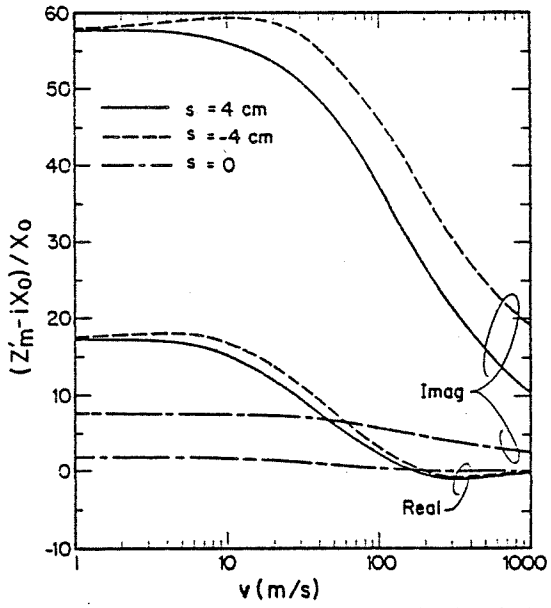


Fig. 13. Normalized response for coaxial sensor a function of v for $f=10$ Hz, $\sigma=10^6$ mho/m, and $\mu/\mu_0=200$, $s=0$, -4, and $+4$ cm

Concluding Remarks

The electromagnetic fields induced in the cylindrical specimen or rope are seen to be influenced by the relative motion of the sensor. However, the effect is quite small unless the motional velocity is on the order

of 10 m/s or higher. The same conclusion would apply to more complicated rope models if the average properties and geometrical dimensions are of the same order.

References

1. H.L. Libby: *Introduction to Electromagnetic Non-Destructive Test Methods* (Wiley Interscience, New York 1971)
2. V.V. Klyuev, M.L. Faingoiz: "Non-destructive testing of moving current conducting articles by means of pass-through converters using the constan: field method," Defektoskopiya 8, 27–31 (1972)
3. H.N. Kritikos, K.S.H. Lee, C.H. Papas: "Electromagnetic reflectivity of nonuniform jet streams," Radio Sci. 2, 991–995 (1967)
4. R.H. Ott, G. Hufford: "Scattering by an arbitrarily shaped conductor in uniform motion relative to the source of an incident spherical wave," Radio Sci. 3, 857–861 (1968)
5. J.R. Wait, D.A. Hill: "Electromagnetic interaction between a conducting cylinder and a solenoid in relative motion," Preliminary Report to US Bureau of Mines on Contract No. HO155008 (9 January 1979)
6. L.D. Landau, E.M. Lifshitz: *Electrodynamics of Continuous Media* (Pergamon Press, Oxford, 1960, Sect. 4.9, p. 205)
7. D.A. Hill, J.R. Wait: "Scattering by a slender void in a homogeneous conducting wire rope," Appl. Phys. 16, 391–398 (1978)

FIELDS OF A HORIZONTAL LOOP OF ARBITRARY SHAPE BURIED IN A TWO LAYER EARTH

by

JAMES R. WAIT and DAVID A. HILL
ERL/NOAA and ITS/NTIA
U.S. Department of Commerce
Boulder, Colorado 80309

Abstract - Expressions have been derived for the magnetic field in air produced by a buried horizontal loop of arbitrary shape. Numerical results are presented for both circular and rectangular loops. Rectangular loops produce an azimuthal magnetic field component which is not present in the case of a circular loop. The results have application to source location in mine rescue techniques. In such cases, frequencies in the audio range are employed and the assumption of a uniform current in the source loop is well justified.

INTRODUCTION

In communicating with and/or locating trapped miners, we had earlier suggested that a feasible source would be a wire loop that could be excited by a portable transmitter. A great deal of effort has gone into the problem by various groups in the U.S. and elsewhere. An accessible and very well written account can be found in the prize-winning paper by Large, Ball and Farstad [1973].

In a previous analysis, we considered the problem of a small horizontal loop or vertical magnetic dipole located in the bottom region of a two-layer earth. The results were quasi-static in the sense that all significant distances in the problem were small compared with a free space wavelength. Using numerical integration, the magnitude of the ratio of the horizontal to the vertical magnetic field was examined for an observer on the earth's surface. This

was shown to have diagnostic features that could be used as the basis of a source location technique, in spite of the fact that the curves were modified to some extent by the layer structure. [Wait, 1971; Wait and Spies, 1971a].

Here we extend the earlier analysis to allow for the finite extent of the source loop. Also, we derive explicit expressions for the fields that are valid everywhere. In order to render the problem some generality, displacement currents in the air and in the ground are retained at least in the initial formulation.

First of all we deal with a circular loop of radius a. When a tends to zero we then recover the field expressions given earlier for a magnetic dipole. We then consider a loop of finite size with any specified shape. In particular, we deal with one of rectangular form.

BASIC FORMULATION

The model for the circular loop is illustrated in Fig. 1. The earth is taken to be a two layer structure where the upper layer or slab of thickness b is characterized by electrical properties σ_1, ε_1, and μ_1. The lower semi-infinite region has corresponding properties σ_2, ε_2, and μ_2. With respect to a polar coordinate system (ρ, ϕ, z), the earth's surface is $z = 0$ and the lower interface of the upper slab is $z = -b$. The loop of radius a, carrying a total uniform current I, is located in the plane $z = -h$ and is coaxial with the z axis. The region $z > 0$ is assumed to be free space with electrical constants (ε_o, μ_o).

The source current and all associated electromagnetic fields are taken to vary as $\exp(i\omega t)$.

The source condition for the surface current density $j_\phi(\rho)$ in the plane $z = -h$ is given as follows

$$j_\phi(\rho) = I\delta(\rho - a) \tag{1}$$

where $\delta(\rho - a)$ is the unit impulse function. Here we find it convenient to apply the Fourier-Bessel transform in order to obtain the desired spectral form for the source field. Thus we have the pair

$$j_\phi(\rho) = \int_0^\infty f(\lambda) J_n(\lambda\rho)\lambda d\lambda \tag{2}$$

and

$$f(\lambda) = \int_0^\infty j_\phi(\rho) J_n(\lambda\rho)\rho d\rho \tag{3}$$

where n is an integer to be selected and J_n is a Bessel function of order n. Clearly, for the filamental current model,

$$f(\lambda) = IJ_n(\lambda a)a \tag{4}$$

By symmetry it is evident that the electromagnetic fields have only non-vanishing components E_ϕ, H_ρ and H_z. A subscript 1, 2, or 0 is added to these quantities when they refer specifically to the upper slab, lower region or free space respectively. In particular, we have the source conditions

$$H_{2\rho}(-h + 0) - H_{2\rho}(-h - 0) = j_\phi(\rho) \tag{5}$$

$$E_{2\phi}(-h + 0) - E_{2\phi}(-h - 0) = 0 \tag{6}$$

that must be met.

In view of the symmetry of the problem, it is apparent that the fields in any of the regions can be obtained from a magnetic Hertz vector that has only an axial component Π^* that we dub the "Hertz potential". Thus

$$E_\phi = i\mu\omega\partial\Pi^*/\partial\rho \tag{7}$$

$$H_\rho = \partial^2\Pi^*/\partial\rho\partial z \tag{8}$$

$$H_z = (-\gamma^2 + \partial^2/\partial z^2)\Pi^* \tag{9}$$

where

$$\gamma^2 = i\mu\omega(\sigma + i\varepsilon\omega).$$

Now because Π^* satisfies

$$\left(\frac{1}{\rho}\frac{\partial}{\partial\rho}\rho\frac{\partial}{\partial\rho} + \frac{\partial^2}{\partial z^2} - \gamma^2\right)\Pi^* = 0 \tag{10}$$

we easily deduce that solutions, finite at $\rho = 0$, have the form

$$\Pi^* = J_o(\lambda\rho)\exp(\mp uz) \tag{11}$$

where

$$u = (\lambda^2 + \gamma^2)^{1/2}.$$

Here λ is the transverse wave number than can be identified with the variable λ in equ. (2). In particular, we note that H_ρ is made up of linear combinations of solutions of the form $J_1(\lambda\rho)\exp(\mp uz)$. [on noting that $dJ_o(x)/dx = -J_1(x)$]. Now it is clearly evident we should choose $n = 1$ in (2), (3), and (4). Thus, our source current density, in the plane $z = -h$, should be given by

$$j_\phi(\rho) = Ia \int_o^\infty J_1(\lambda a)J_1(\lambda\rho)\lambda d\lambda \tag{12}$$

We are now in the position to write down the desired formsfor the Hertz potentials in the three regions:

$$\Pi_1^* = p \int_o^\infty A[e^{-u_1 z} + R_o e^{u_1 z}] \frac{J_1(\lambda a)}{u_2} J_o(\lambda\rho)d \tag{13}$$

$$\Pi_2^* = p \int_o^\infty [e^{-u_2|z+h|} + R_\perp e^{2u_2 b}\ e^{u_2(z-h)}] \frac{J_1(\lambda a)}{u_2} J_o(\lambda\rho)d\lambda \tag{14}$$

$$\Pi_o^* = p \int_o^\infty T_o e^{-u_o z} \frac{J_1(\lambda a)}{u_2} J_o(\lambda\rho)d\lambda \tag{15}$$

where the five functional coefficients p, A, R_o, $R_\perp$ and T_o are not yet known. Other multiplicative factors have been inserted to simplify the interpretation of the final results.

In order that (5) and (6) be satisfied, we readily deduce that $p = Ia/2$. The other four coefficients can be deduced by insisting that the tangential fields E_ϕ and H_ρ be continuous at the two interfaces $z = 0$ and $z = -b$. This algebraic process yields, for the reflection coefficients,

$$R_o = (N_1 - N_o)/(N_1 + N_o) \tag{16}$$

and
$$R_\perp = (N_2 - Y_1)/(N_2 + Y_1) \tag{17}$$

where $N_1 = u_1/i\mu_1\omega$, $N_2 = u_2/i\mu_2\omega$, $N_o = u_o/i\mu_o\omega$ and Y_1 are appropriate admittances. Here
$$Y_1 = -\left.\frac{H_{1\rho}}{E_{1\phi}}\right]_{z=-b} = N_1 \frac{1 - R_o e^{-2u_1 b}}{1 + R_o e^{-2u_1 b}} \tag{18}$$

Actually these results are immediately obvious if one bears in mind the transmission line analogy for such problems.

To relate A and T_o we write down the matching equations for continuity of H_ρ at $z = 0$ and $z = -b$:
$$u_1(1 - R_o)A = u_o T_o \tag{19}$$

$$u_1[e^{u_1 b} - R_o e^{-u_1 b}]A = u_2[e^{u_2 b} - R_\perp e^{u_2 b}]e^{-u_2 h} \tag{20}$$

Thus
$$T_o = \frac{u_2}{u_o}[(1 - R_o)(1 - R_\perp)e^{u_2 b}/(e^{u_1 b} - R_o e^{-u_1 b})]\, e^{-u_2 h} \tag{21}$$

and
$$A = [(u_2/u_1)(1 - R_\perp)e^{u_2 b}/(e^{u_1 b} - R_o e^{-u_1 b})]\, e^{-u_2 h} \tag{22}$$

which completes our task of finding the unknown coefficients.

Now using the identity
$$1 - R_\perp = 2Y_1/(N_2 + Y_1) \tag{23}$$

it is not difficult to show that
$$\frac{T_o}{u_2} = \frac{1}{u_o}\left(\frac{2N_o}{N_1 + N_o}\right)\left(\frac{2N_1}{N_2 + N_1}\right)[1 - R_o R_2 e^{-2u_1 b}]^{-1}\, e^{-u_2(h-b)}\, e^{-u_1 b} \tag{24}$$

where
$$R_2 = (N_1 - N_2)/(N_1 + N_2) \tag{25}$$

The right hand side of (24) can clearly be interpreted as the product of two transmission coefficients (in large parentheses) and a propagation factor $\exp[-u_2(h-b) - u_1 b]$ corresponding to the one way transmission loss from the source to the bottom of the upper slab and then through the slab to the surface. The bracketed factor, when expanded, can be interpreted as the effect of multiple reflections within the slab, e.g.,

$$[1 - R_o R_2 e^{-2u_1 b}]^{-1} = 1 + R_o R_2 e^{-2u_1 b} + (R_o R_2)^2 e^{-4u_1 b} + \ldots \tag{26}$$

The field quantities of special interest are the magnetic components $H_{o\rho}$ and H_{oz} in the free space region. These are obtained from

$$H_{o\rho} = \partial^2 \Pi_o^* / \partial\rho\partial z \tag{27}$$

and

$$H_{oz} = (-\gamma_o^2 + \partial^2/\partial z^2)\Pi_o^* \tag{28}$$

where $\gamma_o^2 = -\varepsilon_o \mu_o \omega^2$.

A special case of particular interest is when all distances are small compared with the free space wavelength. Thus, we can say that $|\gamma_o \ell| << 1$ where ℓ is a typical distance. This amounts to setting $\gamma_o = 0$ in the general formulae derived above. Furthermore, to simplify the discussion we set $\mu_1 = \mu_2 = \mu_o$ then, for example, $N_1/N_2 = u_1/u_2$ and $N_o/N_1 = u_o/u_1 = \lambda/u_1$.

Using the preceding simplifications, we find without difficulty that

$$T_o = \frac{u_2}{u_o} T = \frac{u_2}{\lambda} T \tag{29}$$

where

$$T = \frac{\left(\frac{2\lambda}{u_1 + \lambda}\right)\left(\frac{2u_1}{u_1 + u_2}\right) \exp[-u_2(h - b) - u_1 b]}{1 - \left(\frac{u_1 - \lambda}{u_1 + \lambda}\right)\left(\frac{u_1 - u_2}{u_1 + u_2}\right) \exp[-2u_1 b]} \tag{30}$$

where $u_1 = (\lambda^2 + \gamma_1^2)^{1/2}$ and $u_2 = (\lambda^2 + \gamma_2^2)^{1/2}$. The desired field components in the quasi-static approximation can be written

$$H_{o\rho} = b_o P \quad \text{and} \quad H_{oz} = b_o Q \tag{31}$$

where

$$b_o = I(\pi a^2)/(2\pi h^3)$$

$$P = \frac{h^3}{2} \int_0^\infty \lambda^2 T(\lambda) e^{-\lambda z} J_1(\lambda\rho) \frac{2J_1(\lambda a)}{\lambda a} d\lambda \tag{32}$$

and

$$Q = \frac{h^3}{2} \int_0^\infty \lambda^2 T(\lambda) e^{-\lambda z} J_o(\lambda\rho) \frac{2J_1(\lambda a)}{\lambda a} d\lambda \tag{33}$$

The limiting case of a magnetic dipole is obtained by letting a become vanishingly small whence $2J_1(\lambda a)/(\lambda a) \to 1$. in the above expressions. The generalization of (30) to a three-layered earth is indicated in the Appendix.

HORIZONTAL LOOP OF ANY SHAPE

It is actually a very simple matter to generalize the above results to a horizontal loop whose profile is non-circular. To this end we write down the Hertz potential $d^2\Pi_o^*$ in the free space region for a current loop of elemental area $dx'dy'$ located at $(x',y',-h)$ with reference to the cartesian system of coordinates (x,y,z). Thus,

$$d^2\Pi_o^* = \frac{I dx'dy'}{4\pi} \int_o^\infty T(\lambda) e^{-\lambda z} J_o\left(\lambda[(x - x') + (y - y')^2]^{1/2}\right) d\lambda$$

for the usual quasi-static approximation wherein $\gamma_o = 0$ and $u_o = \lambda$. Then, of course,

$$\Pi_o^* = \frac{IA}{4\pi} \int_o^\infty T(\lambda) e^{-\lambda z} f(\lambda) d\lambda \tag{35}$$

where

$$f(\lambda) = \frac{1}{A} \int_{Area} \int \left(J_o\, \lambda[(x - x')^2 + (y - y')^2]^{1/2}\right) dx'dy' \tag{36}$$

and A is the area of the loop.

The desired magnetic field components expressed in cartesian coordinates are now obtained from

$$H_{ox} = \partial^2\Pi_o^*/\partial x \partial z \tag{37}$$

$$H_{oy} = \partial^2\Pi_o^*/\partial y \partial z \tag{38}$$

and

$$H_{oz} = \partial^2\Pi_o^*/\partial z^2 \tag{39}$$

In carrying out these operations we note that

$$\partial J_o(\lambda\hat{\rho})/\partial x = -J_1(\lambda\hat{\rho})\lambda\partial\hat{\rho}/\partial x = -J_1(\lambda\hat{\rho})\lambda(x - x')/\hat{\rho}$$

where $\hat{\rho} = [(x - x')^2 + (y - y')^2]^{1/2}$. Then we may write

$$H_{ox} = b_o P_x \tag{40}$$

$$H_{oy} = b_o P_y \tag{41}$$

$$H_{oz} = b_o P_z \tag{42}$$

where

$$P_{\substack{x \\ y}} = \frac{h^3}{2}\int_o^\infty \lambda^2 T(\lambda) e^{-\lambda z} f_{\substack{x \\ y}}(\lambda) d\lambda \tag{43}$$

and

$$P_z = \frac{h^3}{2}\int_o^\infty \lambda^2 T(\lambda) e^{-\lambda z} f(\lambda) d\lambda \tag{44}$$

where $b_o = IA/(2\pi h^3)$

Here

$$f_x(\lambda) = \frac{1}{A}\iint_{\text{Area}} J_1(\lambda\hat{\rho})\frac{x - x'}{\hat{\rho}}\,dx'dy' \tag{45}$$

and

$$f_y(\lambda) = \frac{1}{A}\iint_{\text{Area}} J_1(\lambda\hat{\rho})\frac{y - y'}{\hat{\rho}}\,dx'dy' \tag{46}$$

and $f(\lambda)$ is given by (36). One may note that

$$f_x(\lambda) = -\lambda^{-1}\partial f(\lambda)/\partial x \tag{47}$$

and

$$f_y(\lambda) = -\lambda^{-1}\partial f(\lambda)/\partial y. \tag{48}$$

An approach to evaluate (36) is to introduce new variables (r,θ) defined by

$$x' - x = r\cos\theta$$

$$y' - y = r\sin\theta$$

The element of area then becomes $rdrd\theta$ and

$$f(\lambda) = \frac{1}{A}\int_o^{2\pi}\int_o^{r_o(\theta)} J_o(\lambda r) r\,dr d\theta \tag{49}$$

where $r = r_o(\theta)$ is the equation for the profile of the loop that is contained in the plane $z = -h$. Using the Bessel function identity

$$\int_0^{\alpha} J_o(\alpha)\alpha d\alpha = \alpha J_1(\alpha) \tag{50}$$

it follows that

$$f(\lambda) = \frac{1}{A\lambda} \int_0^{2\pi} J_1\big(\lambda r_o(\theta)\big) r_o(\theta) d\theta \tag{51}$$

Of course, if $r_o(\theta) = a$, we obtain

$$f(\lambda) = \frac{2}{\lambda a} J_1(\lambda a) \tag{52}$$

which is the expected value.

REDUCTION OF INTEGRALS

Strictly speaking, (39) to (51) are valid only when the projection of the observation point (x,y) in the plane of the loop ($z = -h$) lies inside the loop. When the observation point lies outside the loop, (49) becomes

$$f(\lambda) = \frac{1}{A} \int_{\theta_1}^{\theta_2} \int_{r_i(\theta)}^{r_o(\theta)} J_o(\lambda r) r dr d\theta \ , \tag{53}$$

where θ_1 and θ_2 are the tangent angles and r_i is the inner radius as shown in Figure 2. The r integration can again be performed analytically by use of (50):

$$f(\lambda) = \frac{1}{A\lambda} \int_{\theta_1}^{\theta_2} [J_1(\lambda r_o(\theta))\, r_o(\theta) - J_1(\lambda r_i(\theta))\, r_i(\theta)] d\theta \ . \tag{54}$$

When the projection of the observation point lies on the loop boundary, (51) and (54) are equivalent.

In order to evaluate $f_x(\lambda)$ and $f_y(\lambda)$, we utilize the following identities involving $\hat{\rho}$:

$$\frac{\partial \hat{\rho}}{\partial x} = - \frac{\partial \hat{\rho}}{\partial x'} \quad \text{and} \quad \frac{\partial \hat{\rho}}{\partial y} = - \frac{\partial \hat{\rho}}{\partial y'} \ . \tag{55}$$

Thus (47) can be written

$$f_x(\lambda) = \frac{1}{A\lambda} \iint_{\text{Area}} \frac{\partial}{\partial x'} J_o(\lambda \hat{\rho}) dx' dy' \ . \tag{56}$$

The x' integration can be performed analytically to yield

$$f_x(\lambda) = \frac{1}{A\lambda}\int_{y_1'}^{y_2'}[J_o(\lambda\hat{\rho})\Big|_{x'=x_2'(y)} - J_o(\lambda\hat{\rho})\Big|_{x'=x_1'(y)}]dy' , \qquad (57)$$

where y_2' and y_1' are the upper and lower limits of y' and x_2' and x_1' are the upper and lower limits of x' and are functions of y. In a completely analagous manner, $f_y(\lambda)$ can be written

$$f_y(\lambda) = \frac{1}{A\lambda}\int_{x_1'}^{x_2'}[J_o(\lambda\hat{\rho})\Big|_{y'=y_2'(x)} - J_o(\lambda\hat{\rho})\Big|_{y'=y_1'(x)}]dx' . \qquad (58)$$

Thus, $f(\lambda)$, $f_x(\lambda)$, and $f_y(\lambda)$ have all been reduced to a single integral.

RECTANGULAR LOOP

Another case of some interest is the rectangular loop, since this shape might be quite feasible for underground workings. Thus, for a rectangle with dimensions $2s$ by 2ℓ, the vertices in the plane $z = -h$ would be located at $(s,\ell,)$, $(-s,\ell)$, $(-s,-\ell)$ and $(s,-\ell)$. In the (r,θ) system the vertices would be located at (r_1,θ_1), (r_2,θ_2), (r_3,θ_3) and (r_4,θ_4) where

$$r_1 = [(s - x)^2 + (\ell - y)^2]^{1/2}, \quad r_2 = [(s + x)^2 + (\ell - y)^2]^{1/2}$$

$$r_3 = [(s + x)^2 + (\ell + y)^2]^{1/2} \text{ and } r_4 = [(s - x)^2 + (\ell - y)^2]^{1/2}.$$

The corresponding angles are defined by

$$\cot\theta_1 = \frac{s - x}{\ell - y}, \quad \cot\theta_2 = \frac{-s - x}{\ell - y}, \quad \cot\theta_3 = \frac{s + x}{\ell + y} \text{ and } \cot\theta_4 = \frac{s - x}{-\ell - y}$$

Also we note that

$$\begin{aligned} r_o(\theta) &= \frac{\ell - y}{\sin\theta} \text{ for } \theta_1 \text{ to } \theta_2 \\ &= -\frac{s + x}{\cos\theta} \text{ for } \theta_2 \text{ to } \theta_3 \\ &= -\frac{\ell + y}{\sin\theta} \text{ for } \theta_3 \text{ to } \theta_4 \\ &= \frac{s - x}{\cos\theta} \text{ for } \theta_4 \text{ to } \theta_1 \end{aligned} \qquad (59)$$

Thus (51) for the rectangular loop takes the form

$$f(\lambda) = \frac{1}{A\lambda}\left\{\int_{\theta_1}^{\theta_2} J_1\left[\lambda\frac{(\ell - y)}{\sin\theta}\right]\frac{\ell - y}{\sin\theta}\,d\theta + \int_{\theta_2}^{\theta_3} J_1\left[-\lambda\frac{s + x}{\cos\theta}\right]\left[\frac{-(s + x)}{\cos\theta}\right]d\theta\right.$$
$$\left. + \int_{\theta_3}^{\theta_4} J_1\left[-\lambda\frac{(\ell + y)}{\sin\theta}\right]\left[\frac{-(\ell + y)}{\sin\theta}\right]d\theta + \int_{\theta_4}^{\theta_1} J_1\left[\lambda\frac{s - x}{\cos\theta}\right]\left[\frac{s - x}{\cos\theta}\right]d\theta\right\} \tag{60}$$

The integrals in (60) can be evaluated either by direct numerical integrations on θ or by the following series approach.

These integrals are of two types that can be defined as

$$\int_0^{\theta_o} \frac{1}{\cos\theta} J_1\left(\frac{\beta}{\cos\theta}\right)d\theta = C(\beta,\theta_o) \tag{61}$$

and

$$\int_{\theta_o}^{\pi/2} \frac{1}{\sin\theta} J_1\left(\frac{\beta}{\sin\theta}\right)d\theta = S(\beta,\theta_o) \tag{62}$$

These can be handled by using the series formulas for the Bessel function, i.e.,

$$J_1(\alpha) = \sum_{m=0}^{\infty} B_m\alpha^{2m+1} \tag{63}$$

where

$$B_m = (-1)^m\frac{1}{m!(m + 1)!2^{2m+1}}$$

Then clearly

$$C(\beta,\theta_o) = \sum_{m=0}^{\infty} B_m\beta^{2m+1}\,C_m(\theta_o) \tag{64}$$

and

$$S(\beta,\theta_o) = \sum_{m=0}^{\infty} B_m\beta^{2m+1}\,S_m(\theta_o) \tag{65}$$

where

$$C_m(\theta_o) = \int_0^{\theta_o}\frac{1}{(\cos\theta)^{2m+2}}\,d\theta \tag{66}$$

and

$$S_m(\theta_o) = \int_{\theta_o}^{\pi/2}\frac{1}{(\sin\theta)^{2m+2}}\,d\theta \tag{67}$$

These are integrals of a standard type and we may write

$$C_o(\theta_o) = \tan \theta_o \tag{68}$$

$$C_1(\theta_o) = \tan \theta_o + \frac{\tan^3 \theta_o}{3} \tag{69}$$

$$C_2(\theta_o) = \frac{\sin \theta_o}{5 \cos^5 \theta_o} + \frac{4}{15} \frac{\sin \theta_o}{\cos^3 \theta_o} + \frac{8}{15} \tan \theta_o \tag{70}$$

For higher order values we have the recurrence formula

$$C_m(\theta_o) = \frac{\sin \theta_o}{(2m + 1)\cos^{2m+1} \theta_o} + \frac{2m}{2m + 1} C_{m-1}(\theta_o) \tag{71}$$

Similarly

$$S_o(\theta_o) = \cot \theta_o \tag{72}$$

$$S_1(\theta_o) = \cot \theta_o + \frac{\cot^3 \theta_o}{3} \tag{73}$$

$$S_2(\theta_o) = \frac{\cos \theta_o}{5 \sin^5 \theta_o} + \frac{4}{15} \frac{\cos \theta_o}{\sin^3 \theta_o} + \frac{8}{15} \cot \theta_o \tag{74}$$

and, for higher values,

$$S_m(\theta_o) = \frac{\cos \theta_o}{(2m + 1)\sin^{2m+1} \theta_o} + \frac{2m}{2m + 1} S_{m-1}(\theta_o) \tag{75}$$

In the evaluation of $f_x(\lambda)$ and $f_y(\lambda)$ for the rectangular loop, (57) and (58) take the following forms:

$$f_x(\lambda) = \frac{1}{\lambda A} \int_{-\ell}^{\ell} [J_o(\lambda \hat{\rho})\big|_{x'=s} - J_o(\lambda \hat{\rho})\big|_{x'=-s}] dy' \, . \tag{76}$$

and

$$f_y(\lambda) = \frac{1}{\lambda A} \int_{-s}^{s} [J_o(\lambda \hat{\rho})\big|_{y'=\ell} - J_o(\lambda \hat{\rho})\big|_{y'=-\ell}] dy' \tag{77}$$

In general the evaluation of (76) and (77) requires numerical integration.

NUMERICAL RESULTS

In this section we present numerical results for the fields of both circular and rectangular buried loops. The half space is taken to be homogeneous ($\sigma_1 = \sigma_2$ and $\varepsilon_1 = \varepsilon_2$), and the frequency is sufficiently low that displacement currents

are negligible ($\sigma_1 >> \omega\varepsilon_1$). The following dimensionless parameters are utilized in presenting the numerical results:

$$Z = z/h, \quad H = h(\omega\mu_o\sigma_1)^{1/2}, \quad D = (x^2 + y^2)^{1/2}/h, \quad \text{and} \quad \phi = \text{Arc tan } (y/x) . \tag{78}$$

Although computer programs were written to evaluate the fields at any arbitrary location above the half-space, all results are presented for the observer at the surface ($Z = 0$).

The results for the circular loop were obtained by numerical integration of (32) and (33). In Figures 3 and 4, we illustrate the vertical and horizontal magnetic fields for various loop sizes for the static case ($H = 0$). As expected, the response is stretched out as a/h is increased. Of course, the results are independent of ϕ for circular loops.

The results for rectangular loops were obtained by numerical integration of (43) and (44). The results for the horizontal fields are given terms of radial and azimuthal components P_ρ and P_ϕ:

$$P_\rho = P_x \cos \phi + P_y \sin \phi \tag{79}$$

and

$$P_\phi = P_y \cos \phi - P_x \sin \phi \tag{80}$$

The normalized loop dimensions S and L are defined as

$$S = s/h \quad \text{and} \quad L = \ell/h . \tag{81}$$

In Figures 5 and 6, $|P_z|$ and $|P_\rho|$ are shown for various size rectangular loops for $S/L = 2$ and $\phi = 0°$. Due to symmetry, P_ϕ is zero for $\phi = 0°$. Note that for $S = 0$ the results reduce to those of the circular loop for $a/h = 0$. This simply confirms the result that a small loop looks like a magnetic dipole regardless of the shape.

In Figures 7 and 8, the ϕ dependence of all three components is shown for two different size loops. Because of symmetry, P_ϕ is zero at $\phi = 0°$ and $90°$, and only the range from $\phi = 0°$ to $90°$ need be shown. Note that the

A worthwhile further extension of the present analysis is to allow for tilts of the source loop relative to the air/earth interface. The formulation for this case is complicated by the vertical components of the source currents but no fundamental difficulty should be encountered. Of course, the implementation of the numerical task would not be trivial. This is certainly a valid subject for further effort.

Acknowledgements

We would like to thank Robert McDonald and Jeri L. Bacon for their help in preparing the illustrations and manuscript.

APPENDIX B

The Three-Layer Case

With reference to Fig. 13, it not difficult to show that the function $T(\lambda)$ analogous to (30) is given by

$$T(\lambda) = D^{-1}\left(\frac{2u_2}{u_2 + u_3}\right)\left(\frac{2u_1}{u_1 + u_2}\right)\left(\frac{2\lambda}{u_1 + \lambda}\right)\exp[-u_3(h - c) - u_2(c - b) - u_1 b] \quad (1)$$

where

$$D = 1 - \left(\frac{u_2 - u_3}{u_2 + u_3}\right)\left(\frac{u_2 - u_1}{u_2 + u_1}\right)\exp[-2u_2(c - b)]$$

$$- \left(\frac{u_1 - \lambda}{u_1 + \lambda}\right)\left(\frac{u_1 - u_2}{u_1 + u_2}\right)\exp[-2u_1 b] \quad (2)$$

$$- \left(\frac{u_1 - \lambda}{u_1 + \lambda}\right)\left(\frac{u_2 - u_3}{u_2 + u_3}\right)\exp[-2u_1 b - 2u_2(c - b)]$$

where $u_m = (\lambda^2 + \gamma_m^2)^{1/2}$, $\gamma_m^2 = i\sigma_m\mu_o\omega$ for $m = 1,2,3$. Here $\mu_m = \mu_o$ and all displacement currents are ignored.

The three quantities in large parentheses on the right-hand side of (1) are the transmission coefficients for the interfaces at $z = -c$, $-b$ and 0 respectively. The total complex phase is given by the exponential term in (1). The total effect of the internal reflections are included in the expression for D given by (2).

The expression for D was given incorrectly in the report by Wait and Spies [1971b]. I am grateful to Dr. Thurlow W.H. Caffey, who pointed this out.

REFERENCES

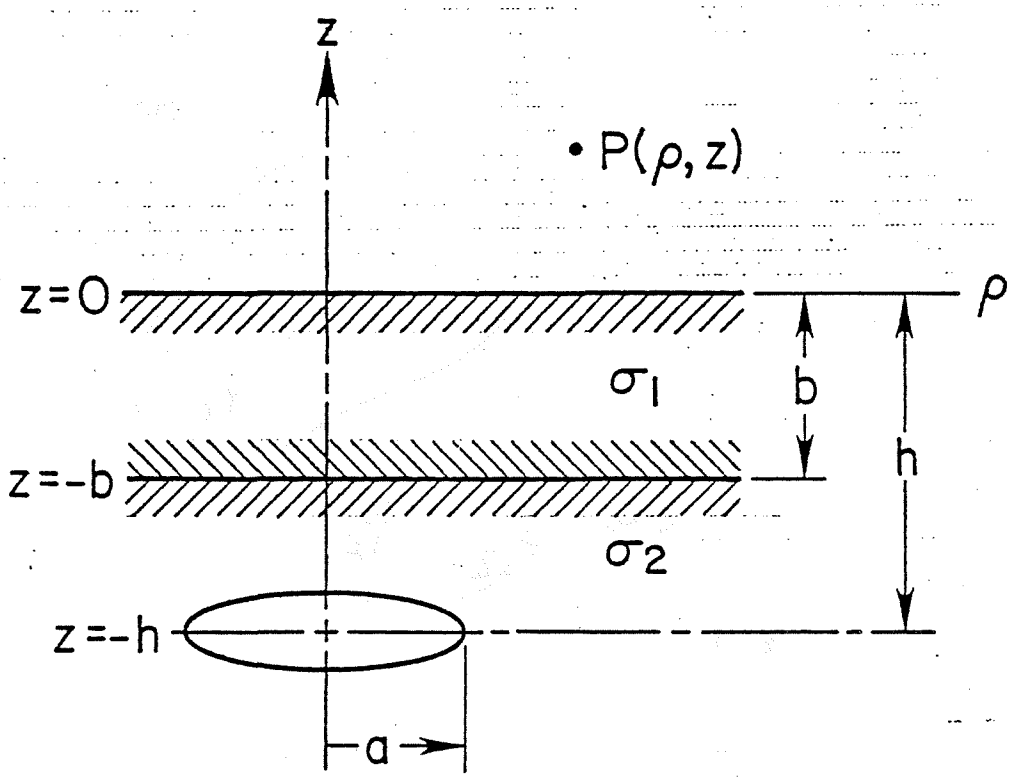
CHANG, D.C., (1973), Characteristics of a horizontal loop antenna over a multi-layered, dissipative half-space, *IEEE Trans.*, AP-21, No. 6, 871-874.

LARGE, D.G., BALL, L., and FARSTAD, A.J., (1973), Radio transmission to and from underground coal mines - theory and experiment, *IEEE Trans.*, COM-21, No. 3, 194-202.

WAIT, J.R., and SPIES, K.P. (1971a), Electromagnetic fields of a small loop buried in a stratified earth, *IEEE Trans.*, AP-19, No. 5, 717-718.

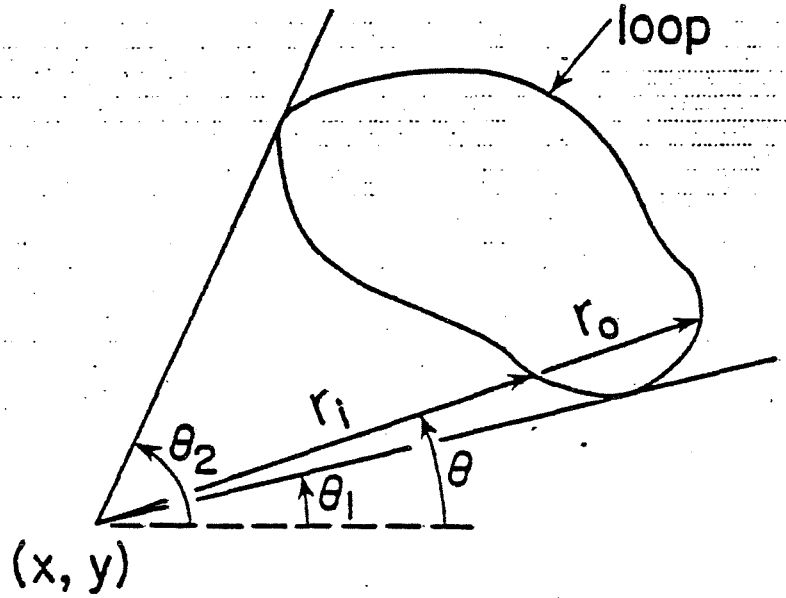
WAIT, J.R., and SPIES, K.P., (1971b), Evaluation of the surface EM fields for a buried magnetic dipole, *AFCRL Rep. 52*, (available from N.T.I.S., Springfield, Va. 22151).

WAIT, J.R., (1971), Electromagnetic induction technique for locating a buried source, *IEEE Trans.*, GE-9, No. 2, 95-98.



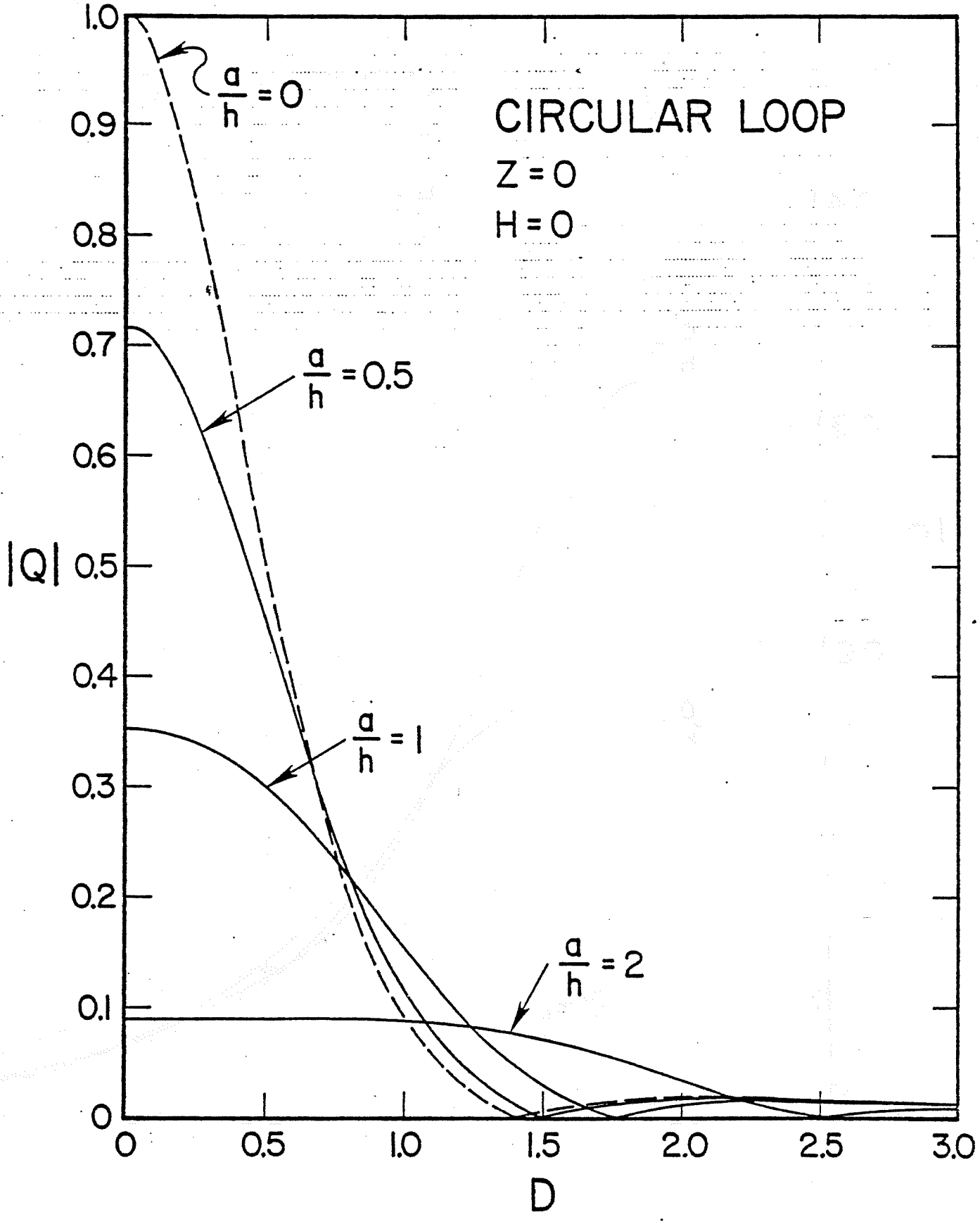
Circular loop of radius a buried in a two layer earth.

Fig. 1



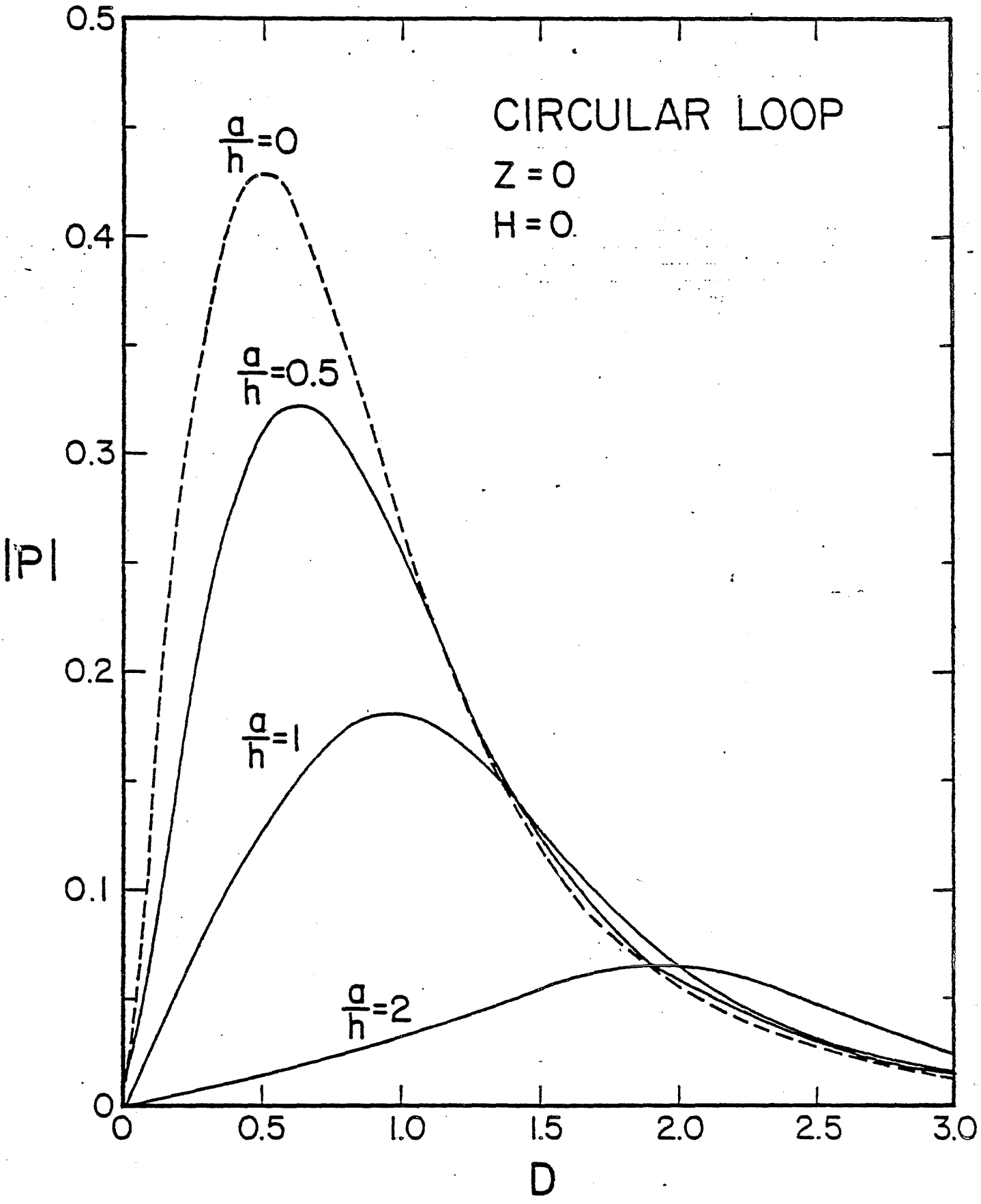
Geometry for a loop of arbitrary shape.

Fig. 2



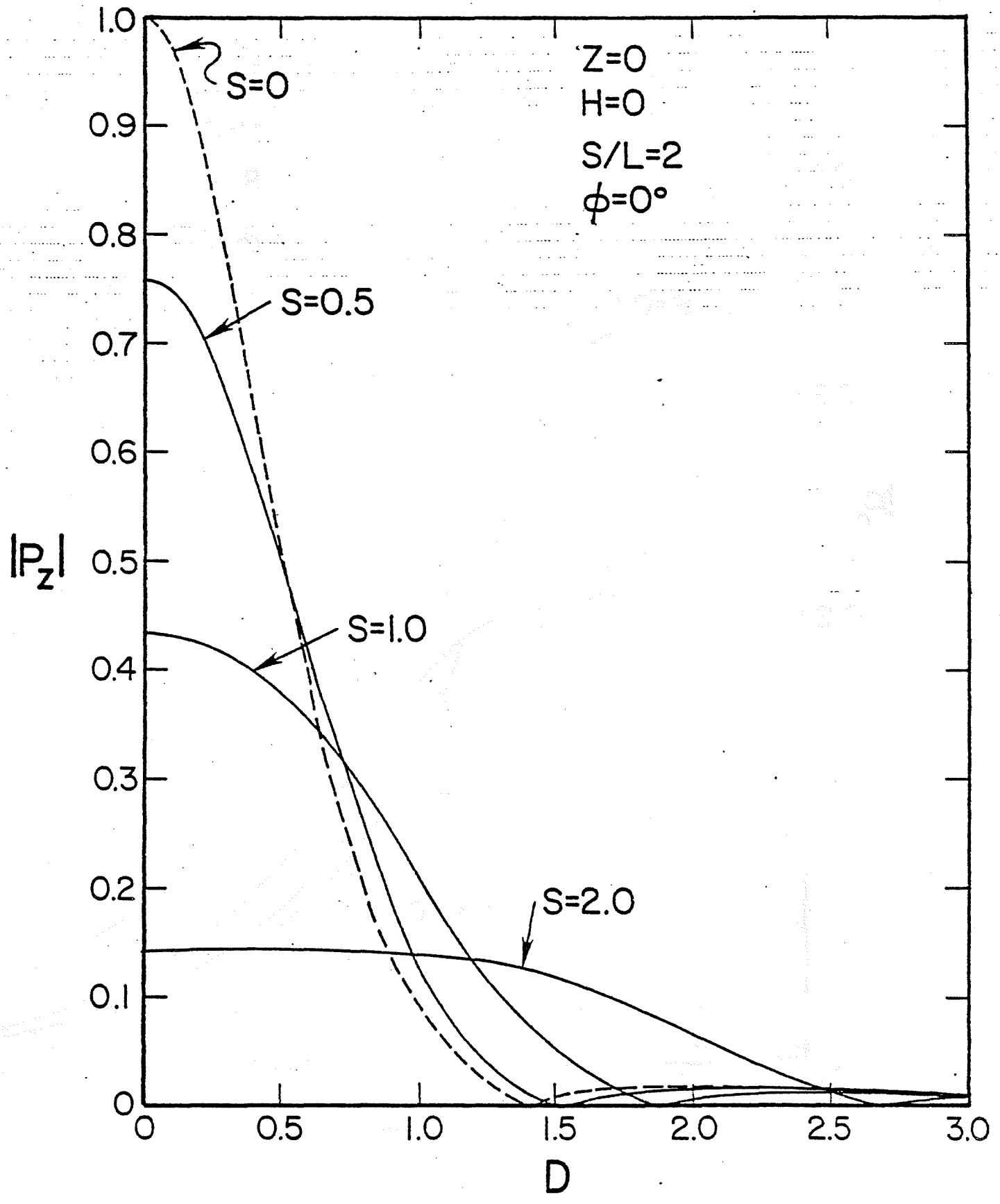
Vertical component of normalized magnetic field for circular loops of various sizes.

Fig. 3



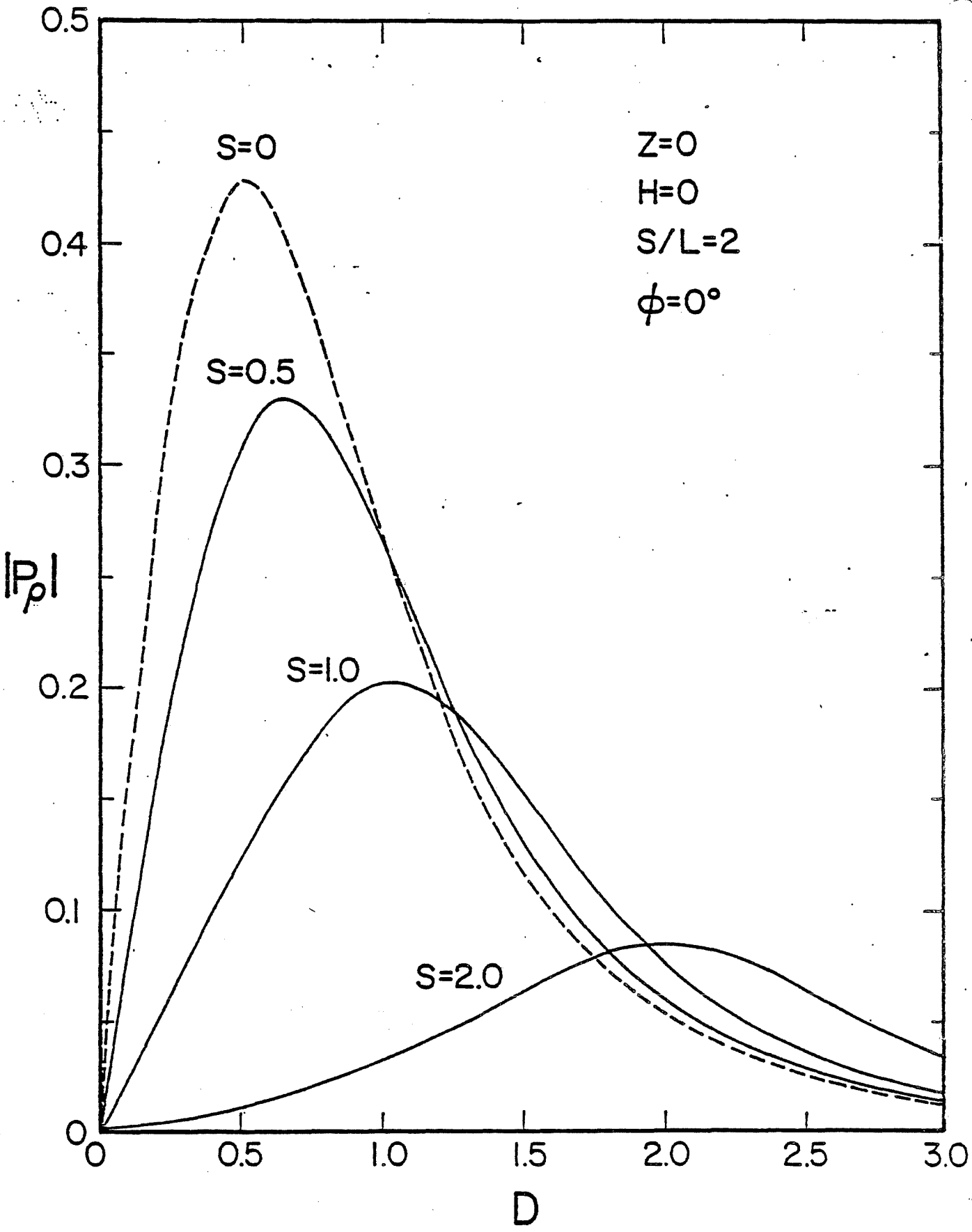
Horizontal component of normalized magnetic field for circular loops of various sizes.

Fig. 4



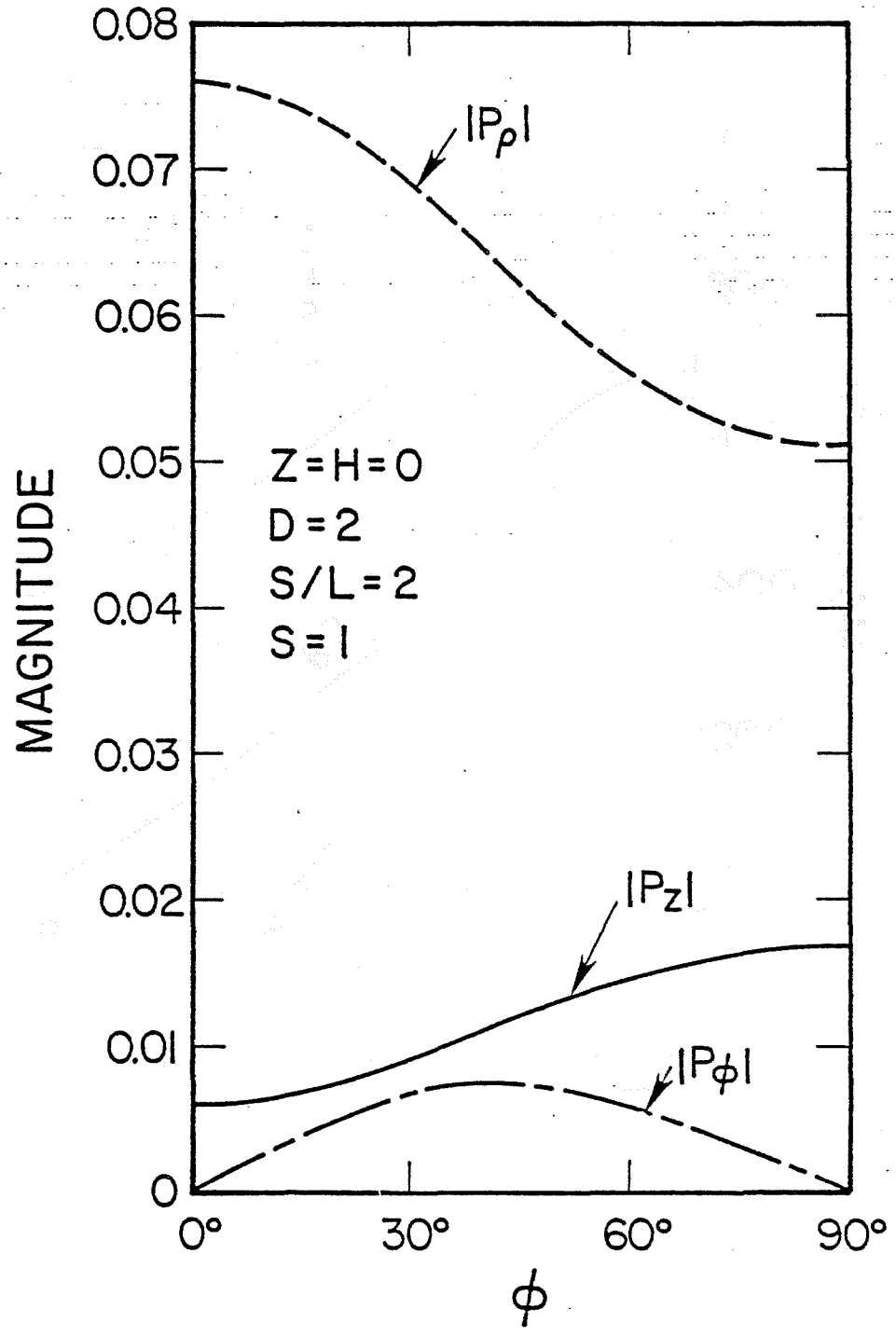
Vertical component of normalized magnetic field for rectangular loops of various sizes.

Fig. 5



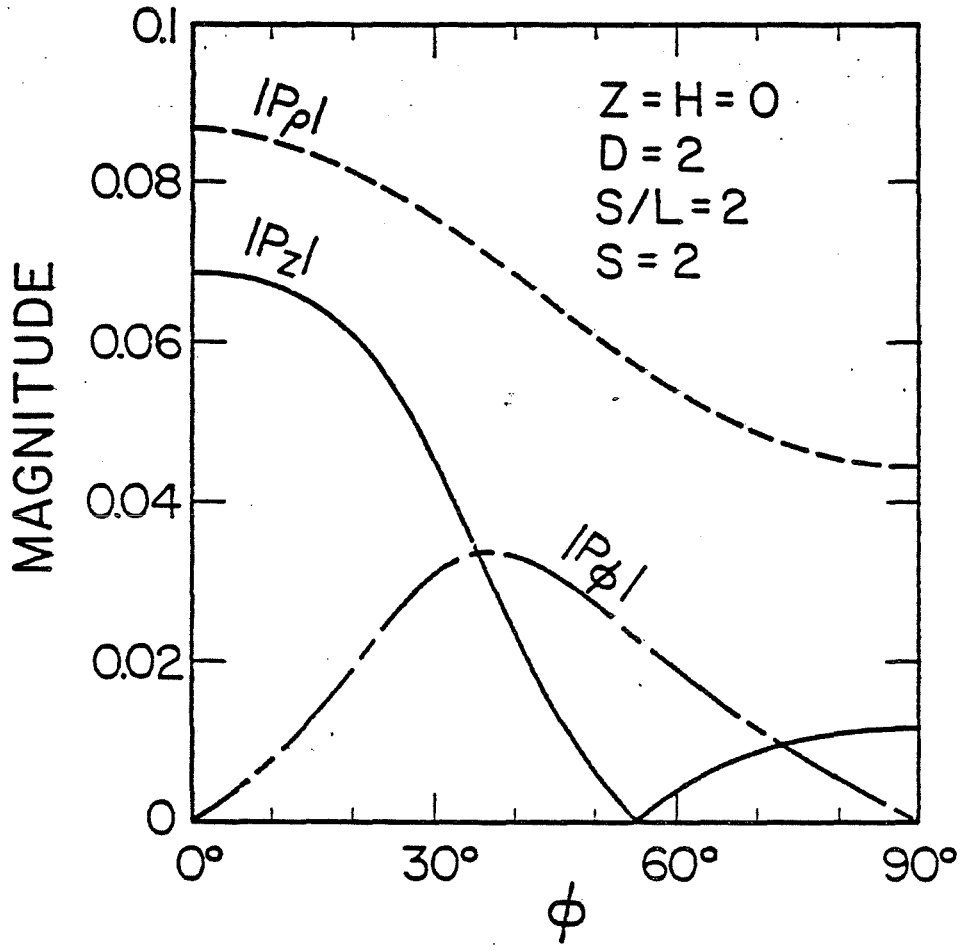
Radial component of normalized magnetic field for rectangular loop of various sizes.

Fig. 6



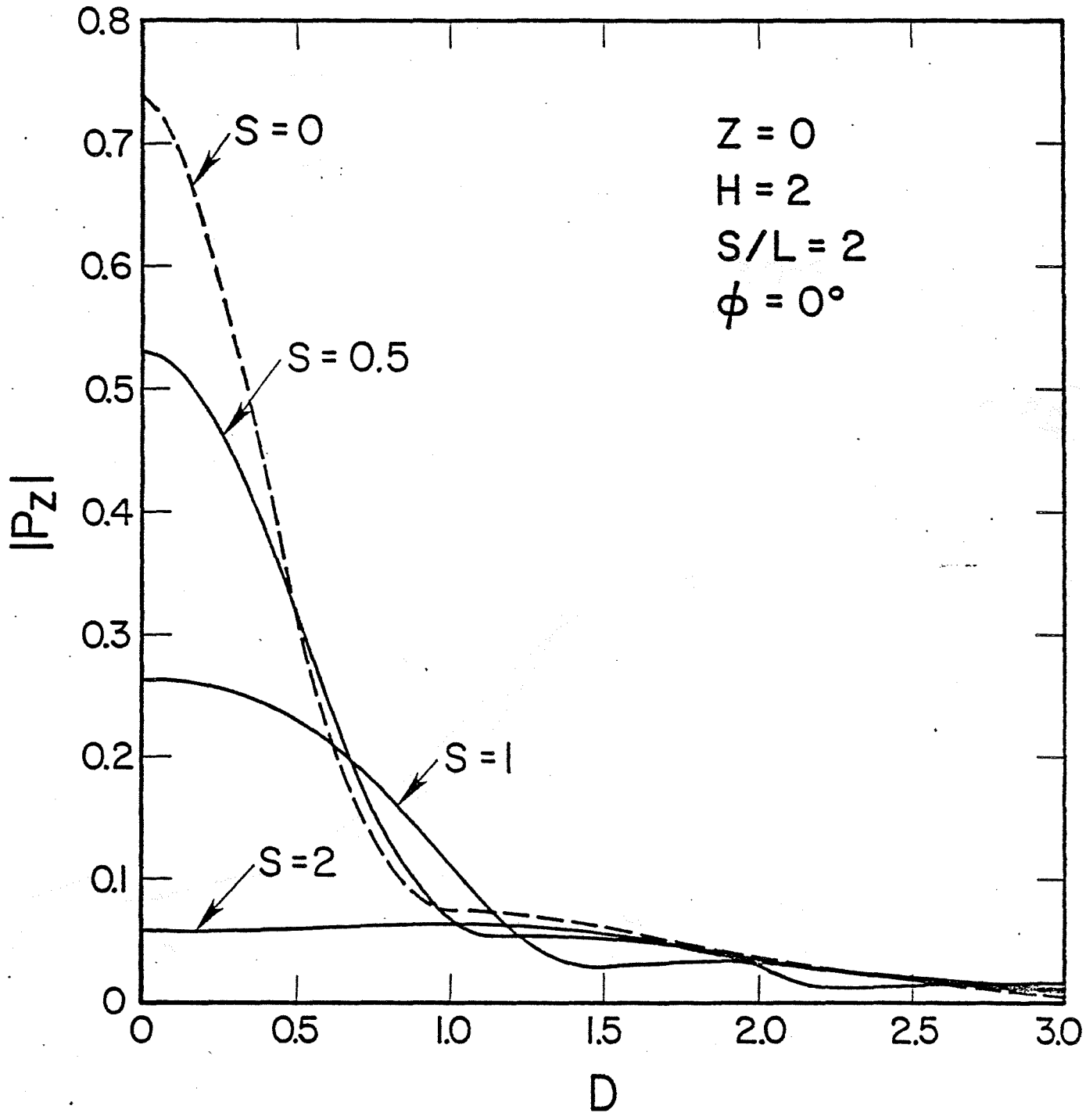
The azimuthal dependence of the three components of magnetic field for a rectangular loop.

Fig. 7



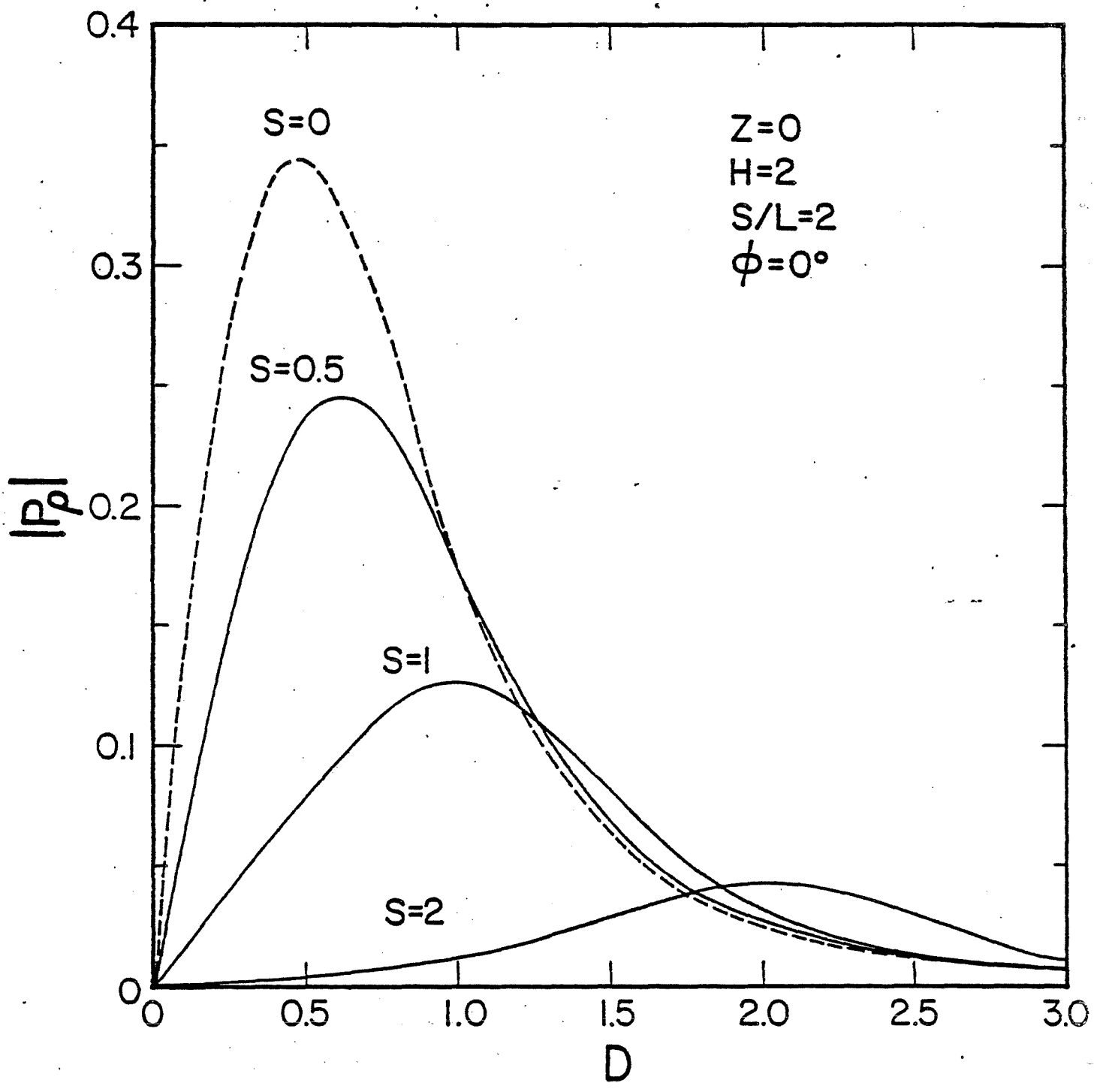
The azimuthal dependence of the three components of magnetic field for a larger rectangular loop (S = 2).

Fig. 8



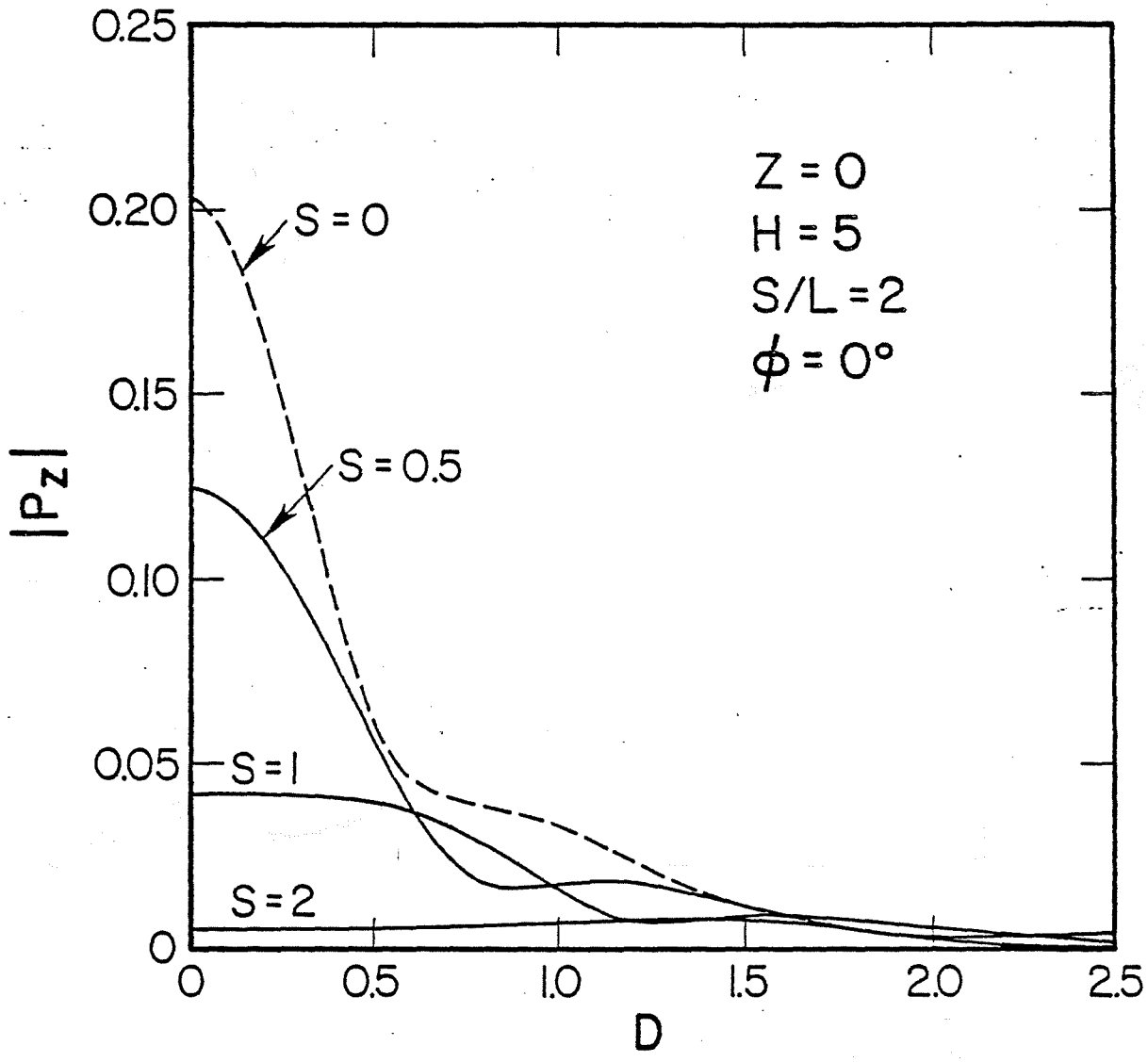
Vertical component of normalized magnetic field for a rectangular loop for H = 2.

Fig. 9



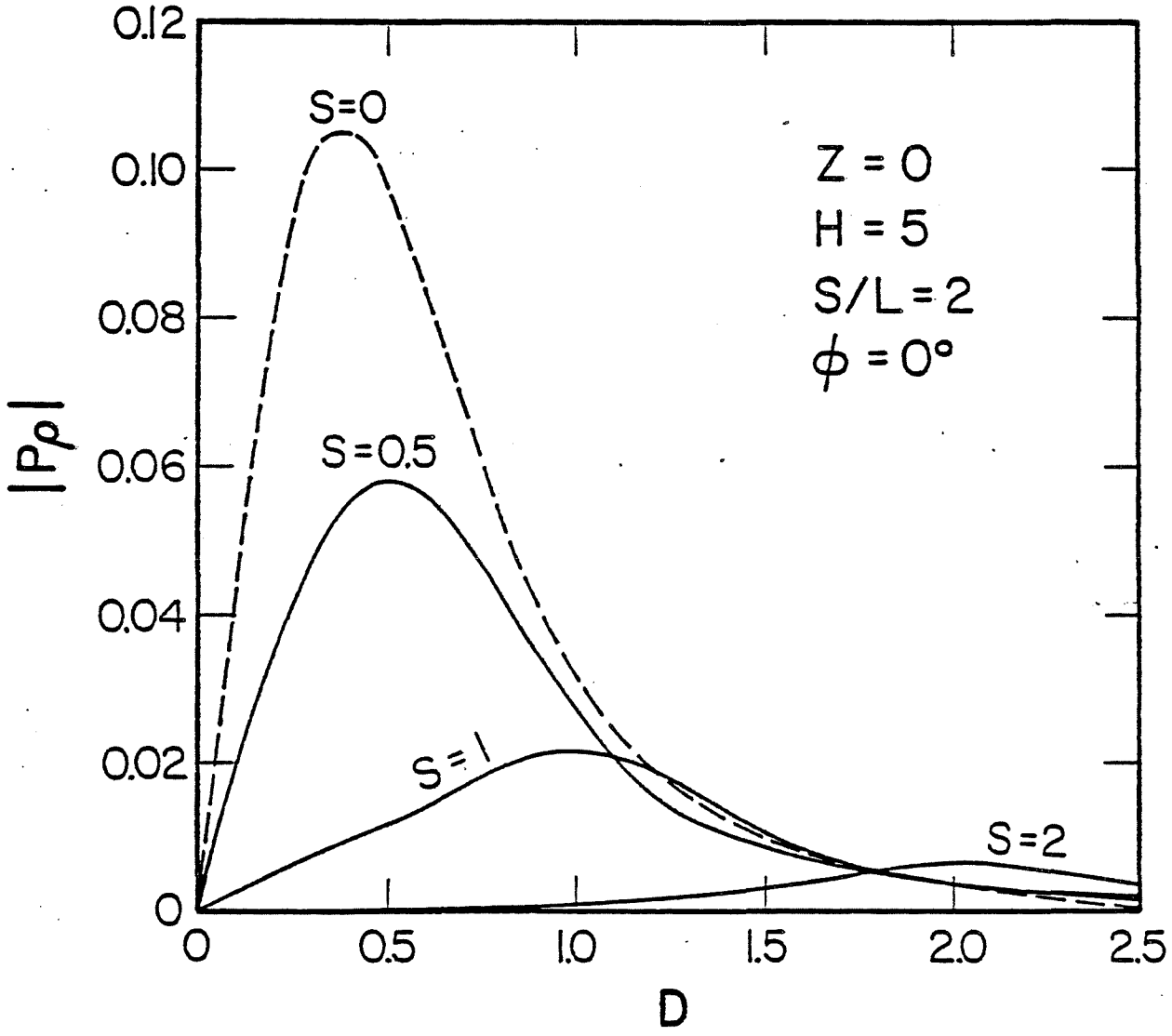
Radial component of normalized magnetic field for a rectangular loop for H = 2.

Fig. 10



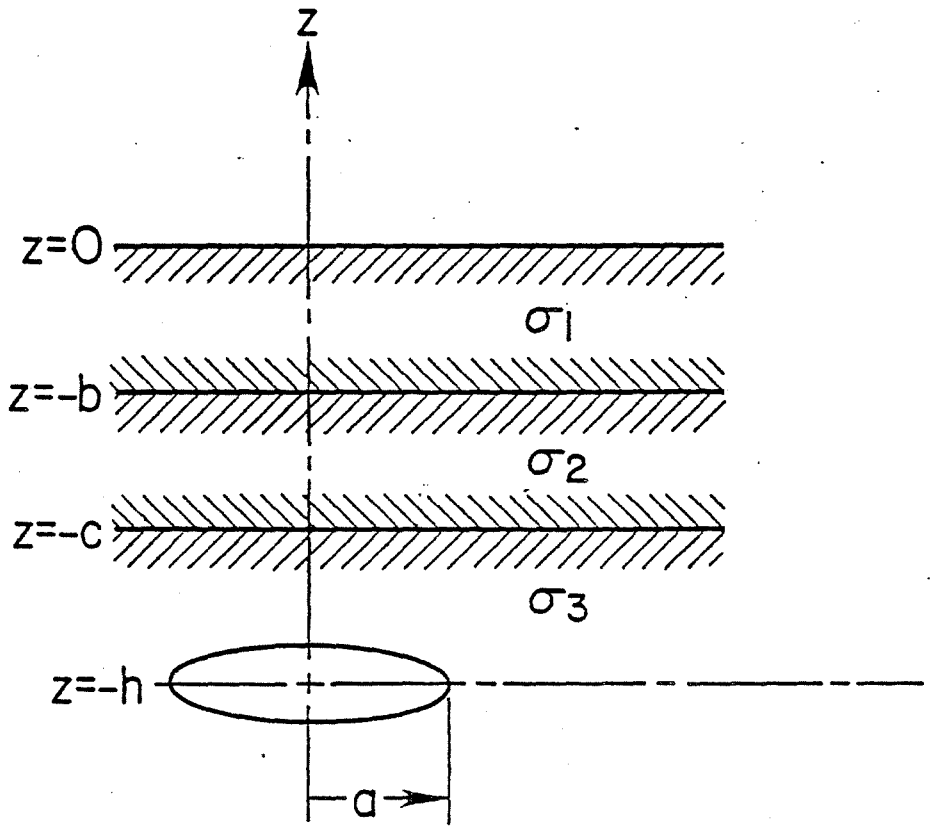
Vertical component of normalized magnetic field for a rectangular loop for H = 5.

Fig. 11



Radial component of normalized magnetic field for a rectangular loop for H = 5.

Fig. 12



Magnetic dipole buried in three layer earth

Fig. 13